TO MY PARENTS

AN EXPERIMENTAL INVESTIGATION
INTO
THE CONSOLIDATION CHARACTERISTICS OF GAP-GRADED SOIL

A Thesis submitted to the
University of London
(Imperial College of Science & Technology)
for the degree of
Master of Philosophy in the Faculty of Engineering

by

ANWAR MUHAMMAD MEMON
B.E. (Civil)

Soil Mechanics Section,
Civil Engineering Department,
Imperial College,
London SW7.

November 1973.

ABSTRACT

The consolidation characteristics of gap-graded soil have been studied from oedometer and triaxial tests. Gap-grading has been provided by mixing kaolin with ground quartz at different ratios by weight. The effects of stress increment ratio on the behaviour of settlement and dissipation of excess pore water pressure are investigated. Both isotropic and anisotropic consolidation have been divided into two groups. In group A, stress increment ratio is kept constant, and in B the ratio is varied in the successive stages of consolidation. It is shown that the Terzaghi theory cannot predict at all the dissipation of excess pore water pressure when small stress increment ratios are used. The effects of possible errors are examined and are shown not to account fully for the discrepancy between theory and observation.

Constant head permeability tests are carried out at the end of primary consolidation in both the oedometer and triaxial tests. The relationships between the effective stress and void ratio, coefficients of compressibility, permeability and consolidation are also studied.

The effects of small pressure increments on the compressibility characteristics of 70% sand - 30% clay mixture are examined in a specially designed hydraulic oedometer as well as in the triaxial tests. Due to the small pressure increments, the excess pore water pressure is found to dissipate very rapidly and not to correspond with the Terzaghi theory at all. Large secondary compression also accompanies the primary consolidation which is difficult to separate. Wahl's curve-fitting method is used to analyse the results and is shown to be useful in such cases.

The microstructure of these sand-clay mixtures, before and after consolidation, is examined, using the Scanning Electron Microscope. It is suggested that a threshold shear stress effect is observed. For example, when large stress increment ratios are applied, the threshold shear strength between particles is exceeded and the consequent pore

pressure response is controlled by the relative compressibilities of the pore fluid and soil skeleton. However, when small increments are applied the shear strength between the particles ratards the compression of the skeleton and so a smaller pore pressure response, and very rapid dissipation is measured.

ACKNOWLEDGEMENTS

The work described in this thesis was carried out in the Soil Mechanics Section of the Department of Civil Engineering, Imperial College of Science and Technology, University of London, under the general supervision of Professor A. W. Bishop.

The author is extremely grateful to Mr. A.E. Skinner, who suggested the topic, supervised the research programme and reviewed the manuscript.

The author wishes to thank his colleagues, in particular Mr. W. M. Maguire, who assisted him in many ways during the course of the work. Sincere appreciation is also expressed to Mrs. E. Gibbs and Messrs. D. T. Evans, L. F. Spall, E. W. Harris, F. D. Evans and C. Gagg for their help in the laboratory.

The author further wishes to thank Mr. and Mrs. Skinner for their kind hospitality on the occasions he had the opportunity to visit them at their home.

Thanks are extended to Miss Niblock for typing the manuscript.

This work was made possible by a grant from the University of Sind, Jamshoro, Pakistan, to whom the author is highly obliged. The financial assistance provided by Wali Muhammad Trust for a period of three months is also gratefully acknowledged.

Finally, the author wishes to express his deepest gratitude to his wife, Najma, for the patience she has shown during the difficult period and the encouragement she has given throughout.

CONTENTS

NOTE: All plates and figures appear at the end of their respective chapters.

1. BRIEF REVIEW OF LITERATURE ON ONE-DIMENSIONAL CONSOLIDATION AND SAND-CLAY MIXTURES.

1.1 Introduction

In 1923 Karl Terzaghi presented a theory of consolidation which was fundamental to the development of Soil Mechanics. His theory was based on the assumption that void ratio and permeability were linear functions of 'effective stress', and were independent of time.

Although Terzaghi's theory enabled engineers to analyse the consolidation behaviour of stressed soil masses, his linearisation of relationships between void ratio, and permeability with respect to effective stress have been shown to lead, in some cases, to a significant difference compared with real soil behaviour.

1.2 Terzaghi's theory

The classical theory of one-dimensional consolidation (Terzaghi, 1923, 1943) is based on the following assumptions:

(i) The soil is homogeneous and fully saturated.

(ii) The pore water and soil grains are incompressible in comparison with the clay skeleton.

(iii) Compression of the soil skeleton and flow of water occur in one and the same direction.

(iv) Stresses are uniformly distributed over any horizontal cross-section of the soil, and so result in identical strains on any horizontal cross-section.

(v) Flow of water through the soil takes place in accordance with Darcy's law.

(vi) The coefficient of permeability k is constant during consolidation under the applied stress increment.

(vii) Only small strains, and correspondingly small changes in void ratio e, are involved.

From these assumptions, the basic equation of consolidation becomes

$$\frac{1}{1+e}\ \frac{\partial e}{\partial t} = \frac{k}{\gamma_w}\ \frac{\partial^2 u}{\partial z^2} \qquad \ldots \qquad (1.1)$$

In addition Terzaghi made the following assumptions:

(viii) The relationship between void ratio e, and effective stress p', is linear and independent of time, therefore,

$$\frac{de}{dp} = \text{constant} = -a_v, \text{ the volume compressibility.}$$

Hence taking into consideration assumption (viii), the equation (1.1) becomes:

$$\frac{\partial u}{\partial t} = \frac{k\,(1+e)}{\gamma_w\, a_v}\ \frac{\partial^2 u}{\partial z^2} \qquad \ldots \qquad (1.2)$$

$$\therefore \quad \frac{\partial u}{\partial t} = c_v\ \frac{\partial^2 u}{\partial z^2} \qquad \ldots \qquad (1.3)$$

Where, $c_v = \frac{k(1+e)}{\gamma_w a_v} = \frac{k}{\gamma_w m_v}$ is the coefficient of consolidation

e = void ratio

p' = effective stress

k = coefficient of permeability

a_v = coefficient of compressibility

$m_v = \frac{(a_v)}{1+e}$ Coefficient of volume compressibility

γ_w = the density of water

t = time from the start of consolidation

z = vertical distance from some chosen datum

u = the excess pore-water pressure.

A particular solution of the differential equation (1.3) depends upon the initial boundary conditions. For instance the case of a layer of clay sitting on an impermeable base and loaded instantaneously, drainage taking place at the top surface only, the following boundary conditions are imposed (Terzaghi 1943):

Datum for z is taken at the base of the clay layer

For $t = 0$ and $0 \leq z < H$, $u = u_o$

$0 \leq t \leq \infty$ and $z = 0$, $\frac{\partial u}{\partial z} = 0$

$0 \leq t \leq \infty$ and $z = H$, $u = 0$

$t = \infty$ and $0 \leq z \leq H$, $u = 0$

A solution in terms of excess pore pressure is established by means of Fourier's series.

$$u = u_o \frac{4}{\pi} \sum_{N=0}^{N=\infty} \frac{1}{(2N+1)} \sin\left[\frac{(2N+1)\pi z}{2H}\right] \exp\left[-(2N+1)^2 \pi^2 T/4\right] \quad . \quad . \quad . \quad (1.4)$$

Where u_o = initial excess pore water pressure

H = thickness of clay (the maximum drainage path)

T = a pure number, known as the time factor and is defined as follows

$$T = \frac{c_v t}{H^2} \quad . \quad . \quad . \quad (1.5)$$

During the process of consolidation the excess water continues to escape from the top and the settlement goes on with a decrease of void ratio. The equation for the settlement at the time t can be written as

$$S_{(t)} = m_v \left(u_o H - \int_o^H u\,dz\right) \quad . \quad . \quad . \quad (1.6)$$

Substituting the value of u from equation (1.4) and integrating, the following solution is obtained in terms of settlement at any time t

$$S_{(t)} = m_v u_o H \left[1 - \frac{8}{\pi^2} \sum_{N=0}^{N=\infty} \frac{1}{(2N+1)^2} \exp \left\{ -(2N+1)^2 \pi^2 T/4 \right\} \right] \quad \ldots \quad (1.7)$$

In equation (1.7) term $m_v u_o H = S_{(\infty)}$ (the ultimate settlement). Hence equation (1.7) can be written in the following form to give average degree of consolidation U

$$\text{where } U = \frac{\text{settlement at any time } t}{\text{settlement at any time } t = \infty}$$

$$\text{i.e. } U = 1 - \frac{8}{\pi^2} \sum_{N=0}^{N=\infty} \frac{1}{(2N+1)^2} \exp \left[-(2N+1)^2 \pi^2 T/4 \right] \quad \ldots \quad (1.8)$$

which can further be written as the function of time factor T

$$\text{i.e. } U = 100 f(T) \quad \ldots \quad (1.9)$$

In comparing test data with predictions from Terzaghi's theory, differences can often be noticed. These may be attributed to;

(a) k not being constant for the imposed stress increment, that is $k = f(p')$.

(b) e may not be a linear function of p'

In addition,

(c) both e and k could be dependent on time.

Investigators have looked at these variations and have developed theories taking into account these limitations of Terzaghi's theory.

1.3 Other Theories of Consolidation considering e and k dependent on Time

Observations concerning the process of secondary consolidation (i.e. e and k functions of time) were first reported by Gray (1936) and Buisman (1936). An empirical approach to this problem was first given by Buisman (1936) with subsequent refinements by Koppejan (1948) and Zeevaert (1957), in which primary and secondary consolidation displacements were considered as separate and serial. The secondary consolidation is considered to succeed the primary consolidation after the excess pore pressure has dissipated, and is proportional to the logarithm of time.

However, rational theories of secondary consolidation have treated the process of both primary and secondary consolidation as occurring concurrently. It is indicated by Christie (1964) that Merchant was the first to make a rational approach to revise Terzaghi's consolidation theory in 1939. Later Taylor and Merchant (1940) and Taylor (1942) presented theories on the process of primary and secondary consolidation where a fluid flow mechanism coupled with a visco-elastic effective stress-strain relationship was envisaged. This conception, proposed by Taylor and Merchant (1940), was shown by Christie, to be equivalent to a model based on a Hookean spring in series with a Kelvin body for effective stress-strain relationship of a clay layer, which has both instantaneous and time dependent components. Later other investigators (Ishii, 1951;

Tan, 1953; 1957; Gibson and Lo, 1961) used the same model. This model responds to an increase in effective stress, by compressing the Hookean spring immediately, but compression of the spring in the Kelvin body is delayed by viscous flow in the dashpot.

In recent years investigators have paid more attention to visco-plastic behaviour of soil, and a number of rheological models have been suggested. Lately, Barden (1965) has proposed a non-linear rheological model by introducing a non-linear dashpot. In addition, advances have been made by considering the influence of strains in two and three dimensions. Theories of three-dimensional consolidation have been advanced by Biot (1956), Mandel (1957) and Tan (1953, 1957). Some others have brought about refinements in 2 - 3-dimensional stress-strain conditions. These proposed theories, though valuable contributions, are in many ways imperfect. For example, none of them takes into account the variation of compressibility and permeability besides other limitations. Again, the sophisticated mathematical treatments are complex and sometimes involve new soil parameters which are difficult to determine experimentally. These complexities have restricted their practical application.

1.4 Effects of load increment ratio

In addition to the time, another factor has to be considered: viz. the effect of the pressure increment ratio. It was first shown by Langer (1936) that, by reducing the loading increments, the resistance to compression increases. Van Zelst (1948), Lewis (1950),

Matlock and Dawson (1951), Northey (1956), and others have observed the influence of the load duration and the load increment ratio on pressure-void ratio relationship. They have shown that the compressibility is affected by long duration of previous load increment and small load increment ratio. They have also reported that the coefficient of consolidation depends upon the consolidation pressure and the magnitude of the pressure increment duration involved. Taylor (1942), Leonards and Ramiah (1959), and Hamilton and Crawford (1959), have noted an increase in the coefficient of consolidation as the load increment ratioincreased. Tests on freeze-dried Kaolin, by Leonards and Altschaeffl (1965), indicated marked reduction in compressibility as the load increment ratio is reduced.

A few studies (Newland and Allely, 1960; Leonards and Girault, 1961; Wahls, 1962), indicate that the ratio of the secondary compression per log. cycle of time to the total primary compression increases in a consistent pattern with decreasing load increment ratio. Unfortunately, with the exception of Leonards and Girault (1961), none of them have measured pore pressures and also the pressure increment ratios used were less than one.

The rate of pore pressure dissipation is highly dependent on the pressure increment ratio, whether small or large. Crawford (1965), Raymond (1965) and Tan (1968) have observed that when small increments are used during consolidation testing the rate of dissipation of pore pressure increases. This phenomenon has also been reported by Leonards and Girault (1961), and they have shown that the rate of excess pore pressure dissipation can be reliably predicted from Terzaghi's theory, provided the applied load increment ratio

is sufficiently large. If the load increment ratio is smaller than some critical value, the Terzaghi theory cannot predict, even approximately, the rate of excess pore pressure dissipation. This is an important factor which has a wider influence on the consolidation parameters and must be taken into consideration by consolidation theories.

A literature survey undertaken showed that not many theories take into consideration the effects of rate of loading and magnitude of pressure increments.

1.5 Non-linear theories of consolidation

Attention has recently been focussed on the variable behaviour of the consolidation coefficients of soils during consolidation. Schiffman (1958) has considered variations in the rate of loading and variations in the coefficient of permeability, but has assumed the coefficient of compressibility to remain constant during the process of consolidation. Richart (1957) has solved, by means of finite differences, the problem considering variable void ratio. Lo (1960) has attempted to take into account the variability of the coefficient of consolidation. Treatment based on large strain theory given by McNabb (1960) and Mikasa (1965) considers the compressibility and permeability varying but in such a way that the coefficient of consolidation remains constant. Hansbo (1960) has considered variable permeability for the solution to the problem of the consolidation of clays by sand drains. Schiffman and Gibson (1964) have considered the effect of the variation in coefficients of permeability and compressibility with depth. A non-linear small strain theory has been presented by

Barden and Berry (1965). Their theory assumes that the void ratio is a log function of permeability and a log function of effective stress. The relationship they obtained, due to the coefficient of permeability as a function of effective stress, could be regarded as similar to Schiffman's (1958) theory.

Examining these theories closely, it could be seen that most of them have limitations, besides being mathematically complicated. For instance, Schiffman (1958) accounted only for variation of the coefficient of permeability with effective stress. His assumption, that the coefficient of permeability decreases and the coefficient of compressibility remains constant with effective stress, leads to the decrease in coefficient of consolidation as the soil consolidates, whereas, many normally consolidated clays exhibit an increase in the coefficient of consolidation with increasing effective stress. McNabb (1960) and Mikasa (1965), on the other hand, have considered the coefficient of consolidation as constant. Schiffman and Gibson (1964) have ignored secondary effects. Barden and Berry (1965) considered only small strains, which limits the scope of their theory. Apart from these limitations, unfortunately, most of the above theories are difficult to apply in practice because of the difficulty of obtaining the relevant soil parameters.

Recently other theories have been advanced which also consider the problem of non-linearity of consolidation parameters during 1-D consolidation. Davis and Raymond (1965) have considered the coefficients of compressibility and permeability decreasing with increasing pressure, whereas the coefficient of consolidation is assumed to remain constant, and strains to be small.

Another theory formulated by Gibson et al.(1967) is free from the limitation of small strain and can take into account the variation of soil compressibility and permeability during consolidation, thus removing the shortcomings in Davis and Raymond's theory. Poskitt (1969) has published a non-linear consolidation theory for normally consolidated clays which considers variable compressibility, permeability and finite strain. But he has ignored the effects of structural viscosity.

1.6 Davis and Raymond's, and Gibson et al. theories compared with Terzaghi's theory

A brief resume of the formulation of the governing differential equations, advanced by Davis and Raymond (1965) and Gibson et al (1967) is given below. These theories are simultaneously compared with Terzaghi's linear theory of consolidation.

(a) Davis and Raymond's non-linear theory of 1-D consolidation

Davis and Raymond (1965) suggested a modification to Terzaghi's theory which appears to go a long way in overcoming the inadequacy of assuming e to be a linear function of p' and k constant. Instead they adopt the empirical linear relationship between e and $\log_{10} p'$ so that coefficient of compressibility can be shown to be given by

$$m_v = \frac{A}{p'} \qquad . \; . \; . \; . \qquad (1.10)$$

where A is a constant which depends on e and C_c*.

---

* Compressibility index as defined by Taylor, 1948, p. 218.

Davis and Raymond pointed out that for normally consolidated soils, the coefficient of consolidation c_v is usually observed to change much less than the coefficient of compressibility m_v, during any pressure increment. Thus there is some empirical justification for assuming c_v to remain constant,

$$\text{i.e.} \qquad c_v = \frac{k}{m_v \gamma_w} = \text{constant} \qquad . \ . \ . \ . \qquad (1.11)$$

This can be seen to be equivalent to assuming that, as the soil particles move closer together, the decrease in permeability k is proportional to the decrease in compressibility m_v.

Instead of assumptions (vi) and (viii), Davis and Raymond adopted equations (1.10) and (1.11) to derive the following differential equation for a thin layer of soil in which total stress p may be considered constant with depth,

$$\text{i.e.} \qquad c_v \frac{\partial^2 w}{\partial z^2} = \frac{\partial w}{\partial t} \qquad . \ . \ . \ . \qquad (1.12)$$

$$\text{where} \qquad w = \log_{10} \frac{p'}{p'_f} = \log_{10} \frac{p'_f - u}{p'_f}$$

p' = the current effective stress

p'_f = final effective stress

u and z = as defined previously.

Equation (1.12) is identical in form to that of Terzaghi's ordinary differential equation and can be solved in the same way since the boundary conditions for oedometer test are similar in terms of u and w. These conditions are (Davis and Raymond, 1965)

$t = 0$ and $0 \leq z \leq H$ and $u = p'_f - p'_i$ then $w = \log \frac{p'_i}{p'_f}$

$0 \leq t \leq \infty$ and $z = H$ and $\frac{\partial u}{\partial z} = 0$ then $\frac{\partial w}{\partial z} = 0$

$0 \leq t \leq \infty$ and $z = 0$ and $u = 0$ then $w = 0$

$t = \infty$ and $0 \leq z \leq H$ and $u = 0$ then $w = 0$

where p'_i = the initial effective stress at time $t = 0$

Hence

$$w_z = \log_{10} \frac{p'_f - u}{p'_f} = \left[\log_{10} \frac{p'_i}{p'_f} \right] \sum_{N=0}^{N=\infty} \frac{2}{M} \left(\sin M \frac{z}{H}\right) \exp \left[-M^2 T \right] \quad . \quad . \quad . \quad . \quad (1.13)$$

where $M = (2N+1) \frac{\pi}{2}$

and $T = \frac{c_v t}{H^2}$, the time factor as defined by Terzaghi's theory.

Apparently Gray (1936) obtained this solution. He also assumed that $\frac{a_v (1 + e)}{k}$ and a layer of finite thickness was constant. In his solution he uses a transformation attributed to Van Dusen (Bureau of Standards) which is not shown in his paper. In addition he does not give a solution for the degree of settlement.

From equation (1.13) therefore

$$\frac{p'_f - u}{p'_f} = \left(\frac{p'_i}{p'_f}\right)^B \quad . \quad . \quad . \quad . \quad (1.14)$$

where $B = \sum_{N=1}^{N=\infty} \frac{2}{M} \left(\sin M \frac{z}{H}\right) \exp\left[-M^2 T\right]$

The equation (1.14) can further be expressed in the following simplified form in terms of pore pressure:

$$\frac{u}{u_o} = \frac{p'_f}{p'_f - p'_i} \left[1 - \left(\frac{p'_i}{p'_f}\right)^B\right] \quad . \quad . \quad . \quad . \quad (1.15)$$

where $u_o = p'_f - p'_i$. is the applied stress increment and B is equal to Terzaghi's value of $\frac{u}{u_o}$ which can be obtained from (1.4) by dividing throughout by u_o. While the equation (1.15) gives different values of pore pressure compared with Terzaghi's equation, it leads to the identical expression for the average degree of consolidation U, which is given in equation (1.8).

(b) Gibson, England and Hussey's finite non-linear 1-D consolidation theory

In 1967 Gibson et al. published a general theory of one-dimensional consolidation which might be considered as a step ahead of Davis and Raymond's (1965) theory. In addition to relieving the limitations of assumptions (vi) and (viii) in Terzaghi's

theory, the assumption of small strain (vii) has also been eliminated by Gibson et al. Furthermore, Darcy's law is recast in a form in which the relative velocity of the soil skeleton and the pore fluid is related to the excess pore pressure gradient.

For the particular case of a horizontal clay layer that is sufficiently thin, such as laboratory samples or natural strata a few feet thick, for which self weight effects are negligible, the equation governing the void ratio, e, is

$$\frac{\partial}{\partial a}\left[c_F \frac{\partial e}{\partial a}\right] = \frac{\partial e}{\partial t} \quad . \quad . \quad . \quad . \quad (1.16)$$

where a = the initial vertical distance of an element of the soil skeleton from some horizontal datum plane which is embedded in the soil skeleton.

and c_F = the quantity related to the coefficient of consolidation c_v of Terzaghi's theory by the following expression:

$$c_F = \left(\frac{1 + e_o}{1 + e}\right) c_v \quad . \quad . \quad . \quad . \quad (1.17)$$

Here e_o = the (uniform) initial void ratio.

In order to linearise the differential equation (1.16), c_F may be assumed to remain constant during consolidation under specific pressure increments such that

$$c_F \frac{\partial^2 e}{\partial a^2} = \frac{\partial e}{\partial t} \quad . \quad . \quad . \quad . \quad (1.18)$$

Equation (1.18) has an important feature in not imposing any restriction on the relationship between effective stress and void ratio, such as assumption (viii) as expressed in equation (1.3) used in the derivation of Terzaghi's expression.

Gibson et al. (1967) have given the following solution to equation (1.18) for the case of an initially thin layer of uniform voids ratio e_o when subjected to an instantaneous increment in applied pressure, which is held constant during the subsequent 1-D consolidation

$$e = e_f + \frac{4}{\pi}(e_o - e_f) \sum_{N=0}^{N=\infty} \frac{(-1)^N}{(2N+1)} \exp\left[-(2N+1)^2 \pi^2 T_o\right] \cos\left[\frac{(2N+1)\pi a}{2H_o}\right] \quad . \quad . \quad . \quad . \quad (1.19)$$

where e_f = the final voids ratio at the end of primary consolidation under the increment

H_o = the length of the initial maximum drainage path at the start of consolidation under the applied pressure increment

and $T_o = \frac{c_F t}{4H_o^2}$ . . . . (1.20)

The datum plane is defined as the plane across which there is no flow of pore fluid and the dimension 'a' is measured from this plane. By putting $a = H_o - z$, where z is the initial distance of a particular element of the soil skeleton from the nearest drainage

surface, so that the equation (1.19) can be expressed in the following alternative form;

$$\frac{e - e_f}{e_o - e_f} = \frac{4}{\pi} \sum_{N=0}^{N=\infty} \frac{1}{(2N+1)} \sin \frac{(2N+1)\pi z}{2H_o}$$

$$\exp \left[-(2N+1)^2 \pi^2 T_o \right] . \quad . \quad . \quad (1.21)$$

The right hand side of this equation is identical in form to the right hand side of Terzaghi's equation (1.4) when u_o is divided throughout. However in equation (1.21) the time factor T_o obtained by Gibson et al. (1967) is one fourth of the time factor given by Terzaghi's theory.

The average degree of consolidation U of the clay layer is given by;

$$U = 1 - \frac{8}{\pi^2} \sum_{N=0}^{N=\infty} \frac{1}{(2N+1)^2} \exp \left[-(2N+1)^2 \pi^2 T_o \right] . \quad . \quad . \quad (1.22)$$

Here again this equation is identical in form to Terzaghi's equation (1.8), with the exception that $T_o = T/4$.

There is no doubt that the theories by Davis and Raymond (1965) and Gibson et al. (1967) are very important achievements towards the realistic considerations of soil behaviour during the consolidation process. However, both the theories may still be considered short of being absolutely perfect. These theories do not

consider the effects of structural viscosity which occur when e and k are function of time. The Davis and Raymond theory has an additional limitation, due to the restrictions to small strains, whereas the theory by Gibson et al. (1967) is free from this restriction and can deal with large strains.

However, all the theories described incorporate the assumption of homogeneous behaviour of the soil structure.

1.7 Sand and Clay Mixtures (Introduction)

This research project was designed to study the influence of soil structure. In order to produce a soil structure which influenced the results of consolidation, mixtures of clay and fine sand, with varying ratios, were tested.

Although this clay and sand mixture can in one sense be considered to be homogeneous in the form used in consolidation theory, the soil structure produced by mixing these materials creates some form of interaction which can be considered to result from a form of non-homogeneity.

1.8 Brief résumé of literature on soil mixtures

A few investigators have considered these types of materials. Gilboy (1928) seems to have been the first to investigate the compressibility of sand-mica mixtures. After a very long break Trollope and Zaffar (1956) and Kenney (1966) carried out shear tests to determine the strength of soil mixtures. Kondner and Vendrell (1964) have formulated an empirical formula to determine the coefficient of consolidation of mixtures of clay minerals. With the

exception of Gilboy (1928) and Kondner and Vendrell (1964), it looks as if no one has attempted to advance the investigation of soil mixtures under consolidation. However, a brief detail of the work done in the field of soil mixtures is given below.

Gilboy (1928) studied the compressibility characteristics of soil mixtures. For this purpose he chose smooth round quartz grains of 0.5 mm average size to constitute the sand fraction, and pure white mica, of average 0.02 mm thickness and 0.417 to 0.589 mm grain size, being the other constituent of the mixture. Various percentages of sand and mica were prepared by weight. Both constituents were thoroughly mixed by shaking in a dry state. Later on the mixture so obtained was hammered till compaction by this means had been achieved. The compacted sand and mica mixture was then placed in the compression apparatus* for testing. The compression of the material was carried out by cyclic loading.

The test results were plotted on a linear graph to obtain the relationship between void ratio and pressure increment for each sand-mica mixture. From the study of experimental results Gilboy (1928) came to the following conclusions:
That the presence of the flat mica grains has a marked effect on the compressibility of the mixture under load, on its expansion after release of pressure, and on the limiting void ratios consistent with equilibrium. The test results further indicate that the characteristic behaviour of fine-grained sediments, such as silts and clays, is principally ascribable to the presence of flat grains. Gilboy (1928) also found out that the compressibility characteristics of any given fine-grained soil may be reproduced on a macroscopic

---

*Riehle Universal hand-operated screw testing machine. For details of the apparatus and its assembly, see Gilboy (1928).

scale by selecting a proper mixture of coarse sand and mica. This demonstrates that any system of analysis or classification of soils which neglects the presence and effects of flat-grain constituents will be incomplete and erroneous.

Recently Kondner and Vendrell (1964) have proposed an empirical formula, in terms of coefficients of consolidation of individual component soils, to determine the coefficient of consolidation of clay mixtures. The consolidation tests on clay mineral mixtures have been carried out in the oedometer and the test results have been correlated with a proposed mathematical formulation.

Kondner and Vendrell pointed out the difficulty of predicting the behaviour of clay mixtures as a function of the properties of the component clays. They also showed that this mixture, or interaction, response is not a simple linear function of the composition. Consequently, the generalised principle of superposition may not be valid, and the presence of a particular clay component that may be present in small quantities may exert a great influence on the engineering behaviour of such a mixture.

In order to overcome these difficulties, and obtain correct values for the coefficient of consolidation of a mixture under a given stress, they have formulated an expression in terms of coefficients of consolidation of the individual components and of the clay mixture as a whole. The formulation of the expression is based on the clay

mineral interaction response studies of plasticity characteristics and consolidation test results. It is indicated that the response properties of the clay mineral mixtures are such that the change of these properties (indices), due to change in composition, is proportional to a constant plus a particular value of the property about which the composition change is occurring. In terms of coefficient of consolidation, the above observation by Kondner and Vendrell (1964) was expressed in the following linear differential equation:

$$\frac{dc_v}{dp} + Ac_v = k \quad . \quad . \quad . \quad . \quad (1.23)$$

and the final solution, after taking into consideration the percentages and coefficients of consolidation of individual components of clay mineral mixtures, was given by them as follows:

$$c_v = c_{v_1} e^{-AP} + c_{v_2} (1 - e^{-AP}) \quad . \quad . \quad . \quad (1.24)$$

where c_v = coefficient of consolidation

c_{v_1} = coefficient of consolidation of one component of mixture

c_{v_2} = coefficient of consolidation of second component of mixture

P = dimensionless composition variable

where $P = \frac{100 - P_1}{P_1} = \frac{P_2}{P_1}$

P_1 = percentage by weight of one clay mineral

P_2 = percentage by weight of second clay mineral

A and k = numerical constants

e = base of natural logarithms.

The numerical constant A can be determined by rearranging and taking the logarithm of equation (1.24), as given below:

$$AP = \log_{10}\left[\left(\frac{c_{v_1} - c_{v_2}}{c_v - c_{v_2}}\right)^{2.3}\right] \quad . \quad . \quad . \quad . \quad (1.25)$$

Equation (1.24), thus represents the interaction response of a two-component system (two clay minerals mixed together) and equation (1.25) enables the dimensionless parameter, A, to be determined.

The investigation of compressibility characteristics of sand-mica mixtures, by Gilboy (1928), and the consolidation behaviour of clay mineral mixtures, by Kondner and Vendrell (1964) may be considered as a valuable contribution towards Soil Mechanics. However, the information on this aspect of the subject is still in its infancy. Gilboy dealt with the one-dimensional compression of sand-mica mixtures in the dry state and consequently, no information was obtained about the usual consolidation parameters. As such, his results are of little value to foundation engineers, who are normally concerned with saturated soils.

On the other hand Kondner and Vendrell (1964) have considered the consolidation properties of a mixture, both components of which are cohesive clay soils. If their argument of interaction response between the two components of a clay mixture is correct and that it depends upon the physio-chemical properties of the individual components, then the consolidation characteristics of clay

mixtures cannot be considered as representative of sand-clay mixtures. Further, Kondner and Vendrell admit that, because of the variability of soil mixtures in general, the above formulation has limited scope in its applicability. The other drawback to Kondner and Vendrell's expression is the constant coefficient of consolidation of individual components. This means that the slightest variation in the coefficient of consolidation of the component clays of the mixture would affect the constant A, and invalidate the whole expression.

Some work on the strength characteristics of sand-clay mixtures has been done. These indicate that mixtures in which the clay content is about 20% undergo a striking change in behaviour. For example, Trollope and Zaffar (1956) did some drained triaxial tests on sand-clay mixtures to determine their shear strength. They concluded that for material containing 20% kaolin (by weight), a condition was established in which the true cohesion was independent of the effective stress system, which of course conflicts with the common belief that, for normally consolidated soils, true cohesion is proportional to effective stress. This, according to the authors, is due to the specific soil structure, which in turn shows the importance of the contribution of the inter-particle forces in determining the fundamental cohesion parameters.

The consolidation behaviour of clay-sand mixtures with less than 30% clay indicates the non-plastic nature of the material. A discussion of this is deferred to later chapters.

The residual strength of mineral (in fine-grained states) and mixtures has been studied by Kenney (1966). He reported that the strength properties of mineral mixtures depend upon the mineral compositions and their physico-chemical properties.

Emphasis on the soil structure, for determining true mechanical properties of any soil, is shown by most of the investigators. The effects of particle arrangements, their shapes, stresses and strains between them, the chemical reaction, etc. create so many complexities that the whole problem of structural study becomes very involved. Nevertheless, in this study the influence of different compositions of sand and clay will be studied, in an attempt to investigate the influence of soil structure on consolidation behaviour.

2. INDEX PROPERTIES. CONSOLIDATION AND CONSTANT HEAD PERMEABILITY TESTS IN 4" DIA. CONVENTIONAL OEDOMETER.

2.1 Introduction

The reason for choosing gap-graded soil was due to the experimental results of triaxial dissipation tests carried out by Skinner and the author (1970) on a soil from a test pit near Stocks Reservoir. The particle size distribution of this soil showed only a small percentage of silt size material. Triaxial test results are discussed in the next chapter.

There was not enough material for the proposed test programme so the consolidation tests were carried out on artificially prepared samples. Hand mixing of sand was used to produce a gap-graded soil in the laboratory.

Extensive experimental work was undertaken to investigate the consolidation properties of these mixtures, both under isotropic and anisotropic stress conditions. At the end of consolidation stages, constant head permeability tests were conducted also. Results of the tests were analysed using Terzaghi's one-dimensional consolidation theory. Before presenting the oedometer test results, the physical properties such as Atterberg limits, particle size distribution etc., of the material used are given in the following section.

2.2 Index Properties

The sand-clay mixtures were prepared from the well-ground quartz and commercially manufactured kaolin. As will be seen from the particle size distribution curves in Figure 2.2, 95% of kaolin was less than .002 mm, and similarly almost 98% of quartz was below 0.2 mm, i.e. fine sand and silt. A gap between the grading was achieved by the absence of the medium and coarse silt size

particles. Atterberg limits for the following mixtures of sand and clay were also determined.

Clay % by weight	Sand % by weight
90	10
80	20
70	30
50	50
30	70
20	80
10	90

To achieve uniform mixtures the sand and clay were initially mixed in the dry state. A clean polythene bag was used for this purpose. The sand and clay of a particular mixture were put in the bag and thoroughly agitated. After this process the mixture of sand-clay was transferred to a porcelain dish, where it was stirred with a spatula while distilled water was added. The required amount of water to give a LI of 1.5 to 2.5 was poured in and the stirring continued until a fairly consistent mixture of sand and clay had been achieved. The material was then left for curing in the polythene bag before starting the consolidation tests.

The index properties were determined according to the British Standard 1377, (1967). The summary of these properties is given in Table no. 2.1. As the sand content of the mixture increases, the liquid and plastic limit decreases and so does the plasticity index, whereas the specific gravity increases. The mixtures containing 20% and less clay act as non-plastic material. In other words 20% clay content is the minimum at which the sand-clay mixture exhibits significant plasticity. This is in agreement with the index property results of similar sort of material reported

by Trollope and Zafar (1956). Thus the value of plasticity index of 8.3 for 80% sand and 20% clay may be considered as the boundary between plastic and non-plastic behaviour of the material in this particular case. Most probably when clay content is less than 20% the sand grains form a structure which is almost independent of the clay component of the mixture. But when the clay content is increased a dispersed sand grain skeleton is created which would not be able to exist on its own.

2.3 Experimental Programme

One dimensional consolidation tests of sand-clay mixtures were carried out in the 4" diameter Bishop type oedometer. Tests using constant and varying stress increment ratios were performed on each mixture. These are labelled as Group A and Group B. The former refer to consolidation tests performed using constant stress increment ratios and the latter to tests using varying stress increment ratios. The stress increment ΔP in the case of Group A tests was such that its ratio with effective stress PO' at the end of the previous stage was 2, for all the consolidation stages. Table no. 2.2 gives the number of stages and the details of ΔP and PO' for both the groups. In addition to the consolidation stages two swelling stages were carried out before removing the sample from the oedometer.

A part of each consolidated sample was impregnated with carbowax and the rest was air-dried for a microstructure study using Stereo Electron Microscope. Chapter 5 is completely devoted to these studies.

The programme of experimental investigation included constant head permeability tests which were conducted at the end of primary consolidation, when the pore pressure had almost dissipated. The tests were performed by applying a small excess pressure to the base of the sample, the top being free to drain.

2.4 Description of the apparatus

(i) 4" dia. Oedometer

A 4" diameter by $1\frac{1}{2}$" high Bishop's modified oedometer was connected at the base to a self-compensating mercury control system on one side and a pressure transducer on the other as shown in Figure No. 2.1.

The oedometer consists of 6" dia. by 1" thick brass base plate with a 3" dia. (UNI A80 KV) ceramic porous stone fitted in the recess at the centre of the base plate. Two 1/8" dia. ports come out from the base of the porous stone. On one side, a P.S.G. type pressure transducer is attached for the measurement of pore water pressure while on the other side an AB10 Klinger valve is connected. The base plate has an annular recess for a rubber O-ring seal. Six studs are provided at the spacing of 60^{o} angle intervals and are screwed on to the base. The sample is placed in a 4" dia. by $1\frac{1}{2}$" high by $\frac{1}{2}$" thick stainless steel ring. This consolidation ring sits on the O-ring when in position. The top cap passes through the six studs and sits on the consolidation ring. A groove is provided in the top cap in which another O-ring is seated. This O-ring sits between the top cap and the consolidation ring which provides effective sealing at the top. By means of six screws the top cap is tightened. This clamps the consolidation ring in position and also makes both top and bottom of the ring water-tight. A loading cap having 4" dia. (UNI A80 KV) ceramic coarse porous stone is placed at the top of the sample and the load is applied through it in the standard Bishop-type press. The pore water is allowed to drain freely from the top of the sample. The flow and deformation of the sample are one-dimensional.

(ii) Apparatus for constant head permeability test

At the end of primary consolidation the samples were subjected to a constant excess hydrostatic pressure at the base in order to determine the coefficients of permeability. A self-compensating mercury control (see Bishop and Henkel, 1962) was devised for this purpose.

As will be seen from the Figure 2.1, the lower mercury pot is sitting on a fixed base and connected through a nylon tube to the upper mercury pot which is supported by an adjustable hanger. The top of the lower pot is in turn connected to the Klinger valve of the oedometer via a saran tubing, whereas the top of the upper pot is open to air. A scale is fixed on the bench around which 1/8" I.D. saran tube is clipped in the manner as shown in the figure. The saran tube is de-aired and then an air bubble is introduced for measuring the quantity* of water flowing into the sample during permeability test.

The constant head permeability tests carried out in this manner were satisfactory except in the case of 80% and 90% sand sample which posed some problems. These were for example loss of head due to the large flow of water into the samples and the limited capacity of the reservoir (mercury pot) to provide uninterrupted water supply until the steady state of flow had been achieved.

(iii) The pressure transducer

For the measurement of pore water pressure a P.S.G. pressure transducer (manufactured by Electro Mechanisms Ltd.) with a range of 0 - 100 p.s.i. was connected to the base of the oedometer as shown in Figure 2.1. It has a circular inlet through which

---

* The calibration of the saran tubing gives 21.7 inches movement of an air bubble per c.c.

the water pressure is applied. Four resistance strain gauges connected in the form of a wheatstone bridge are secured to its walls. The method of construction provides self-compensation against changes of resistance with temperature. The transducer is connected to a readout meter (a Boulton and Paul type C61 transducer meter) which enables the transducer output to be nulled. This meter was itself connected to a strip chart 'potentiometer' recorder which records pore pressure variations during the consolidation process.

(iv) Chart recorder

The recorder which automatically records the output signals due to the variation in pressure is connected via the C61 meter to the pressure transducer. The change in the pore water pressure during the consolidation process is recorded on a chart which is driven at a constant speed. During or after the test P.W.P. can be computed from a prior calibration test. The needle of the recorder is so arranged that when brought to the centre, i.e. at the 50th division on the scale (total 100 divisions) attached, the output voltage of the transducer has been nulled and thus the existing pore pressure in the sample is obtained by calibrating the transducer with the C61 readout. Before commencing the consolidation test, the scale factor and recorder pen position were set depending upon the pressure increment. During the test,the recorder pen travels either to the left or right indicating a rise or fall in P.W.P. respectively. The time can be measured from the speed at which the chart moves. Two speeds were available. The fast speed provided one inch travel in six minutes, whereas on the slow speed the chart speed was one inch per hour. The advantage of the recorder is that a continuous record of pore pressure behaviour is obtained.

2.5 Calibration of pressure transducer

Before calibration of the pressure transducer, the whole apparatus was thoroughly de-aired, as described in the following section. An additional disc cap was then clamped to the top cap. The oedometer was next filled with de-aired water and connected via nylon tubing to a dead weight 'Budenberg ' pressure gauge calibrator. By adding weights to the dead weight gauge tester, known pressures were transmitted to the transducer. Simultaneously decade reading of the C61 was noted for each pressure increment (0 - 100 p. s. i. pressure range). In addition the recorder response was noted for high, medium and low sensitivity settings of C61 meter. The calibration graphs p. s. i. per number of decade divisions against decade division were plotted. The values of pore pressure at particular times were normally computed from the chart obtained from the recorder, besides cross checks were made using the calibration graphs.

2.6 De-airing of the apparatus

Before starting the consolidation tests, the oedometer and the entire system were thoroughly de-aired. Initially the pressure transducer was disconnected and the de-aired distilled water was flushed across the port at the base of the oedometer. Air trapped in the passage, porous stone and the Klinger valve was thus forced out through the other end of the port. Next freshly boiled distilled water was injected with the help of a syringe inside the pressure transducer. The tendency of air bubbles to stick to the walls of the transducer was eliminated in this way. The oedometer was then placed under de-aired water in a basin and the pressure transducer along with its fittings was screwed into its base (Figure 2.1).

The oedometer was then filled up with de-aired water and sealed with a top plate. A mercury pot was connected via nylon tubing filled with de-aired water to the top plate and oedometer was left overnight under a pressure of 100 p. s. i. In this way the remaining air bubbles still entrapped in the system were dissolved in the water which was flushed out under a differential head of water. Simultaneously the system was also completely checked for possible leaks.

2.7 Preparation of samples

The method of preparing the sand-clay has already been described in section 2.2. The initial moisture content of the samples varied, depending upon the percentage of the constituents and their index properties. In order to have soft and fully saturated samples, the moisture content was intended to be very high (Table 3.2). As a result these samples, except with high sand content, were normally in the form of thin paste lying between 1.5 to 2.5 liquidity index.

To eliminate any air bubbles trapped in the voids while mixing, the material was placed in a vacuum dessicator and subjected to a vacuum before preparing a sample. In addition, an attempt was made to keep the initial moisture content of the two samples of the mixture as near as possible for test groups A and B. However, the results of void ratio etc., were worked out from final moisture content and the weight of the sample. The initial water content of the samples is shown in Table 2.3.

2.8 The procedure of consolidation test

Before proceeding with the consolidation test, the apparatus was ensured to be free from the trapped air bubbles as described earlier. A piece of Whatman's No. 54 filter paper already soaked in de-aired distilled water was placed over the porous stone in order to prevent clogging and to facilitate the removal of sample after the test. The steel sample ring was then placed on the base plate. A weighed quantity of sand-clay mixture was slowly poured into the ring whose inside wall was previously coated with a thin film of silicone grease to assist in decreasing side friction. Great care was taken to prevent air being trapped while pouring the material into the consolidation ring. As soon as the ring was filled up to the brim, the top surface was carefully levelled with the help of a metal piece. Another soaked Whatman's filter paper was neatly placed on the top surface of the sample. The retaining ring was next clamped in position. The loading cap containing the top drainage porous stone was slowly lowered until it came in contact with the sample.

The oedometer pot was placed in the Bishop-type oedometer press, and its hanger was brought into position. Initial readings of both the C61 meter and the dial gauge (resolution 10^{-4} inch) were noted. The chart recorder was switched on to the fast speed with its needle set as explained in section 2.4(iv). The consolidation test commenced with the application of a load increment and the readings of the settlement were taken in the usual manner. Simultaneously, the pore pressure variation was recorded on the strip recorder.

The load increments were applied as shown in Table 2.2. With the exception of samples containing 80% and 90% sand, the duration of each load increment was about 24 hours. One problem encountered with the samples having a large proportion of clay was that some extrusion occurred through the gap between the top cap and sample ring, specially during the first stage of consolidation. These and other factors influencing the test results will be discussed later.

2.9 The procedure of constant head permeability test (C.H.T.)

Before commencing a constant head permeability test an air bubble was introduced in the saran tubing and its initial position was recorded with respect to the scale rule as described in section 2.4(ii). The upper self-compensating mercury pot was positioned so that the differential head between the two pots produced a constant hydrostatic pressure of 1.0 p.s.i. (or 27.69 inches constant head of water) at the base of the sample. At the end of primary consolidation when pore pressure had almost dissipated the permeability test was started by opening the Klinger valve of the oedometer. Immediately the bubble came into action by moving towards the sample. Readings of the leading meniscus of the air bubble were taken at suitable time intervals. A note of the displacement dial gauge over the sample was also taken. This indicated slight swelling of the sample at the beginning of a C.H.T. The permeability test was allowed to run till a steady state had been achieved. The samples containing a high clay content required more time to reach the steady state than those of a high sand content. As such, the duration of the permeability test depended upon the percentage of the constituents in a mixture.

Since there was no control on the top drainage of the sample, the computation of the coefficient of permeability had to be based on the rate of flow of water into the sample. To avoid disturbance caused by the seepage force, the permeability tests were carried out from the third stage of consolidation onwards in both groups A and B.

2.10 Test Results and Discussions

(a) Time-Settlement Relationship

The settlement-log time curves of pure clay and sand-clay mixtures are shown in Figures 2.3(a) to 2.74(a). With the exception of the first stages of Group B tests, the plot of excess pore pressure against log of time for each stage of consolidation is also given under its respective settlement curve, Figures 2.3(b) to 2.74(b). The influence of the effective stress increment ratio $\frac{\Delta P}{Po'}$, on the secondary consolidation was not included in this phase of the programme. Therefore the increment ΔP was applied immediately after the primary consolidation.

As is evident from the time-settlement diagrams, the deformation due to the first increment is much larger than the subsequent loading increments. Since the samples were very soft the extrusion at the first stage of consolidation was considerable. Besides this, the bedding and perhaps the effects of shock loading made it difficult to analyse the results of the first stage correctly. These effects can be noticed from time-settlement figures of pure clay and samples with only a small sand content. Consequently the void ratio has also been severely affected in some cases, as for instance in the case of 90% and 70% clay samples (Figures 2.94 and 2.96) where the void ratio at the first stages seems to be in error. On the other hand, samples with 50% or more of sand appear to be less affected, perhaps due to the low compressibility.

In order to examine the effects of the load increment ratio on the time-rate of consolidation, the experimental time-settlement curves of 50% - 50% sand-clay mixtures have been compared with Terzaghi's theoretical curve fitted at t_{50} as shown in Figures 2.39(a) to 2.47(a). It will be seen from the shapes of experimental and theoretical curves that Terzaghi's theory predicts the rate of settlement reasonably

accurately up to U = 70%. However, there is comparatively less correspondence between the theoretical curve and the experimental curve of the fifth stage of consolidation Group B test where $\frac{\Delta P}{Po'}$ is less than 1.0 (i.e. $\frac{P}{Po'} = 0.5$). Similarly, the experimental curves of the rest of the samples are likely to correspond closely with Terzaghi's theoretical curve, with the exception of the last stage in Group B where some discrepancy may be expected. Identical behaviour to this has also been observed by Leonards and Girault (1961), Christie (1965) and Tan (1967). The consolidation tests carried out by Leonards and Girault (1961) using $\frac{\Delta P}{Po'} = 1.0$, 0.25 and 0.22 successively showed that the shape of the time-settlement curve is greatly affected when small $\frac{\Delta P}{Po'}$ is used. Looking back at the settlement curves of 50% - 50% sand-clay mixture, it will be seen that the observed rate of consolidation has the tendency to be slightly faster in the beginning than predicted by Terzaghi's theory. However, towards the end of consolidation (about U = 70% and beyond) the rate of settlement becomes slower than the theoretical. This is generally due to the influence of secondary and creep effects, causing delay in the consolidation process. As far as sand-clay mixtures containing 80% and 90% sand are concerned, their non-plastic nature (section 2.2) having low compressibility gives rise to high time-rate of consolidation. Because of this considerably flat shaped curves are obtained, Figures 2.58(a) to 2.74(a) (with the exception of the first stages of consolidation). Hence, sometimes it becomes quite difficult to determine the consolidation parameters using Casagrande's log time fitting method, particularly when small and instantaneous settlement occurs with small load increments.

(b) Pore Pressure Characteristic

The dissipation of pore pressure was measured during each stage of consolidation and is shown in Figures 2.3(b) to 2.74(b) in terms of excess pore pressure versus log of time. For comparison graphs of settlement and dissipation of pore pressure are given on the same page. In the case of the Group B tests, the first increment was very small and the measurement of pore water pressure was not successful. In the case of the Group A tests, the pore pressure response of the first stage of consolidation was also difficult to monitor. This difficulty enforced as a limitation of the equipment and was the function of the measuring system and the insensitivity of pressure transducer at low stresses and perhaps the side friction.

The flexibility of the measuring system may be mainly due to the entrapped air, temperature changes and volumetric expansion of the system itself. In general, the flexibility of the measuring systems gives rise to three effects:

(i) With the application of pressure increment some water must flow from the sample into the measuring device which creates the difference in the measuring system and in the pore fluid. Thus there can be a considerable timelag before equilibrium is reached.

(ii) Even if no drainage is permitted during a pressure increment, some water must flow to the connecting leads, valves etc., which are likely to expand and cause the pressure difference throughout.

(iii) The stress distribution between the soil skeleton and the pore phase may be altered by the change in overall compressibility of the pore phase caused by the excessive flexibility of the measuring device.

The effects of system flexibility have been investigated by Whitman, Richardson, Healy (1961), Bishop and Henkel (1962), Gibson (1963), Northey and Thomas (1965), Christie (1965) and many others. Their studies have shown that besides the compressibility of the soil skeleton and the duration of the previous increment, the flexibility of the measuring system also greatly influences the response time and the maximum pore pressure build-up. Whitman et al. (1961) were first to present the following approximate expression for the pore pressure response of a saturated clay specimen in terms of the flexibility of the measuring system.

$$\frac{\Delta uB}{\Delta uA} = \frac{1}{1+B} \qquad \ldots \ldots \ldots \qquad 2.1$$

where $B = G/AHm_v$

m_v = coefficient of compressibility (sq. in/lb)

G = flexibility of the measuring system (cu. in/p. s.i.)

H = thickness of sample (in.)

A = area of the oedometer (sq. in.)

ΔuA = pore pressure which would exist at the base of a sample if there were no measuring system.

ΔuB = measured pore pressure

A more rigorous analysis is given by Gibson (1963) which is based on Terzaghi's theory of consolidation, and examines the equilibrium pore pressure as well as the time taken to reach various degrees of equilibrium. Perloff, Nair and Smith (1965) have developed a mathematical solution by which the effect of the volume change in

the measuring system is taken into account in the evaluation of pore pressure build-up throughout the consolidation test specimen as a function of time. Northey and Thomas (1965) looked into the response of pore pressure measuring devices when applied to determine the pressure build-up in oedometer tests. The pore pressure build-up has also been studied by them in relation to the speed of loading, the effects of oedometer wall friction and the sensitivity of the pressure transducer. Christie (1965) obtained the following analytical expression for the excess of pore water pressure u at any point in the sample, which is based on Terzaghi's theory of consolidation:

$$u = 2u_o \sum_{n=1}^{\infty} \frac{(\alpha_n^2 + C^2)}{\alpha_n (\alpha_n^2 + C^2 + C)} e^{-\alpha_n^2 T} \sin \frac{\alpha_n z}{H}$$

$$-2 (u_o - p_{mo}) \sum_{n=1}^{\infty} \frac{(\alpha_n^2 + C^2)}{\alpha_n (\alpha_n^2 + C^2 + C)} e^{-\alpha_n^2 T} \cos \alpha_n \sin \frac{\alpha_n z}{H}$$

..... 2.2

where $C = AHm_v/G$

and α_n is positive root of $\alpha \tan \alpha = C$,

u_o is the initial pressure in the sample,

p_{mo} is the initial pressure in the measuring system.

For the excess pore water pressure at the base of the sample $z = H$.

The theoretical effects of flexibility of the measuring system in terms of $\frac{u}{u_o}$ versus T given by Christie is shown in Figure 2.19. In the conventional oedometer the initial pressure in the measuring device, $p_{mo} = 0$, thus the pore water pressure at the base of the sample increases from zero to a peak value and then dissipates.

From this figure it will be seen that when the value of C is decreasing, the peak pressure reduces and the time lag in the process of pore pressure dissipation increases.

In the tests reported here the flexibility of the measuring device was of the order of 6.45×10^{-5} cu. in./p.s.i. Assuming that there was no air in the system,* the values of C in case of 50% - 50% sand-clay mixtures have been calculated and are given in Table 2.4. It is interesting to note that the value of C is very high except in the last stages of Group A and B. This would suggest that theoretically maximum P.W.P. response should be 98% in all cases except where $\frac{\Delta P}{Po'}$ is reduced to 0.5 (fifth stage of Group B). While the actually measured pore pressure values are much less and vary between 83% to 62% in Group A and 92% to 56% in Group B, as shown in Figures 2.83 and 2.84. Therefore the measuring system itself is effectively rigid in relation to the soil tested and can not be wholly responsible for the variation of peak pore pressure with $\frac{\Delta P}{Po'}$ or rapid rate of pore pressure dissipation with small $\frac{\Delta P}{Po'}$.

The other factors which are likely to influence the pore pressures are:

(i) incomplete saturation
(ii) leakage
(iii) temperature
(iv) clogging of the porous stone
(v) the side friction.

Briefly, their effects on the pore pressure are discussed as follows.

It is difficult to say whether the samples in the oedometer tests were fully saturated. But the B values (Bishop and Henkel 1962) obtained from the isotropic consolidation tests were almost unity as described in Chapter 3. It is therefore assumed that the samples

* It has already been said that the pressure transducer and the oedometer were thoroughly de-aired.

tested in the oedometer were fully saturated, and that the discrepancies in the pore pressure response and in the time lag are not due to this reason.

Tan (1968) has examined the effects of leakage on both the average rate of consolidation and the pore pressure dissipation. He has shown that the leakage at the base of the oedometer would result in a considerable acceleration of rate of pore pressure dissipation and the average rate of consolidation. In the tests reported here there was no obvious leakage. If there had been a leak, the pore pressure dissipation would have been very rapid. It will be seen from Figure 2.1 that an O-ring was provided with annular recess of oedometer base plate which served as an effective sealing. Besides this the whole apparatus was thoroughly checked for leakage prior to testing. So leakage is not responsible for the slower rate of pore pressure dissipation for the large load increment ratios.

The temperature variation can cause changes in the viscosity of the pore fluid and therefore the permeability of the sample. This in turn can accelerate or decelerate the pore pressure changes depending upon the rise or fall of temperature respectively. Finn (1951) has reported that the coefficient of consolidation is also affected by the temperature variations. Besides this the differential expansion or contraction of the various parts of the instrument can cause flexibility problems. However, since all the tests were carried out in the temperature controlled room ($20^{o}C$) the effect of temperature cannot be the factors influencing the results in this case.

The permeability of the ceramic porous stone (UNI A80 KV) used in the oedometer was of the order of 1.7×10^{-2} cm/sec. This is higher than the permeability of the material tested. Bishop and Gibson (1963) made an analytical study of the effects due to plugging of the porous stones. Their calculations show that the porous stones

used at Imperial College are free from being clogged. Hence the different rates of pore pressure dissipation for various values of load stress increment ratio cannot be attributed to this error either.

The other most important problem inherent in the conventional oedometer is the side friction during the consolidation process. Consequently the pore pressure and the settlement measurements are likely to be affected by this factor. Taylor (1942) showed that 10 - 30% of the applied pressure could be transferred to the walls of the oedometer by frictionor adhesion during tests on the Boston Blue Clay. Between 0.15 to 0.30 coefficient of side friction in conventional tests have been reported by Hansbo (1960), Nakase (1963) and Northey and Thomas (1965). However, their studies have shown that the side friction is dependent on the consolidation pressure, that is, it is high at the small pressure and rapidly decreases with the increasing pressure. The rate at which side friction develops is dependent on at least two factors:

(i) the rate of strain,

(ii) the rate of pore pressure dissipation.

An appreciable amount of side friction accompanies the development of initial (immediate) compression. Thereafter, the friction increases (at a decreasing rate) and undoubtedly affects the rate of pore pressure dissipation (Leonards and Girault, 1961). This is perhaps one of the reasons why the first stages of both the groups A and B tests where the increments were 0.875 p. s. i. and 1.75 p. s. i. respectively were not successful. However, it still does not account for the higher peak pore pressure with the increasing $\frac{\Delta P}{Po'}$ as in the case of the second and third stages of the Group B tests, and the decrease in the peak pore pressure following the smaller $\frac{\Delta P}{Po'}$ (i.e. 1.0 and 0.5) as in the case of the fourth and fifth stages of consolidation.

While still on the subject, it must be pointed out that Kallstenius (1963) has shown that friction is higher for soft wall materials than for hard materials of equal surface smoothness. In the present work, the consolidation tests were carried out in hard stainless steel rings lubricated with silicone grease, which minimized the side friction affects to a considerable extent (Martin 1962, Hansbo 1960, and Kallstenius 1963). Thus side friction is not expected to have an appreciable effect on the observed peak pore pressure, which has been increasing or decreasing with $\frac{\Delta P}{Po'}$, and decreasing consistently with constant $\frac{\Delta P}{Po'}$ in spite of high consolidation pressure. Besides this, similar behaviour of pore pressure dissipation was observed in the hydraulic oedometer (Chapter no. 4).where the side friction is considerably smaller than in a conventional oedometer.

In regard to the electro-chemical effects in pore fluid, these were minimized by remoulding with distilled water, and are considered to be not at all serious in the material under consideration.

Now it will be seen that the characteristics of pore pressures are highly dependent on the structural viscosity and the magnitude of load increment ratio and its duration.

The families of time-pore pressure relationship curves of pure clay and the sand-clay mixtures are shown in Figures 2.75 to 2.90. From these diagrams it can be noticed that the samples of 100% clay show as high as 90% to 95% build-up of pore pressure when $\frac{\Delta P}{Po'}$ is constant (Group A) or increasing (Group B). The pore pressure build-up of sand-clay mixtures containing higher proportions of clay (i.e. more than 30% clay) is also of the same order as that of pure clay. But sand-clay mixtures containing 80% and more sand show an appreciable decrease in the pore pressure response to an extent of 50% or less than the applied stress. Looking at curves

of pore pressure dissipation under Group B tests, it can be observed that with the increase of $\frac{\Delta P}{Po'}$ the peak pore pressure increases, but as the $\frac{\Delta P}{Po'}$ decreases, the pore pressure response also decreases. This effect can be seen after the third stage of consolidation when a small $\frac{\Delta P}{Po'}$ of 1.0 and 0.5 is applied following the previous $\frac{\Delta P}{Po'}$ of 3.0. A decrease in the peak pore pressure with successive load increments is also evident from the Group A tests when $\frac{\Delta P}{Po'} = 2.0$ is applied to all the stages of consolidation.

The pore pressure plots also indicate in general a delay in the build-up of maximum pore pressure. This trend is more conspicuous in the case of sand-clay mixtures containing a higher proportion of clay. Barry and Wilkinson (1969) have shown that the pore pressure response is related to the structural viscosity of the material. The concept and the effects of the visco-elastic material on pore pressure dissipation are discussed as follows.

Conventionally, the consolidation process of fine grained soil is divided into primary consolidation and secondary compression, as suggested by Gray (1936) and Buisman (1936). Whereas actually the primary and secondary consolidation occur concurrently, as pointed out by Taylor and Marchant (1940) and Taylor (1942). They proposed a visco-elastic effective stress-strain relationship which is equivalent to a model based on a Hooken spring in series with a Kelvin body having both instantaneous and time-dependent components (Christie 1964). Since then many investigators have suggested modification in their proposed rheological models (e.g. Ishii 1951; Tan 1953, 1959; Gibson and Lo 1961; Murayama and Shibata 1964; Barden 1965; Wu et al 1966).

Barry and Wilkinson (1969) studied the effects of structural viscosity on the pore pressure build-up under undrained conditions.

An analytical expression based on the rheological models by Barden (1965) and Wu, Resendiz and Neukirchner (1966) has been formulated by them. They have shown that the time required for the pore pressure build-up depends upon the structural viscosity of a particular soil and the stress increment ratio. In other words, a sufficiently large time will be required for the build-up of maximum pore pressure when small $\frac{\Delta P}{Po'}$ is used on a soil having large structural viscosity. Barry and Wilkinson (1969) showed that the theoretical time for 95% pore pressure build-up of Kaolinite under undrained conditions is 0.3 seconds and 1.3 minutes when $\frac{\Delta P}{Po'}$ of 1.0 and 0.25 is used respectively. The experimental time for maximum pore pressure build-up of pure kaolin (Figure 2.76, Group B) for the fourth stage ($\frac{\Delta P}{Po'}$ = 1.0) and the fifth stage ($\frac{\Delta P}{Po'}$ = 0.5) is about 2.0 and 3.0 minutes respectively. Keeping in view the pore pressure measurements in the conventional oedometer (drained conditions), the agreement between the theoretical and experimental is quite reasonable.

Barry and Wilkinson pointed out that if the soil is of viscous nature and behaving as a non-linear Kalvin element, then the rate of build-up in pore pressure for a small $\frac{\Delta P}{Po'}$ will occur very slowly, perhaps over a number of days. Similar effects were observed by the writer in the triaxial and hydraulic oedometer consolidation tests on 70% sand - 30% clay mixture samples under very small $\frac{\Delta P}{Po'}$. It was noticed that after the completion of consolidation tests when the drainage valves were closed, the pore pressure started building up very slowly to a certain value in 24 hours, suggesting a continuous relaxation of the soil specimens being damped by the visco-elastic behaviour of the soil structure. Further discussion on this is given in Chapter 4, however, this phenomenon shows that the sand-clay mixtures have a considerable structural viscosity, due to which delay in the maximum pore pressure build-up is caused in all of

them, as shown in Figures 2.77 and 2.86 (except those containing 80% and 90% sand) particularly when $\frac{\Delta P}{Po'}$ is decreased as fourth and fifth stages of consolidation.

The other most important factor seems to be the duration of load increment ratio. The effects of duration on the pore pressure dissipation have been studied by Northey and Thomas (1965). It is shown by them that rapid loading (at 20 minute intervals) leads to a sharper pore-pressure response when compared with standard 24-hour-cycle loading. The difference is assigned to the effect on pore pressure of greater rigidity of the soil structure build-up as a result of the secondary consolidation of the 24-hour cycle. That is, during the secondary consolidation, the soil builds bonds which will resist further compression and prevent the full development of pore pressure under new increment of pressure applied to the soil. This phenomenon of the stiffening of the structure has been observed by Taylor (1942), Skempton and Northey (1952), Leonards and Ramiah (1959), Christie (1965), Bjerrum (1967) and many others. Though the tests reported here were carried out for normal duration, however the effects of secondary consolidation cannot be ignored specially near the end of the primary consolidation.

It will be seen from the pore pressure graphs that the decrease in the response time and the peak pore pressure is very pronounced for the fourth and fifth stages of consolidation (Group B) where $\frac{\Delta P}{Po'}$ is smaller than previous $\frac{\Delta P}{Po'}$. Similar effects are also noticeable in the case of the last stage of Group A tests, but to a lesser extent. From this it appears that the rigid structure which is built up within the soil tends to resist further compression, i.e. a part of the load is carried by the structural bonds, as suggested by Taylor (1942), instead of wholly being transferred to the pore water instantaneously. Similar conclusions were drawn by Whitman, Richardson and Healy (1961). They further pointed out that it is difficult to measure pore pressure accurately whenever the stiffness of the mineral approaches that of the water.

The above observations and the arguments suggest that in the absence of interparticle bonding and structural viscosity, the maximum pore pressure build-up should be equal to the applied stress increment ΔP and instantaneous. As regards the second and third stages of consolidation, where $\frac{\Delta P}{Po'}$ is 2.0 and 3.0 respectively, it can be noticed that the pore pressure has built up very well to an extent of even 98% and 99% in some cases (see Figures 2.76, 2.79, 2.82). The response time to peak pore pressure is also reduced. This whole phenomenon of rise in the peak pore pressure in no way means that the interparticle bonding is absent, but could mean that the large load increments may be creating very high shear stresses due to the displacement of particles during the consolidation process in a conventional oedometer. Consequently these shear stresses overcome the resistance due to the interparticle bonding and cause a considerable breaking up of bonds. This may not happen in the case of small load increments where the resistance to compression increases, as pointed out by Langer (1936). Thus for the large increments, a greater portion of the applied load will be transferred to the pore water resulting in a higher peak pore pressure than in the case of the subsequent smaller load increments.

On the other hand, in the case of Group A tests where the load increments are doubled, even then the peak pore pressure of the subsequent stages decreases, particularly in the fourth stage. This suggests that after every consolidation stage the particles come closer and closer, resulting in very tight packing and higher interparticle bonding which create even more resistance every time. To overcome this resistance and to achieve a higher peak pore pressure it is not only necessary to apply a higher load increment, but also to increase the $\frac{\Delta P}{po'}$ from its previous value. In other words, even if the increments are doubled to keep the $\frac{\Delta P}{Po'}$ constant, the peak pore pressure will

continue to deteriorate, unless $\frac{\Delta P}{Po'}$ is also increased. The effects of constant $\frac{\Delta P}{Po'}$ on the peak pore pressure are clearly demonstrated by the 80% sand samples, as shown in Figure 2.87. However, it must be pointed out that exceedingly low peak pore pressure in the case of 80% and 90% sand samples, could be due to the lack of clay content, causing low compressibility, very tight packing of sand grains , and therefore highly stiff structures. Consequently, when a load increment is applied to such types of soils, most of the pressure is transmitted to the sand grains, which do not pass the same on to the pore water, but to each other, thus causing very low peak pore pressure, as shown in Figures 2.87 to 90.

Primarily it was desired to fit Terzaghi's theoretical curve to the 50% dissipation of pore pressure curves obtained from the tests. Since in many tests the samples did not produce a 100% response of pore water pressure, the 50% point was difficult to achieve. However, the approximate comparison between the theoretical and the experimental curves can be vizualised.

It will be seen from the excess P.W.P. diagrams, that the rate of pore pressure dissipation is greatly influenced by the load increment ratio $\frac{\Delta P}{Po'}$. That is, tests with large $\frac{\Delta P}{Po'}$ show a slower rate of pore pressure dissipation than those with small $\frac{\Delta P}{Po'}$. These effects can be seen from the Group B diagrams where in the second and third states $\frac{\Delta P}{Po'}$ is 2.0 and 3.0, and that of the fourth and fifth stages is 1.0 and 0.50 respectively. The rate of pore pressure dissipation of the second and third stages is slower and likely to be in better agreement with Terzaghi's theoretical curve. Whereas in the case of the fourth and fifth stages the rate of pore pressure dissipation tends to be much faster and may not correspond with the theoretical curve at all. For Group A tests, better agreement between the theoretical and experimental curves can be expected. These effects are better demonstrated in the next chapter where the two curves

have actually been fitted. However, the influence of $\frac{\Delta P}{Po'}$ on the excess pore pressure dissipation has been observed by many investigators, e.g. Leonards and Giraults (1961), Crawford (1965), Raymond (1965), Davis and Raymond (1965), Barden (1965), Tan (1968) and Som (1968).

On the effects of $\frac{\Delta P}{Po'}$ Leonards and Girault (1961) concluded that the rate of excess pore pressure dissipation can be reliably predicted from Terzaghi's theory, provided the applied load increment ratio is sufficiently large. However, if the $\frac{\Delta P}{Po'}$ is smaller than the critical value (in this case less than 1.0), Terzaghi's theory cannot predict, even approximately, the rate of excess pore pressure dissipation. Northey and Thomas (1965) and Christie (1965) reported similar behaviour of pore pressure using small $\frac{\Delta P}{Po'}$ for a duration of 24 hours. Davis and Raymond (1965) have formulated a non-linear small strain theory and have shown that the rate of pore pressure dissipation is highly dependent on the $\frac{\Delta P}{Po'}$ and may not be satisfactorily predicted by Terzaghi's theory. However on the other hand, it has been shown that the rate of settlement is not much affected by the load increment ratio.

From the test results presented here, similar behaviour to that quoted by the above quoted research workers is confirmed. Further to that, it is pointed out that besides the $\frac{\Delta P}{Po'}$, the proportion of sand and clay in a mixture also greatly affects the rate of pore pressure dissipation, as demonstrated by the results of 80% and 90% sand samples. It can be seen from Figures 2.87(b) to 2.90(b) that the rate of pore pressure dissipation is becoming faster and faster for each successive consolidation stage, regardless of the magnitude of $\frac{\Delta P}{Po'}$. Also the build-up of maximum pore pressure decreases in the subsequent stages. This type of behaviour is mainly due to the incompressible nature of the sample containing more sand. For

these samples the pressure transducer must also be too soft, as shown in Table 2.4. Thus it is not likely that Terzaghi's theoretical curve would correspond with the experimental curves of sand-clay mixtures containing a small quantity of clay in relation to sand.

(c) Pressure-Void Ratio Relationship

The calculations of pressure-void ratio are based on the void ratio at the end of the test. The e - log P' relationships of pure clay and the sand-clay mixtures are shown in Figures 2.93 to 2.100. It will be seen from these graphs that all the samples show a linear e - log P' relationship, although slightly displaced in relation to each other.

The void ratio-pressure curves of Group and B tests of individual samples have been assembled on one graph in order to compare them with eath other and to investigate the influence of load increment ratio. In most cases the void ratio of the constant $\frac{\Delta P}{Po'}$ test is slightly higher than that of the varying $\frac{\Delta P}{Po'}$. This in spite of the initial void ratio of the two identical samples being almost the same (see initial water content given in Table 2.3). Whereas the two void ratio curves of 80% and 30% clay samples agree with each other rather well as shown in Figures 2.95 and 2.98. However, the overall agreement between the e - log P' curves obtained from the Group A and B tests seems quite reasonable considering the difficulties such as bedding errors, deformation of the apparatus and the extrusion of the material during consolidation process. The other factor which is likely to cause some descrepancies in void ratio is incomplete saturation.

It has already been said that the samples were fully saturated, therefore the errors in the void ratio cannot be due to this effect. As far as bedding and the deformation of the apparatus is concerned,

Som (1968) found that if the settlement is large then these effects are insignificant. However, due to the soft nature of the sample, the extrusion of the material during all the oedometer tests was noticeable and cannot be ignored. The influence of this can be realized from the e - log P' curve of 90% clay sample, as shown in Figure 2.94. In this case a significant amount of material was squeezed out around the porous stone when initial increment of 1.75 p.s.i. was applied. Thus there is a considerable difference at the beginning of the void ratio-pressure relationships of Group A and B tests. Matlock and Dawson (1951) investigated the effects of extrusion of the material on e - log P' curve. They checked the reduced dry weight of the specimen against the calculated original value, and found that the loss of soil during the consolidation process almost exactly compensated the apparently lowered void ratio. They have shown that it is because of the extrusion of the material which causes these discrepancies and not the $\frac{\Delta P}{Po'}$.

The other important factor is the duration of the load increment. The effects of this on the normally consolidated clays have been studied by Lewis (1950), Northey (1956), Leonards and Ramiah (1959)and Simons (1965). Lewis used pressure increment duration of 24 hours and 48 hours, Northey 20 minutes and 24 hours, Leonard and Ramiah 4 hours, 1 day and 1 week, and Simons 5 hours, 1 day and 1 week. They all came to the conclusion that the effect of load increment duration on the void ratio pressure relationship was insignificant. In the present series of tests the load increments were applied for the normal duration (24 hours) only, and therefore the e - log P' curves are not likely to be affected by this effect at all.

Now looking back to the e - log P' curves, it seems that the difference between the two curves from the A and B tests may be mainly due to the extrusion of material, as suggested by Matlock and

Dawson (1951) but not due to variation in $\frac{\Delta P}{Po'}$ as shown from the triaxial tests (Chapter no. 3). This is contrary to what Newland and Allely (1956, 1960), obtained from their consolidation tests on very high sensitivity clay. They further suggested that the e - log P' shape is affected by the magnitude of the first load increment. It will be seen from the e - log P' relationship that there is no change in the shape of curves due to the different initial increments, i.e., there is no influence of the magnitude of the first increments on the shape of e - log P' curves in this case.

In general the e - log P' curves of the sand-clay mixtures curves containing high clay content are steeper than those containing more proportion of sand. This is expected for the clay, being more compressible than the sand.

(d) Compressibility Characteristics

The coefficient of volume compressibility m_v, is defined as

$$m_v = \frac{\Delta H}{H} \times \frac{1}{\Delta P'}$$

where H is the initial height before starting the test, ΔH is the change in height due to the load increment $\Delta P'$ from effective stress Po' to (Po' + $\Delta P'$).

The relationship between the coefficient of compressibility and the log of average effective stress of all the samples is shown in Figures 2.101 to 2.108. Each graph represents both Group A and B tests. The m_v calculations are based on the primary consolidation only.

As expected, m_v decreases with increasing effective stress. In general, m_v in the initial stages is large and decreases in the following stages of consolidation. This can be seen from the figures

where the slope of the curve changes continuously from the very steep initial position to a flat section towards the end of the pressure range. The initial steep line starts curving between 1.0 p.s.i. to 4 p.s.i. and then begins to flatten. In the pressure range used it appears that the compressibility of the samples with more than 50% clay is much the same as pure clay (see Table 2.3 for the numerical value of m_v). Whereas the mixtures containing 80% and more sand exhibit considerably lower compressibility, indicating the domination of sand particles when material has switched over from plastic to non-plastic nature. A similar reduction in the compressibility of sand-mica mixtures with decreasing mica constituents was demonstrated by Gilboy (1928). The flat shape mica grains in his case may be linked to the kaolin particles in this case, though the former are many times bigger in size than the latter. Thus the comparatively low compressibility of the sand-clay mixtures containing higher proportion of sand is reasonable and associated with the basic non-plastic properties of that material.

Further discussion and the comparison between these compressibilities and those obtained from the triaxial tests are deferred to Chapter 3. However, it was pointed out by Som (1968) that the side friction during the consolidation in a conventional oedometer can greatly affect m_v at low stresses. He carried out hydraulic oedometer tests also and observed that the m_v curves from these tests lay between the curves of the first and second loadings of a conventional oedometer. Since in the hydraulic oedometer changes in the height and pore water pressure were measured over a small central area of the sample, the effects of side friction were largely eliminated. Therefore the m_v values obtained from the hydraulic oedometer should be free from this effect and be more reliable than those of conventional oedometer tests. As such, there could be some

doubt about m_v reported here but only those of the first stages of consolidation where small increments were applied which could have been affected by side friction. Later on, after the second stage of consolidation, larger increments were applied, due to which the side friction must have been reduced (see Leonards and Girault, 1961). Thus it is fair to say that the m_v values of the rest of the consolidation stages should be relatively free from this effect and may be considered as reasonable.

(e) Coefficient of Permeability

The coefficient of permeability k was measured at the end of each consolidation stage in the manner described earlier. The permeability was calculated after the steady state flow condition had been reached. The following familiar equation has been applied to evaluate the permeability:

$$k = \frac{Q}{iA} = \frac{Q}{A} \times \frac{H}{h},$$

where Q = rate of flow

A = Cross-sectional area of the sample

i = $\frac{h}{H}$ hydraulic gradient

h = hydraulic head

H = the drainage path (sample thickness).

For achieving correct steady state flow, the plots similar to those shown in Figure 2.92 were drawn. These graphs represent the volume change Δv between two times t_1 and t_2 divided by $(t_2 - t_1)$ to get flow rate Q, which was plotted against $\sqrt{\frac{2}{t_1+t_2}}$ on arithmetic scale. When steady state flow of water was deemed to have been reached, the graph of Q vs $\sqrt{2}t^{-\frac{1}{2}}$ curved and became parallel to the $\sqrt{2}t^{-\frac{1}{2}}$ axis.* The Q is taken from here to

---

* where $t_1 + t_2 = t$

evaluate k. This method eliminates the possibilities of picking Q before the steady state flow had been reached. Gibson (1963, 1970) has given an analytical solution for in situ constant head permeability test and has shown that the steady state can be more accurately predicted from Q vs $t^{-\frac{1}{2}}$ relationship. A similar sort of solution for one-dimensional constant head permeability test has also been given by Tan (1968).

It has already been said that the diameter of the sample was 4 inches, whereas that of the bottom porous stone in the conventional oedometer was 3 inches. Due to this $\frac{1}{2}$ inch wide impermeable annular boundary was created at the bottom. Thus the flow of water near the sides was a radial flow. The equation of rate of flow $Q = k.A.i$ is strictly applicable to the one-dimensional flow, therefore the coefficient of permeability was in error by a certain percentage. So in order to take into account the error in k due to the radial flow, a relaxation solution was used as explained in Appendix A. It was found that the coefficient of permeability k obtained using the simple I-D formula was 12.5% less than the actual one which included the effects of both vertical and horizontal flow near the impermeable annular boundary.

The coefficient of permeability k_s has also been calculated from the equation $k_s = c_{vs} \times m_v \times \gamma_w$, where c_{vs} is the coefficient of consolidation measured from the settlement curve, m_v and γ_w are the coefficient of compressibility and unit weight of water respectively. The relationship of k with effective stress and that of k_s with average effective stress is given in Figures 2.109 to 2.116. In general both k and k_s decrease with increasing effective stress, the former being somewhat larger than the latter. The relationship between k and k_s with the log of effective stress is linear in almost all cases. With the exception of 80% and 90%

sand sample, the correspondence between the respective values of k and k_s obtained from Group A and B tests is reasonably good within the experimental errors. However, in the case of 80% and 90% sand samples (see Figures 2.115 and 2.116) there is comparatively a wide scatter of points, particularly those of the actually measured ones. This can be mainly due to the experimental difficulties such as head lost due to the water flowing through the apparatus itself during the permeability test. On the other hand, k_s could have been affected by slight error in c_{vs} values obtained from log time fitting method.

As regards the validity of Darcy's law, there is some controversy on the factors which can cause deviation in the law. For instance the permeability tests on saturated kaolinite and compacted silty clay by Mitchell and Younger (1966) indicate deviation from Darcy's law at very low hydraulic gradients. They have further pointed out that the migration of fine particles, that is actual change in soil fabric during the flow, can occur and lead to non-Darcy effects. Hansbo (1960) also suggested that Darcy's law may not be valid for low porosities and low hydraulic gradients. On the other hand Olsen (1965) and Matyas (1966) cast doubt on the existence of any deviation from Darcy's law, even at small gradients provided the specimen is fully saturated. Olsen (1965) however, suggested that non-Darcy flow can occur due to particle migration caused by seepage forces. In spite of some disagreement, all of them agree about the non-existence of a threshold gradient for flow.

Since in the present study fully saturated specimens were tested, and the hydraulic gradient was sufficiently high, Darcy's law was assumed to apply. Anyhow, the concept of movement of fine particles due to the seepage forces is not ruled out and may be one of the factors causing some discrepancies in the overall magnitude of coefficient of permeability k, particularly in the case of samples with more sand content.

(f) Coefficient of Consolidation

The computations of coefficient of consolidation c_{vs} have been made in accordance with Terzaghi's theory ($c_{vs} = \frac{TH^2}{t}$), from the settlement time curves at t_{50}. using Casagrande's log time fitting method. The variations of c_{vs} with log of average effective stress for the corresponding consolidation stages of all the tests are given in Figures 2.117 to 2.124.

In general the c_{vs} increases with the effective stress. Looking at Figure 2.117 representing c_{vs} - log P' relationship of 100% clay, it can be observed that for constant $\frac{\Delta P}{Po'}$, the c_{vs} is increasing with effective stress. Similarly for varying $\frac{\Delta P}{Po'}$, c_{vs} also increases as long as the $\frac{\Delta P}{Po'}$ is increasing. However, as soon as the $\frac{\Delta P}{Po'}$ is reduced, the trend of c_{vs} is suddenly changed, showing a slight decrease in its value. The increase in the coefficient of consolidation has also been observed by Lewis (1950), Leonards and Ramiah (1959) and Hamilton and Crawford (1959). An almost similar picture is envisaged from c_{vs} - log P' graphs of sand-clay mixtures as shown in Figures 2.118 to 2.124, although in general there is a decrease in the slope of these curves when the $\frac{\Delta P}{Po'}$ ratio is reduced. It must be pointed out here that the c_{vs} of the fifth stage of (Group B test) 80% sand sample and that of the fourth and fifth stage (Group B) and the fourth stage of (Group A) 90% sand samples was checked by using Taylor's $\sqrt{t}$ fitting method. It was found that the c_{vs} values at these stages are actually higher than those obtained from the log time fitting method as shown in Figures 2.123 and 2.124. As a matter of fact it was the instantaneous and small settlement of 80% and 90% samples which made it difficult to determine correct t_{50} values from almost flat log time-settlement curves. Now, looking at the Table 2.3 it can be noticed that the order of magnitude of c_{vs} of 80% and 90% sand samples is considerably higher than the rest

of sand-clay mixtures. Whereas the order of magnitude of c_{vs} of kaolin and the sand-clay mixtures containing 30% and more clay seems almost within the same range for the corresponding consolidation stages.

The coefficient of consolidation c_{v*} has also been calculated from the well-known formula $c_{v*} = \frac{k}{m_v \times \gamma_w}$ where k and m_v are the actually measured coefficients of permeability and the compressibility respectively, and γ_w is the unit weight of water. Since m_v is for average stress Po' to (Po' +ΔP), therefore the values of k for the corresponding average effective stress obtained from the k-log P' graphs have been used. By examining the c_{v*} values (Table 2.3) it can be noticed that almost identical picture to that of c_{vs} is envisaged. That is c_{v*} is increasing with the effective stress, confirming the trend of coefficient of consolidation obtained from the time-settlement curves. The comparison of c_{v*} with corresponding values of c_{vs} shows that the former is considerably higher than the latter in most cases. There is no apparent reason for the higher c_{v*} values.

Since coefficient of consolidation is related to both k and m_v, it would be reasonable to look at the variations in both c_{vs} and c_{v*} in relation to these parameters. As already shown in the preceding sections, k and m_v decrease with effective stress, however their ratio ($c_v = \frac{k}{m_v \cdot \gamma_w}$) consistently gives an increasing coefficient of consolidation. Apparently it is m_v which is decreasing more than k at the corresponding stages of consolidation, causing a regular increase in both c_{vs} and c_{v*} values. It is known that Terzaghi's theory is based on the assumptions that during consolidation, the coefficients of consolidation, compressibility and permeability remain constant. However, none of these assumptions is valid for the soil under consideration. Recently some non-linear theories have been

proposed which consider variations in the consolidation parameters (Schiffman, 1958; Davis and Raymond, 1965; Barden and Berry, 1965; Gibson, et al., 1967; and Poskitt, 1969). Schiffman (1958) considered the variation of permeability, but the compressibility has been assumed to remain constant. Davis and Raymond (1965) have found that if compressibility does not remain constant during consolidation, but varies according to linear e-log P' relationship, the dissipation of maximum pore pressure is a function of the load increment ratio. Similarly, if m_v and k decrease in such a way that c_v remains constant, the rate of settlement is independent of load increment ratio and is identical to that given by Terzaghi's theory. It has already been seen that e-log P' relationship is linear and that rate of pore pressure dissipation is a function of $\frac{\Delta P}{Po'}$. However, the coefficient of consolidation is increasing with the effective stress and is not constant as assumed by Davis and Raymond. In spite of this, it is interesting to note that Davis and Raymond's theory is at least approximately satisfied, that is the rate of settlement is correctly predicted by Terzaghi's theory for U= 60% - 70%, as shown in Figures 2.39(a) to 2.47. A more general case of the above problem has been solved by Barden and Berry (1965) taking into consideration variation of k. Gibson, England and Hussey (1967) and Poskitt (1969) have also given large strain non-linear consolidation theories. However the assumptions inherent in all the theories, that the coefficient of consolidation remains constant with the effective stress, may be satisfactory in some cases but certainly not in the case of sand-clay mixtures. That is m_v and k of the sand-clay mixtures is varying in such a way that c_v does not remain constant, as assumed by the above theories, but increases with the effective stress. A further discussion is deferred to the next chapter, where the consolidation parameters obtained under isotropic consolidation are also considered.

NUMBER OF MIXTURE	PERCENTAGE OF		SPECIFIC GRAVITY GS	LIQUID LIMIT W_L	PLASTIC LIMIT W_P	PLASTICITY INDEX I_P
	CLAY	SAND				
1	100	0	2.577	64.0	36.0	28.0
2	90	10	2.586	58.0	32.0	26.0
3	80	20	2.595	53.0	29.0	24.0
4	70	30	2.604	46.0	26.0	20.0
5	50	50	2.622	35.0	19.0	16.0
6	30	70	2.641	23.0	12.0	11.0
7	20	80	2.650	17.0	8.7	8.3
8	10	90	2.660	—	—	—
9	0	100	2.700	—	—	—

TABLE No. 2.1

ATTERBERG LIMITS AND SPECIFIC GRAVITY OF SAND AND CLAY MIXTURES

TEST GROUP A

Stage No.	Pressure Range p.s.i.	Load Increment ΔP p.s.i.	Initial Effective Stress Po' p.s.i.	Effective Stress Increment Ratio ΔP/Po'
1	0-1.75	1.75	-	-
2	1.75-5.25	3.50	1.75	2
3	5.25-15.75	10.50	5.25	2
4	15.75-47-25	31.50	15.75	2
5	47.25-15.75	-31.50	47.25	-
6	15.75-1.75	-14.00	15.75	-

TEST GROUP B

1	0-0.875	0.875	-	-
2	0.875-2.625	1.75	0.875	2
3	2.625-10.50	7.875	2.625	3
4	10.50 -21.00	10.50	10.50	1
5	21.00 -31.50	10.50	21.00	0.5
6	31.50 -21.00	-10.5	31.50	-
7	21.00 -0.875	-20.125	21.00	-

TABLE 2.2

Consolidation programme of Oedometer tests

100% CLAY (Test Group A)
Initial Water Content = 90.0%

Stage No.	Pressure Range p.s.i.	$m_v = \frac{1}{H} \times \frac{\Delta H}{\Delta P}$ sq. cm/gms $\times 10^{-4}$	$c_{vs} = \frac{T_{50} H^2}{t_{50}}$ sq. cm/sec $\times 10^{-4}$	$c_{v*} = \frac{k(\text{average})}{m_v \times \gamma_w}$ sq. cm/sec $\times 10^{-4}$	$k = \frac{Q}{Axi}$ cm/sec $\times 10^{-8}$	$k_s = m_v \times c_{vs} \times \gamma_w$ cm/sec $\times 10^{-8}$
1	0- 1.75	3.134	4.05	-	-	12.68
2	2.75- 5.25	1.133	4.46	12.35	18.11	8.45
3	5.25-15.75	0.372	8.68	25.26	8.24	3.23
4	15.75-47.25	0.042	13.40	112.76	3.96	0.63
	100% CLAY (Test Group B)					
	Initial Water Content - 89.22%					
1	0- 0.875	8.371	1.94	-	-	16.27
2	0.875- 2.625	2.491	4.81	-	-	11.98
3	2.625-10.50	0.791	9.12	18.96	10.28	7.21
4	10.50- 21.00	0.504	7.68	16.35	6.96	3.86
5	21.00- 31.50	0.038	7.76	160.52	5.24	0.29
	90% CLAY-10% SAND Mixture (Test Group A)					
	Initial Water Content = 87.07%					
1	0. 1.75	3.135	10.88	-	-	34.11
2	1.75- 5.25	1.133	10.19	13.24	14.84	11.55
3	5.25-15.75	0.372	14.51	27.95	7.46	5.40
4	15.75-47.25	0.047	24.50	95.34	4.17	1.15
	90% CLAY-10% SAND Mixture (Test Group B)					
	Initial Water Content = 86.86%					
1	0- 0.875	11.150	3.80	-	-	42.31
2	0.875- 2.625	2.58	6.31	-	-	16.32
3	2.625-10.50	1.014	12.66	8.28	6.74	12.85
4	10.50- 21.00	0.516	13.73	10.66	4.26	7.08
5	21.00- 31.50	0.037	21.15	101.35	3.34	0.79

TABLE 2.3

(continued)

Results of Oedometer Consolidation Tests

80% CLAY-20% SAND Mixture (Test Group A)
Initial Water Content = 68%

Stage No.	Pressure Range p.s.i.	$m_v = \frac{1}{H} \times \frac{\Delta H}{\Delta P}$ sq. cm/gms $\times 10^{-4}$	$c_{vs} = \frac{T_{50} \cdot H^2}{t_{50}}$ sq. cm/sec $\times 10^{-4}$	$c_{v*} = \frac{k(\text{average})}{m_v \times \gamma_w}$ sq. cm/sec $\times 10^{-4}$	$k = \frac{Q}{Axi}$ cm/sec $\times 10^{-8}$	$k_s = m_v \times c_{vs} \times \gamma_w$ cm/sec $\times 10^{-8}$
1	0- 1.75	3.454	3.88	-	-	13.40
2	1.75- 5.25	1.115	6.70	12.91	13.88	7.47
3	5.25-15.75	0.409	10.05	23.84	7.60	4.10
4	15.75-47.25	0.051	13.07	94.11	3.40	0.66

80% CLAY-20% SAND Mixture (Test Group B)
Initial Water Content = 66.25%

1	0- 0.875	4.949	2.29	-	-	13.61
2	0.875- 2.625	1.772	4.54	-	-	8.05
3	2.625-10.50	0.647	10.34	8.90	5.15	6.96
4	10.50 - 21.00	0.423	11.84	10.40	3.79	5.01
5	21.00 - 31.50	0.026	14.65	138.4	3.46	0.37

70% CLAY-30% SAND Mixture (Test Group A)
Initial Water Content = 60.67%

1	0- 1.75	3.692	3.16	-	-	11.67
2	1.75- 5.25	1.152	5.95	9.90	10.56	6.85
3	5.25-15.75	0.375	10.67	20.80	6.32	3.99
4	15.75-47.2	0.035	13.88	128.57	3.35	0.49

70% CLAY-30% SAND Mixture (Test Group B)
Initial Water Content = 59.51%

1	0. 0.875	5.054	2.17	-	-	10.97
2	0.875- 2.625	1.654	4.70	-	-	7.78
3	2.625-10.50	0.586	7.90	14.50	7.37	4.63
4	10.50 - 21.00	0.413	10.81	15.01	5.43	4.46
5	21.00 - 31.50	0.029	16.75	168.96	4.50	0.48

TABLE 2.3

(continued)

50% CLAY-50% SAND Mixture (Test Group A)
Initial Water Content = 38.87%

Stage No	Pressure Range p.s.i.	$m_v = \frac{1}{H} \times \frac{\Delta H}{\Delta P}$ sq. cm/gms x 10^{-4}	$c_{vs} = \frac{T_{50} \cdot H^2}{t_{50}}$ sq. cm/sec x 10^{-4}	$c_{v*} = \frac{k(\text{average})}{m_v \times \gamma_w}$ sq. cm/sec x 10^{-4}	$k = \frac{Q}{Axi}$ cm/sec x 10^{-8}	$k_s = m_v \times c_{vs} \times \gamma_w$ cm/sec x 10^{-8}
1	0- 1.75	2.87	3.38	-	-	7.63
2	1.75- 5.25	0.845	5.38	7.69	6.23	4.55
3	5.25-15.75	0.312	11.30	12.50	2.91	3.52
4	15.75-47.25	0.035	25.00	51.42	1.40	0.88
50% CLAY-50% SAND Mixture (Test Group B) Initial Water Content = 38.97%						
1	0- 0.875	3.244	4.65			15.08
2	0.875- 2.625	1.279	3.53			4.51
3	2.625-10.50	0.302	8.43	30.13	7.85	4.36
4	10.50 - 21.00	0.295	9.55	18.30	3.52	2.82
5	21.00 - 31.50	0.020	11.81	165.0	3.05	0.23
30% CLAY-70% SAND Mixture (Test Group A) Initial Water Content = 32.28%						
1	0- 1.75	1.764	4.24	-	-	7.48
2	1.75- 5.25	0.618	10.35	20.06	11.84	6.40
3	5.25-15.75	0.207	20.97	40.10	6.40	4.35
4	15.75-47.25	0.011	44.15	436.36	3.93	0.47
30% CLAY-70% SAND Mixture (Test Group B) Initial Water Content = 32.04%						
1	0- 0.875	4.844	2.57	-	-	12.44
2	0.875- 2.625	1.279	7.77	-	-	9.95
3	2.625-10.50	0.300	20.00	35.0	9.10	5.99
4	10.50 - 21.00	0.190	24.91	41.05	6.89	4.74
5	21.00 - 31.50	0.015	36.73	42.0	5.90	0.54

TABLE 2.3

(continued)

20% CLAY-80% SAND Mixture (Test Group A)
Initial Water Content = 29.33%

Stage No	Pressure Range p.s.i.	$m_v = \frac{1}{H} \times \frac{\Delta H}{\Delta P}$ sq. cm/gms x 10^{-4}	$c_{vs} = \frac{T_{50} \cdot H^2}{t_{50}}$ sq. sm/sec x 10^{-3}	$c_{v*} = \frac{k(\text{average})}{m_v \times \gamma_w}$ sq. cm/sec. x 10^{-3}	$k = \frac{Q}{Axi}$ cm/sec x 10^{-8}	$k_s = m_v \times c_{vs} \times \gamma_w$ cm/sec x 10^{-8}
1	0- 1.75	1.398	0.70	-	-	9.62
2	1.75- 5.25	0.398	3.18	6.03	22.52	12.62
3	5.25-15.75	0.112	5.03	16.34	16.97	5.65
4	15.75-47.25	0.012	14.15	121.66	13.75	1.67
20% CLAY-80% SAND Mixture (Test Group B) Initial Water Content = 25.97%						
1	0- 0.875	2.504	0.61	-	-	15.38
2	0.875- 2.625	0.600	1.64	-	-	9.82
3	2.625-10.50	0.192	10.77	25.78	46.76	10.67
4	10.50 - 21.00	0.087	13.71	52.07	51.12	11.96
5	21.00 - 31.50	0.010	6.72	423.0	37.47	0.65
10% CLAY-90% SAND Mixture (Test Group A) Initial Water Content = 27.33%			x 10^{-2}	x 10^{-2}	x 10^{-8}	x 10^{-8}
1	0- 1.75	0.483	0.43	-	-	20.97
2	1.75- 5.25	0.140	2.21	12.62	173	30.93
3	5.25-15.75	0.057	3.46	28.50	156	19.68
4	15.75-47.25	0.010	2.49	145.00	142	2.57
10% CLAY-90% SAND Mixture (Test Group B) Initial Water Content = 27.23%						
1	0- 0.875	1.115	0.37	-	-	40.87
2	0.875- 2.625	0.272	2.30	-	-	62.14
3	2.625-10.50	0.082	4.44	48.78	337	36.25
4	10.50 - 21.00	0.065	4.35	46.92	302	28.20
5	21.00 - 31.50	0.008	4.31	346.87	262	3.40

TABLE 2.3

50% CLAY-50% SAND Mixture

Group A

Stage No	P p. s. i.	Effective Stress after consolidation p. s. i.	Compressibility of the soil m_v sq. in/lbs x 10^{-3}	Height of the sample H. inches	$C = AHm_v/G$	Pore Pressure at the Base u/u_o (Theoretical) (Christie, 1965)	$u/\Delta P$ (Actually Measured)
1	1.75	1.75	15.37	1.50	4493	0.98	0.64
2	3.50	5.25	5.97	1.42	1643	0.98	0.83
3	10.50	15.75	2.20	1.35	578	0.98	0.82
4	31.50	47.25	0.25	1.26	60	0.98	0.62

Group B

1	0.875	0.875	22.81	1.50	6667	0.98	-
2	1.75	2.625	8.99	1.46	2557	0.98	0.80
3	7.875	10.05	3.53	1.38	949	0.98	0.92
4	10.50	21.00	2.07	1.31	529	0.98	0.88
5	10.50	31.50	0.14	1.27	34	0.85	0.56

TABLE 2.4

Theoretical and measured pore pressure at the base of the sample

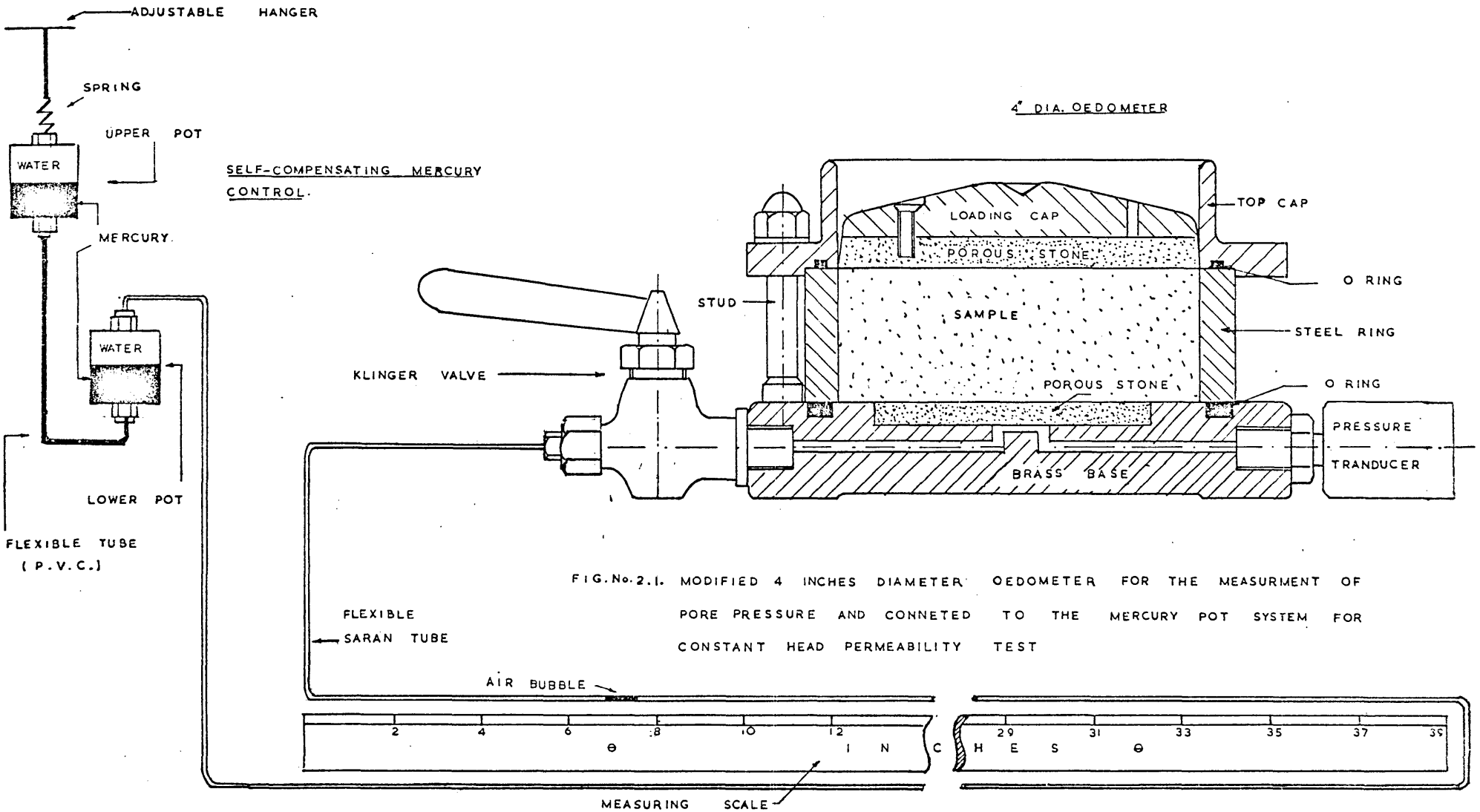

FIG. No. 2.1. MODIFIED 4 INCHES DIAMETER OEDOMETER FOR THE MEASURMENT OF PORE PRESSURE AND CONNETED TO THE MERCURY POT SYSTEM FOR CONSTANT HEAD PERMEABILITY TEST

PARTICLE SIZE DISTRIBUTION

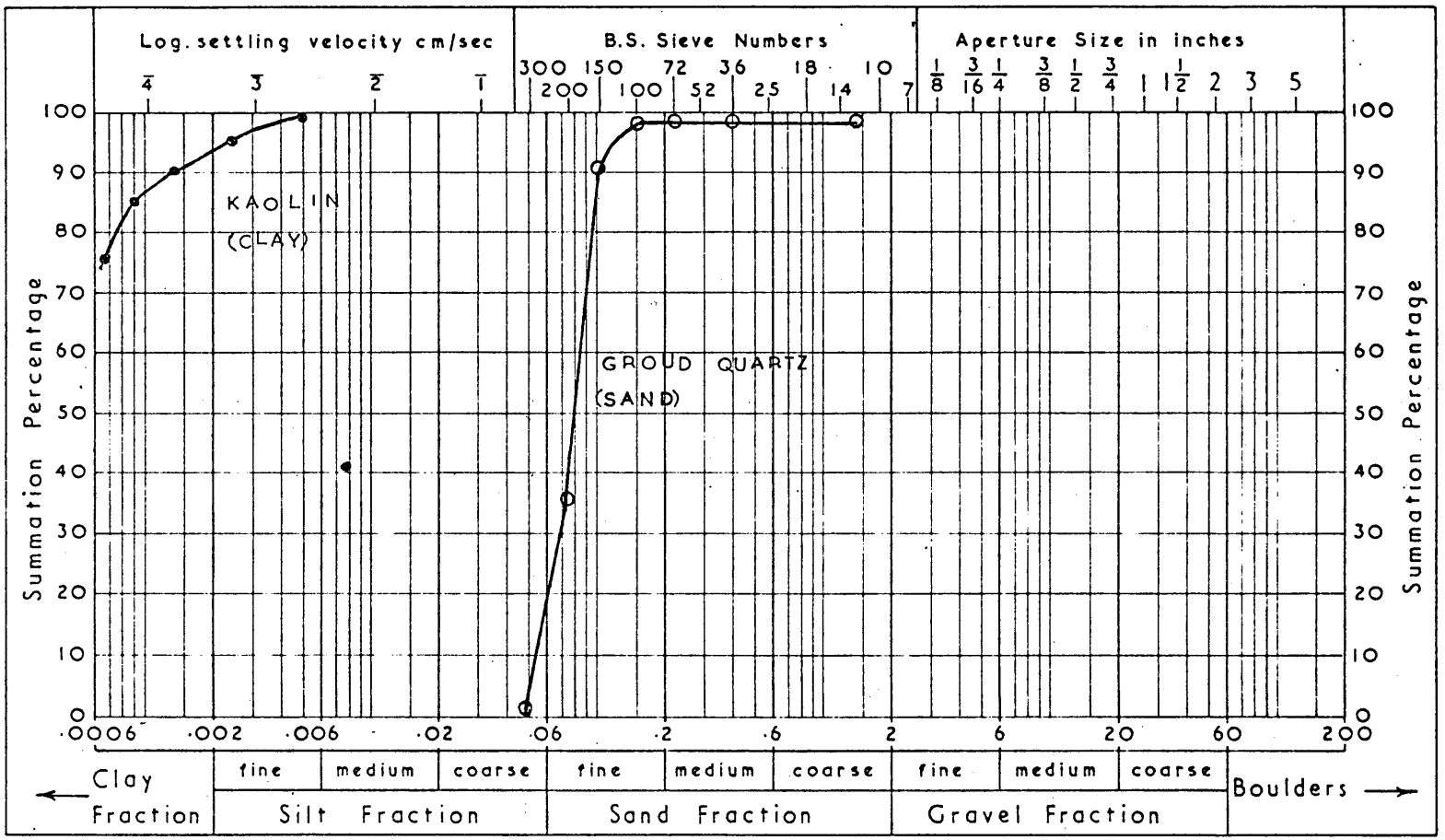

FIG. NO. 2-2

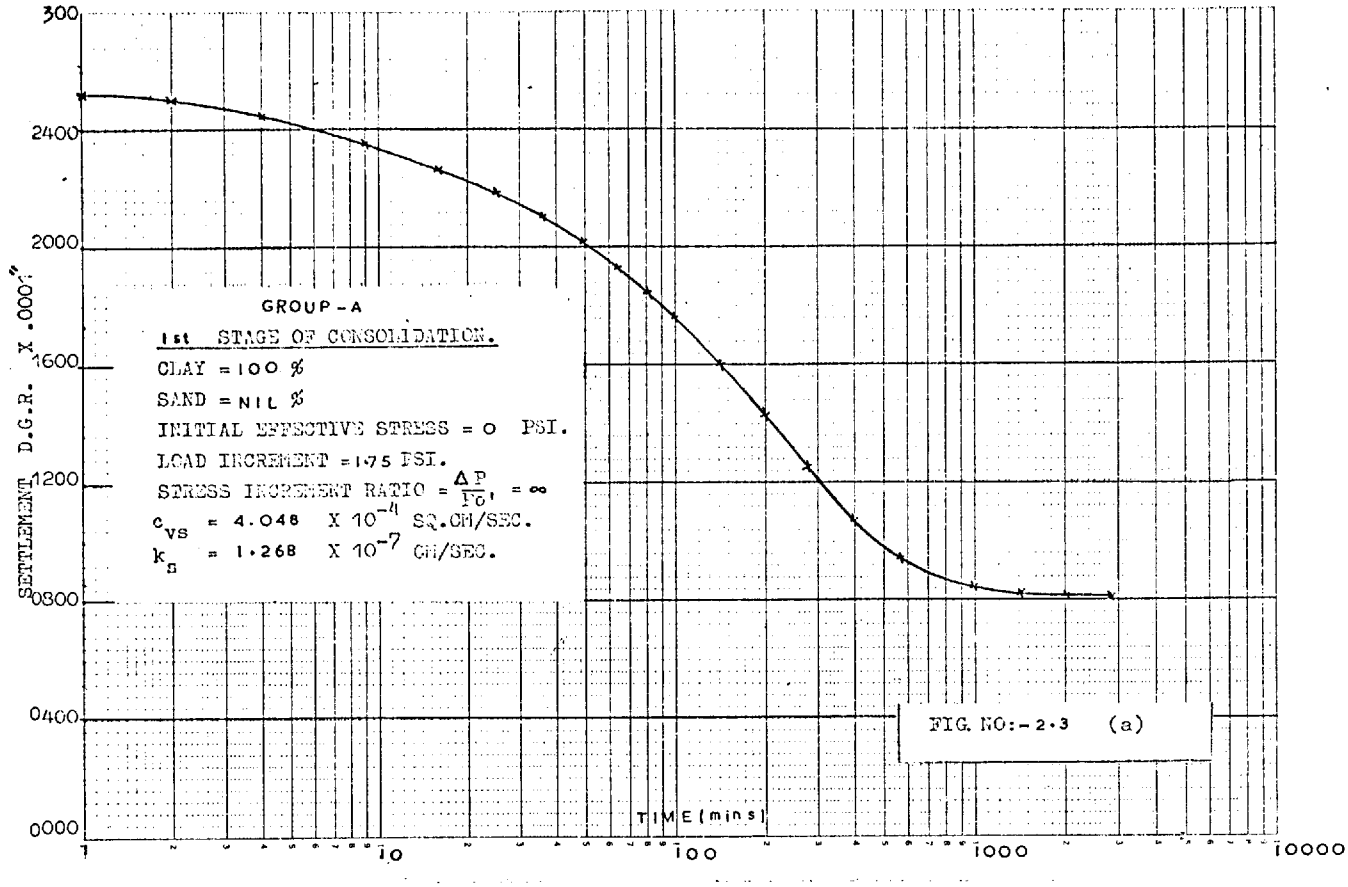

FIG. NO:- 2·3 (a)

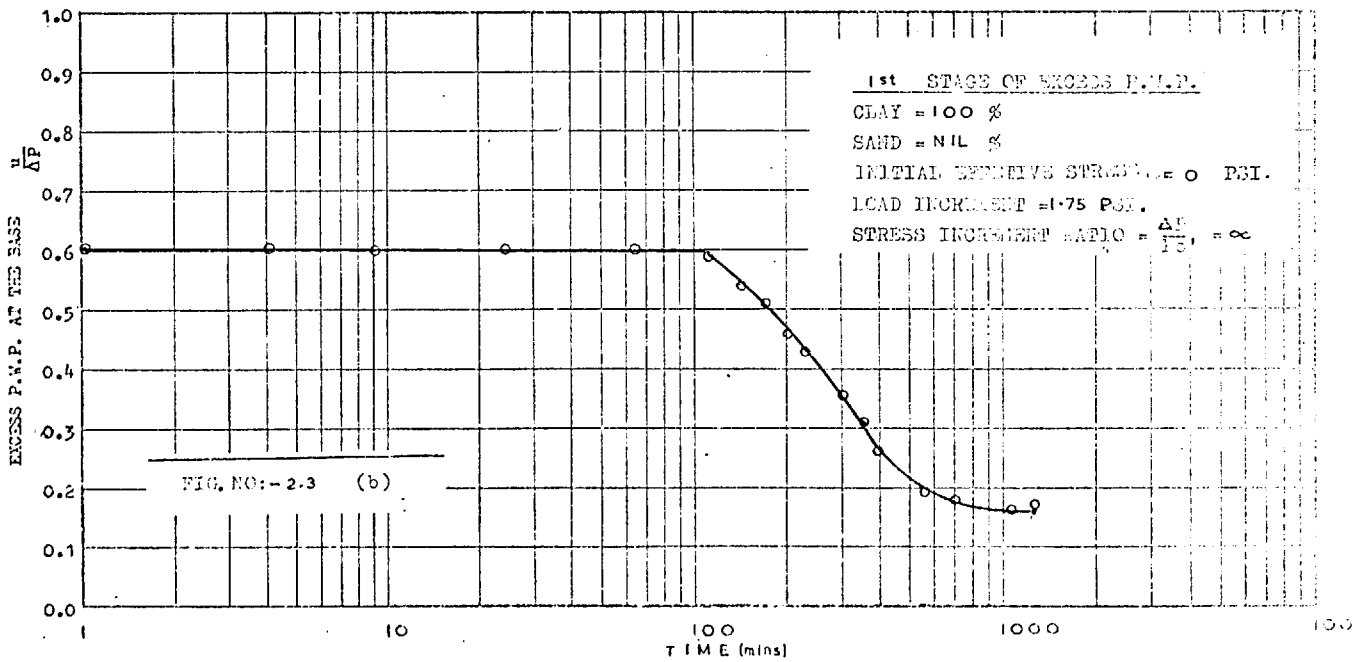

FIG. NO:- 2·3 (b)

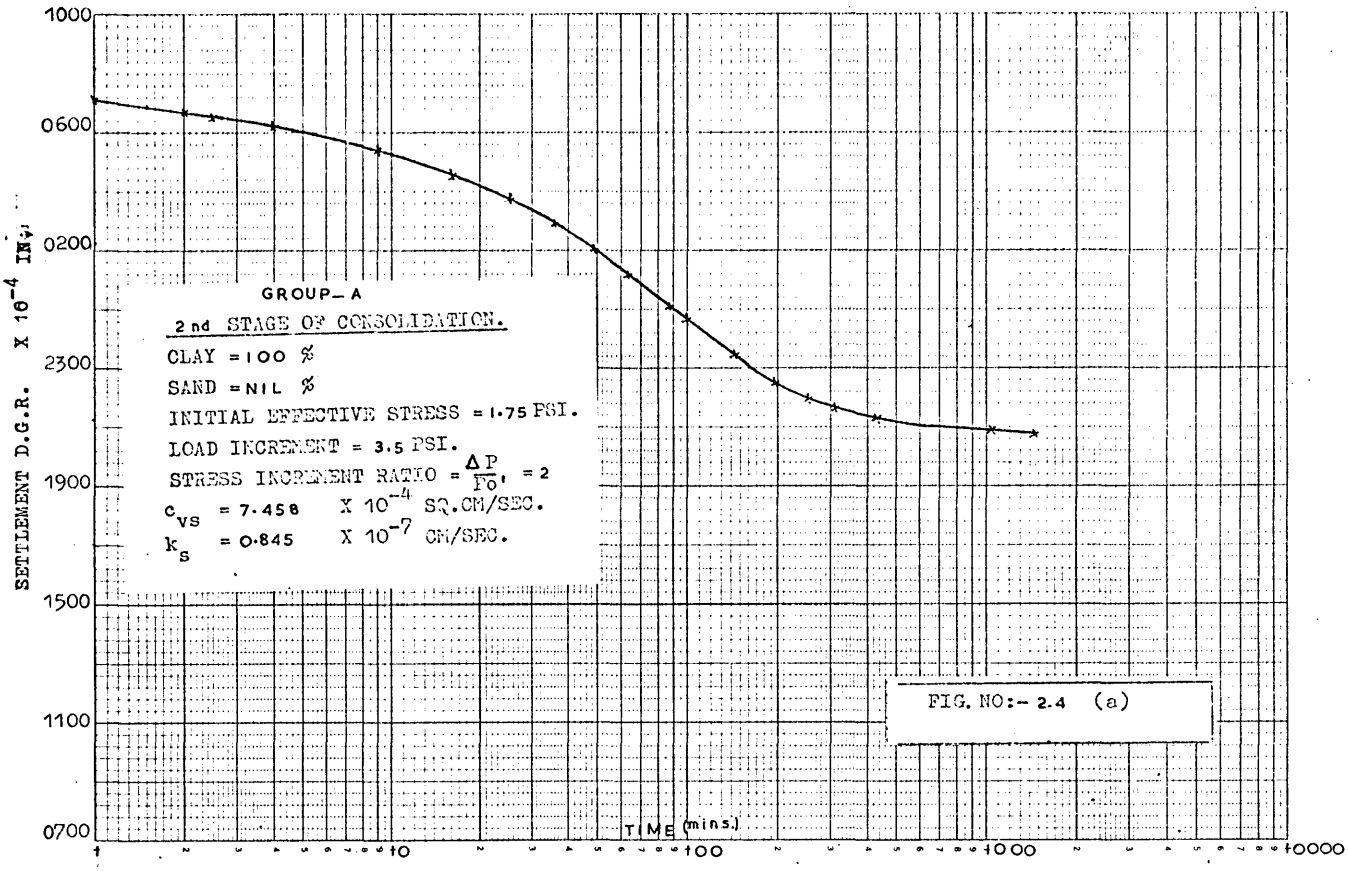

FIG. NO:- 2.4 (a)

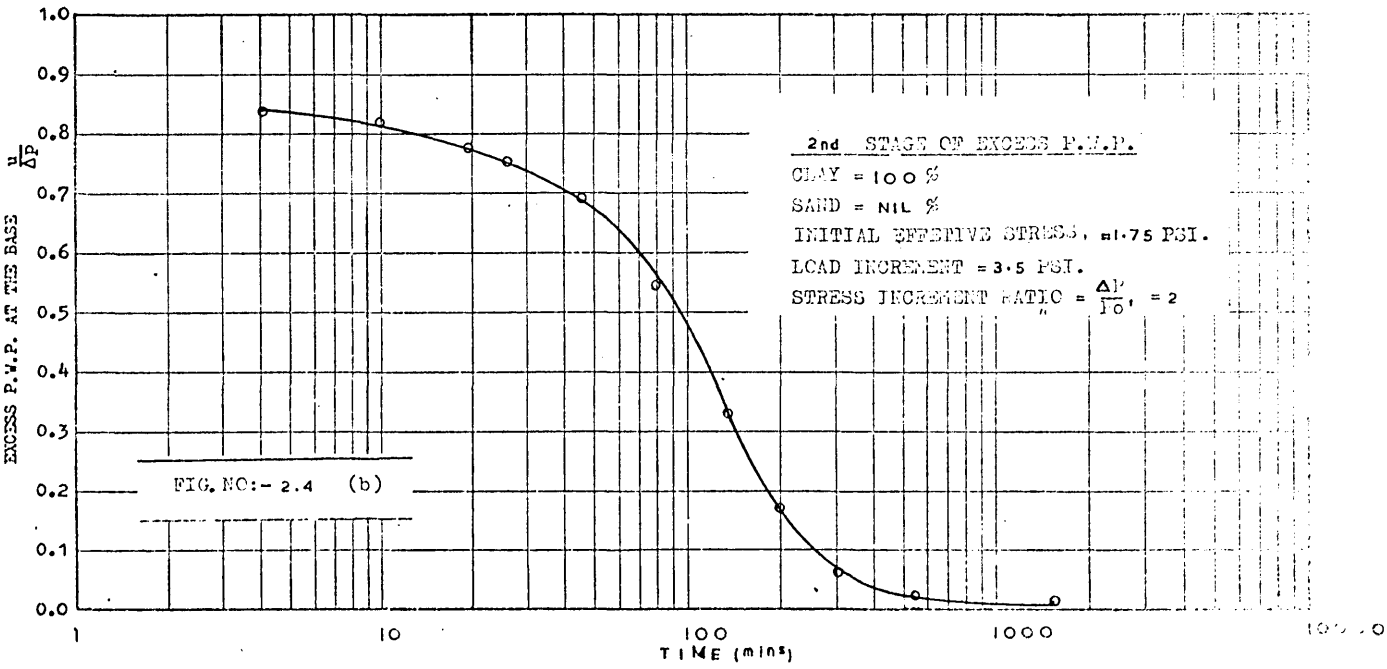

FIG. NO:- 2.4 (b)

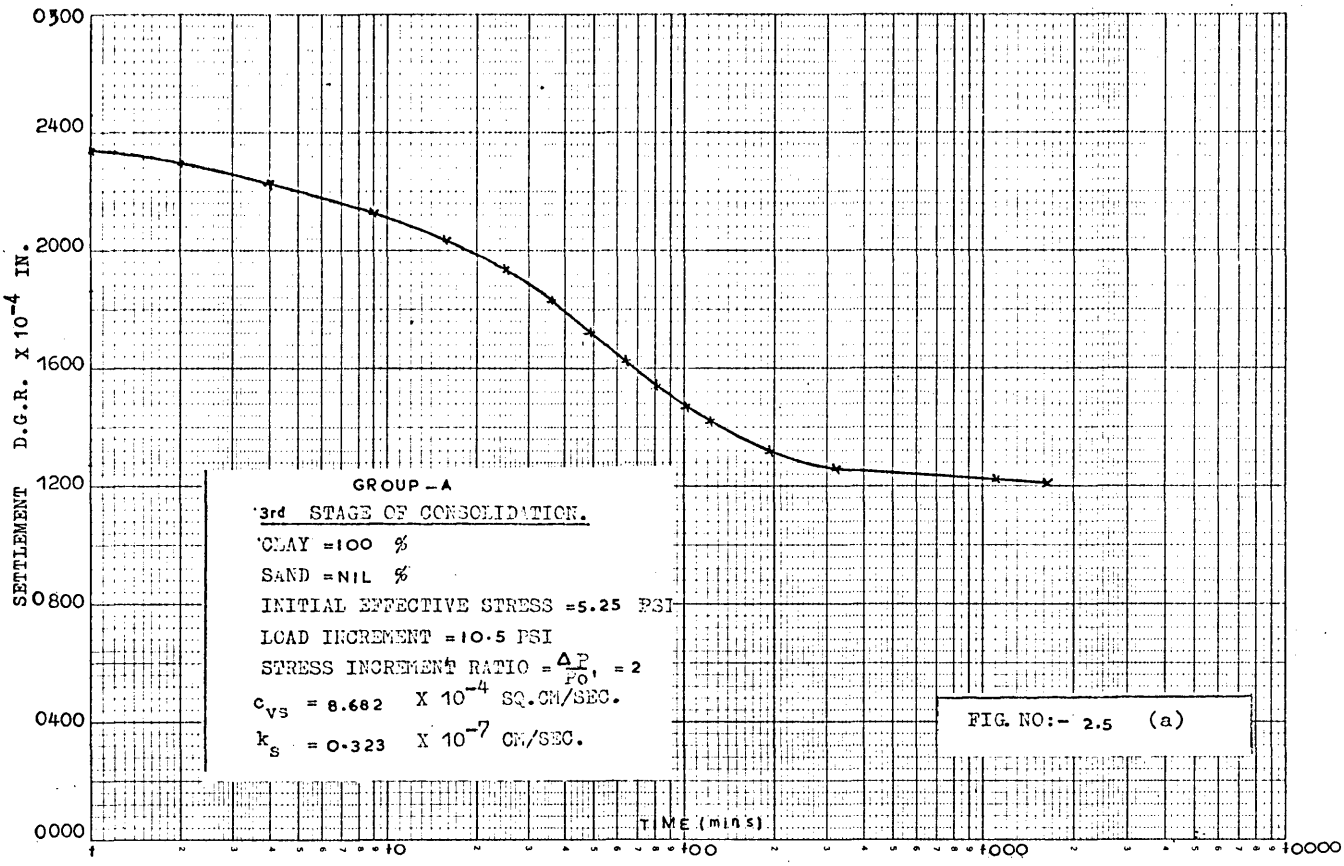
SETTLEMENT D.G.R. X 10^{-4} IN.
0300
2400
2000
1600
1200
0800
0400
0000
TIME (mins)
GROUP – A
3rd STAGE OF CONSOLIDATION.
CLAY =100 %
SAND =NIL %
INITIAL EFFECTIVE STRESS =5.25 PSI
LOAD INCREMENT =10.5 PSI
STRESS INCREMENT RATIO = $\frac{\Delta P}{P_0}$ = 2
c_{vs} = 8.682 X 10^{-4} SQ.CM/SEC.
k_s = 0.323 X 10^{-7} CM/SEC.
FIG. NO:- 2.5 (a)

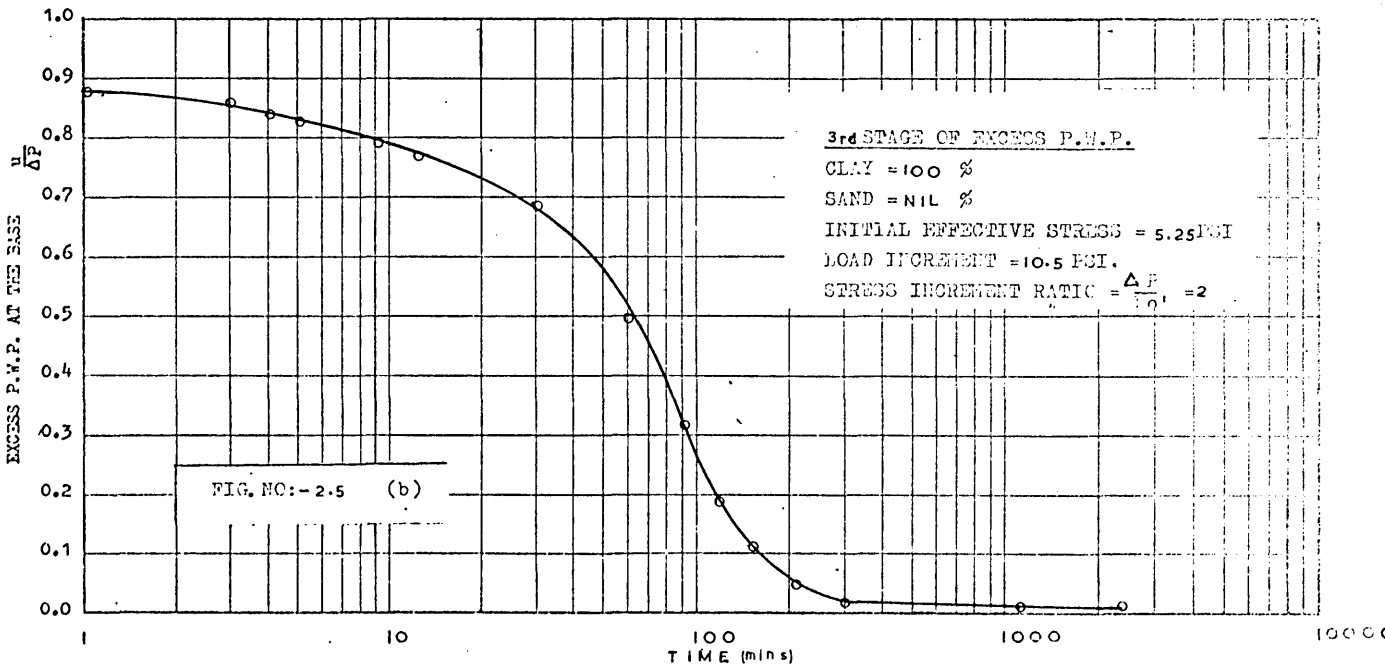
EXCESS P.W.P. AT THE BASE $\frac{u}{\Delta P}$
1.0
0.9
0.8
0.7
0.6
0.5
0.4
0.3
0.2
0.1
0.0
TIME (mins)
3rd STAGE OF EXCESS P.W.P.
CLAY =100 %
SAND =NIL %
INITIAL EFFECTIVE STRESS = 5.25PSI
LOAD INCREMENT =10.5 PSI.
STRESS INCREMENT RATIO = $\frac{\Delta P}{P_0}$ =2
FIG. NO:- 2.5 (b)

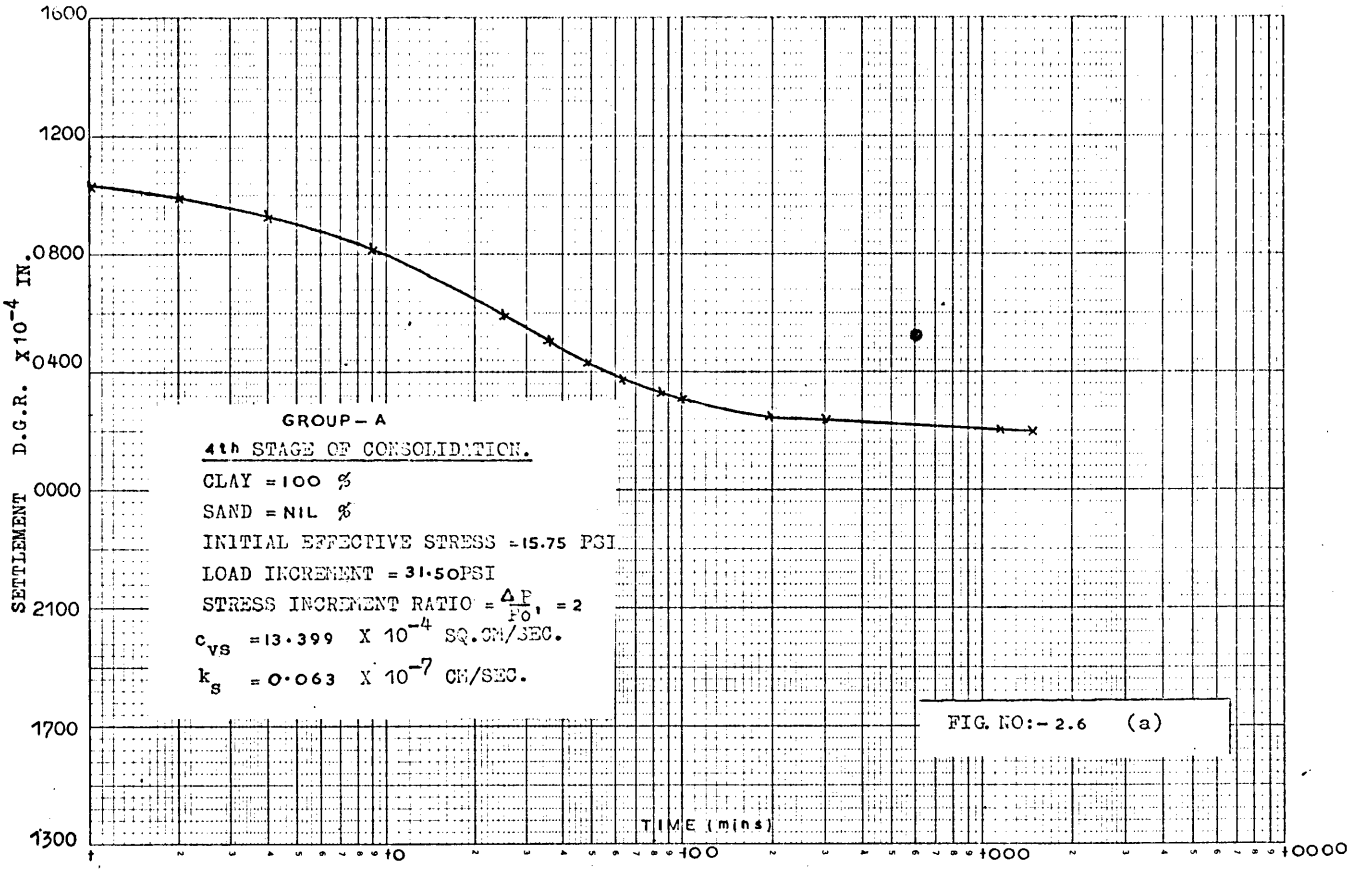
SETTLEMENT D.G.R. $\times 10^{-4}$ IN.
1600
1200
0800
0400
0000
2100
1700
1300
TIME (mins)
1
10
100
1000
10000
GROUP – A
4th STAGE OF CONSOLIDATION.
CLAY = 100 %
SAND = NIL %
INITIAL EFFECTIVE STRESS = 15.75 PSI
LOAD INCREMENT = 31.50PSI
STRESS INCREMENT RATIO = $\frac{\Delta P}{Po}$ = 2
c_{vs} = 13.399 X 10^{-4} SQ.CM/SEC.
k_s = 0.063 X 10^{-7} CM/SEC.
FIG. NO:- 2.6 (a)

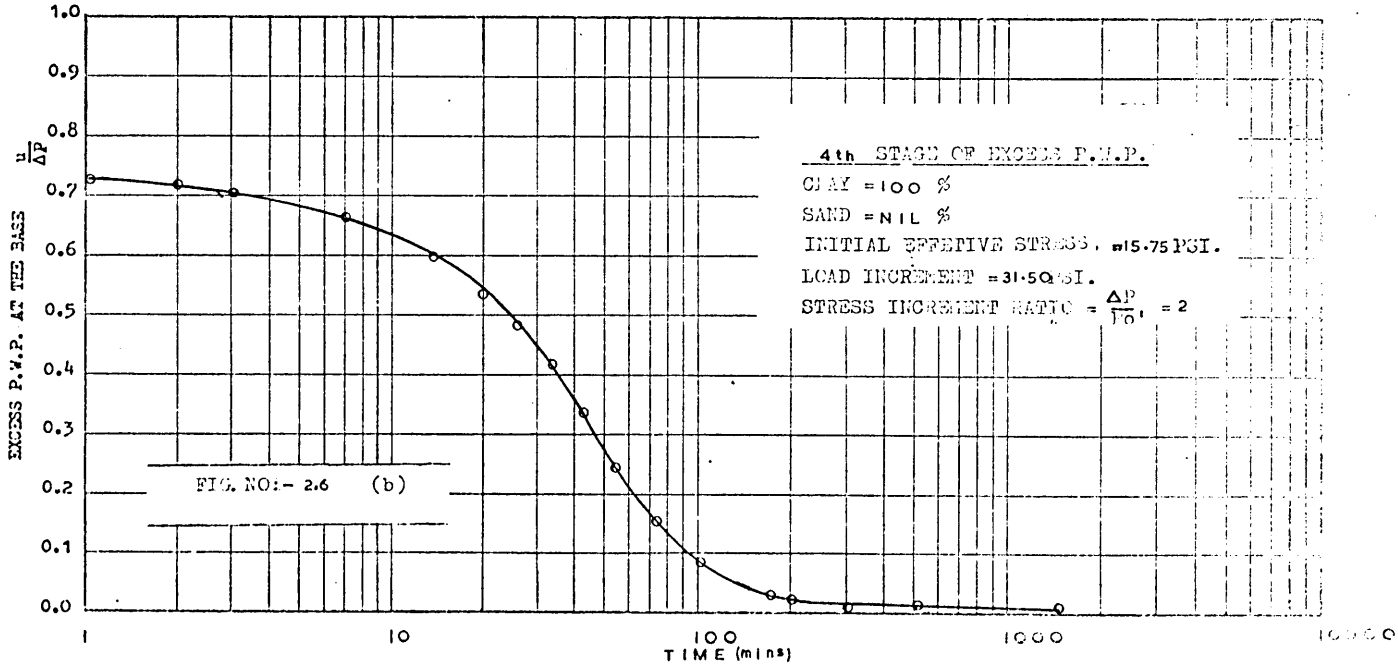
EXCESS P.W.P. AT THE BASE $\frac{u}{\Delta P}$
1.0
0.9
0.8
0.7
0.6
0.5
0.4
0.3
0.2
0.1
0.0
1
10
100
1000
TIME (mins)
4th STAGE OF EXCESS P.W.P.
CLAY = 100 %
SAND = NIL %
INITIAL EFFECTIVE STRESS = 15.75 PSI.
LOAD INCREMENT = 31.50 PSI.
STRESS INCREMENT RATIO = $\frac{\Delta P}{Po}$ = 2
FIG. NO:- 2.6 (b)

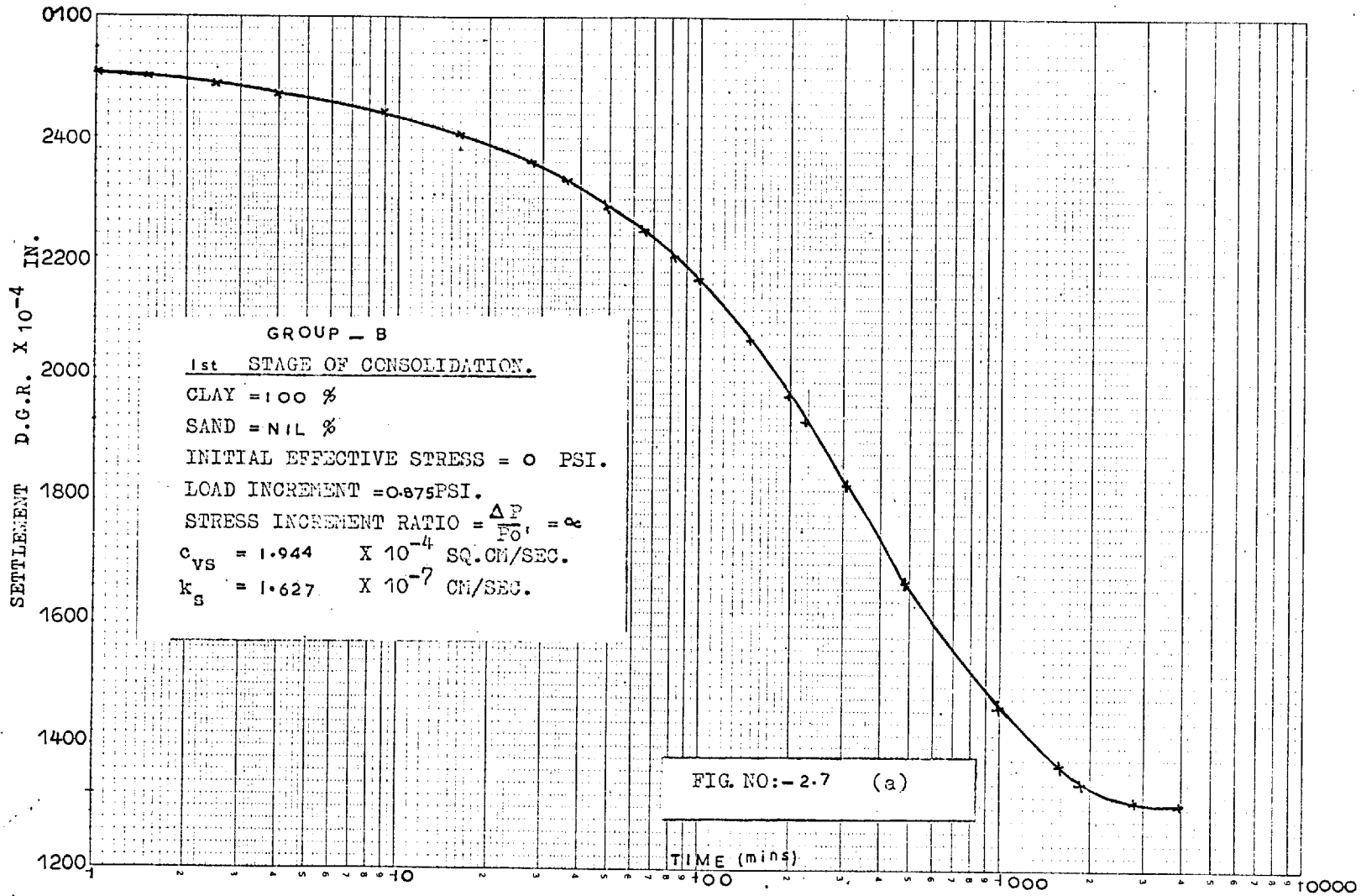
0100
2400
2200
2000
1800
1600
1400
1200
SETTLEMENT D.G.R. X 10^{-4} IN.
GROUP – B
1st STAGE OF CONSOLIDATION.
CLAY = 100 %
SAND = NIL %
INITIAL EFFECTIVE STRESS = 0 PSI.
LOAD INCREMENT = 0.875 PSI.
STRESS INCREMENT RATIO = $\frac{\Delta P}{P_0}$ = ∞
c_{vs} = 1.944 X 10^{-4} SQ.CM/SEC.
k_s = 1.627 X 10^{-7} CM/SEC.
FIG. NO:– 2.7 (a)
TIME (mins)
1
10
100
1000
10000

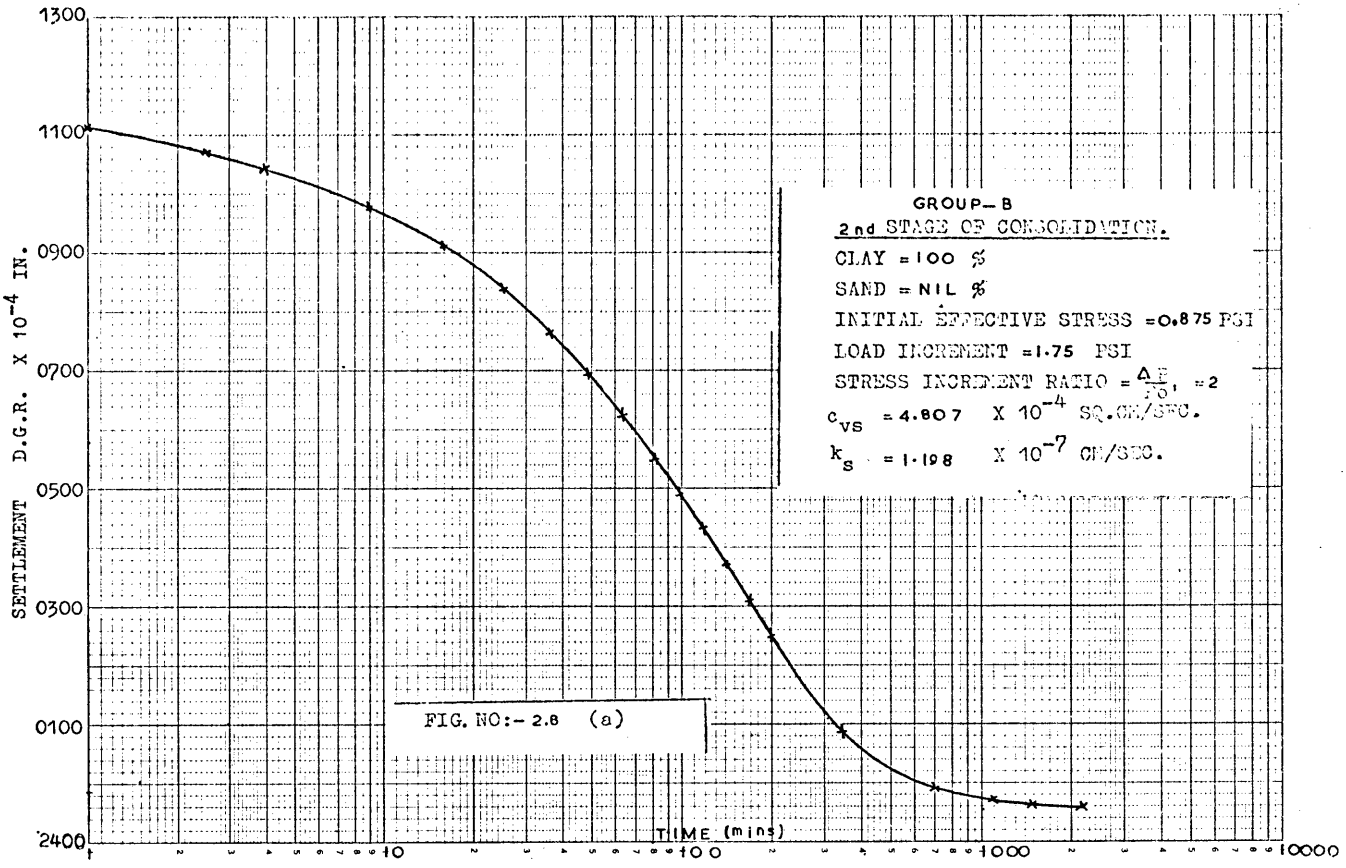

FIG. NO:– 2.8 (a)

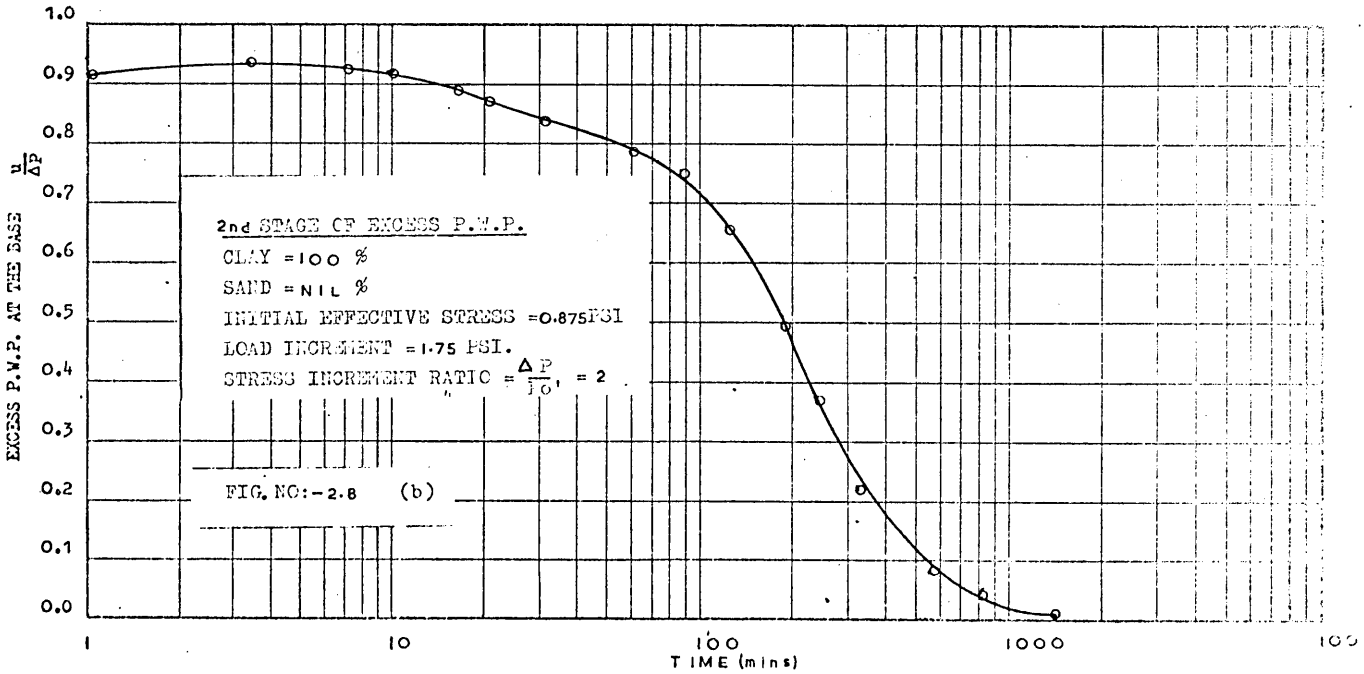

FIG. NO:– 2.8 (b)

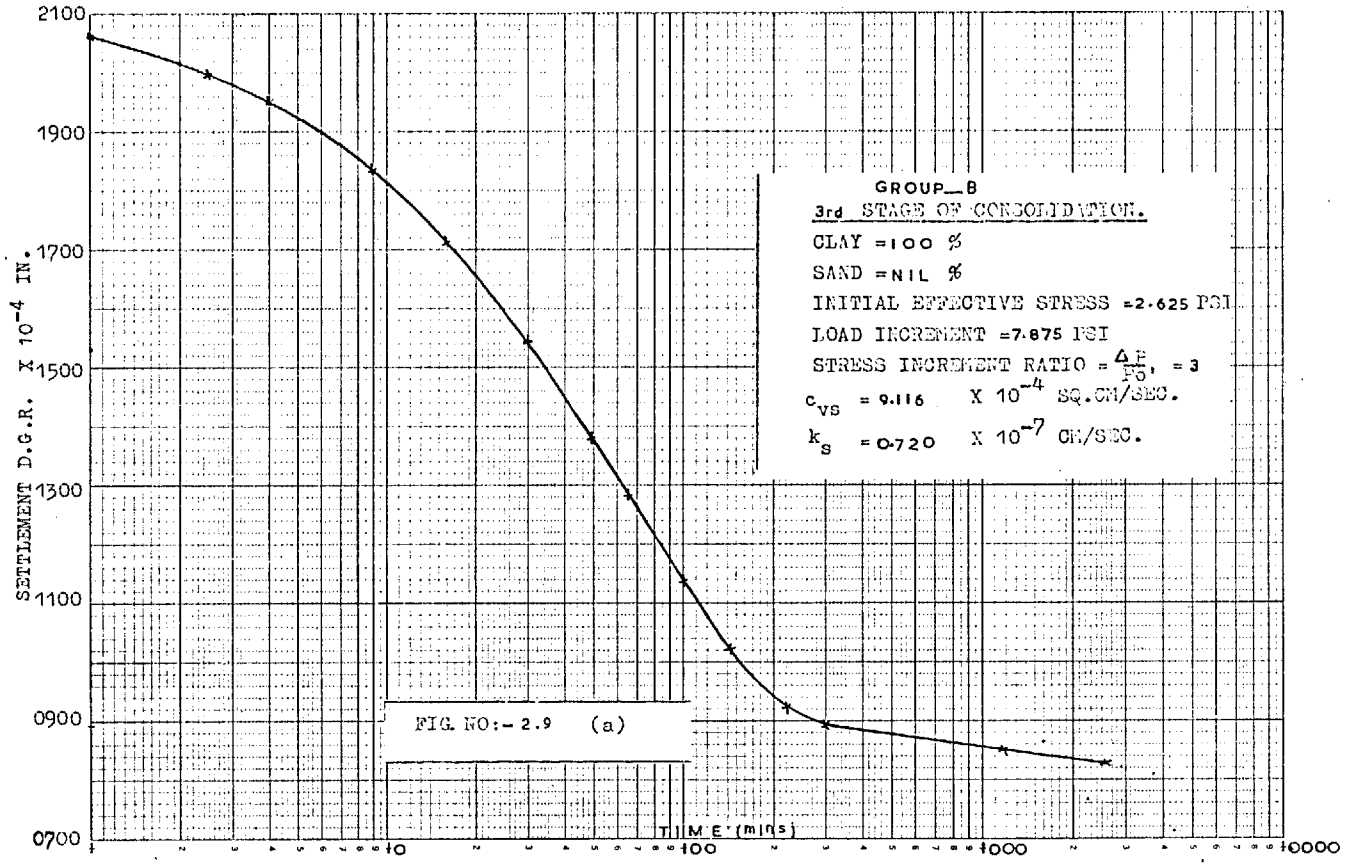

FIG. NO:- 2.9 (a)

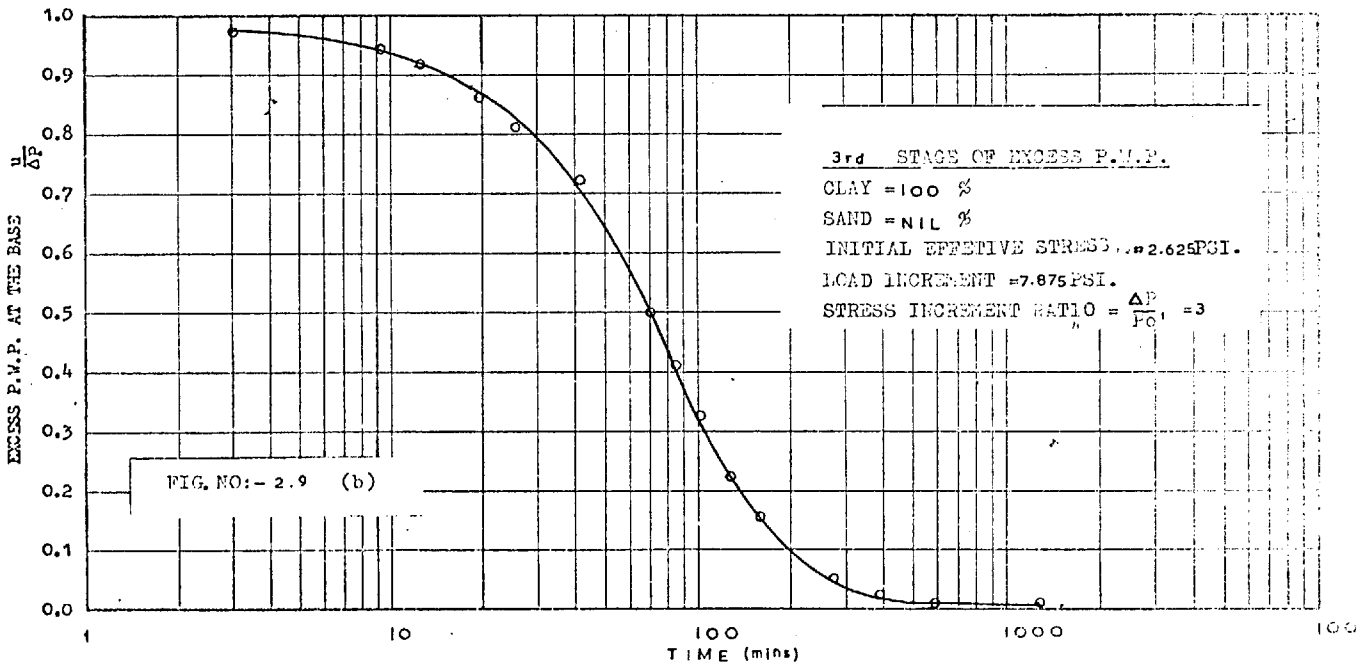

FIG. NO:- 2.9 (b)

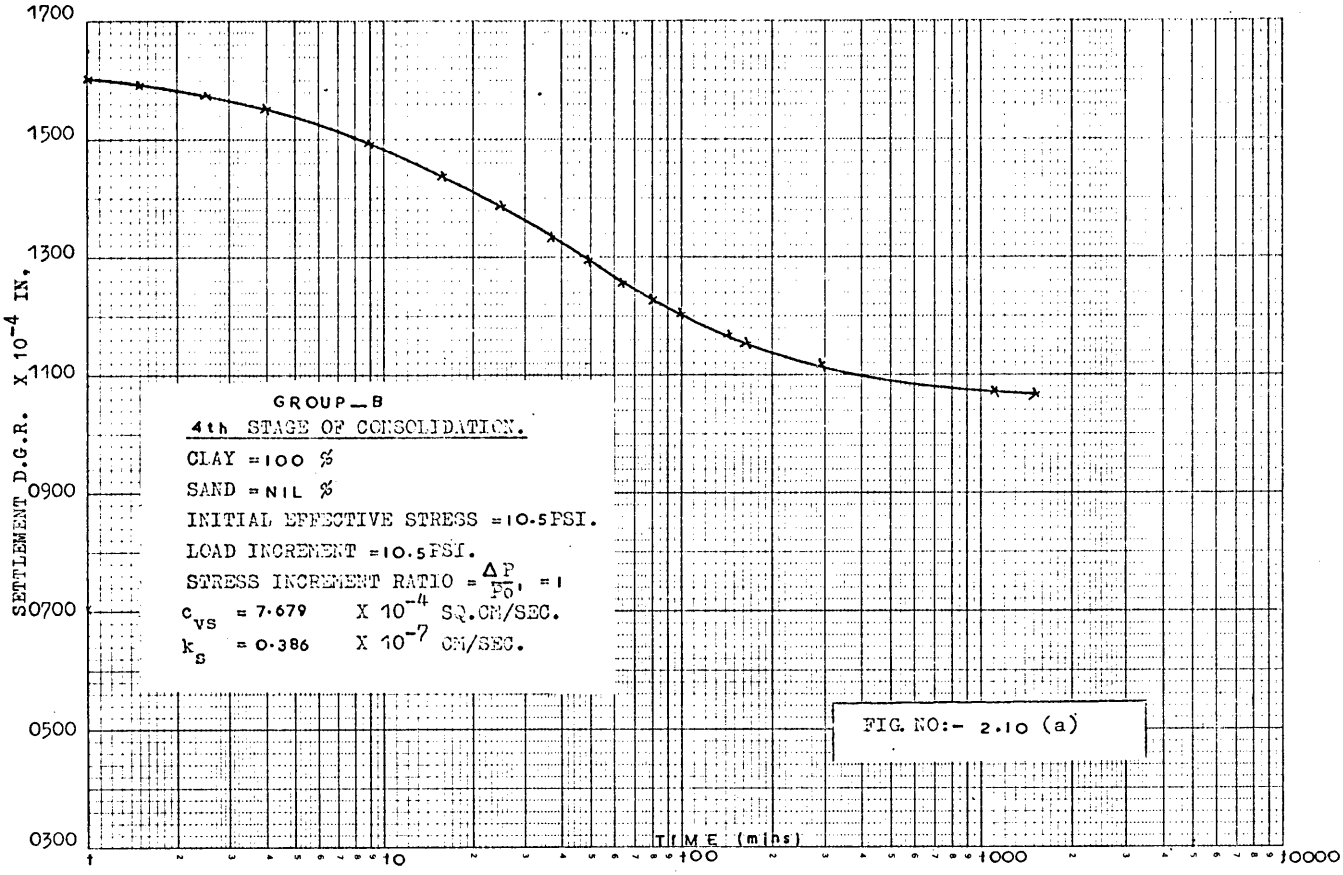

FIG. NO:- 2.10 (a)

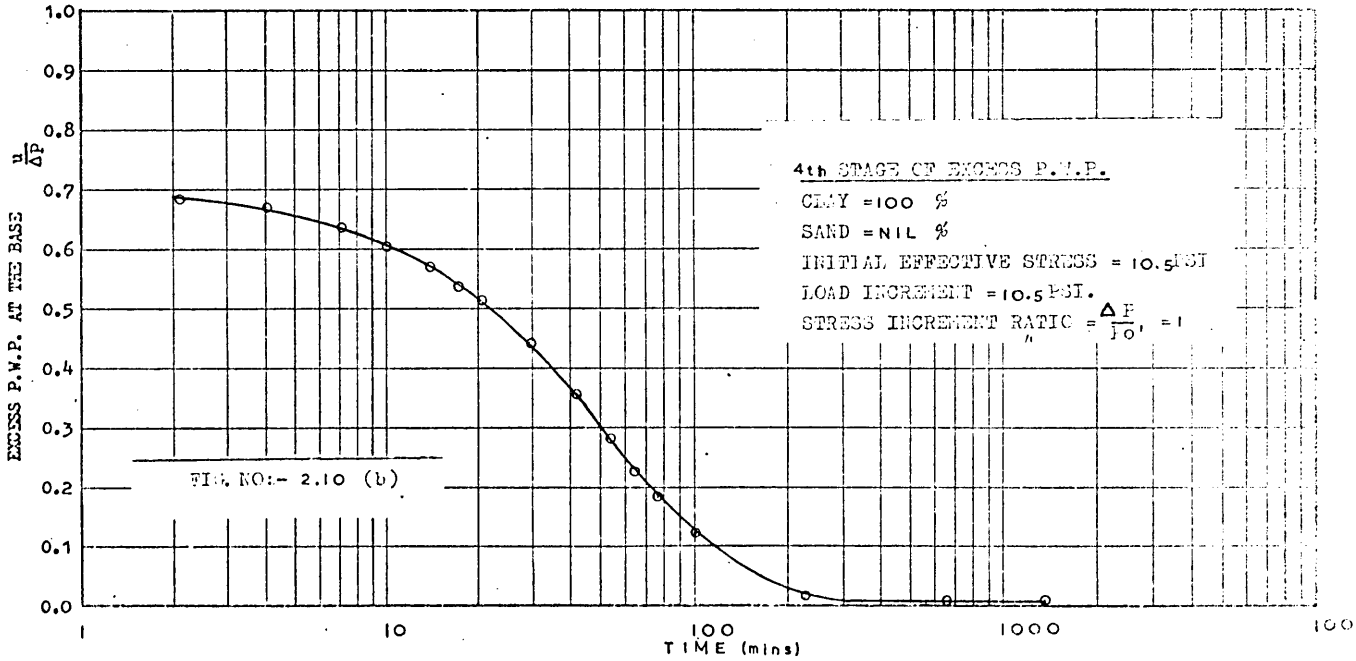

FIG. NO:- 2.10 (b)

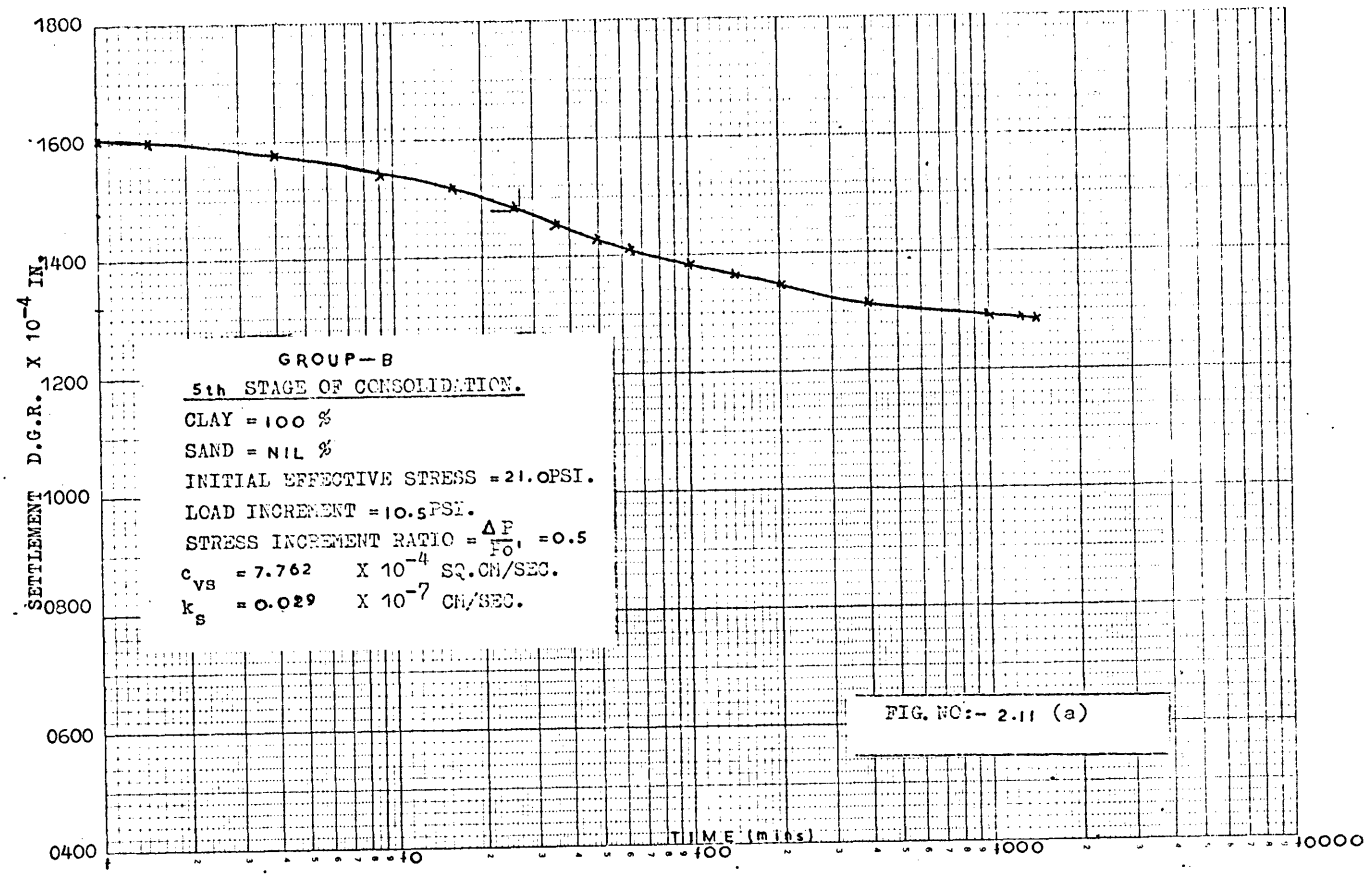

FIG. NO:- 2.11 (a)

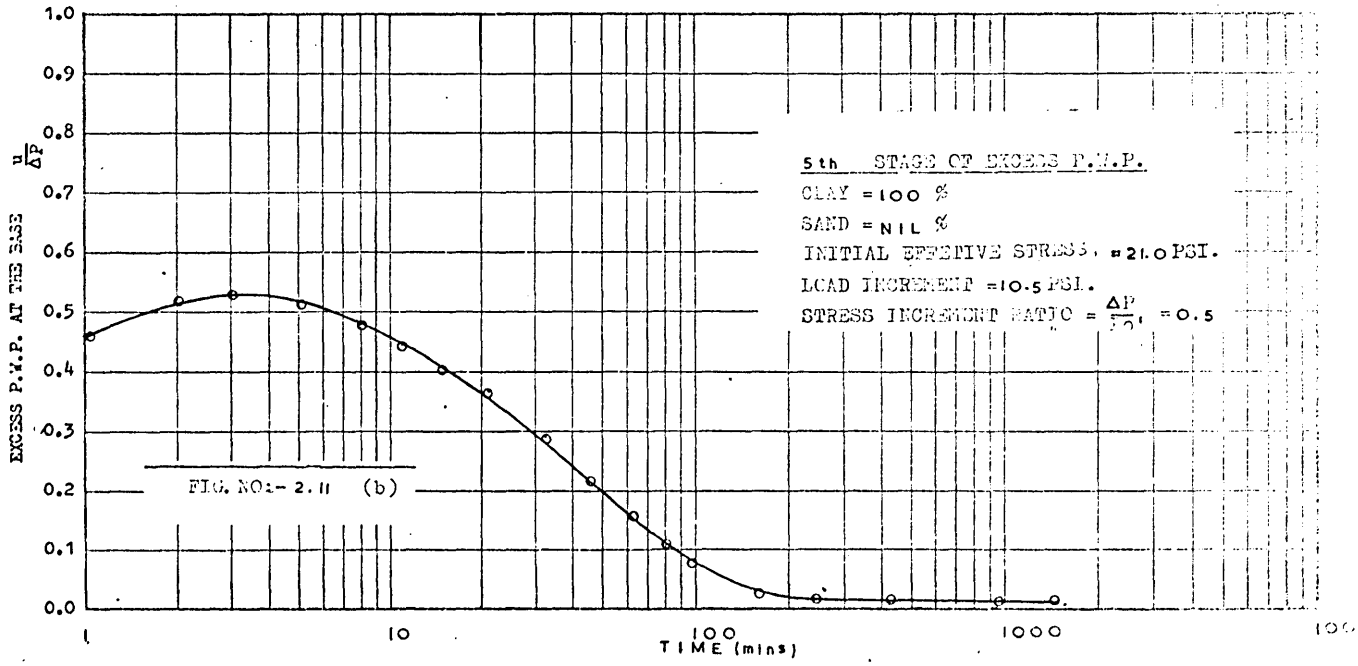

FIG. NO:- 2.11 (b)

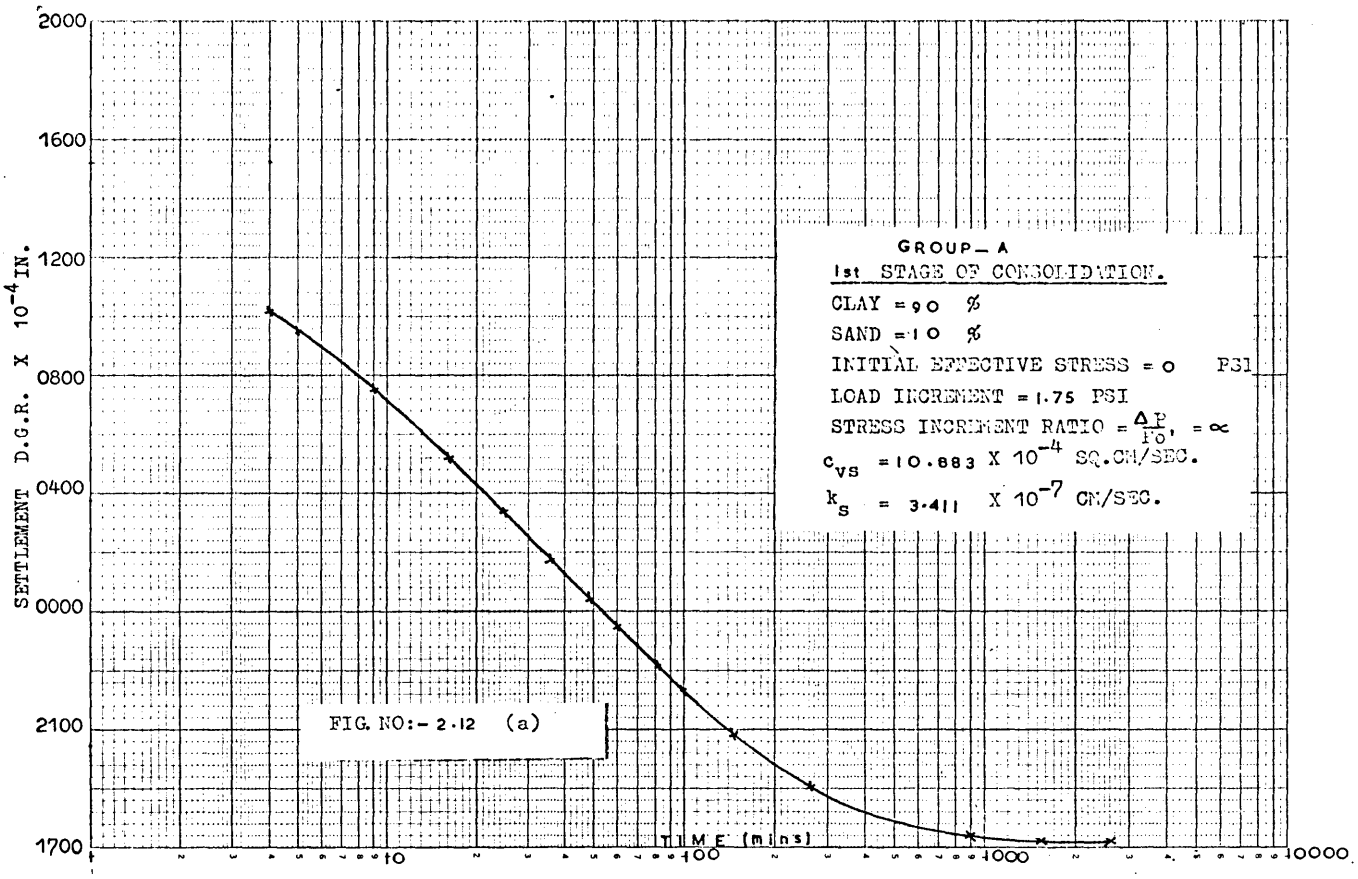
SETTLEMENT D.G.R. X 10^{-4} IN.
2000
1600
1200
0800
0400
0000
2100
1700
TIME (mins)
10
100
1000
10000
GROUP – A
1st STAGE OF CONSOLIDATION.
CLAY = 90 %
SAND = 10 %
INITIAL EFFECTIVE STRESS = 0 PSI
LOAD INCREMENT = 1.75 PSI
STRESS INCREMENT RATIO = $\frac{\Delta P}{P_0}$, = ∝
c_{vs} = 10.883 X 10^{-4} SQ.CM/SEC.
k_s = 3.411 X 10^{-7} CM/SEC.
FIG. NO:- 2.12 (a)

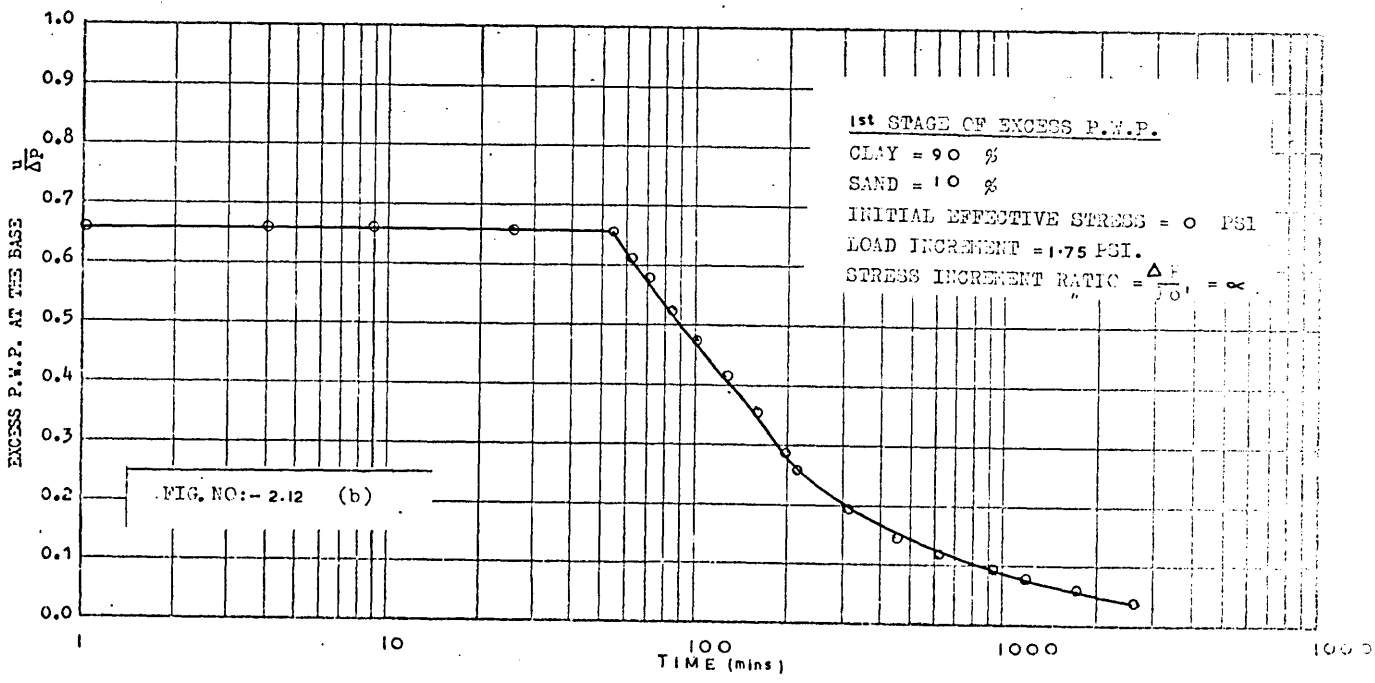
EXCESS P.W.P. AT THE BASE $\frac{u}{\Delta P}$
1.0
0.9
0.8
0.7
0.6
0.5
0.4
0.3
0.2
0.1
0.0
1
10
100
1000
TIME (mins)
1st STAGE OF EXCESS P.W.P.
CLAY = 90 %
SAND = 10 %
INITIAL EFFECTIVE STRESS = 0 PSI
LOAD INCREMENT = 1.75 PSI.
STRESS INCREMENT RATIO = $\frac{\Delta P}{P_0}$, = ∝
FIG. NO:- 2.12 (b)

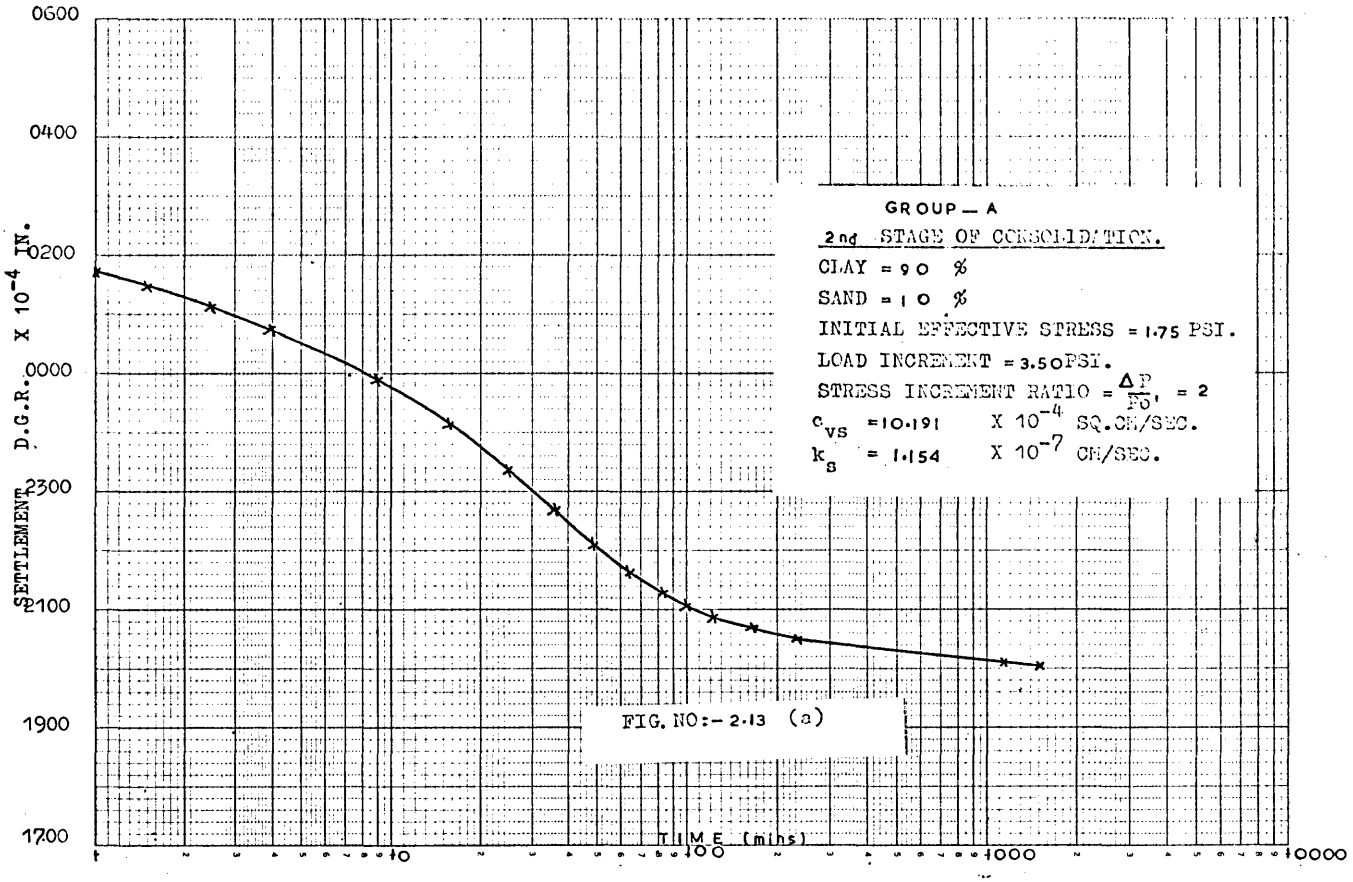

FIG. NO:- 2.13 (a)

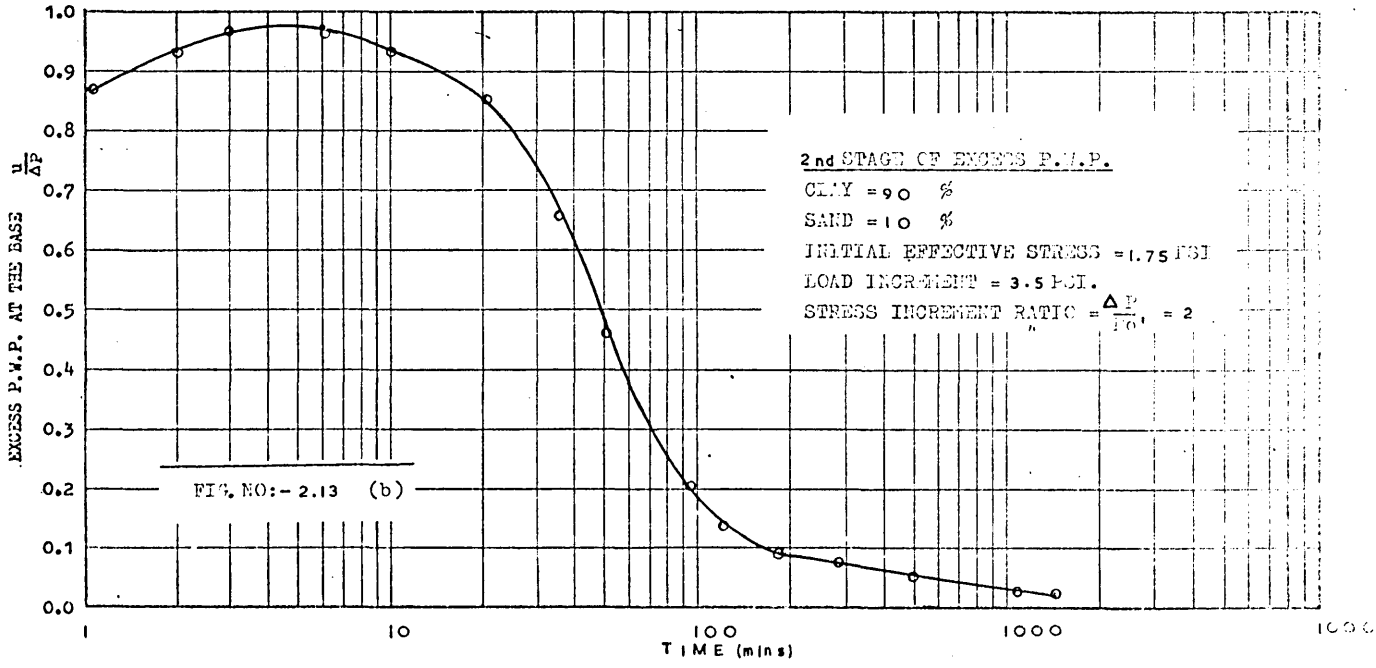

FIG. NO:- 2.13 (b)

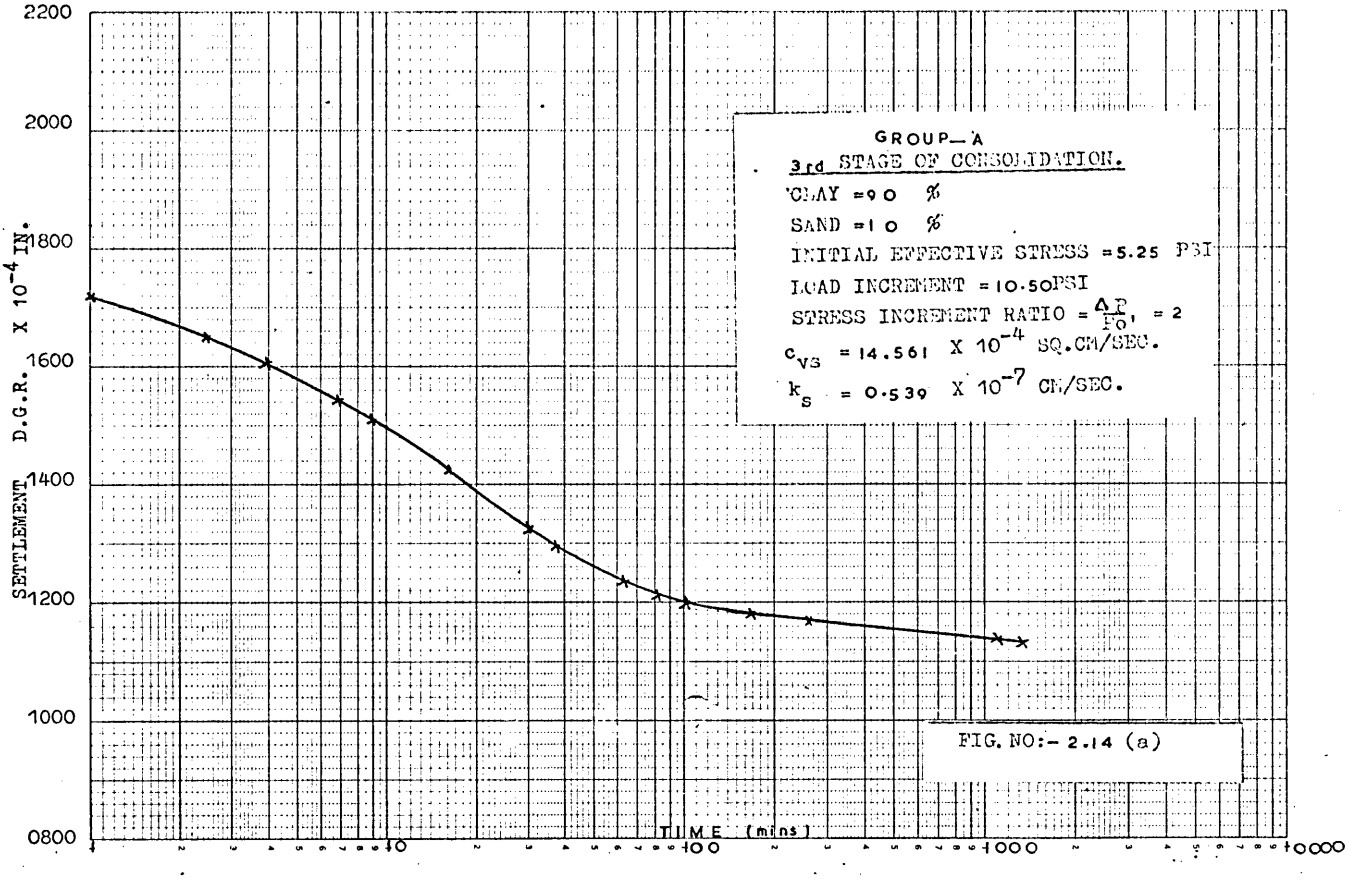

FIG. NO:- 2.14 (a)

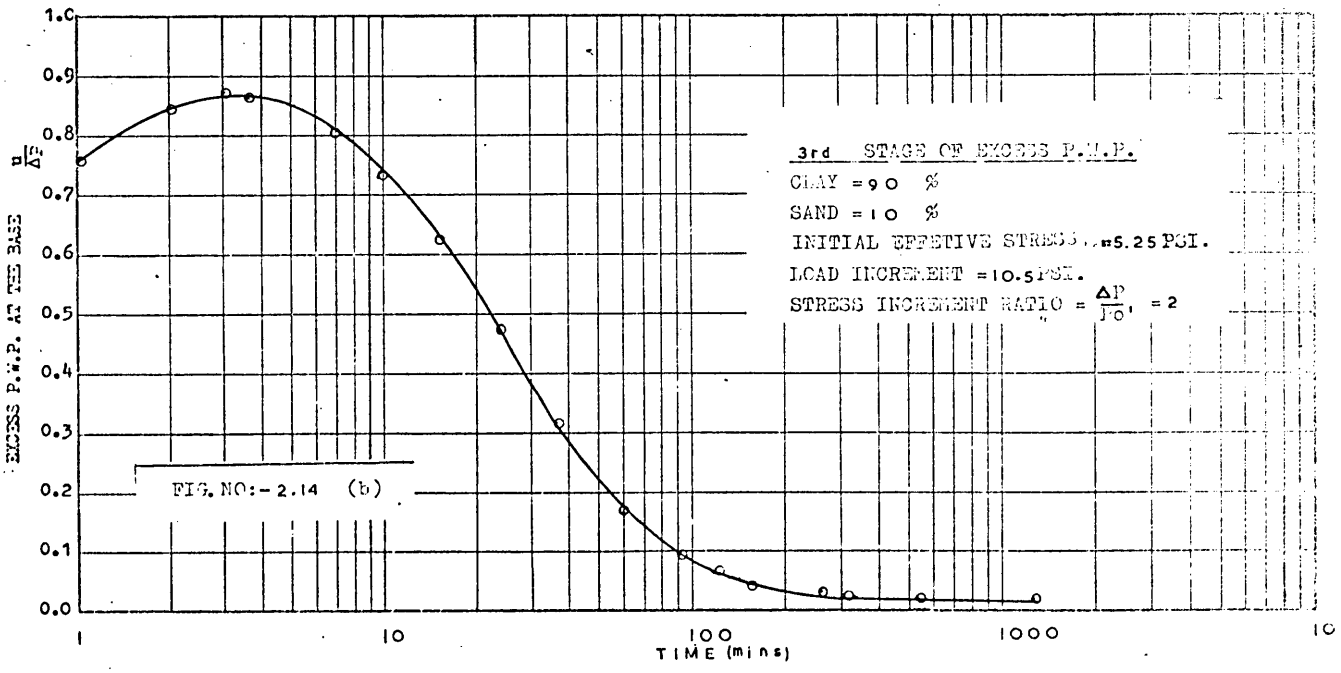

FIG. NO:- 2.14 (b)

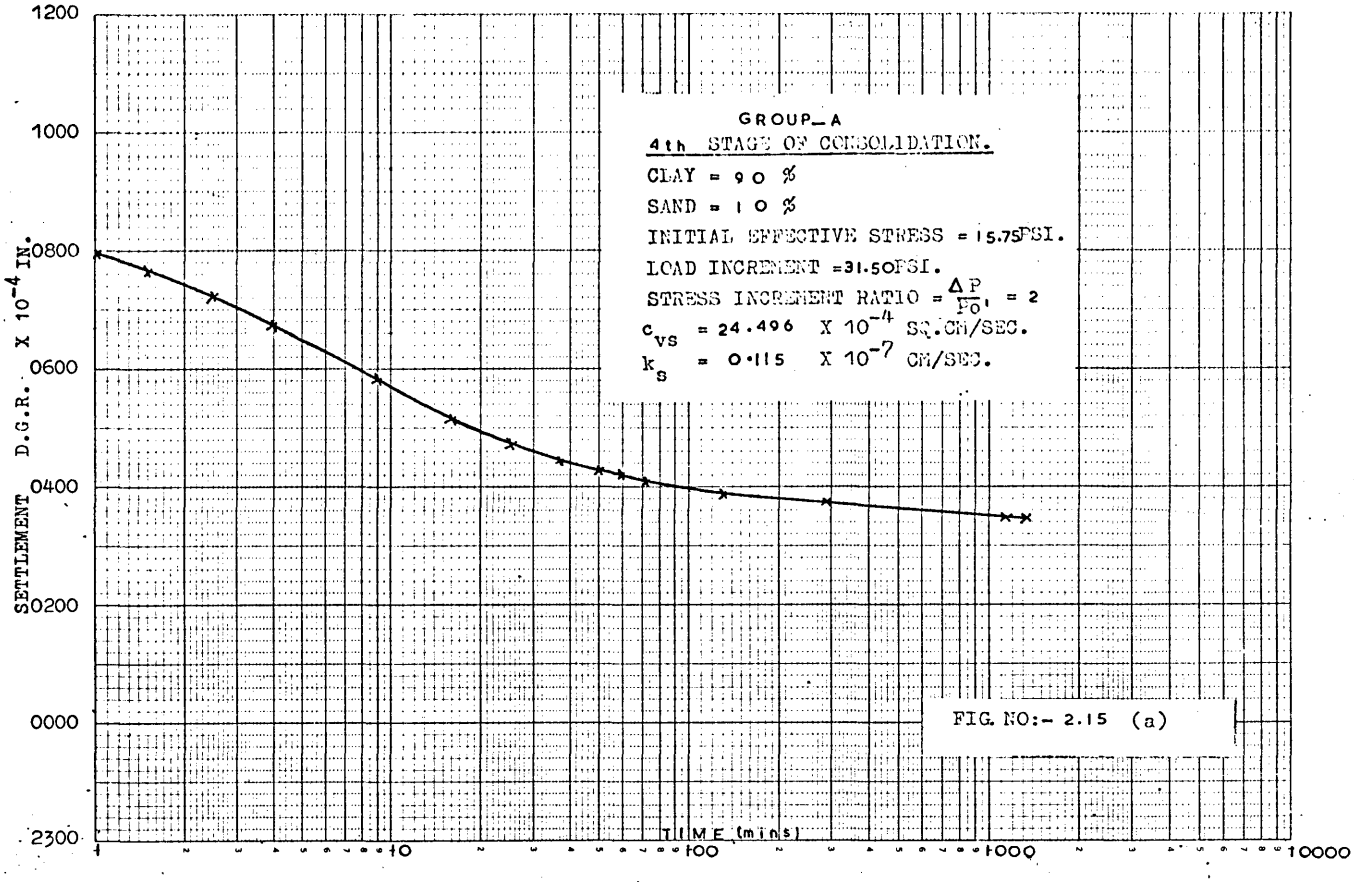

FIG. NO:- 2.15 (a)

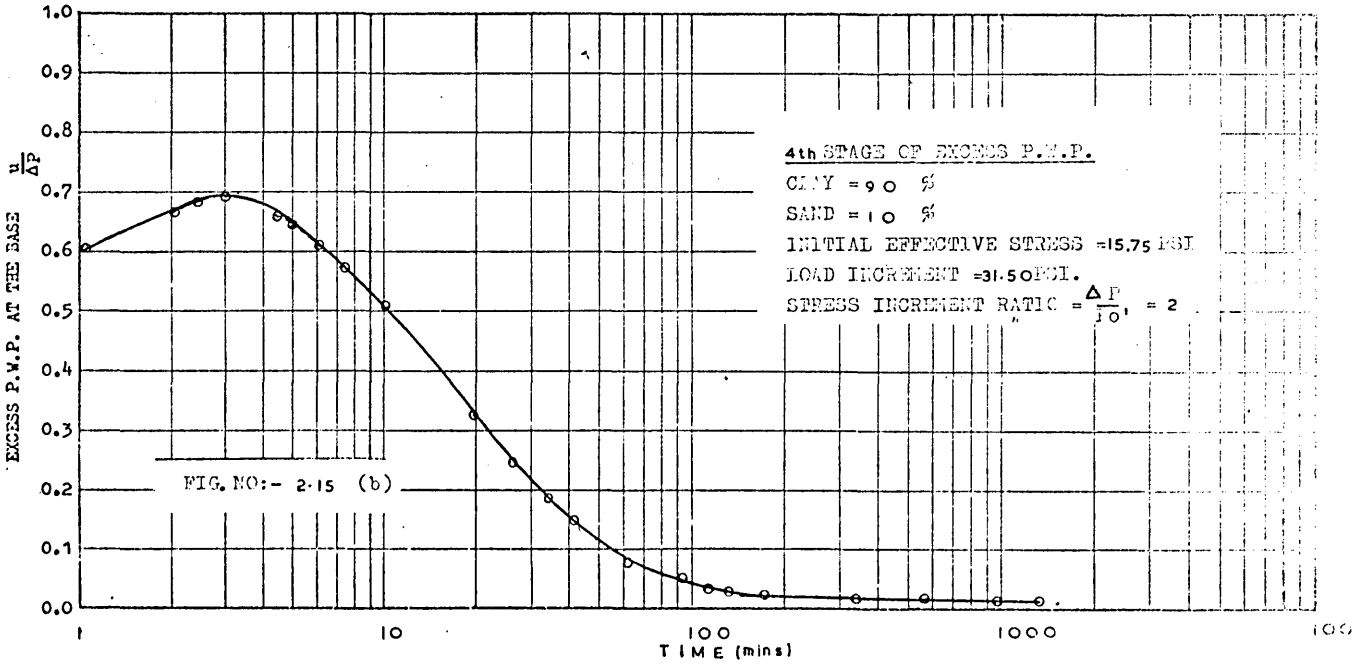

FIG. NO:- 2.15 (b)

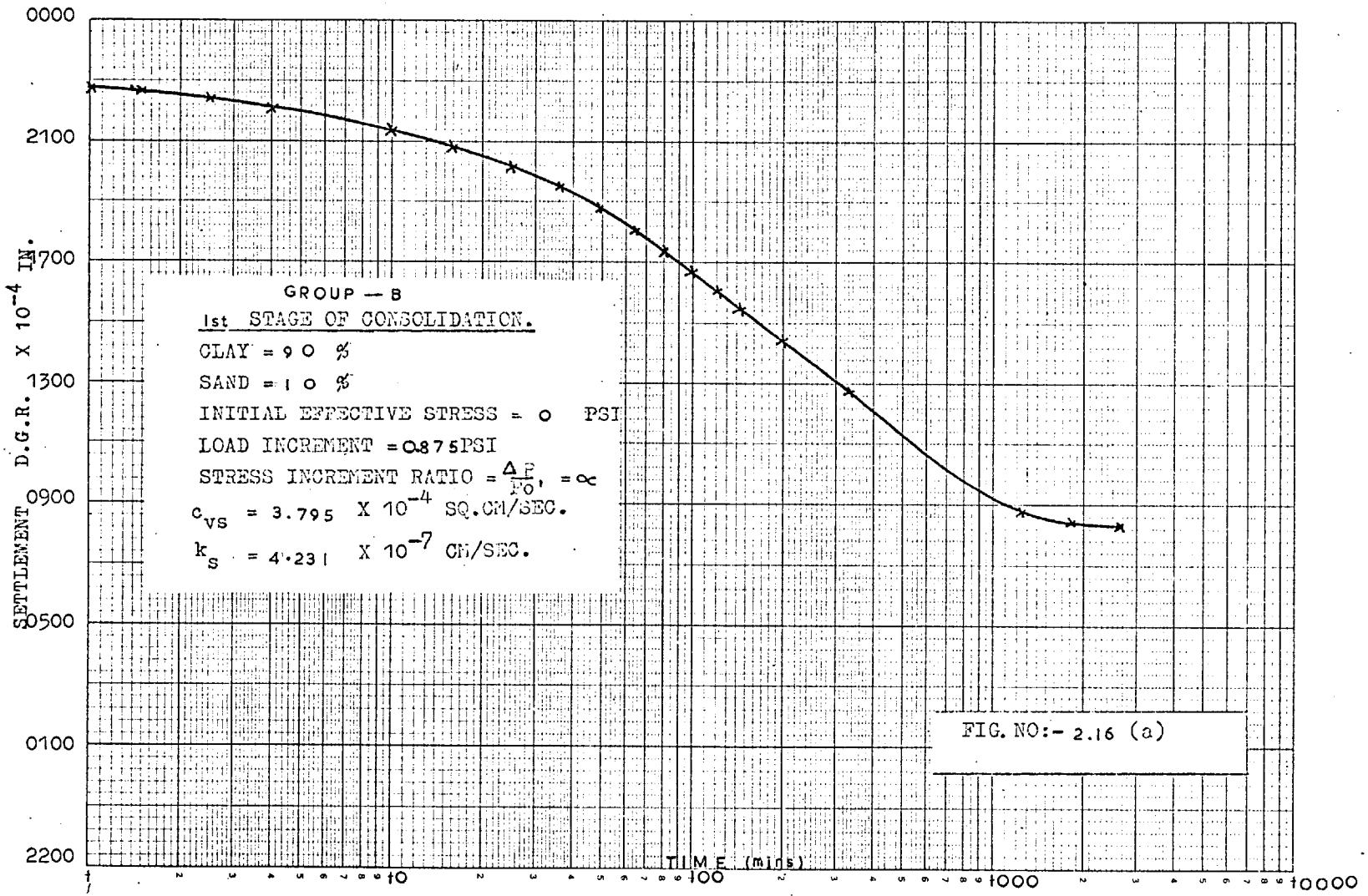
0000
2100
1700
1300
0900
0500
0100
2200
SETTLEMENT D.G.R. X 10^{-4} IN.
GROUP — B
1st STAGE OF CONSOLIDATION.
CLAY = 90 %
SAND = 10 %
INITIAL EFFECTIVE STRESS = 0 PSI
LOAD INCREMENT = 0.875 PSI
STRESS INCREMENT RATIO = $\frac{\Delta P}{P_0}$, = ∞
c_{vs} = 3.795 X 10^{-4} SQ.CM/SEC.
k_s = 4.231 X 10^{-7} CM/SEC.
t
t0
t00
t000
t0000
TIME (mins)

FIG. NO:- 2.16 (a)

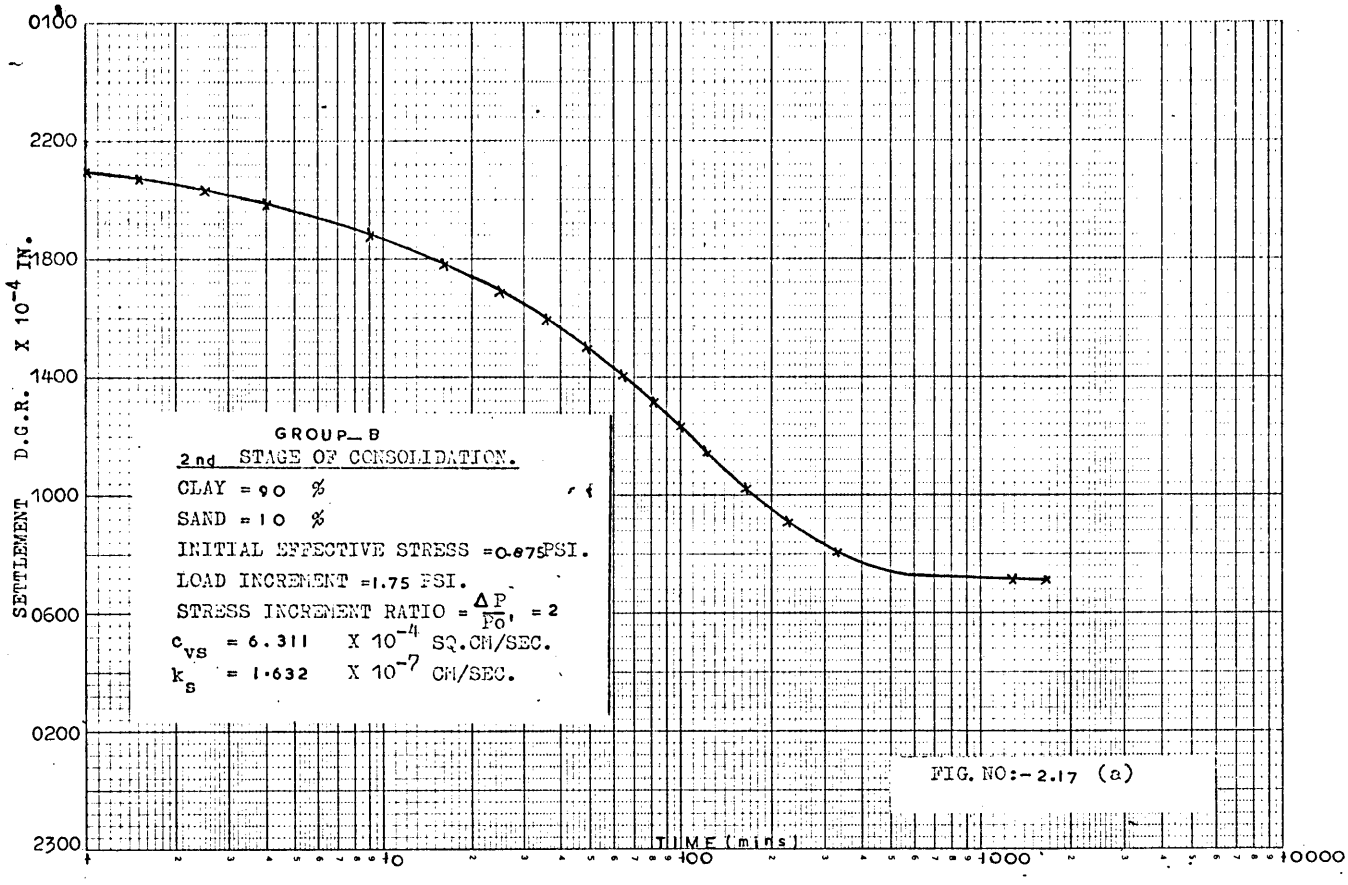

FIG. NO:- 2.17 (a)

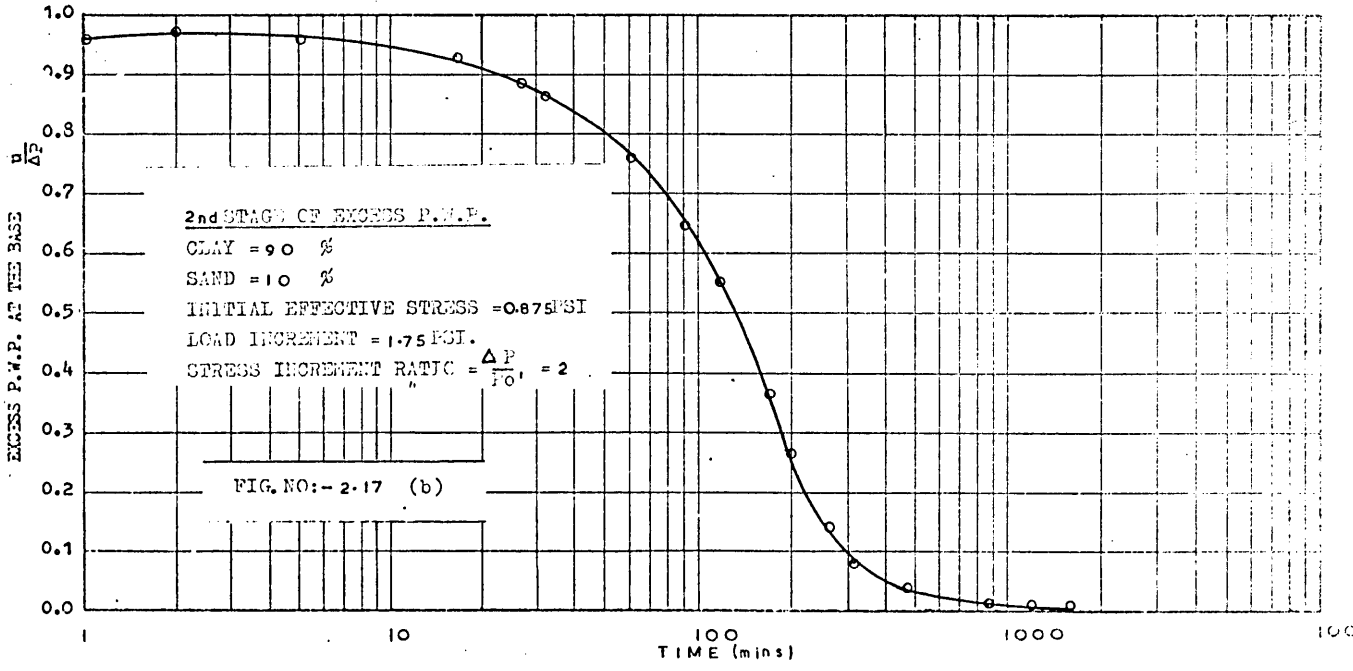

FIG. NO:- 2.17 (b)

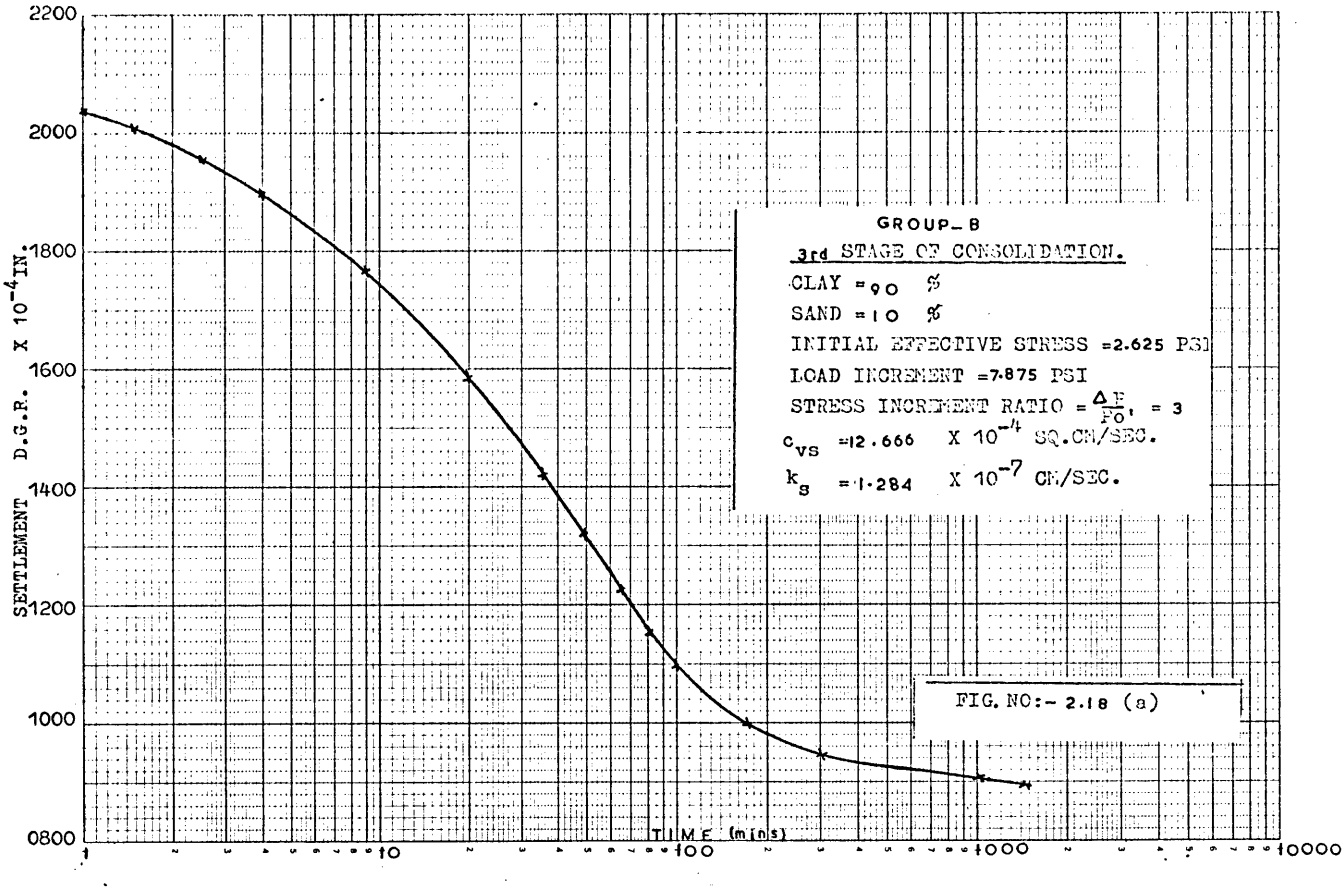

FIG. NO:- 2.18 (a)

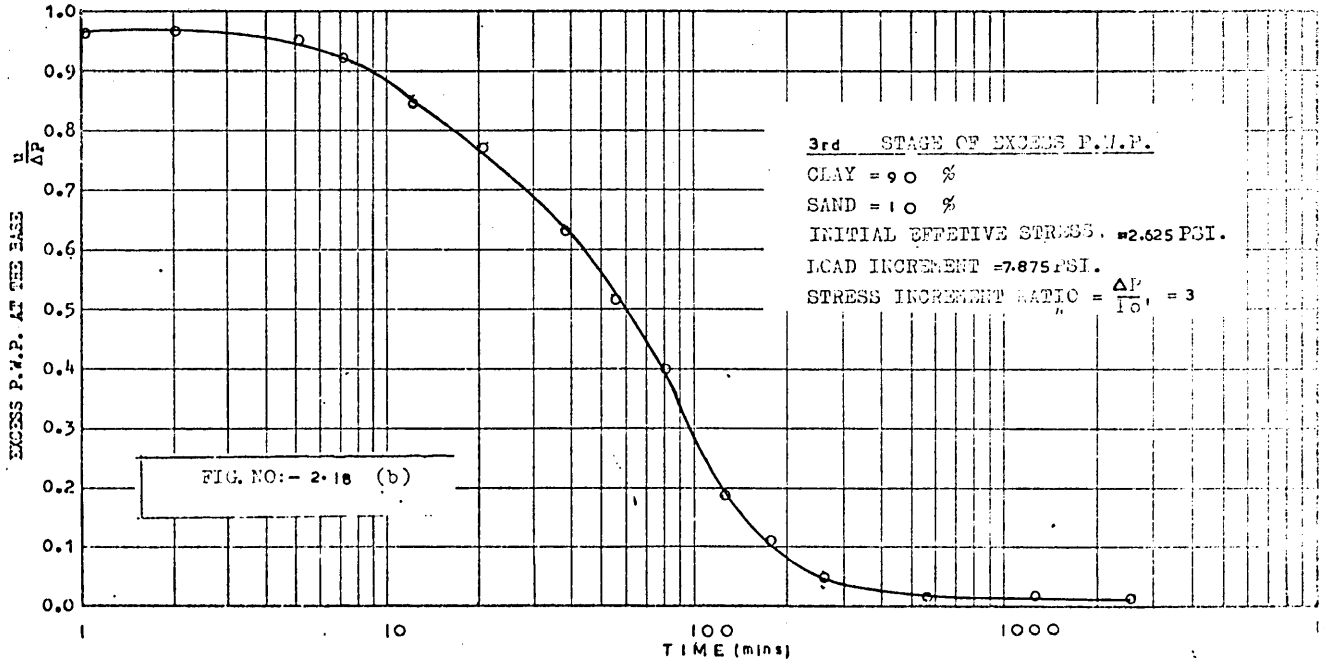

FIG. NO:- 2.18 (b)

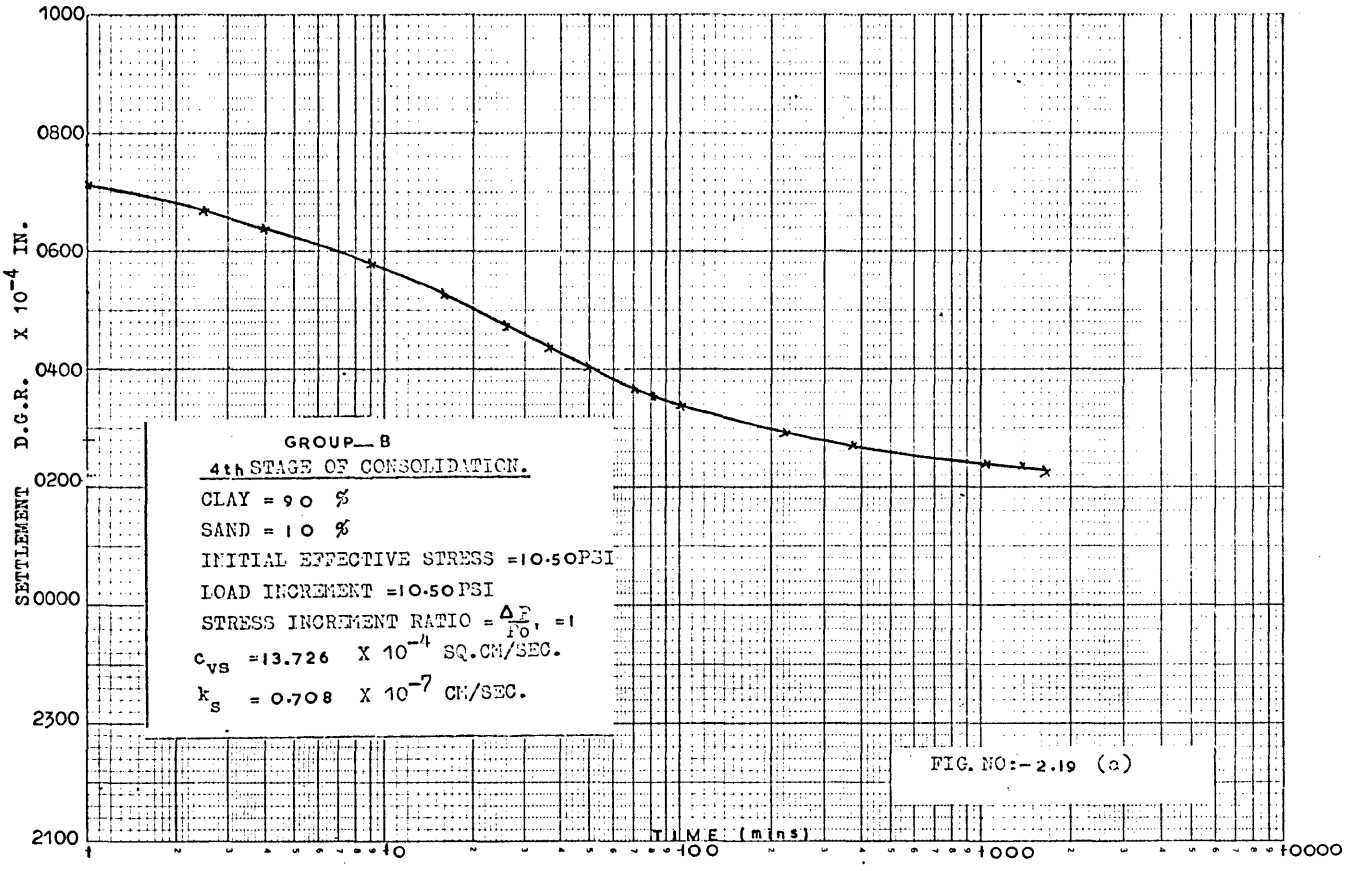

FIG. NO:- 2.19 (a)

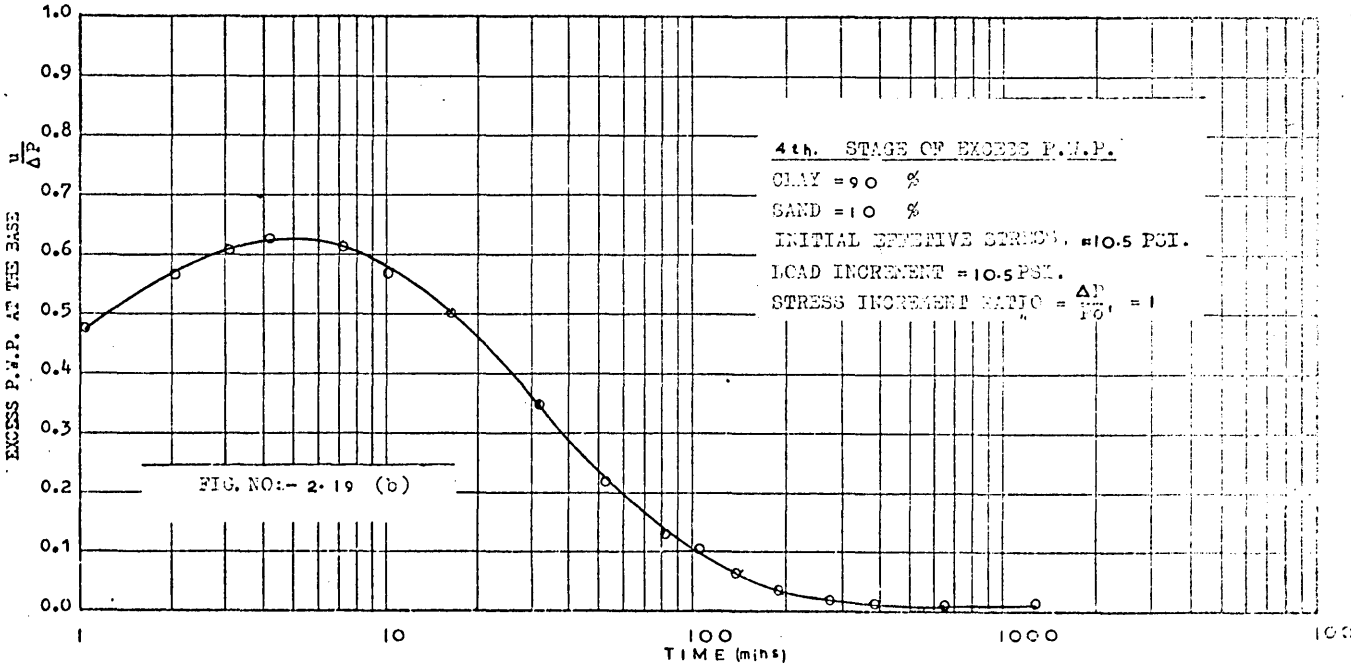

FIG. NO:- 2.19 (b)

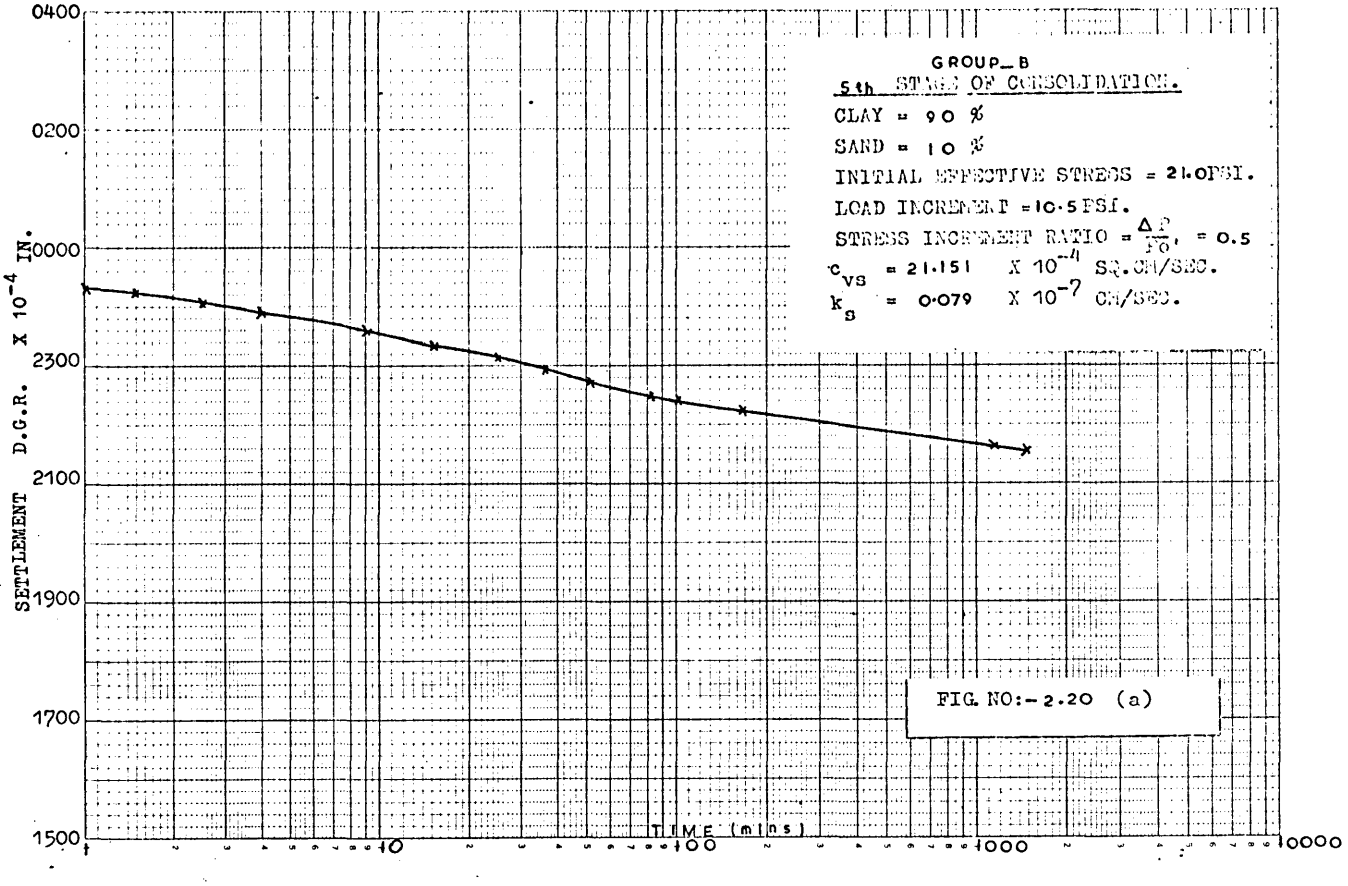
GROUP_B
5th STAGE OF CONSOLIDATION.
CLAY = 90 %
SAND = 10 %
INITIAL EFFECTIVE STRESS = 21.0PSI.
LOAD INCREMENT = 10.5PSI.
STRESS INCREMENT RATIO = ΔP/Po, = 0.5
cvs = 21.151 X 10^-4 SQ.CM/SEC.
ks = 0.079 X 10^-7 CM/SEC.
FIG. NO:- 2.20 (a)
SETTLEMENT D.G.R. X 10^-4 IN.
0400
0200
0000
2300
2100
1900
1700
1500
TIME (mins)
10
100
1000
10000

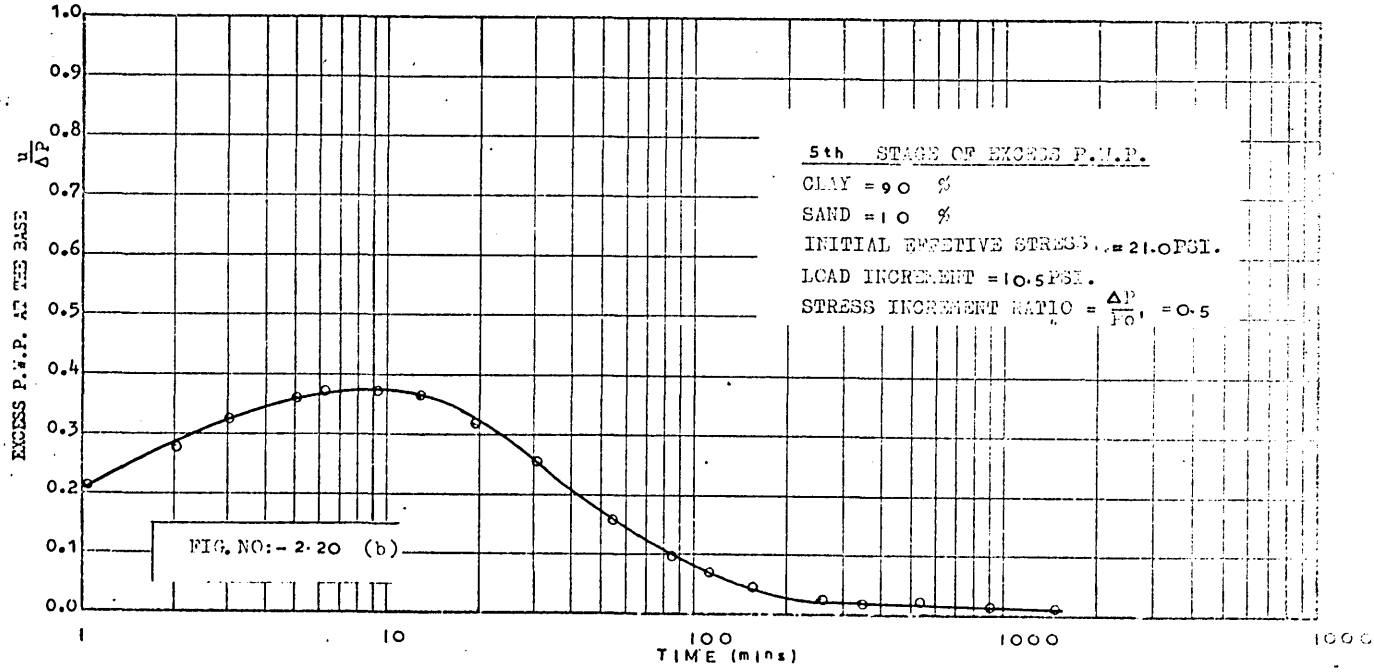
5th STAGE OF EXCESS P.W.P.
CLAY = 90 %
SAND = 10 %
INITIAL EFFECTIVE STRESS = 21.0PSI.
LOAD INCREMENT = 10.5PSI.
STRESS INCREMENT RATIO = ΔP/Po, = 0.5
FIG. NO:- 2.20 (b)
u/ΔP
EXCESS P.W.P. AT THE BASE
1.0
0.9
0.8
0.7
0.6
0.5
0.4
0.3
0.2
0.1
0.0
1
10
100
1000
TIME (mins)

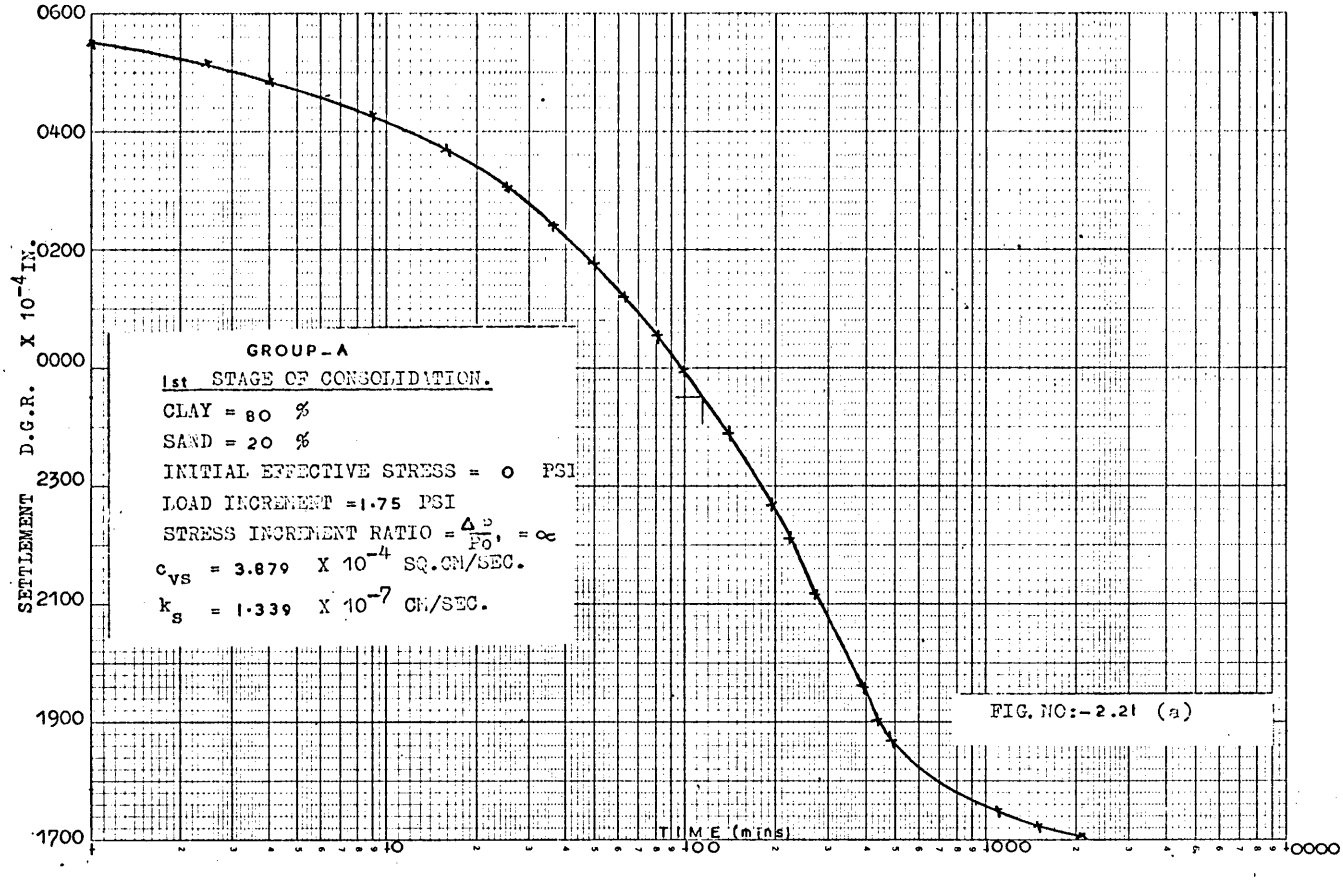

FIG. NO:- 2.21 (a)

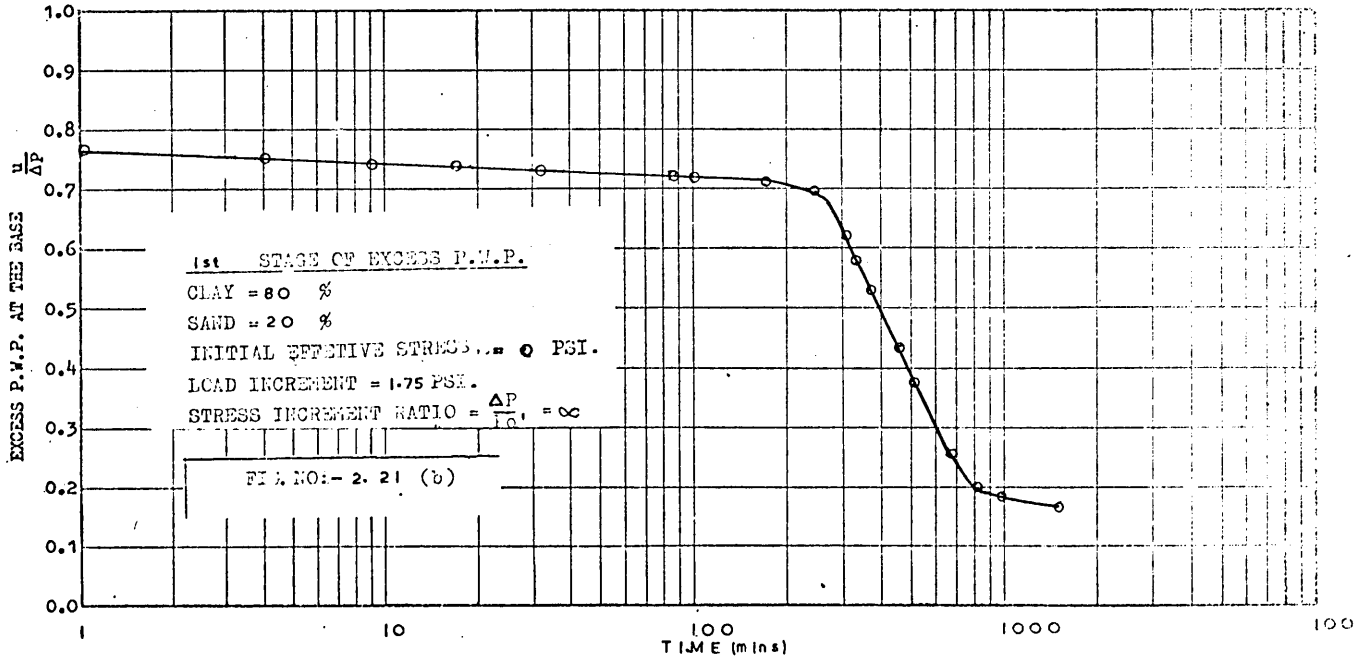

FIG. NO:- 2. 21 (b)

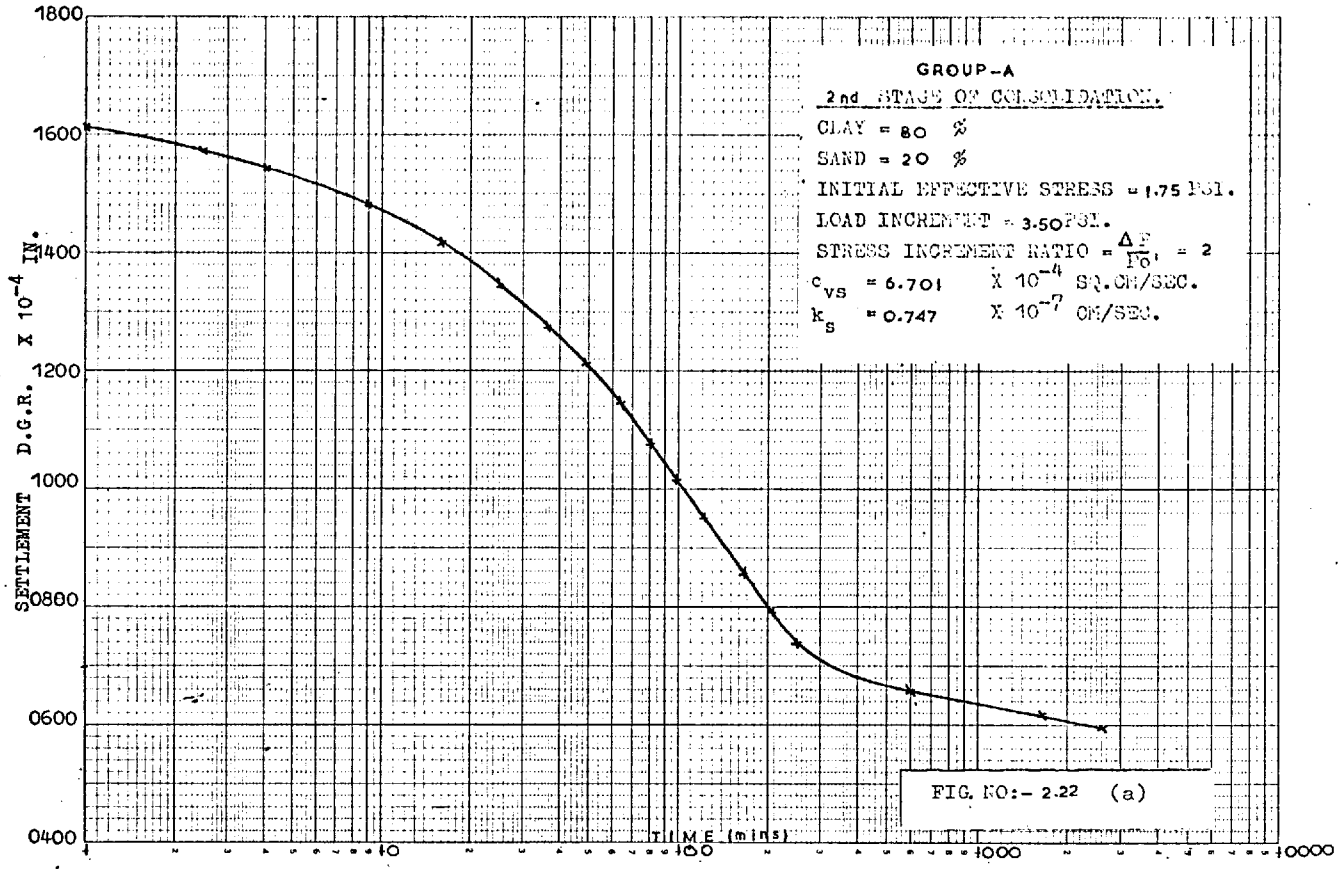

FIG. NO:- 2.22 (a)

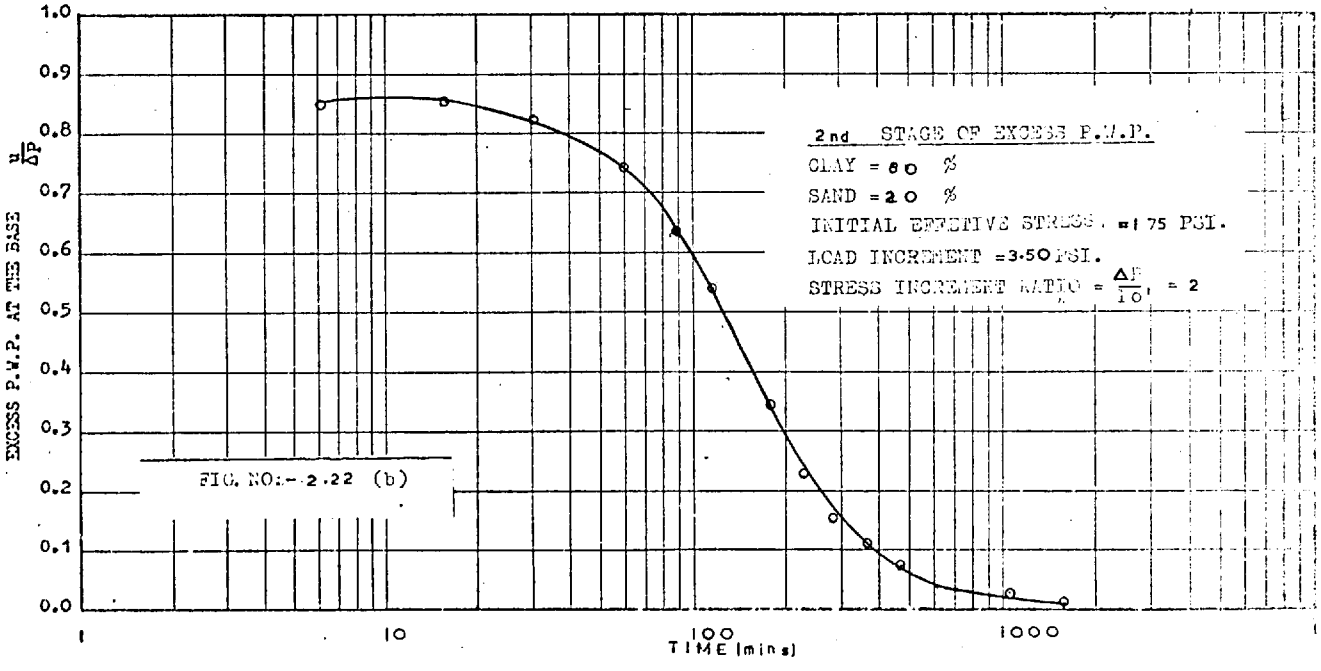

FIG. NO:- 2.22 (b)

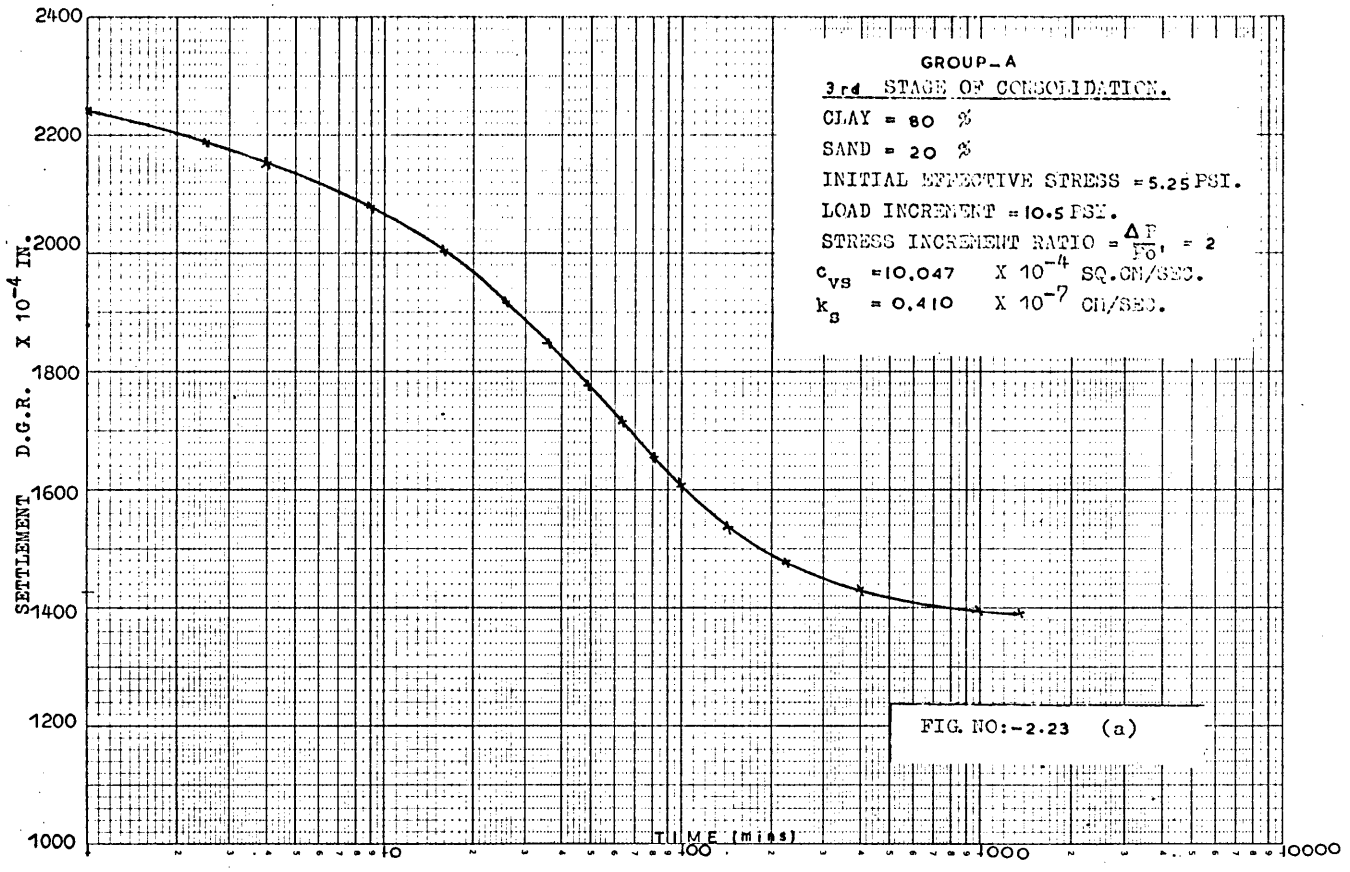

FIG. NO:-2.23 (a)

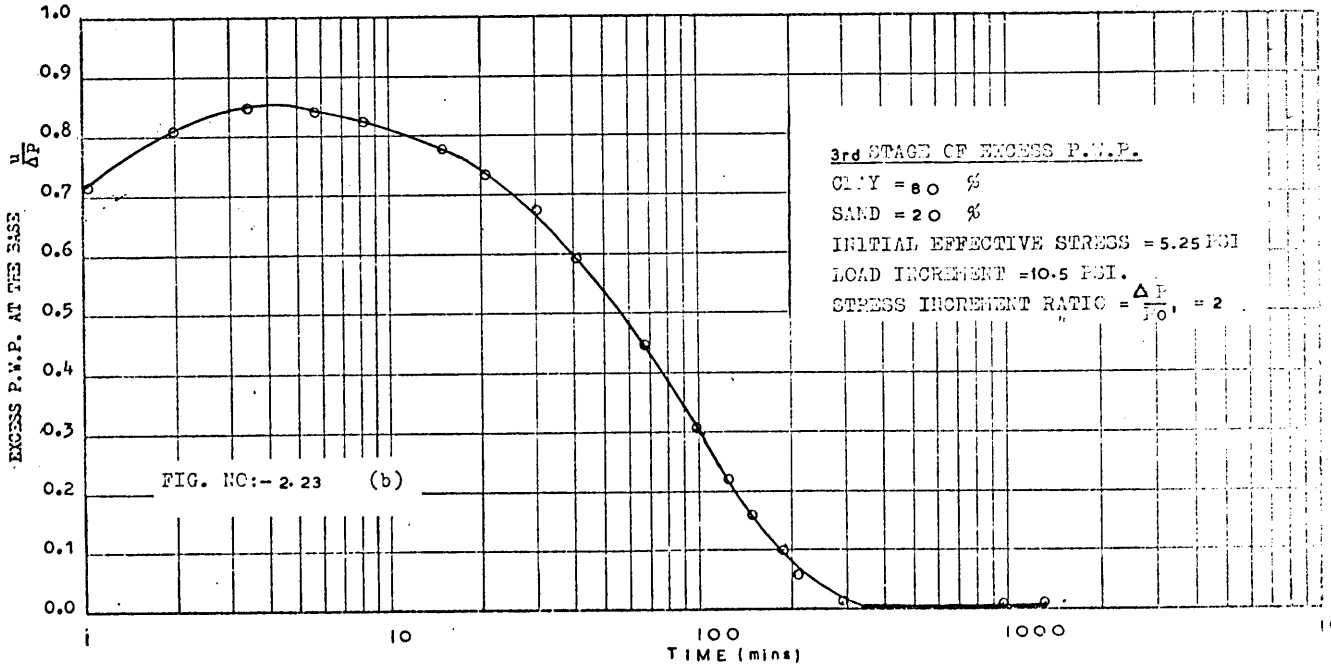

FIG. NO:- 2.23 (b)

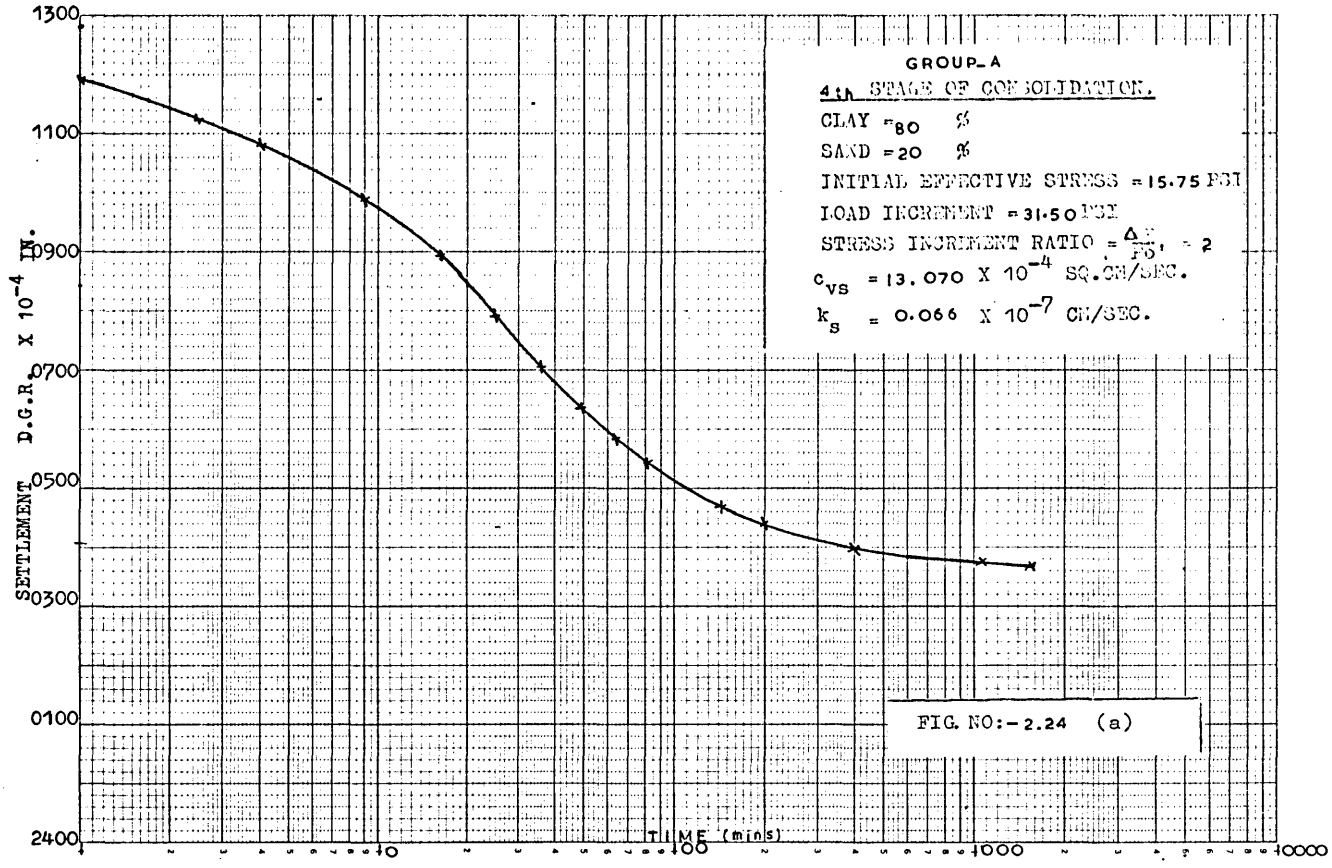

FIG. NO:- 2.24 (a)

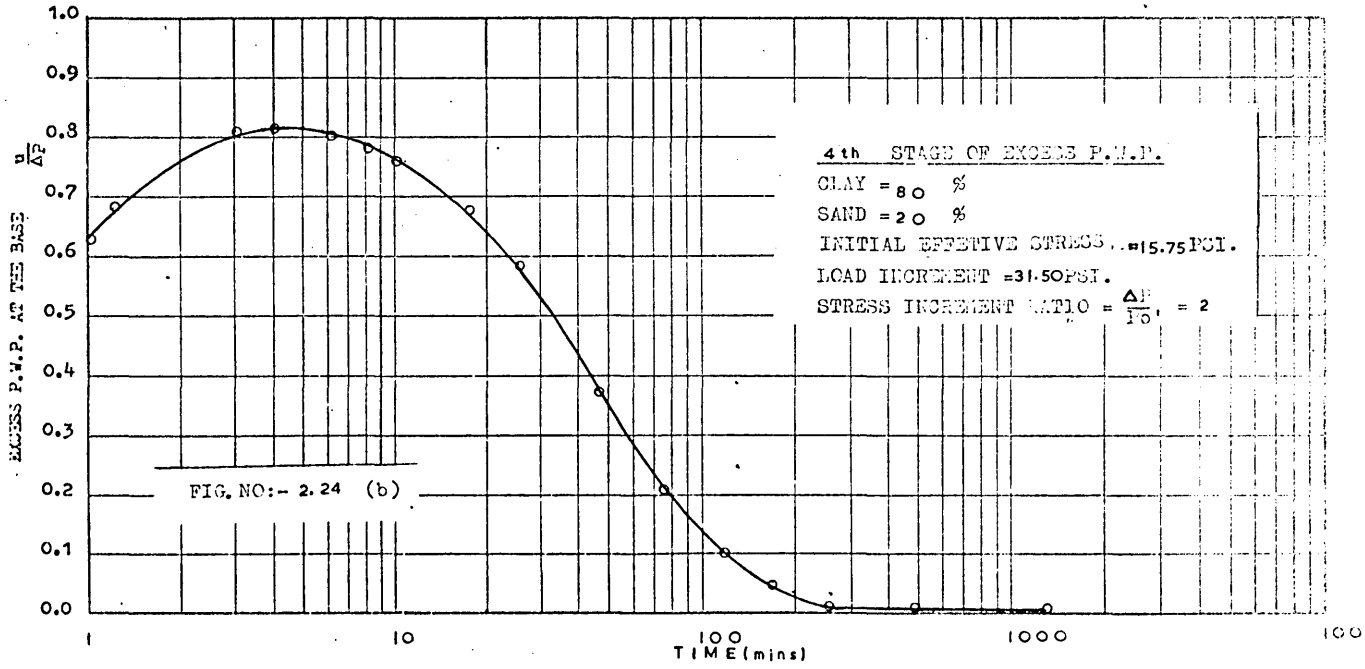

FIG. NO:- 2.24 (b)

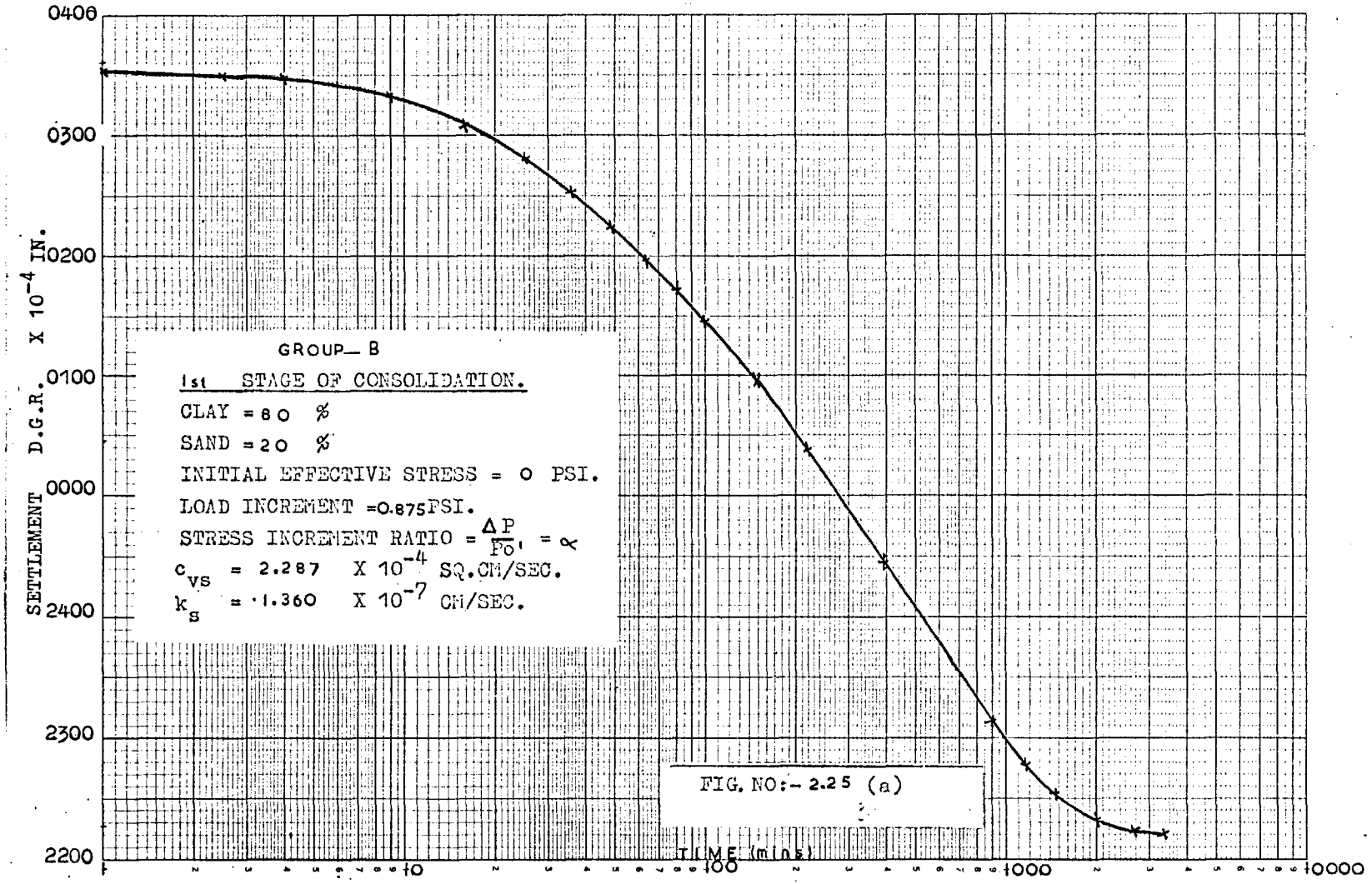
0406
0300
0200
0100
0000
2400
2300
2200
SETTLEMENT D.G.R. X 10^{-4} IN.
GROUP— B
1st STAGE OF CONSOLIDATION.
CLAY = 80 %
SAND = 20 %
INITIAL EFFECTIVE STRESS = 0 PSI.
LOAD INCREMENT =0.875PSI.
STRESS INCREMENT RATIO = $\frac{\Delta P}{Po}$ = ∝
c_{vs} = 2.287 X 10^{-4} SQ.CM/SEC.
k_s = 1.360 X 10^{-7} CM/SEC.
10
100
1000
10000
TIME (mins)

FIG. NO:- 2.25 (a)

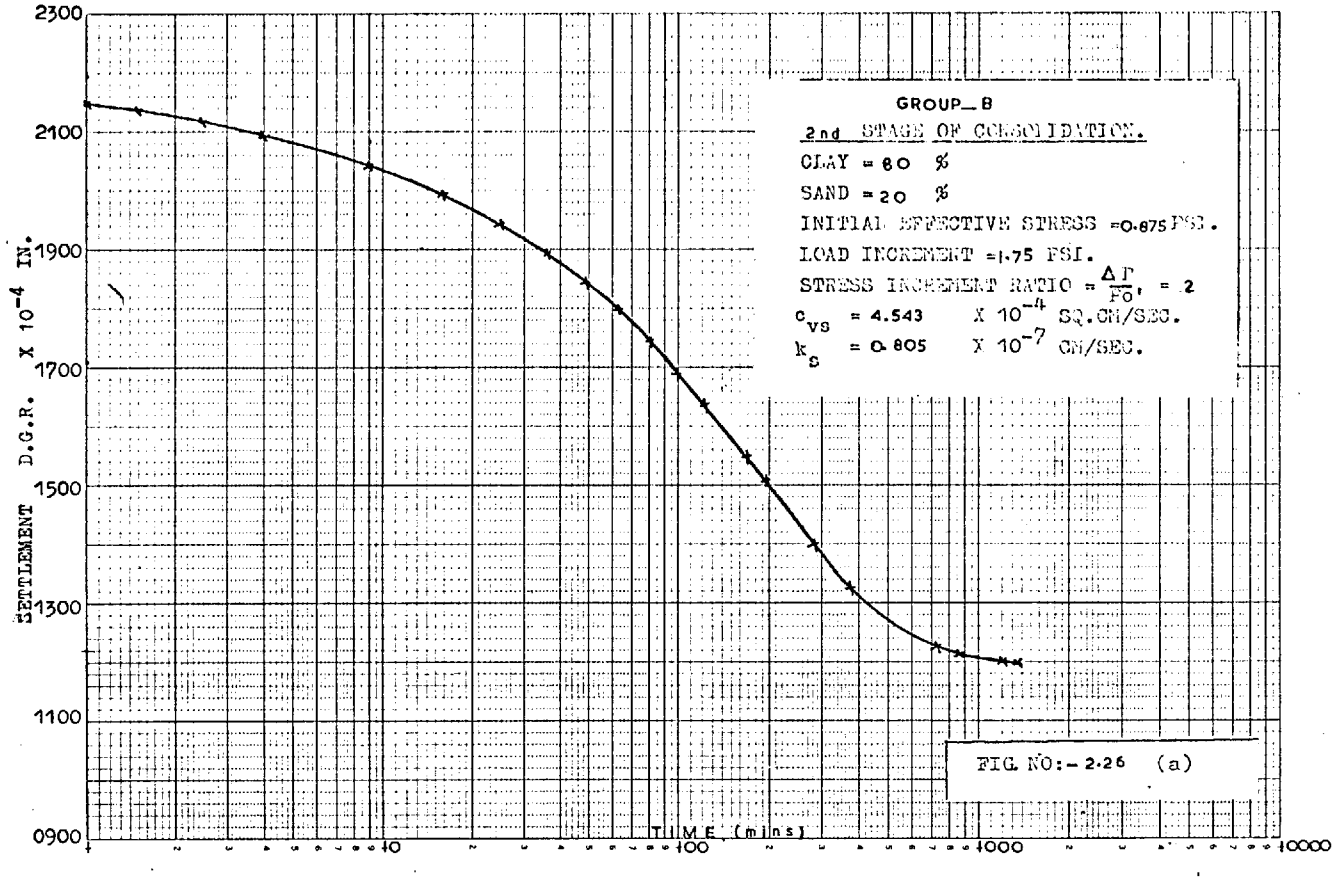

FIG. NO:- 2.26 (a)

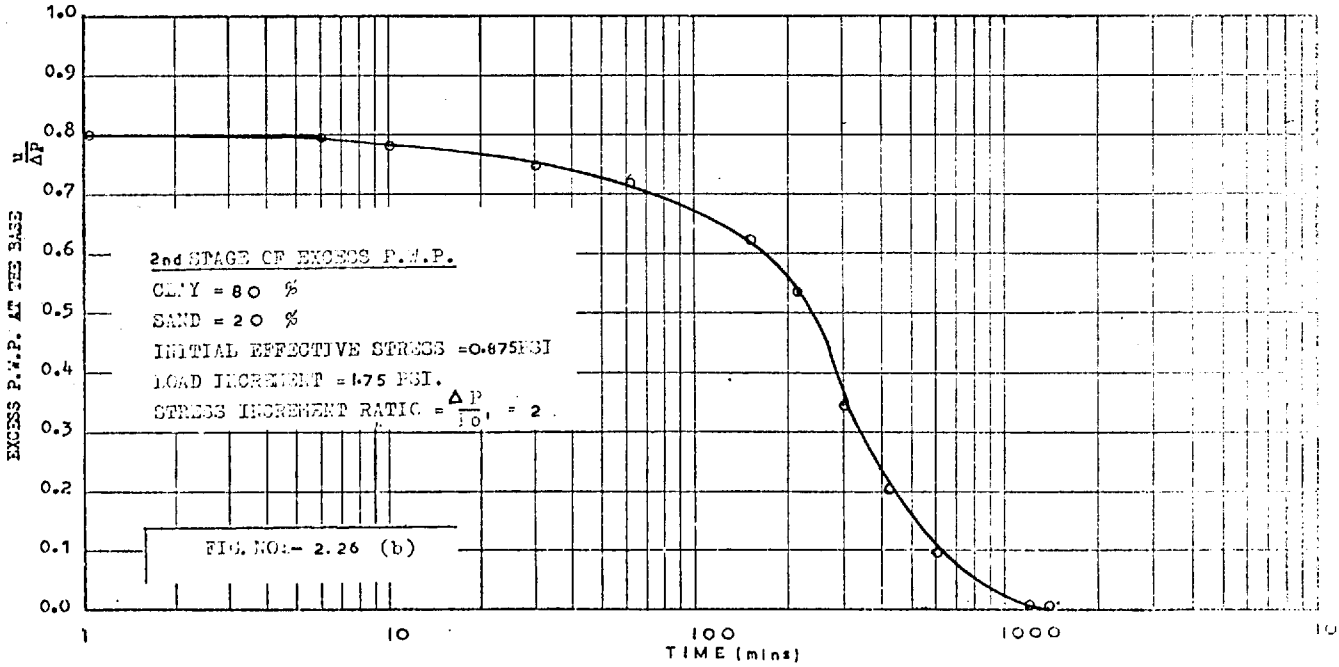

FIG. NO:- 2.26 (b)

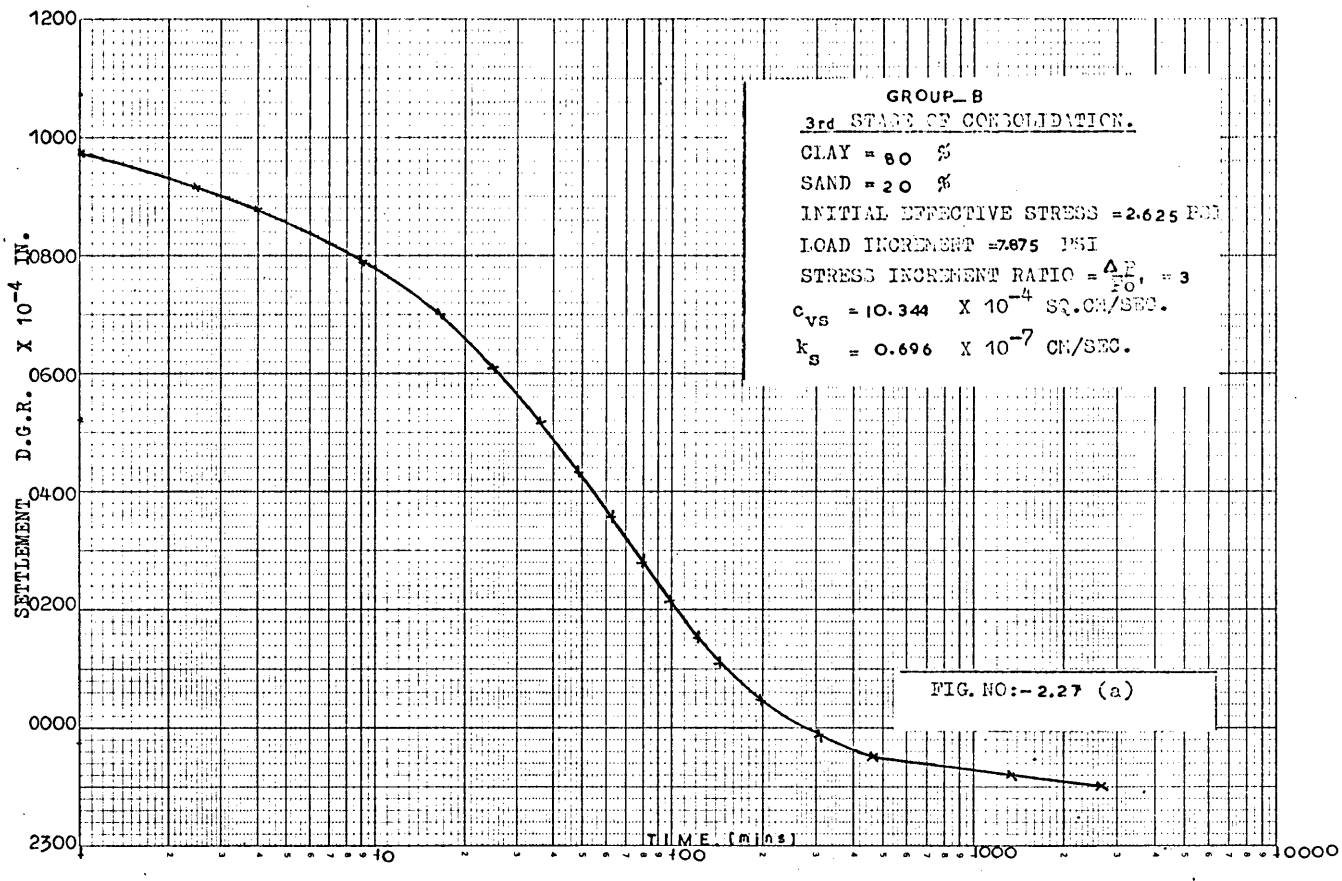
GROUP_B
3rd STAGE OF CONSOLIDATION.
CLAY = 80 %
SAND = 20 %
INITIAL EFFECTIVE STRESS = 2.625 PSI
LOAD INCREMENT = 7.875 PSI
STRESS INCREMENT RATIO = $\frac{\Delta P}{P_o}$ = 3
c_{vs} = 10.344 X 10^{-4} SQ.CM/SEC.
k_s = 0.696 X 10^{-7} CM/SEC.
FIG. NO:- 2.27 (a)
SETTLEMENT D.G.R. X 10^{-4} IN.
TIME (mins)

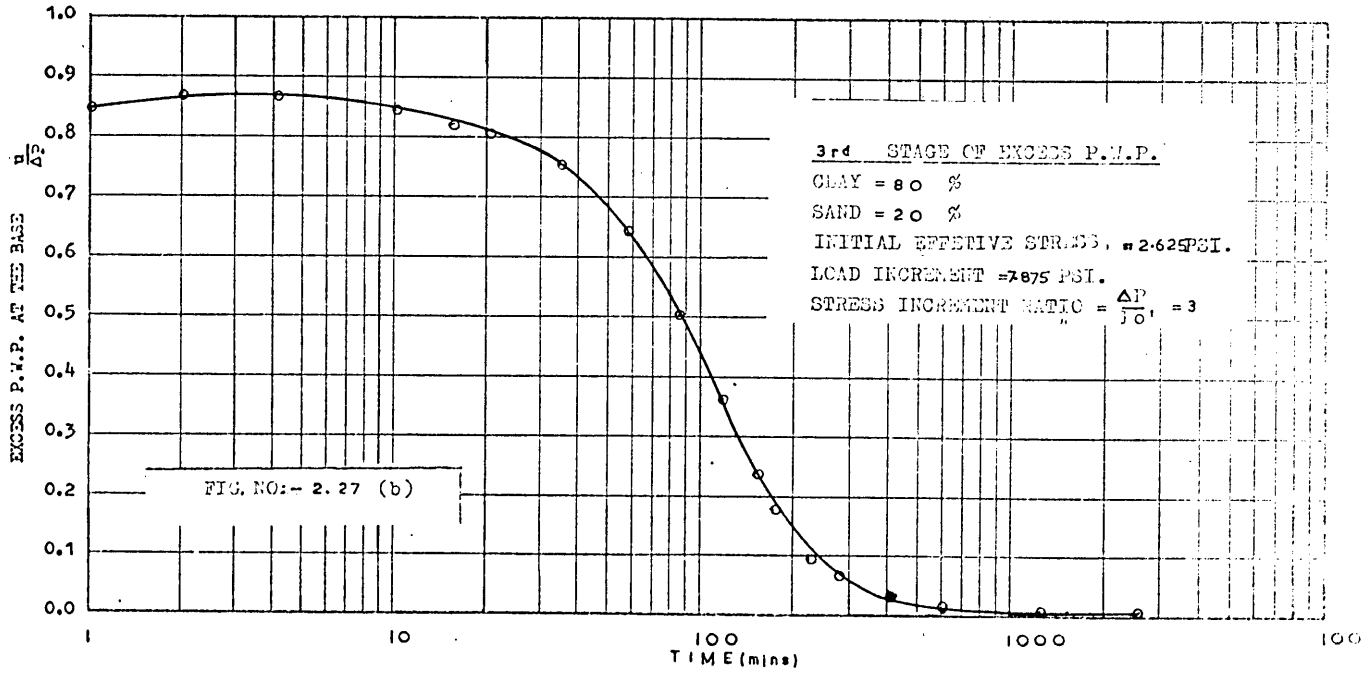
3rd STAGE OF EXCESS P.W.P.
CLAY = 80 %
SAND = 20 %
INITIAL EFFETIVE STRESS = 2.625 PSI.
LOAD INCREMENT = 7.875 PSI.
STRESS INCREMENT RATIO = $\frac{\Delta P}{P_o}$ = 3
FIG. NO:- 2.27 (b)
$\frac{u}{\Delta P}$
EXCESS P.W.P. AT THE BASE
TIME (mins)

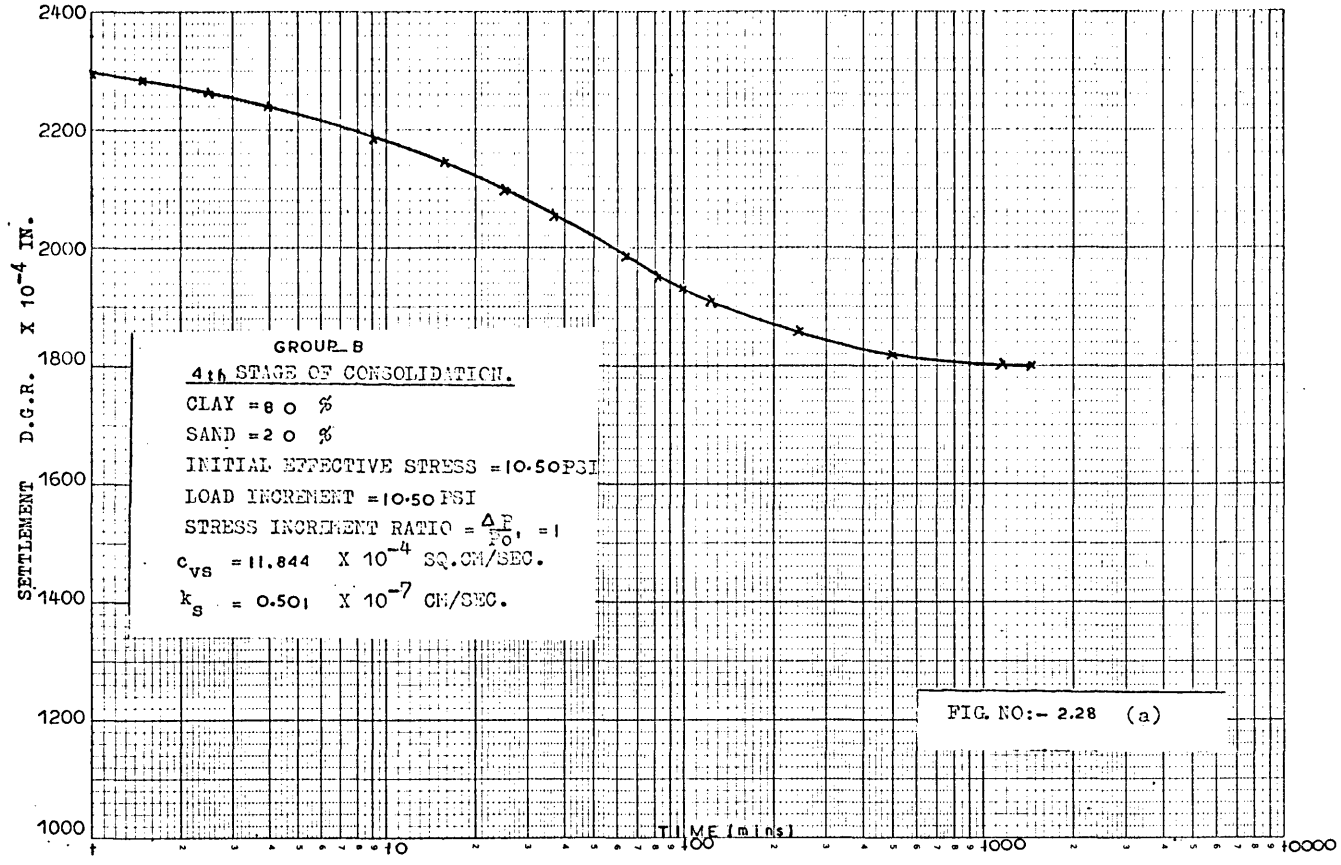

FIG. NO:- 2.28 (a)

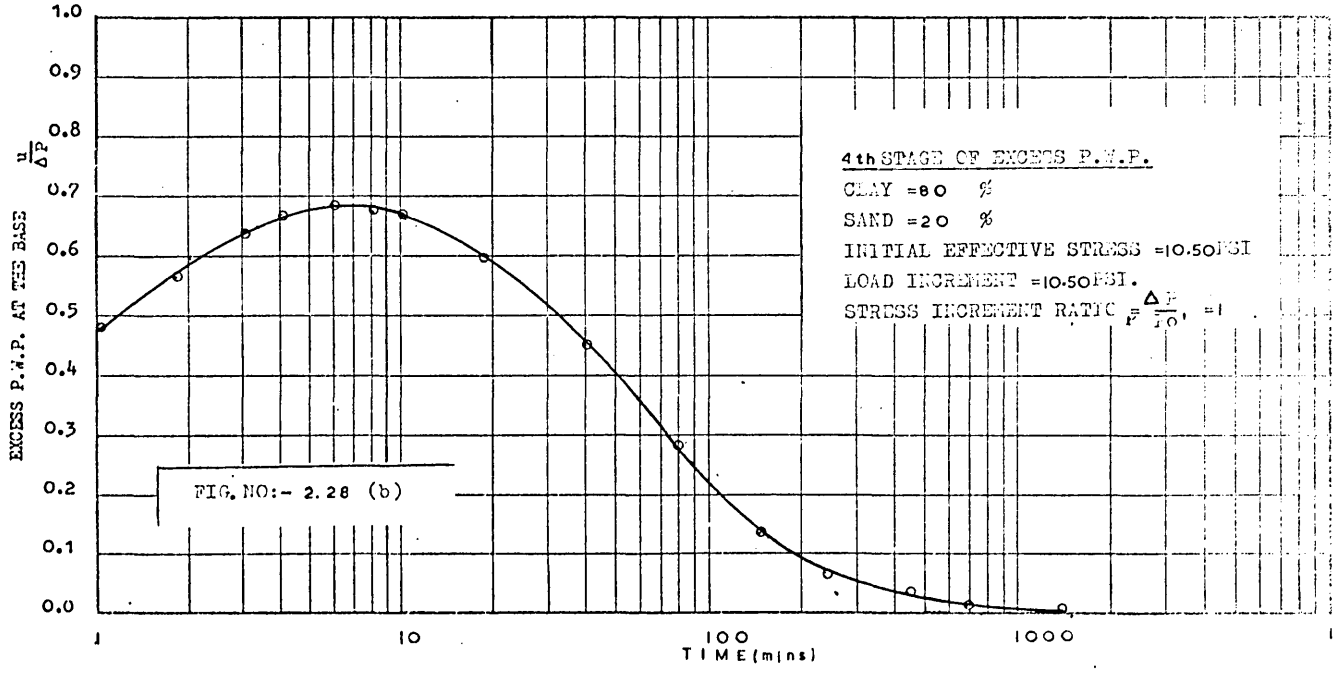

FIG. NO:- 2.28 (b)

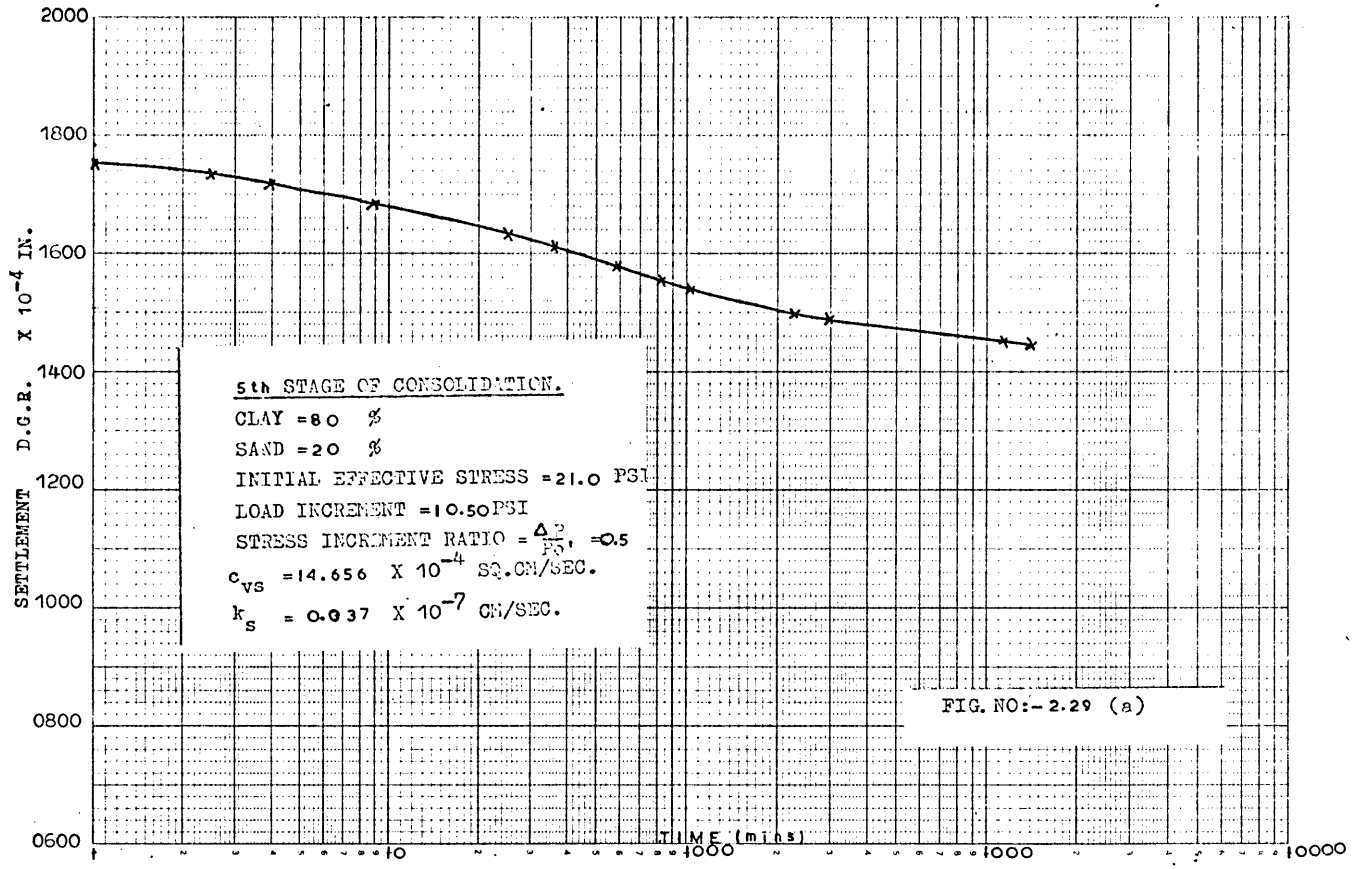

FIG. NO:- 2.29 (a)

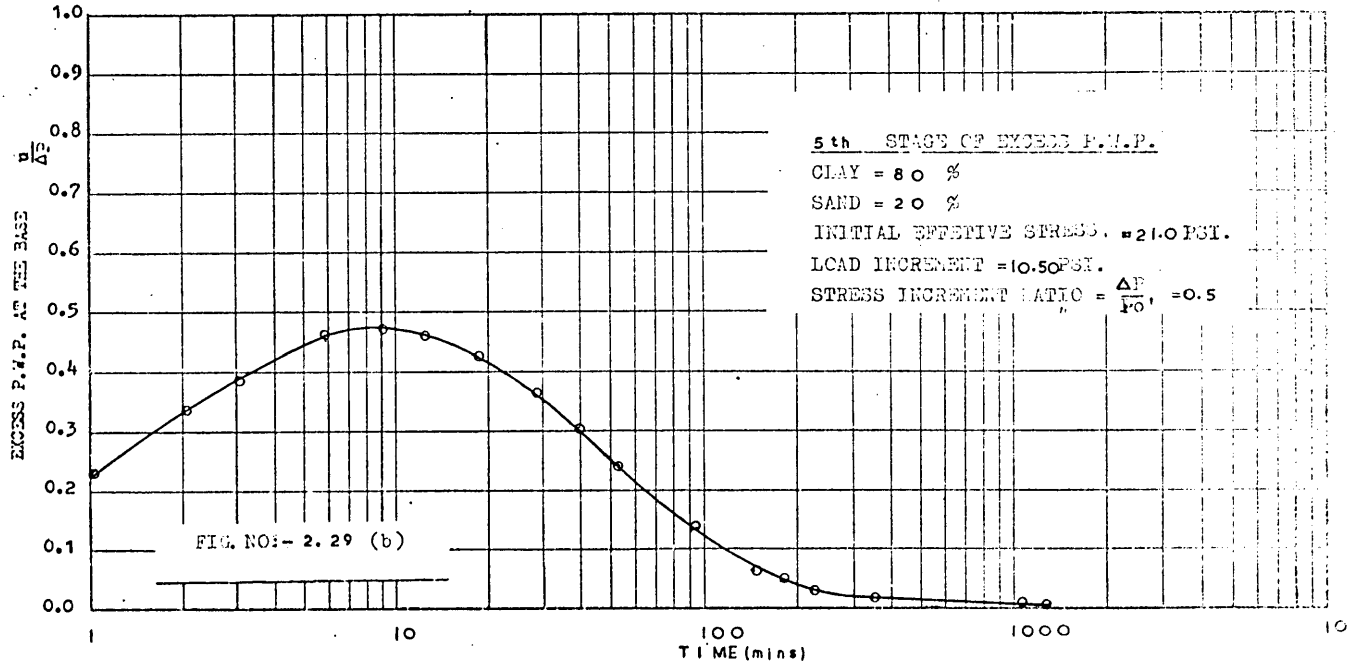

FIG. NO:- 2.29 (b)

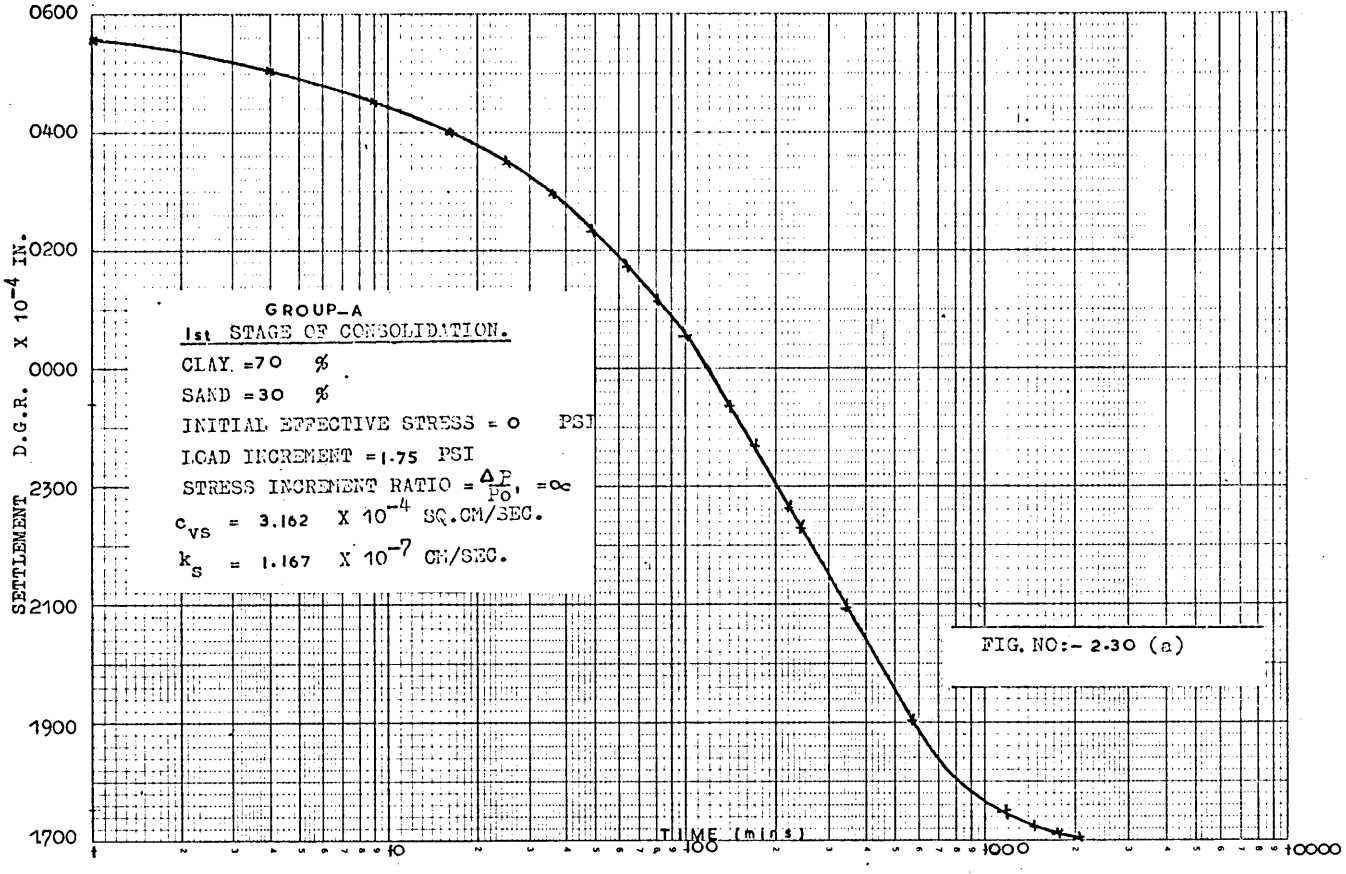

FIG. NO:- 2.30 (a)

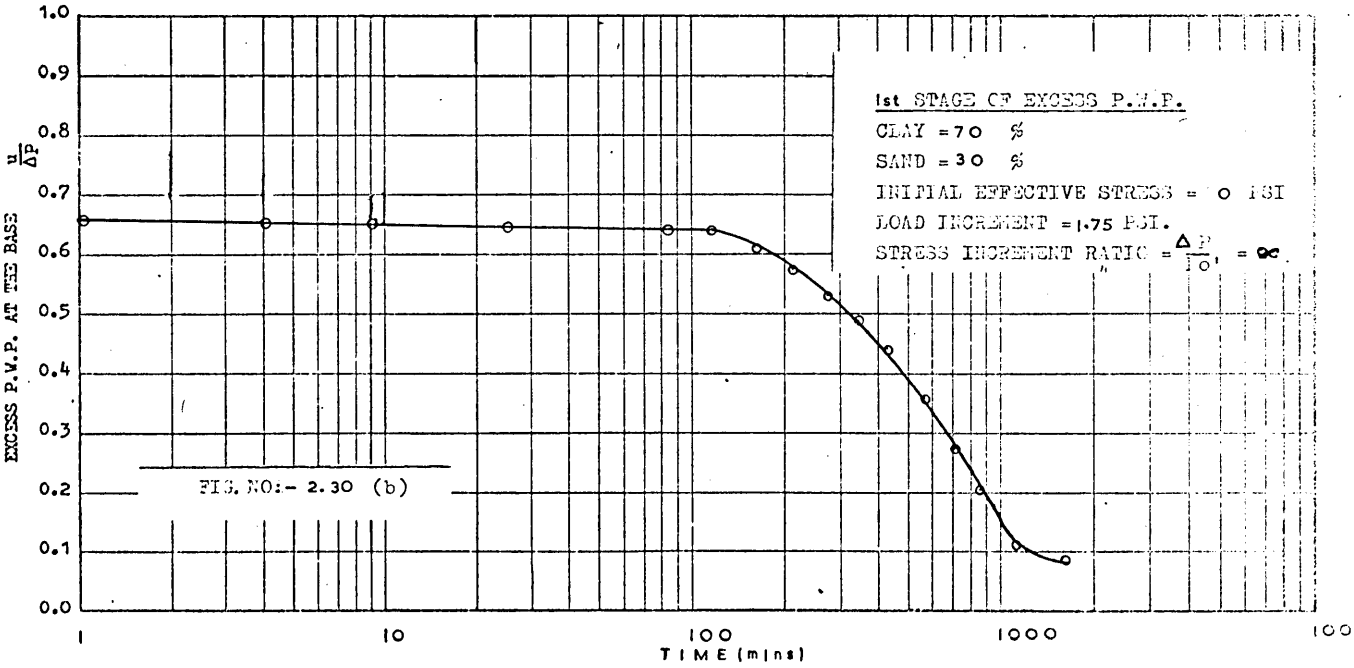

FIG. NO:- 2.30 (b)

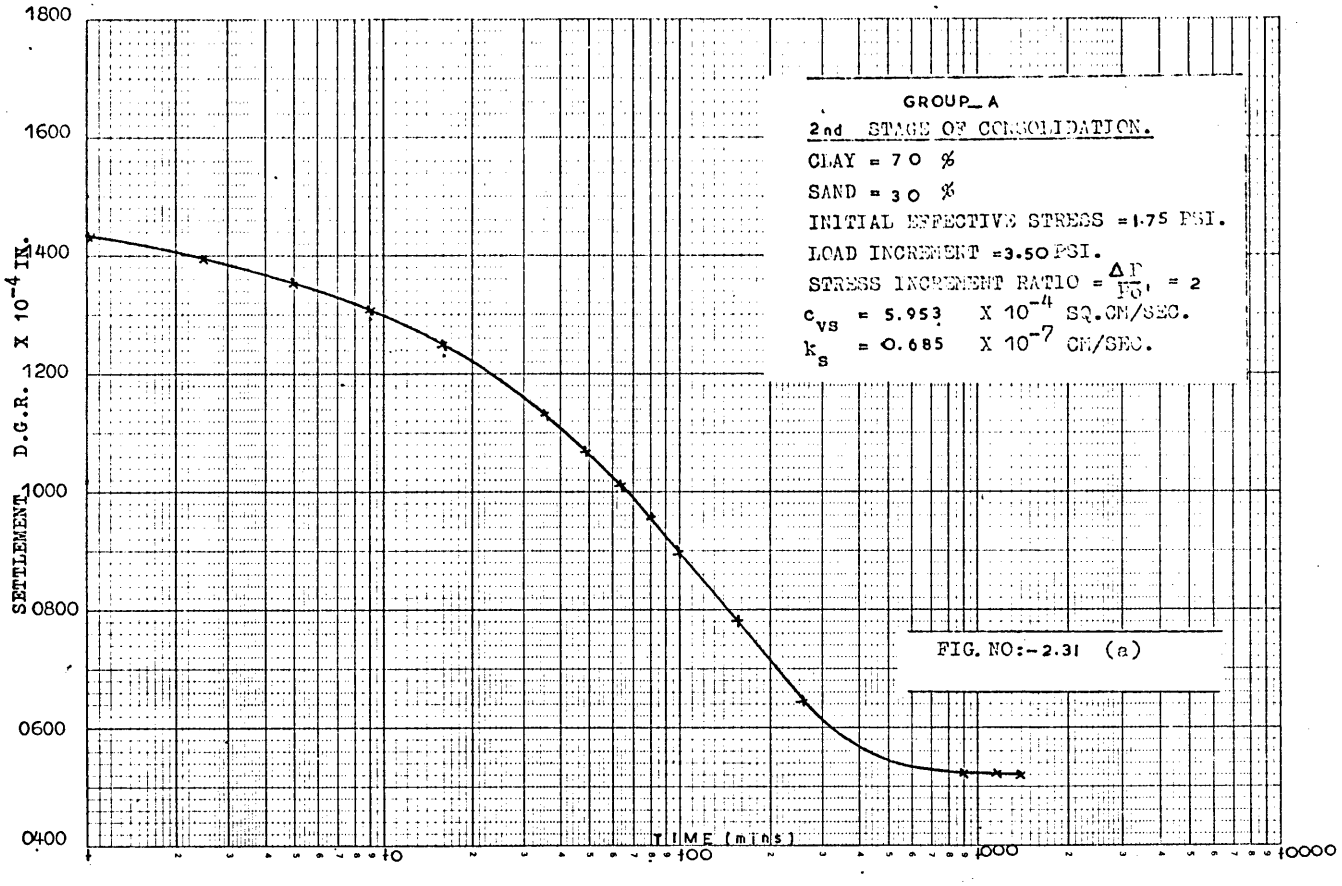

FIG. NO:- 2.31 (a)

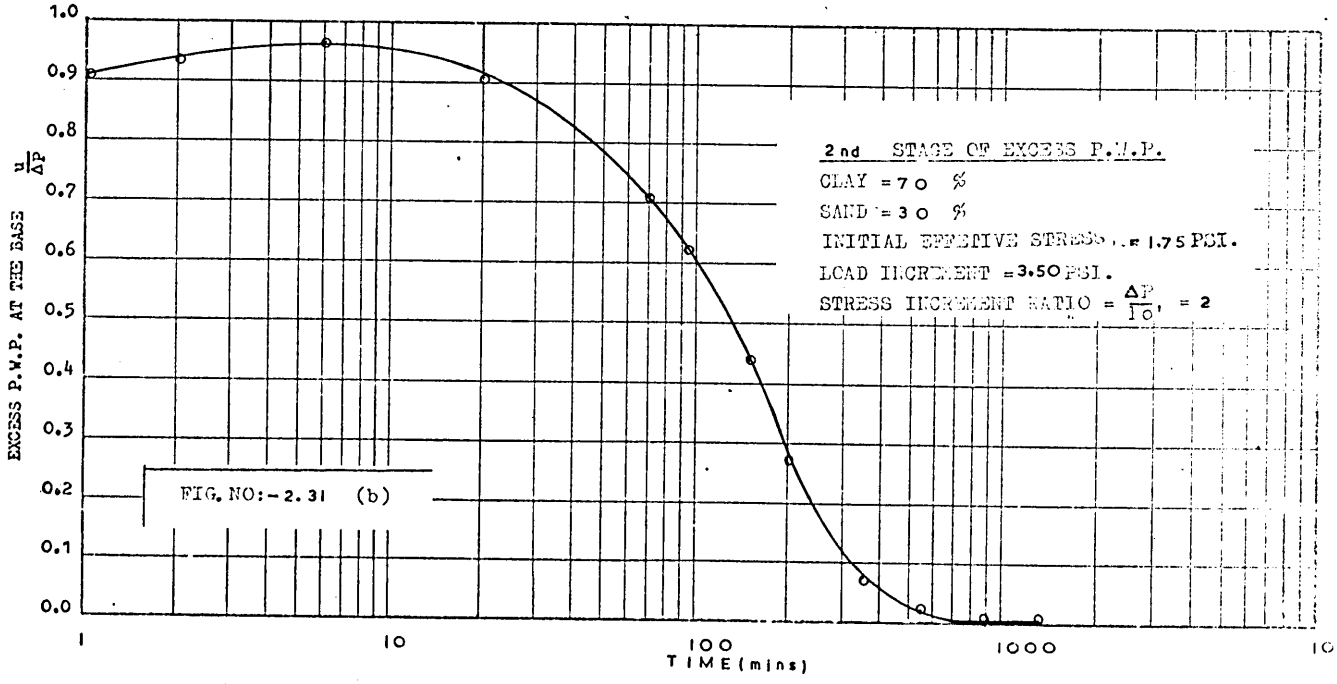

FIG. NO:- 2.31 (b)

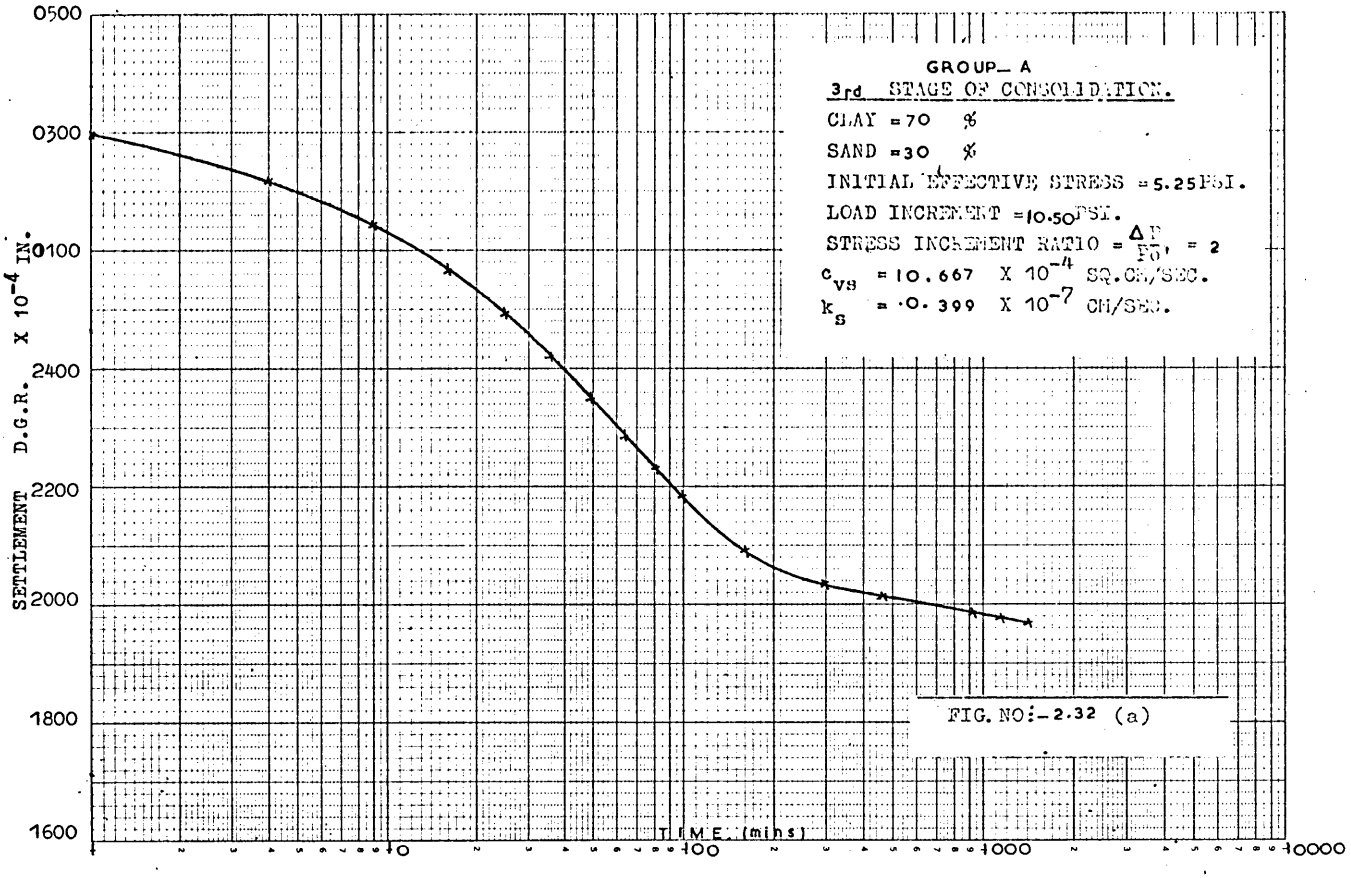

FIG. NO:– 2.32 (a)

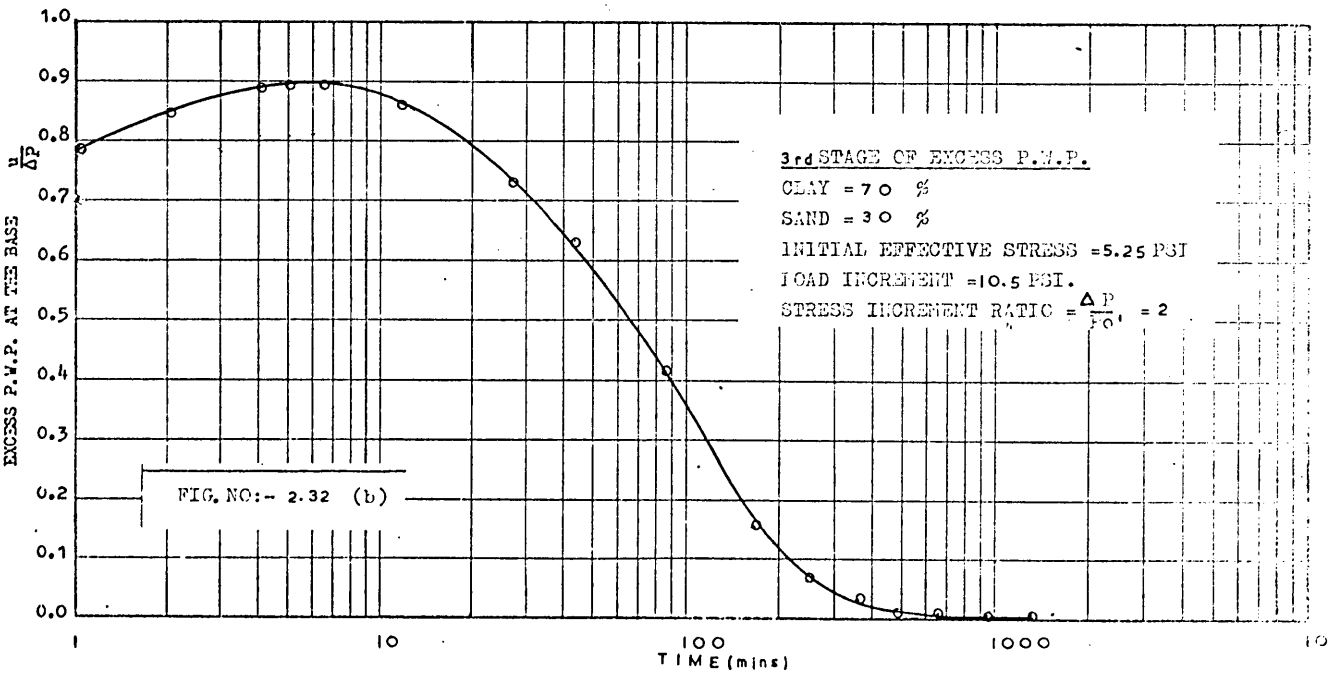

FIG. NO:– 2.32 (b)

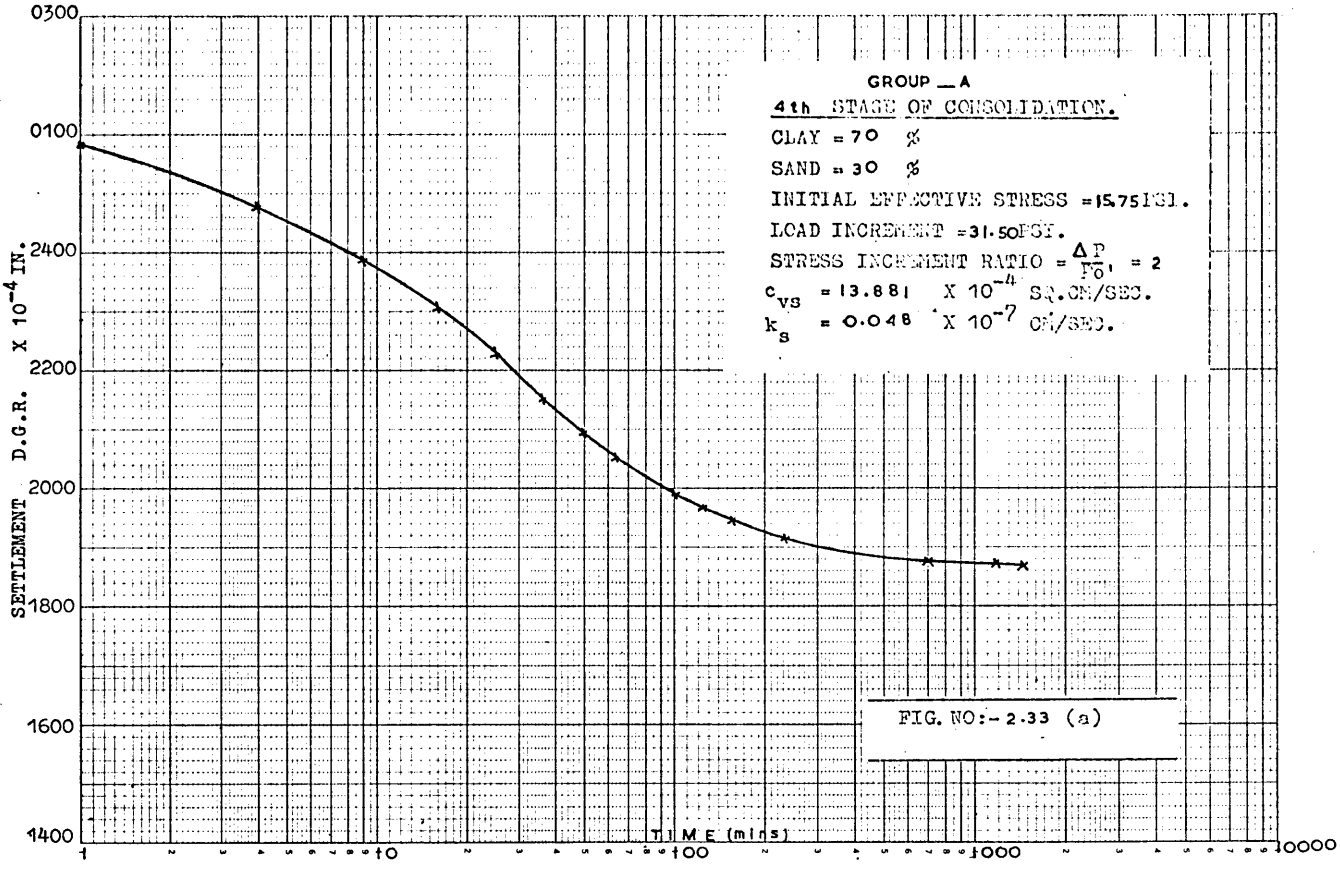

FIG. NO:- 2.33 (a)

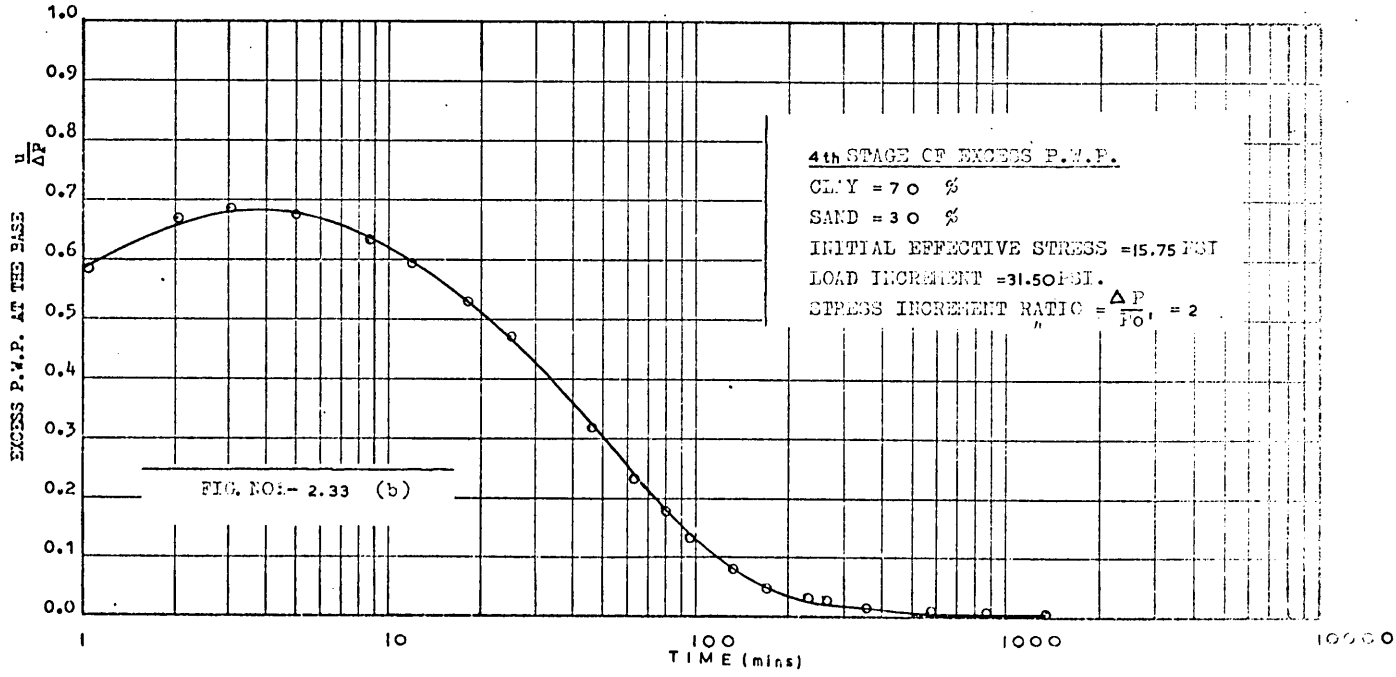

FIG. NO:- 2.33 (b)

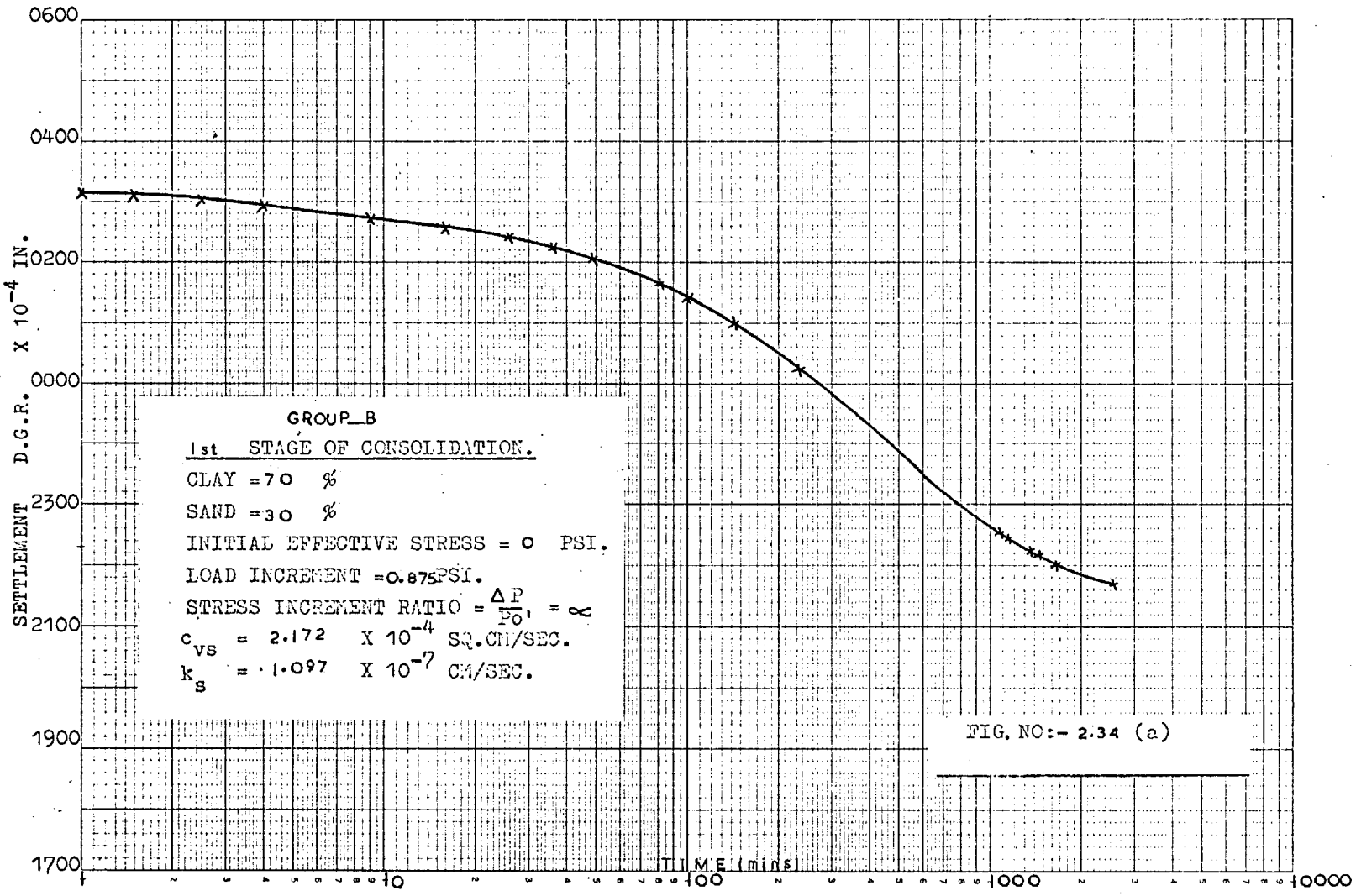
0600
0400
0200
0000
2300
2100
1900
1700
SETTLEMENT D.G.R. X 10^{-4} IN.
GROUP_B
1st STAGE OF CONSOLIDATION.
CLAY =70 %
SAND =30 %
INITIAL EFFECTIVE STRESS = 0 PSI.
LOAD INCREMENT =0.875PSI.
STRESS INCREMENT RATIO = $\frac{\Delta P}{P_0}$ = ∞
c_{vs} = 2.172 X 10^{-4} SQ.CM/SEC.
k_s = 1.097 X 10^{-7} CM/SEC.
TIME (mins)
10
100
1000
10000

FIG. NO:- 2.34 (a)

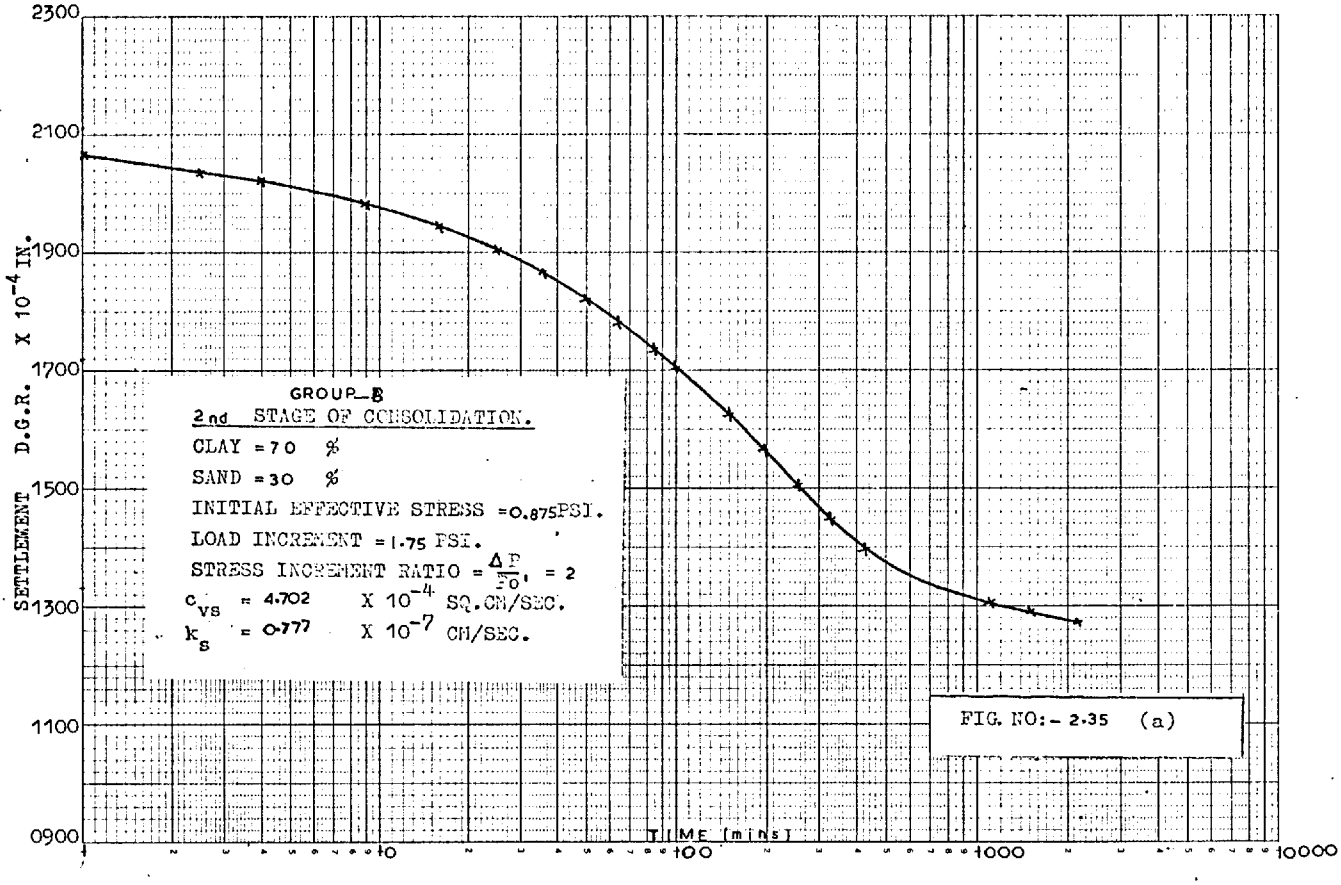

FIG. NO:- 2.35 (a)

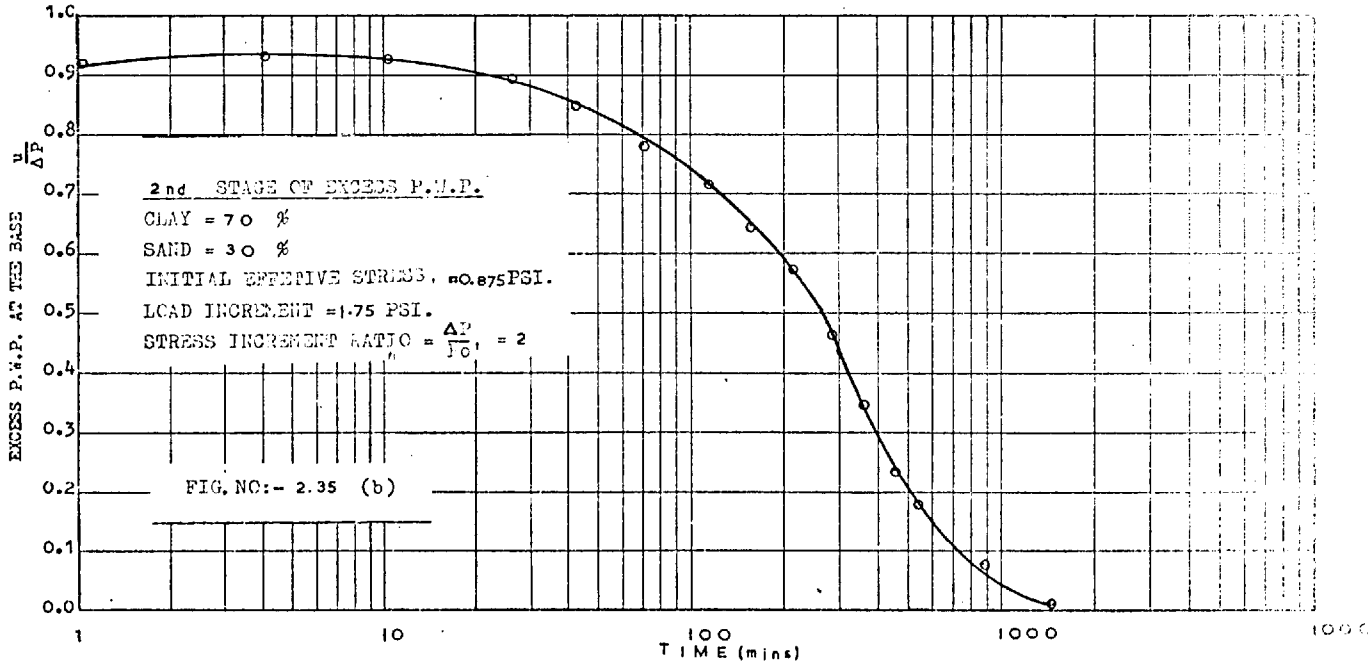

FIG. NO:- 2.35 (b)

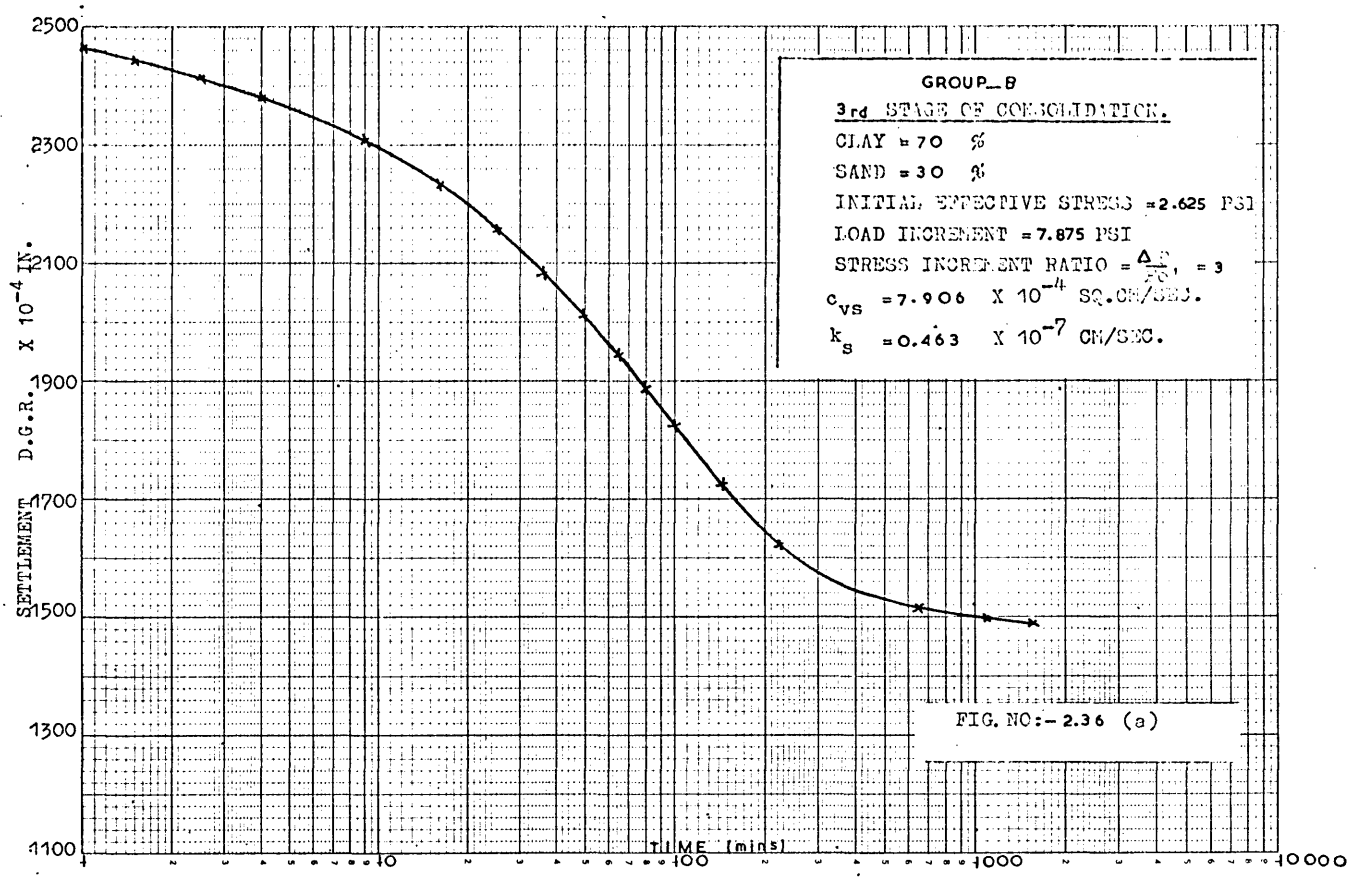

FIG. NO:- 2.36 (a)

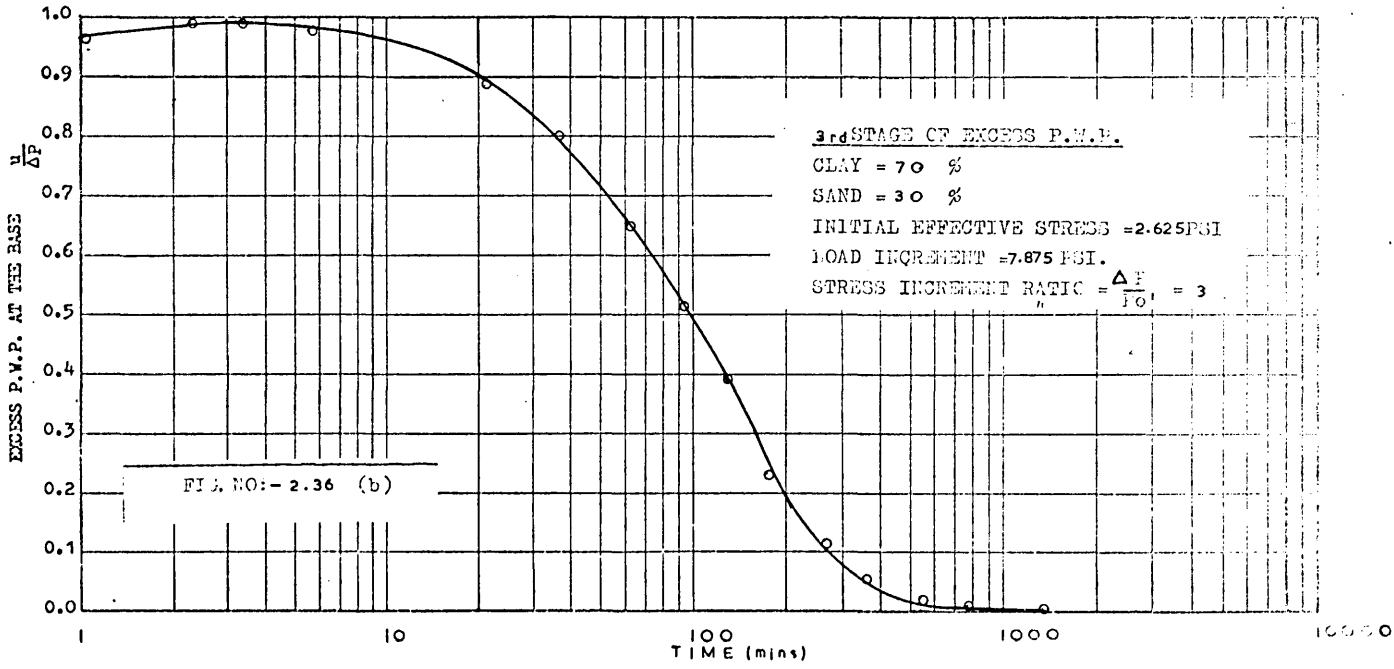

FIG. NO:- 2.36 (b)

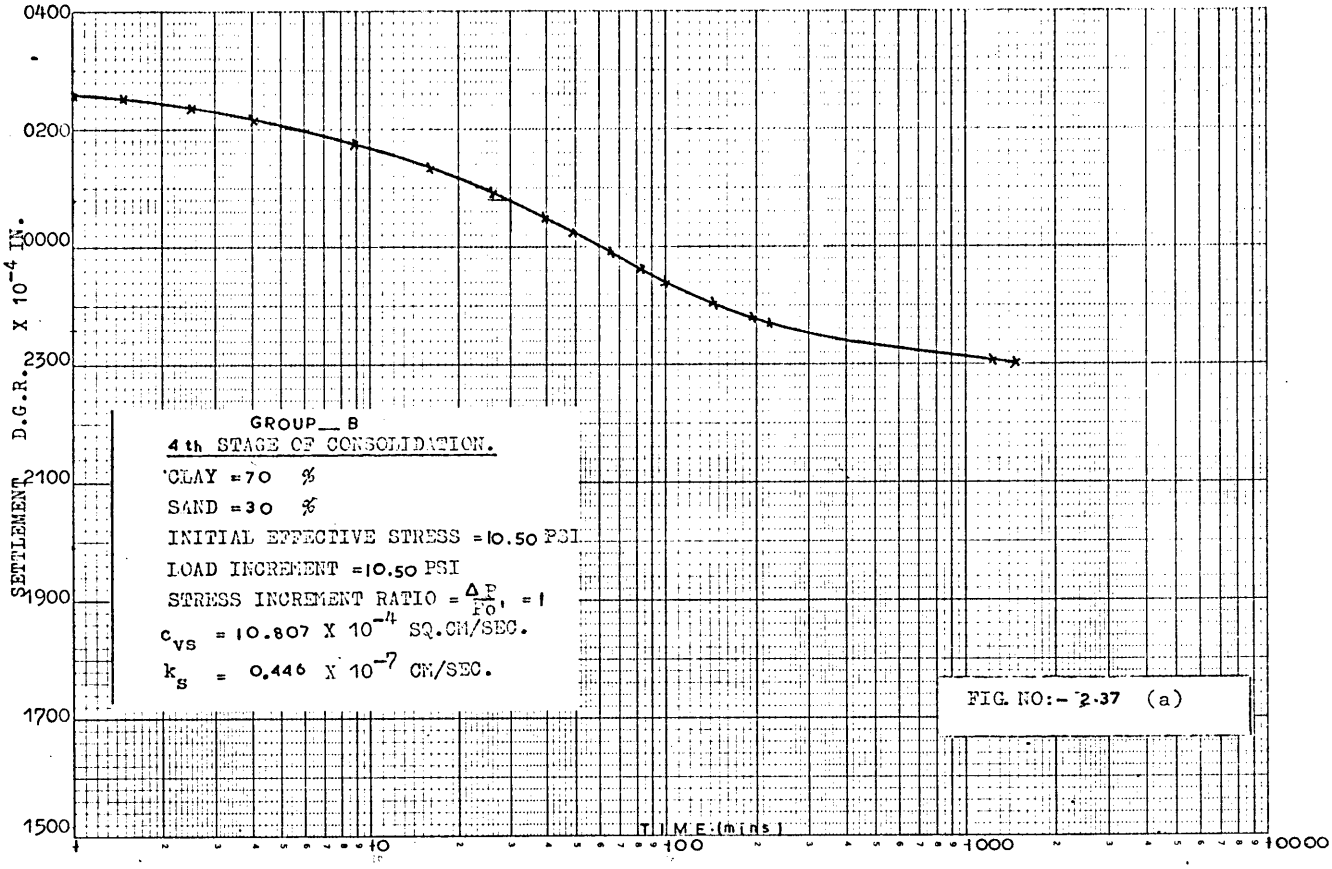
0400
0200
0000
2300
2100
1900
1700
1500
SETTLEMENT D.G.R. X 10^{-4} IN.
TIME (mins)
10
100
1000
10000
GROUP__ B
4th STAGE OF CONSOLIDATION.
CLAY = 70 %
SAND = 30 %
INITIAL EFFECTIVE STRESS = 10.50 PSI
LOAD INCREMENT = 10.50 PSI
STRESS INCREMENT RATIO = $\frac{\Delta P}{P_0}$ = 1
c_{vs} = 10.807 X 10^{-4} SQ.CM/SEC.
k_s = 0.446 X 10^{-7} CM/SEC.
FIG. NO:- 2.37 (a)

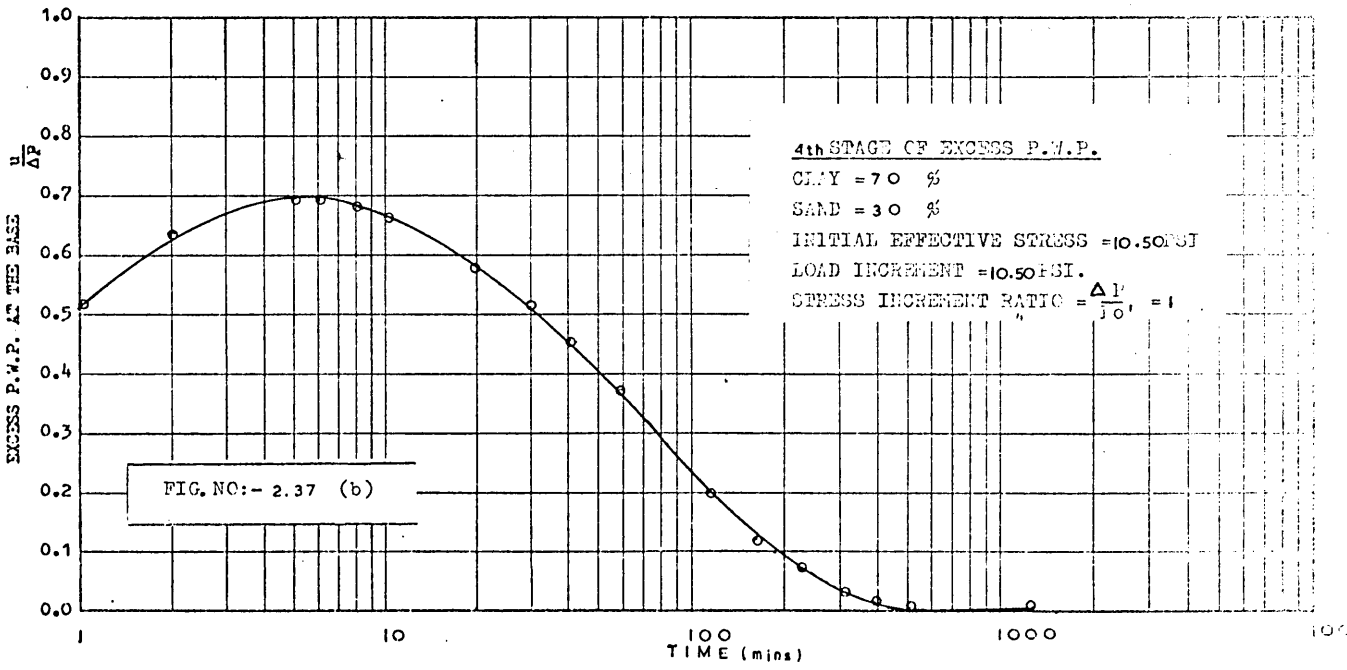
1.0
0.9
0.8
0.7
0.6
0.5
0.4
0.3
0.2
0.1
0.0
EXCESS P.W.P. AT THE BASE $\frac{u}{\Delta P}$
TIME (mins)
1
10
100
1000
4th STAGE OF EXCESS P.W.P.
CLAY = 70 %
SAND = 30 %
INITIAL EFFECTIVE STRESS = 10.50 PSI
LOAD INCREMENT = 10.50 PSI.
STRESS INCREMENT RATIO = $\frac{\Delta P}{P_0}$ = 1
FIG. NO:- 2.37 (b)

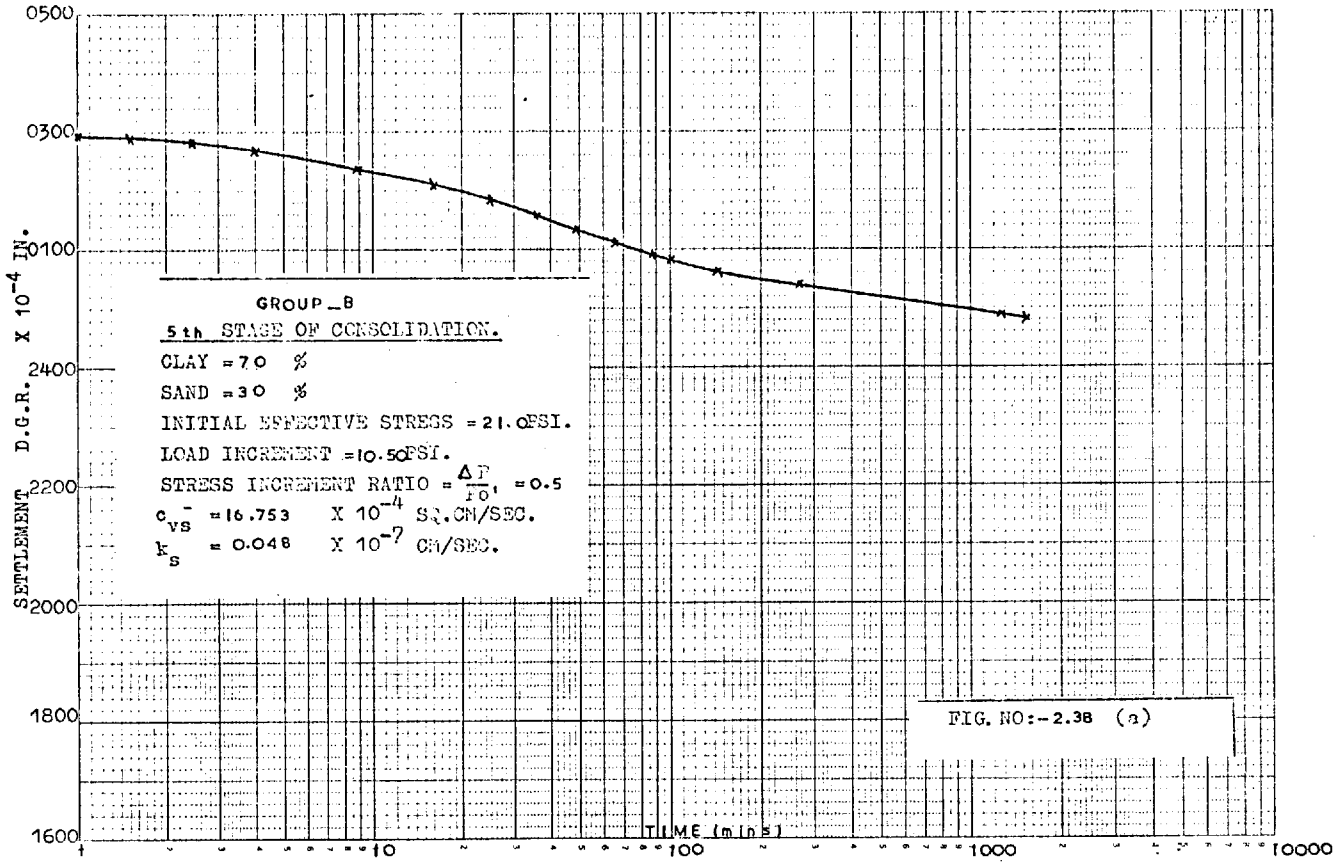

FIG. NO:- 2.38 (a)

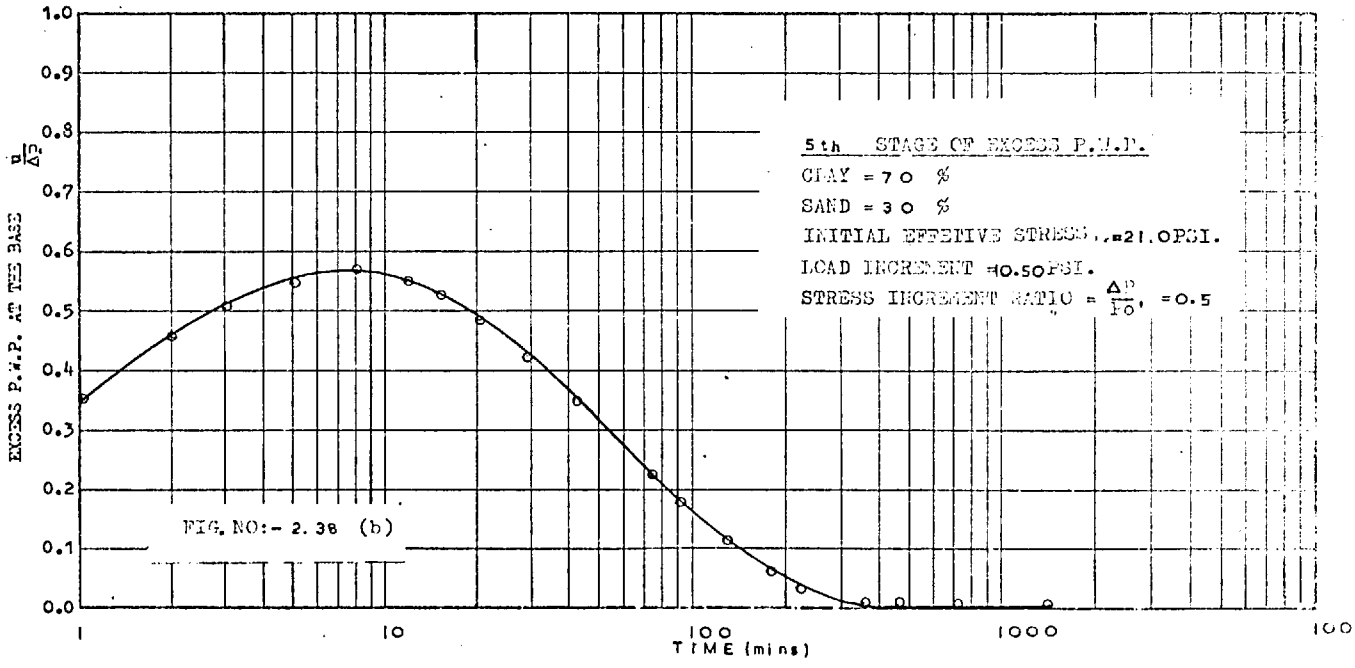

FIG. NO:- 2.38 (b)

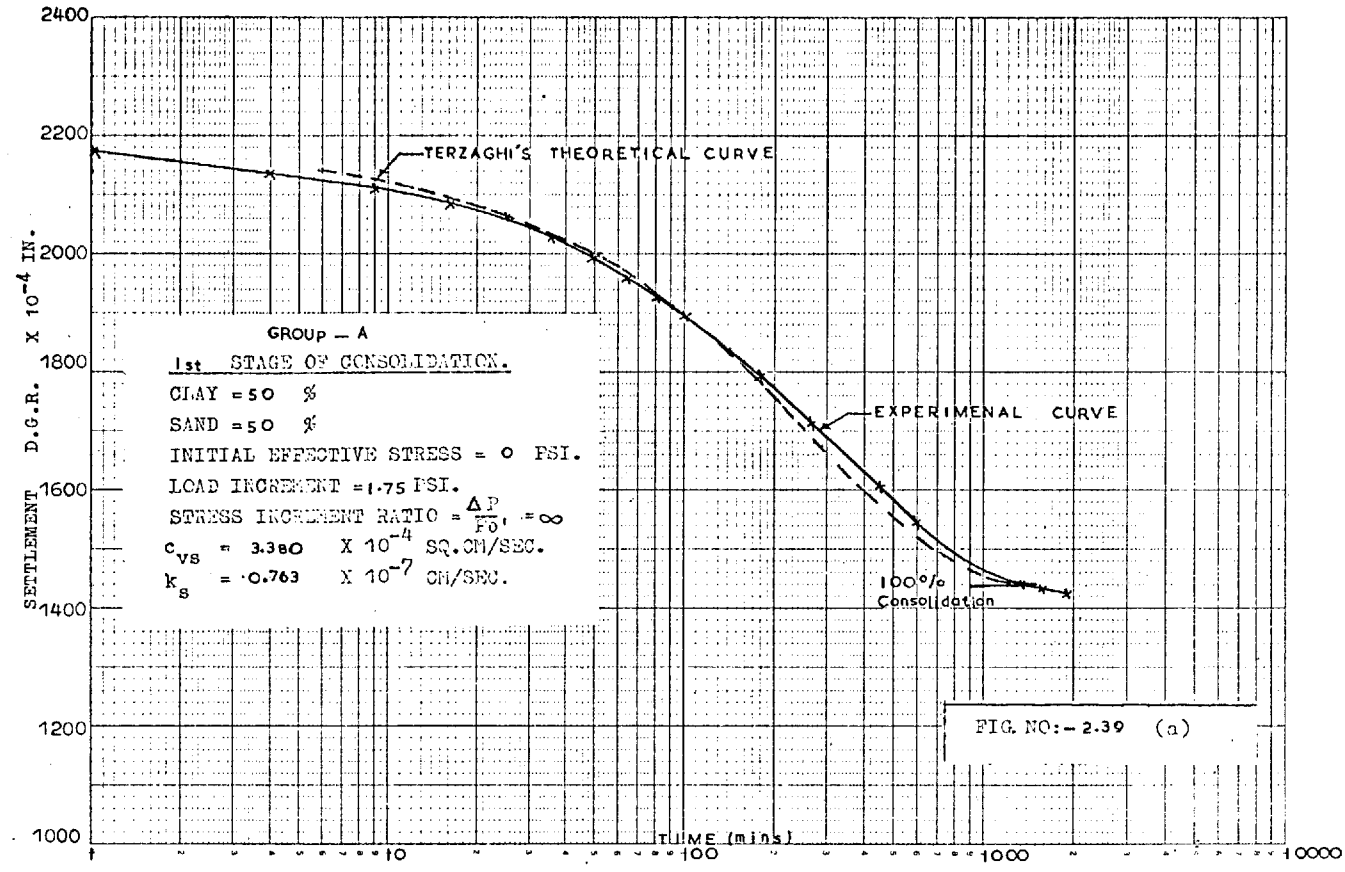

FIG. NO:- 2.39 (a)

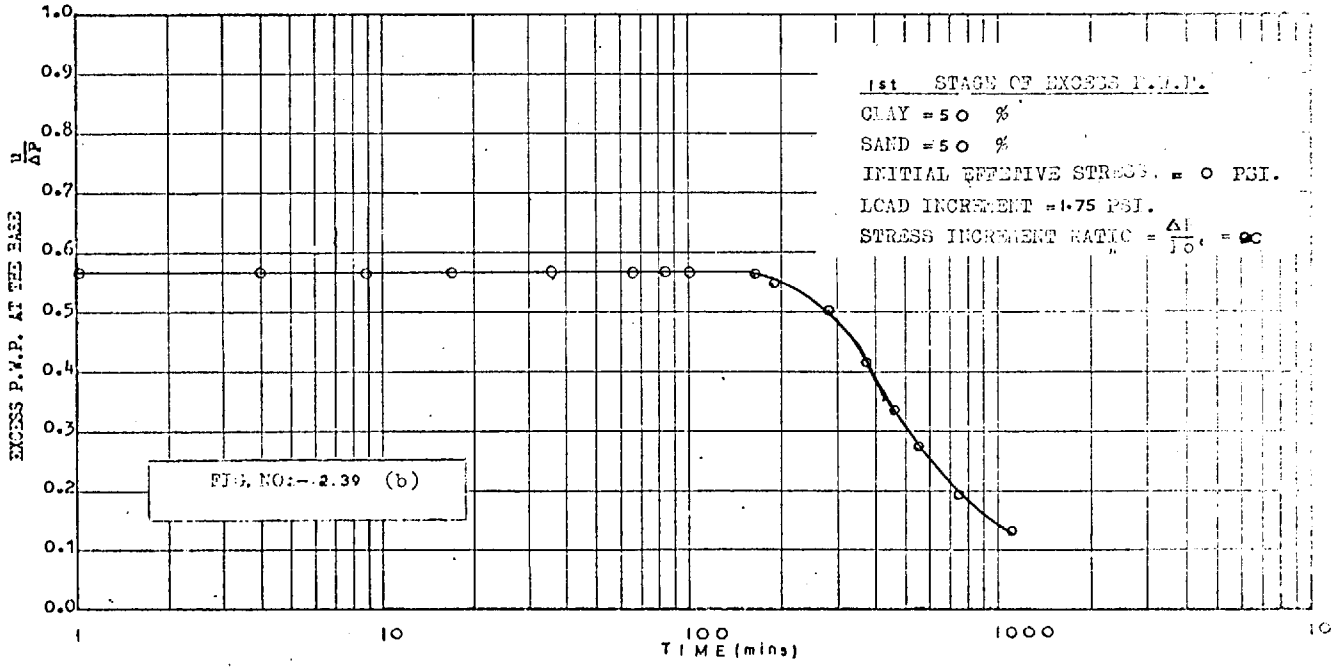

FIG. NO:- 2.39 (b)

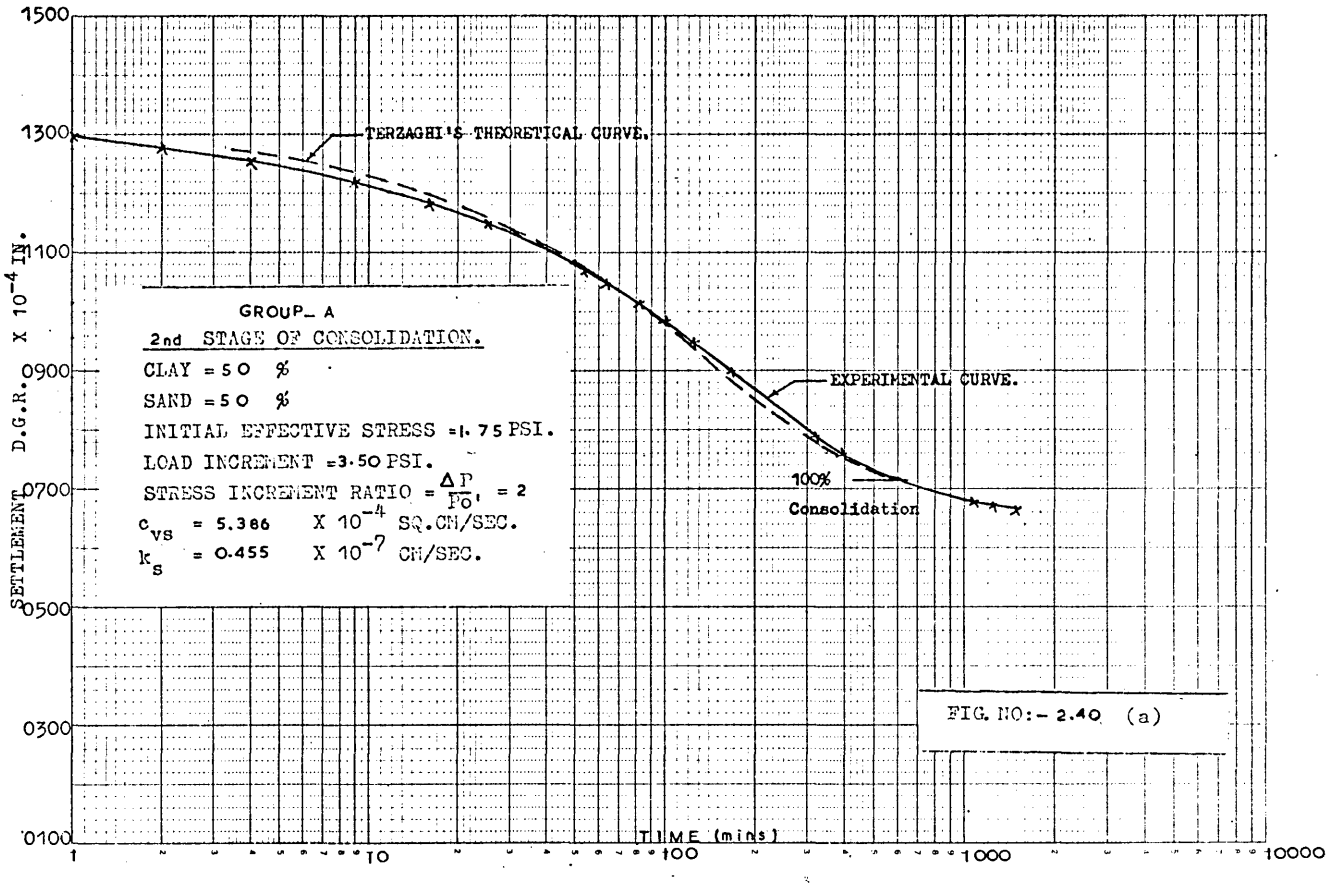

FIG. NO:- 2.40 (a)

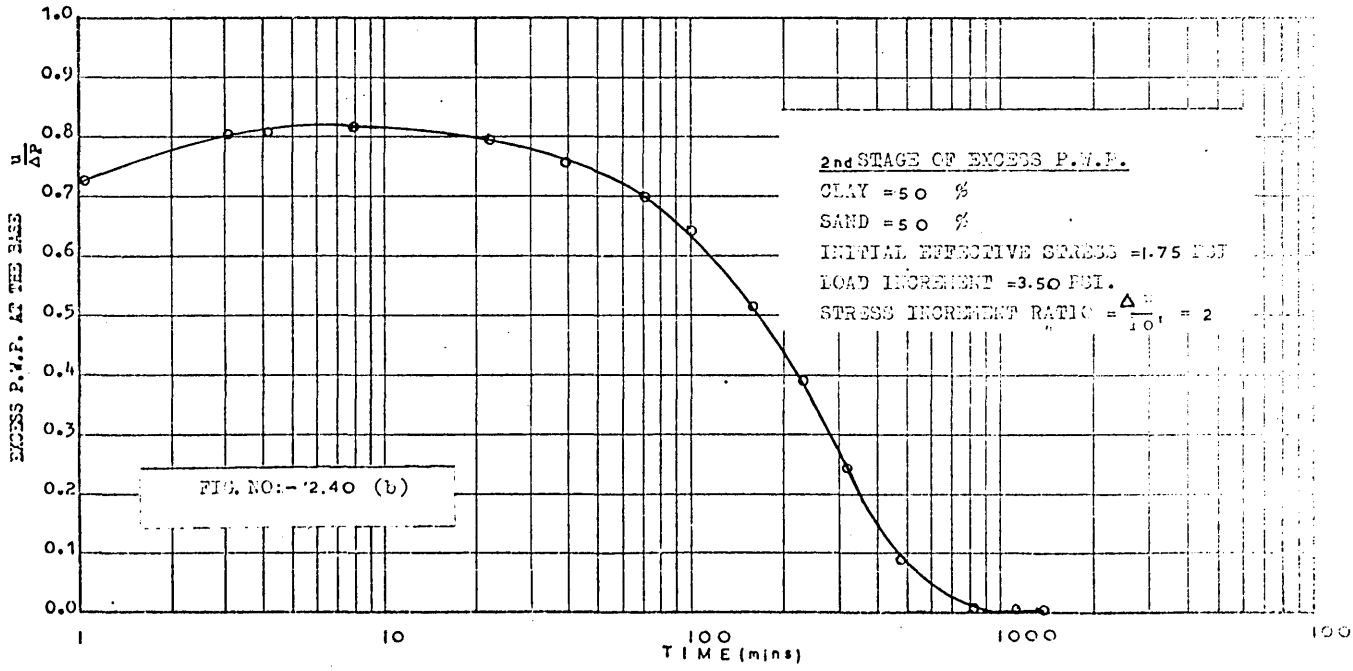

FIG. NO:- 2.40 (b)

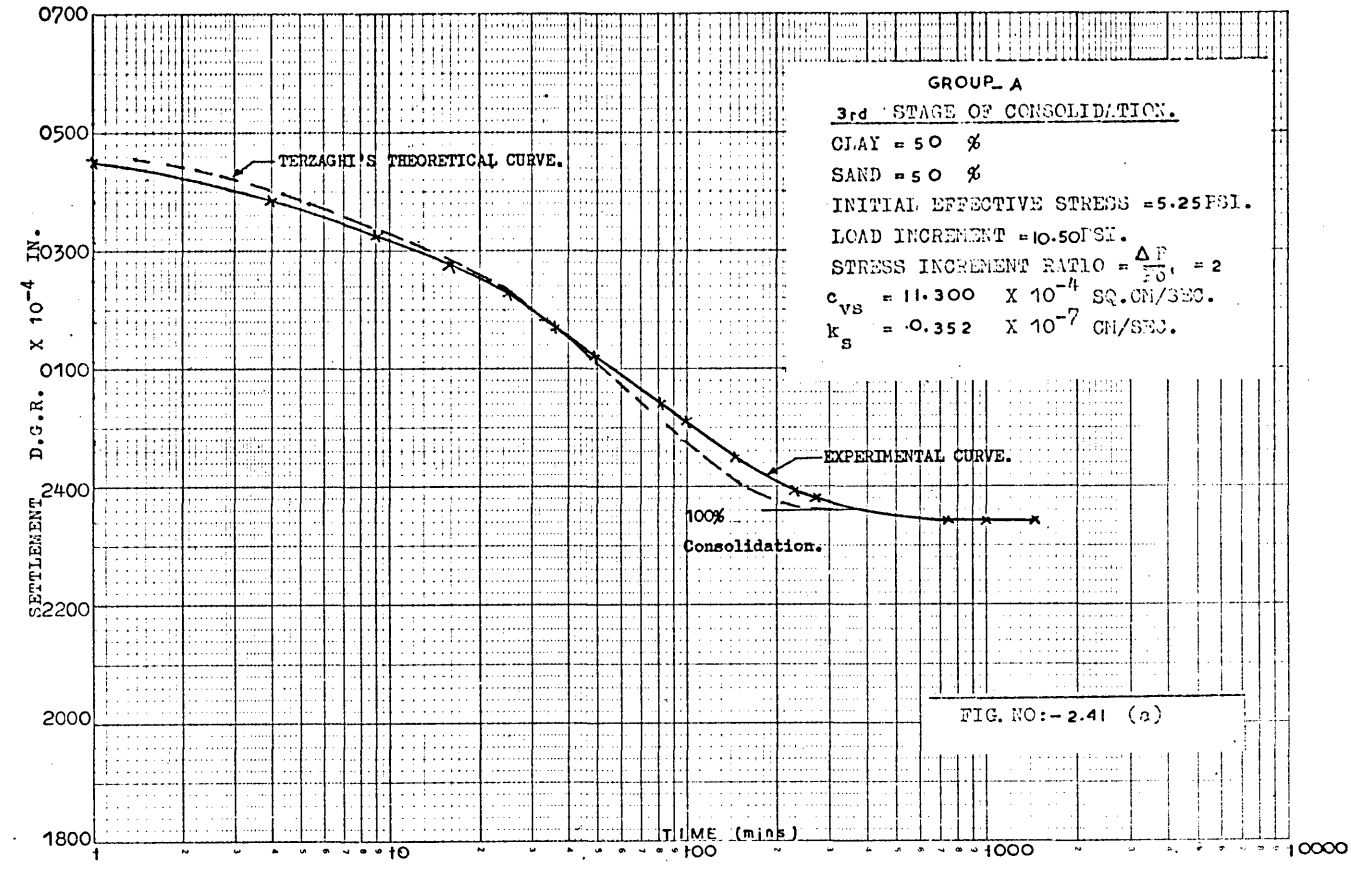

FIG. NO:- 2.41 (a)

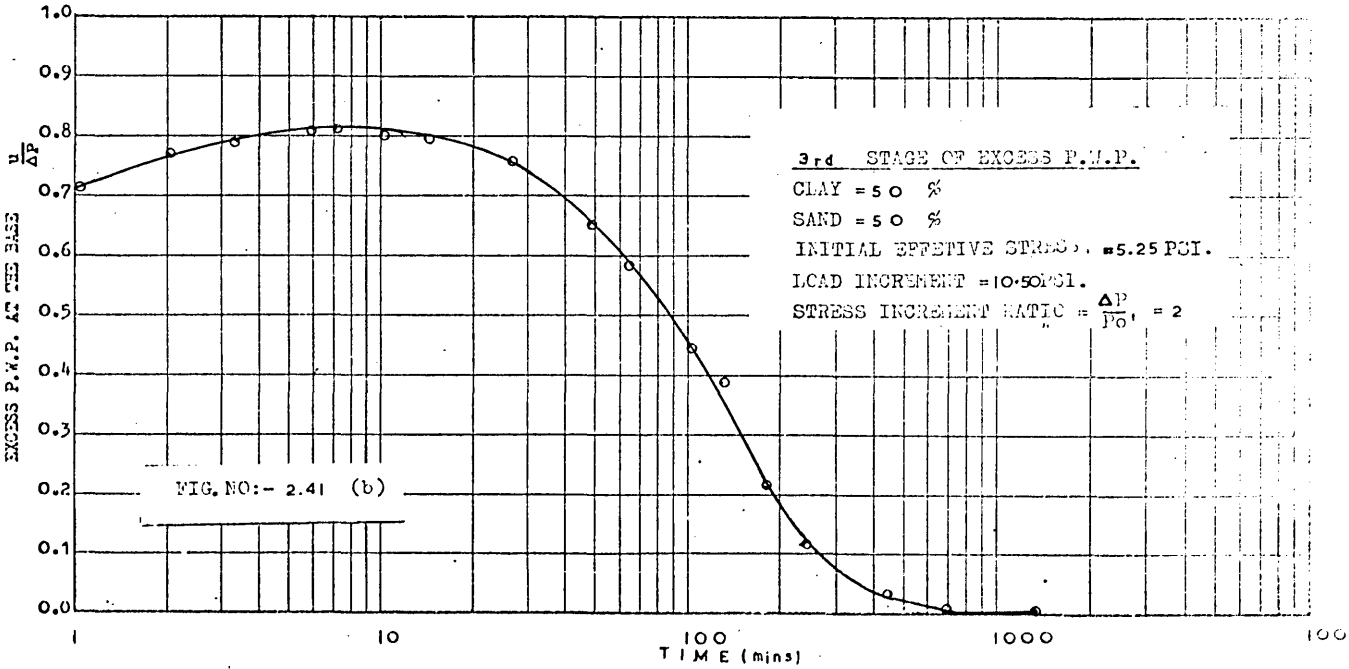

FIG. NO:- 2.41 (b)

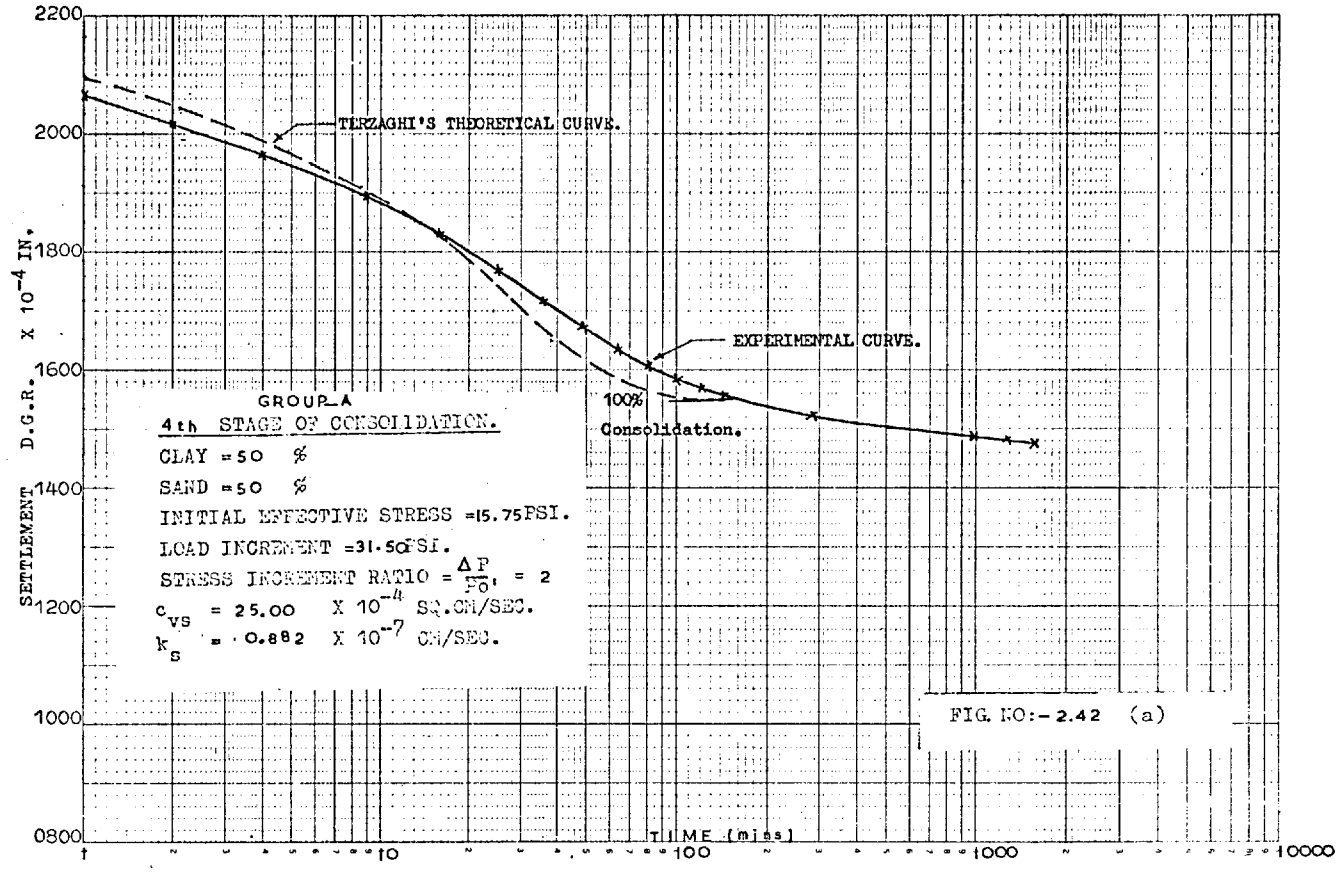

FIG. NO:- 2.42 (a)

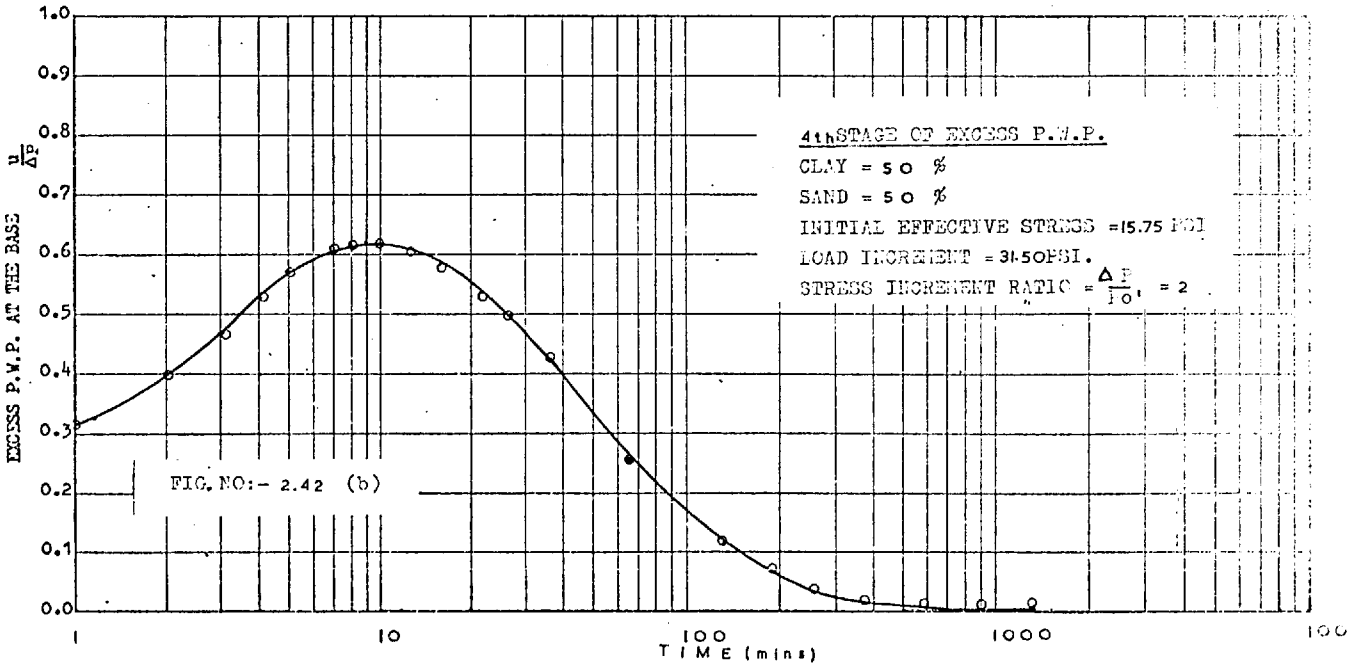

FIG. NO:- 2.42 (b)

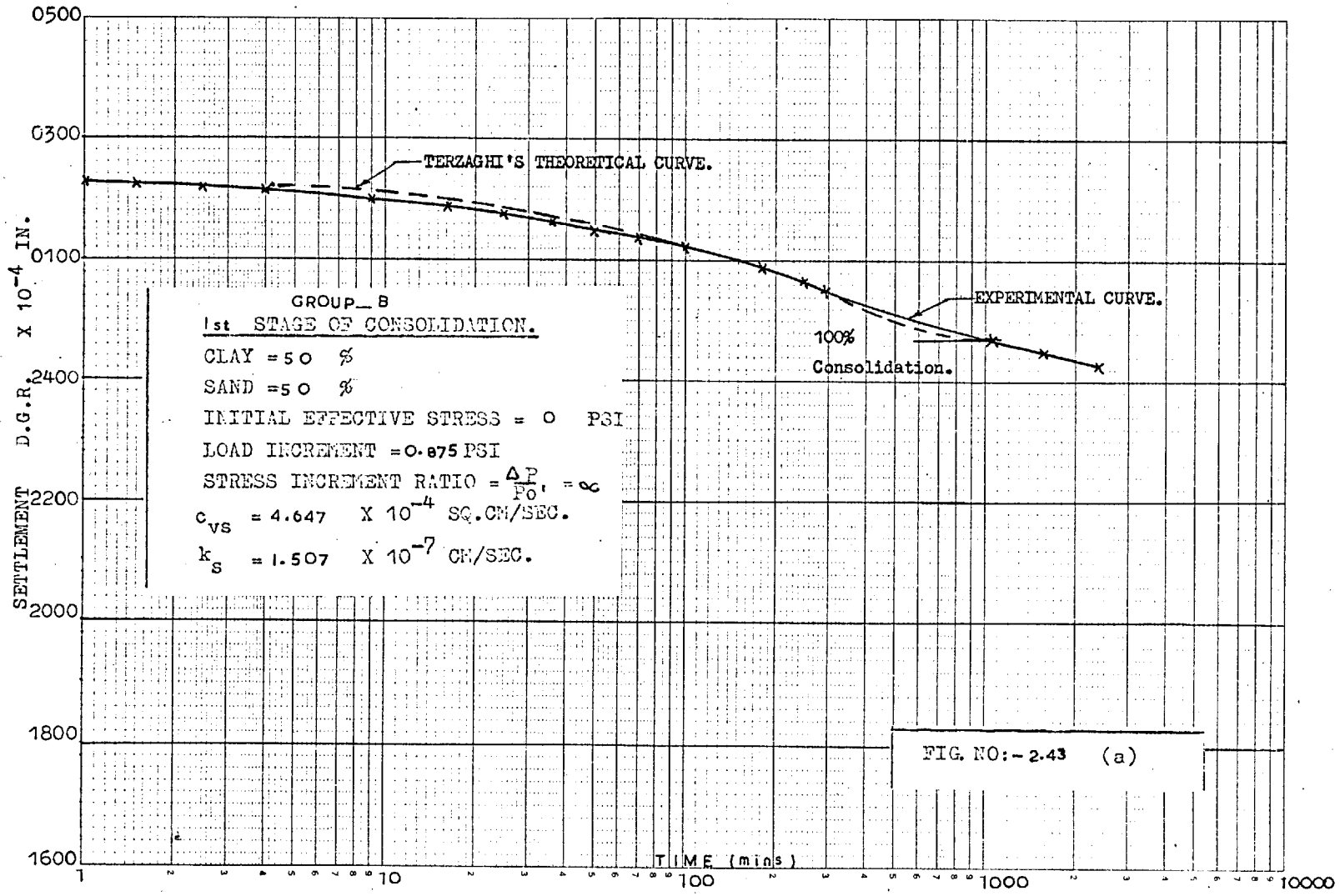
0500
0300
0100
2400
2200
2000
1800
1600
SETTLEMENT D.G.R. X 10^{-4} IN.
TERZAGHI'S THEORETICAL CURVE.
EXPERIMENTAL CURVE.
100% Consolidation.
GROUP_B
1st STAGE OF CONSOLIDATION.
CLAY = 50 %
SAND = 50 %
INITIAL EFFECTIVE STRESS = 0 PSI
LOAD INCREMENT = 0.875 PSI
STRESS INCREMENT RATIO = $\frac{\Delta P}{Po}$ = ∞
c_{vs} = 4.647 X 10^{-4} SQ.CM/SEC.
k_s = 1.507 X 10^{-7} CM/SEC.
1
10
100
1000
10000
TIME (mins)

FIG. NO:- 2.43 (a)

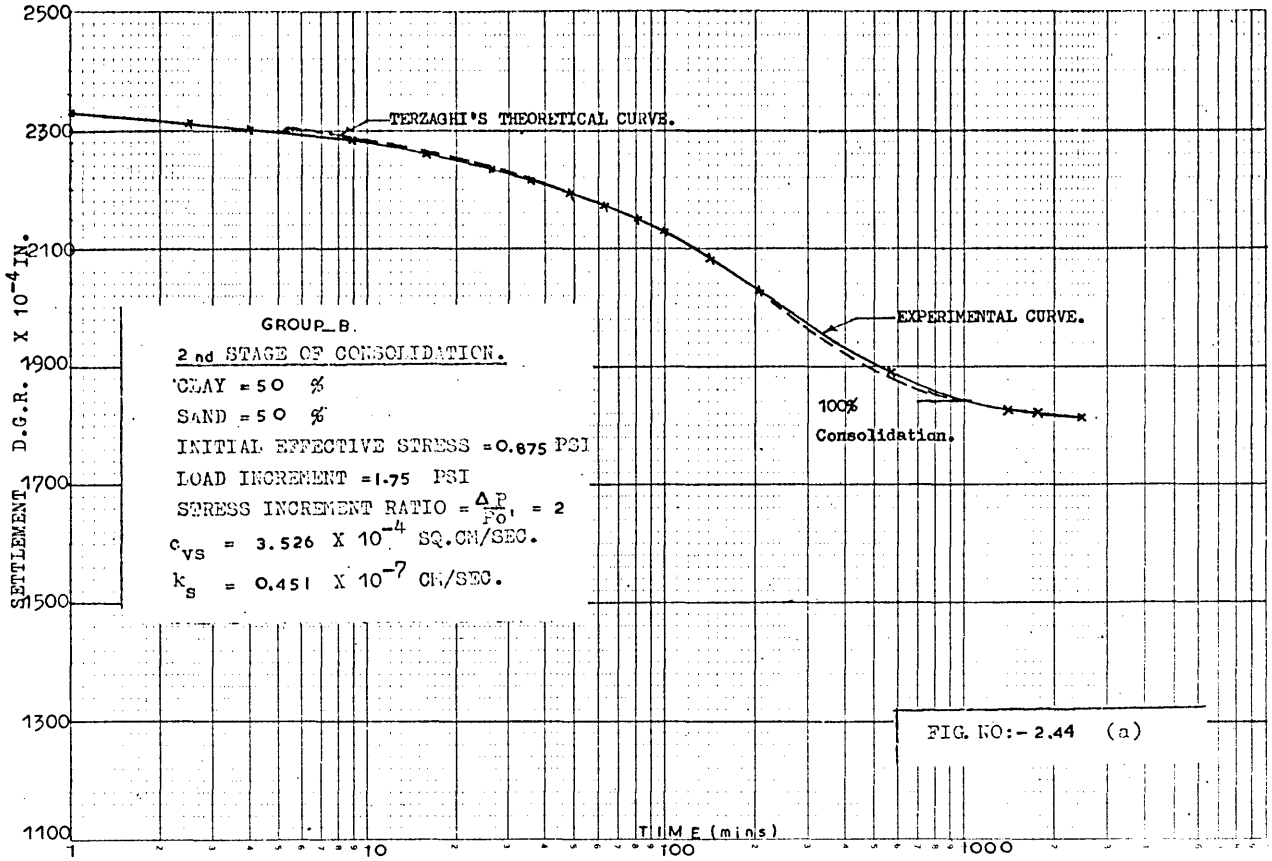

FIG. NO:- 2.44 (a)

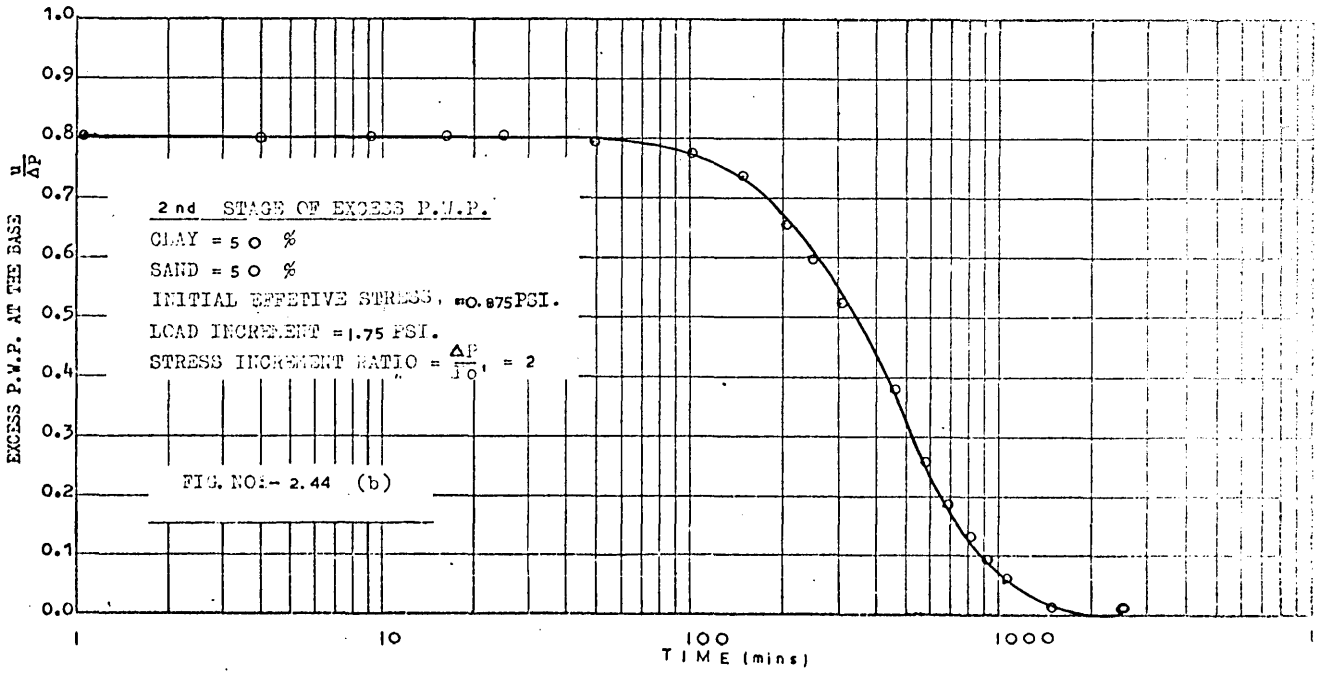

FIG. NO:- 2.44 (b)

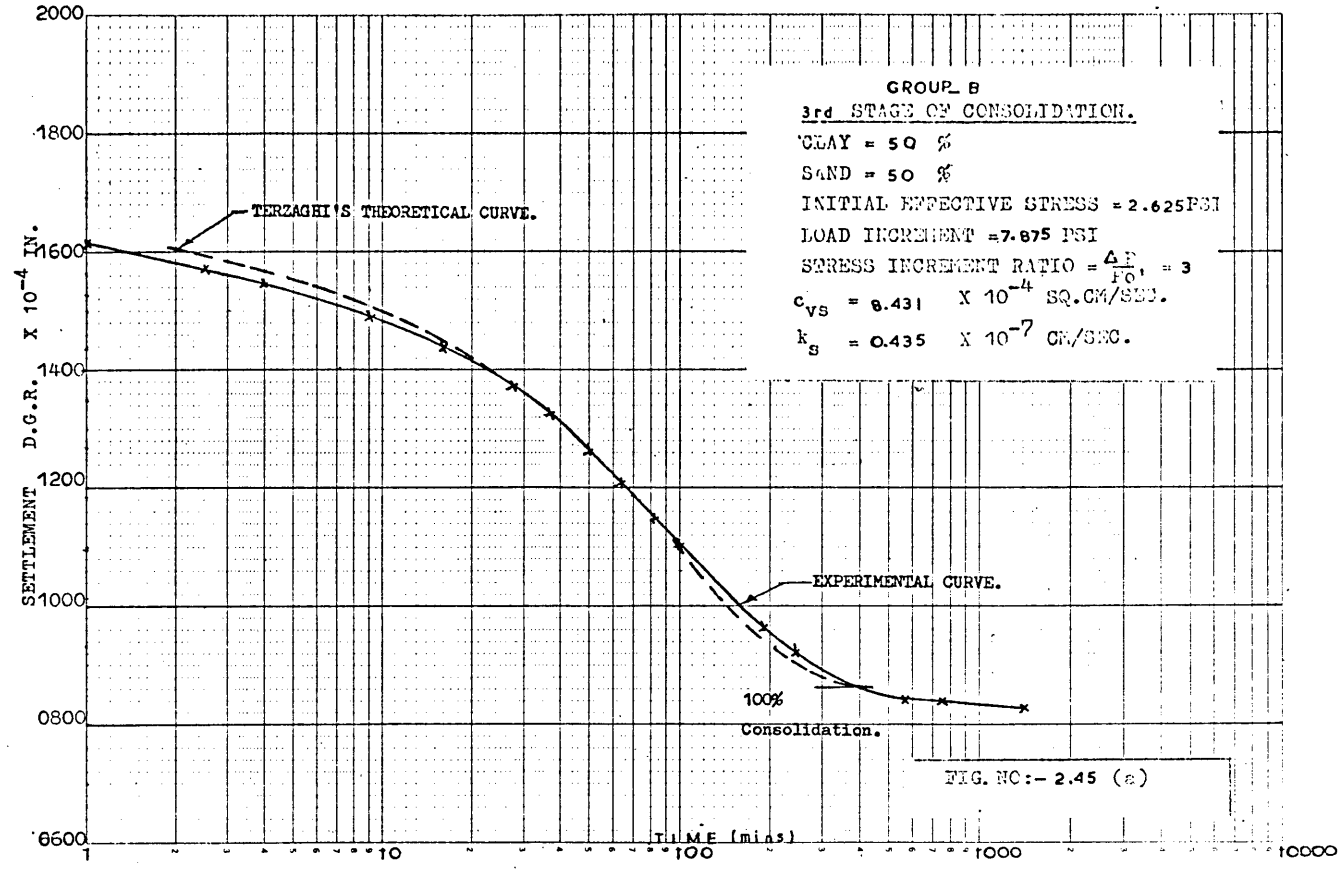

FIG. NO:- 2.45 (a)

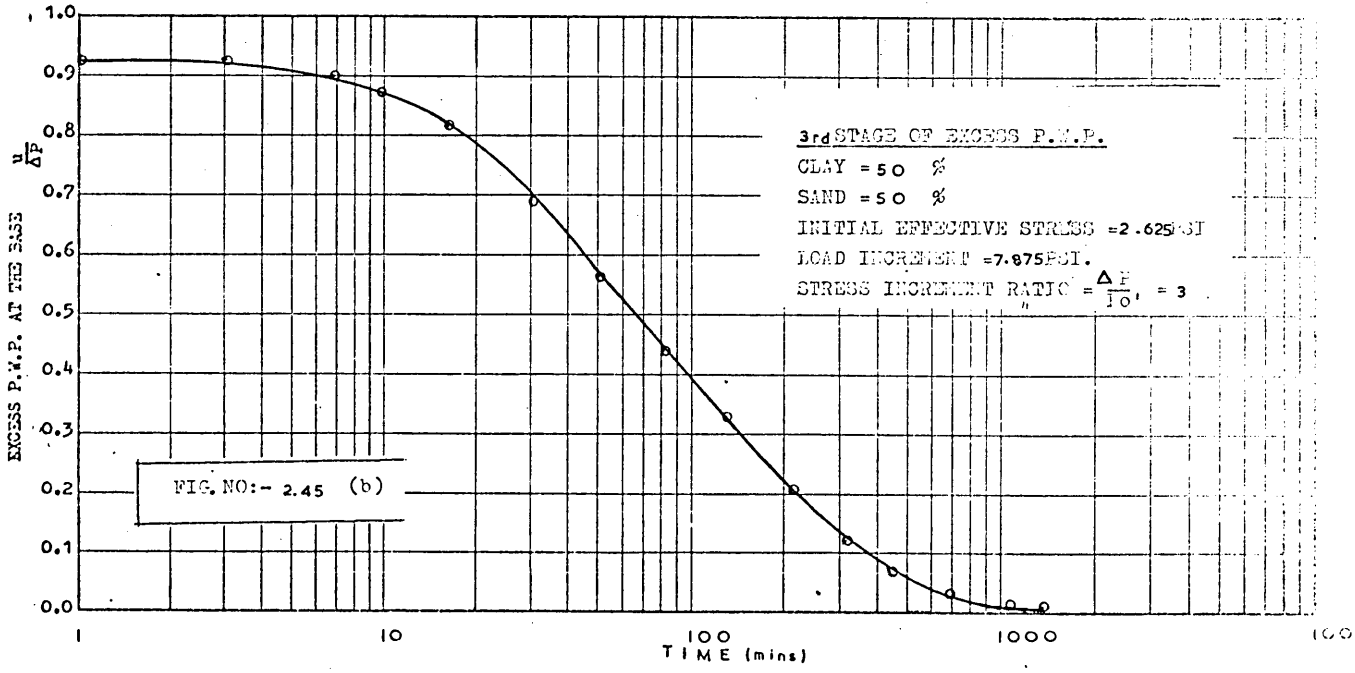

FIG. NO:- 2.45 (b)

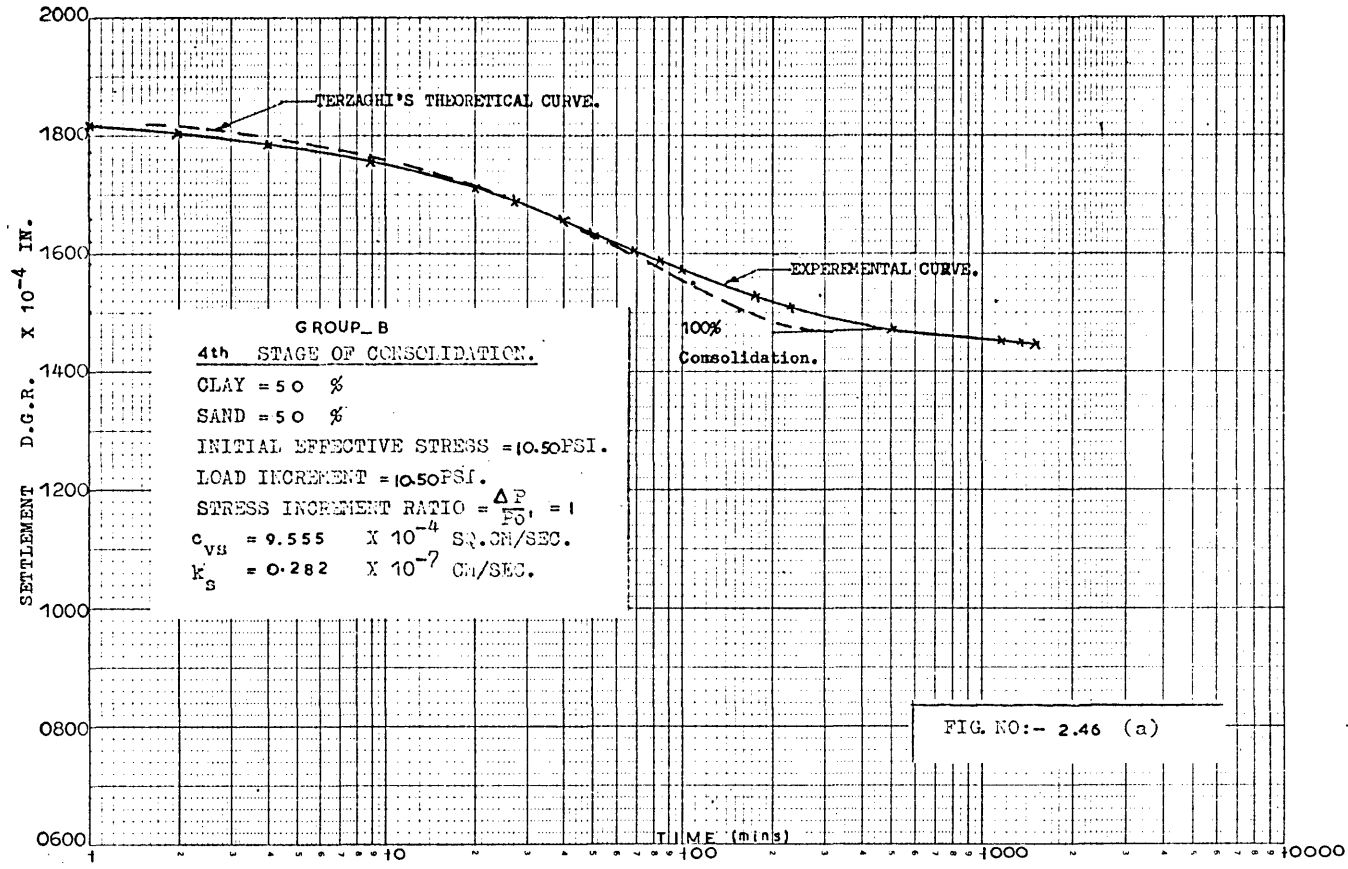

FIG. NO:- 2.46 (a)

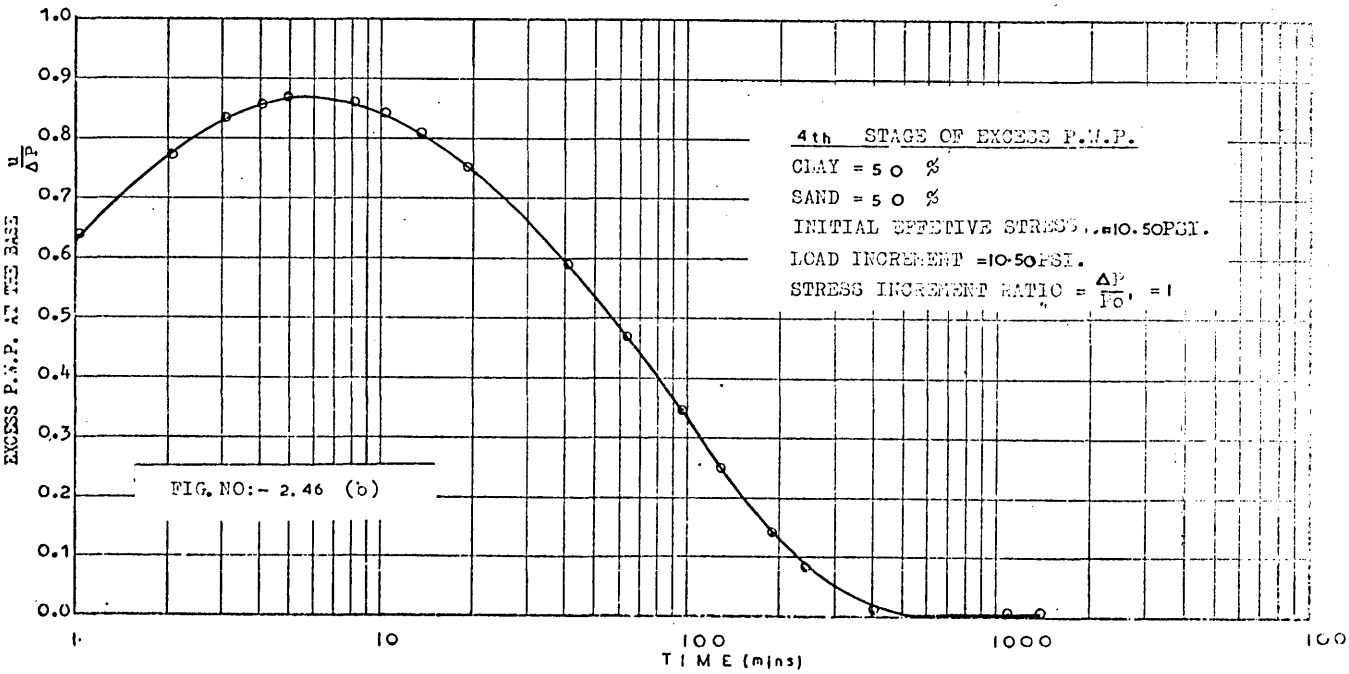

FIG. NO:- 2.46 (b)

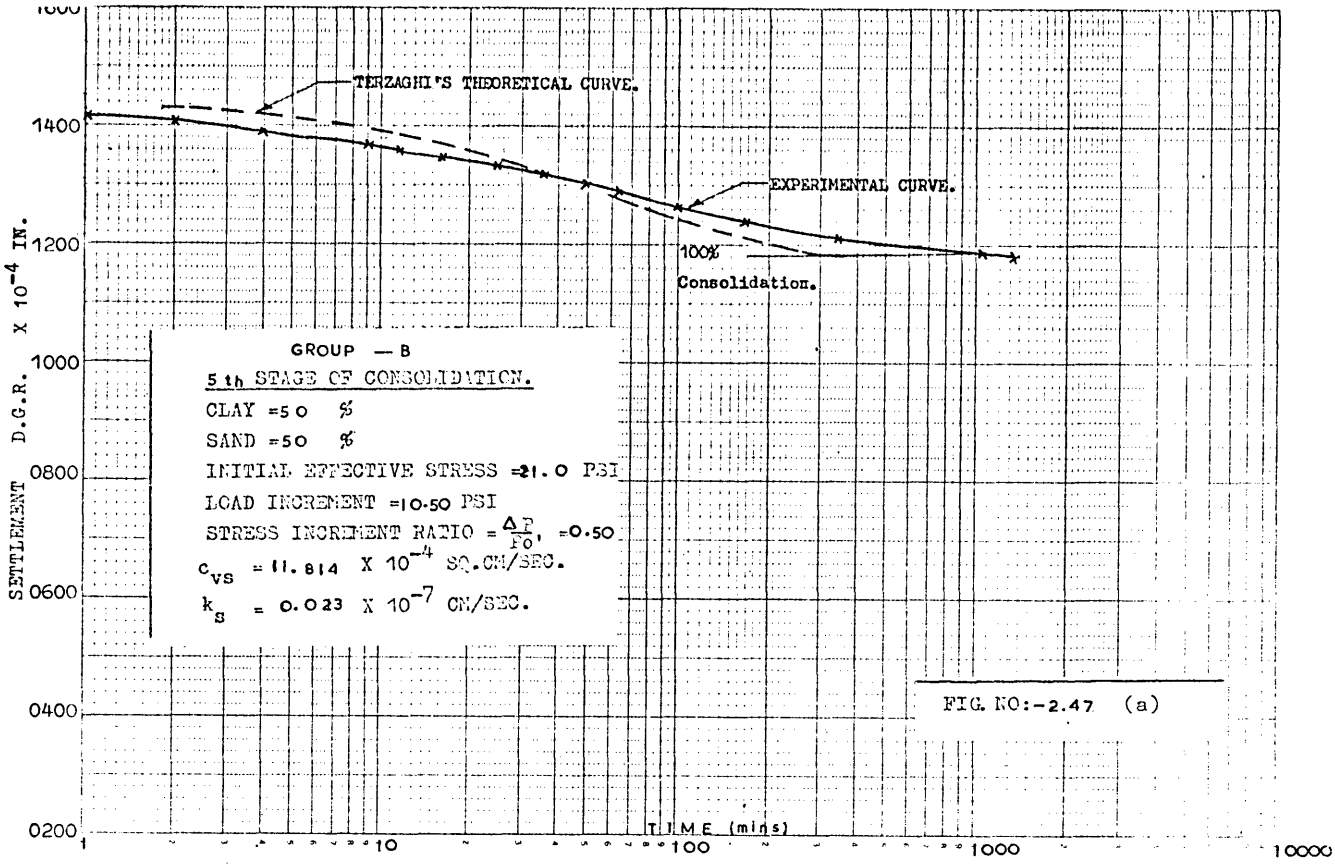

FIG. NO:-2.47 (a)

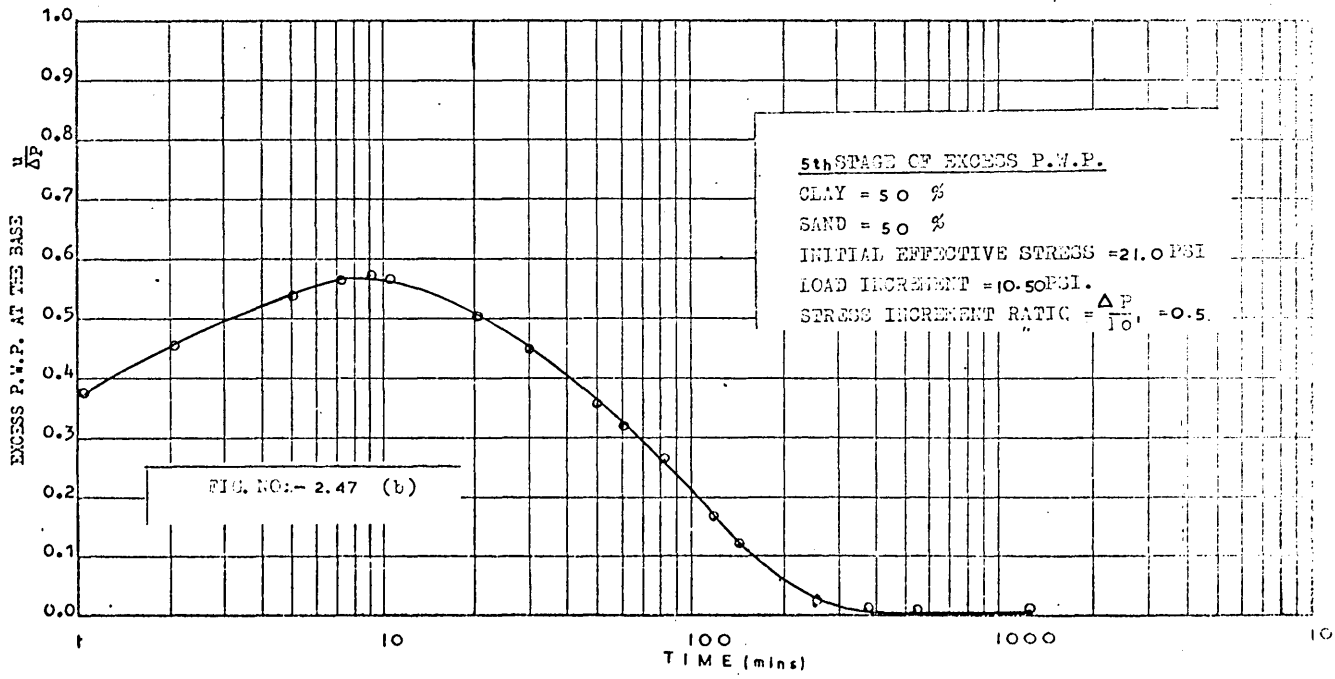

FIG. NO:- 2.47 (b)

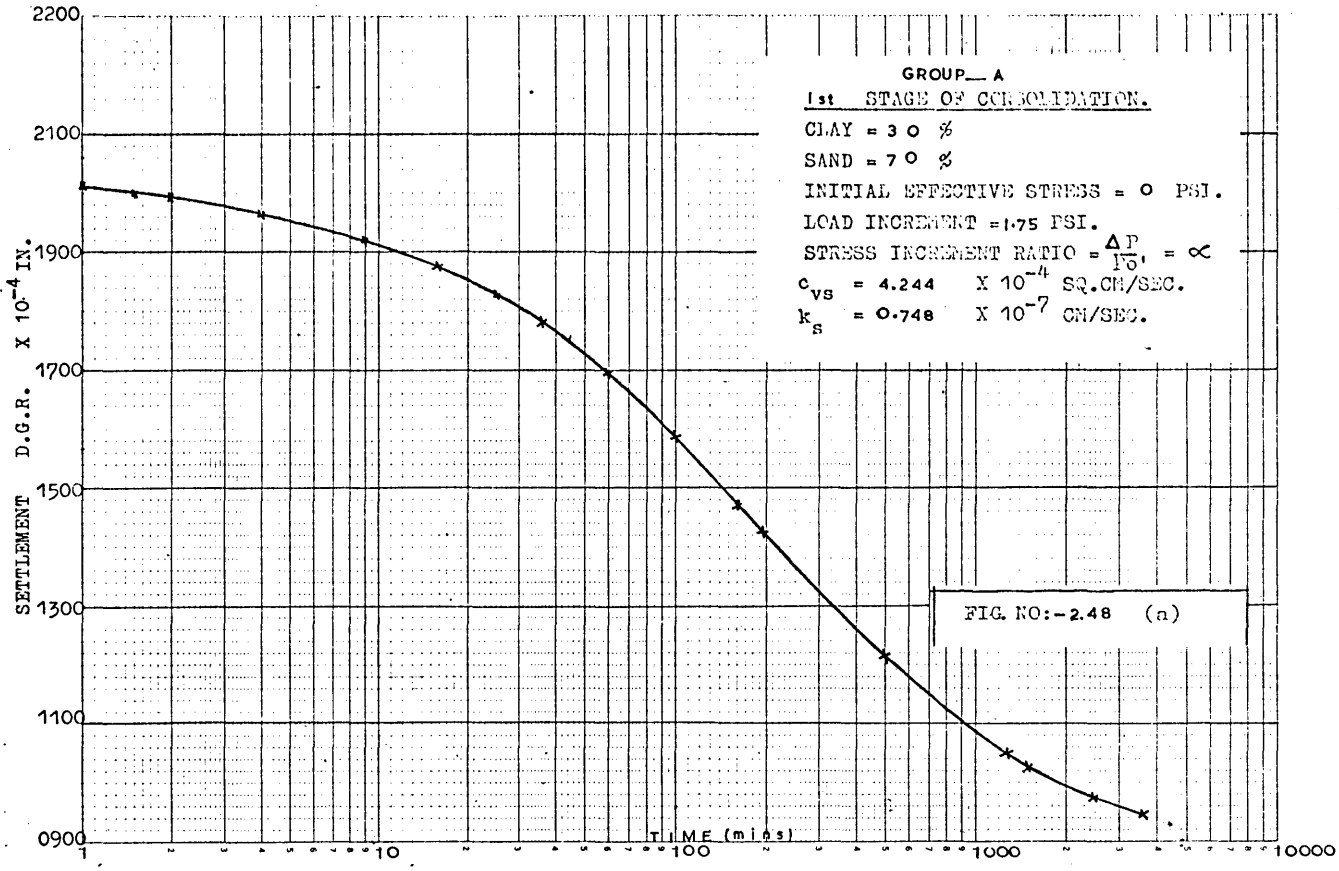

FIG. NO:- 2.48 (a)

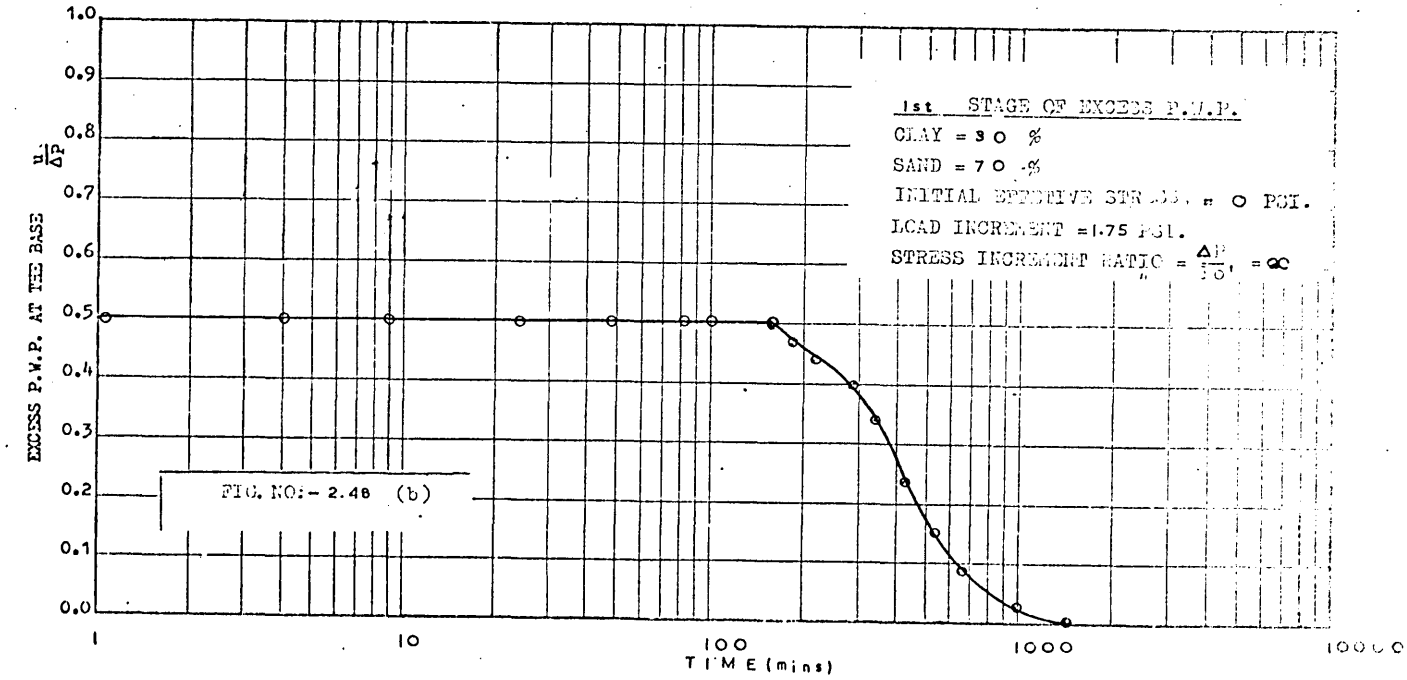

FIG. NO:- 2.48 (b)

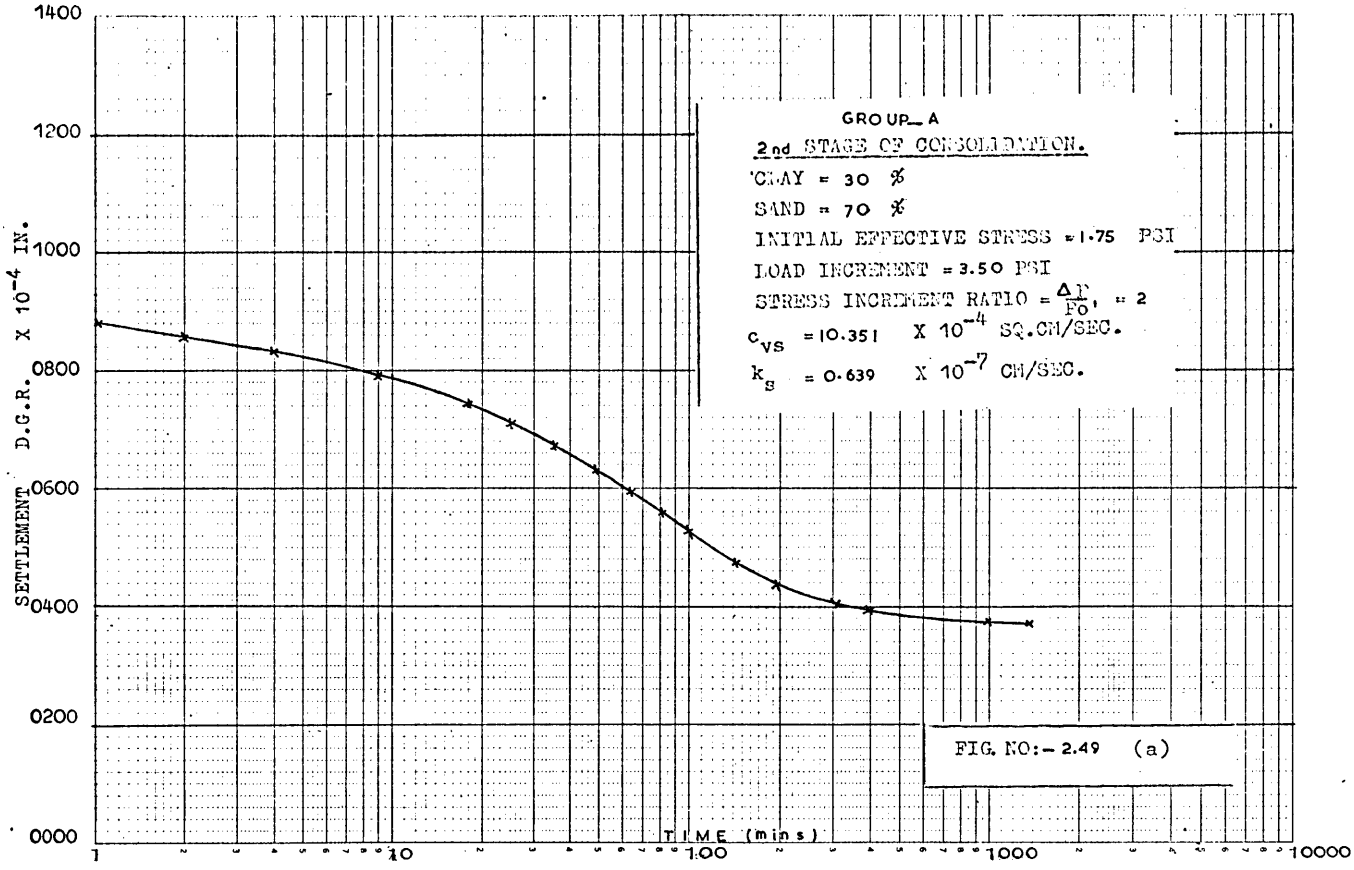

FIG. NO:- 2.49 (a)

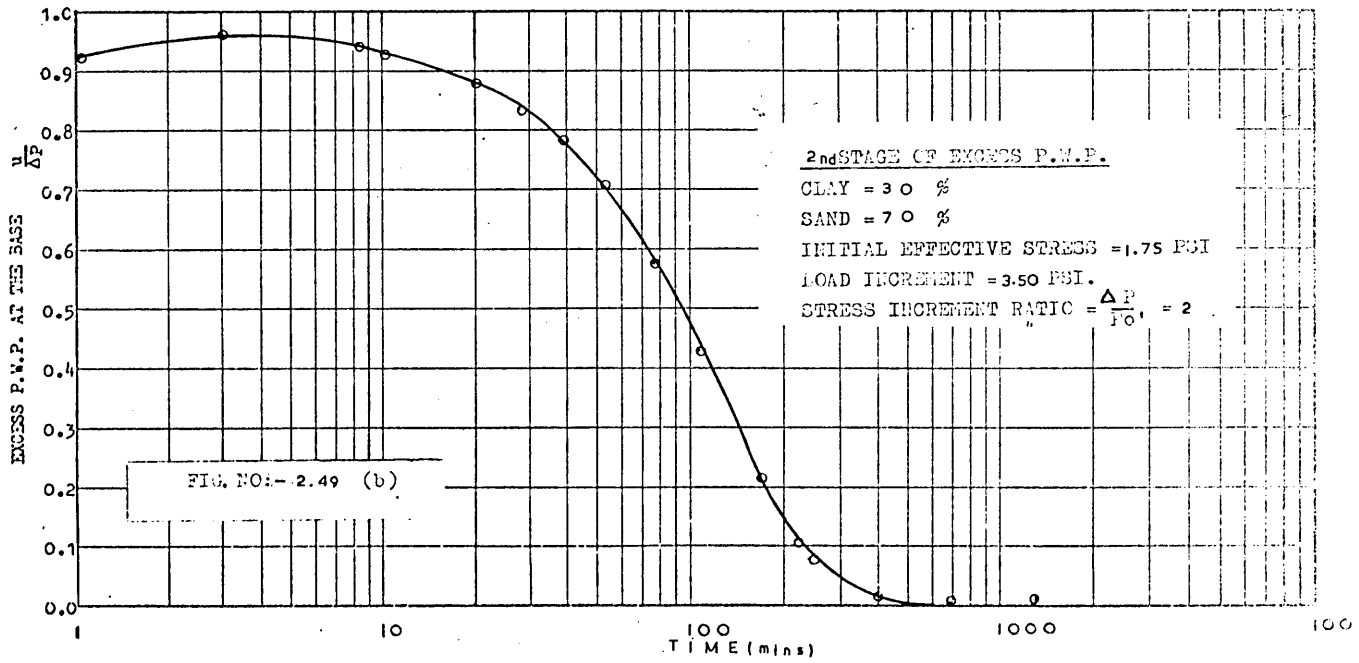

FIG. NO:- 2.49 (b)

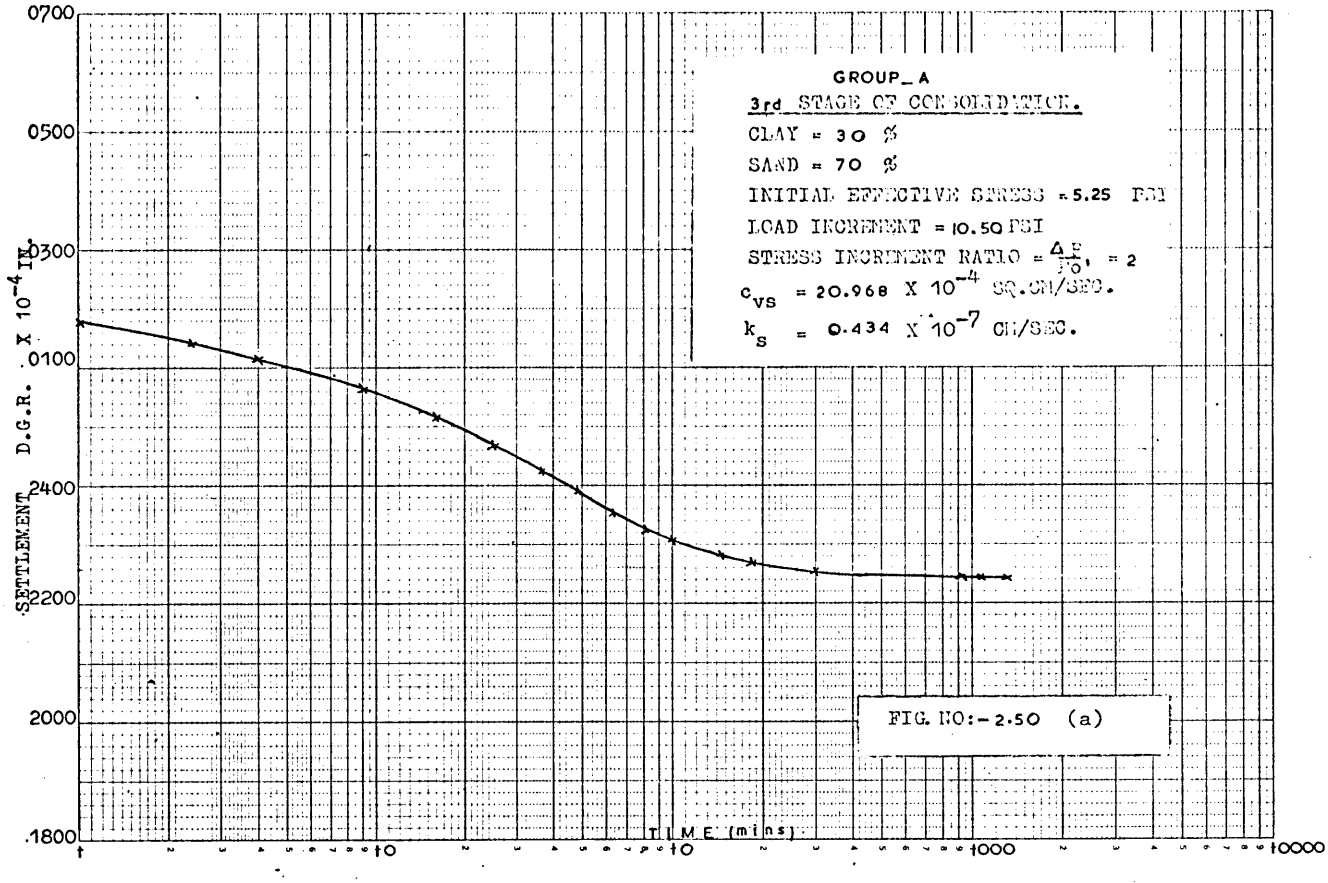

FIG. NO:- 2.50 (a)

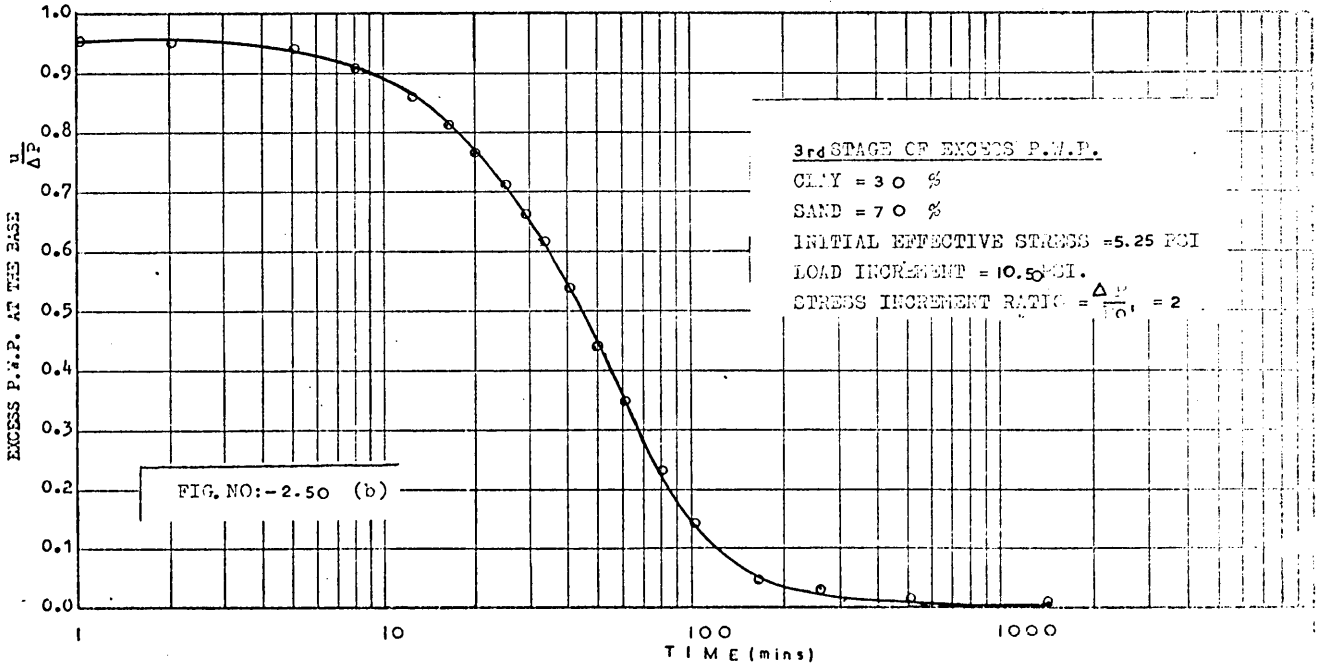

FIG. NO:- 2.50 (b)

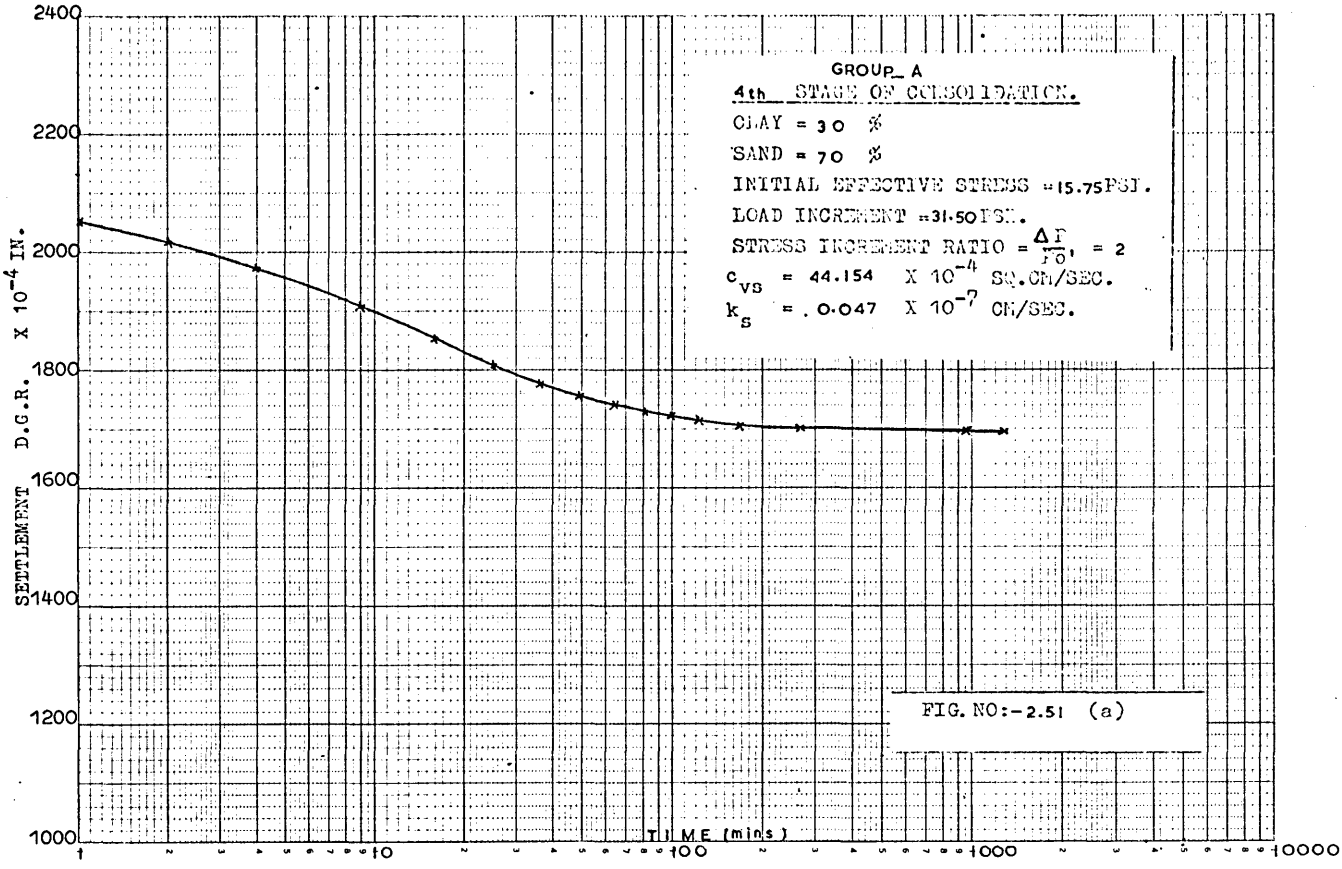

FIG. NO:- 2.51 (a)

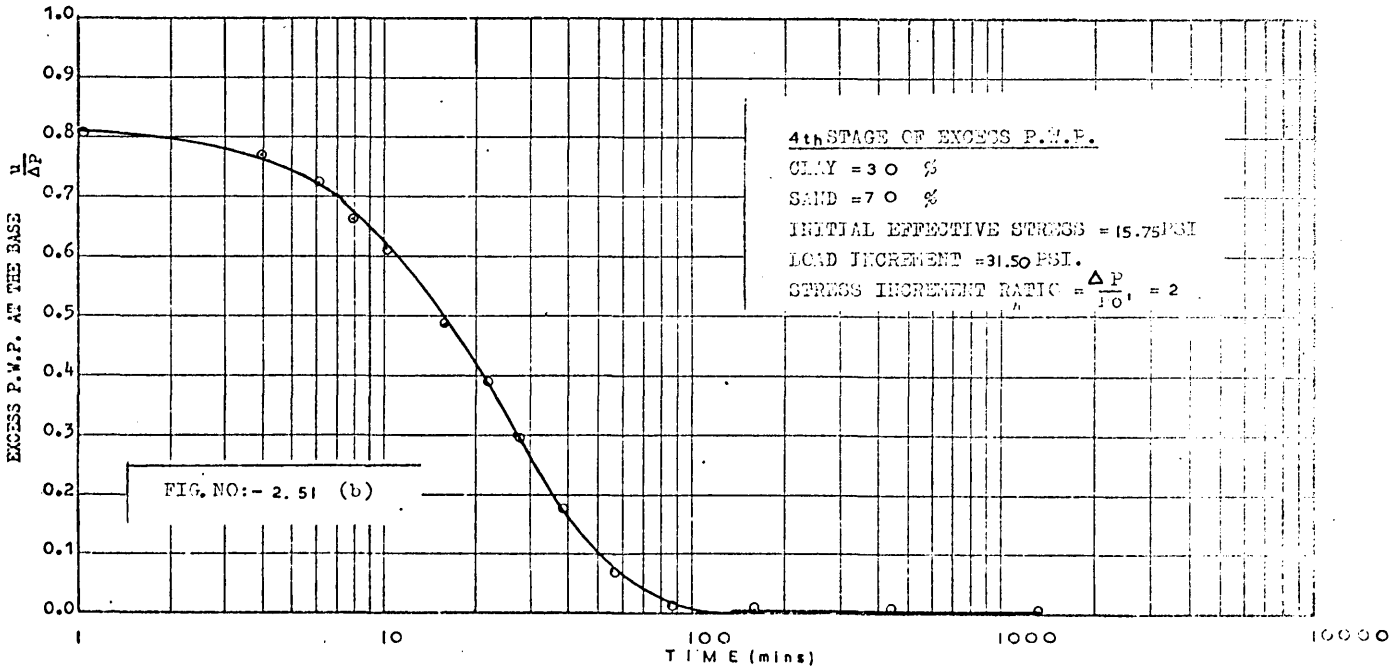

FIG. NO:- 2.51 (b)

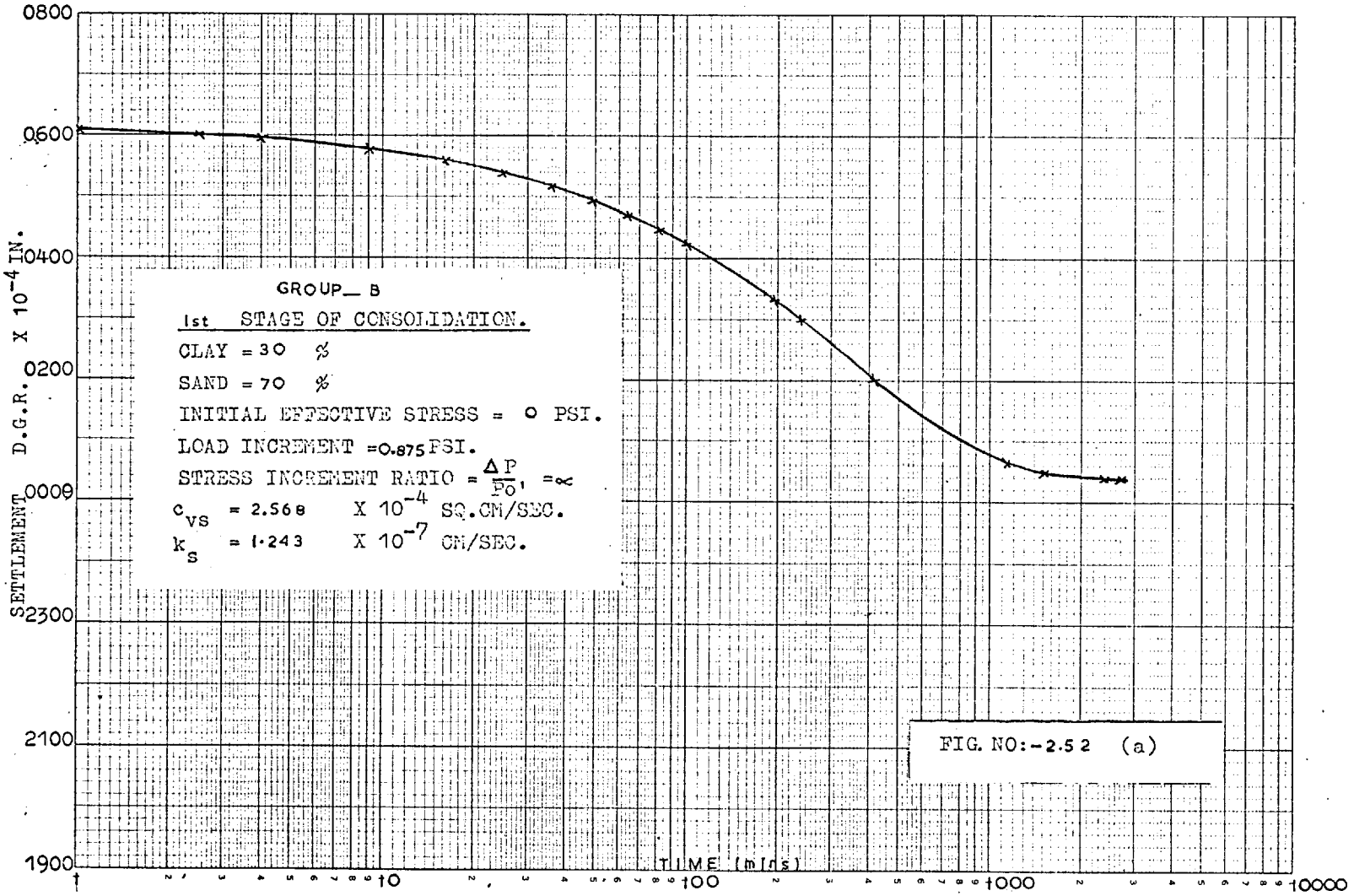
0800
0600
0400
0200
0009
2300
2100
1900
SETTLEMENT D.G.R. X 10^{-4} IN.
GROUP_ B
1st STAGE OF CONSOLIDATION.
CLAY = 30 %
SAND = 70 %
INITIAL EFFECTIVE STRESS = 0 PSI.
LOAD INCREMENT =0.875 PSI.
STRESS INCREMENT RATIO = $\frac{\Delta P}{Po}$ = ∝
c_{vs} = 2.568 X 10^{-4} SQ.CM/SEC.
k_s = 1·243 X 10^{-7} CM/SEC.
TIME (mins)
1
10
100
1000
10000

FIG. NO:-2.5 2 (a)

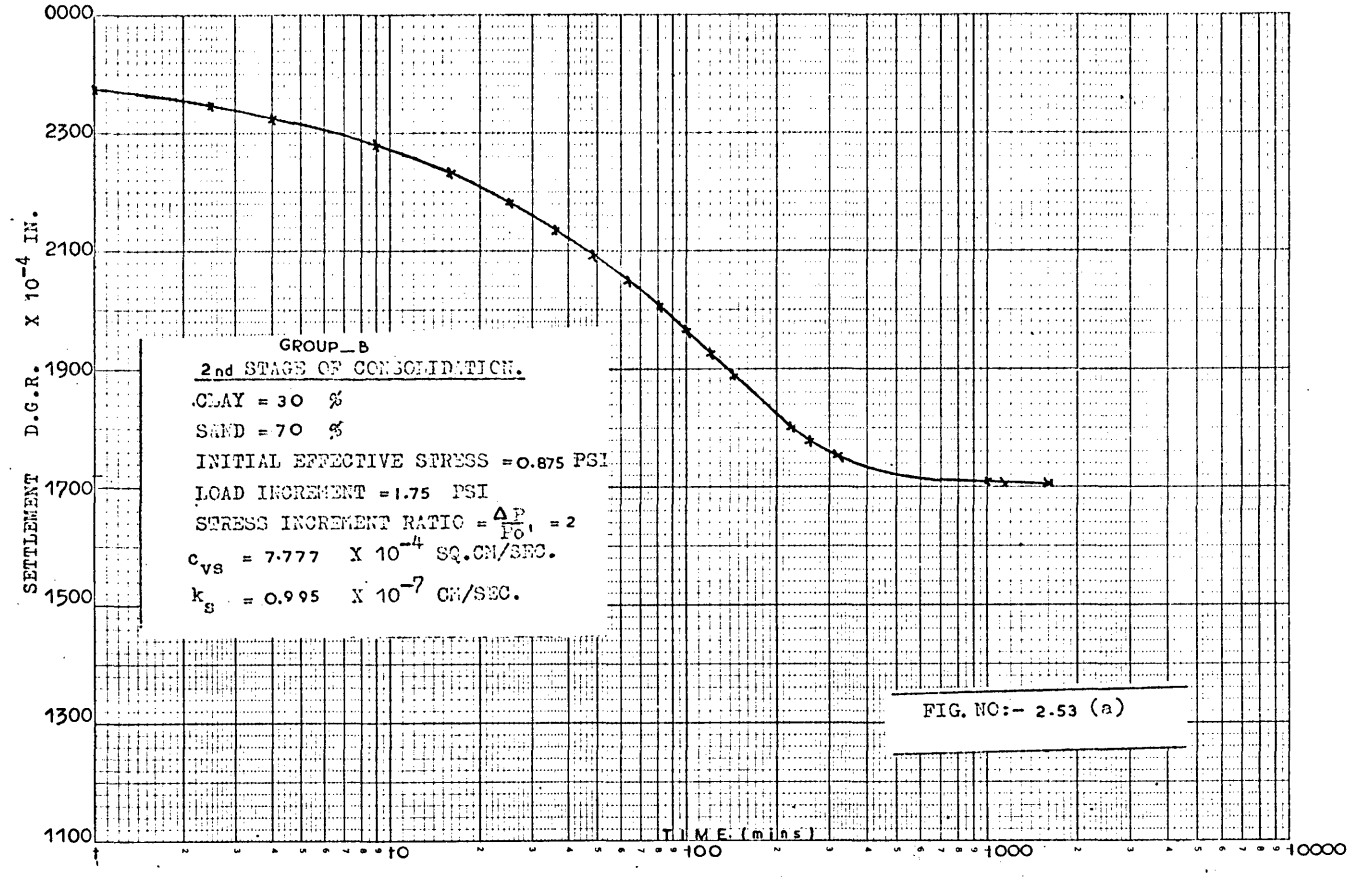

FIG. NO:- 2.53 (a)

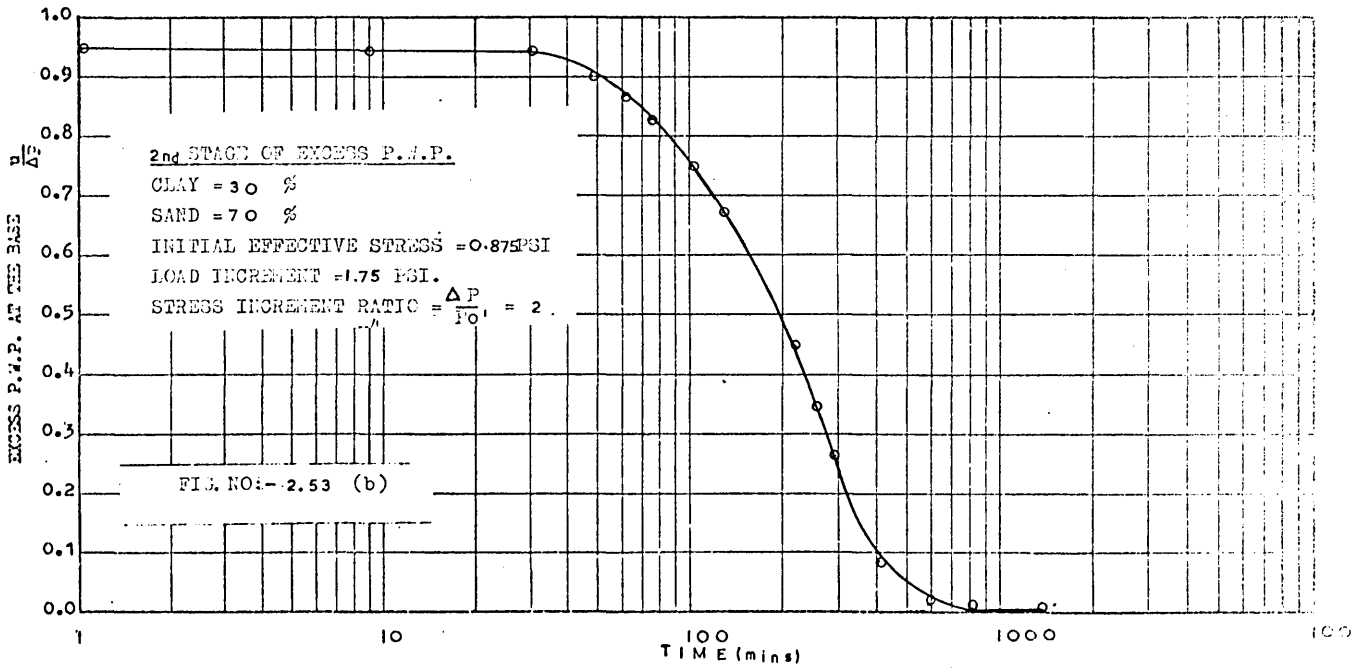

FIG. NO:- 2.53 (b)

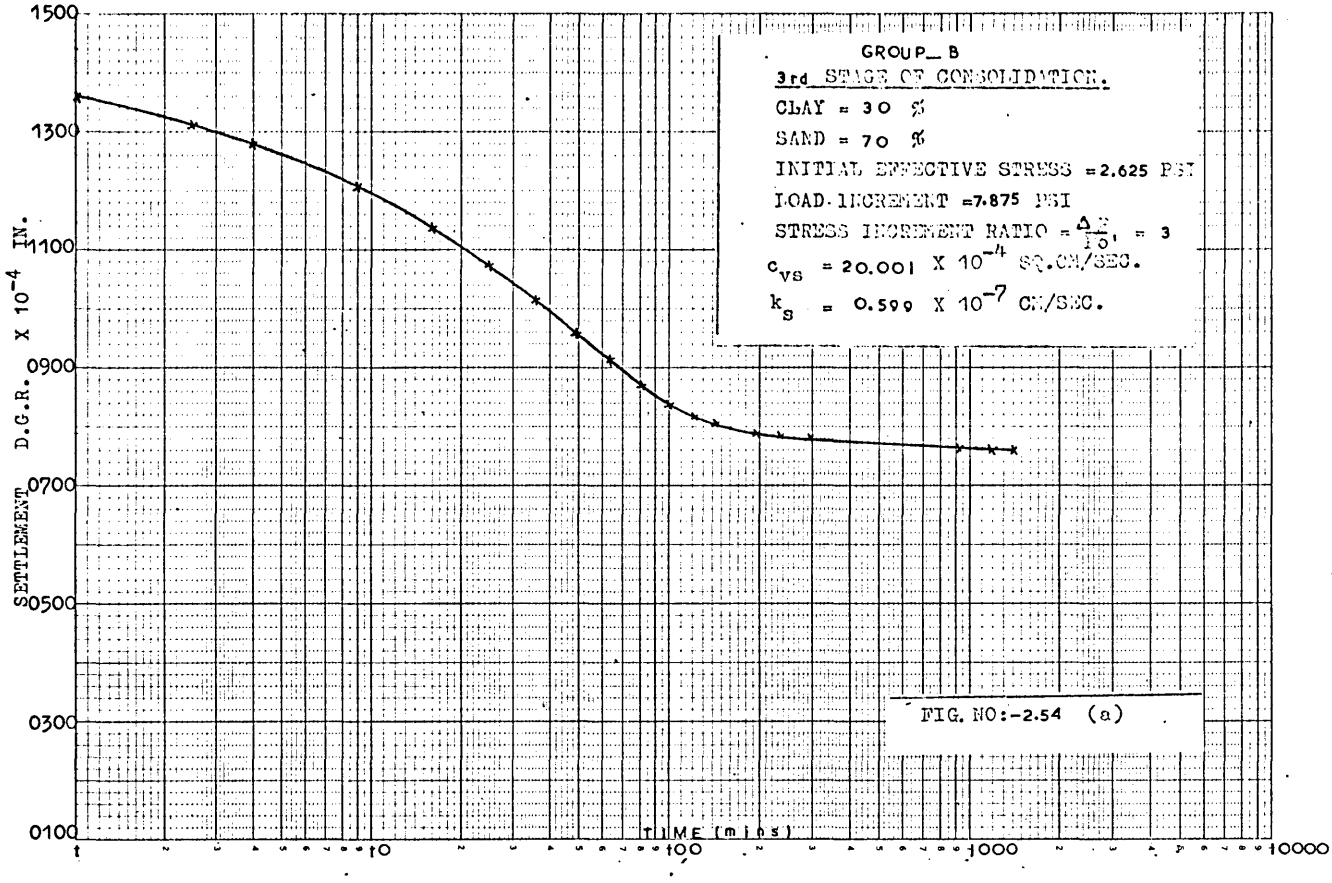

FIG. NO:-2.54 (a)

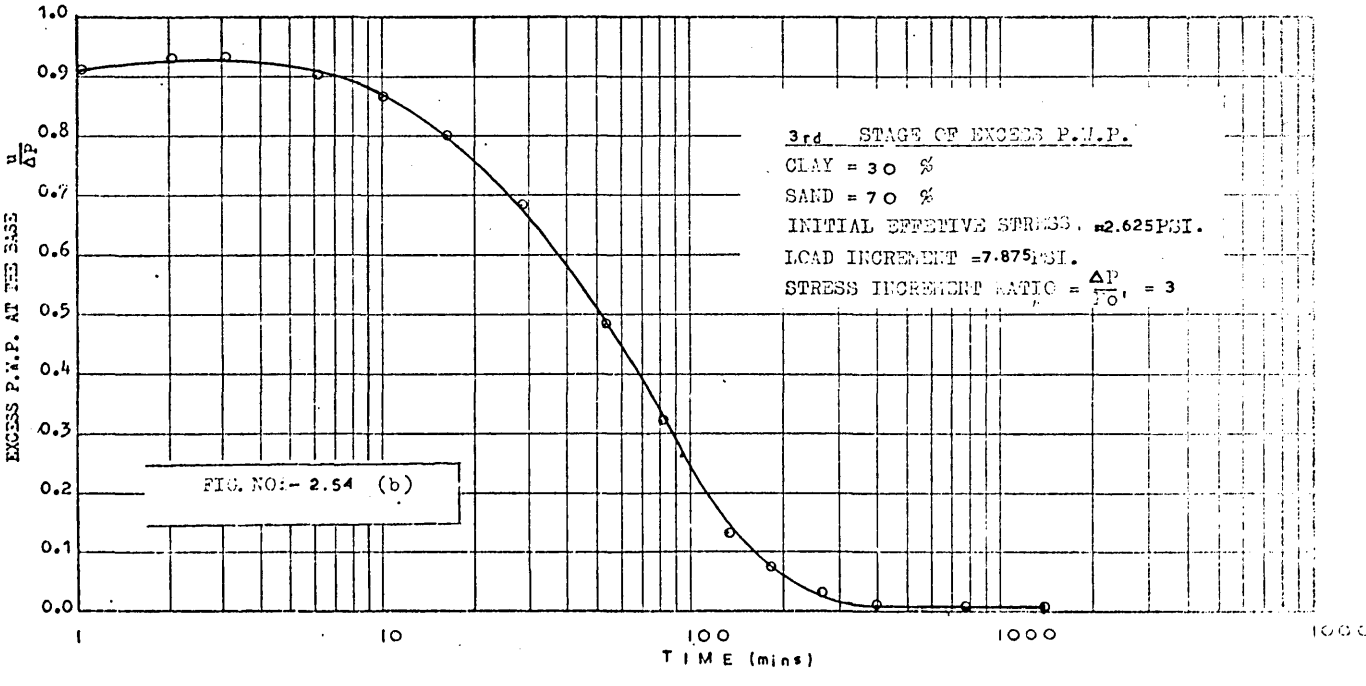

FIG. NO:- 2.54 (b)

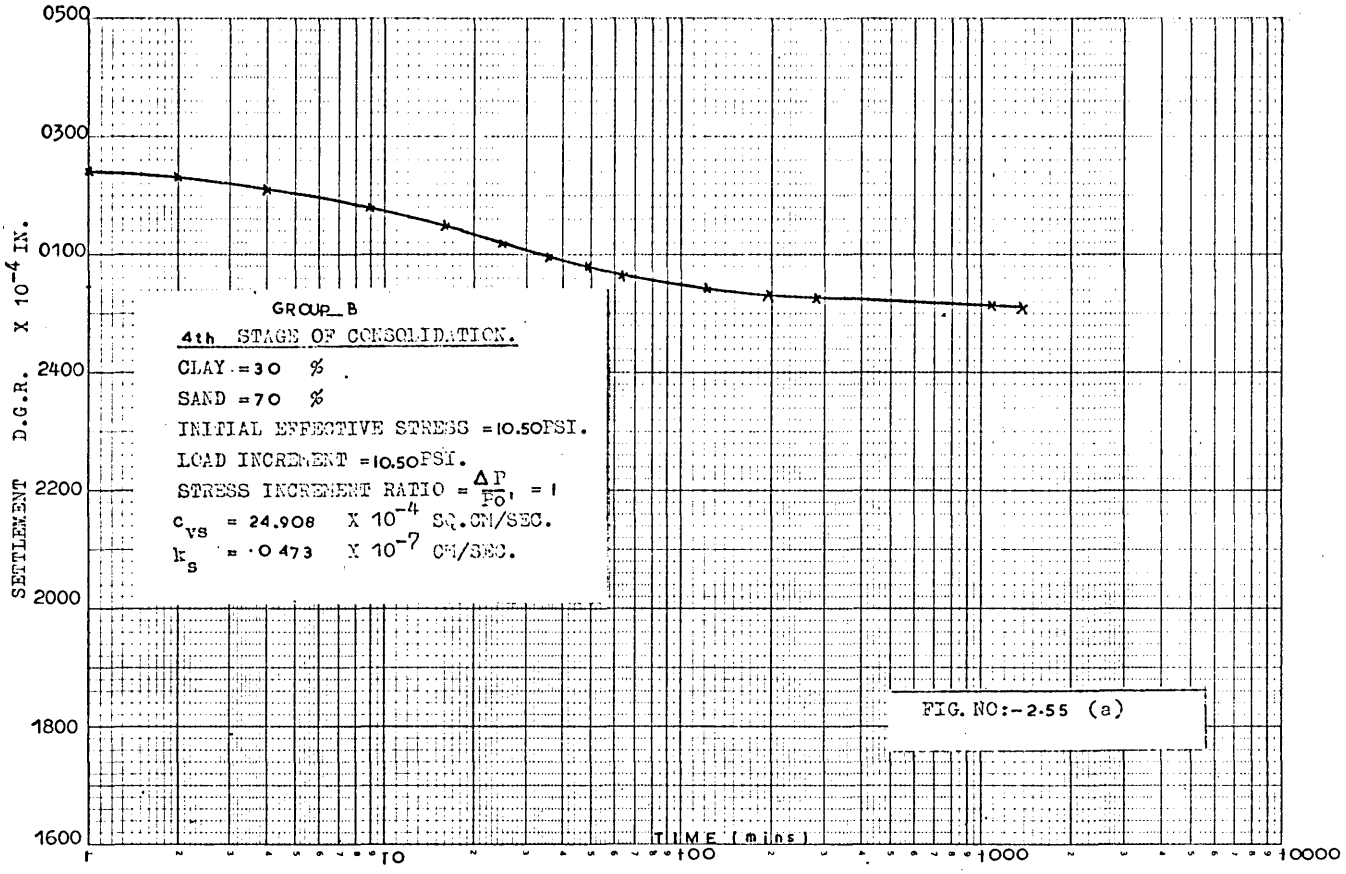
0500
0300
0100
2400
2200
2000
1800
1600
SETTLEMENT D.G.R. X 10^{-4} IN.
GROUP_B
4th STAGE OF CONSOLIDATION.
CLAY =30 %
SAND =70 %
INITIAL EFFECTIVE STRESS =10.50PSI.
LOAD INCREMENT =10.50PSI.
STRESS INCREMENT RATIO = $\frac{\Delta P}{Po}$ = 1
c_{vs} = 24.908 X 10^{-4} SQ.CM/SEC.
k_s = ·0473 X 10^{-7} CM/SEC.
FIG. NO:-2.55 (a)
10
100
1000
10000
TIME (mins)

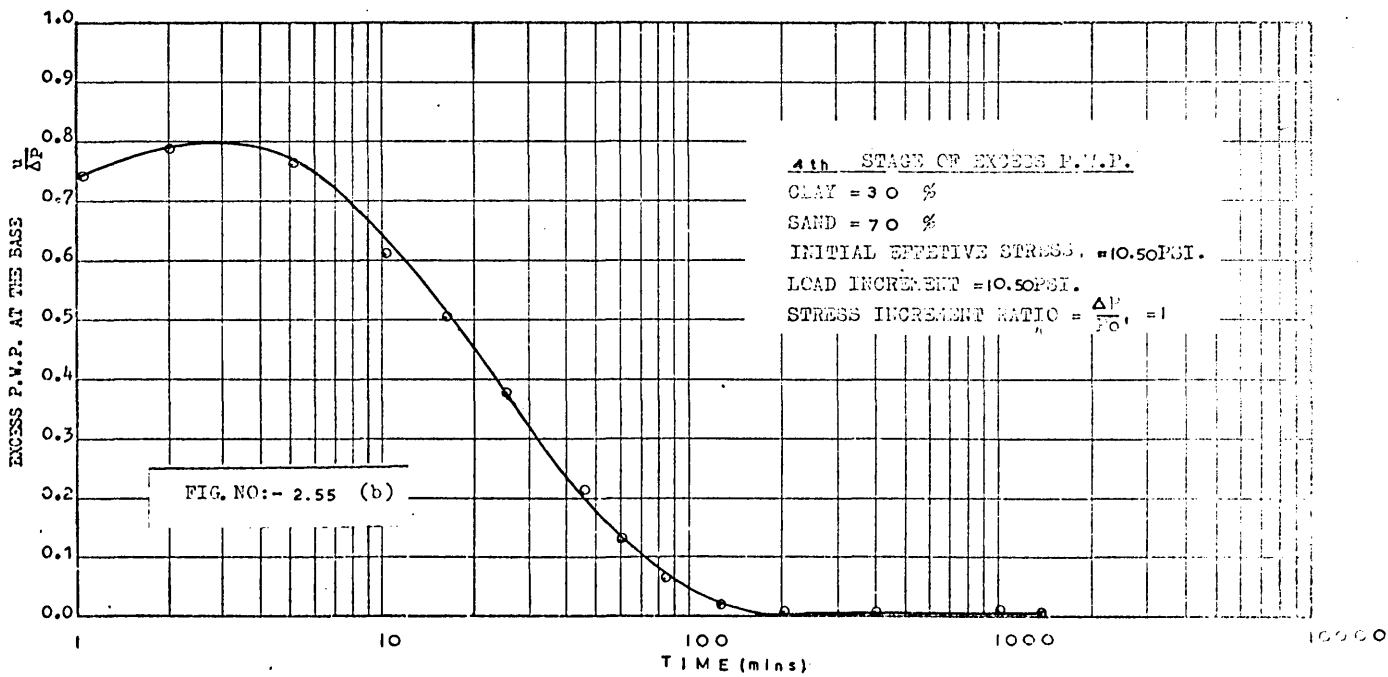
1.0
0.9
0.8
0.7
0.6
0.5
0.4
0.3
0.2
0.1
0.0
$\frac{u}{\Delta P}$
EXCESS P.W.P. AT THE BASS
4th STAGE OF EXCESS P.W.P.
CLAY = 30 %
SAND = 70 %
INITIAL EFFETIVE STRESS. =10.50PSI.
LOAD INCREMENT =10.50PSI.
STRESS INCREMENT RATIO = $\frac{\Delta P}{Po}$ = 1
FIG. NO:- 2.55 (b)
1
10
100
1000
10000
TIME (mins)

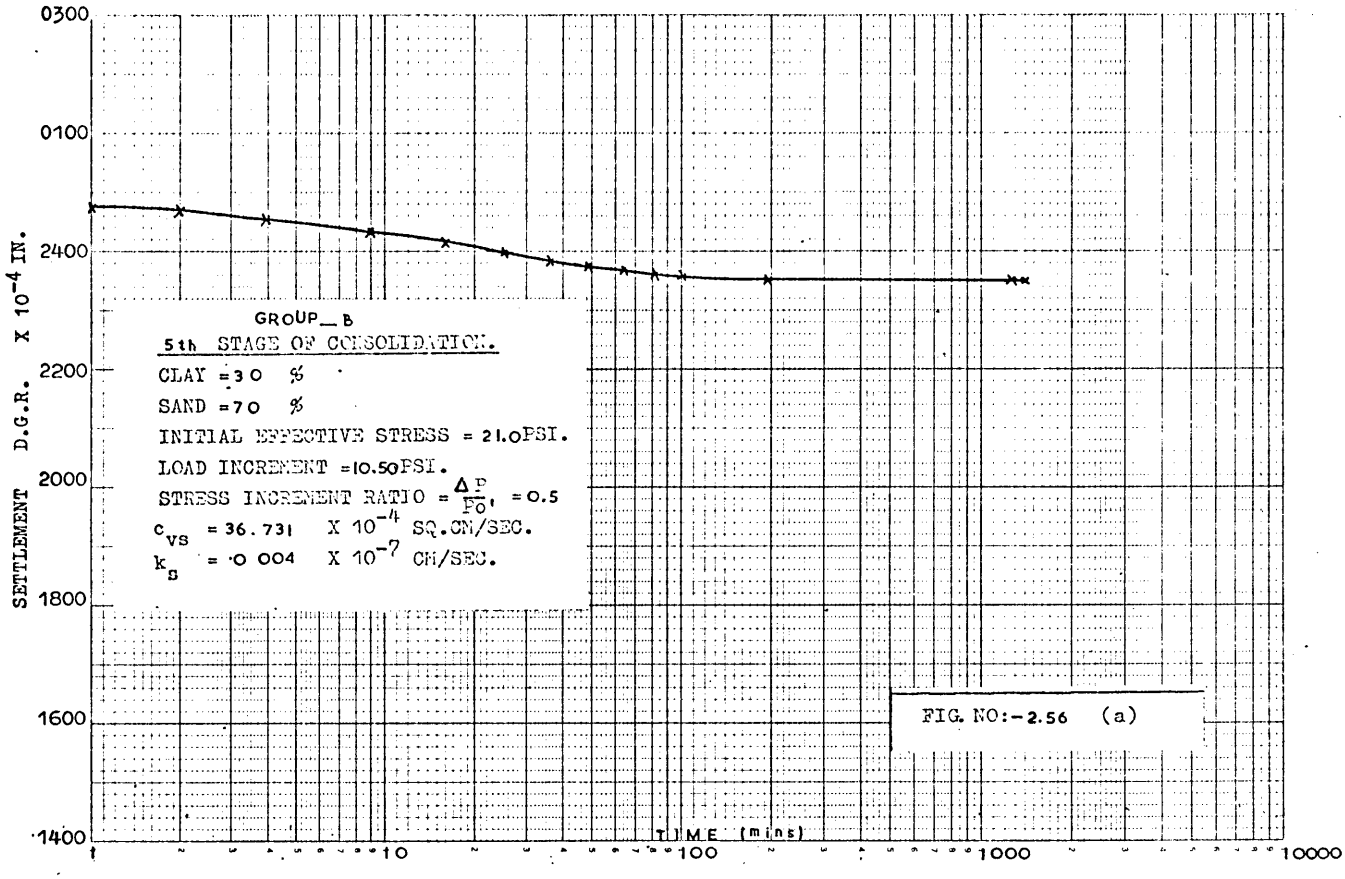
0300
0100
2400
2200
2000
1800
1600
1400
SETTLEMENT D.G.R. X 10^{-4} IN.
GROUP_B
5th STAGE OF CONSOLIDATION.
CLAY = 30 %
SAND = 70 %
INITIAL EFFECTIVE STRESS = 21.0PSI.
LOAD INCREMENT = 10.50PSI.
STRESS INCREMENT RATIO = $\frac{\Delta P}{Po}$ = 0.5
c_{vs} = 36.731 X 10^{-4} SQ.CM/SEC.
k_s = 0.004 X 10^{-7} CM/SEC.
FIG. NO:- 2.56 (a)
1
10
100
1000
10000
TIME (mins)

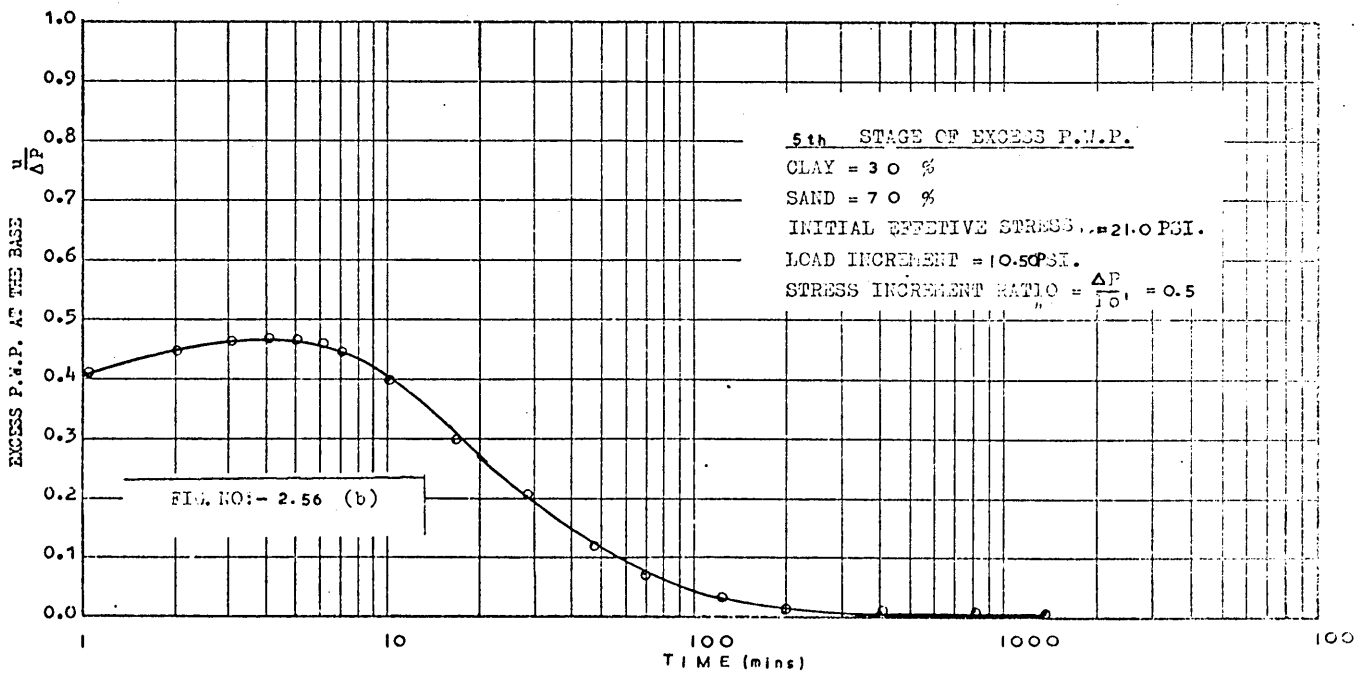
1.0
0.9
0.8
0.7
0.6
0.5
0.4
0.3
0.2
0.1
0.0
EXCESS P.W.P. AT THE BASE $\frac{u}{\Delta P}$
5th STAGE OF EXCESS P.W.P.
CLAY = 30 %
SAND = 70 %
INITIAL EFFECTIVE STRESS = 21.0 PSI.
LOAD INCREMENT = 10.50PSI.
STRESS INCREMENT RATIO = $\frac{\Delta P}{Po}$ = 0.5
FIG. NO:- 2.56 (b)
1
10
100
1000
10000
TIME (mins)

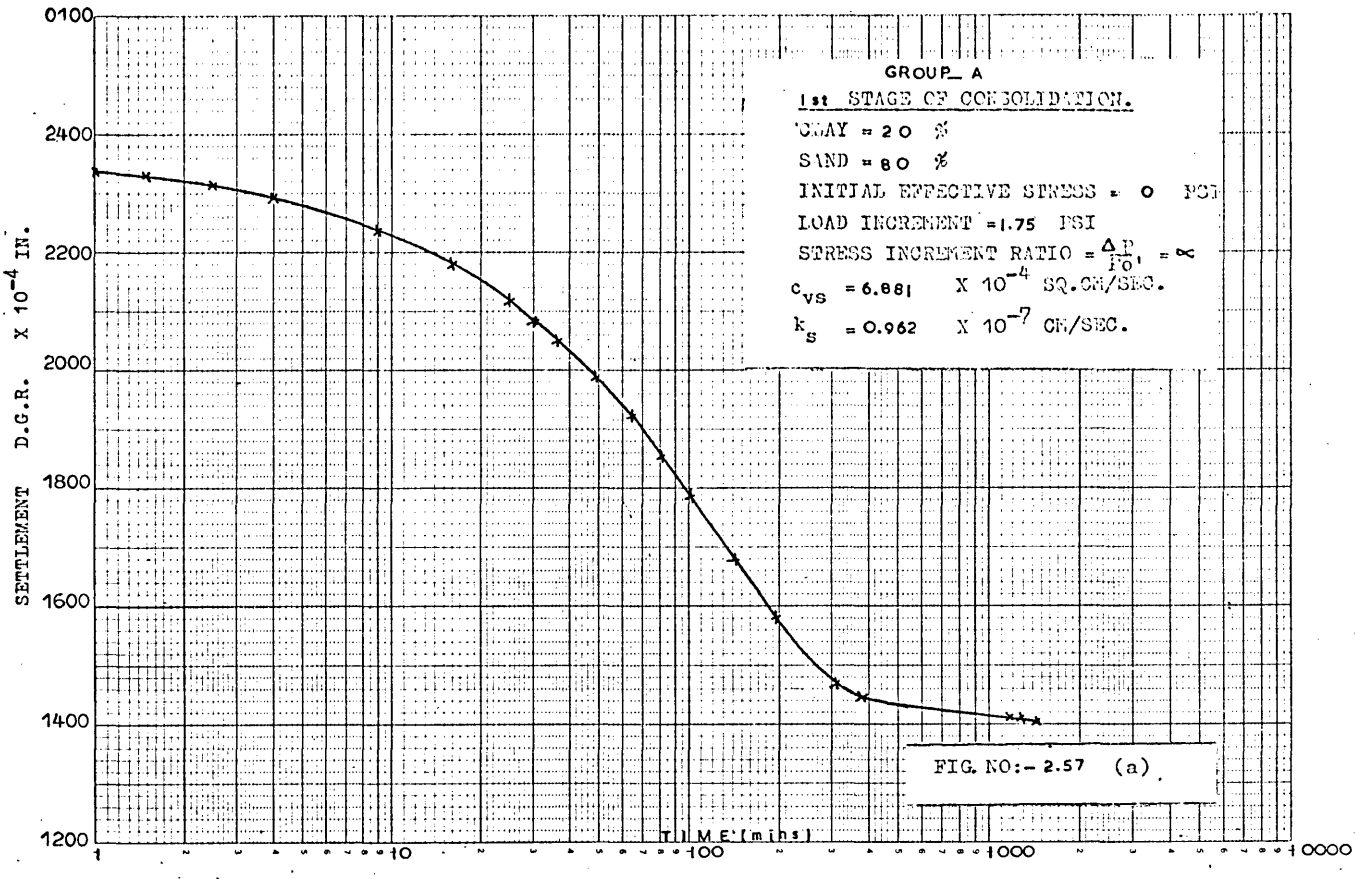

FIG. NO:- 2.57 (a)

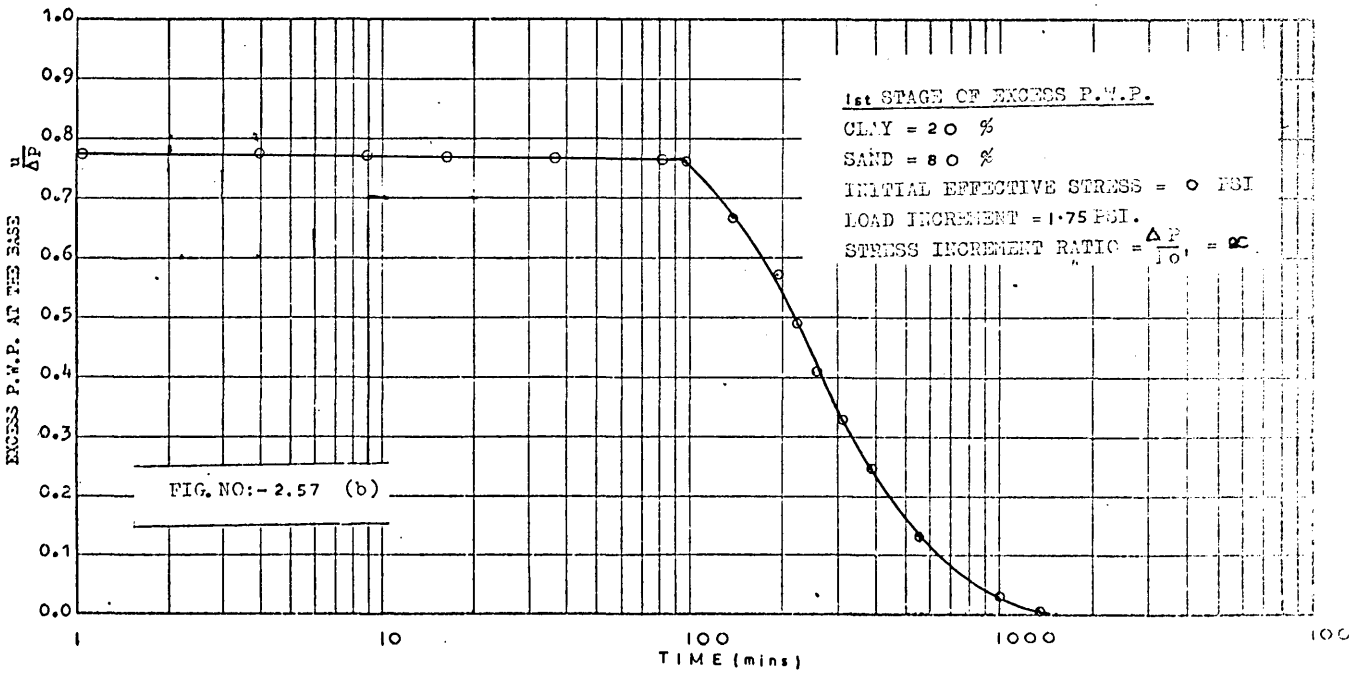

FIG. NO:- 2.57 (b)

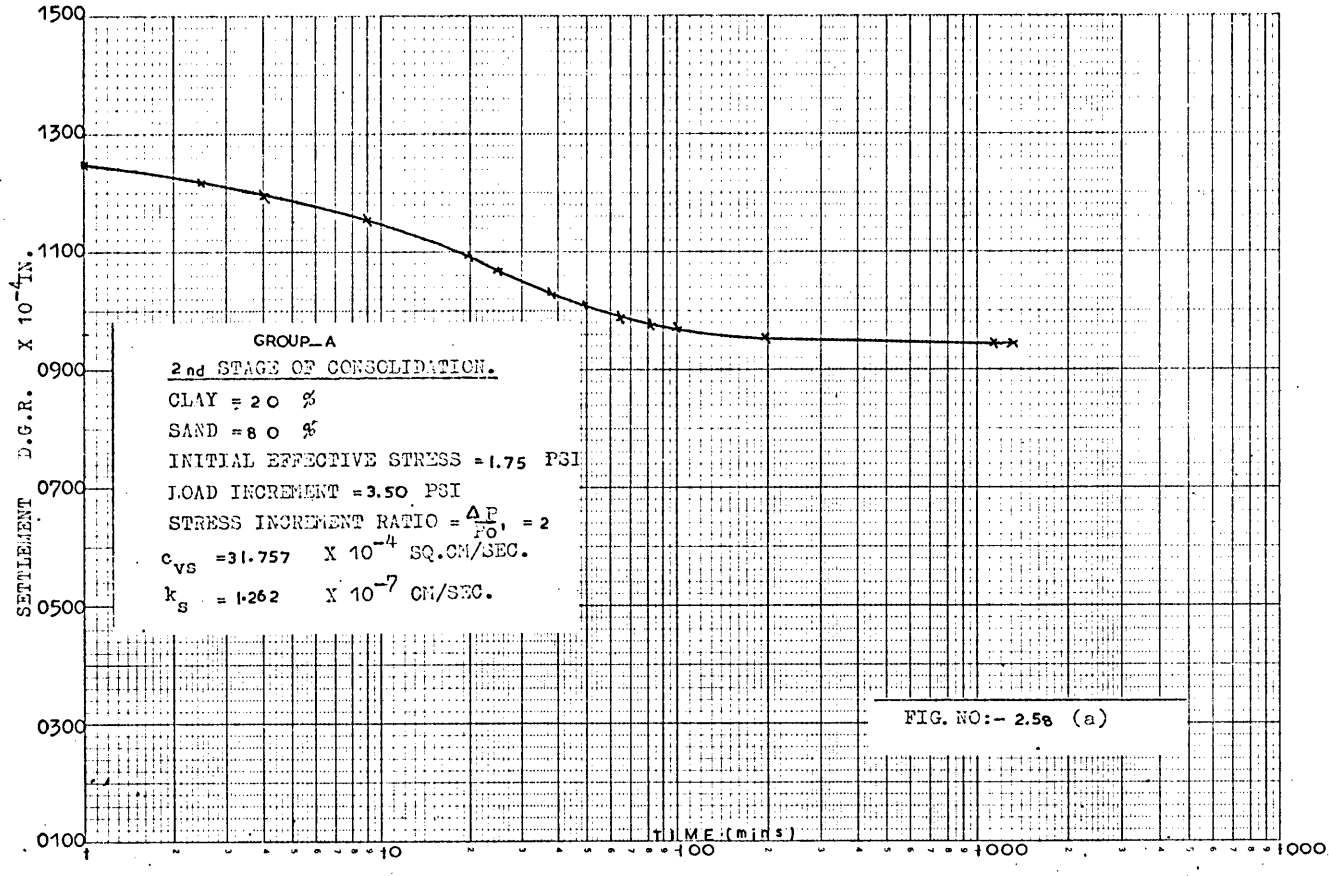

FIG. NO:- 2.58 (a)

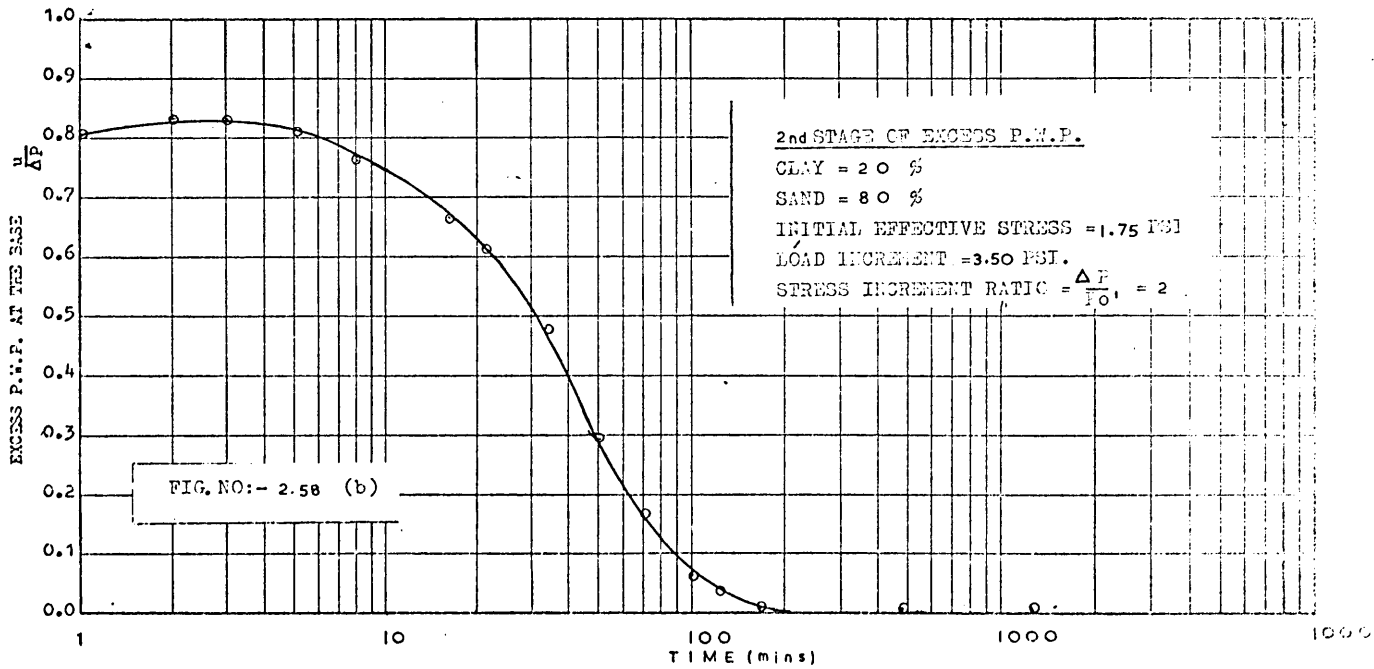

FIG. NO:- 2.58 (b)

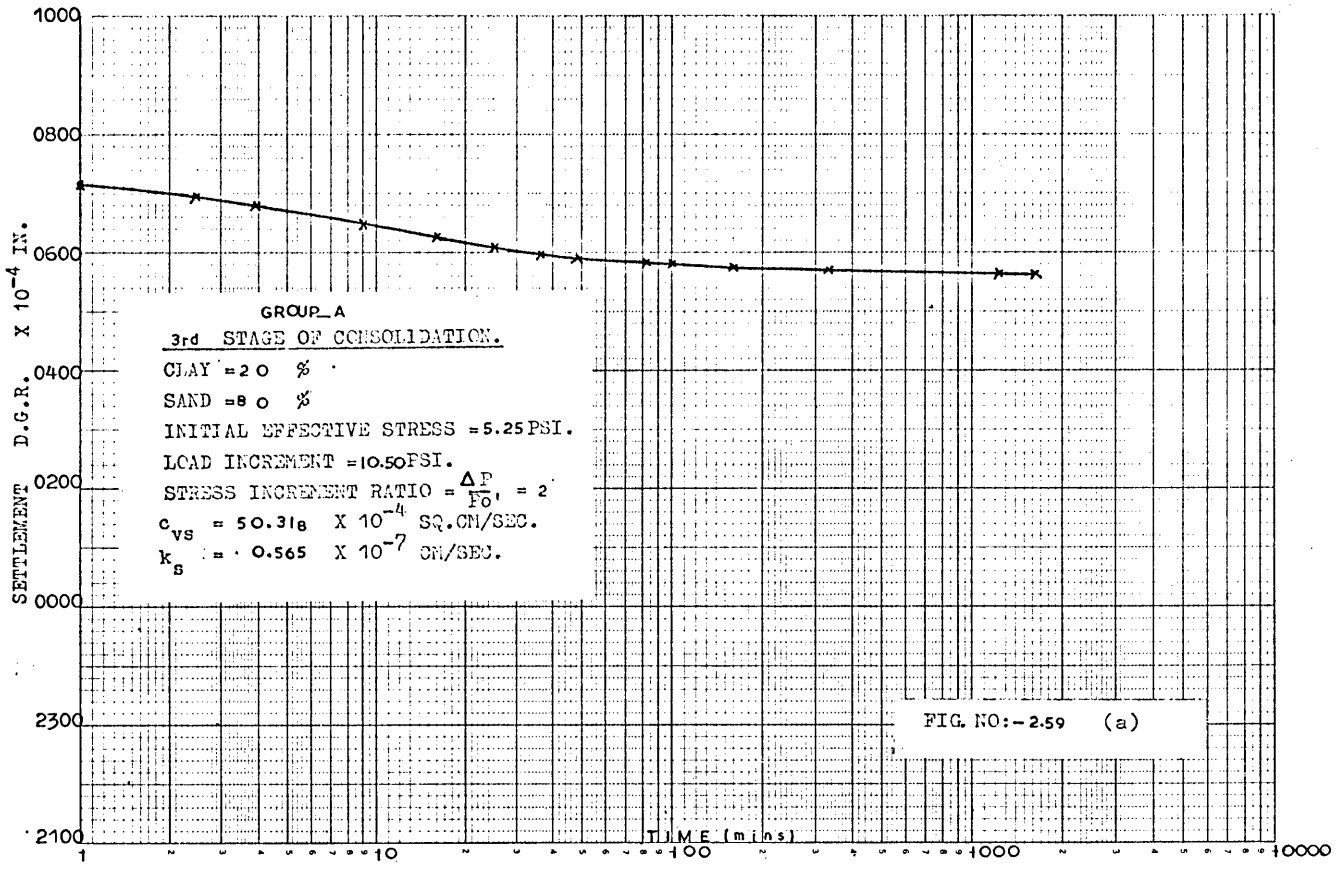
1000
0800
0600
0400
0200
0000
2300
2100
SETTLEMENT D.G.R. X 10^{-4} IN.
GROUP_A
3rd STAGE OF CONSOLIDATION.
CLAY = 20 %
SAND = 80 %
INITIAL EFFECTIVE STRESS = 5.25 PSI.
LOAD INCREMENT = 10.50 PSI.
STRESS INCREMENT RATIO = $\frac{\Delta P}{Po}$ = 2
c_{vs} = 50.318 X 10^{-4} SQ.CM/SEC.
k_s = 0.565 X 10^{-7} CM/SEC.
FIG. NO:- 2.59 (a)
1
10
100
1000
10000
TIME (mins)

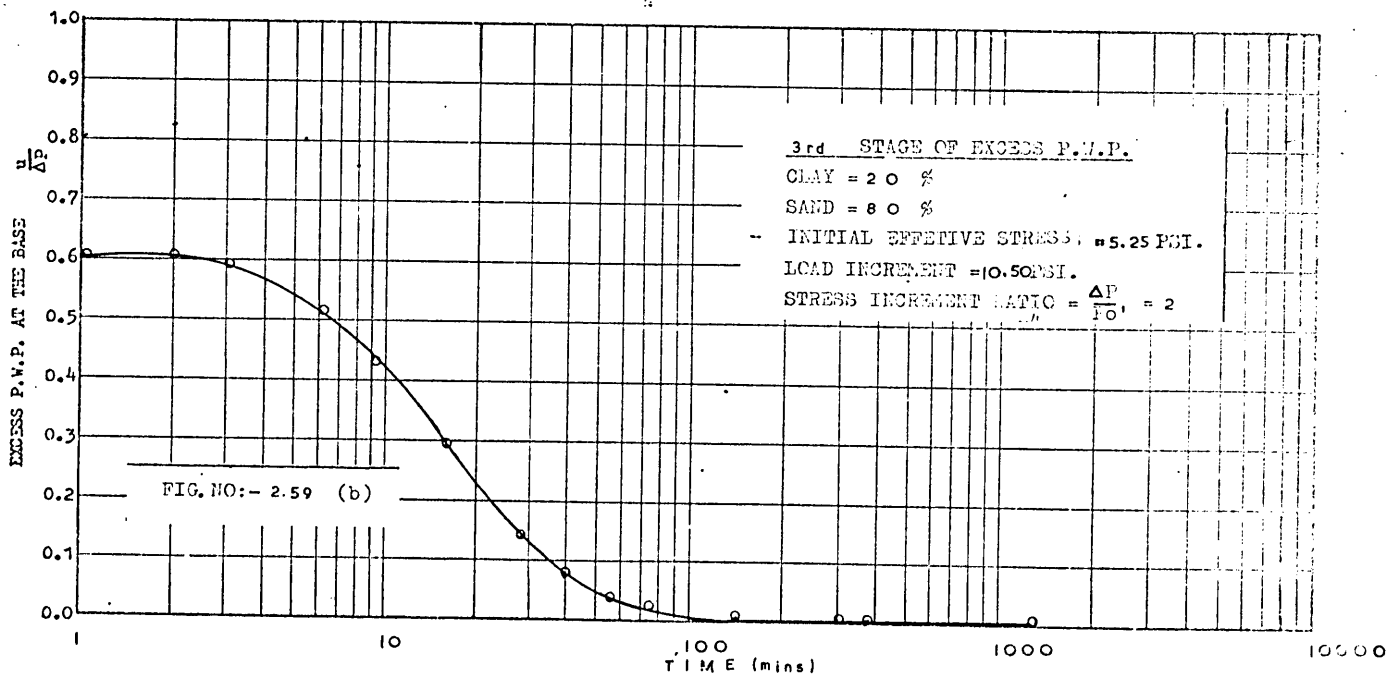
1.0
0.9
0.8
0.7
0.6
0.5
0.4
0.3
0.2
0.1
0.0
$\frac{u}{\Delta P}$
EXCESS P.W.P. AT THE BASE
3rd STAGE OF EXCESS P.W.P.
CLAY = 20 %
SAND = 80 %
INITIAL EFFECTIVE STRESS = 5.25 PSI.
LOAD INCREMENT = 10.50 PSI.
STRESS INCREMENT RATIO = $\frac{\Delta P}{Po}$ = 2
FIG. NO:- 2.59 (b)
1
10
100
1000
10000
TIME (mins)

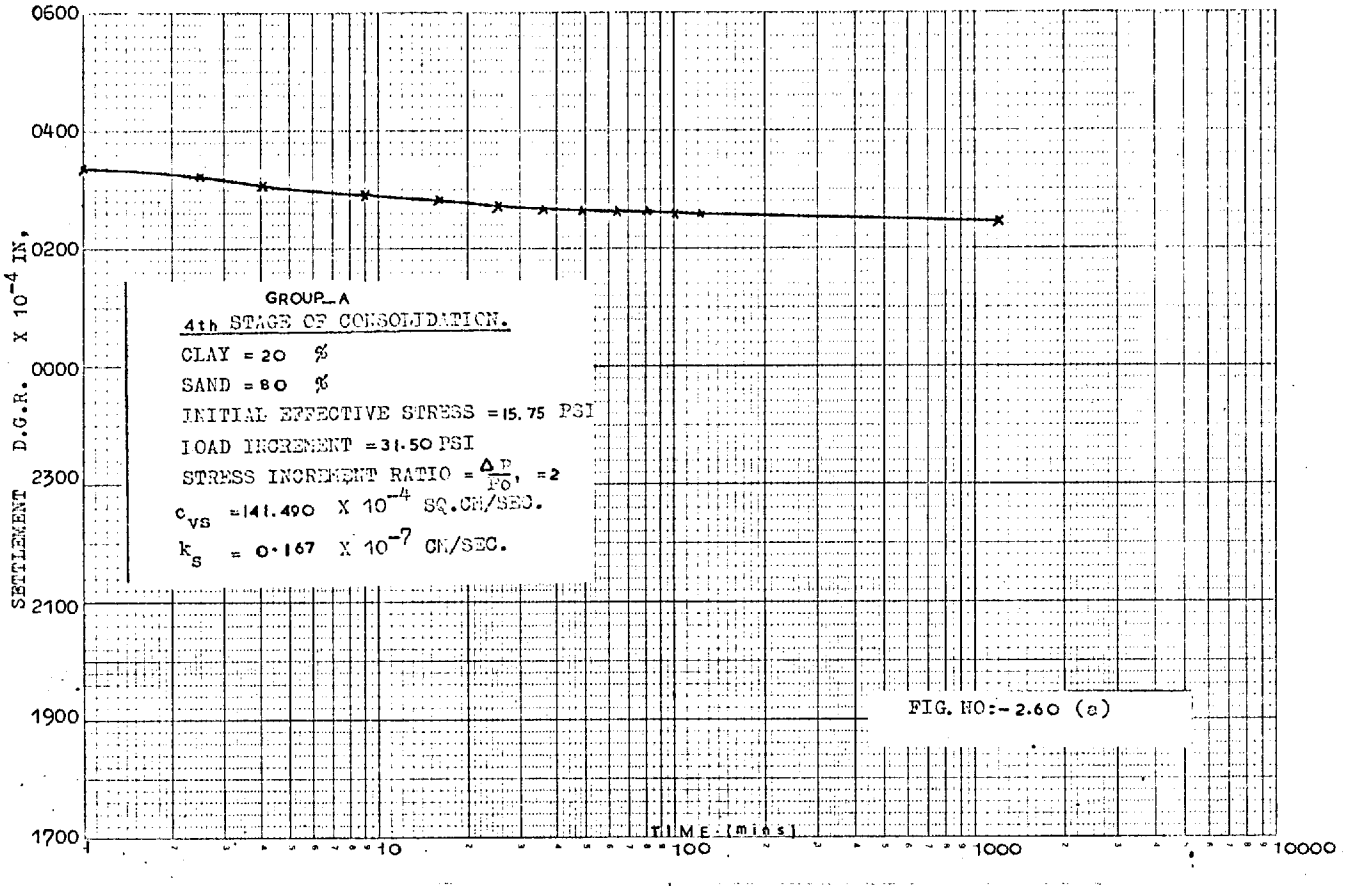

FIG. NO:- 2.60 (a)

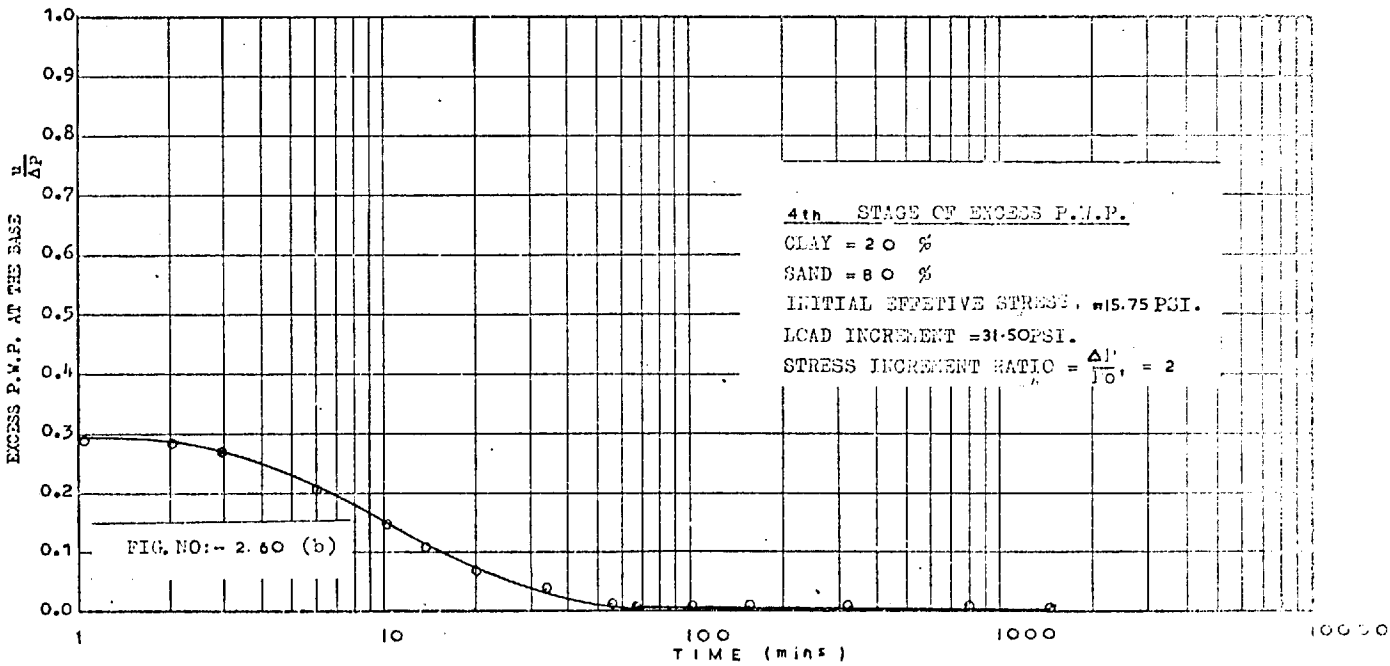

FIG. NO:- 2.60 (b)

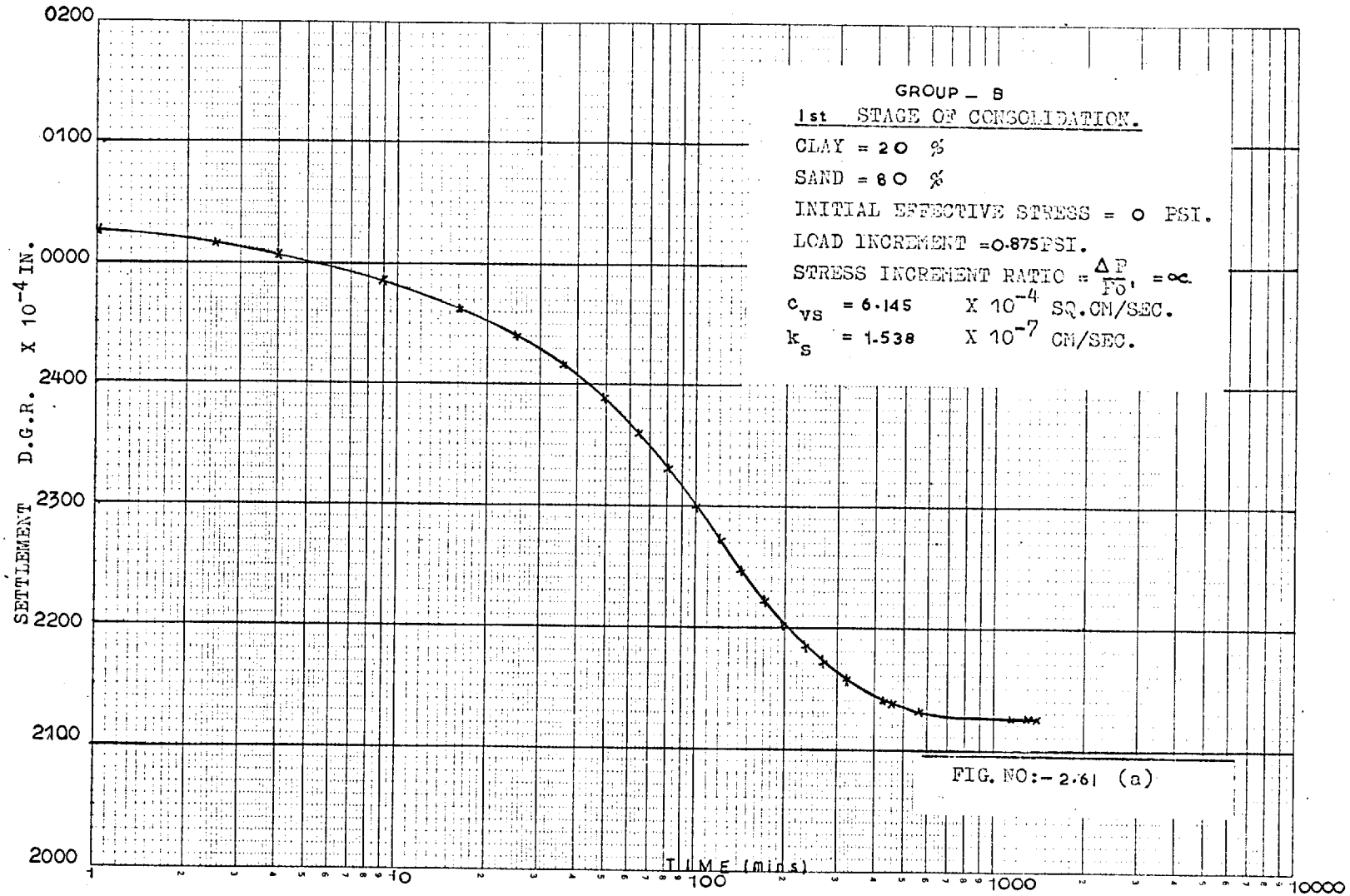
GROUP – B
1st STAGE OF CONSOLIDATION.
CLAY = 20 %
SAND = 80 %
INITIAL EFFECTIVE STRESS = 0 PSI.
LOAD INCREMENT =0.875PSI.
STRESS INCREMENT RATIO = ΔP/P0, = ∞.
c_{vs} = 6.145 X 10^{-4} SQ.CM/SEC.
k_s = 1.538 X 10^{-7} CM/SEC.
SETTLEMENT D.G.R. X 10^{-4} IN.
0200
0100
0000
2400
2300
2200
2100
2000
1
10
100
1000
10000
TIME (mins)

FIG. NO:– 2.61 (a)

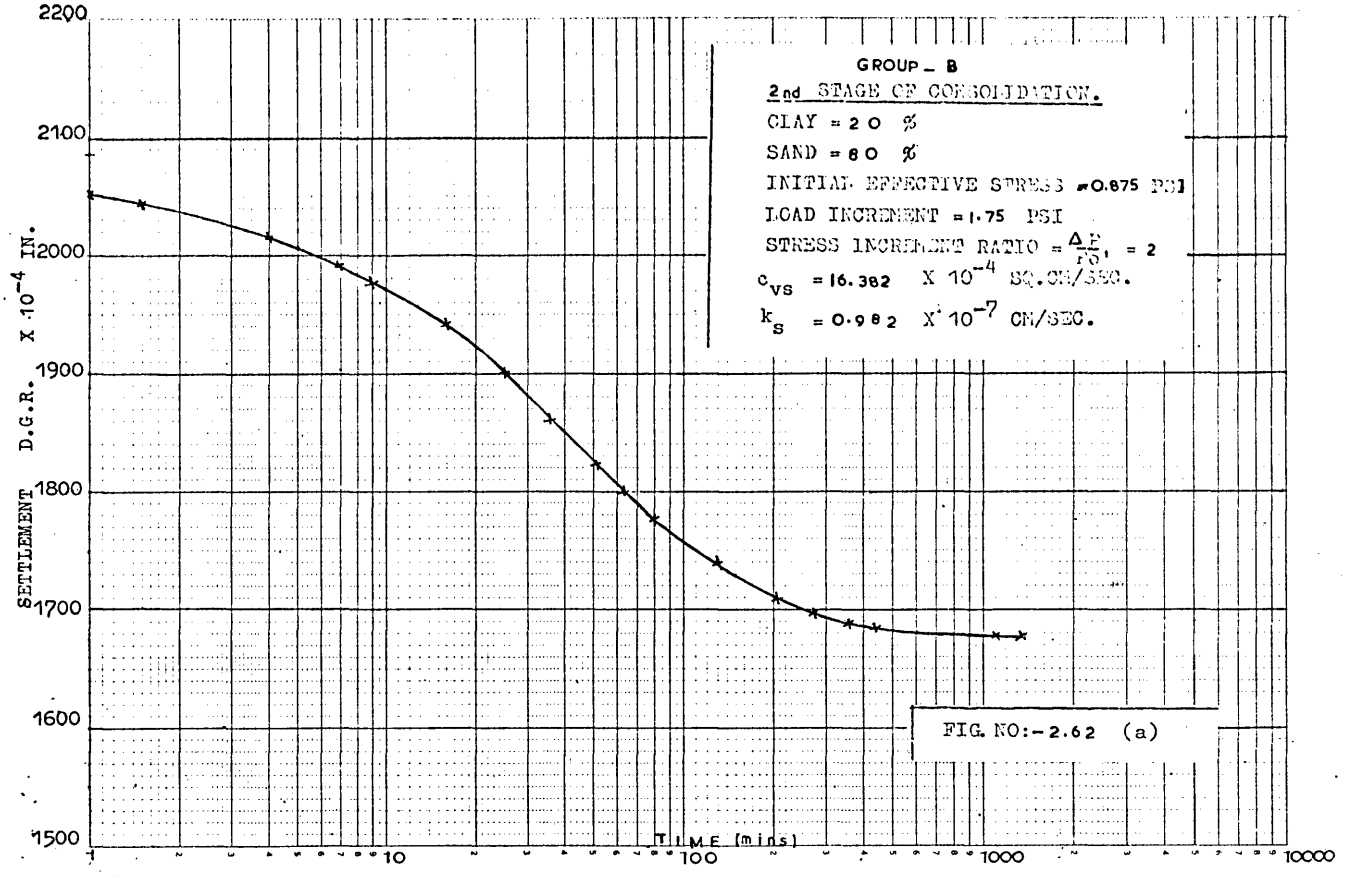

FIG. NO:- 2.62 (a)

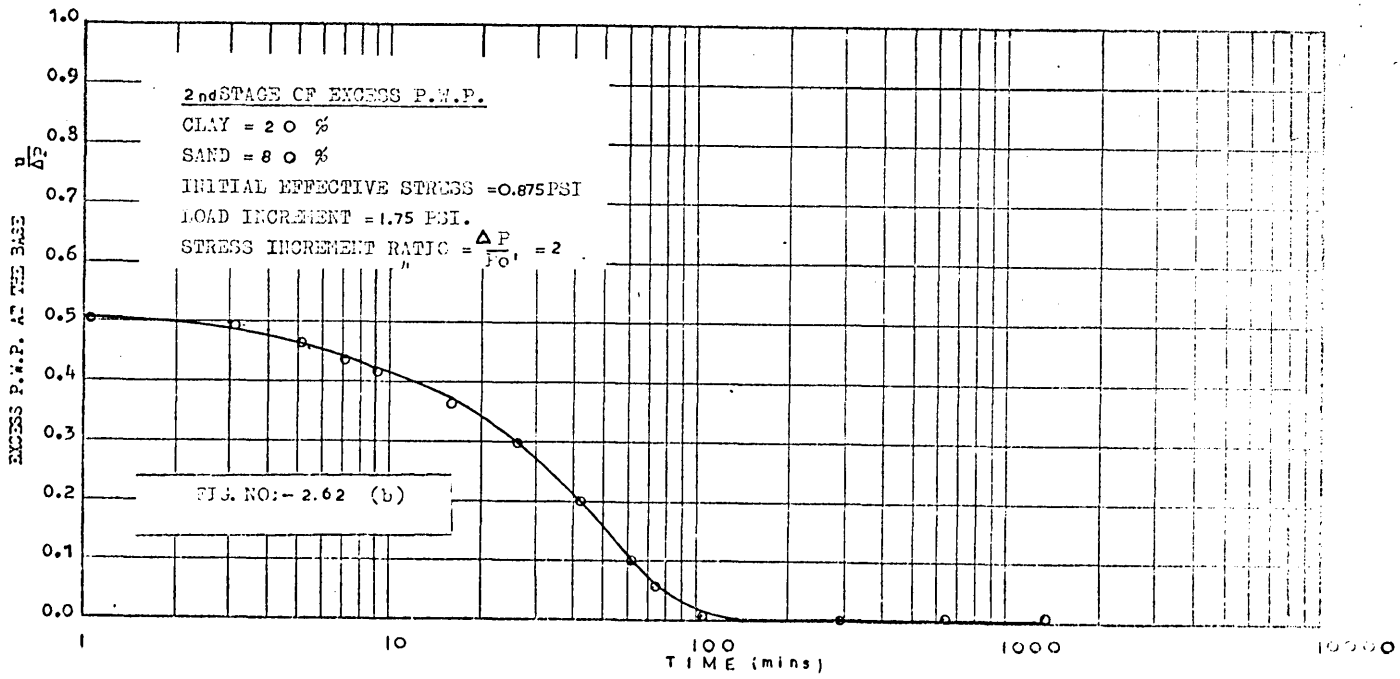

FIG. NO:- 2.62 (b)

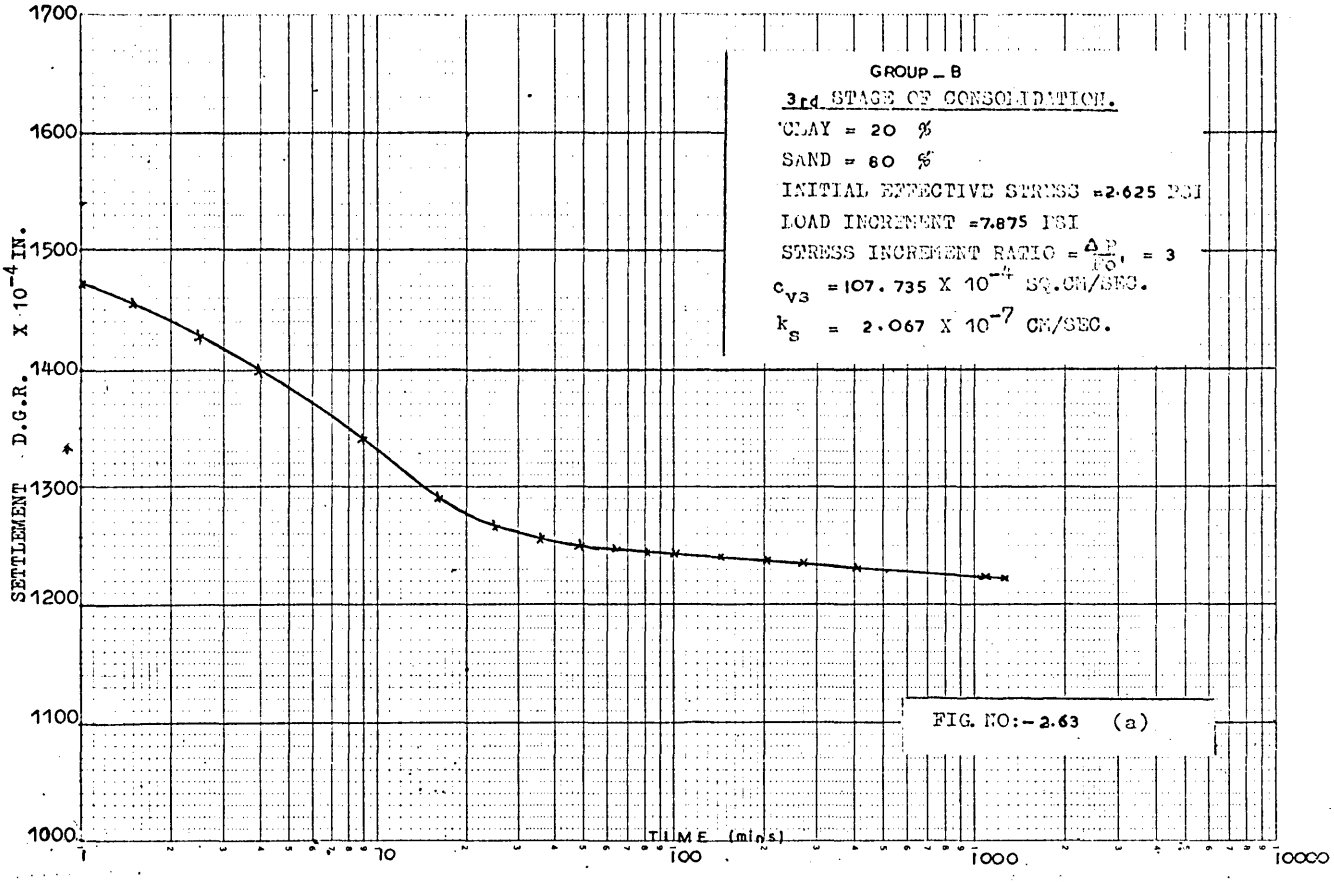

FIG. NO:- 2.63 (a)

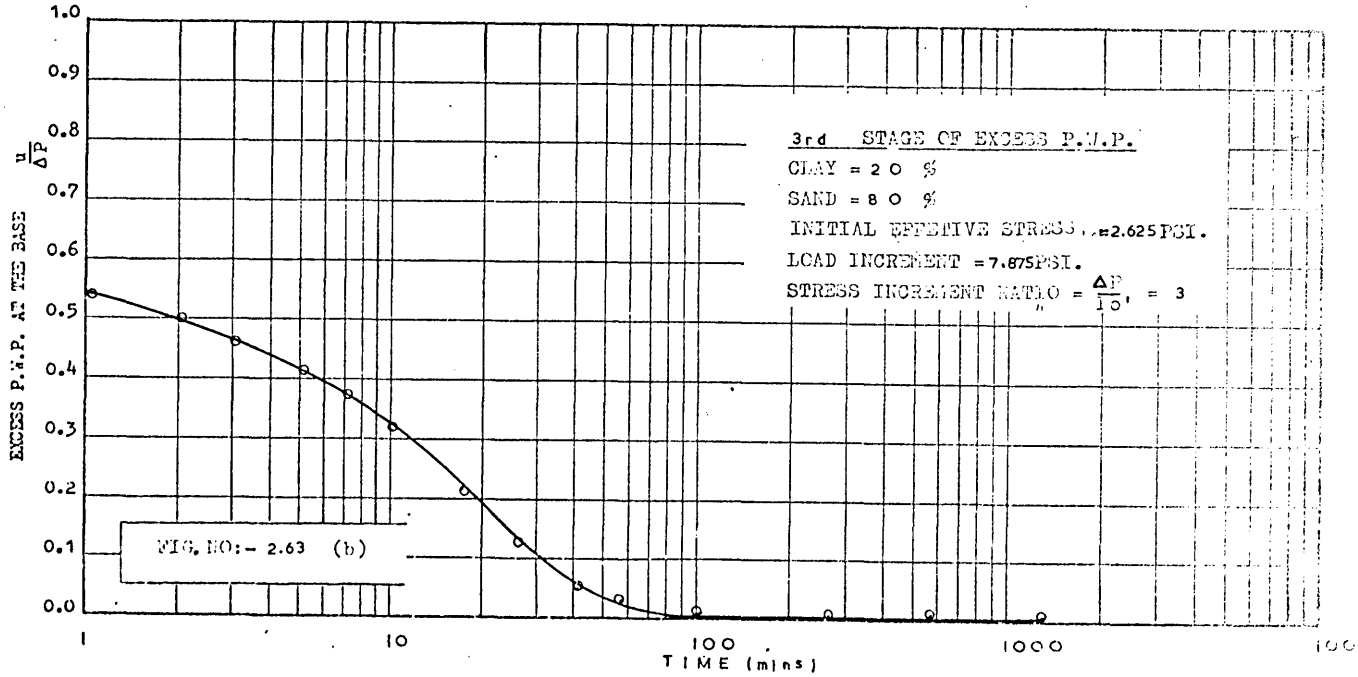

FIG. NO:- 2.63 (b)

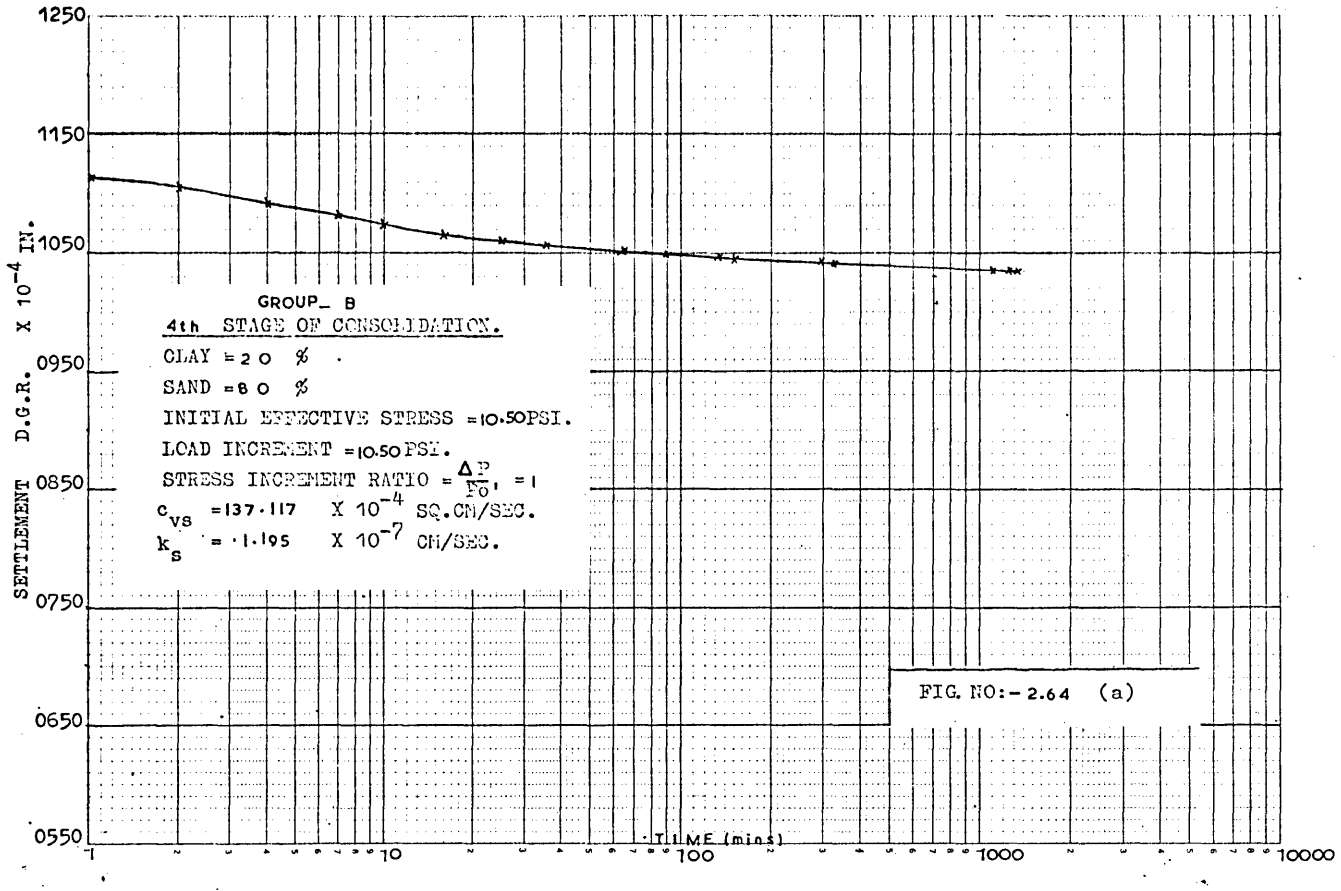
1250
1150
1050
0950
0850
0750
0650
0550
SETTLEMENT D.G.R. X 10^{-4} IN.
TIME (mins)
1
10
100
1000
10000
GROUP_ B
4th STAGE OF CONSOLIDATION.
CLAY = 2 0 %
SAND = 8 0 %
INITIAL EFFECTIVE STRESS = 10·50 PSI.
LOAD INCREMENT = 10·50 PSI.
STRESS INCREMENT RATIO = $\frac{\Delta P}{P_0}$, = 1
c_{vs} = 137·117 X 10^{-4} SQ.CM/SEC.
k_s = ·1·195 X 10^{-7} CM/SEC.
FIG. NO:- 2.64 (a)

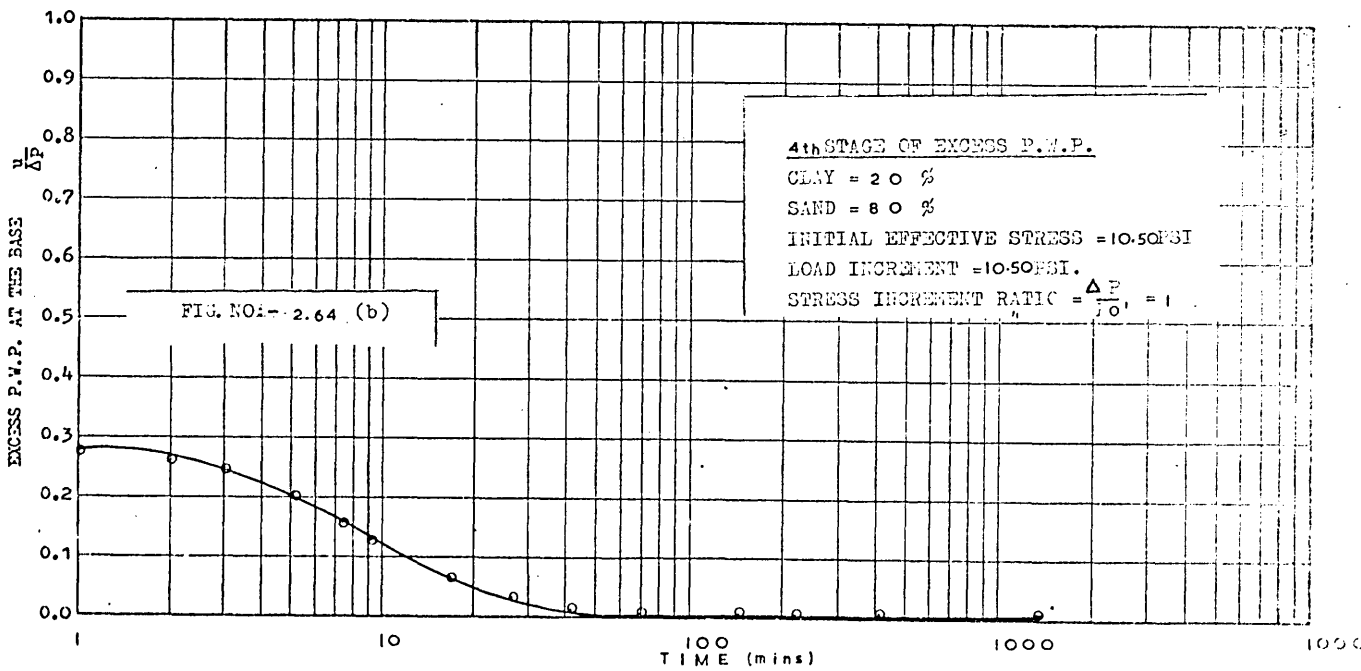
1.0
0.9
0.8
0.7
0.6
0.5
0.4
0.3
0.2
0.1
0.0
EXCESS P.W.P. AT THE BASS $\frac{u}{\Delta P}$
TIME (mins)
1
10
100
1000
10000
4th STAGE OF EXCESS P.W.P.
CLAY = 2 0 %
SAND = 8 0 %
INITIAL EFFECTIVE STRESS = 10·50 PSI
LOAD INCREMENT = 10·50 PSI.
STRESS INCREMENT RATIO = $\frac{\Delta P}{P_0}$, = 1
FIG. NO:- 2.64 (b)

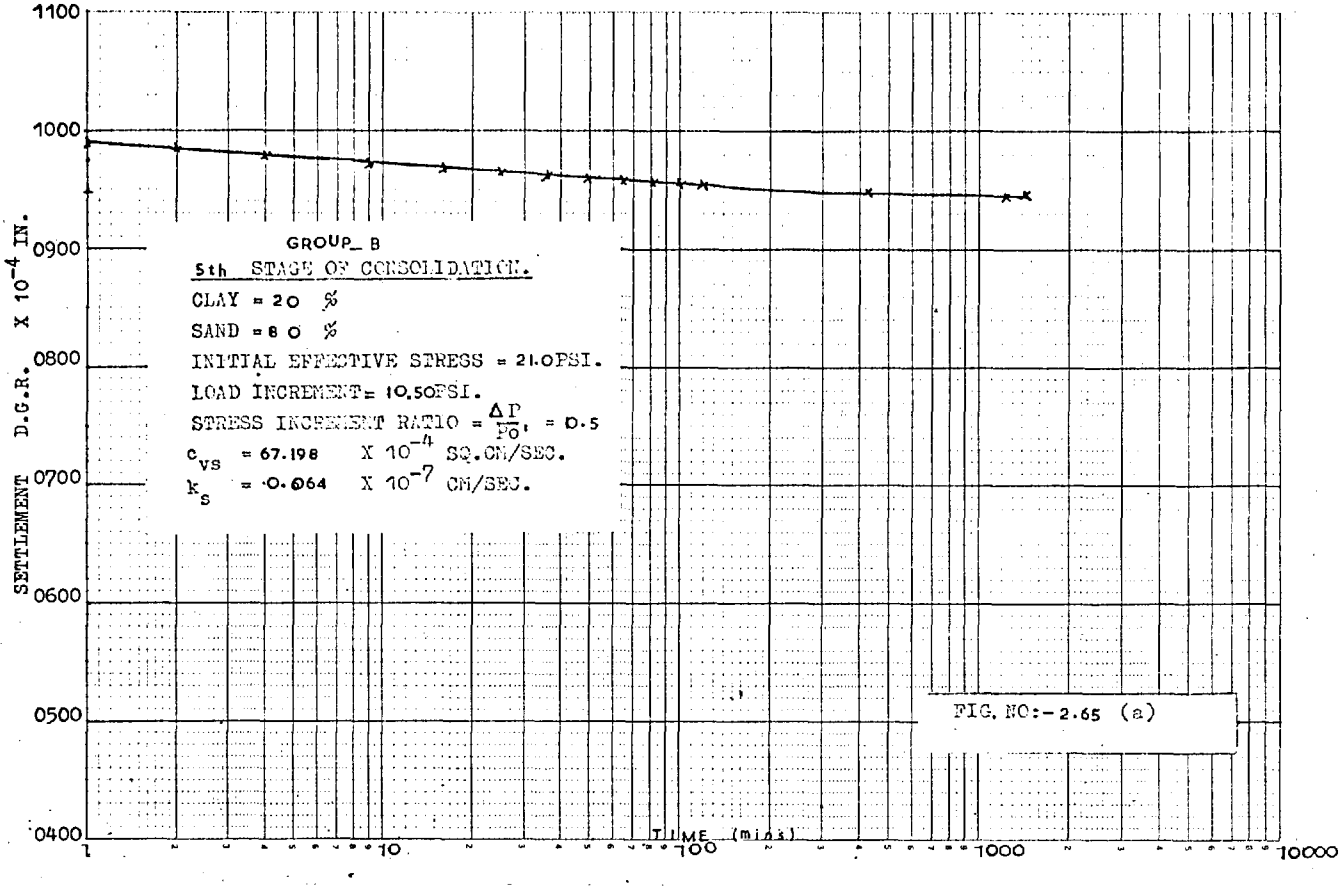
GROUP_ B
5th STAGE OF CONSOLIDATION.
CLAY = 20 %
SAND = 80 %
INITIAL EFFECTIVE STRESS = 21.0PSI.
LOAD INCREMENT= 10.50PSI.
STRESS INCREMENT RATIO = ΔP/Po = 0.5
cvs = 67.198 X 10^-4 SQ.CM/SEC.
ks = 0.064 X 10^-7 CM/SEC.
FIG. NO:- 2.65 (a)
SETTLEMENT D.G.R. X 10^-4 IN.
TIME (mins)
1100
1000
0900
0800
0700
0600
0500
0400
1
10
100
1000
10000

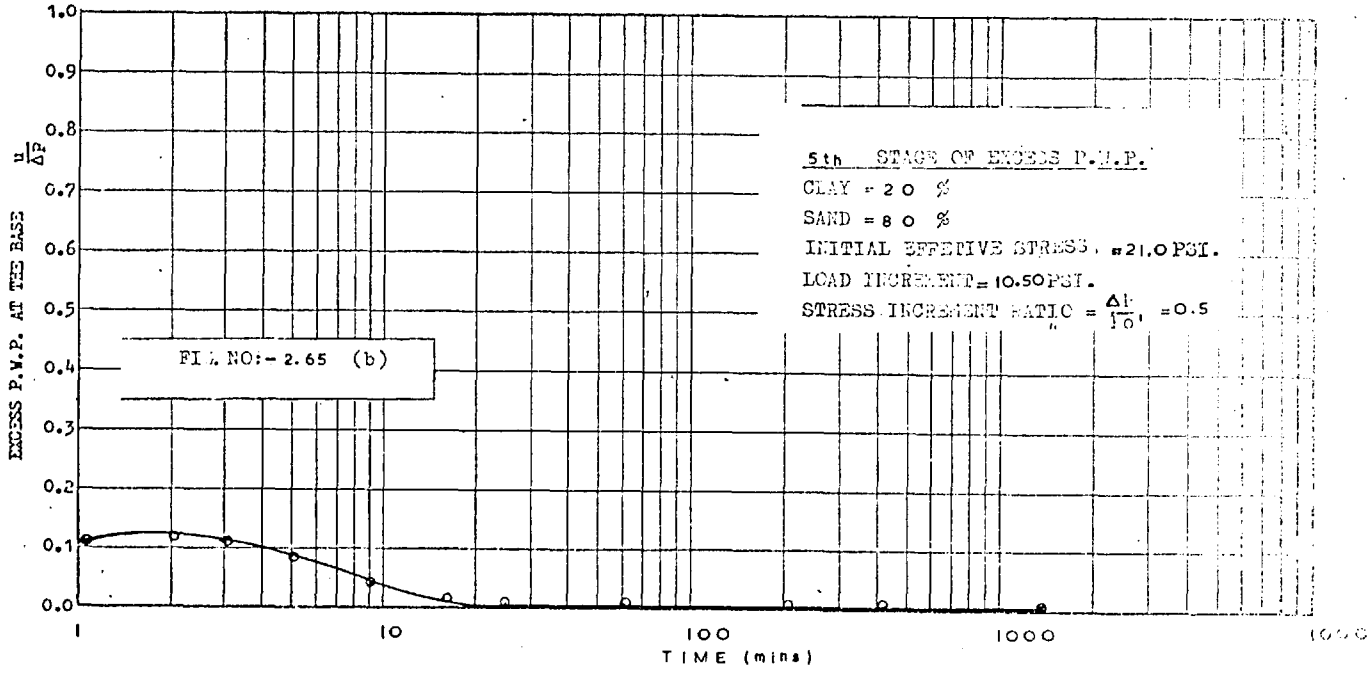
5th STAGE OF EXCESS P.W.P.
CLAY = 20 %
SAND = 80 %
INITIAL EFFECTIVE STRESS = 21.0PSI.
LOAD INCREMENT= 10.50PSI.
STRESS INCREMENT RATIO = Δσ/σ = 0.5
FIG NO:- 2.65 (b)
EXCESS P.W.P. AT THE BASE u/ΔP
TIME (mins)
1.0
0.9
0.8
0.7
0.6
0.5
0.4
0.3
0.2
0.1
0.0
1
10
100
1000
10000

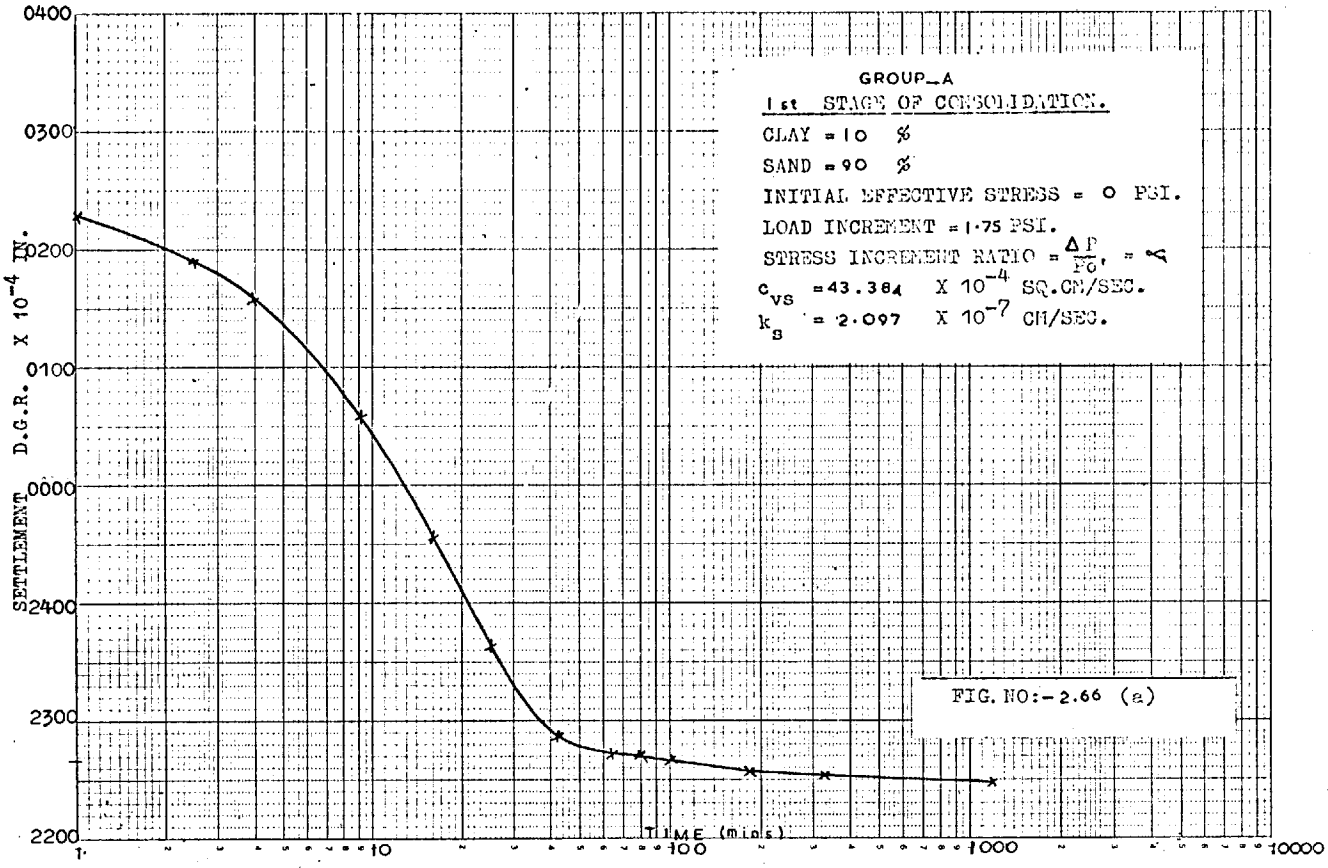

FIG. NO:- 2.66 (a)

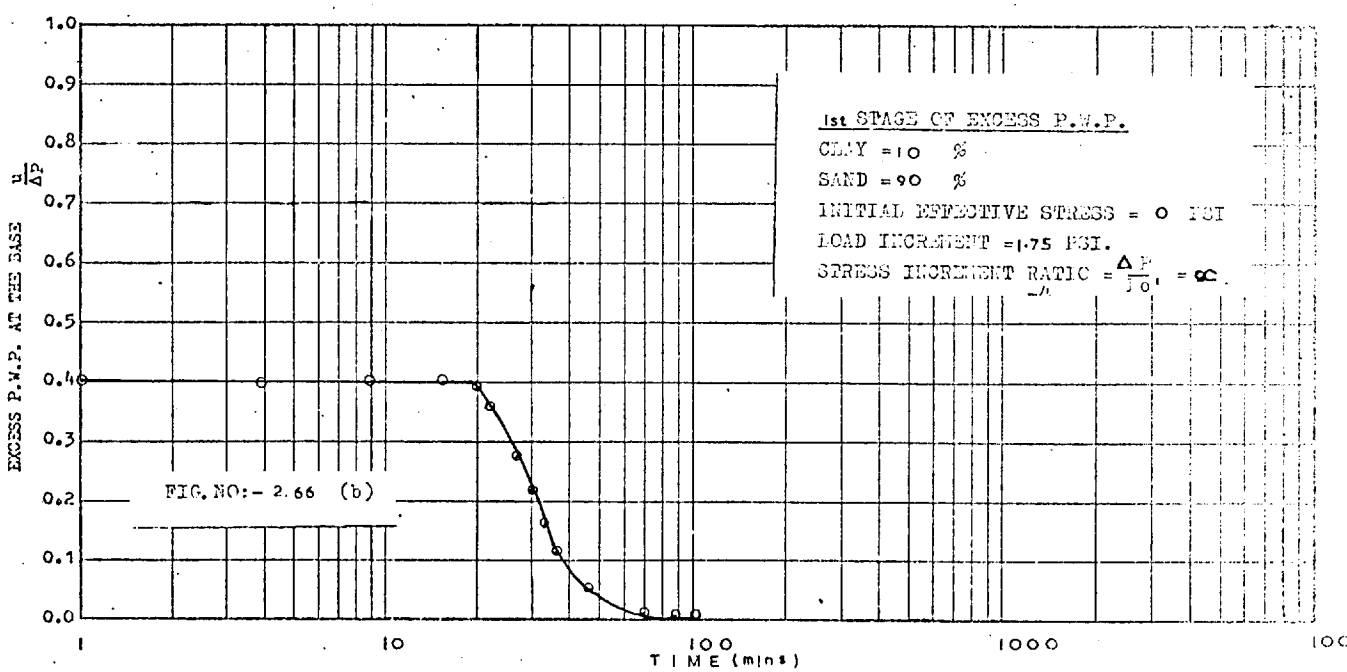

FIG. NO:- 2.66 (b)

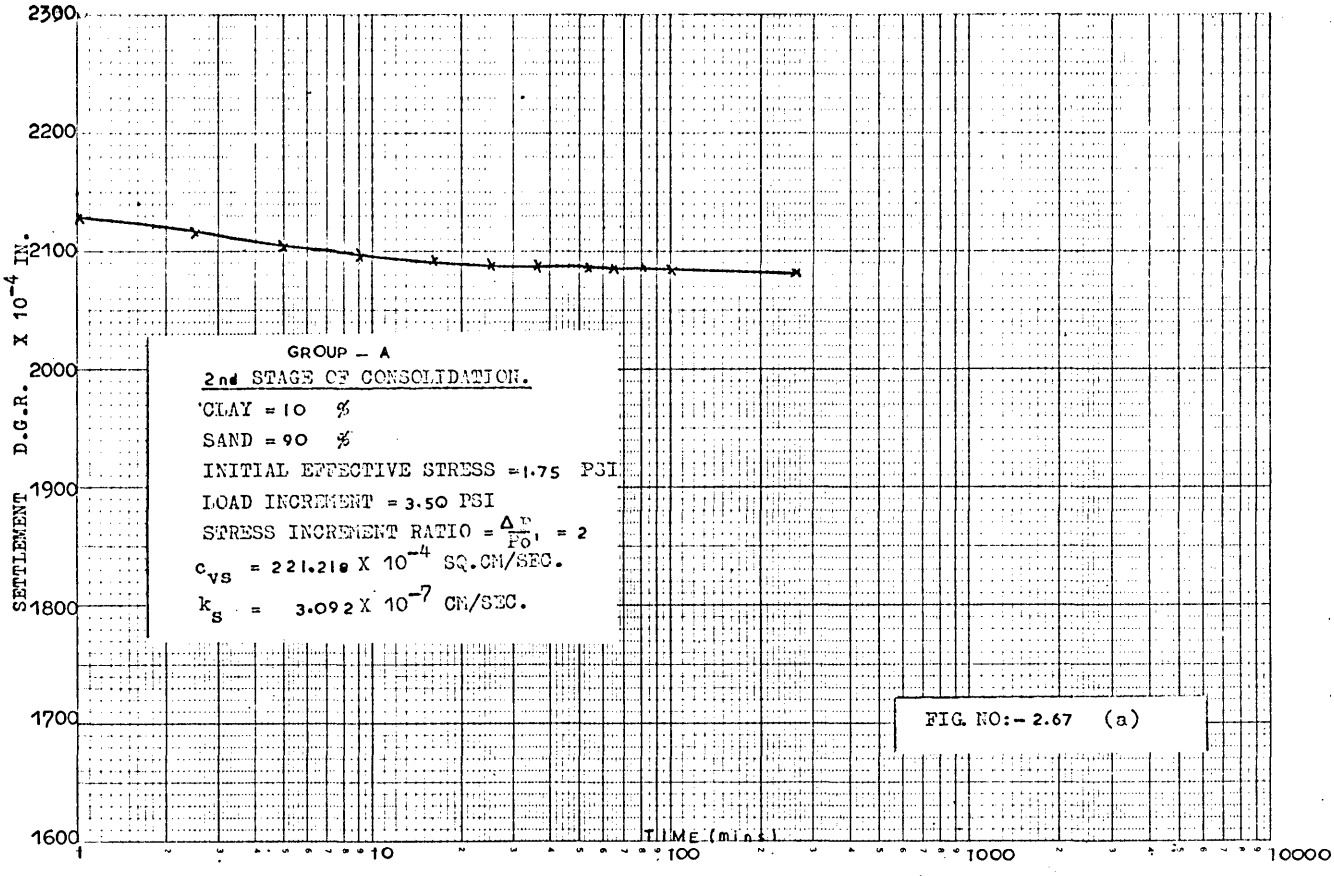

FIG. NO:– 2.67 (a)

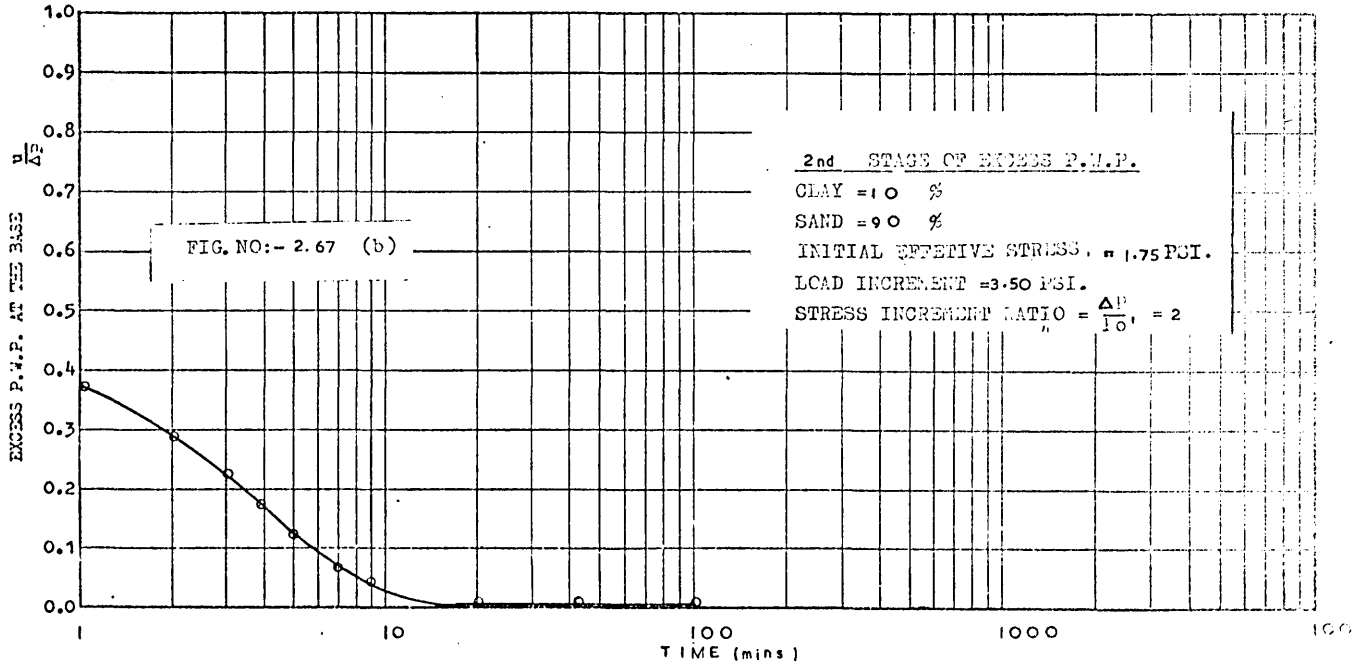

FIG. NO:– 2.67 (b)

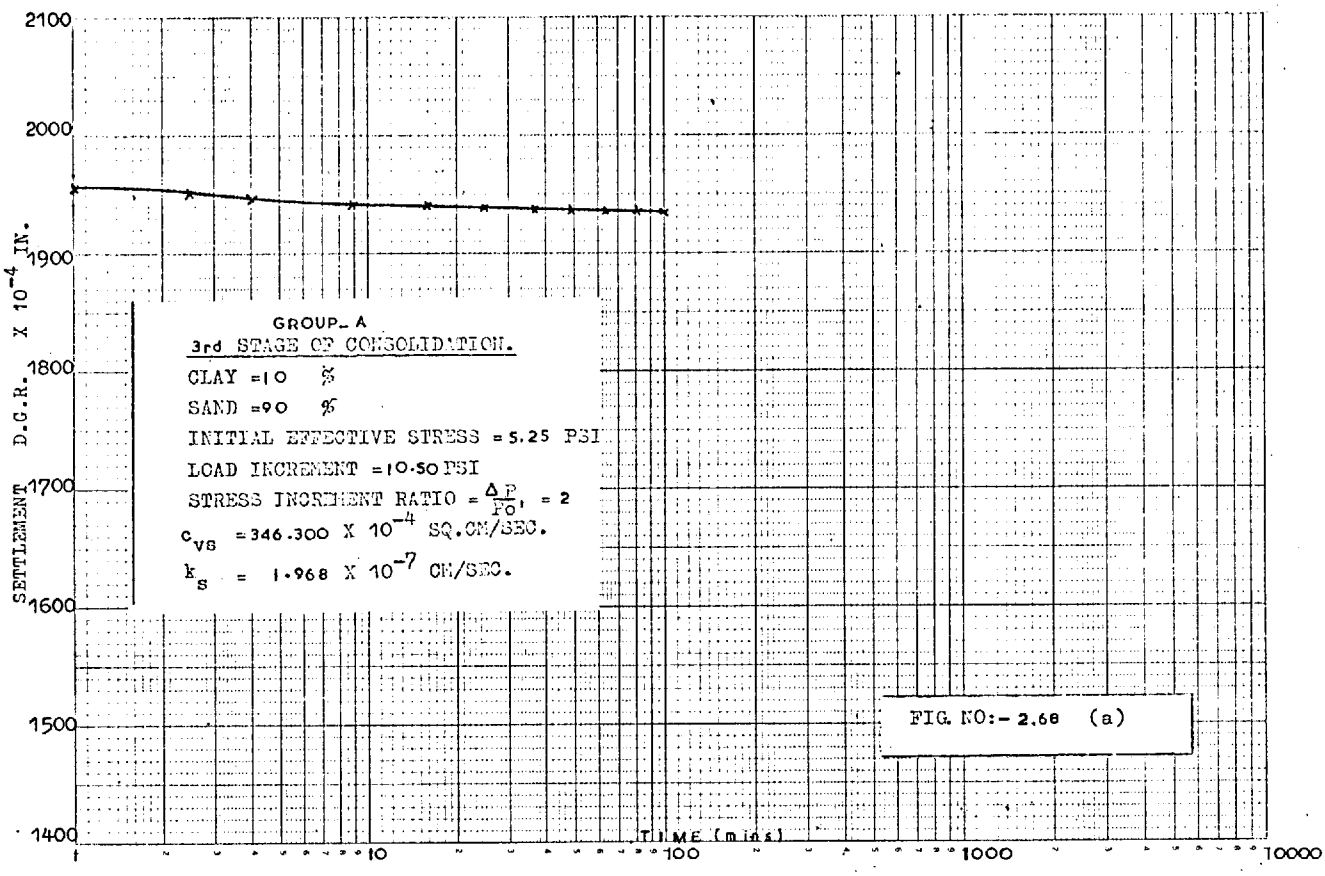
SETTLEMENT D.G.R. X 10^{-4} IN.
2100
2000
1900
1800
1700
1600
1500
1400
TIME (mins)
1
10
100
1000
10000
GROUP- A
3rd STAGE OF CONSOLIDATION.
CLAY =10 %
SAND =90 %
INITIAL EFFECTIVE STRESS = 5.25 PSI
LOAD INCREMENT =10.50 PSI
STRESS INCREMENT RATIO = $\frac{\Delta P}{Fo}$ = 2
c_{vs} = 346.300 X 10^{-4} SQ.CM/SEC.
k_s = 1.968 X 10^{-7} CM/SEC.
FIG. NO:- 2.68 (a)

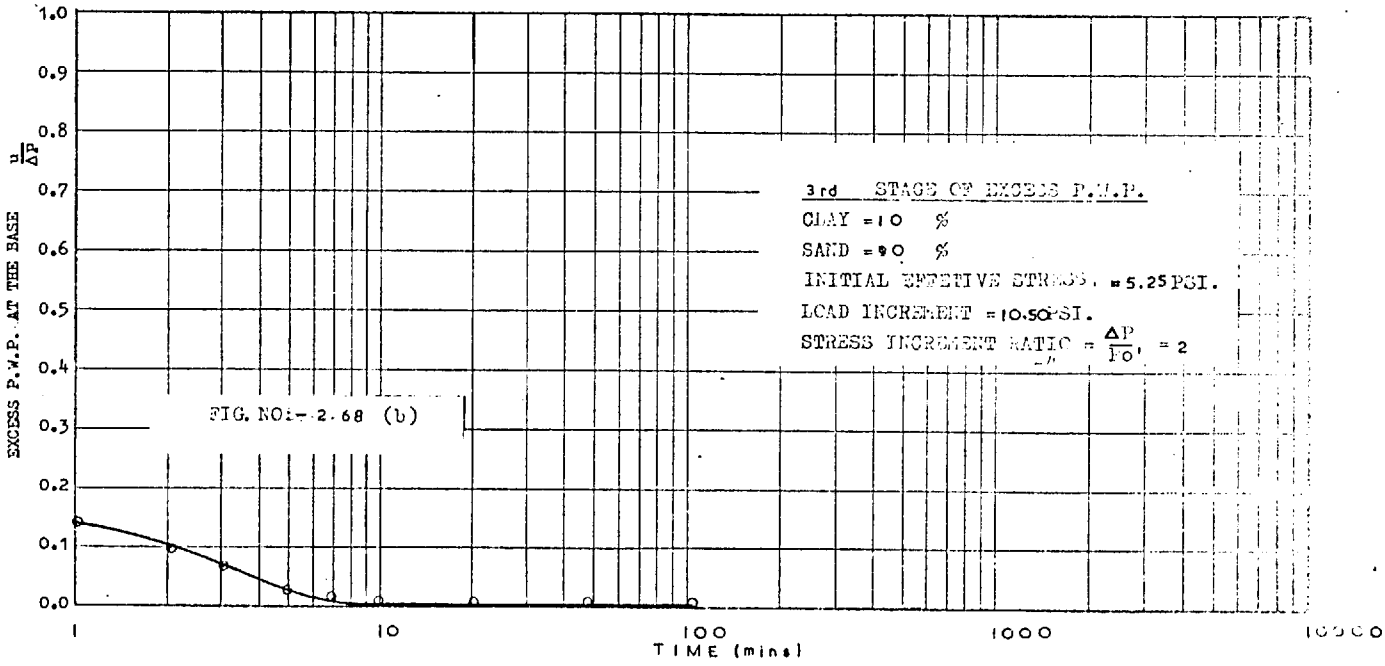
EXCESS P.W.P. AT THE BASE $\frac{u}{\Delta P}$
1.0
0.9
0.8
0.7
0.6
0.5
0.4
0.3
0.2
0.1
0.0
TIME (mins)
1
10
100
1000
3rd STAGE OF EXCESS P.W.P.
CLAY =10 %
SAND =90 %
INITIAL EFFECTIVE STRESS = 5.25 PSI.
LOAD INCREMENT =10.50 PSI.
STRESS INCREMENT RATIO = $\frac{\Delta P}{Fo}$ = 2
FIG. NO:- 2.68 (b)

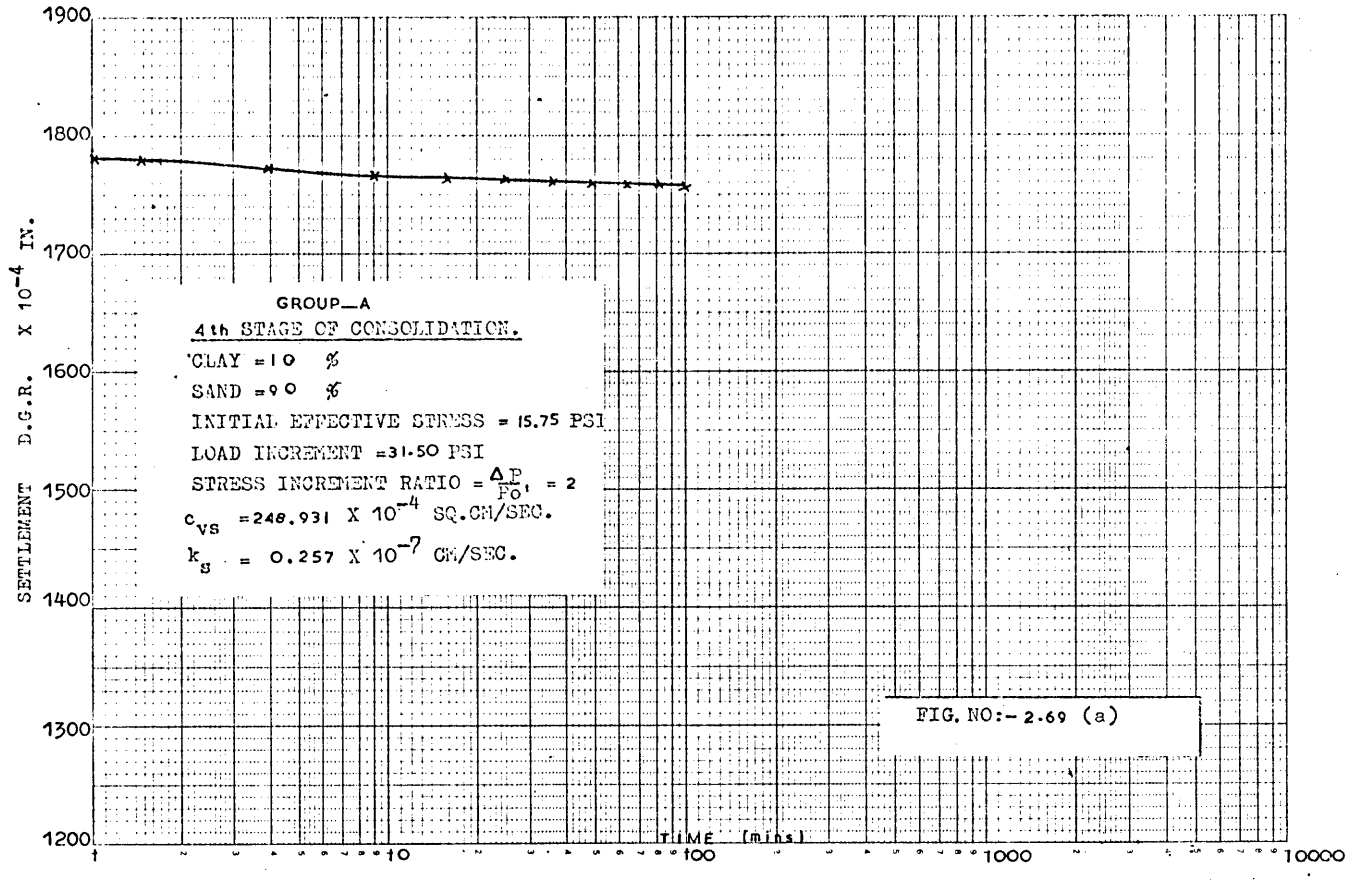

FIG. NO:- 2.69 (a)

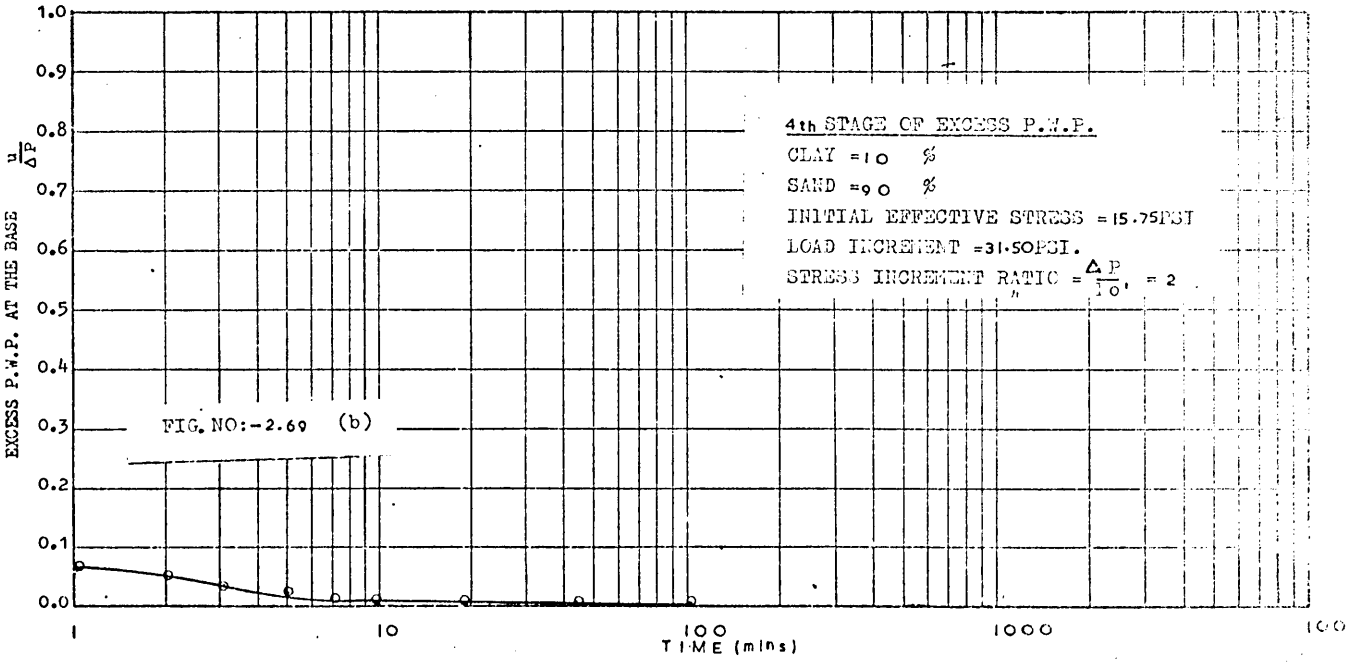

FIG. NO:- 2.69 (b)

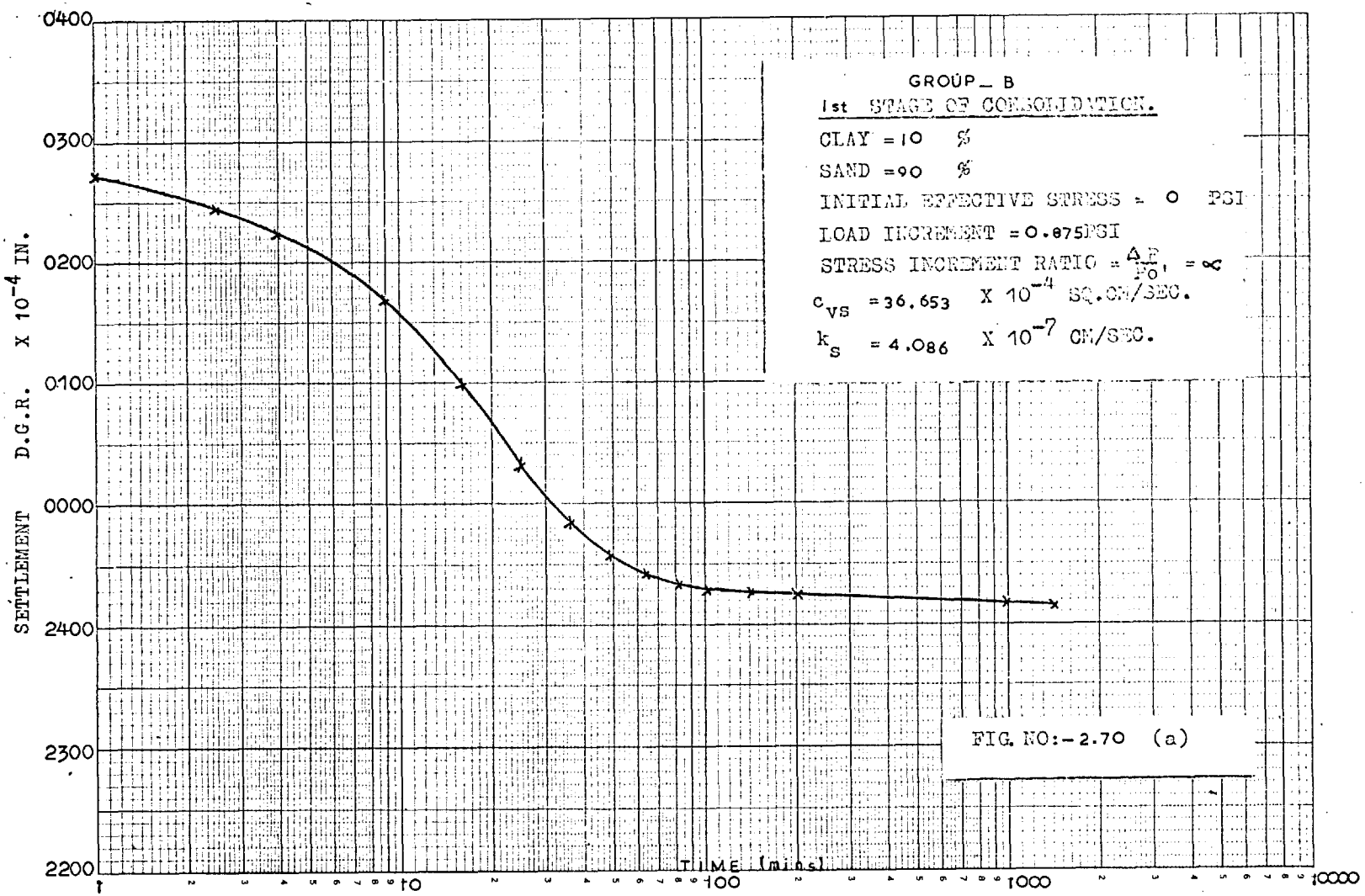
GROUP_ B
1st STAGE OF CONSOLIDATION.
CLAY = 10 %
SAND = 90 %
INITIAL EFFECTIVE STRESS = 0 PSI
LOAD INCREMENT = 0.875PSI
STRESS INCREMENT RATIO = $\frac{\Delta P}{P_0}$ = ∞
c_{vs} = 36.653 X 10^{-4} SQ.CM/SEC.
k_s = 4.086 X 10^{-7} CM/SEC.
FIG. NO:- 2.70 (a)
SETTLEMENT D.G.R. X 10^{-4} IN.
0400
0300
0200
0100
0000
2400
2300
2200
TIME (mins)
1
10
100
1000
10000

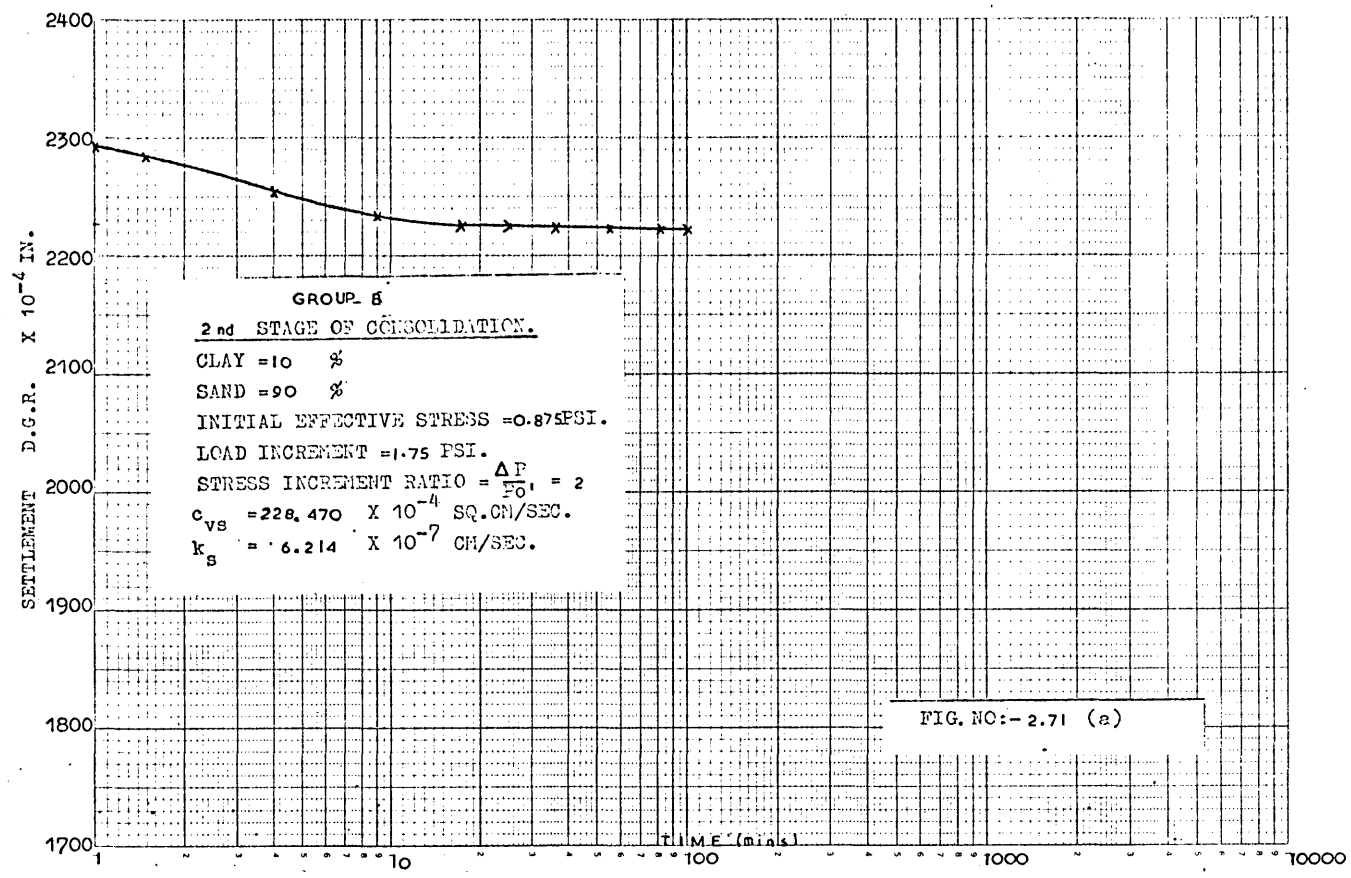

FIG. NO:- 2.71 (a)

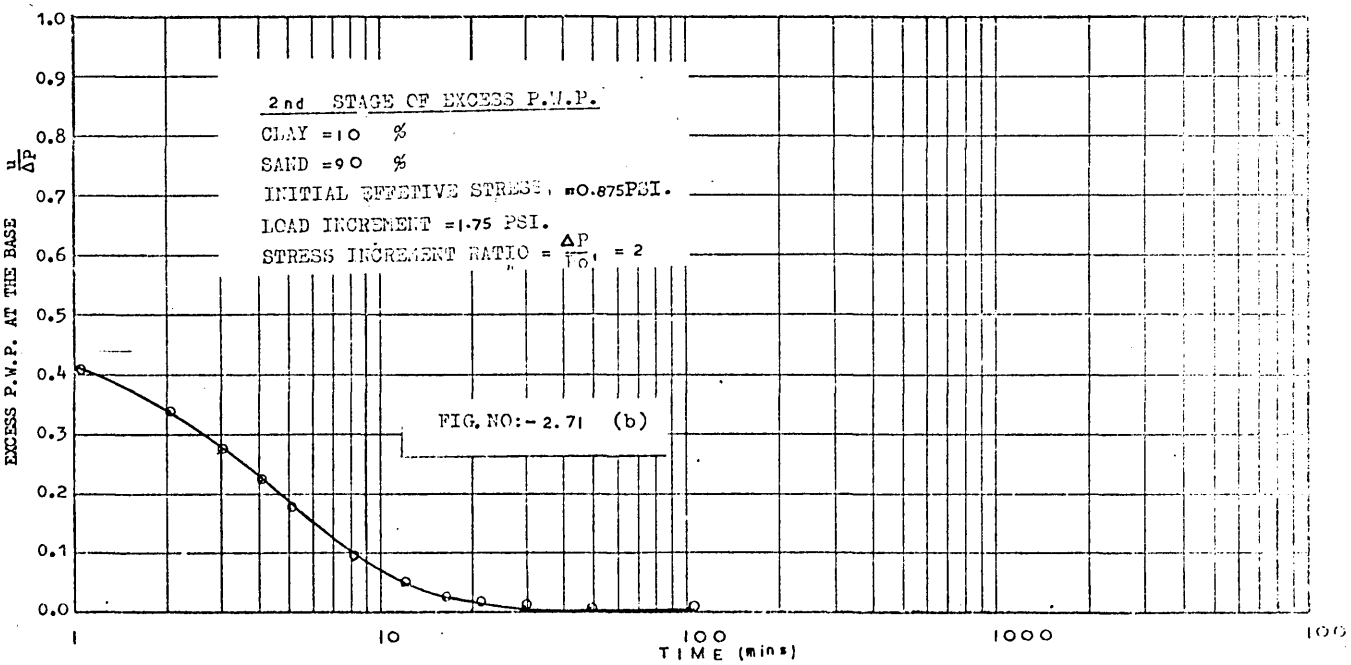

FIG. NO:- 2.71 (b)

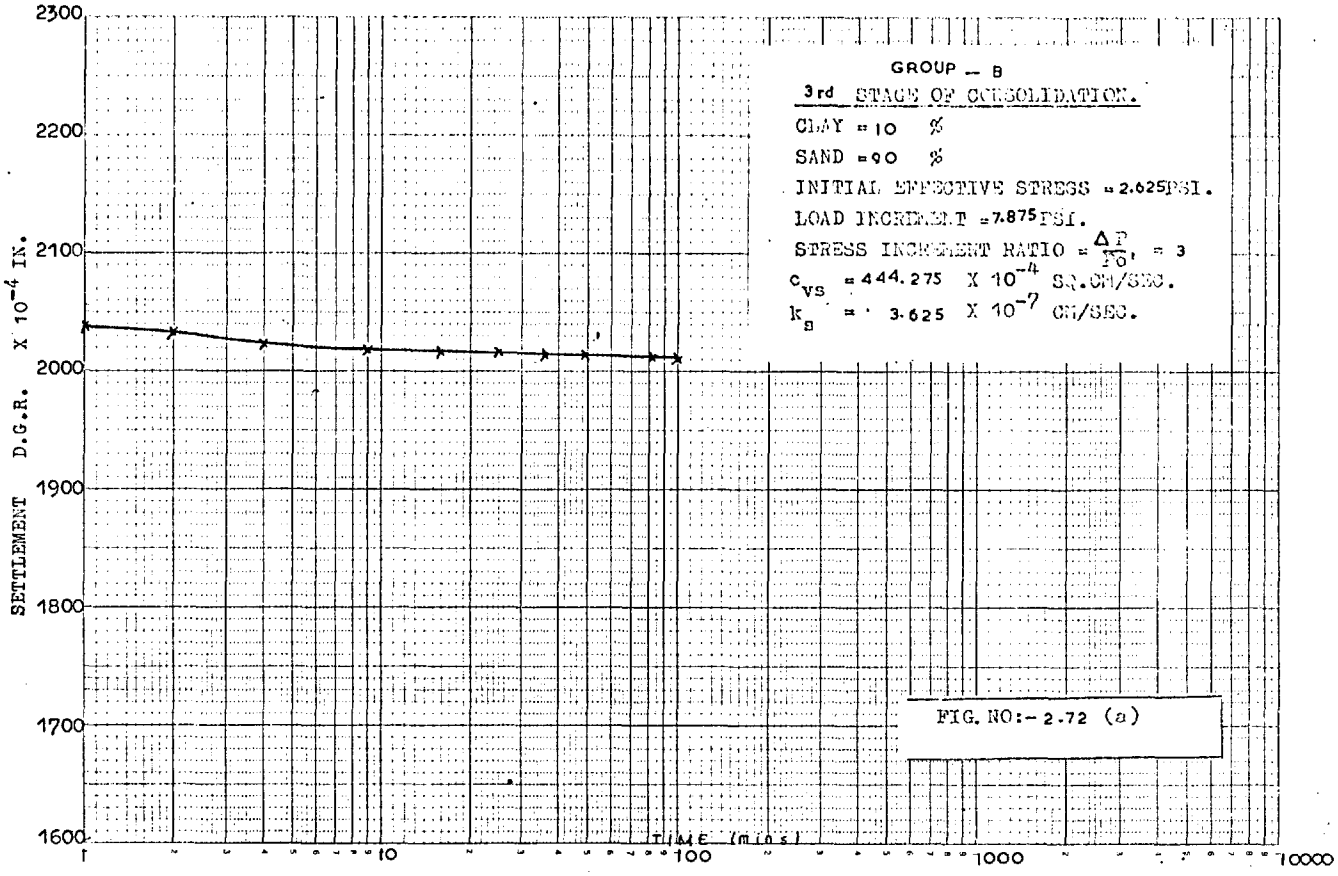

FIG. NO:- 2.72 (a)

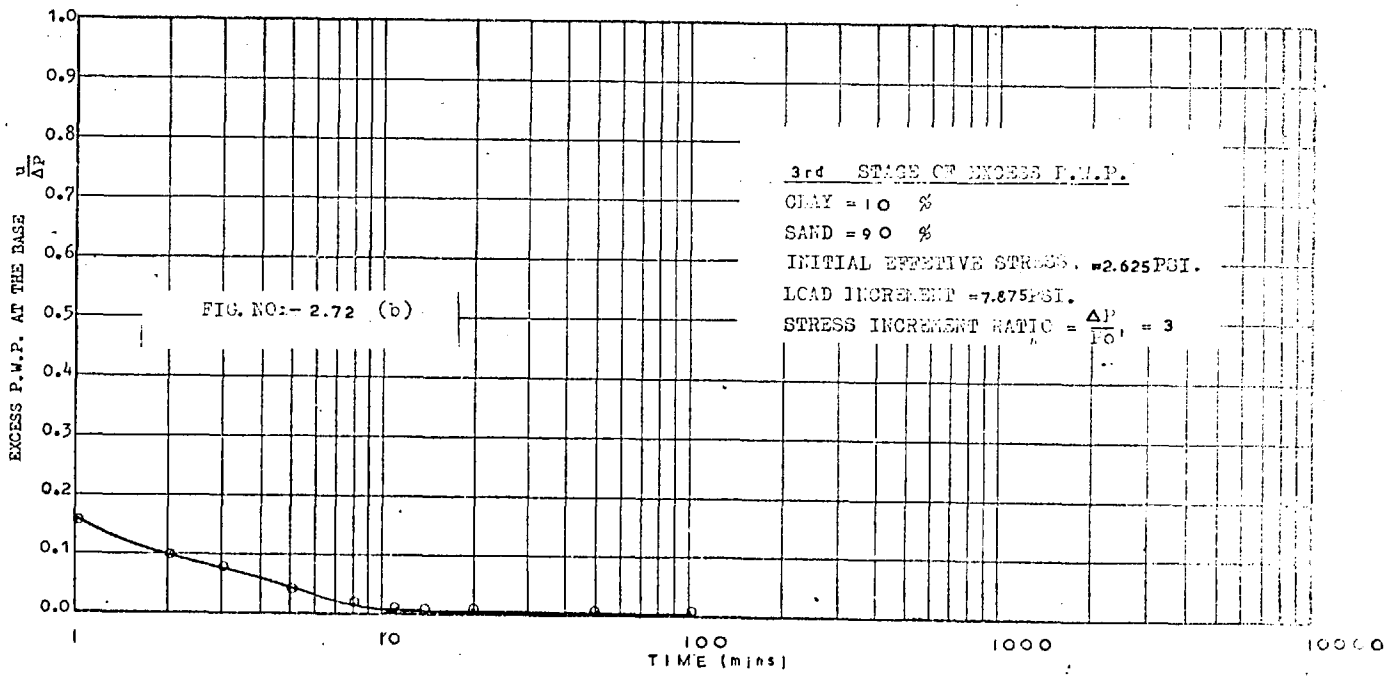

FIG. NO:- 2.72 (b)

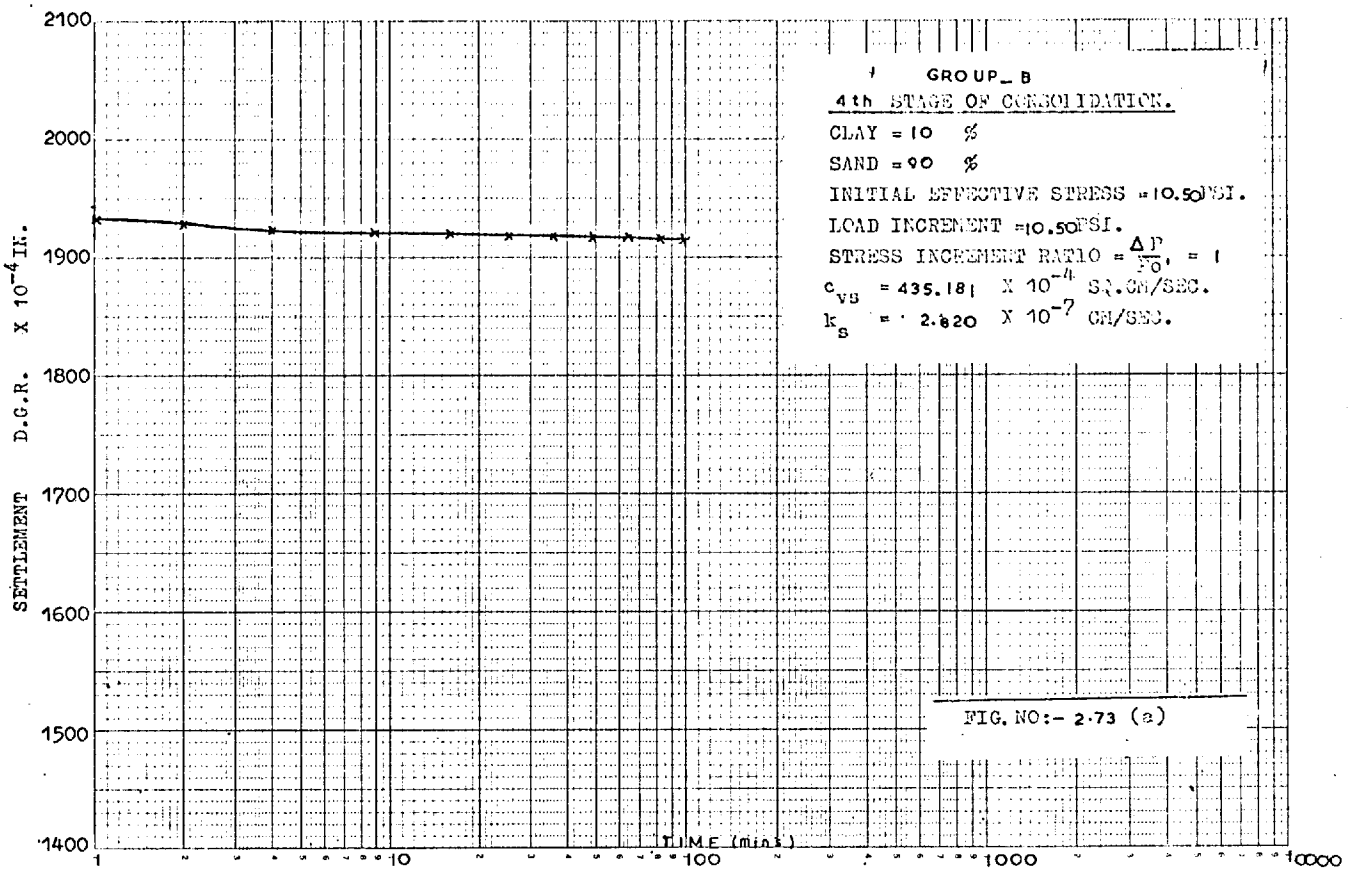
GROUP_B
4th STAGE OF CONSOLIDATION.
CLAY = 10 %
SAND = 90 %
INITIAL EFFECTIVE STRESS = 10.50 PSI.
LOAD INCREMENT = 10.50 PSI.
STRESS INCREMENT RATIO = ΔP/P0 = 1
c_{vs} = 435.181 X 10^{-4} SQ.CM/SEC.
k_s = 2.820 X 10^{-7} CM/SEC.
FIG. NO:- 2.73 (a)
SETTLEMENT D.G.R. X 10^{-4} IN.
TIME (mins)
2100
2000
1900
1800
1700
1600
1500
1400
1
10
100
1000
10000

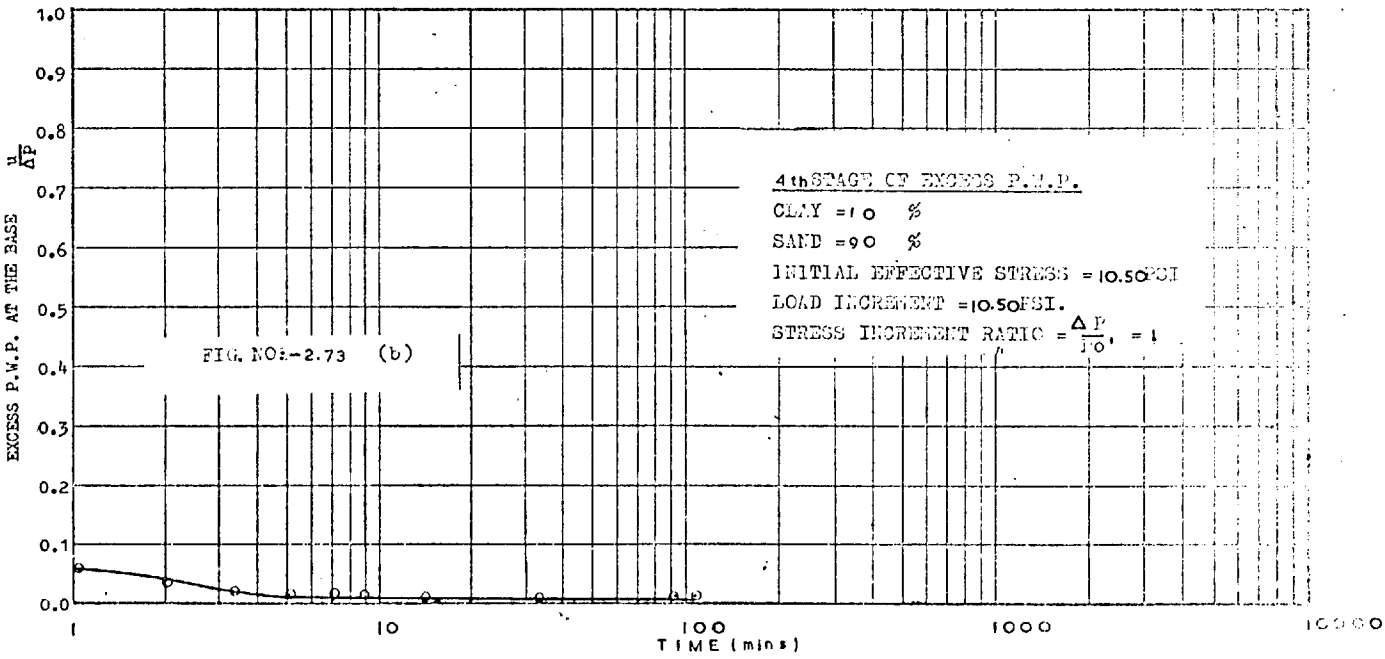
4th STAGE OF EXCESS P.W.P.
CLAY = 10 %
SAND = 90 %
INITIAL EFFECTIVE STRESS = 10.50 PSI
LOAD INCREMENT = 10.50 PSI.
STRESS INCREMENT RATIO = ΔP/P0 = 1
FIG. NO:- 2.73 (b)
EXCESS P.W.P. AT THE BASE u/ΔP
TIME (mins)
1.0
0.9
0.8
0.7
0.6
0.5
0.4
0.3
0.2
0.1
0.0
1
10
100
1000
10000

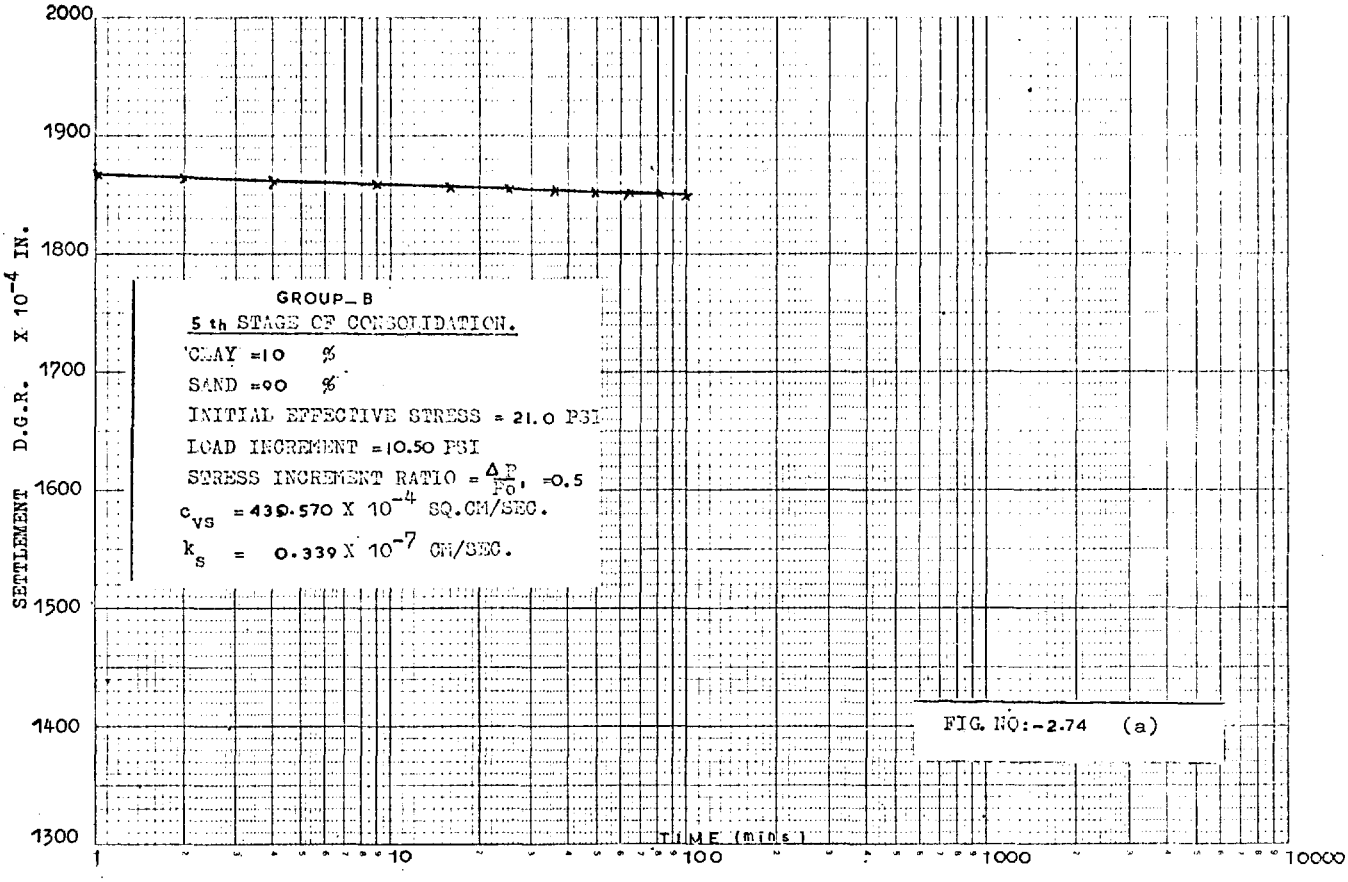

FIG. NO:-2.74 (a)

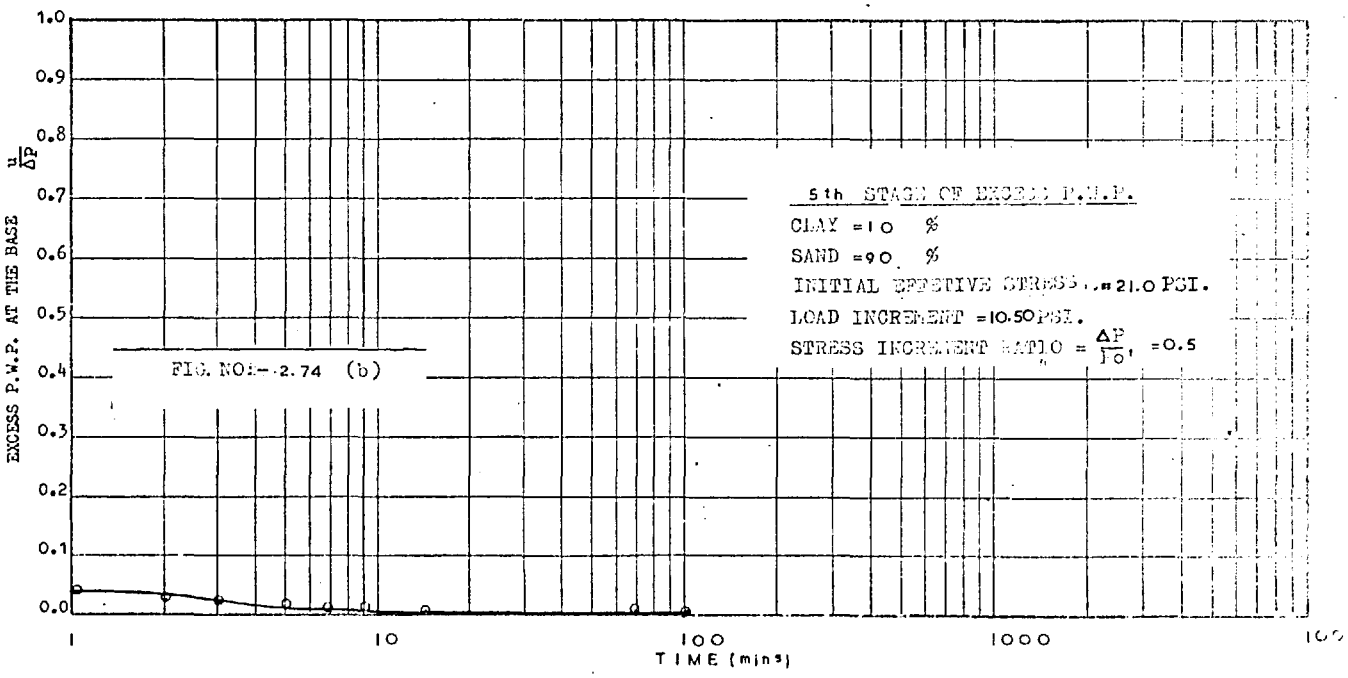

FIG. NO:-2.74 (b)

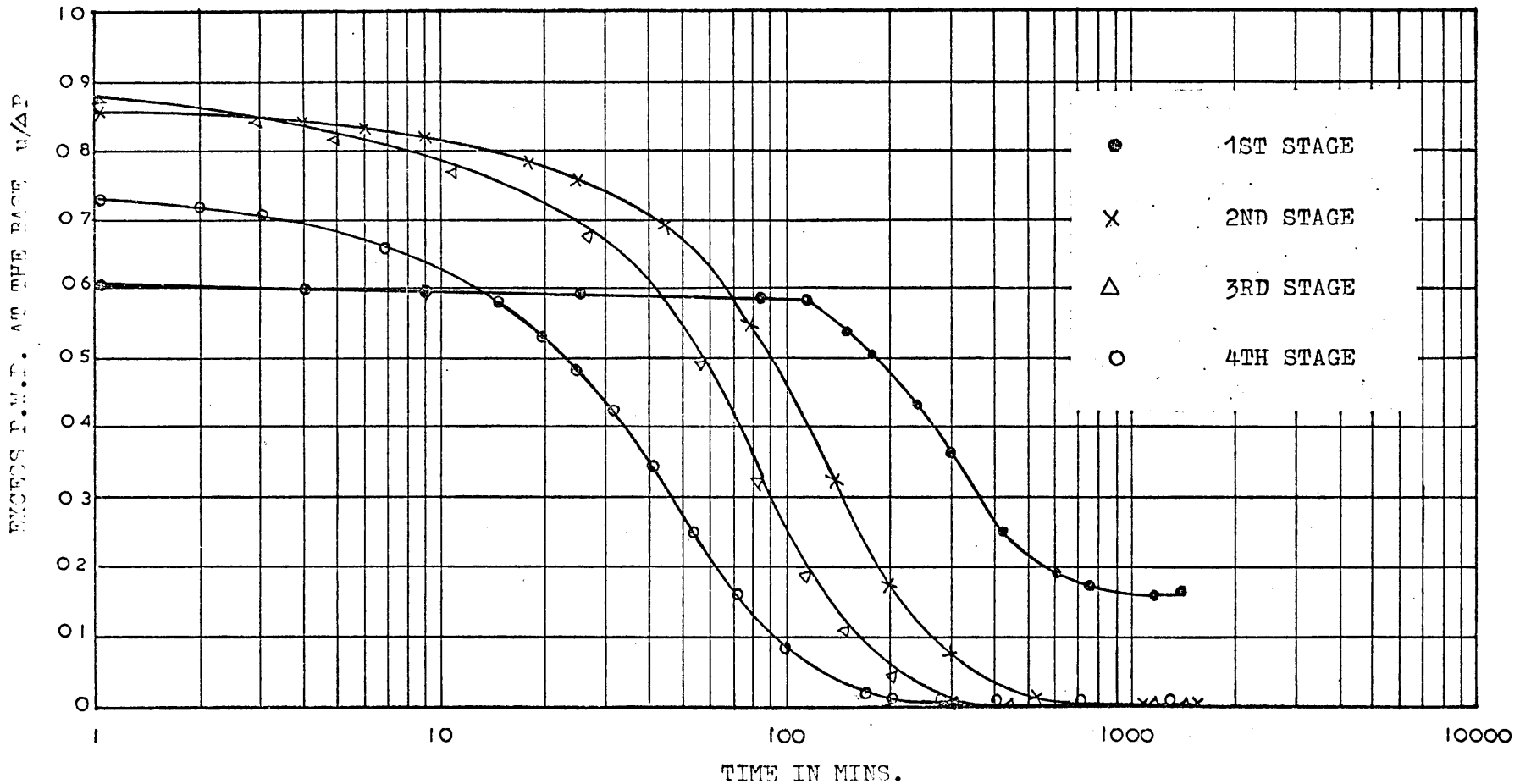

FIGURE NO. 2.75. P.W.P. DISSIPATION CURVES OF 100% CLAY (GROUP A)

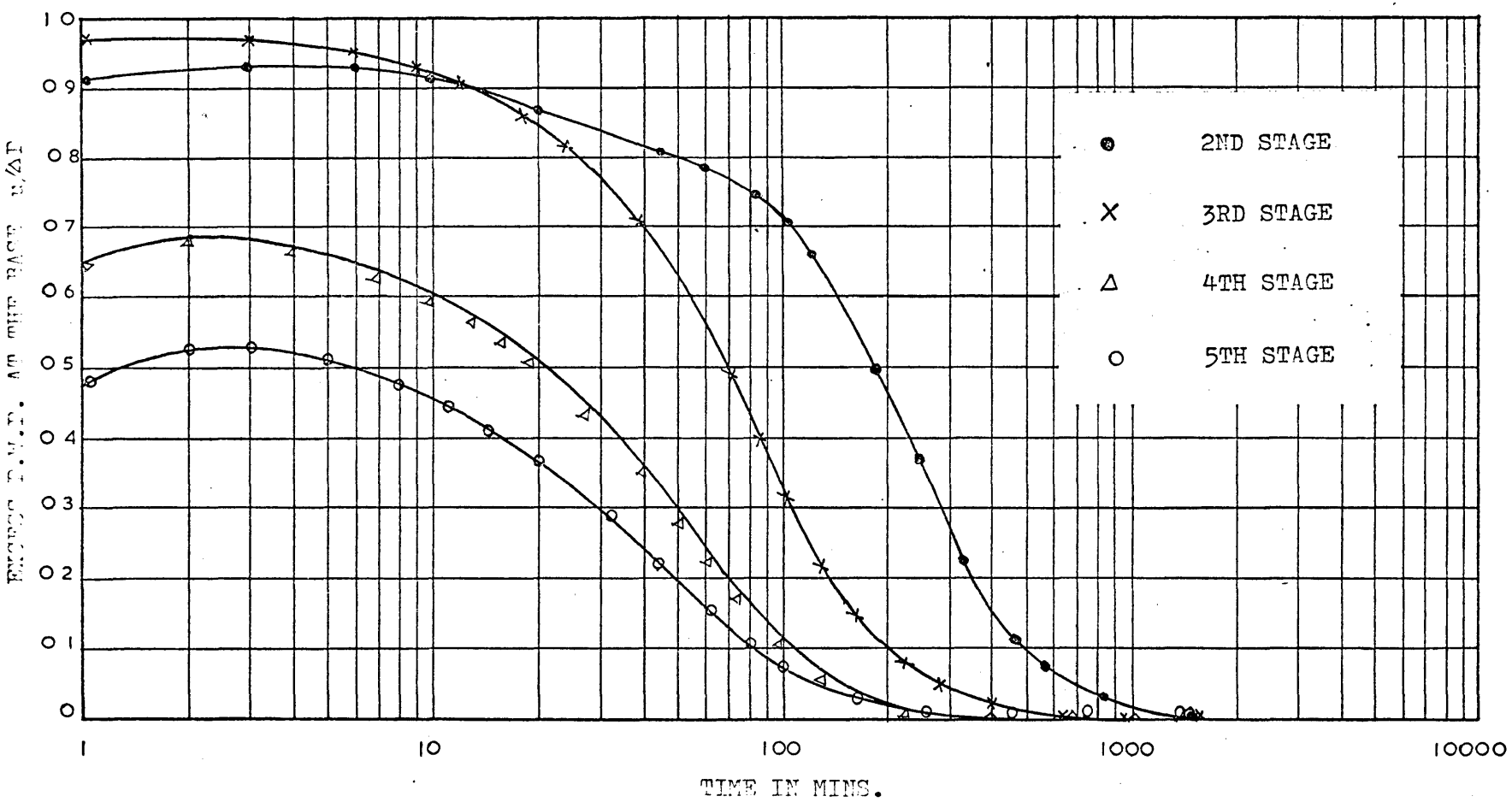

FIGURE NO. 2.76 P.W.P. DISSIPATION CURVES OF 100% CLAY (GROUP B)

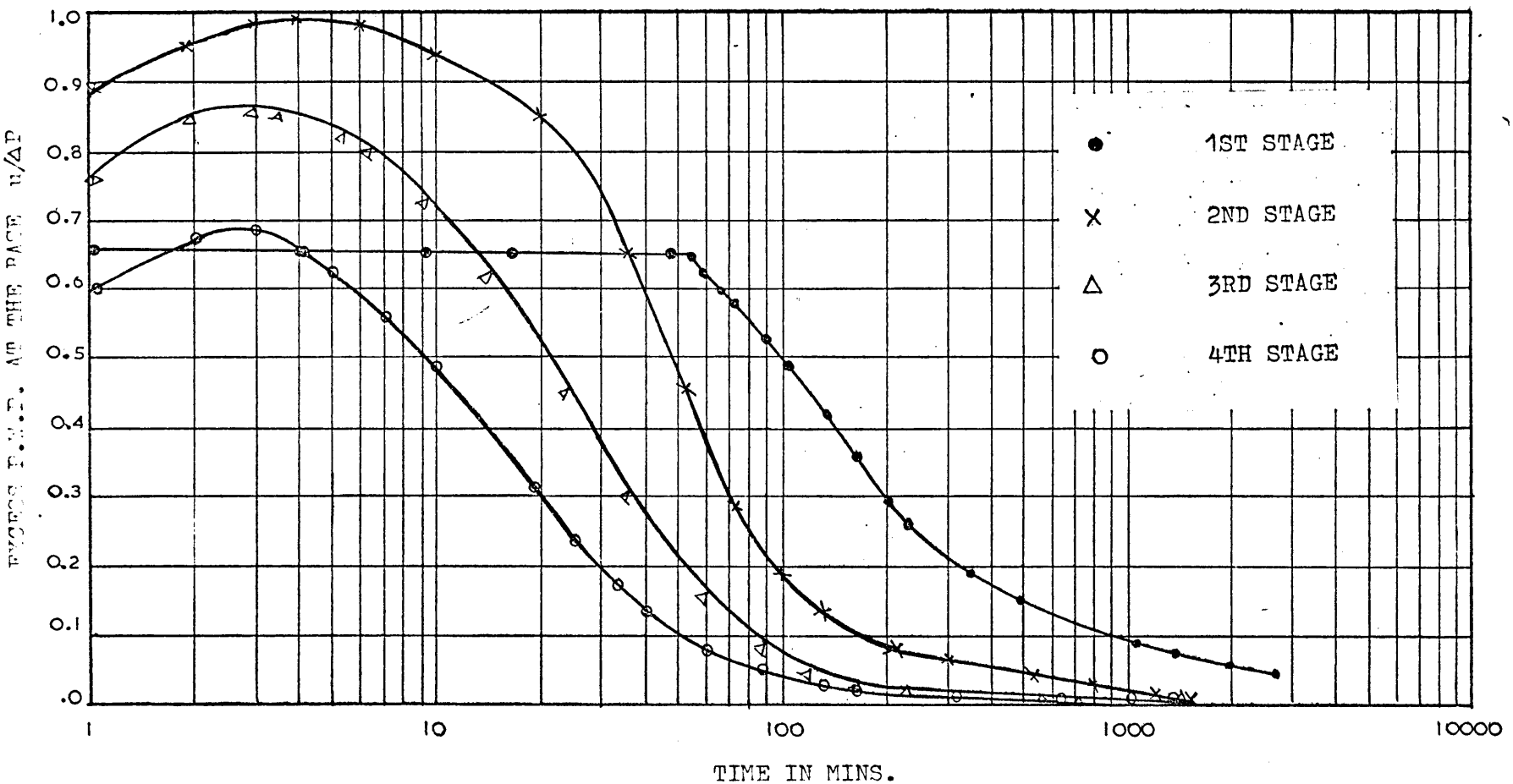

FIGURE NO. 2.77. P.W.P. DISSIPATION CURVES OF 90% CLAY- 10% SAND (GROUP A)

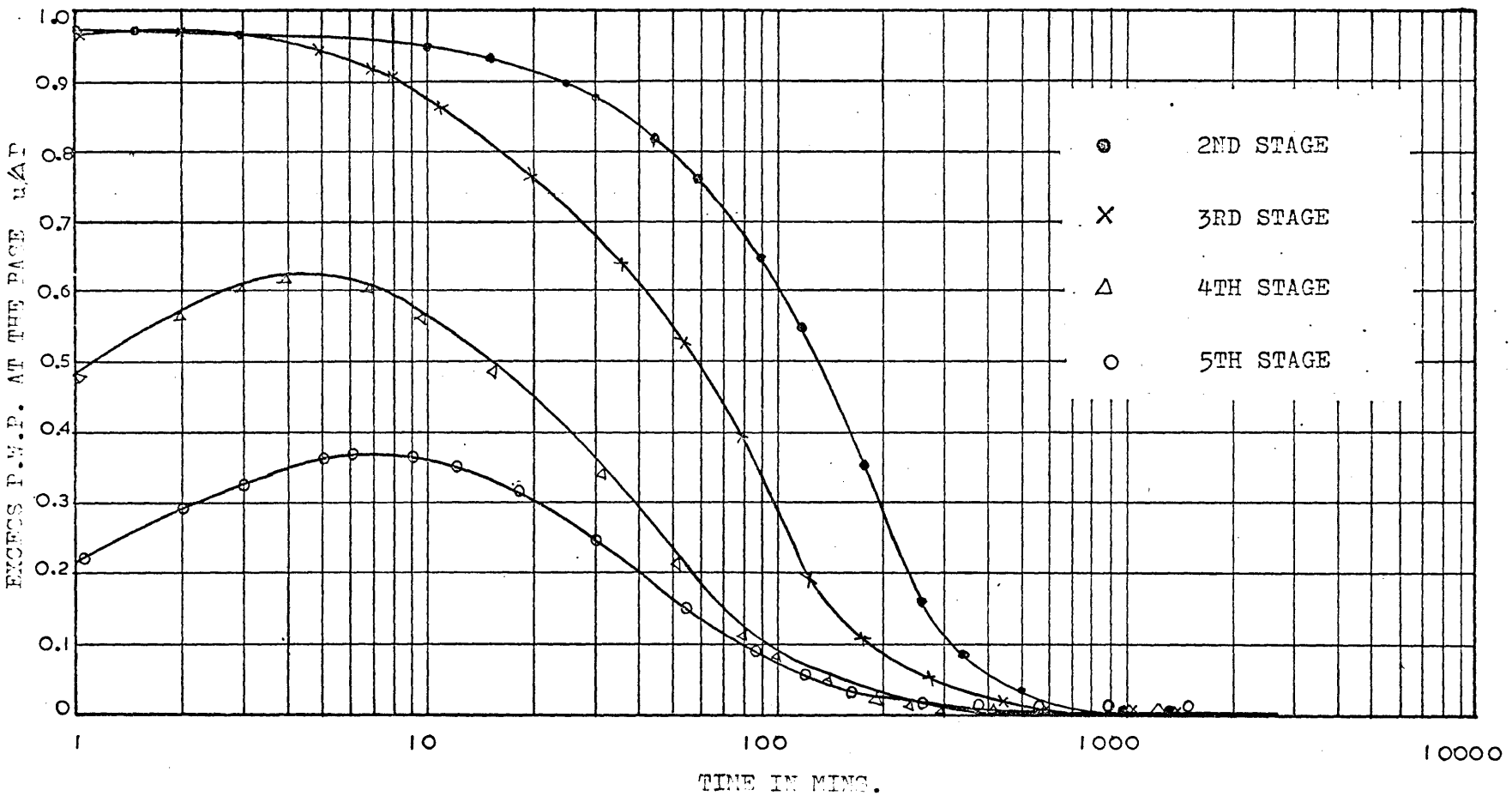

FIGURE NO. 2.78. P.W.P. DISSIPATION CURVES OF 90% CLAY- 10% SAND (GROUP B)

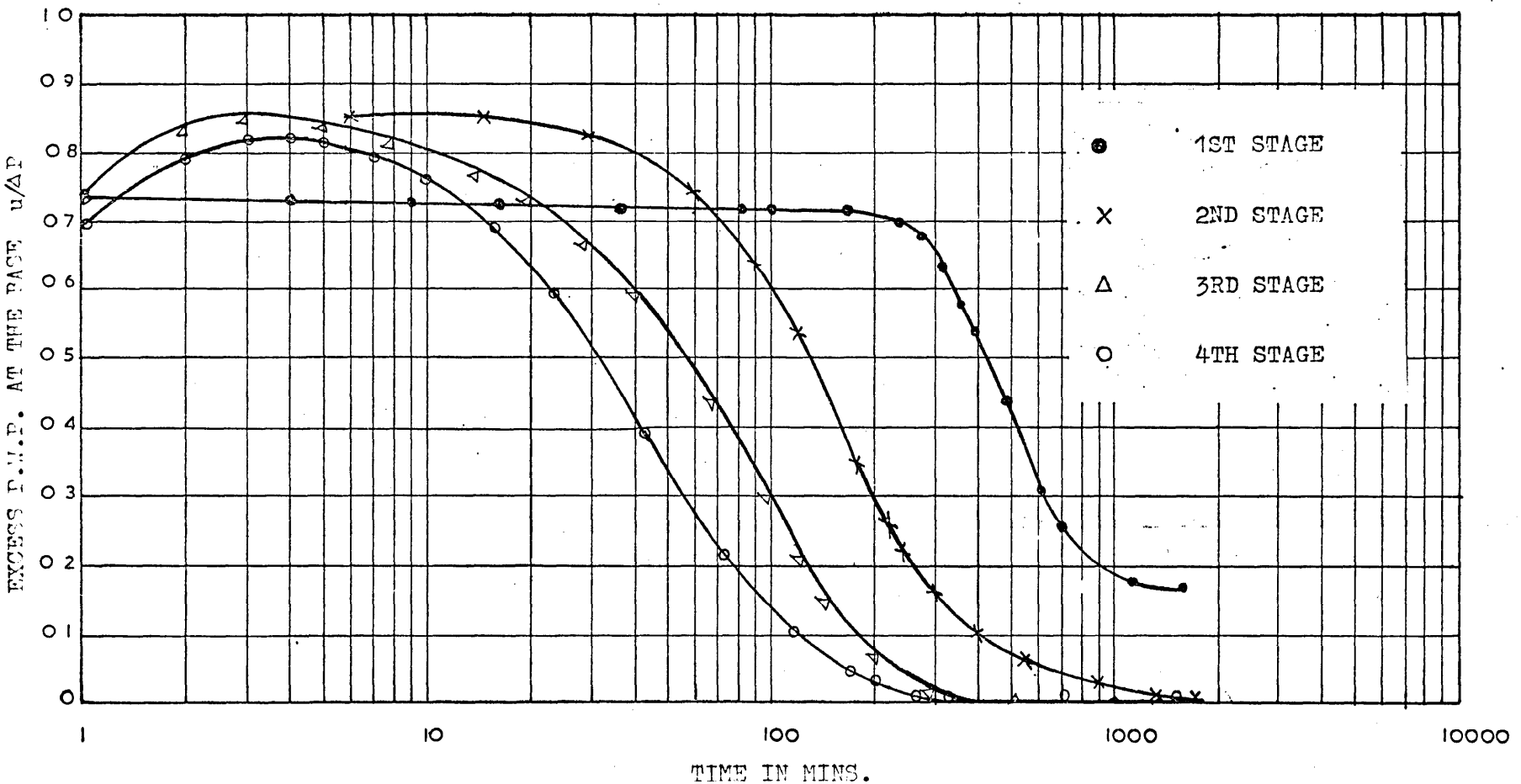

FIGURE NO. 2.79. P.W.P. DISSIPATION CURVES OF 80% CLAY- 20% SAND (GROUP A)

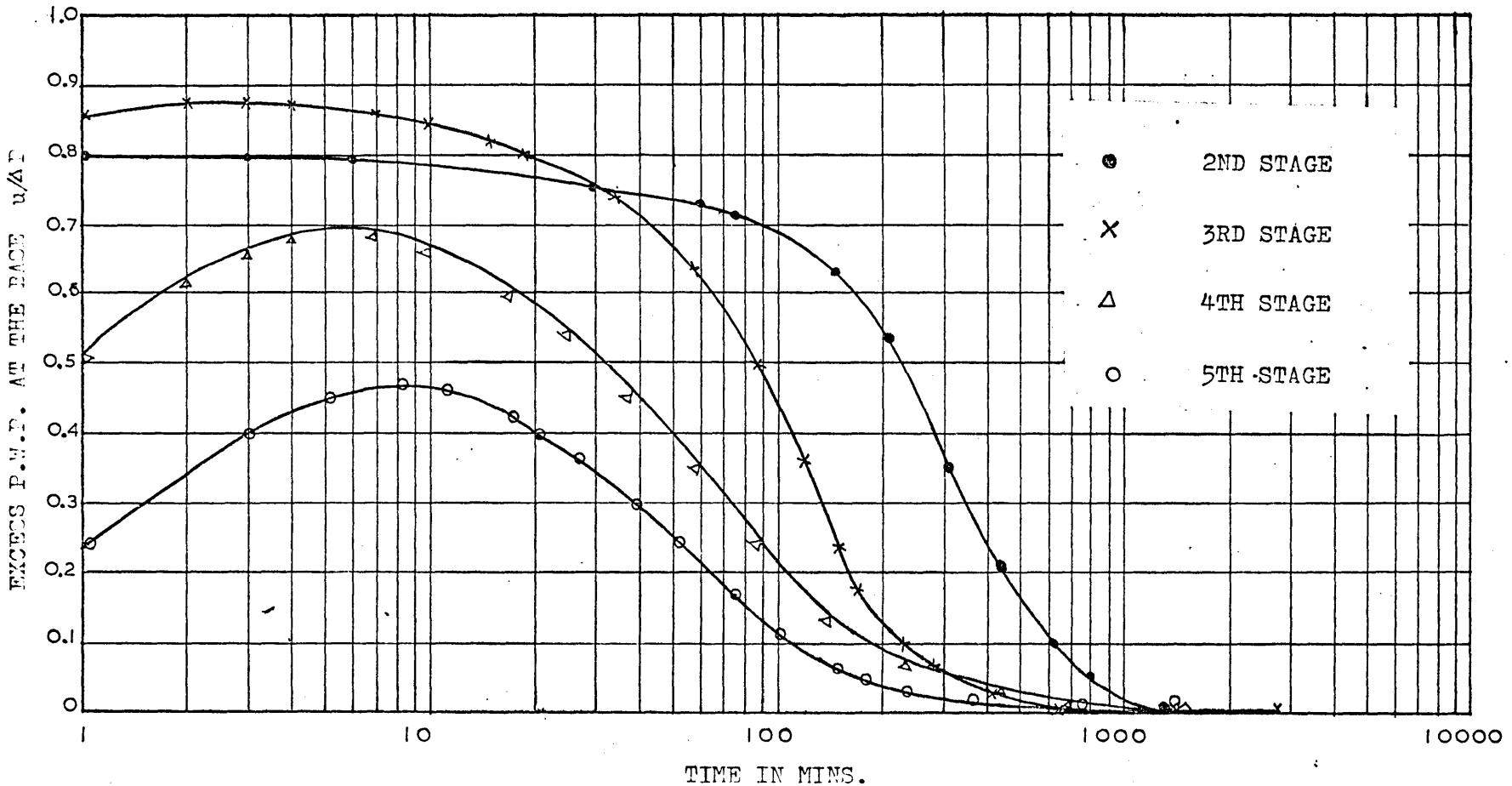

FIGURE NO. 2.80. P.W.P. DISSIPATION CURVES OF 80% CLAY- 20% SAND (GROUP B)

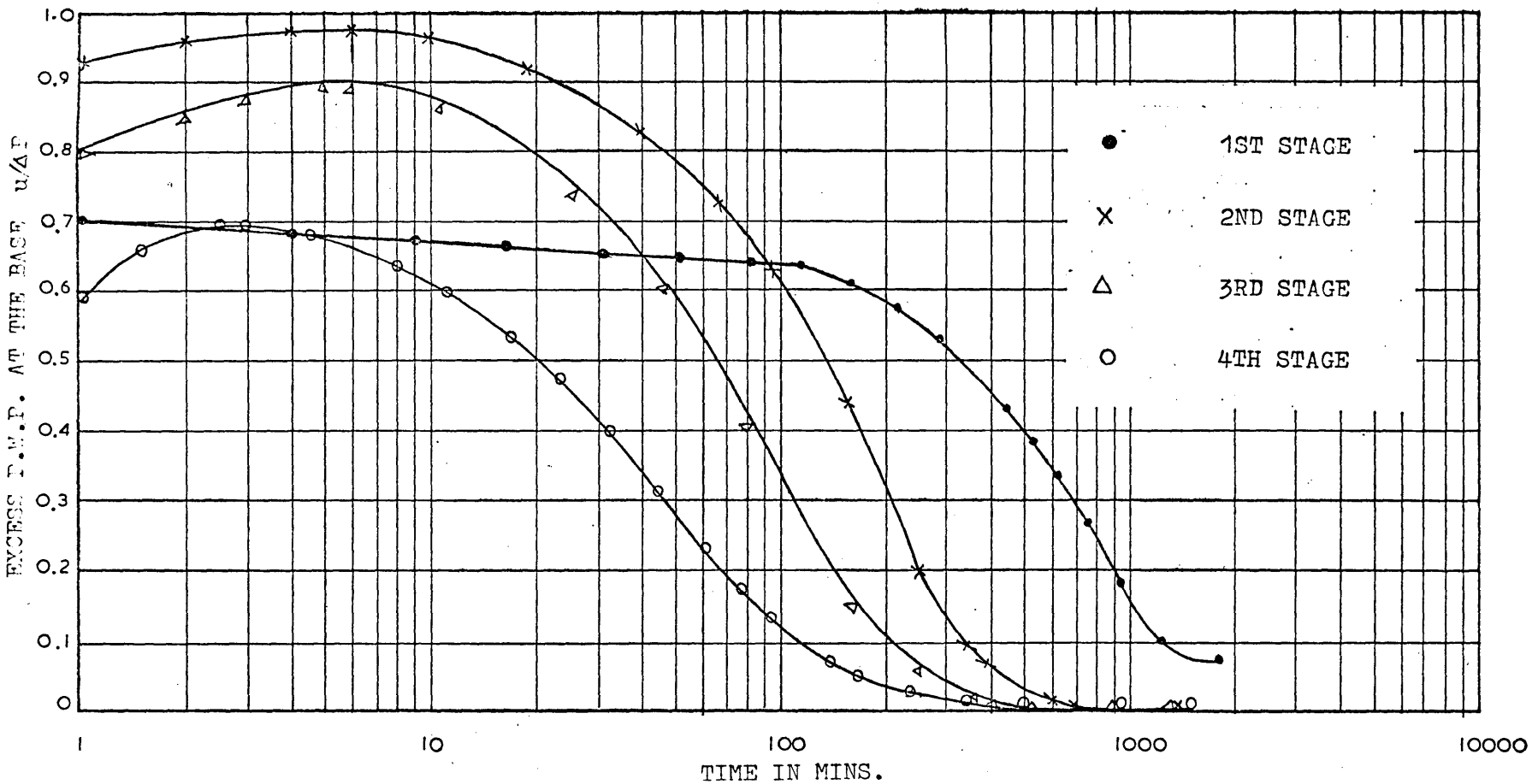

FIGURE NO. 2.81. P.W.P. DISSIPATION CURVES OF 70% CLAY- 30% SAND (GROUP A)

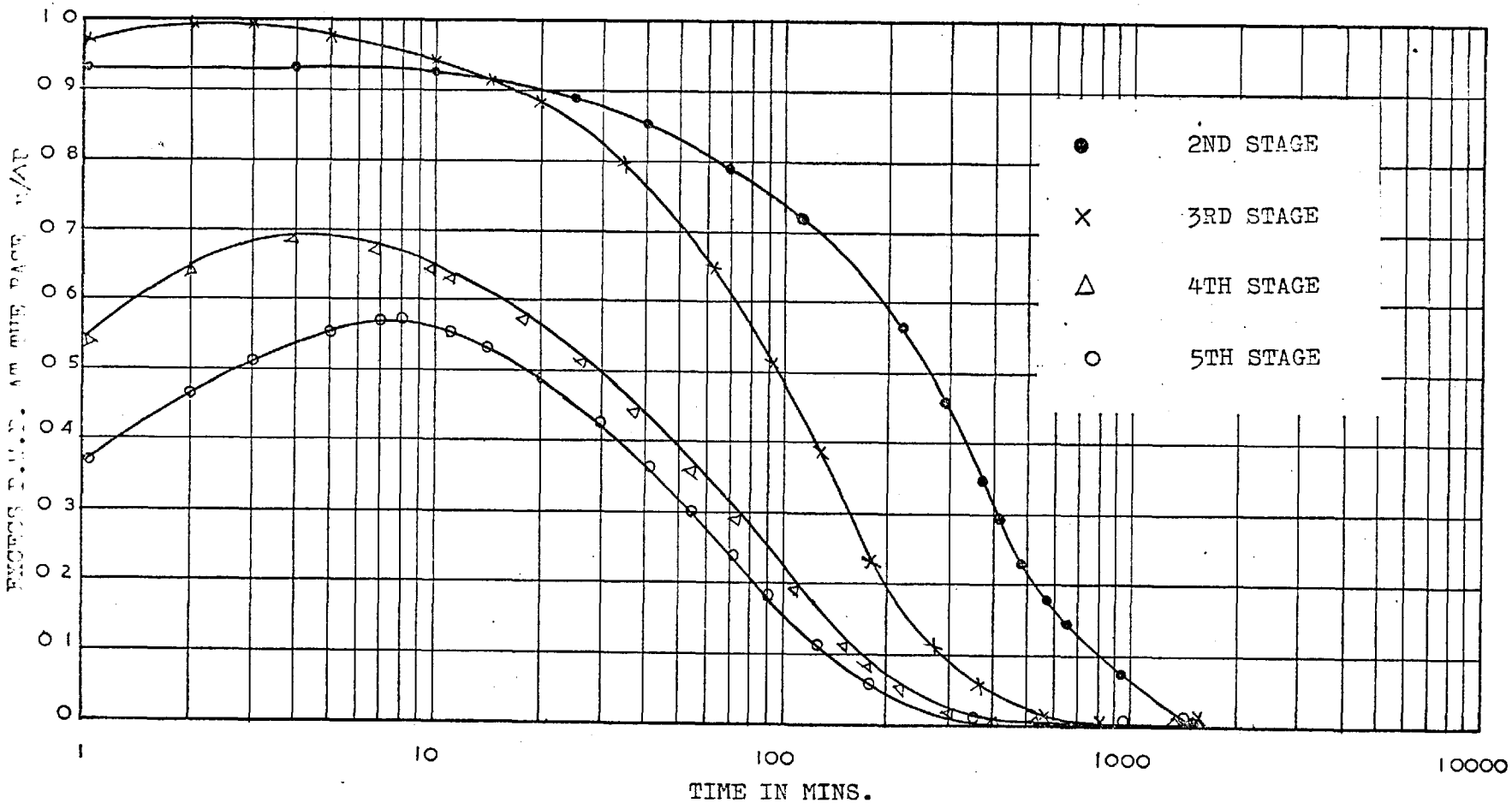

FIGURE NO. 2.82. P.W.P. DISSIPATION CURVES OF 70% CLAY- 30% SAND (GROUP B)

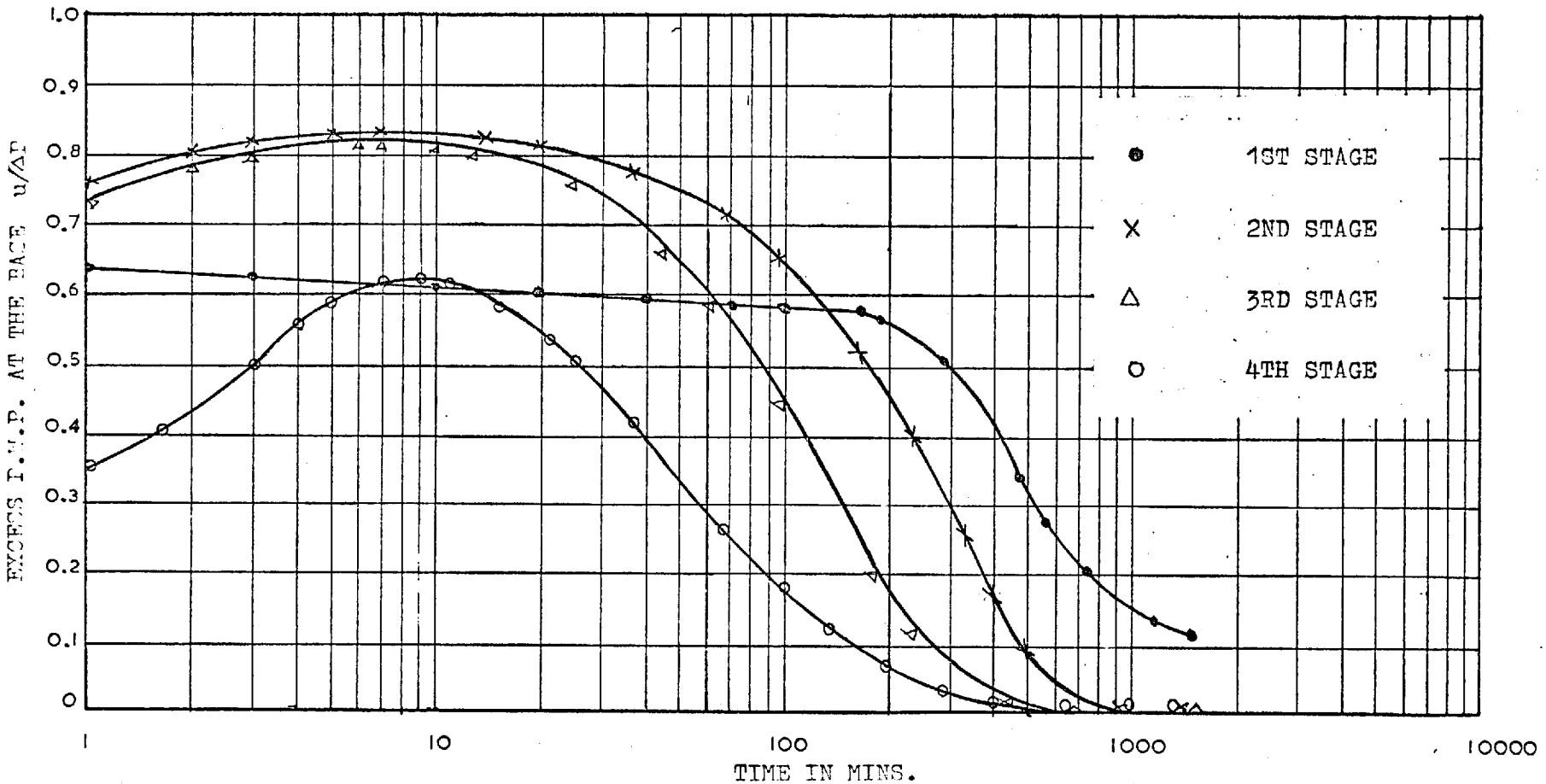

FIGURE NO. 2.83. P.W.P. DISSIPATION CURVES OF 50% CLAY- 50% SAND (GROUP A)

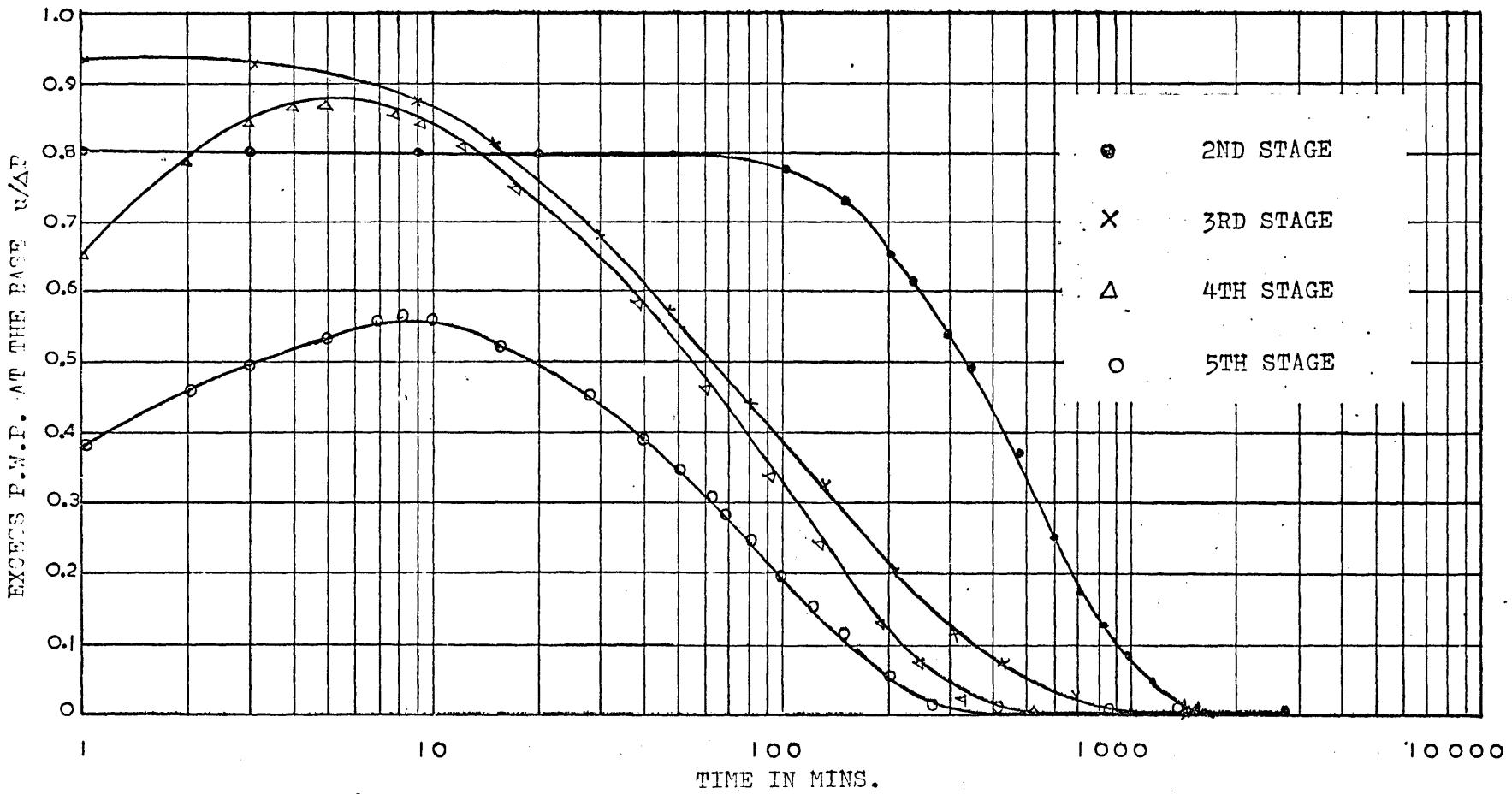

FIGURE NO. 2.84. P.W.P. DISSIPATION CURVES OF 50% CLAY- 50% SAND (GROUP B)

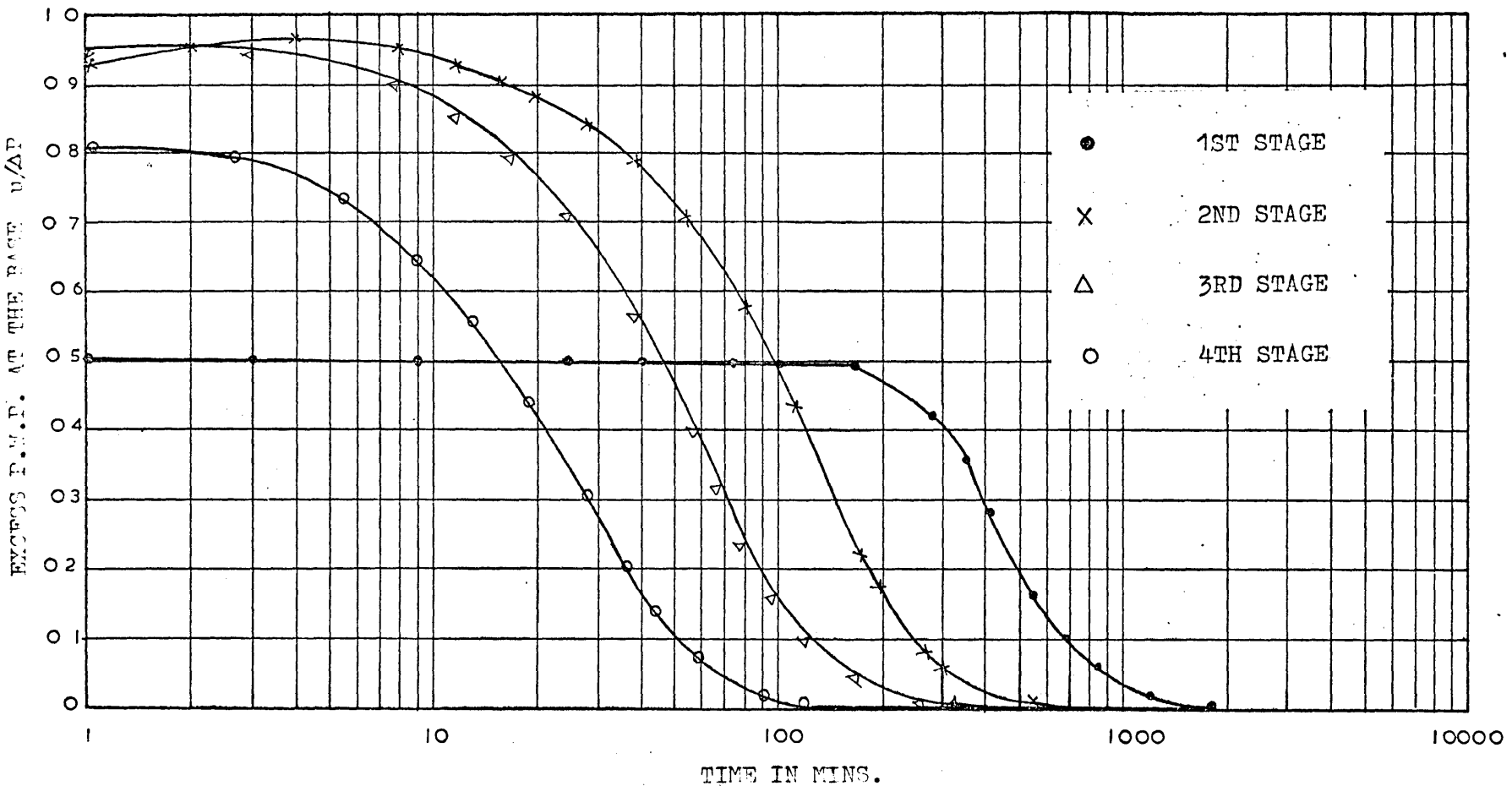

FIGURE NO. 2.85. P.W.P. DISSIPATION CURVES OF 30% CLAY- 70% SAND (GROUP A)

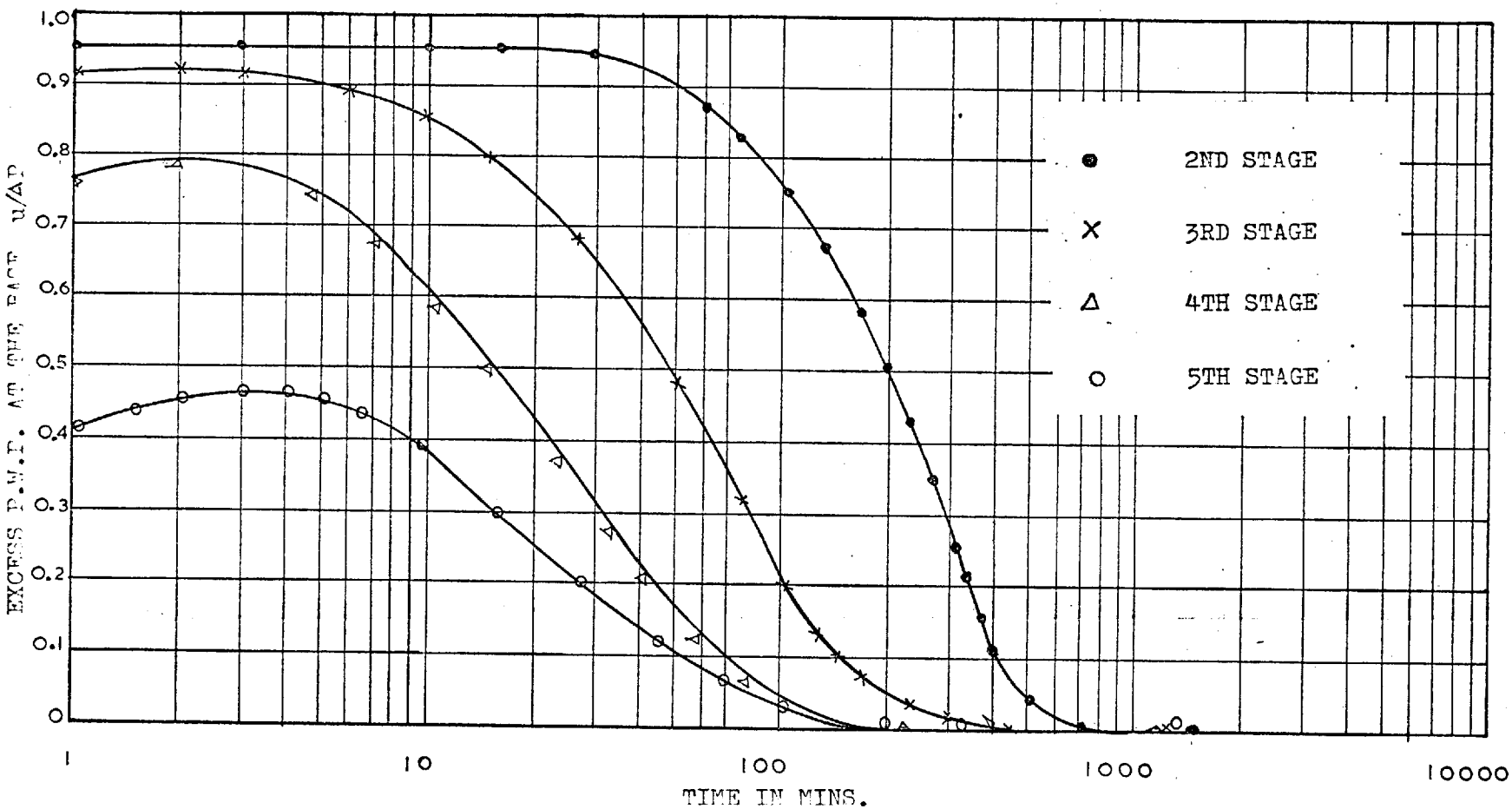

FIGURE NO. 2.86. P.W.P. DISSIPATION CURVES OF 30% CLAY- 70% SAND (GROUP B)

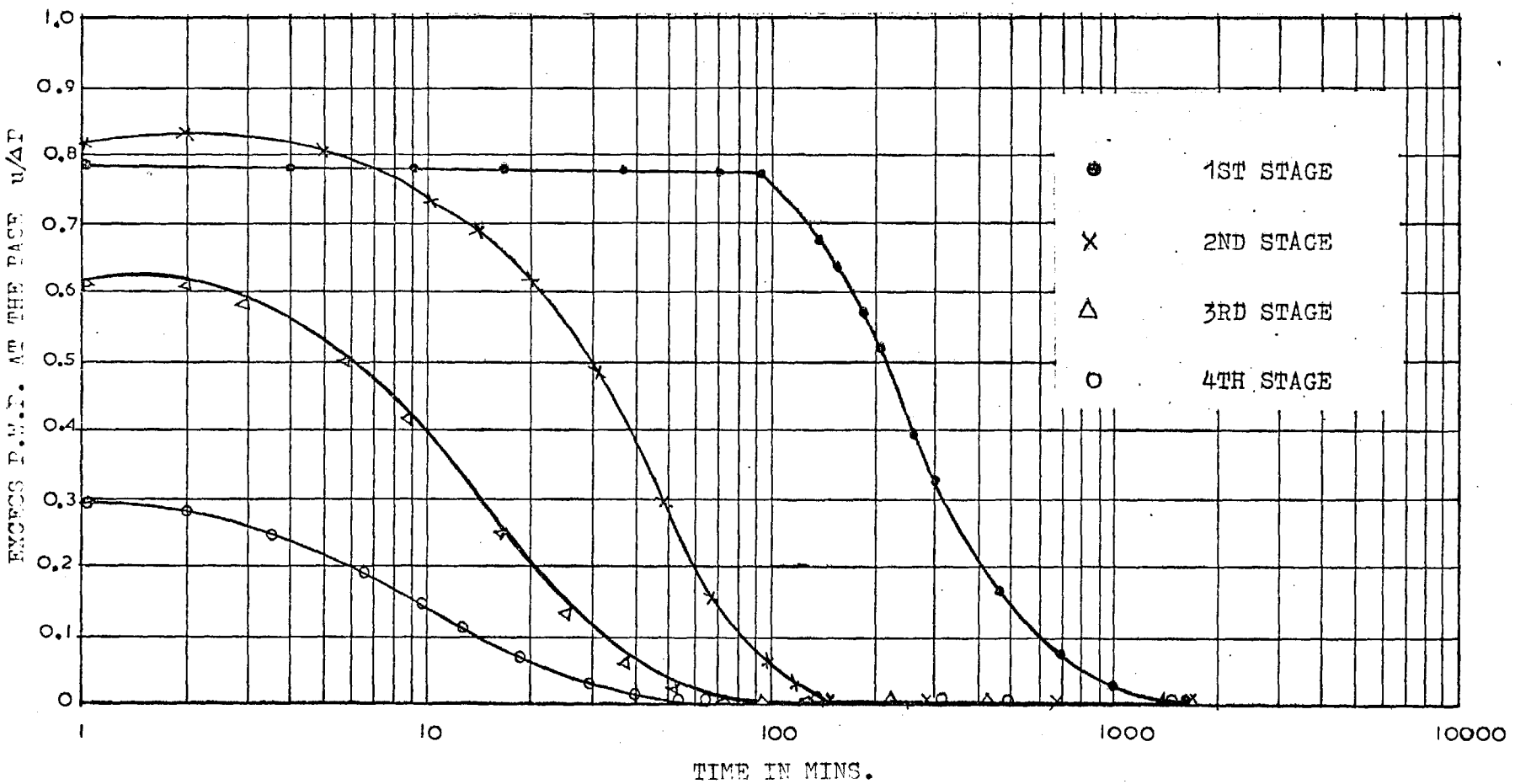

FIGURE NO. 2.87. P.W.P. DISSIPATION CURVES OF 20% CLAY- 80% SAND (GROUP A)

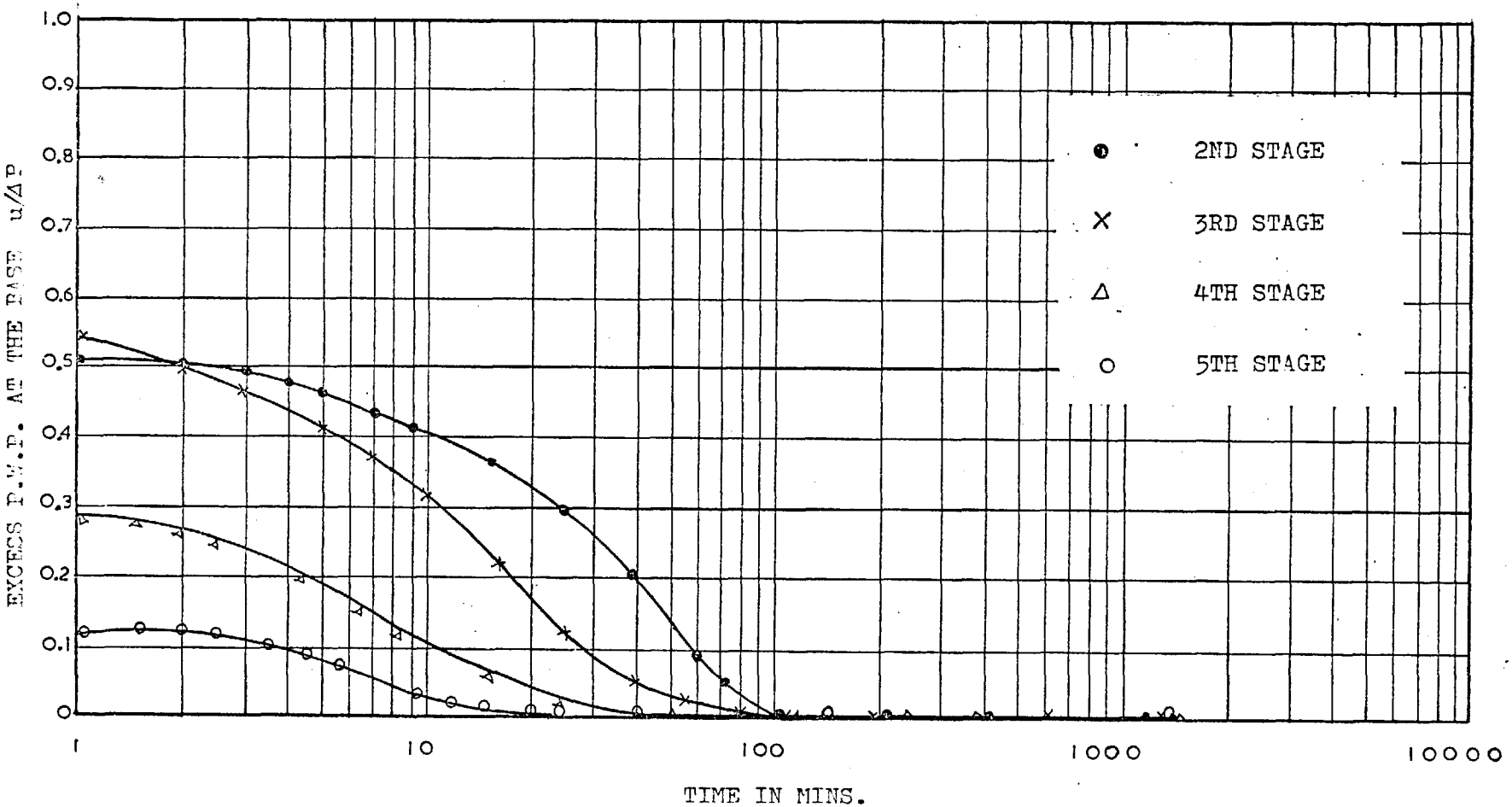

FIGURE NO. 2.88 P.W.P. DISSIPATION CURVES OF 20% CLAY- 80% SAND (GROUP B)

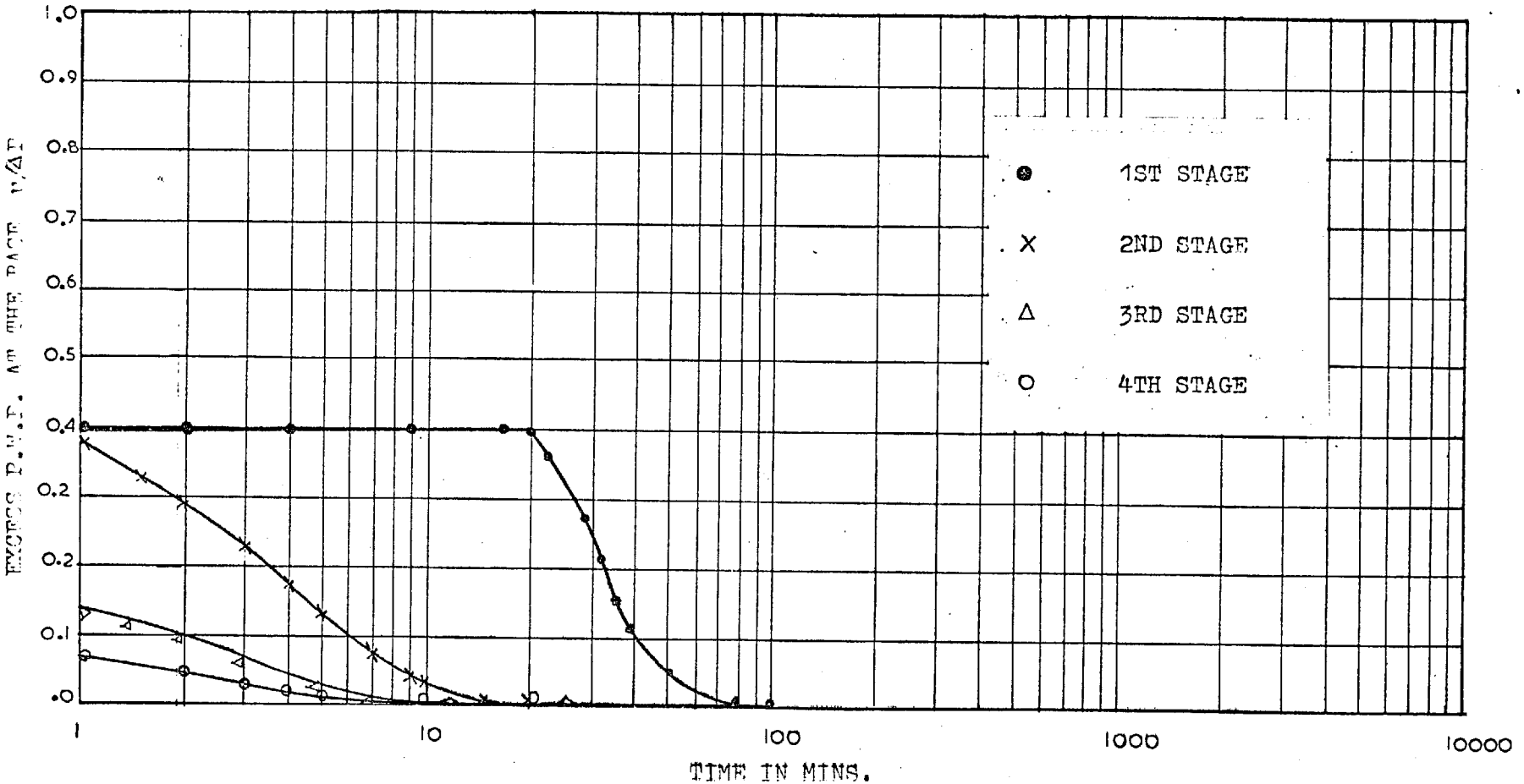

FIGURE NO. 2.88. P.W.P. DISSIPATION CURVES OF 10% CLAY- 90% SAND (GROUP A)

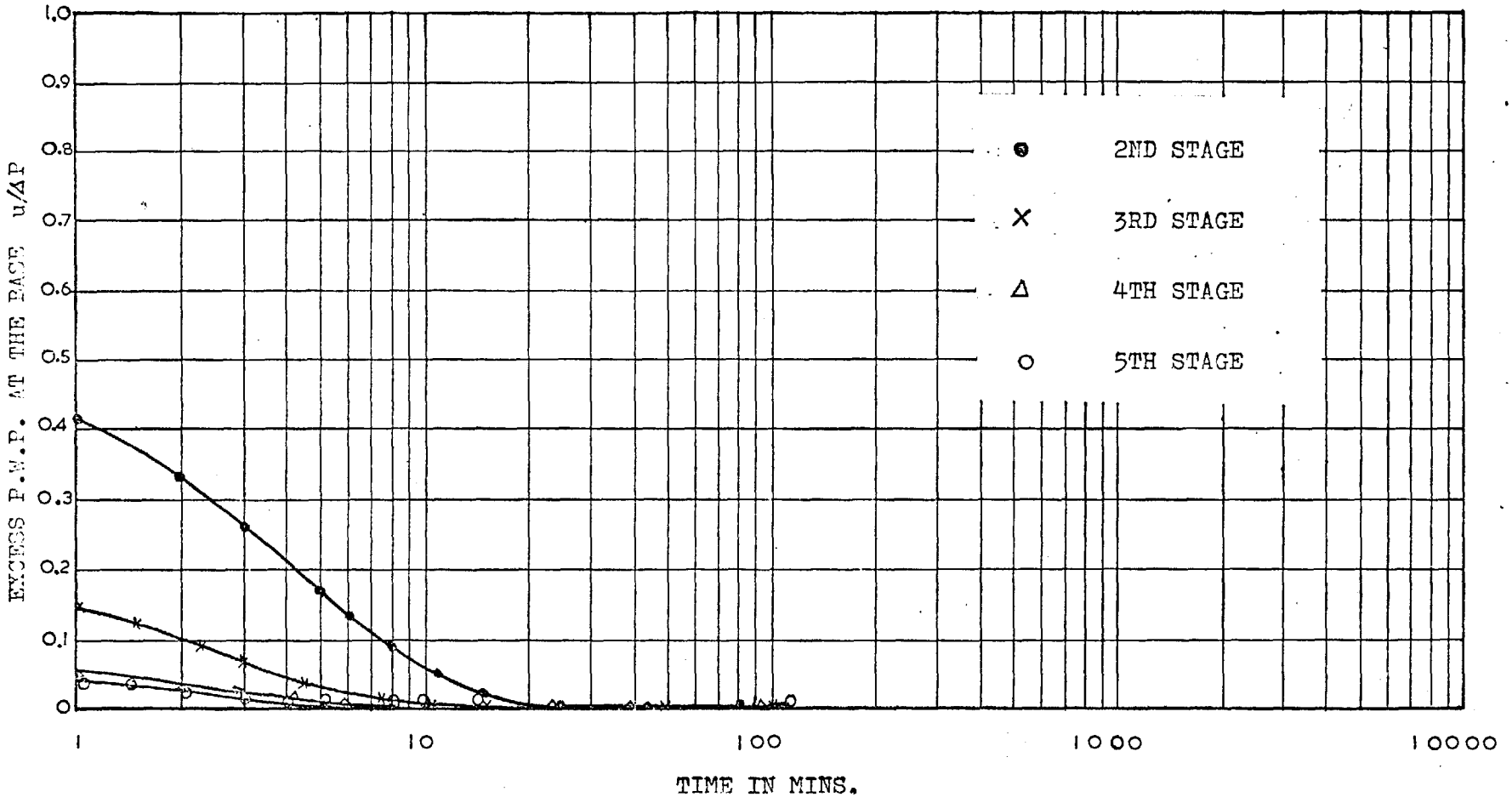

FIGURE NO. 2.90. P.W.P. DISSIPATION CURVES OF 10% CLAY- 90% SAND (GROUP B)

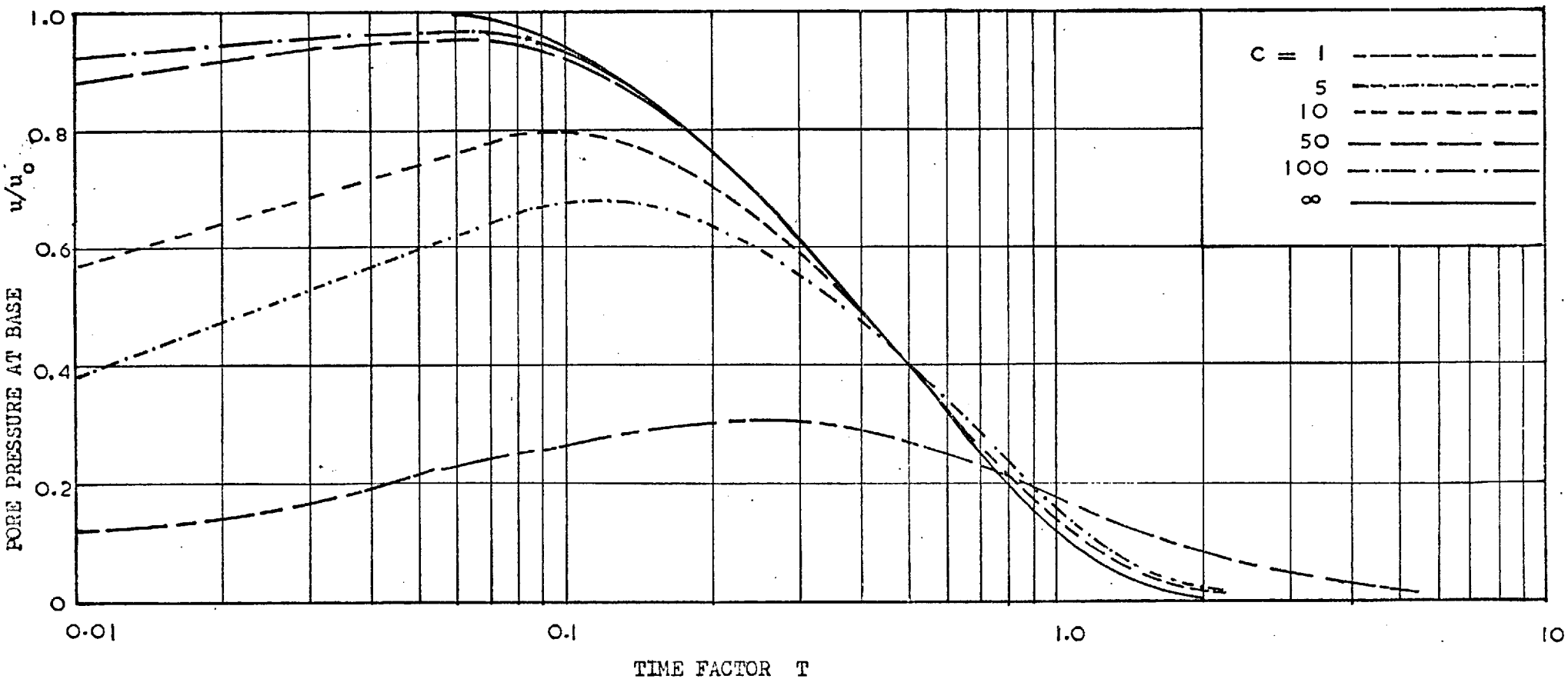

FIG. NO. 2.91 Theoretical effect of flexibility of the pore pressure measuring system on pore pressure at base of sample, Pmo = 0 (After Christie, I.F., 1965).

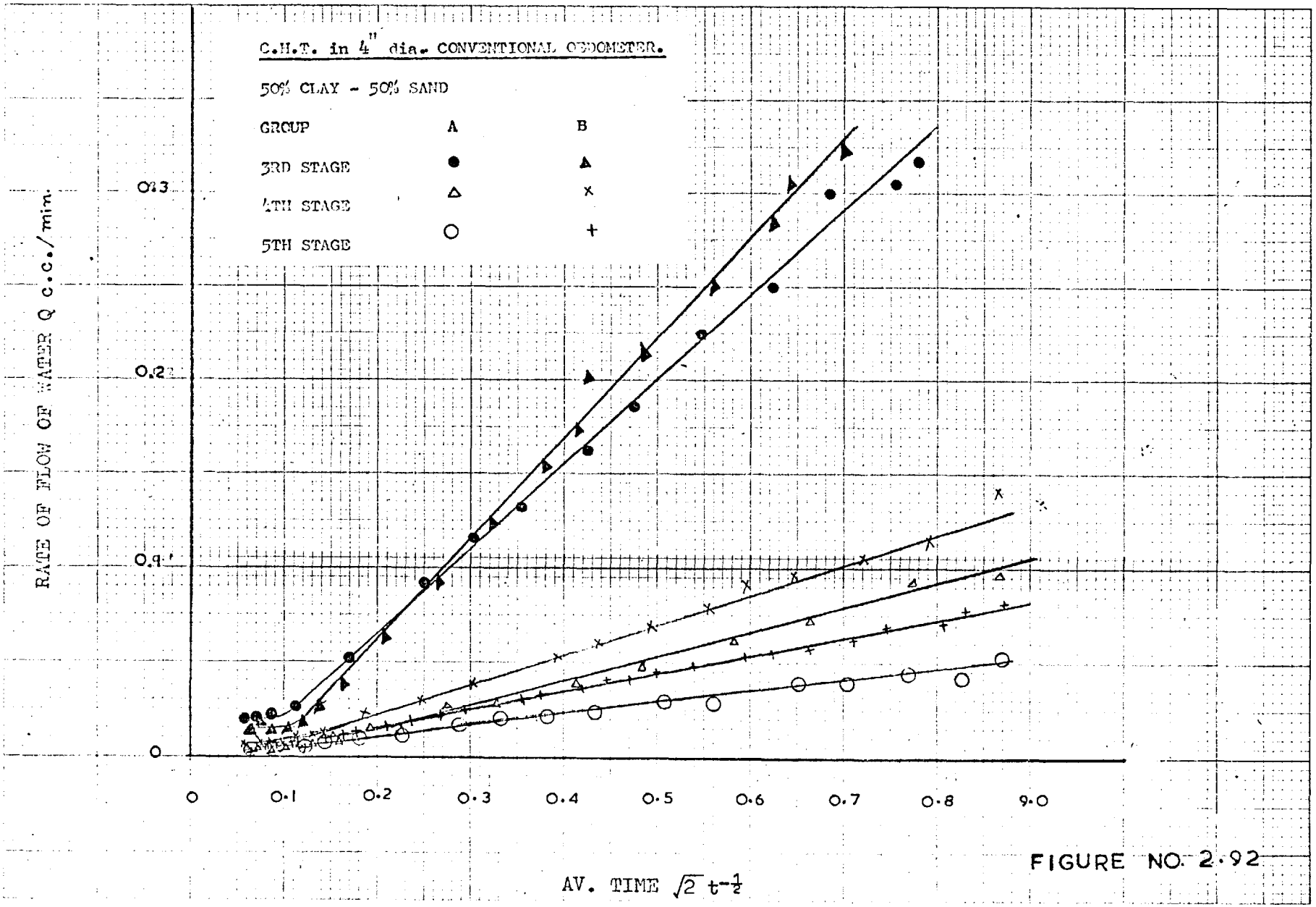

FIGURE NO. 2.92

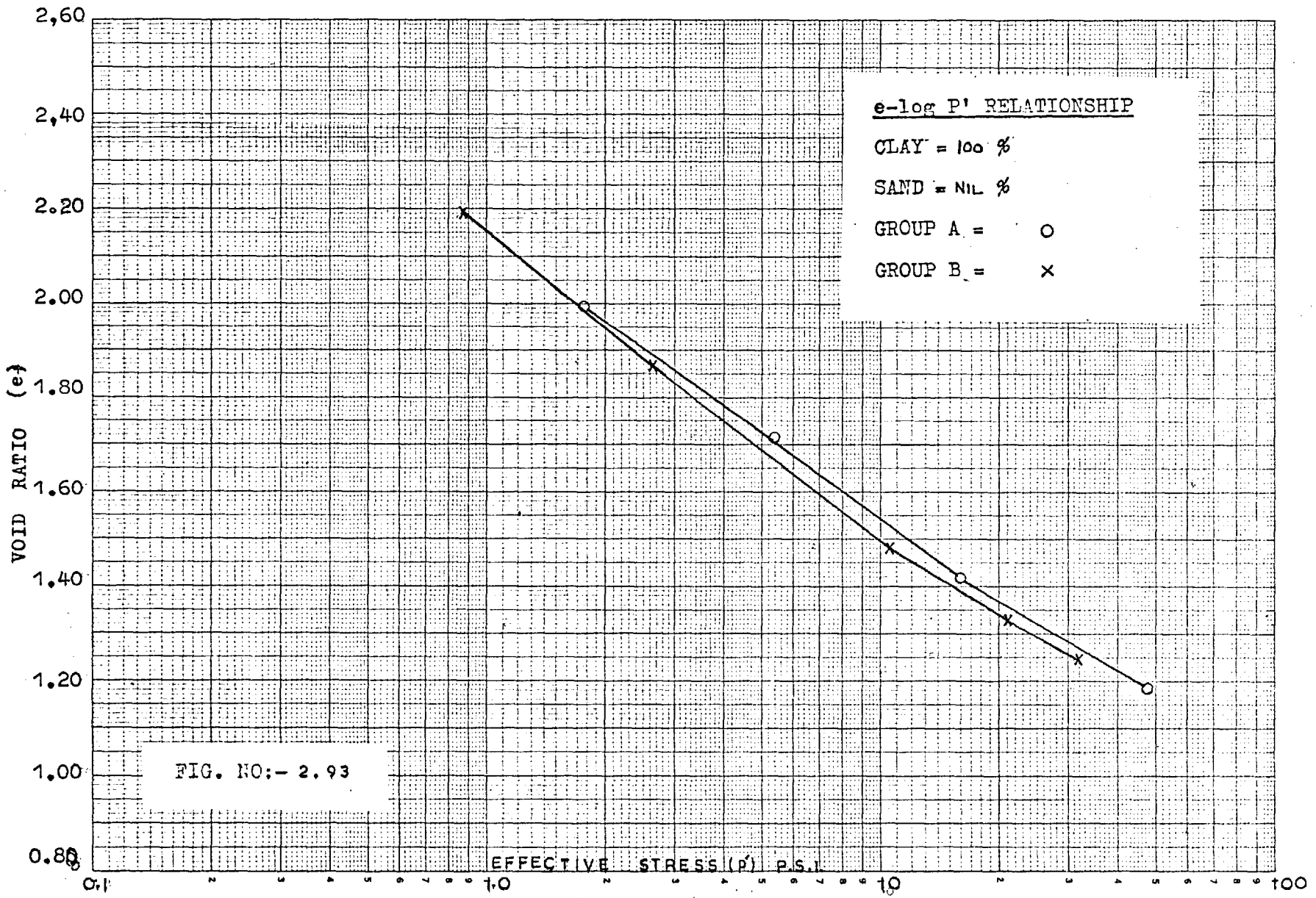
e-log P' RELATIONSHIP
CLAY = 100 %
SAND = NIL %
GROUP A = O
GROUP B = ×
VOID RATIO (e)
2.60
2.40
2.20
2.00
1.80
1.60
1.40
1.20
1.00
0.80
EFFECTIVE STRESS (p') P.S.I
0.1
1.0
10
100

FIG. NO:- 2.93

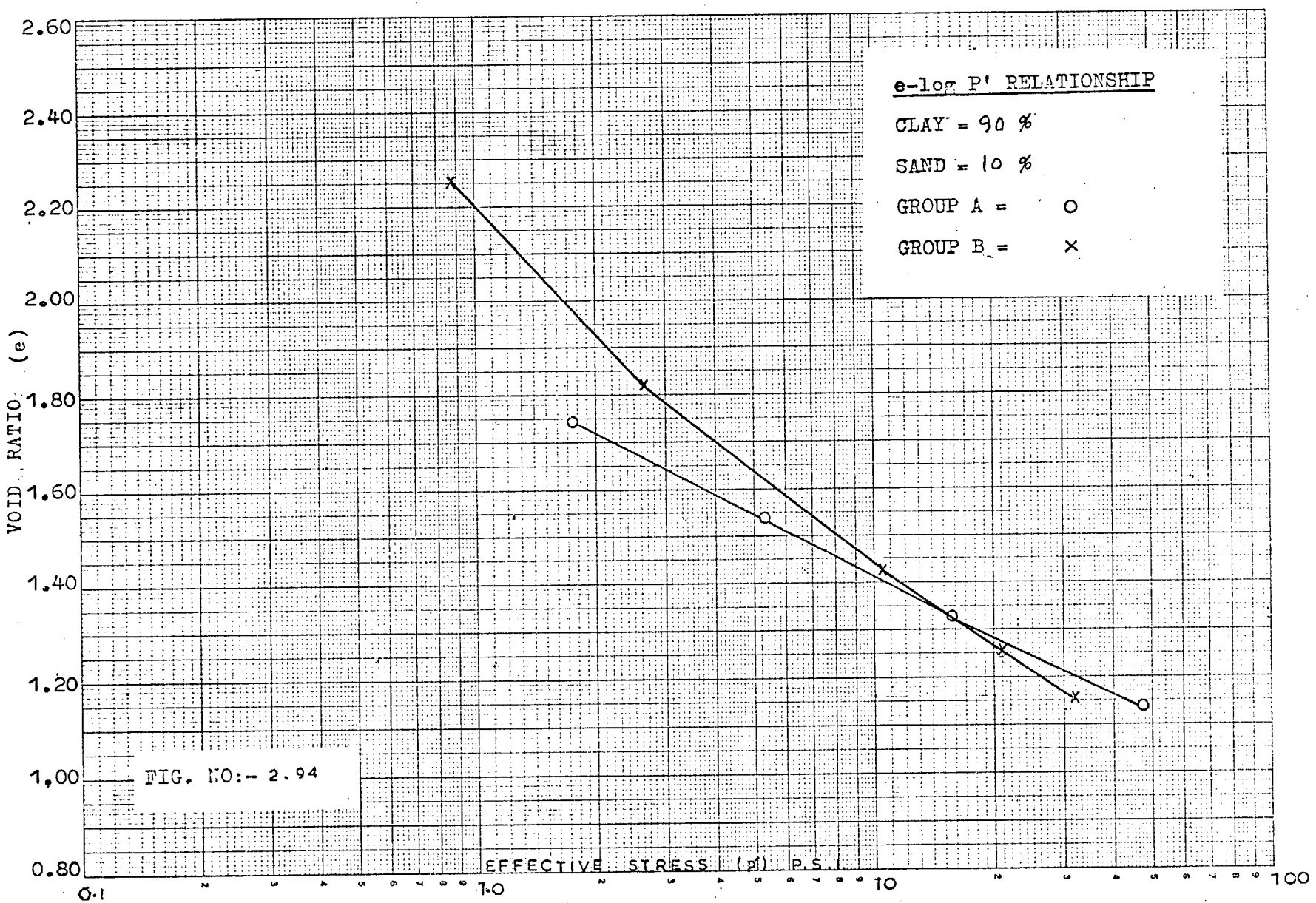
e-log P' RELATIONSHIP
CLAY = 90 %
SAND = 10 %
GROUP A = O
GROUP B = ×
VOID RATIO (e)
2.60
2.40
2.20
2.00
1.80
1.60
1.40
1.20
1,00
0.80
EFFECTIVE STRESS (p) P.S.I.
0.1
1.0
10
100
FIG. NO:- 2.94

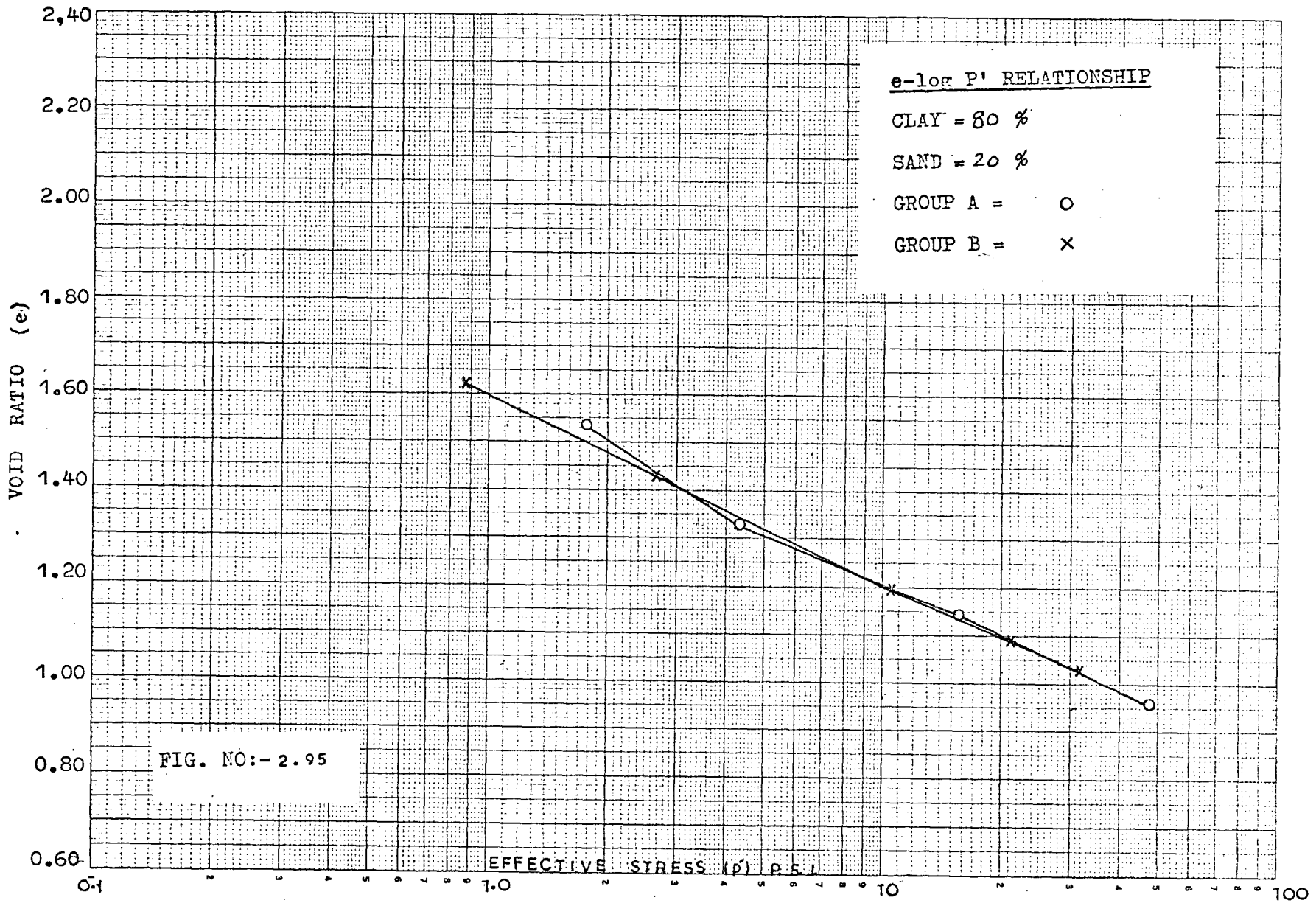
e-log P' RELATIONSHIP
CLAY = 80 %
SAND = 20 %
GROUP A = O
GROUP B = ×
VOID RATIO (e)
2.40
2.20
2.00
1.80
1.60
1.40
1.20
1.00
0.80
0.60
0.1
1.0
10
100
EFFECTIVE STRESS (p') P.S.I.
FIG. NO:- 2.95

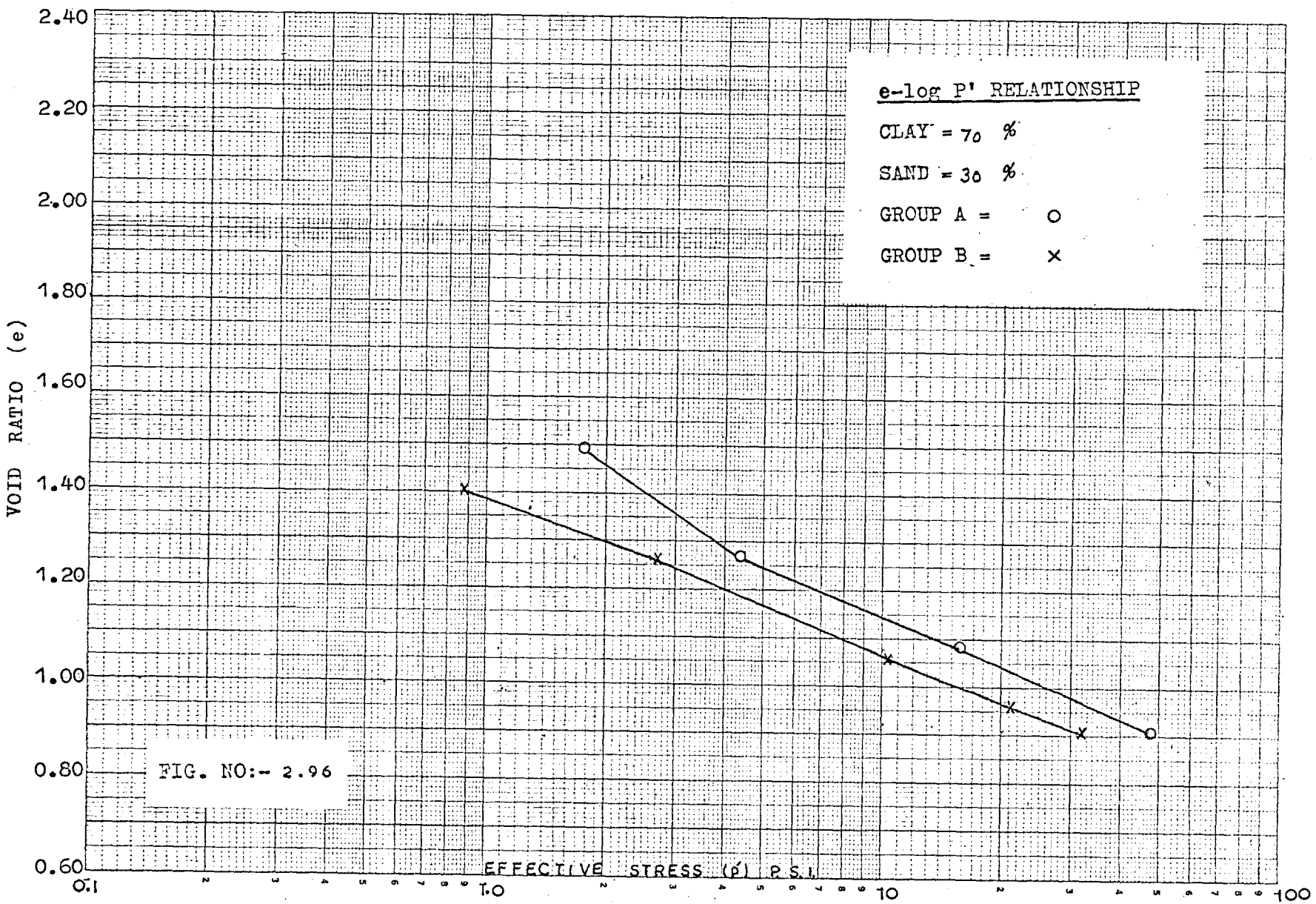
e-log P' RELATIONSHIP
CLAY = 70 %
SAND = 30 %
GROUP A = O
GROUP B = X
VOID RATIO (e)
2.40
2.20
2.00
1.80
1.60
1.40
1.20
1.00
0.80
0.60
0.1
1.0
10
100
EFFECTIVE STRESS (p') P.S.I.
FIG. NO:- 2.96

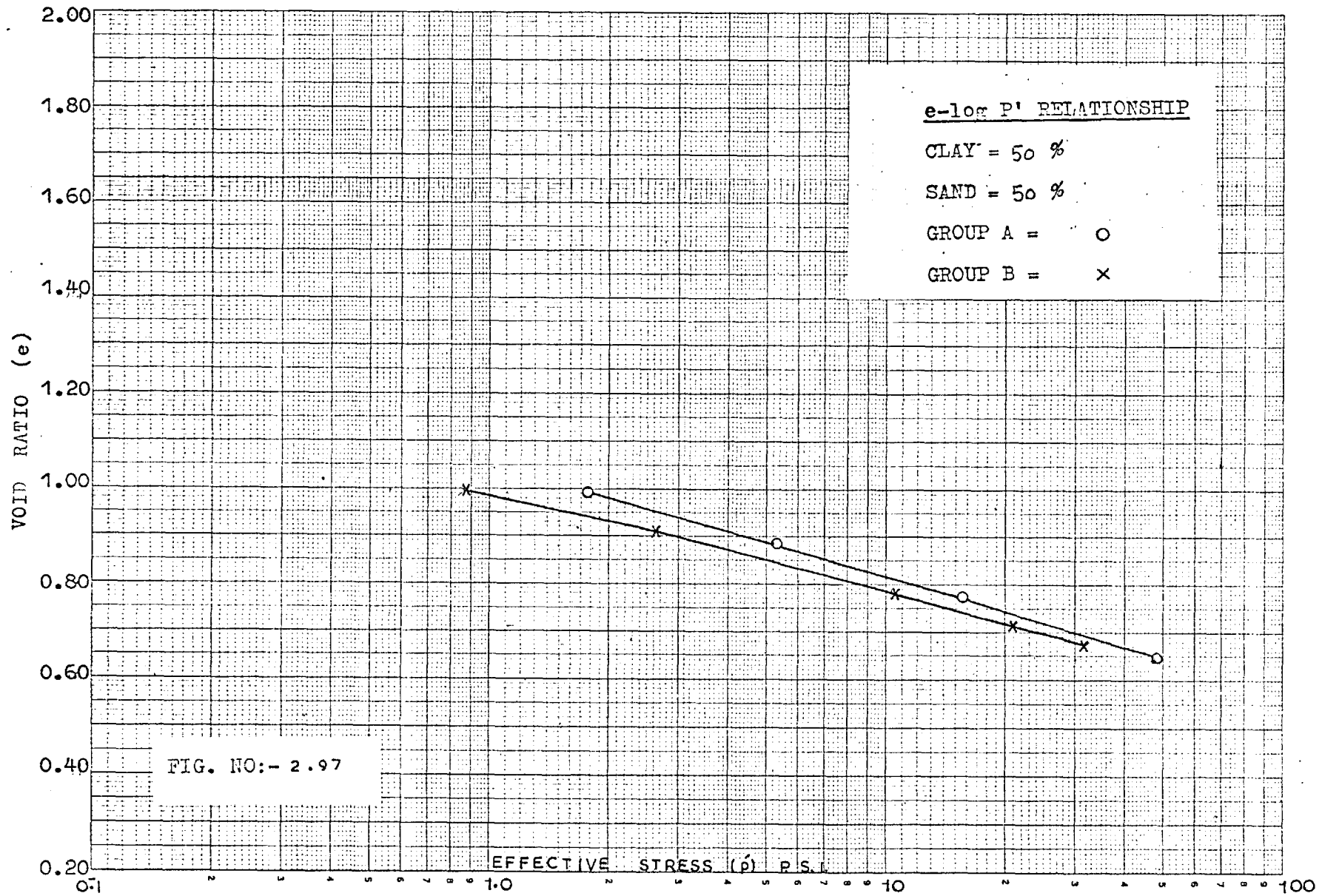
e-log P' RELATIONSHIP
CLAY = 50 %
SAND = 50 %
GROUP A = O
GROUP B = ×
VOID RATIO (e)
2.00
1.80
1.60
1.40
1.20
1.00
0.80
0.60
0.40
0.20
0.1
1.0
10
100
EFFECTIVE STRESS (p') P.S.I.

FIG. NO:- 2.97

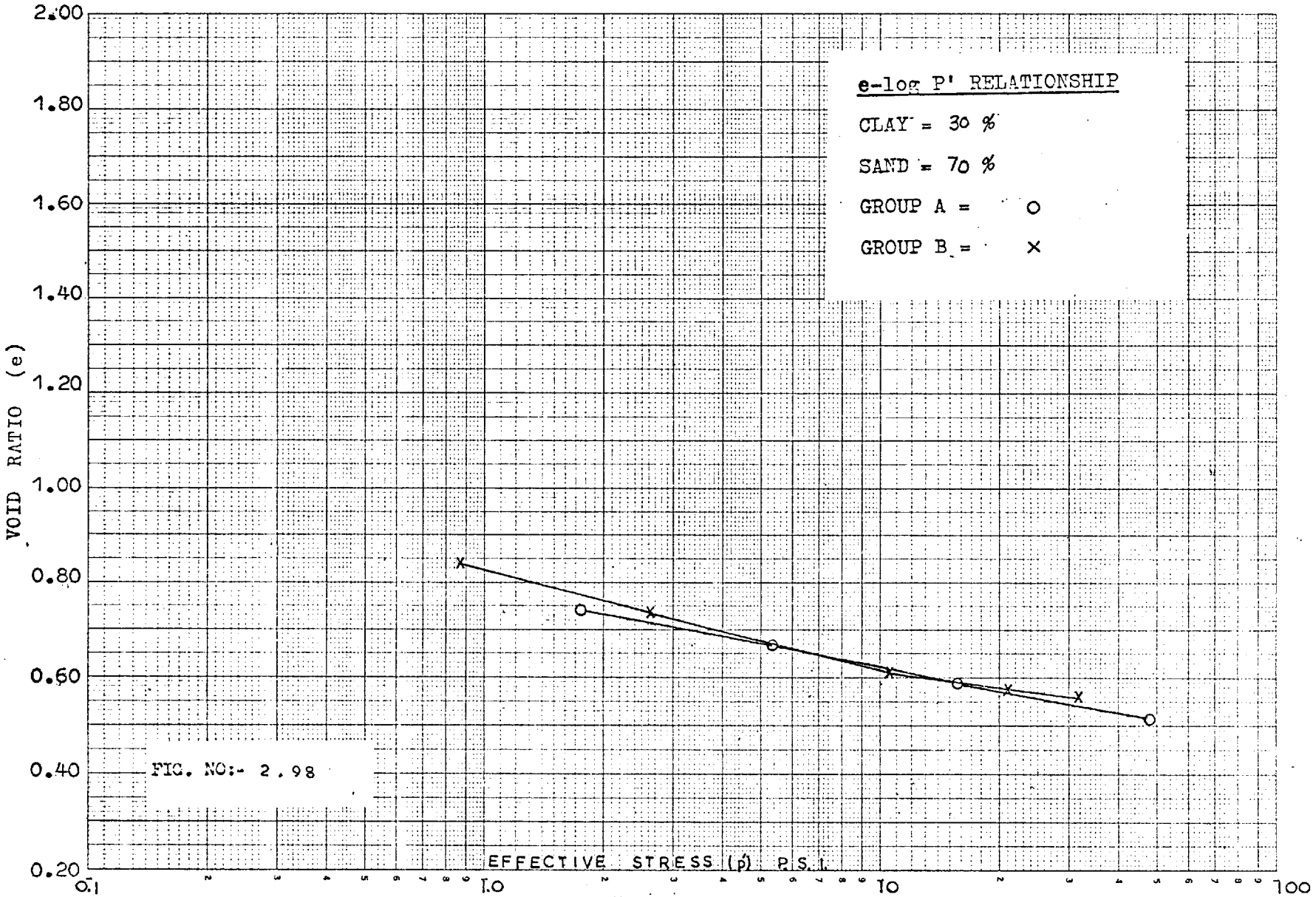
e-log P' RELATIONSHIP
CLAY = 30 %
SAND = 70 %
GROUP A = O
GROUP B = X
VOID RATIO (e)
2.00
1.80
1.60
1.40
1.20
1.00
0.80
0.60
0.40
0.20
0.1
1.0
10
100
EFFECTIVE STRESS (p) P.S.I.
FIG. NO:- 2.98

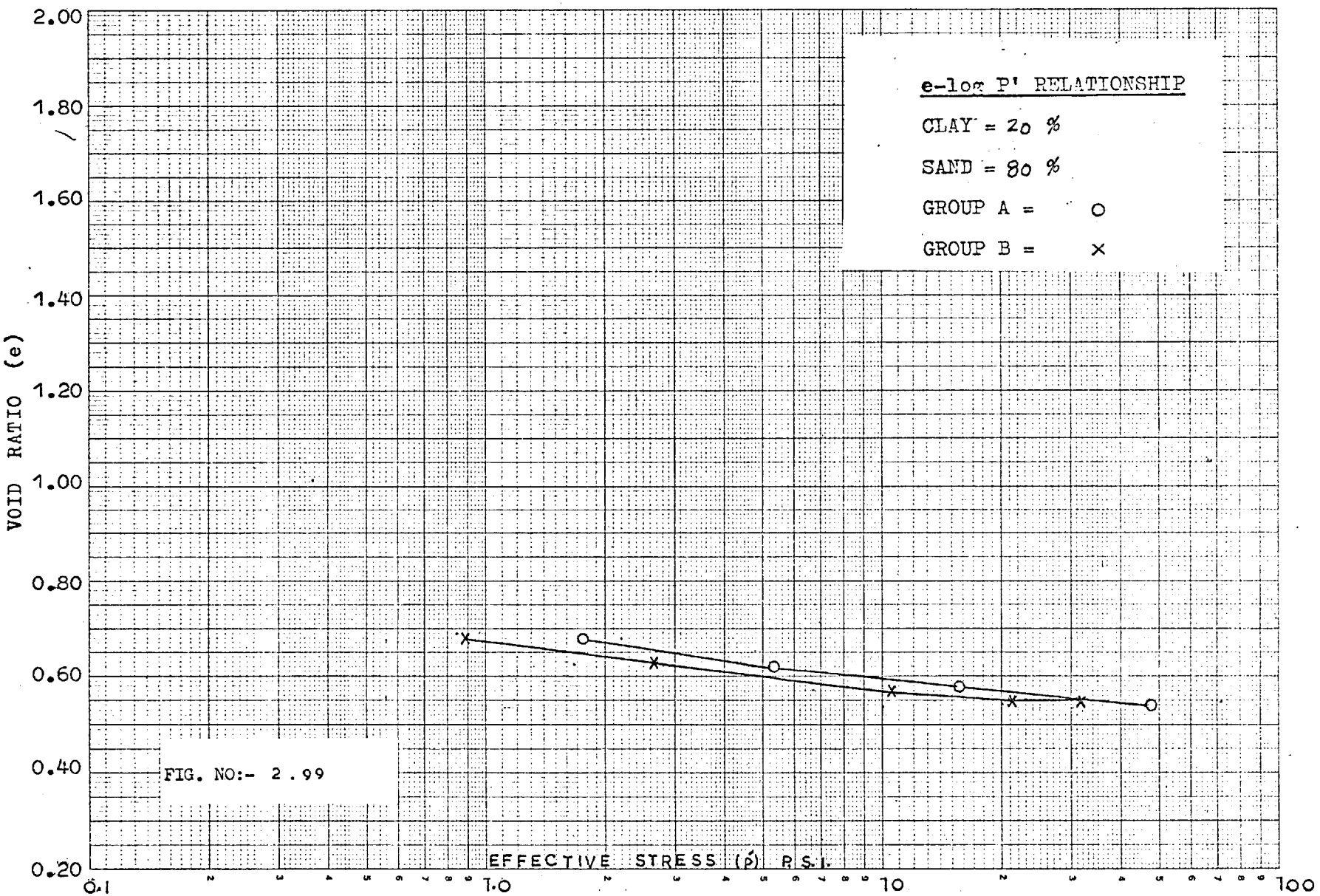
e-log P' RELATIONSHIP
CLAY = 20 %
SAND = 80 %
GROUP A = O
GROUP B = ×
VOID RATIO (e)
2.00
1.80
1.60
1.40
1.20
1.00
0.80
0.60
0.40
0.20
EFFECTIVE STRESS (P) P.S.I.
0.1
1.0
10
100

FIG. NO:- 2.99

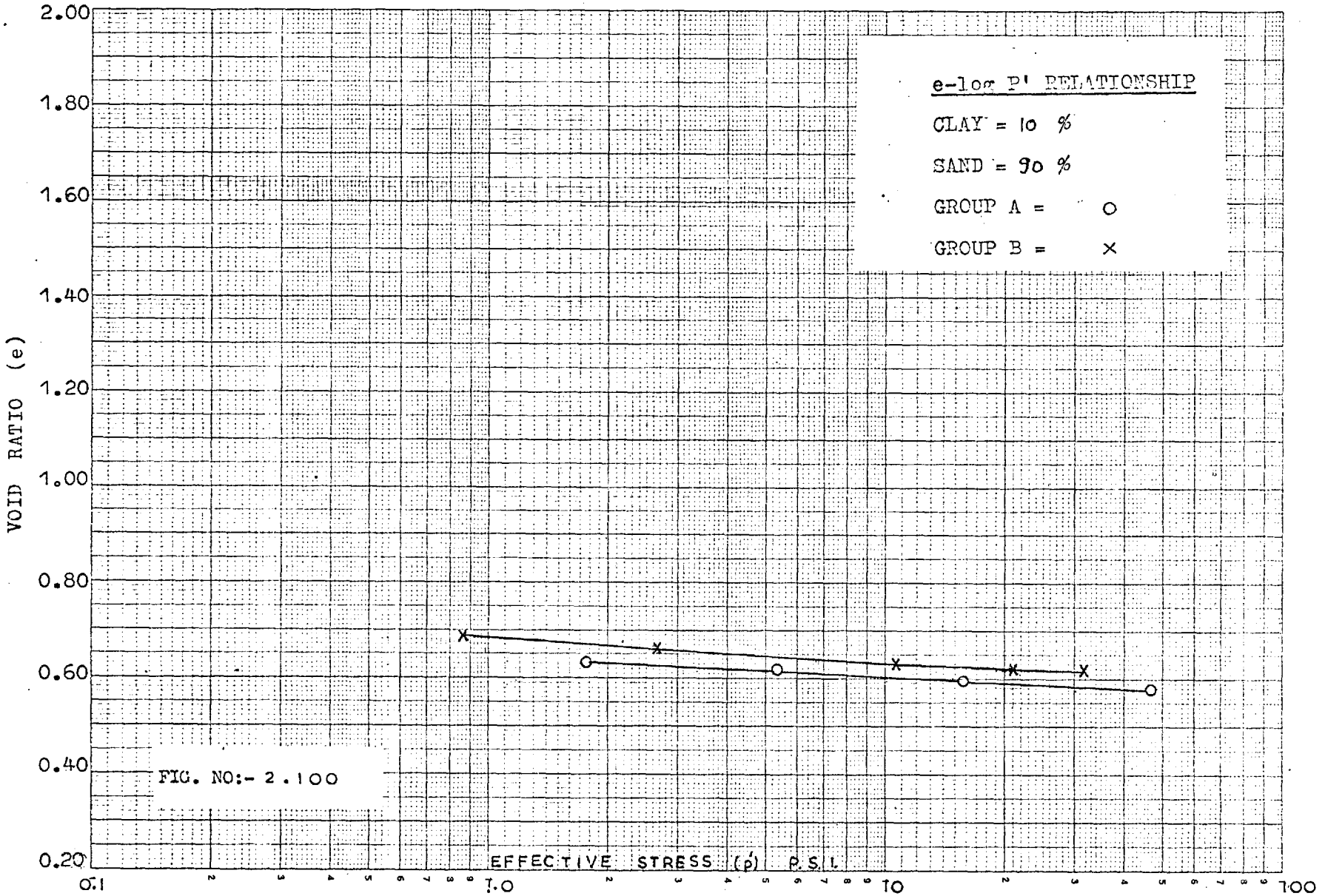
e-log P' RELATIONSHIP
CLAY = 10 %
SAND = 90 %
GROUP A = O
GROUP B = X
VOID RATIO (e)
2.00
1.80
1.60
1.40
1.20
1.00
0.80
0.60
0.40
0.20
EFFECTIVE STRESS (p') P.S.I.
0.1
1.0
10
100
FIG. NO:- 2.100

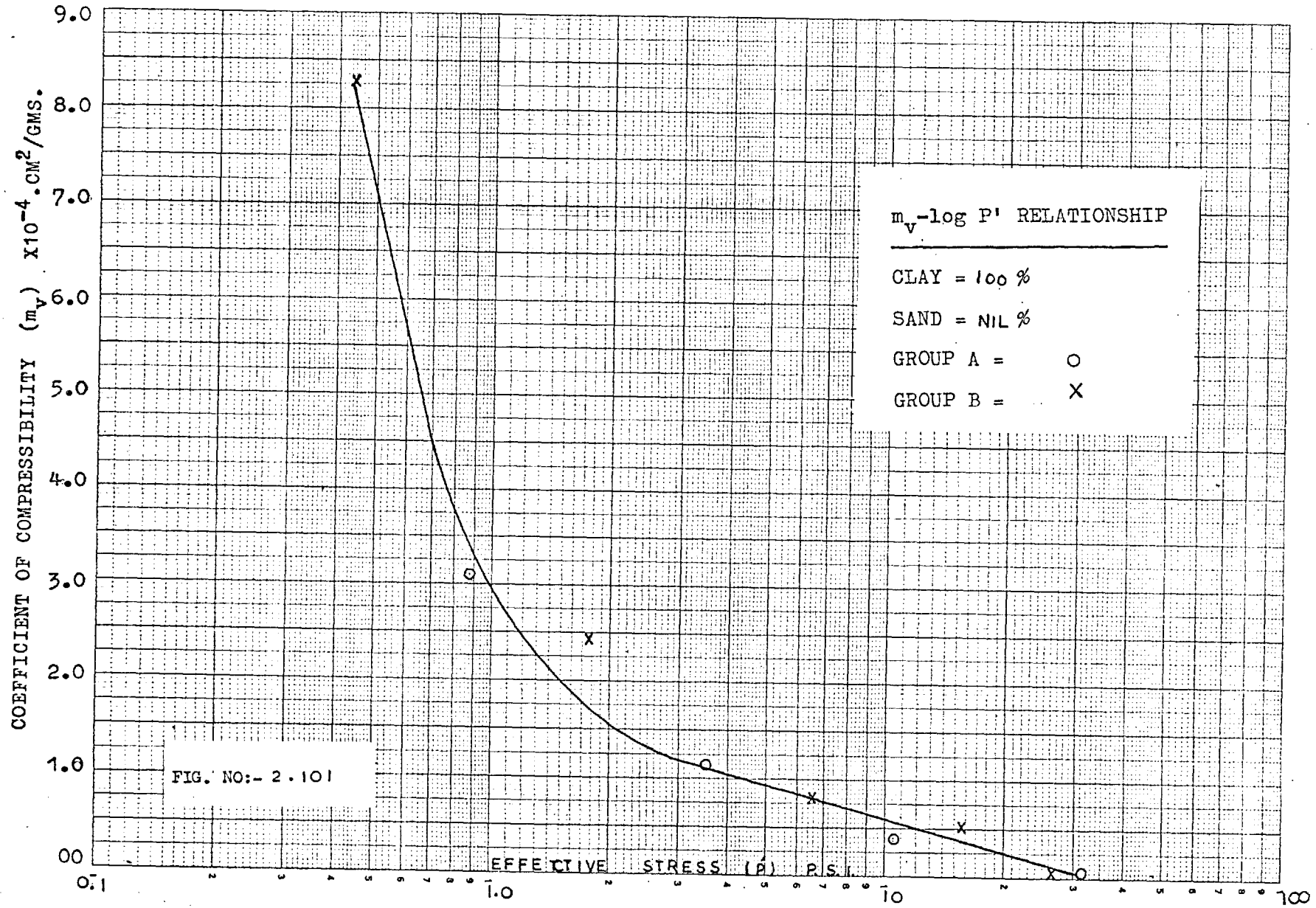
m_v-log P' RELATIONSHIP
CLAY = 100 %
SAND = NIL %
GROUP A = O
GROUP B = X
COEFFICIENT OF COMPRESSIBILITY (m_v) X10^{-4}.CM^2/GMS.
9.0
8.0
7.0
6.0
5.0
4.0
3.0
2.0
1.0
00
0.1
1.0
10
100
EFFECTIVE STRESS (P) P.S.I.

FIG. NO:- 2.101

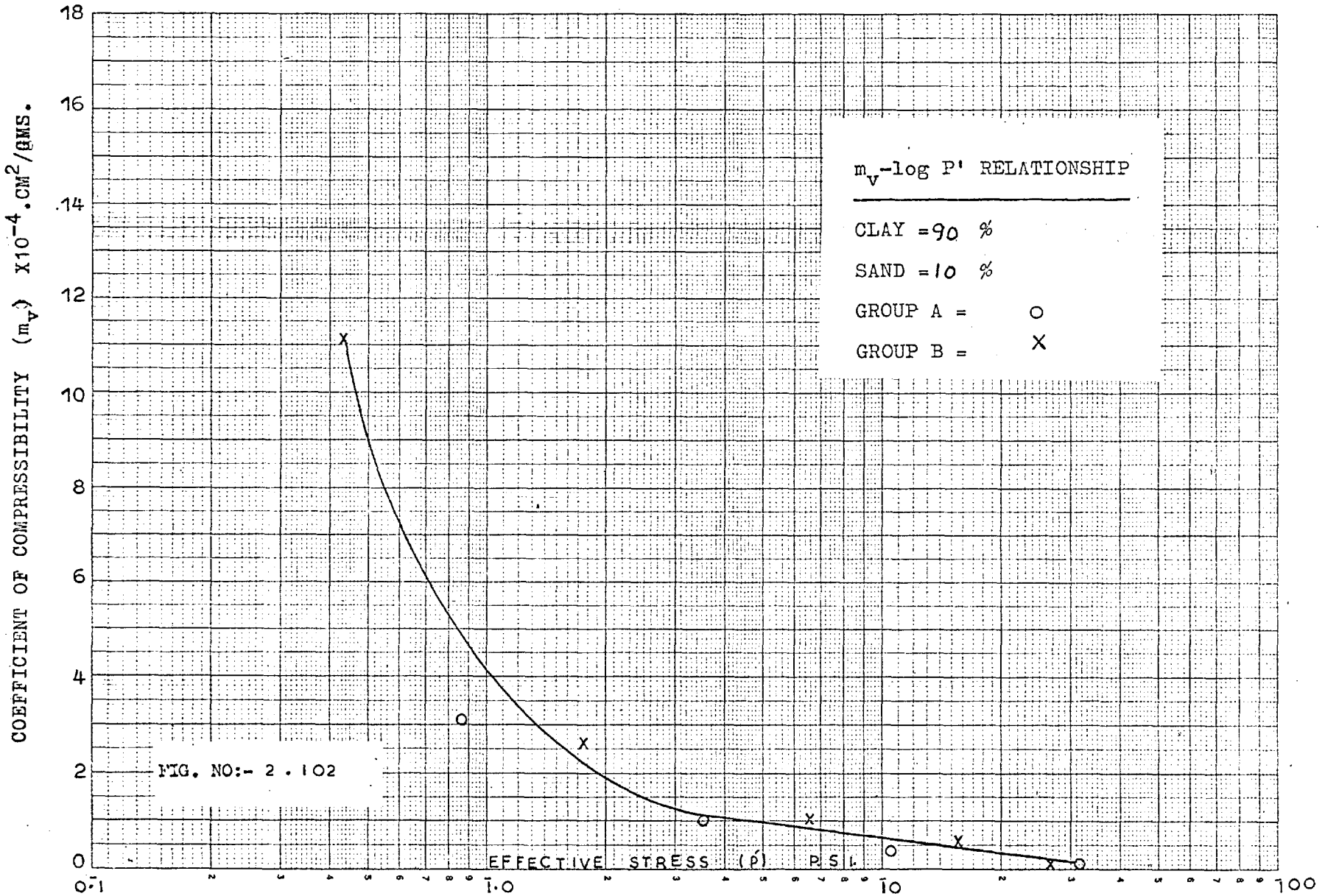
m_v-log P' RELATIONSHIP
CLAY =90 %
SAND =10 %
GROUP A = O
GROUP B = X
COEFFICIENT OF COMPRESSIBILITY (m_v) X10^{-4}.CM^2/GMS.
EFFECTIVE STRESS (ρ) P.S.I.
0·1
1·0
10
100
0
2
4
6
8
10
12
14
16
18

FIG. NO:- 2 . 102

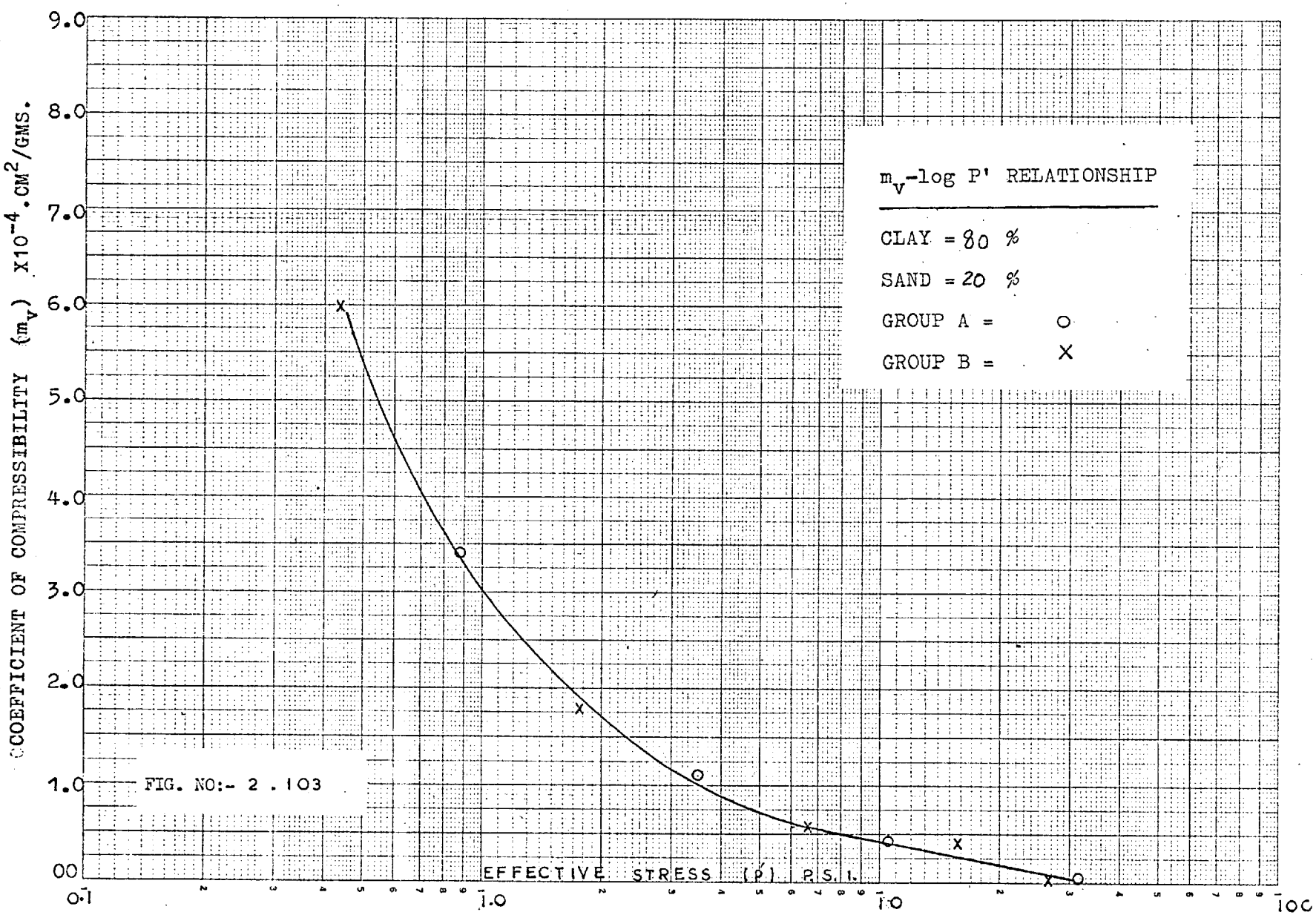
m_v-log P' RELATIONSHIP
CLAY = 80 %
SAND = 20 %
GROUP A = O
GROUP B = X
COEFFICIENT OF COMPRESSIBILITY (m_v) X10^{-4}.CM^2/GMS.
9.0
8.0
7.0
6.0
5.0
4.0
3.0
2.0
1.0
00
0.1
1.0
10
100
EFFECTIVE STRESS (P') P.S.I.

FIG. NO:- 2 . 103

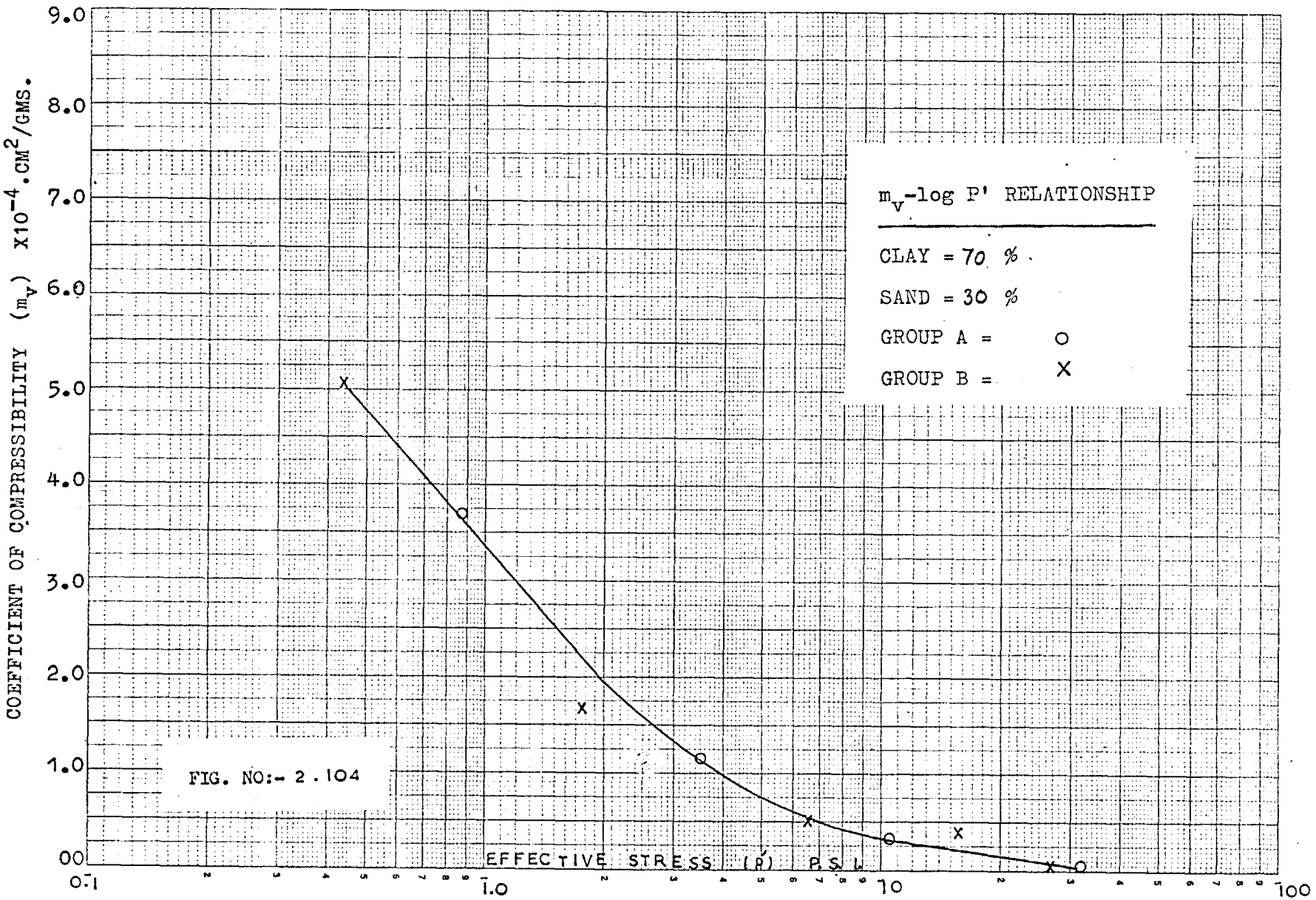
m_v-log P' RELATIONSHIP
CLAY = 70 %
SAND = 30 %
GROUP A = O
GROUP B = X
COEFFICIENT OF COMPRESSIBILITY (m_v) X10^{-4}.CM^2/GMS.
9.0
8.0
7.0
6.0
5.0
4.0
3.0
2.0
1.0
00
0.1
1.0
10
100
EFFECTIVE STRESS (P') P.S.I.

FIG. NO:- 2.104

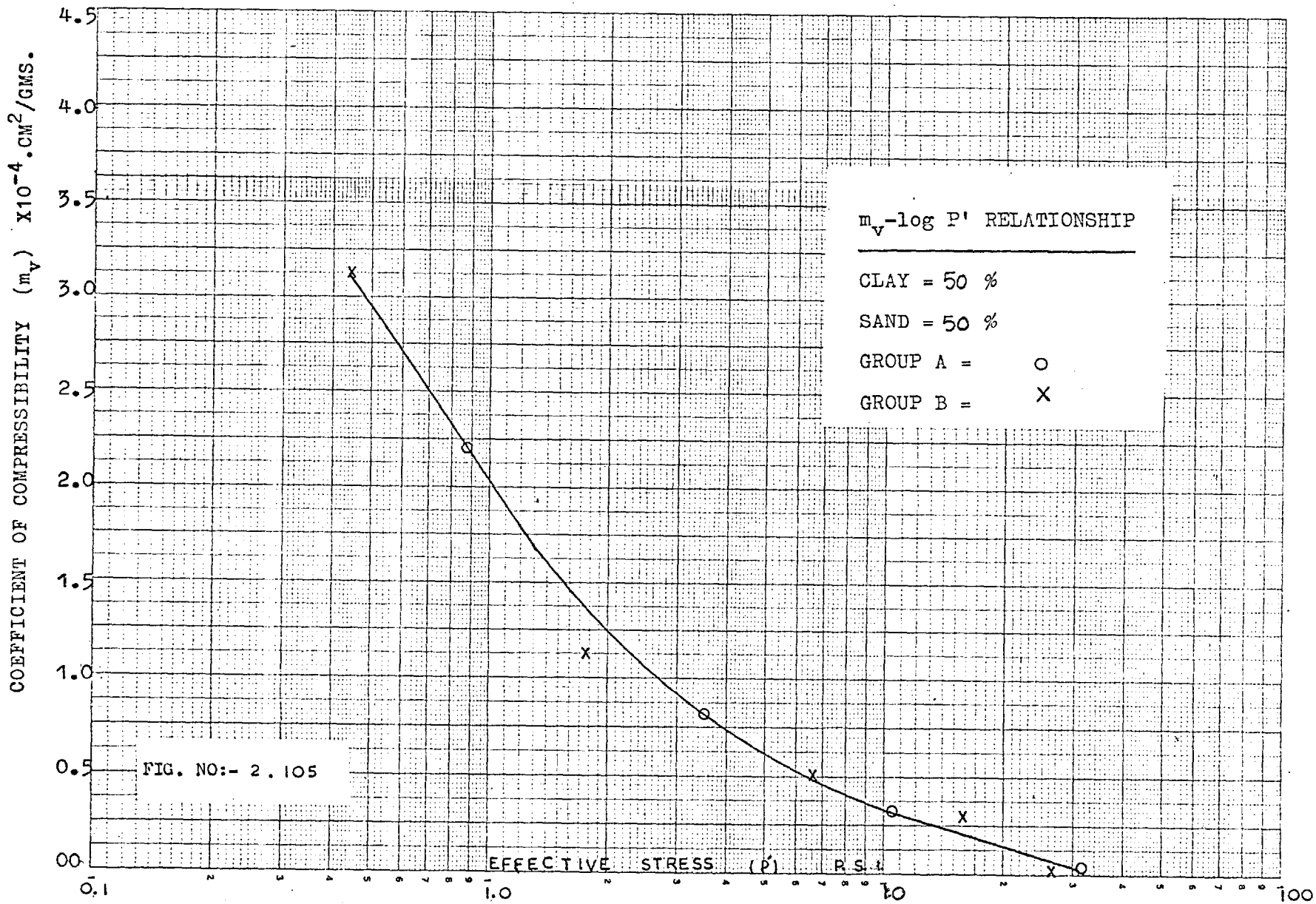
COEFFICIENT OF COMPRESSIBILITY (m_v) X10^{-4}.CM^2/GMS.
4.5
4.0
3.5
3.0
2.5
2.0
1.5
1.0
0.5
00
0.1
1.0
10
100
EFFECTIVE STRESS (P') P.S.I
m_v-log P' RELATIONSHIP
CLAY = 50 %
SAND = 50 %
GROUP A = O
GROUP B = X
FIG. NO:- 2.105

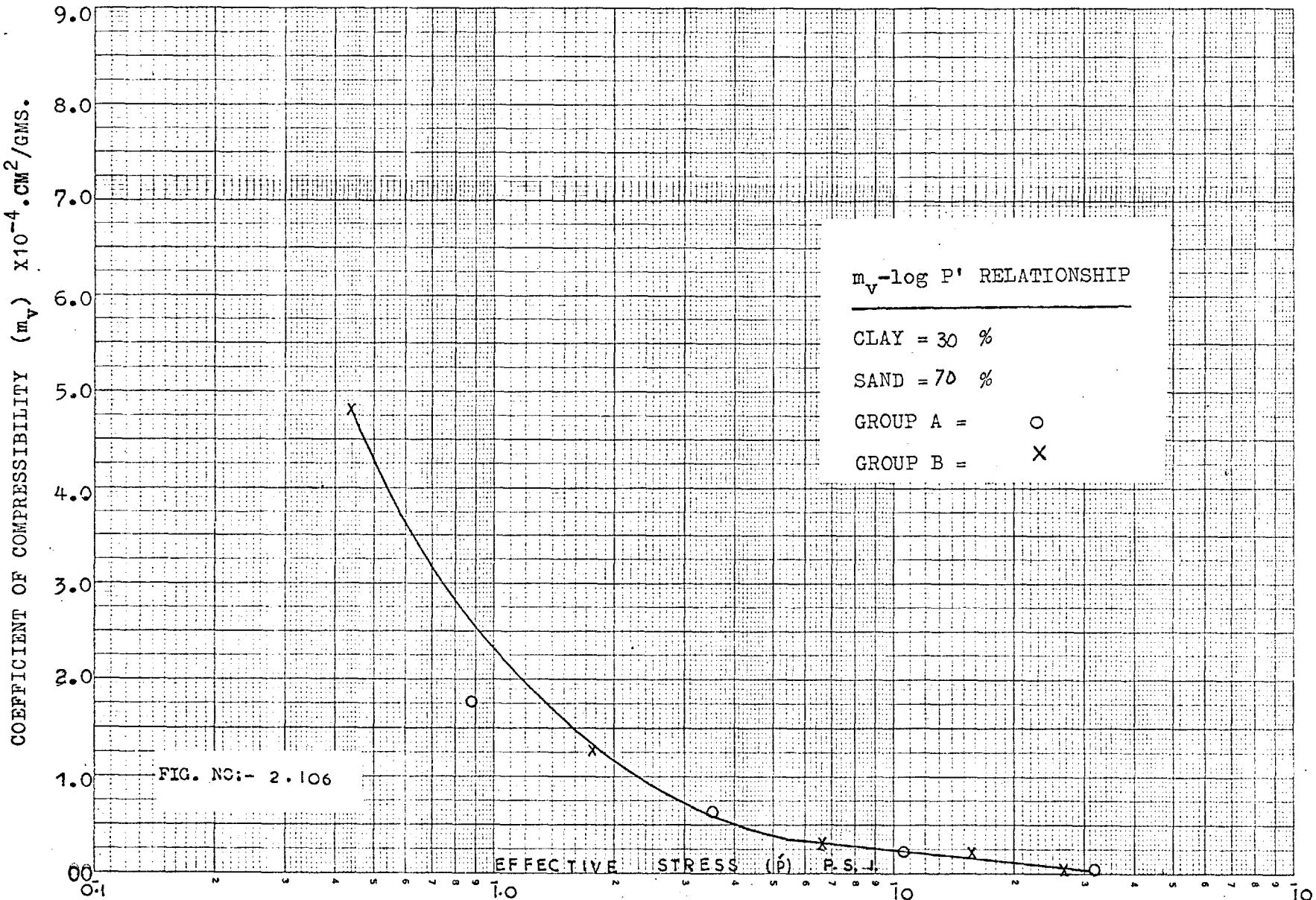
m_v-log P' RELATIONSHIP
CLAY = 30 %
SAND = 70 %
GROUP A = O
GROUP B = X
COEFFICIENT OF COMPRESSIBILITY (m_v) X10^{-4}.CM^2/GMS.
9.0
8.0
7.0
6.0
5.0
4.0
3.0
2.0
1.0
00
0.1
1.0
10
EFFECTIVE STRESS (P') P.S.I.

FIG. NO:- 2.106

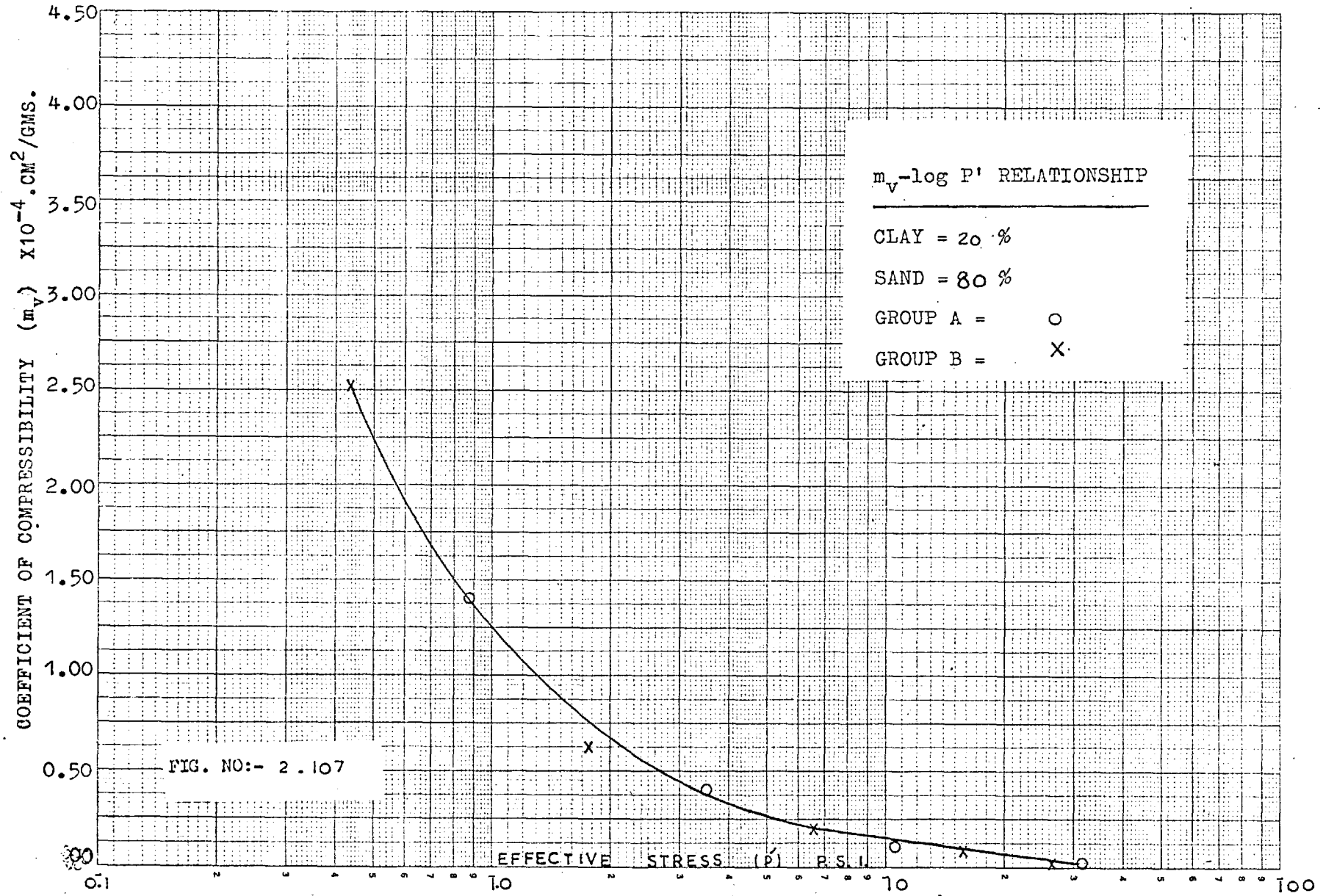
m_v-log P' RELATIONSHIP
CLAY = 20 %
SAND = 80 %
GROUP A = O
GROUP B = X
COEFFICIENT OF COMPRESSIBILITY (m_v) X10^{-4}.CM^2/GMS.
4.50
4.00
3.50
3.00
2.50
2.00
1.50
1.00
0.50
0.00
0.1
1.0
10
100
EFFECTIVE STRESS (P') P.S.I.

FIG. NO:- 2.107

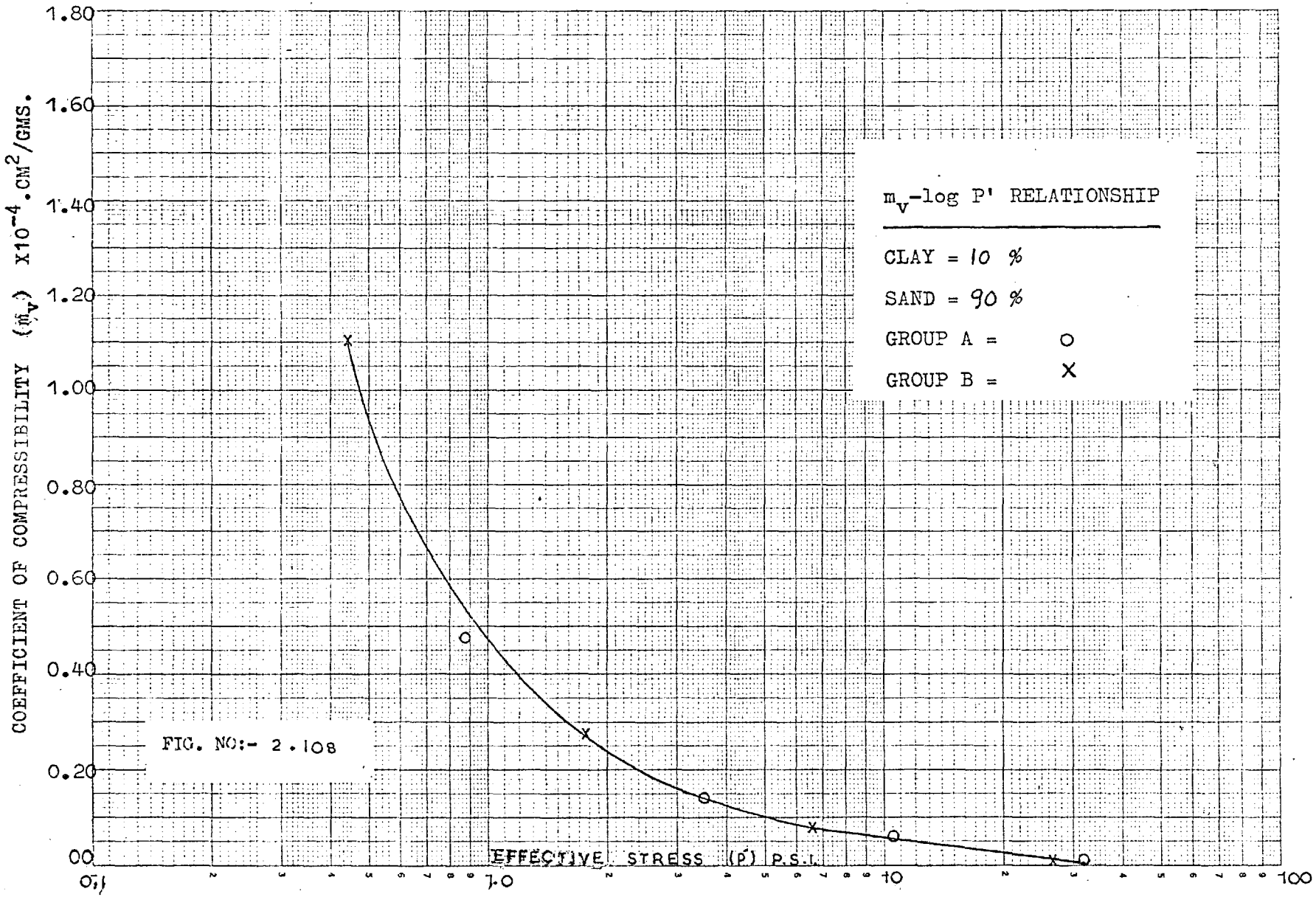
m_v-log P' RELATIONSHIP
CLAY = 10 %
SAND = 90 %
GROUP A = O
GROUP B = X
COEFFICIENT OF COMPRESSIBILITY (m_v) X10^{-4}.CM^2/GMS.
1.80
1.60
1.40
1.20
1.00
0.80
0.60
0.40
0.20
00
0.1
1.0
10
100
EFFECTIVE STRESS (P') P.S.I.

FIG. NO:- 2.108

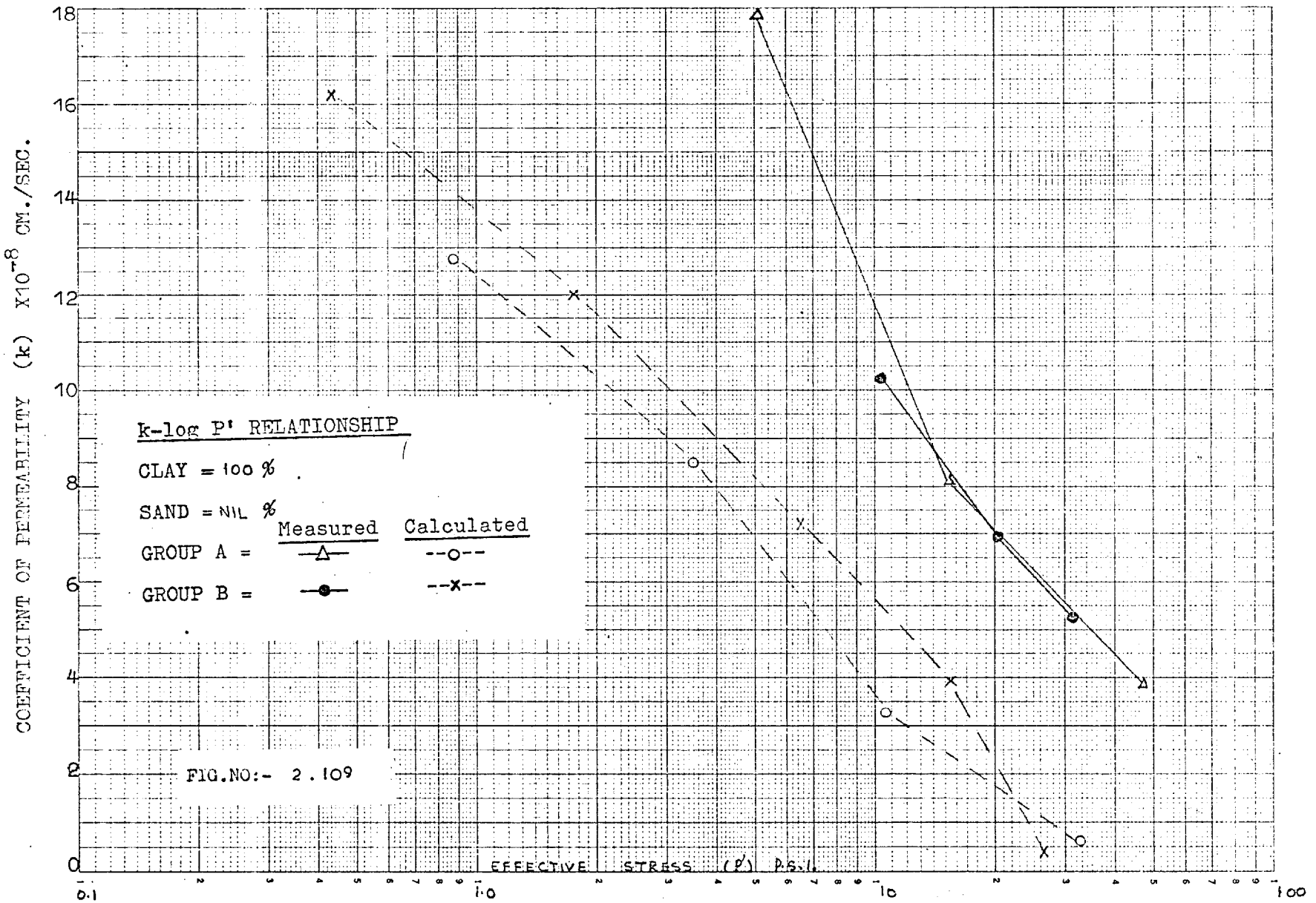
COEFFICIENT OF PERMEABILITY (k) X10⁻⁸ CM./SEC.
18
16
14
12
10
8
6
4
2
0
0.1
1.0
10
100
EFFECTIVE STRESS (P') P.S.I.
k-log P' RELATIONSHIP
CLAY = 100 %
SAND = NIL %
Measured
Calculated
GROUP A =
GROUP B =
FIG.NO:- 2.109

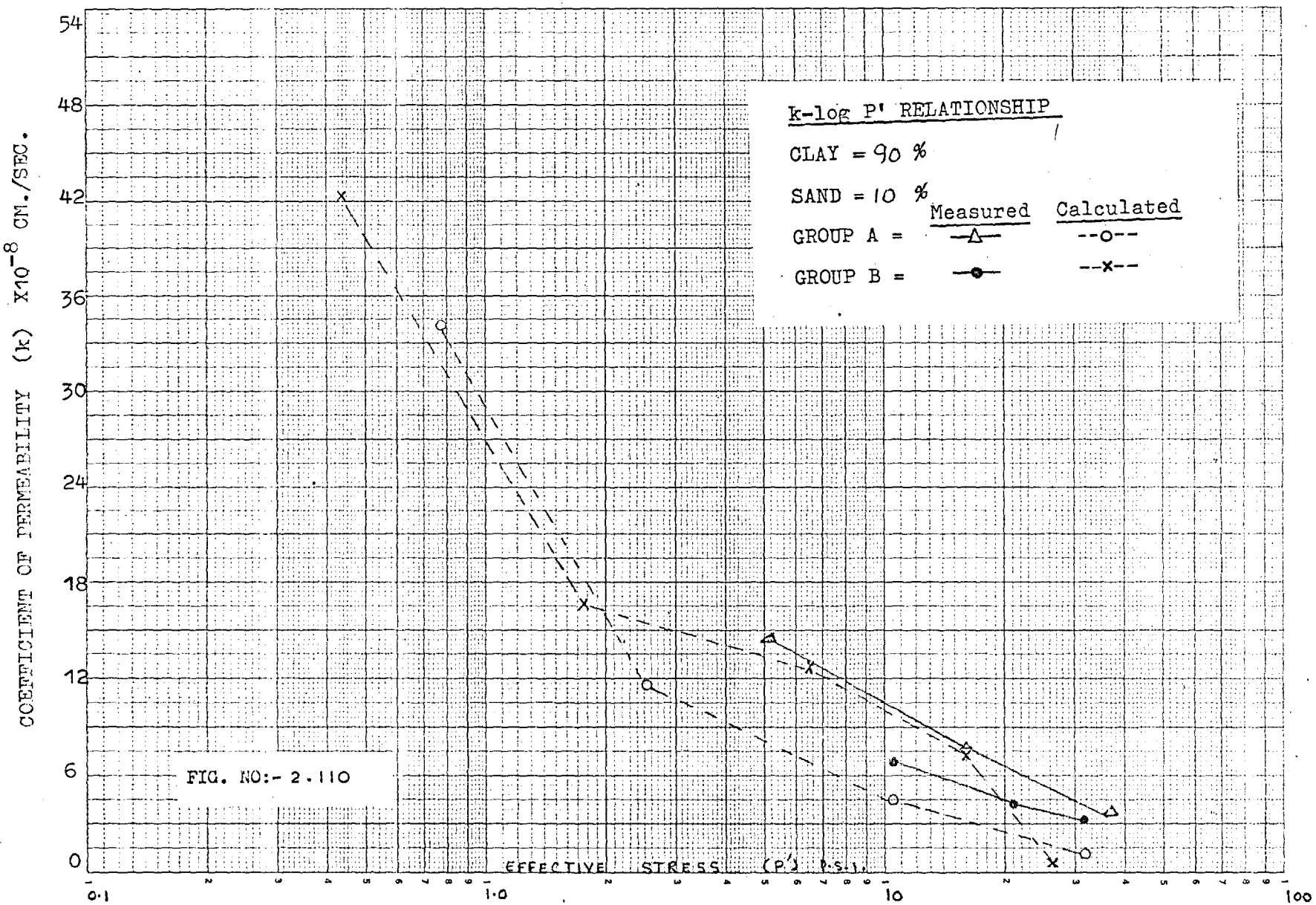
k-log P' RELATIONSHIP
CLAY = 90 %
SAND = 10 %
Measured
Calculated
GROUP A =
GROUP B =
COEFFICIENT OF PERMEABILITY (k) X10⁻⁸ CM./SEC.
54
48
42
36
30
24
18
12
6
0
0·1
1·0
10
100
EFFECTIVE STRESS (P') P.S.I.

FIG. NO:- 2.110

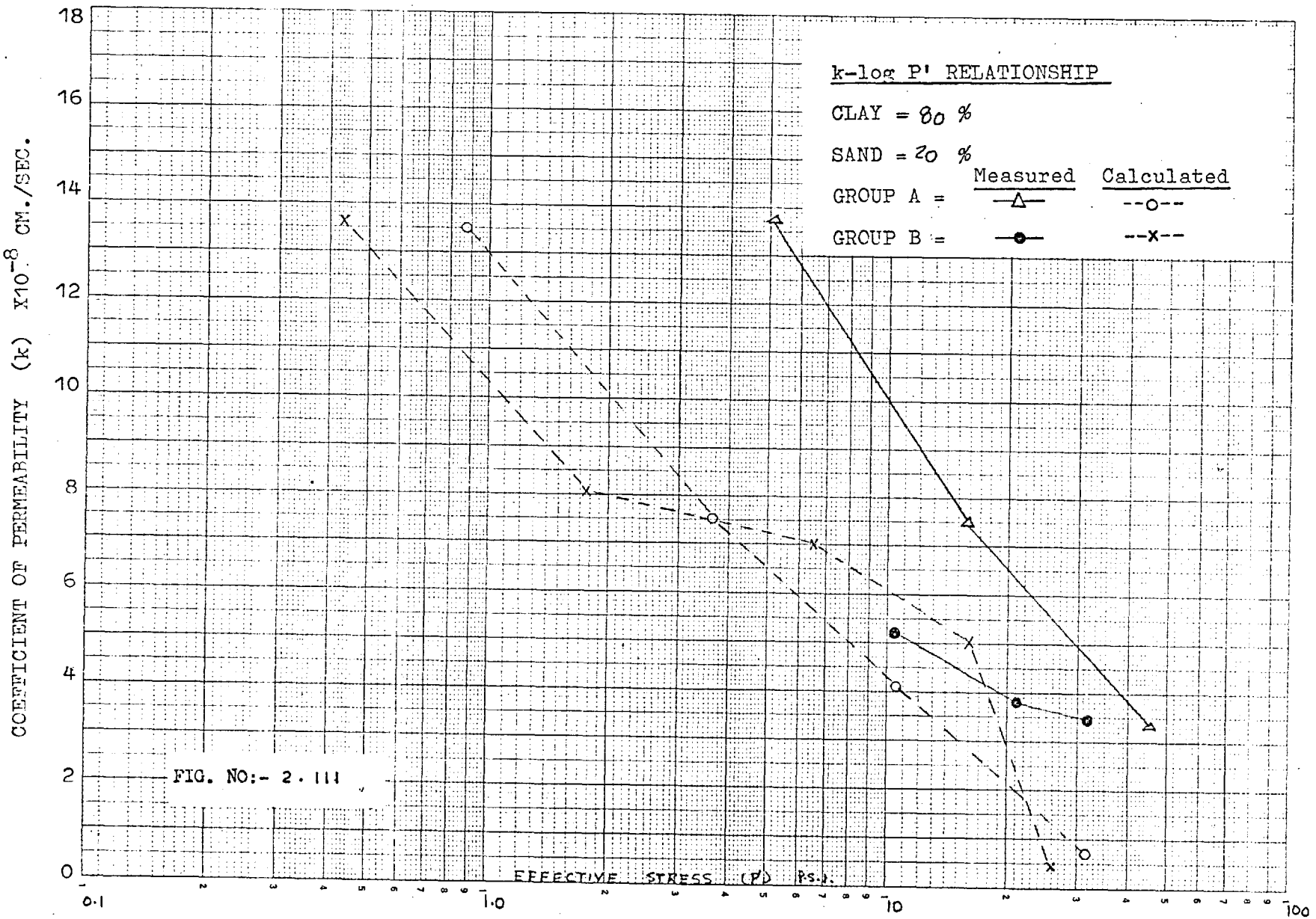
k-log P' RELATIONSHIP
CLAY = 80 %
SAND = 20 %
Measured
Calculated
GROUP A =
GROUP B =
COEFFICIENT OF PERMEABILITY (k) X10⁻⁸ CM./SEC.
EFFECTIVE STRESS (P') Ps.i.
0
2
4
6
8
10
12
14
16
18
0.1
1.0
10
100

FIG. NO:- 2.111

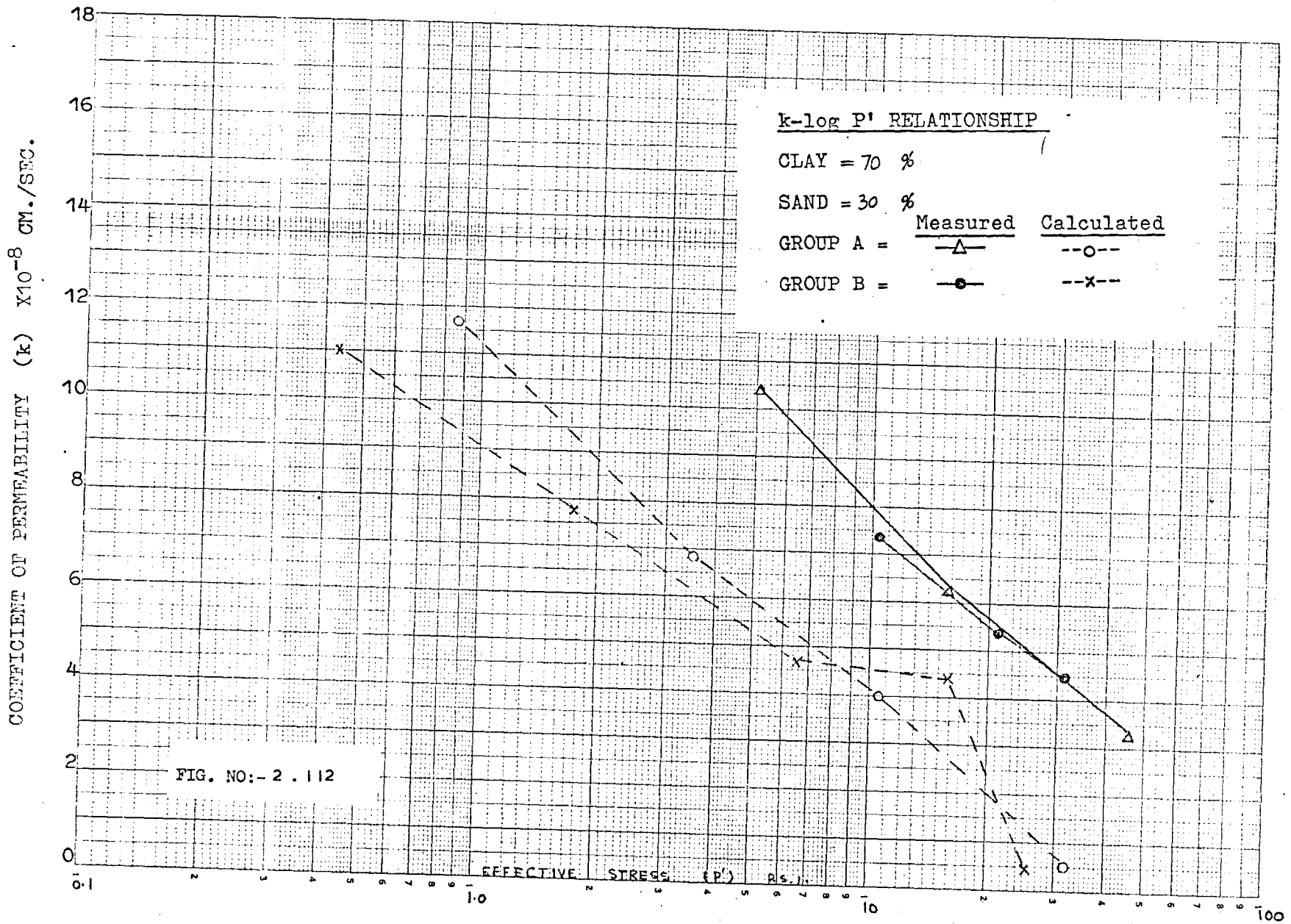
k-log P' RELATIONSHIP
CLAY = 70 %
SAND = 30 %
Measured
Calculated
GROUP A =
GROUP B =
COEFFICIENT OF PERMEABILITY (k) X10⁻⁸ CM./SEC.
EFFECTIVE STRESS (P') Kg./...
0
2
4
6
8
10
12
14
16
18
0·1
1·0
10
100

FIG. NO:- 2 . 112

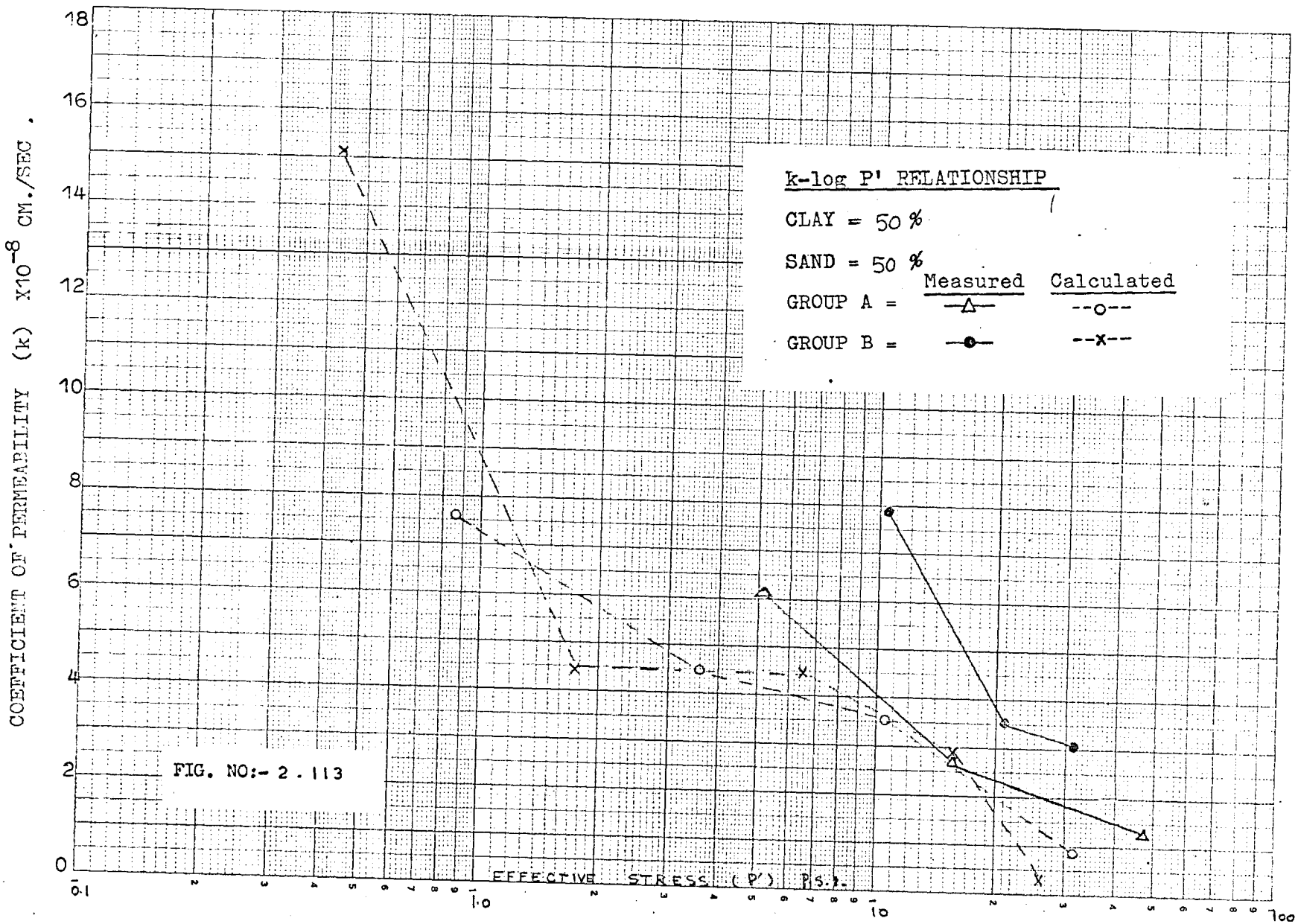
k-log P' RELATIONSHIP
CLAY = 50 %
SAND = 50 %
Measured
Calculated
GROUP A =
GROUP B =
COEFFICIENT OF PERMEABILITY (k) X10⁻⁸ CM./SEC.
EFFECTIVE STRESS (P') P.S.I.
0
2
4
6
8
10
12
14
16
18
0.1
1.0
10
100

FIG. NO:- 2 . 113

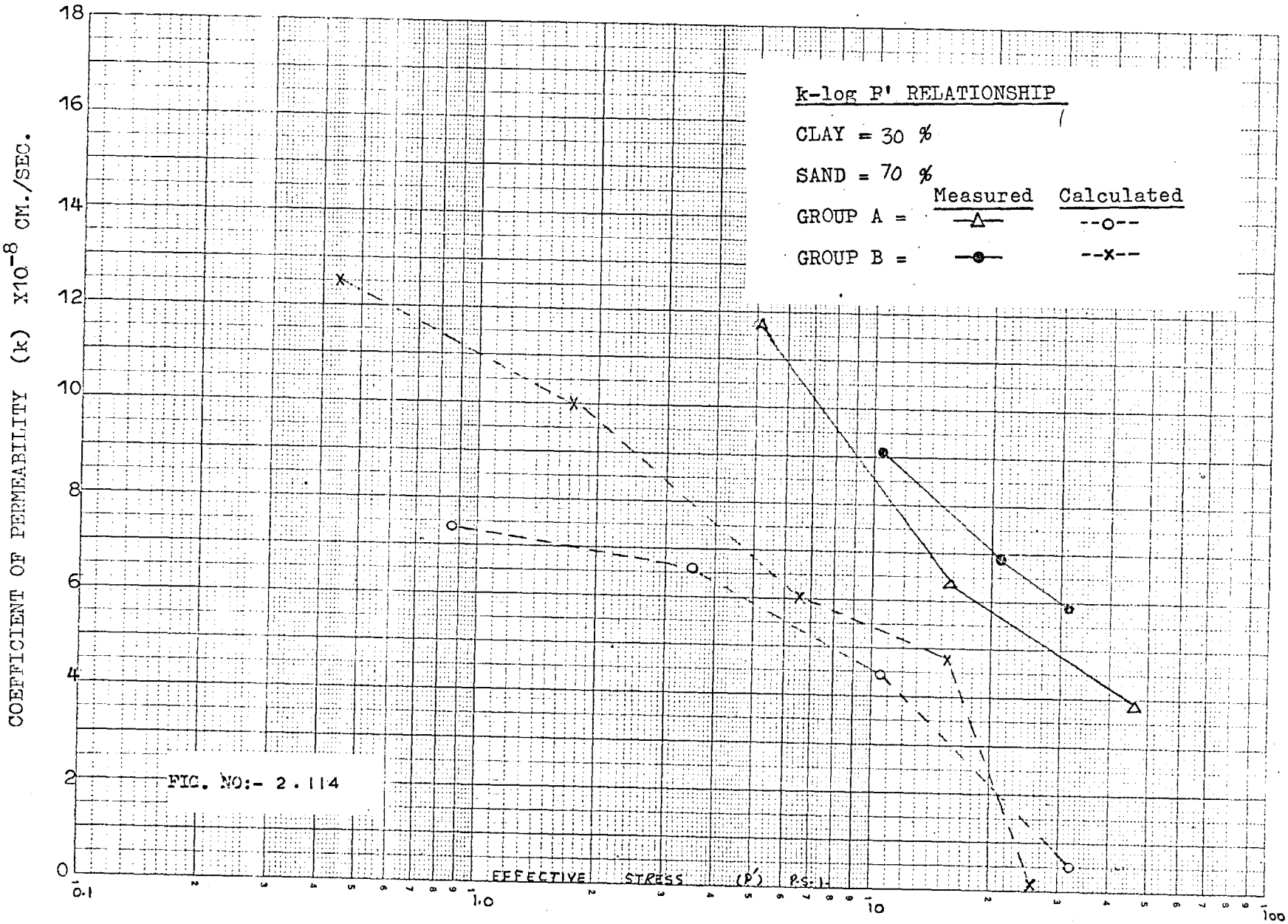
k-log P' RELATIONSHIP
CLAY = 30 %
SAND = 70 %
Measured
Calculated
GROUP A =
GROUP B =
COEFFICIENT OF PERMEABILITY (k) X10⁻⁸ CM./SEC.
EFFECTIVE STRESS (P') P.S.I.
0
2
4
6
8
10
12
14
16
18
0.1
1.0
10
100

FIG. NO:- 2.114

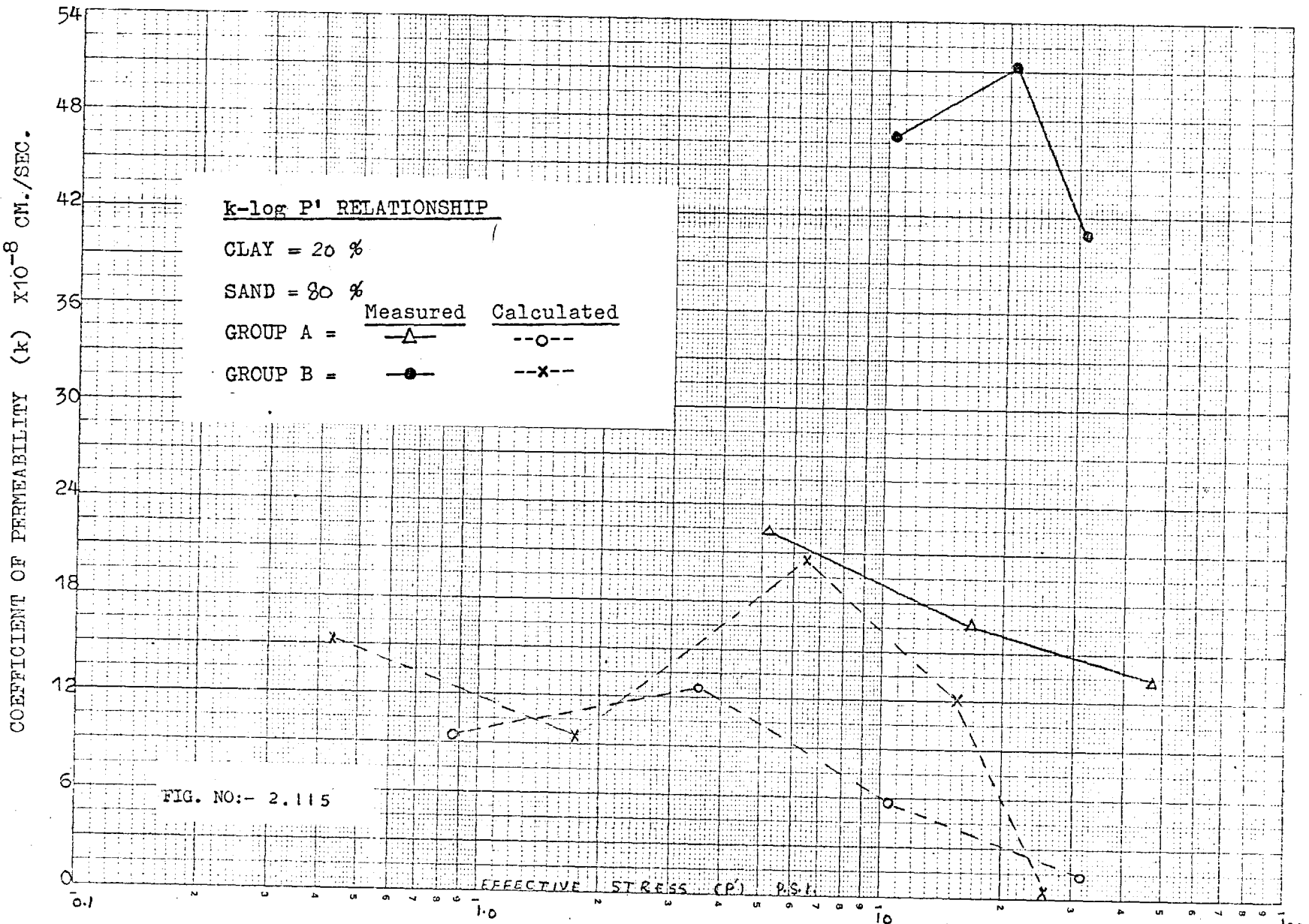
k-log P' RELATIONSHIP
CLAY = 20 %
SAND = 80 %
Measured
Calculated
GROUP A =
GROUP B =
COEFFICIENT OF PERMEABILITY (k) X10⁻⁸ CM./SEC.
54
48
42
36
30
24
18
12
6
0
0.1
1.0
10
100
EFFECTIVE STRESS (P') P.S.I.

FIG. NO:- 2.115

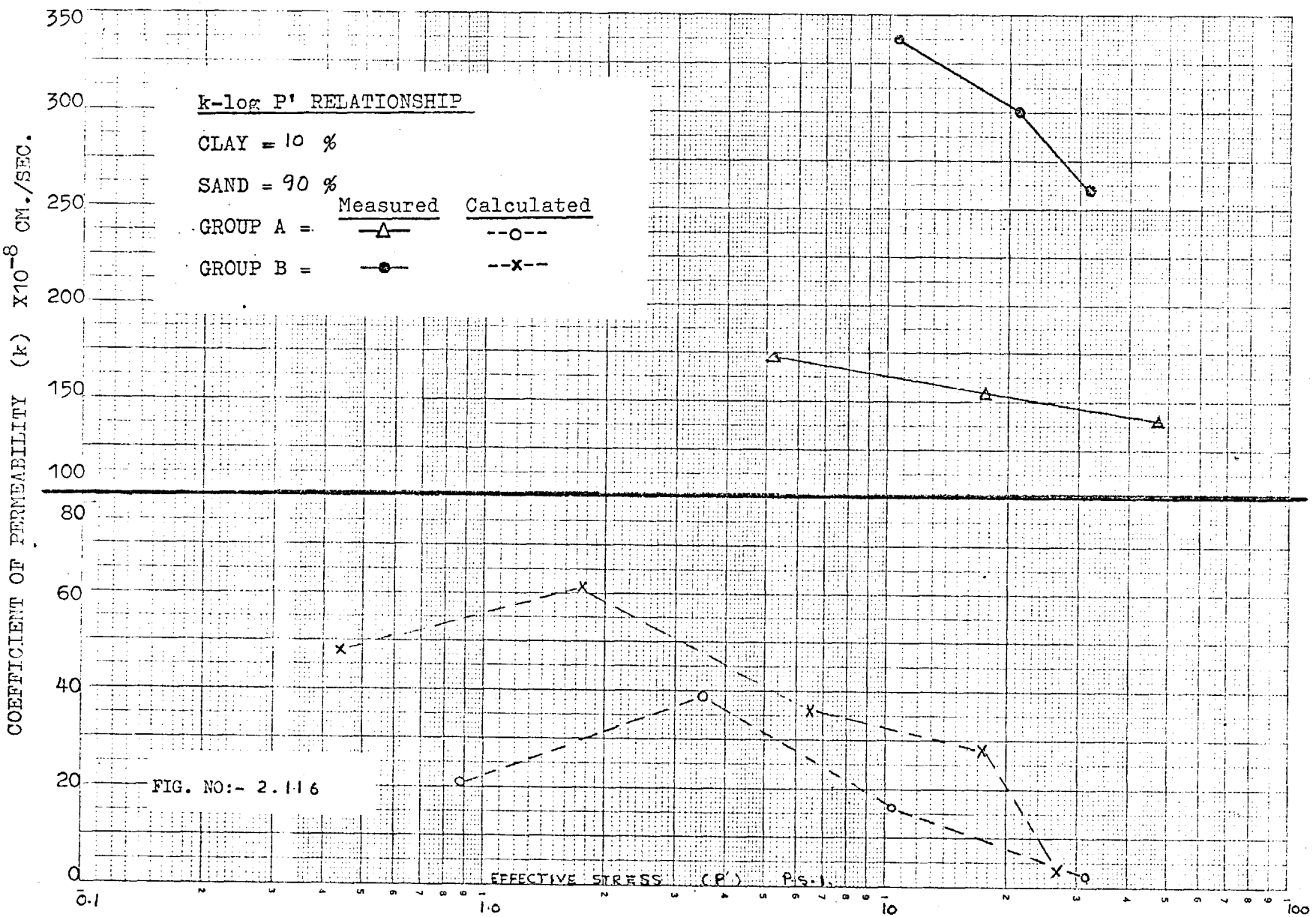
k-log P' RELATIONSHIP
CLAY = 10 %
SAND = 90 %
Measured
Calculated
GROUP A =
GROUP B =
COEFFICIENT OF PERMEABILITY (k) X10⁻⁸ CM./SEC.
EFFECTIVE STRESS (P') P.S.I.
350
300
250
200
150
100
80
60
40
20
0
0.1
1.0
10
100

FIG. NO:- 2.1.16

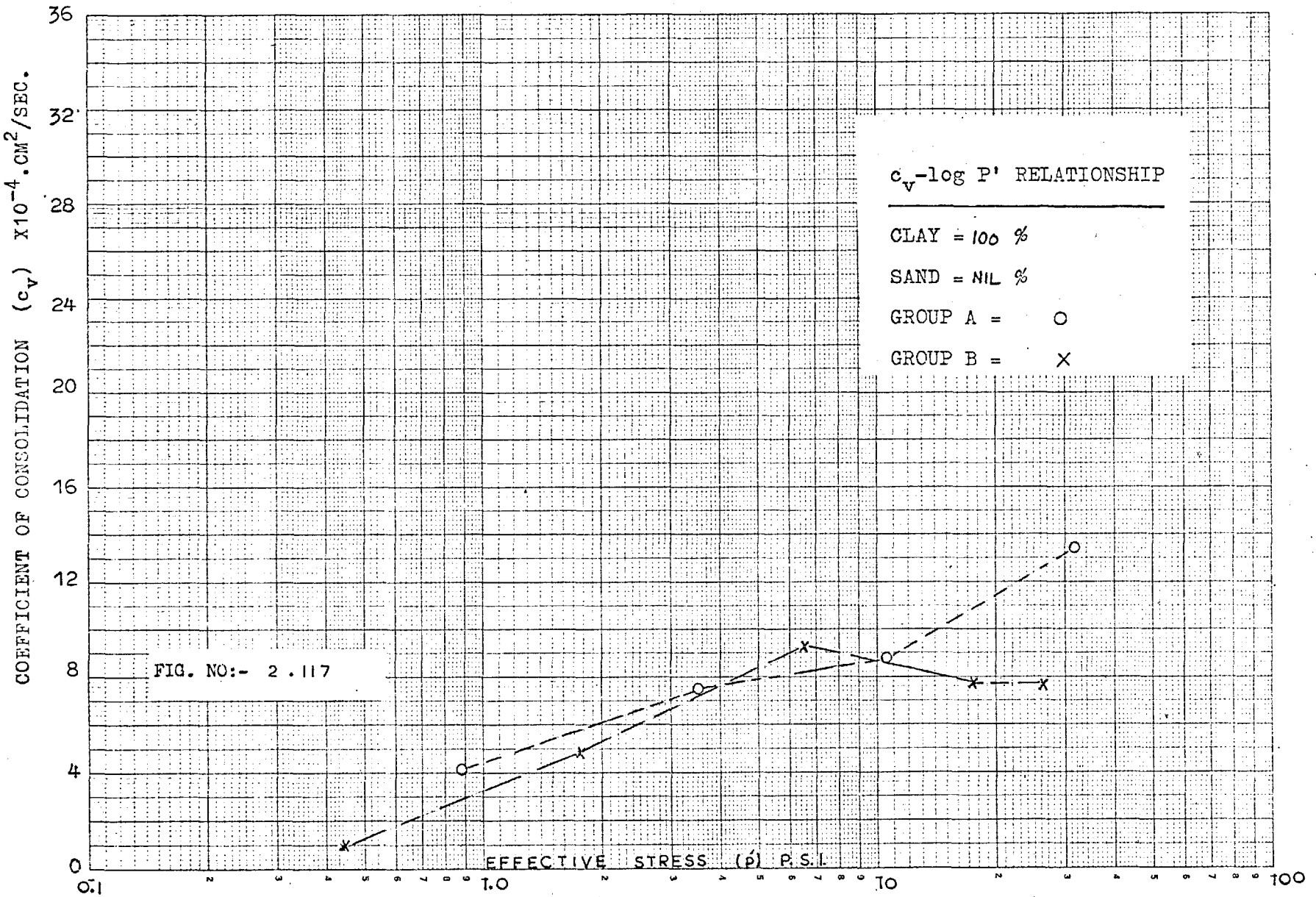
c_v-log P' RELATIONSHIP
CLAY = 100 %
SAND = NIL %
GROUP A = O
GROUP B = X
COEFFICIENT OF CONSOLIDATION (c_v) X10^{-4}.CM^2/SEC.
EFFECTIVE STRESS (p) P.S.I.
0
4
8
12
16
20
24
28
32
36
0.1
1.0
10
100

FIG. NO:- 2.117

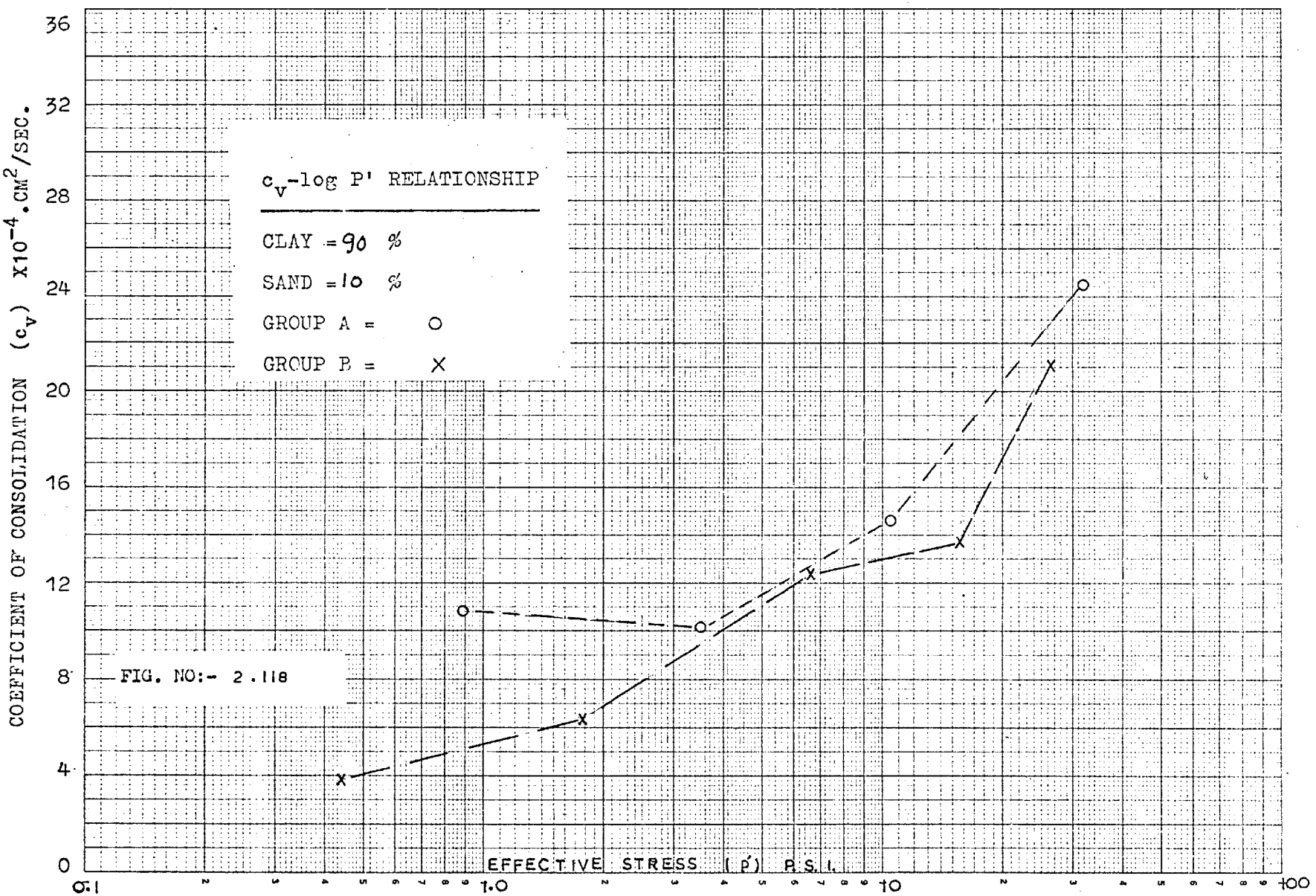
c_v-log P' RELATIONSHIP
CLAY = 90 %
SAND = 10 %
GROUP A = O
GROUP B = X
FIG. NO:- 2.118
COEFFICIENT OF CONSOLIDATION (c_v) X10^{-4}.CM^2/SEC.
EFFECTIVE STRESS (p') P.S.I.
0
4
8
12
16
20
24
28
32
36
0.1
1.0
10
100

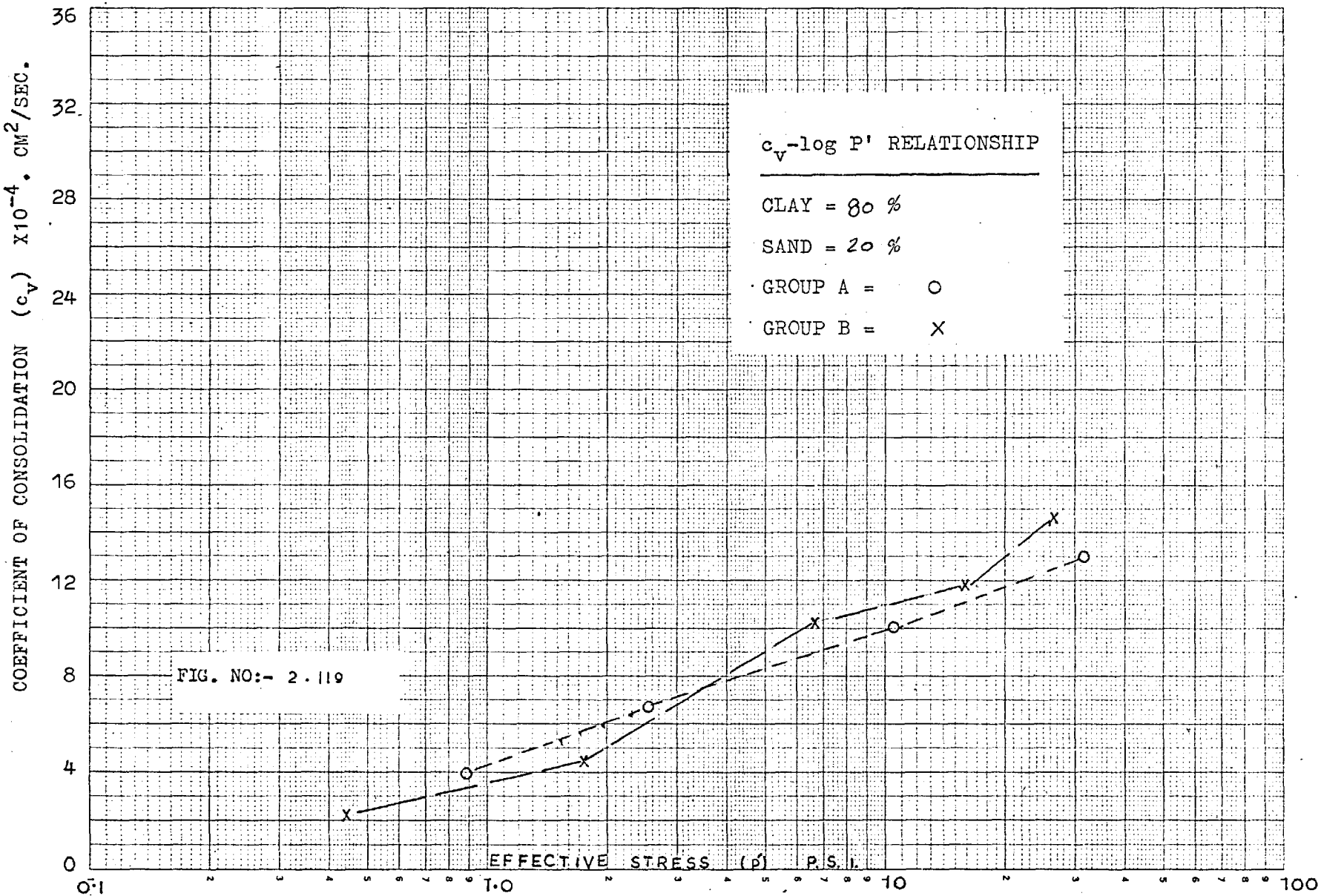
c_v-log P' RELATIONSHIP
CLAY = 80 %
SAND = 20 %
GROUP A = O
GROUP B = X
FIG. NO:- 2.119
COEFFICIENT OF CONSOLIDATION (c_v) X10^{-4}, CM^2/SEC.
EFFECTIVE STRESS (p') P.S.I.
0
4
8
12
16
20
24
28
32
36
0·1
1·0
10
100

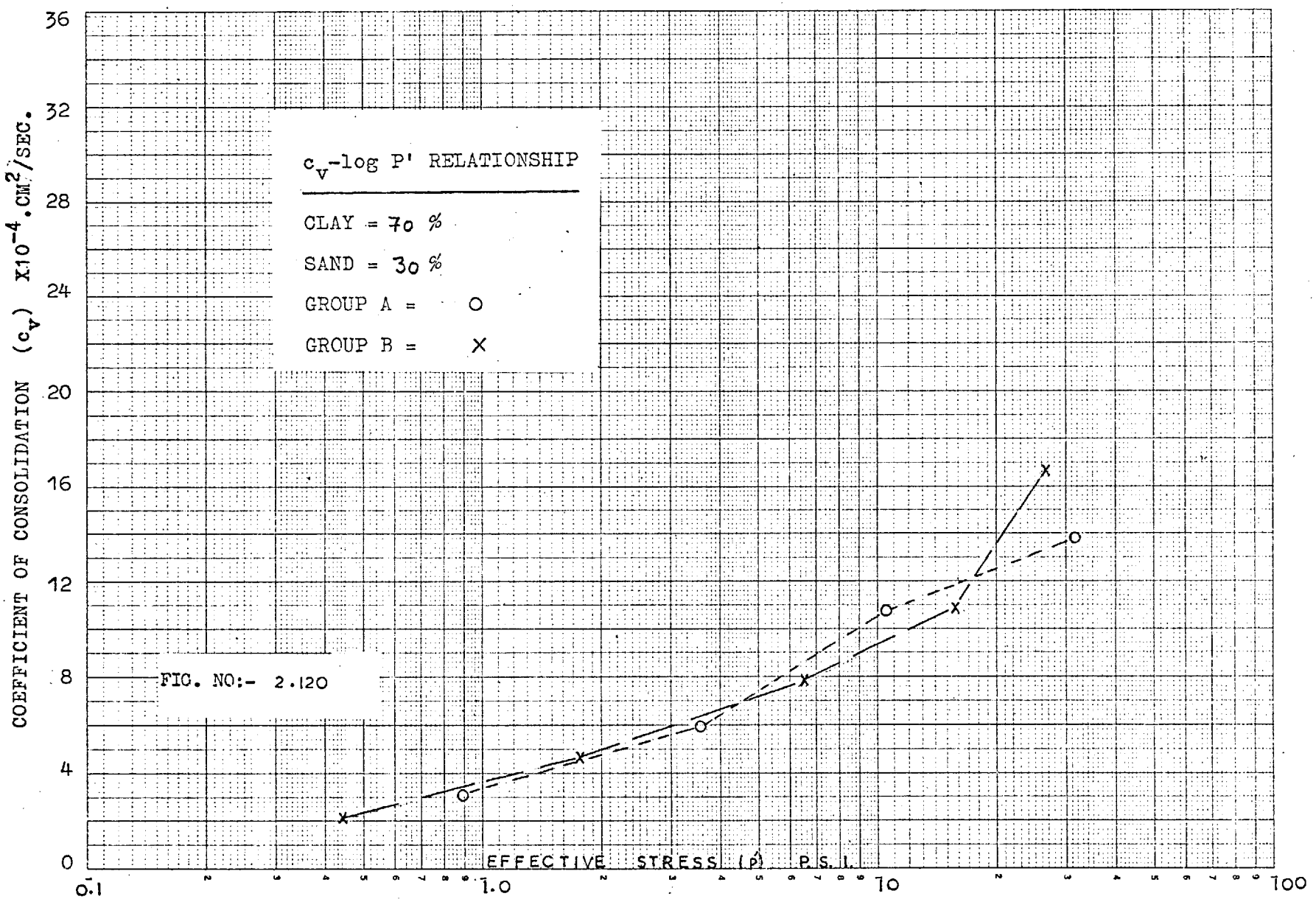
c_v-log P' RELATIONSHIP
CLAY = 70 %
SAND = 30 %
GROUP A = O
GROUP B = X
FIG. NO:- 2.120
COEFFICIENT OF CONSOLIDATION (c_v) X10^{-4}.CM^2/SEC.
EFFECTIVE STRESS (P') P.S.I.
36
32
28
24
20
16
12
8
4
0
0.1
1.0
10
100

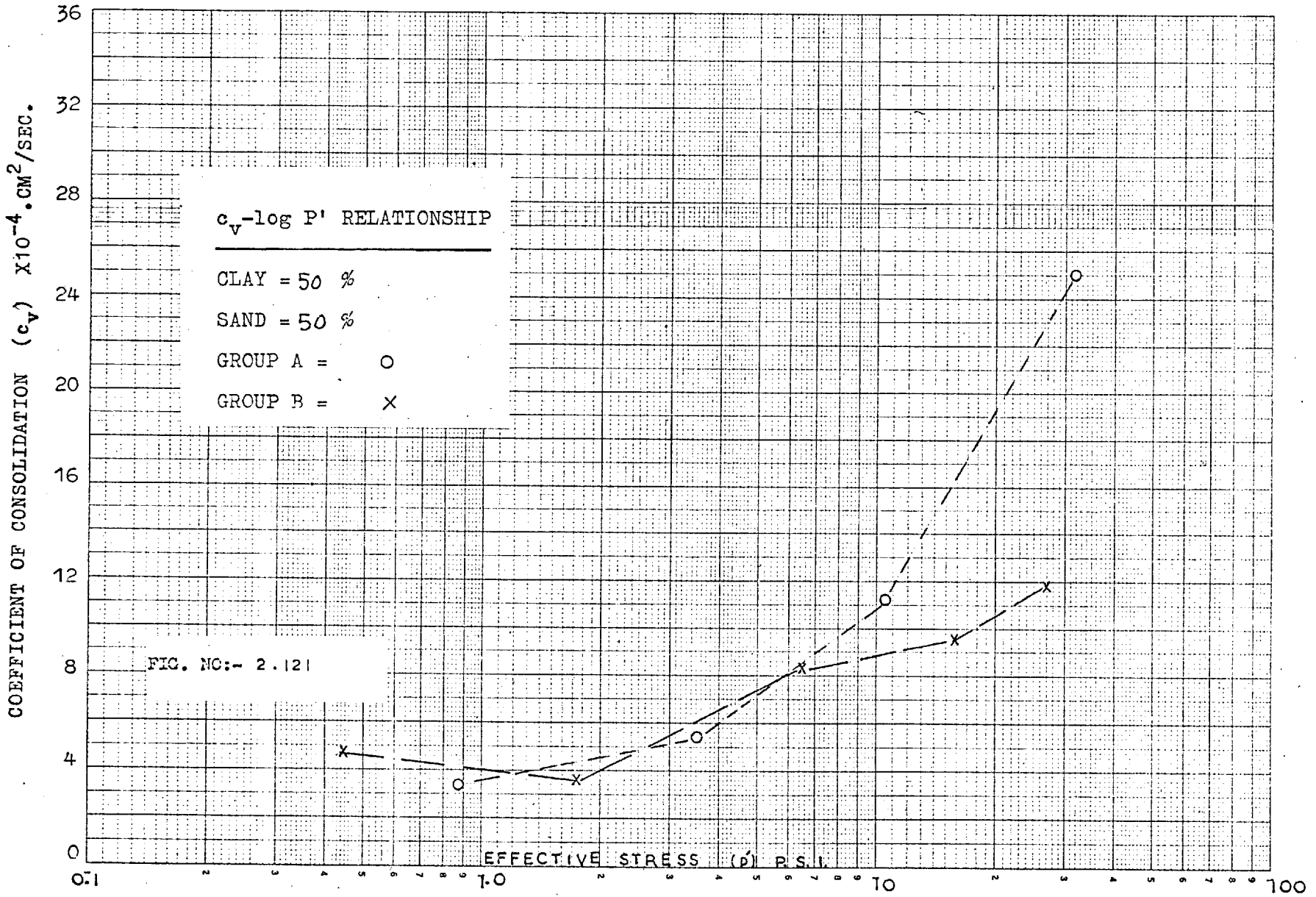
c_v-log P' RELATIONSHIP
CLAY = 50 %
SAND = 50 %
GROUP A = O
GROUP B = X
FIG. NO:- 2.121
COEFFICIENT OF CONSOLIDATION (c_v) X10^{-4}.CM^2/SEC.
EFFECTIVE STRESS (p') P.S.I.
36
32
28
24
20
16
12
8
4
0
0.1
1.0
10
100

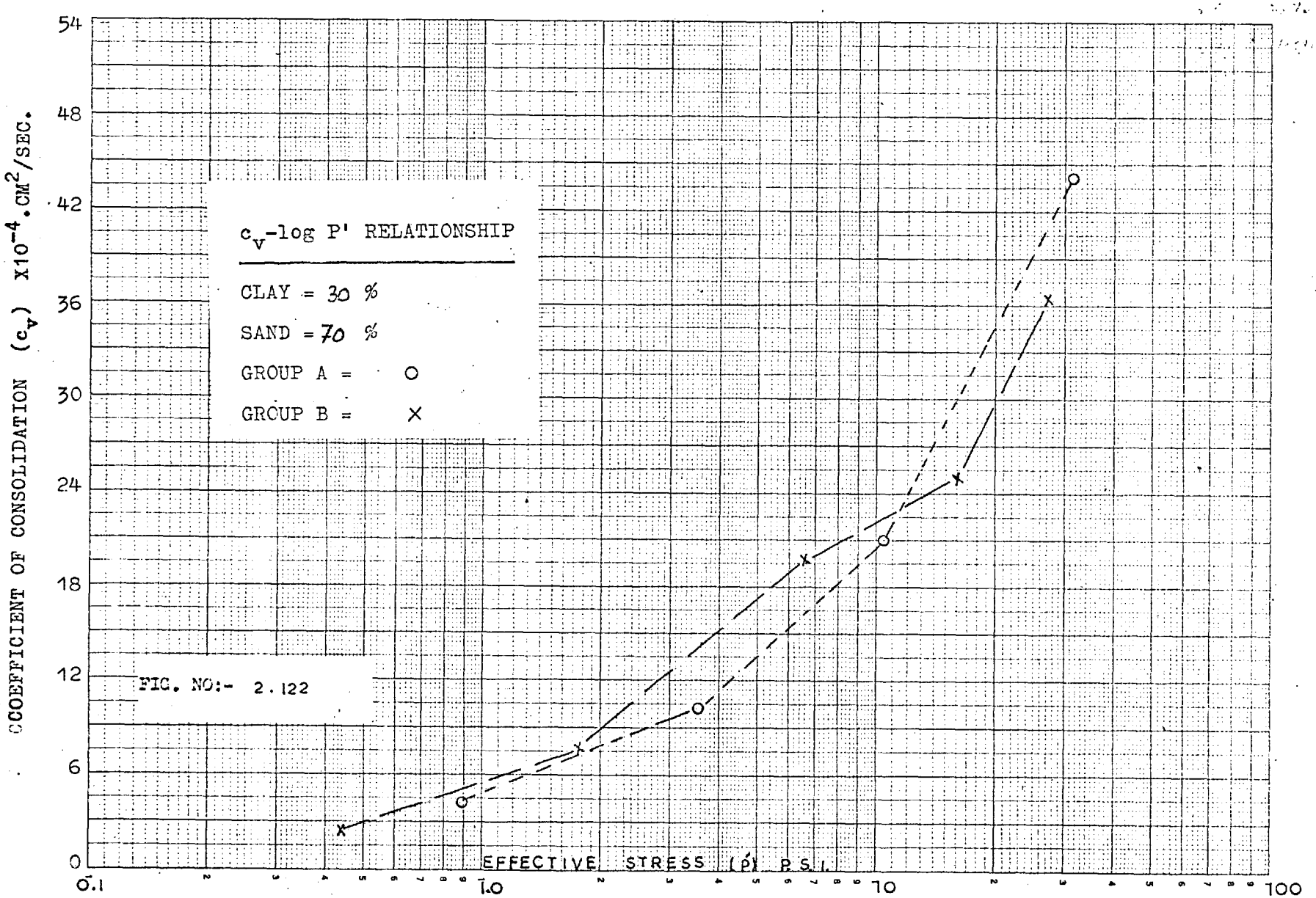
c_v-log P' RELATIONSHIP
CLAY = 30 %
SAND = 70 %
GROUP A = O
GROUP B = X
FIG. NO:- 2.122
COEFFICIENT OF CONSOLIDATION (c_v) X10^{-4}.CM^2/SEC.
54
48
42
36
30
24
18
12
6
0
0.1
1.0
10
100
EFFECTIVE STRESS (P') P.S.I.

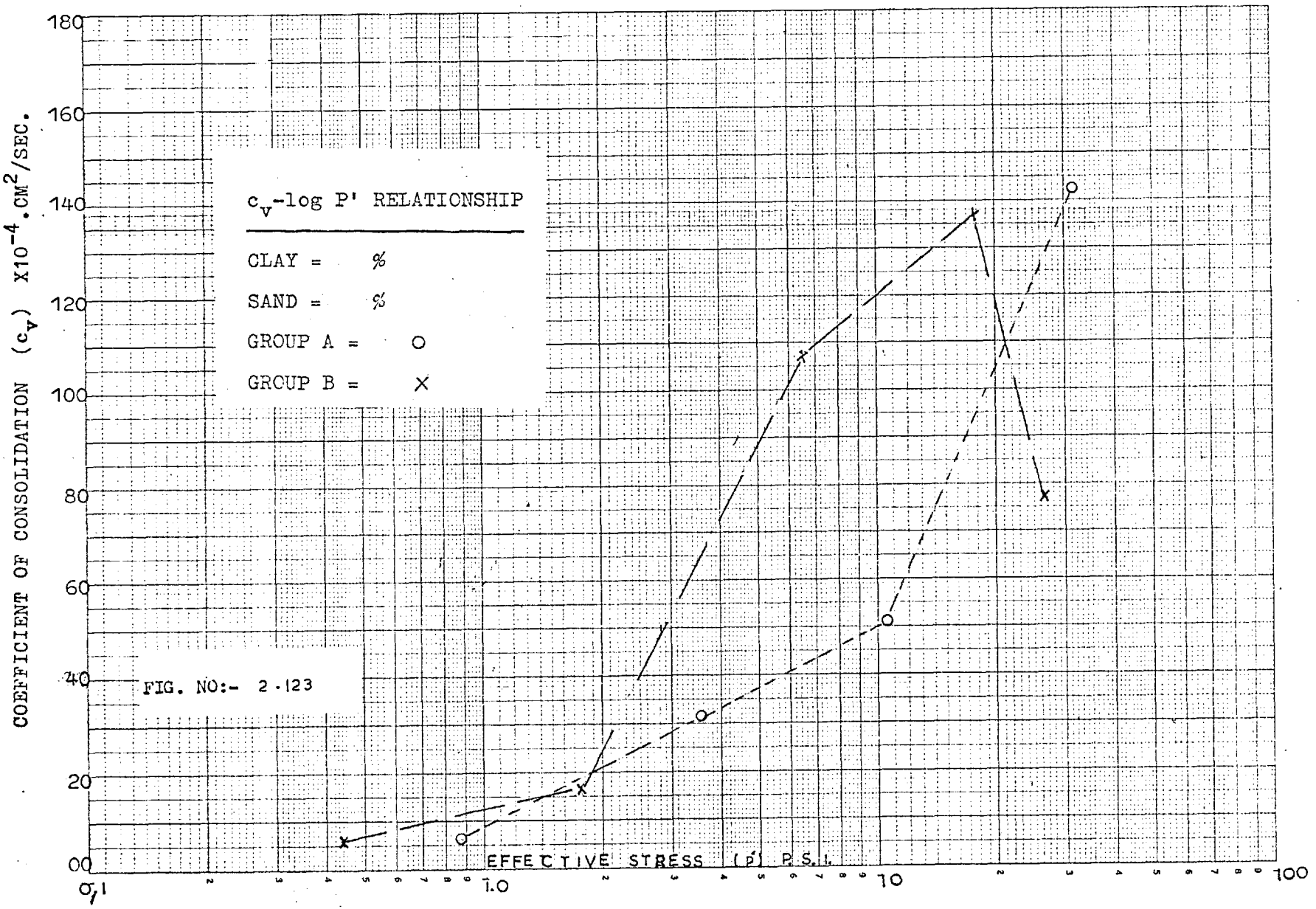
c_v-log P' RELATIONSHIP
CLAY = %
SAND = %
GROUP A = O
GROUP B = X
FIG. NO:- 2·123
COEFFICIENT OF CONSOLIDATION (c_v) X10^{-4}.CM^2/SEC.
EFFECTIVE STRESS (P') P.S.I.
180
160
140
120
100
80
60
40
20
00
σ_1
1.0
10
100

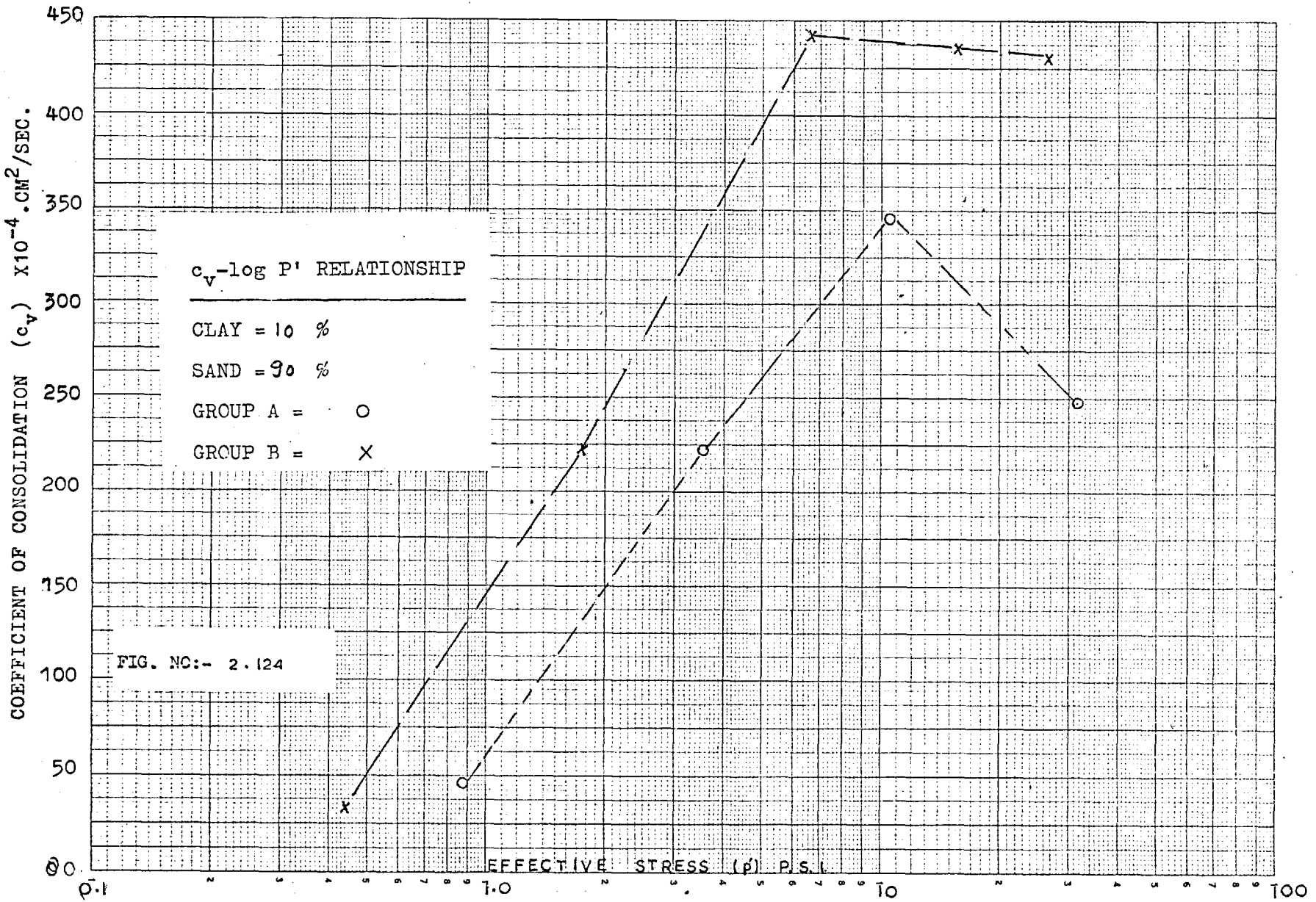
c_v-log P' RELATIONSHIP
CLAY = 10 %
SAND = 90 %
GROUP A = O
GROUP B = X
FIG. NO:- 2.124
COEFFICIENT OF CONSOLIDATION (c_v) X10^{-4}.CM^2/SEC.
EFFECTIVE STRESS (p') P.S.I.
450
400
350
300
250
200
150
100
50
0
0.1
1.0
10
100

3. TRIAXIAL CONSOLIDATION AND CONSTANT HEAD PERMEABILITY TESTS

3.1 Programme of testing

The isotropic consolidation tests on 1.5 in. diameter by 3 in. high cylindrical kaolin and gap-graded soil samples were carried out in the triaxial apparatus. To verify whether the samples were fully saturated, they were subjected to the required cell pressure in steps and B values were determined. The consolidation process was resumed by decreasing back pressure for each stage, while maintaining constant cell pressure. The drainage of pore fluid was allowed to take place from the top only, while the pore water pressure (P.W.P.) was measured at the bottom of the sample.

The test programme was devised on the same lines as described in the previous chapter, namely group A and B tests. In group A the effective stress increment ratio $\frac{\Delta P}{Po'}$ was kept constant for all the stages, while in group B the $\frac{\Delta P}{Po'}$ was varied from one stage of consolidation to another, as shown in Table 3.1. Basically, both groups consisted of five stages of consolidation and two stages of swelling.

3.2 Description of the Apparatus

Details of the triaxial apparatus and the self-compensating mercury control are described by Bishop and Henkel (1962). However, instruments such as the pressure transducer, volume gauges etc. used here are briefly described in the following section.

(a) Instrument for measuring pore water pressure

The change of pore pressure of all the samples was measured at the base by a very stiff Bell and Howell type 4-366 electric pressure transducer having a range of 0 to 100 p.s.i. It converts fluid pressure experienced by the diaphragm of the instrument to a controlled strain

in an excited Wheatsone Bridge of strain gauges windings. This type of transducer is somewhat stiffer than the P.S.G. type described in section 2.4 (iii). The volume change of Bell and Howell type due to deflection of the diaphragm is less than 1×10^{-6} cc/p.s.i. Together with a perspex mounting block and valves the volume change is of the order 1×10^{-5} cc/p.s.i.

The pressure transducer was connected to a strip chart potentiometric recorder via readout meter* which enabled the transducer output to be nulled. Prior to consolidation tests all the transducers were repeatedly calibrated both on the C61 readout meter and chart recorder by adding standard weights to the dead weight calibrator (Budenberg) in the manner explained in Chapter 2. The output from the pressure transducer during a consolidation test was normally recorded and later converted in terms of pore pressure (p.s.i.) at their respective times.

(b) Volume Change Measurements

One of the ends of a parafin volume gauge (Bishop and Henkel, 1962) was connected to the top of the sample from where the drainage had to take place, while another was connected to the self-compensating mercury control. During the consolidation, volume change of the sample was measured by the movement of dyed parafin in a 5.0 cc graduated glass burette. A valve system shown in Figure 3.1 was provided in between the volume gauge and sample, to facilitate the reversing of the flow of water. It was endeavoured, whenever possible, to use the inner burette of the volume gauge and thus avoid errors due to the creeping of the outer perspex cylinder.

---

*A Boulton and Paul type C61 transducer meter.

For the purpose of the constant head permeability test (i.e. C.H.T.) the back pressure was applied via 1/8 in. outer diameter, flexible saran tubing to the base of the sample. Since C.H.T. were carried out under a constant pressure difference of 1.0 p.s.i. (i.e. 27.69 in. hydraulic head of water), the amount of water entering into the sample could not be accurately measured with the parafin volume gauge. Instead, an air-bubble was introduced into the saran tubing which was clipped alongside a measuring scale to work as a rather more precise volume gauge (21.7 inches movement of an air-bubble is equivalent to 1.0 cc.).

(c) Drainage Connections

Before setting up a sample, all the connections were thoroughly checked for any possible leakage. The drainage connection to the top of the sample was made by sealing saran tubing to the perspex loading cap by means of a gland screw and loctite. This lead, passing through a gland in the base of the cell, was connected to the parafin volume gauge via the valve system for reversing flow.

(d) Rubber Membrane

The cylindrical triaxial samples were confined in a latex rubber membrane.before applying cell pressure. Since the samples were prepared from very soft material it was fairly difficult to hold them upright in a 0.008 in. thick rubber membrane. In order to avoid this practical difficulty, slightly thicker rubber membranes which could hold the samples in a vertical position had to be used. Besides that, the thin membranes were likely to get punctured by the sharp edges of sand grains in the sand-clay mixture samples. Due to this leakage was experienced a number of times during the consolidation process, particularly at high effective stresses. This resulted in discarding a great many tests. However, it was found that 0.026 in. (average) thick

rubber membranes were sufficiently stiff to hold these soft samples in the upright position satisfactorily for all practical purposes, and were also strong enough to resist piercing by the sharp corners of sand particles.

(e) Perspex Stand

As mentioned above, the samples were very soft and therefore could not stand on the pedestal of the triaxial base independently. Thus a perspex stand was devised to give additional support to the specimen and prevent it from collapsing down, especially after placing the top cap over it. It simply consisted of a 6 in. high, $\frac{1}{2}$ in. wide and 1/8 in. thick rectangular perspex bar to which 1 in. inside diameter, 1 in. wide and 1/8 in. thick split rings were fixed at both the ends. After the sample had been installed and the membrane sealed to the top cap, the perspex stand was very gently slipped over the top and lowered down in such a way that one end sat on the base of the triaxial cell, while the other end lightly supported the top cap. Plate 3.1 shows a cylindrical specimen supported by a perspex stand. Since the stand was never in contact with the sample directly, it is unlikely that the consolidation process could have been affected due to this.

3.3. Arrangement of the apparatus

Figure 3.1 shows the layout of the apparatus used for consolidation and constant head permeability tests. For measuring pore water pressure a Bell and Howell type 4-366 pressure transducer is connected through a perspex mounting to a klinger valve I at the base of the triaxial cell. For applying constant cell and back pressure, the self-compensating mercury controls are connected to the other two klinger valves. The mercury control systems 1, 2 and 3 are initially connected to the valve assembly at points G, E and A respectively. From here the mercury control No. 3. is directly connected to the klinger valve C situated in the triaxial base to apply a constant all-

round pressure to the sample. The mercury control No. 2. on the other hand, is connected via 5.0 cc parafin volume gauge to the top cap for a constant back pressure against which the consolidation has to take place. Similarly for C.H.T. the desired constant back pressure can be applied at the bottom of the sample through mercury control system No. 1, which is connected via flexible saran tubing clipped around the scale to the klinger valve H.

3.4 Procedure for setting up the sample

First of all, it was ensured that all the connections were properly made to avoid any leakage during the tests. The entire system was also thoroughly de-aired. The drainage lead connecting the top cap was flushed with air-free water using by-pass valve system for reversing flow. The parafin level in the volume gauge was adjusted to the desired position using screw control. The previously de-aired pressure transducer was checked on the readout meter C61.

The cylindrical samples were moulded from the previously prepared material (sections 2.2 and 2.7). Although the material was very soft (liquidity index between 1.5 to 2.5), it was manageable enough to prepare bit by bit a 1.5 in. dia. by 3 in. high (approx.) sample in a 1.5 in. I.D. and 6 in. high brass mould. An already saturated porous stone was placed and covered with a saturated Whatman's No. 54 filter paper. The rubber membrane was stretched in the usual manner and retained under suction. The brass mould containing the sample was then slowly pushed into the stretched membrane. As quickly as possible the brass mould was next hoisted on to the pedestal. A 1.5 in. dia. by 6 in. high wooden dummy was placed on the top of the sample and retained in that position while the brass mould was swiftly pulled out of the stretched membrane. In this way the sample was brought into the grip of the rubber membrane and confined in it. The lower end of the membrane was now clamped to the pedestal with two or three O-rings. Before installing the top cap another soaked

filter paper disc and a saturated porous stone were placed on top of the sample. During setting up every possible care was taken to avoid air being trapped between the sample and membrane. Finally, the membrane was gently stroked upwards; and then the top cap was installed and sealed with O-rings. Next the perspex stand was carefully slipped over the sample as described earlier. After measuring the dimensions of the sample, the triaxial cell was assembled and filled with de-aired water.

3.5 Procedure of consolidation test

In order to verify full saturation of the sample, cell pressure was increased step by step to a required pressure and B value at each step was determined. For applying precise stress increments, the dead weight gauge tester was connected to the triaxial cell through klinger valve M, shown in Figure 3.1. Stress increments were applied by opening valves M, B and C. At each step immediate pore pressure build-up of the sample was recorded. Before applying the next stress increment, the pore pressure was allowed to come to equilibrium. From this, B values of almost 1.0 were usually measured, which indicated that the samples were fully saturated. This is well-demonstrated e.g. in Figures 3.2 and 3.3 showing the build-up of pore pressure against increasing cell pressure for 70% and 30% clay samples. After the desired value of cell pressure had been reached i.e. 95 p.s.i. and 80 p.s.i. for groups A and B respectively, the triaxial cell was disconnected from the dead weight gauge tester by closing valves M and B, and then reconnected through valve A to the previously set self-compensating mercury control No. 3. The sample was then left overnight under its respective cell pressure to allow any trapped air bubbles to dissolve in water. Next morning the tests were started with the first stage of consolidation as planned.

First the self-compensating mercury control No. 2. was set to the required back pressure. Initial readings of the volume gauge and readout meter C61 were taken. The strip recorder was switched on to fast speed and its pen set in position* depending upon the stress increment and working sensitivity of the C61 meter, as described in section 2.4 (iv). The consolidation process was then commenced by opening klinger valve E. As the test continued, volume gauge readings were taken at appropriate time intervals, while the dissipation of pore pressure was being recorded automatically on the chart recorder. During the test, cross-checks of the back pressure values were made by connecting the pressure transducer through klinger valve K to mercury control No. 2. Before doing so the sample was first isolated from the pressure transducer by closing valve I. In this way the pore pressure still to be dissipated was accurately measured, i.e. errors due to the slight change in the strain gauge readings caused by temperature variations were eliminated. The pressure transducer was reconnected by opening valve I after closing K. The consolidation process was allowed to run until the pore pressure had almost been dissipated. And then, before closing the drainage valves C.H.T. for that stage was carried out. For the next stage of consolidation, back pressure was lowered accordingly (Table 3.1) while the cell pressure remained constant. After the completion of the last stage of consolidation, two swelling stages were carried out to bring the sample back to the low effective stress. Finally, the cell pressure was slowly reduced to zero, the triaxial apparatus was dismantled and the sample was unloaded in the usual manner. The final weight, dimensions and moisture content were then obtained.

---

*In the case of the triaxial tests, the chart recorder pen was always set on the left hand side. The pen moved towards the right hand side as the pore pressure dissipated with time.

3.6 Procedure of permeability test (C.H.T.)

Constant head permeability tests were performed after the third, fourth and fifth stages of consolidation and the two swelling stages. First of all the self-compensating mercury control No. 1. was adjusted to the desired pressure, such that the differential pressure between this and the mercury control No. 2 was equivalent to 1.0 p.s.i. An air-bubble was introduced into the saran tubing and its position in relation to the measuring scale was recorded. After the excess pore pressure had been dissipated during consolidation, the constant back pressure was applied at the bottom of the sample for C.H.T. by opening klinger valves G and H (Figure 3.1). The air bubble in the saran tubing immediately began to travel towards the sample. At this instant a certain volume of water was entering into the sample under a constant excess hydrostatic pressure of 1.0 p.s.i. The movement of the air-bubble was recorded at suitable intervals. Readings of the volume gauge connected to the top of the sample were also taken side by side. The permeability test was allowed to run until steady state flow of water had been reached. After the constant head permeability test, valves G and H were closed and the pore pressure was allowed to come to equilibrium before starting the next stage of consolidation. The duration of achieving steady state depended upon the constituents of a sand-clay mixture sample. Sand-clay mixtures containing a high percentage of clay usually took a longer time than those containing less. All the C.H.T. results reported here are based on the amount of water flowing into the sample.

3.7 Results and Discussion

(i) Volume change characteristics

The graphs of volume change with log of time for all the consolidation stages of 100% clay, and sand-clay mixtures are shown in Figures 3.6 (a) to 3.65 (a). Each stage of consolidation was terminated when the pore water pressure had almost dissipated, i.e. secondary consolidation was not studied in detail. Since drainage was permitted only from the top of the sample, the time taken to reach 100% primary consolidation was generally long, particularly with those of high clay content.

Terzaghi's theoretical curve has been fitted at t_{50} to the experimental curves of 70% and 30% clay samples. It will be seen from Figures 3.26 (a) to 3.35 (a) and 3.46 (a) to 3.55 (a) that there is quite good correspondence between the predicted and the observed rates of consolidation up to U = 70%, although at the beginning slight disagreement is evident. In some cases the observed volume change at the early stages is slightly faster, and in others somewhat slower than anticipated by theory. Towards the end of consolidation, i.e. after U = 70% or so, the experimental curve begins to deviate because of secondary and creep effects. A similar influence was observed in the oedometer tests. It is interesting to see that the theoretical curve fits well to the volume change curve of the fifth stage Group B tests, where $\frac{P}{Po'} = 0.5$. In the previous observations of the oedometer tests some disagreement between the two curves was noticed for this stress increment ratio. The consolidation tests in the oedometer by Leonards and Girault (1961), Wahls (1962) and Tan (1968) have shown that if $\frac{\Delta P}{Po'}$ is less than 1 the experimental curves will tend to deviate from the theoretical one. This happens in the triaxial consolidation tests too, provided the stress increment ratio is further decreased, as demonstrated

in the next chapter. In other words, if $\frac{\Delta P}{P_{o'}}$ is less than 0.5 and is further decreased in the subsequent stages of consolidation, then the large amount of secondary compression accompanies the primary consolidation. Consequently it becomes difficult to estimate the primary consolidation and compare it with Terzaghi's theory. As expected, the consolidation of 80% and 90% sand samples is very rapid in comparison to the sand-clay mixtures containing 70% and less sand. This is of course due to the low compressibility of the material containing more sand.

It may be worth mentioning that during the consolidation process, sharp edges of quartz sometimes punctured the rubber membrane causing a rise in the pore water pressure, and therefore a decrease in the effective stress. Due to this practical difficulty only about 50% of the tests were successful and the rest were discarded as soon as the leakage was detected. Keeping in view the large volume changes of the samples and relatively short durations of the tests, the leakage through the rubber membrane due to the hydraulic pressure gradient and osmotic pressure difference (Poulos, 1964) is considered to be negligible. Since the triaxial consolidation test results are free from all those errors involved in the conventional oedometer tests, these are more reliable. However, the overall settlement characteristics of the soil under consideration are similar for both the isotropic and anisotropic consolidation tests, for instance, up to about 70% average degree of consolidation in both cases agree with Terzaghi's theory.

(ii) Dissipation of pore water pressure

The curves of excess pore water pressure dissipation against log of time are shown in Figures 3.6 (b) to 3.42 (b). Terzaghi's theoretical curve has been fitted to each of them at 50% dissipation.

Unlike the volume change curves, the correspondence between the theoretical and observed excess pore pressure seems to differ for each stage. To examine this behaviour closely, attention is focussed e.g. on the dissipation curves of 70% clay (Figure 3.26 (b) to 3.35 (b) and 30% clay (Figures 3.46 (b) to 3.55 (b)) sand-clay mixture samples. In the case of the first stage of consolidation, the two curves seem to agree with each other quite well in both the Groups A and B tests. The difference between the theoretical and experimental curves widens in the subsequent stages of consolidation. In general the excess pore water dissipates rapidly at the beginning, but later on tends to slow down. The partial or full agreement between the observed and theoretical curves largely depends upon the magnitude of the pressure increment ratio, $\frac{\Delta P}{Po'}$. The effects of stress increment ratio on the pore pressure behaviour can be seen from the Group A and B tests. For $\frac{\Delta P}{Po'} = 2$ (Group A), although initially excess pore pressure dissipates rapidly, it begins to correspond with the theoretical curve afterwards. Similarly the two curves seem to agree with each other in the second and third stages of consolidation, Group B, where $\frac{\Delta P}{Po'}$ is increased successively. But when $\frac{\Delta P}{Po'}$ is reduced from its previous value, as in the fourth and fifth stages (Group B), a very poor fit between the experimental curves and theory is obtained. This phenomenon is significant particularly in the fifth stage, where $\frac{\Delta P}{Po'} = 0.5$. The effects of even smaller stress increment ratios on the pore pressure characteristics can be seen in Chapter 4. The other interesting point to note is the influence of decreasing stress increment ratio on the shape of the excess pore water pressure curves. Looking at the dissipation curves of Group B, it will be seen that the shapes of the first three stages resemble typical curves produced by Terzaghi's theory. But in the last two stages there is slight arrest or intermittance of pore pressure dissipation during the initial part of the consolidation process. Due to this,

a somewhat flat curve of P.W.P. is obtained in the beginning, which makes it different from the theoretical. However, the two curves start to resemble each other afterwards as the pore pressure dissipates smoothly without any further arrest. Similar effects of decreasing stress increment ratio on the excess pore water pressure dissipation curves was observed by Skinner* (1970). It will be seen from his dissipation curves (Figure 3.4) that those of the first and second stages agree well with theory. But when $\frac{\Delta P}{Po'}$ is reduced from 10 to 0.90 and then 0.47 in the third and fourth stages respectively, both the resemblance and correspondence between the experimental and theoretical curves (fitted at 50% dissipation) completely disappear, as shown in Figures 3.5 (a) and (b). Oedometer consolidation tests by e.g. Leonards and Girault (1961), Northey and Thomas (1965) and Christie (1965) have also revealed the influence of stress increment ratio on the dissipation of pore pressures. Davis and Raymond (1965) found that the rate of pore pressure dissipation is a function of stress increment ratio, while the average rate of volume change remains unaffected. Consequently Terzaghi's theory predicts satisfactorily the latter but not the former. This is true at least for the soil under consideration, as shown in the volume change and pore pressure plots given in Figures 3.26 to 3.35 and 3.46 to 3.55 (a) and (b).

In one respect the isotropic consolidation tests reported here are similar to the oedometer tests, i.e. the flow of pore water is substantially in an axial direction. But in the strictest sense the stress-strain conditions in both isotropic and anisotropic consolidation tests are not the same. This is because lateral strains are developed

---

* Unpublished data of isotropic consolidation tests on sandy clay soil (70% sand) from a test pit near Stocks Reservoir. He carried out a triaxial consolidation test under constant back pressure while increasing the cell pressure. (See Table in Figure 3.4).

during consolidation at different rates and at different elevations. Thus each element of the sample is subjected not only to a change in all-round pressure, but also shear stresses which develop during the consolidation process. To take into account factors like these, a number of three-dimensional theories have been formulated. The general theory of 3-D consolidation was proposed by Biot (1941). Since then many research workers (e.g. Biot, 1956; Mandel, 1957; Tan, 1953, 1957; and Gibson and McNamee, 1957, 1963) have brought about various refinements in the three-dimensional theories. However, the main difficulty with these theories is that all of them are mathematically too complex, and involve parameters such as Young's modulus and Poisson's ratio which are sometimes difficult to determine experimentally. This is why these are not very commonly used in engineering practise.

It is shown in the previous chapter, that the build-up of pore pressure largely depends upon the structural viscosity and the magnitude of the pressure increment. Although primary and secondary consolidation start side by side, it is after some time that the effects of the latter are dominant, i.e. after the pore pressure has almost dissipated. From here onwards the structural viscosity plays an important role. Berry and Wilkinson (1969) have shown that the pore pressure build-up under undrained conditions is the function of both the structural viscosity and the magnitude of $\frac{\Delta P}{Po'}$. It appears that structural bonds form at the end of a consolidation stage which are reflected in stiffer behaviour with respect to small stress increments. However, the bonds break readily at larger increments, resulting in higher pore pressure build-up. In order to avoid difficulties associated with this effect, the tests reported here were carried out by lowering the back pressure while maintaining constant cell pressure.

General discussion on the flexibility of the pore pressure measuring device is given in section 2.10 (b). The effects of saturation will now be considered as follows:

B value

B Values are normally measured to find out whether a sample is fully saturated. Skempton (1954) showed that for an element of clay subjected to axi-symmetric loading without allowing drainage, the increase in pore pressure due to increase in total stresses can be expressed as:

$$\Delta u = B \left[\Delta \sigma_3 + A \ (\Delta \sigma_1 - \Delta \sigma_3) \right] \quad \ldots\ldots (3.1)$$

where A and B are pore pressure parameters and $\Delta \sigma_1$ and $\Delta \sigma_3$ are increases in the major and minor principal stresses. When a sample of clay is subjected to all-round pressure $\Delta \sigma_1 = \Delta \sigma_3$, hence equation (3.1) becomes:

$$\Delta u = B \cdot \Delta \sigma_3 \quad \ldots\ldots (3.2)$$

or

$$\frac{\Delta u}{\Delta \sigma_3} = B \quad \ldots\ldots (3.3)$$

It is readily seen from equation (3.3) that the peak pore pressure build-up depends on the value of B. Since B can also be expressed in the form (Bishop and Henkel, 1962),

$$B = \frac{1}{1 + \frac{nC_w}{C_c}} \quad \ldots\ldots (3.4)$$

where n is the initial porosity,

C_w is the compressibility of water,

C_c is the compressibility of soil skeleton,

and for a saturated clay C_w is much smaller as compared to C_c, therefore the value of B is almost equal to 1.0. But in the case of partly saturated soil, the compressibility of air and water together, say C, becomes comparable to C_c, resulting in lower values of B (less than 1.0).

In most of the tests reported here a B value of 1 was normally obtained. For example, the relationship of pore pressure with total stress of 70% and 30% clay samples is plotted in Figures 3.2 and 3.3. It will be seen that the increase in pore pressure Δu equals the increase in applied stress $\Delta\sigma_3$. This shows that the samples were fully saturated and that the results discussed here are free from this effect.

Finally, it is concluded that the dissipation of excess pore water pressure is a function of stress increment ratio. This is evident from both the oedometer and triaxial consolidation tests, i.e. when $\frac{\Delta P}{Po'}$ is increased successively as in the second and third stages of the Group B tests, the excess pore water pressure dissipation is slower in comparison to the subsequent stages of consolidation where $\frac{\Delta P}{Po'}$ is reduced. The oedometer tests have shown that the small stress increments are resisted by the strong bonds, which results in the small pore pressure build-up. Conversely, large stress increment ratios can overcome the resistance offered by the structural bonds, causing full development of pore pressures to the applied stress increments. The same must be true in the case of triaxial tests too.

(iii) Void ratio vs logarithm pressure

The relationship of void ratio, e, with effective stress P' for pure clay and sand-clay mixtures is shown in Figures 3.66 to 3.70. On each graph, curves of e-log P' obtained from groups A and B are shown. As expected, the relationship between the void ratio and

logarithm of effective pressure is linear in all cases. The overall picture is similar to that observed from the oedometer tests, as discussed in section 2.10 (c). There is good agreement between the e-log P' relationships obtained from the Group A and B tests, whereas in the oedometer some scattering of void ratio points and comparatively less correspondence of the relationships from the two groups was largely contributed by the practical difficulties such as side friction, bedding, deformation of the apparatus and most of all the extrusion of the material (Matlock and Dawson, 1951).

Although the duration of each consolidation stage was longer (5 to 6 days) in the triaxial tests, the void ratio seems not have been affected at all. This in line with the studies by Lewis (1950), Northey (1956) and Leonards and Ramiah (1959). The final void ratios calculated from the volume changes in the triaxial tests showed comparatively better agreement with those found from the final water content. The slopes of e-log P' curves of 30% and more clay samples are steeper than those containing less clay. This is of course due to the more compressible nature of the former in relation to the latter.

(iv) Coefficient of compressibility

The volume change due to increases in three principal effective stresses, i.e. $\Delta\sigma_1' = \Delta\sigma_2' = \Delta\sigma_3'$ (axi-symmetric pressure) is

$$\frac{\Delta V}{V} = - C_c \cdot \frac{\Delta\sigma_1' + \Delta\sigma_2' + \Delta\sigma_3'}{3} \qquad \ldots\ldots (3.5)$$

or $$\frac{\Delta V}{V} = - C_c \cdot \Delta\sigma_3' \qquad \ldots\ldots (3.6)$$

where C_c is the average compressibility over the range of volume change under consideration. C_c has been plotted against the average effective stress, as shown in Figures 3.71 to 3.76. In general, the compressibility

decreases in the subsequent stages of consolidation in much the same way as m_v in the oedometer tests. Initially higher C_c values are obtained which decrease sharply in the later stages as the effective stress increases. Also the lower compressibilities of 10% and 20% clay samples are associated with the large sand content. It is obvious that the compressibility values obtained from the triaxial tests are free from those errors involved in the conventional oedometers, particularly side friction and the extrusion of material. This in fact is well-demonstrated by the correspondence between C_c-log P' curves of Group A and B tests.

Comparing the two compressibilities m_v and C_c of the respective materials (see Tables 2.3 and 3.2 respectively), it will be seen that the former are much lower than the latter. The lower values of m_v are partly due to the practical difficulties mentioned above and mainly due to the different stress-strain conditions involved in the isotropic and anisotropic consolidation tests. Skempton and Bishop (1954) showed that for normally consolidated clays the compressibility m_v, as measured in the oedometer, is closely equal to the true compressibility C_c. In more silty or sandy clays, however, m_v may be appreciably less than C_c. This difference is due to the following reasons.

In the particular case of consolidation under a vertical pressure with zero lateral strain, as in the oedometer and in natural beds of sedimentary deposits,

$$\Delta\sigma_2' = \Delta\sigma_3' = K_0 \cdot \Delta\sigma_3' \qquad \ldots\ldots (3.7)$$

where K_0 is defined as the coefficient of earth pressure at rest, and the volume change may be written in the form

$$\frac{\Delta V}{V} = - C_c \cdot \Delta\sigma_1' \cdot S_d \left[1 + K_0 \left(\frac{1}{S_d} - 1\right)\right] \ldots\ldots (3.8)$$

where S_d is the structural parameter which is a function of the dilatancy* of the soil (Skempton and Bishop, 1954). As an example, in fairly loose sands at small strains $S_d \simeq 0.33$ and $K_0 = 0.40$, by substituting these values in equation (3.8), it therefore follows that:

$$\frac{\Delta V}{V} = - C_c \cdot 0.6 \cdot \Delta\sigma_1'$$

and hence $m_v = 0.6\ C_c$.

For normally consolidated clays of moderate or high plasticity, $K_0 = (1 - \sin\phi')$. For example, say $\phi = 26^\circ$, in which case $K_0 \simeq 0.6$, and therefore S_d may approach 1.0, it follows that:

$$\frac{\Delta V}{V} = - C_c \cdot \Delta\sigma_1'$$

and hence $m_v = C_c$.

The m_v values less than C_c in the present series of tests suggests that the sand-clay mixture of this type, if existing in nature would have a lower value of the parameters K_0 and S_d. It may therefore be concluded that the difference between m_v and C_c is due to the different stress-strain conditions in the oedometer and triaxial tests.

---

* Volume change consequent upon the application of a shear stress. In ideal linear isotropic elastic or perfectly plastic materials the dilatancy is zero, but may have quite large positive or negative values in soils.

(v) Coefficient of Permeability

Constant head permeability tests were carried out at the end of primary consolidation and the swelling stages. The coefficient of permeability k was calculated from the relationship $k = \frac{Q}{i \times A}$, where i denotes hydraulic gradient, A the cross-sectional area of the sample and Q the rate of flow of water. To determine the rate of flow at steady state Q was plotted against the average time

$$\sqrt{\frac{2}{t_1 + t_2}} = \sqrt{2}t^{-\frac{1}{2}} \quad *$$

similar to e.g. Figure 2.92. Coefficients of permeability k_s and k_p were indirectly calculated from the relationships $k_s = c_{vs} \cdot C_c \cdot \gamma_w$ and $k_p = c_{vp} \cdot C_c \cdot \gamma_w$, respectively. In these equations c_{vs} and c_{vp} are the coefficients of consolidation calculated from settlement and P.W.P. dissipation curves, C_c is the coefficient of compressibility and γ_w is the unit weight of water. Variations of coefficient of permeability with effective stress of pure clay and the mixtures are shown in Figures 3.77 to 3.83. k_s and k_p have been plotted against average effective stress. The results have also been summarised in Table. 3.2.

It will be seen from the k-log P' relationship that k, k_s and k_p are decreasing with the effective stress. Some scatter of the points, particularly that of k_s and k_p, can be observed at the earlier stages. Later on these points converge into a narrow band and begin to correspond with each other reasonably well. Except in the initial portion of the curve where there is a sudden drop, the coefficient of permeability is decreasing steadily with the effective stress. Slightly increased values of k_p are obtained from the fifth stage Group B tests, which are mainly due to

---

* where $t_1 + t_2 = t$

the higher values of c_{vp} at those stages. As shown earlier, the dissipation of excess P.W.P. is greatly affected by the small stress increment ratio, for which the fit of Terzaghi's theory is not good, consequently the c_{vp} values are very high at these stages. However, Terzaghi's theory can still anticipate well the volume change which has resulted in appropriate c_{vs} values such that the computed k_s agrees with the measured k.

Before proceeding further, it is emphasised that the direct constant head permeability tests (C.H.T.) are thought to be free from errors due to plugging of porous stone (Bishop and Gibson 1963), temperature variation etc. Also the flow of water during C.H.T. was one-dimensional. Comparing the actually measured permeabilities from the oedometer tests with these it will be seen that the latter are lower than the former. It is not surprising because in the oedometer the diameter of the porous stone was a bit smaller than that of the sample due to which the the flow of water was not one-dimensional. Using relaxation method for axi-symmetrical flow (Appendix A) it was found that the coefficients of permeability should be 12.5% more than those calculated from the one-dimensional formula $Q = K \cdot i \cdot A$. On the other hand, values of computed permeabilities k_s of the triaxial tests are higher than those of the oedometer tests; which is of course due to the lower values of the coefficient of compressibility in the latter case (see Tables 2.3 and 3.2).

The permeability tests reported here are based on the assumption that Darcy's law is applicable. There are various arguments about the validity of Darcy's law and under what conditions it is true, (e.g. Hansbo 1960; Olsen 1965; Mitchell and Younger 1966; Matyas, 1966). However, it is agreed by all of them that Darcy's law holds good provided the samples are fully saturated and tested under a sufficiently high hydraulic gradient. Both of these conditions were satisfied while carrying out constant head permeability tests.

(vi) Coefficient of Consolidation

Using Terzaghi's expression $c_v = \frac{TH^2}{t}$ where T is the theoretical time factor, H the drainage path and t the actual time, both coefficients of consolidation c_{vs} and c_{vp} have been calculated from the volume change and P.W.P. dissipation curves respectively. Casagrande's curve fitting method has been used to determine t_{50} from the settlement curves. In the case of pore water pressure curves, time at 50% dissipation has been used to calculate c_{vp}. For each stage of consolidation the height of the sample was corrected depending upon the subsequent volume changes. The coefficient of consolidation c_{v*} has also been calculated indirectly using the expression $c_{v*} = \frac{k}{C_c \cdot \gamma_w}$, where k and C_c are coefficients of permeability and compressibility respectively at average effective stress.

The values of c_{vs}, c_{vp} and c_{v*} of 100% clay and sand-clay mixture from Group A and B tests are summarised in Table 3.2. Also c_{vs} and c_{vp} are plotted against average effective stress, as shown in Figures 3.84 to 3.90. On the whole, the coefficient of consolidation increases with the effective stress. The trend of increasing c_{vs}, c_{vp} and c_{v*} is associated with constant $\frac{\Delta P}{Po'}$ (Group A) and increasing $\frac{\Delta P}{Po'}$ (Group B). But when $\frac{\Delta P}{Po'}$ is reduced, as in the fourth and fifth stages of Group B tests, c_{vs} and c_{v*} are also slightly decreased. It is interesting to note the c_{vs} and c_{v*} of the successive consolidation stages of various samples seem to agree reasonably well with each other. In contrast, c_{vp} values are severely affected particularly when $\frac{\Delta P}{Po'}$ is reduced. This is expected because of rapid dissipation of excess P.W.P. when small $\frac{\Delta P}{Po'}$ is used, resulting in higher values of c_{vp}. As a matter of fact the disagreements between c_{vs} and c_{vp} are in line with the investigations by e.g. Leonards and Girault (1961), Davis and Raymond (1965) and Skinner (1970) who have shown that Terzaghi's theory cannot predict the

dissipation of excess P.W.P. when small stress increment ratios are applied.

From Table 3.2 it can be seen that ratio c_{vs}/c_{vp} is the function of stress increment ratio $\frac{\Delta P}{Po'}$. The ratio of c_{vs}/c_{vp} decreases with the decrease in $\frac{\Delta P}{Po'}$. The effects of stress increment ratio have also been observed by Leonards and Girault (1961), Tan (1968) Skinner (1970) and Garga (1970). Leonards and Girault (1961) investigated the effects of $\frac{\Delta P}{Po'}$ as well as the nature of the pore fluid and also the influence of side friction on undisturbed sensitive Mexico clay in a specially designed oedometer with the facility of measuring dissipation of excess P.W.P. Skinner (1970) carried out isotropic consolidation tests on the remoulded sandy clay near Stocks Reservoir site, as mentioned earlier. These results are tabulated in Table 3.3, which clearly indicates that when $\frac{\Delta P}{Po'}$ decreases the ratio c_{vs}/c_{vp} also decreases and vice versa. A similar picture emerges from the tests carried out on 100% clay and the sand-clay mixtures, as shown in Table. 3.2 In Group B tests when $\frac{\Delta P}{Po'}$ is reduced (fourth and fifth stages) the value of c_{vs}/c_{vp} decreases, which is due to the large increase in c_{vp} and to some extent the decrease in c_{vs}. However, when $\frac{\Delta P}{Po'} = 2$ is kept constant in the successive stages of consolidation the variations in c_{vs} and c_{vp} are very small, thus c_{vs}/c_{vp} obtained from Group A test is almost constant for all the consolidation stages. These results further demonstrate the fact that the dissipation of P.W.P is a function of $\frac{\Delta P}{Po'}$ and that the coefficient of consolidation calculated from it using Terzaghi's theory may be an over-estimate. Since in the field $\frac{\Delta P}{Po'}$ is normally less than 1 and decreases with depth, the implications of the results can obviously be appreciated from the above discussions.

As described in Chapter 1, Terzaghi's theory is based on the assumptions that the coefficient of consolidation, compressibility and permeability are constant and the e-log P' relationship is independent of time. But this is not true in many soils, including London clay, as shown by Garga (1970); and at least, in the case of material considered here. During the decade or so attempts have been made by many research workers to present non-linear theories by considering variations in some of the consolidation parameters. For instance Schiffman (1958) considered variations in the coefficient of permeability, but assumed the coefficient of compressibility to remain constant. McNabb (1960) and Mikasa (1965) have formulated theories which take into account variation of compressibility and permeability but in such a way that the coefficient of consolidation remains constant. On similar assumptions one dimensional non-linear theory for small strains has been presented by Davis and Raymond (1965), and for large strain by Gibson, England and Hussey (1967)*. Barden and Berry (1965) have considered the variation of permeability and the effects of structural viscosity (creep). This is a small strain theory and is not applicable to highly compressible soils or to large pressure increments. A non-linear theory of consolidation presented by Poskitt (1969) incorporates the results of Barden and Berry (1965), Davis and Raymond (1965) and Gibson et al (1967). Garga (1970) made an attempt to analyse the consolidation results of London clay using both the Davis and Raymond, and Poskitt theories, and found that the behaviour of the clay was so non-linear that these theories did not actually apply. The results of sand-clay mixture and pure kaolin presented here clearly indicate variation in coefficients of consolidation, compressibility and permeability. The assumptions by different research

---

* Coefficient of consolidation C_F introduced by Gibson et al (1967) is different from c_v of Terzaghi's theory and can be assumed to remain constant during consolidation under a specific pressure increment. (See Chapter 1).

workers that the compressibility and permeability vary in such a way that the coefficient of consolidation remains constant, are not valid for the tests reported here. Non-linear theories are no doubt more refined than Terzaghi's theory, however they still have some limitations.

TEST GROUP A

Stage No	Cell Pressure p.s.i	Back Pressure p.s.i.	Stress increment ΔP p.s.i.	Effective Stress increment ratio $\Delta P/Po'$
1	95	94	1	-
2	"	92	2	2
3	"	86	6	2
4	"	68	18	2
5	"	14	54	2
6	"	68	-54	-
7	"	94	-26	-

TEST GROUP B

1	80	79	1	-
2	"	77	2	2
3	"	68	9	3
4	"	56	12	1
5	"	44	12	0.5
6	"	56	-12	-
7	"	79	-23	-

TABLE 3.1

Consolidation Programme of Triaxial Tests

100% CLAY (Test Group A)

Stage No.	Po' psi	$\frac{\Delta P}{Po'}$	e	C_c sq. cm/gms x 10^{-4}	c_{vs} sq. cm/sec x 10^{-4}	c_{vp} sq. cm/sec x 10^{-4}	c_{v*} sq. cm/sec x 10^{-4}	c_{vs}/c_{vp}	k cm/sec x 10^{-8}	k_s cm/sec x 10^{-8}	k_p cm/sec x 10^{-8}
1	-	-	1.87	7.08	3.78	2.36	2.62	1.60	-	26.75	16.71
2	1	2	1.74	2.84	4.8	3.27	3.94	1.46	-	13.62	8.81
3	3	2	1.62	1.57	5.94	4.73	5.66	1.25	8.19	9.33	7.42
4	9	2	1.45	0.63	9.15	8.68	1.05	5.26	5.26	5.78	5.5
5	27	2	1.26	0.22	17.27	13.15	13.18	1.31	1.87	3.83	2.92
100% CLAY (Test Group B)											
1	-	-	1.88	7.63	3.15	1.82	2.43	1.92	-	24.0	13.91
2	1	2	1.76	3.37	8.08	2.78	3.32	2.90	-	27.0	9.37
3	3	3	1.61	1.24	7.15	6.23	6.29	1.15	6.70	8.68	6.51
4	12	1	1.37	0.55	8.36	11.66	9.80	0.71	3.62	4.59	6.40
5	24	0.5	1.26	0.49	6.27	25.0	8.57	3.64	3.64	3.07	12.25
80% CLAY-20% SAND Mixture (Test Group A)											
1	-	-	1.60	8.08	2.32	2.62	2.10	.89	-	18.78	21.17
2	1	2	1.45	1.32	3.25	2.82	8.63	1.15	-	10.61	9.19
3	3	2	1.32	1.55	6.02	5.03	5.35	1.20	7.67	9.36	7.77
4	9	2	1.17	0.87	2.02	2.88	5.36	.71	1.93	1.50	2.15
5	17	2	0.97	0.36	15.7	12.1	5.55	1.29	0.98	5.64	4.69
80 CLAY-20% SAND Mixture (Test Group B)											
1	-	-	1.60	7.89	2.3	1.9	2.15	1.20	-	18.01	14.91
2	1	2	1.41	2.86	5.2	3.5	3.98	1.47	-	15.02	10.20
3	3	3	1.32	1.31	8.1	4.9	5.87	1.63	7.34	10.54	6.46
4	12	1	1.13	0.58	8.6	11.7	8.44	.73	4.44	5.0	6.76
5	24	0.5	1.03	0.51	9.0	28.2	7.45	.32	4.47	4.57	14.34

TABLE 3.2

Results of Triaxial (isotropic) Consolidation Test (continued)

70% CLAY-30% SAND Mixture (Test Group A)

Stage No	Po' psi	$\frac{\Delta P}{Po'}$	e	C_c sq. cm/gms x 10^{-4}	c_{vs} sq. cm/sec x 10^{-4}	c_{vp} sq. cm/sec x 10^{-4}	c_{v*} sq. cm/sec x 10^{-4}	c_{vs}/c_{vp}	k cm/sec x 10^{-8}	k_s cm/sec x 10^{-8}	k_p cm/sec x 10^{-8}
1	-	-	1.55	5.93	3.97	4.97	3.44	.80	-	23.5	29.5
2	1	2	1.45	4.72	3.71	2.76	2.62	1.34	-	17.5	12.8
3	3	2	1.30	1.60	5.00	4.00	5.75	1.25	8.9	8.01	6.43
4	9	2	1.14	0.52	9.07	9.10	11.15	1.00	4.0	4.6	4.7
5	27	2	1.01	0.22	15.38	14.19	11.81	1.08	1.4	3.4	3.2
70% CLAY-30% SAND Mixture (Test Group B)											
1	-	-	1.56	6.83	3.22	3.68	2.98	.88	-	22.0	25.1
2	1	2	1.44	2.85	5.79	2.86	4.35	2.27	-	16.5	8.1
3	3	3	1.35	1.40	6.73	4.72	6.07	1.43	7.3	9.37	6.5
4	12	1	1.14	0.57	9.47	11.12	9.82	.85	4.5	5.42	6.4
5	24	0.5	1.04	0.30	8.34	33.0	14.00	.25	3.6	2.42	9.6
50% CLAY-50% SAND Mixture (Test Group A)											
1	-	-	0.96	2.76	1.77	1.80	2.17	.97	-	4.87	5.0
2	1	2	0.92	1.38	4.01	2.80	3.62	1.43	-	5.54	3.9
3	3	2	0.88	0.91	4.85	4.34	4.61	1.12	6.92	4.40	3.9
4	9	2	0.81	0.42	9.42	8.51	8.09	1.10	5.28	4.00	3.6
5	27	2	0.72	0.16	13.14	14.50	16.87	.90	1.89	2.1	2.3
50% CLAY-50% SAND Mixture (Test Group B)											
1	-	-	0.93	2.17	1.40	1.77	2.76	.80	-	3.1	3.8
2	1	2	0.90	1.79	3.37	2.44	2.79	1.38	-	6.0	4.4
3	3	3	0.86	0.32	7.10	6.45	12.5	1.10	5.17	2.3	2.1
4	12	1	0.82	0.30	8.22	10.16	11.33	.81	4.68	2.5	3.1
5	24	0.5	0.7	0.20	7.43	29.27	15.0	.25	3.43	1.5	5.9

TABLE 3.2

(continued)

30% CLAY-70% SAND Mixture (Test Group A)

Stage No.	Po' psi	$\frac{\Delta P}{Po'}$	e	C_c sq. cm/gms x 10^{-4}	c_{vs} sq. cm/sec x 10^{-4}	c_{vp} Sq. cm/sec x 10^{-4}	c_{v*} sq. cm/sec x 10^{-4}	c_{vs}/c_{vp}	k cm/sec x 10^{-8}	k_s cm/sec x 10^{-8}	k_p cm/sec x 10^{-8}
1	-	-	0.888	10.39	3.44	2.89	2.54	1.19	-	35.7	29.95
2	1	2	0.76	4.0	7.47	4.01	3.70	1.86	-	29.6	15.91
3	3	2	0.67	1.48	11.46	7.50	5.54	1.53	8.92	17.0	11.06
4	9	2	0.56	0.43	21.24	17.32	12.09	1.22	5.06	8.55	7.43
5	27	2	0.47	0.17	36.33	35.05	20.0	1.03	3.26	6.26	6.04
30% CLAY-70% SAND Mixture (Test Group B)											
1	-	-	1.003	14.94	2.48	2.08	1.77	1.19	-	37.06	31.14
2	1	2	0.91	4.44	3.75	2.80	3.24	1.34	-	16.63	12.42
3	3	3	0.69	1.23	7.68	5.60	5.85	1.37	5.48	9.44	6.92
4	12	1	0.57	0.40	14.04	16.58	12.50	.84	4.70	5.68	6.71
5	24	0.5	0.51	0.23	11.81	91.18	18.26	0.13	4.35	2.77	21.41
20% CLAY-80% SAND Mixture (Test Group A)									x 10^{-7}	x 10^{-7}	x 10^{-7}
1	-	-	0.76	16.22	20.28	3.82	2.83	5.31	-	32.90	6.20
2	1	2	0.55	2.11	16.61	8.96	13.50	1.85	-	3.50	1.90
3	3	2	0.51	0.70	36.8	25.00	30.70	1.47	1.91	2.60	1.75
4	9	2	0.46	0.22	94.97	81.9	75.00	1.45	1.53	2.10	1.83
5	27	2	0.42	0.09	106.4	158.2	127.70	0.67	0.93	1.00	1.51
10% CLAY-90% SAND Mixture (Test Group B)				x 10^{-4}	x 10^{-2}	x 10^{-2}	x 10^{-2}		x 10^{-5}	x 10^{-5}	x 10^{-5}
1	-	-	0.78	12.94	6.21	.23	2.04	26.00	-	8.00	0.31
2	1	2	0.63	0.85	3.09	2.38	28.23	1.29	-	2.26	0.20
3	3	3	0.61	0.82	26.5	1.20	26.22	2.20	2.1	2.18	0.98
4	12	1	0.55	0.80	44.5	4.0	25.00	1.11	2.05	3.56	3.20
5	24	0.5	0.54	0.78	55.4	48.2	24.35	1.14	1.92	4.35	3.10

TABLE 3.2

Soil	Po'	$\frac{\Delta P}{Po'}$	Coefficient of Consolidation. sq. cm/ sec. c_{vs} (from Δ_v)	c_{vp} (from Δ_u)	c_{vs}/c_{vp}	Reference
Undisturbed	2.8	2.0	12.5	12.9	0.97	Leonards and
Mexico City	15.6	3.0	1.46	0.93	1.57	Girault. (1961)
Clay.	74.4	0.15	0.13	9.14	0.014	
Remoulded	-	-	5.40	6.50	0.830	Skinner (1970)
Sandy Clay	1.0	10	3.90	3.03	1.28	(unpublished)
Soil from	11.0	0.90	3.8	7.2	0.53	
stock	21.0	0.47	2.5	10.90	0.23	
reservoir test pit.						
M6	0	∞	5.6	4.30	1.31	Garga (1970)
Boulder clay	6.0	0.67	9.92	8.71	1.14	
fill remould	2.0	0.33	9.36	12.36	0.89	

TABLE 3.3

Consolidation Results Compared.

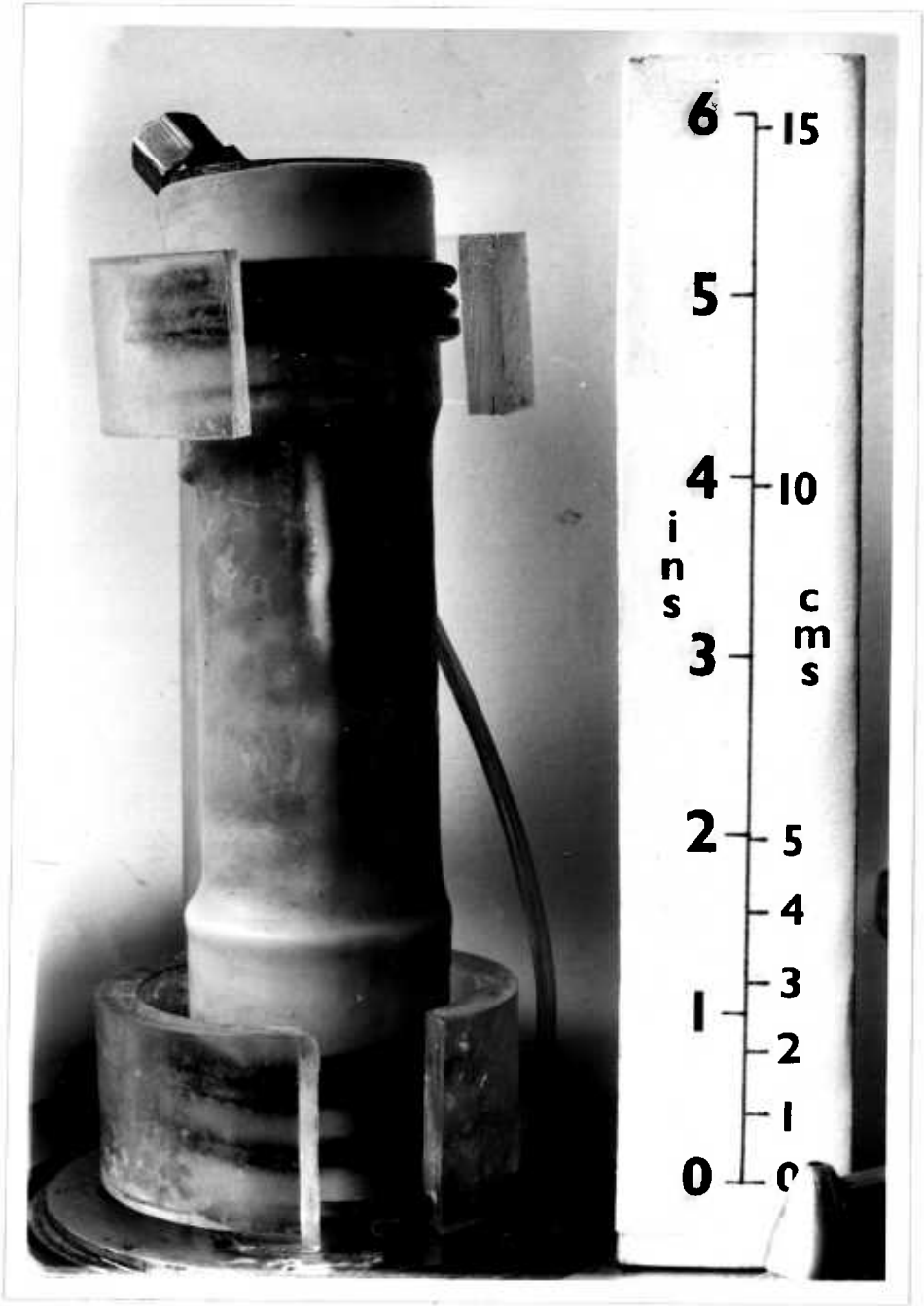

Plate 3.1 Perspex stand holding the triaxial cylindrical sample in position.

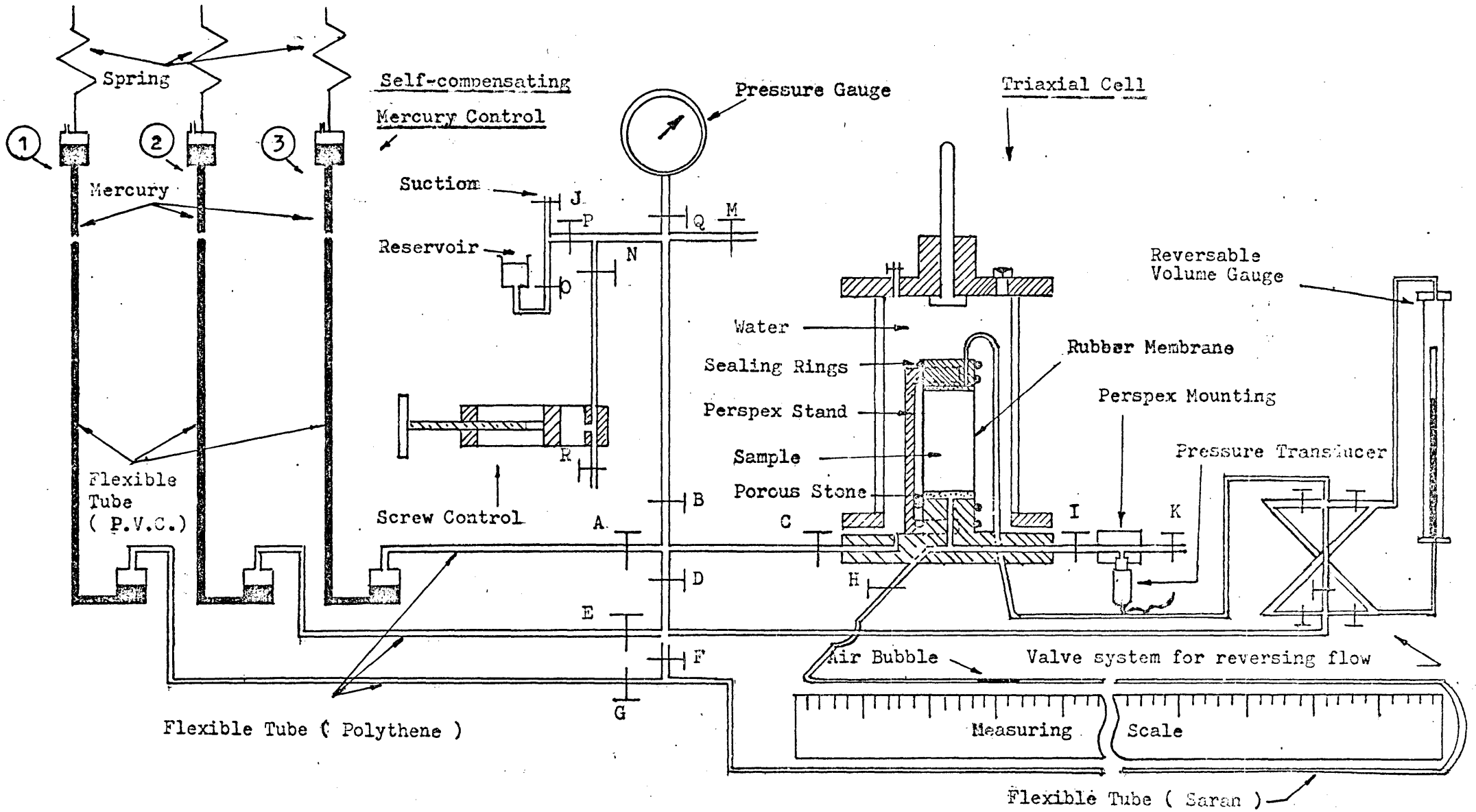

Fig. No. 3.1. The layout of self-compensating mercury control and the apparatus for triaxial consolidation tests with the pore-pressure dissipation and constant head permeability measuring system.

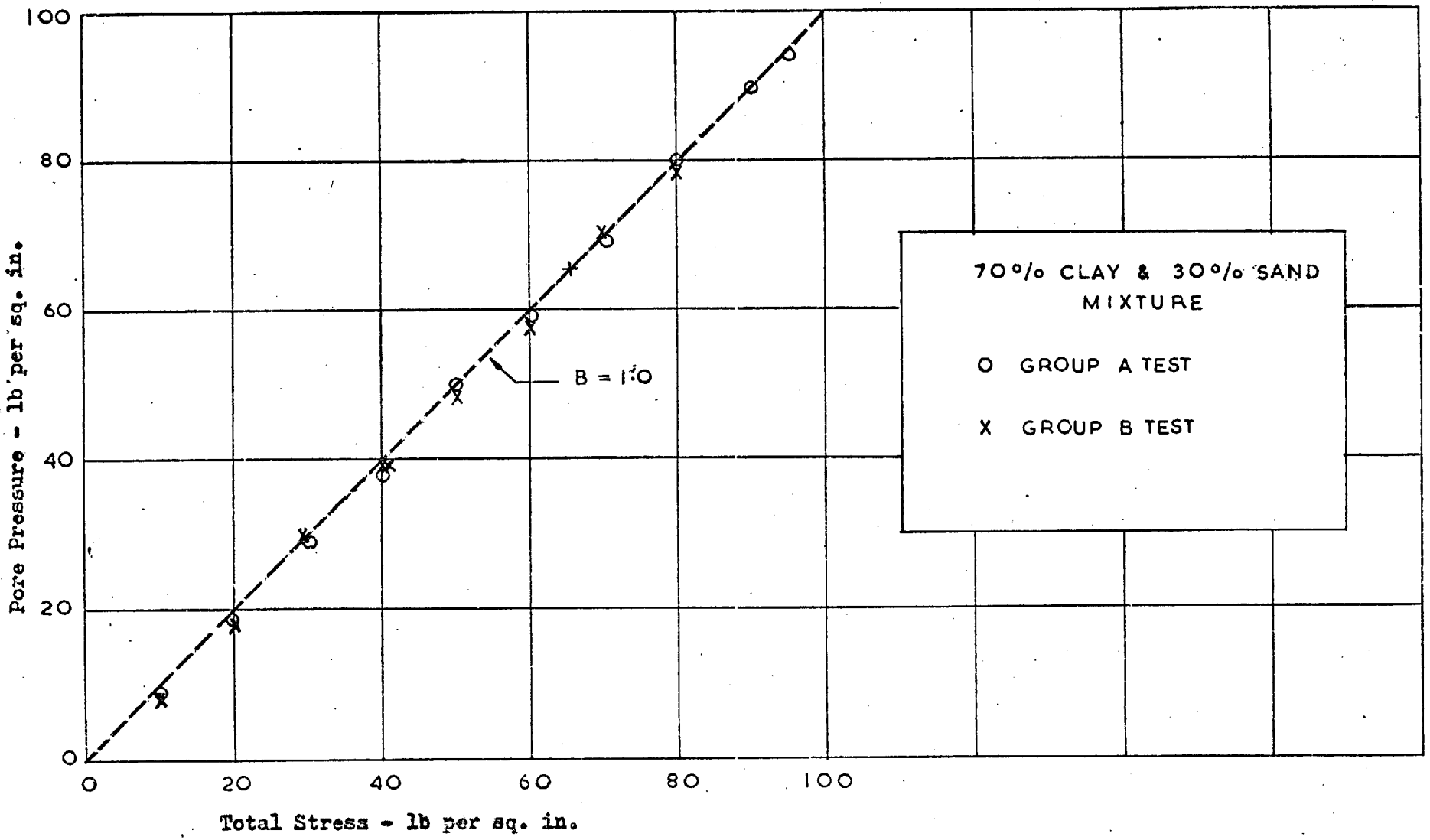

Figure No. 3.2, The build-up of pore pressure against increasing cell pressure (B value).

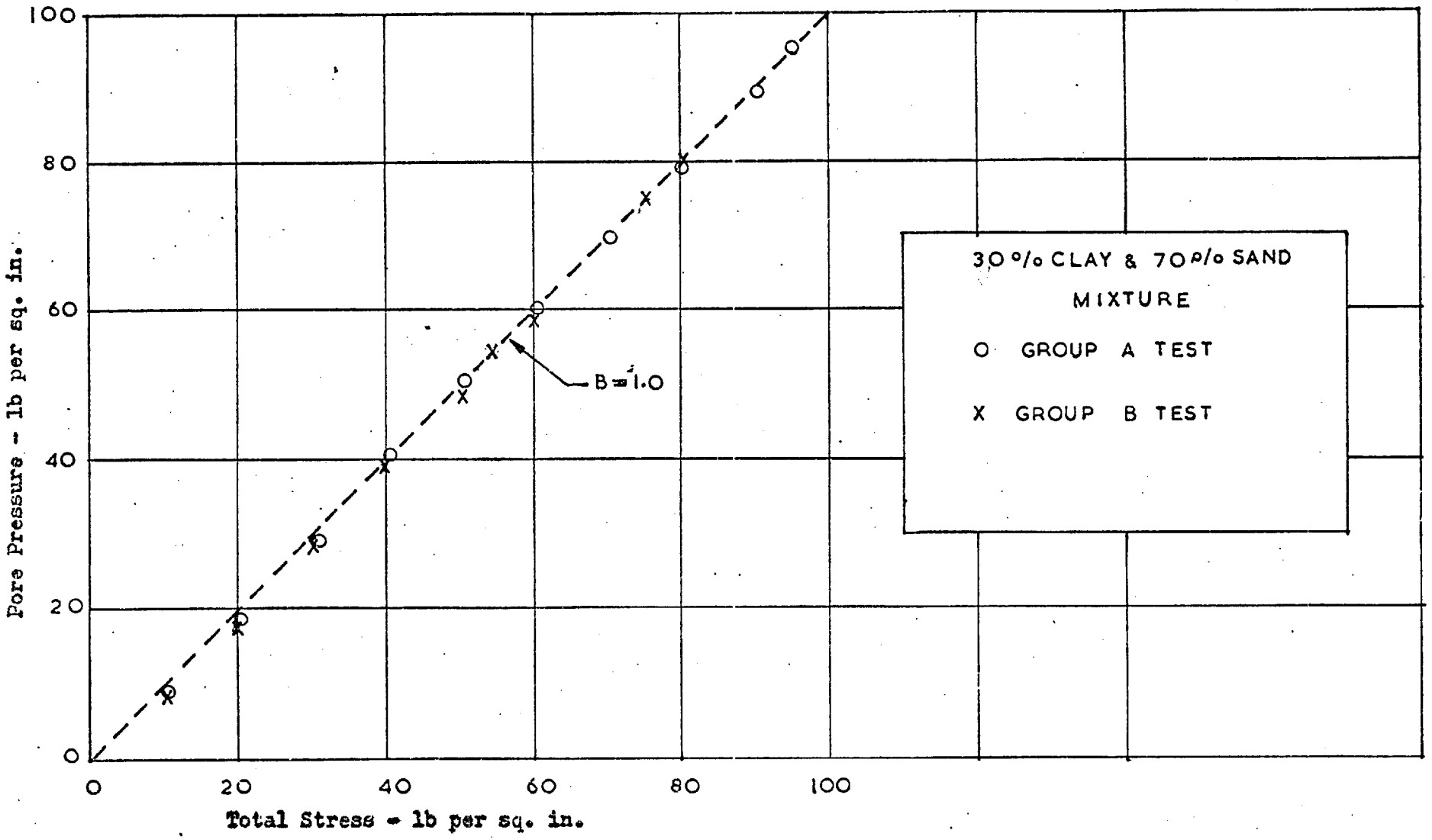

Figure No. 3.3, The build-up of pore pressure against increasing cell pressure (B value).

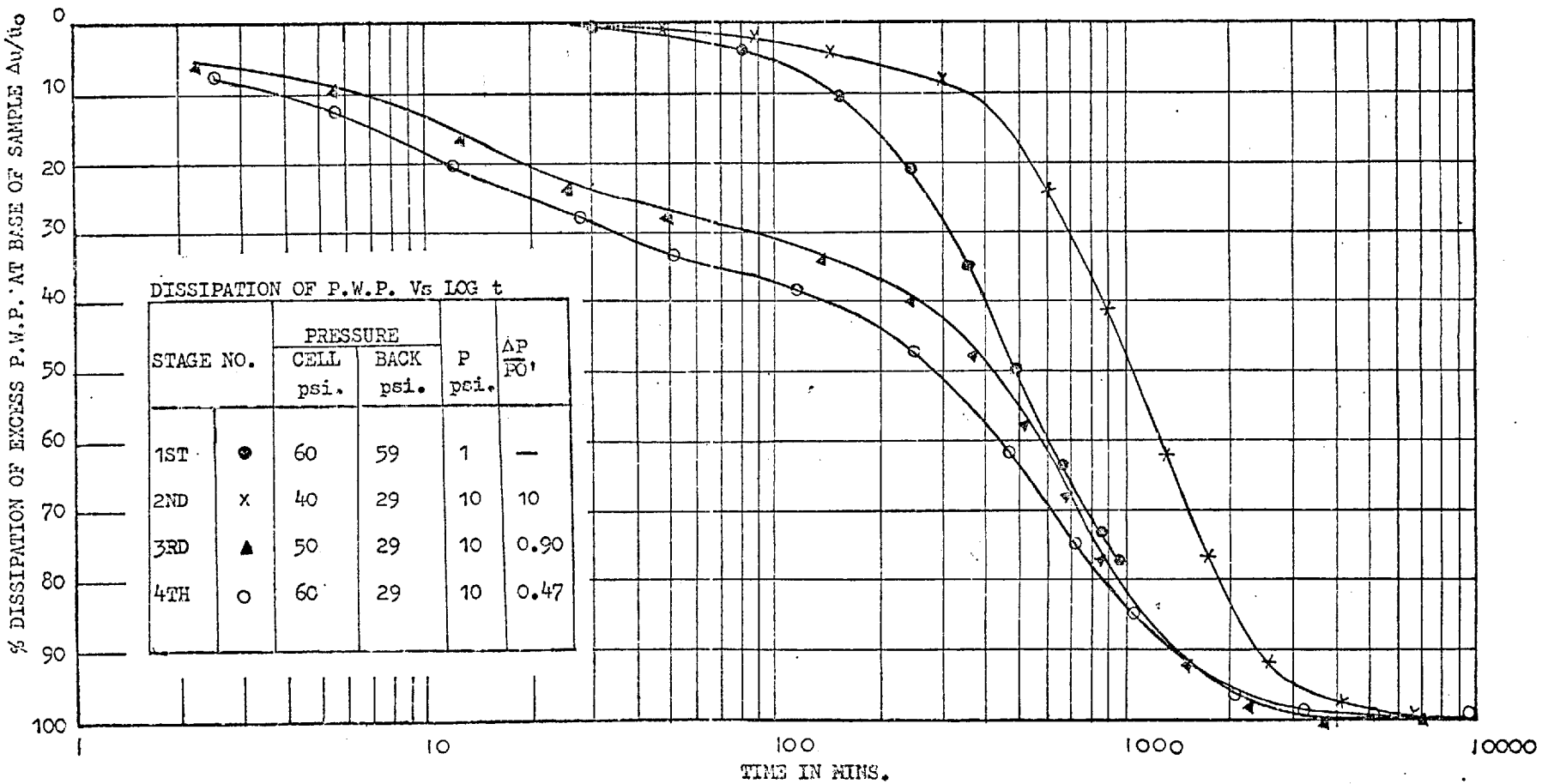

FIGURE NO. 3.4 :- The relationship between the percentage dissipation of pore water pressure and the logarithm of time during the isotropic consolidation. (After Skinner A.E., 1970)

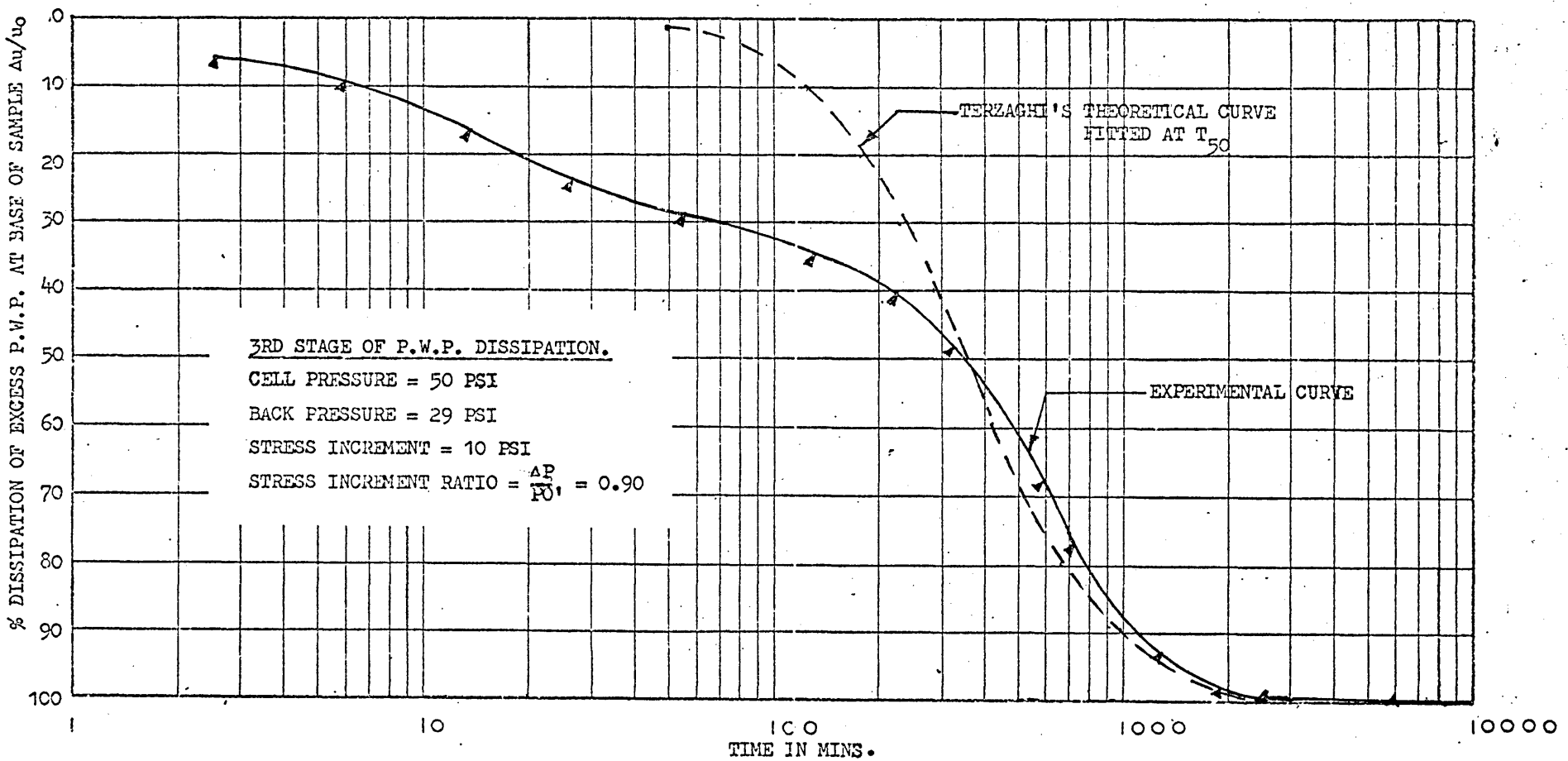

FIGURE NO. 3.5(a) :- Terzaghi's theoretical curve fitted at T_{50} to the experimental curve of percentage dissipation of pore water pressure obtained by Skinner A.E., (1970)

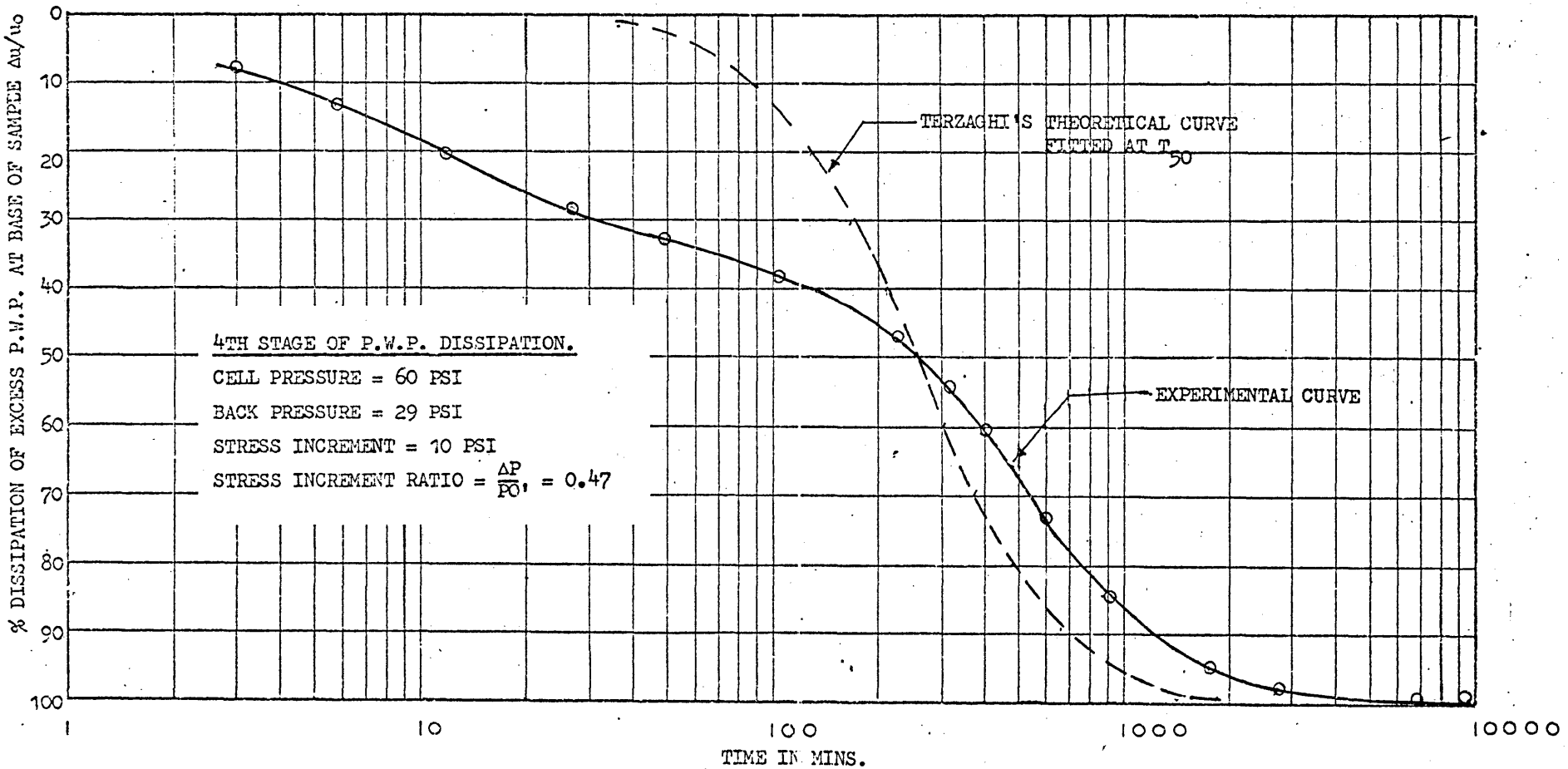

FIGURE NO. 3.5 (b) :- Terzaghi's theoretical curve fitted at T_{50} to the experimental curve of percentage dissipation of pore water pressure obtained by Skinner A.E., (1970)

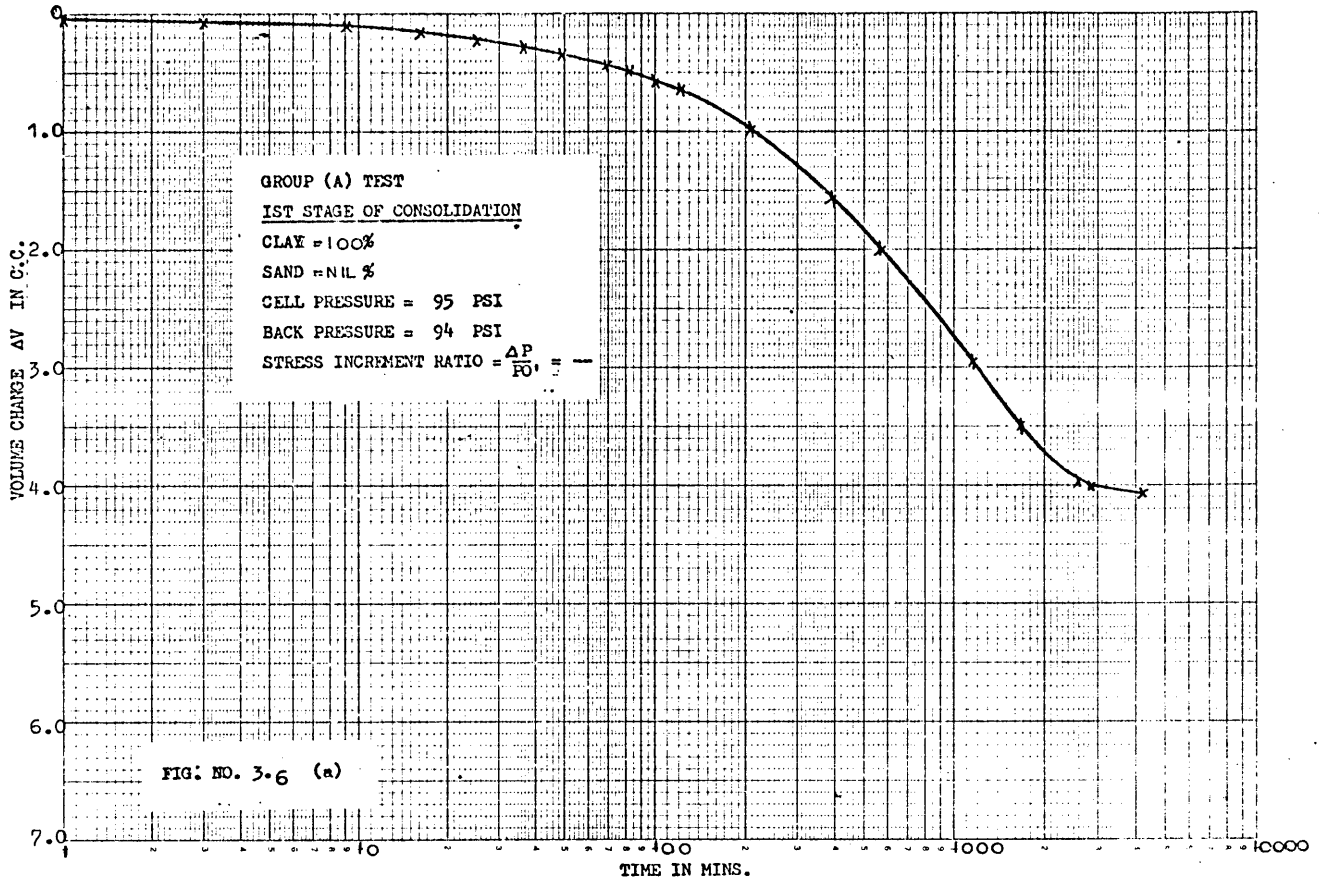

FIG. NO. 3.6 (a)

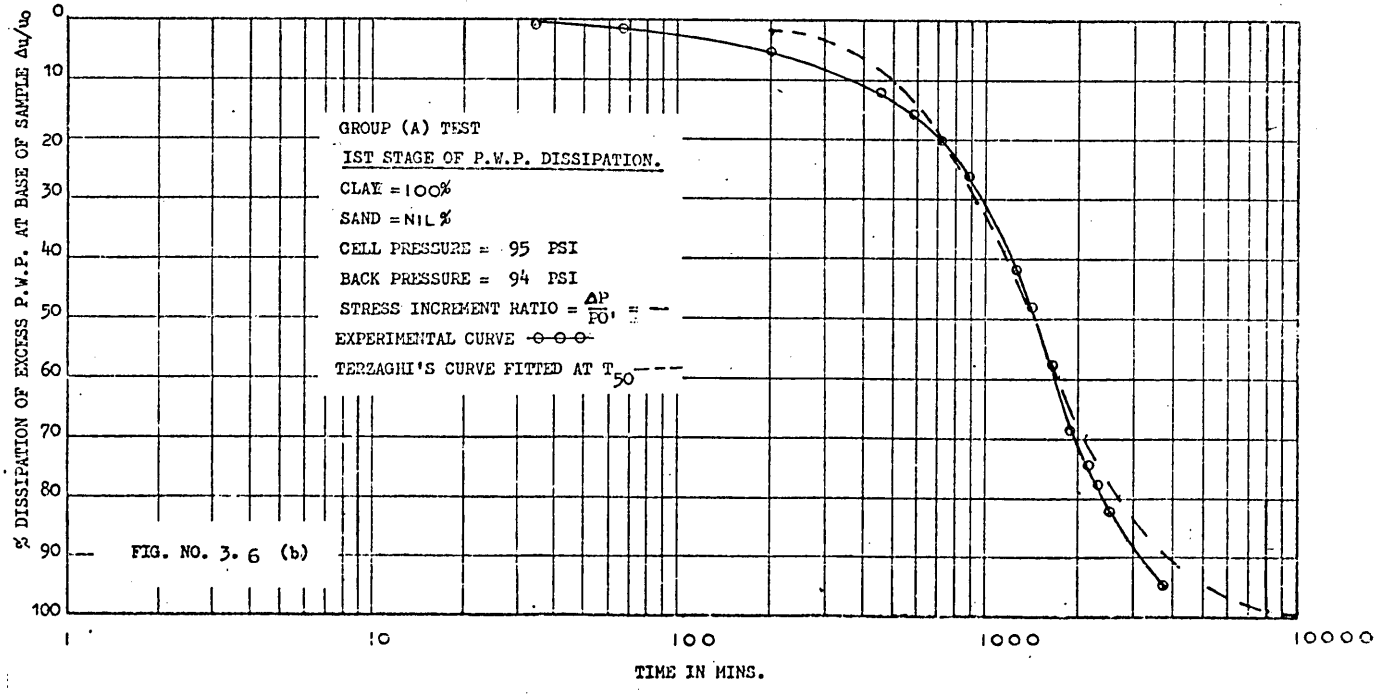

FIG. NO. 3.6 (b)

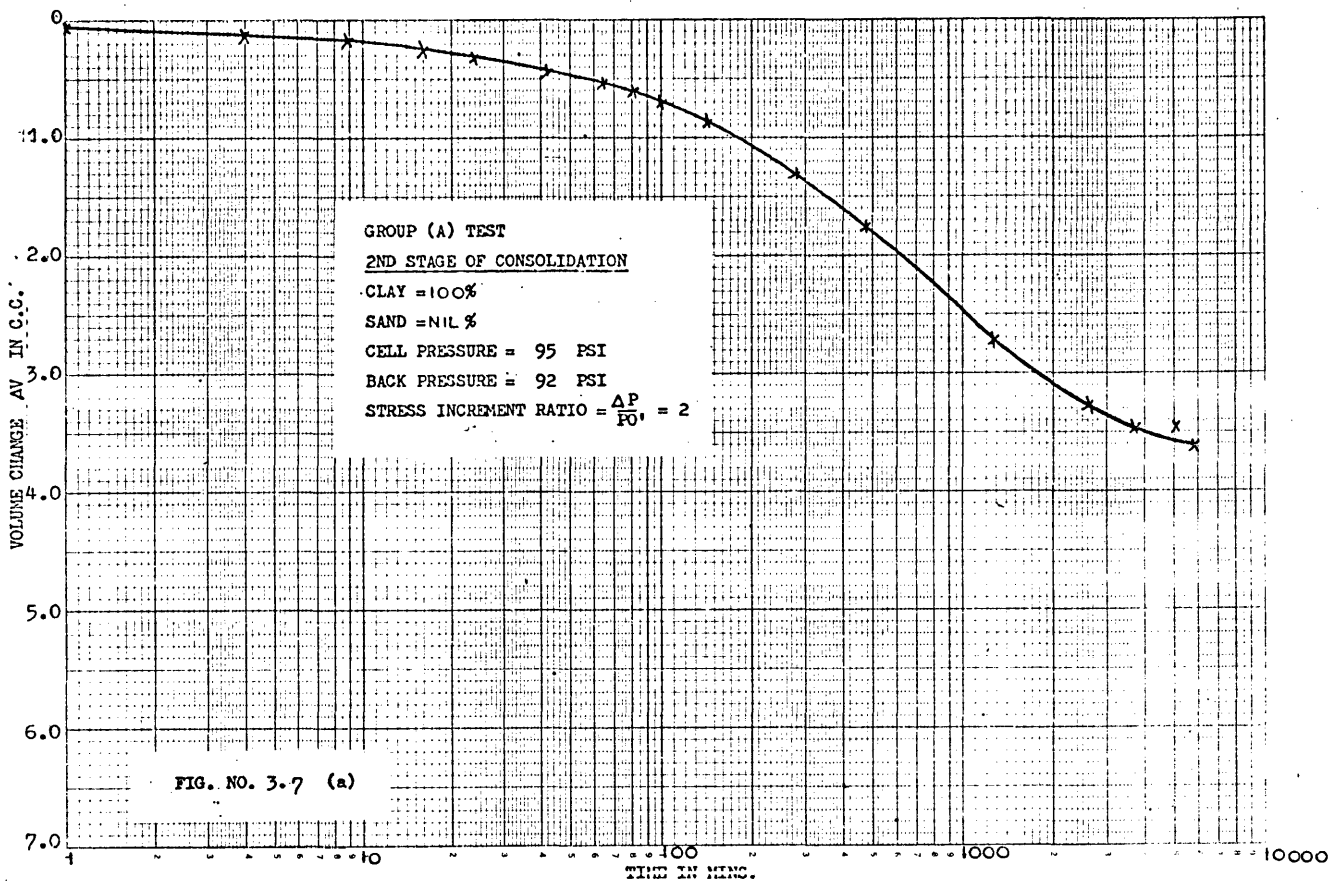

FIG. NO. 3.7 (a)

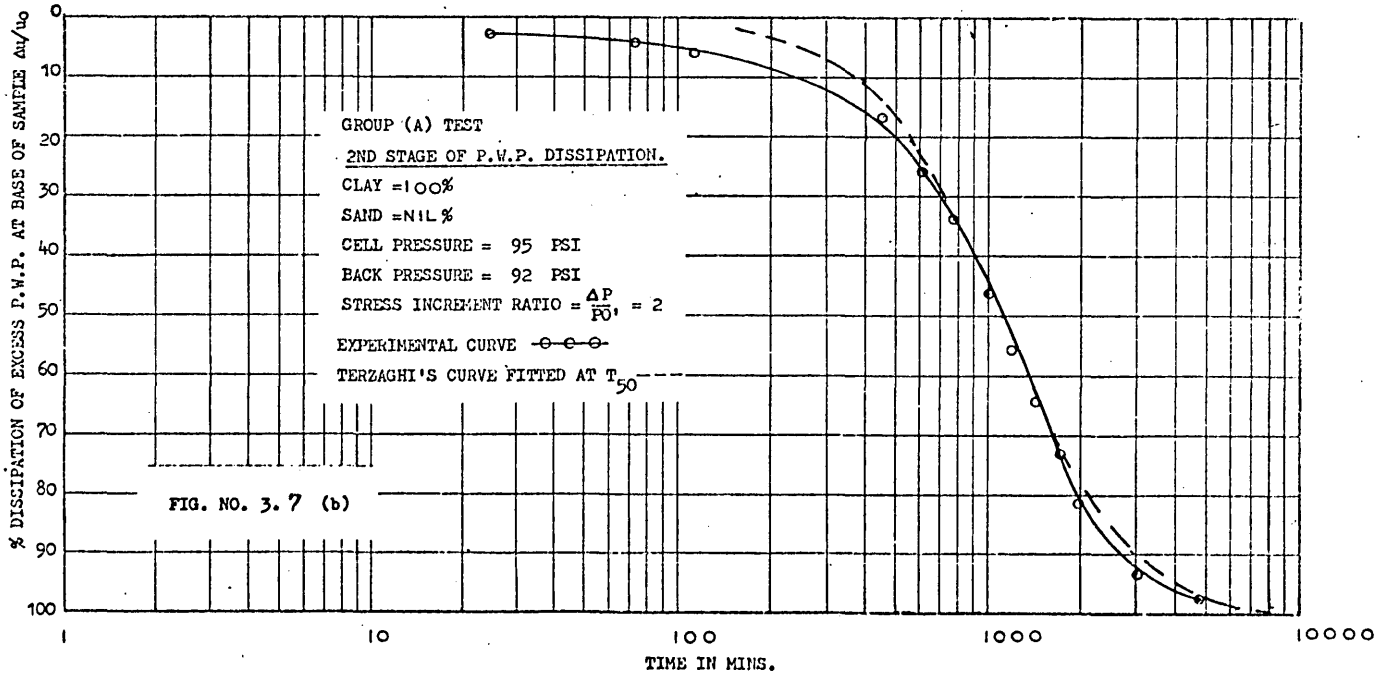

FIG. NO. 3.7 (b)

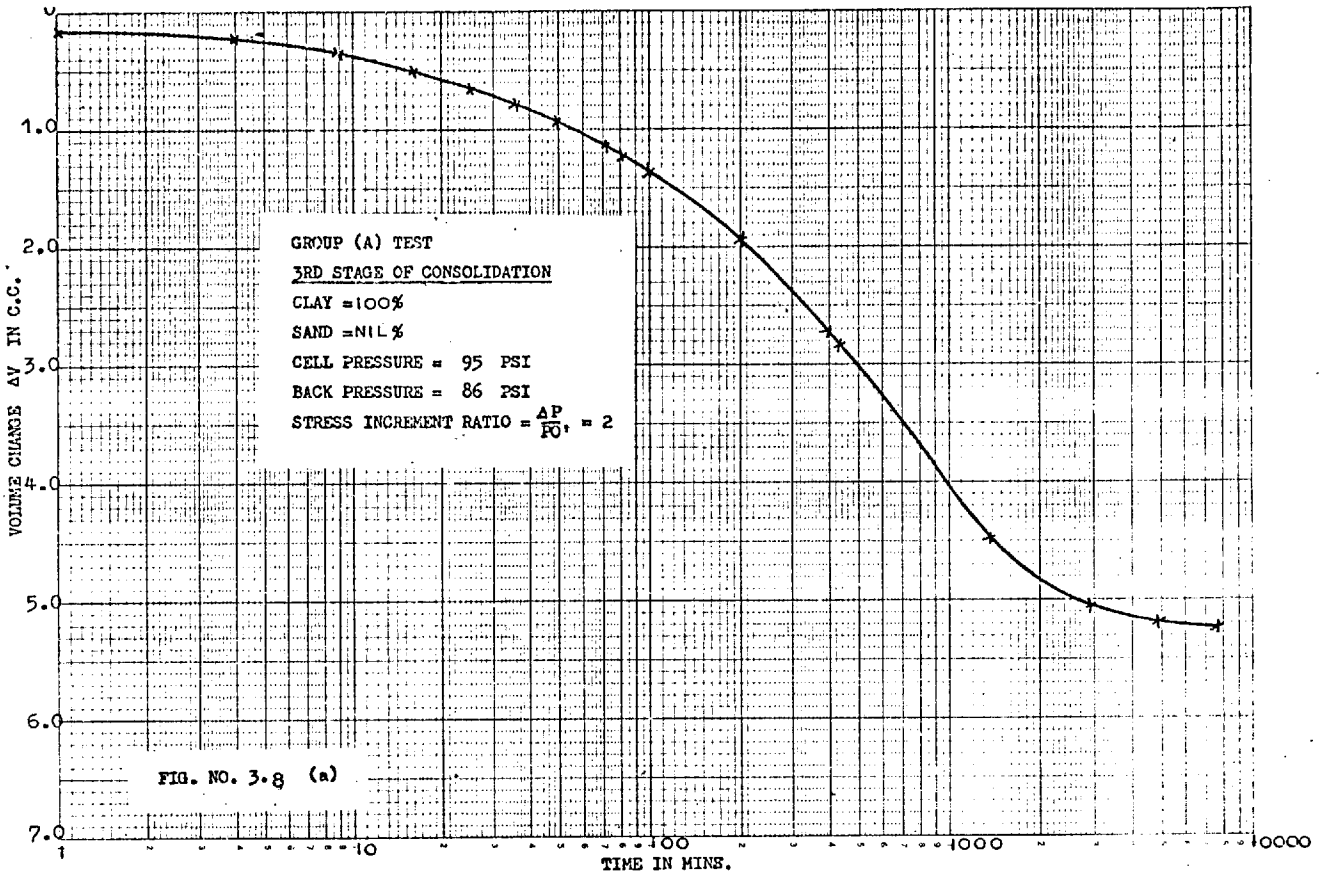

FIG. NO. 3.8 (a)

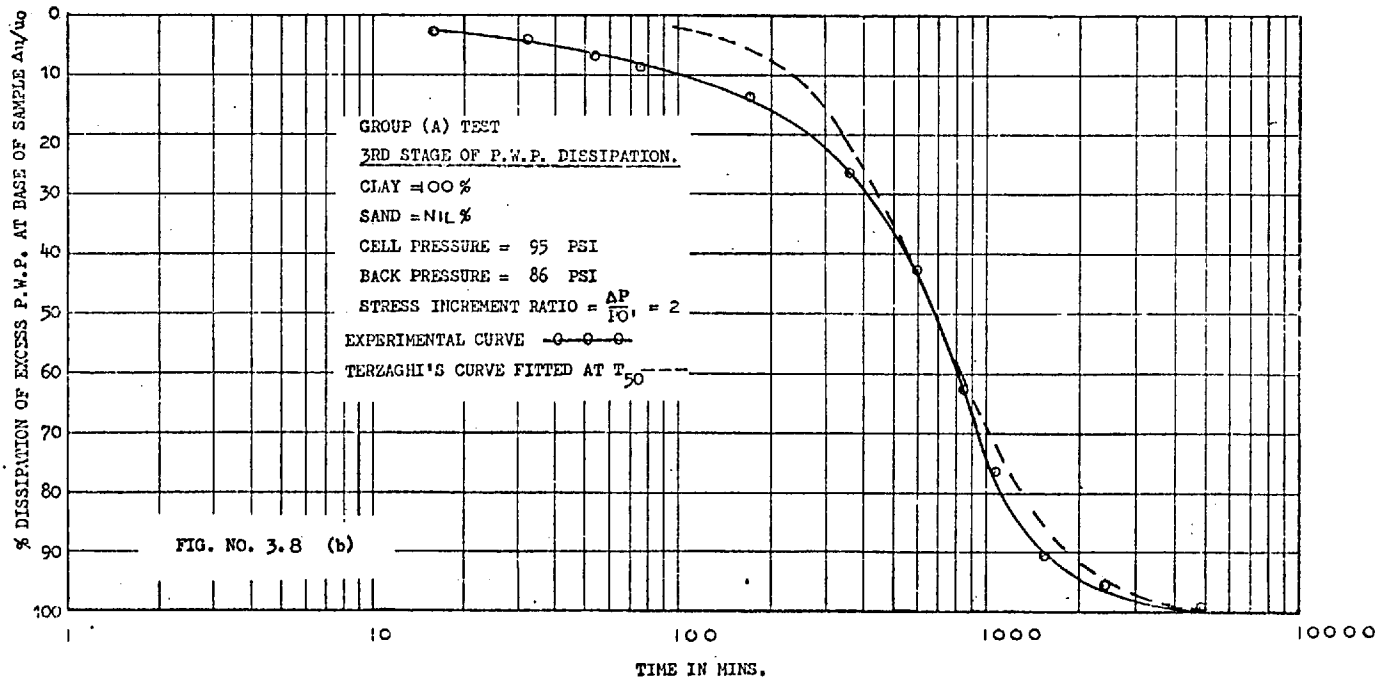

FIG. NO. 3.8 (b)

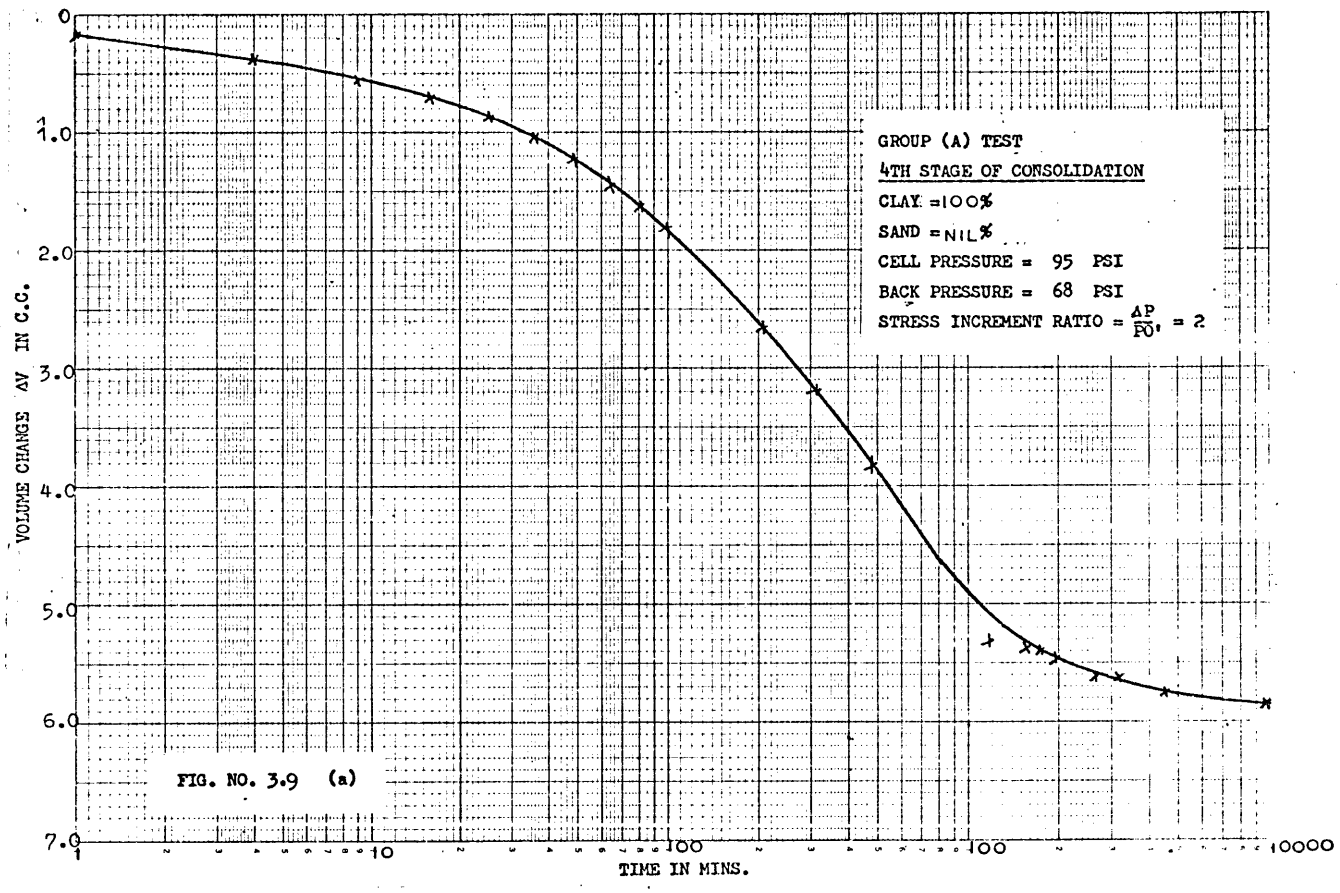

FIG. NO. 3.9 (a)

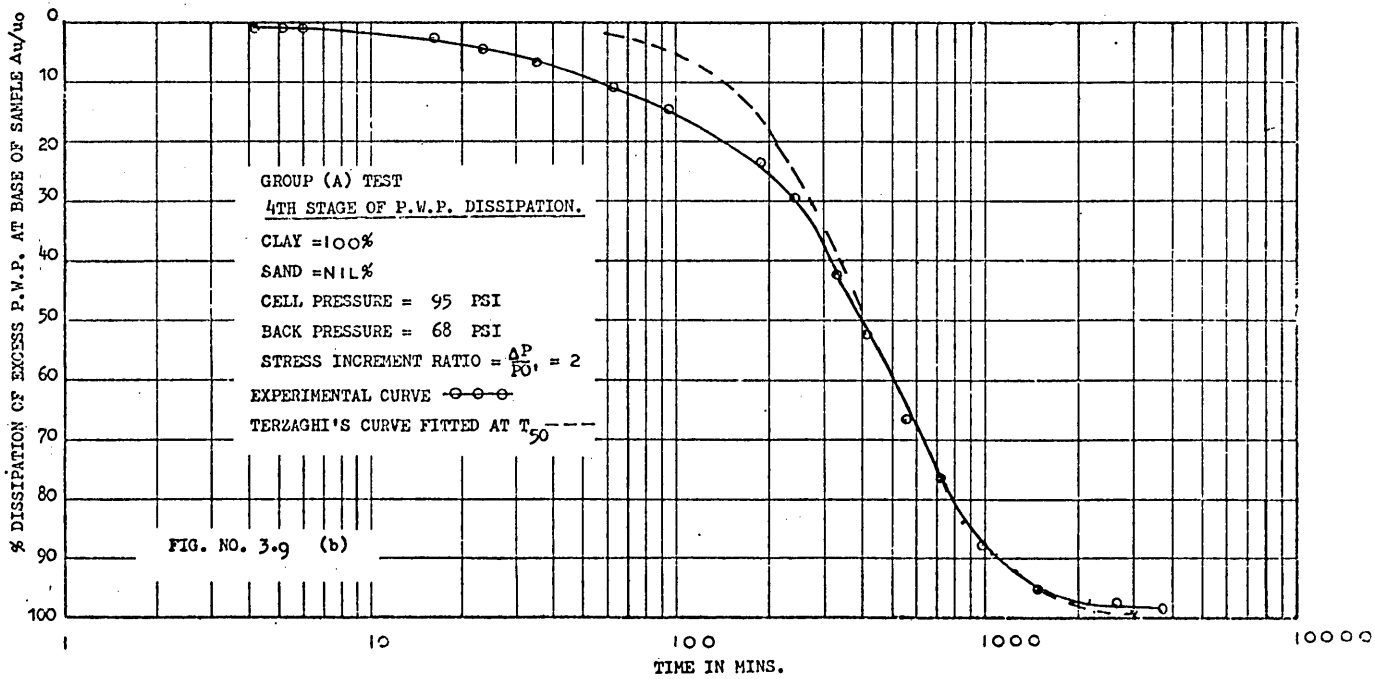

FIG. NO. 3.9 (b)

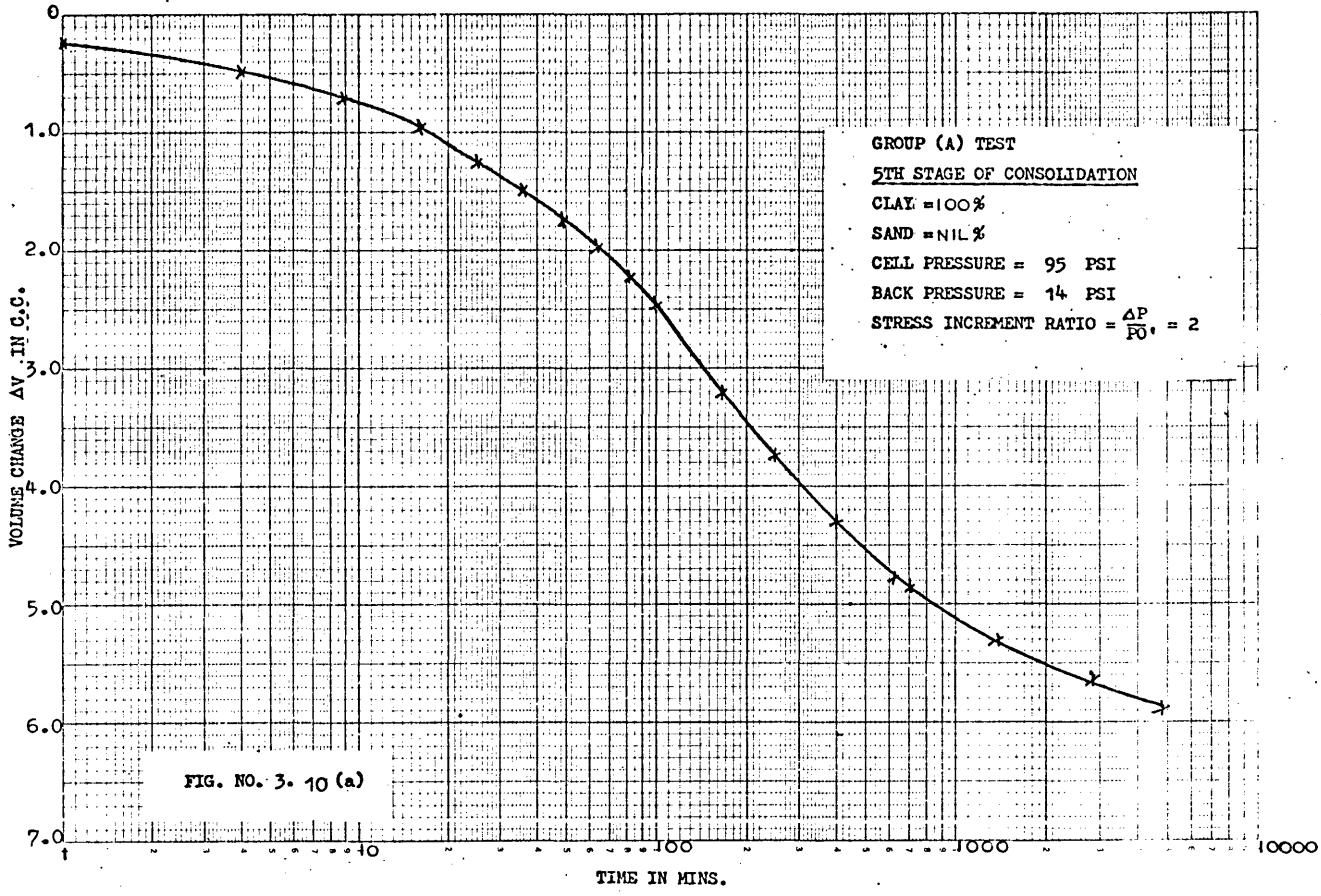

FIG. NO. 3.10 (a)

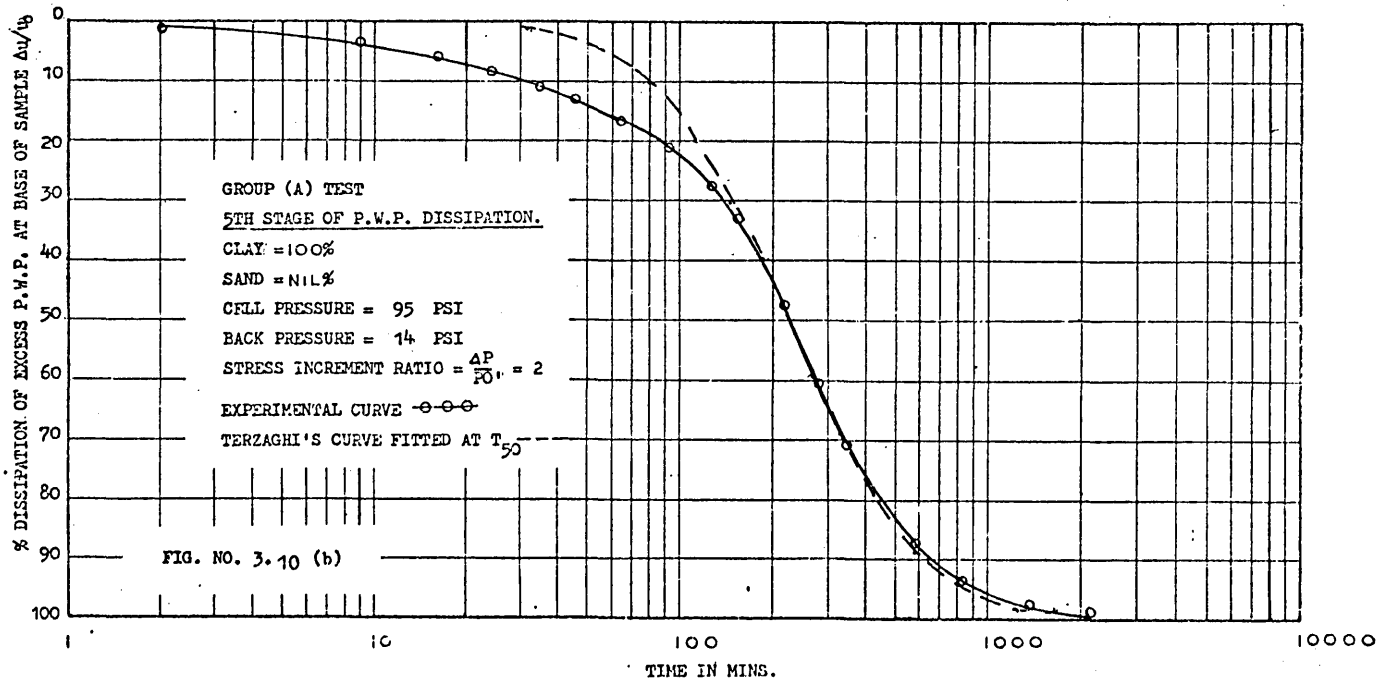

FIG. NO. 3.10 (b)

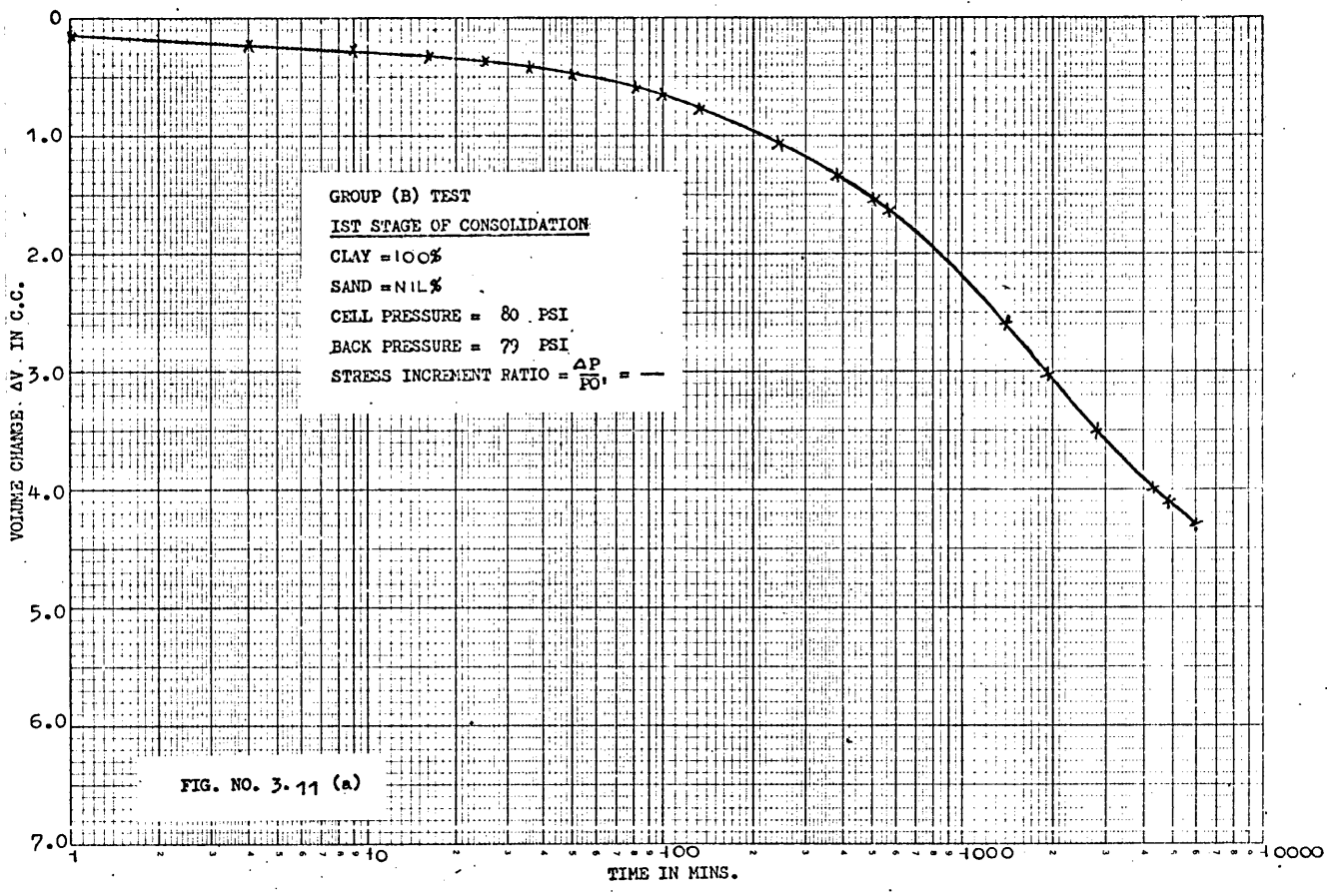

FIG. NO. 3.11 (a)

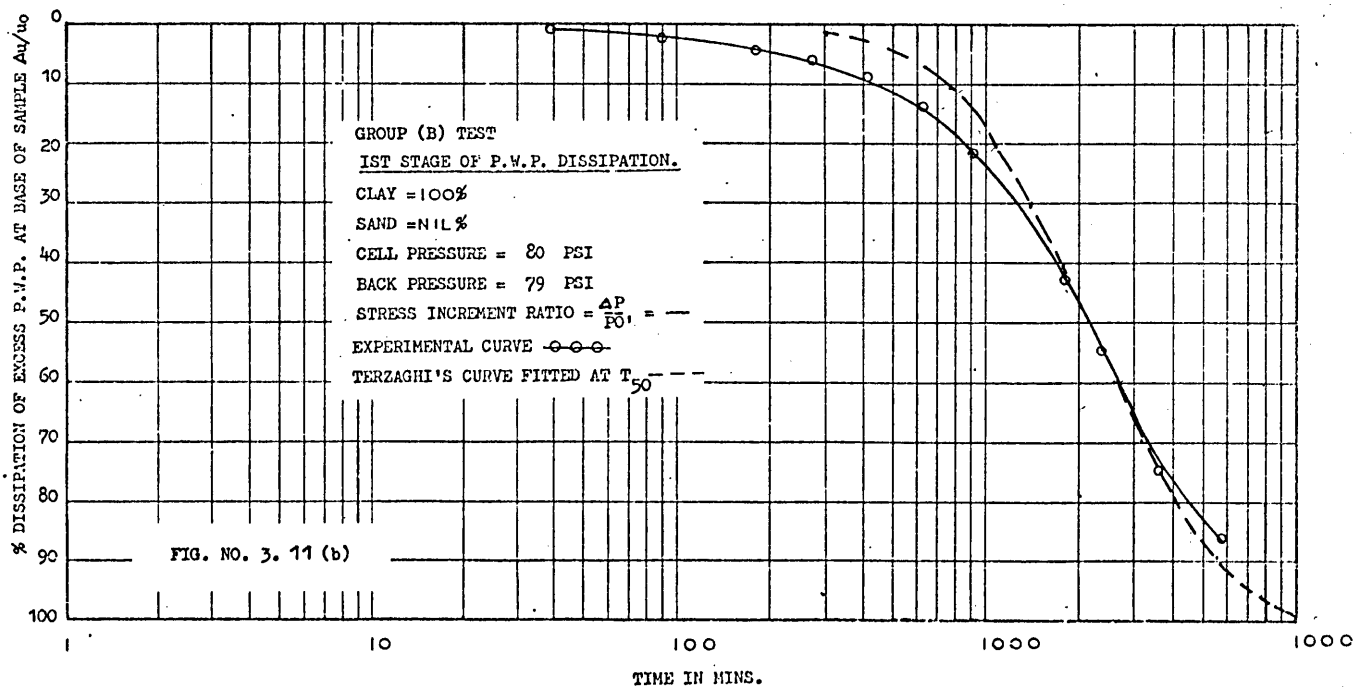

FIG. NO. 3.11 (b)

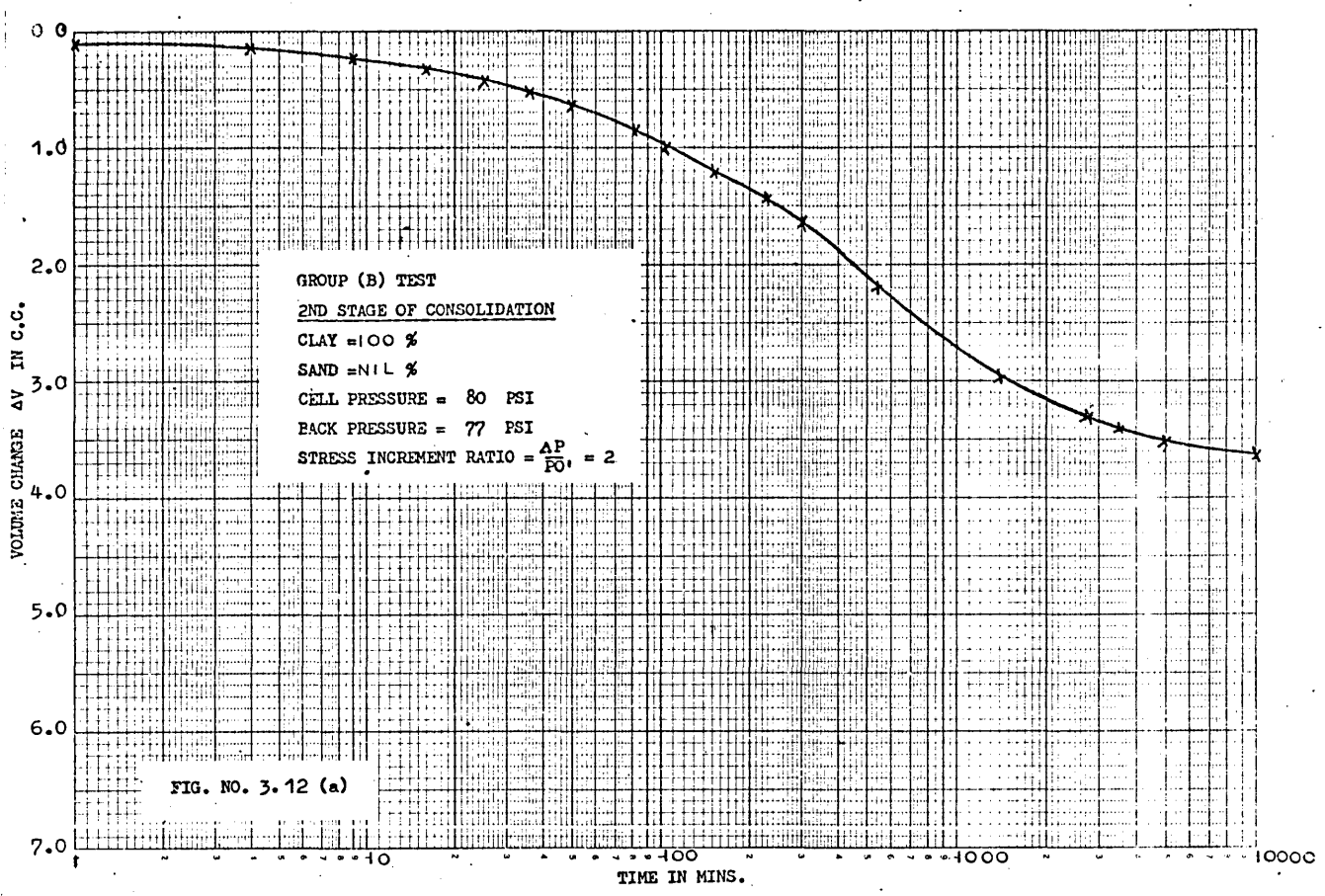

FIG. NO. 3.12 (a)

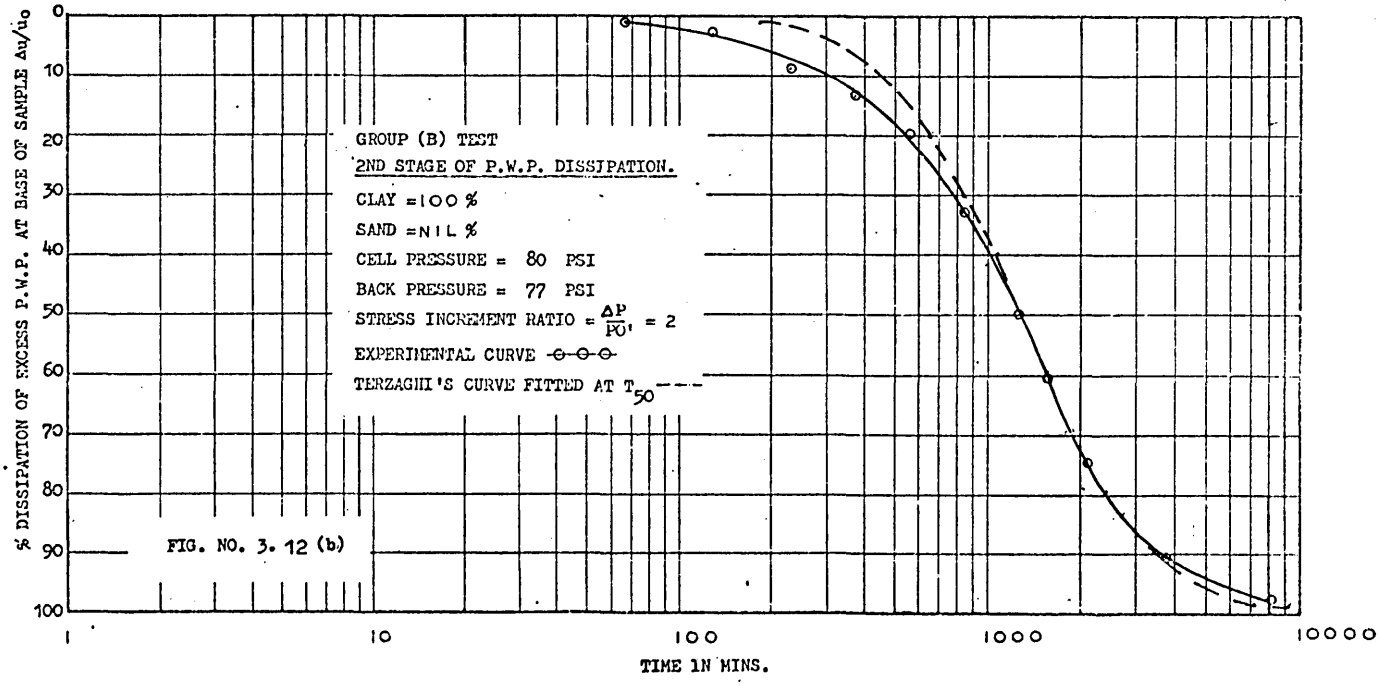

FIG. NO. 3.12 (b)

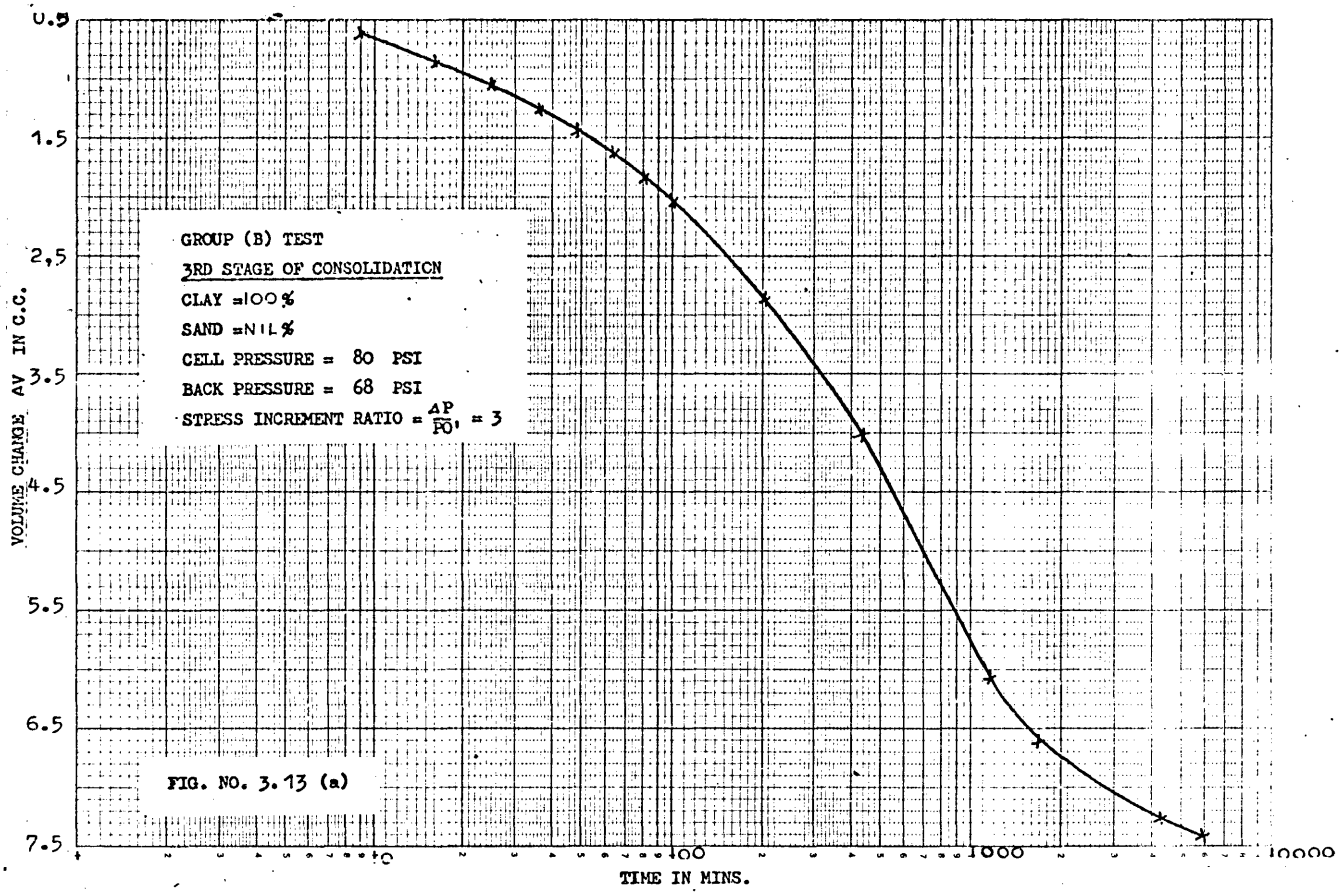

FIG. NO. 3.13 (a)

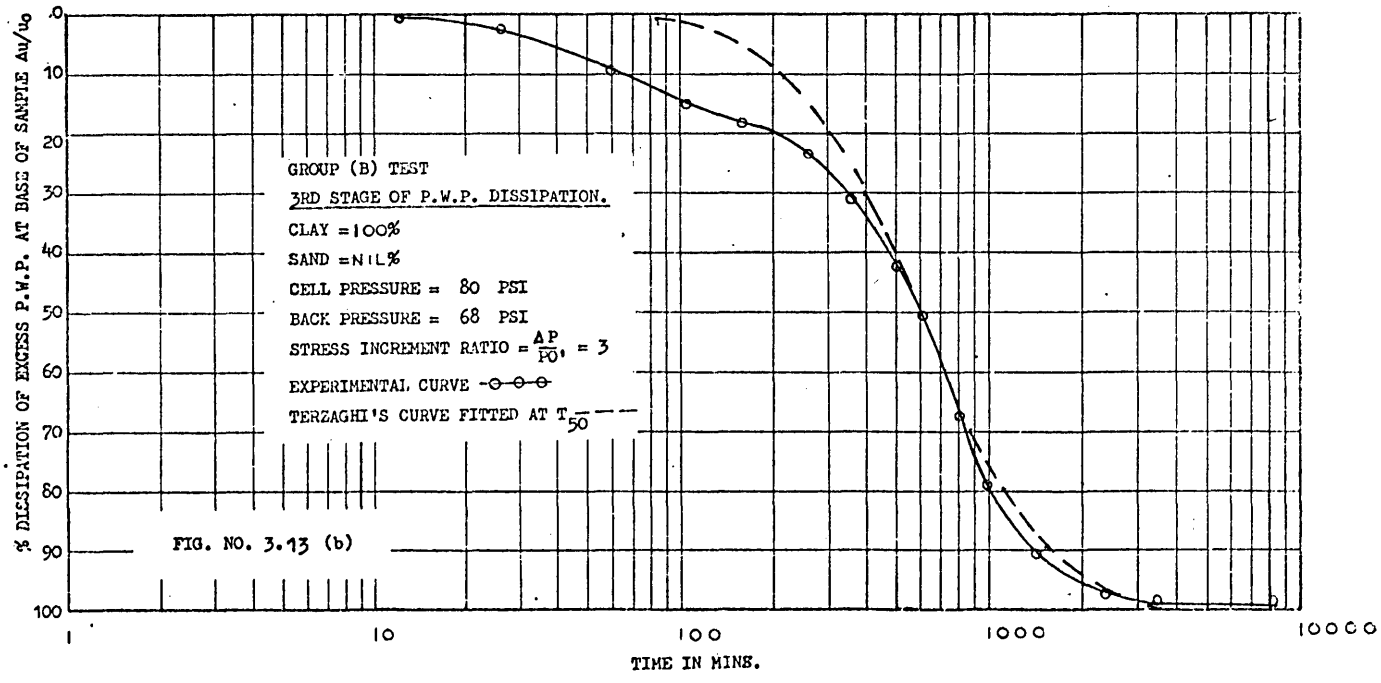

FIG. NO. 3.13 (b)

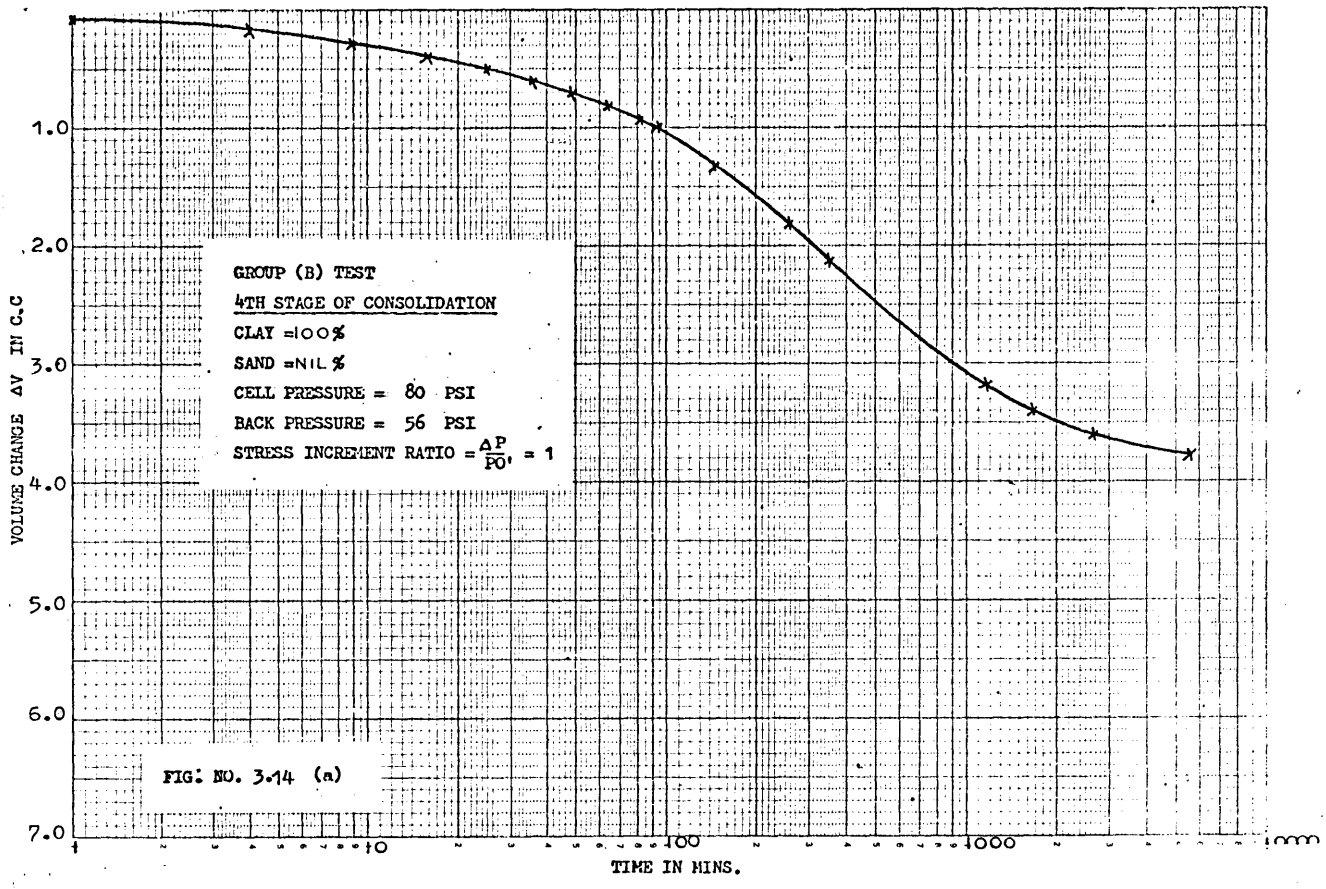

FIG. NO. 3.14 (a)

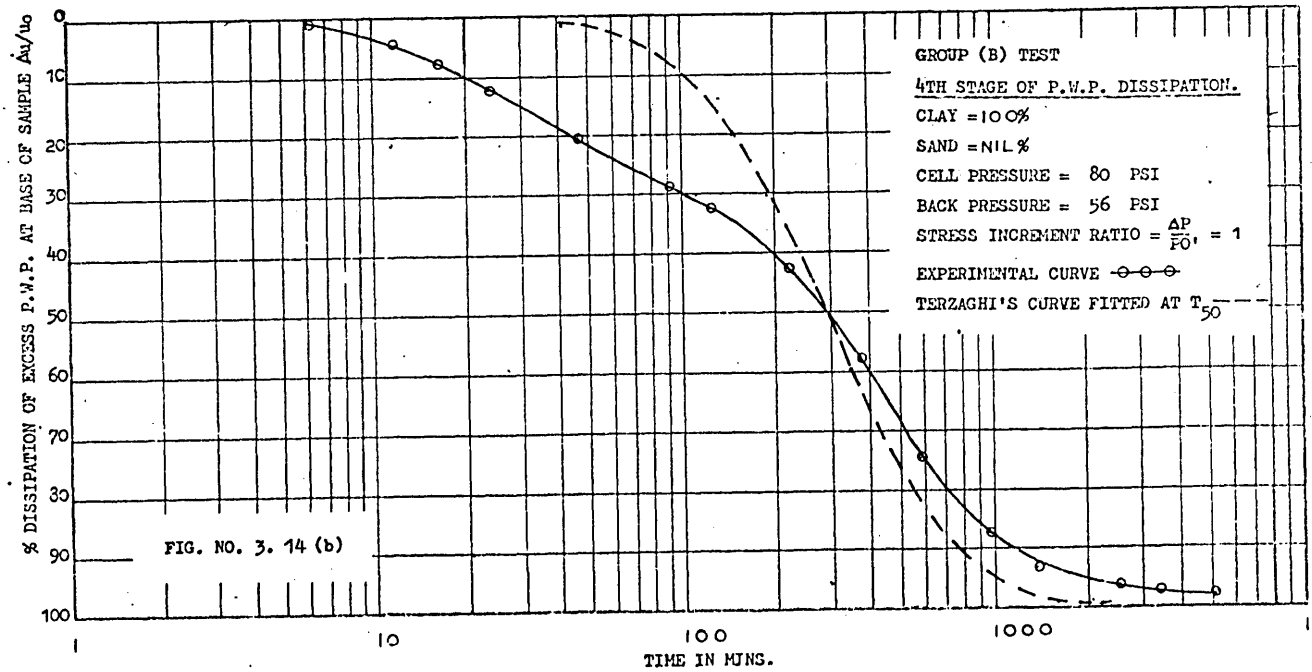

FIG. NO. 3. 14 (b)

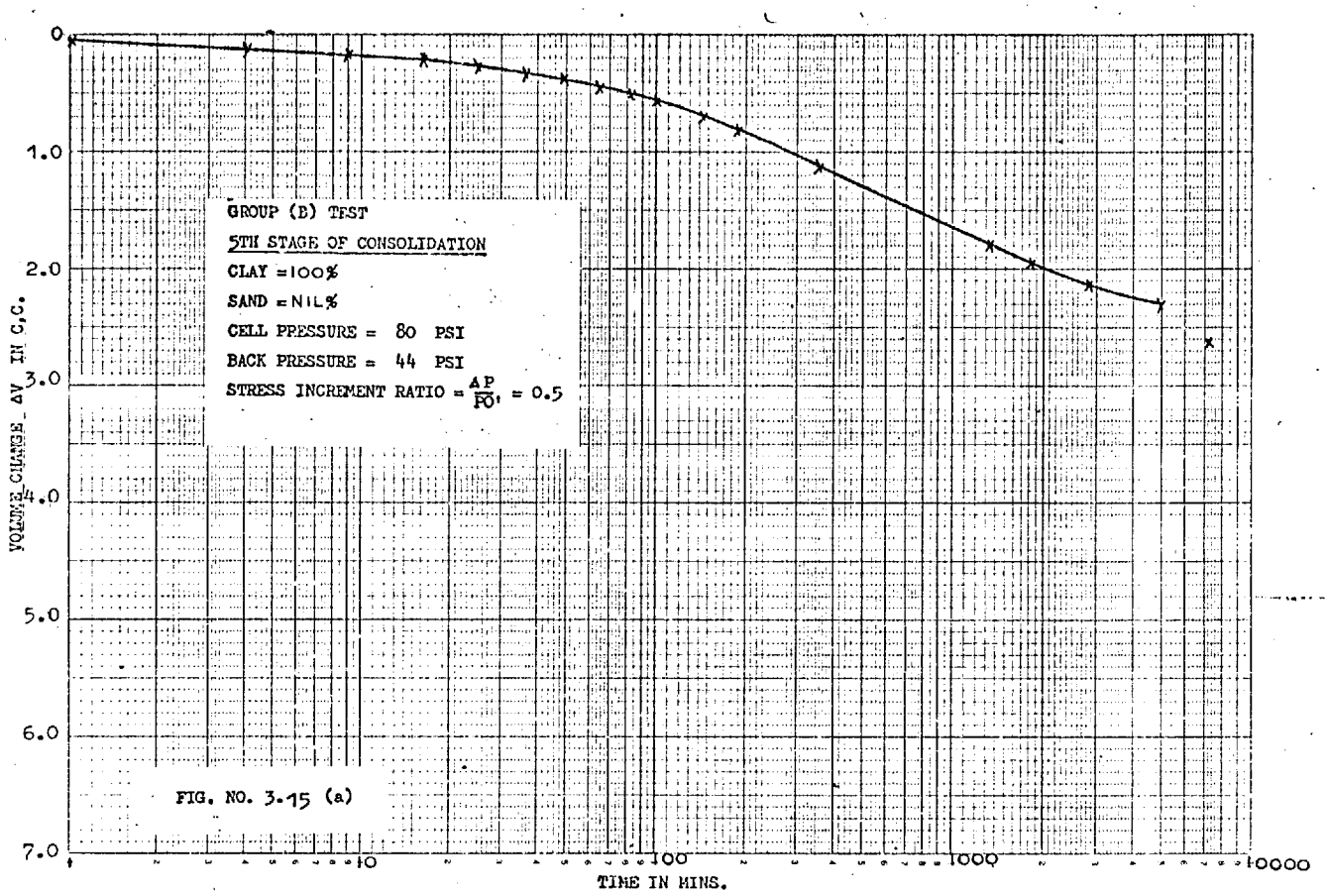

FIG. NO. 3.15 (a)

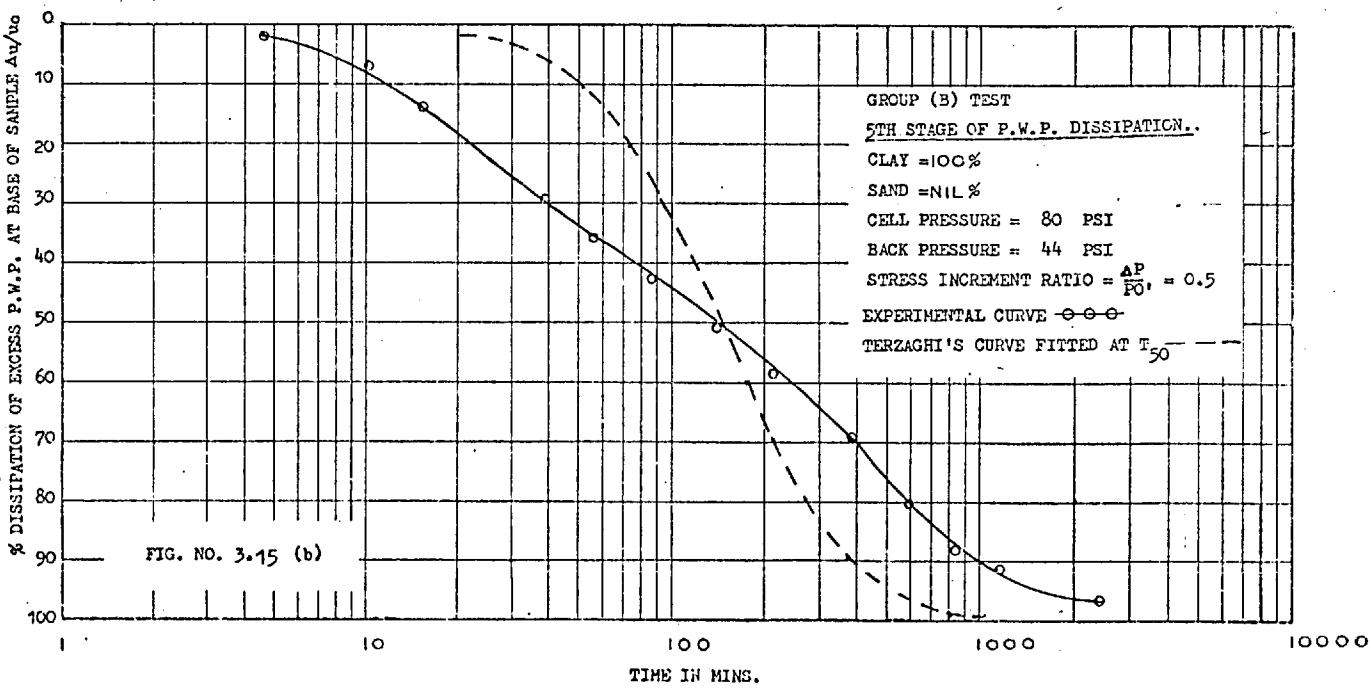

FIG. NO. 3.15 (b)

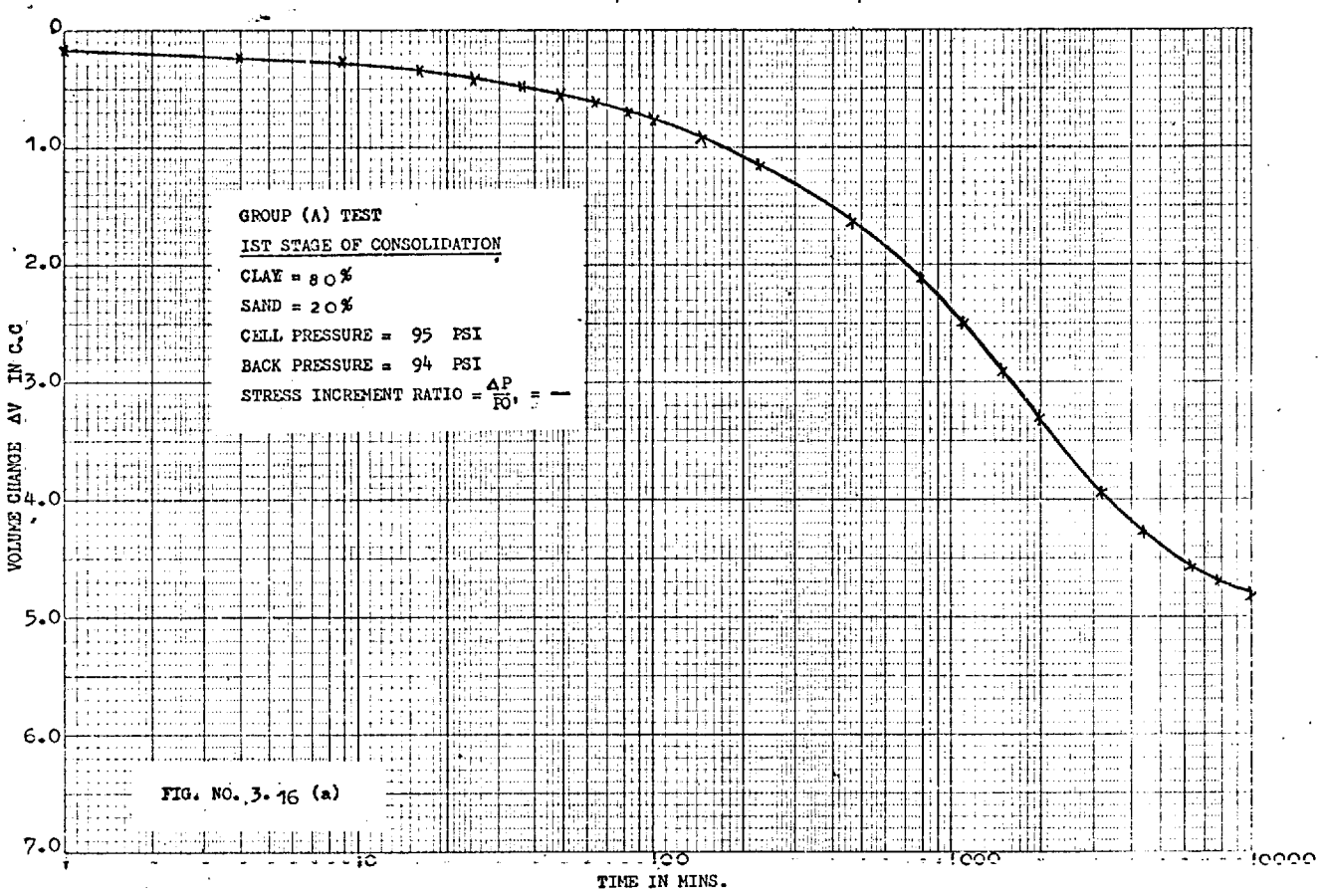

FIG. NO. 3.16 (a)

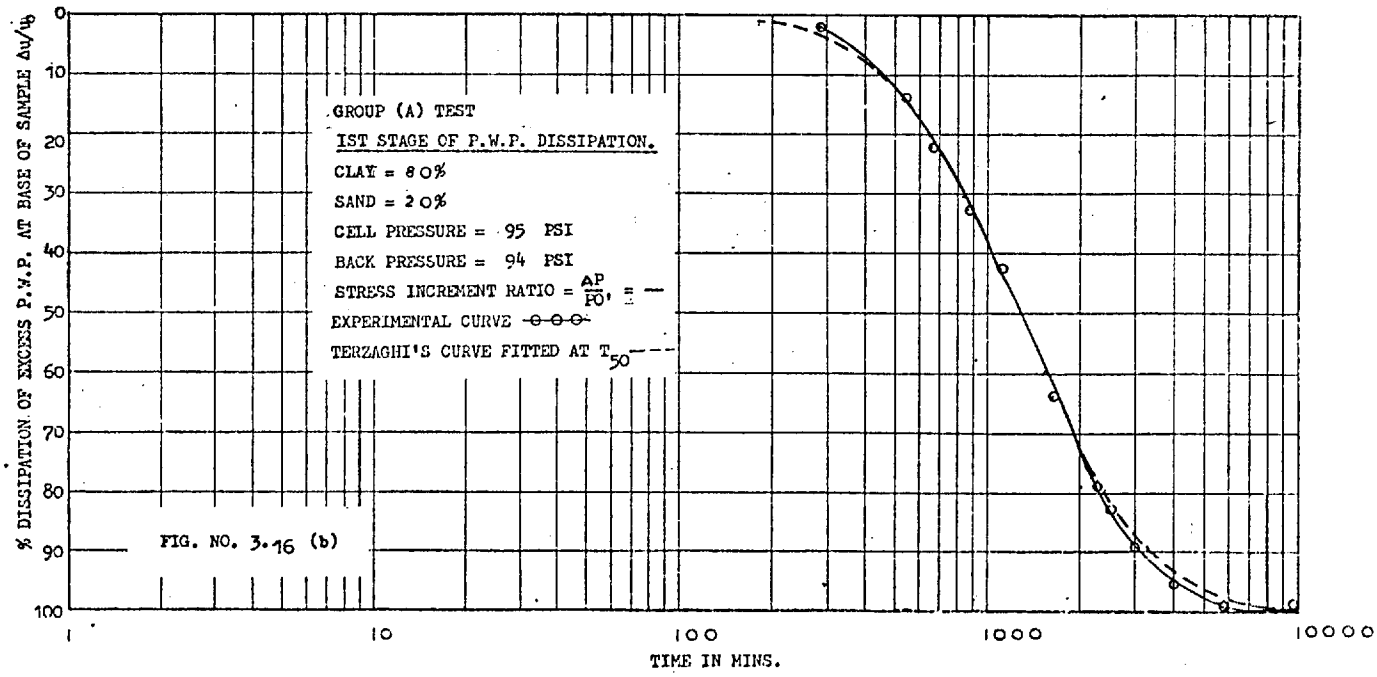

FIG. NO. 3.16 (b)

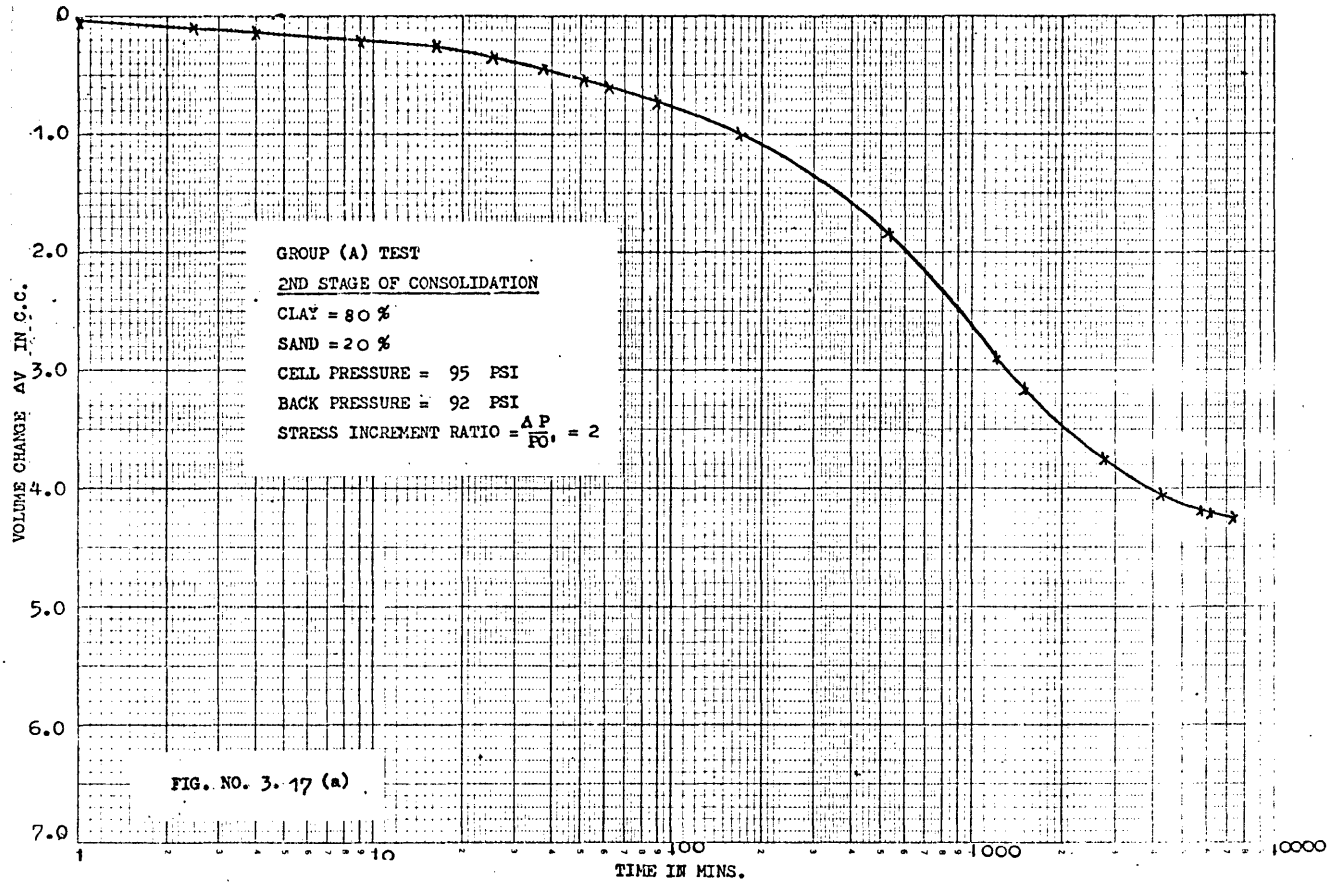

FIG. NO. 3.17 (a)

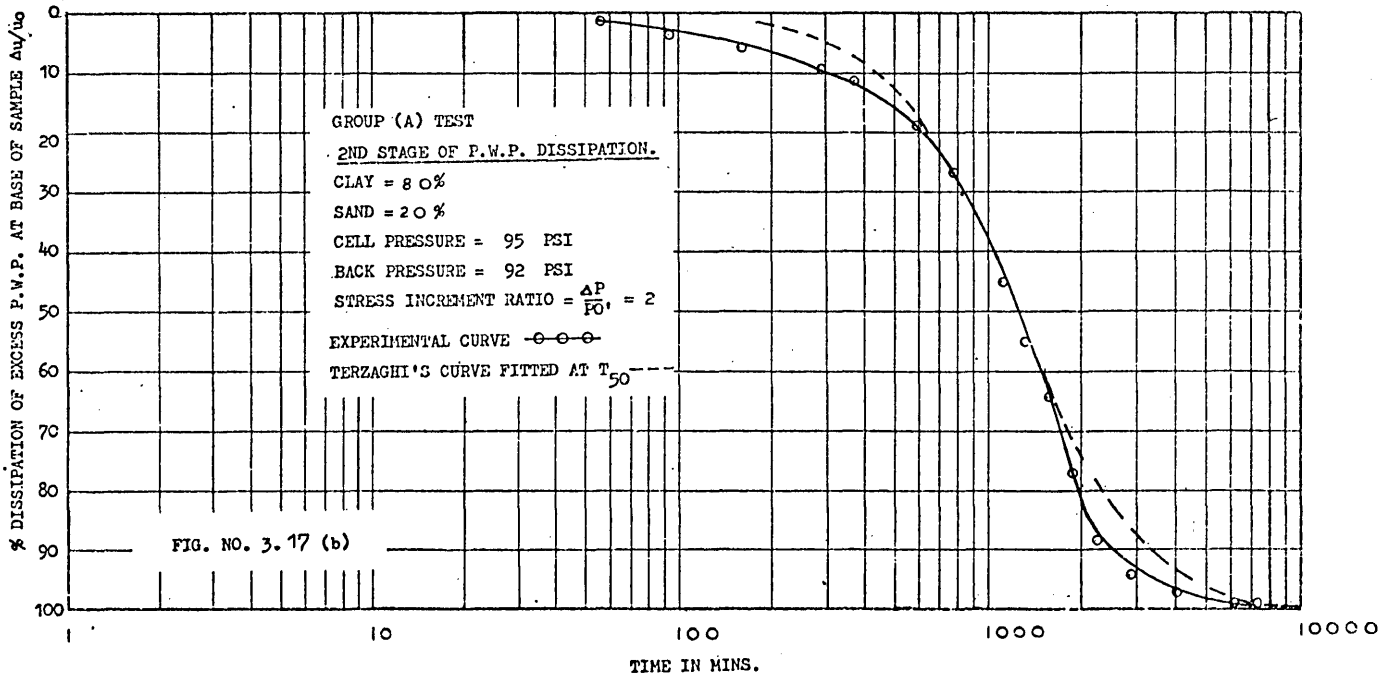

FIG. NO. 3.17 (b)

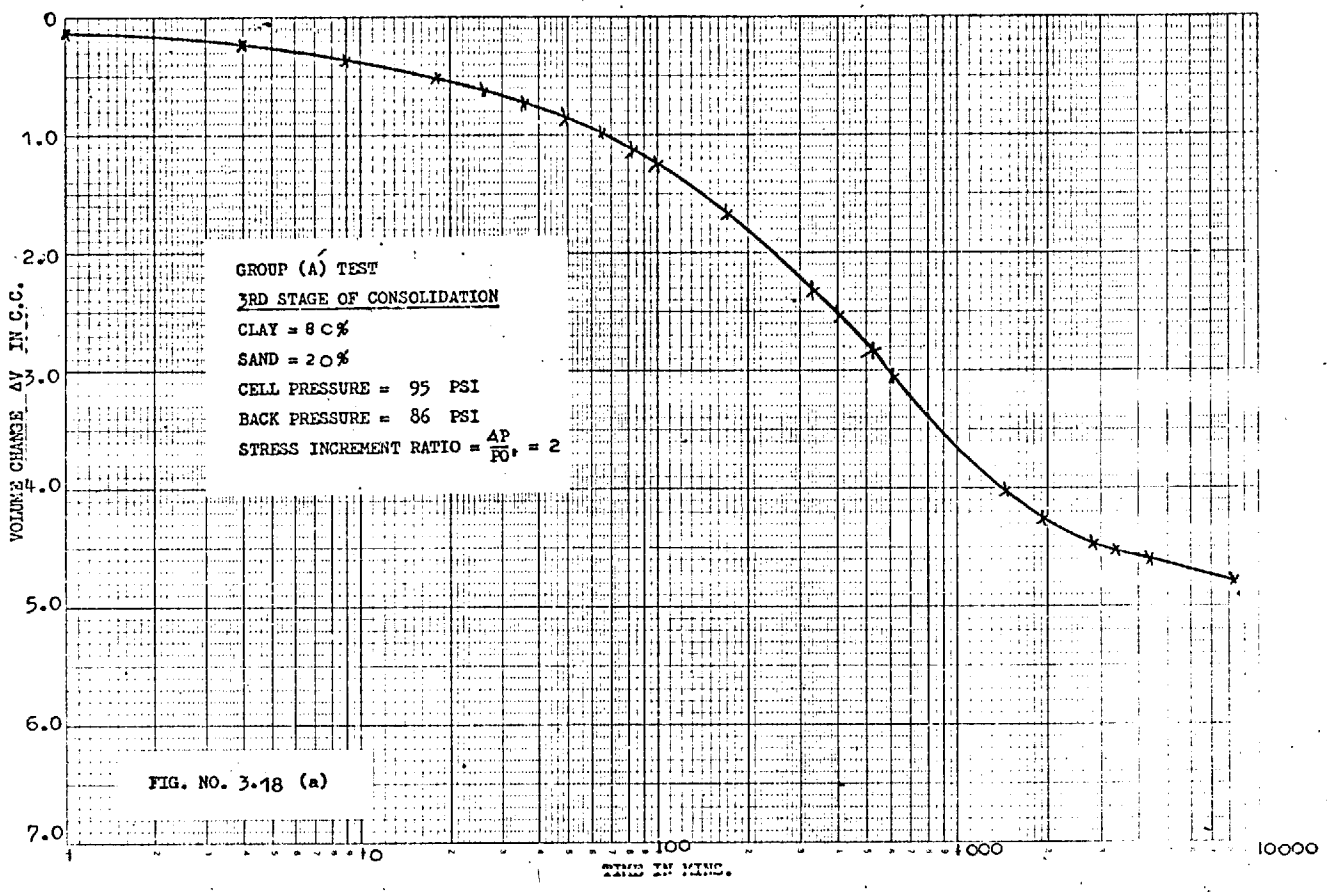

FIG. NO. 3.18 (a)

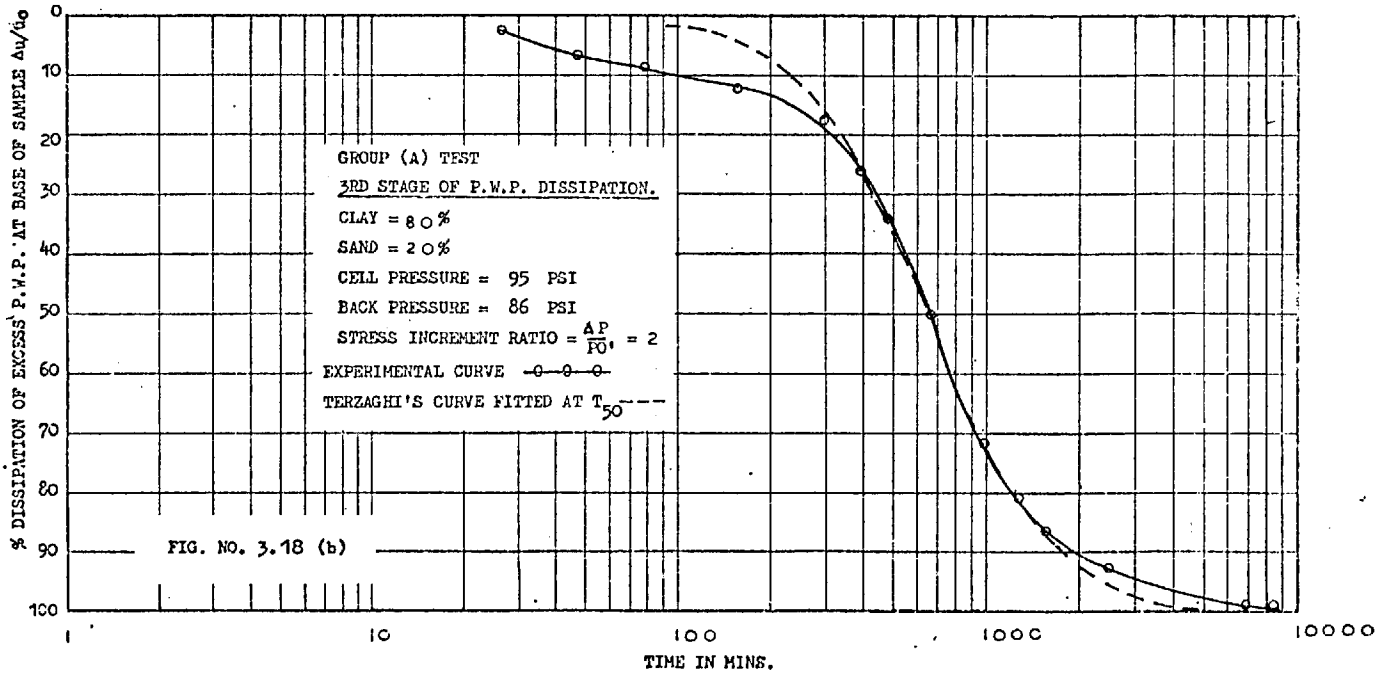

FIG. NO. 3.18 (b)

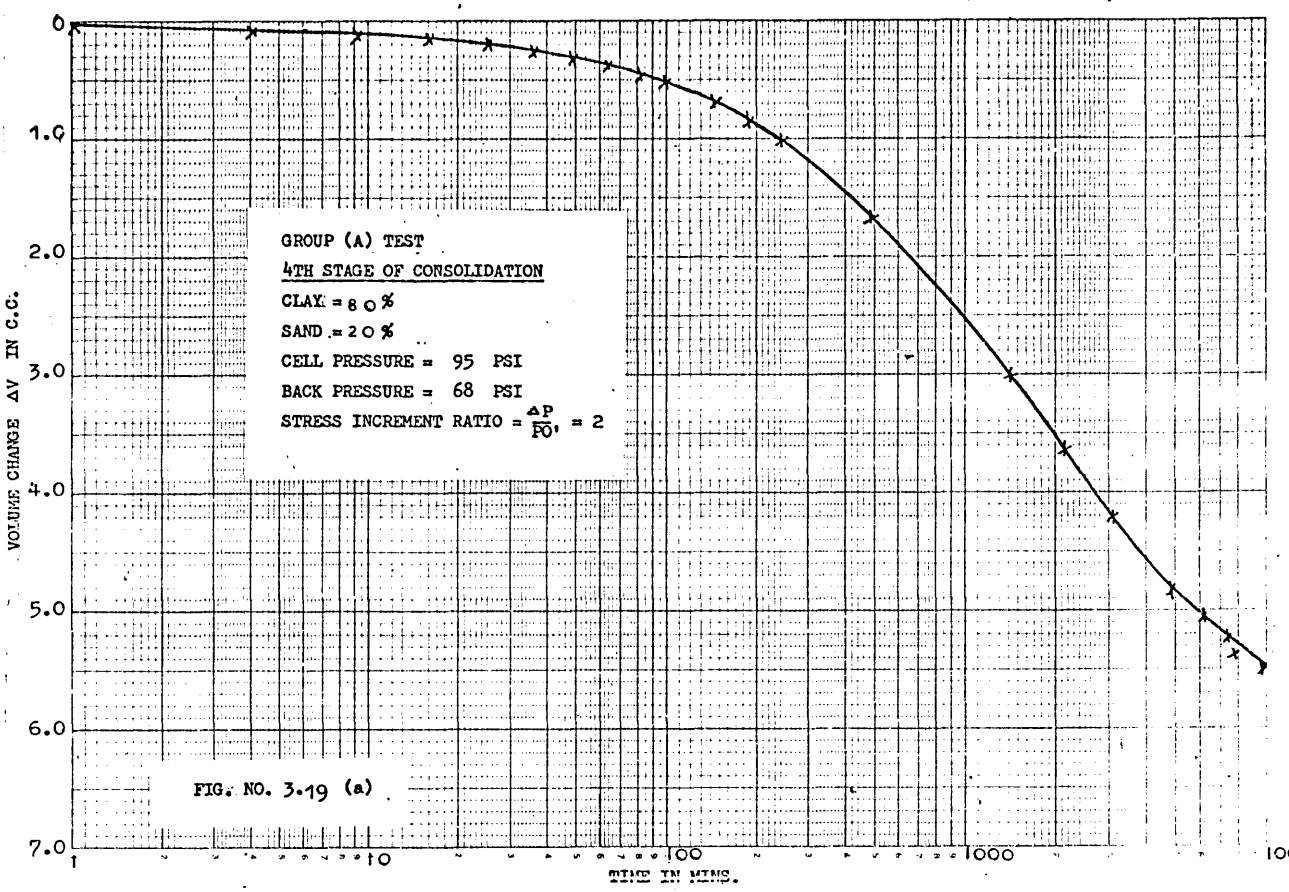

FIG. NO. 3.19 (a)

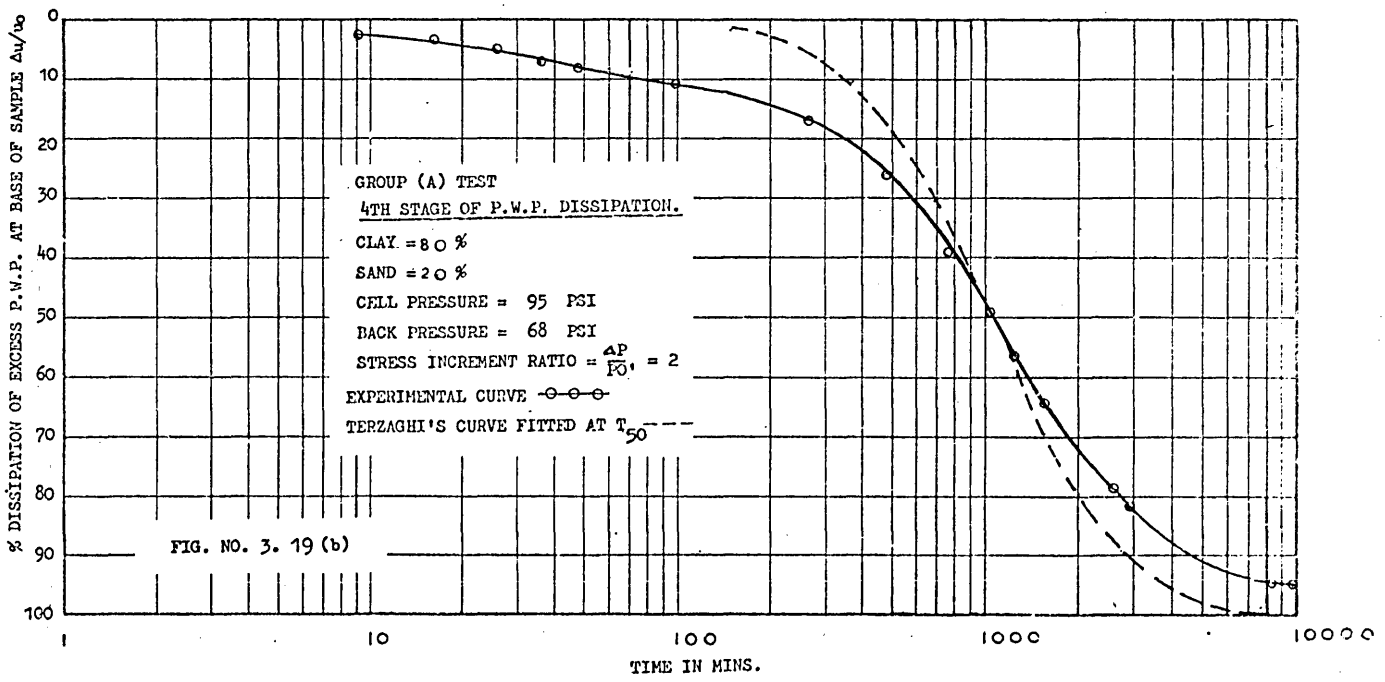

FIG. NO. 3. 19 (b)

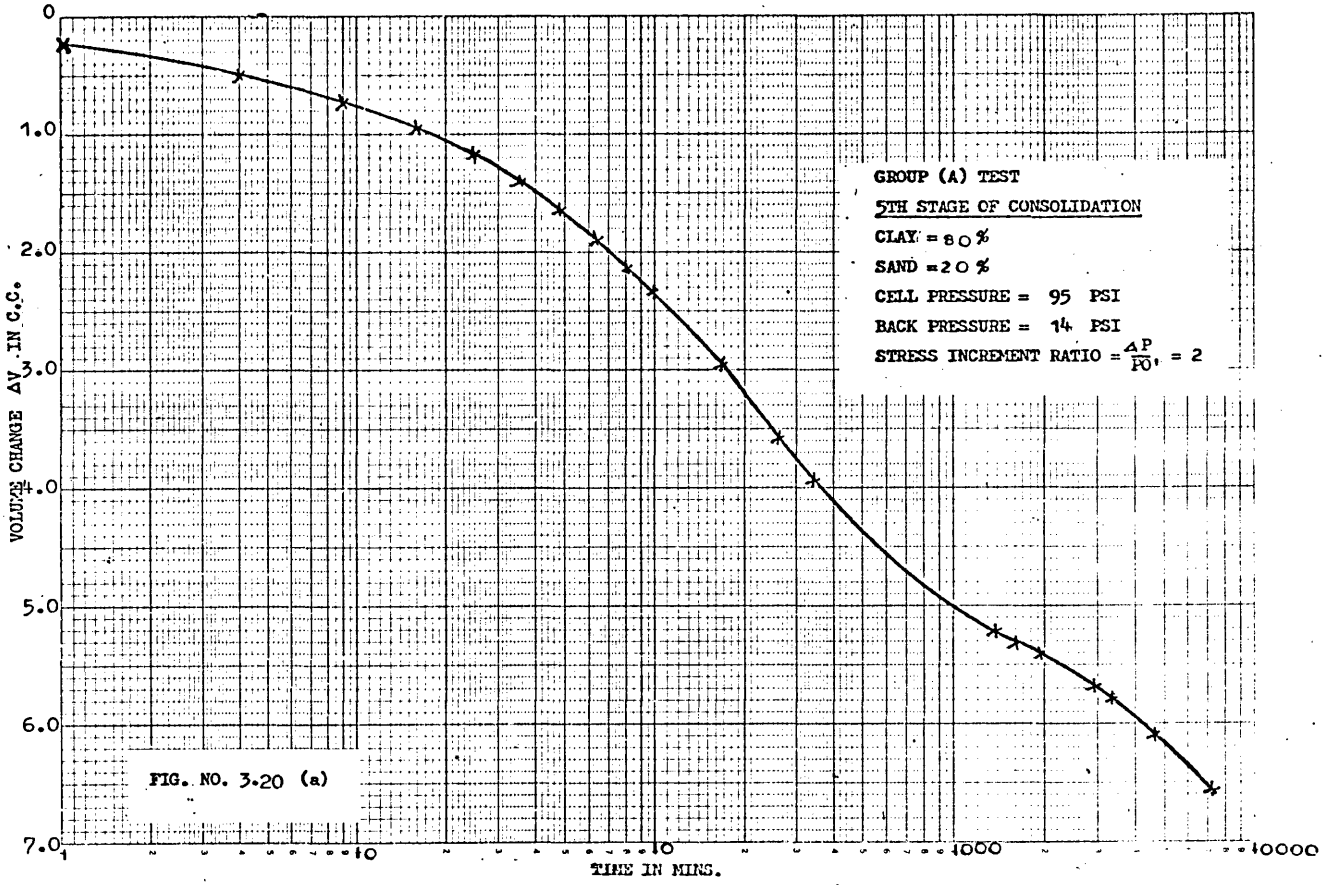

FIG. NO. 3.20 (a)

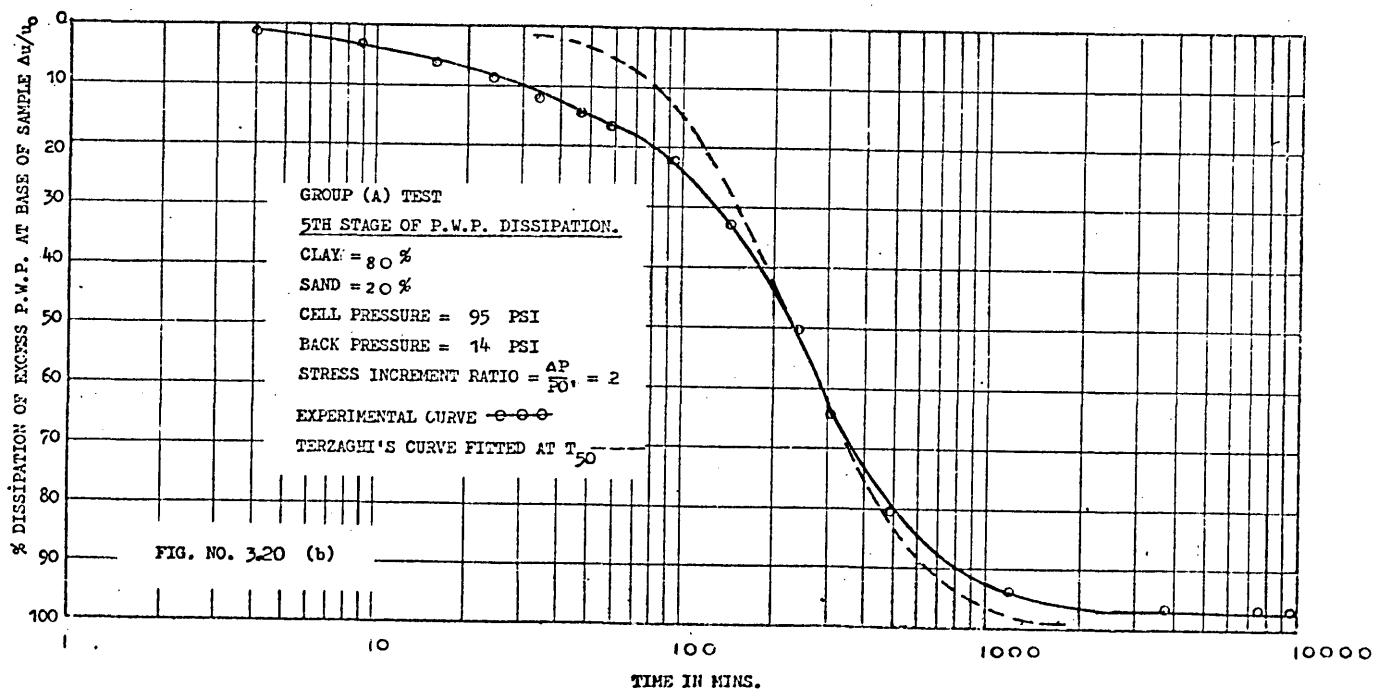

FIG. NO. 3.20 (b)

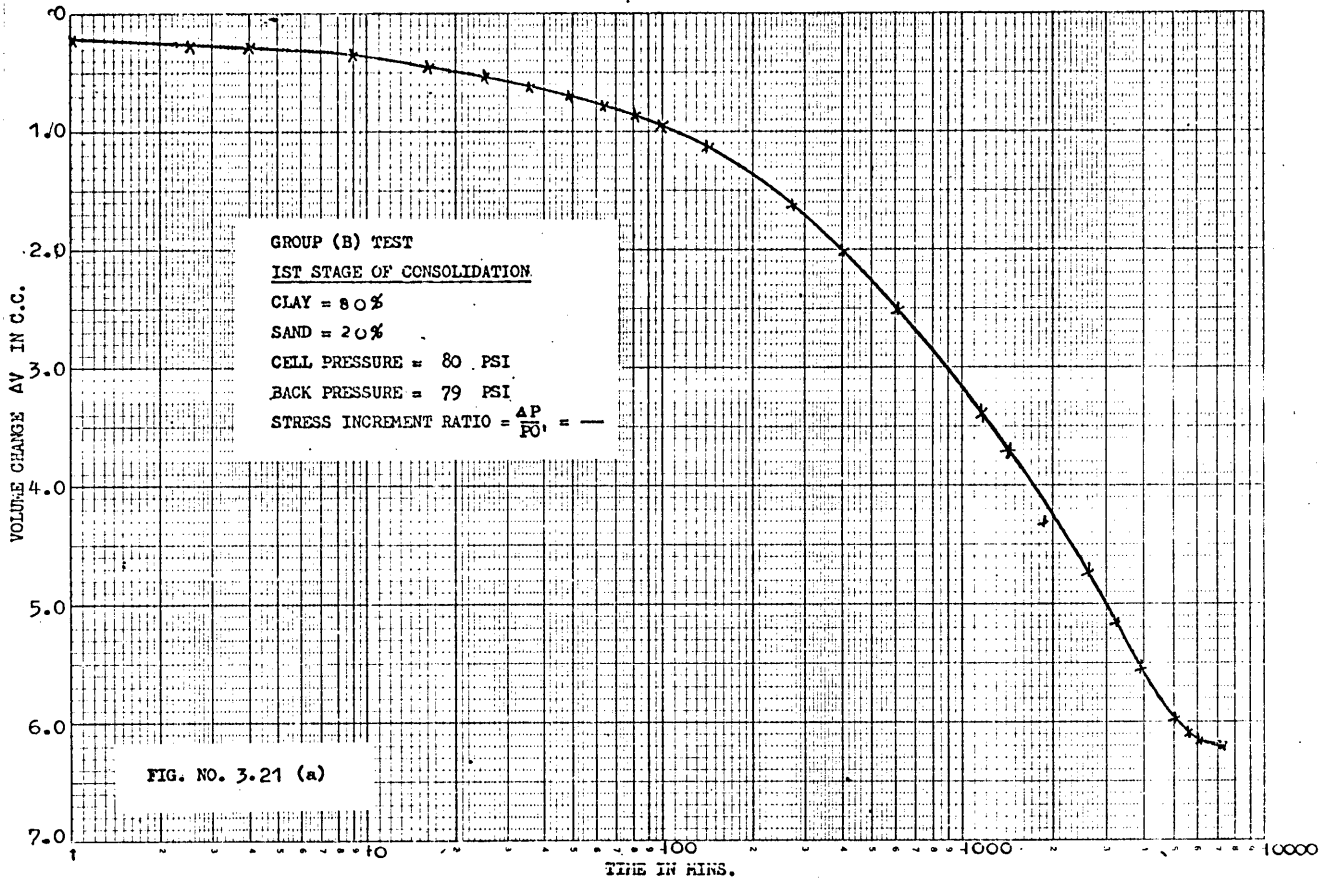
VOLUME CHANGE ΔV IN C.C.
TIME IN MINS.
GROUP (B) TEST
IST STAGE OF CONSOLIDATION
CLAY = 80%
SAND = 20%
CELL PRESSURE = 80 PSI
BACK PRESSURE = 79 PSI
STRESS INCREMENT RATIO = ΔP/P0 = —
FIG. NO. 3.21 (a)

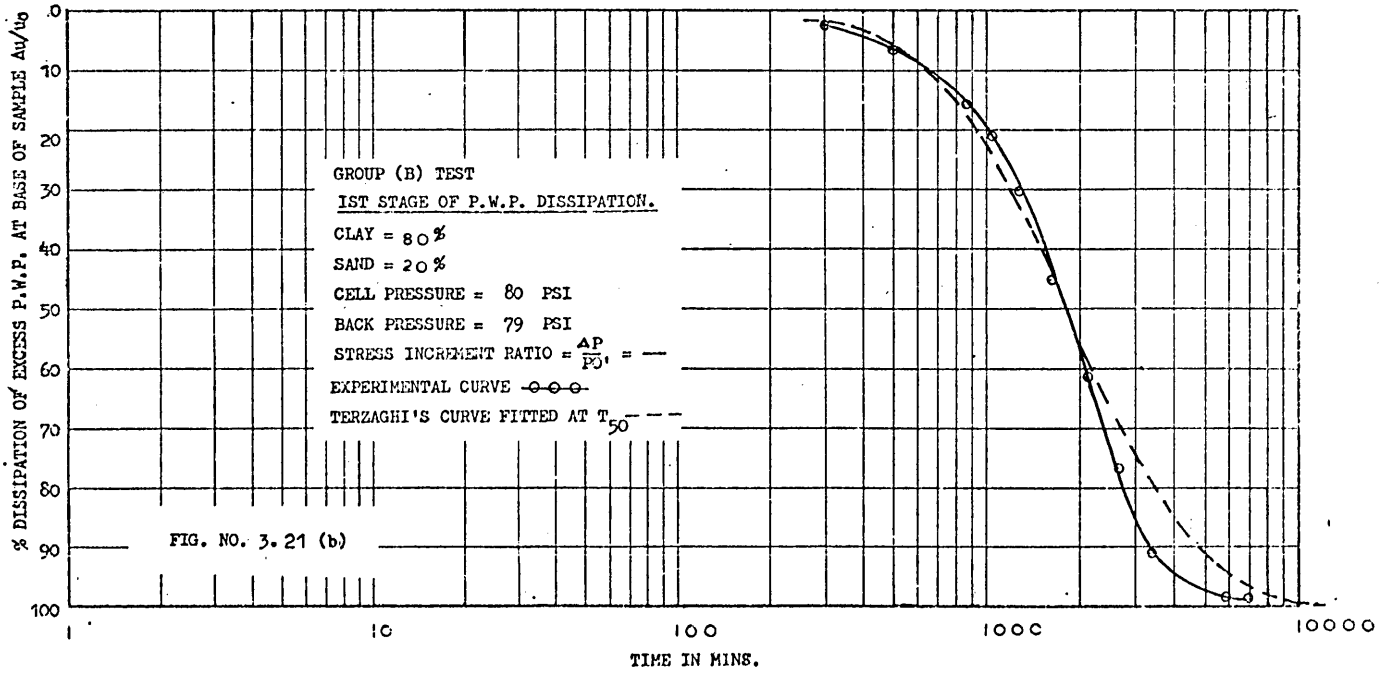
% DISSIPATION OF EXCESS P.W.P. AT BASE OF SAMPLE Δu/u0
TIME IN MINS.
GROUP (B) TEST
IST STAGE OF P.W.P. DISSIPATION.
CLAY = 80%
SAND = 20%
CELL PRESSURE = 80 PSI
BACK PRESSURE = 79 PSI
STRESS INCREMENT RATIO = ΔP/P0 = —
EXPERIMENTAL CURVE -o-o-o-
TERZAGHI'S CURVE FITTED AT T50 - - -
FIG. NO. 3.21 (b)

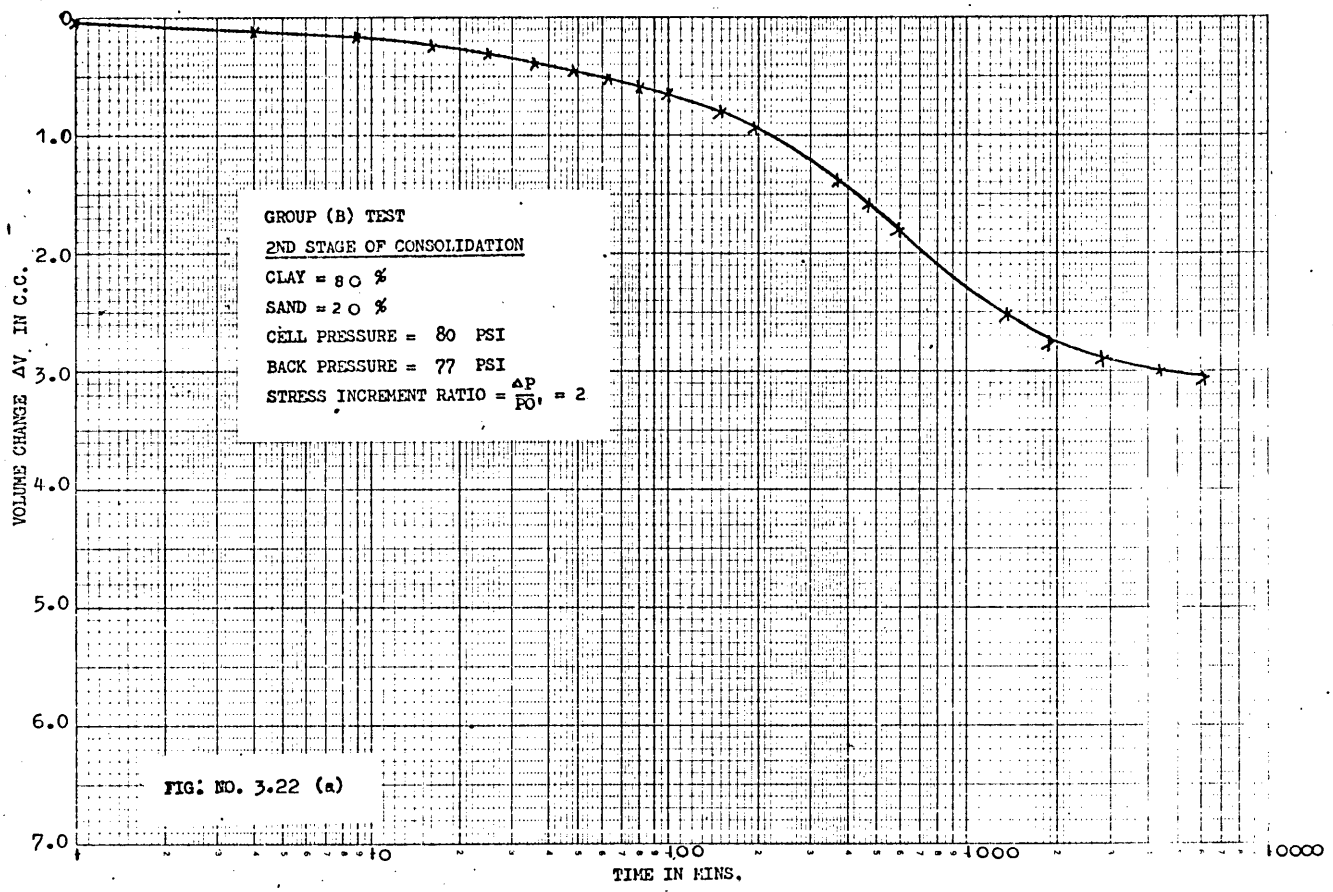
VOLUME CHANGE ΔV IN C.C.
0
1.0
2.0
3.0
4.0
5.0
6.0
7.0
GROUP (B) TEST
2ND STAGE OF CONSOLIDATION
CLAY = 80 %
SAND = 20 %
CELL PRESSURE = 80 PSI
BACK PRESSURE = 77 PSI
STRESS INCREMENT RATIO = ΔP/P0, = 2
FIG. NO. 3.22 (a)
1
10
100
1000
10000
TIME IN MINS.

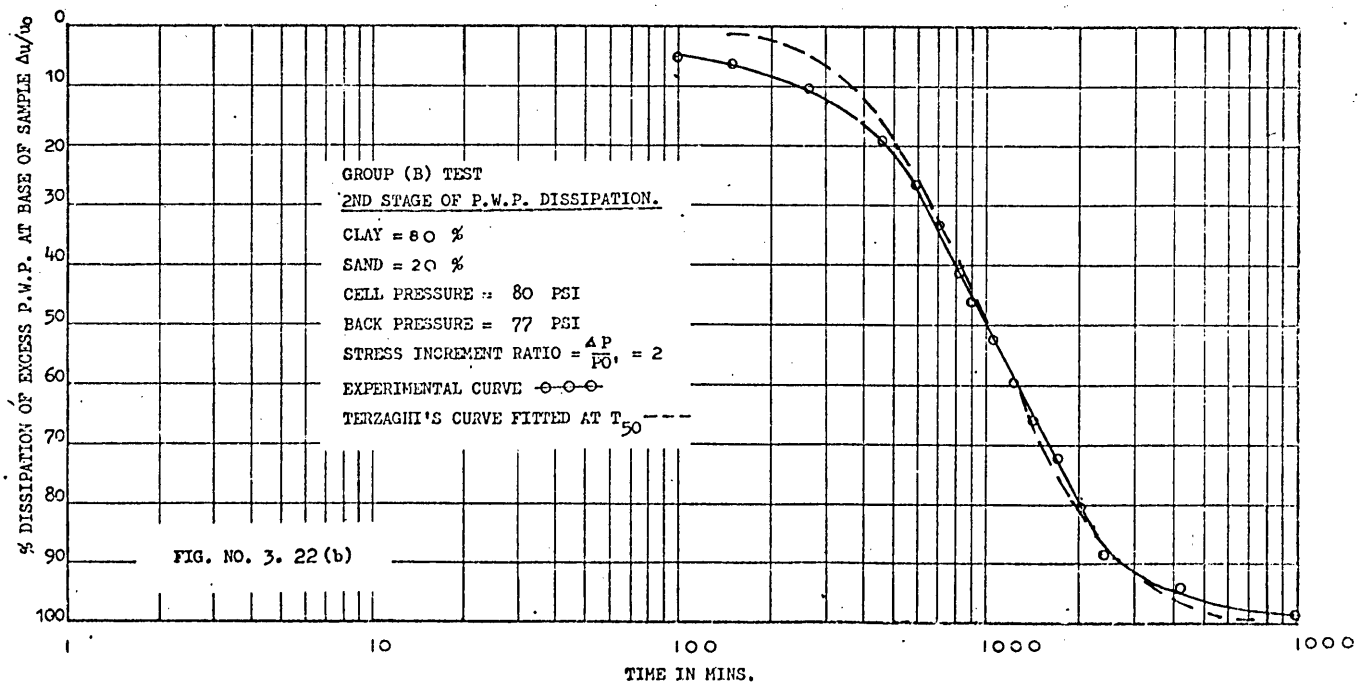
% DISSIPATION OF EXCESS P.W.P. AT BASE OF SAMPLE Δu/u0
0
10
20
30
40
50
60
70
80
90
100
GROUP (B) TEST
2ND STAGE OF P.W.P. DISSIPATION.
CLAY = 80 %
SAND = 20 %
CELL PRESSURE = 80 PSI
BACK PRESSURE = 77 PSI
STRESS INCREMENT RATIO = ΔP/P0, = 2
EXPERIMENTAL CURVE
TERZAGHI'S CURVE FITTED AT T50
FIG. NO. 3. 22 (b)
1
10
100
1000
10000
TIME IN MINS.

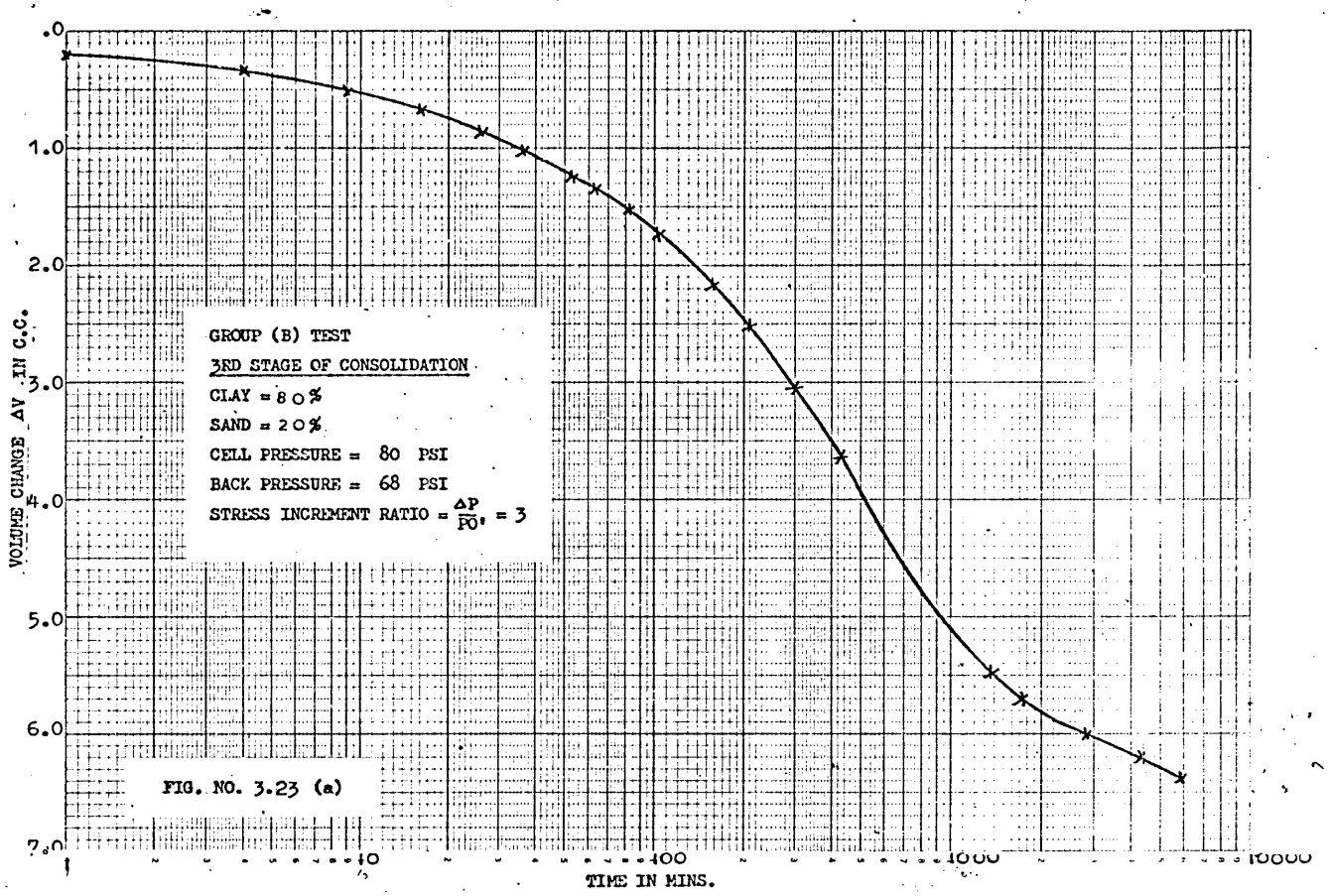

FIG. NO. 3.23 (a)

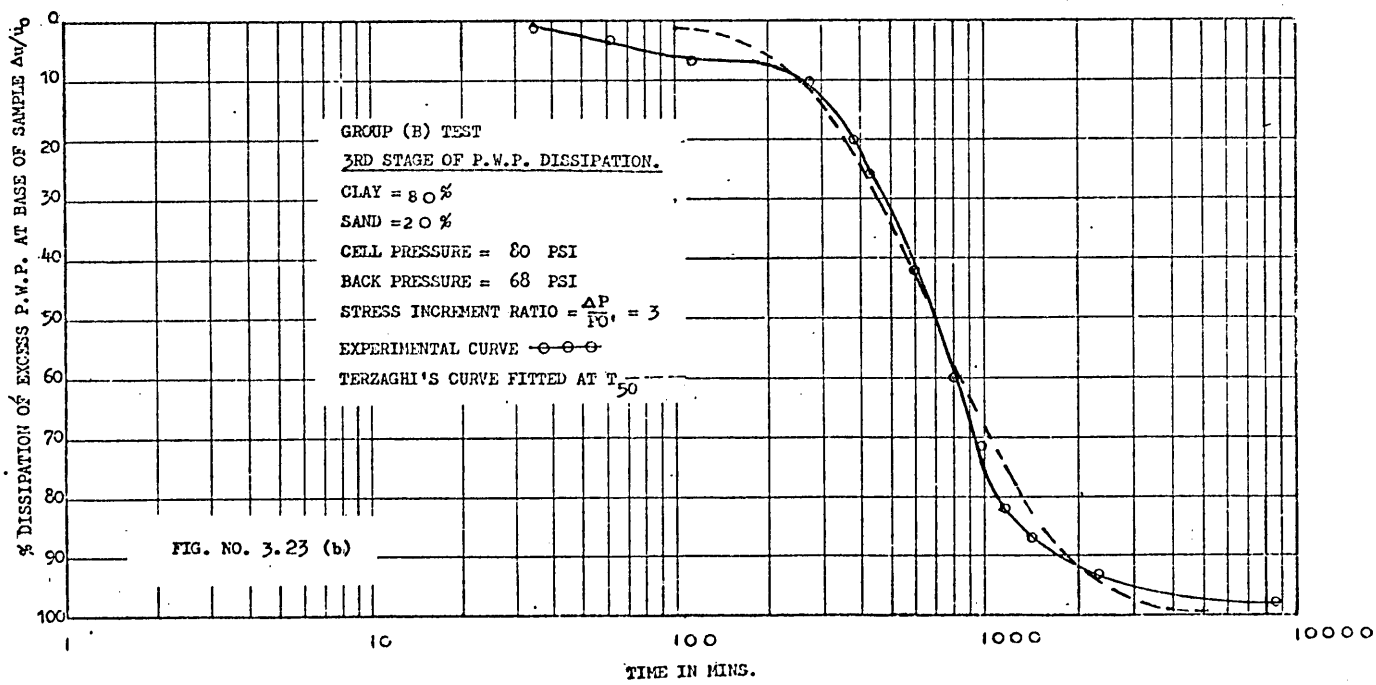

FIG. NO. 3.23 (b)

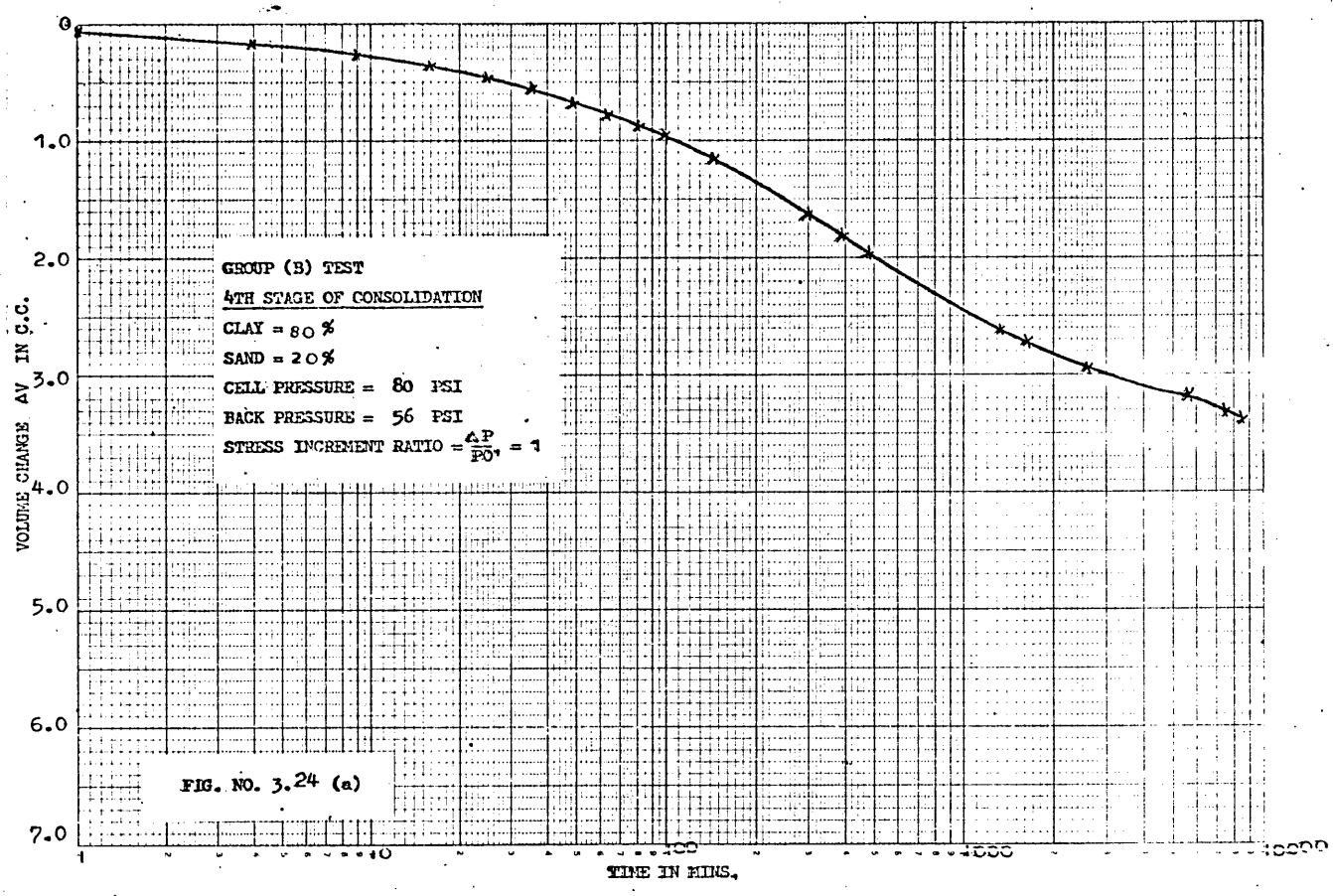

FIG. NO. 3.24 (a)

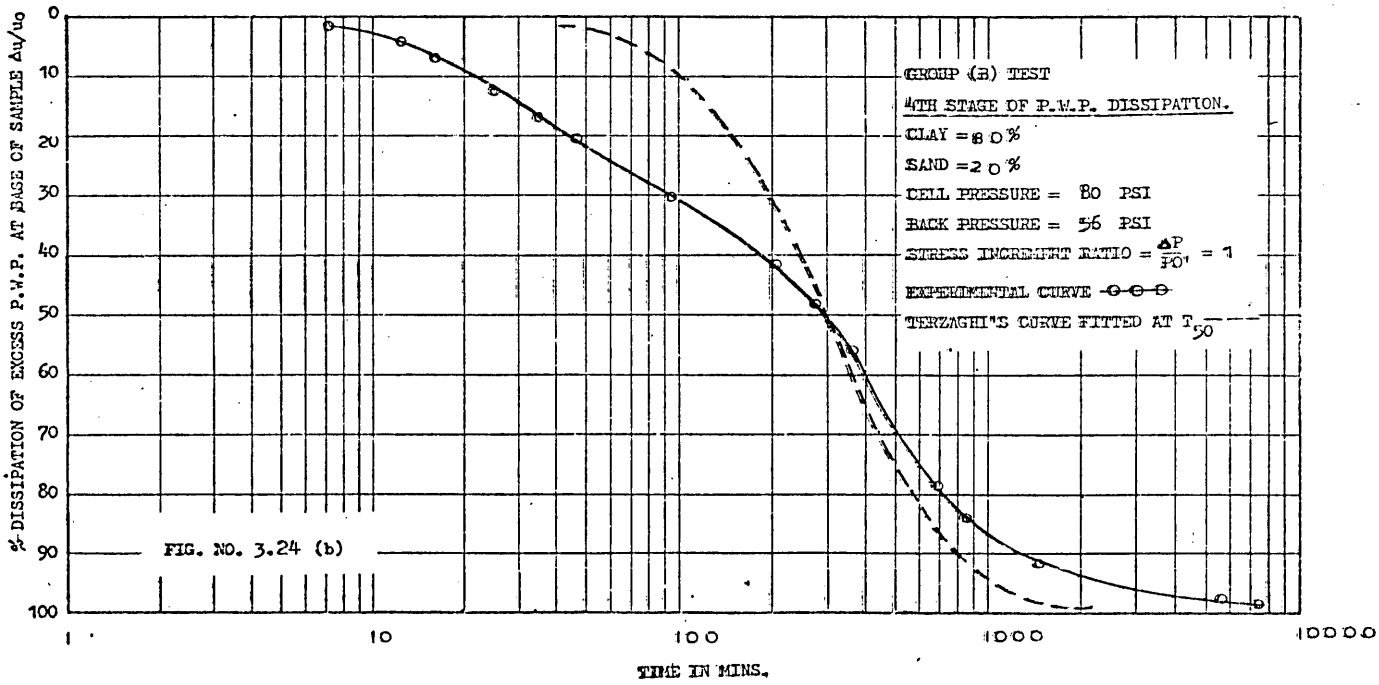

FIG. NO. 3.24 (b)

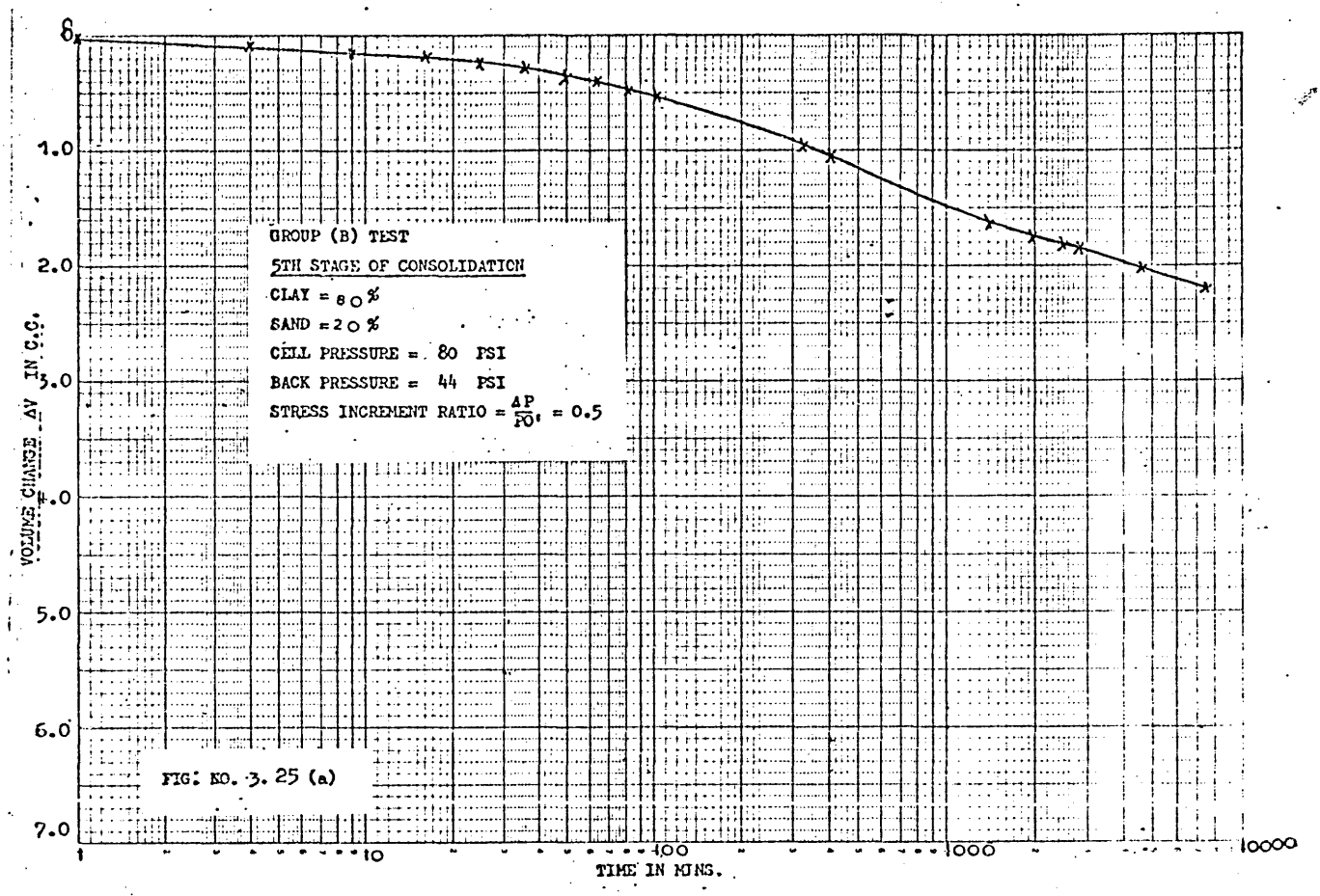

FIG. NO. 3.25 (a)

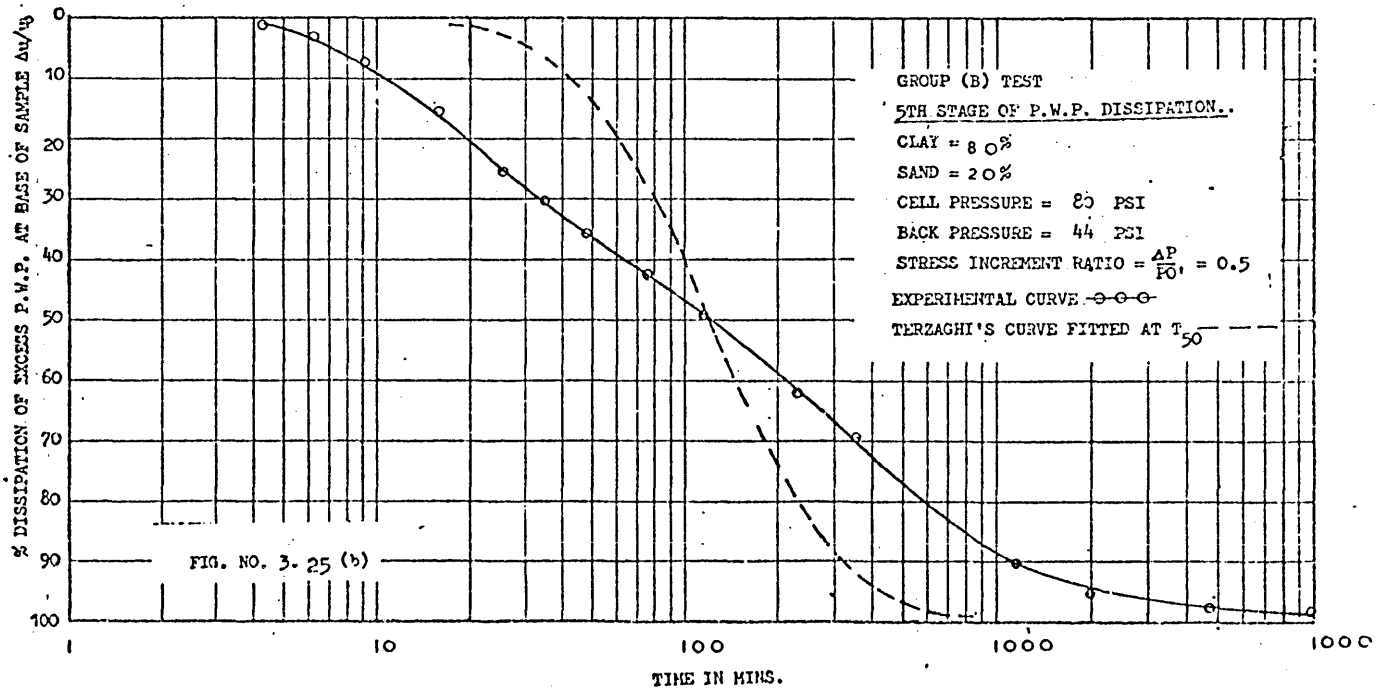

FIG. NO. 3.25 (b)

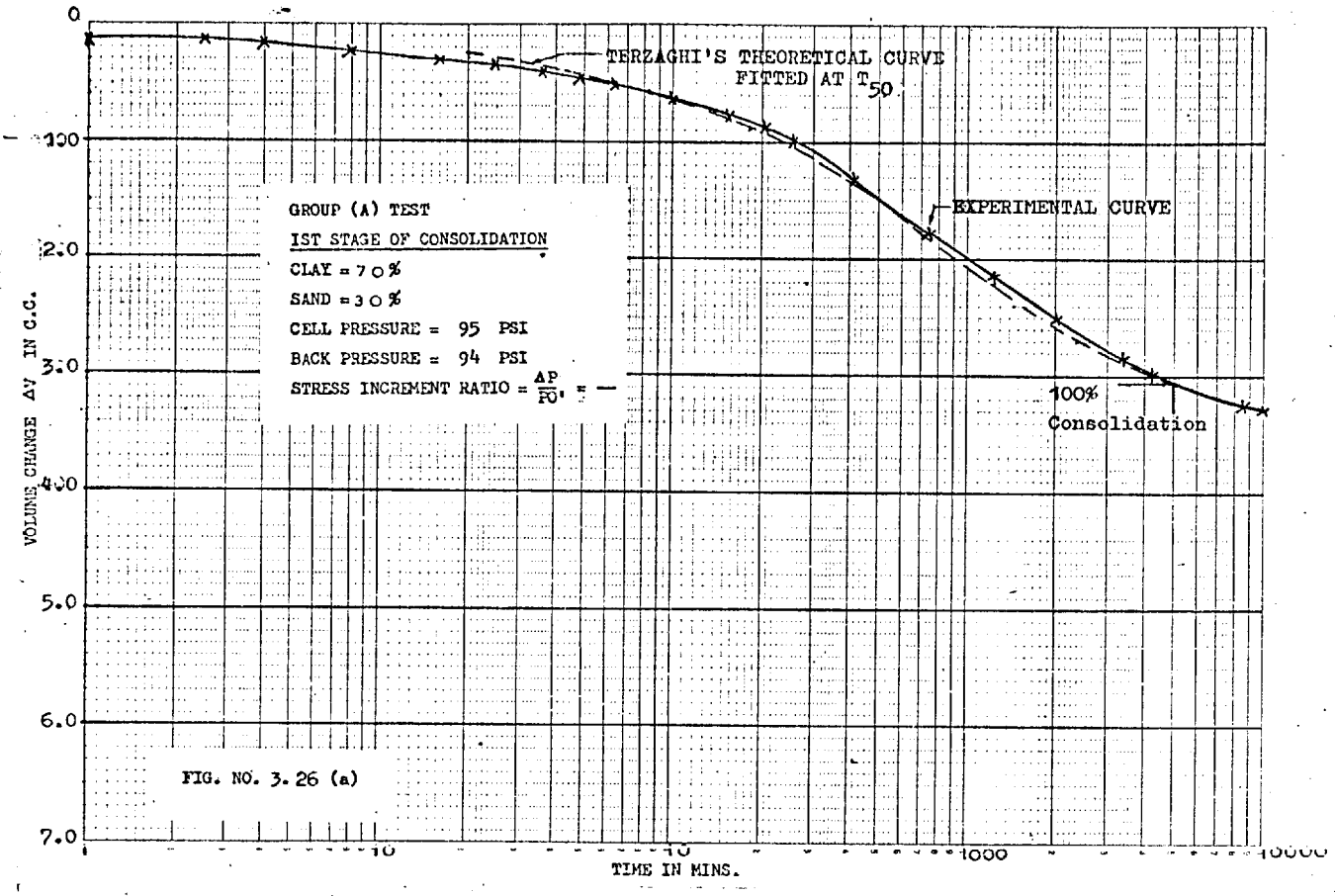

FIG. NO. 3.26 (a)

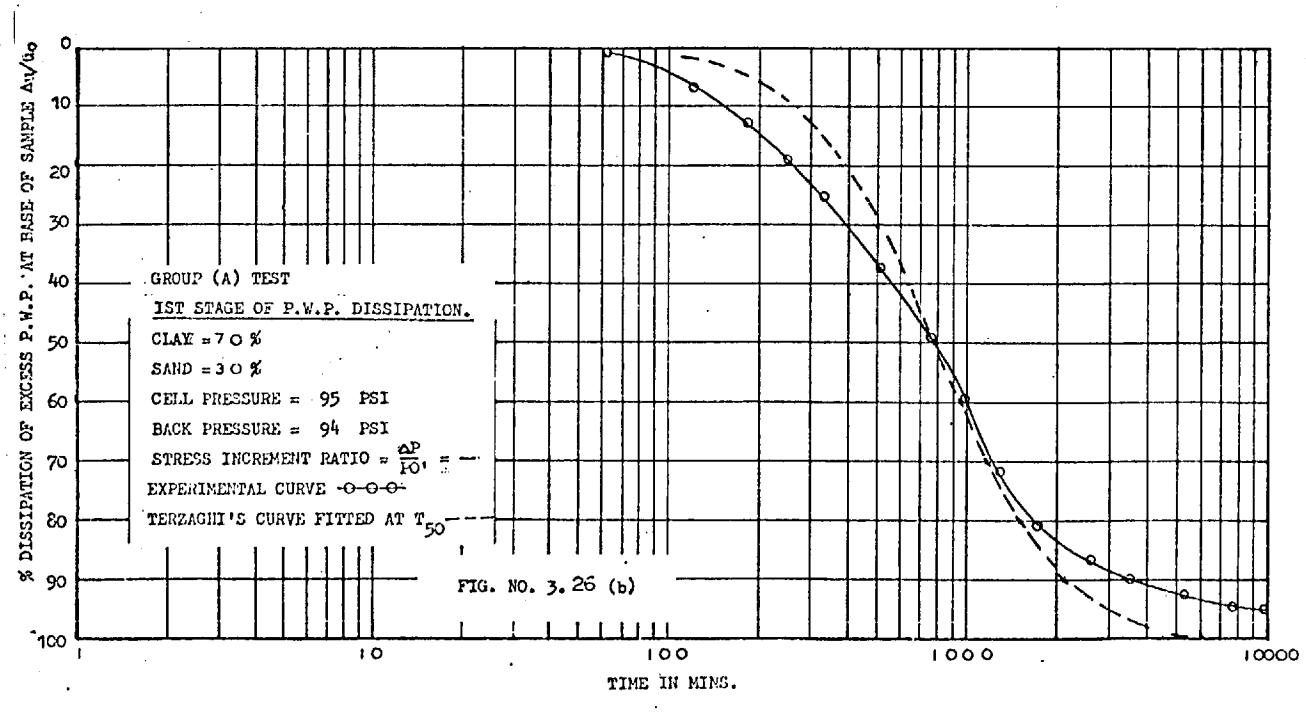

FIG. NO. 3.26 (b)

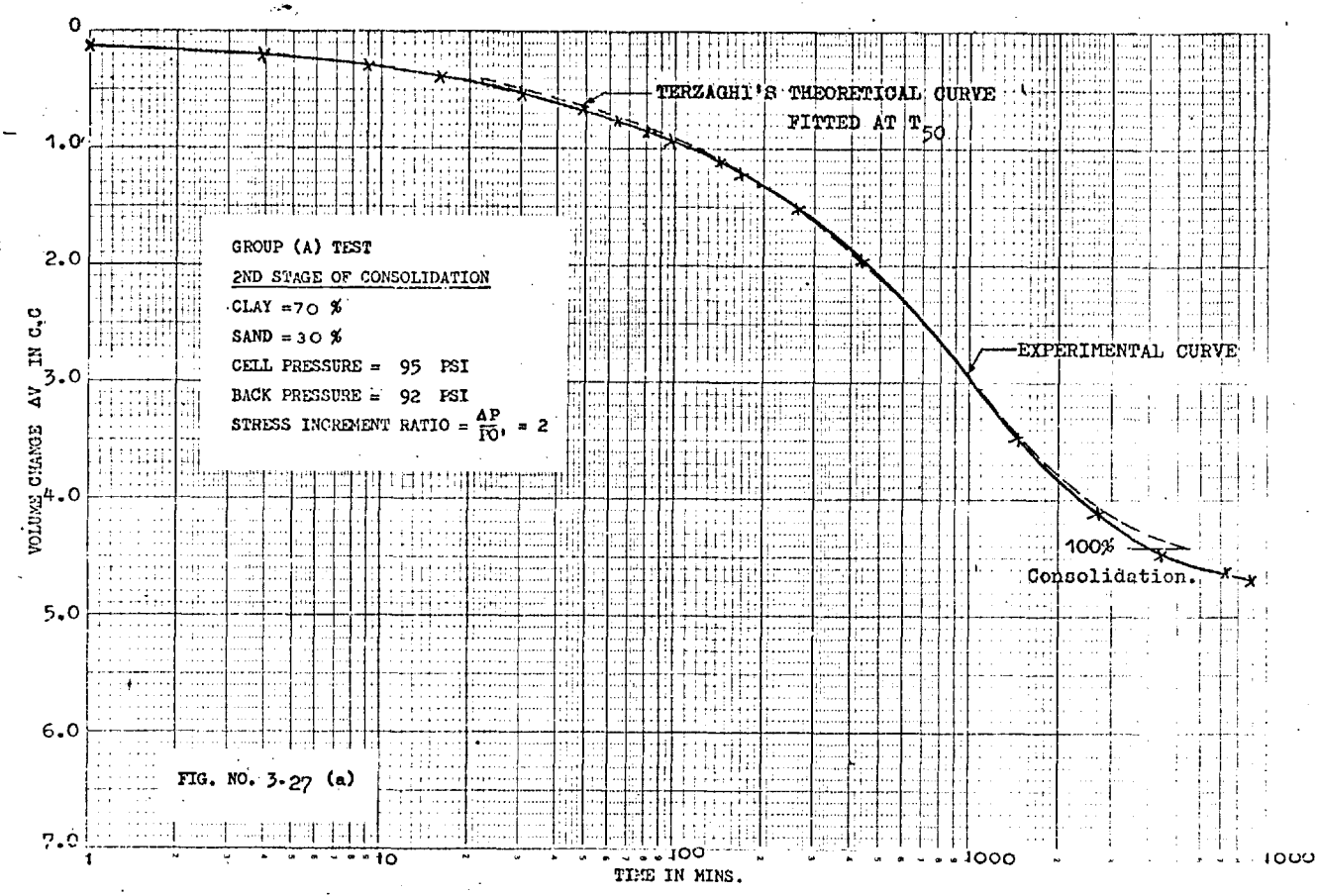

FIG. NO. 3.27 (a)

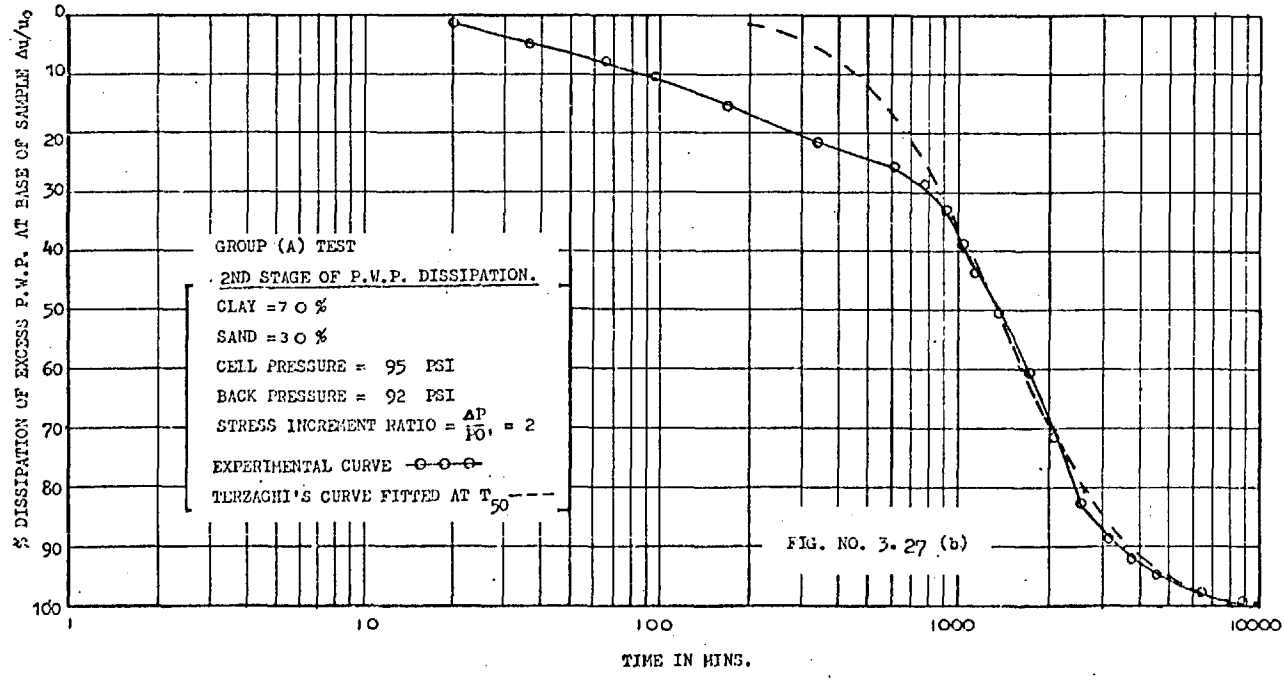

FIG. NO. 3.27 (b)

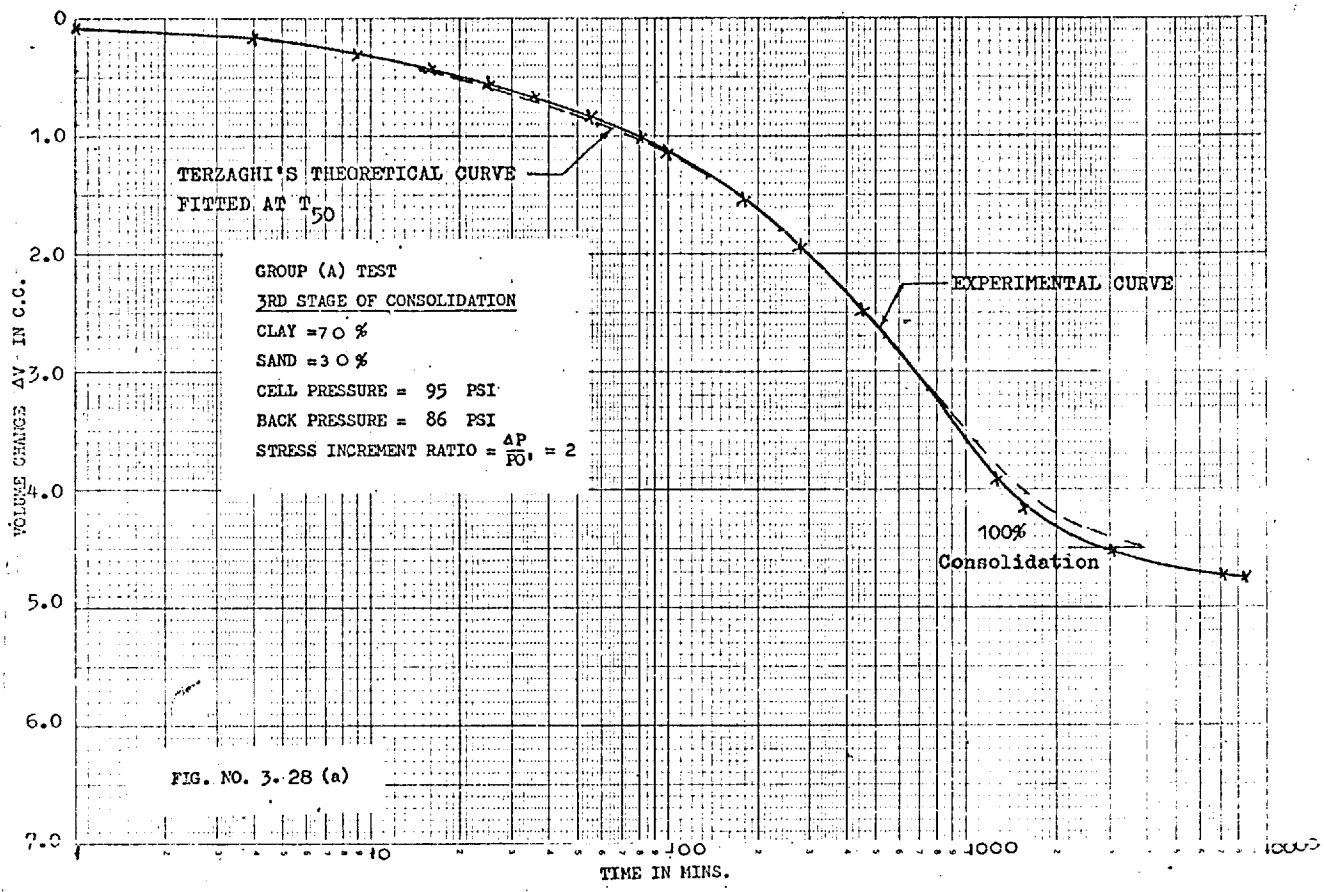

FIG. NO. 3.28 (a)

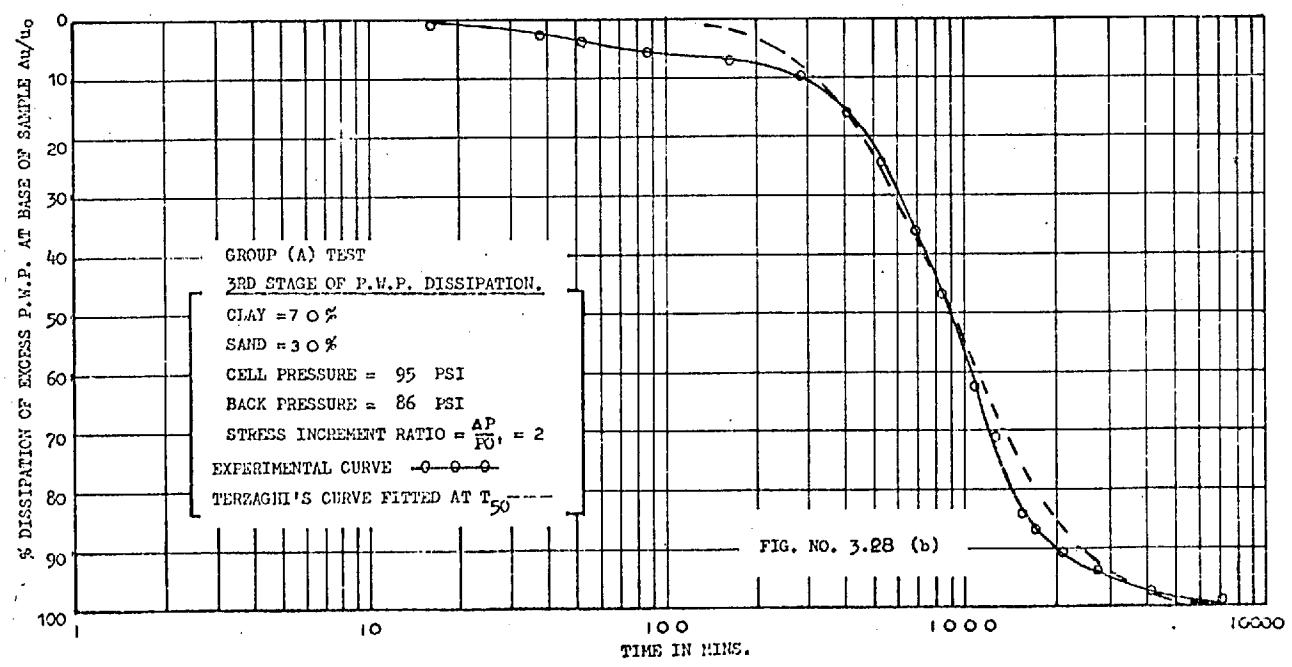

FIG. NO. 3.28 (b)

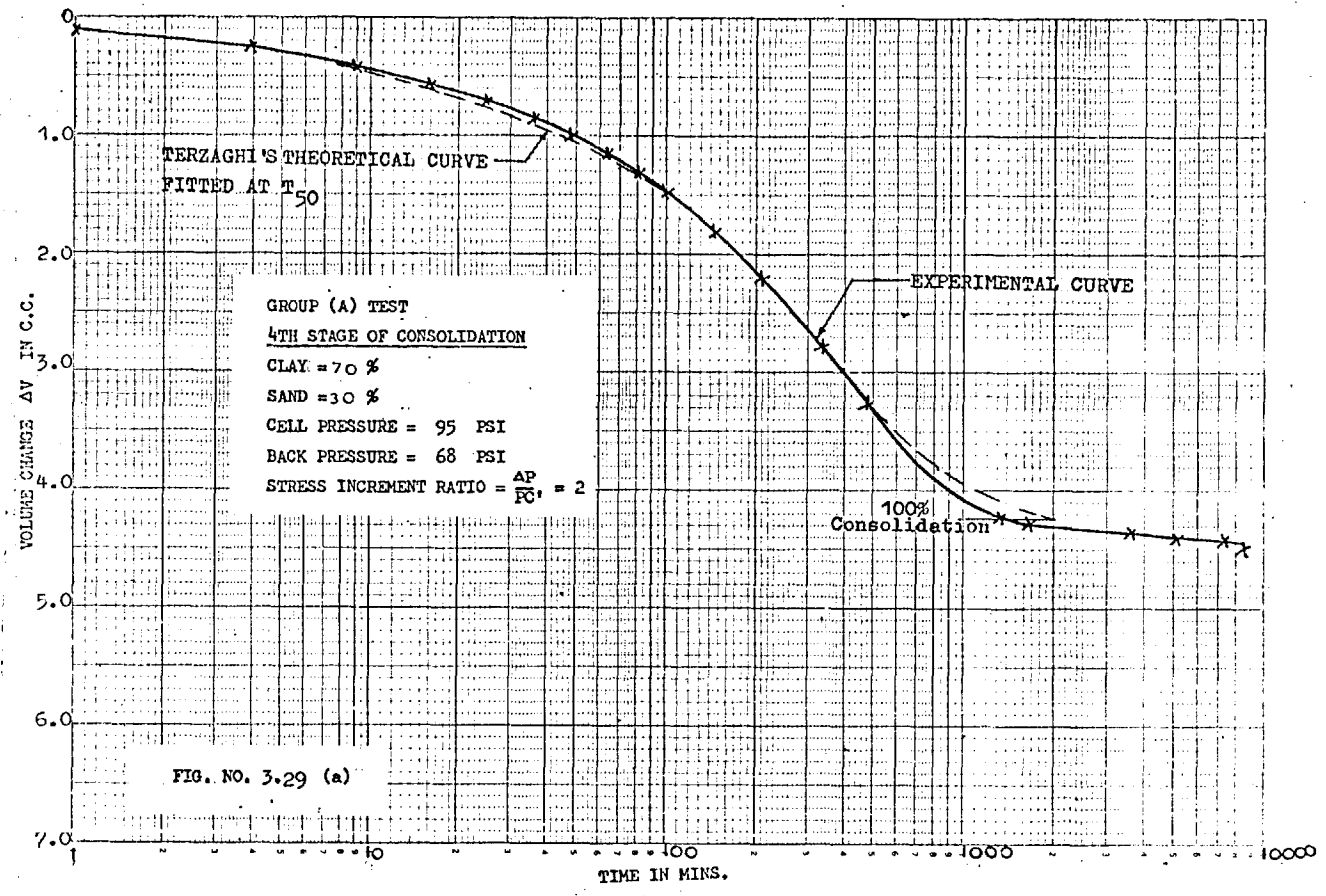

FIG. NO. 3.29 (a)

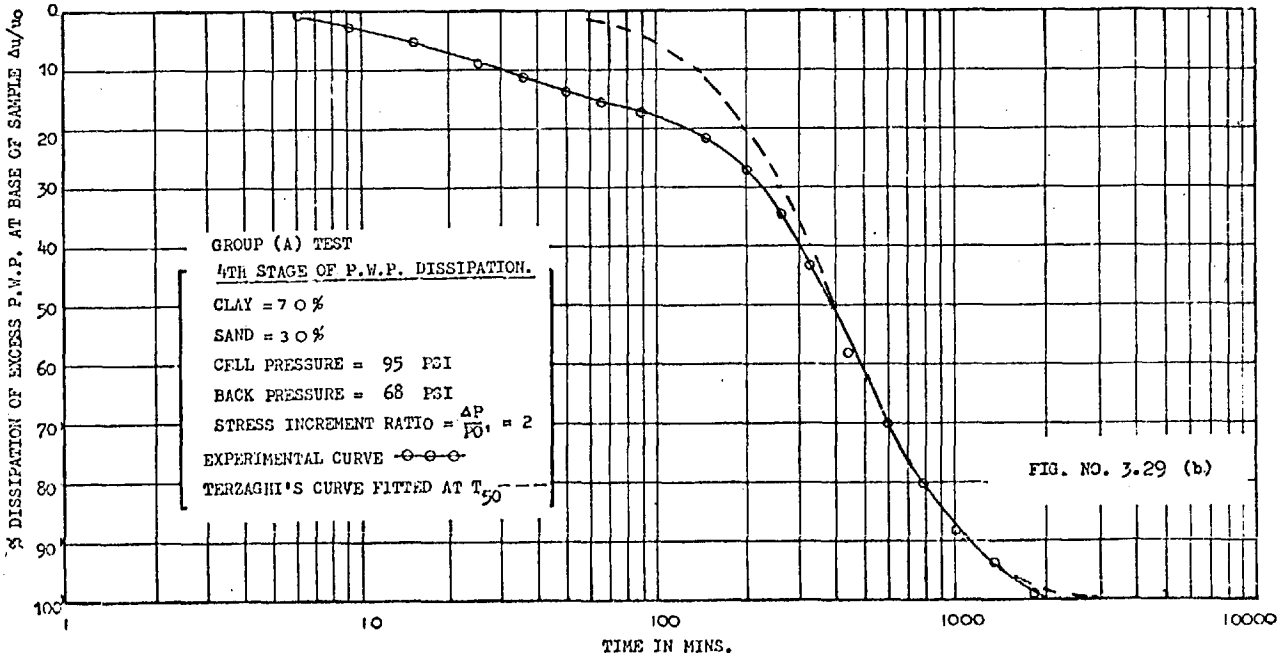

FIG. NO. 3.29 (b)

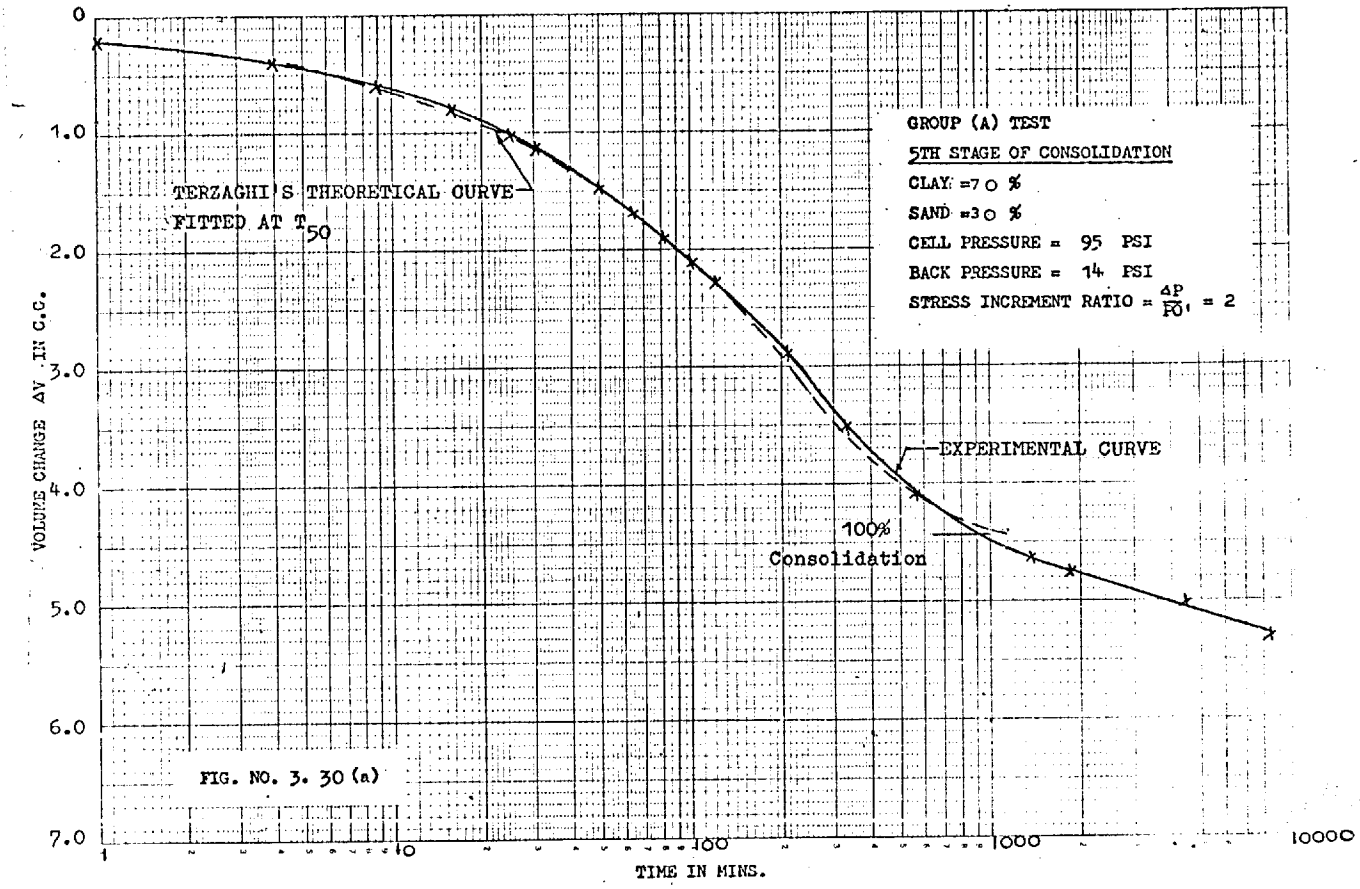

FIG. NO. 3. 30 (a)

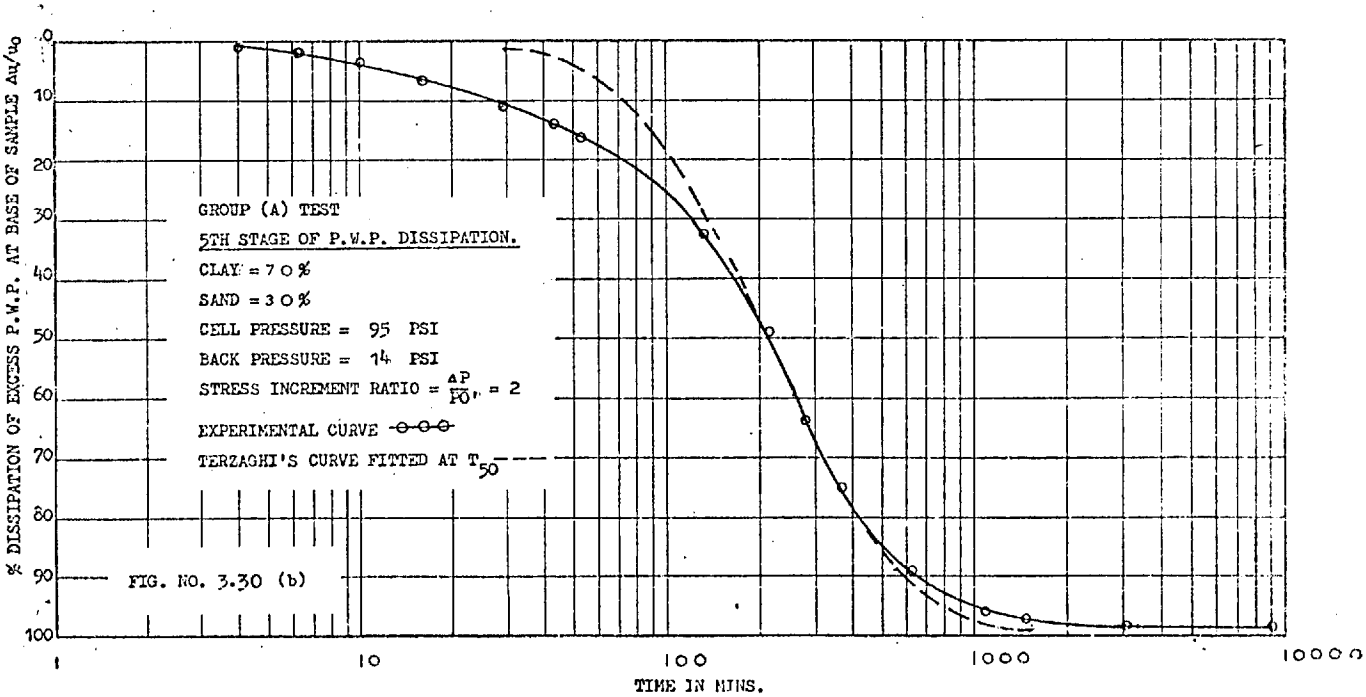

FIG. NO. 3.30 (b)

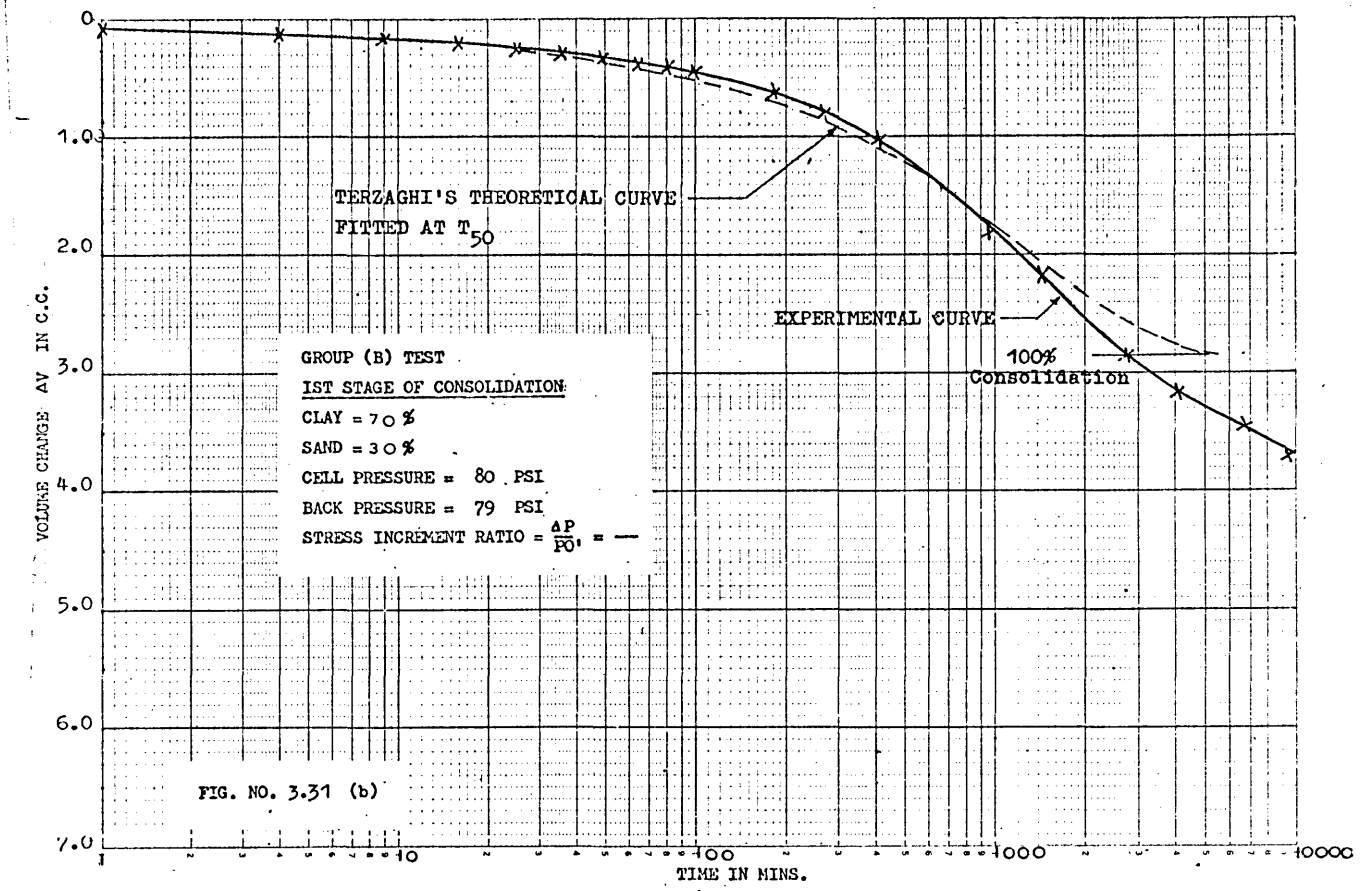

FIG. NO. 3.31 (b)

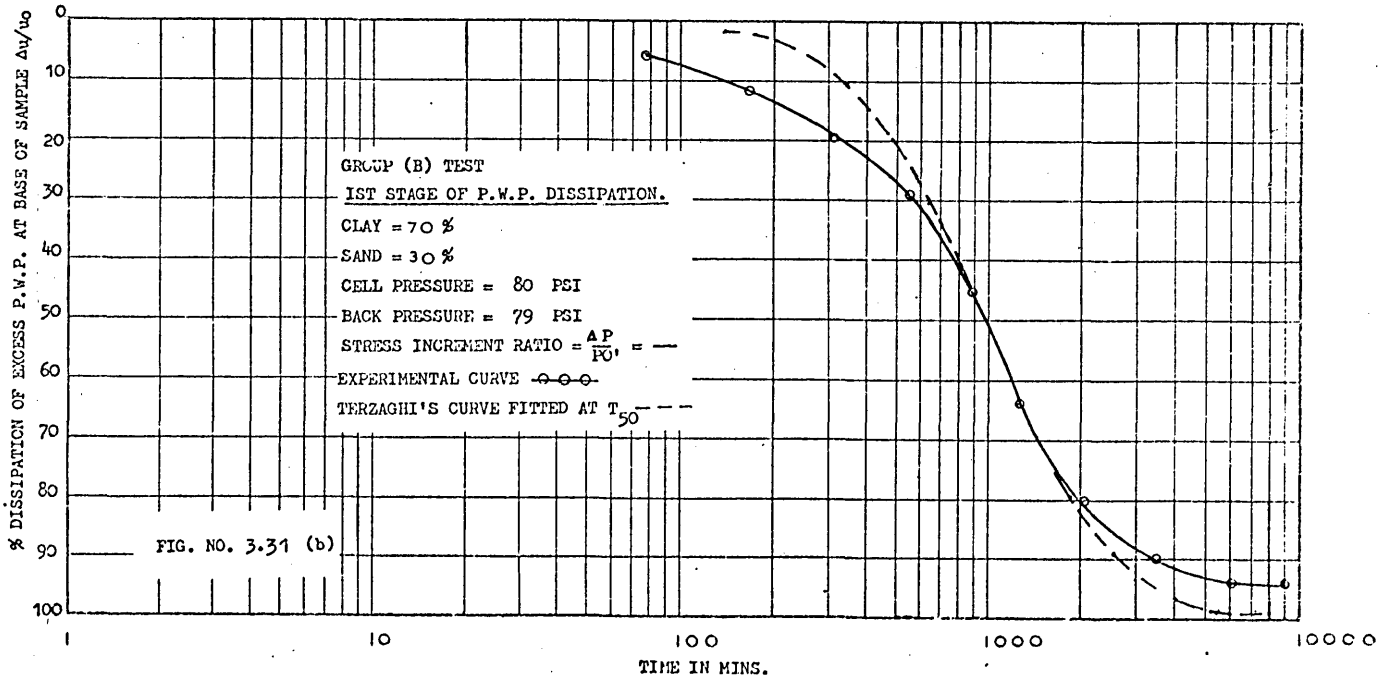

FIG. NO. 3.31 (b)

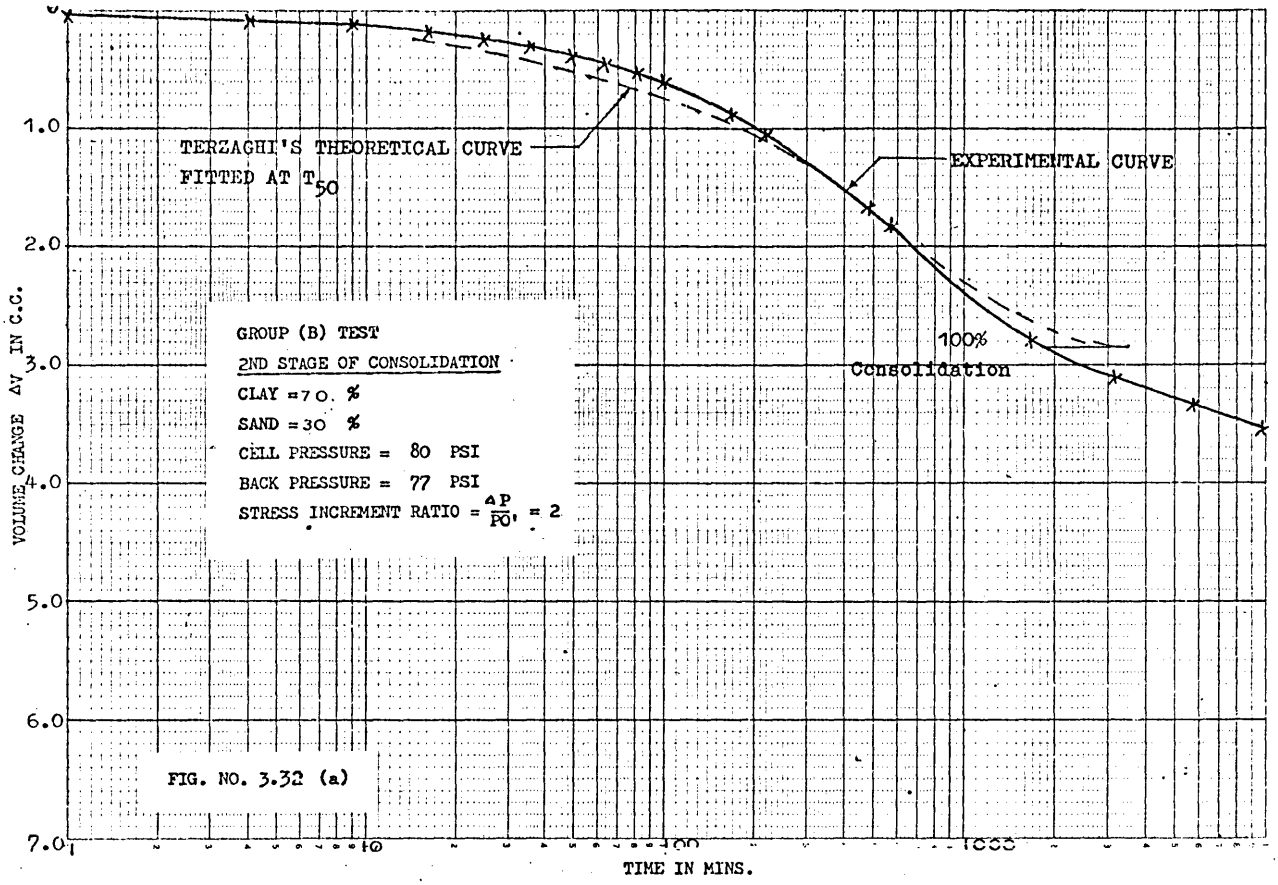

FIG. NO. 3.32 (a)

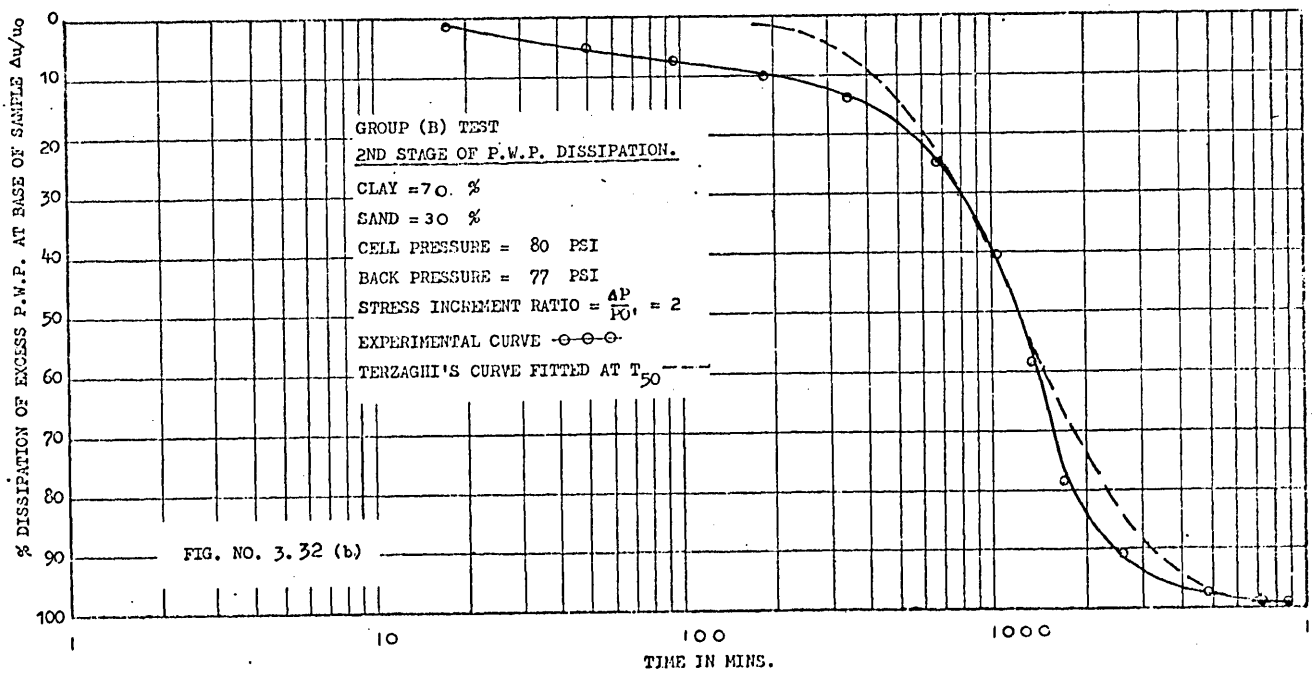

FIG. NO. 3.32 (b)

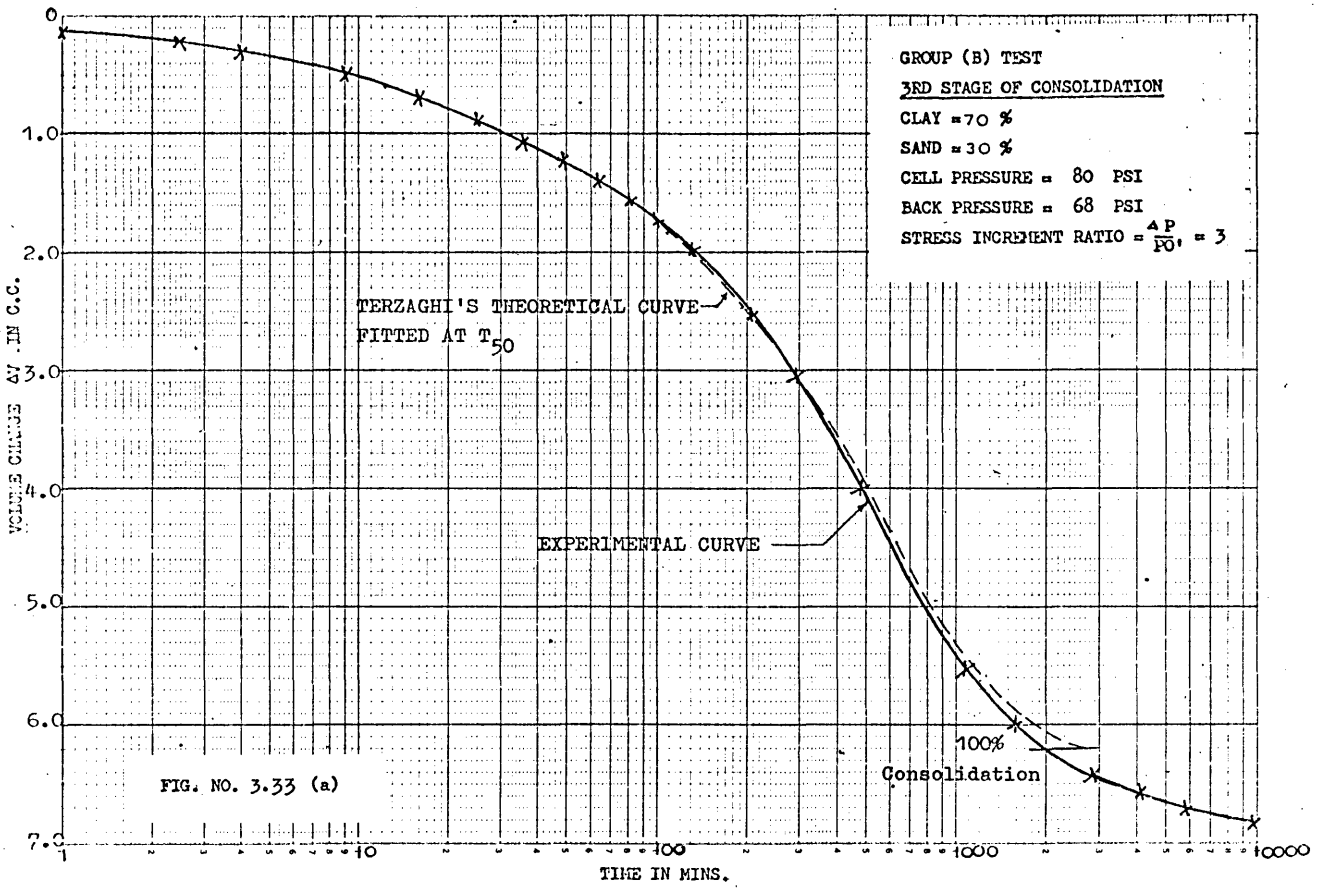
GROUP (B) TEST
3RD STAGE OF CONSOLIDATION
CLAY = 70 %
SAND = 30 %
CELL PRESSURE = 80 PSI
BACK PRESSURE = 68 PSI
STRESS INCREMENT RATIO = ΔP/P0 = 3
TERZAGHI'S THEORETICAL CURVE FITTED AT T50
EXPERIMENTAL CURVE
100% Consolidation
FIG. NO. 3.33 (a)
VOLUME CHANGE Δv IN C.C.
TIME IN MINS.

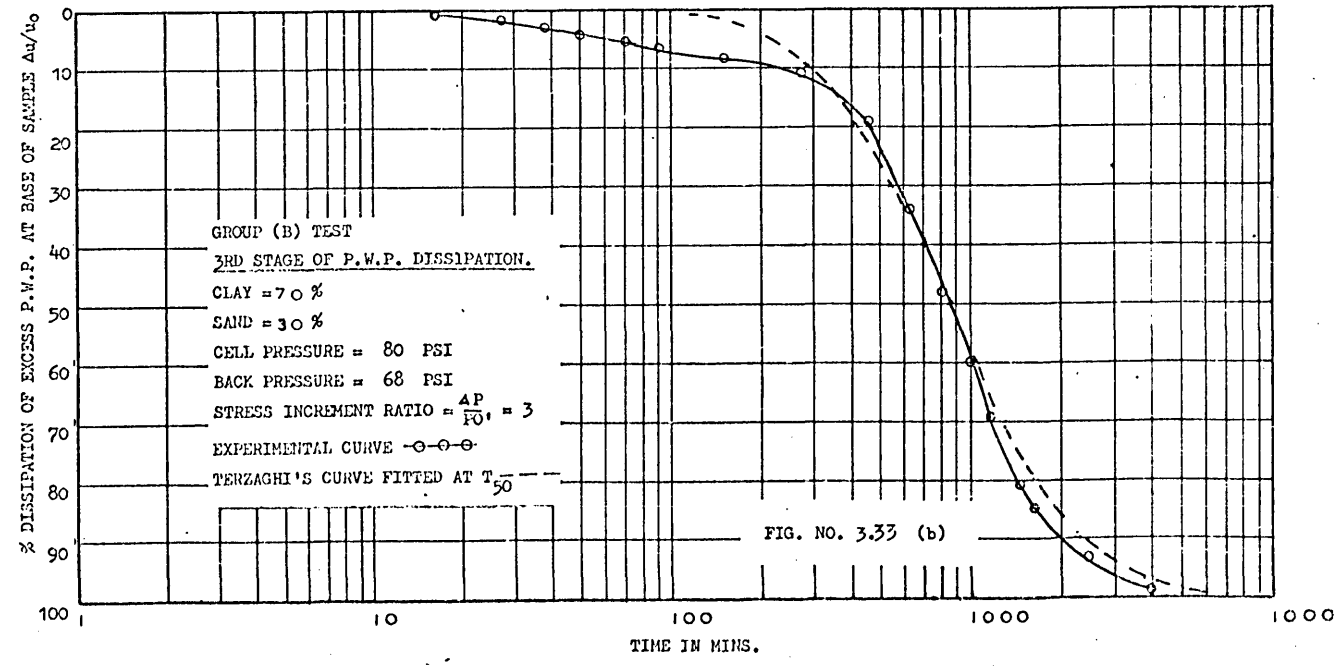
GROUP (B) TEST
3RD STAGE OF P.W.P. DISSIPATION.
CLAY = 70 %
SAND = 30 %
CELL PRESSURE = 80 PSI
BACK PRESSURE = 68 PSI
STRESS INCREMENT RATIO = ΔP/P0 = 3
EXPERIMENTAL CURVE
TERZAGHI'S CURVE FITTED AT T50
FIG. NO. 3.33 (b)
% DISSIPATION OF EXCESS P.W.P. AT BASE OF SAMPLE Δu/uo
TIME IN MINS.

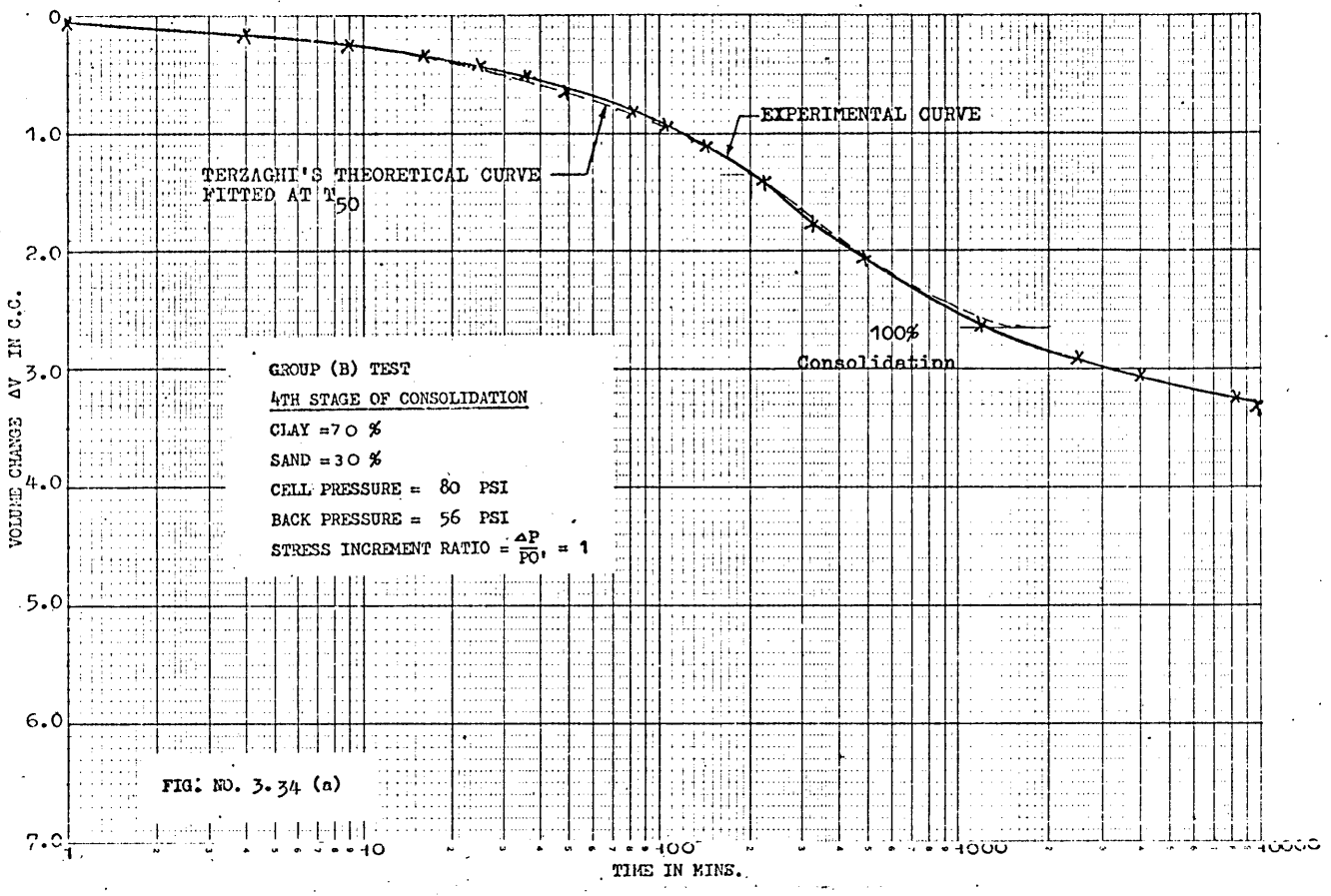

FIG. NO. 3.34 (a)

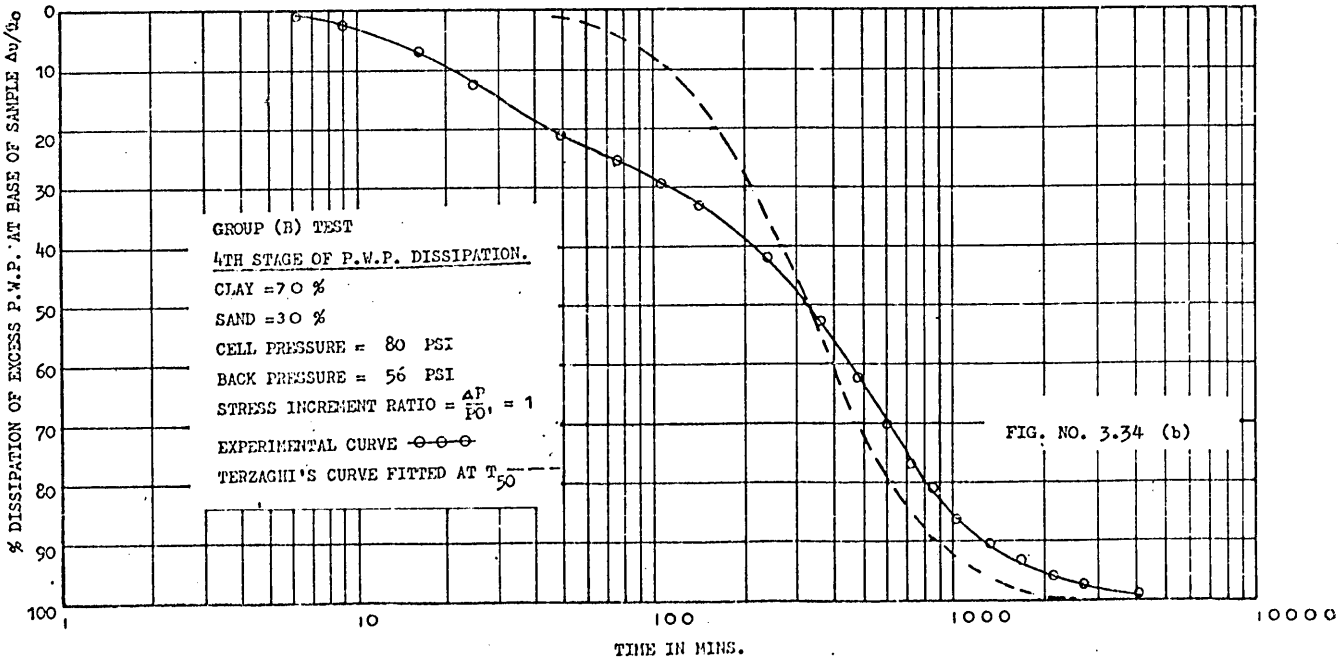

FIG. NO. 3.34 (b)

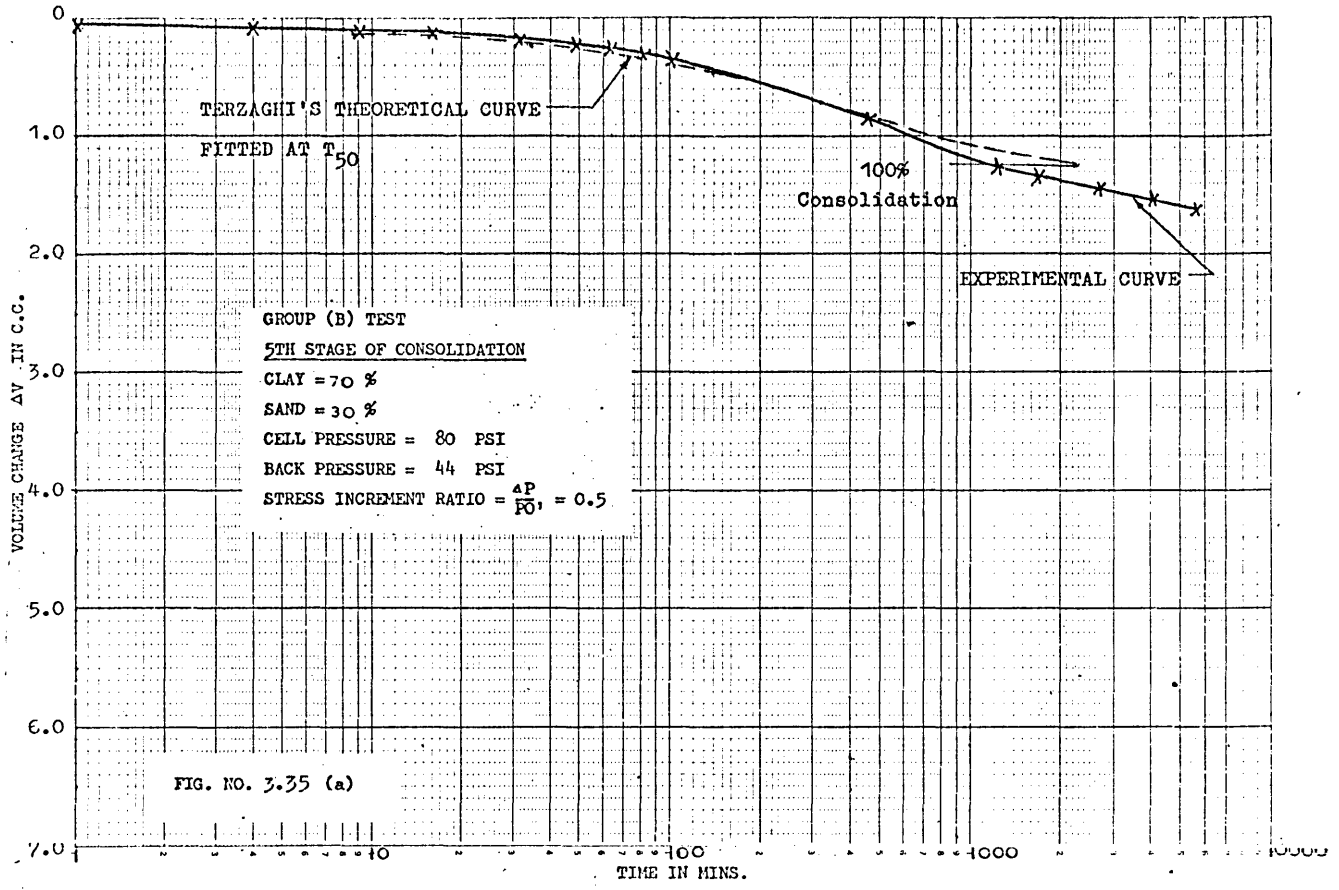

FIG. NO. 3.35 (a)

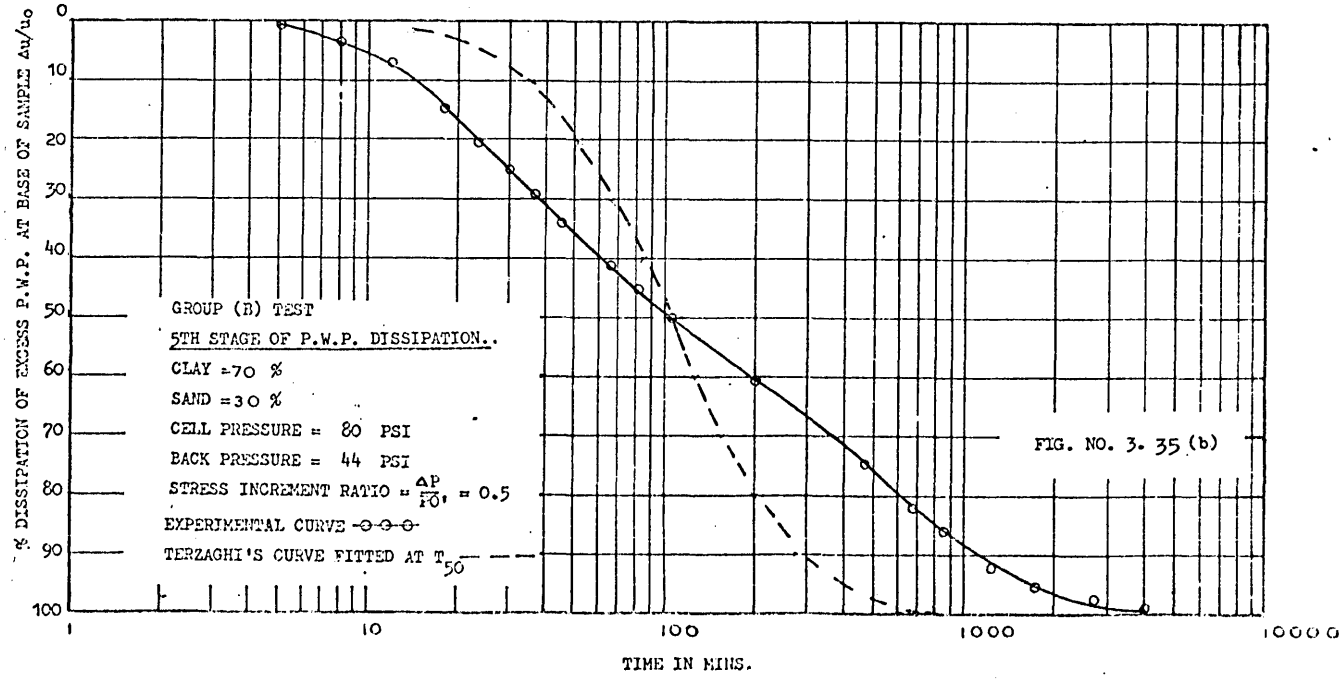

FIG. NO. 3. 35 (b)

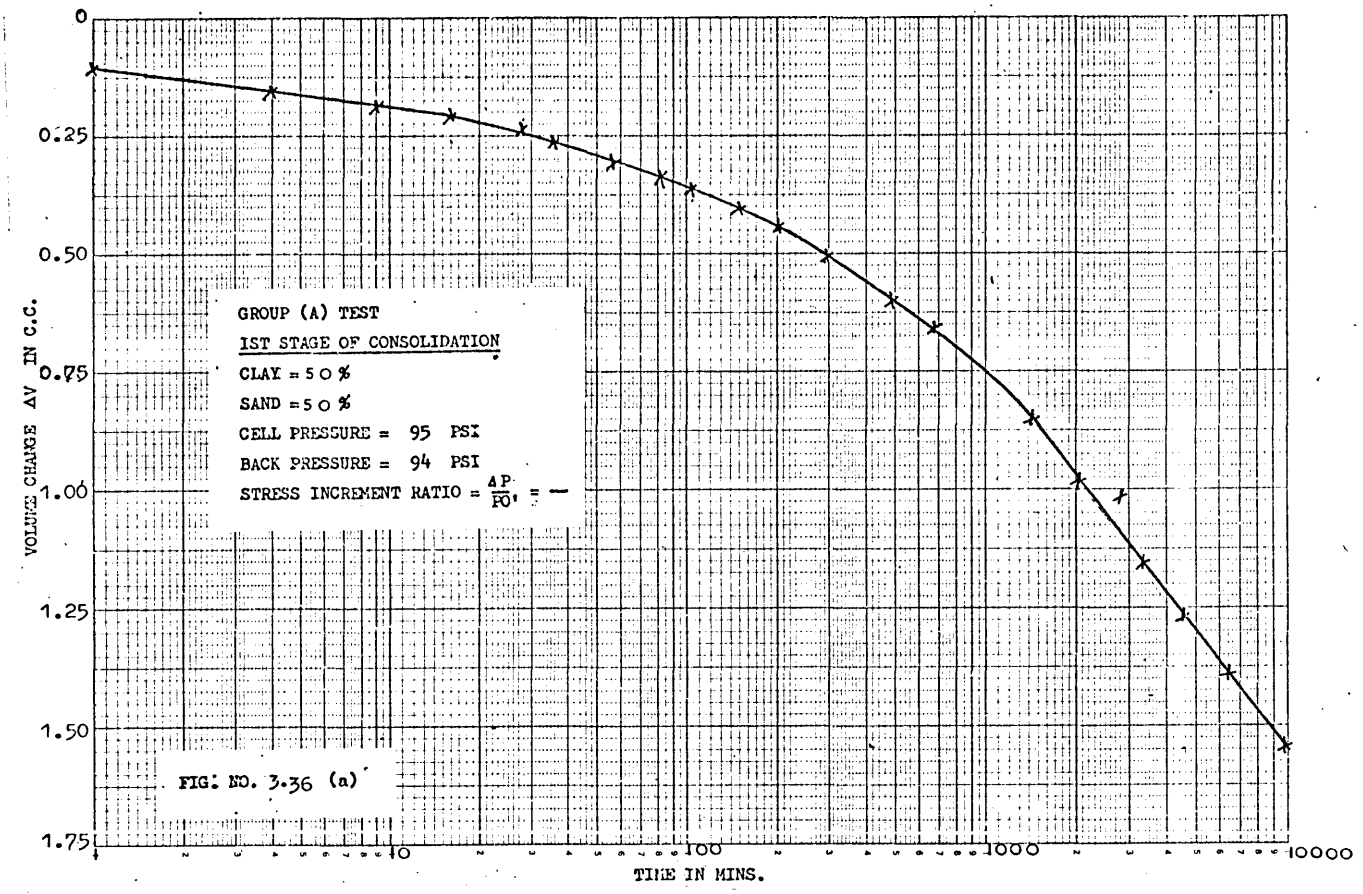

FIG. NO. 3.36 (a)

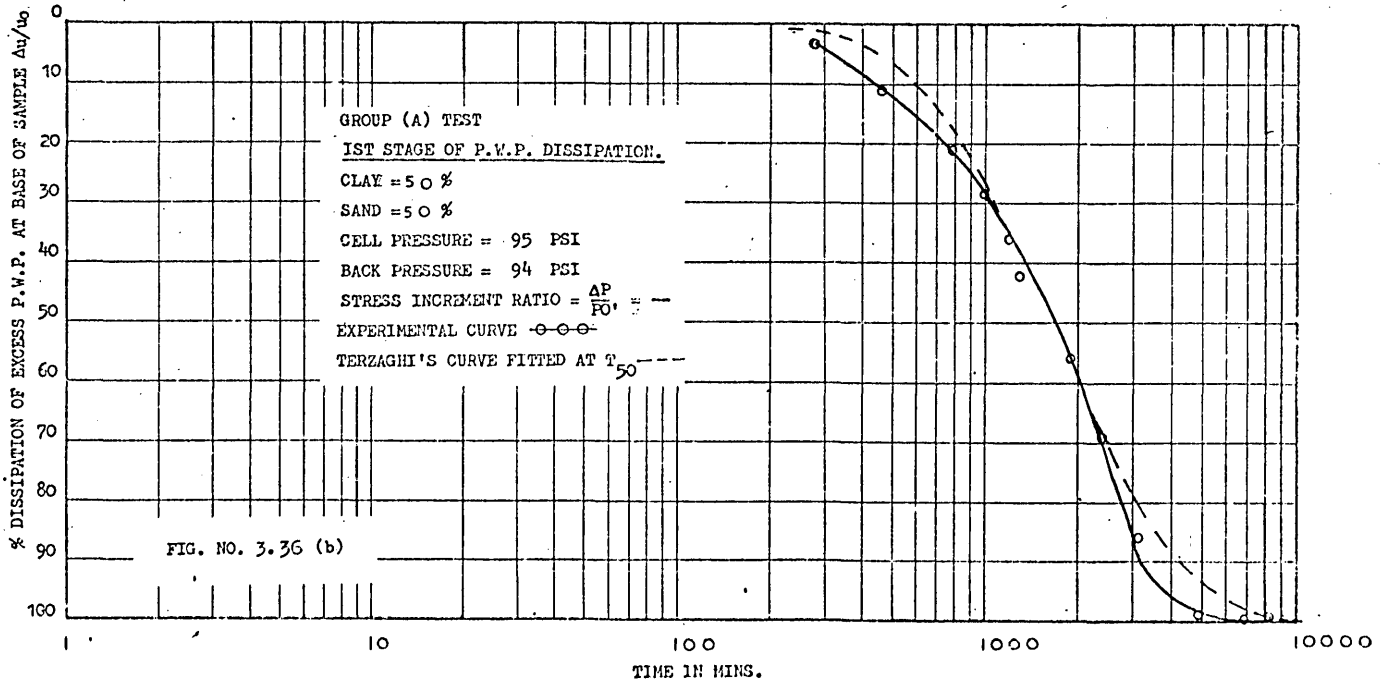

FIG. NO. 3.36 (b)

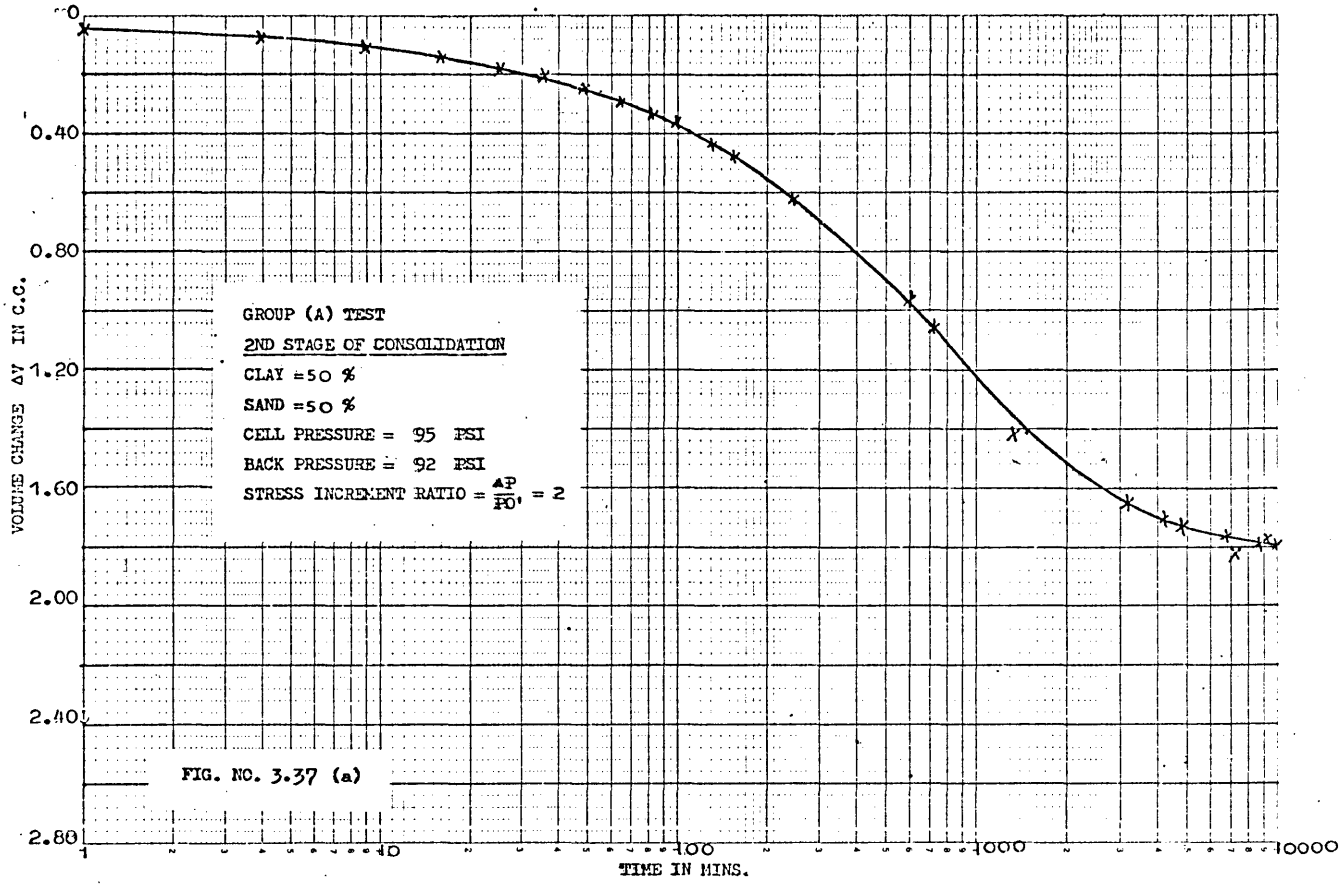

FIG. NO. 3.37 (a)

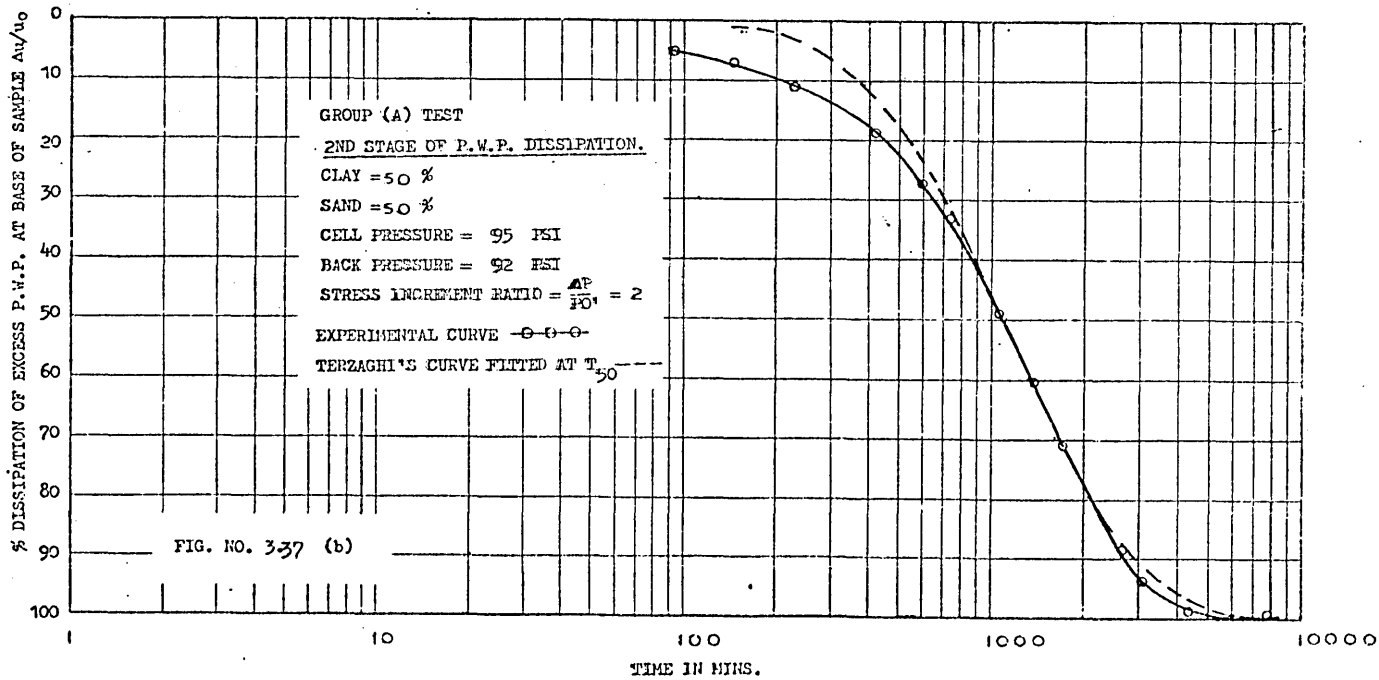

FIG. NO. 3.37 (b)

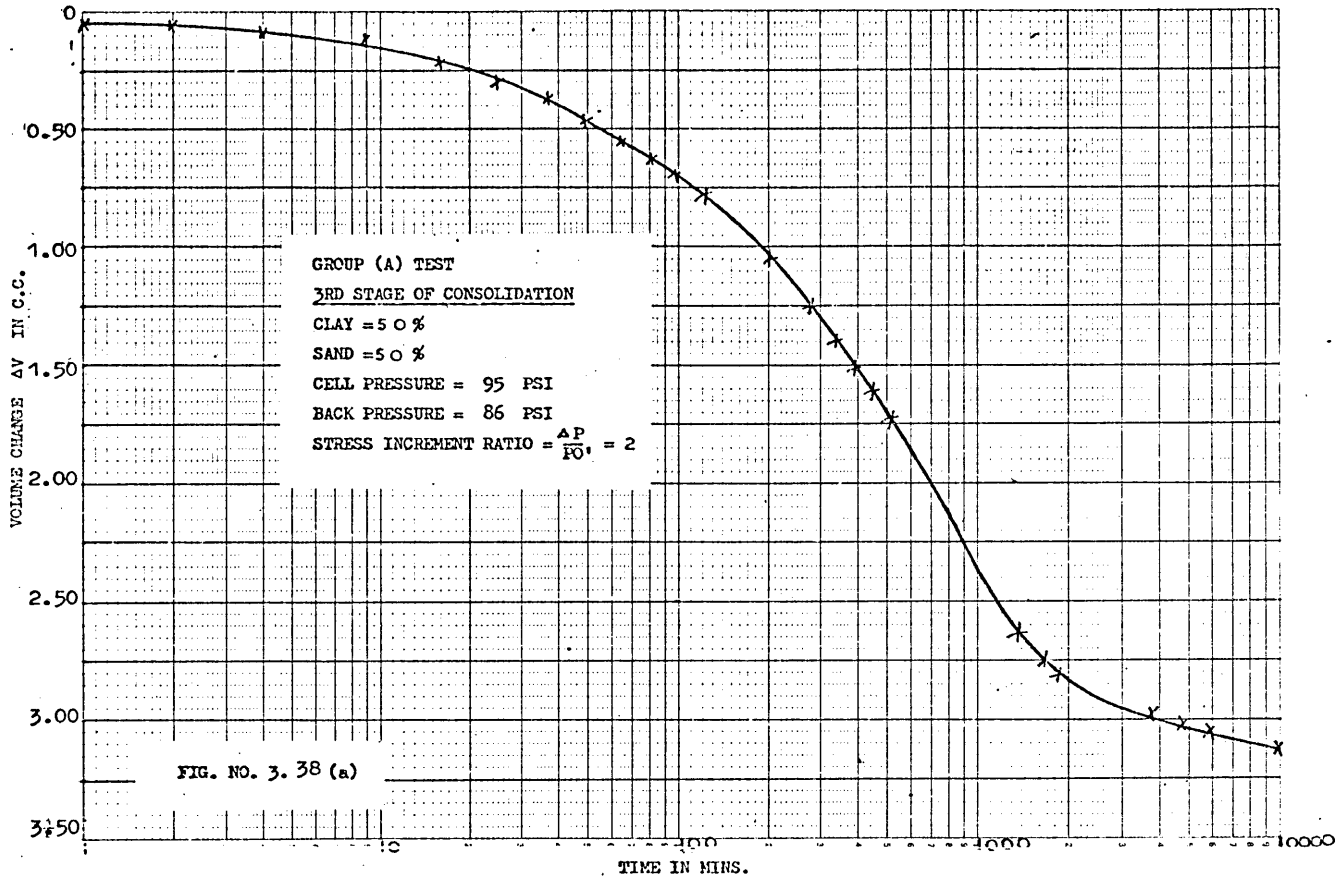

FIG. NO. 3.38 (a)

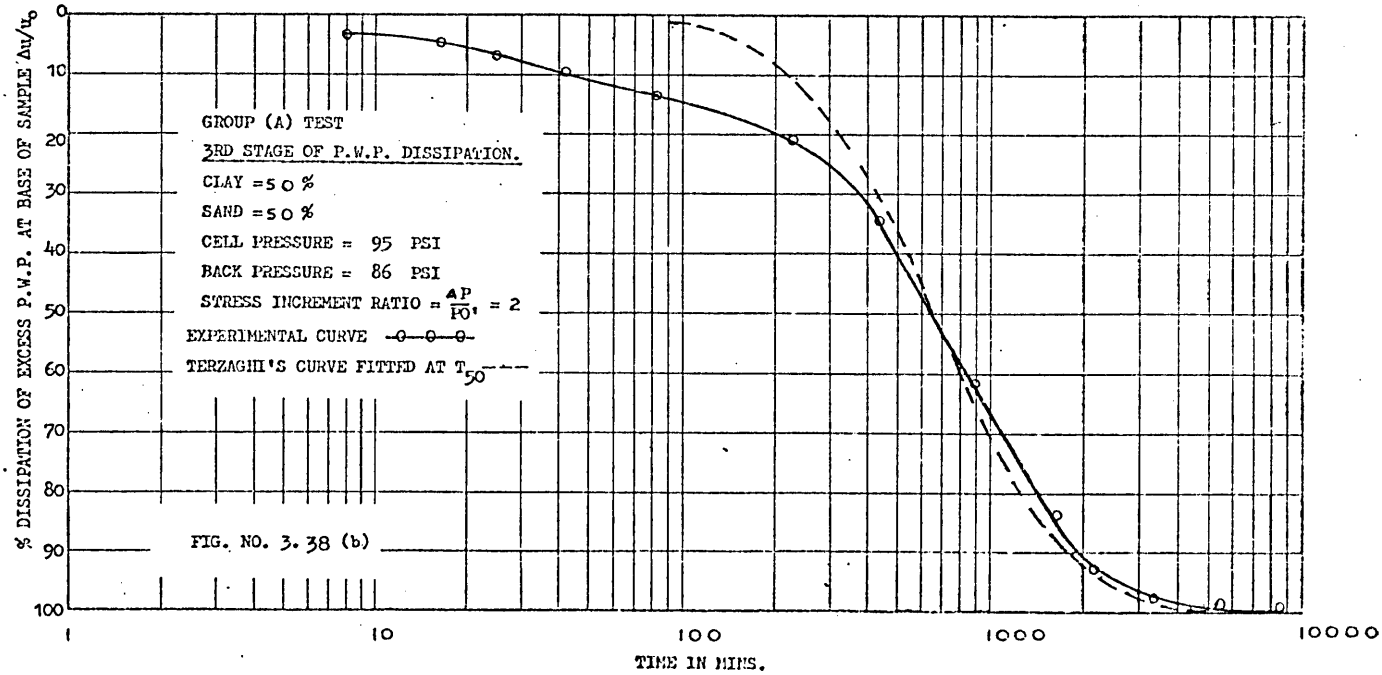

FIG. NO. 3.38 (b)

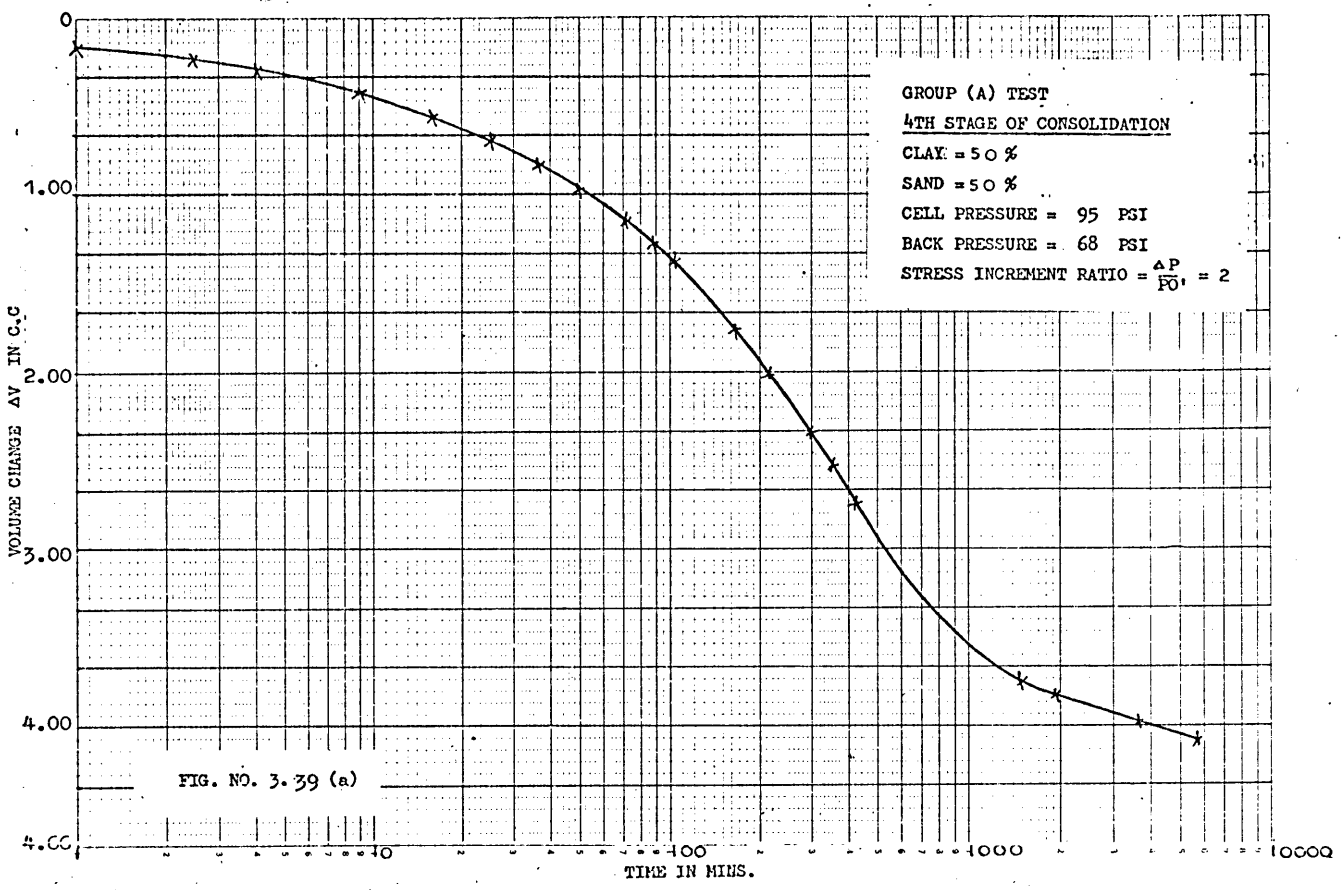

FIG. NO. 3.39 (a)

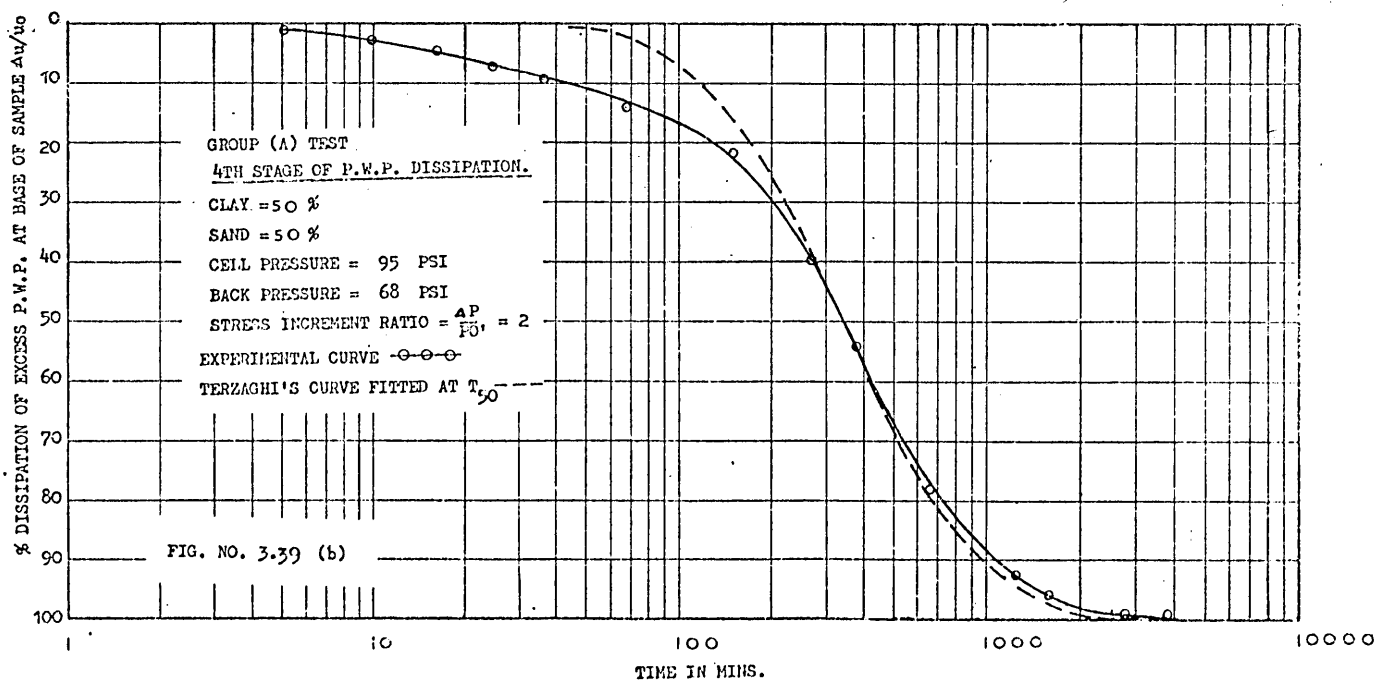

FIG. NO. 3.39 (b)

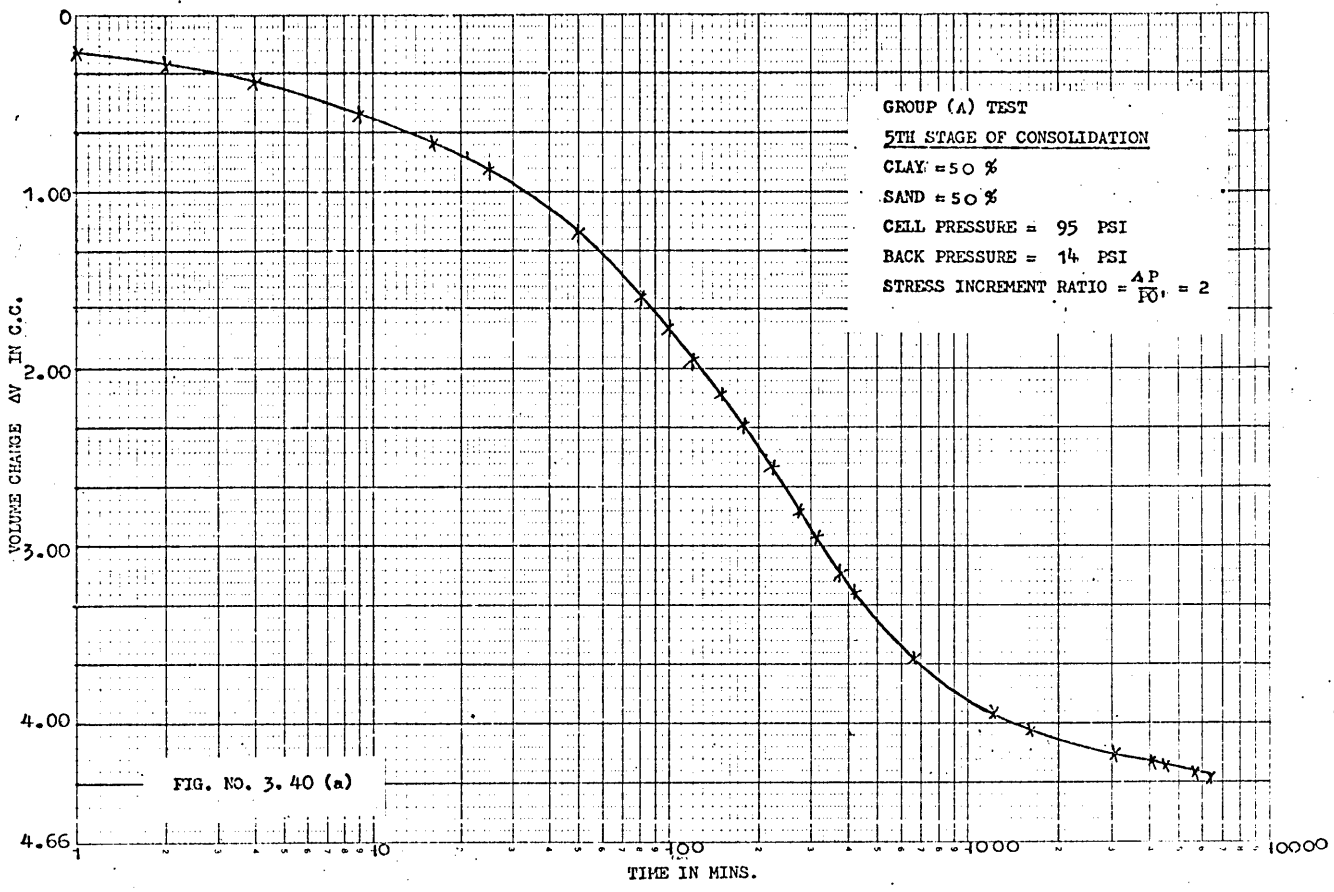

FIG. NO. 3.40 (a)

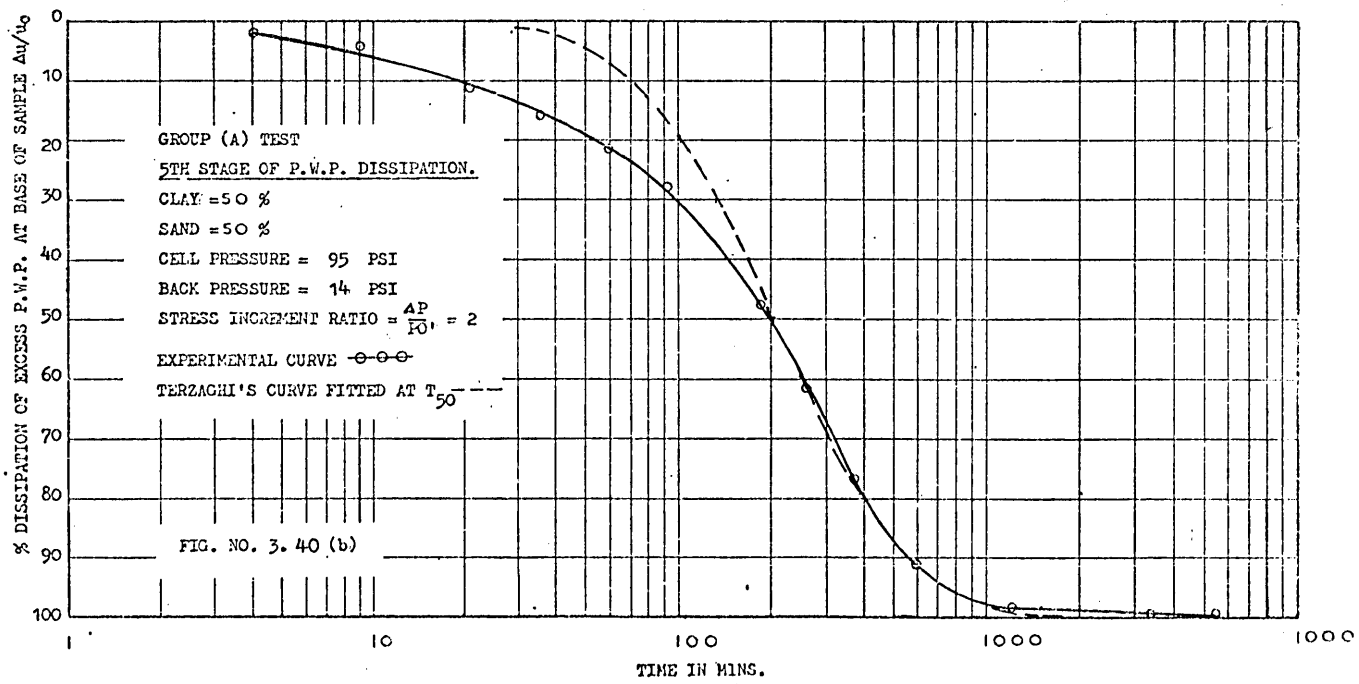

FIG. NO. 3.40 (b)

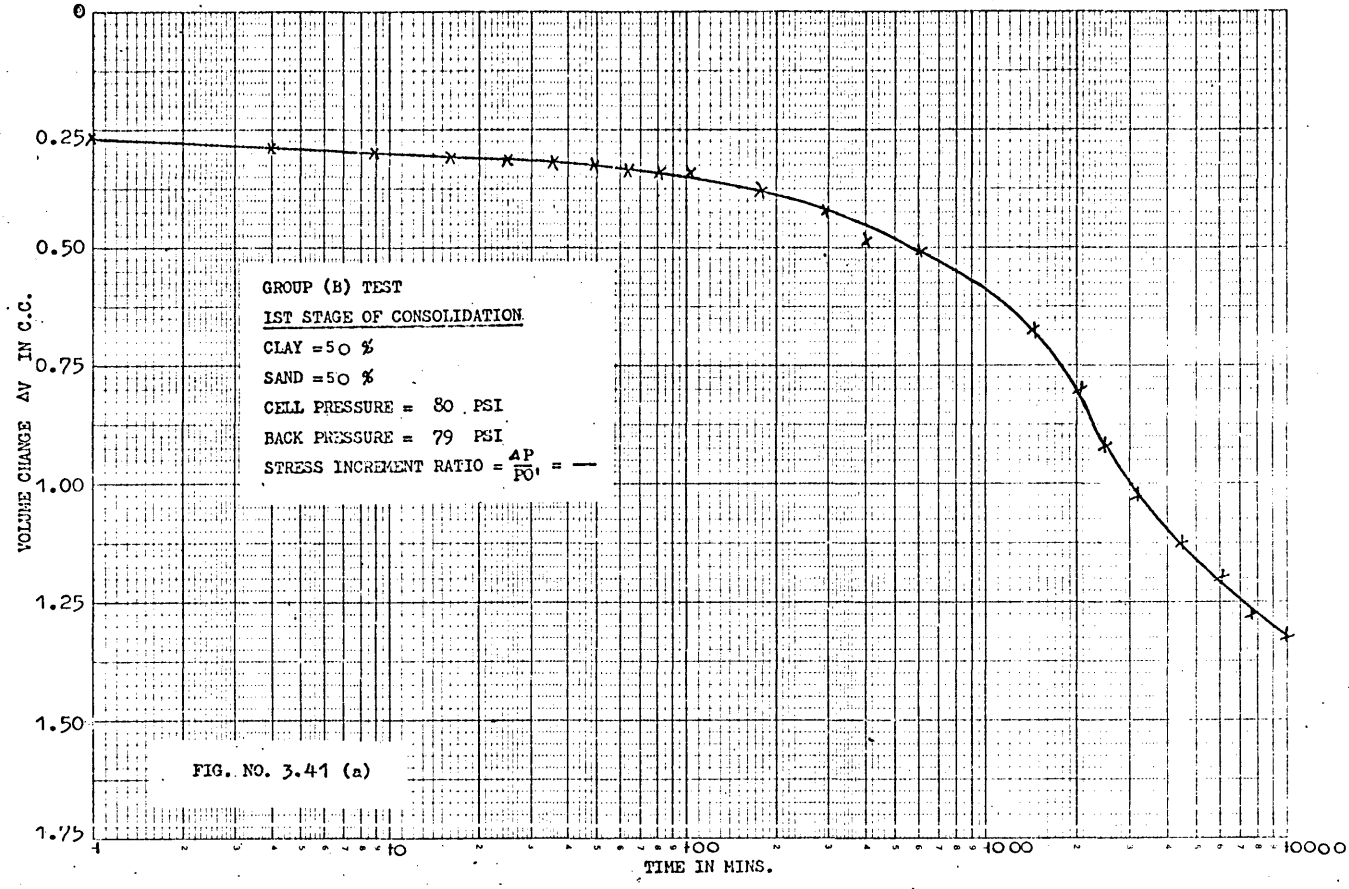

FIG. NO. 3.41 (a)

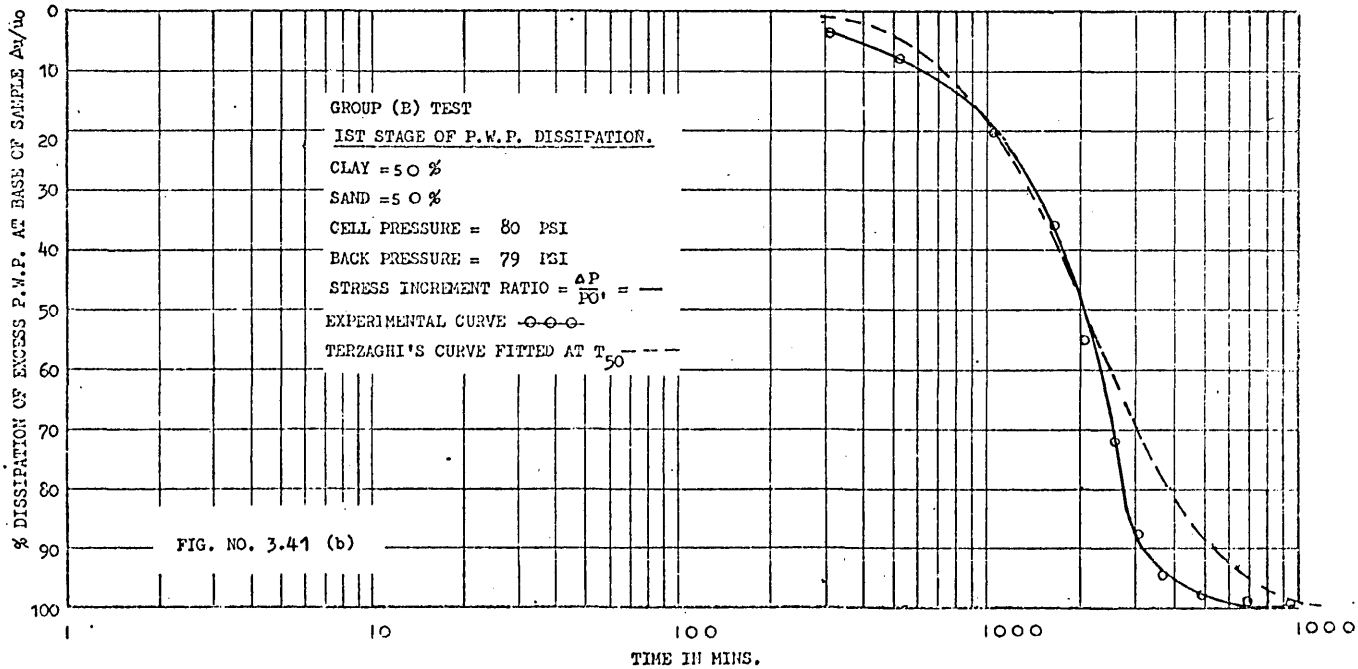

FIG. NO. 3.41 (b)

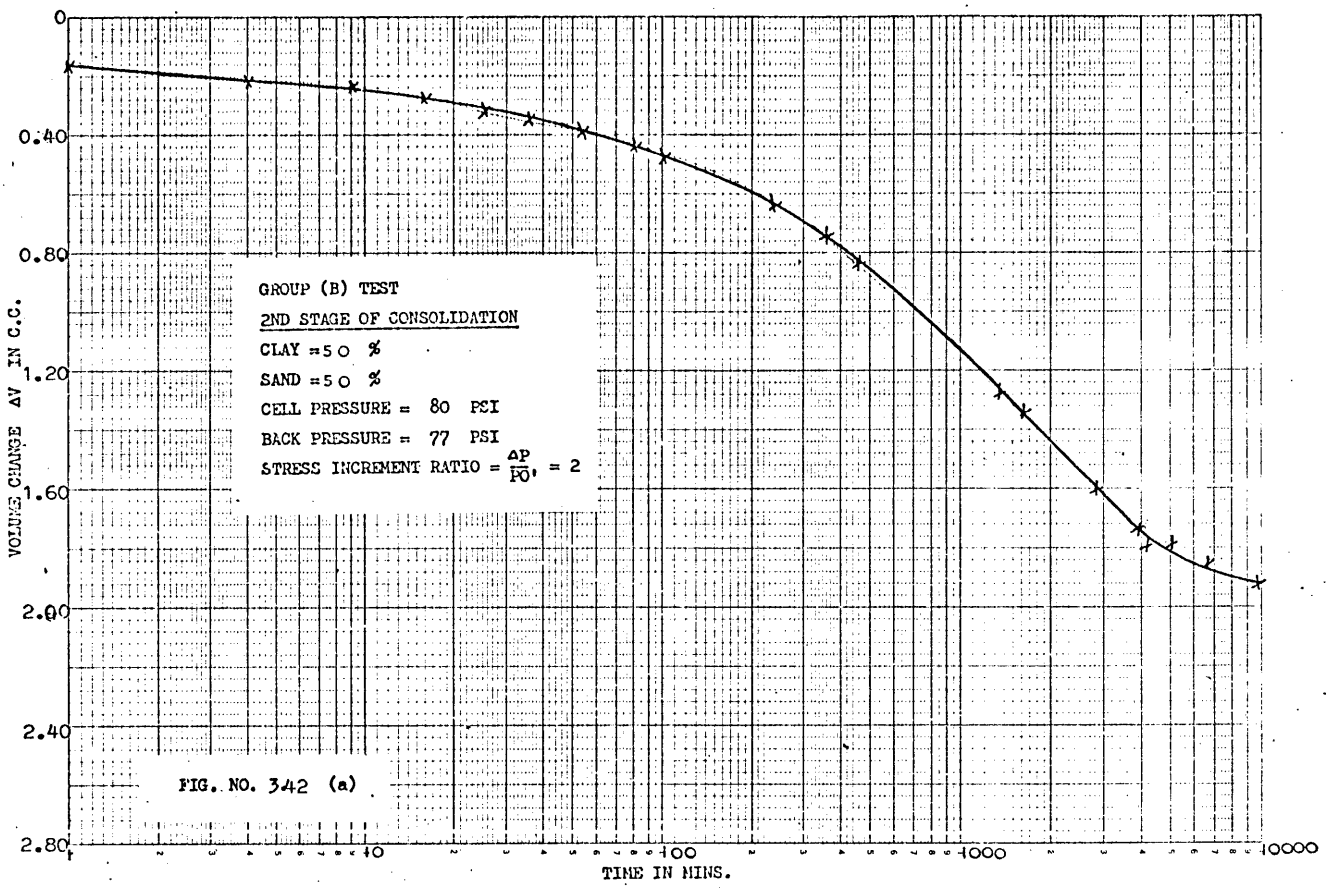

FIG. NO. 342 (a)

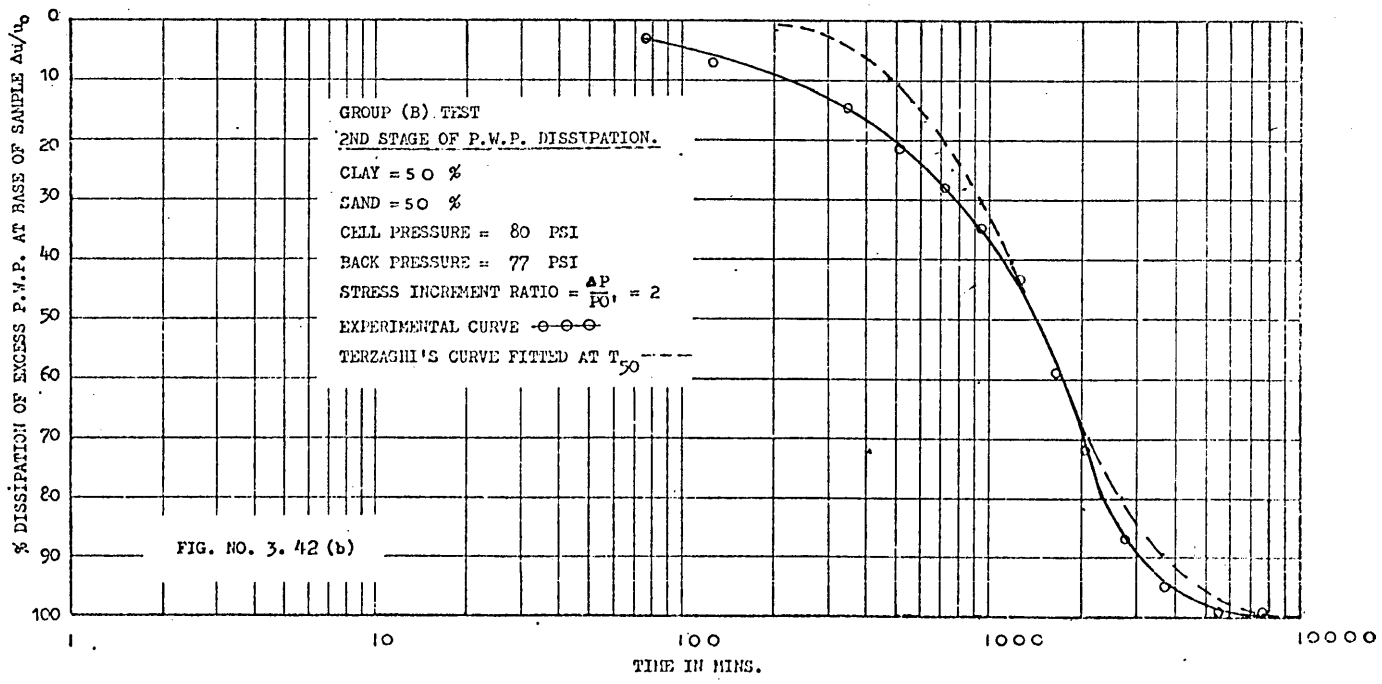

FIG. NO. 3. 42 (b)

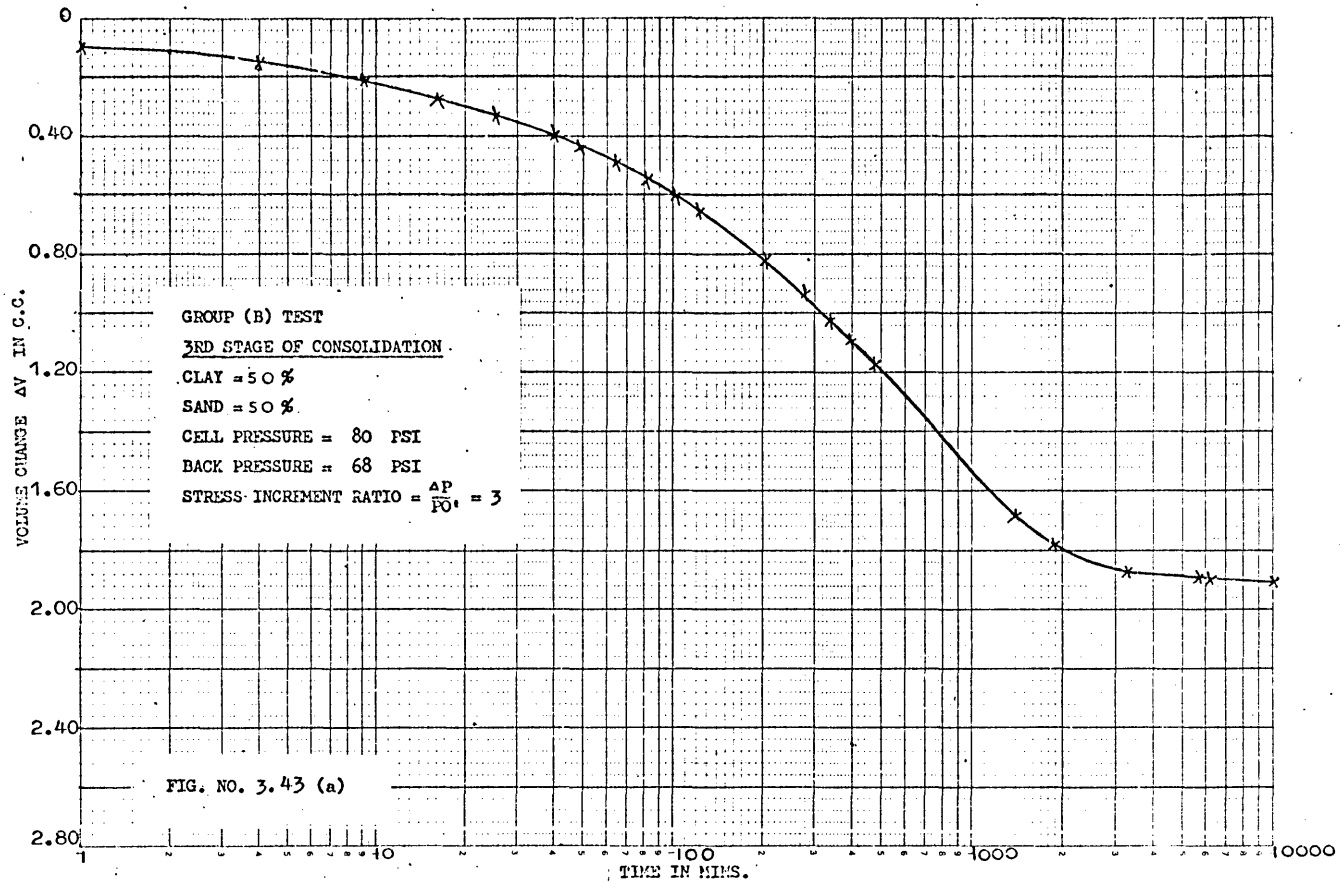

FIG. NO. 3.43 (a)

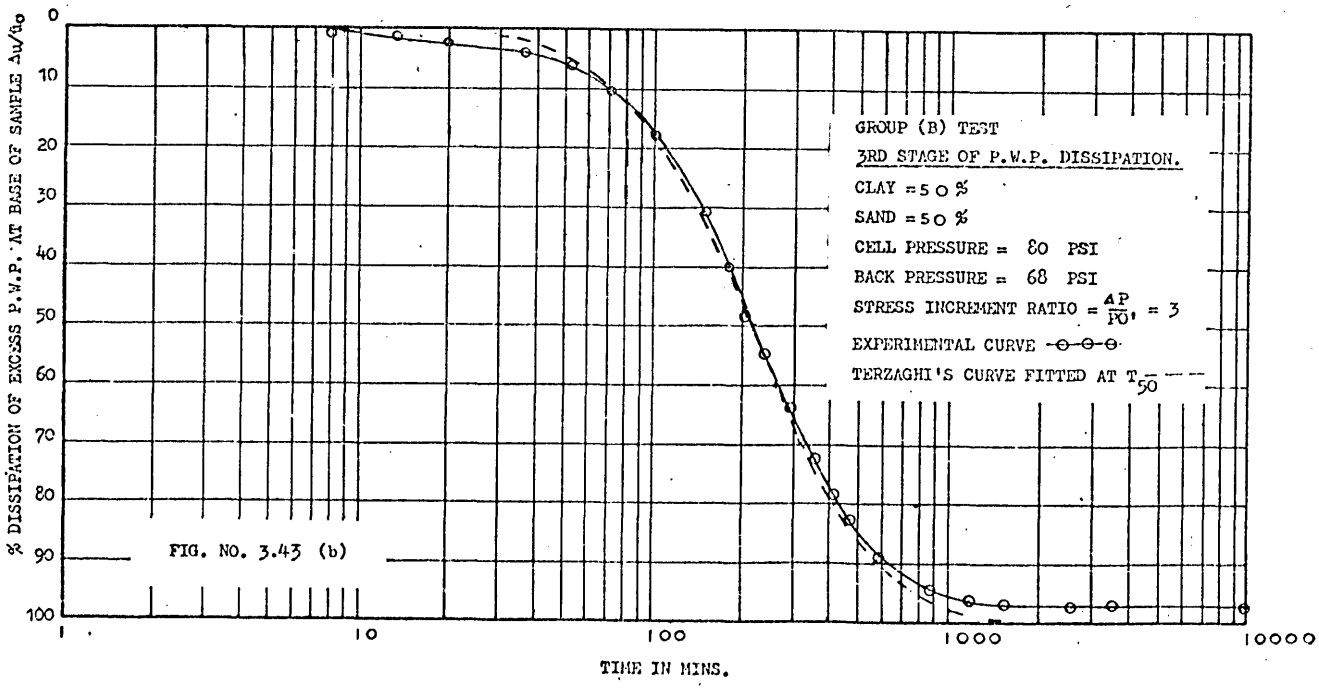

FIG. NO. 3.43 (b)

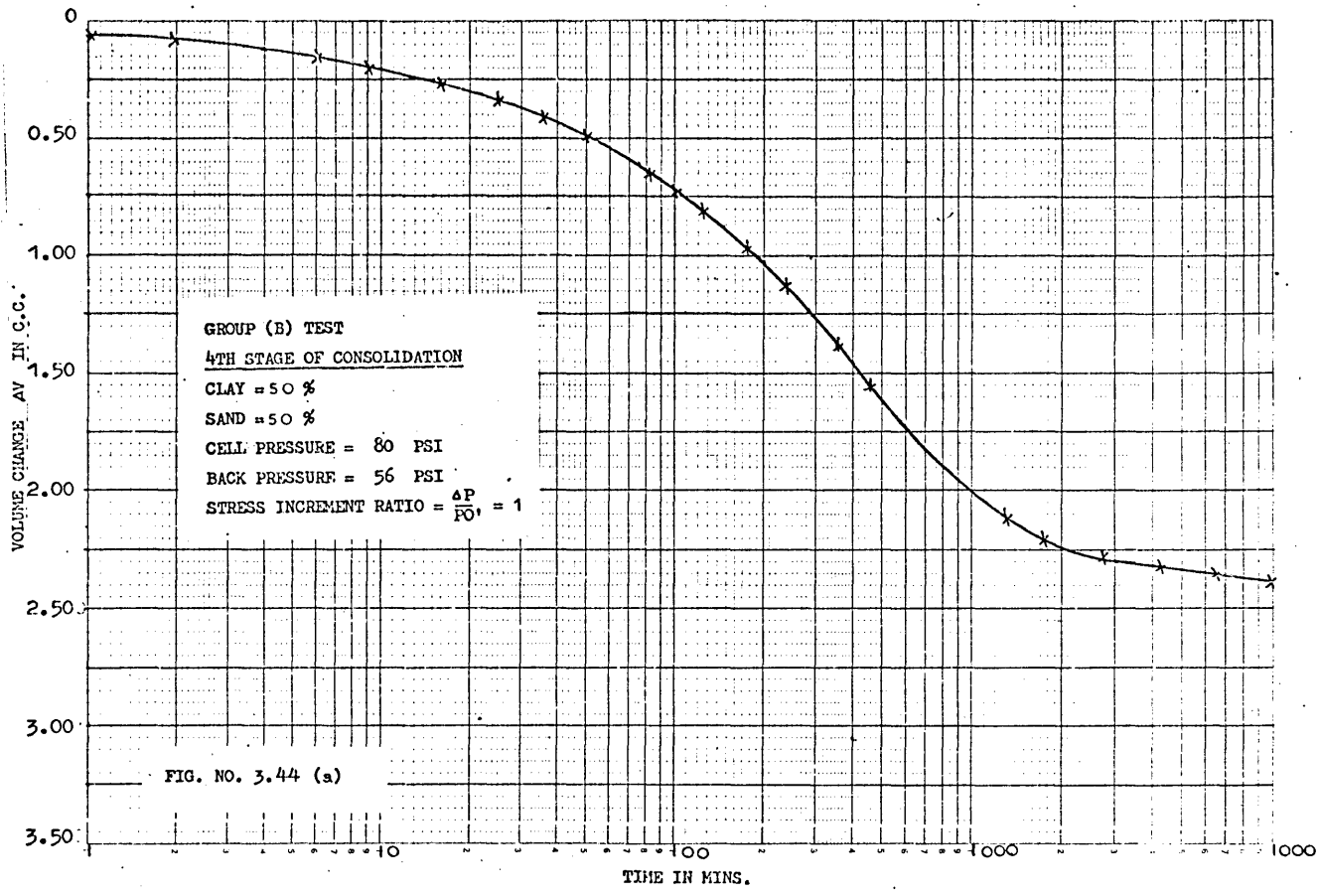

FIG. NO. 3.44 (a)

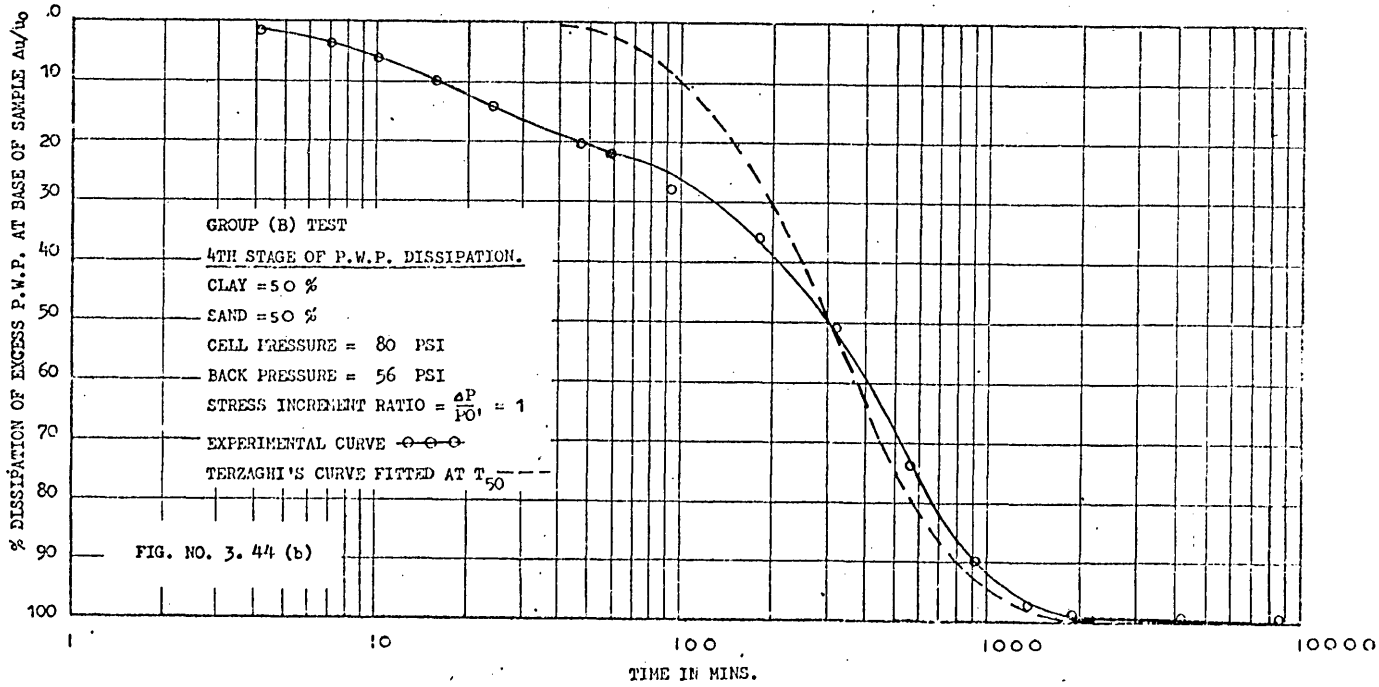

FIG. NO. 3.44 (b)

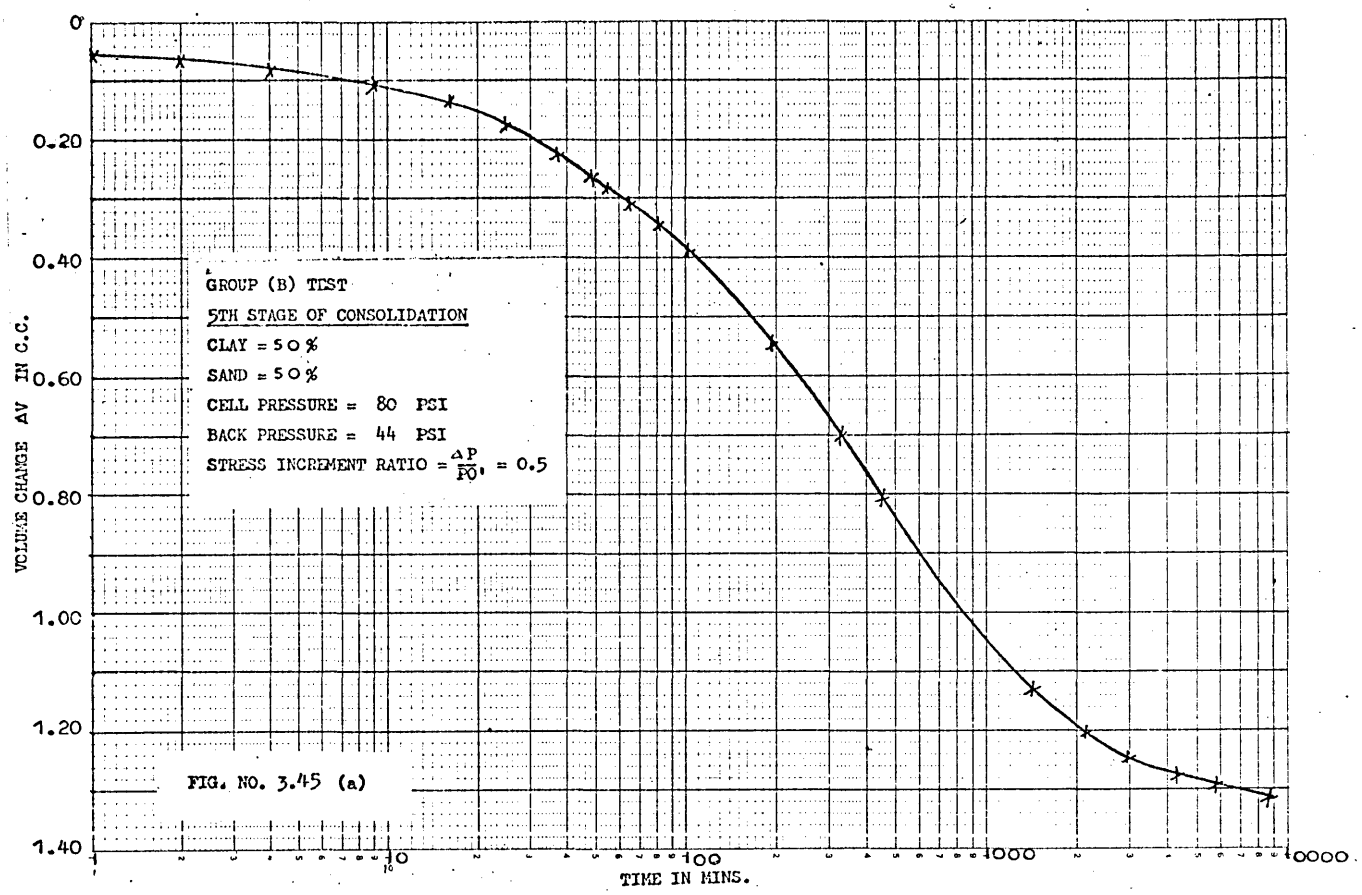

FIG. NO. 3.45 (a)

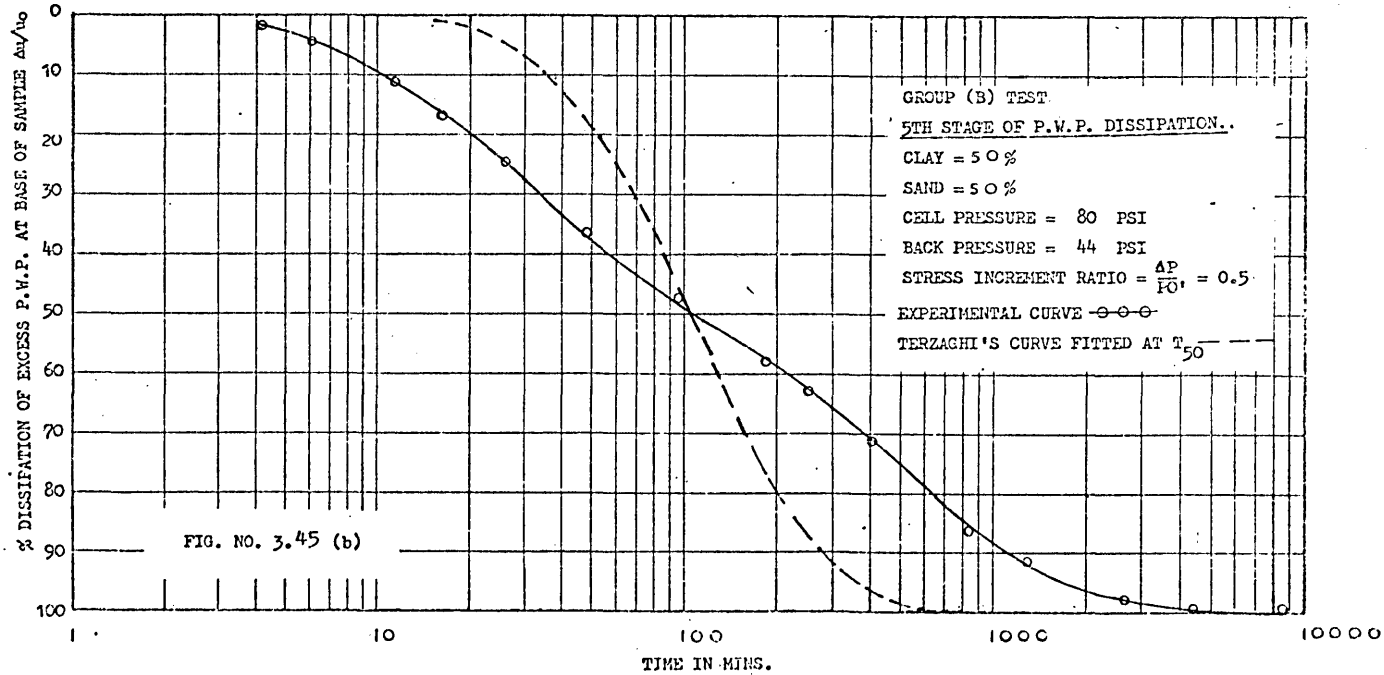

FIG. NO. 3.45 (b)

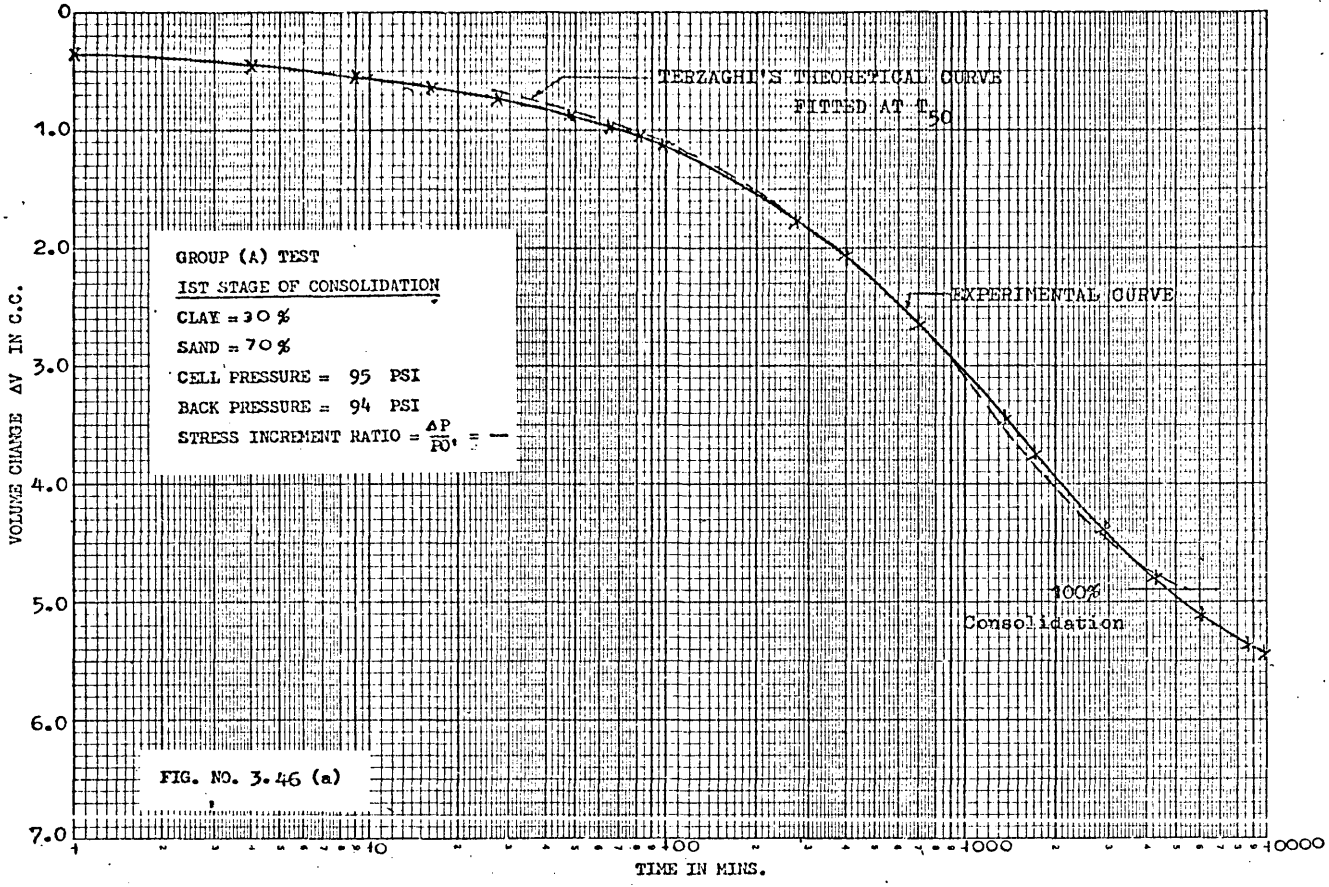

FIG. NO. 3.46 (a)

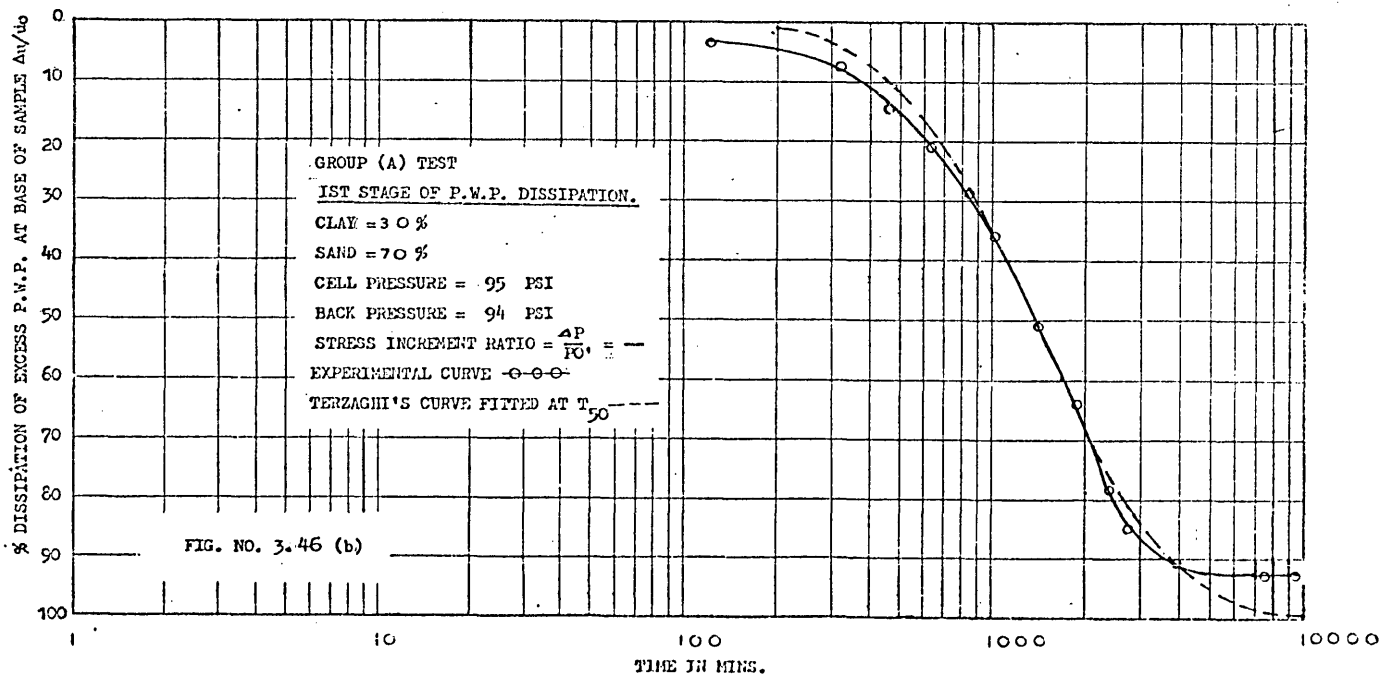

FIG. NO. 3.46 (b)

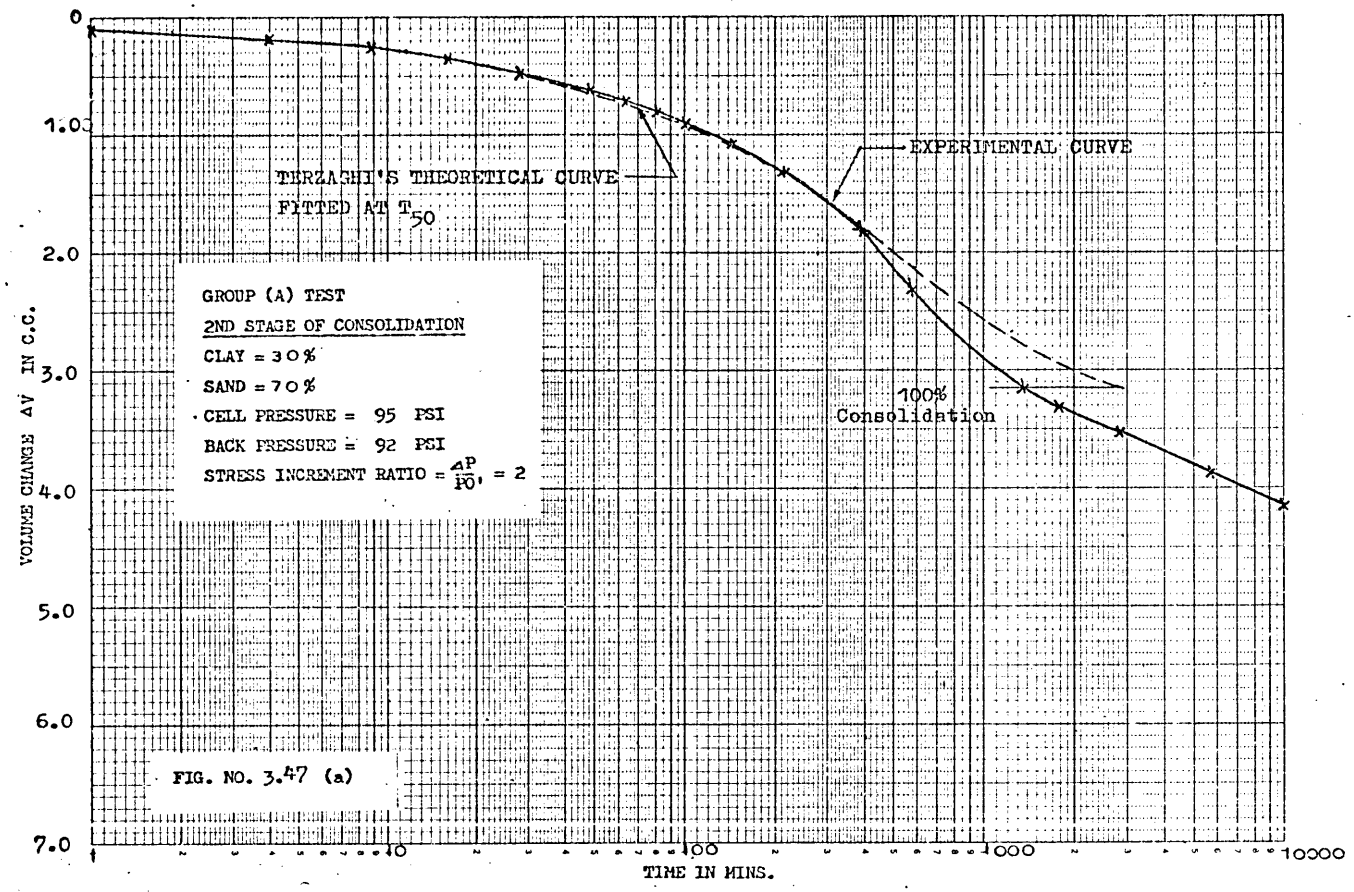

FIG. NO. 3.47 (a)

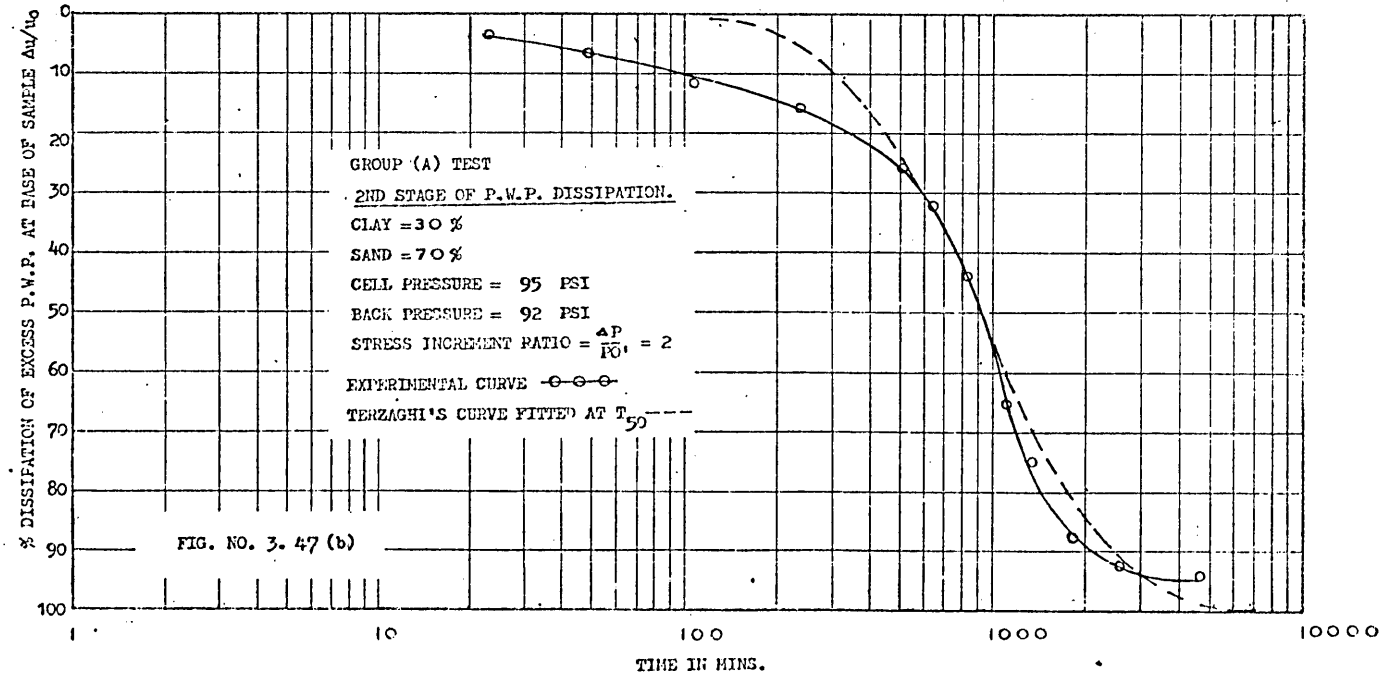

FIG. NO. 3. 47 (b)

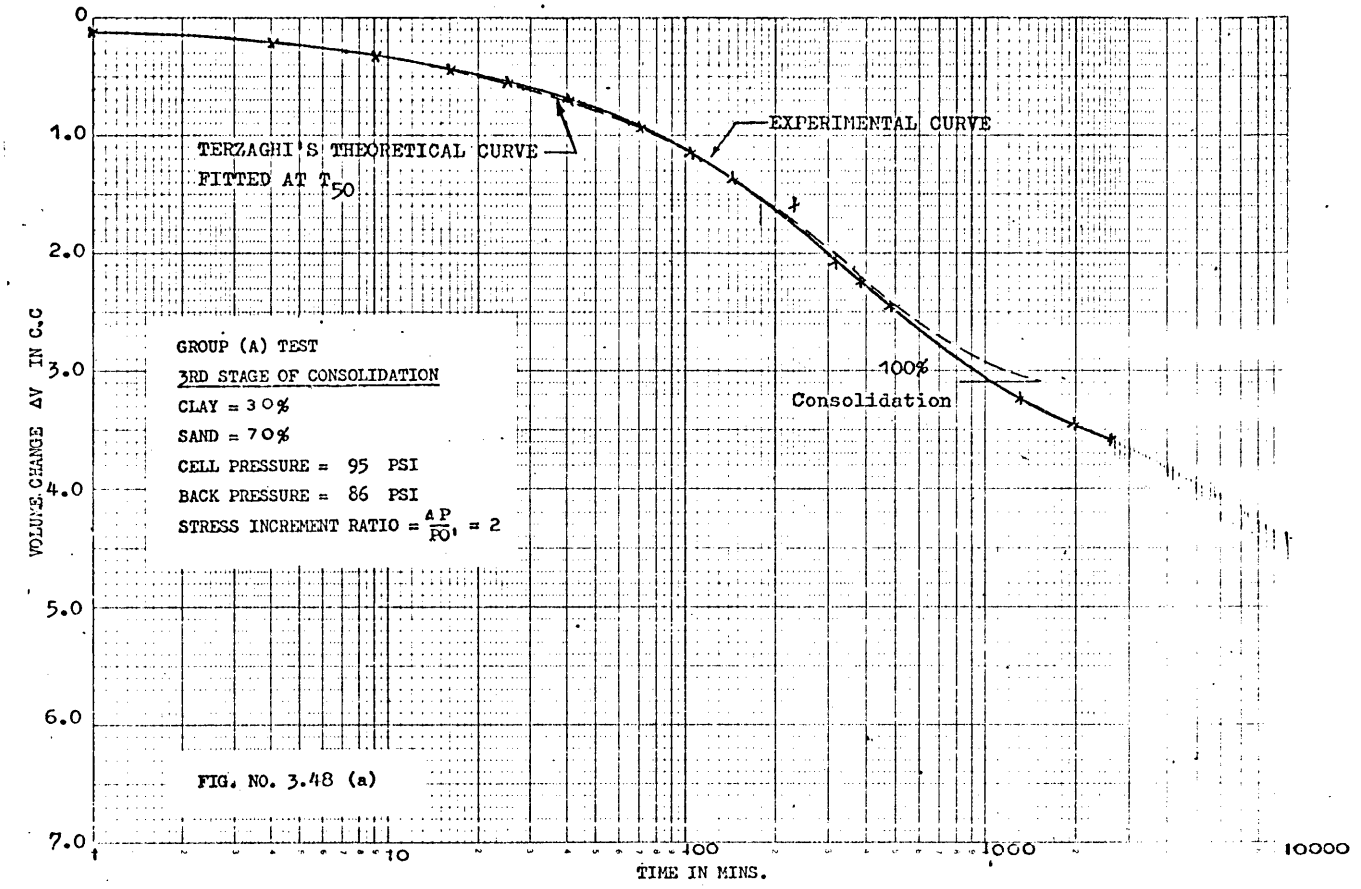

FIG. NO. 3.48 (a)

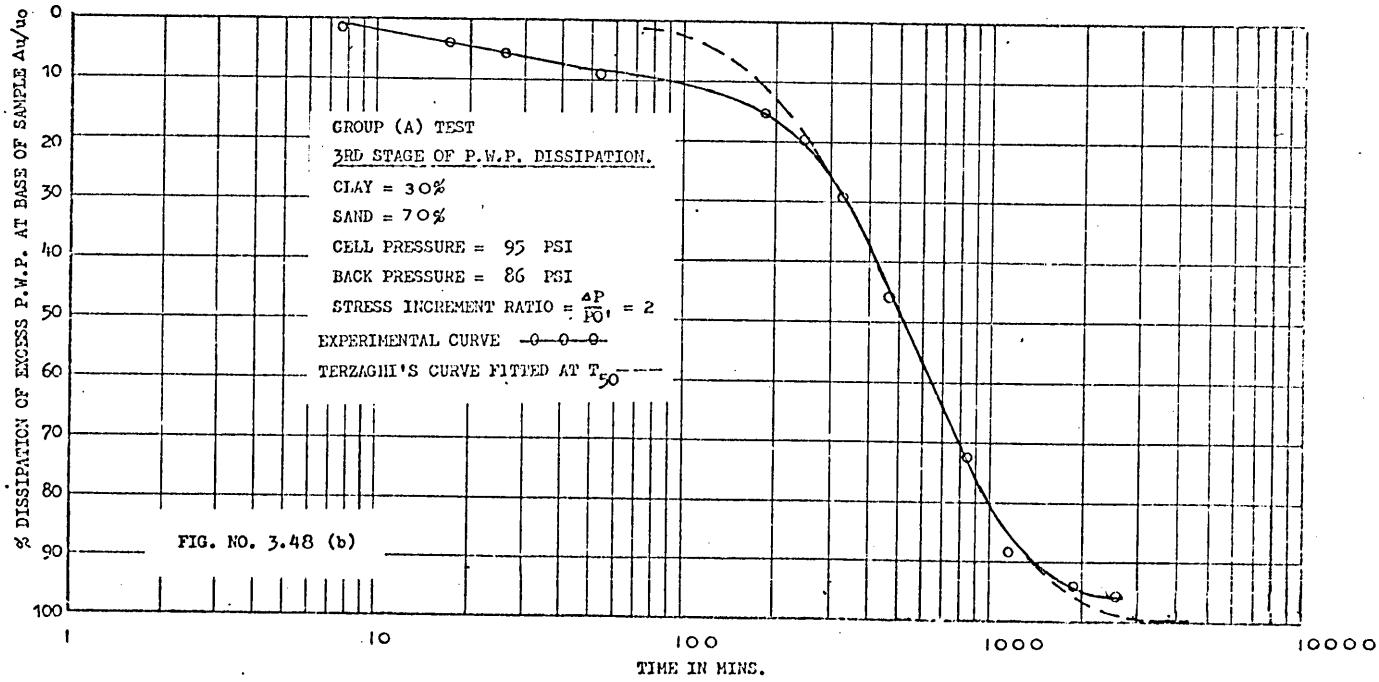

FIG. NO. 3.48 (b)

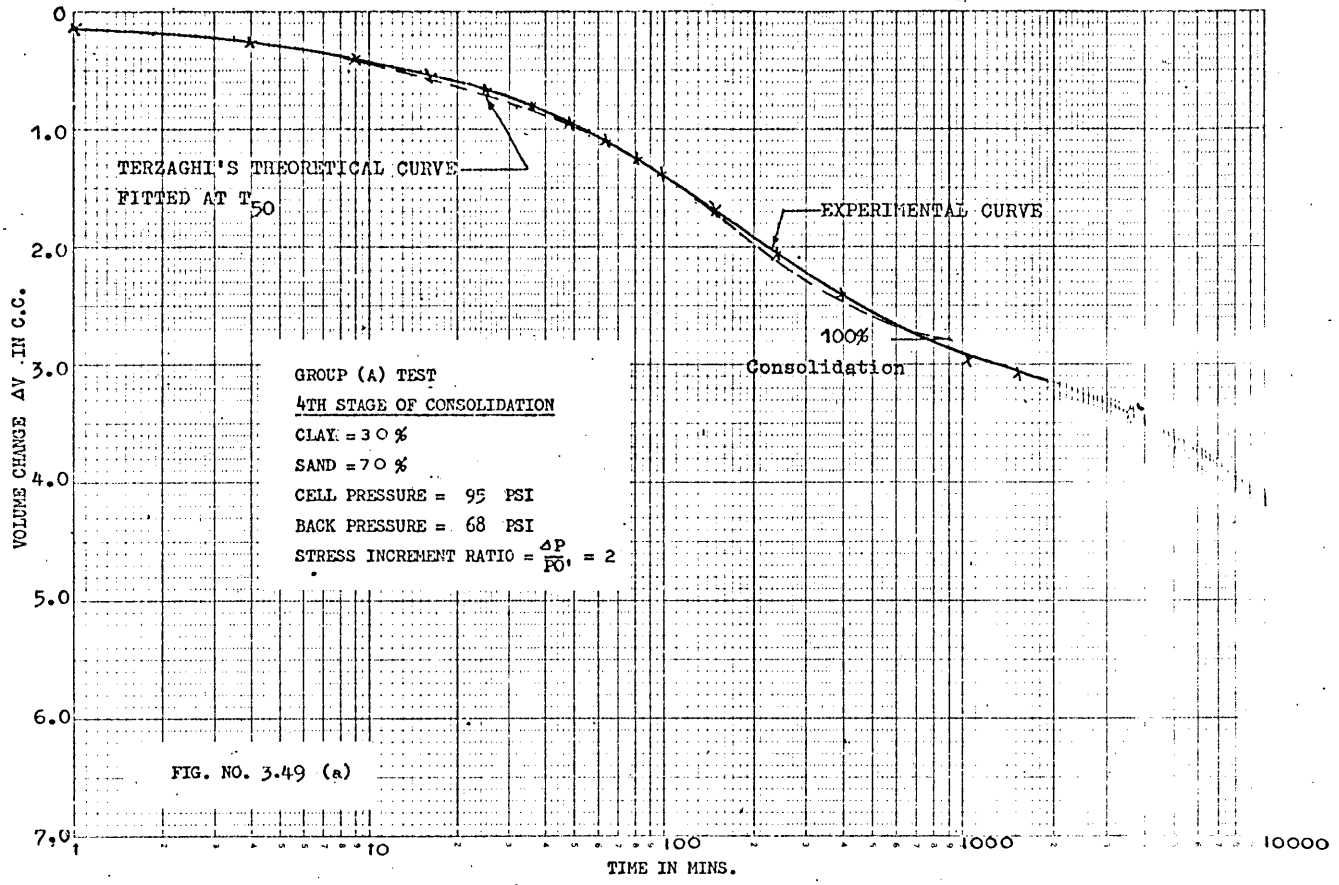

FIG. NO. 3.49 (a)

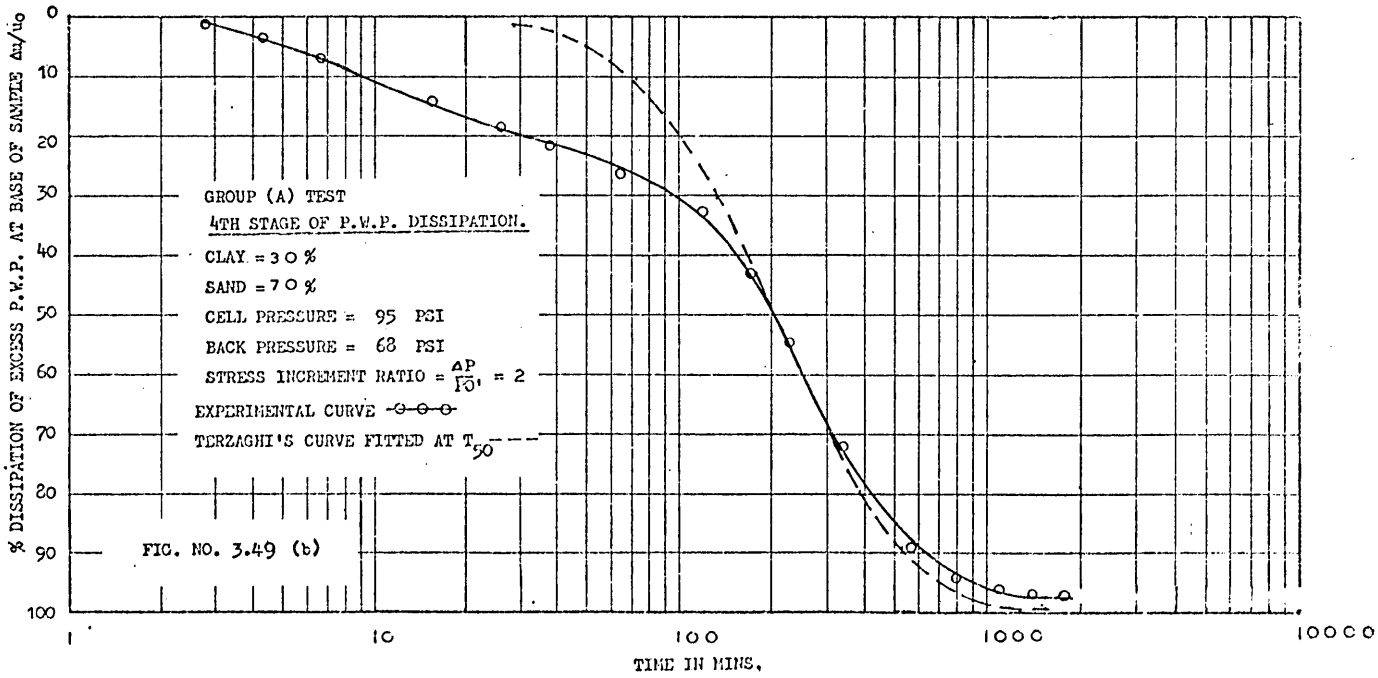

FIG. NO. 3.49 (b)

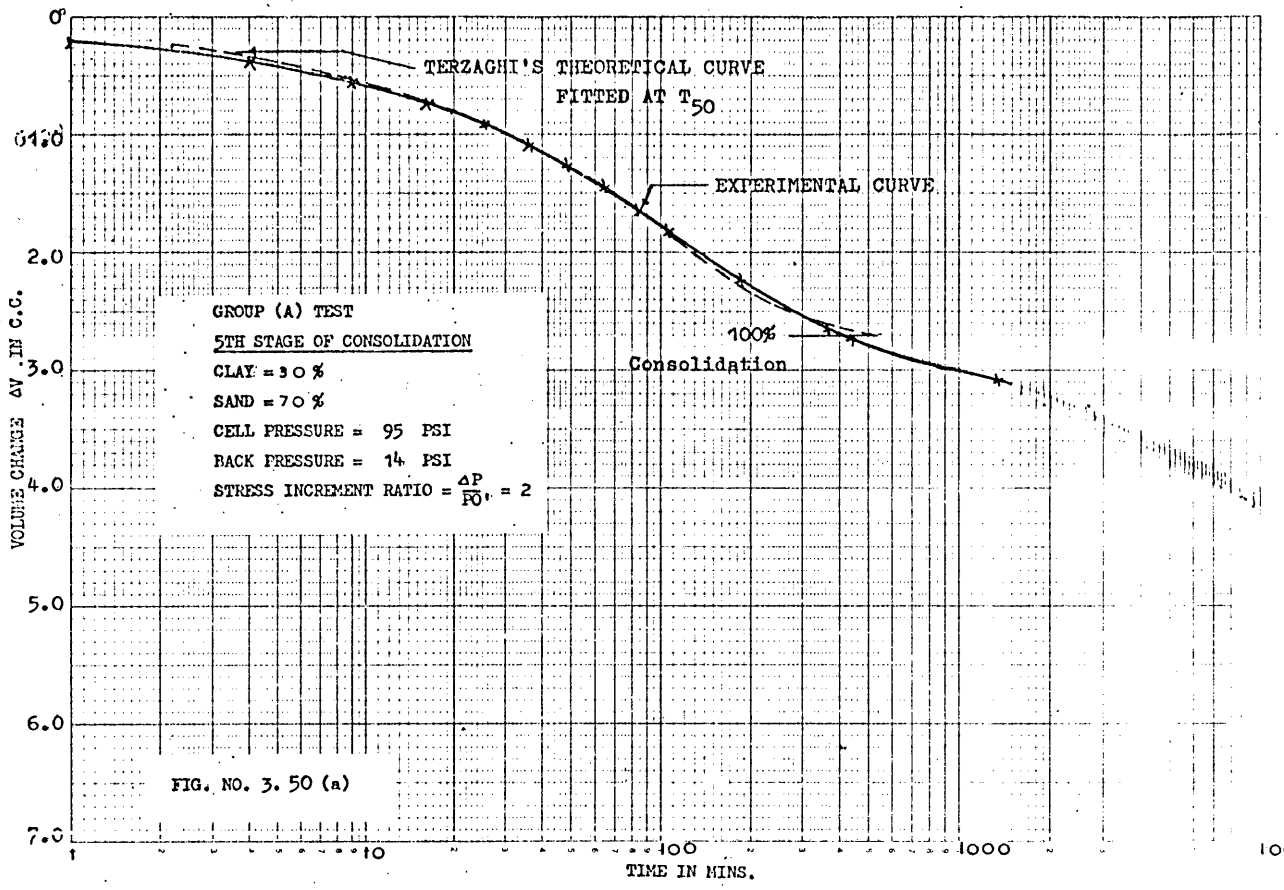

FIG. NO. 3.50 (a)

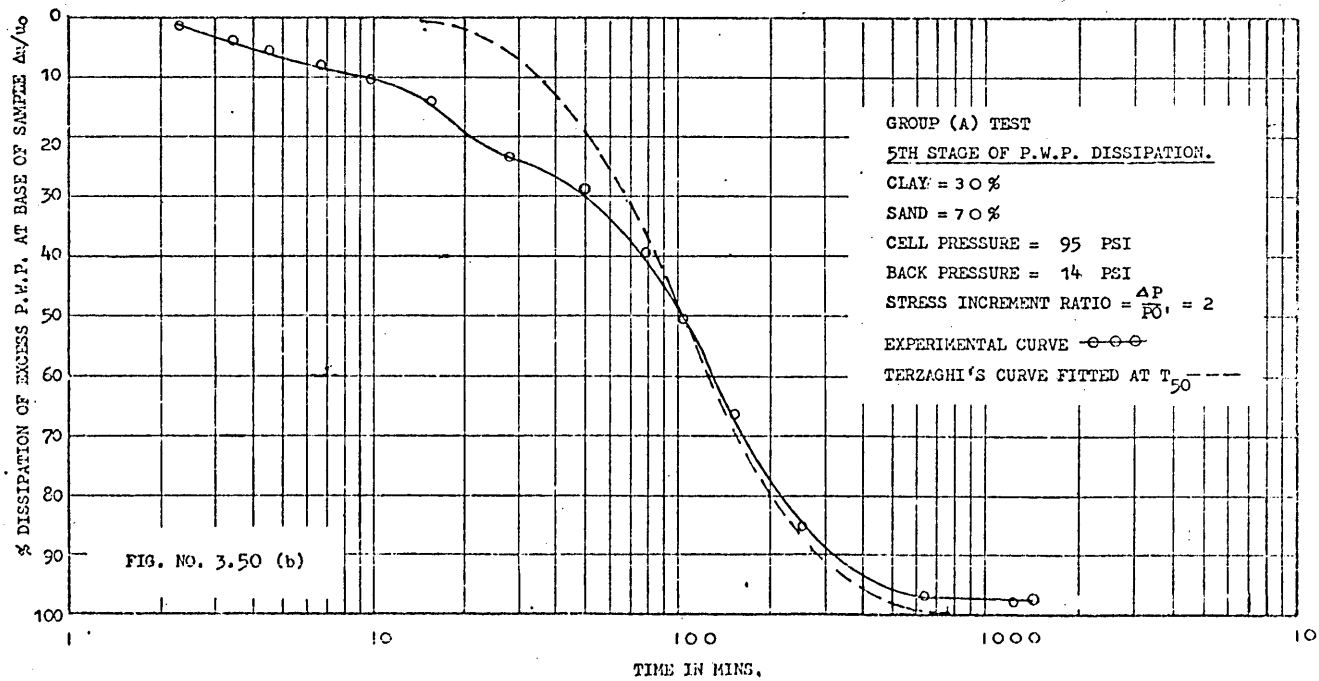

FIG. NO. 3.50 (b)

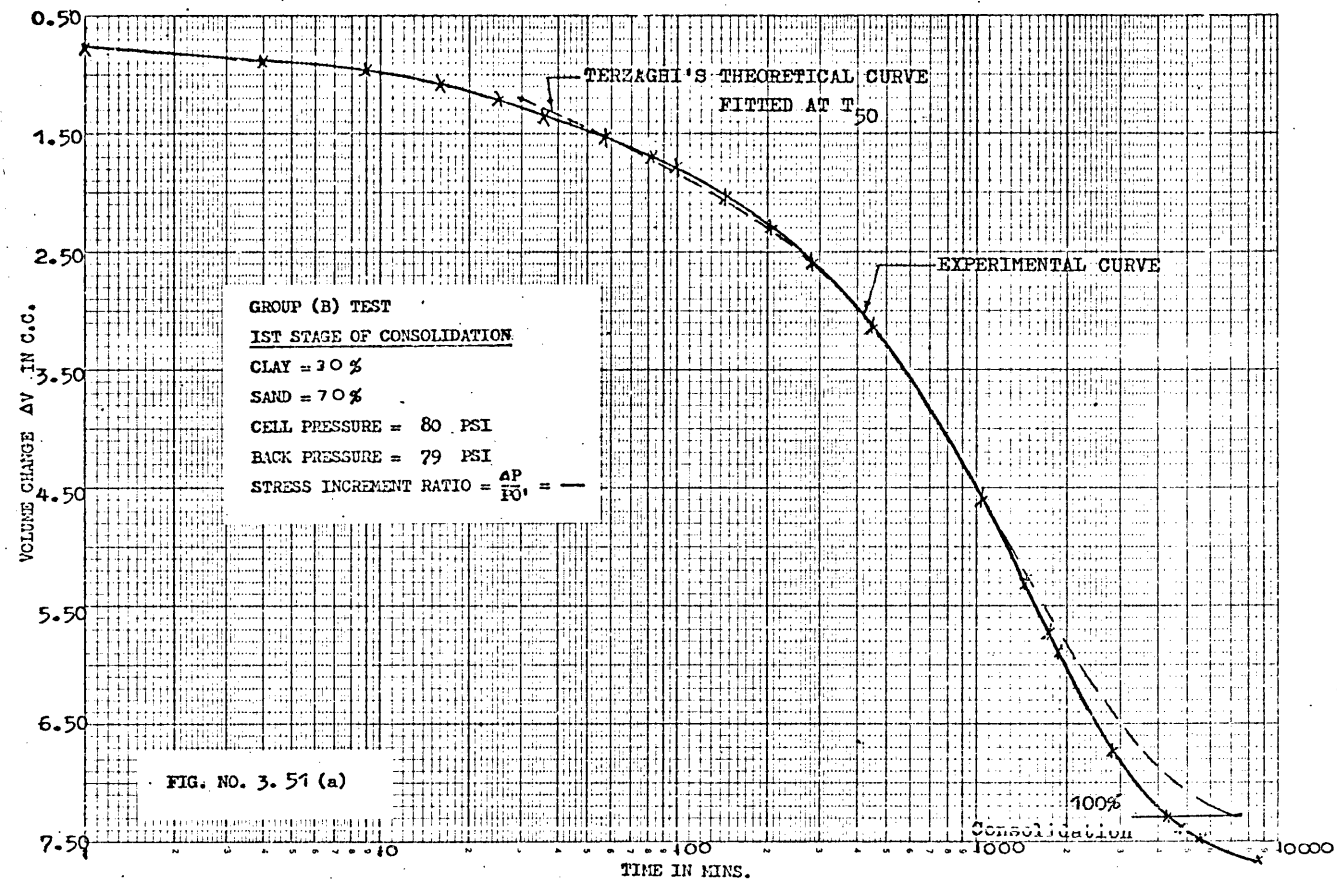

FIG. NO. 3.51 (a)

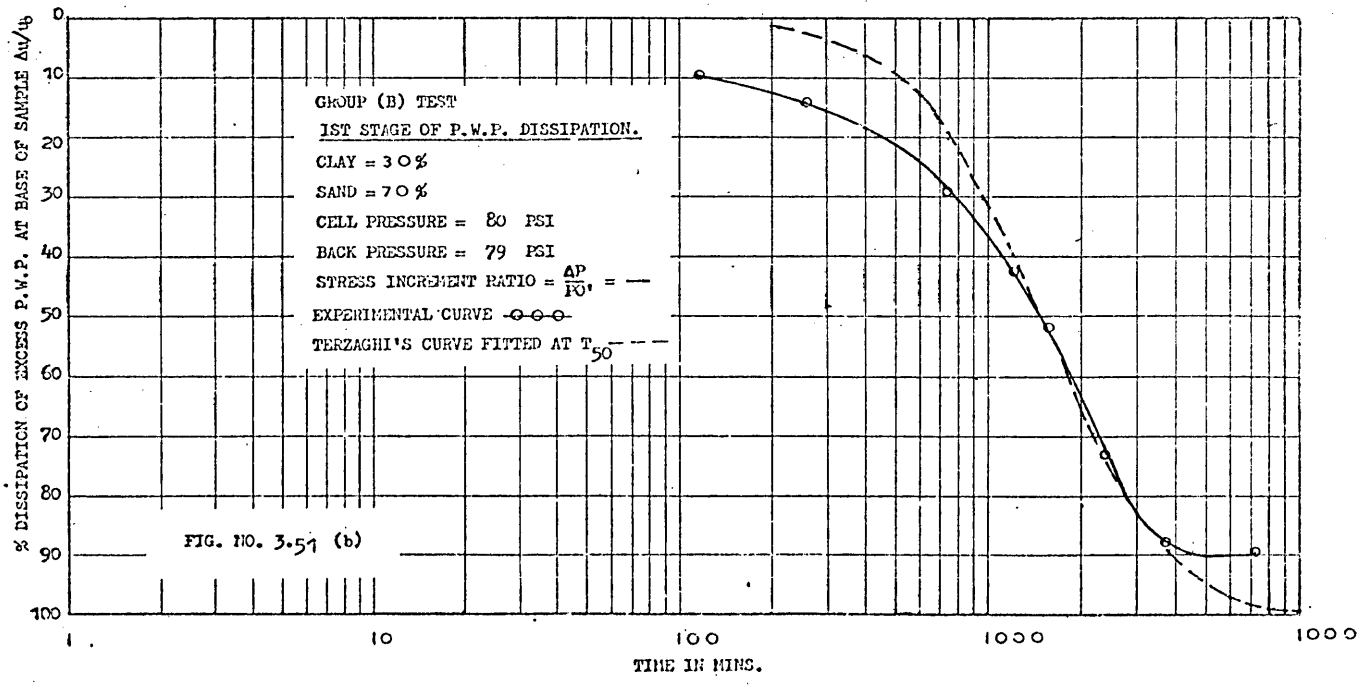

FIG. NO. 3.51 (b)

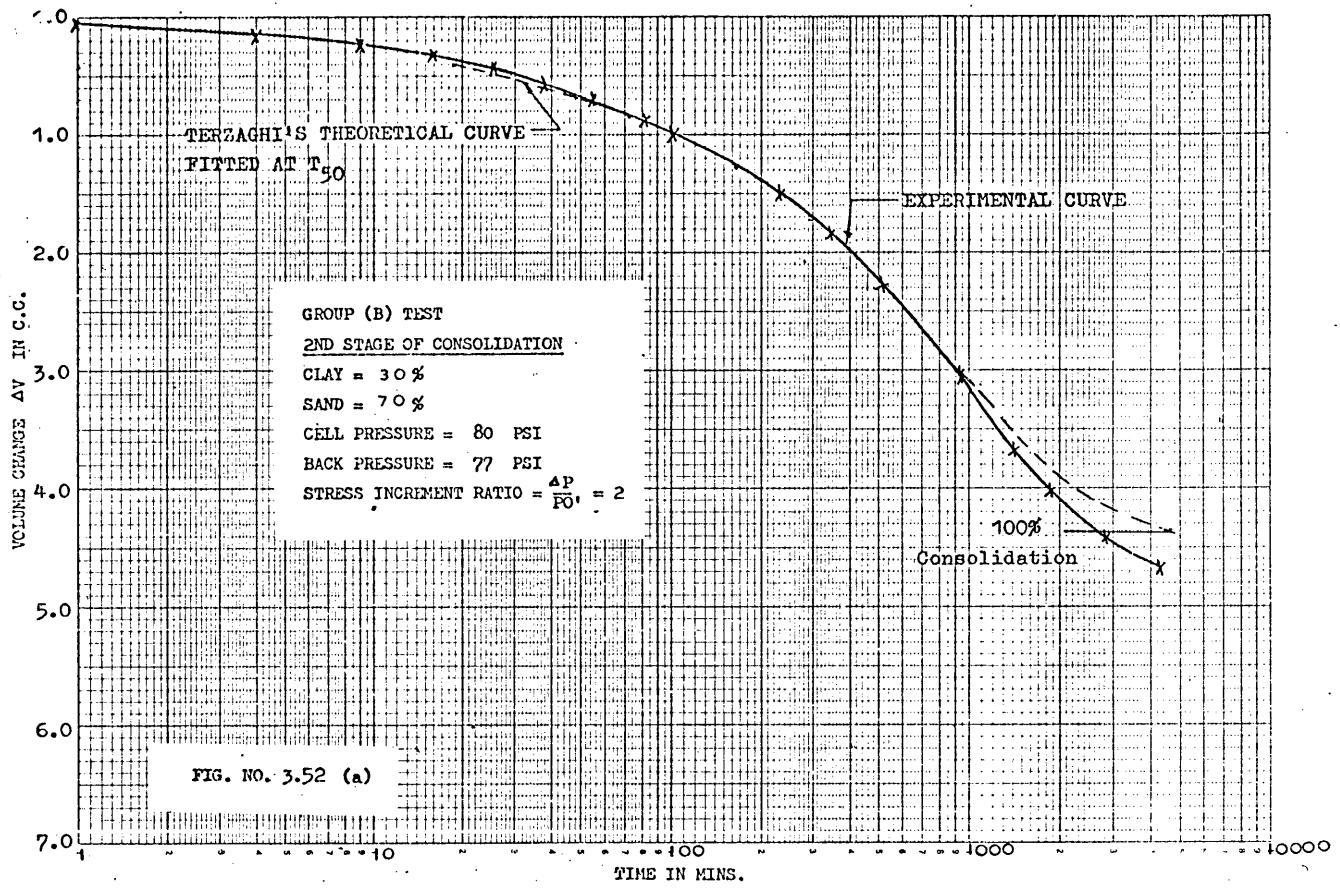

FIG. NO. 3.52 (a)

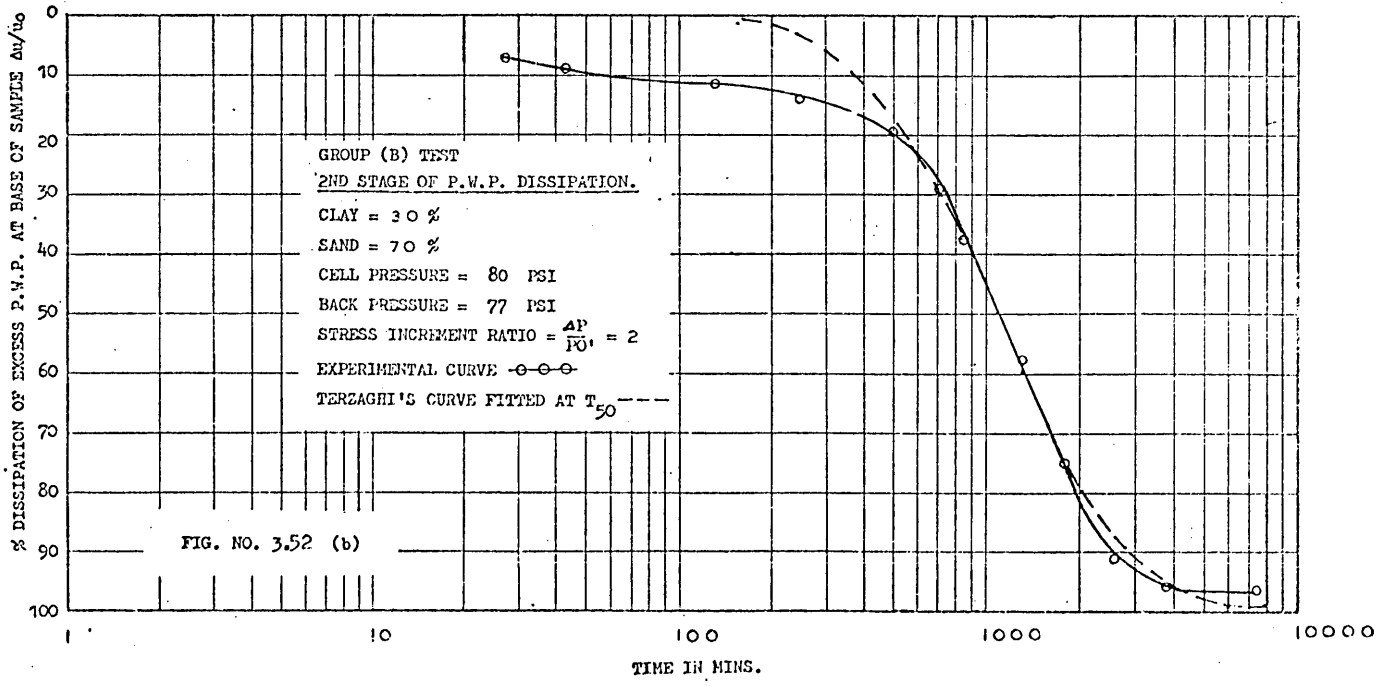

FIG. NO. 3.52 (b)

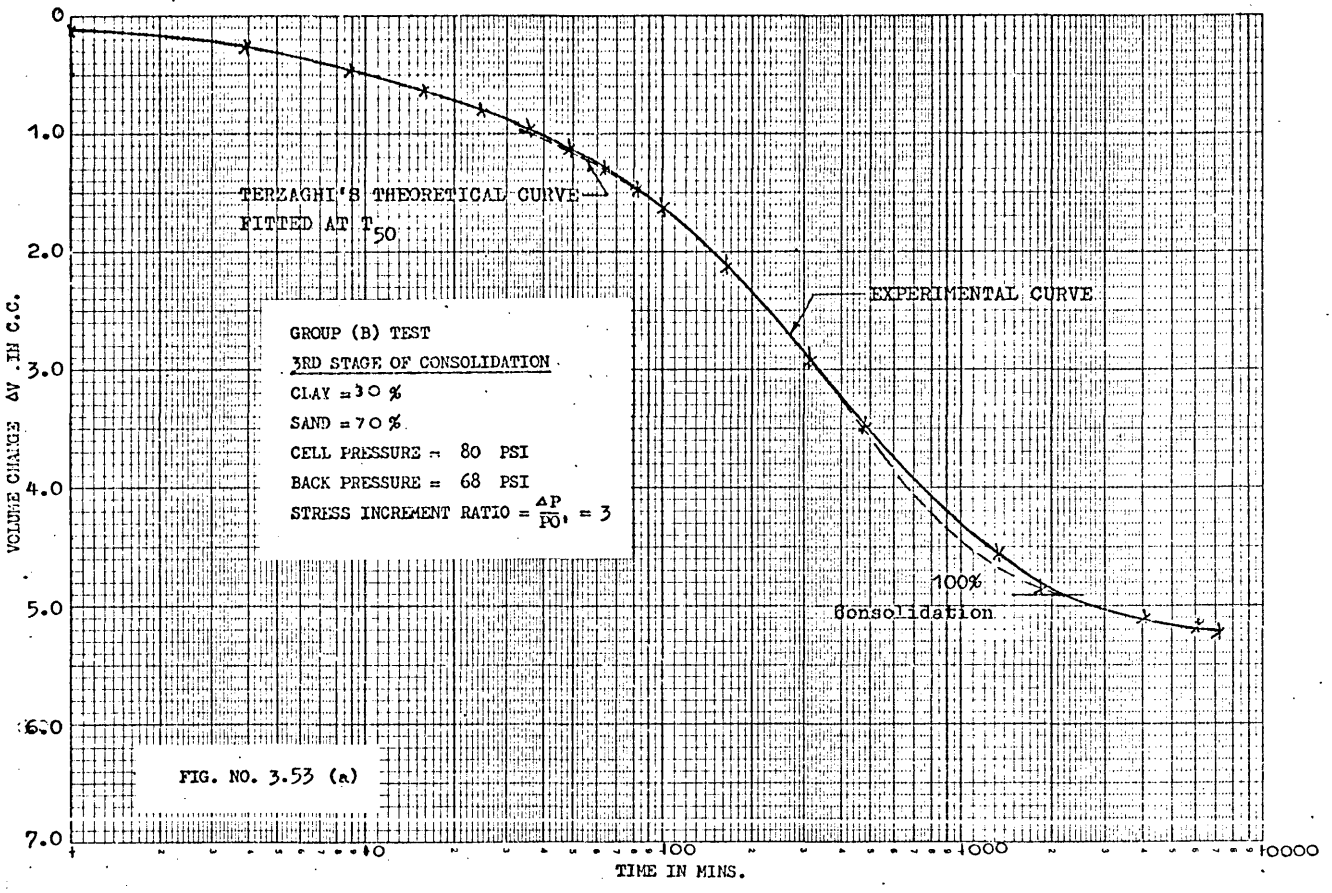

FIG. NO. 3.53 (a)

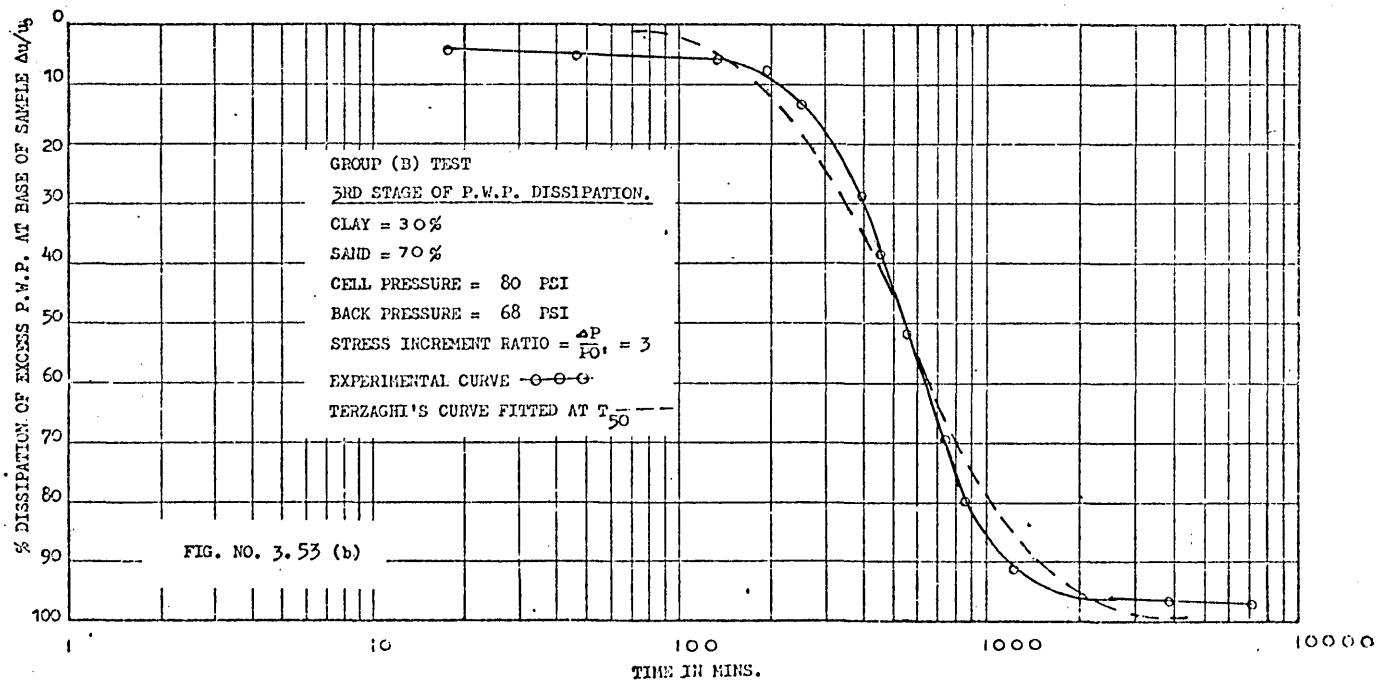

FIG. NO. 3.53 (b)

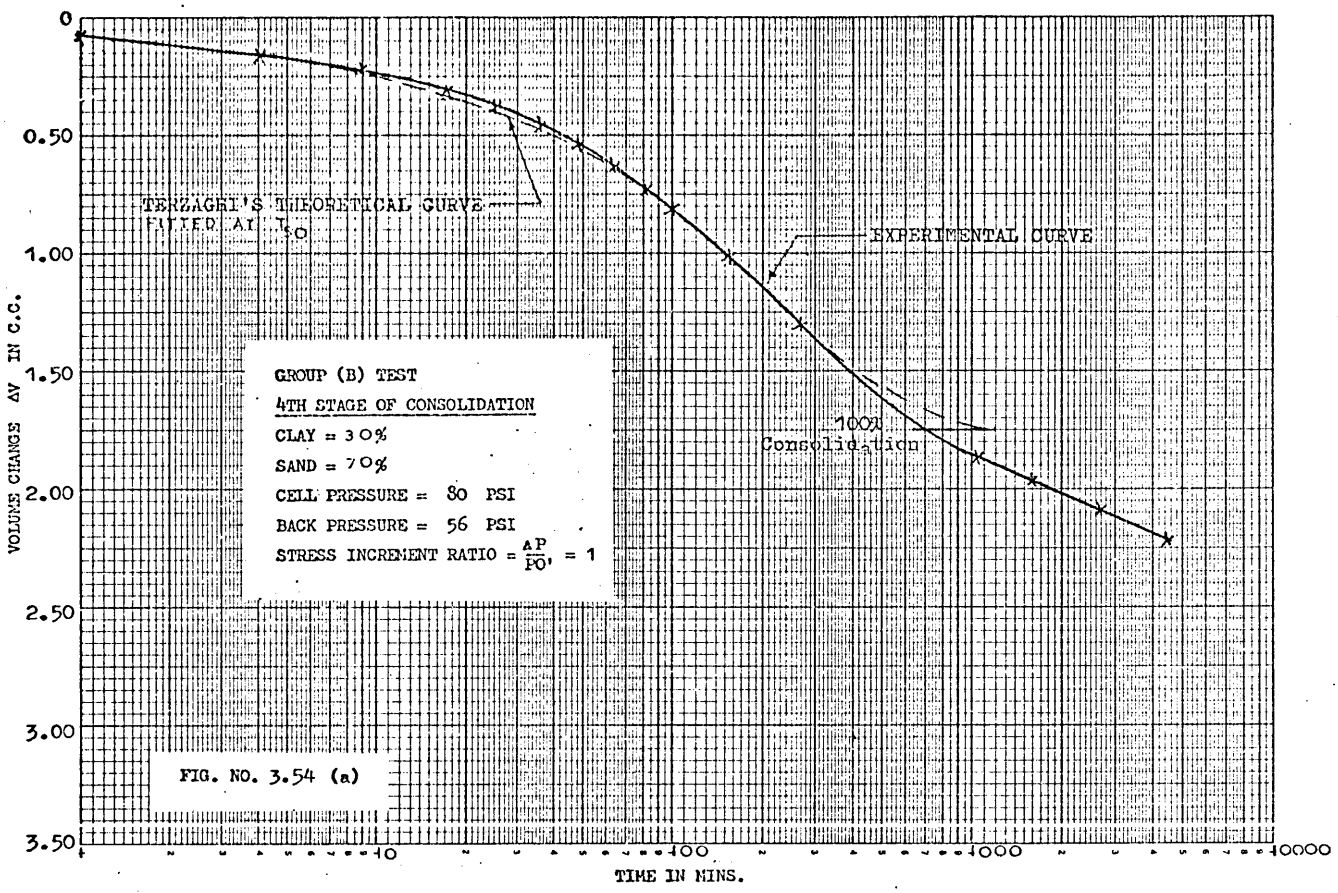

FIG. NO. 3.54 (a)

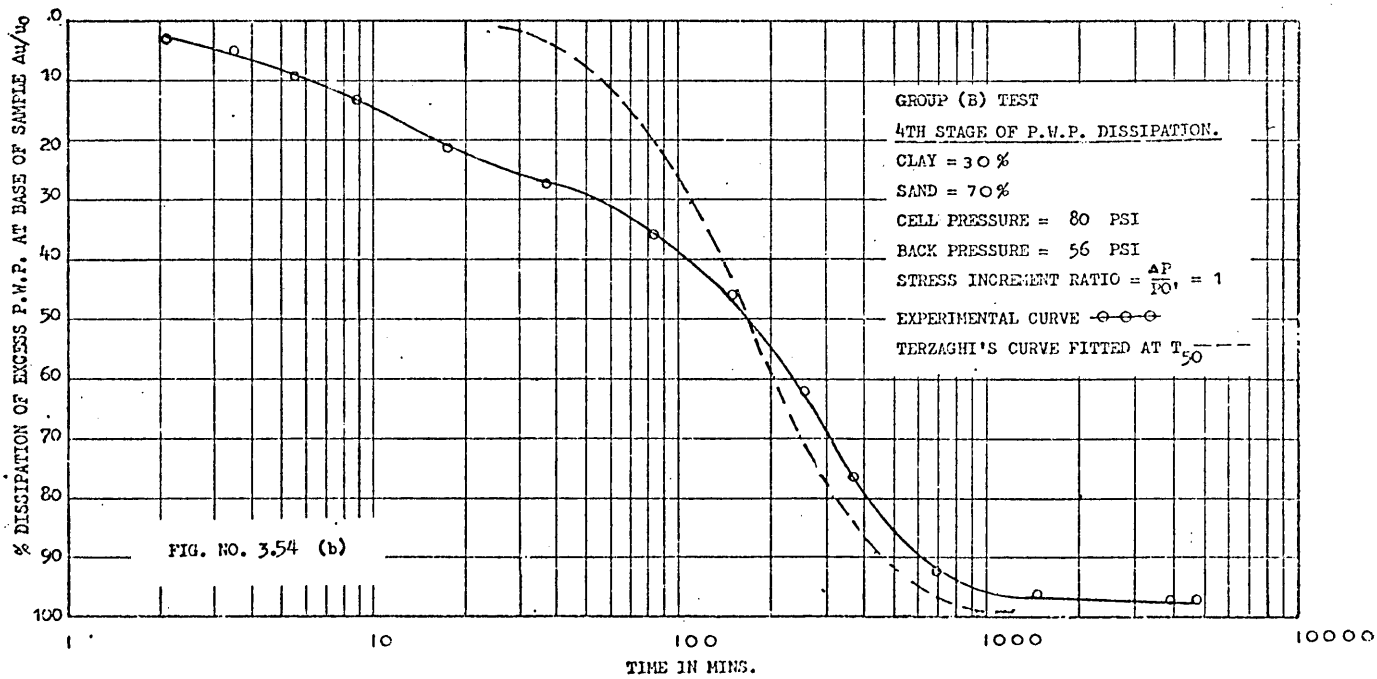

FIG. NO. 3.54 (b)

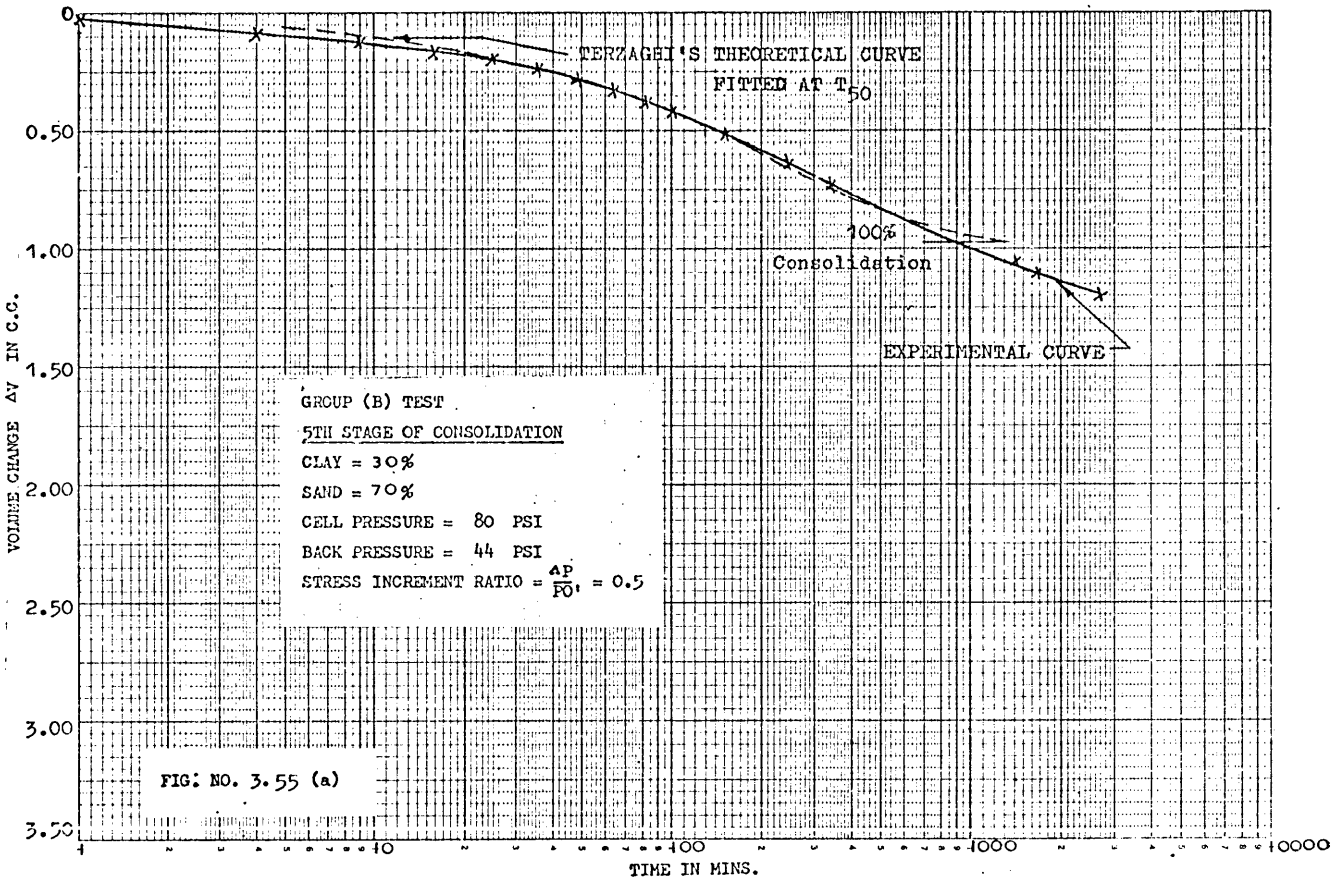

FIG. NO. 3.55 (a)

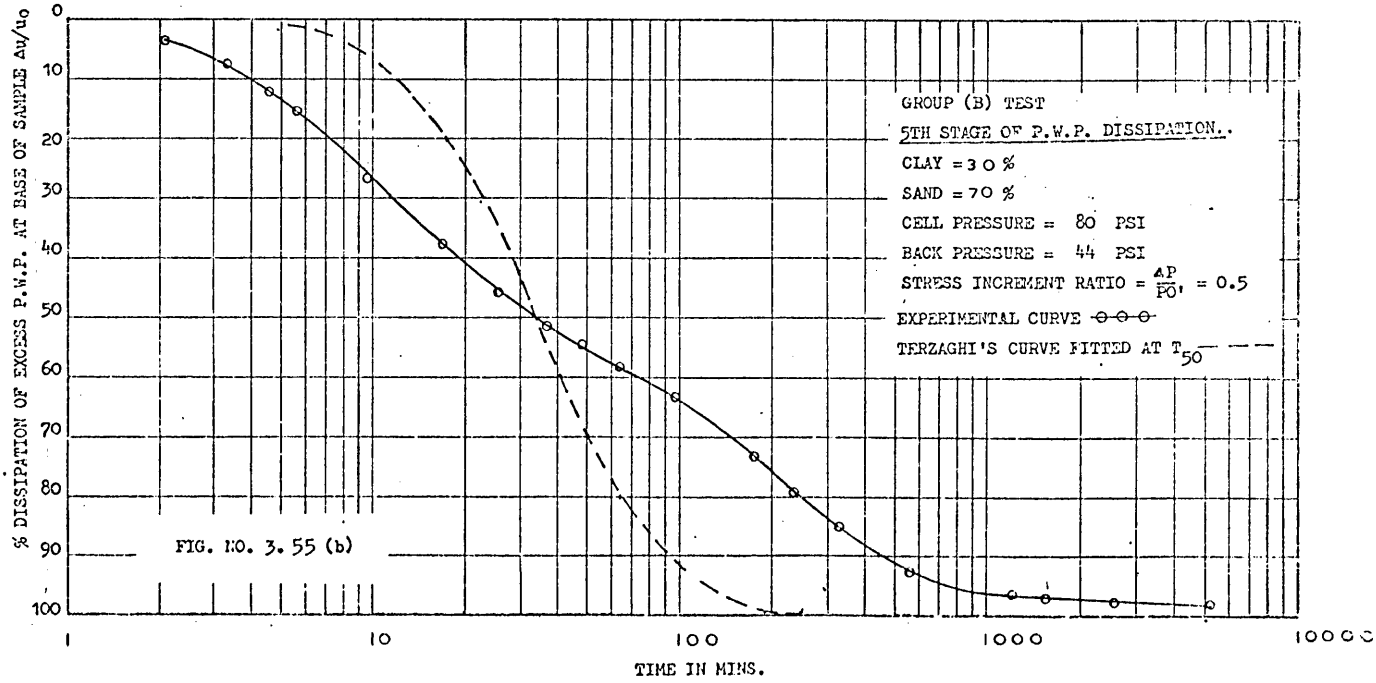

FIG. NO. 3.55 (b)

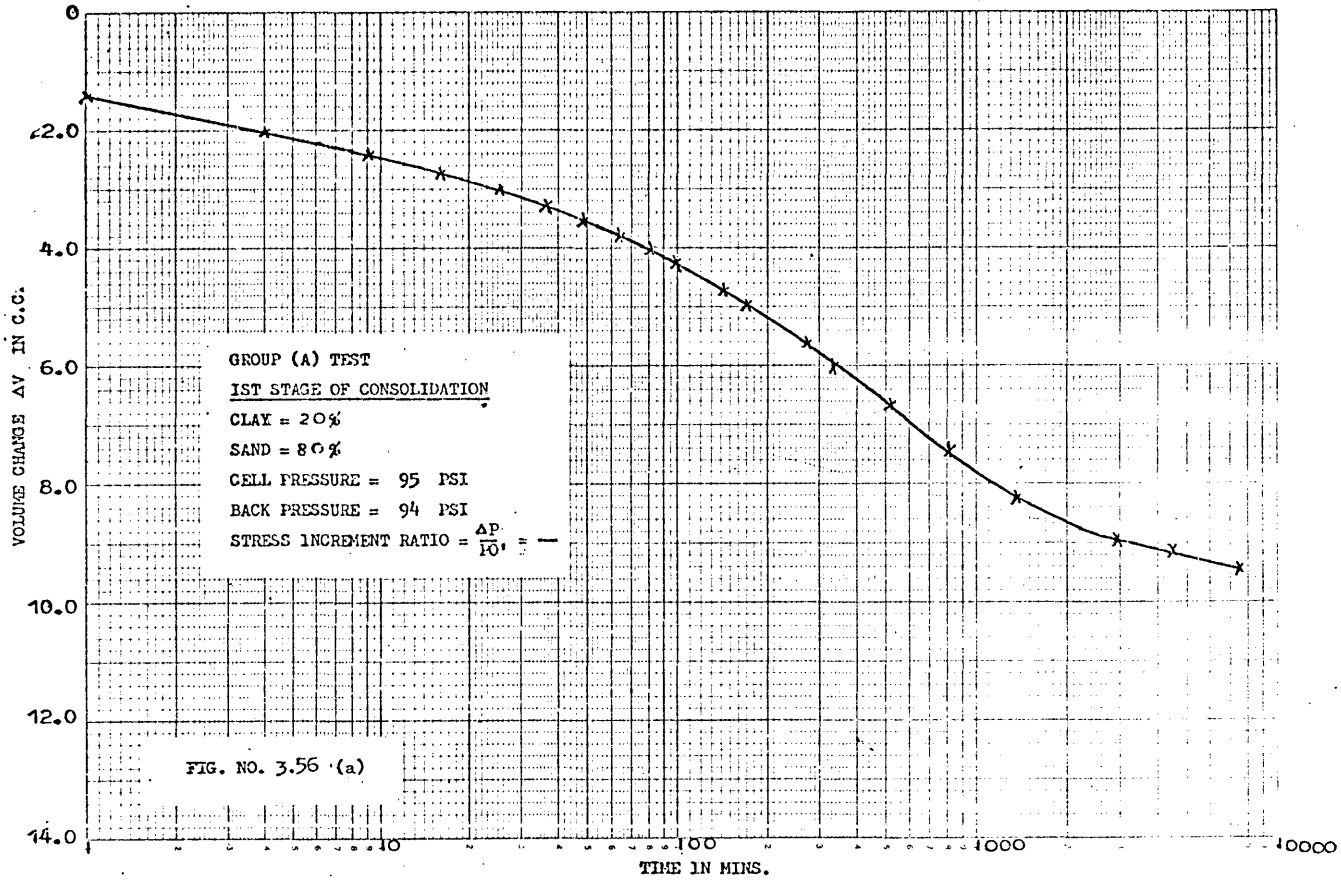

FIG. NO. 3.56 (a)

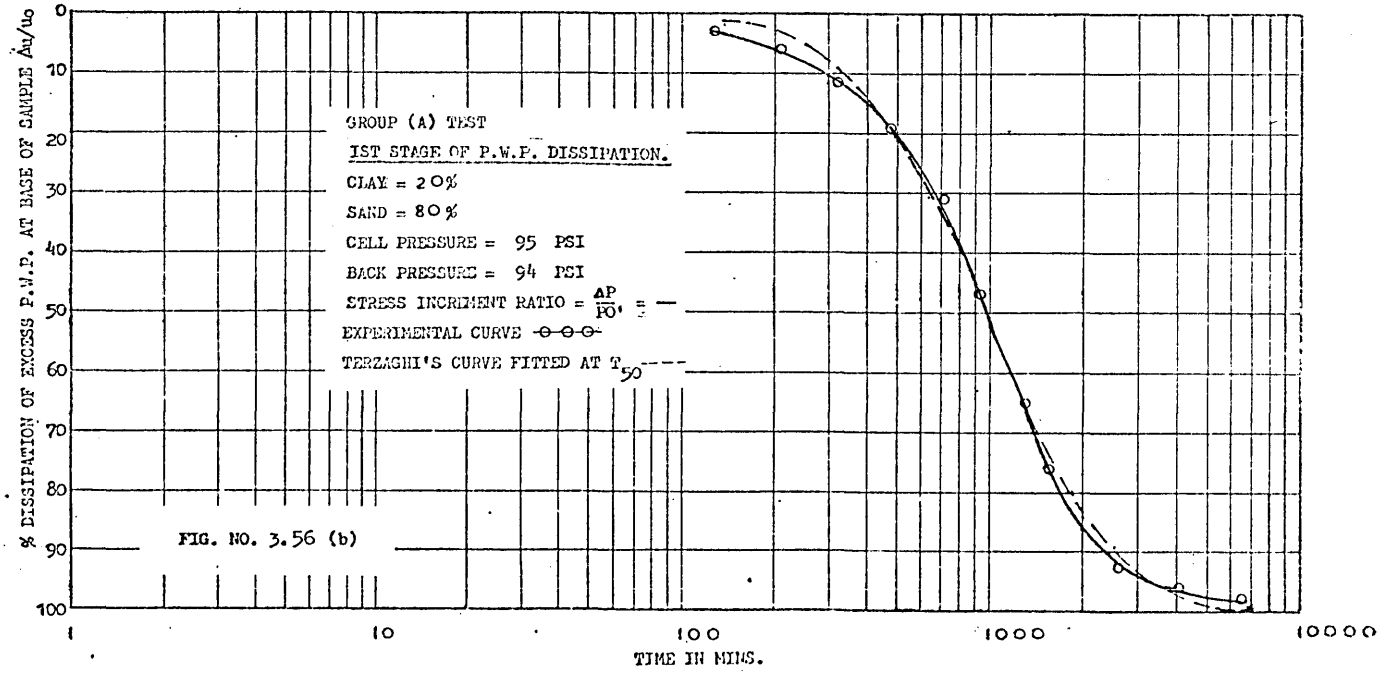

FIG. NO. 3.56 (b)

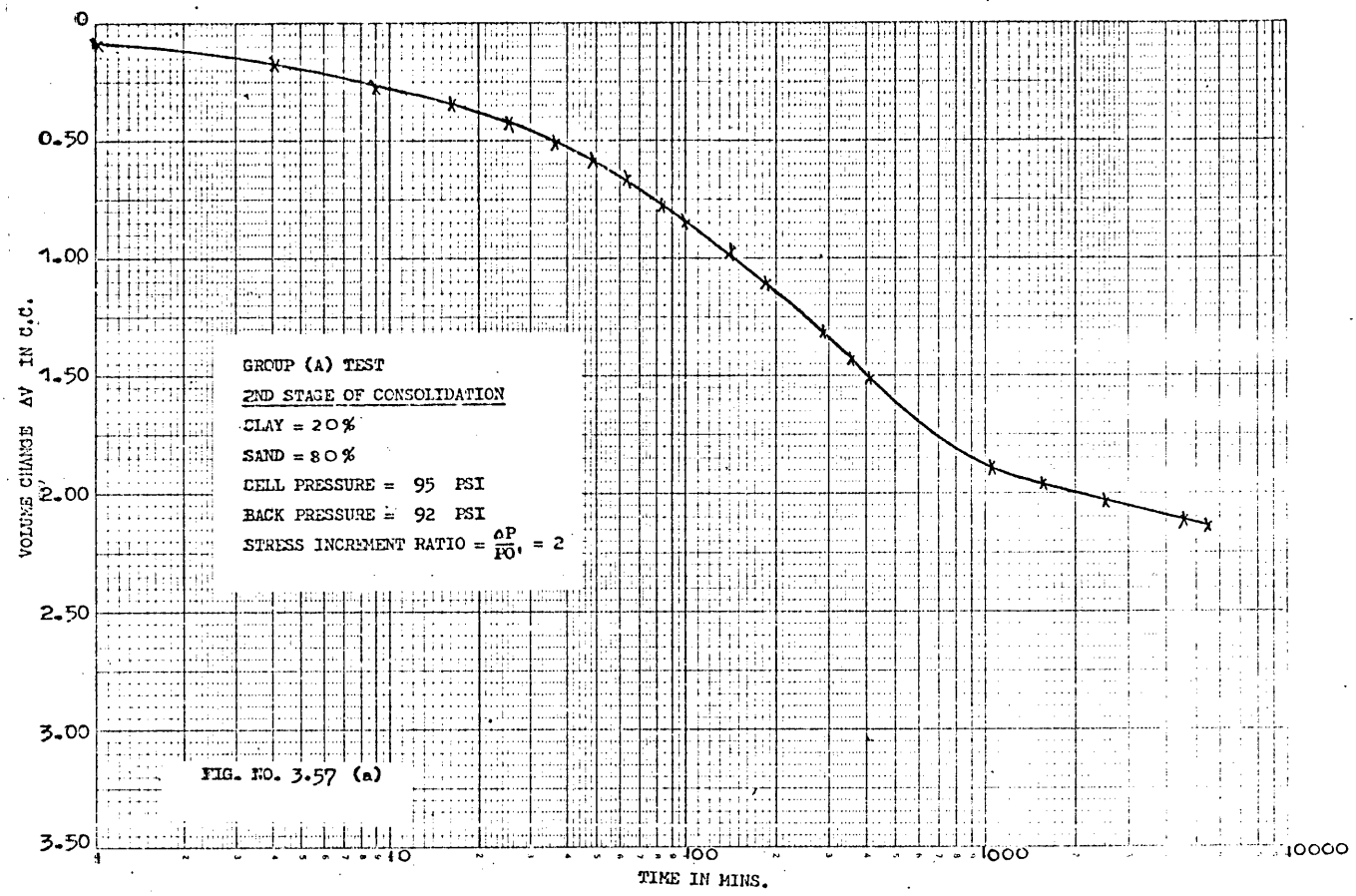

FIG. NO. 3.57 (a)

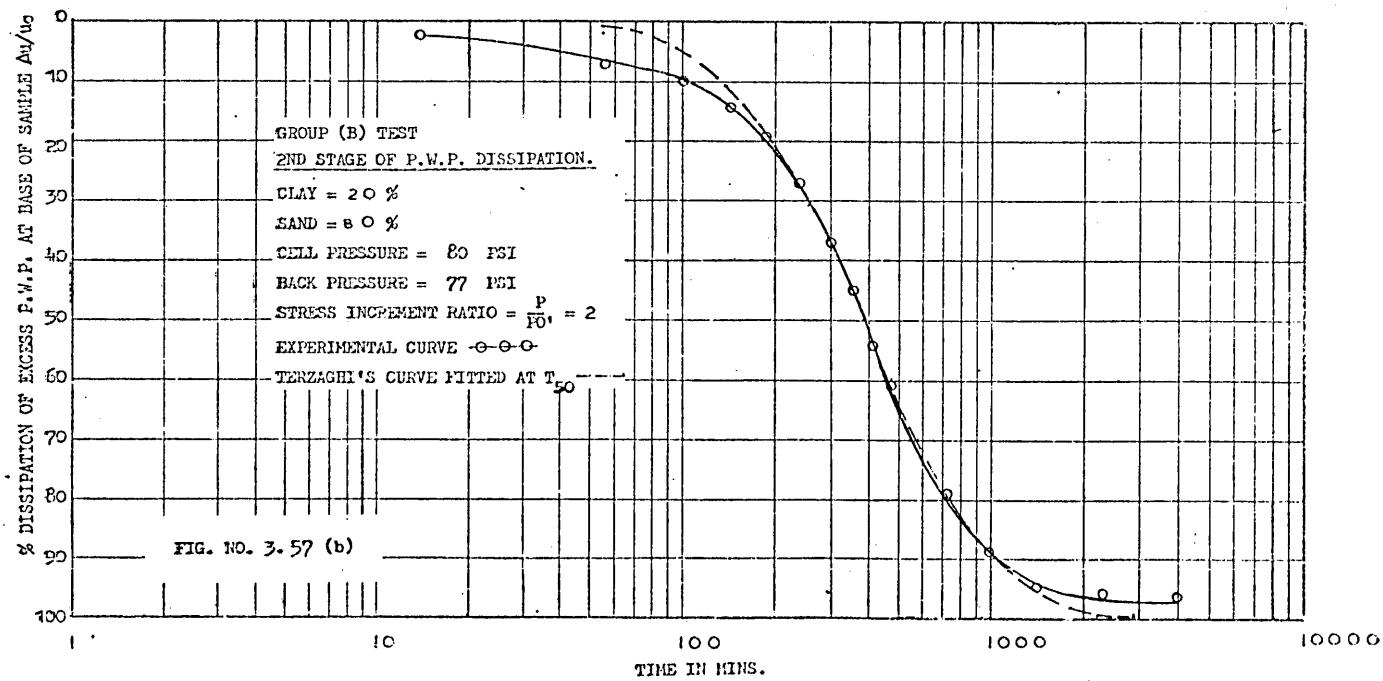

FIG. NO. 3.57 (b)

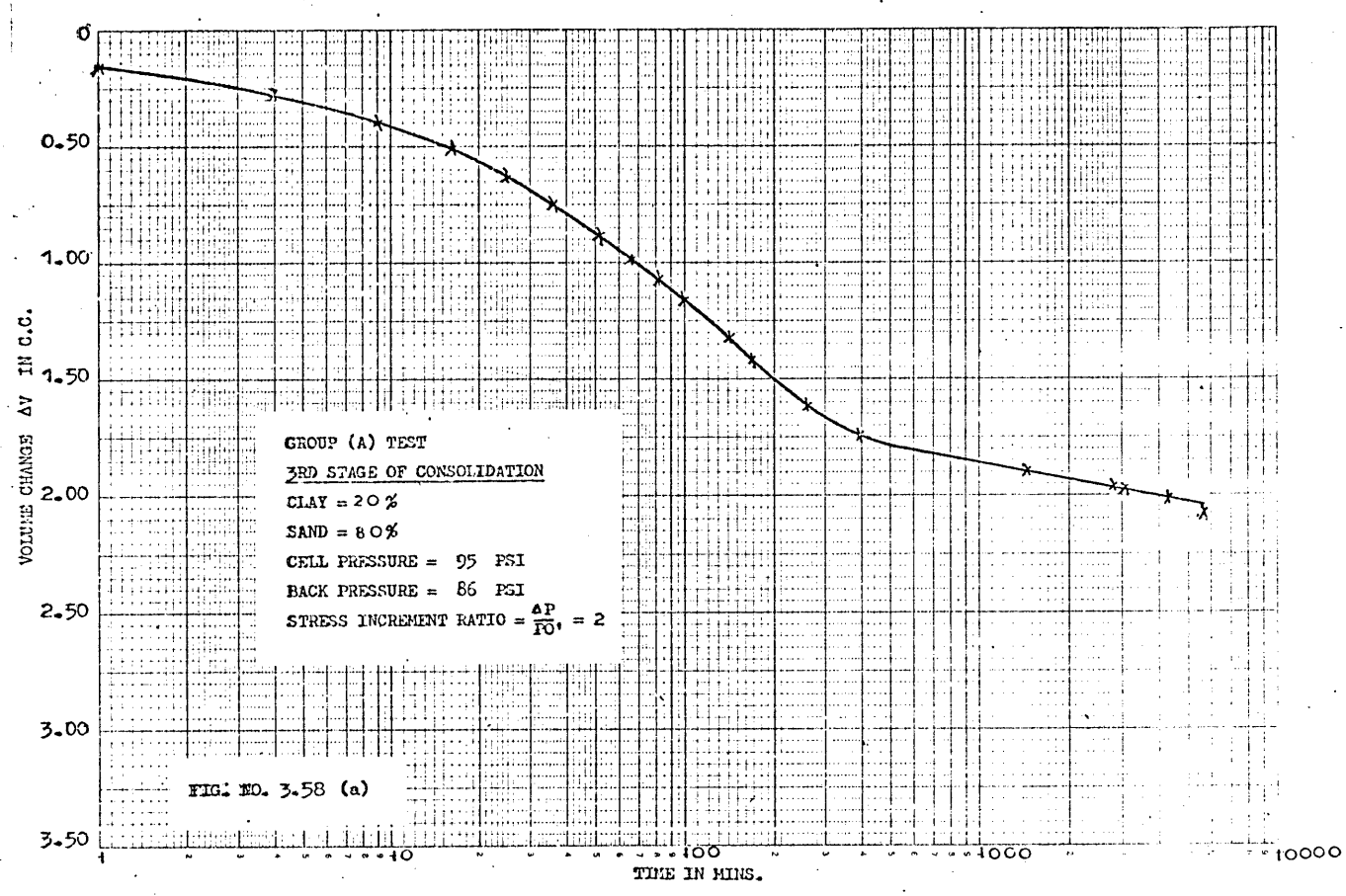

FIG. NO. 3.58 (a)

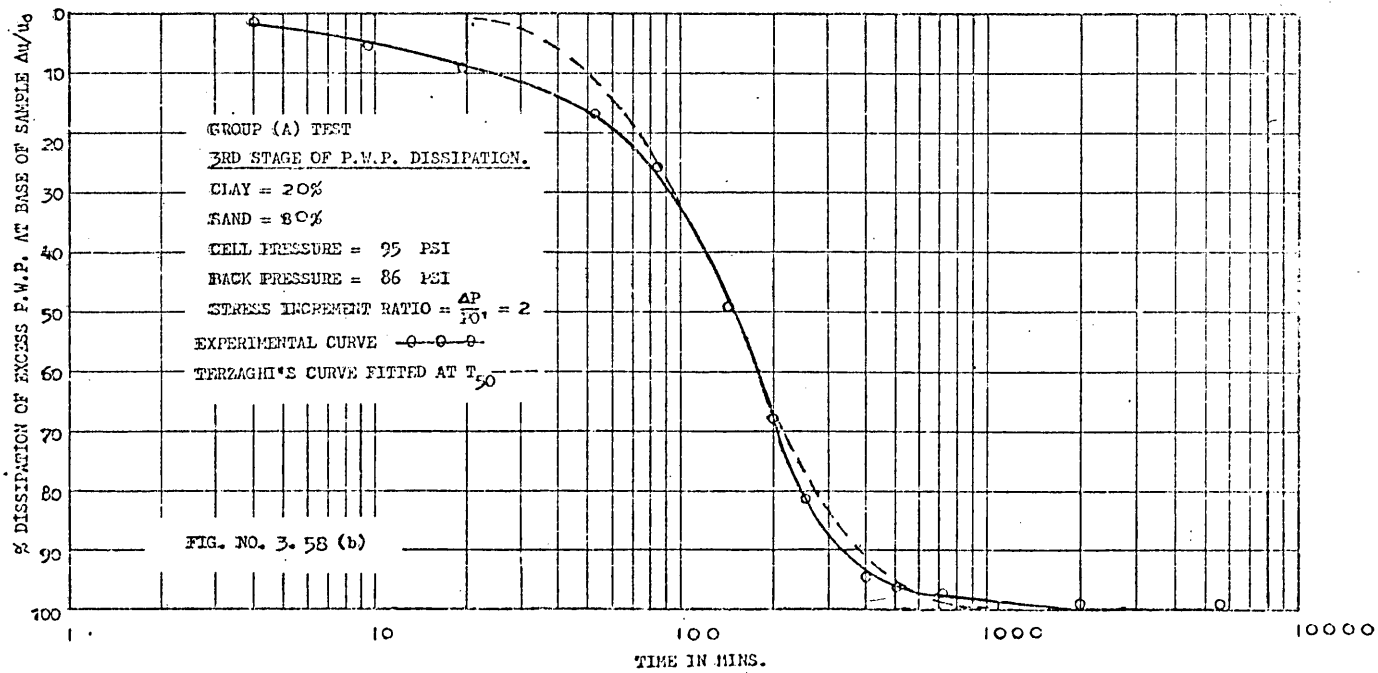

FIG. NO. 3.58 (b)

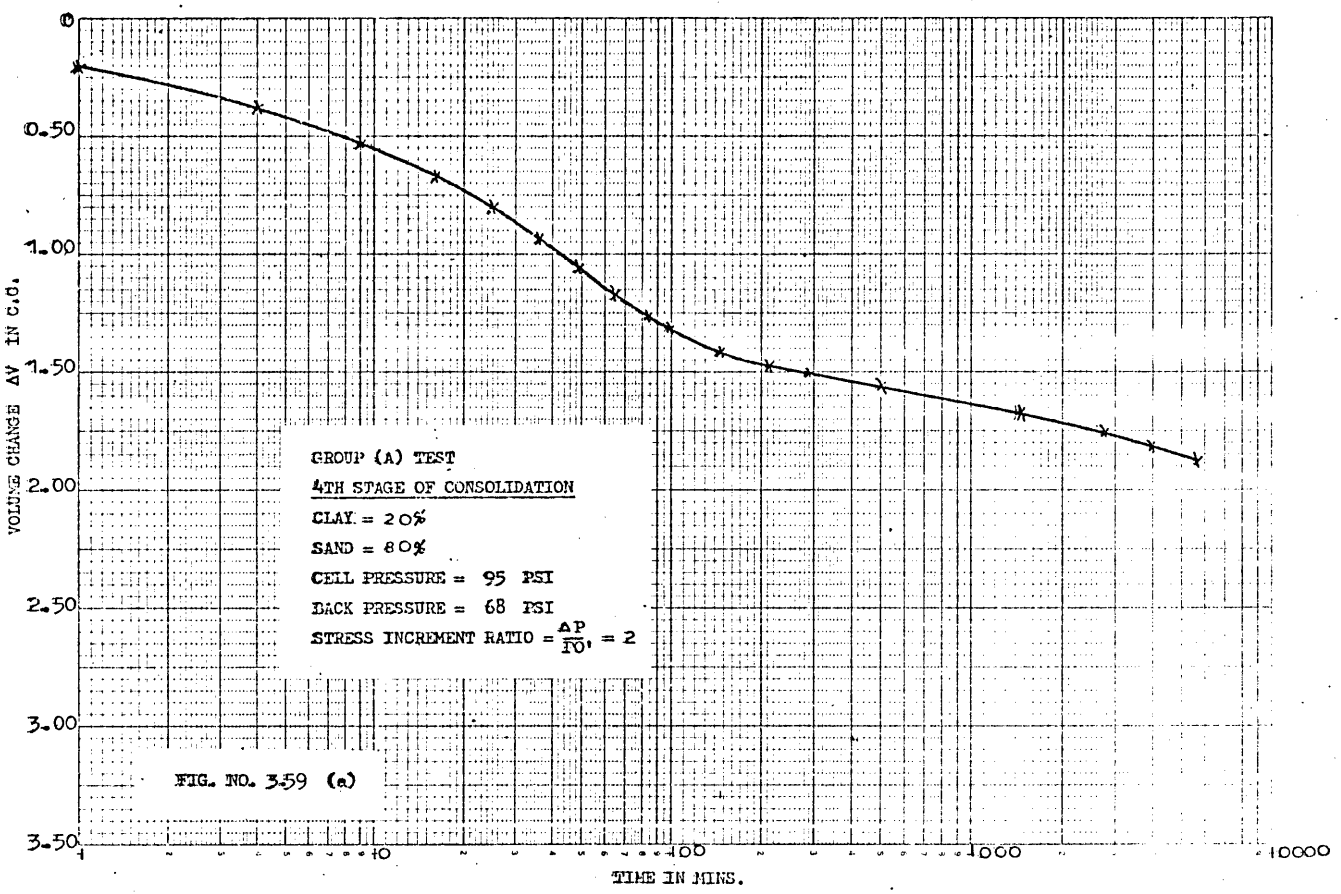

FIG. NO. 3.59 (a)

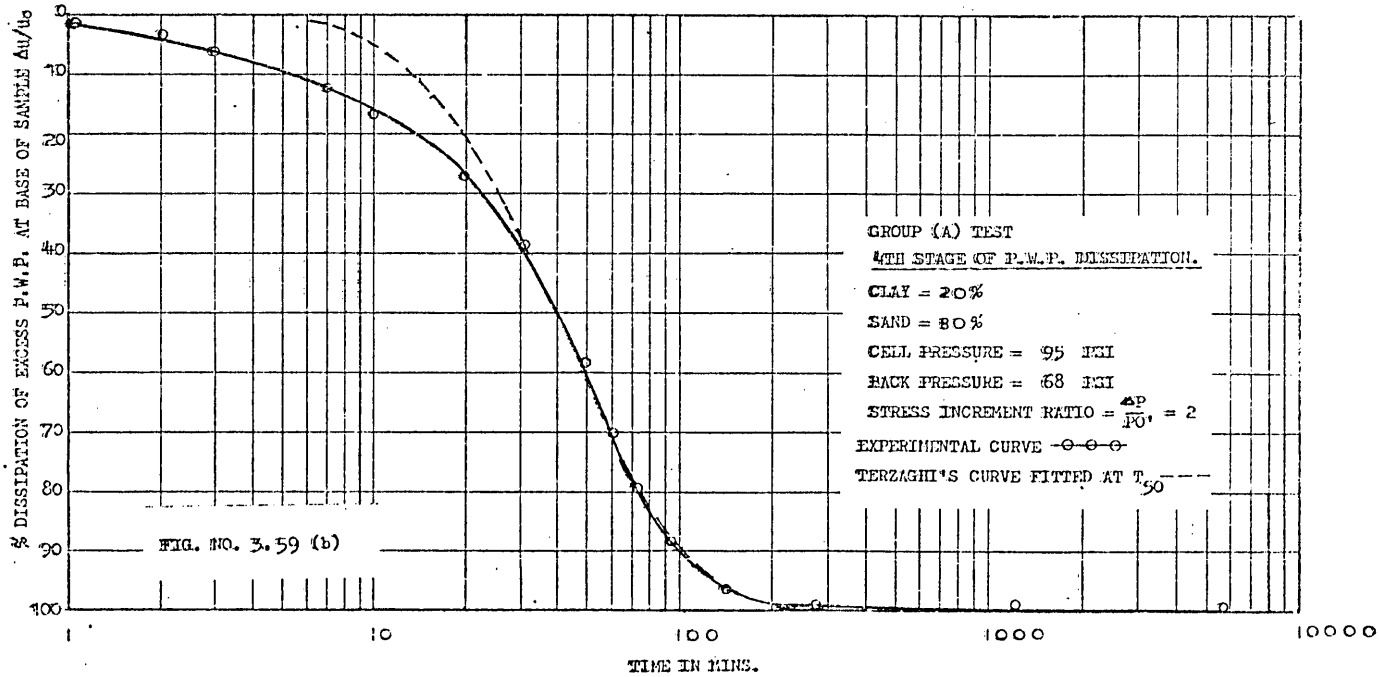

FIG. NO. 3.59 (b)

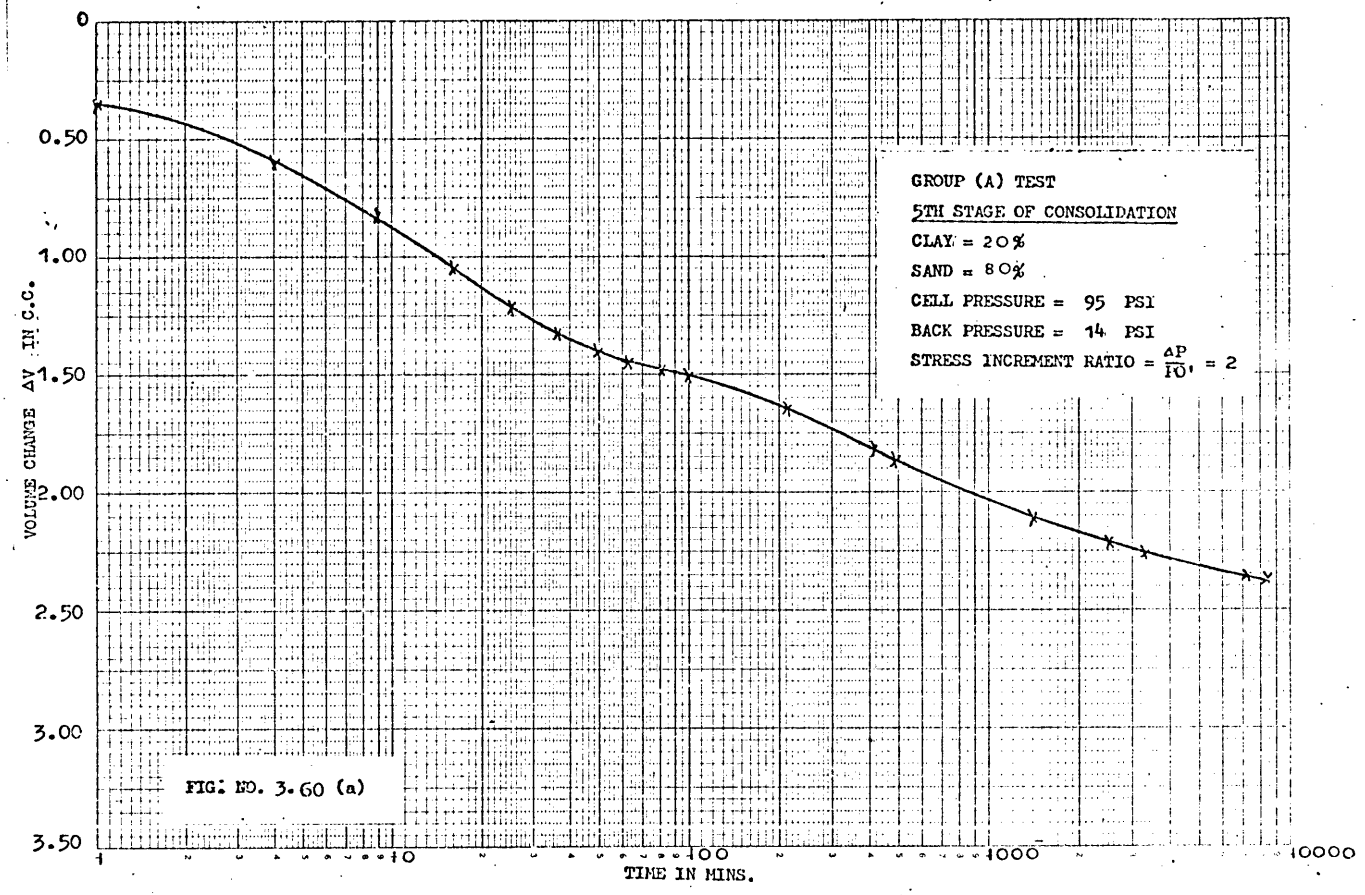

FIG. NO. 3.60 (a)

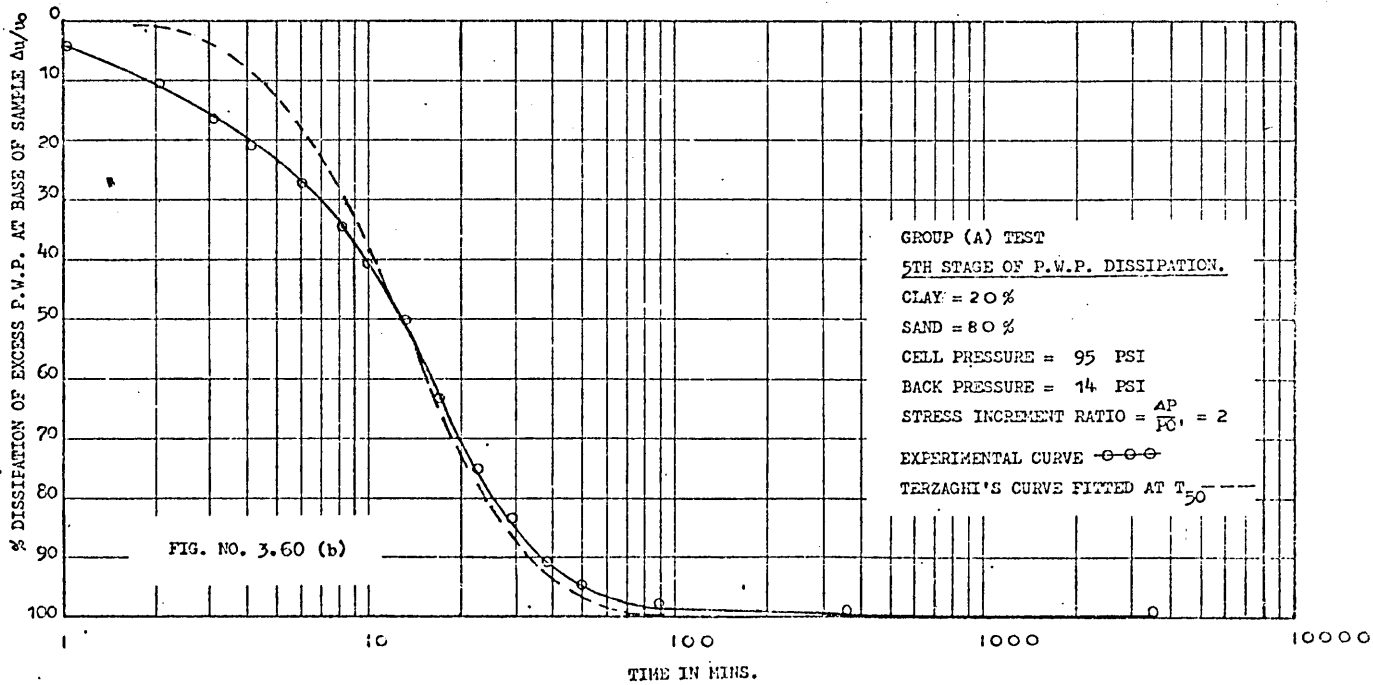

FIG. NO. 3.60 (b)

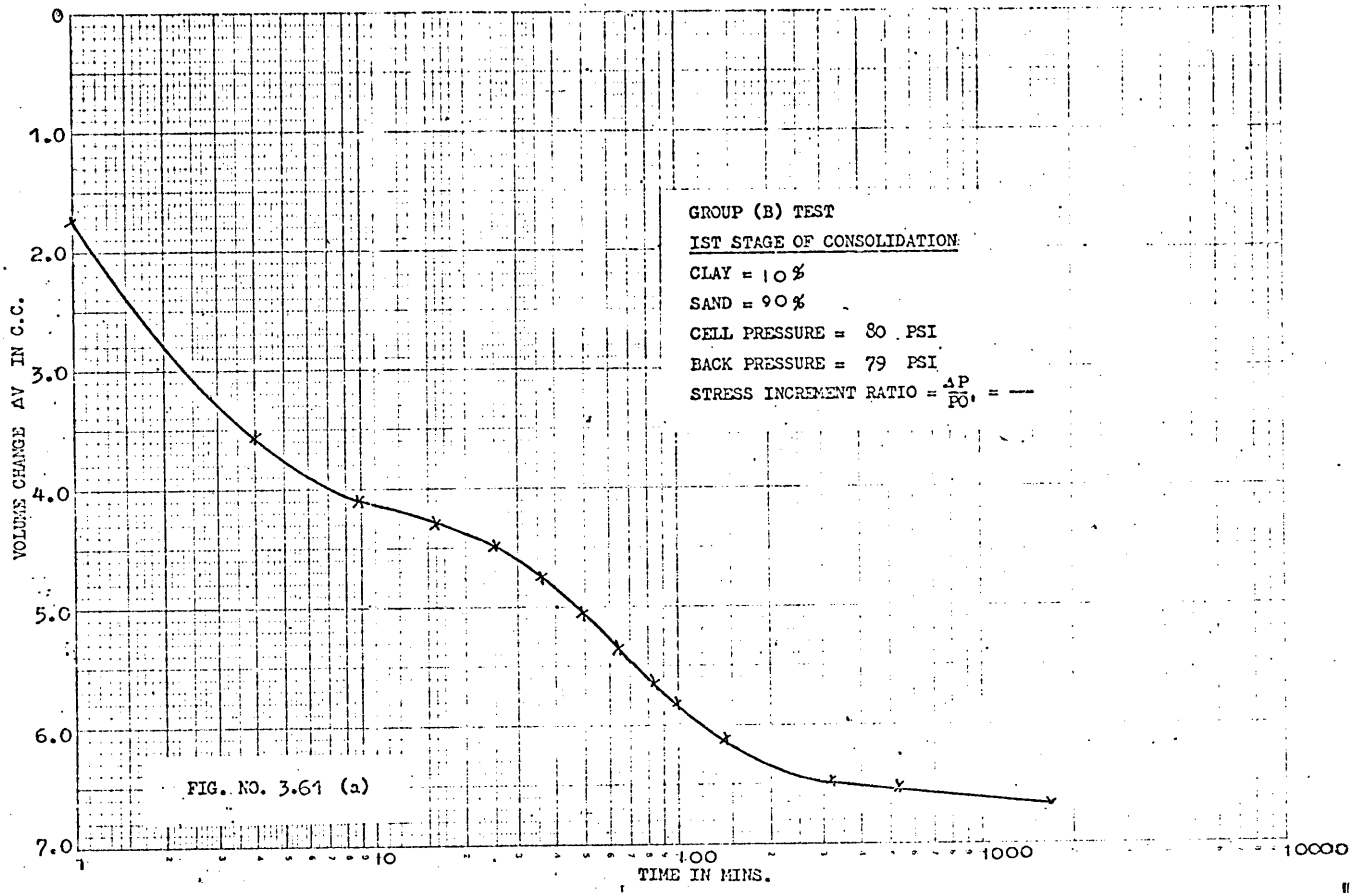
VOLUME CHANGE ΔV IN C.C.
0
1.0
2.0
3.0
4.0
5.0
6.0
7.0
1
10
100
1000
10000
TIME IN MINS.
GROUP (B) TEST
IST STAGE OF CONSOLIDATION
CLAY = 10 %
SAND = 90 %
CELL PRESSURE = 80 PSI
BACK PRESSURE = 79 PSI
STRESS INCREMENT RATIO = ΔP/P0' = —
FIG. NO. 3.61 (a)

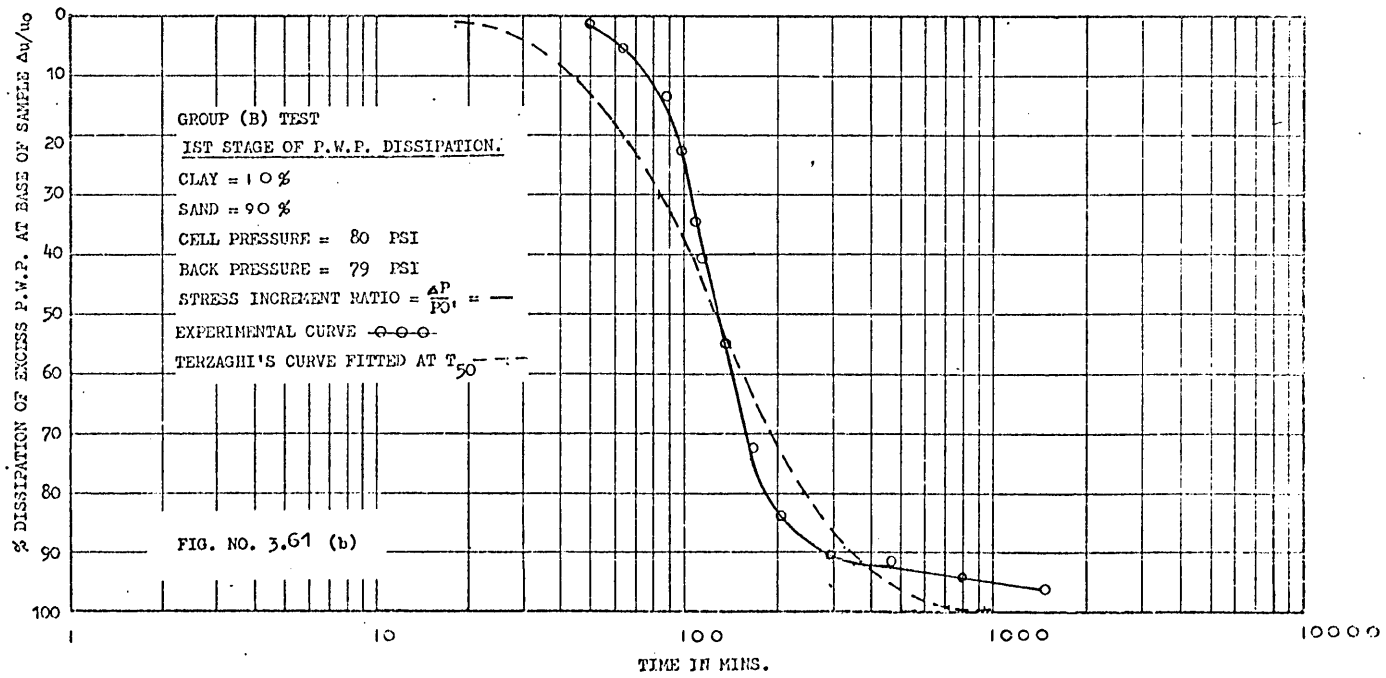
% DISSIPATION OF EXCESS P.W.P. AT BASE OF SAMPLE Δu/uo
0
10
20
30
40
50
60
70
80
90
100
1
10
100
1000
10000
TIME IN MINS.
GROUP (B) TEST
IST STAGE OF P.W.P. DISSIPATION.
CLAY = 10 %
SAND = 90 %
CELL PRESSURE = 80 PSI
BACK PRESSURE = 79 PSI
STRESS INCREMENT RATIO = ΔP/P0' = —
EXPERIMENTAL CURVE -o-o-o-
TERZAGHI'S CURVE FITTED AT T50 — - —
FIG. NO. 3.61 (b)

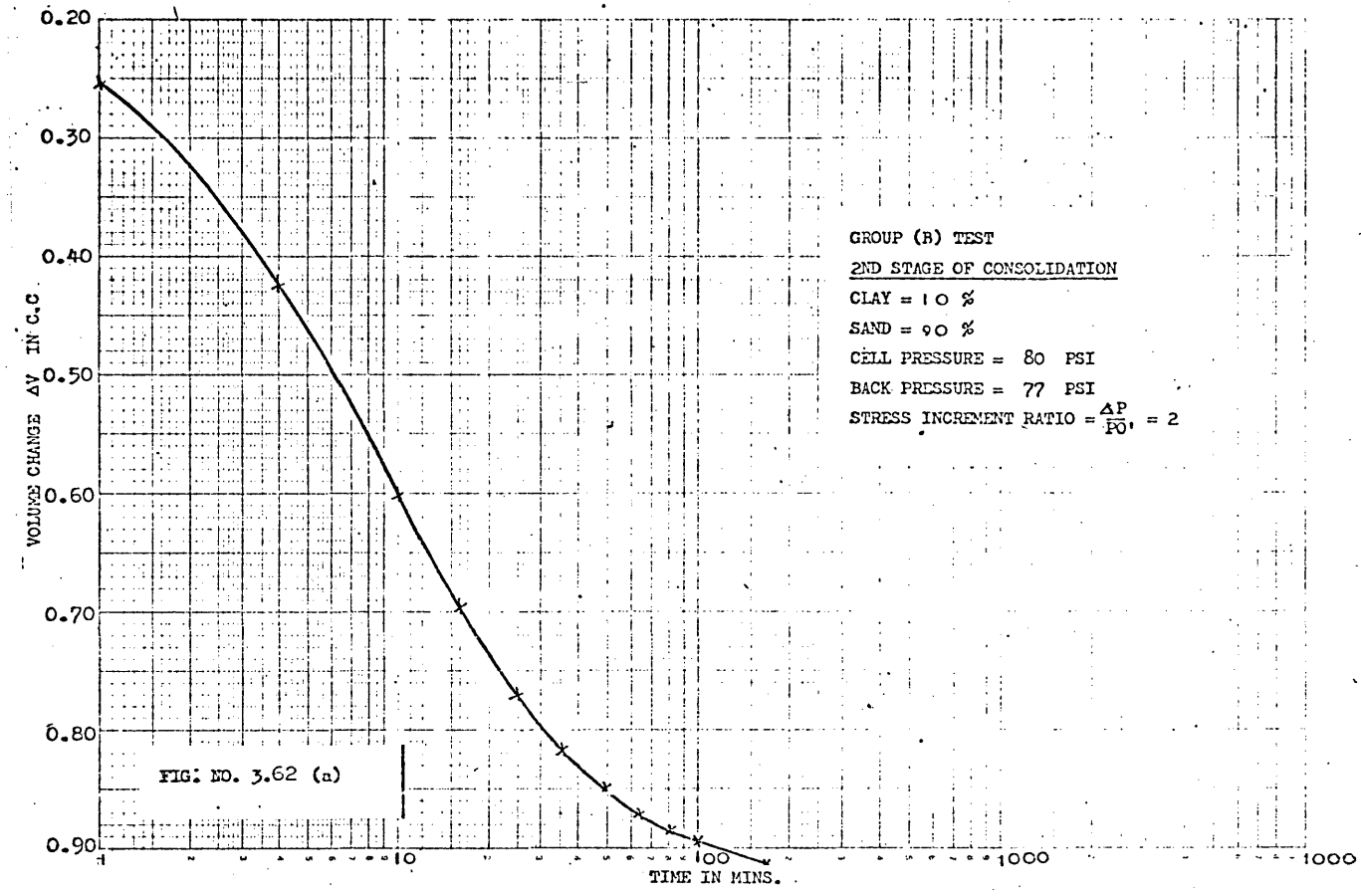

FIG. NO. 3.62 (a)

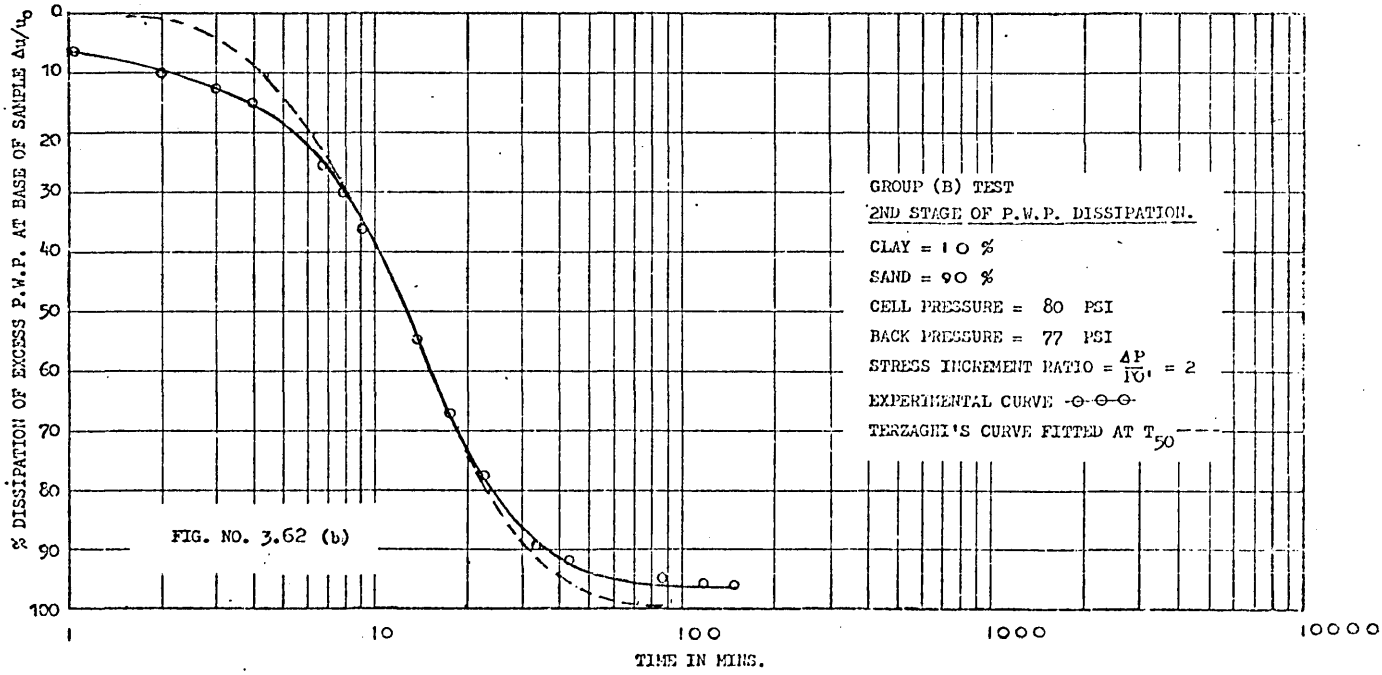

FIG. NO. 3.62 (b)

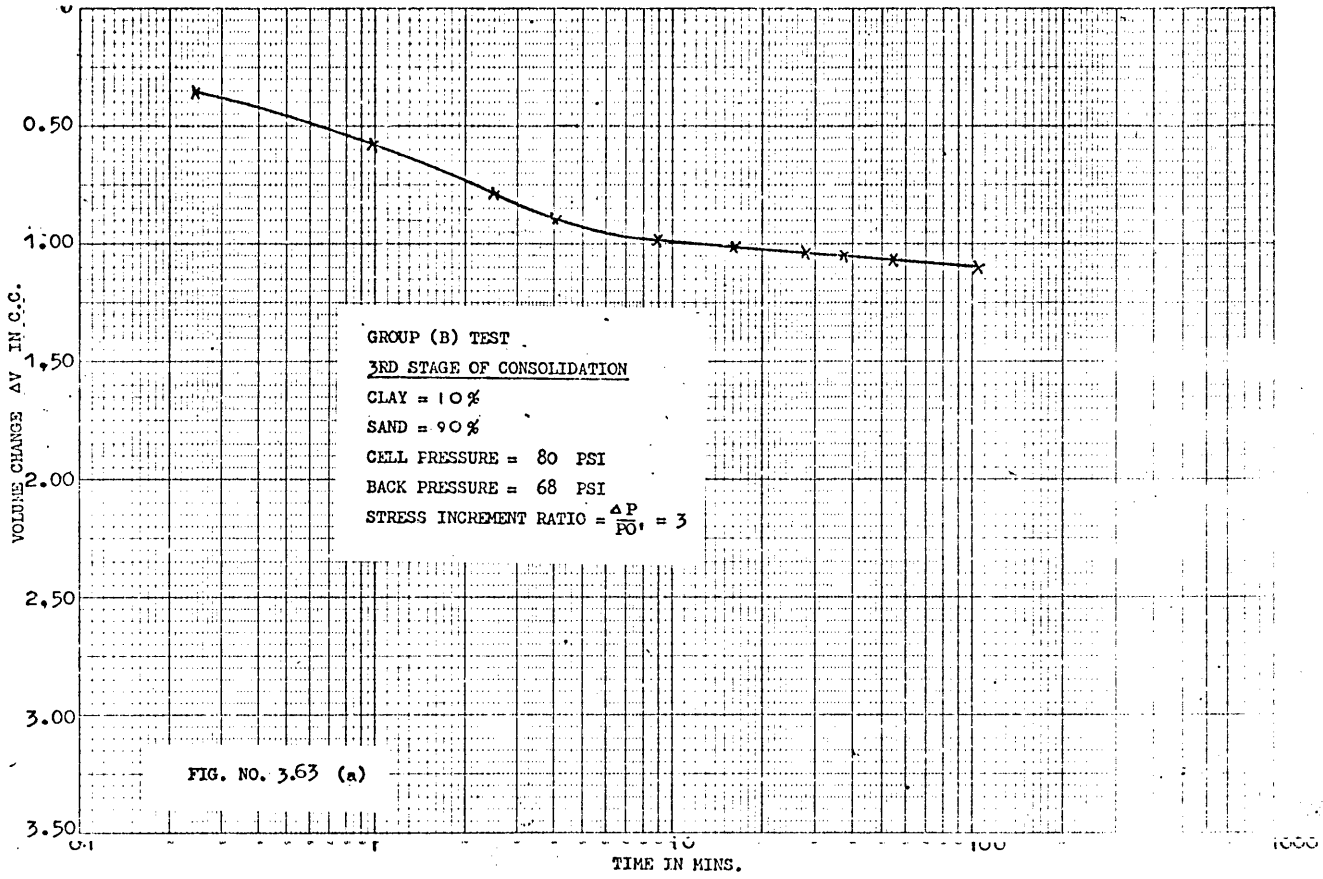

FIG. NO. 3.63 (a)

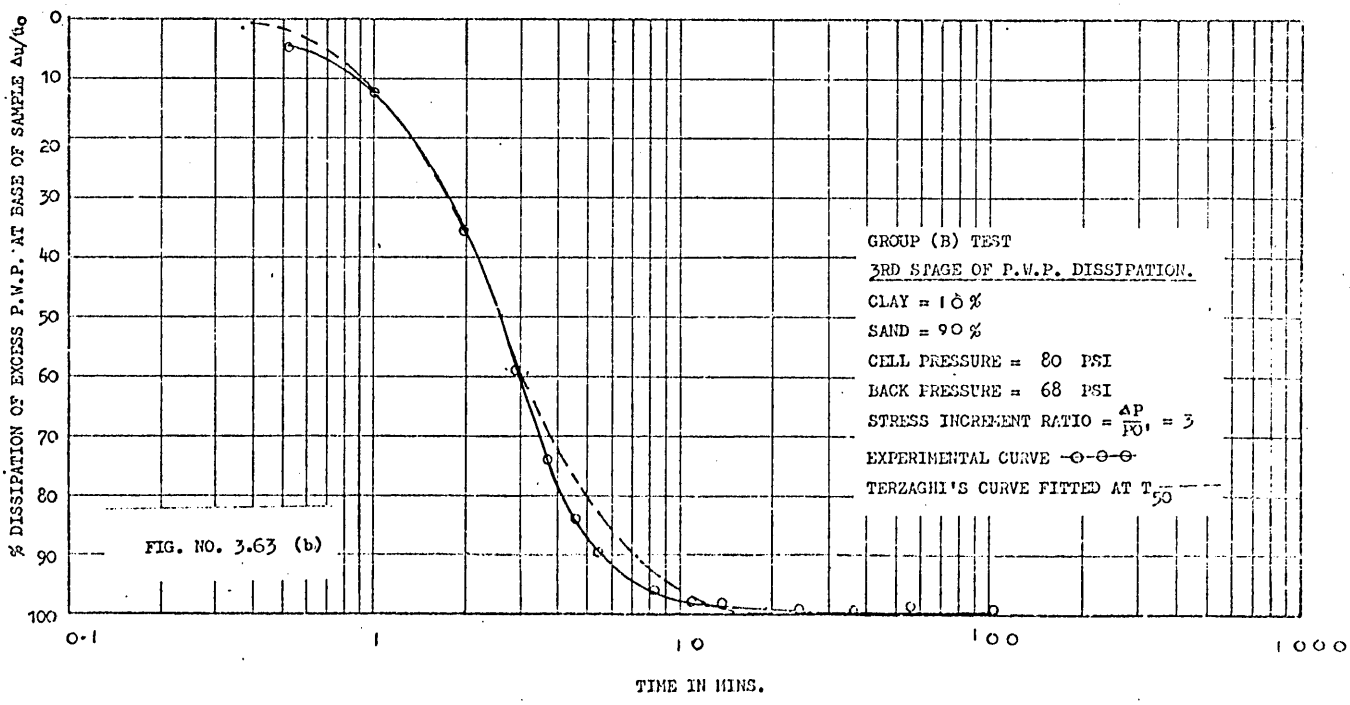

FIG. NO. 3.63 (b)

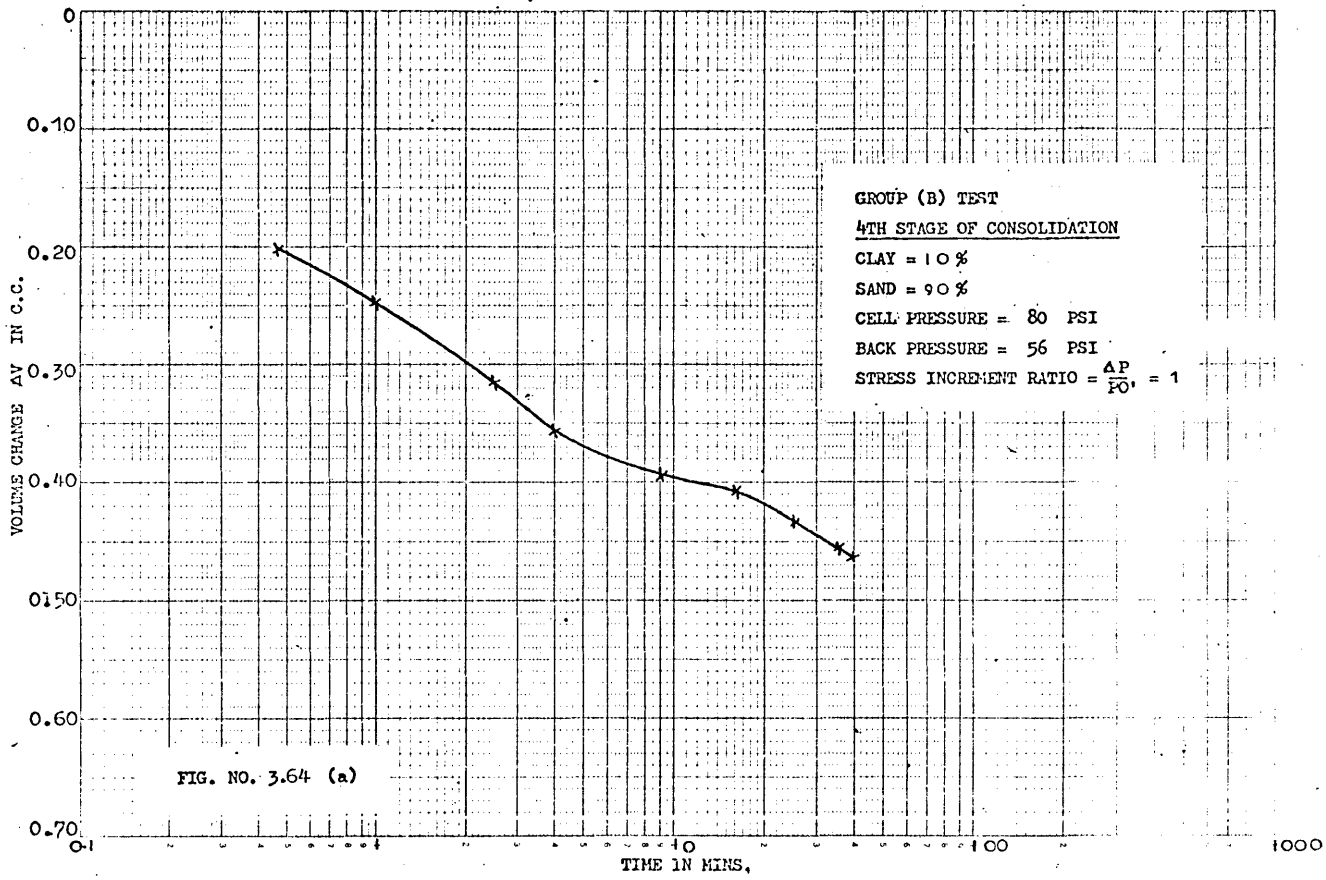

FIG. NO. 3.64 (a)

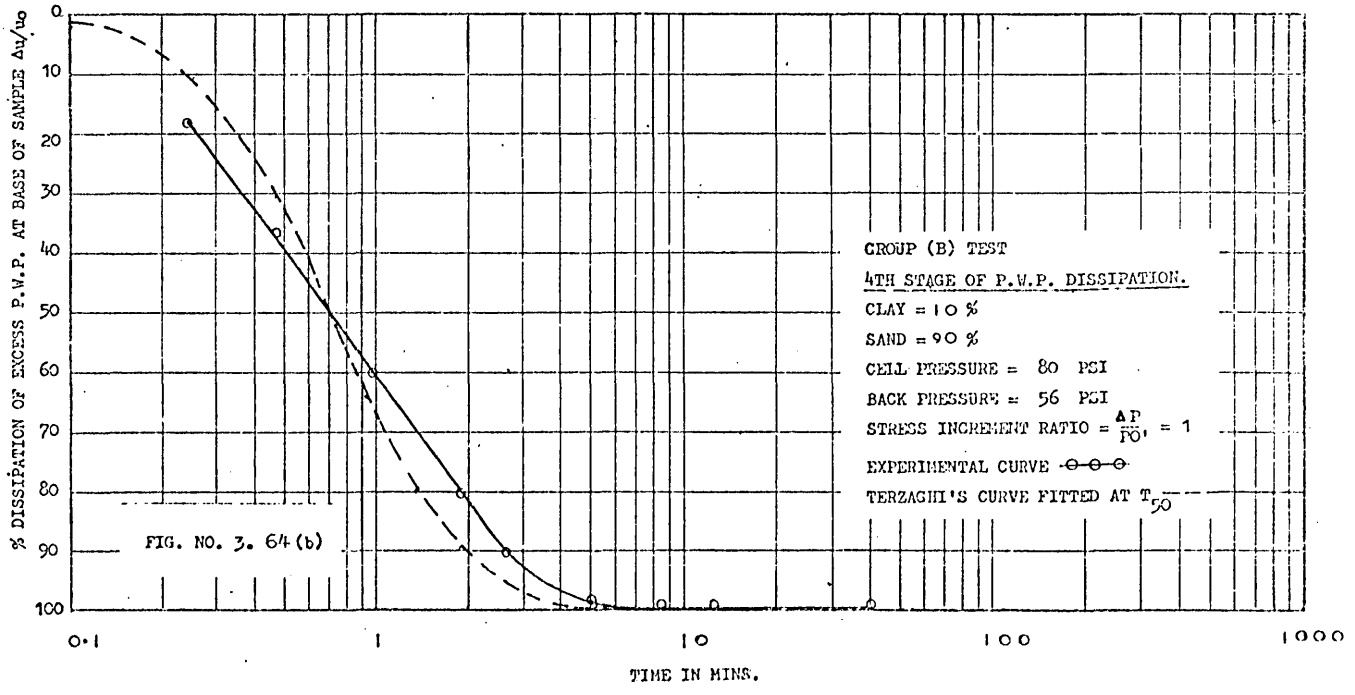

FIG. NO. 3. 64 (b)

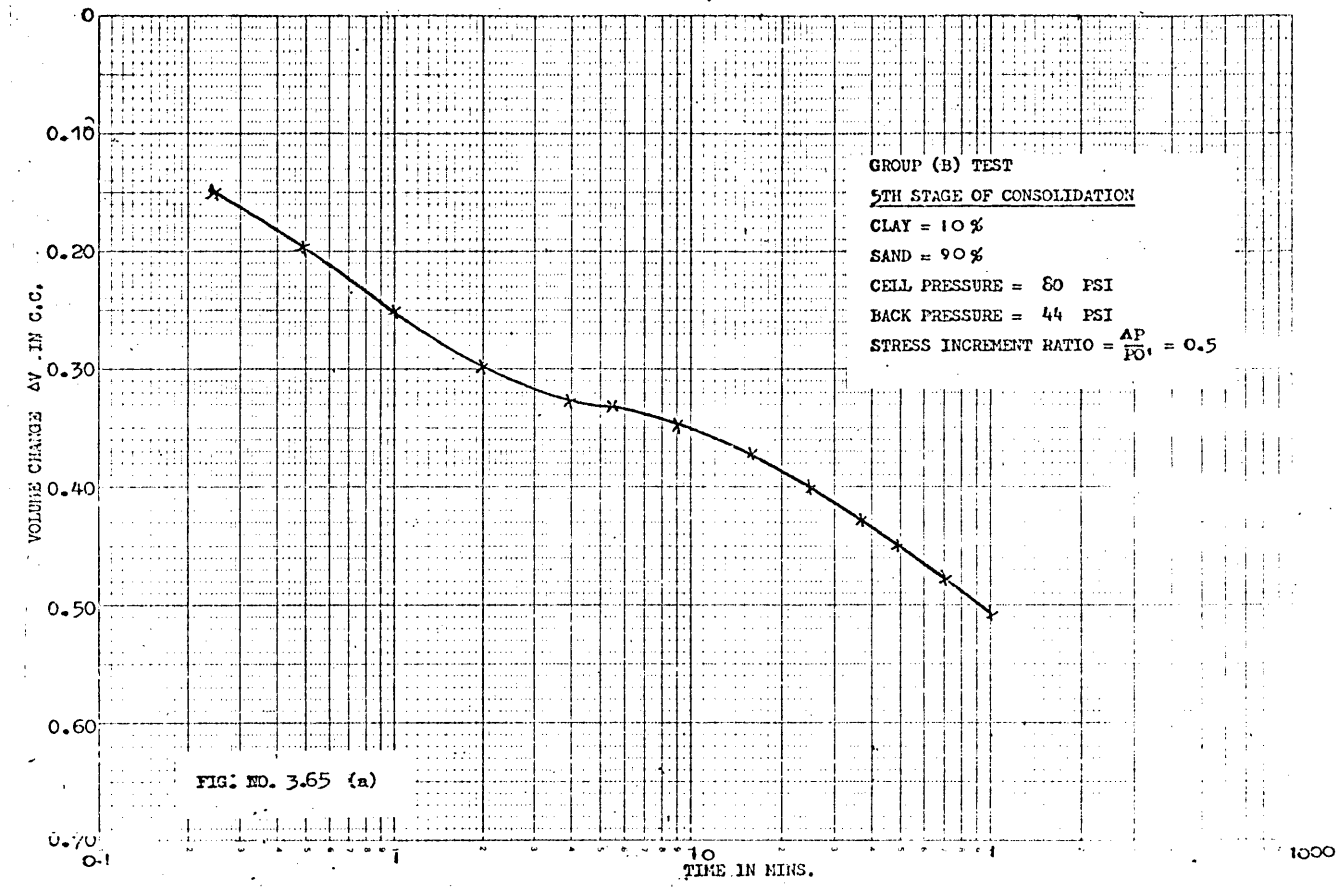

FIG. NO. 3.65 (a)

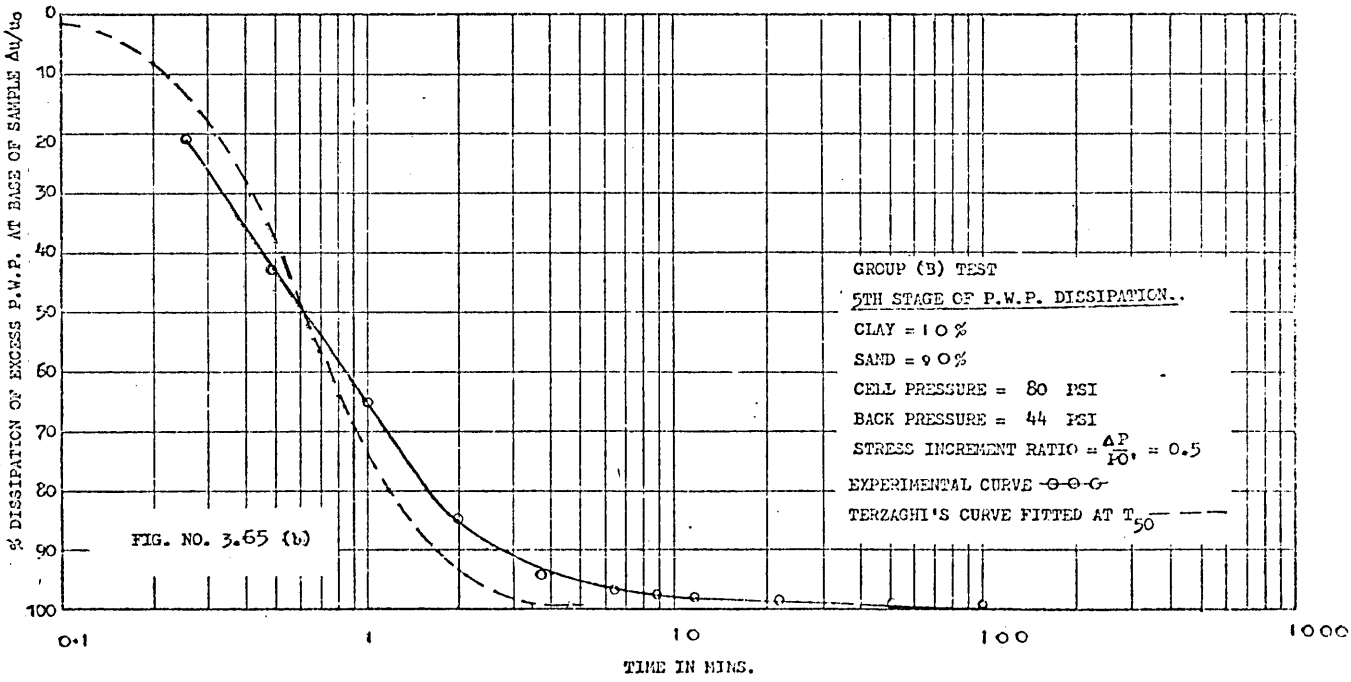

FIG. NO. 3.65 (b)

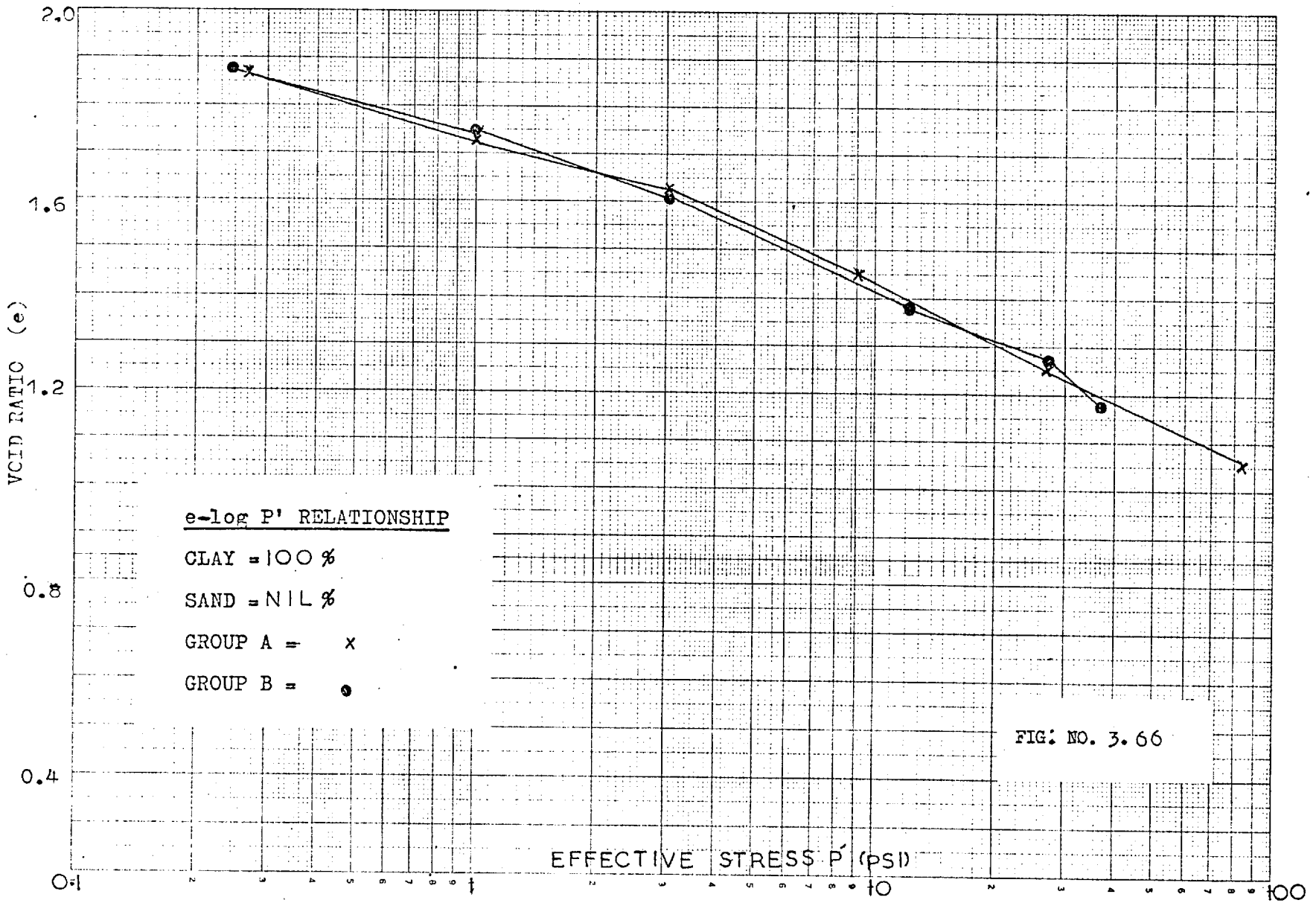
2.0
1.6
1.2
0.8
0.4
VOID RATIO (e)
e-log P' RELATIONSHIP
CLAY = 100 %
SAND = NIL %
GROUP A = x
GROUP B = ●
0.1
1
10
100
EFFECTIVE STRESS P' (PSI)

FIG. NO. 3.66

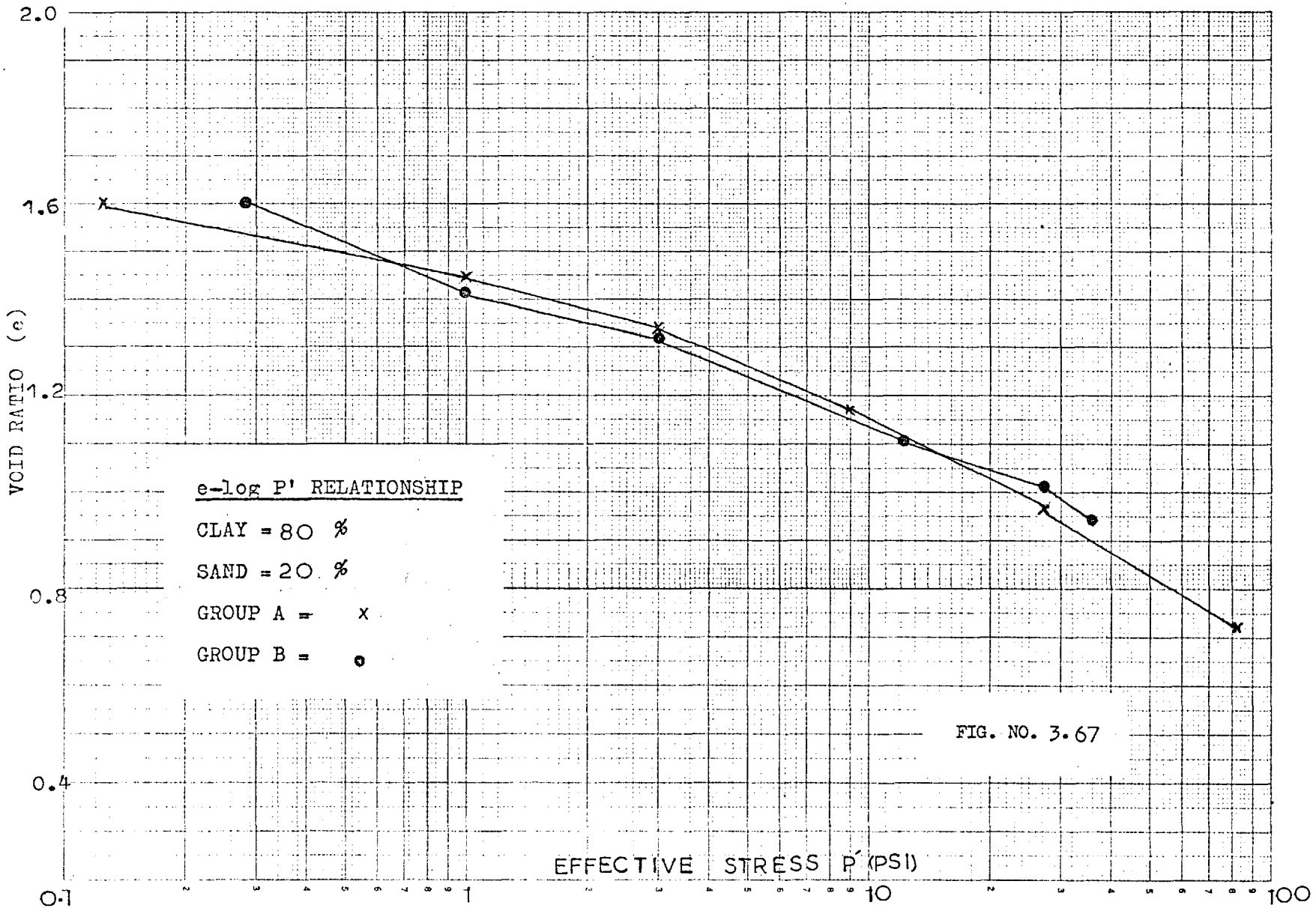
2.0
1.6
1.2
0.8
0.4
VOID RATIO (e)
e-log P' RELATIONSHIP
CLAY = 80 %
SAND = 20 %
GROUP A = x
GROUP B = o
0.1
1
10
100
EFFECTIVE STRESS P' (PSI)

FIG. NO. 3.67

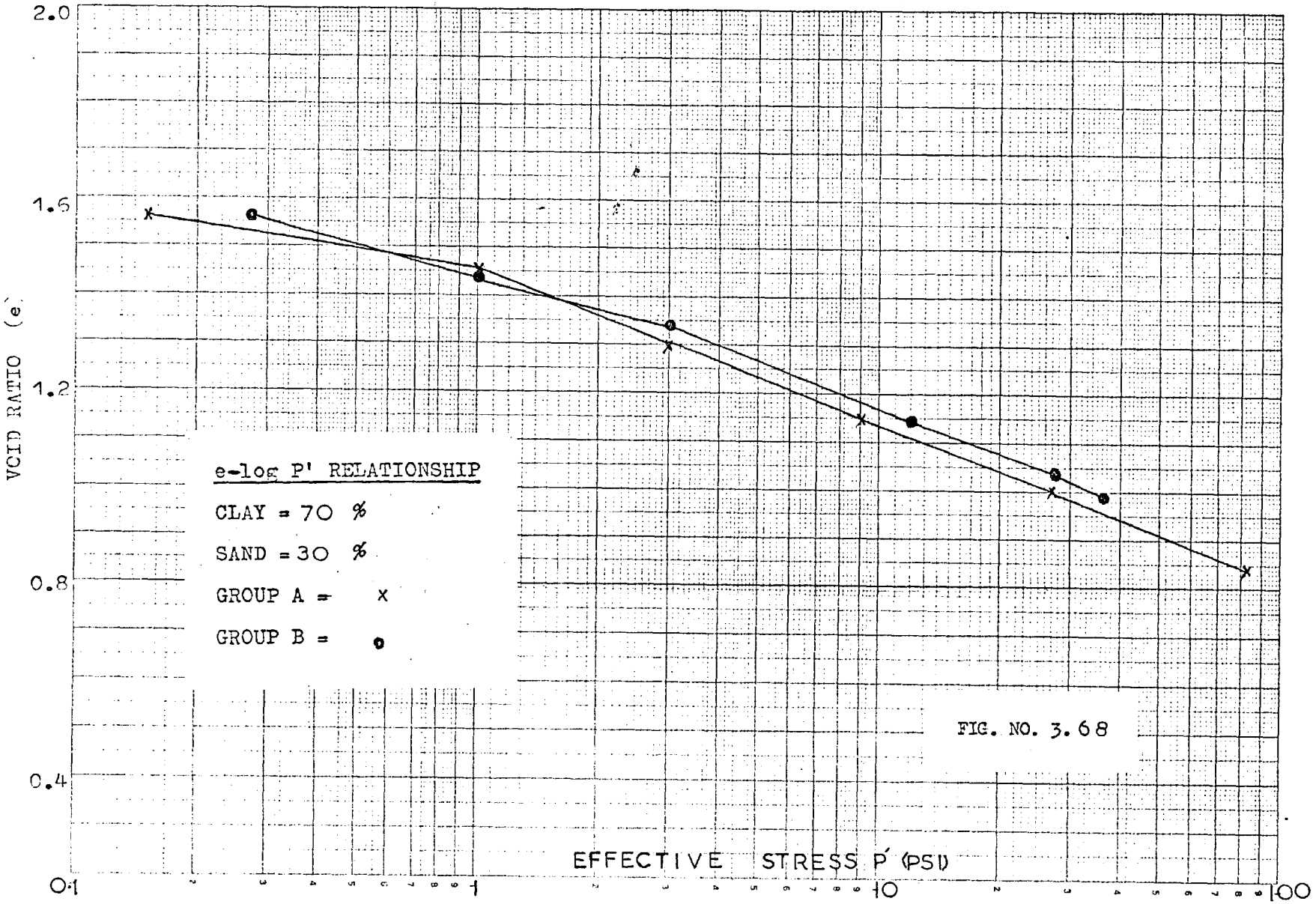
2.0
1.6
1.2
0.8
0.4
VOID RATIO (e)
e-log P' RELATIONSHIP
CLAY = 70 %
SAND = 30 %
GROUP A = x
GROUP B = o
0.1
1
10
100
EFFECTIVE STRESS P' (PSI)

FIG. NO. 3.68

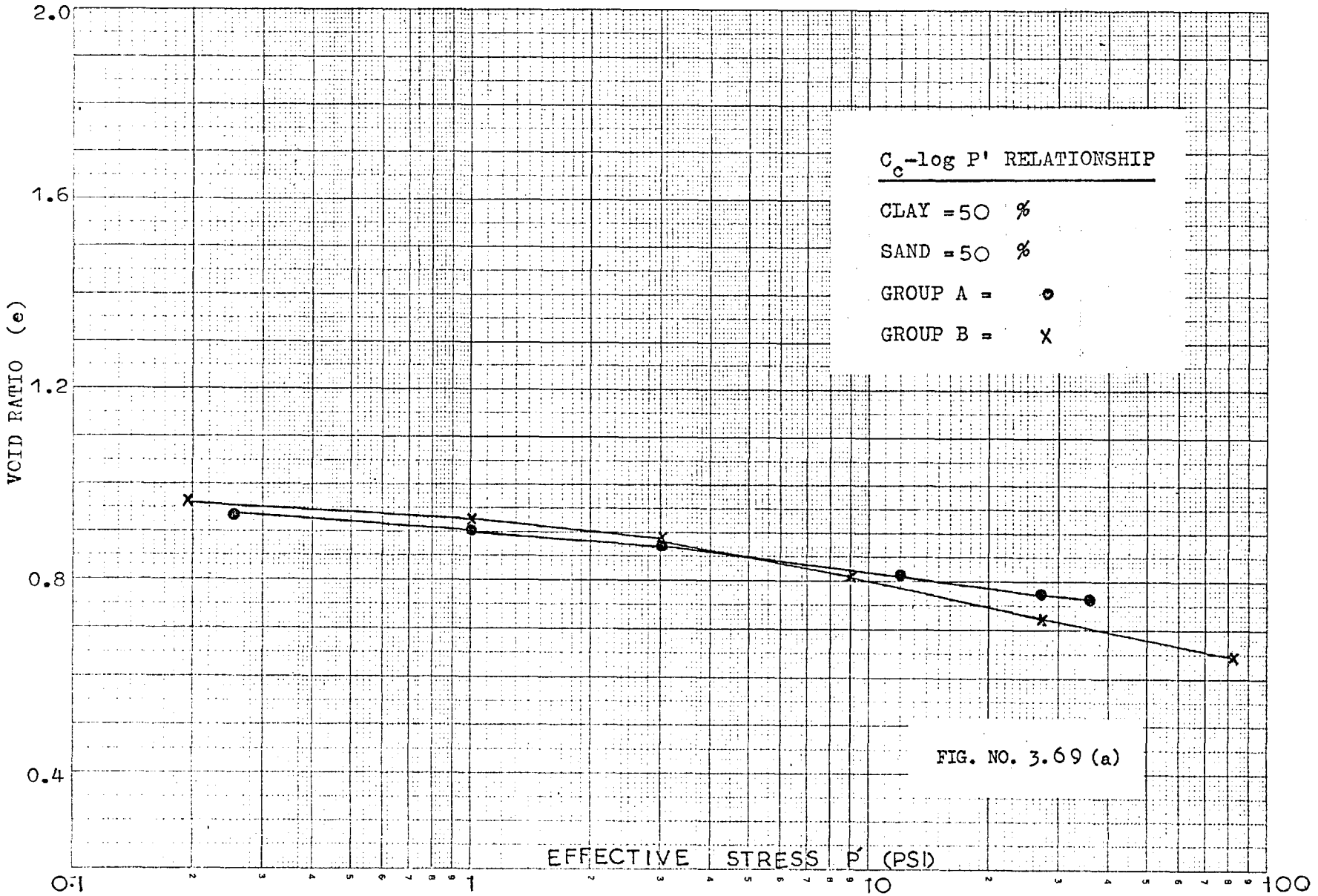
C_c-log P' RELATIONSHIP
CLAY = 50 %
SAND = 50 %
GROUP A =
GROUP B =
VOID RATIO (e)
2.0
1.6
1.2
0.8
0.4
EFFECTIVE STRESS P' (PSI)
0.1
1
10
100
FIG. NO. 3.69 (a)

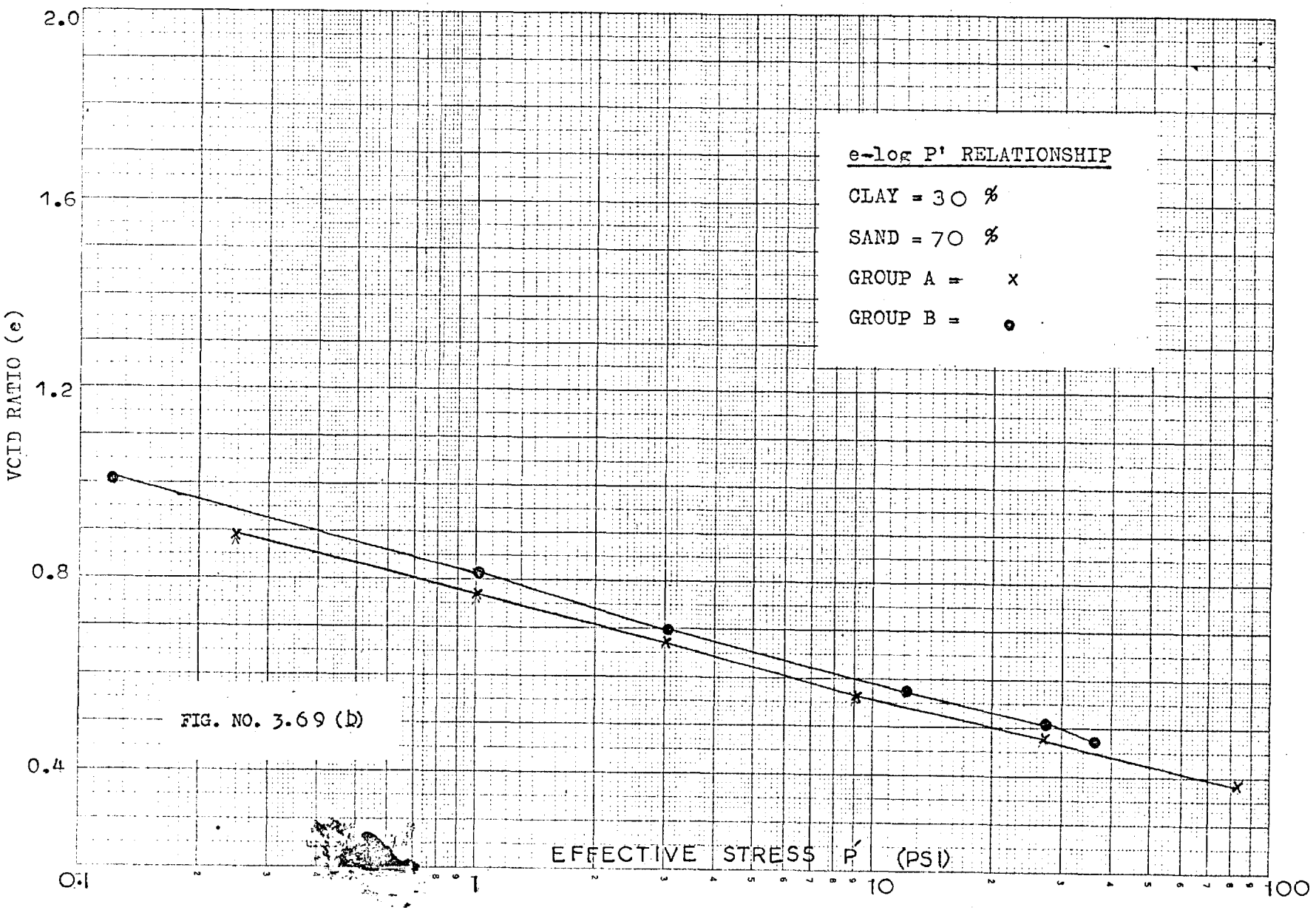
e-log P' RELATIONSHIP
CLAY = 30 %
SAND = 70 %
GROUP A = x
GROUP B = o
VOID RATIO (e)
2.0
1.6
1.2
0.8
0.4
0.1
1
10
100
EFFECTIVE STRESS P' (PSI)

FIG. NO. 3.69 (b)

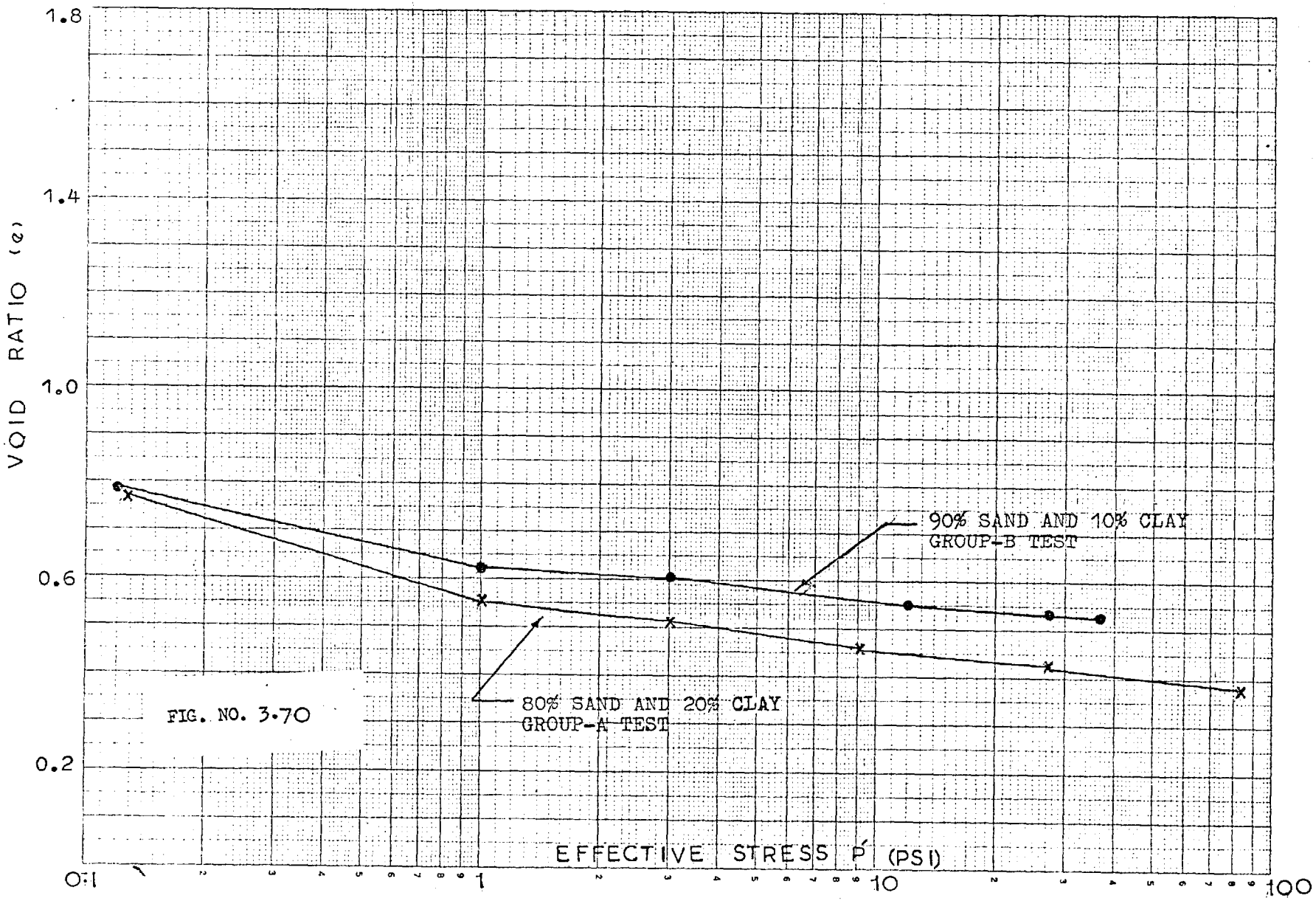
1.8
1.4
1.0
0.6
0.2
VOID RATIO (e)
0.1
1
10
100
EFFECTIVE STRESS P' (PSI)
90% SAND AND 10% CLAY
GROUP-B TEST
80% SAND AND 20% CLAY
GROUP-A TEST

FIG. NO. 3.70

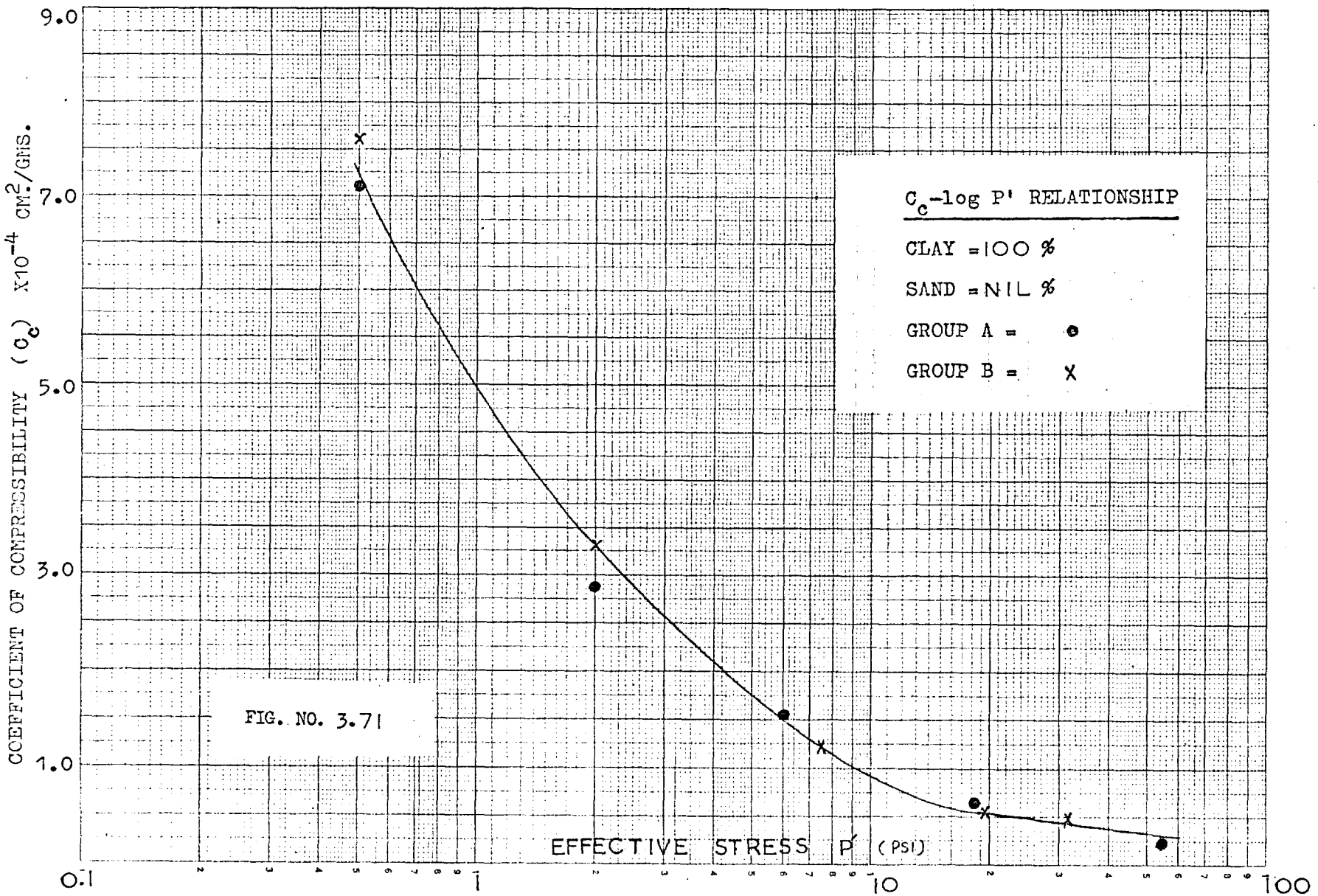
9.0
7.0
5.0
3.0
1.0
COEFFICIENT OF COMPRESSIBILITY (C_c) X10^{-4} CM^2/GMS.
0.1
1
10
100
EFFECTIVE STRESS P' (PSI)
C_c-log P' RELATIONSHIP
CLAY =100 %
SAND = NIL %
GROUP A =
GROUP B =
FIG. NO. 3.71

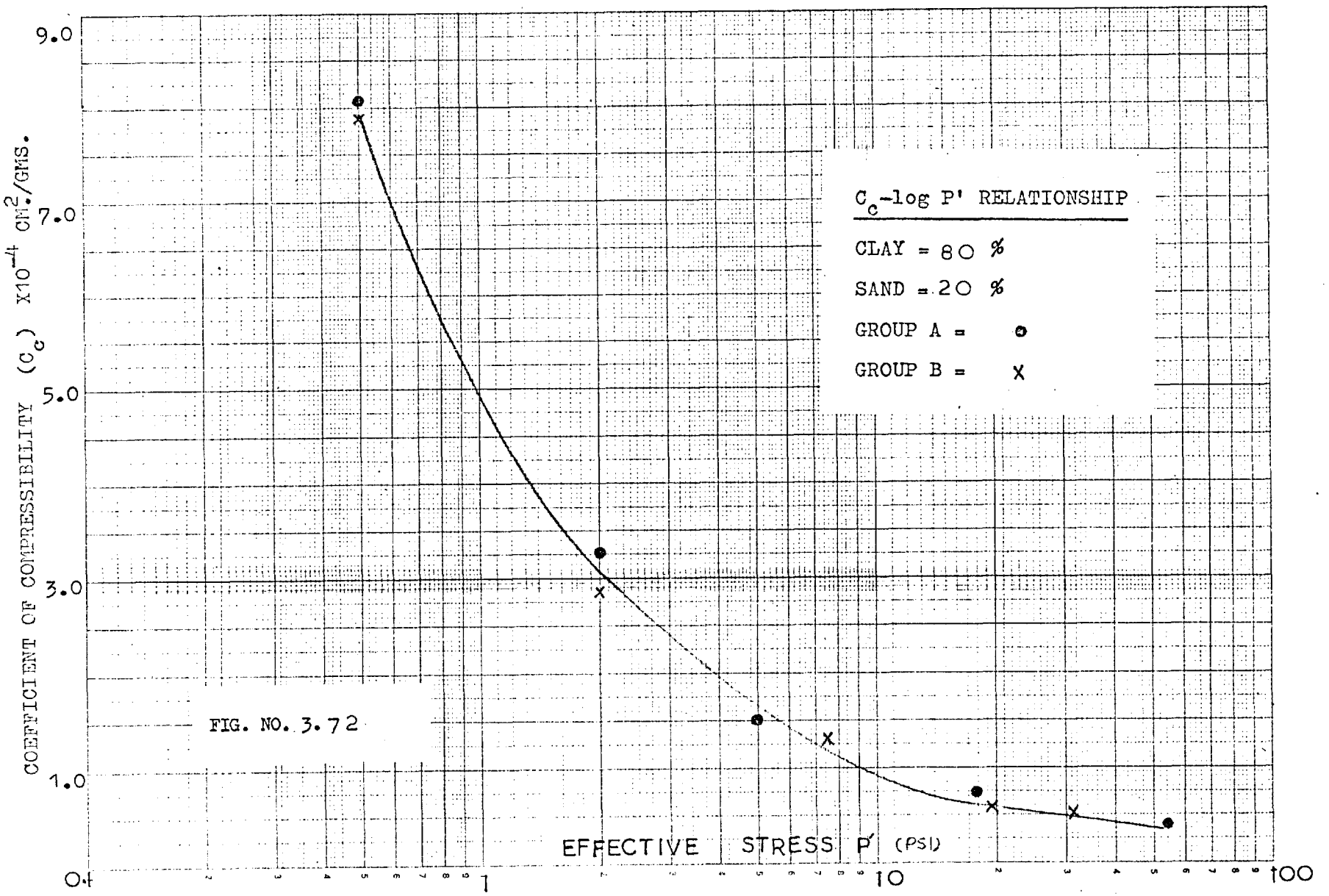
C_c-log P' RELATIONSHIP
CLAY = 80 %
SAND = 20 %
GROUP A =
GROUP B = X
COEFFICIENT OF COMPRESSIBILITY (C_c) X10^{-4} CM.^{2}/GMS.
9.0
7.0
5.0
3.0
1.0
0.4
1
10
100
EFFECTIVE STRESS P' (PSI)

FIG. NO. 3.72

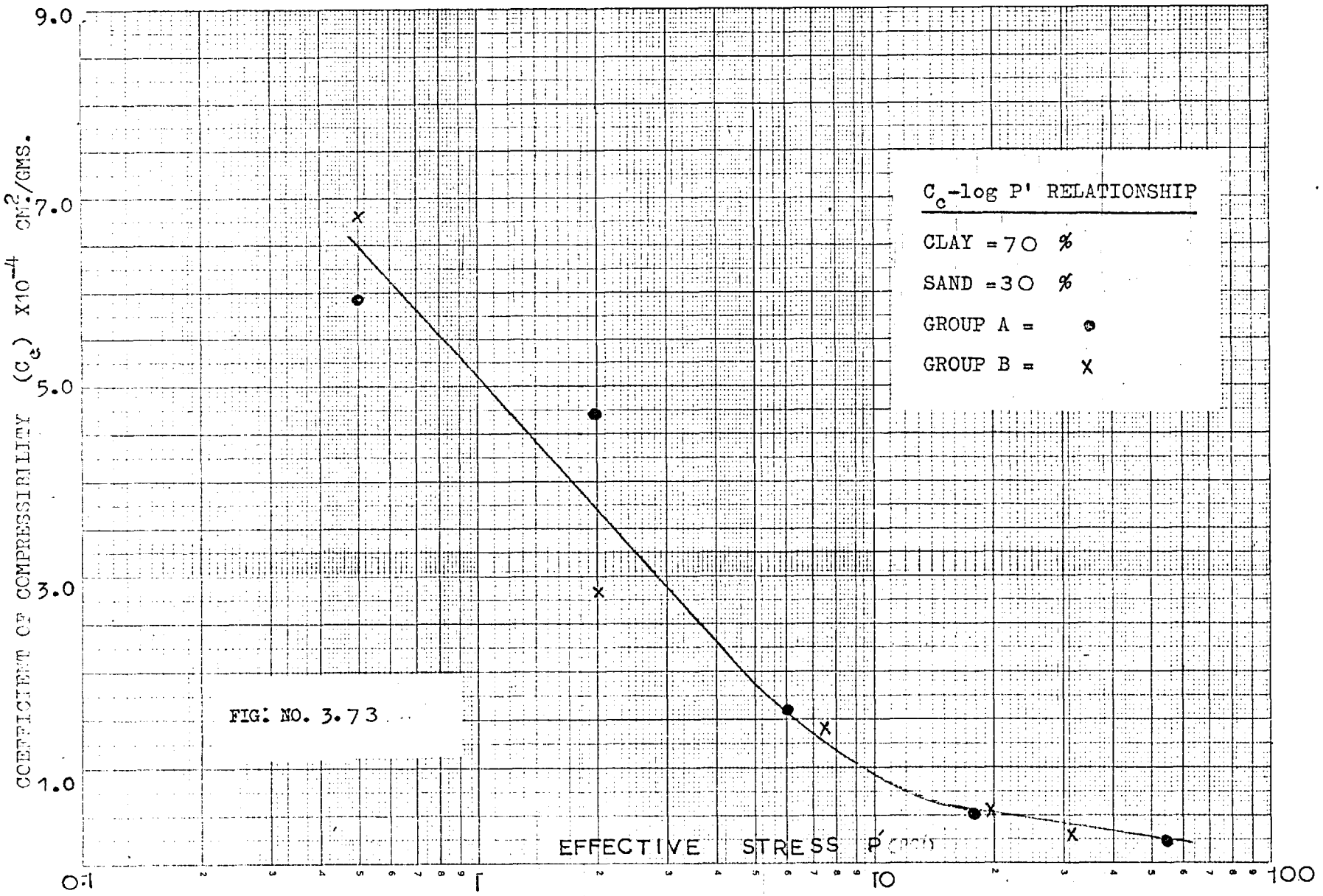
9.0
7.0
5.0
3.0
1.0
COEFFICIENT OF COMPRESSIBILITY (C_c) X10^{-4} CM^2/GMS.
0.1
1
10
100
EFFECTIVE STRESS P'
C_c-log P' RELATIONSHIP
CLAY = 70 %
SAND = 30 %
GROUP A =
GROUP B =
FIG. NO. 3.73

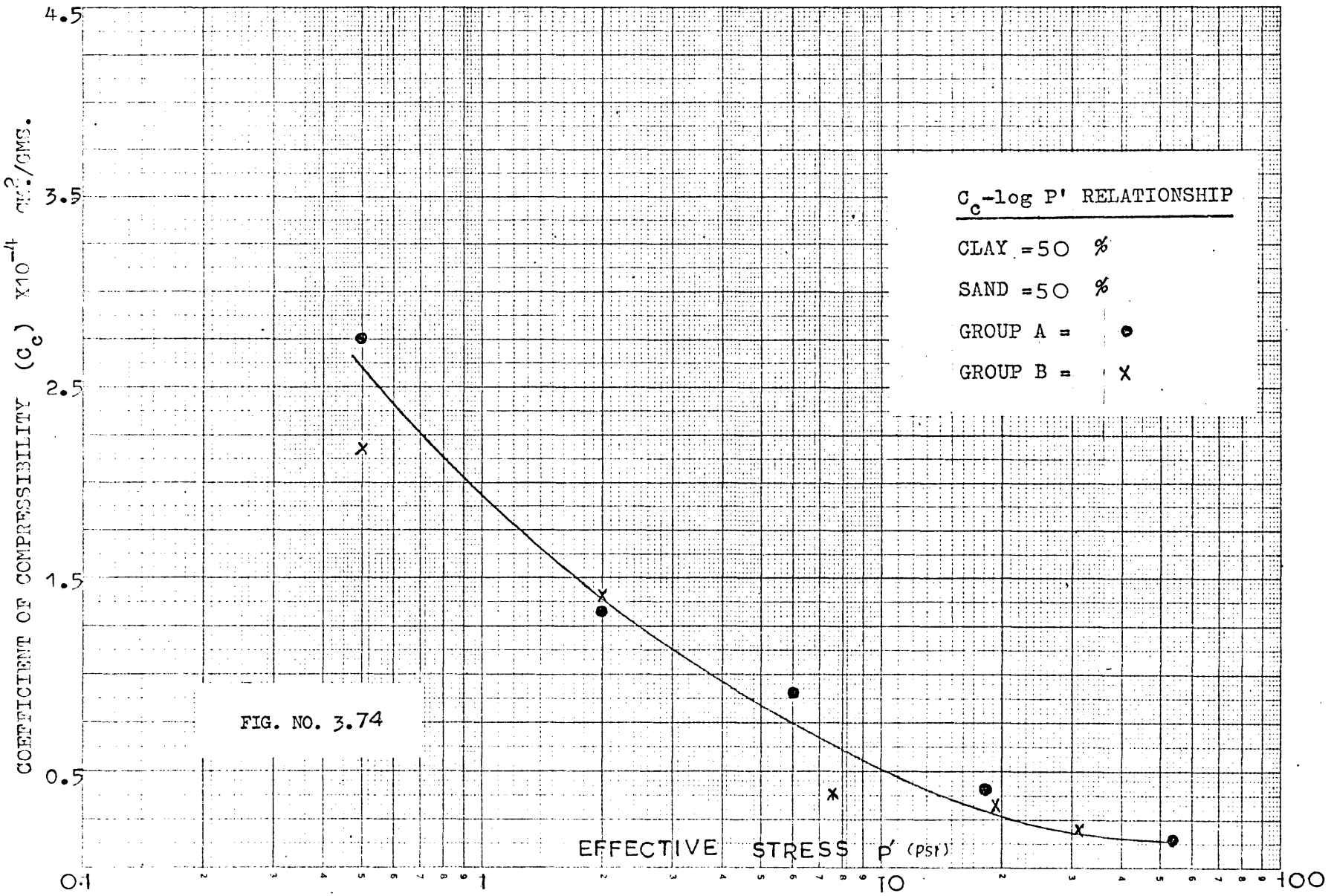
C_c-log P' RELATIONSHIP
CLAY =50 %
SAND =50 %
GROUP A =
GROUP B =
COEFFICIENT OF COMPRESSIBILITY (C_c) X10^{-4} cm^2/GMS.
EFFECTIVE STRESS P' (psf)
4.5
3.5
2.5
1.5
0.5
0.1
1
10
100

FIG. NO. 3.74

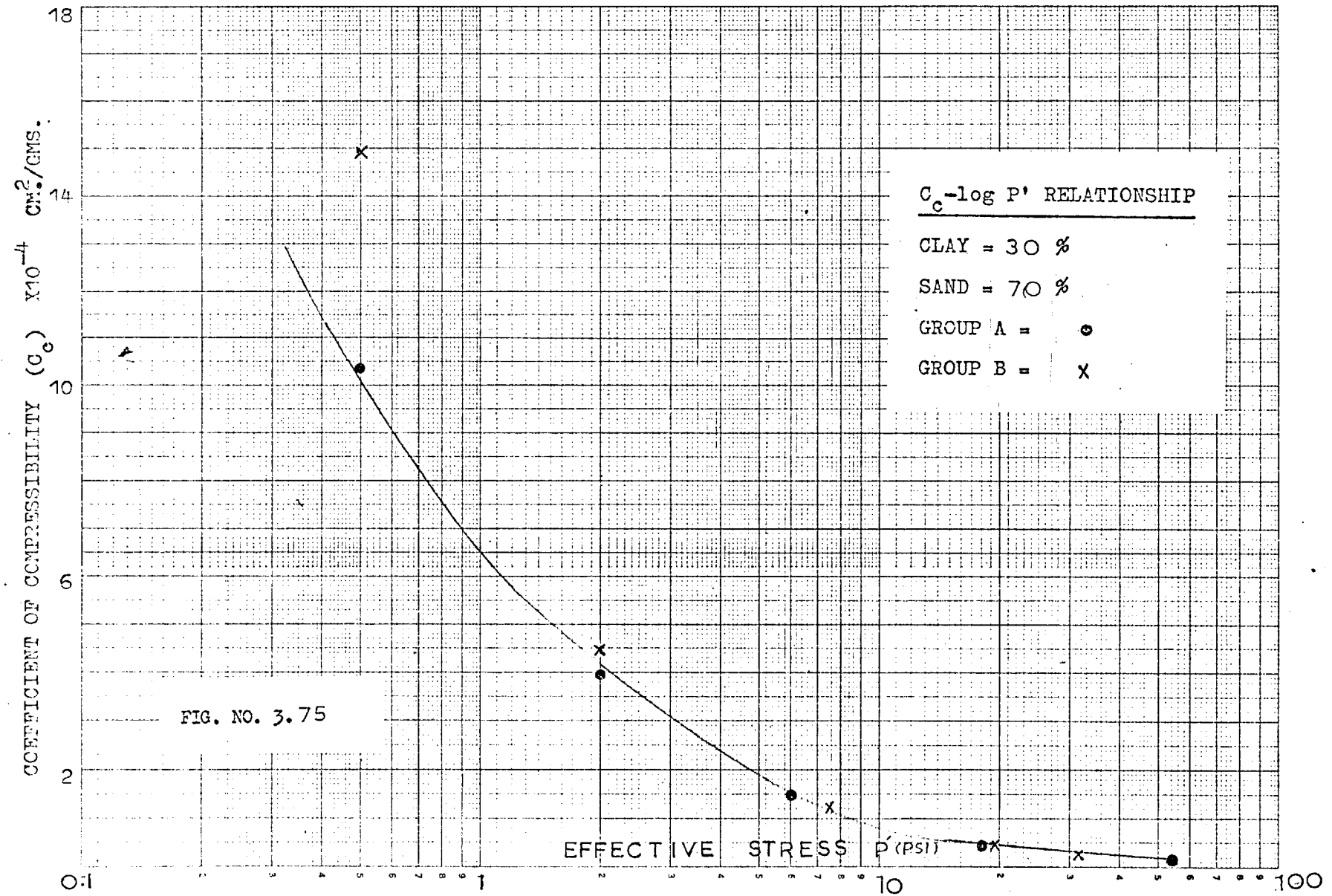
C_c-log P' RELATIONSHIP
CLAY = 30 %
SAND = 70 %
GROUP A =
GROUP B =
COEFFICIENT OF COMPRESSIBILITY (C_c) X10^{-4} CM.^{2}/GMS.
EFFECTIVE STRESS P' (PSI)
18
14
10
6
2
0.1
1
10
100

FIG. NO. 3.75

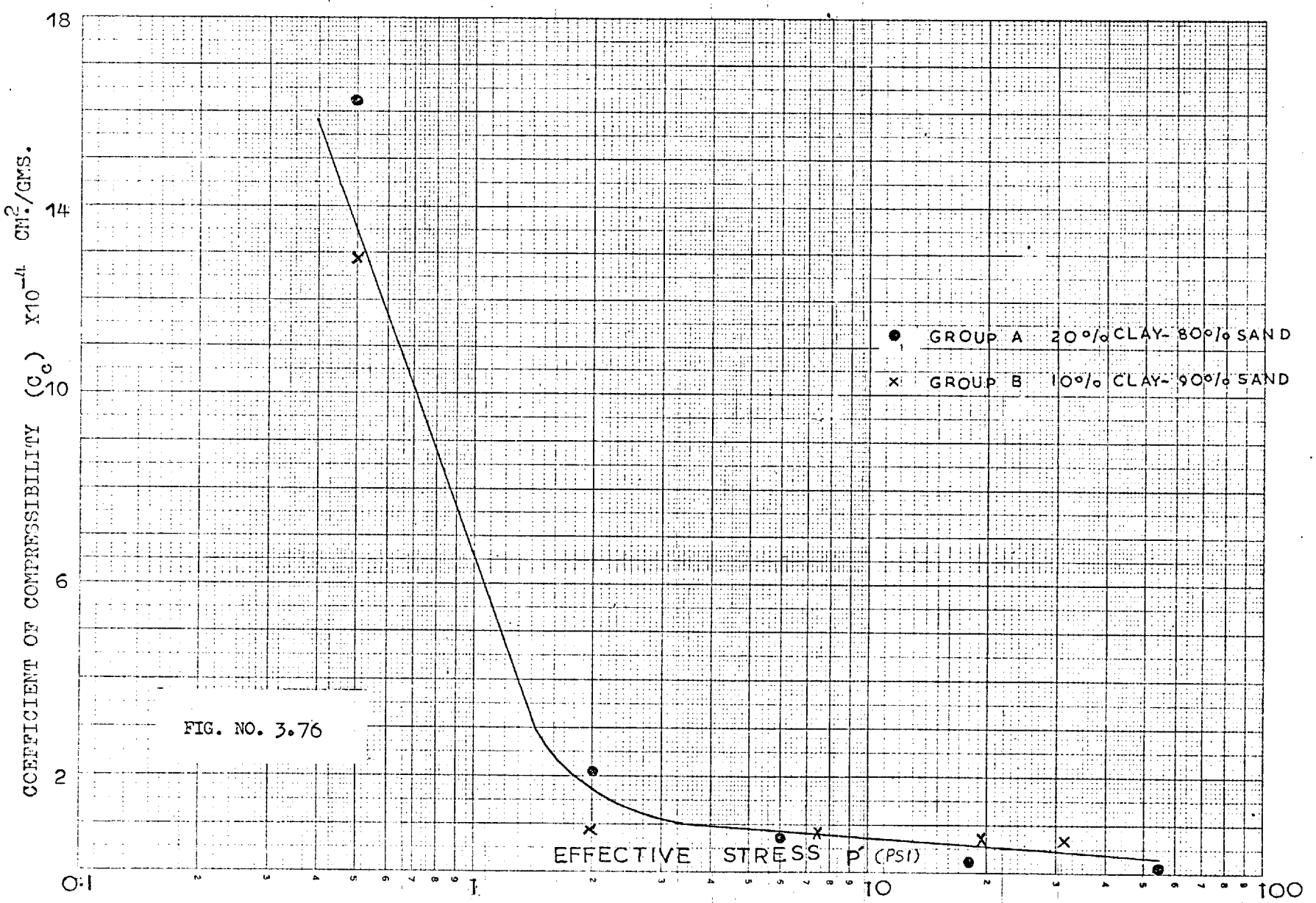
COEFFICIENT OF COMPRESSIBILITY (C_c) X10^{-4} CM^2./GMS.
18
14
10
6
2
0·1
1
10
100
EFFECTIVE STRESS P' (PSI)
GROUP A 20% CLAY- 80% SAND
GROUP B 10% CLAY- 90% SAND
FIG. NO. 3.76

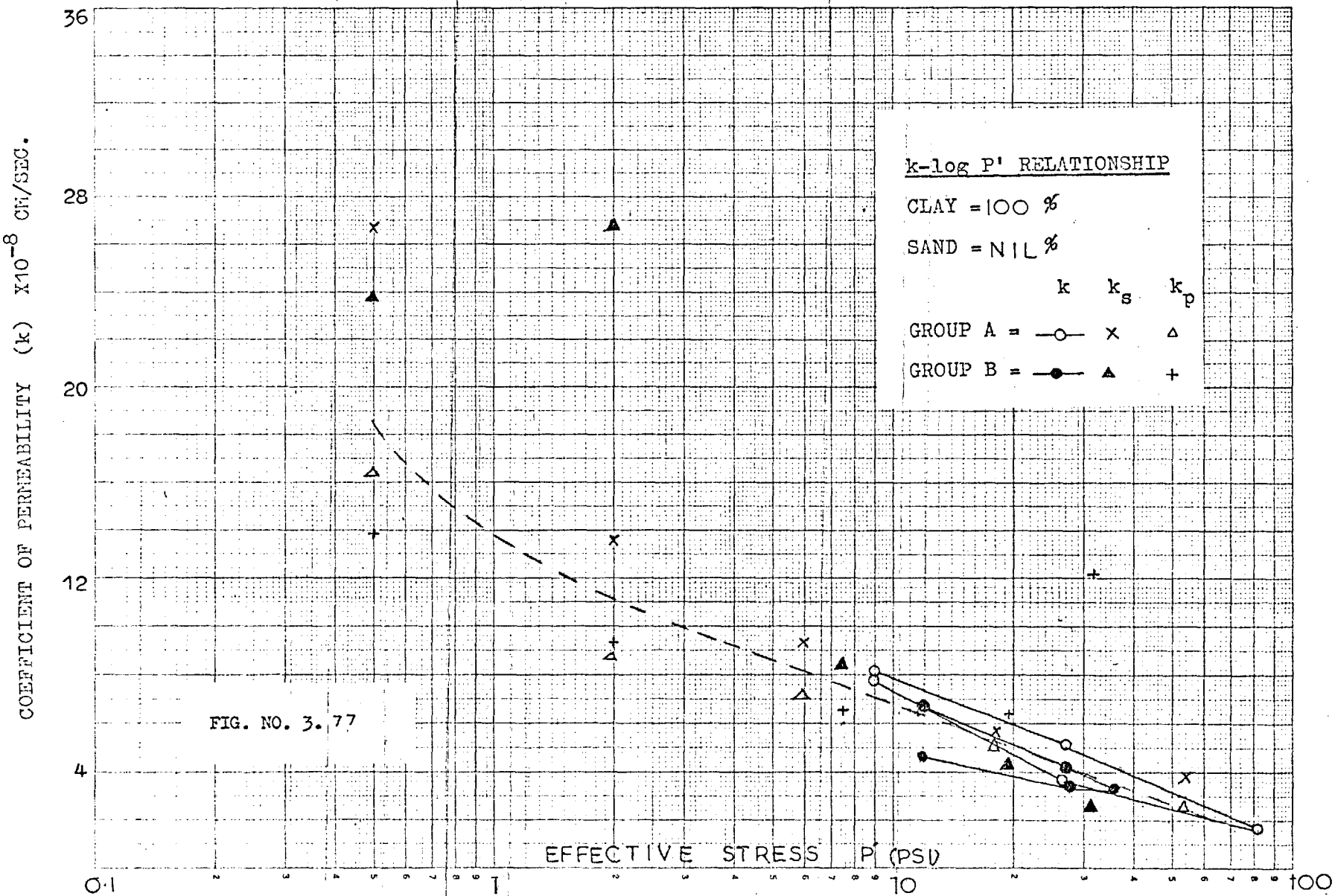
k-log P' RELATIONSHIP
CLAY = 100 %
SAND = NIL %
k k_s k_p
GROUP A =
GROUP B =
COEFFICIENT OF PERMEABILITY (k) X10^-8 CM/SEC.
36
28
20
12
4
0·1
1
10
100
EFFECTIVE STRESS P' (PSI)

FIG. NO. 3.77

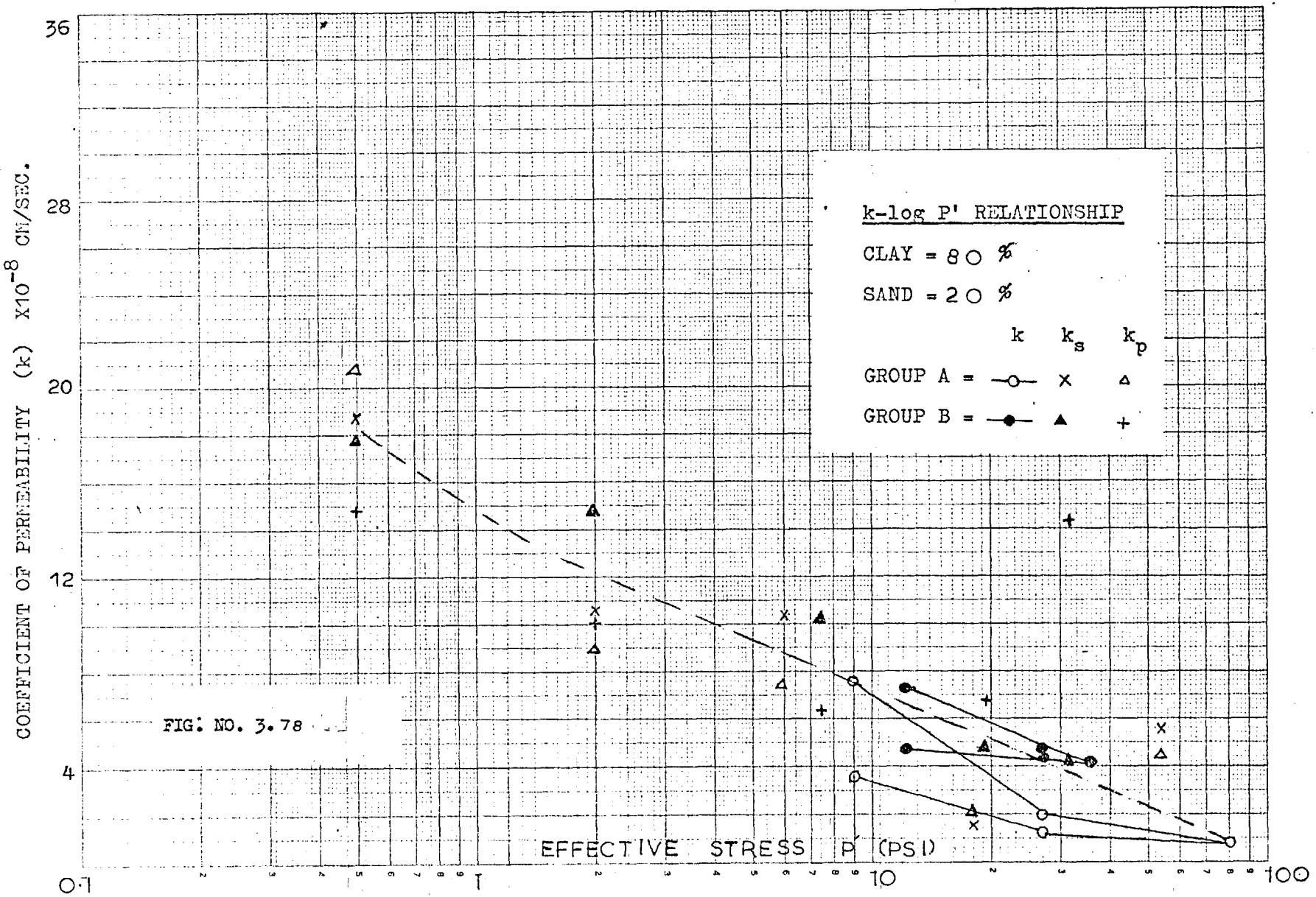
k-log P' RELATIONSHIP
CLAY = 80 %
SAND = 20 %
k k_s k_p
GROUP A =
GROUP B =
COEFFICIENT OF PERMEABILITY (k) X10^{-8} CM/SEC.
36
28
20
12
4
0·1
1
10
100
EFFECTIVE STRESS P' (PSI)

FIG. NO. 3.78

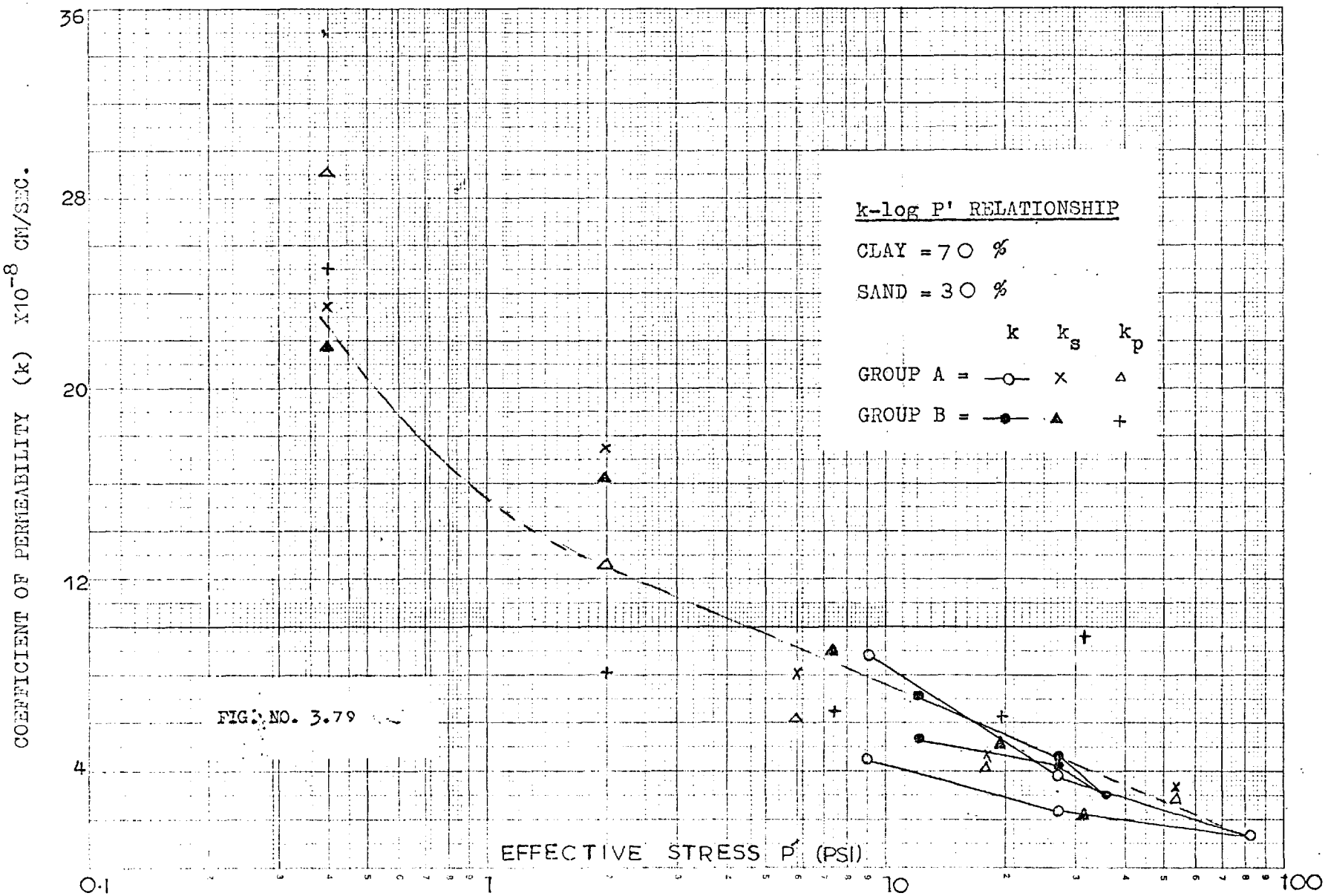
k-log P' RELATIONSHIP
CLAY = 70 %
SAND = 30 %
k k_s k_p
GROUP A =
GROUP B =
COEFFICIENT OF PERMEABILITY (k) X10^-8 CM/SEC.
36
28
20
12
4
0.1
1
10
100
EFFECTIVE STRESS P' (PSI)

FIG. NO. 3.79

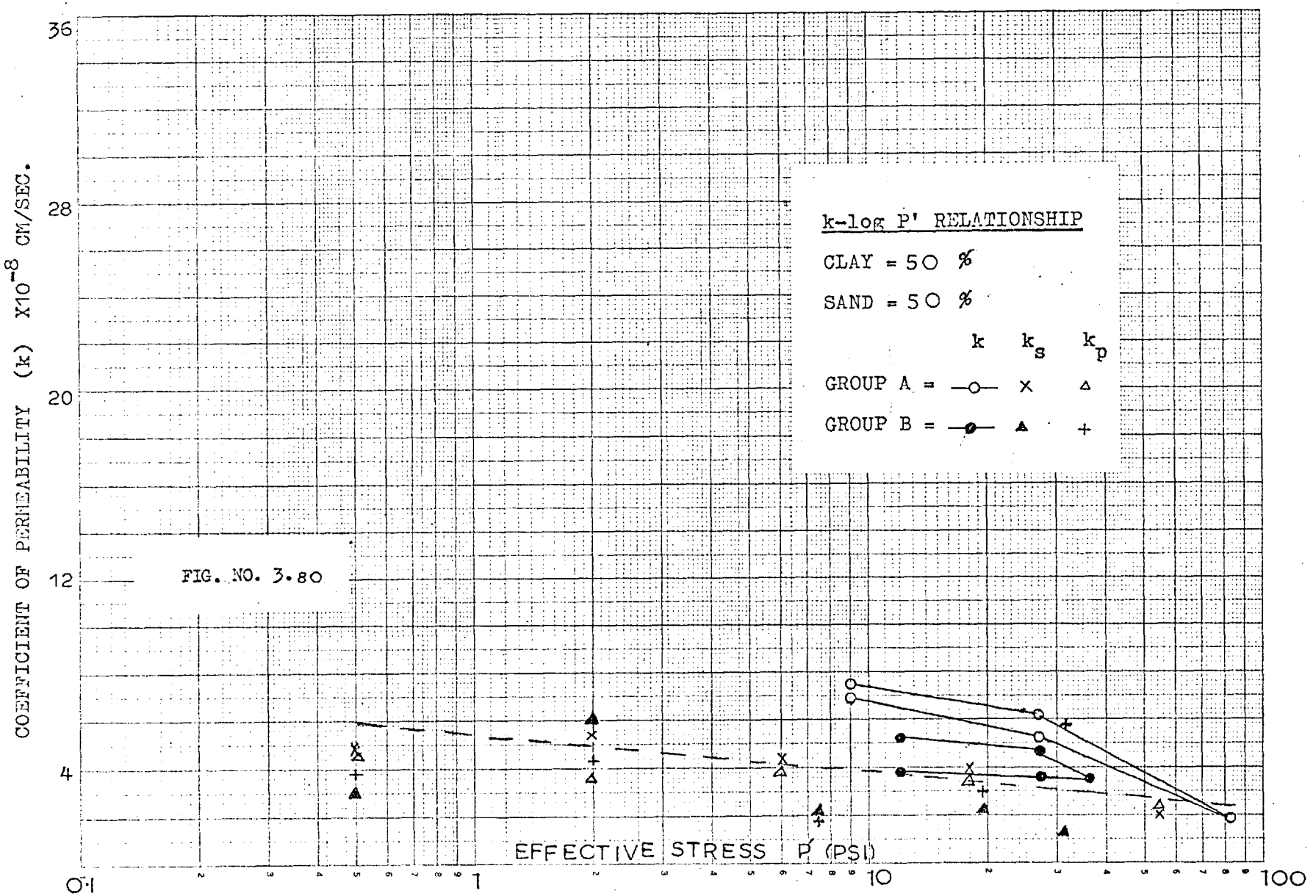
k-log P' RELATIONSHIP
CLAY = 50 %
SAND = 50 %
k k_s k_p
GROUP A =
GROUP B =
FIG. NO. 3.80
COEFFICIENT OF PERMEABILITY (k) X10^{-8} CM/SEC.
36
28
20
12
4
EFFECTIVE STRESS P' (PSI)
0·1
1
10
100

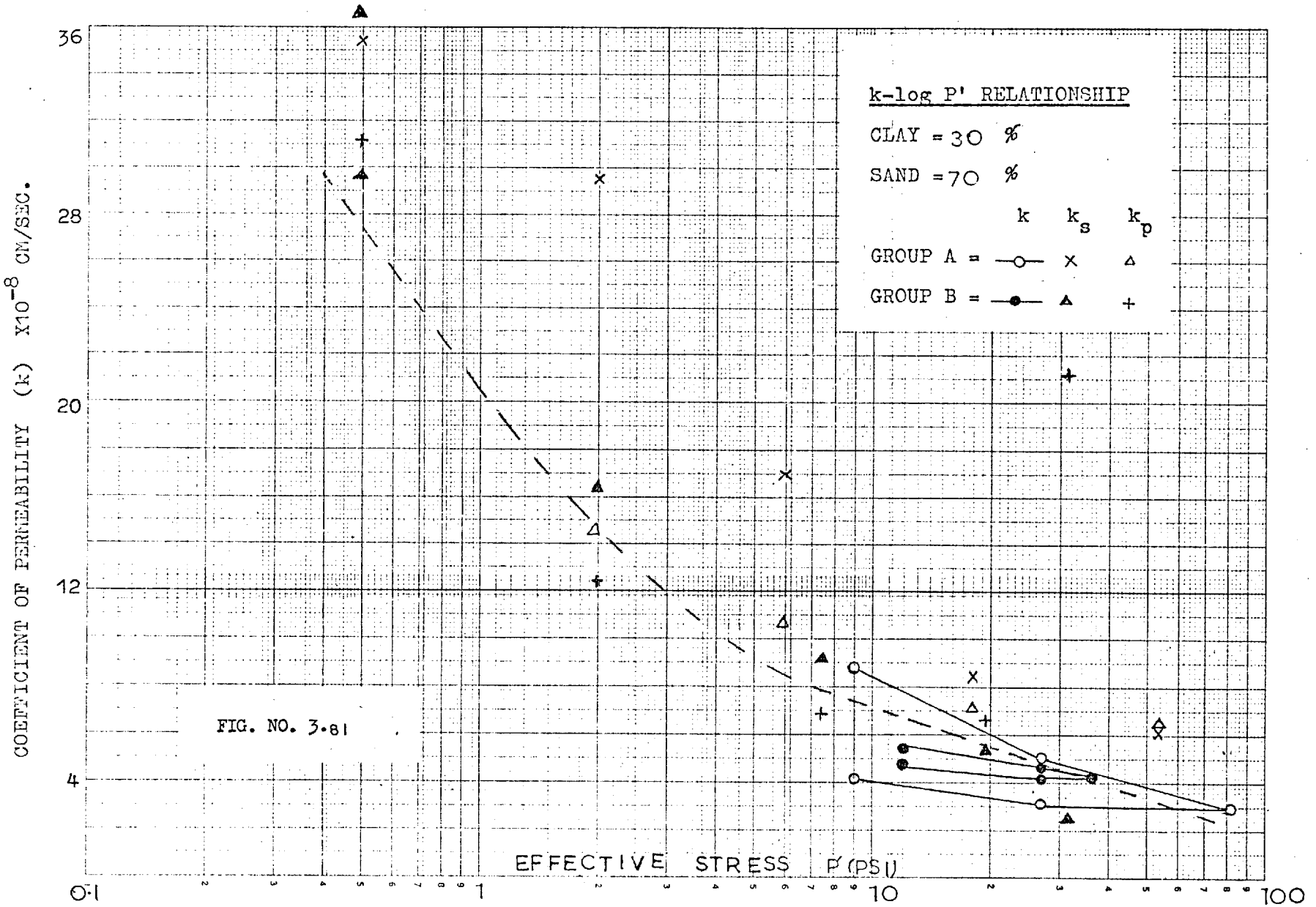
k-log P' RELATIONSHIP
CLAY = 30 %
SAND = 70 %
k k_s k_p
GROUP A =
GROUP B =
COEFFICIENT OF PERMEABILITY (k) X10^{-8} CM/SEC.
36
28
20
12
4
0·1
1
10
100
EFFECTIVE STRESS P' (PSI)

FIG. NO. 3.81

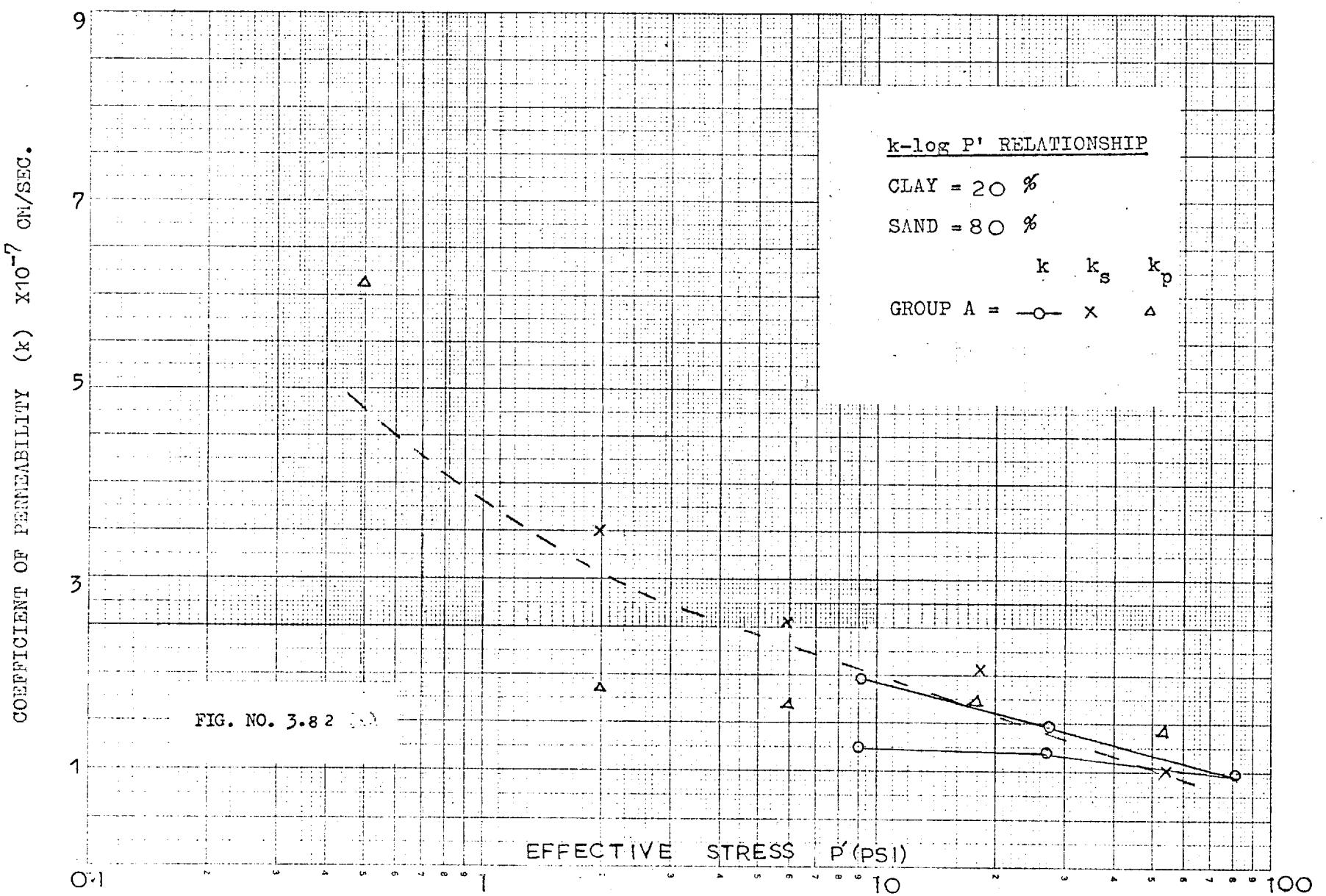
k-log P' RELATIONSHIP
CLAY = 20 %
SAND = 80 %
k k_s k_p
GROUP A =
COEFFICIENT OF PERMEABILITY (k) X10^{-7} CM/SEC.
EFFECTIVE STRESS P' (PSI)
9
7
5
3
1
0.1
1
10
100

FIG. NO. 3.8 2

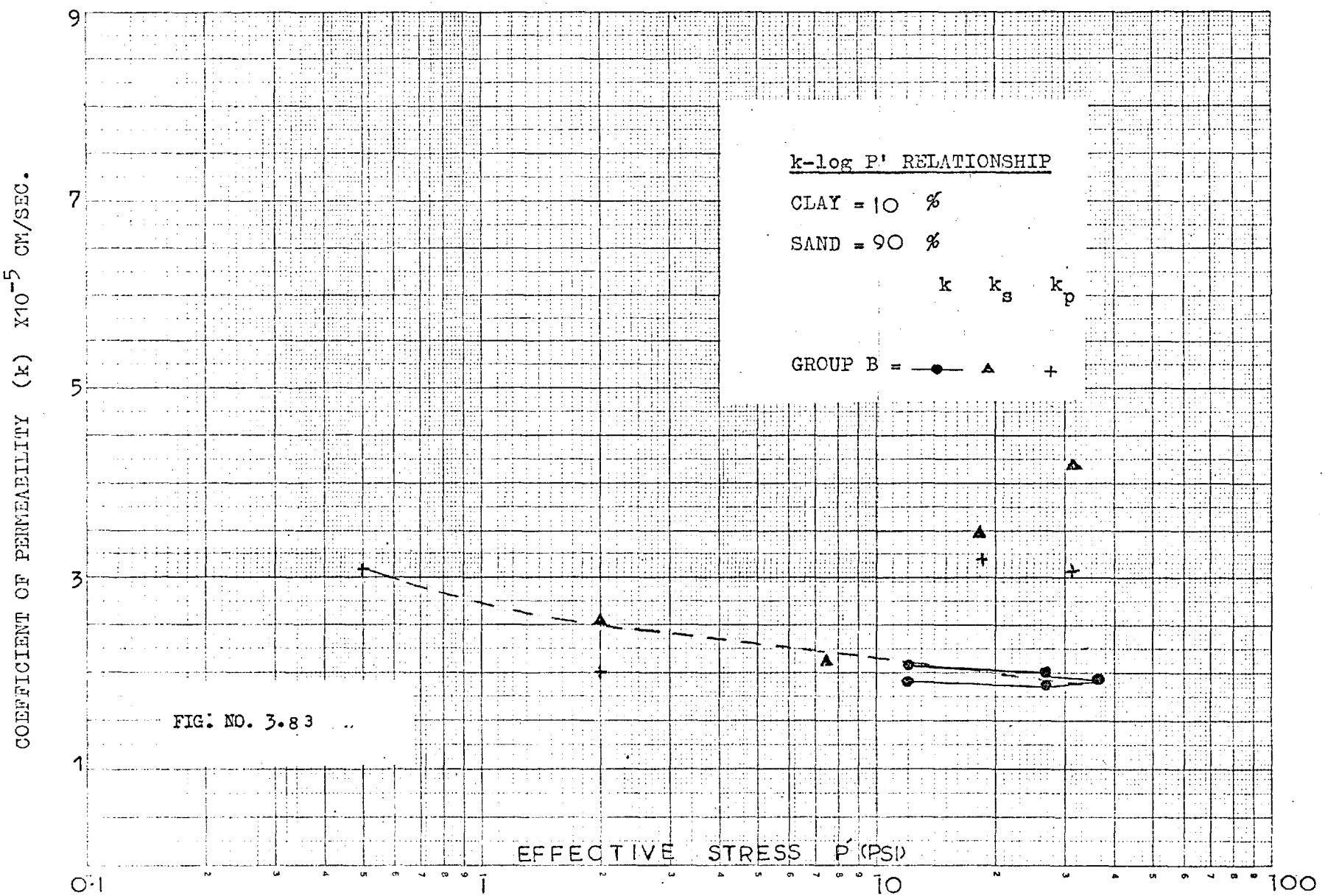
k-log P' RELATIONSHIP
CLAY = 10 %
SAND = 90 %
k k_s k_p
GROUP B =
COEFFICIENT OF PERMEABILITY (k) X10^{-5} CM/SEC.
9
7
5
3
1
0·1
1
10
100
EFFECTIVE STRESS P' (PSI)

FIG. NO. 3.8 3

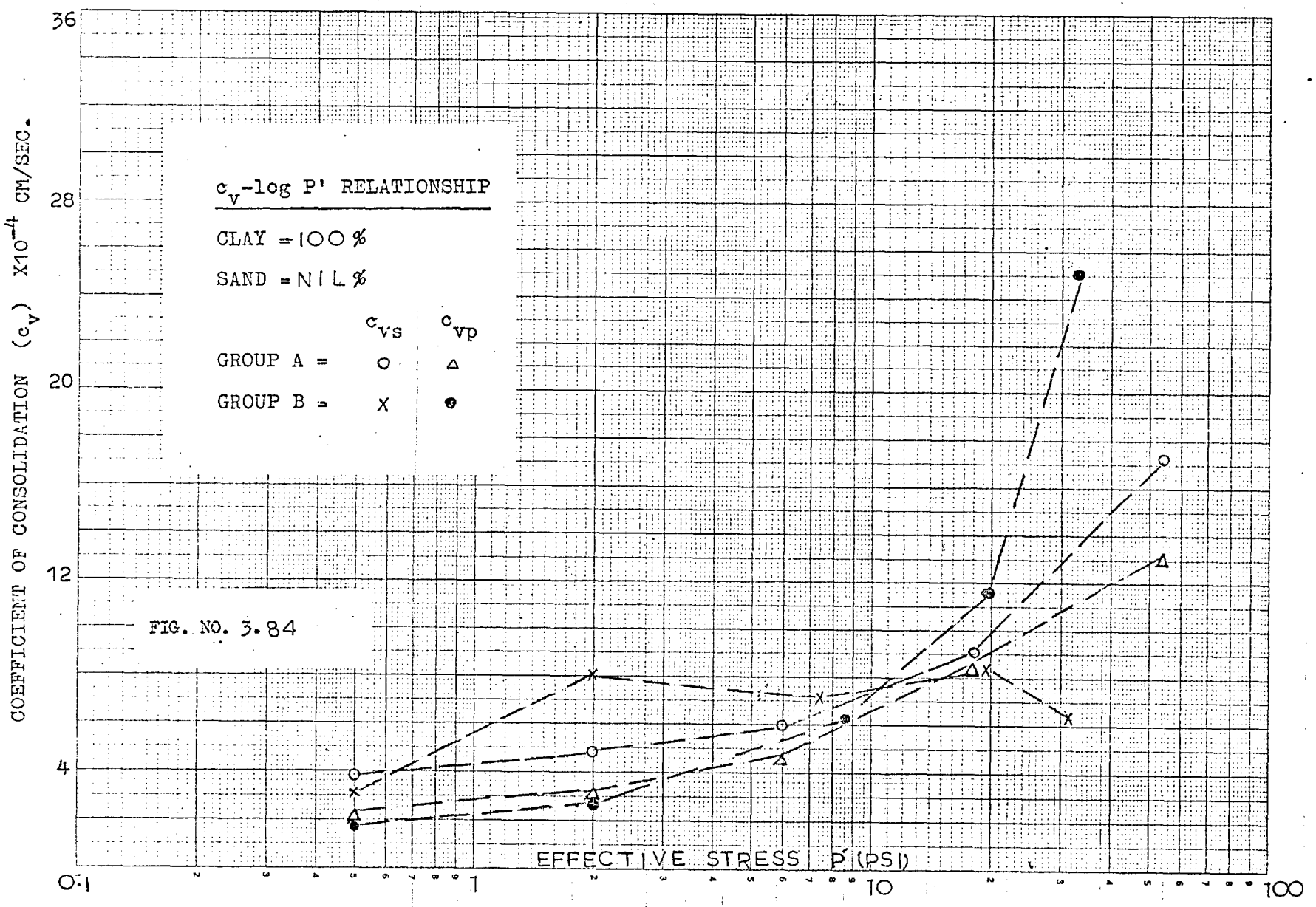
c_v-log P' RELATIONSHIP
CLAY = 100 %
SAND = NIL %
c_{vs} c_{vp}
GROUP A = O Δ
GROUP B = X ●
FIG. NO. 3.84
COEFFICIENT OF CONSOLIDATION (c_v) X10^{-4} CM/SEC.
36
28
20
12
4
0·1
1
10
100
EFFECTIVE STRESS P' (PSI)

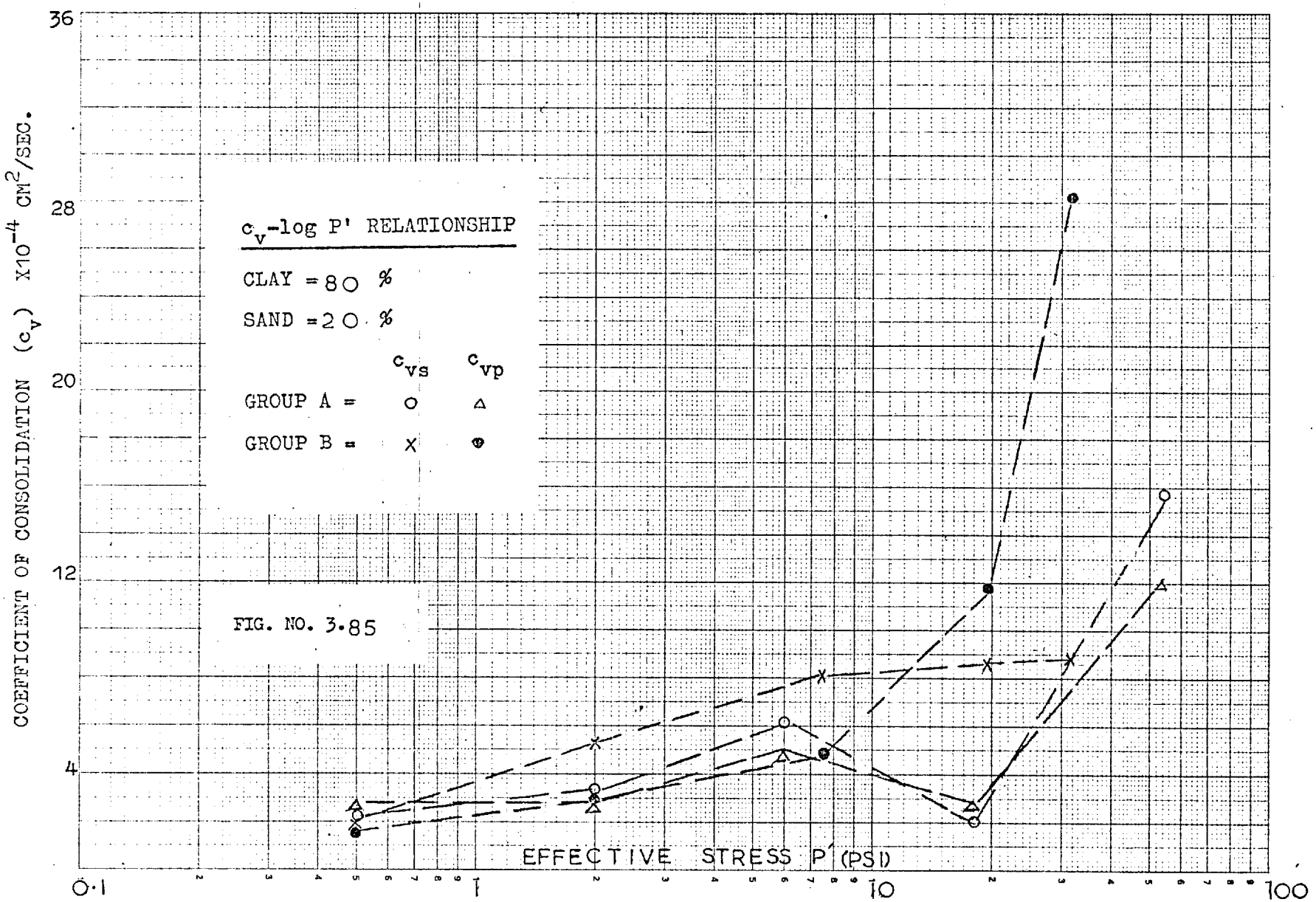
c_v-log P' RELATIONSHIP
CLAY = 80 %
SAND = 20 %
c_{vs} c_{vp}
GROUP A = O Δ
GROUP B = X ⊕
FIG. NO. 3.85
COEFFICIENT OF CONSOLIDATION (c_v) X10^{-4} CM^2/SEC.
36
28
20
12
4
EFFECTIVE STRESS P' (PSI)
0·1
1
10
100

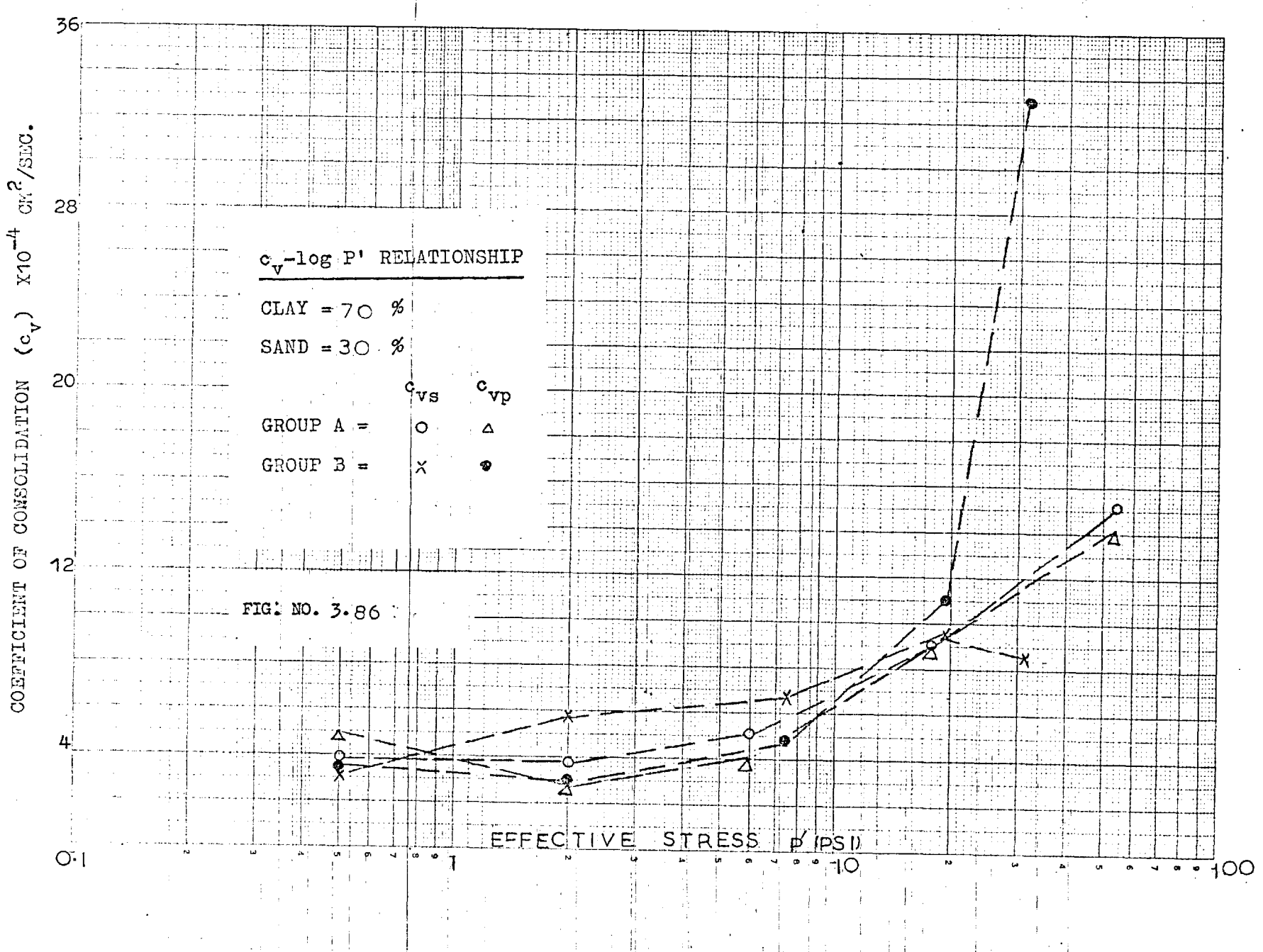
c_v-log P' RELATIONSHIP
CLAY = 70 %
SAND = 30 %
c_{vs} c_{vp}
GROUP A = O Δ
GROUP B = X ●
FIG. NO. 3.86
COEFFICIENT OF CONSOLIDATION (c_v) X10^{-4} CM^2/SEC.
36
28
20
12
4
0·1
1
10
100
EFFECTIVE STRESS P' (PSI)

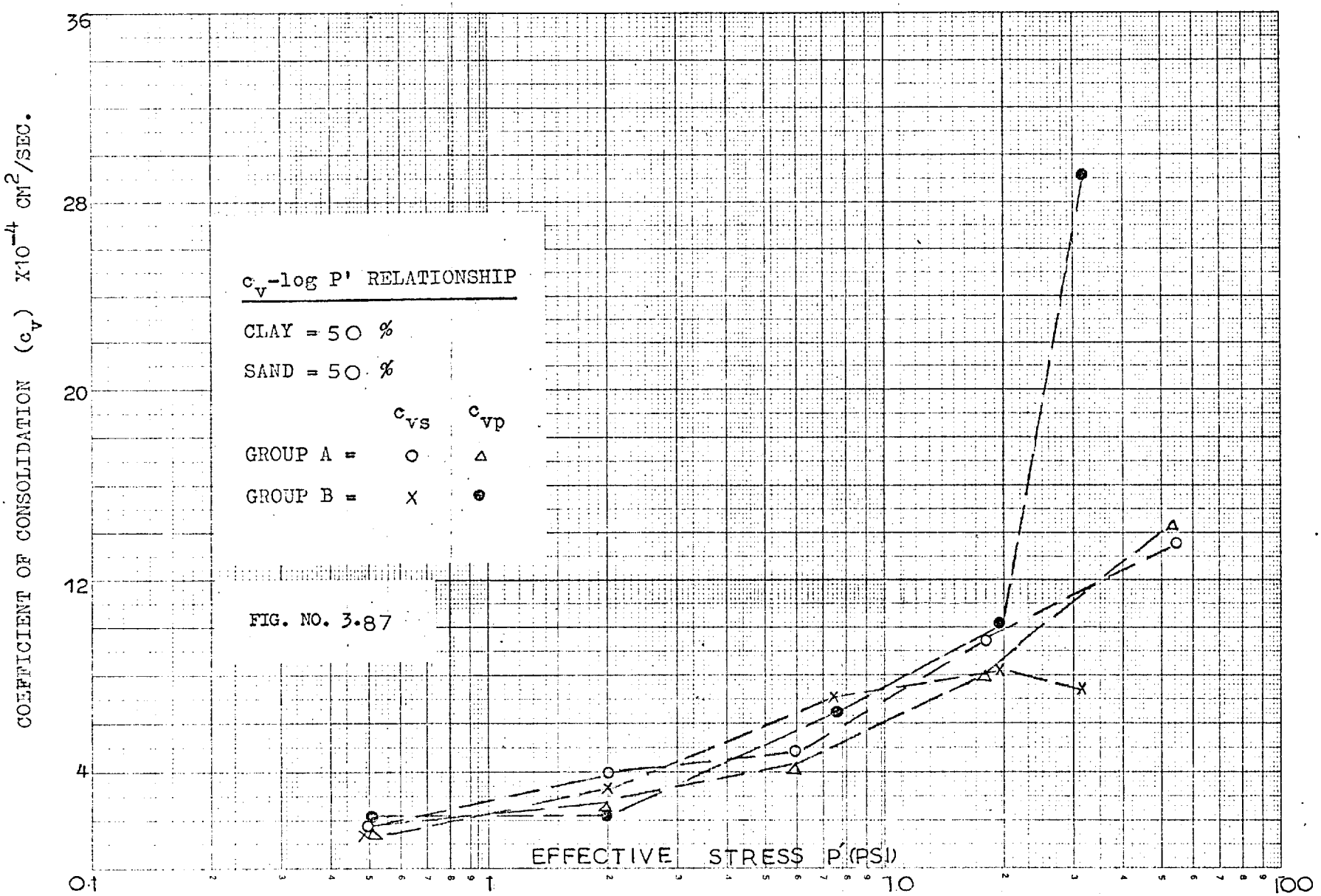
c_v-log P' RELATIONSHIP
CLAY = 50 %
SAND = 50 %
c_{vs} c_{vp}
GROUP A = O Δ
GROUP B = X ⊛
FIG. NO. 3.87
COEFFICIENT OF CONSOLIDATION (c_v) X10^{-4} CM^2/SEC.
36
28
20
12
4
0.1
1
10
100
EFFECTIVE STRESS P' (PSI)

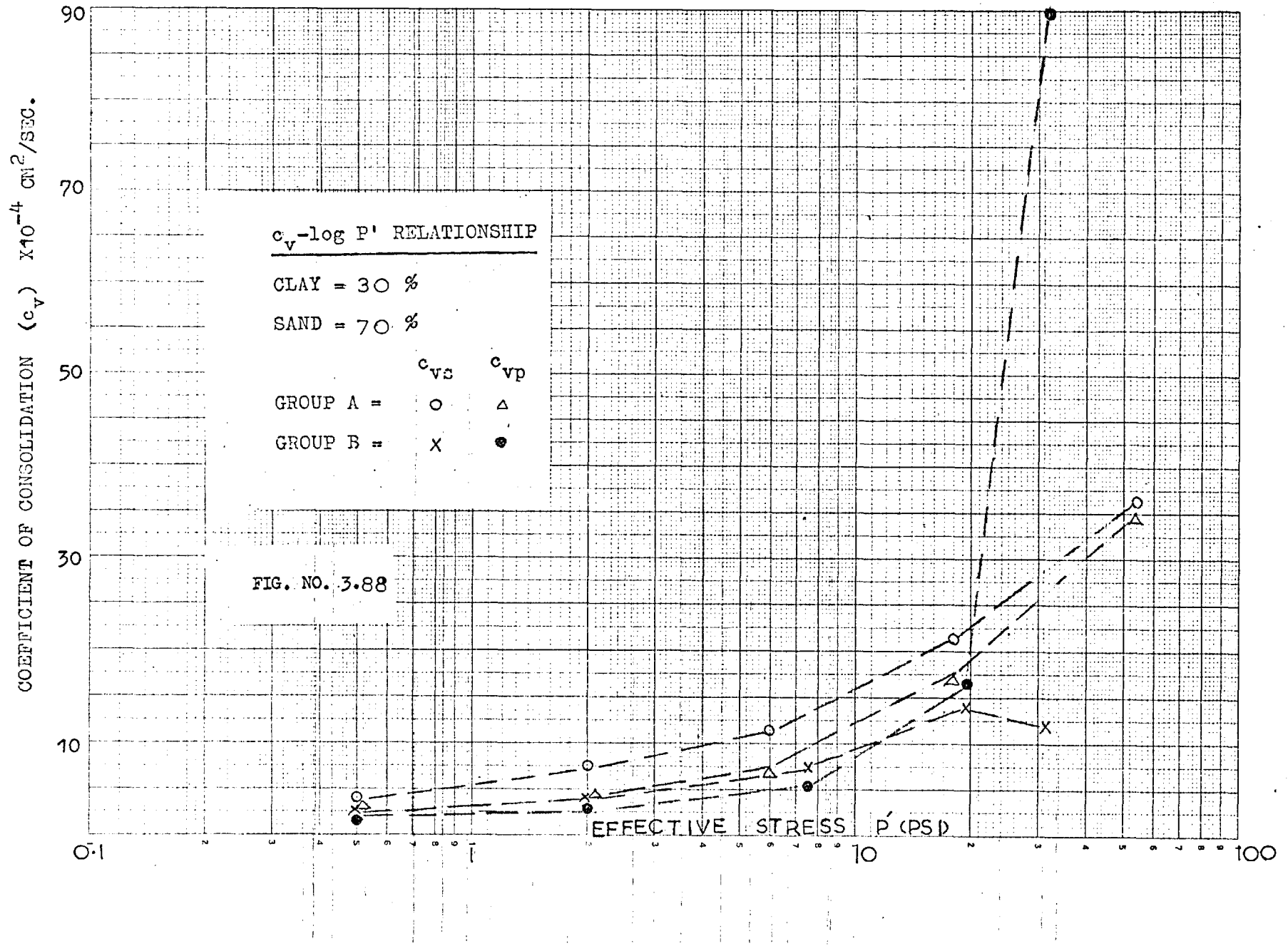
c_v-log P' RELATIONSHIP
CLAY = 30 %
SAND = 70 %
c_{vs} c_{vp}
GROUP A = ○ △
GROUP B = × ●
FIG. NO. 3.88
COEFFICIENT OF CONSOLIDATION (c_v) X10^{-4} CM^2/SEC.
90
70
50
30
10
0·1
1
10
100
EFFECTIVE STRESS P' (PSI)

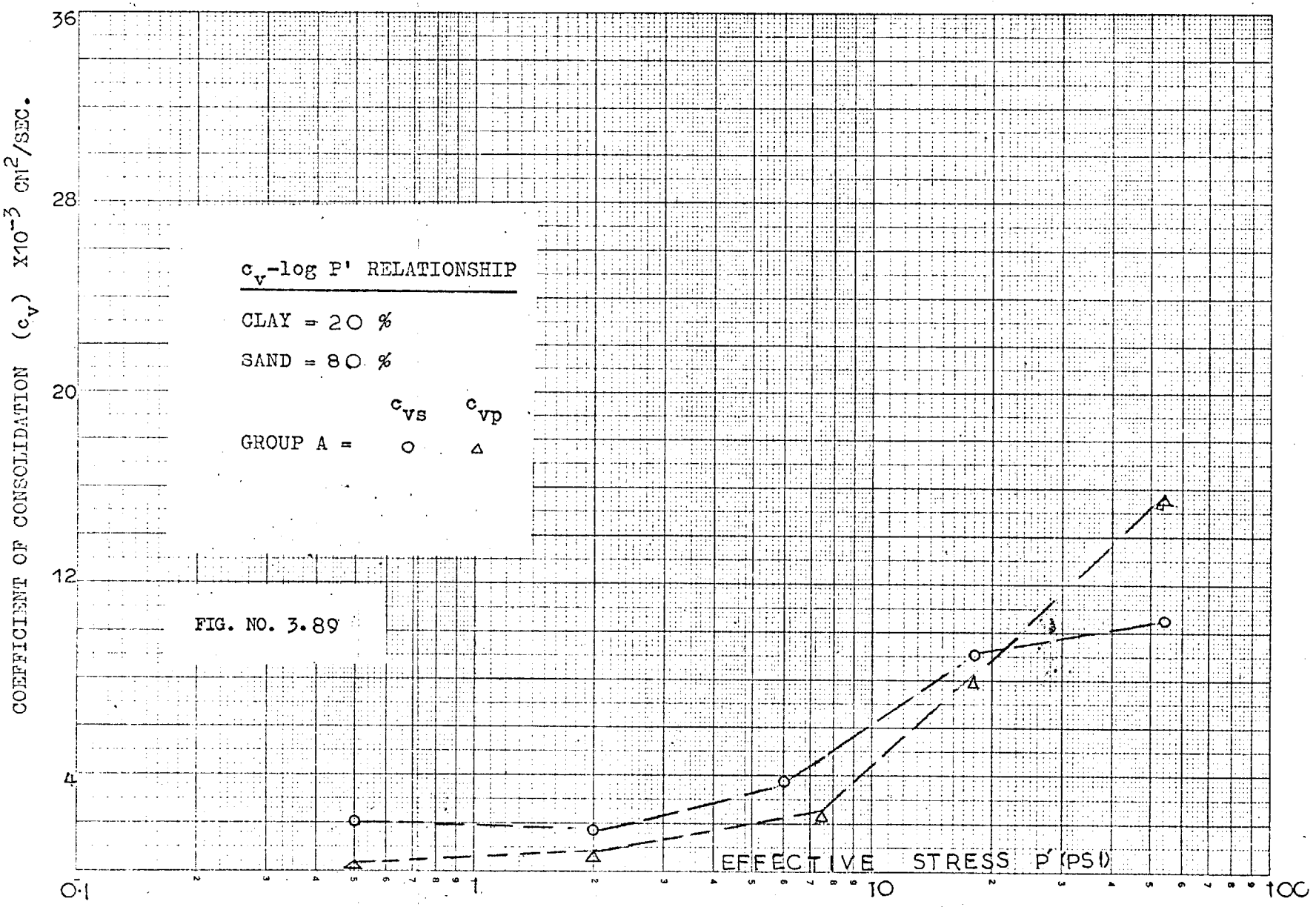
c_v-log P' RELATIONSHIP
CLAY = 20 %
SAND = 80 %
c_{vs} c_{vp}
GROUP A = ○ △
FIG. NO. 3.89
COEFFICIENT OF CONSOLIDATION (c_v) X10^{-3} CM^2/SEC.
36
28
20
12
4
0·1
1
10
100
EFFECTIVE STRESS P' (PSI)

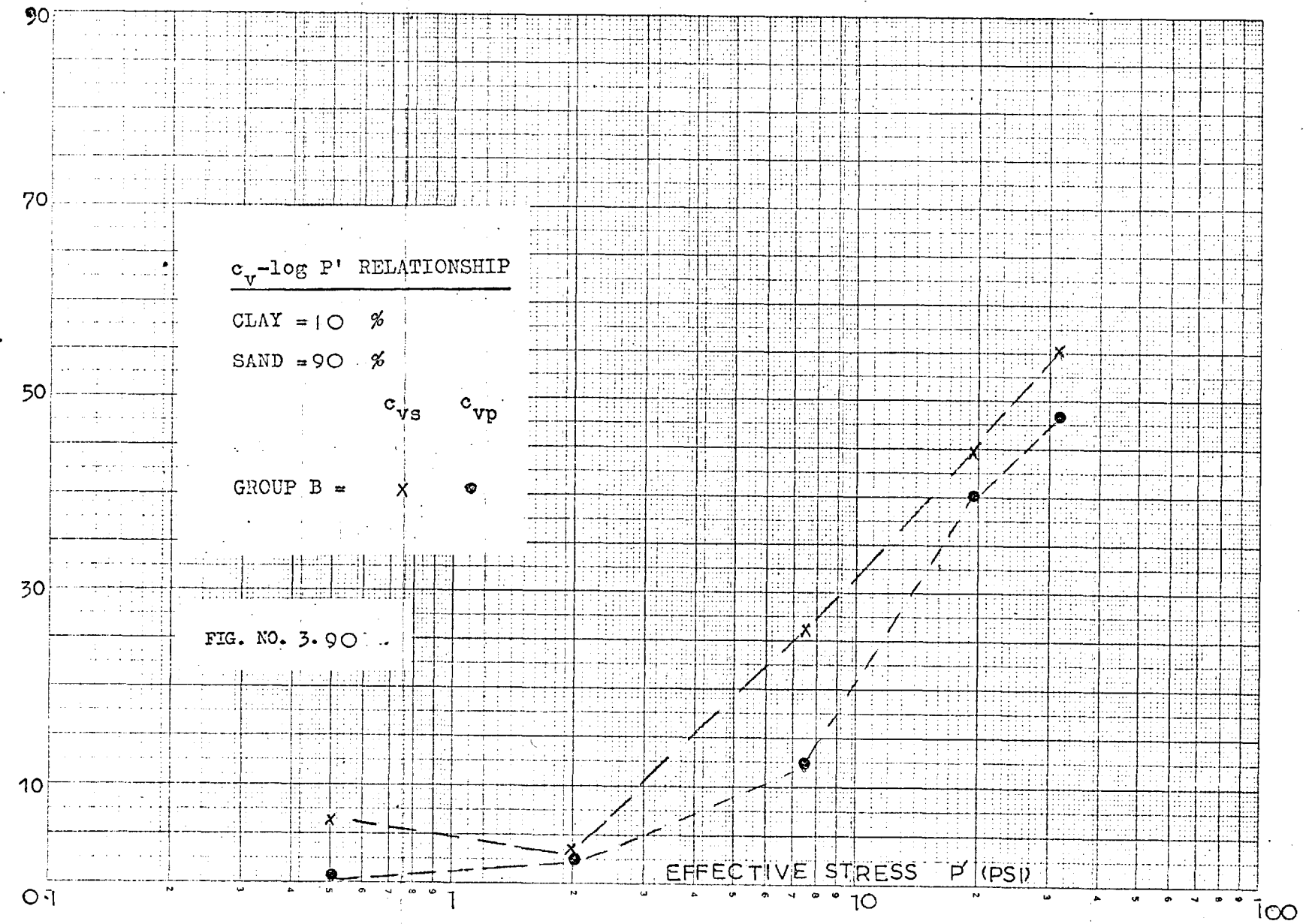
c_v-log P' RELATIONSHIP
CLAY = 10 %
SAND = 90 %
c_{vs} c_{vp}
GROUP B =
FIG. NO. 3.90
COEFFICIENT OF CONSOLIDATION (c_v) X10^{-2} CM^2/SEC.
EFFECTIVE STRESS P' (PSI)
90
70
50
30
10
0.1
1
10
100

4. HYDRAULIC OEDOMETER AND TRIAXIAL CONSOLIDATION TESTS USING SMALL PRESSURE INCREMENTS

4.1 Apparatus for consolidation tests

In order to determine the compressibility characteristics and pore pressure phenomenon of a soil under very small pressure increments (0.5 p.s.i.), the consolidation tests were carried out in the hydraulic oedometer and the triaxial apparatus. A small hydraulic system was devised in which a dead weight was applied to a ram of a standard rotating bush triaxial cell. The necessity for this type of system had arisen from the practical difficulties of adjusting the self-compensating mercury control to the required back pressures accurately. The volume change of the samples was measured by the movement of an air-bubble in saran tubing connecting the apparatus and the pressure system. A parafin volume gauge was also used particularly where large volume change was expected. In the hydraulic oedometer additional settlement measurements at the centre of the sample were recorded using an oil-filled dial gauge.

The consolidation tests reported in this chapter were carried out on 70% sand - 30% clay mixture only. The choice of this particular mixture was based on its special characteristics of behaving like a plastic material in spite of containing more sand.

4.2 Details of the apparatus

(a) General description of the "Hydraulic" oedometer

The hydraulic oedometer designed by Skinner at Imperial College, mainly consists of a 7 in. (inside dia.) by 12 in. high cell in which the essential oedometer components are enclosed as illustrated in Figure 4.1.

As will be seen, the perspex cylinder is sandwiched between the chromium plated brass base and the top cap. A 4.0 in. dia. and 0.5 in. thick ceramic porous stone (UNI A80KV) rests in the central recess of the base. The stainless steel 4.0 in. (inside dia.) by 2.0 in. high oedometer ring containing a sample is placed over the porous stone. The oedometer ring is sealed to the base by pressing an O-ring into position with a brass sleeve ring. A 4. in. dia. and 0.25 in. thick vyon filter disc sits on the top of the sample. A 4.0 in. inside dia. stainless steel guide cylinder bearing the vyon filter ring in its lower limb is sealed with an O-ring to the top of the oedometer ring. Six 0.25 in. dia. tie rods passing through the annular platform on the top of the guide cylinder are screwed to the base. With the help of six lock nuts, the guide cylinder is firmly tightened in position to the odometer ring. An adiprene rubber membrane loading cap of 4.0 in. outside dia. which has a vyon filter ring fitted to its lower end, passes through the guide cylinder and rests on the vyon filter disc sitting on top of the sample. For measuring axial deformation, an oil-filled dial gauge, calibrated in 10^{-4} in. divisions, is clamped to an adjustable perspex supporting spider, such that its travelling arm rests on the centre of the loading cap.

The hydraulic oedometer is designed to permit drainage from either or both ends of a sample. For the top drainage, saran tubing is fitted in such a way that it communicates with the vyon filter ring provided in the guide cylinder. The other end of the saran tubing is connected via a volume gauge to a pressure system against which the drainage is to take place. Similarly for the bottom drainage, a pressure system can be connected through one of the ports to the porous stone resting on the base plate. A pressure transducer is installed in another port at the base for observing the pore water pressure characteristics of a sample. Individual parts of the hydraulic oedometer can be seen in the photograph given in plate no. 4.1.

(b) Modification

Due to ineffective sealing and considerable side friction between the adiprene rubber membrane loading cap (Figure 4.2) and the guide cylinder walls, the following two types of loading caps were used instead:

i) 2.5 in. (outside) dia. hollow brass top cap, as shown in Figure 4.3, which will from now onwards be referred to as "Rigid" loading cap,

ii) 3.5 in. (outside) dia. hollow perspex cylinder top cap, to which a 0.026 in. thick latex rubber membrane diaphragm sealed at one end with O-ring, as shown in Figure 4.4. This will be referred to as "Flexible" loading cap.

The rigid or flexible loading cap can be installed after setting up the sample and clamping the guide cylinder in position. In order to make the system water-tight, an 0.026 in. thick rubber membrane jacket is sealed to the upper end of the loading cap. Later it is rolled along the outer wall of the loading cap and folded back upwards to be sealed to the projecting annular ring provided at the top of the guide cylinder, as shown in Figures 4.3 and 4.4. In the case of the flexible loading cap, the travelling rod of the oil-filled dial gauge sits on a 0.5 in. dia. brass disc placed at the centre of the diaphragm. The communication between the top of the sample and the drainage lead for both types of caps can be maintained through the vyon filter. Since the loading cap is not in direct contact with the guide cylinder, the question of side friction between the two does not arise at all.

4.3 Layout of the dead weight pressure system

To apply small pressure increments of 0.5 p.s.i. accurately, a simple dead weight pressure system, as shown in plate 4.2, was used. It will be seen from the schematic layout of the pressure system, (Figure 4.5) that it is primarily a "loaded ram" method of obtaining a constant pressure. The apparatus consists of two triaxial cells A and B with rotating bush heads, sitting side by side on a wooden frame. These are, in effect, small accumulators in which dead weights applied to the 5/8 in. dia. rams are used to maintain constant cell and back pressures. The principal difficulties of such a type of pressure system are friction, leakage and volumetric capacity. To avert the problems due to the friction, an electric motor is connected to the rotating rotating bushings constructed in the top caps of triaxial cell (see Bishop and Henkel, 1962). Similarly, the difficulty of the excessive leakage is met by filling half of these cells with castor oil. The volumetric capacity of the pressure system was sufficiently large as compared to the volume change of the sample during the individual stages of consolidation. However, a small oil container is provided to refill the oil in the cells whenever necessary. This can be done by connecting the oil reservoir to the pressure source and pumping oil into it by means of a screw control, till the ram has risen to its full volumetric capacity.

To maintain a constant cell pressure, the hydraulic pressure source A is connected through nylon tubing to the hydraulic oedometer or triaxial apparatus at the base. For applying a constant back pressure against which the consolidation is to take place, the pressure source B is connected via saran tubing to the top of the sample. During the process of consolidation volume changes can be measured by both 5.0 c.c. parafin volume gauge and the movement of an air bubble in the saran tubing simultaneously, as described in the previous chapters.

A Bell and Howell type 4-366 electric pressure transducer (0-100 p. s. i. range) with a very small volumetric change under pressure is mounted on one of the sides of the hydraulic oedometer or triaxial base for measuring the pore pressure of a sample. The other end of the transducer is connected to the perspex block T-junction through the klinger valves n and e. To this T-junction the pressure sources A and B are connected by the valves d-g, and b-f respectively. The purpose of these additional connections is to check the pressure increments prior to commencing a consolidation stage. Secondly, to cross-check the cell or back pressure during the consolidation process to determine the exact amount of pore pressure still to be dissipated for a pressure increment applied. These extra connections are useful when working on the high sensitivity of C61 transducer meter, particularly due to slight variation in the room temperature* ($\pm$ 0.5 ^{o}C). Before starting the consolidation tests both pressure sources were calibrated for the pressure output against the dead weight gauge tester (Budenberg). Figures 4.6(a) and (b) show the pressure output (in p. s. i.) against the dead weights (in grams) placed on the hangers of pressure sources A and B respectively.

4.4 Procedure of testing

(a) Setting up of sample in the Hydraulic Oedometer

Before installing a sample, the whole layout of various connections and drainage leads emerging from the hydraulic oedometer and those of pressure system were thoroughly checked for leakage. Earlier the de-aired water was flushed through different leads to ensure that the entire system was free from any trapped air. Similarly the ceramic porous stone (UNI A80 kv) was saturated before placing it into the central recess of the base plate as shown in Figure 4.1. A soaked Whatman's no. 54

---

* All tests were carried out in the temperature controlled room +20^{o}C.

filter paper was then slid over the porous stone. Next the sample ring was brought into position and sealed to the base by means of an O-ring pressed with the help of a brass sleeve ring into the annular groove. The soil paste was then put into the sample ring bit by bit. When the oedometer ring was filled up to the brim, a metal piece with a smooth edge was used to level the top surface of the sample. In this way, an almost 1.0 inch thick sample was achieved. On the top of the sample a saturated filter paper and vyon filter disc were placed gently one over the other.

After the sample had been set, the guide cylinder was slowly lowered down with the help of 6 tie rods screwed in the oedometer base plate to sit on the sample ring. An O-ring was provided in between the sample ring and the guide cylinder to seal the two, using lock nuts. Next, the loading cap wearing a rubber membrane jacket was gently allowed to rest on the vyon filter disc already sitting on the top of the sample. The free end of the rubber membrane was rolled back upwards and sealed to the annular ring projecting vertically from the guide cylinder, as shown in Figures 4.3 and 4.4. During this operation every possible effort was made to avoid air being trapped in between the sample and loading cap assembly. To further ensure this, de-aired water was flushed through the top drainage lead in the guide cylinder to bleed from the opposite side. Now an oil-filled dial guage supported by a perspex spider was placed on the loading cap. In the case of the flexible loading cap, the travelling rod of the dial gauge was allowed to rest on a 0.5 in. dia. brass disc previously placed on the diaphragm, as shown in Figure 4.4. The other parts of the hydraulic oedometer were next assembled in the manner described earlier.

The cylindrical 1.5 in. dia. by 3 in. high sample for the triaxial consolidation test was prepared in a similar way to that described in section 3.4

(b) Method of consolidation test

After assembling the apparatus, the cell was filled with de-aired water in the usual way. The cell pressure of both the hydraulic oedometer and the triaxial was raised through the dead weight gauge tester (Buderberg) in steps to 80 p. s. i. At each step of pressure increment, pore pressure was measured to determine B values and verify whether the samples were fully saturated. After the cell pressure had been increased to a required value, the pressure lead was disconnected from the gauge tester and reconnected to the hydraulic pressure source A through the klinger valve, c, as shown in Figure 4.5. The sample was then left overnight under constant cell pressure to allow any trapped air to dissolve in water.

The next morning the consolidation process was started with the first stage followed by the rest of the stages of consolidation (Table 4.1) in the following manner.

Before commencing a consolidation stage the dead weight pressure source B was set to a desired back pressure. The initial position of the air bubble in relation to the measuring scale, the volume gauge and dial gauge readings along with that of the readout meter C61 for the pore pressure measurements were noted. The chart recorder was switched on to the fast speed and its needle set in position depending upon the stress increment and working sensitivity* as described in section 2.4 (iv). Now, to begin the consolidation process, klinger valve, a, of the pressure source B was opened and the constant back pressure applied to the top of the sample. During the test volume change and axial deformation readings of the sample were taken at the appropriate time intervals in the normal way, while dissipation of pore water pressure

*For small stress increments the readout meter C61 was set on the high sensitivity which gave 74 divisions per p. s. i. on the chart recorder. similarly, for large increments the medium sensitivity was used, which represented 7.5 divisions per p. s. i. on the recorder.

was recorded automatically on the chart recorder.

As the test continued, the pore pressure which remained to be dissipated at any time was often cross-checked by connecting the back pressure source B to the pressure transducer through the perspex block T-junction, as shown in the layout (Figure 4.5). To do so the sample was first isolated from the transducer by closing valve, o. Pressure source B was then connected to the transducer by opening valves b, f, e and n. After determining the value of back pressure (P.W.P. still to be dissipated) the transducer was reconnected to the sample by first closing valves n, e, f and b and then opening valve o. A similar method was adopted to check the precise amount of stress increment before commencing a consolidation stage. These cross-checks were made in view of slight variations in the room temperature, which affected the transducer and, consequently, the readings, particularly on the high working sensitivity of the C61 readout meter.

Except for the first stage of consolidation, the volumetric capacity of pressure source B was quite large in comparison to the volume change of the sample at any stage. However, before starting a consolidation stage pressure source B was always adjusted to its full volumetric capacity by refilling the required quantity of oil. This was normally done by connecting the oil container through nylon tubing to the klinger valve, m. After opening valves h and j the oil was slowly pumped into the pressure accumulator by means of a screw control. In the case of the first stage, where the volume change of a specimen was larger than the capacity of the pressure source, the oil was refilled only after isolating the sample from the source. In the same way, whenever pressure source A needed to be set, the oil container was connected through klinger valve, k. In order to avoid disturbance due to the oil pumping process, the apparatus containing the sample was first disconnected by closing the valve, c. After the oil had been filled in, the cell was reconnected by opening valve c after closing k.

In the case of the hydraulic oedometer, the duration of a pressure increment was normally 24 hours, whereas for triaxial tests it varied from 5 to 7 days during the first 11 stages, and 24 hours for the last 4 stages of consolidation. Finally, two swelling stages were carried out before dismantling the apparatus and unloading the sample.

4.5 Results and Discussion

The settlement and pore water pressure characteristics of 30% clay - 70% sand mixture observed from the hydraulic oedometer and triaxial tests are assembled in Figures 4.7 to 4.42. Only two hydraulic oedometer tests could be carried out, one with the rigid loading cap and another with the flexible loading cap. Unfortunately, leakage developed in both of them during the 10th and 11th stages of of consolidation, where large pressure increments had been applied. Consequently these tests were stopped and could not be continued to the schedules 15 stages (see Table 4.1); also time did not permit the repetition of the tests.

In each figure relationships of settlement and pore pressure dissipation with log t and $\sqrt{t}$ are given. This is done in order to facilitate the comparison of the two relationships on different scales, as well as with each other. The plots of time-settlement illustrate the effects of stress increment ratio on the time-rate of consolidation. There are three distinctively shaped time-settlement curves. For large stress increment ratio a settlement curve is obtained which, with the exception of secondary compression, corresponds to the typical Terzaghi curve. This will be referred to as the Type I curve (e.g. see figures of the 10th and 11th stages of consolidation). From this type of curve, end of primary consolidation i.e. when the excess pore pressure has almost dissipated, can be estimated quite accurately

using the Casagrande construction. For a very small stress increment ratio a Type III is obtained. Due to large secondary compression this curve deviates considerably from that of Terzaghi's theoretical. Neither Casagrande's nor Taylor's time-fitting method can estimate the primary consolidation in this case (e.g. Figures 4.14, 4.25 and 4.30 (a) and (c)), while for intermediate $\frac{\Delta P}{Po'}$ a transition curve Type II is obtained which lies between Type I and III. These three types of curve confirm the earlier observations of Leonards and Girault (1961); Wahls (1962) and Tan (1968) as to the effects of $\frac{\Delta P}{Po'}$ on the time rate of consolidation.

Within its limits, Terzaghi's theory of consolidation is a simplified mathematical interpretation of a highly complicated phenomenon. Basic assumptions of constant permeability and compressibility, over a given pressure increment, and a void ratio effective stress relationship, independent of time (no creep), are responsible for most of the discrepancies between the observed and predicted behaviour of a soil. Deviation of rate of settlement and dissipation of excess pore water pressure from Terzaghi's theory have been adequately demonstrated by the curves of the hydraulic oedometer and triaxial tests reported here. Although the duration of a pressure increment was very small, nevertheless the results indicate very high secondary effects. To deal with the secondary effects Buisman (1936) was amongst the first to present an empirical analysis in which primary and secondary consolidation were considered as two separate entities, i.e. primary consolidation is succeeded by secondary compression after the excess pore water has dissipated. But judging from the time-settlement graphs reported here, it is evident that secondary consolidation occurs before the pore pressures have fully dissipated and that its

magnitude increases with time as the P.W.P. ceases to dissipate. It seems that primary and secondary consolidation processes begin together almost instantaneously with the application of load increment. One of the first attempts to rationalize Terzaghi's theory of consolidation was made by Merchant (1939) and Taylor and Merchant (1940) who suggested that primary consolidation and secondary compression occur concurrently, with the component due to secondary compression developing at a rate which is proportional to the amount of residual secondary compression (Christie, 1964). Since then refinements in the classical theory have been brought about by many research workers. Amongst the latest are Gibson and Lo (1961), Wahls (1962) Murayama and Shibata (1964), and Barden (1965). Gibson and Lo (1961) proposed a theory in which the compressibility of an element of the soil skeleton is represented by a rheological model comprising a Hookean spring in series with a Kelvin body. Murayama and Shibata (1964) assumed that the behaviour of the clay skeleton could be analysed with the behaviour of a mechanical model consisting of an independent Hookean spring connected in series with a modified Kelvin element composed of a Hookean spring, a slider and a dashpot. The non-linear theory by Barden (1965) assumes the soil skeleton to behave as a mechanical model consisting of a linear spring coupled in parallel with a non-linear dashpot. This model does not have instant compression, since the whole spring is damped by the dashpot.

Berre and Iversen (1972) while investigating the influence of sample thickness on the rate of compression and pore pressure dissipation for a soft normally-consolidated clay exhibiting large secondary compression, used the theories of Gibson and Lo (1961) and Barden (1965). They concluded that the Gibson and Lo theory does not agree with the experimental curves at low values of time. But Barden's theoretical time-compression curve agreed well with

the experimental curves both at high and low values of time. However, the theoretical pore pressures were found to be too low at low values of time. Nevertheless theoretical treatment of structural viscosity by Barden (1965) indicates that its effects would be exhibited to a marked extent only in tests with thin samples and small stress increment ratio. This is well illustrated by the experimental curves of 1.0 inch thick samples consolidated in the hydraulic oedometers (Figures 4.7 to 4.27 (a) and (c)). The effects of structural viscosity can also be seen from the curves of 3 inch high triaxial sample (Figures 4.28 to 4.42 (a) and (c)), particularly for small $\frac{\Delta P}{Po'}$.

Dissipation curves for excess pore water pressure of all the stages of consolidation from the hydraulic oedometer and triaxial tests are given in Figures 4.7 (b) to 4.42 (b). Terzaghi's theoretical curve has been fitted to all of them at 50% dissipation. It will be seen that a better correspondence between the theoretical and observed curves is obtained only at those stages where large stress increment ratio has been applied (tenth and eleventh stages). But when small $\frac{\Delta P}{Po'}$ is used the pore pressure seems to dissipate rapidly in the beginning and then slow down after 50% dissipation. Absolutely no correspondence between the experimental and Terzaghi's theoretical curve is achieved in these cases. From these dissipation curves the influence of structural viscosity of the material under consideration is very well demonstrated. Leonards and Girault (1961) observed similar behaviour i.e. rapid dissipation of pore water pressure with small stress increment ratio. According to Leonards and Altschaeffl (1964) when stress increment ratio is small, slippage between particles occurs at a limited number of contact points. The compressibility will therefore be smaller than would be the case if a larger $\frac{\Delta P}{Po'}$ were applied. Because the consolidation process is accelerated when the compressibility is reduced, pore pressure dissipation will be more rapid for a small $\frac{\Delta P}{Po'}$ than for a large one.

The relationship of P.W.P. dissipation in p.s.i. against root of time is also plotted, as shown in Figures 4.7 (d) to 4.42 (d), to indicate initial and final P.W.P. at the consolidation stages. In the case of the hydraulic oedometer tests, the duration of the pressure increment was about 24 hours, and that of the triaxial tests was 5 - 7 days, except in the last six stages. Before applying a pressure increment, pore pressure of the sample was allowed to reach equilibrium under undrained conditions. During this time, the pore pressure began to rise slowly to a certain limit in both the hydraulic oedometer and triaxial samples. For instance, compare Figures 4.18(d) and 4.19(d) where pore pressure of a hydraulic oedometer developed from 79.0 p.s.i. to 79.06 p.s.i. In the case of a triaxial sample drainage valves were allowed to remain closed overnight before proceeding with another stage of consolidation; the pore pressure e.g. third and fourth stages of consolidation (Figures 4.30 (d) and 4.31(d)) developed by less than 0.20 p.s.i. which is about 10% of the total effective stress at these stages. It seems that if drainage is prevented, the creep strains will induce excess pore pressure and cause concomitant reduction in shear strength (Leonards and Altschaeffl, 1964). During this time, the continuous relaxation of the soil specimen is also being damped by the visco-elastic behaviour of the soil structure. Study on the build-up of excess pore pressure under undrained conditions by Berry and Wilkinson (1969) indicates that the increase in pore pressure is closely related to the structural viscosity and the magnitude of a pressure increment ratio, as discussed in Chapter 2. The other distinct feature of the pore pressure dissipation curves (Figures 4.7 to 4.42 (b) and (d)) is that they seldom dissipate to 100%, i.e. residual P.W.P. of about 2% to 5% remains after the primary consolidation is supposed to have been reached. During primary consolidation the deformation is controlled essentially by the permeability and com-

pressibility of the soil skeleton, while during secondary compression only small excess hydrostatic pore pressures remain and the compression is a form of the viscous resistance of the soil skeleton. Looking back at the pore pressure dissipation curves, another interesting thing to note is the intermittence or arresting of P. W. P. during the consolidation process. This phenomen can be observed in both the hydraulic oedometer and triaxial tests, particularly when small stress increments are applied. For example, in the second stage of consolidation (Figure 4.8 (b), 4.19 (b) and 4.29 (b)), the pore pressure dissipates fairly rapidly in the beginning, then after about 40% to 50% dissipation, becomes very slow. This arresting of the pore pressures is thought to be due to interparticle action, such as concurrent breaking and mending of bonds while moving closer in a tight packing, as will be discussed in the next chapter. Similar behaviour of the pore pressure under small stress increment ratios has been observed by Skinner (1970) and the author, as described in the previous chapter.

One of the main advantages of a hydraulic oedometer is to eliminate or minimize the errors involved in the conventional oedometer (see Chapter 2). The flexibility of the pore pressure measuring device has been shown to be sufficiently stiff for the soil under consideration, i. e. pore pressure behaviour is not due to this effect. However, due to small stress increments, even slight leakage through the rubber membrane or drainage connections could cause some discrepancies in the test results. In the hydraulic oedometer, with flexible loading cap, differences between the volume change and axial deformation are considerable. This seems to have been caused by the malfunction of the volume gauge rather than anything else. Otherwise, had there been any internal leakage, the pore pressure would have risen to the cell pressure when the drainage valves were allowed to remain closed for some time. Besides, the difference

could also have been due to the flexibility of the tubing connecting the sample to the volume gauge. At the instant when consolidation is started, the pressure in the system drops from equilibrium pore pressure to the applied back pressure, creating an initial volume change in the system. The results of the triaxial test seem to be relatively free from these errors. This can be seen by comparing compressibilities of this test with those of 70% sand samples from the group A and B tests described in Chapter 3, at the same effective stresses. They show good agreement with each other.

Curve-fitting method for determining t_{50} and T_{50}

The fact that primary and secondary consolidation begin simultaneously with the application of a pressure increment means that the void ratio at t_{100} (end of primary) must be due to both. But after t_{100} the change in void ratio is caused by secondary compression alone. It is presumed that primary consolidation comes to an end at t_{100}, regardless of the shape and type of the settlement curve. In other words, if primary consolidation stops in the case of Type I curve, then it must do the same for Type II as well as Type III. Wahls (1962) has proposed a curve-fitting method which can prove useful where Casagrande's method for determining 100% primary consolidation may be difficult to use.

A summary of Wahls' (1962) primary and secondary consolidation equations and his curve-fitting method is given below.

Wahls developed the consolidation equation by considering a rheological model. Although the consolidation process is assumed to involve primary and secondary consolidation, two separate rheological mechanisms are developed, one for each phenomenon. They are later connected in series. The fundamental concepts of primary

consolidation are expressed in terms of the rheological model, namely Kelvin body. This consists of an elastic spring connected in parallel to a viscous dashpot. When pressure is applied to the Kelvin model, the pressure is initially supported by the dashpot and gradually transferred to the spring as the system compresses. After the entire pressure is supported by the spring, the maximum deformation is supposed to have been reached and the process stops. Hence the spring is analogous to the intergranular structure of the soil, and the dashpot is analogous to the pore water.

To model the primary behaviour Wahls uses an infinite series of Kelvin bodies. Thus the deformation equation of the rheological model for primary consolidation is

$$R_1 = A_p \Delta P \left[1 - \frac{8}{\pi^2} \sum_{n=0}^{\infty} \frac{1}{(2n+1)^2} e^{-\left[(2n+1)\pi/2\right]^2 T} \right] \quad \ldots\ldots (4.1)$$

Where R_1 denotes compression of the primary mechanism,

A_p denotes coefficient of compressibility for primary mechanism,

ΔP denotes pressure increment,

T denotes Terzaghi's dimensionless time factor,

e denotes base of natural logarithm.

Equation (4.1) can also be written in the following simple form:

$$R_1 = A_p \Delta P \, f(T) \quad \ldots\ldots (4.2)$$

where

$$f(T) = 1 - \frac{8}{\pi^2} \sum_{n=0}^{\infty} \frac{1}{(2n+1)^2} e^{-\left[(2n+1)\pi/2\right]^2 T}$$

is the primary time factor function.

Similarly, the equation for secondary compression is based on the assumptions that

(i) the magnitude of secondary compression is a function of the maximum value of effective stress sustained; the void ratio, and time and is independent of the magnitude of the pressure increment.

(ii) The rate of secondary compression is a function of time.

(iii) The time required for the development of the linear relationship between secondary compression and logarithm of time is related to the time required for the completion of primary consolidation.

(iv) The coefficient of secondary compression, C_α, is a function of total pressure and void ratio. C_α is assumed to be constant for the duration of a given pressure increment and can be determined from the total pressure and the void ratio at the completion of primary consolidation.

To fulfil these assumptions a viscous dashpot has been introduced with each Kelvin body of the primary model. Thus the final equation for the compression of secondary mechanism, R_2, of the infinite series of secondary dashpot is

$$R_2 = C_f \frac{8}{\pi^2} \sum_{n=0}^{\infty} \frac{1}{(2n+1)^2} \log_{10} \left[1+\left(\frac{2n+1}{2} \pi \right)^2 T \right] \quad \ldots\ldots (4.3)$$

where C_f denotes secondary coefficient.

The deformation equation for the secondary effects can also be written as

$$R_2 = C_\alpha \; h(t) \quad \ldots\ldots (4.4)$$

where C_α is the coefficient of secondary compression which is closely approximated on a semi-logarithm plot by a straight line with a slope equal to $0.9215\ C_f$ (Wahls' particular case) and

$$h(T) = 1.08516 \quad \frac{8}{\pi^2} \quad \sum_{n=0}^{\infty} \quad \frac{1}{(2n+1)^2} \quad \log_{10} \left[1 + \left(\frac{2n+1}{2} \pi \right)^2 \quad T \right]$$

is the secondary time factor function.

The total compression, R_T, due to primary and secondary consolidation can be obtained by adding equations (4.2) and (4.4), i.e.

$$R_T = R_1 + R_2 = A_p \Delta P \quad f(T) + C_\alpha \qquad h(T)$$

$$\text{or} = A_p \Delta P \left[f(T) + \frac{C_\alpha}{A_p \Delta P} \qquad h(T) \right] \qquad \ldots\ldots (4.5)$$

This equation is for the complete consolidation process.

The relevant parameters for the above expression can be determined by using Wahls' (1962) curve-fitting method, shown in Figure 4.43. His method has been used to determine 50% primary consolidation from the settlement curves of the hydraulic oedometer and triaxial tests reported here. The coefficient of consolidation has been calculated at t_{50} using an appropriate time factor related to $C_\alpha / \Delta R_{TI}$. Wahls' curve-fitting method is outlined as follows:

(i) The final slope, C_α, on the semi-logatithmic plot of the experimental curve is first determined.

(ii) Refer to Figure 4.43 (i). The compression, R_{TI}, at the tangent intercept point is found, i.e. (1) the intersection of the line of maximum slope and the line of secondary slope for Type I curve (a)., (2) the point of tangency of the curve to the line of secondary compression for Type II* curve (b).

---

*Wahls' Type II curve is the extreme case and may be considered the same as the author's Type III.

(iii) Next ΔR_{TI}, the compression at the tangent intercept point is found by subtracting the theoretical zero, R_0 from R_{TI}.

(iv) R_M and $R_0 + \frac{1}{2} \Delta R_{TI}$ is calculated, and from the test curve the corresponding time coordinate, t_M, (i.e. t_{50}) is determined.

(v) Lastly, the relevant theoretical time factor, T, is found. To do this $C_\alpha / \Delta R_{TI}$ is first calculated and then the time factor T_M (i.e. T_{50}) corresponding to R_M is determined from Figure 4.43(ii)(a) for the Type I curve, or from Figure 4.43 (ii)(b) for the Type II curve.

The above Wahls' curve-fitting method has been used to determine the time at 50% primary consolidation. The coefficient of consolidation is calculated on the basis of this time which will be discussed later. The test results of particular interest herein are the effects of the pressure increment ratio on the shape of the settlement-time curves and the secondary compression characteristics. The coefficient of secondary compression C_α in units of void ratio change per logarithm of cycle time has been plotted against the stress increment ratio $\frac{\Delta P}{Po'}$ and the effective stress P'. It will be seen from Figure 4.44 that the values of C obtained from the hydraulic oedometer tests fall within a range of values .001 to .006. Slightly larger values of C_α are obtained from the triaxial tests (Figure 4.4). However, it is evident from these graphs that the coefficient of secondary compression is independent of the stress increment ratio and the consolidation pressure. It must be pointed out here that in the twelfth to fifteenth stages of consolidation (triaxial) a decrease in C_α value can be observed. This seems to have been caused by very small $\frac{\Delta P}{Po'}$ applied after the large one. Perhaps similar reduction C_α would have been obtained

in hydraulic oedometers also if small stress increments had also been applied at the end of the tests. The above results conform with the findings of Newland and Allely (1960) whose experiments on Whangamarino clay indicated that the slope of the secondary compression curve is independent of consolidation pressure. Tan (1968) also observed similar behaviour of remould remoulded clays. Referring back to the settlement-time curve (Figures 4.7 to 4.42 (a) and (c)), it can be seen that the large stress increment ratios give large primary consolidation, consequently the ratio of secondary to primary consolidation will become small and vice versa. This is in agreement with the test results of Newland and Allely (1960), Leonards and Girault (1961) and Wahls (1962).

The relationship of void ratio against effective stress of 70% sand - 30% clay mixture obtained from anisotropic (axial deformation) and isotropic consolidation is shown in Figures 4.46 and 4.47 respectively. The values of void ratios are also summarized in Tables 4.2, 4.3 and 4.4. In the case of the flexible loading cap, it is assumed that the thrust of the dial gauge (about 3 lbs at full stroke) is uniformly distributed by the 1/8 inch thick vyon filter disc used as the upper boundary filter. This is an approximation, the real distribution would depend on the flexing of the vyon filter. The effects of this approximation are not very significant, as can be seen from the initial points of the two tests. In the e-log P' plots with dotted lines represent void ratio e_p due to primary consolidation only, and the solid lines represent total void ratio $e = e_p + e_s$ which include both the primary and secondary consolidation. The duration of each increment was large enough to allow full primary consolidation. In the case of the hydraulic oedometers the duration was about 24 hours, whereas in the triaxial tests it varied from 5 to 7 days. However, it is evident from the void ratio graphs that large secondary compression

had occurred after 100% primary consolidation. This confirms in a general way the proposal by Taylor (1942) that there is a primary e-log P' curve obtained by allowing just sufficient time for primary consolidation, while below, and roughly parallel to this curve, are other curves for successively longer duration of increments. The difference between the two e-log P' curves is due to the change in void ratio by an amount of secondary compression in excess of primary consolidation. The void ratio change Δe_s due to secondary compression largely depends upon the duration of a pressure increment after primary consolidation has ceased. Similarly the magnitude of Δe_s in relation to that of primary consolidation Δe_p seems to depend on the stress increment ratio. This effect can be seen clearly from the settlement curves where the larger the $\frac{\Delta P}{Po'}$, the greater the total settlement, therefore the larger the total void ratio change during an increment. Thus Δe_s represents a smaller percentage of the total void ratio change when $\frac{\Delta P}{Po'}$ is increased. Conversely, when small $\frac{\Delta P}{Po'}$ is used, Δe_s represents a large percentage of the total void ratio change in comparison to Δe_p (duration of the pressure increment being the same for both cases).

The coefficient of compressibility, m_v, has been calculated from the volume change as well as the void ratio determined from axial deformation of the samples in hydraulic oedometers, i.e.

$$m_v = \frac{\Delta V}{\Delta P} \cdot \frac{1}{(1+V_0)} = \frac{\Delta e}{\Delta p} \cdot \frac{1}{(1+e_0)}$$

where V_0 and e_0 correspond to a pressure Po; and V and e are the change in volume and void ratio due to pressure increase from Po to (Po + Δ P). Similarly, the coefficient of compressibility C_c due to isotropic consolidation has been determined from the volume change using equation (3.6). The relationships of the coefficient of compressibility m_v and C_c with the average maximum principal

effective stress are shown in Figure 4.48. In general m_v and C_c decrease with the effective stress in a similar way as in the conventional oedometer and triaxial tests reported in the previous chapters. The compressibility values of 70% sand sample obtained from the hydraulic oedometer tests, are however, higher than those of conventional oedometers. It has already been shown that in the conventional oedometer compressibilities can be affected by side friction, extrusion of material deformation of the apparatus, etc. These difficulties are eliminated in the hydraulic oedometers. Looking back at the compressibility graph, it will be seen that the m_v and C_c values lie within a narrow band of scattered points. Since the duration of the pressure increments was relatively very small, m_v and C_c seem to have been least affected by the stress increment ratio. Som (1968) found that after a long duration (90 days or so) the magnitude of subsequent loading has marked effect on the compressibility, i.e. long rest periods followed by large stress increment ratio will give large compressibility and vice versa.

The coefficient of consolidation c_v has been calculated at 50% primary consolidation. Wahls' (1962) curve-fitting method is used to estimate 100% primary consolidation from the settlement curves, as described earlier. The theoretical time factor T_M (i.e. T at 50% primary consolidation) at which the compression is equal to one-half the compression at the tangent intercept point is related to the ratio of C_α to ΔR_{TI}, the compression at intercept point. The time factor T_M was obtained from the $T_M - C_\alpha/\Delta R_{TI}$ relationship, Figure 4.43 (ii). It can also be seen that when the ratio $C_\alpha/\Delta R_{TI} \leq 0.2$, the time factor is approximately the same as Terzaghi's theory i.e. $T_{50} = 0.198$. The T_M itself then increases or decreases as $C_\alpha/\Delta R_{TI}$ which itself depends upon the shape of the settlement curve. For large $\frac{\Delta P}{Po'}$ as in the tenth and eleventh

stages, T_M was almost the same as Terzaghi's theoretical. But for small $\frac{\Delta P}{Po'}$ where abnormally high amounts of secondary compression blended with primary consolidation showing no distinction between the two, i.e. Type II and III curves, as mentioned earlier, T_M was different. For such type of curves corrected values of T_M were determined using Wahls' theoretical curves (Figures 4.43 (ii) (a) and (b)). The time $t_M = t_{50}$ at 50% primary consolidation for the individual experimental curve was determined. H, the height of the sample at each stage of consolidation, was known. The coefficient of consolidation c_{vs} was then calculated using the relationship

$$c_{vs} = \frac{T_M \, H^2}{t_M}$$

Since Wahls has taken into consideration the secondary effects, the dimensionless time factor T_M in this expression will not be the same as Terzaghi's theoretical, except when the coefficient of secondary compression C_α tends to be zero.

Figures 4.49, 4.50 and 4.51 show the relationship between coefficients of consolidation with effective stress. c_{vp} calculated at 50% dissipation* of excess pore water pressure has also been plotted. The summary of c_{vs} and c_{vp} values obtained from the hydraulic oedometer and triaxial tests is given in the respective Tables 4.2, 4.3 and 4.4. It will be seen that c_{vs} and c_{vp} values do not correspond with each other, excepting those of the tenth and eleventh stages where large stress increment ratio has been used. As $\frac{\Delta P}{Po'}$ is reduced in the successive stages of consolidation, c_{vp} increases, whereas c_{vs} decreases. With the increase of $\frac{\Delta P}{Po'}$ from 0.111 to 1.0 and 2.0 in the tenth and eleventh stages respectively,

---

* According to Terzaghi's theory, average consolidation of 68% should occur at 50% dissipation of excess pore pressure (e.g. Figures 4.28(a) to 4.42(a)).

(Table 4.1), c_{vp} decreases and c_{vs} increases in such a way that the two values agree well with each other. In these stages, i.e. the tenth and eleventh, the proportion of primary to secondary is larger. But, again when small $\frac{\Delta P}{Po'}$ is used as in the twelfth to fifteenth stages, Figure 4.51, the values of c_{vp} increase and those of c_{vs} decrease. For small stress increment ratio, the proportion of primary to secondary is smaller. Thus it can be concluded that both c_{vs} and c_{vp} are the functions of secondary to primary consolidation. Also, the high values of c_{vp} are associated with the rapid dissipation of excess pore water pressure and the low values of c_{vs} are related to the slow overall settlement. Similar conclusions were drawn by Leonards and Altschaeffl (1964) on the consolidation characteristics of freeze-dried kaolin, and it was remarked that the degree of consolidation and rate of pore pressure dissipation can be distinct entities.

Since c_{vp} has been calculated using Terzaghi's theory, and c_{vs} is determined using Wahls' (1962) analysis, the comparison of the two may not be totally correct. However, for the sake of argument it will be seen that the ratio of c_{vs}/c_{vp} obtained from isotropic and anisotropic consolidation tests supports the conclusions arrived at before in Chapter 3. That is the ratio of time at 50% dissipation of excess pore water pressure to the time at 50% settlement increases as the stress increment ratio decreases. For larger stress increment ratio c_{vs}/c_{vp} is larger. The values of c_{vs}/c_{vp} are mainly due to the rapid dissipation of excess pore pressure giving higher values of c_{vp}. It may be mentioned here that there is no significant difference between the c_{vs} values calculated from the volume change and axial deformation of the sample in the hydraulic oedometer tests. Besides this an almost similar picture of the consolidation behaviour of 70% sand sample emerges from both the hydraulic oedometer and triaxial

tests. The above results are in full agreement with the work by Leonards and Girault (1961), Skinner (1970) and Garga (1970), as tabulated in Table 3.3, which shows that a good agreement between c_{vs} and c_{vp} can be obtained for large increment ratios only.

Finally, it is suggested that when the secondary component of consolidation is significant and it becomes difficult to use Casagrande's or Taylor's time fitting method, in such cases Wahls' (1962) curve-fitting method may prove useful for analysing the results.

4.6 Advantages of the hydraulic oedometer

Hydraulic oedometers have been previously designed and used by e.g. Lowe et al (1964), Whitman and Miller (1965), Rowe and Barden (1966). They have successfully employed the principle of hydraulic loading system in the design of consolidation cells which have been satisfactorily used to study the consolidation characteristics of soil. At Imperial College Som (1968) used a high pressure oedometer to investigate the consolidation behaviour of London clay. There are a number of advantages of the hydraulic oedometer over the conventional type, for instance:

(i) As in the original design, Figure 4.1, and later modified, Figure 4.4., uniform pressure on the sample can be maintained by applying the pressure on a flexible rubber membrane which allows free deformation of the sample. This is difficult to achieve in the conventional oedometer due to the rigid loading cap.

(ii) By providing a small porous stone at the base, pore water pressure dissipation can be measured at a central area. Similarly, settlement can also be measured at the centre of the sample. In doing so, the effects of side friction can be eliminated to a great extent.

(iii) Errors due to deformation of the apparatus can be reduced to a negligible proportion.

(iv) Inevitable shock loading due to the dead weight lever system in the conventional oedometer is completely avoided by the hydraulic pressure system.

(v) In the conventional oedometer there is no control over the drainage, which begins immediately with the application of a load increment. Thus the pore pressure has no time to reach its peak. Whereas the drainage is under full control in the hydraulic oedometer. Employing a rigid measuring system, high pore pressure response can be achieved during undrained loading before commencing the consolidation process.

(vi) As the consolidation can be carried out against back pressures; any trapped air can be dissolved into solution to ensure full saturation before consolidation is begun. Besides, the stress conditions due to back pressure are more similar to field conditions.

(vii) Consolidation characteristics can be well studied from the volume change, direct settlement and the pore pressure variations observed in a hydraulic oedometer.

Stage No.	Cell Pressure psi	Back Pressure psi	Stress Increment ΔP psi	Stress Increment Ratio $\Delta P/Po'$
1 (saturation)	80	7.90	1.0	---
2	"	78.50	0.50	0.50
3	"	78.0	0.50	0.333
4	"	77.50	0.50	0.250
5	"	77.0	0.50	0.200
6	"	76.50	0.50	0.166
7	"	76.0	0.50	0.142
8	"	75.50	0.50	0.125
9	"	75.0	0.50	0.111
10	"	70.0	5.0	1.0
11	"	50.0	20.0	2.0
12	"	49.50	0.50	0.01666
13	"	49.0	0.50	0.01639
14	"	48.5	0.50	0.01612
15	"	48.0	0.50	0.01587

TABLE 4.1

Consolidation Programme of Hydraulic Odeometer and Triaxial Tests

Stage No	Po' psi	$\frac{\Delta P}{Po'}$	VOLUME CHANGE e	m_v Sq. cm/gms x 10^{-4}	$C\alpha/\Delta R_{TI}$	T_M	c_{vs} Sq. cm/sec x 10^{-4}	c_{vs}/c_{vp}	AXIAL DEFORMATION e	m_v Sq. cm/gms x 10^{-4}	$C\alpha/\Delta R_{TI}$	T_M	c_{vs} Sq. cm/sec x 10^{-4}	c_{vs}/c_{vp}
1	-	-	.903	10.31	0.052	.198	1.59	1.272	.903	14.36	-	.197	1.51	1.21
2	1.0	0.50	.77	3.24	0.018	.197	1.40	0.021	.72	3.77	0.04	.197	1.80	0.027
3	1.5	0.333	.746	2.45	0.464	.209	1.95	0.011	.696	2.57	0.04	.197	1.84	0.010
4	2.0	0.250	.73	1.08	1.190	.075	0.70	0.003	.681	1.65	1.20	.075	1.0	0.005
5	2.5	0.20	.713	2.70	0.34	.206	1.83	0.010	.671	2.91	0.26	.198	1.66	0.009
6	3.0	0.166	.695	1.13	0.55	.214	1.12	0.006	.654	1.46	0.60	.213	0.96	0.005
7	3.5	0.142	.683	1.88	0.51	.213	1.42	0.007	.646	1.36	0.63	.210	1.08	0.005
8	4.0	0.125	.6711	1.14	0.932	.150	0.74	0.003	.638	1.13	1.08	.11	0.48	0.002
9	4.5	0.111	.663	1.40	1.20	.075	0.37	0.001	.631	0.89	1.05	.125	0.82	0.004
10	5.0	1.0	.654	0.95	0.14	.197	9.64	1.036	.6266	1.07	0.075	.197	9.64	9.64
11	10.0	2.0	.594	0.48	0.25	.198	24.23	1.20	.5667	0.32	0.074	.197	26.40	26.40

TABLE 4.2

Consolidation tests in the Hydraulic Oedometer with Rigid loading cap

			VOLUME CHANGE						AXIAL DEFORMATION					
Stage No.	Po' psi	$\frac{\Delta P}{Po'}$	e	m_v sq. cm/gms x 10^{-4}	$C_\infty/\Delta R_{TI}$	T_M	c_{vs} sq. cm/sec x 10^{-4}	c_{vs}/c_{vp}	e	m_v sq. cm/gm x 10^{-4}	$C_\infty/\Delta R_{TI}$	T_M	c_{vs} sq. cm/sec x 10^{-4}	c_{vs}/c_{vp}
1	-	-	0.98	26.76	0.25	.198	5.73	1.58	0.98	21.14	0.01	.197	4.51	1.25
2	1.0	0.50	0.64	6.88	0.39	.208	2.53	0.014	0.70	2.70	0.30	.202	2.23	0.012
3	1.5	0.333	0.60	5.02	0.57	.214	3.38	0.014	0.68	2.20	0.16	.197	1.25	0.005
4	2.0	0.250	0.57	3.69	0.52	.213	1.81	0.0056	0.67	1.36	0.56	.214	1.03	0.003
5	2.5	0.20	0.55	3.66	0.44	.219	1.30	0.0031	0.66	1.74	0.42	.209	1.00	0.002
6	3.0	0.166	0.52	2.90	0.79	.181	0.97	0.0017	0.65	1.16	0.79	.180	0.80	0.0014
7	3.5	0.142	0.51	2.70	0.66	.205	0.91	0.0016	0.64	1.02	0.51	.214	0.81	0.0014
8	4.0	0.125	0.50	2.45	1.33	.05	0.45	0.0008	0.638	0.94	1.30	.055	0.41	0.0007
9	4.5	0.111	0.48	3.25	0.86	.15	0.50	0.0008	0.633	0.94	0.74	.190	0.63	0.001
10	5.0	1.0	0.47	3.60	0.26	.198	10.77	0.912	0.628	0.74	0.03	.197	14.29	1.21

TABLE 4.3

Consolidation tests in the Hydraulic Oedometer with Flexible loading cap

Stage No.	Po' p.s.i.	$\frac{\Delta P}{Po'}$	e	C_c sq. cm/gms x 10^{-4}	$C_\alpha/\Delta R_{TI}$	T_M	c_{vs} sq. cm/gm x 10^{-4}	c_{vs}/c_{vp}
1	-	-	.960	11.70	0.27	0.21	1.69	1.25
2	1.0	0.50	.804	4.00	0.51	0.213	5.38	0.60
3	1.5	0.333	.776	2.69	1.33	0.05	1.72	0.017
4	2.0	0.250	.753	0.96	1.62	0.033	0.87	0.007
5	2.5	0.20	.746	2.03	1.80	0.03	0.85	0.008
6	3.0	0.166	.731	1.16	1.20	0.076	0.60	0.004
7	3.5	0.142	.724	1.50	0.41	0.21	2.01	0.01
8	4.0	0.125	.715	1.11	1.53	0.038	0.30	0.001
9	4.5	0.111	.708	0.39	1.35	0.05	0.57	0.002
10	5.0	1.0	.700	0.72	0.14	0.197	10.26	1.01
11	10.0	2.0	.654	0.26	0.13	0.197	17.82	0.89
12	30.0	0.0166	.592	0.04	1.76	0.025	0.80	0.002
13	30.5	0.0163	.5918	0.16	2.53	0.015	2.34	0.006
14	31.0	0.0161	.5908	0.15	1.81	0.030	0.74	0.007
15	31.5	0.0158	.5897	0.15	2.11	0.019	0.40	0.0008

TABLE 4.4

Triaxial Consolidation Test

Plate 4.1 Individual parts of the Hydraulic Oedometer

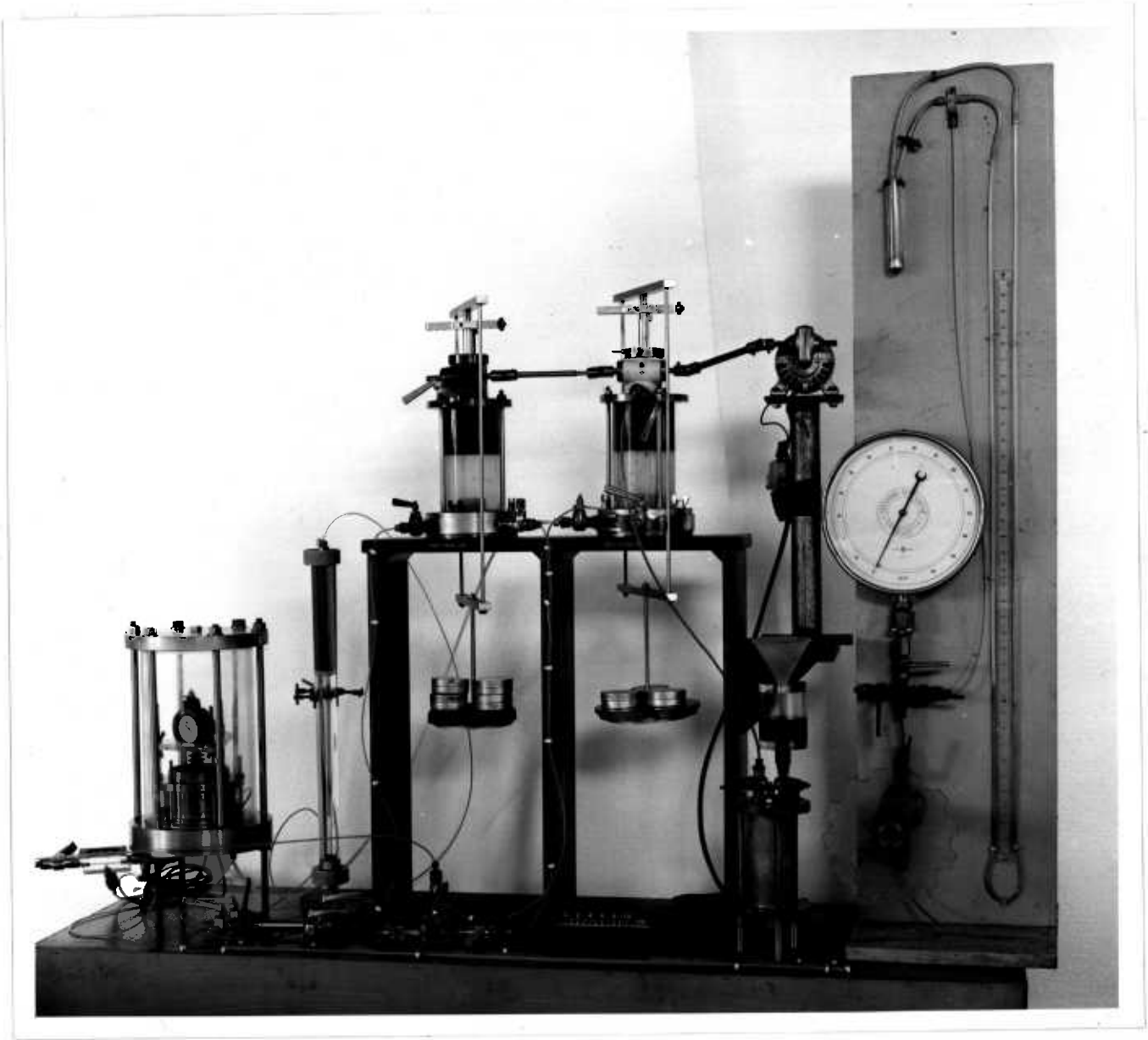

Plate 4.2 Dead weight pressure system connected to the Hydraulic Oedometer.

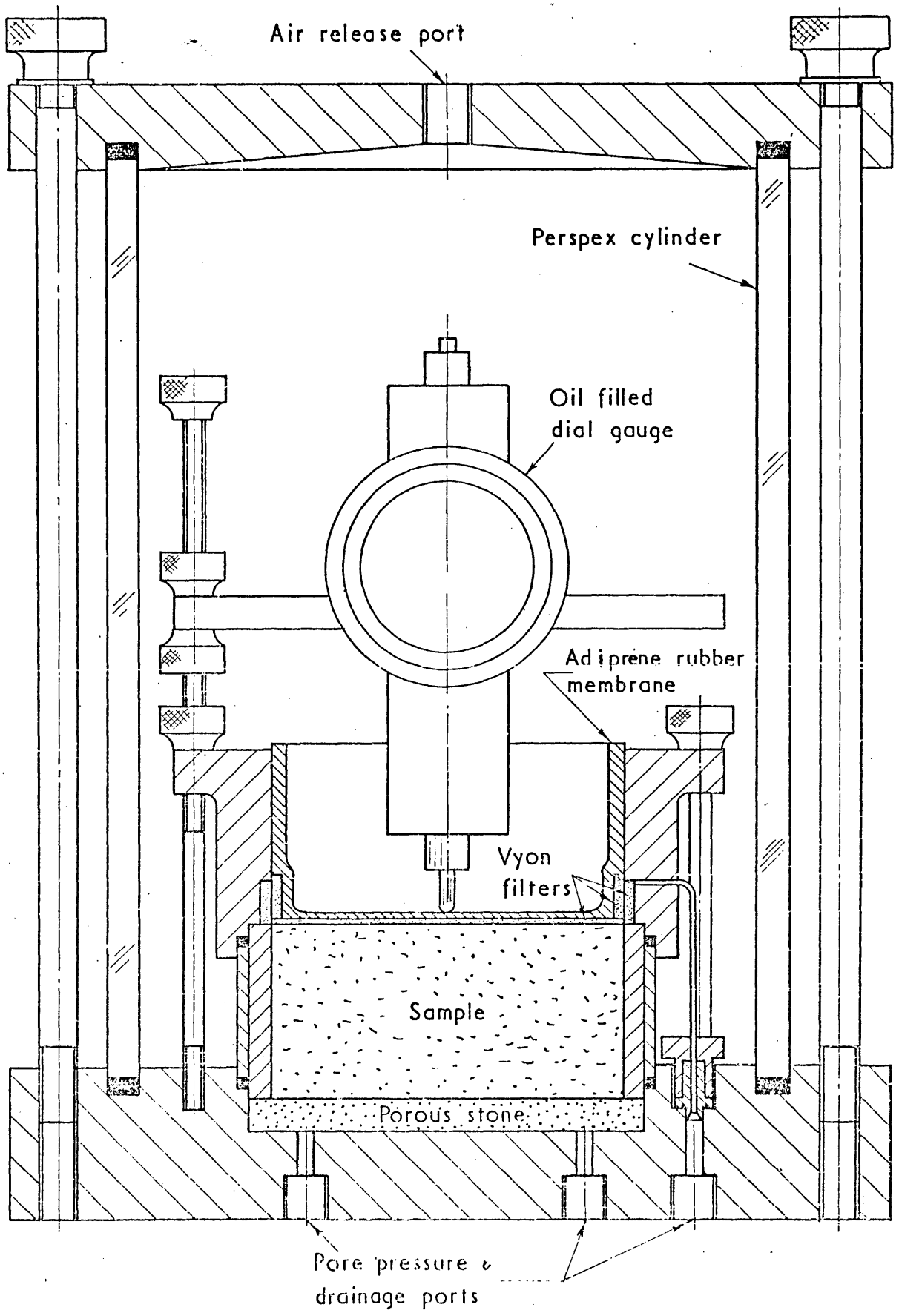

Fig 4·1 HYDRAULIC OEDOMETER

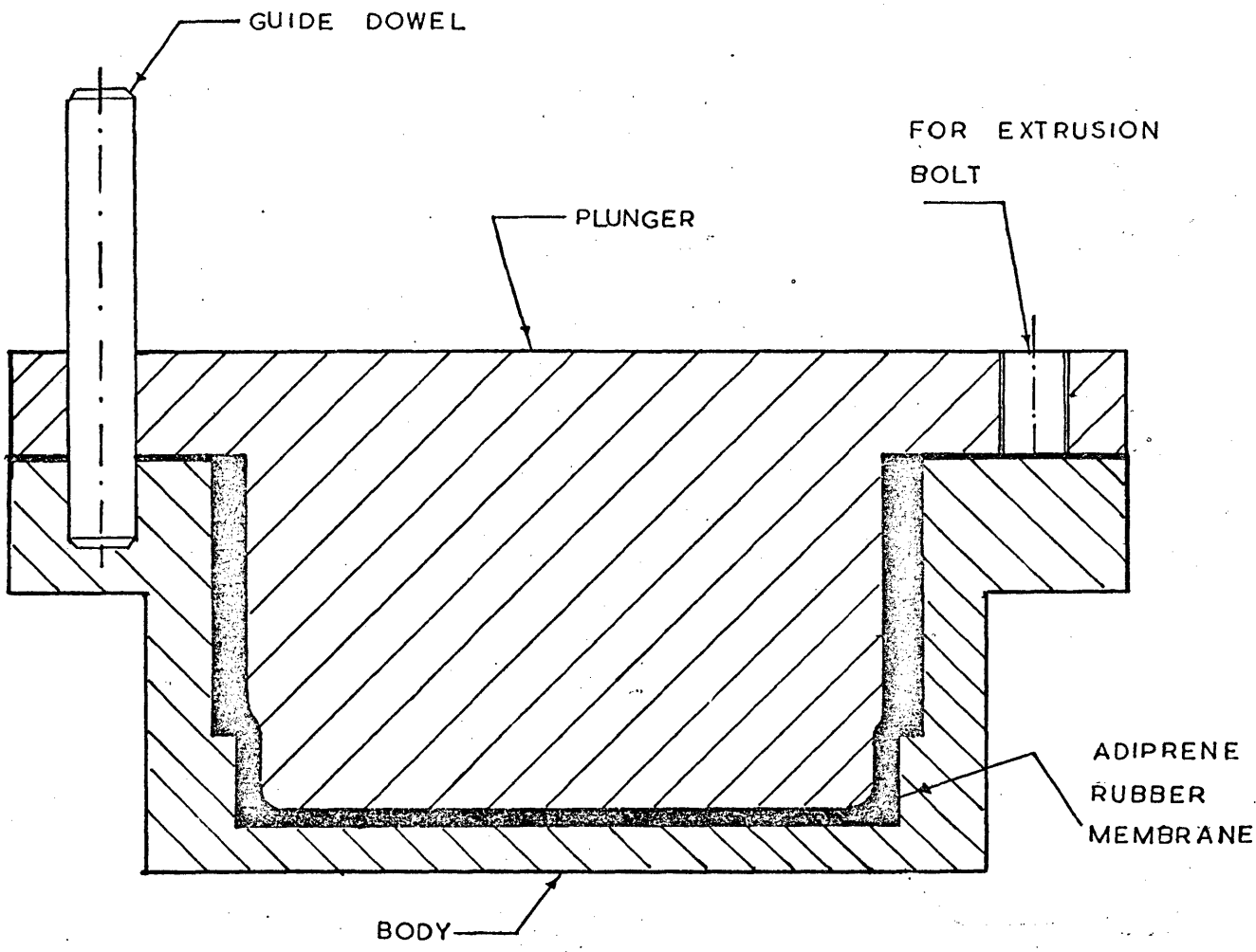

FIGURE NO. 4.2. Stainless steel mould for casting an Adiprene rubber membrane

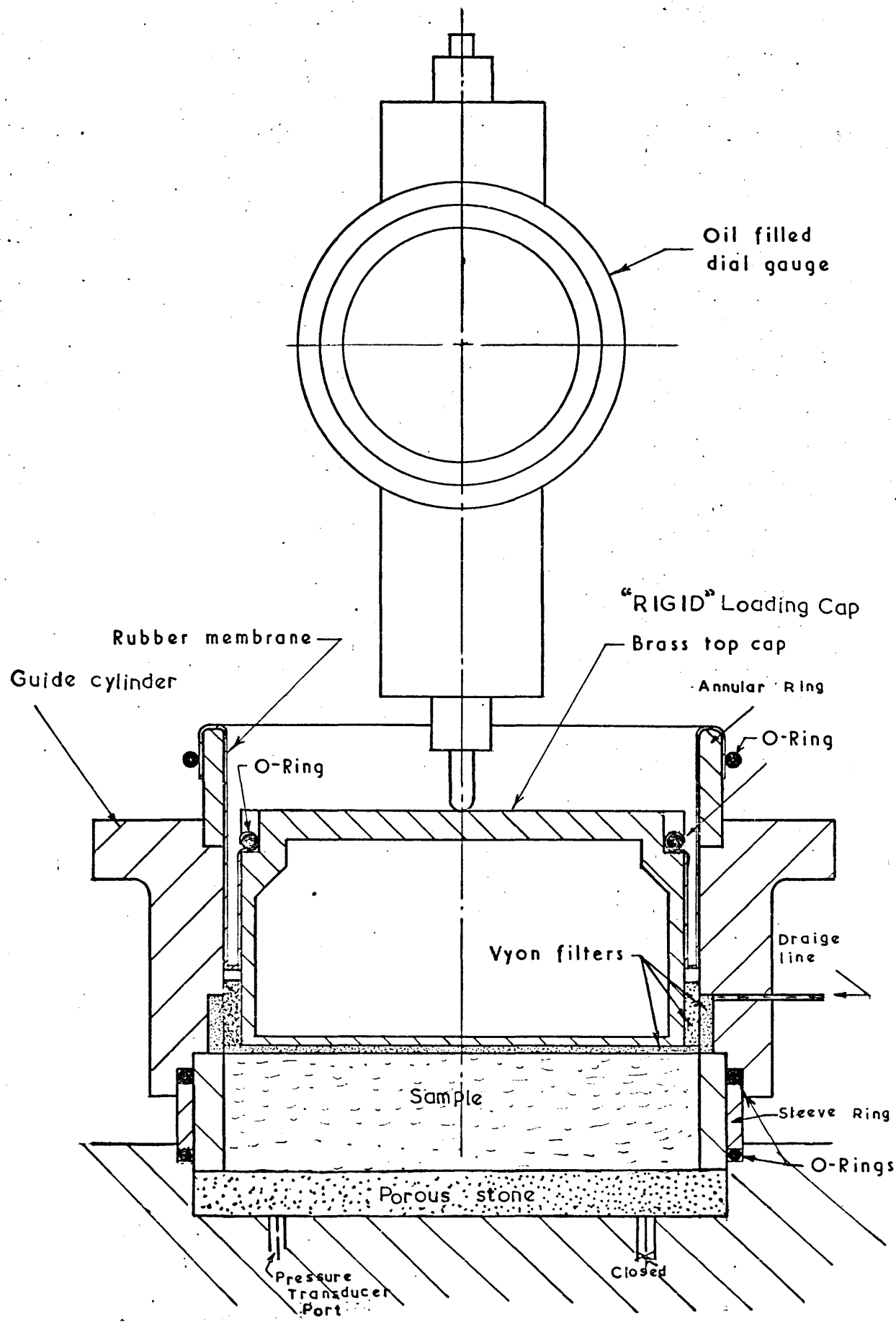

FIGURE NO. 4.3. " RIGID " LOADING CAP SITTING ON 1.0 INCH THICK SAMPLE IN THE HYDRAULIC OEDOMETER.

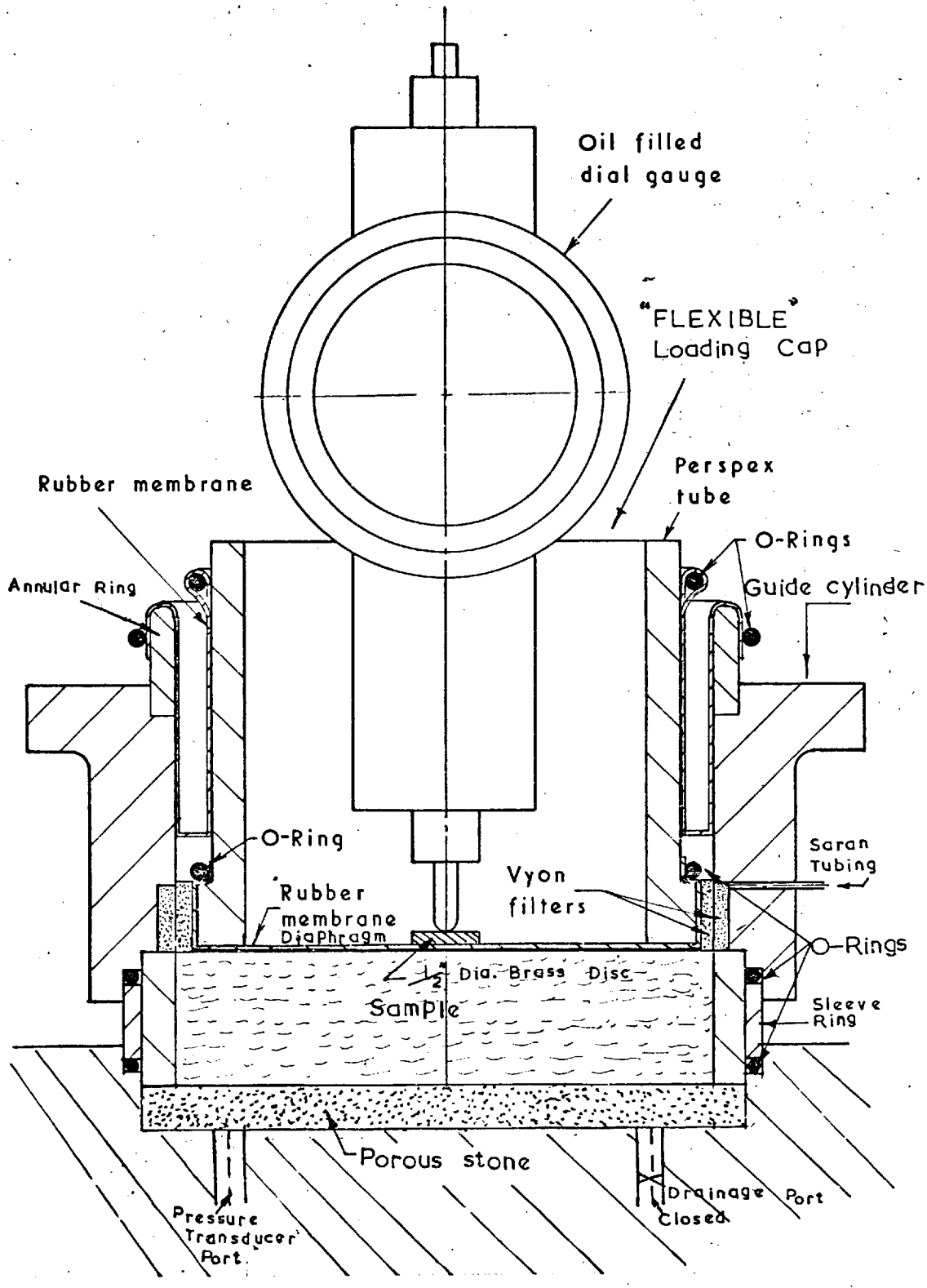

FIGURE NO. 4.4. " FLEXIBLE " LOADING CAP SITTING ON 1.0 INCH THICK SAMPLE IN THE HYDRAULIC OEDOMETER.

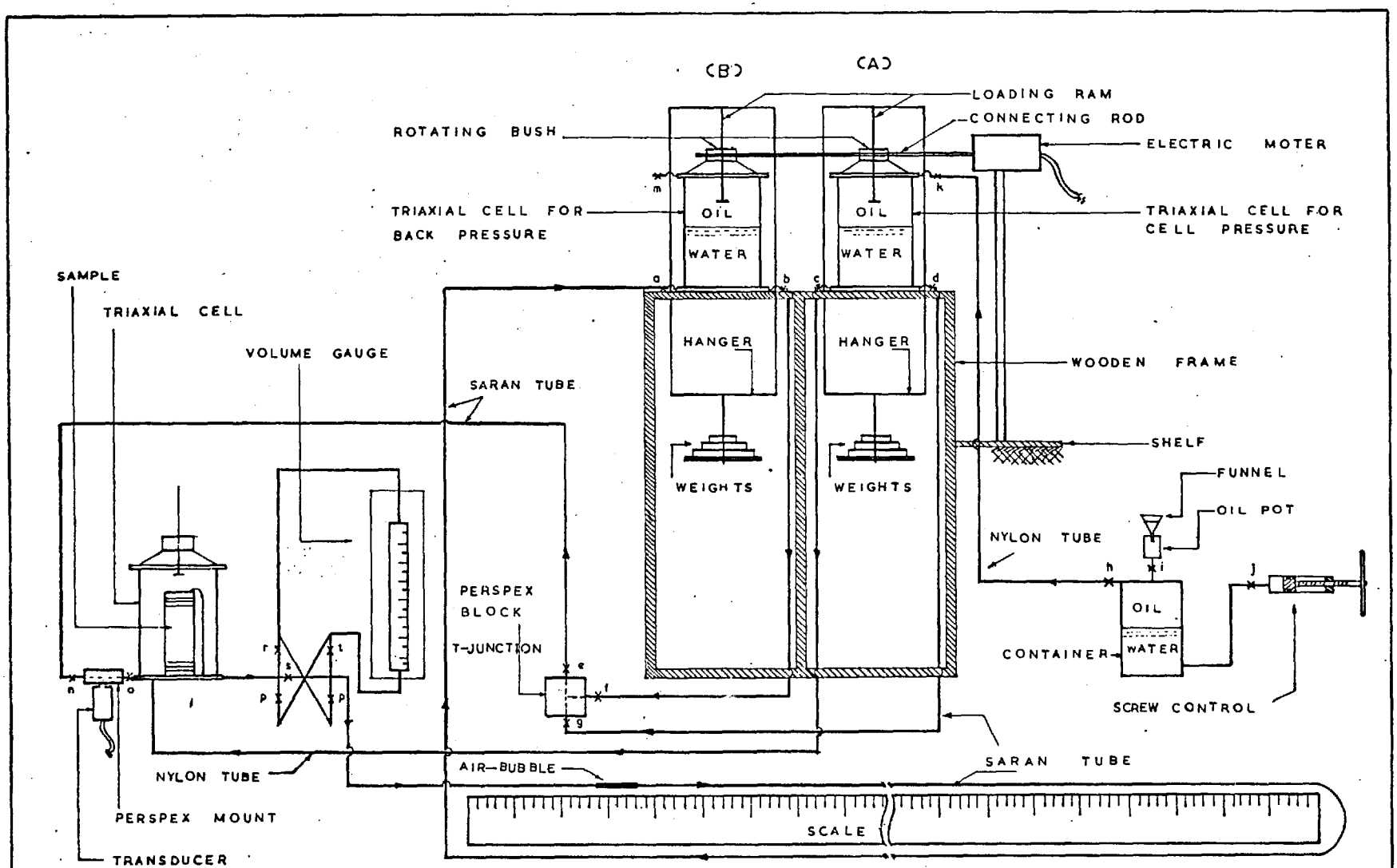

FIG. NO. 4.5 THE LAYOUT OF THE PRESSURE SYSTEM FOR THE APPLICATION OF SMALL STRESS INCREMENTS

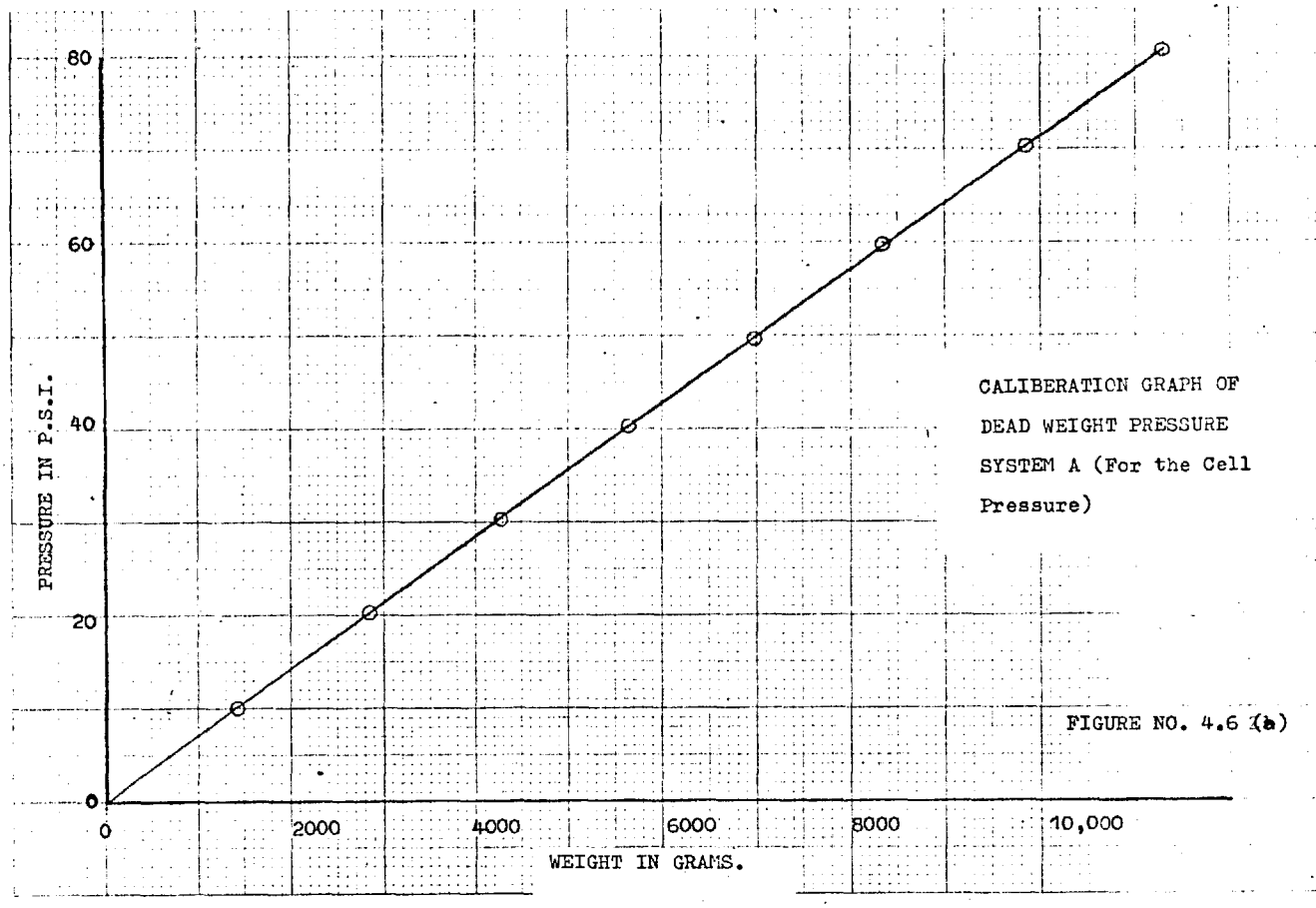

CALIBERATION GRAPH OF DEAD WEIGHT PRESSURE SYSTEM A (For the Cell Pressure)

FIGURE NO. 4.6 (a)

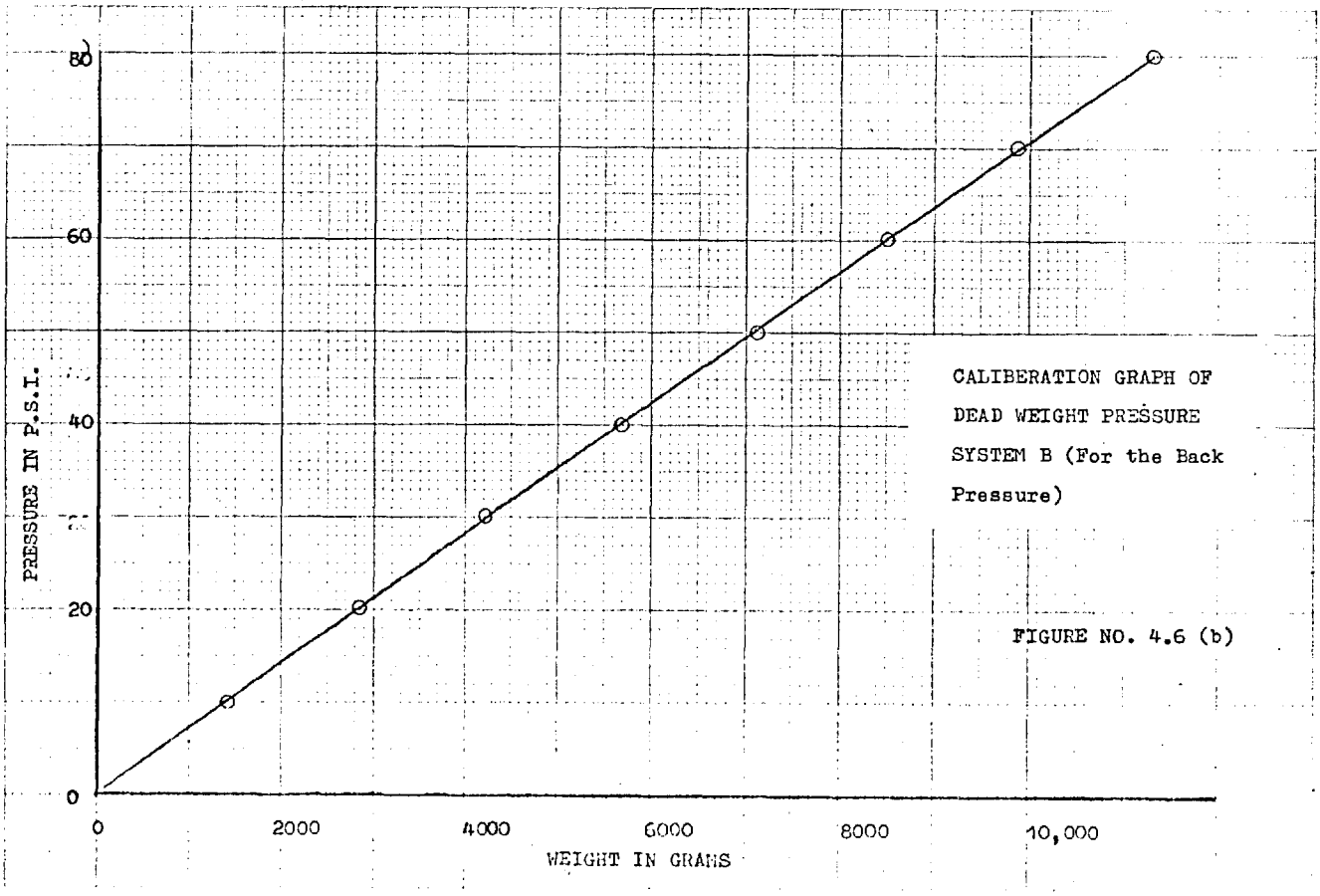

CALIBERATION GRAPH OF DEAD WEIGHT PRESSURE SYSTEM B (For the Back Pressure)

FIGURE NO. 4.6 (b)

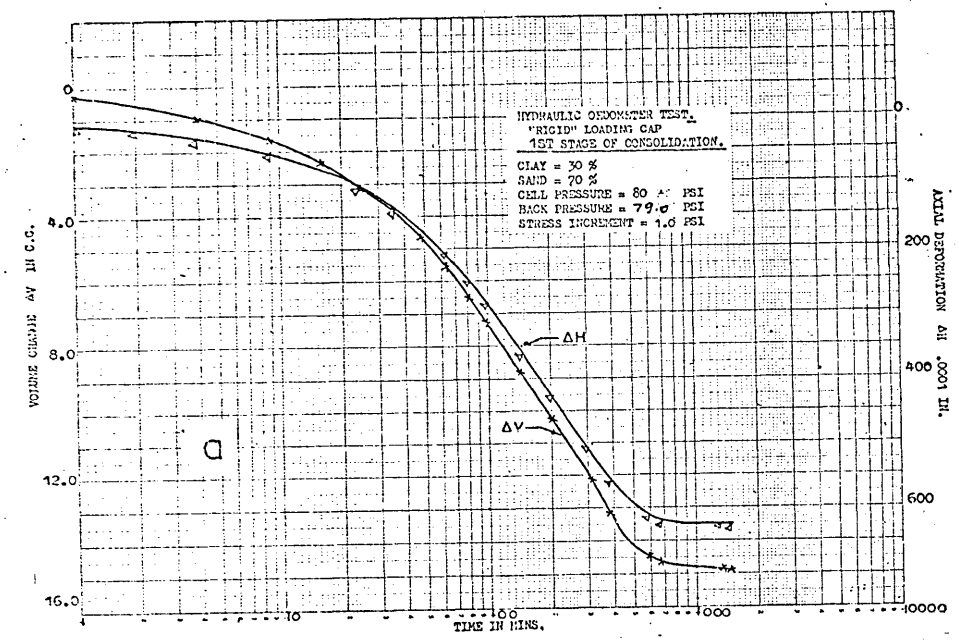

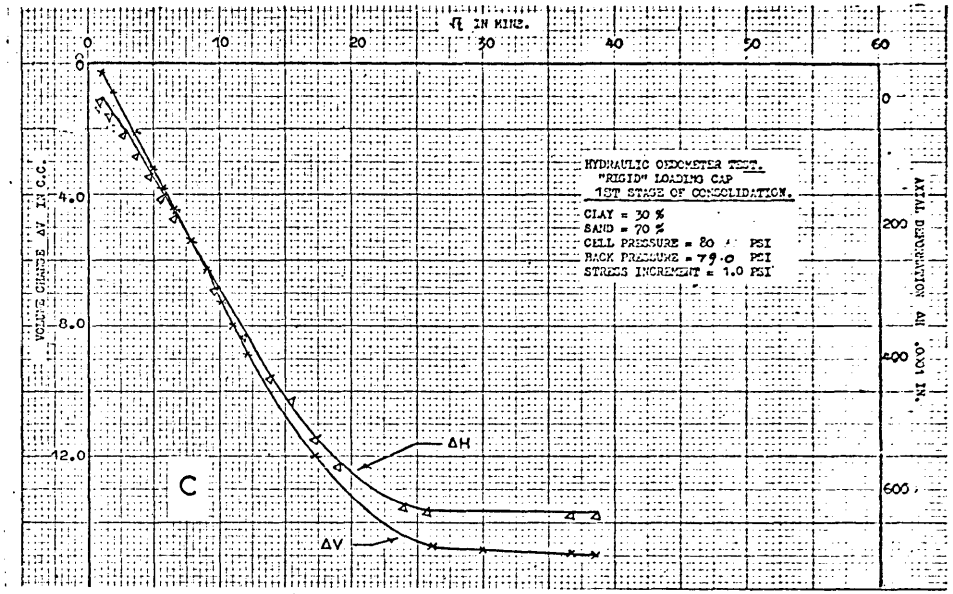

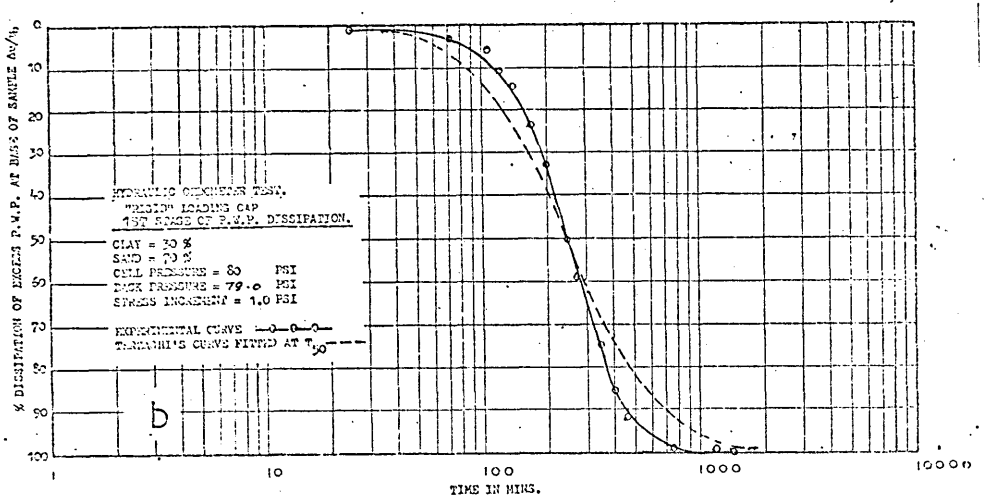

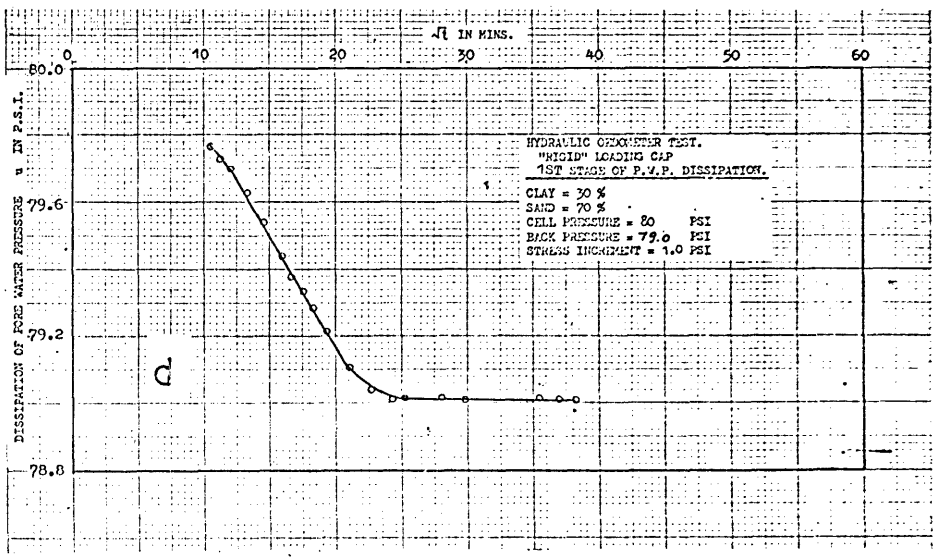

FIG. NO. 4.7 (1st. Stage)

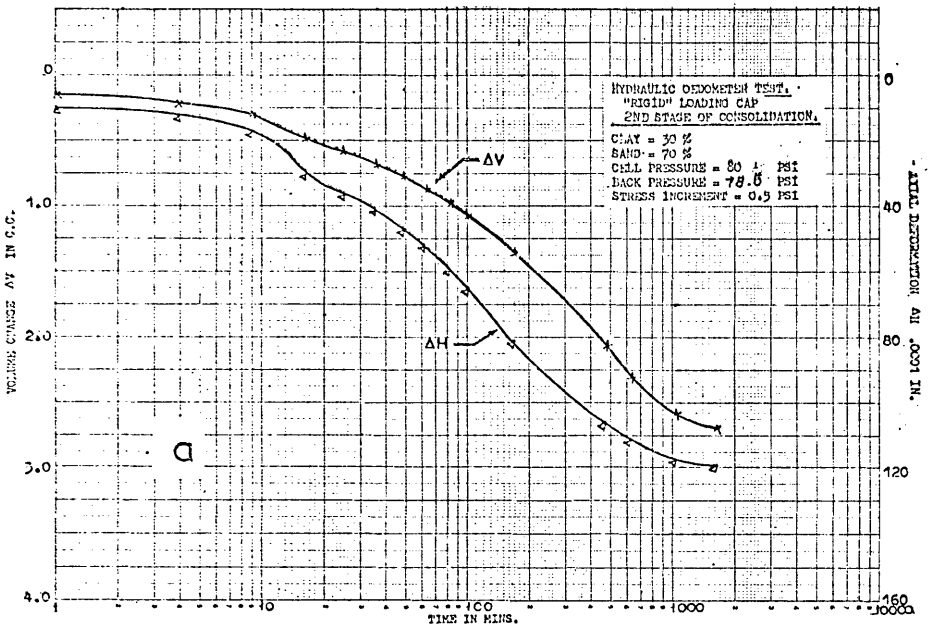

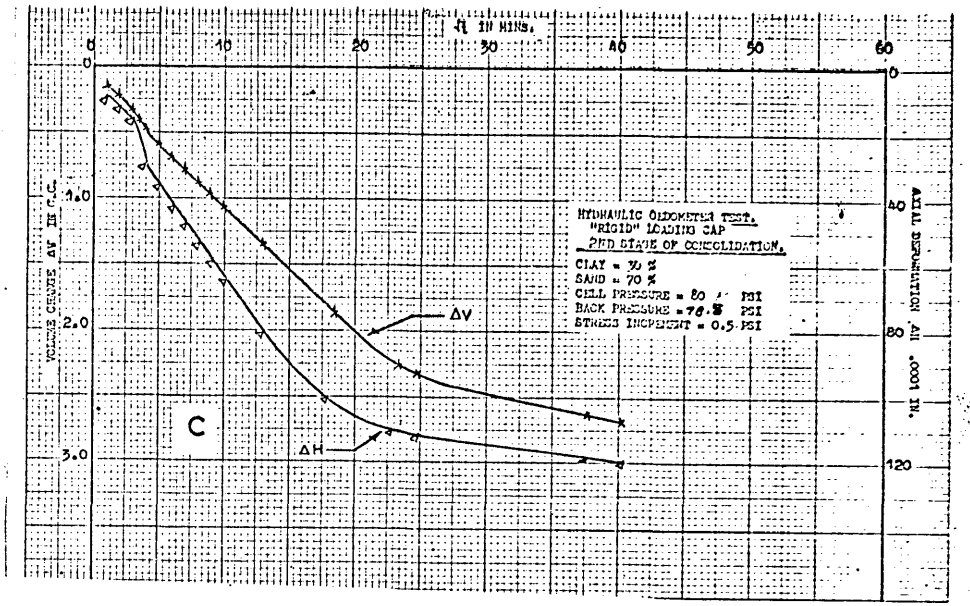

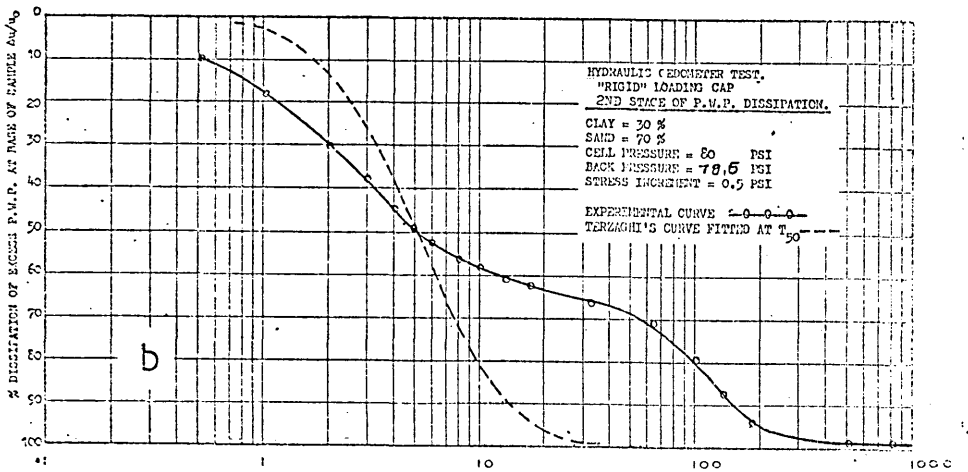

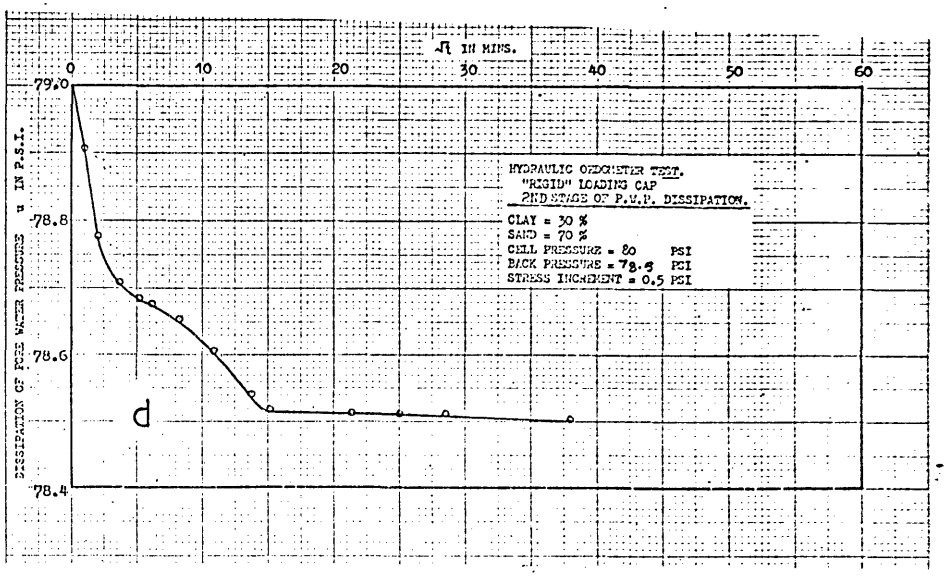

FIG. NO. 4.8 (2nd. Stage)

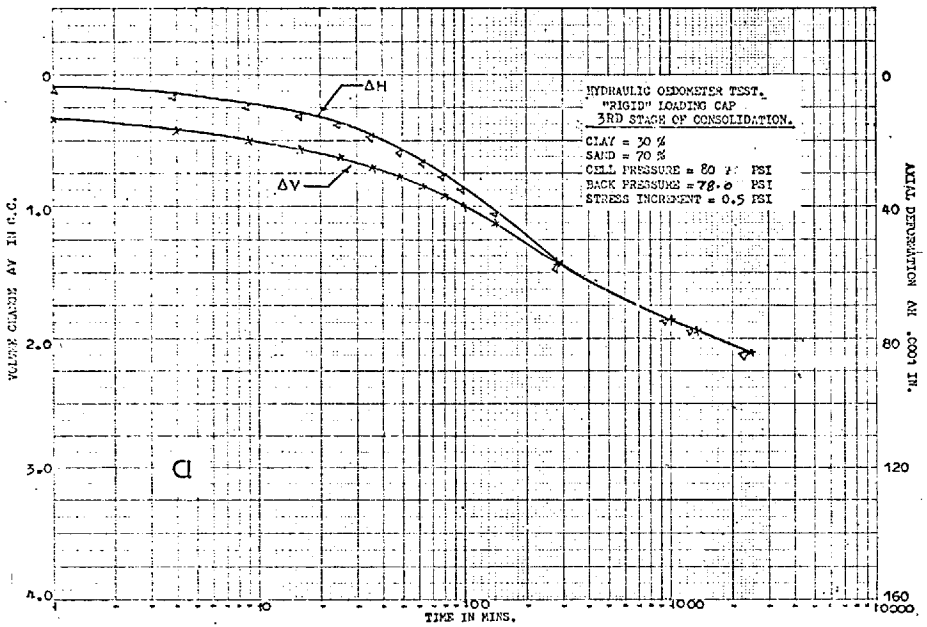

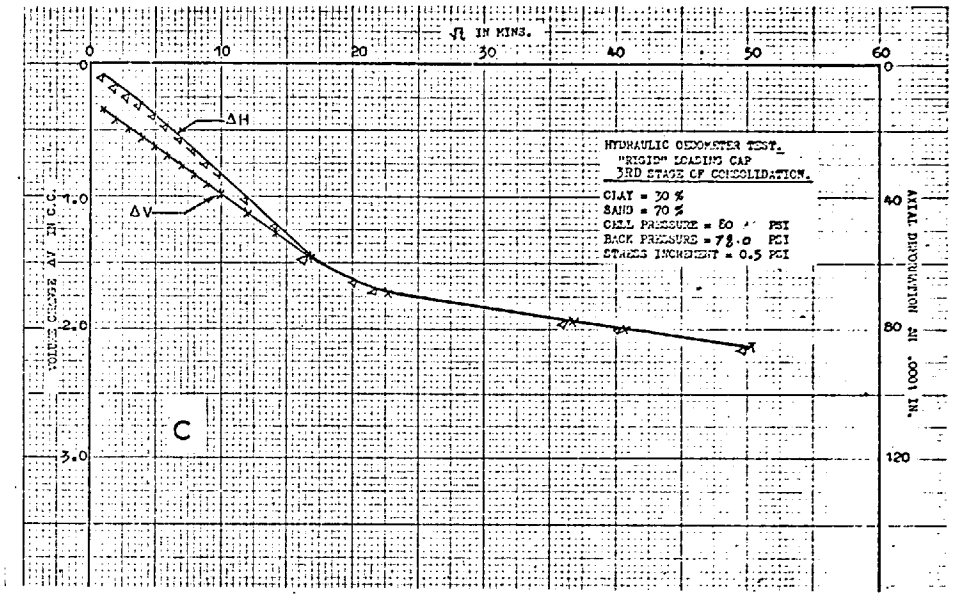

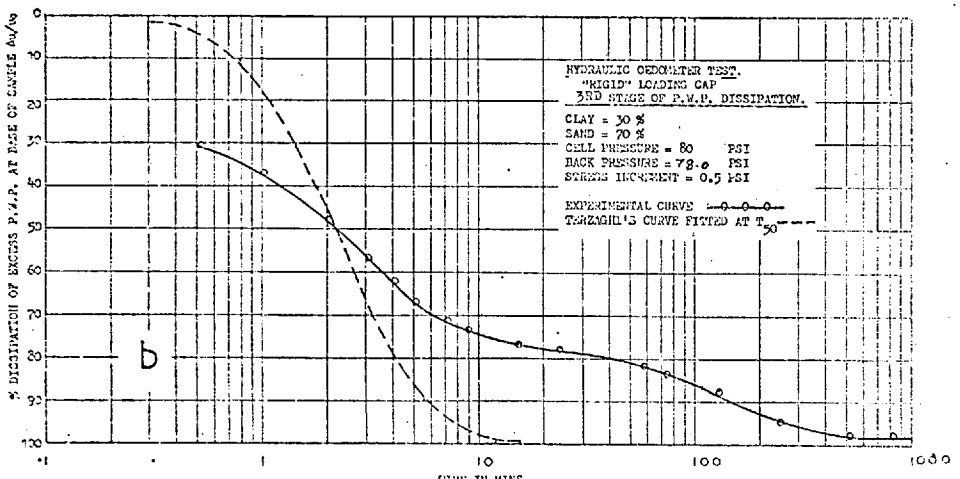

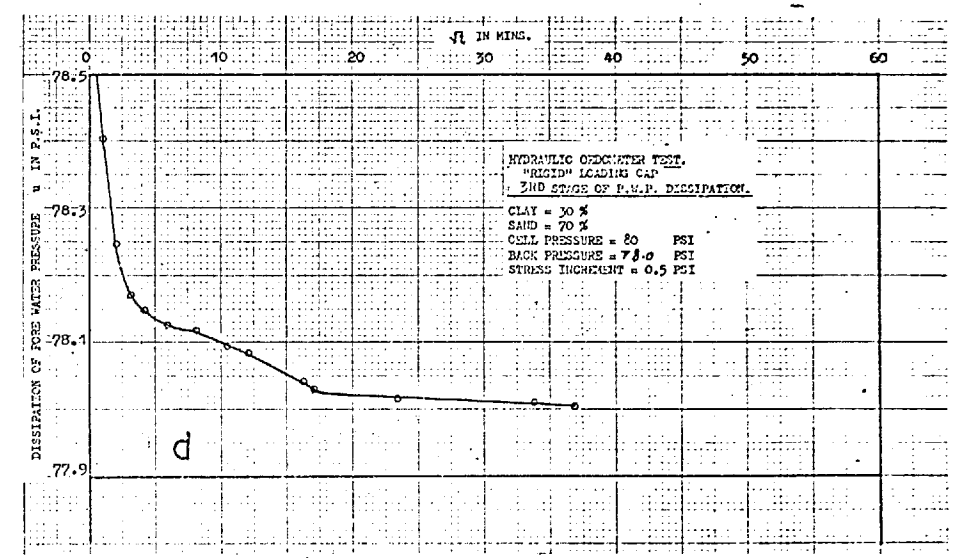

FIG. NO. 4.9 (3rd. Stage)

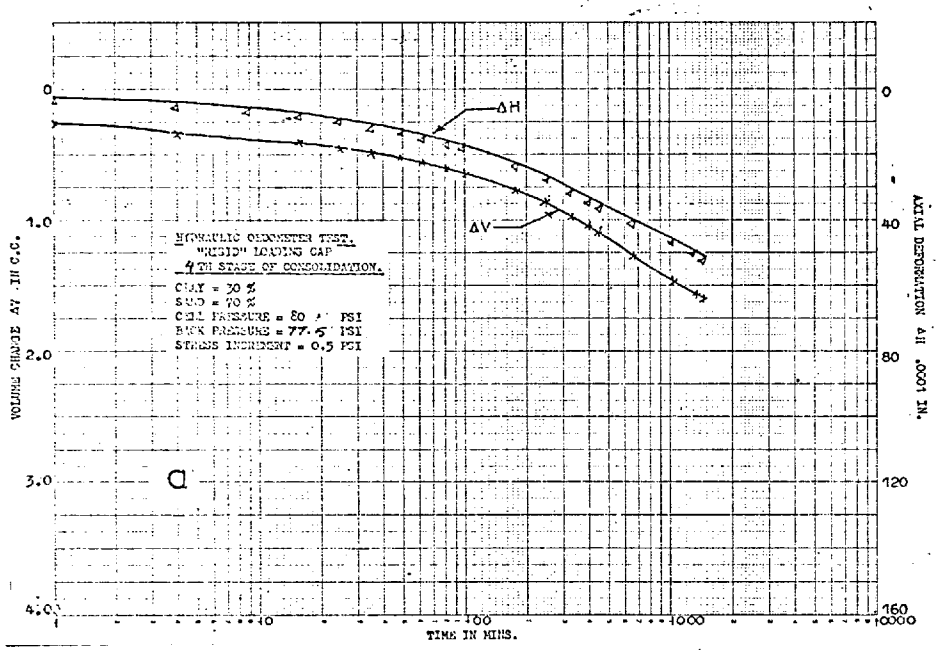

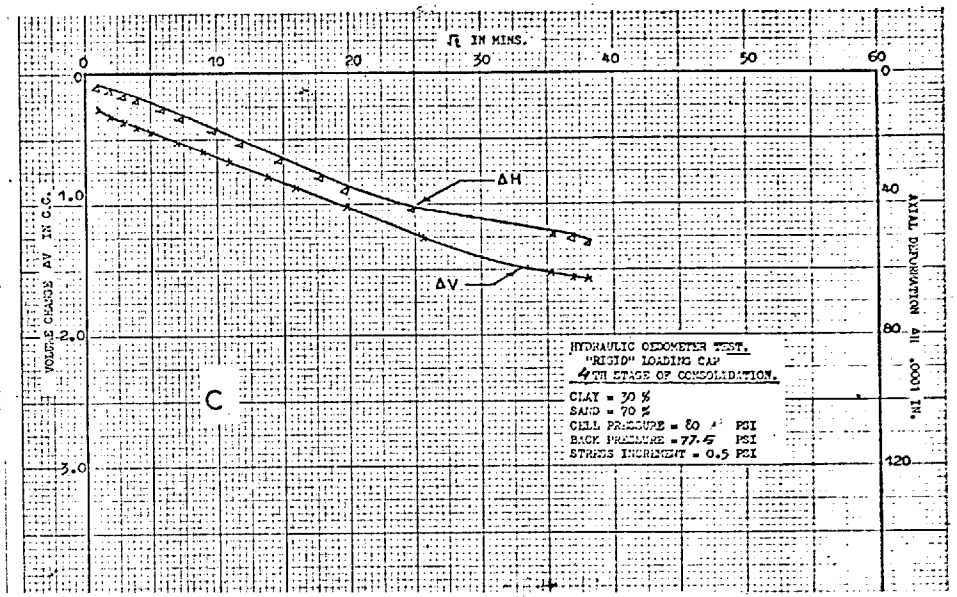

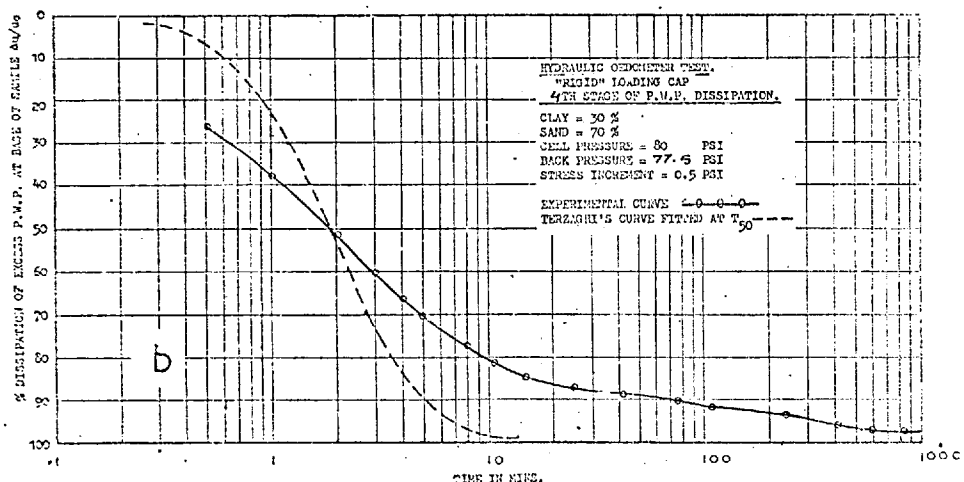

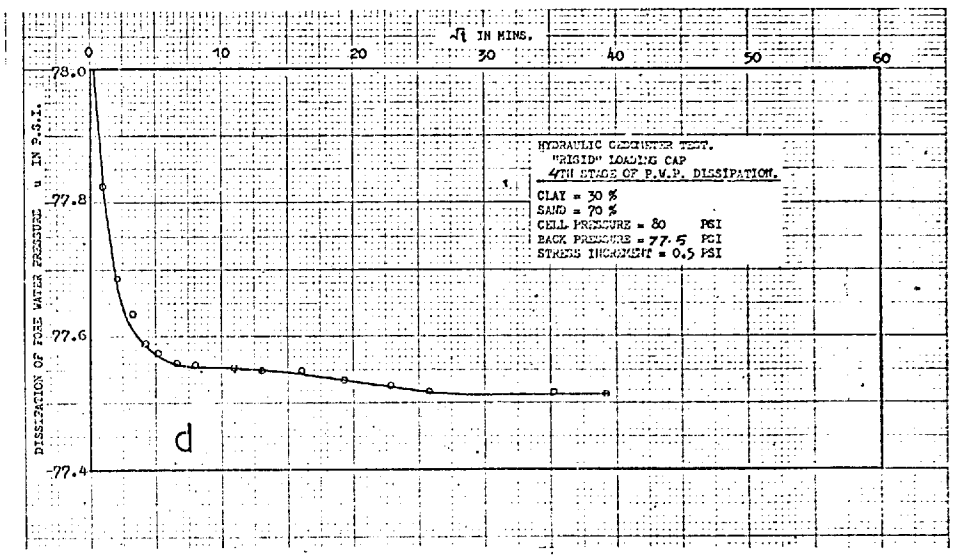

FIG. NO. 4. 10 (4th Stage)

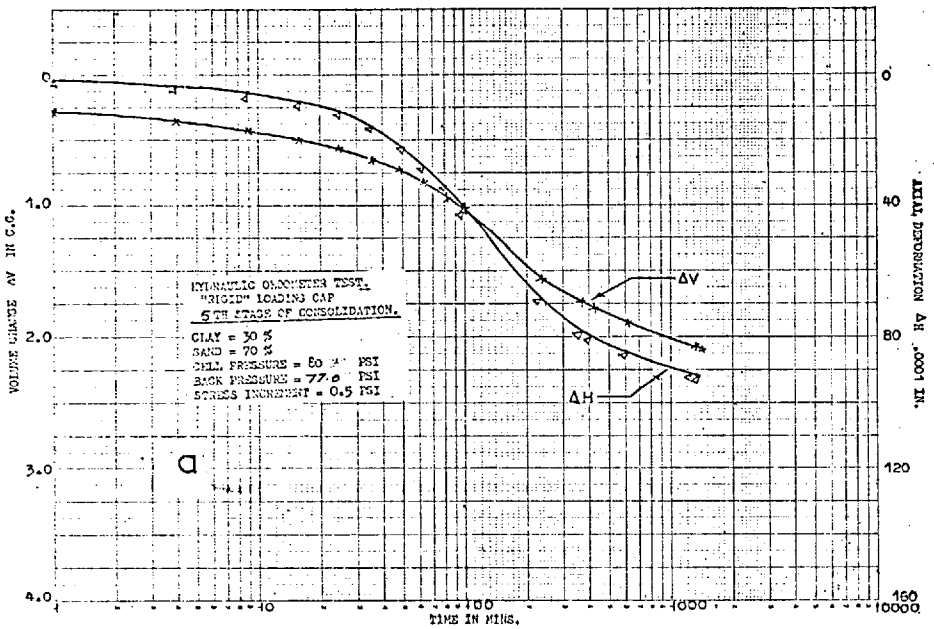

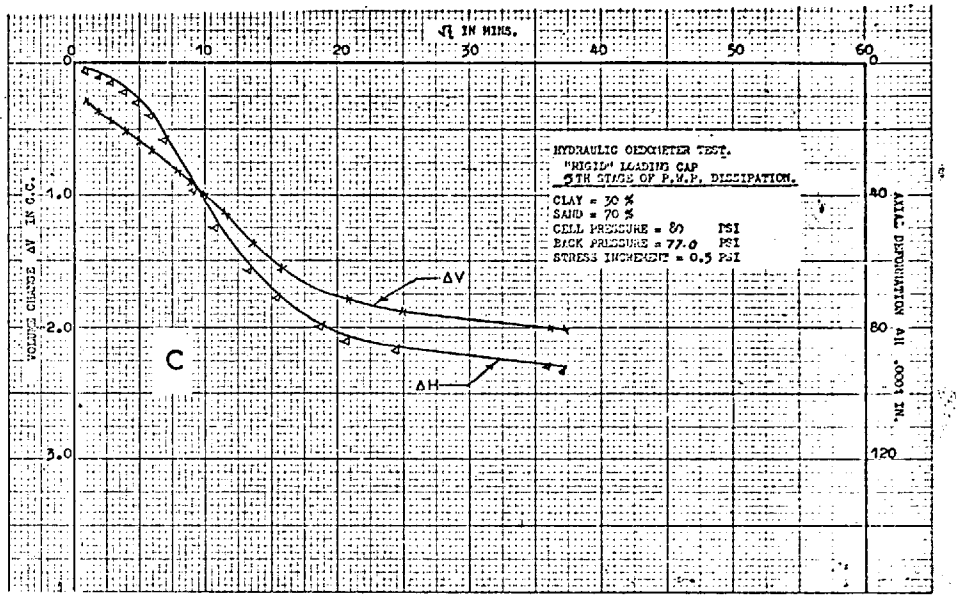

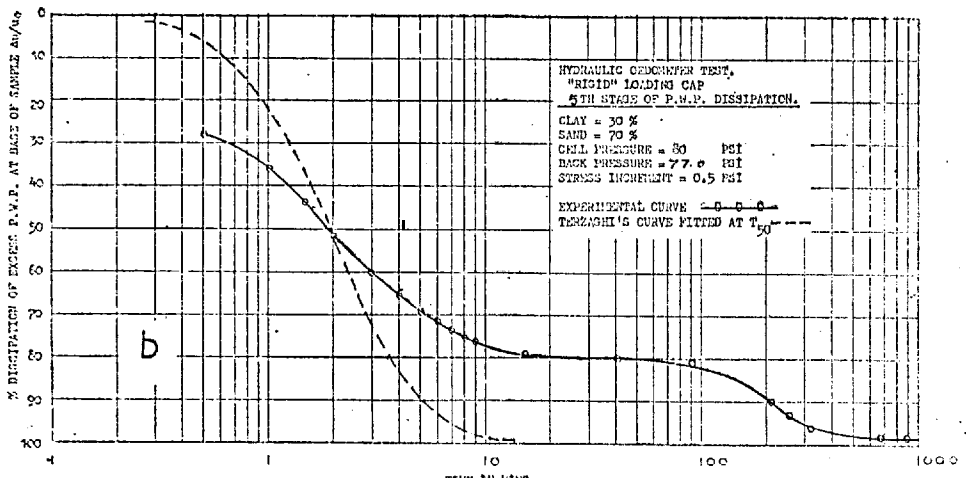

FIG. NO. 4. 11 (5th. Stage)

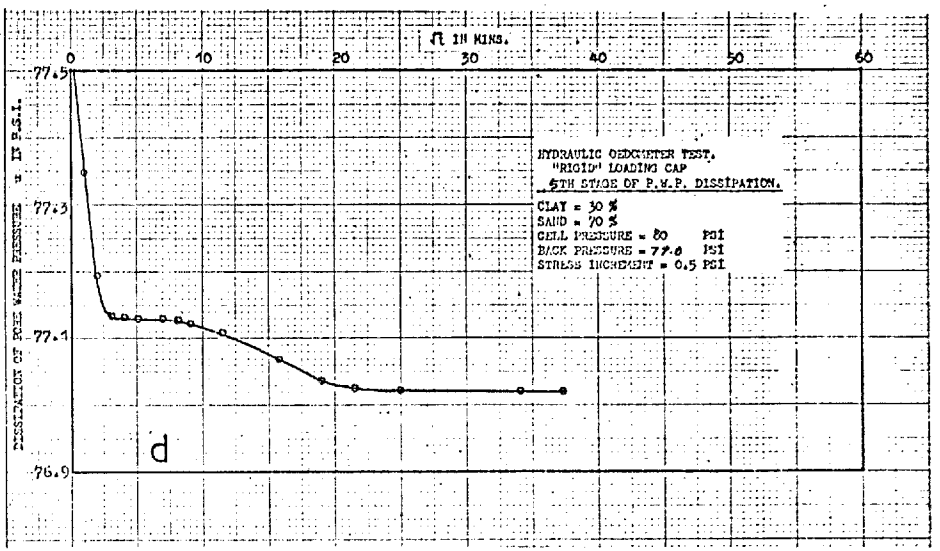

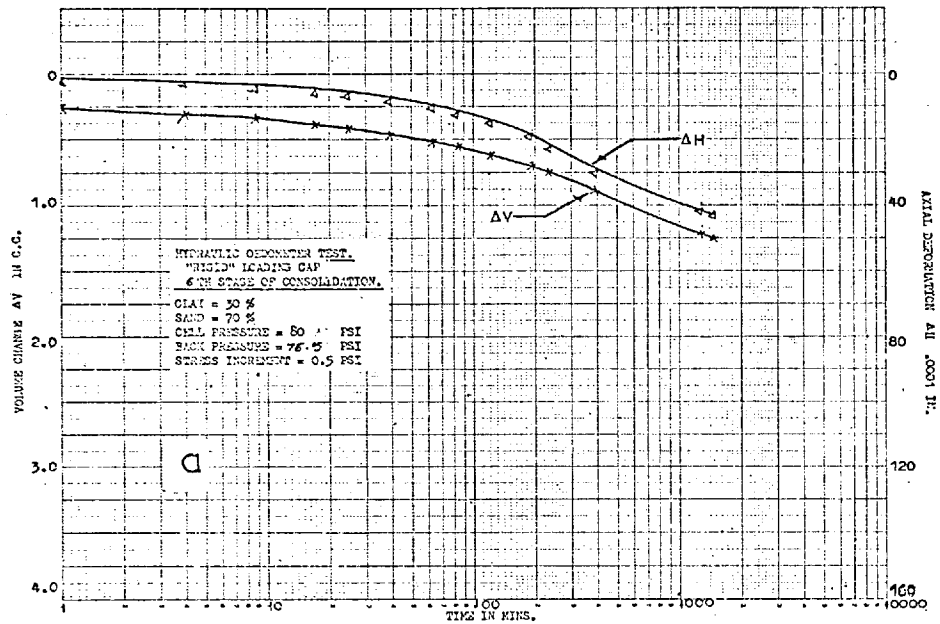

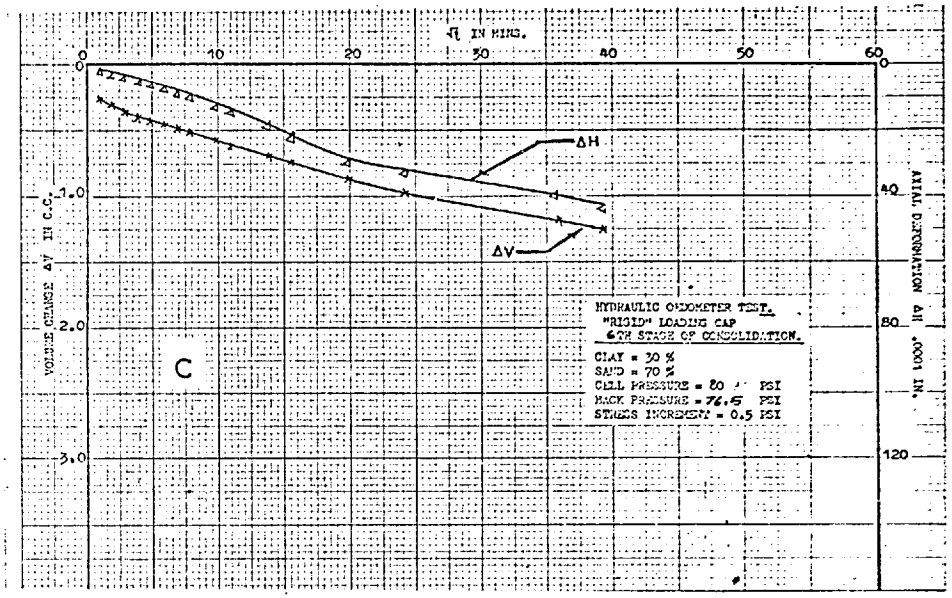

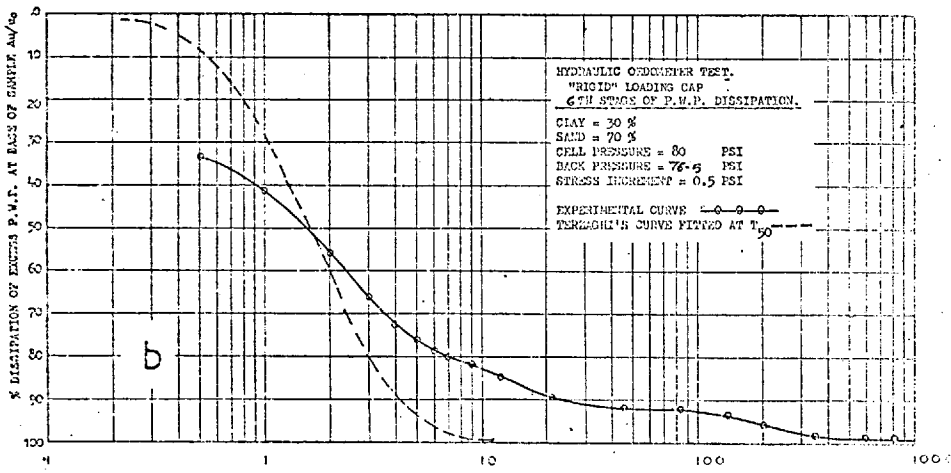

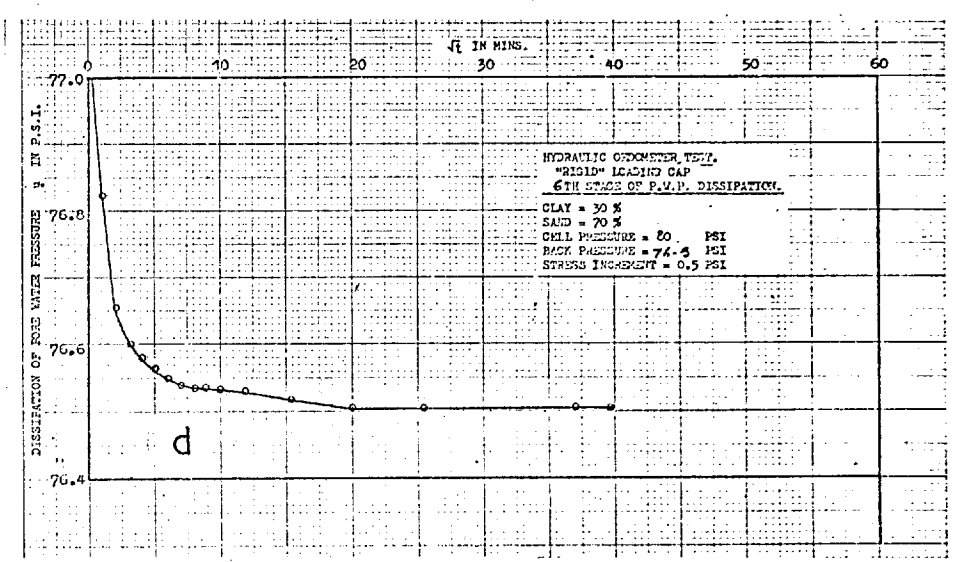

FIG. NO. 4.12 (6th. Stage)

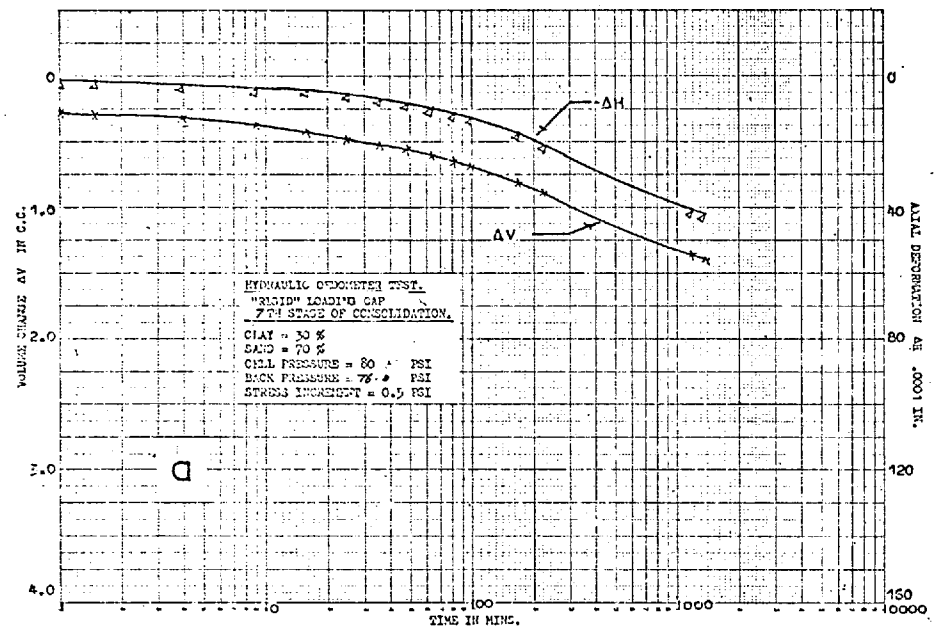

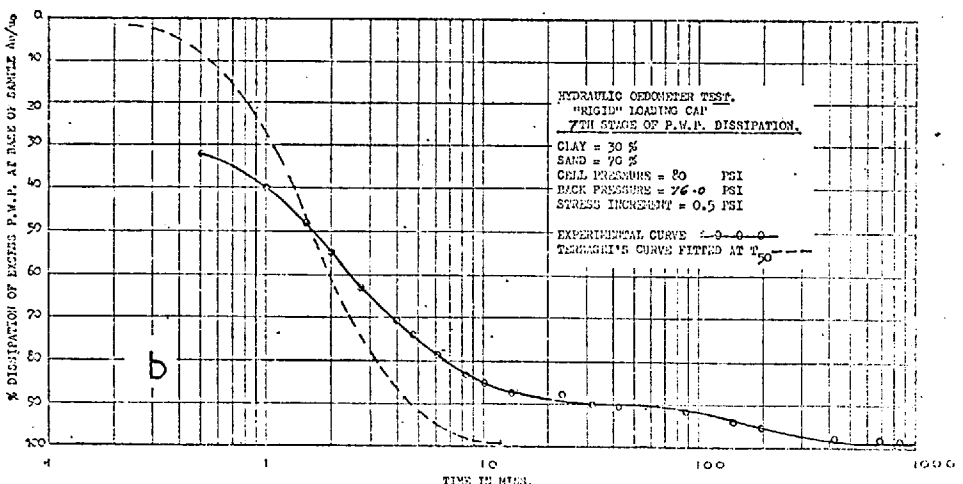

FIG. NO. 4. 13 (7th. Stage)

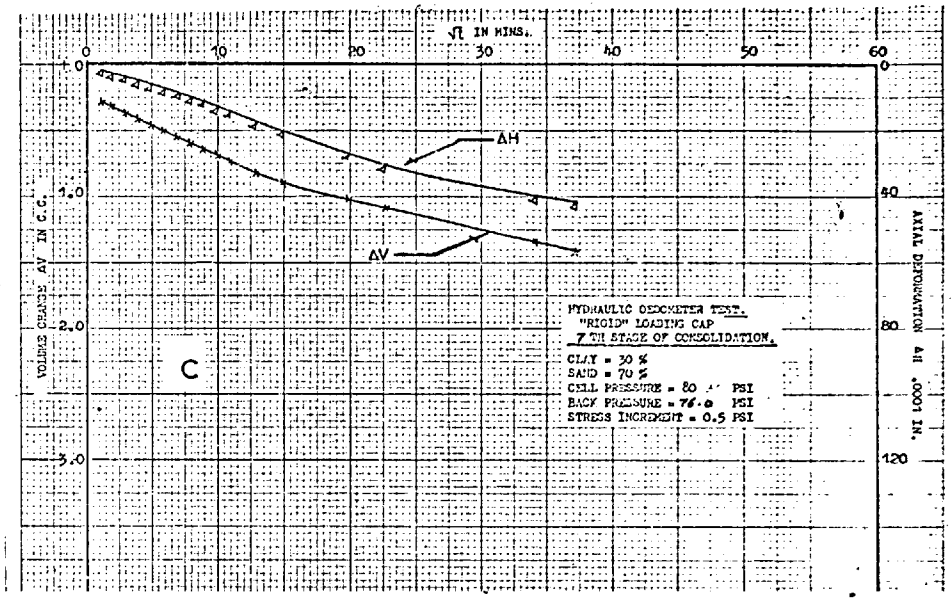

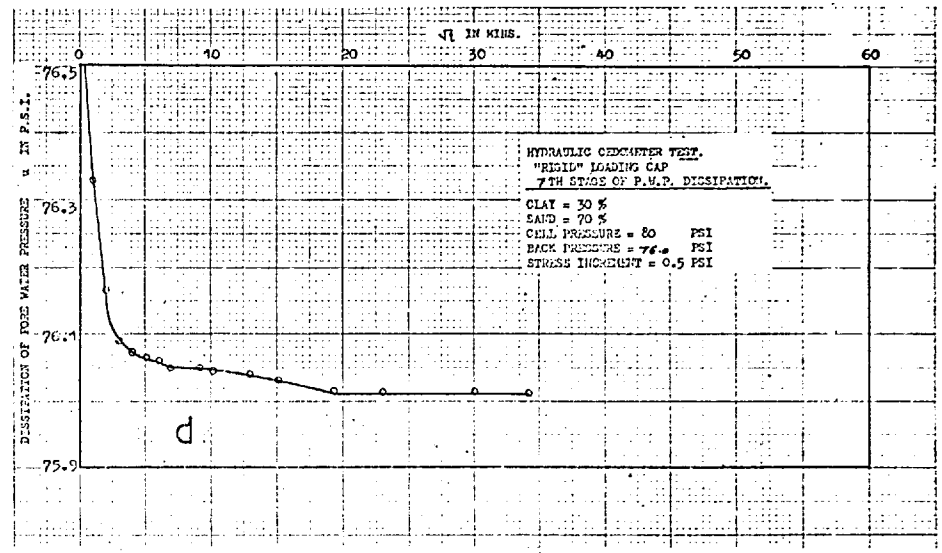

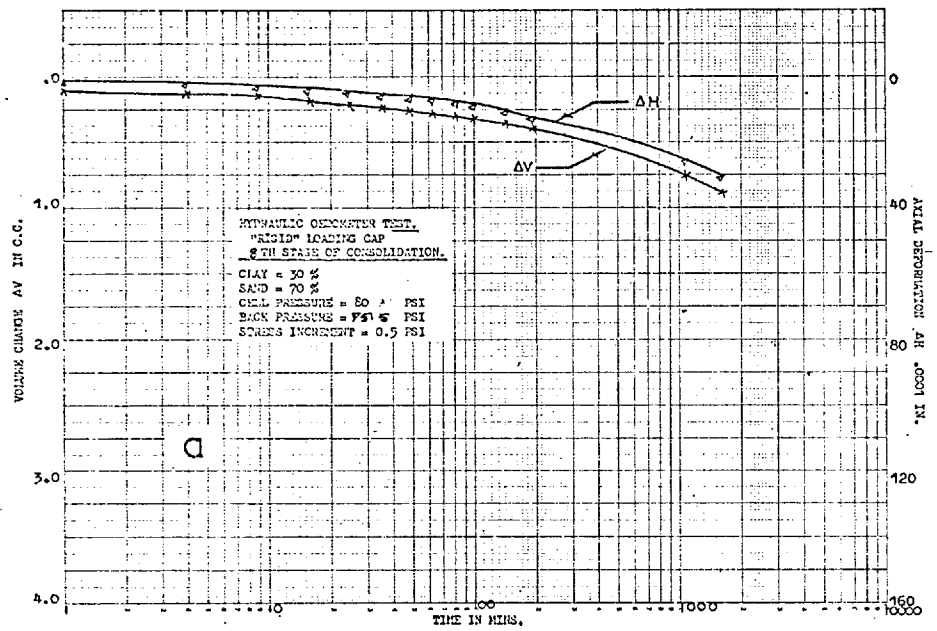

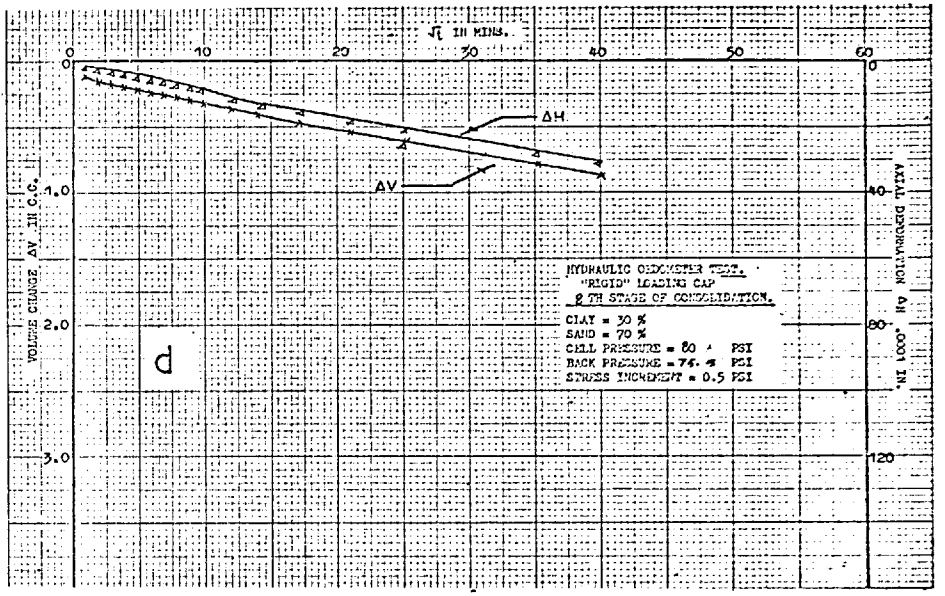

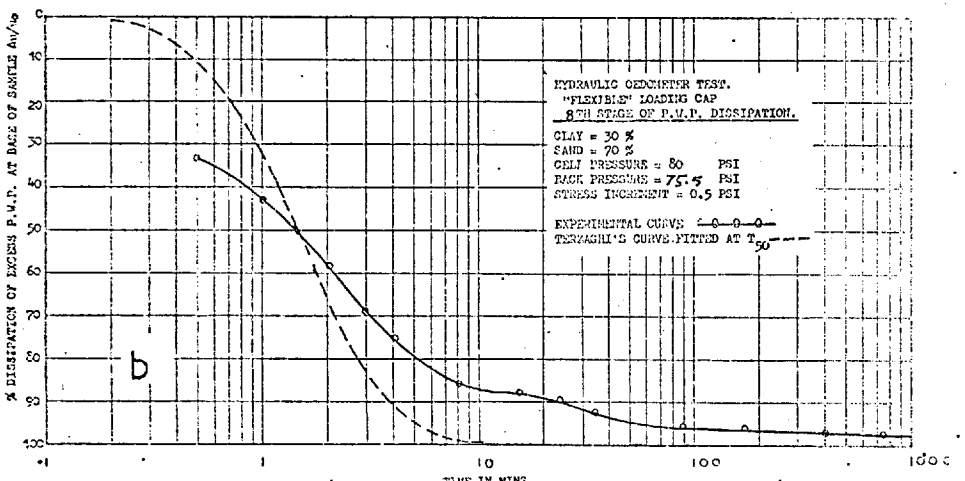

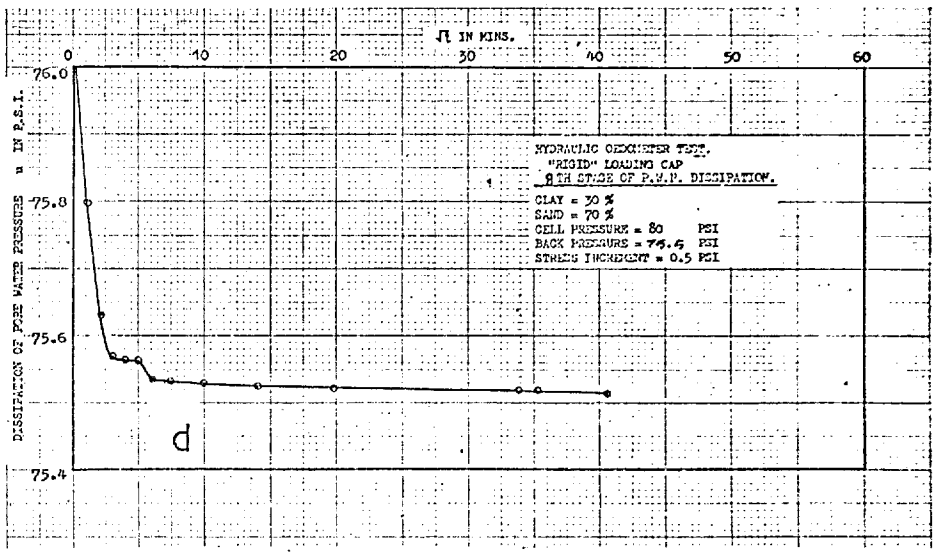

FIG. NO. 4. 14 (8th. Stage)

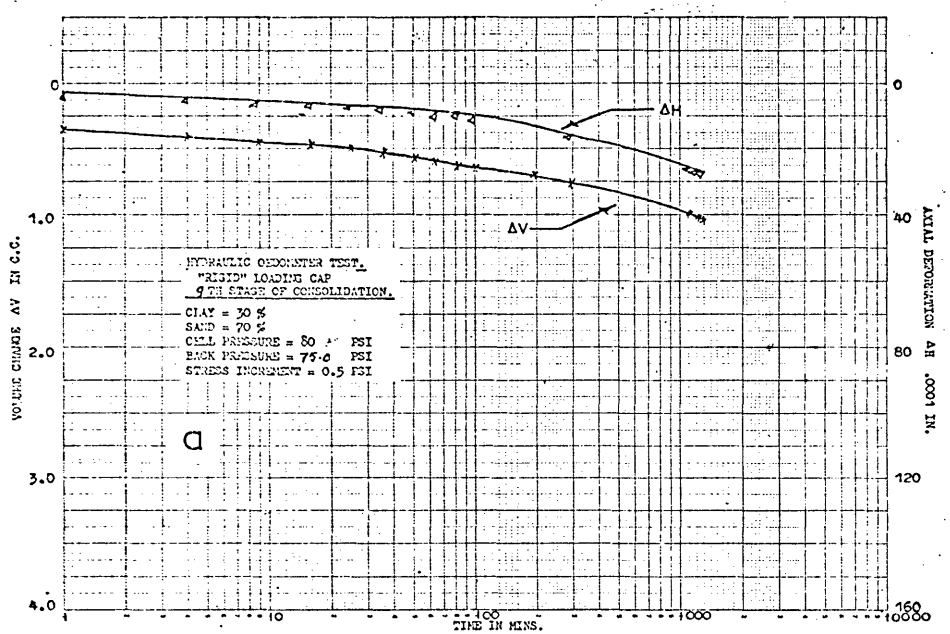

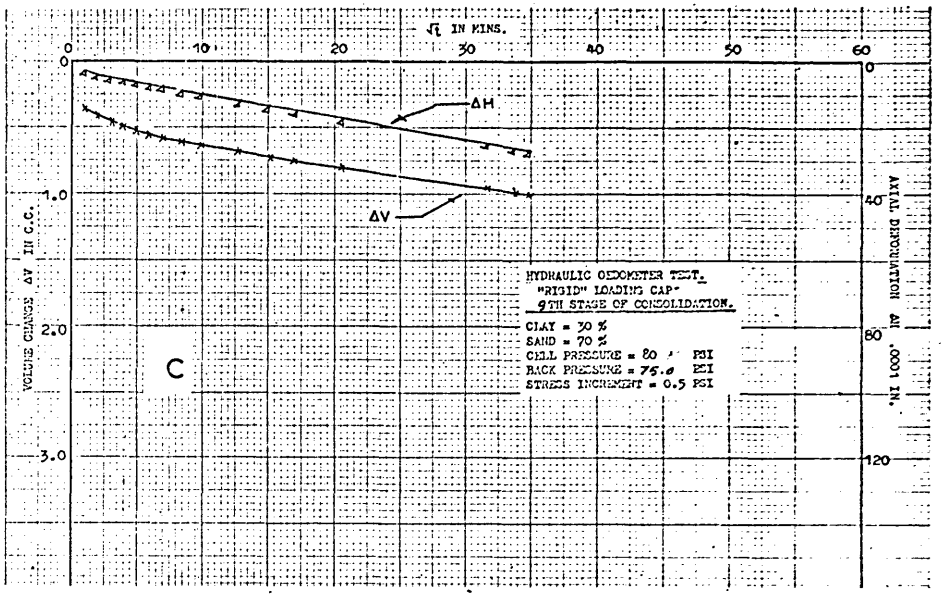

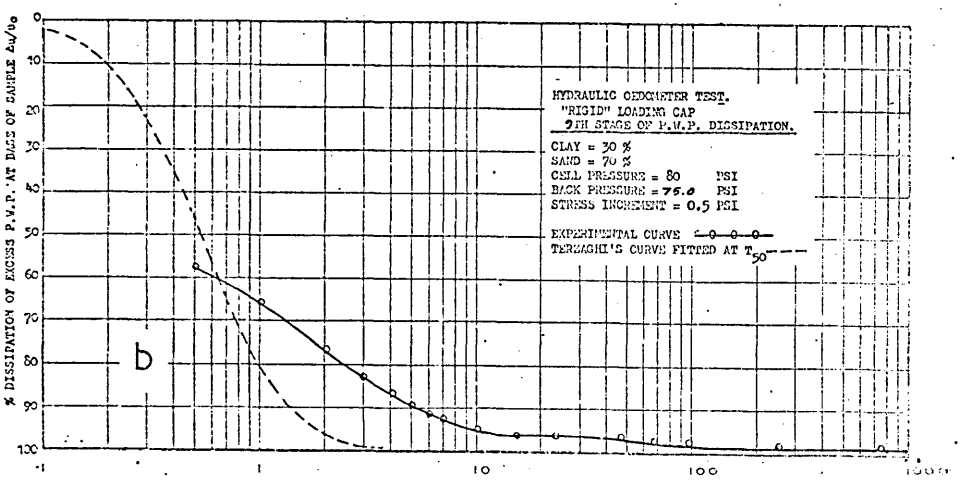

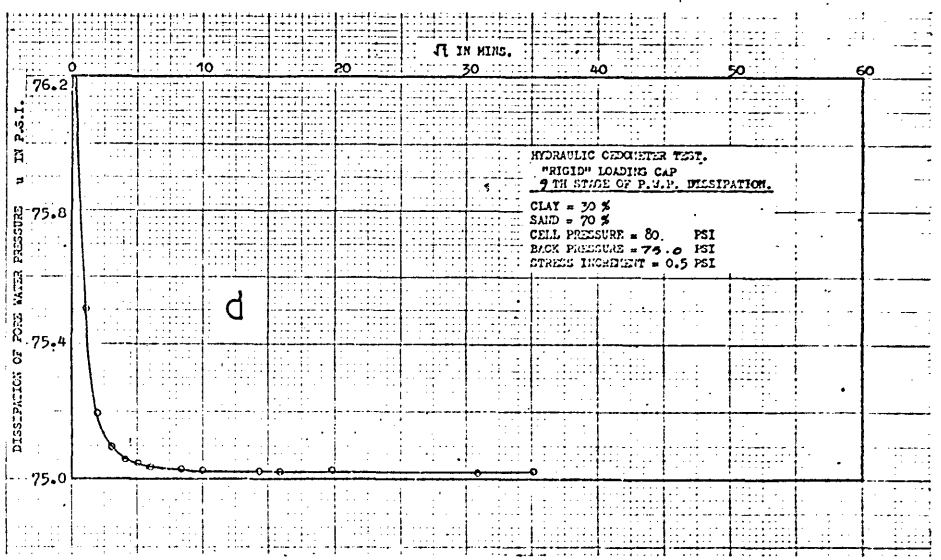

FIG. NO. 4.15 (9th. Stage)

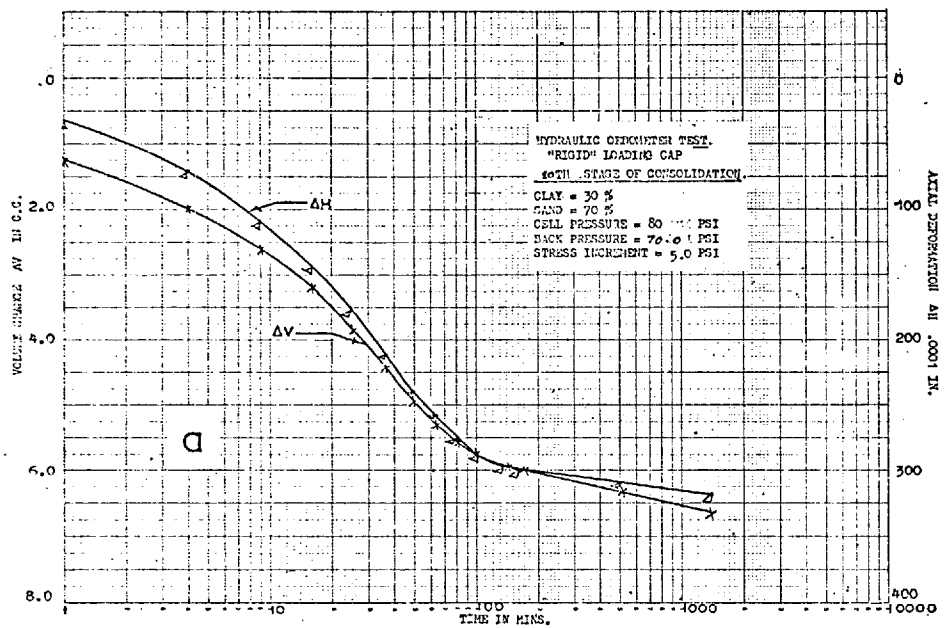

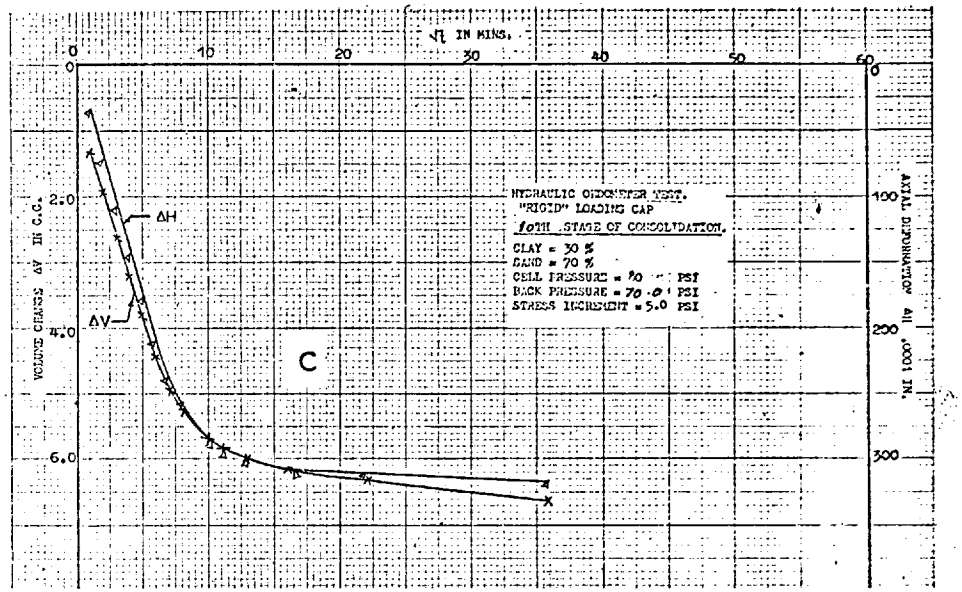

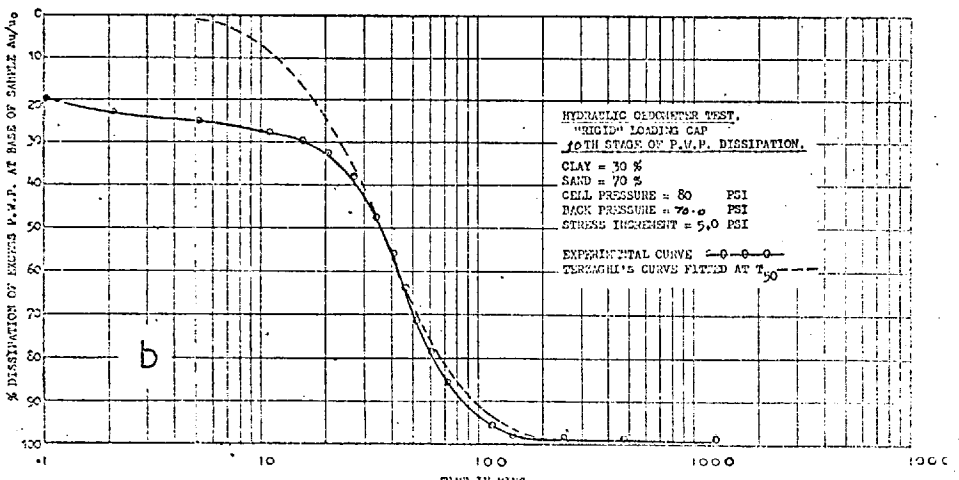

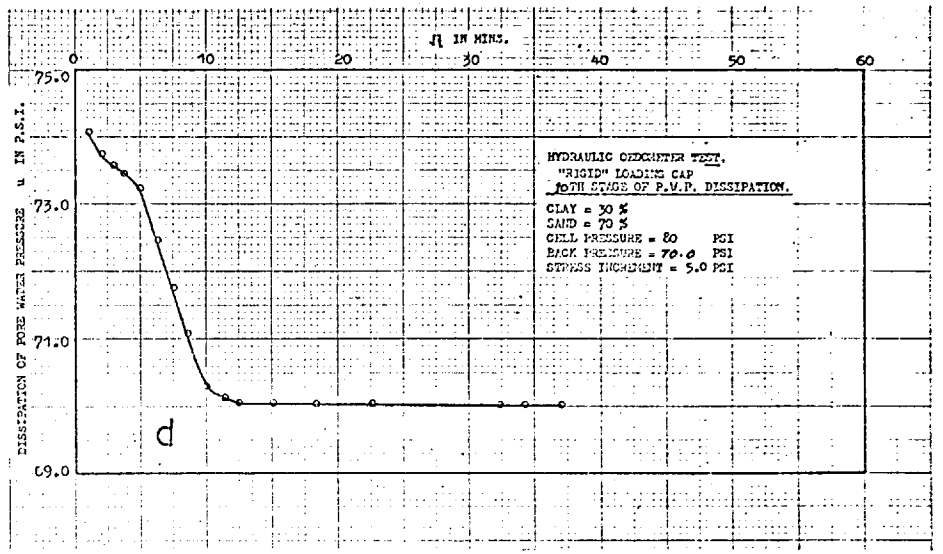

FIG. NO. 4.16 (10th. Stage)

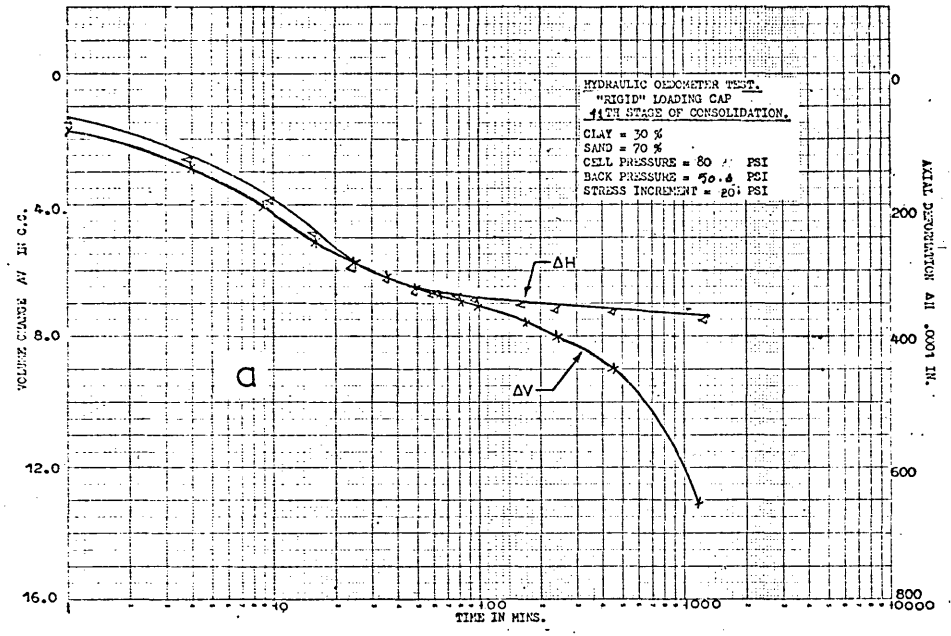

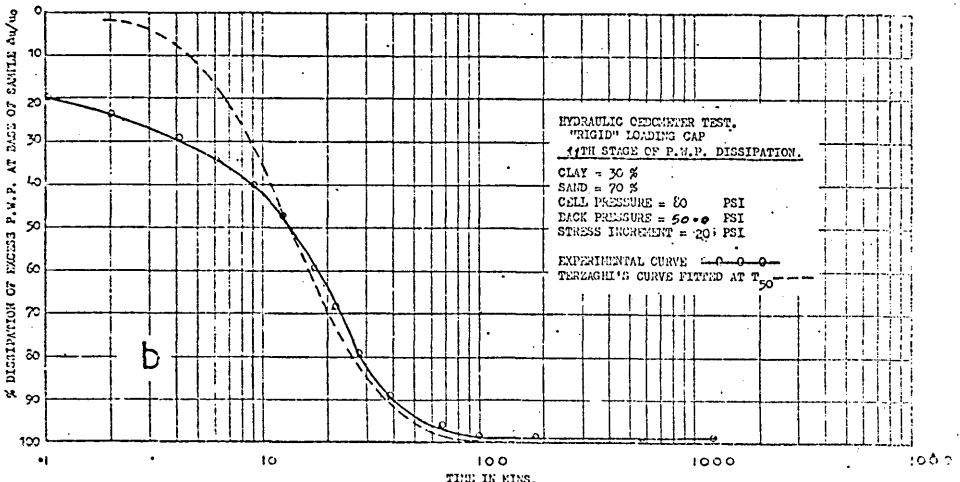

FIG. NO. 4. 17 (11th. Stage)

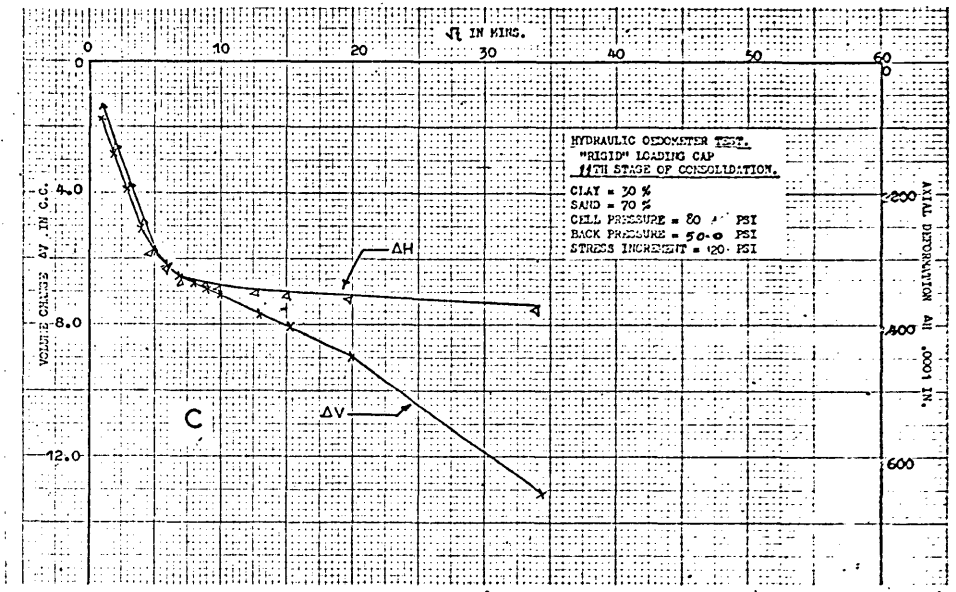

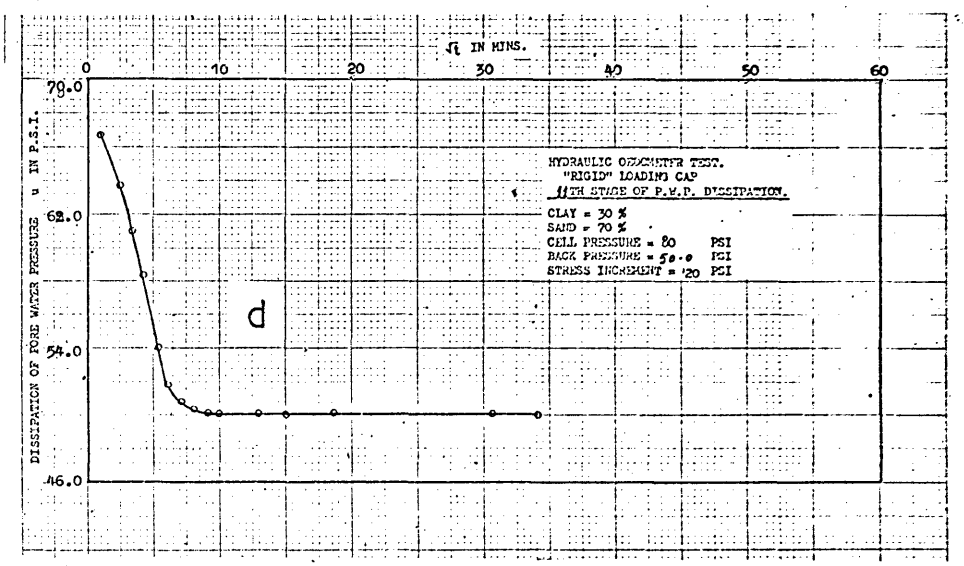

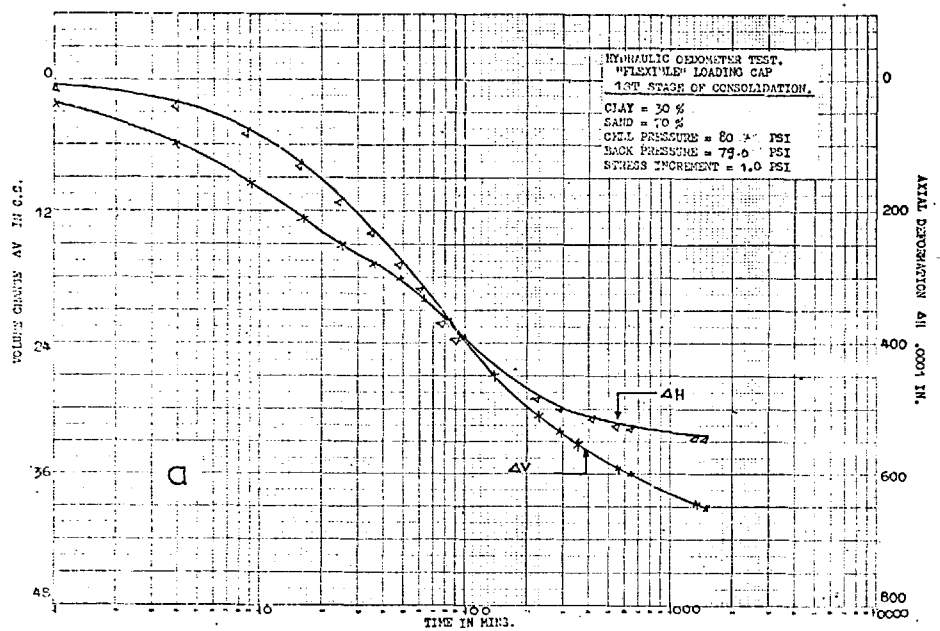

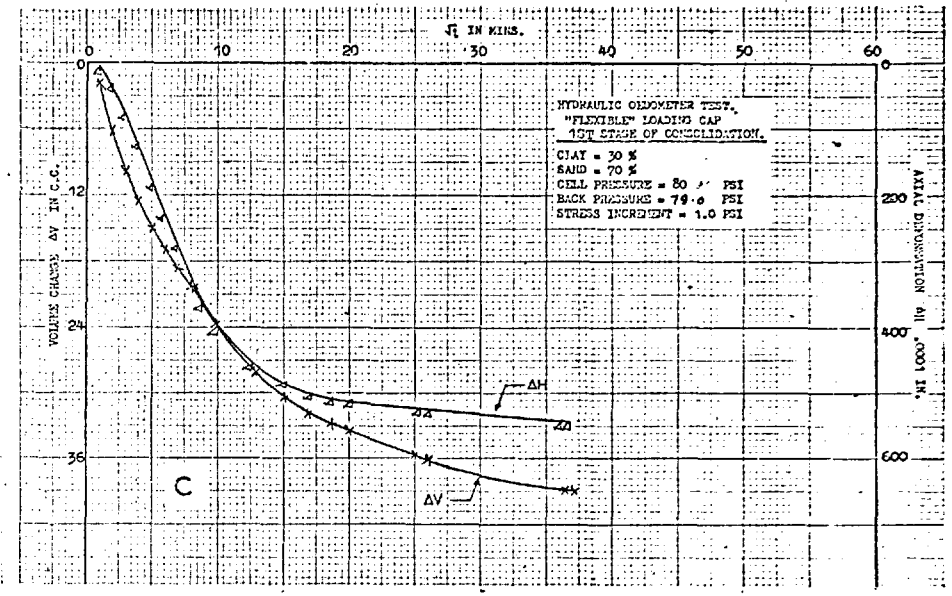

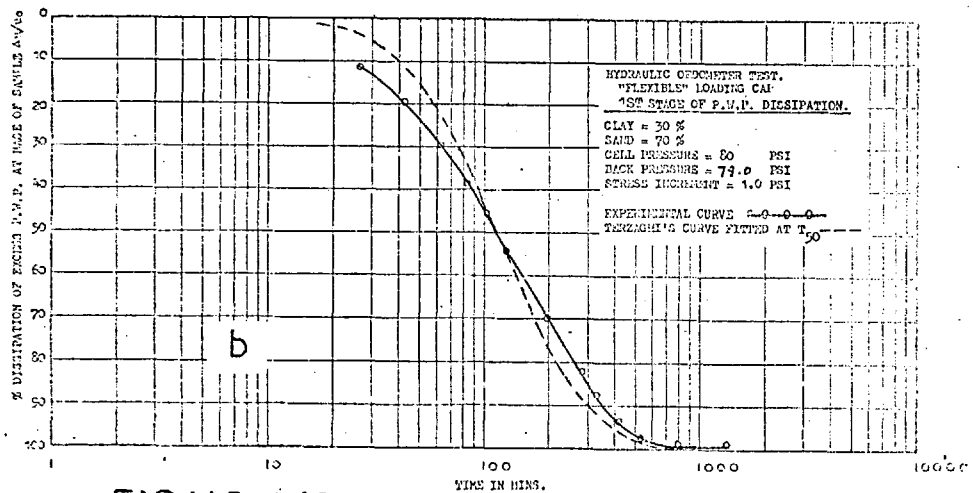

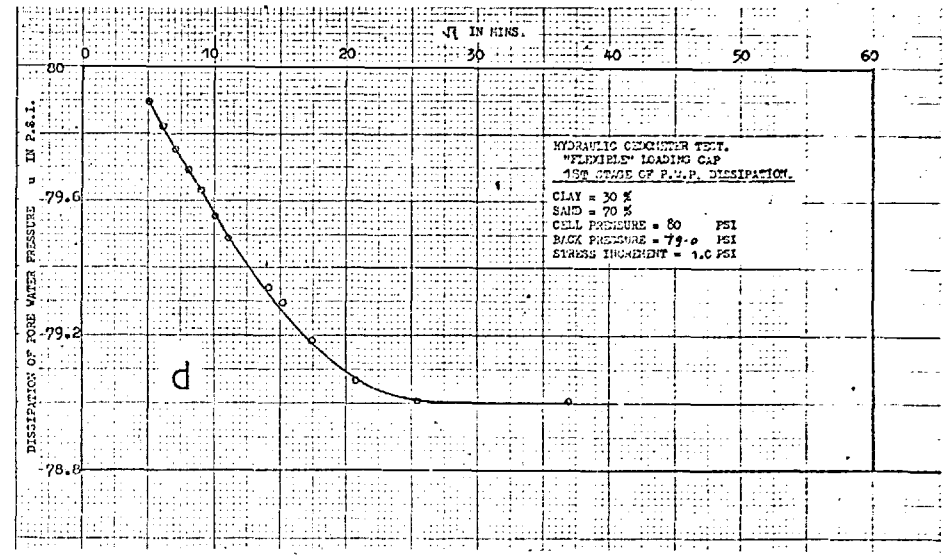

FIG.NO.4.18 (1st. Stage)

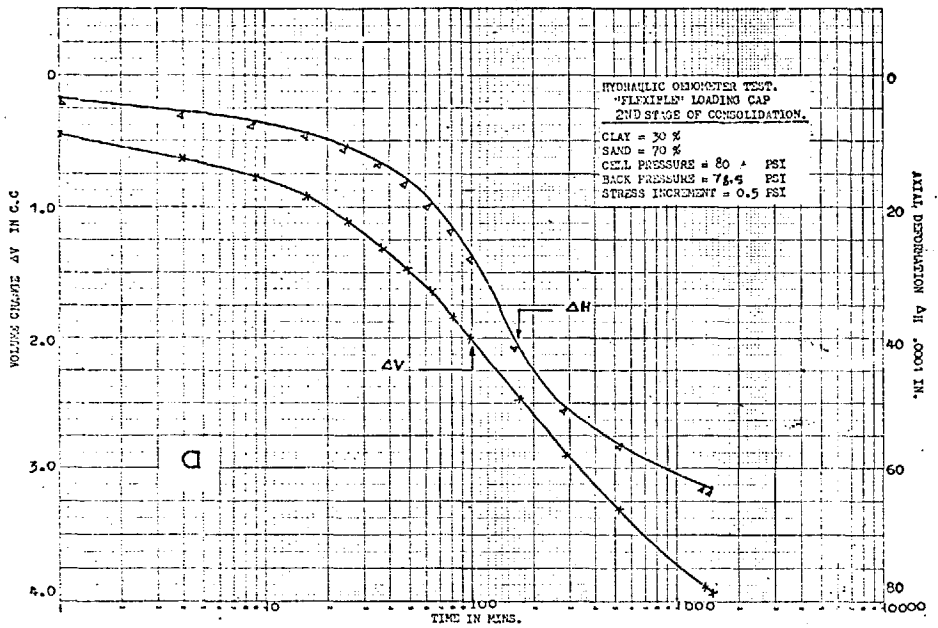

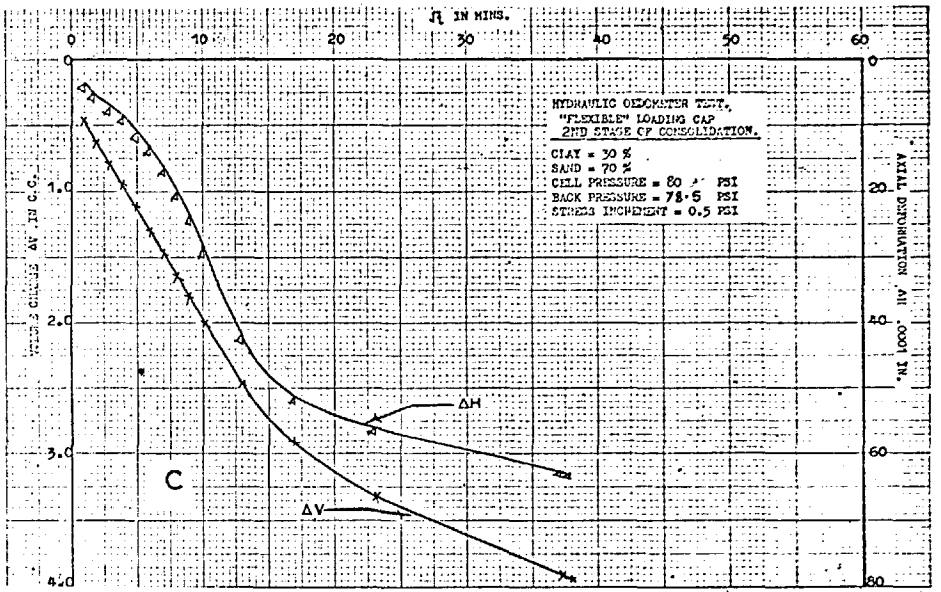

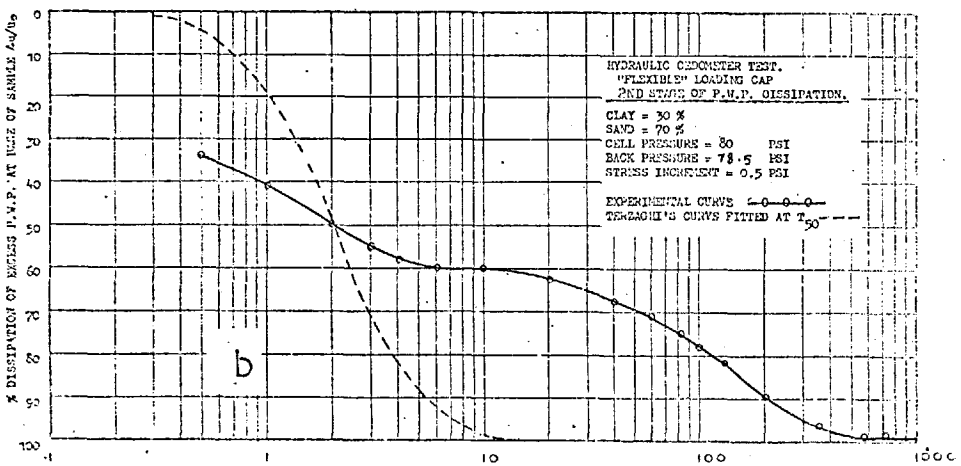

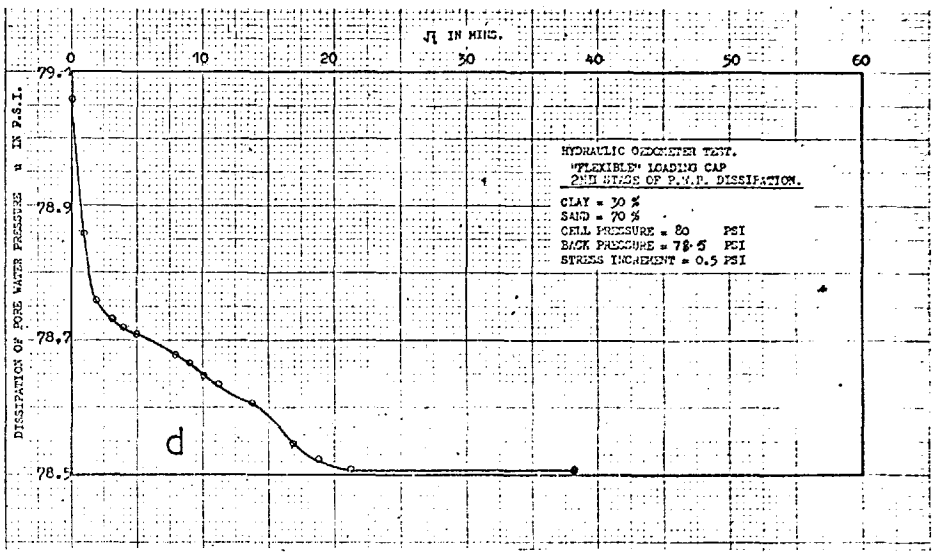

FIG.NO. 4.19 (2nd Stage)

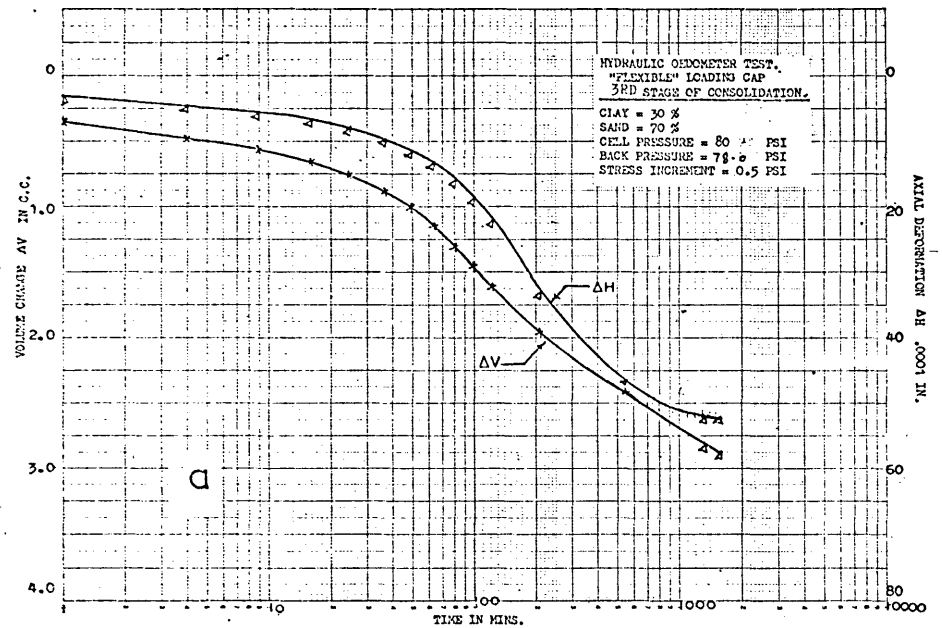

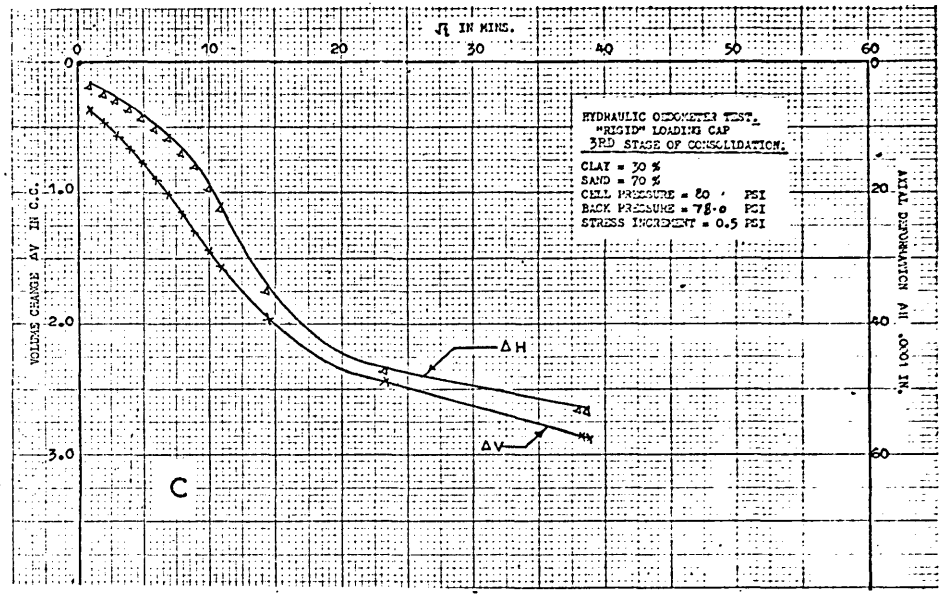

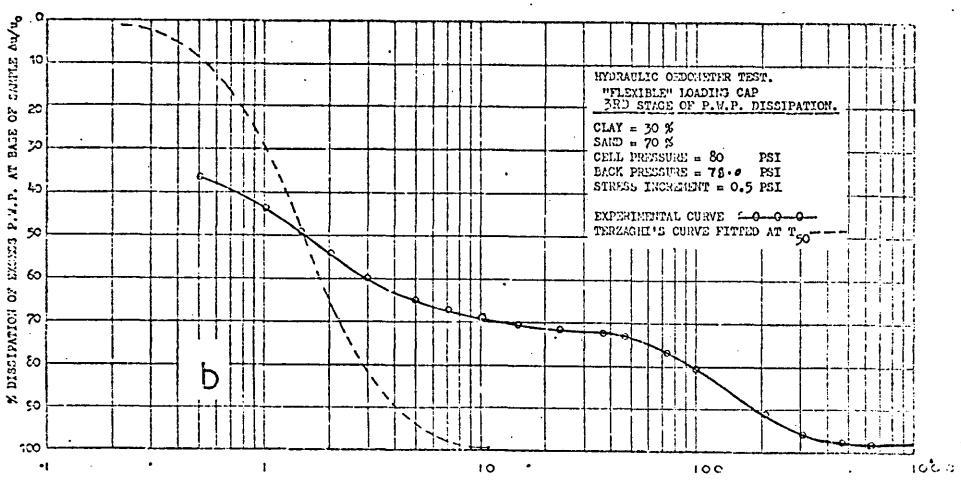

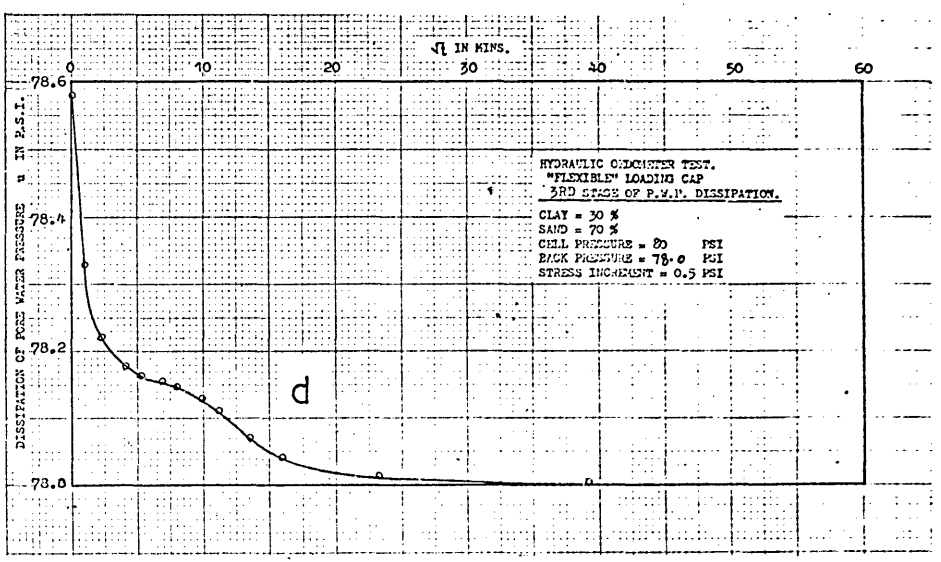

FIG. NO. 4.20 (3rd Stage)

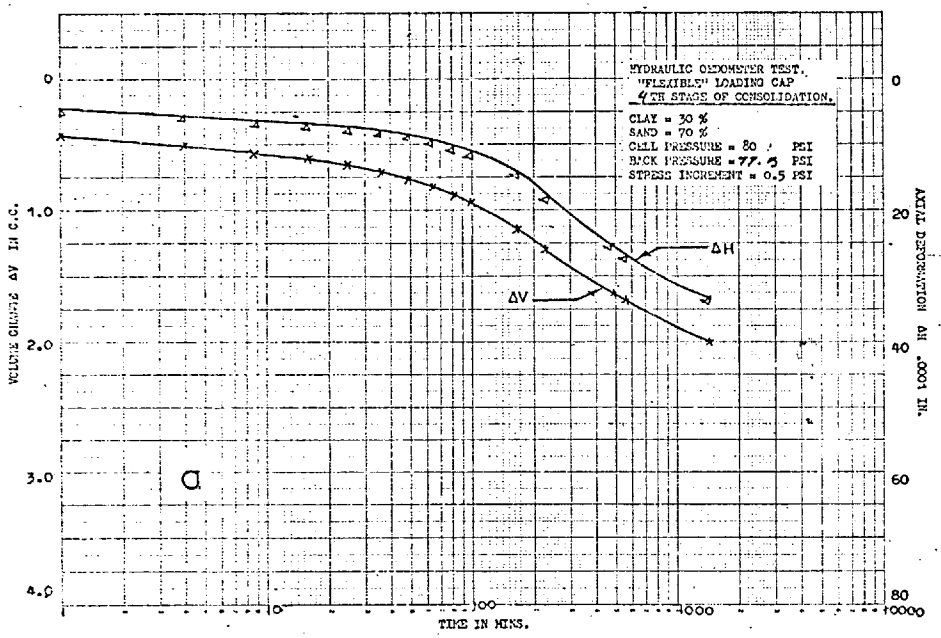

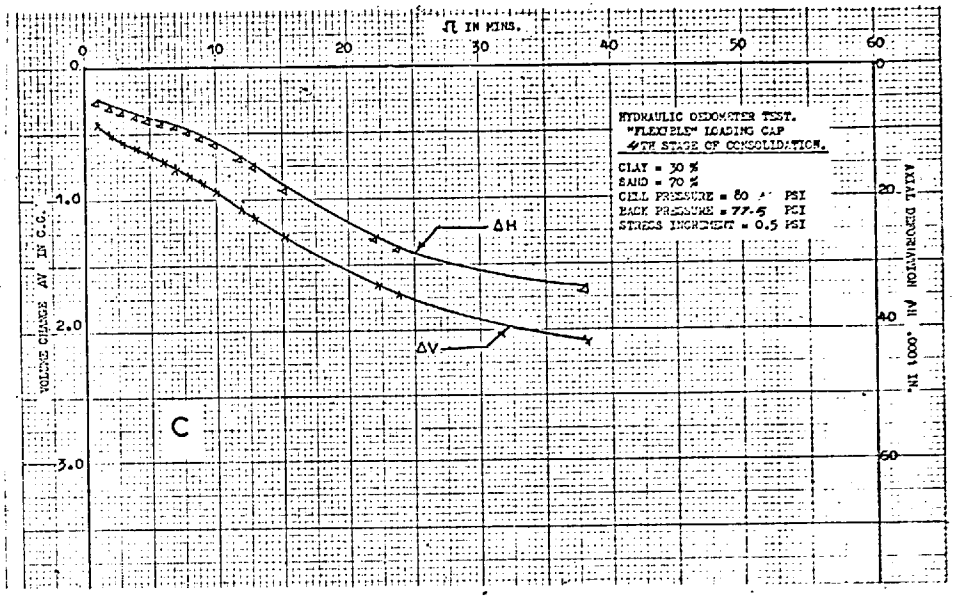

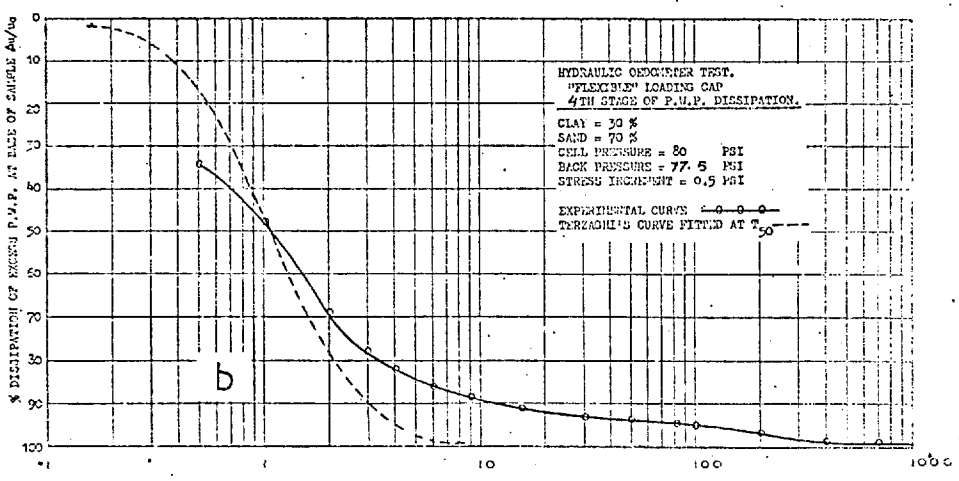

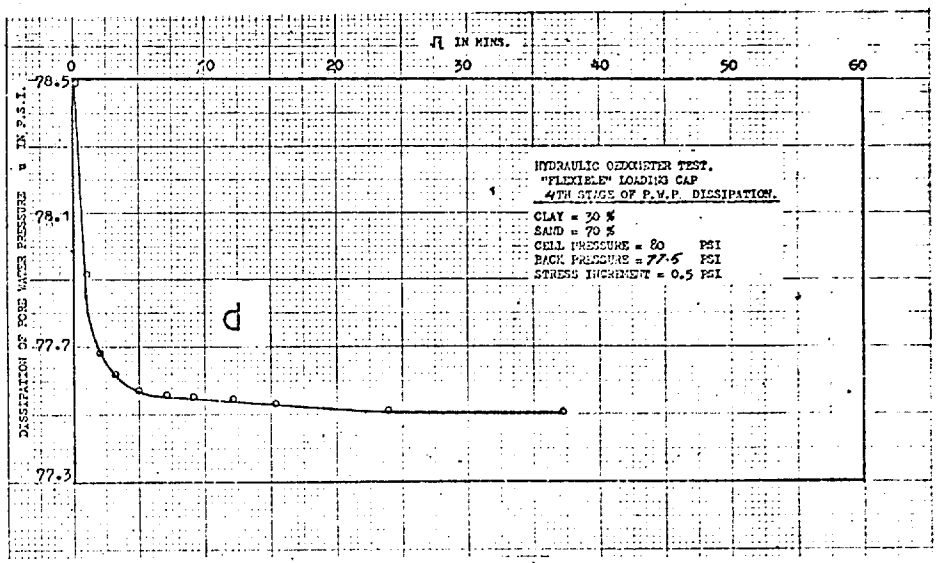

FIG.NO. 4. 21 (4th. Stage)

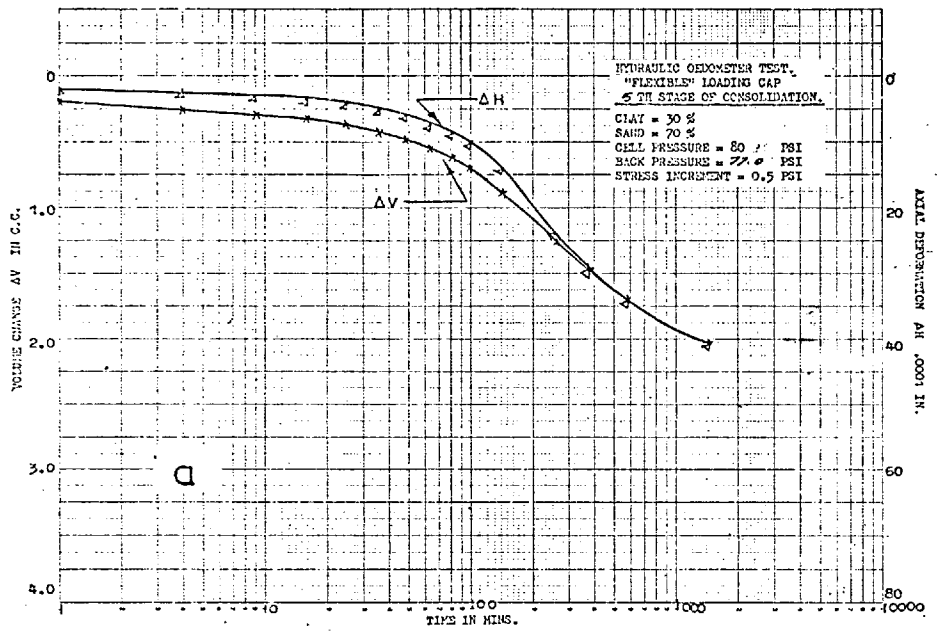

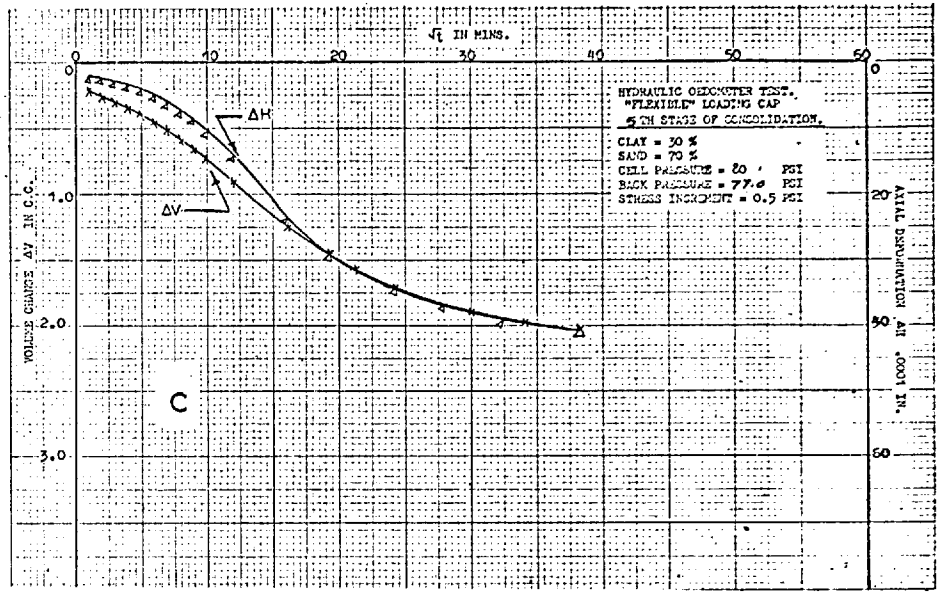

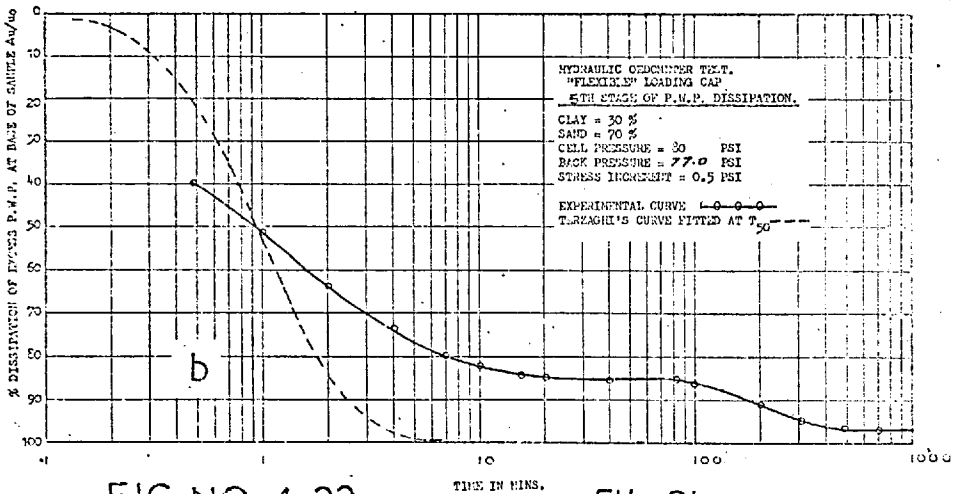

FIG. NO. 4.22 (5th. Stage)

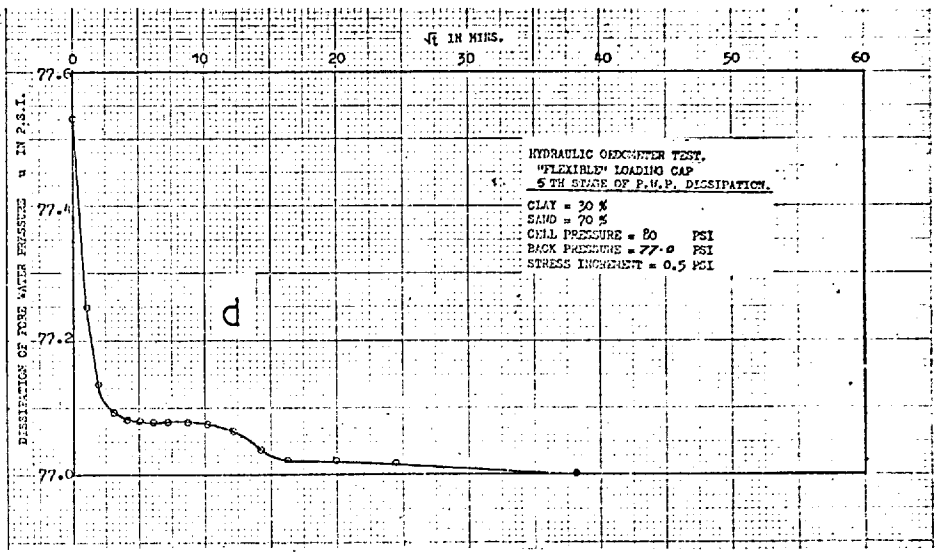

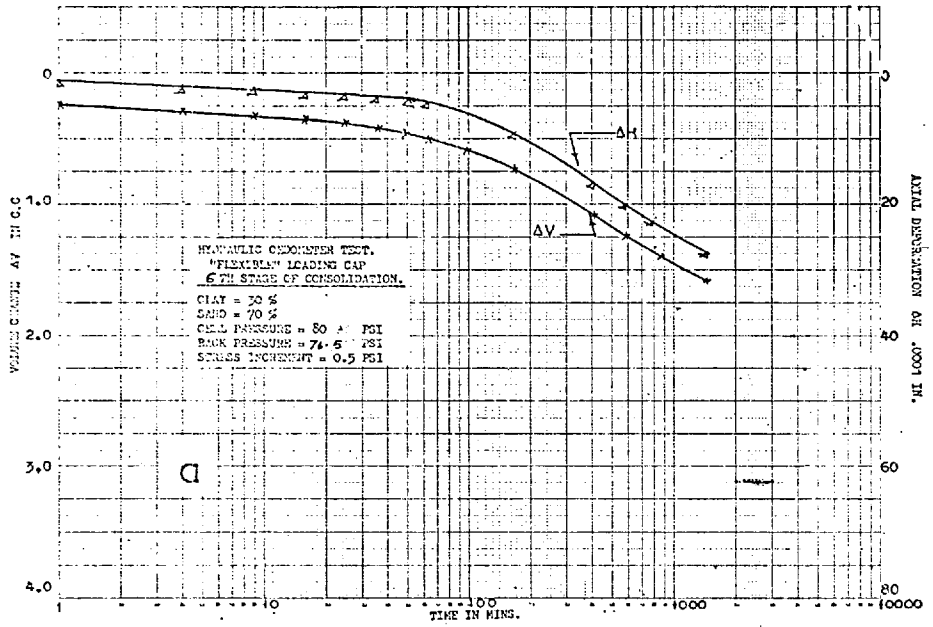

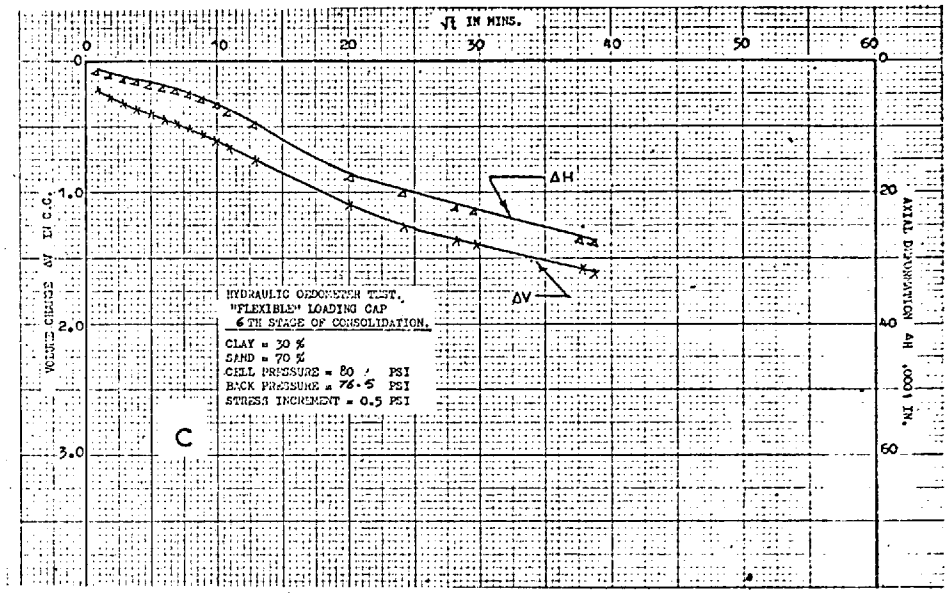

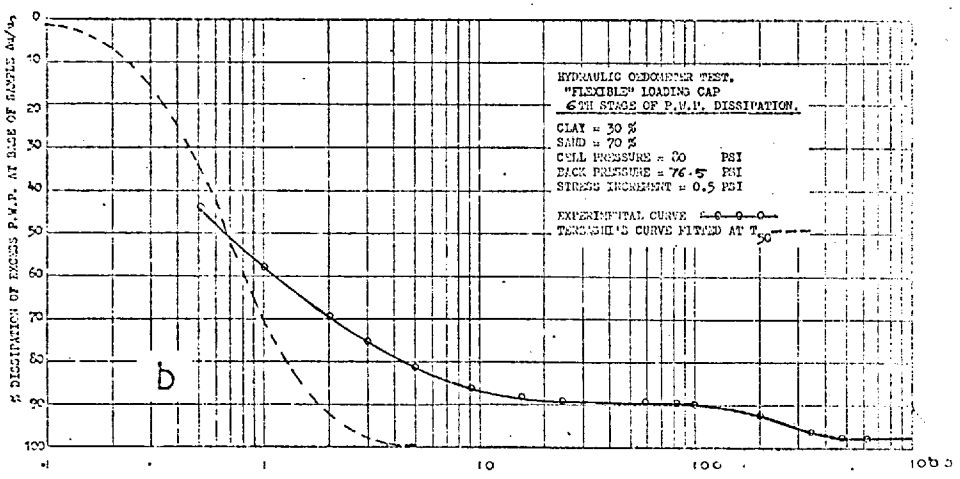

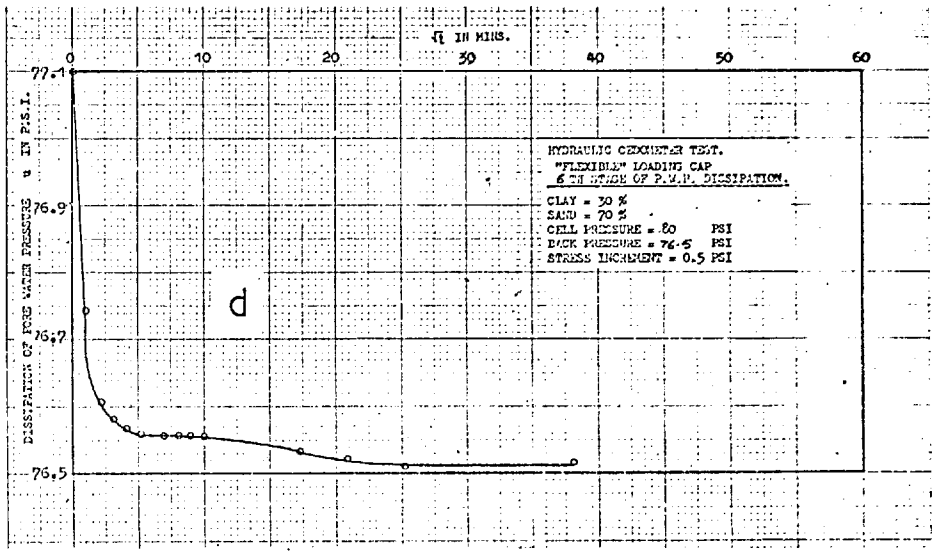

FIG. NO. 4. 23 (6th. Stage)

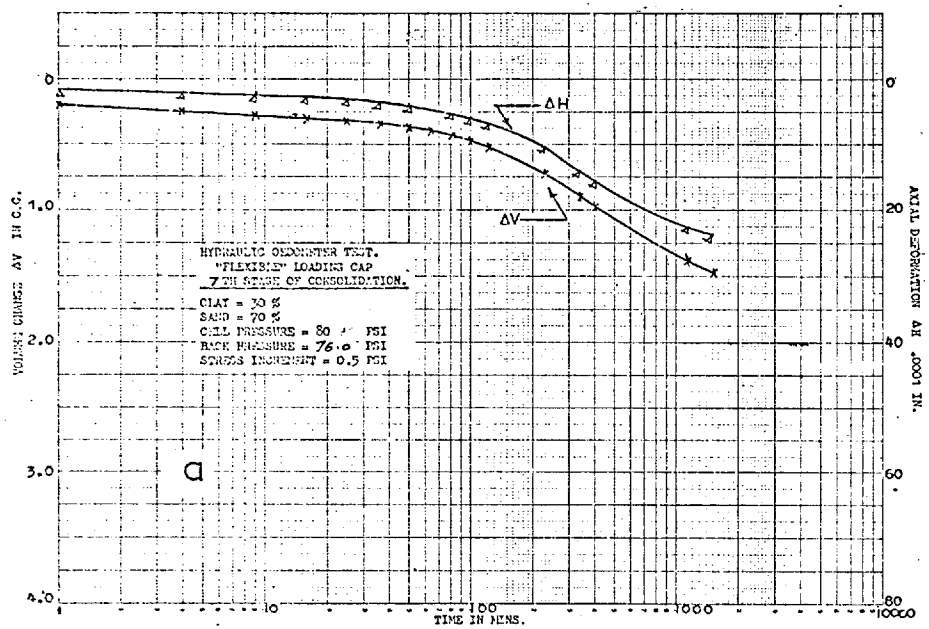

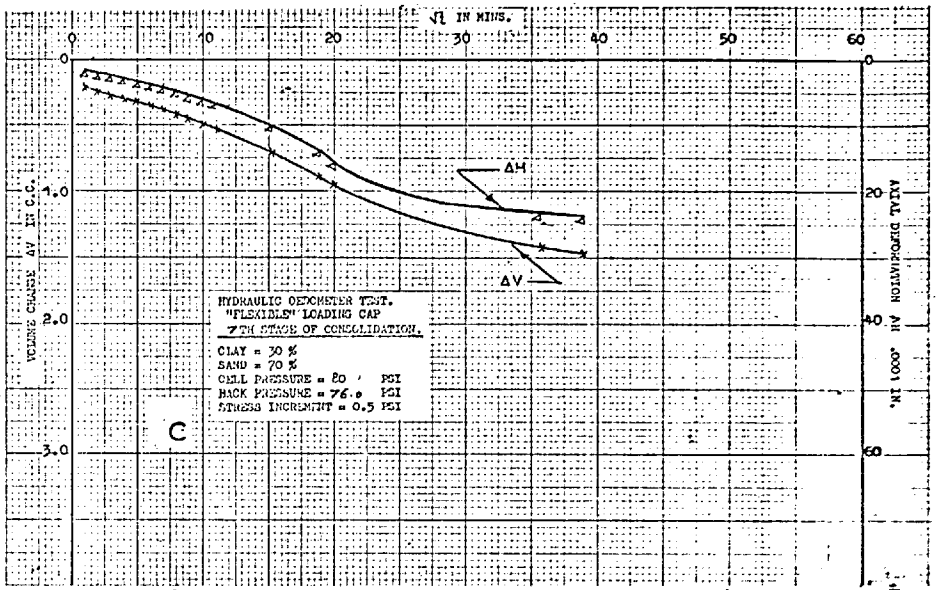

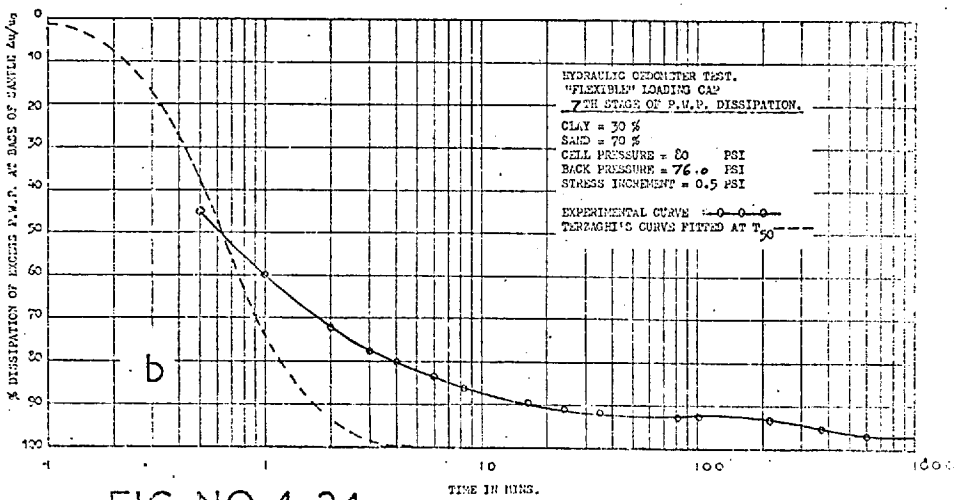

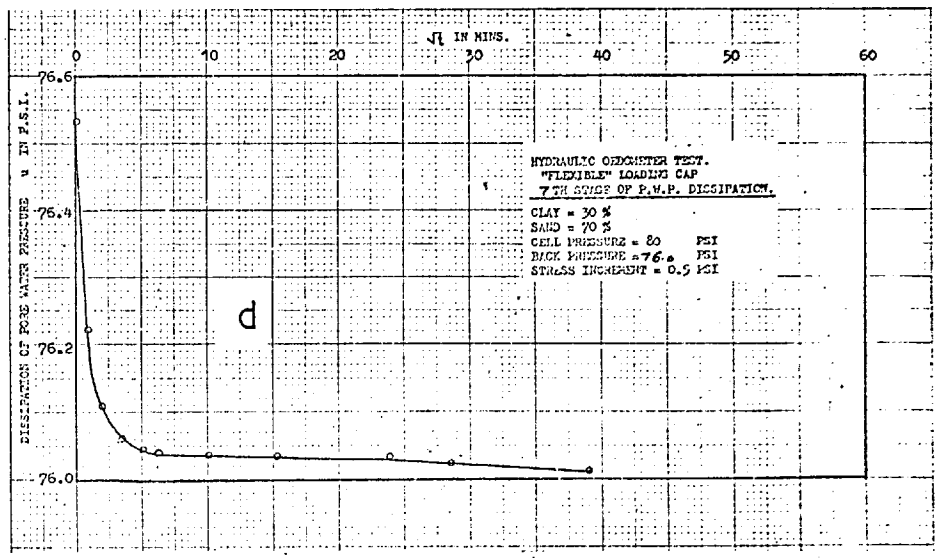

FIG. NO. 4. 24 (7th Stage)

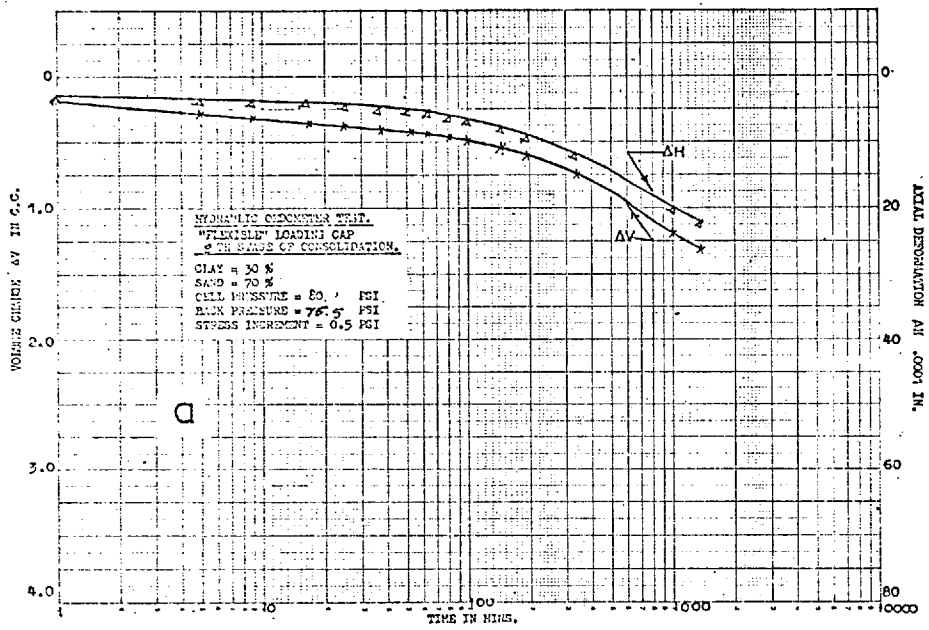

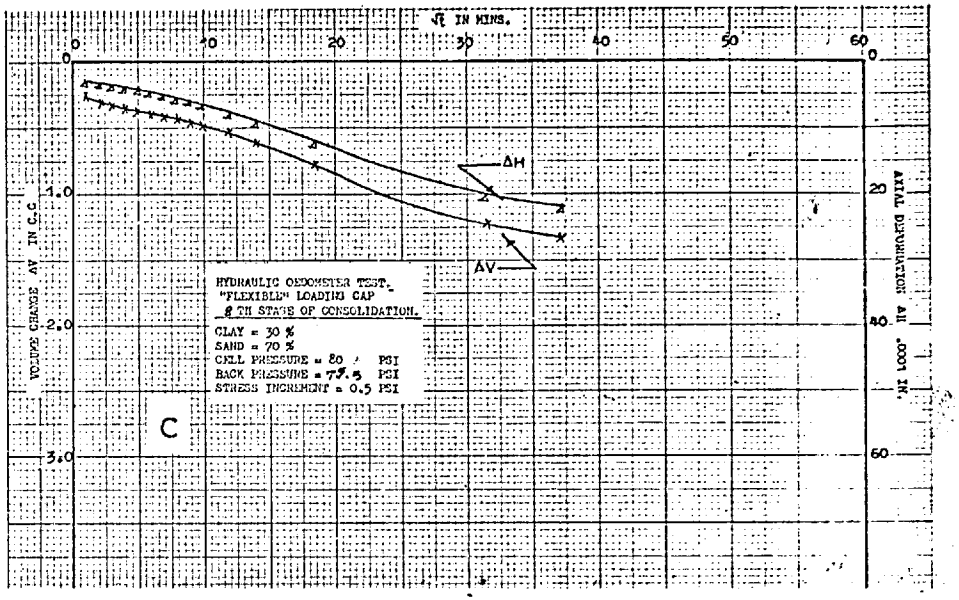

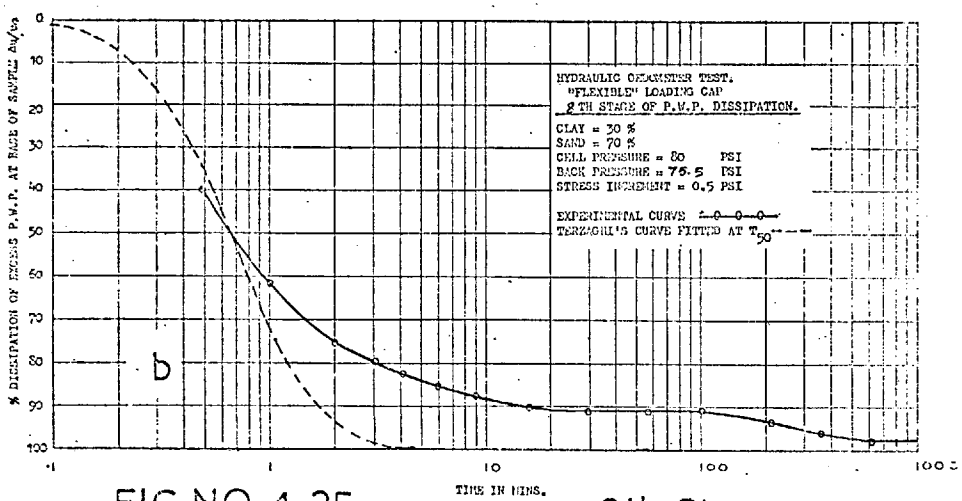

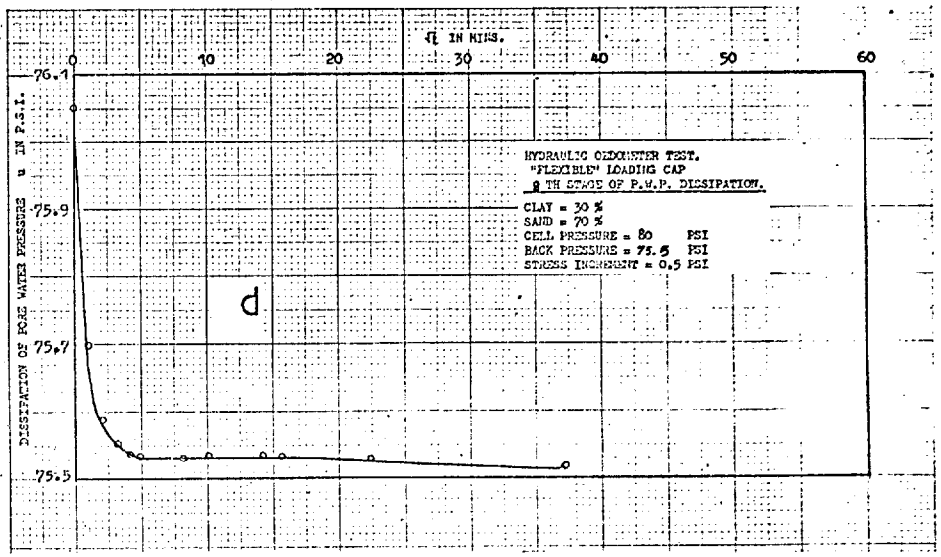

FIG. NO. 4.25 (8th Stage)

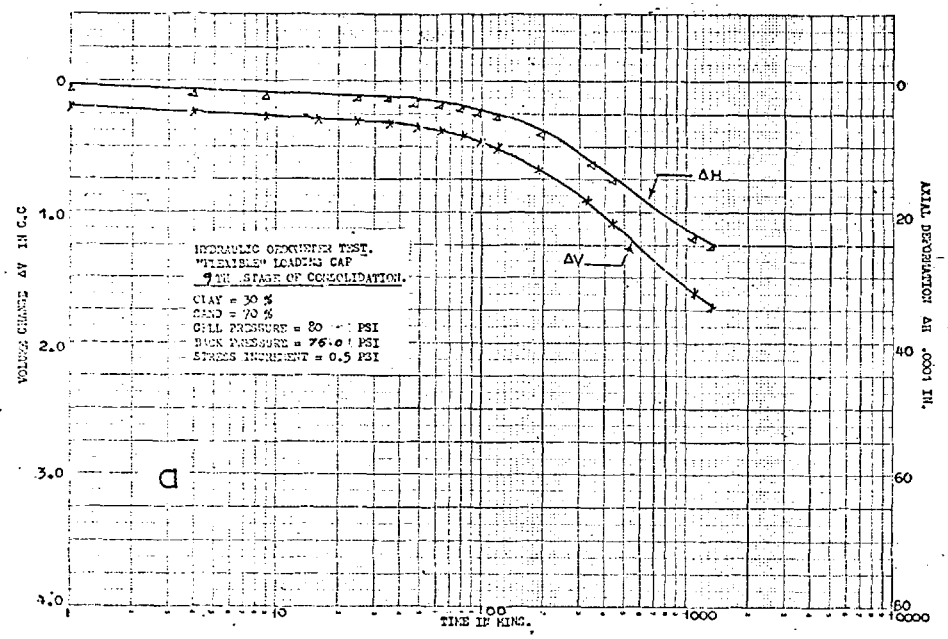

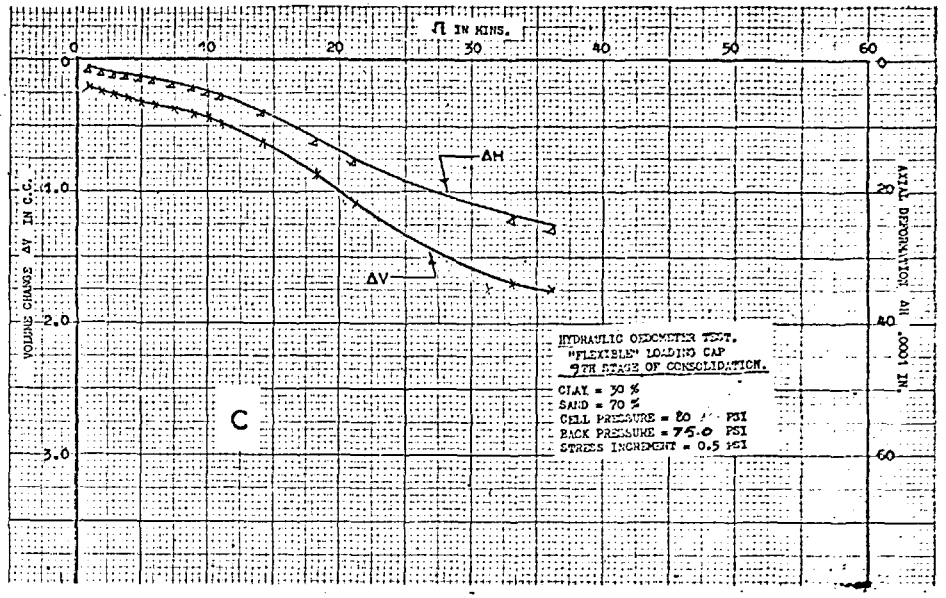

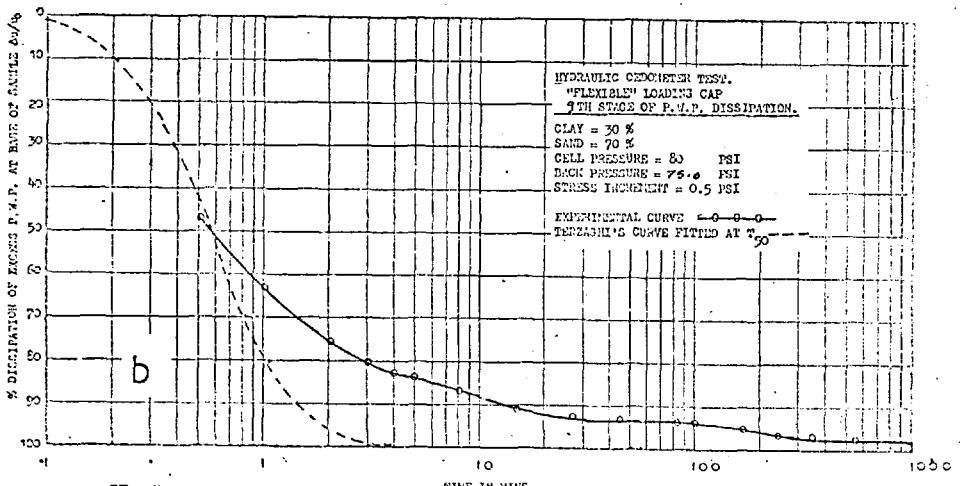

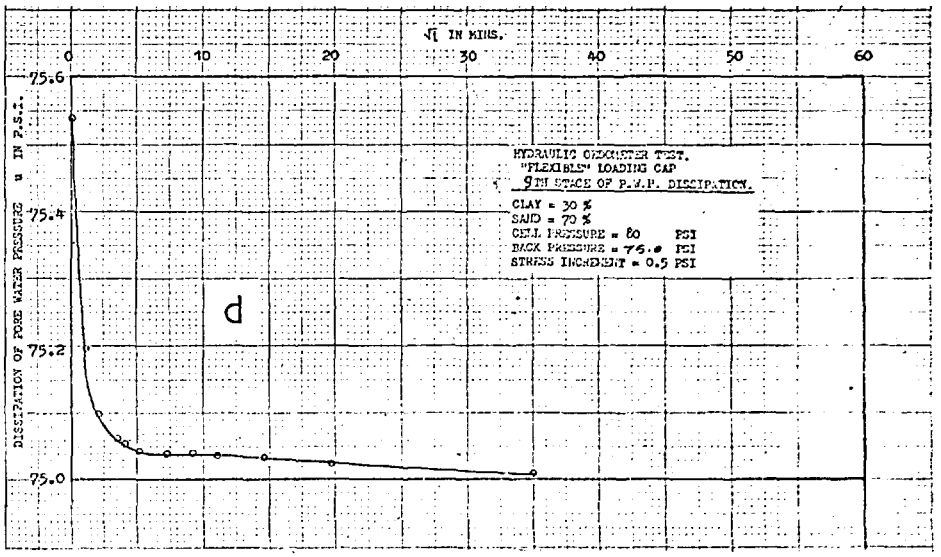

FIG. NO. 4. 26 (9th. Stage)

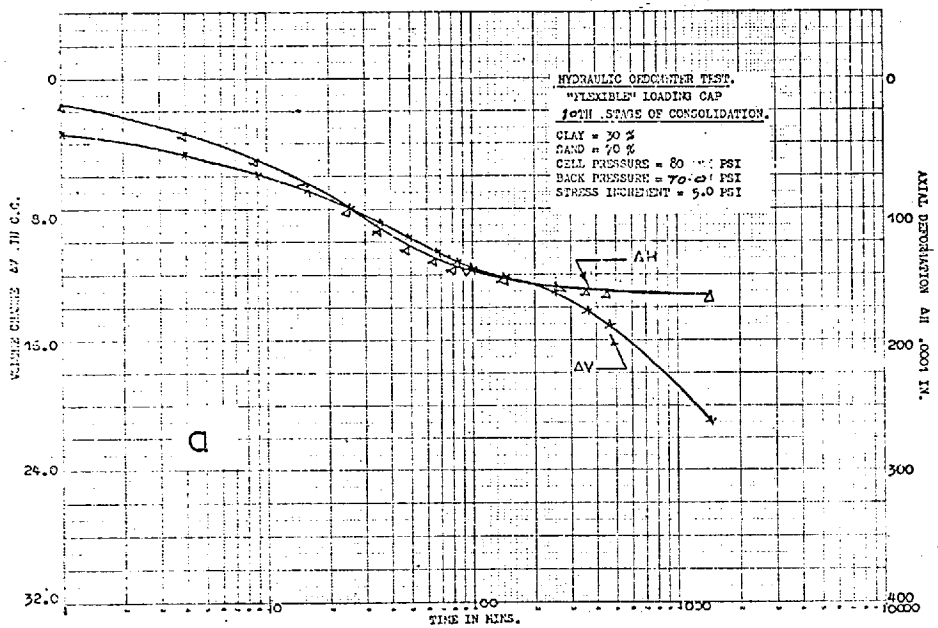

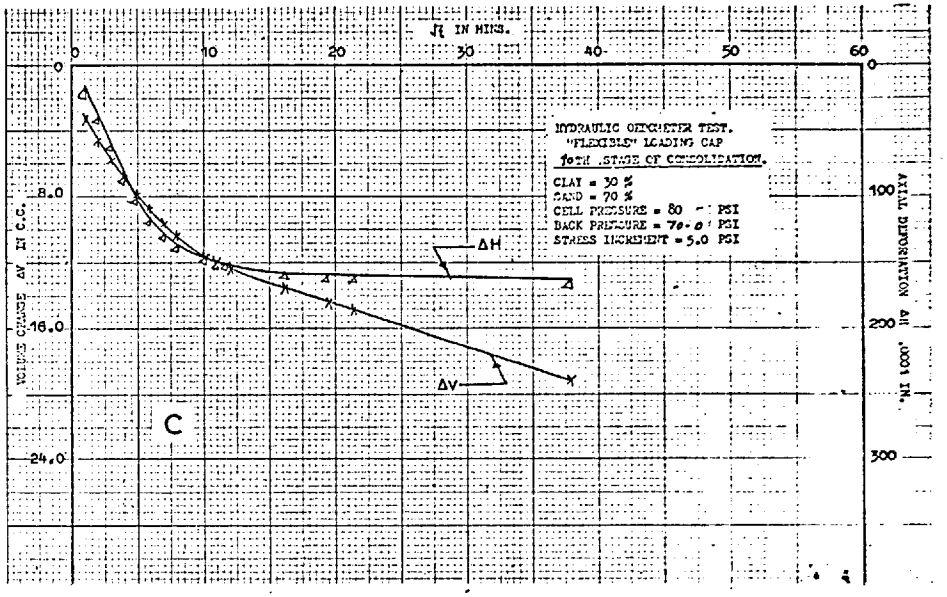

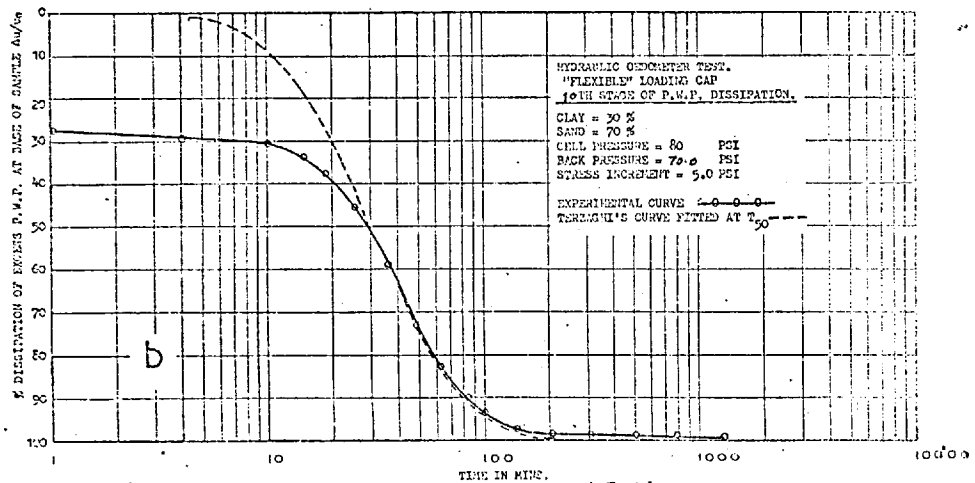

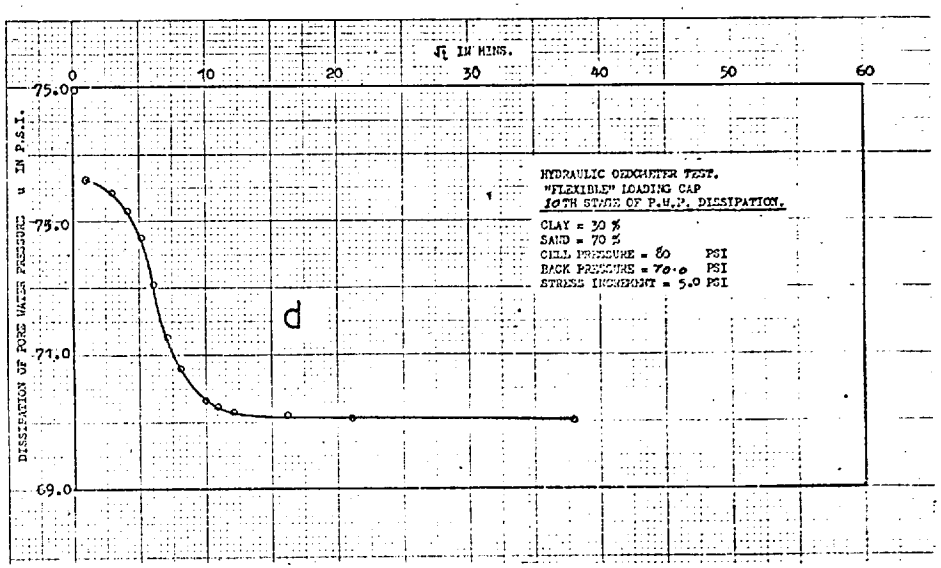

FIG. NO. 4.27 (10th. Stage)

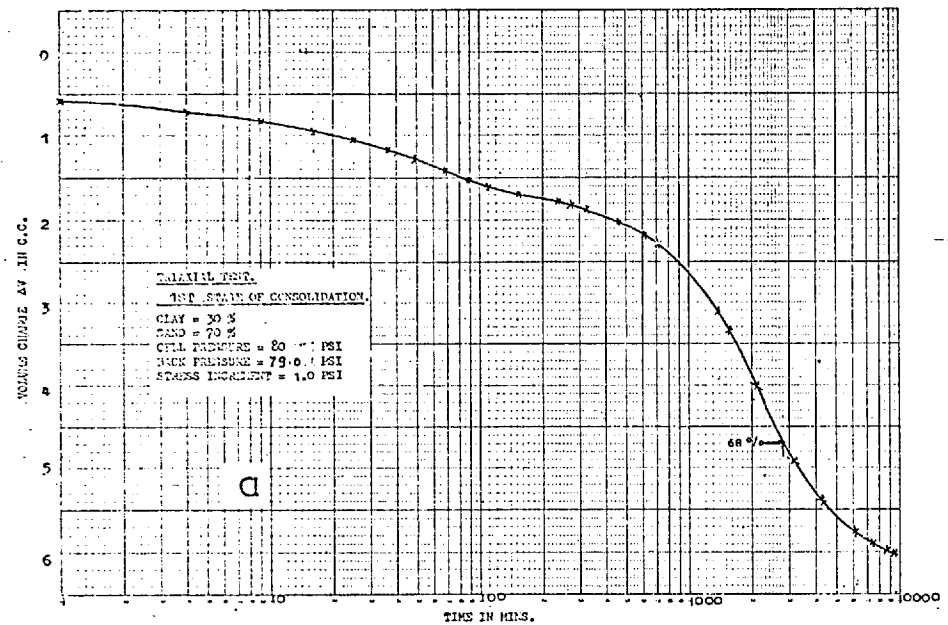

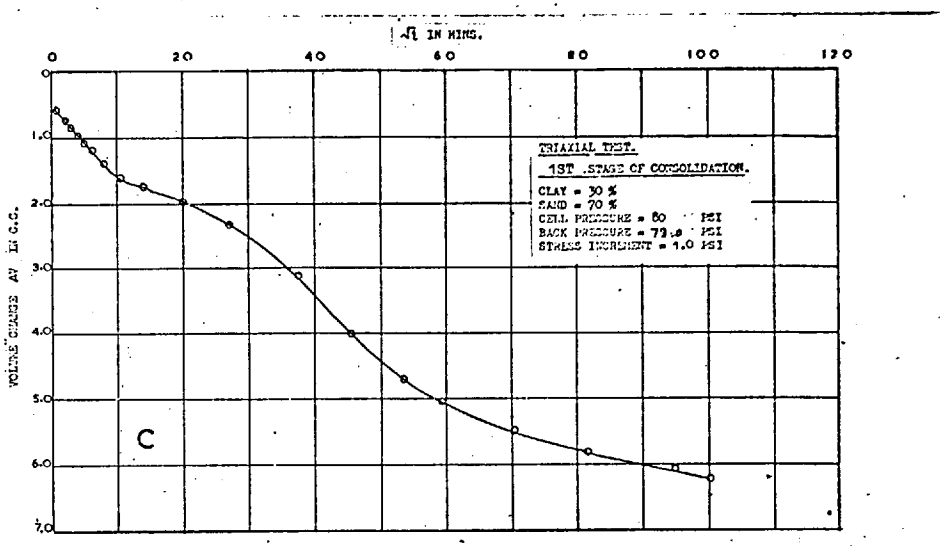

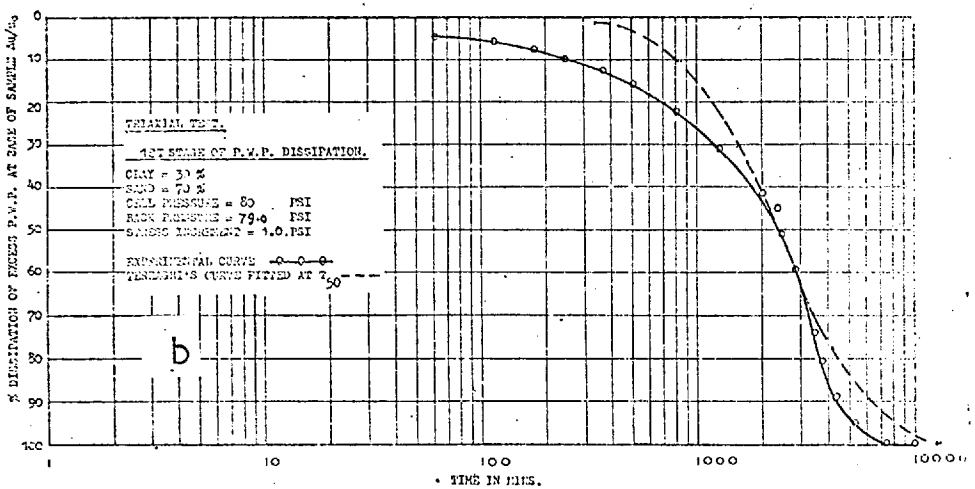

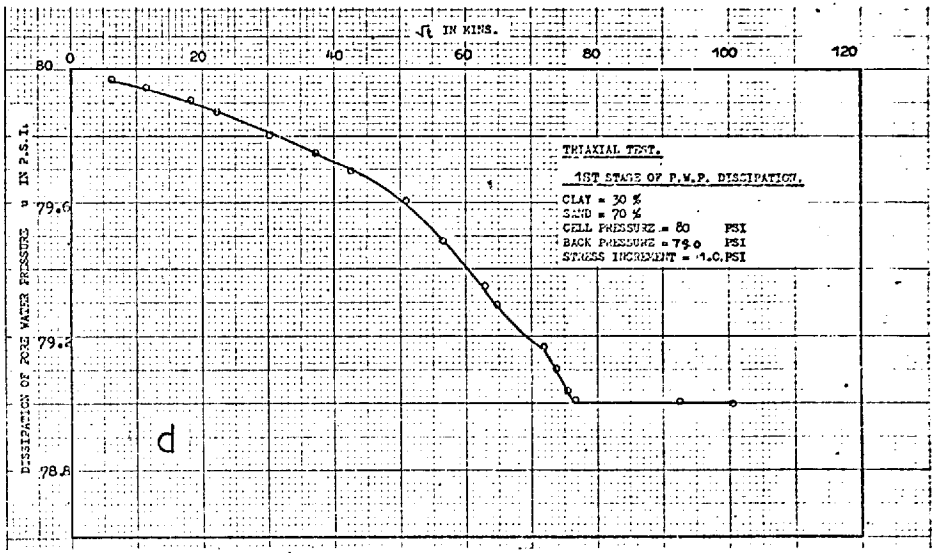

FIG. NO. 4.28 (Ist. Stage)

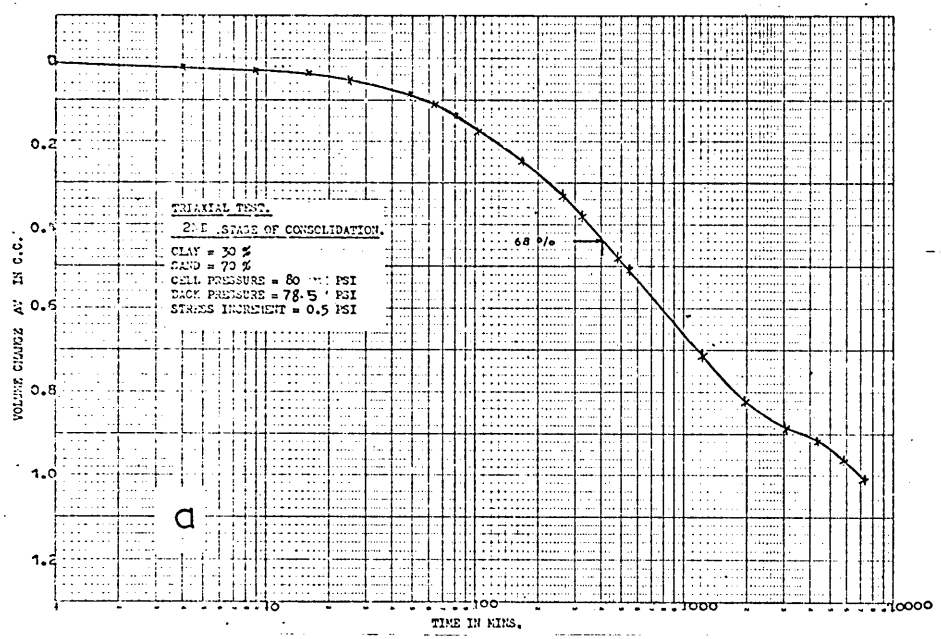

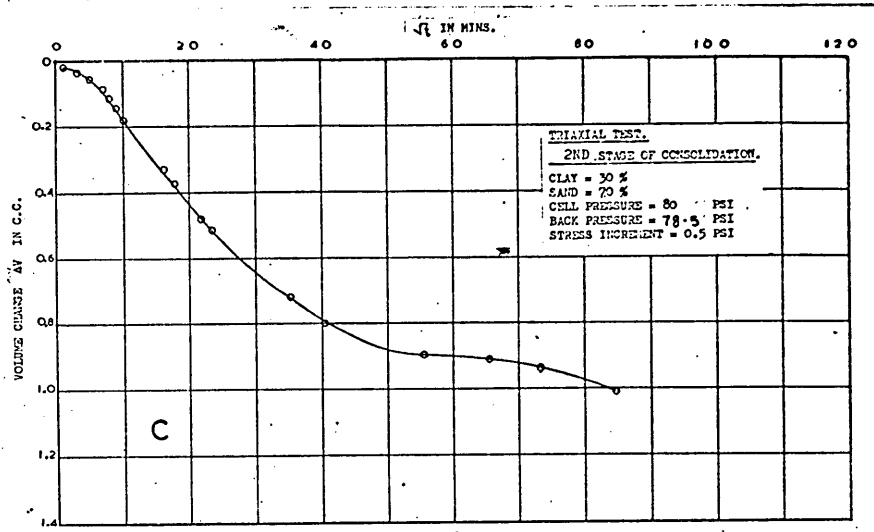

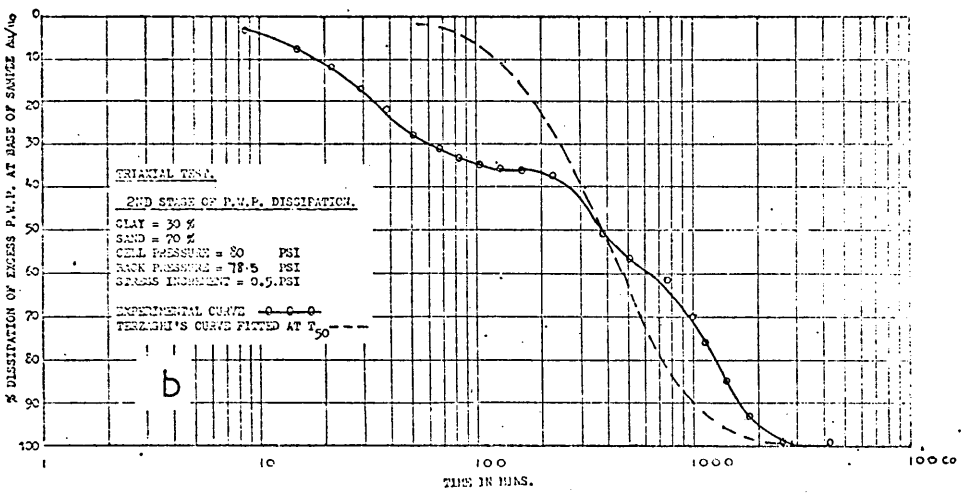

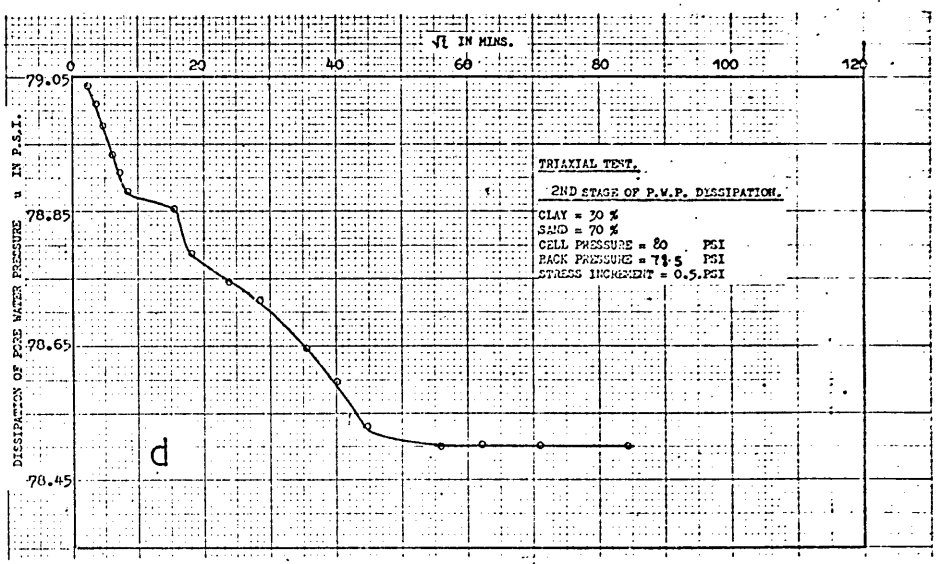

FIG.NO. 4.29 (2nd. Stage)

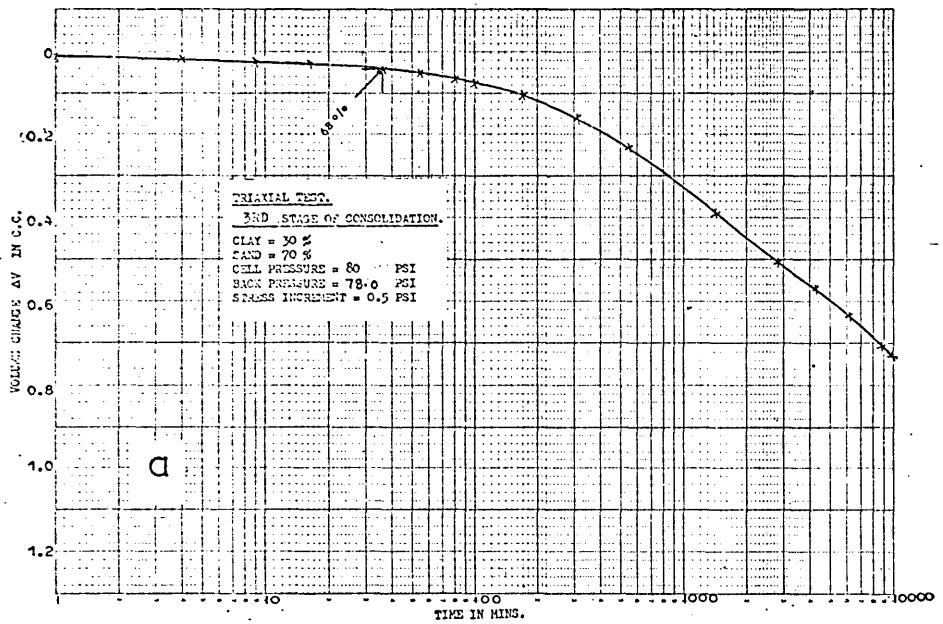

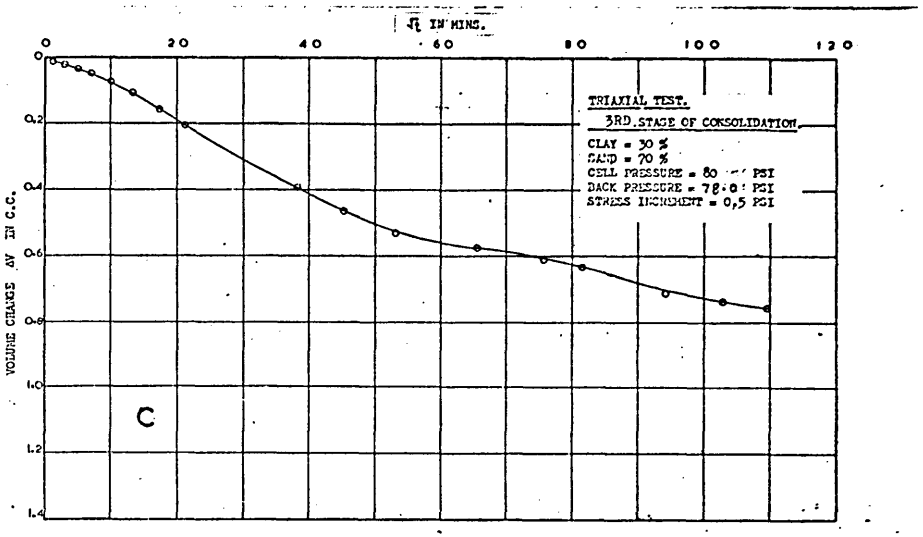

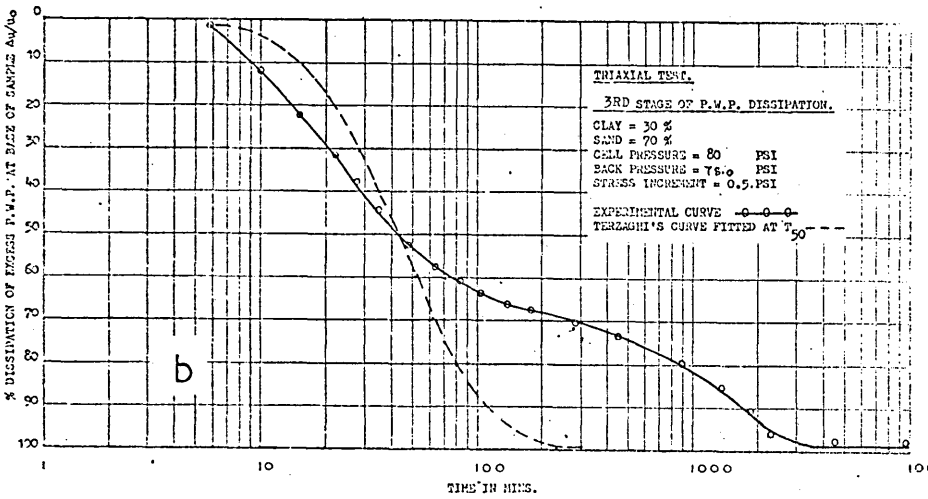

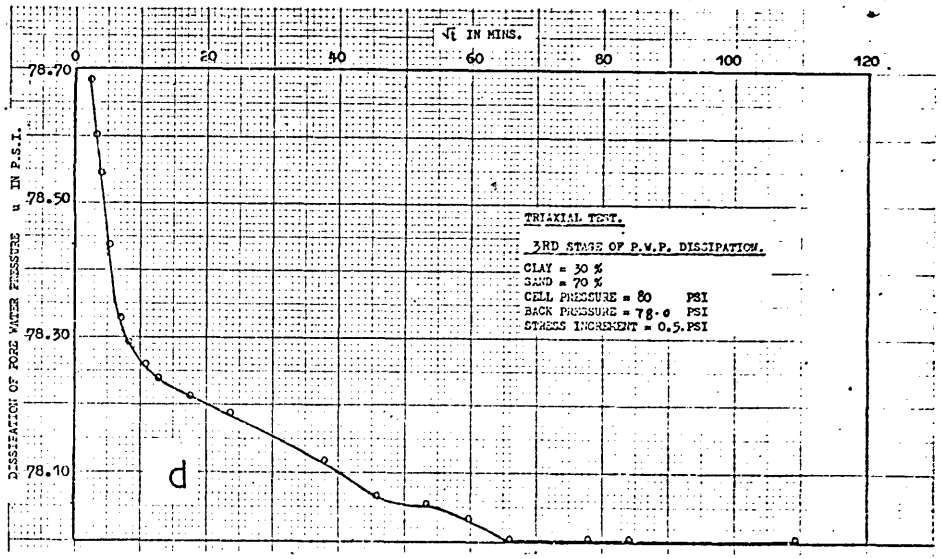

FIG.NO. 4. 30 (3rd Stage)

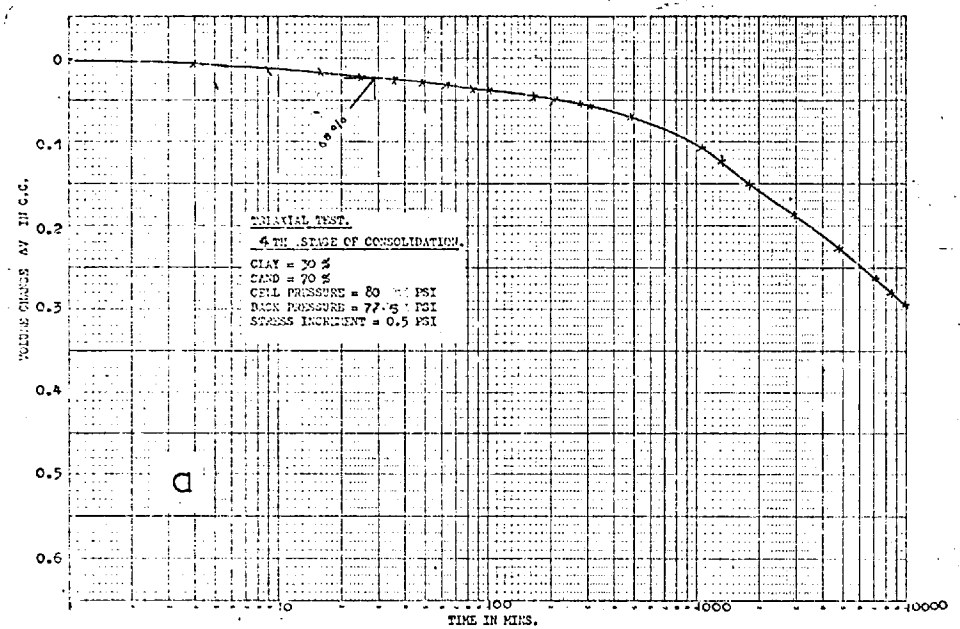

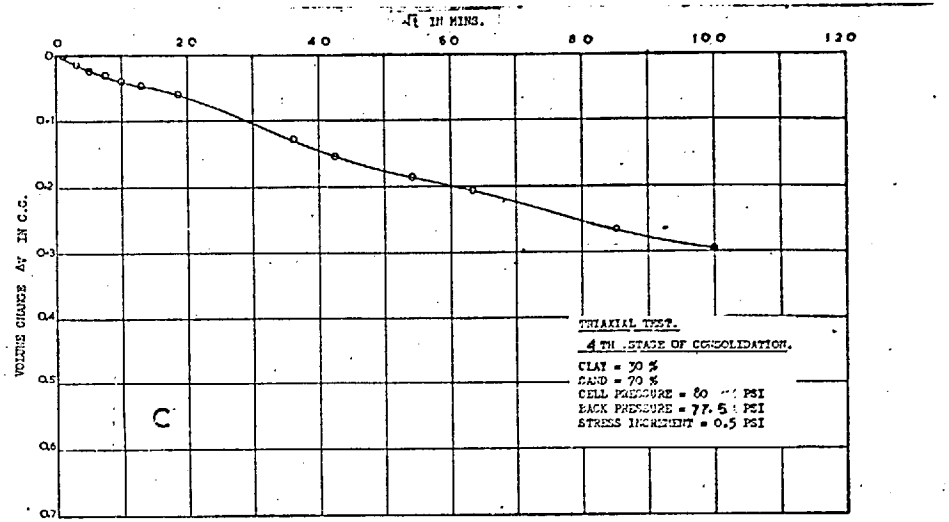

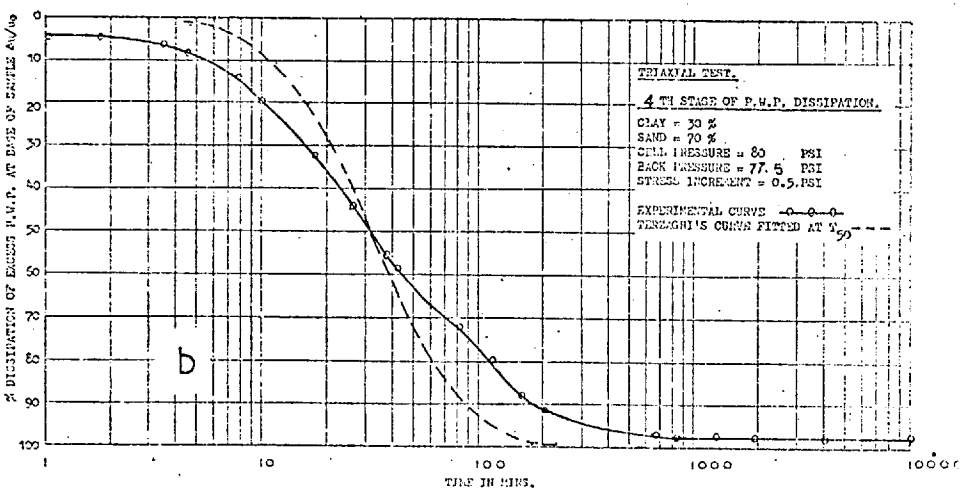

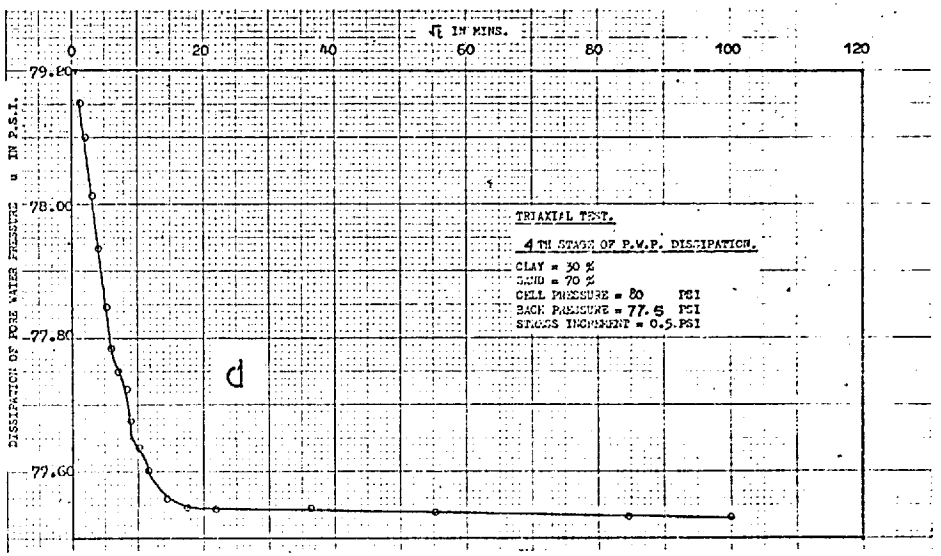

FIG.NO. 4.31 (4th Stage)

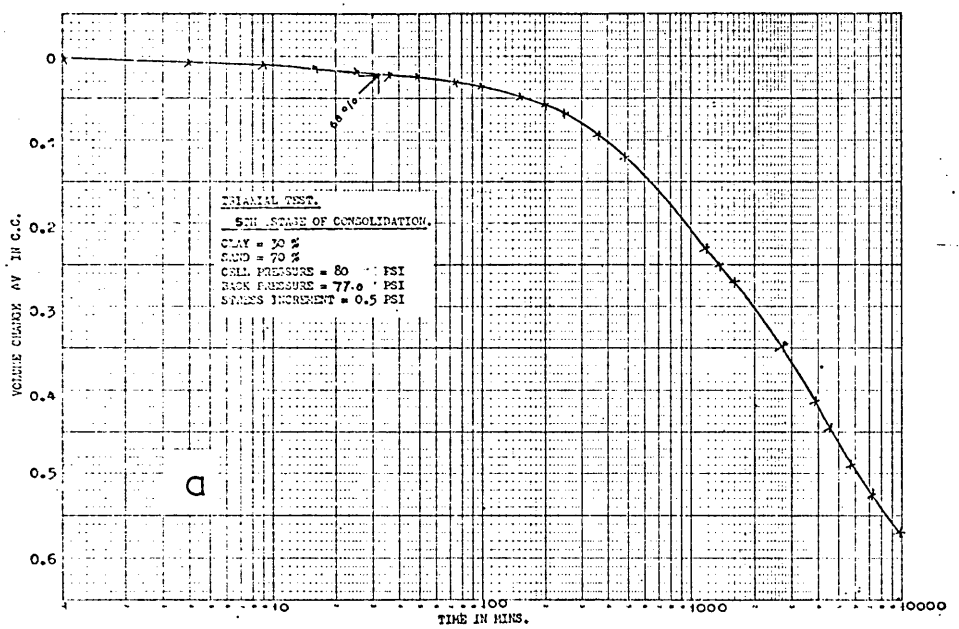

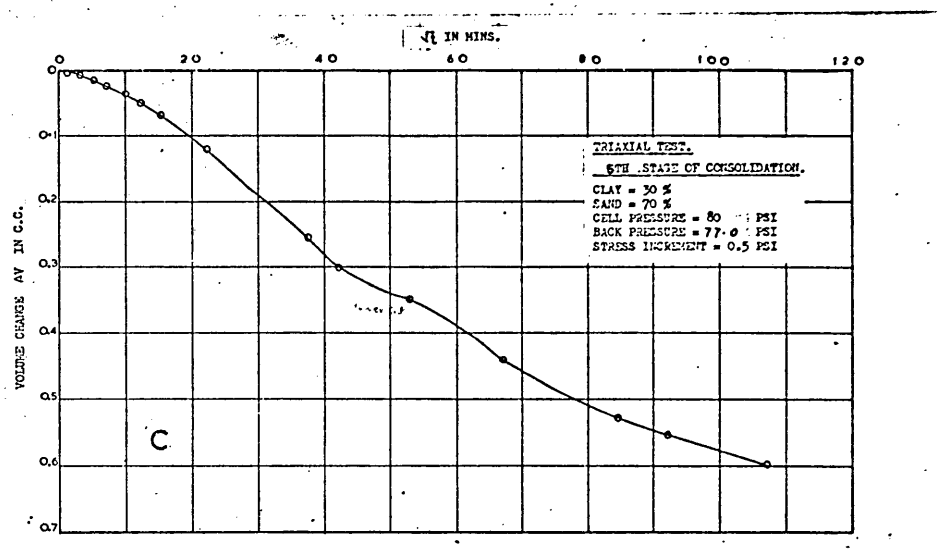

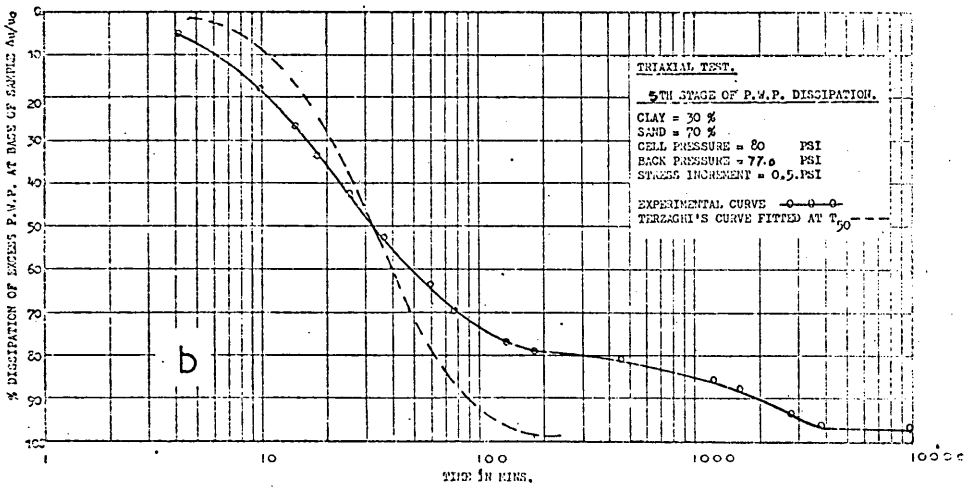

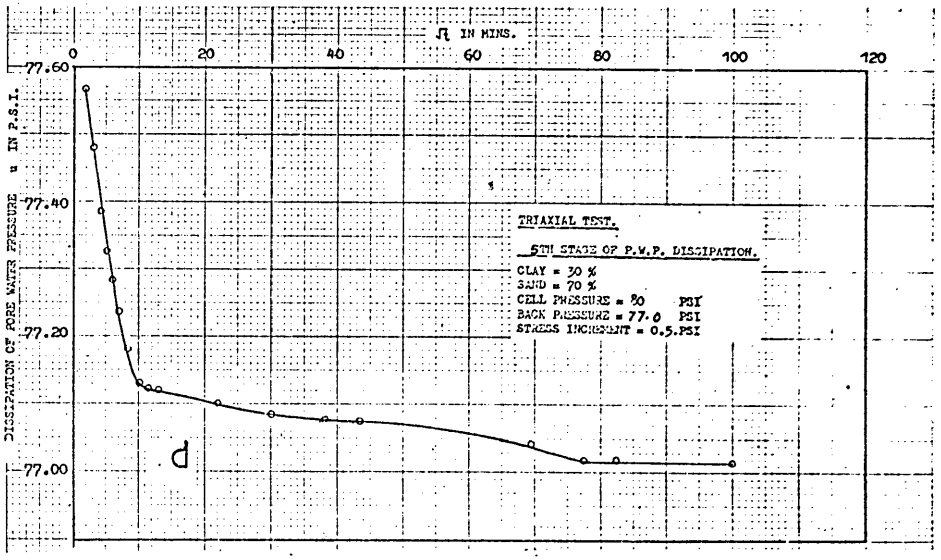

FIG.NO. 4.32 (5th. Stage)

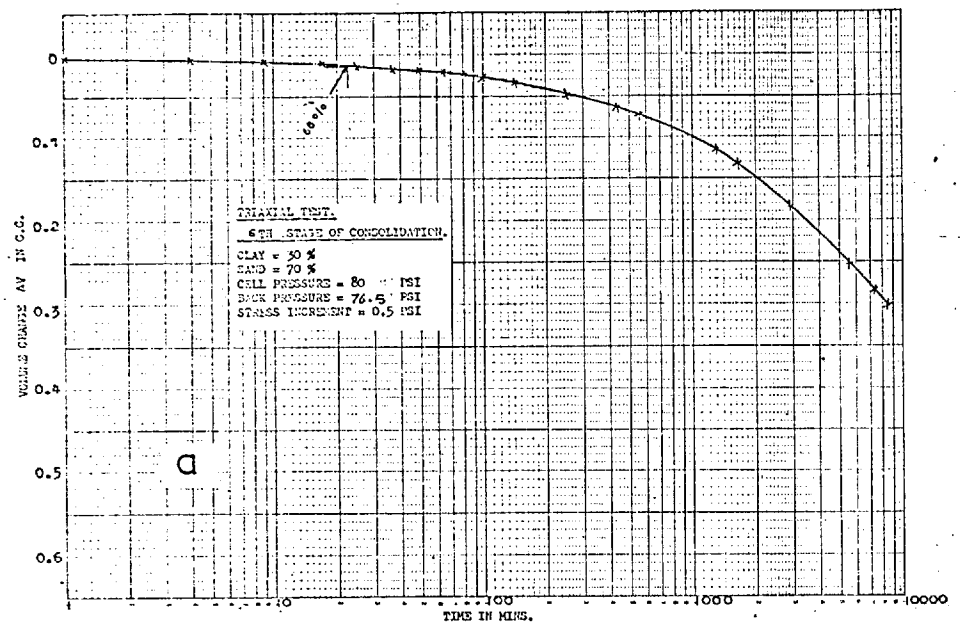

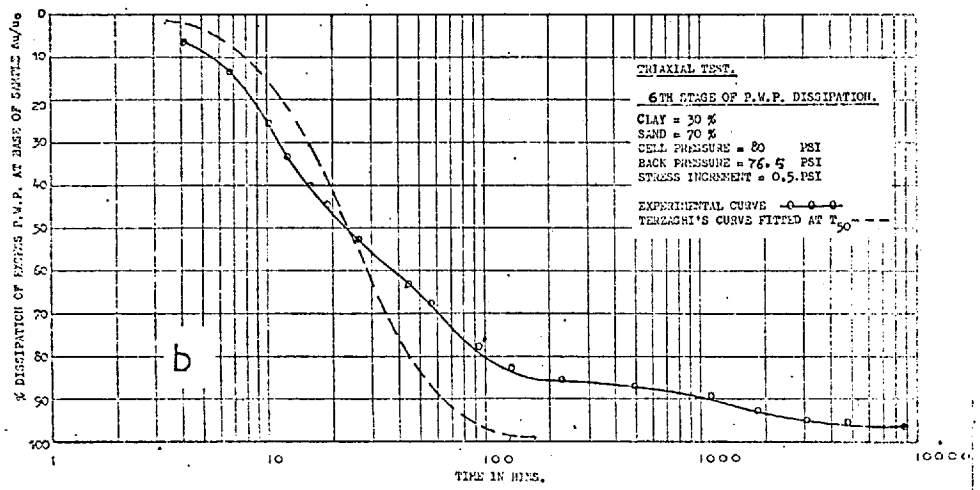

FIG. NO. 4. 33 (6th. Stage)

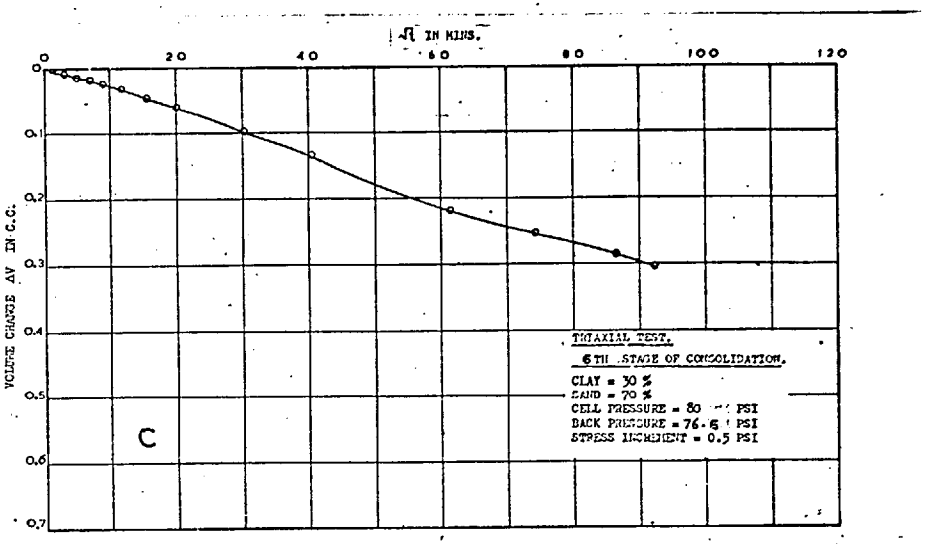

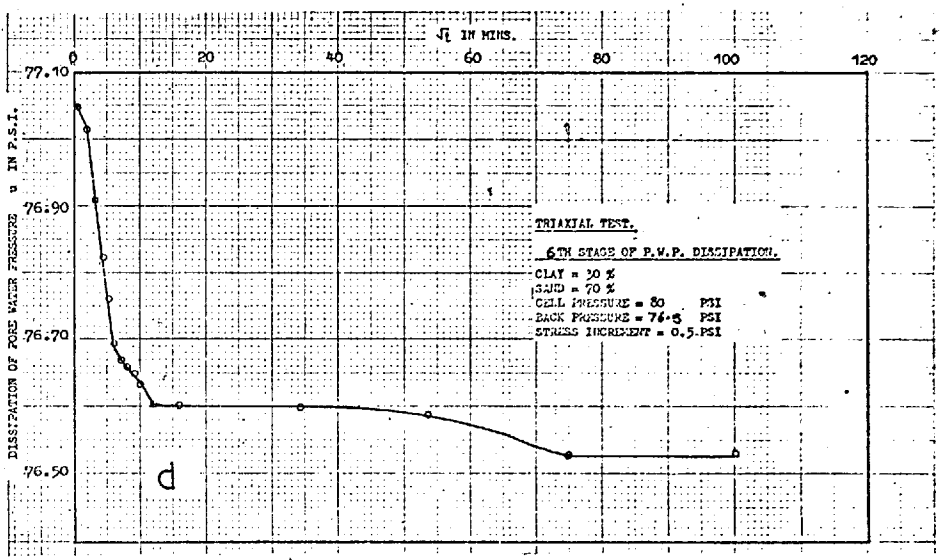

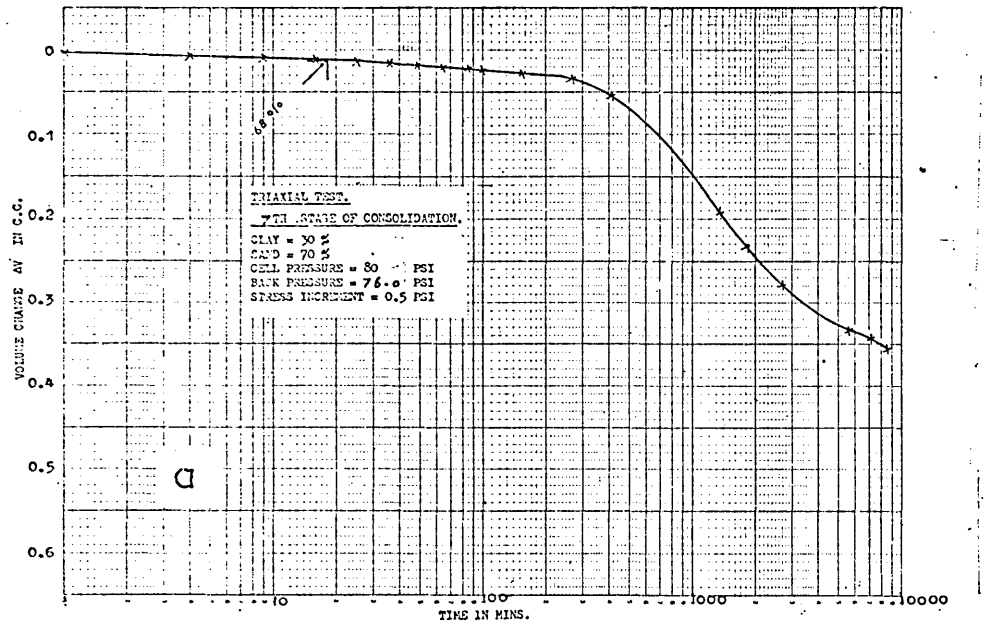

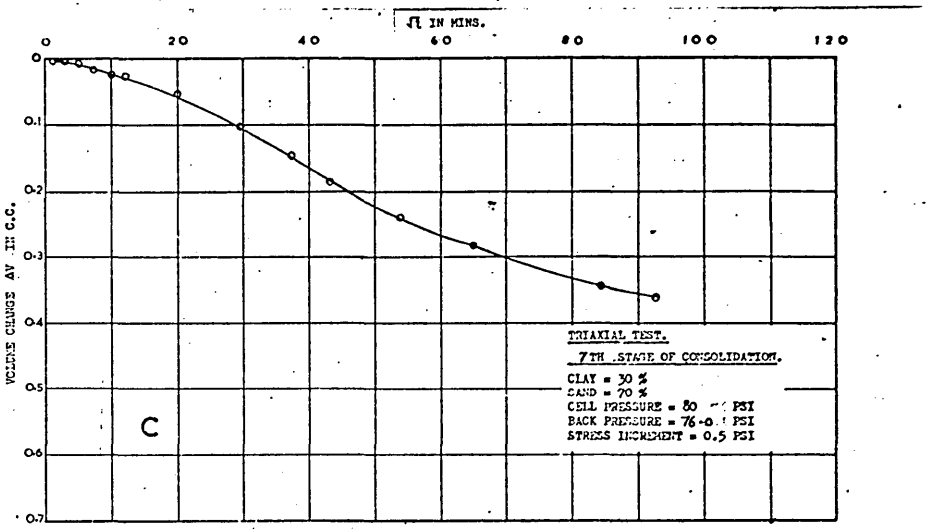

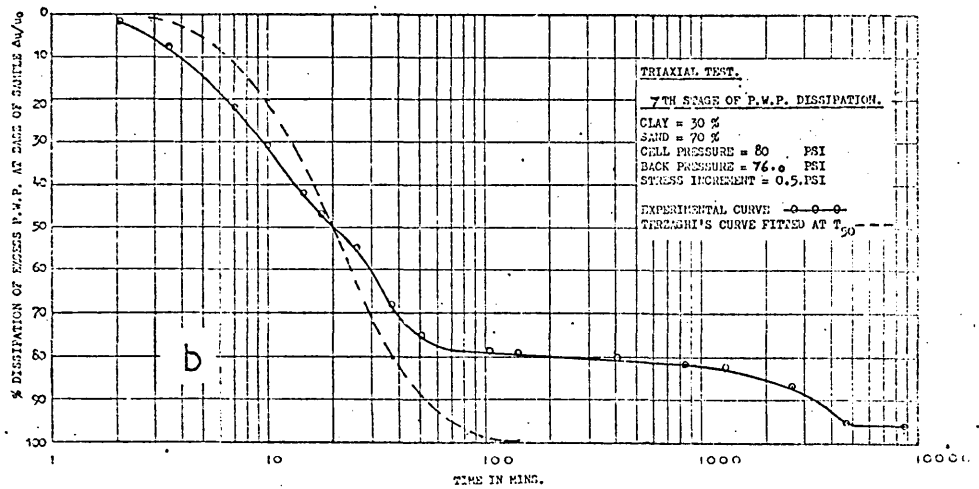

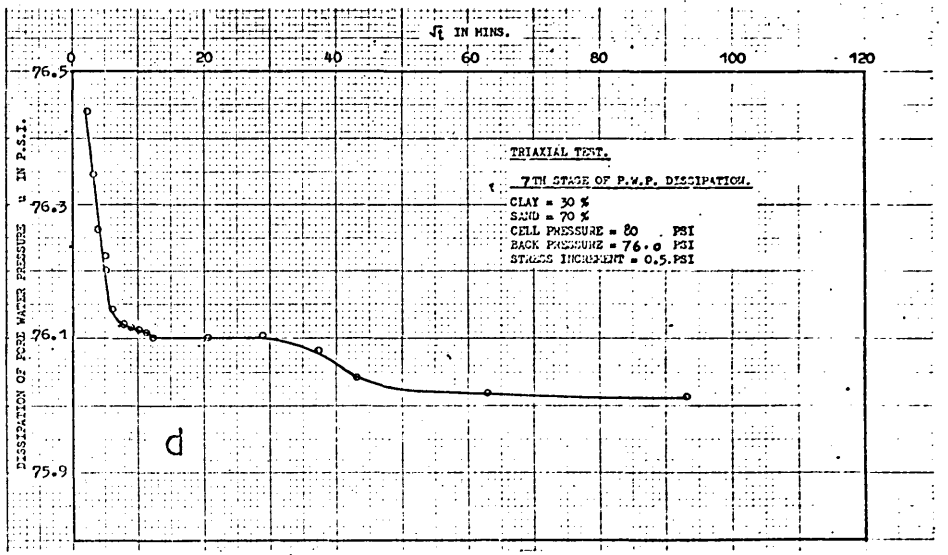

FIG. NO. 4.34 (7th. Stage)

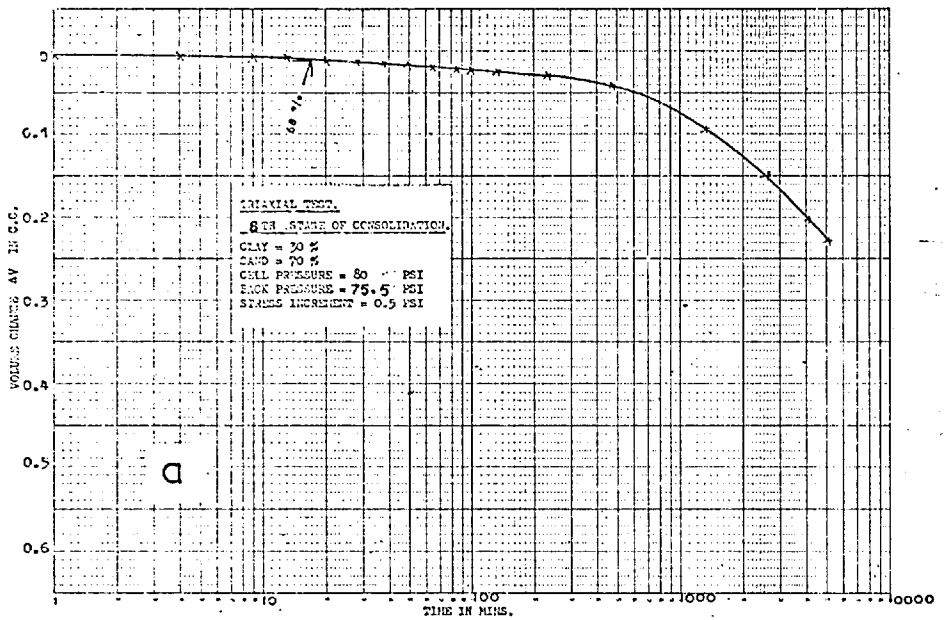

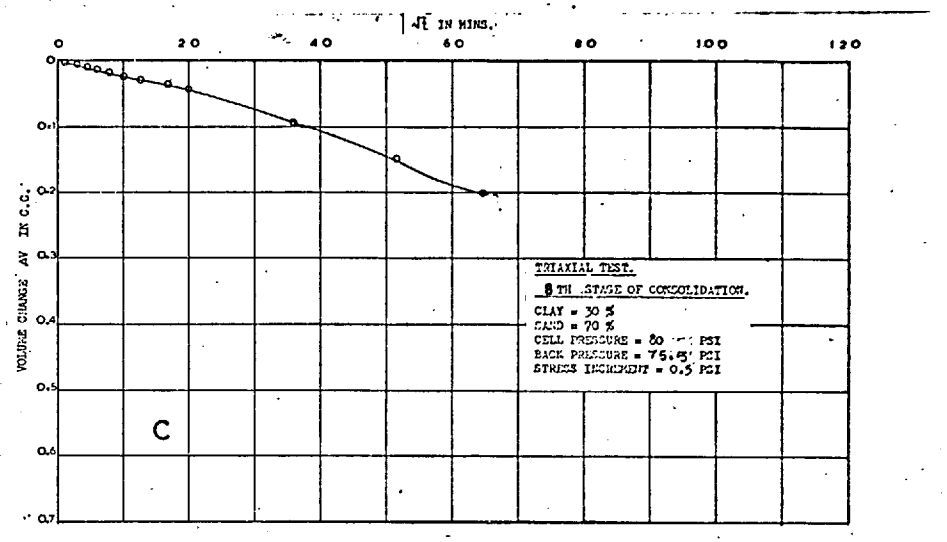

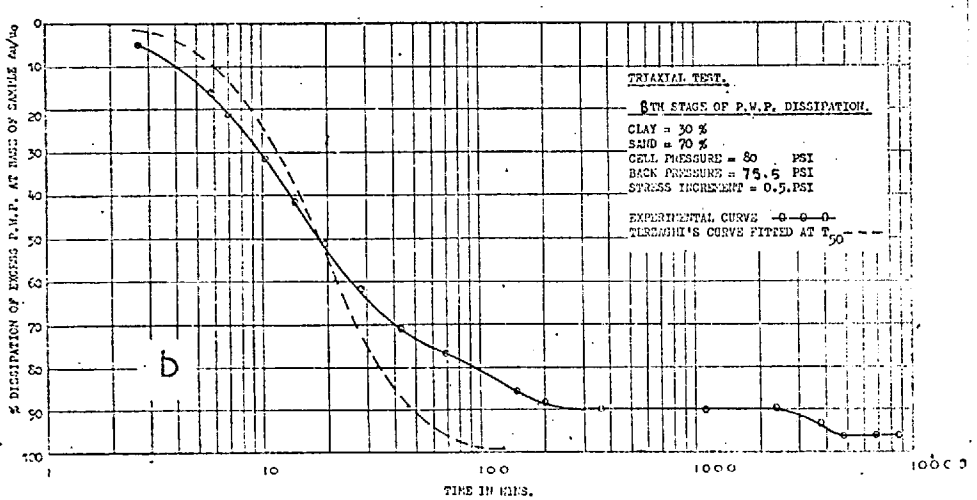

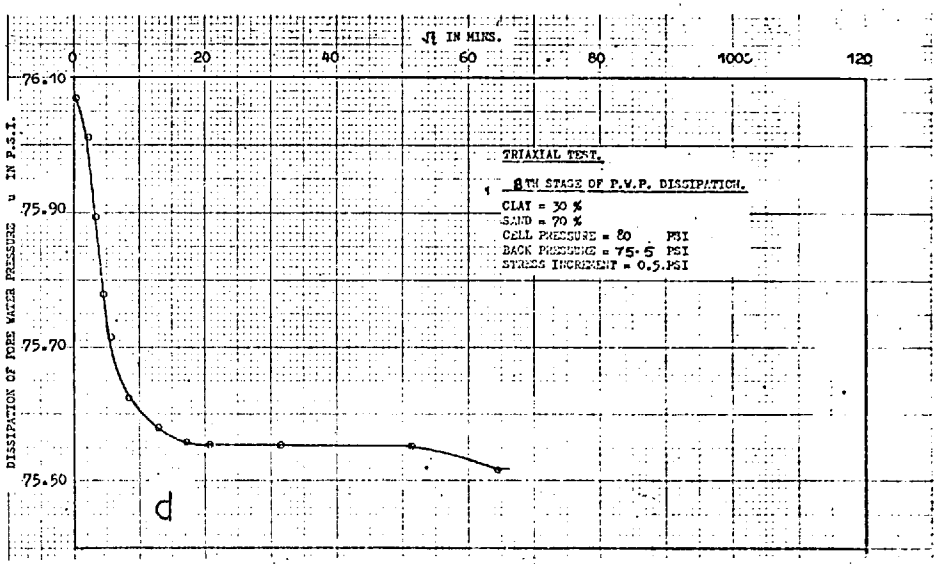

FIG. NO. 4. 35 (8th. Stage)

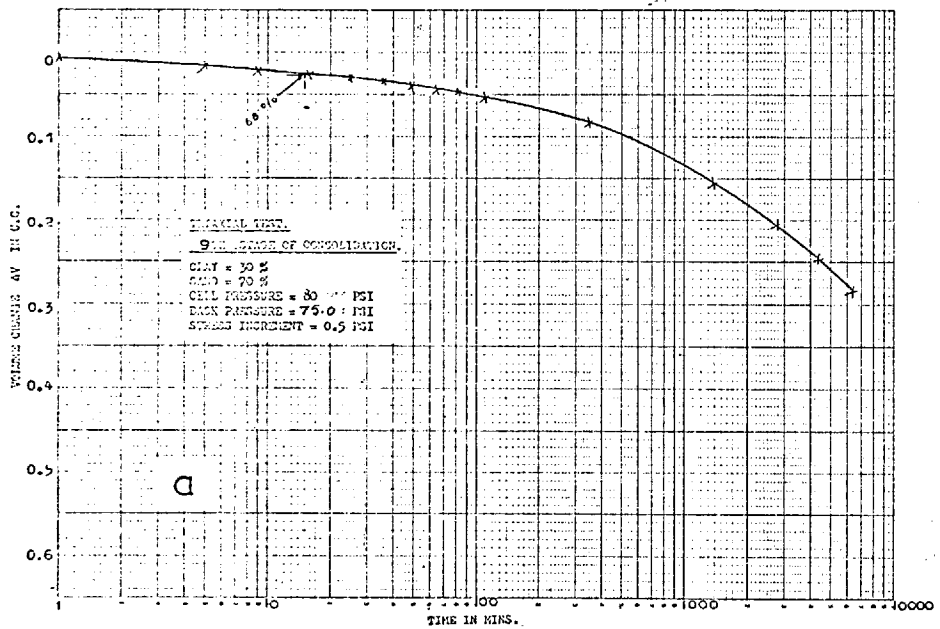

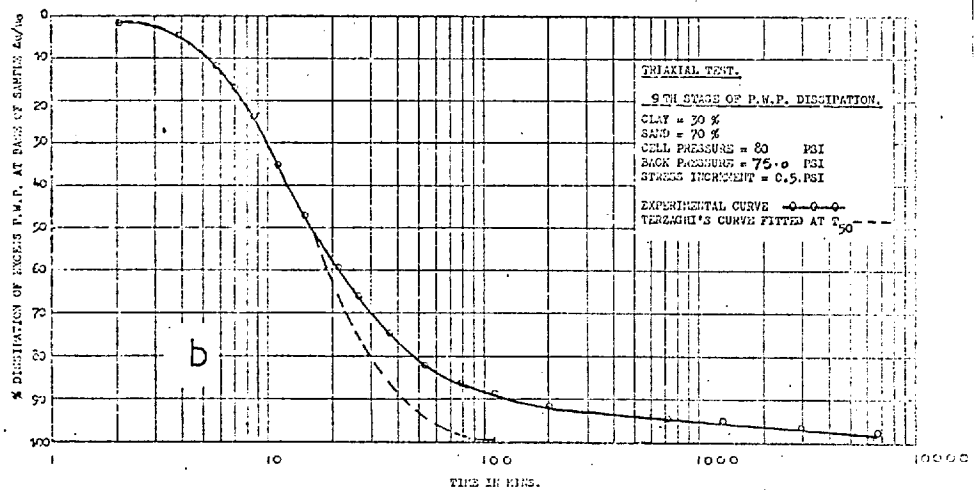

FIG.NO.4.36 (9th. Stage)

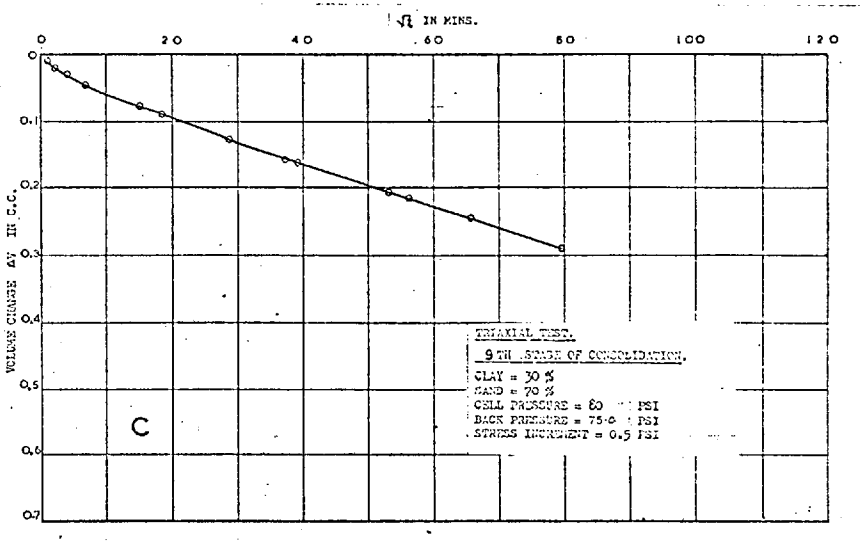

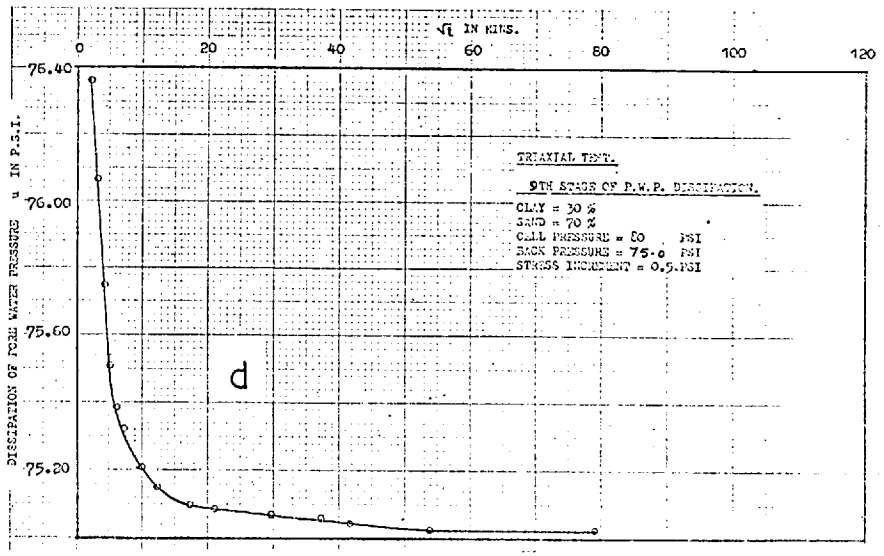

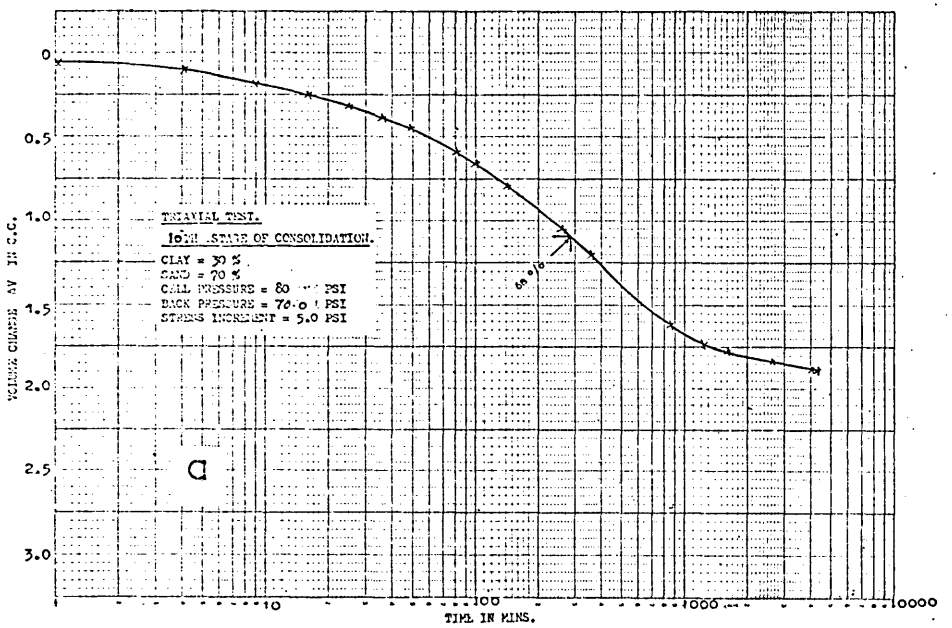

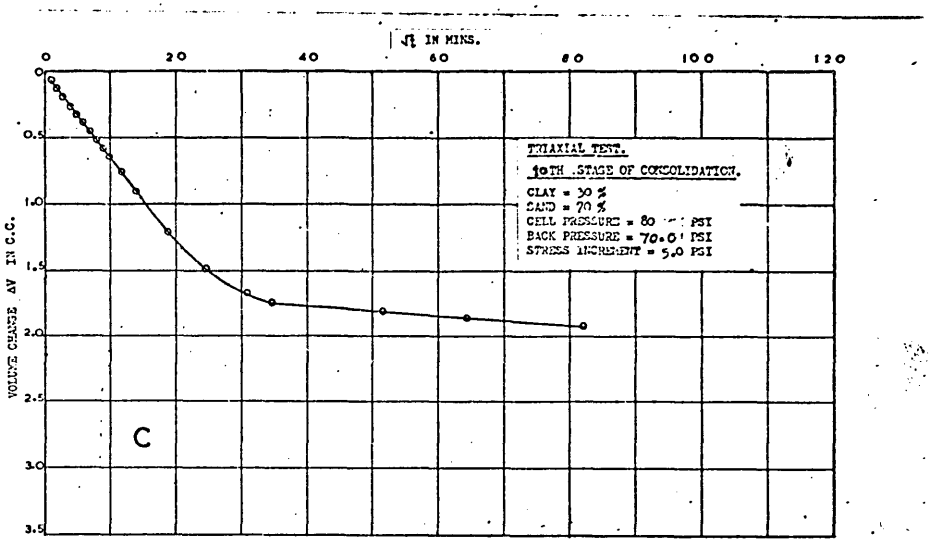

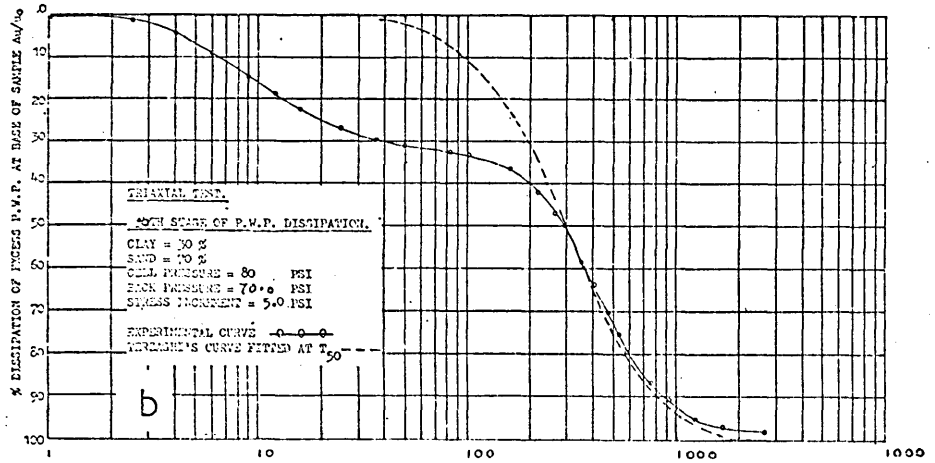

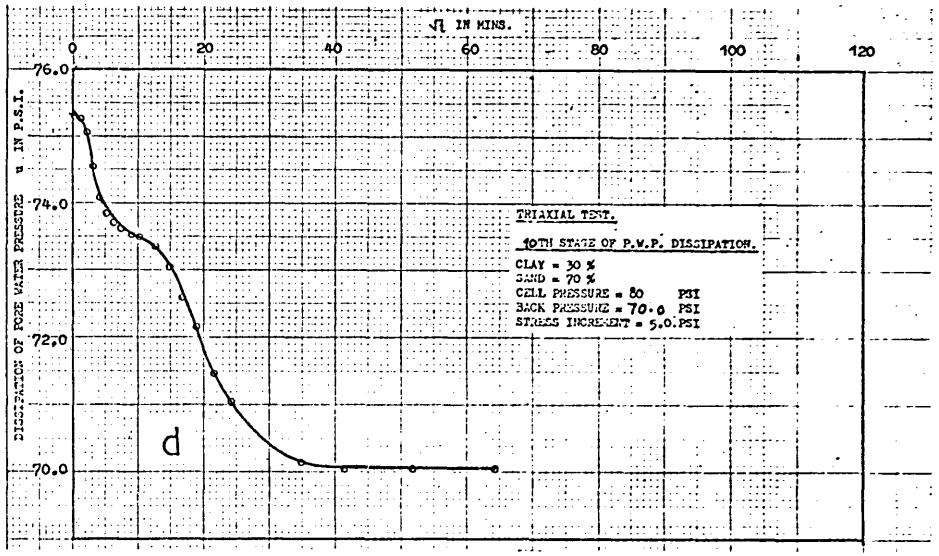

FIG. NO. 4.37 (10th. Stage)

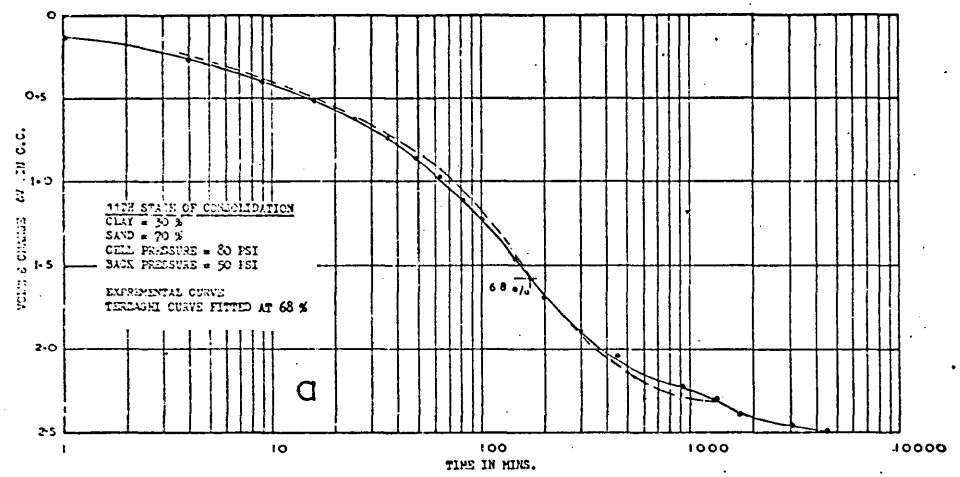

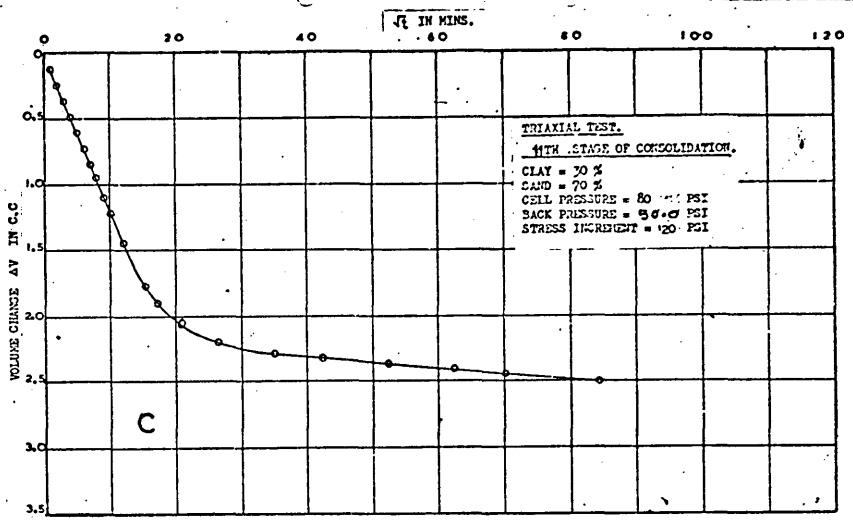

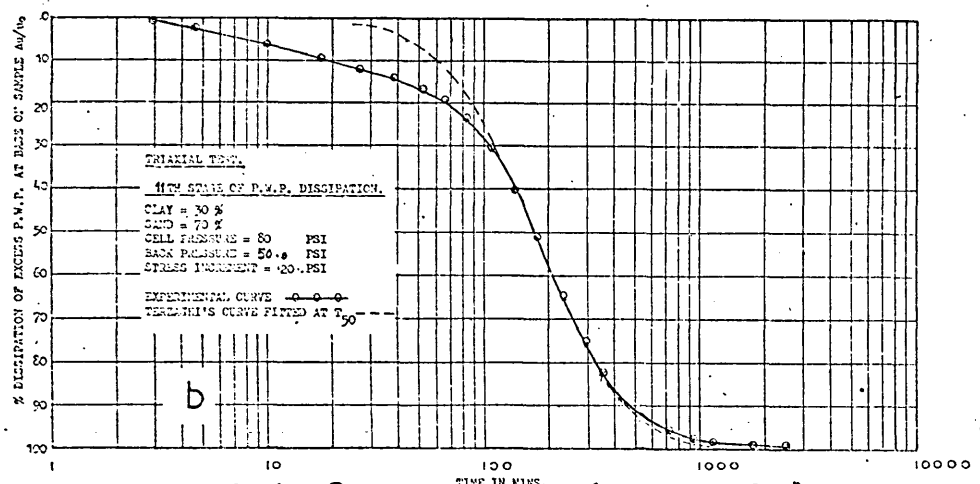

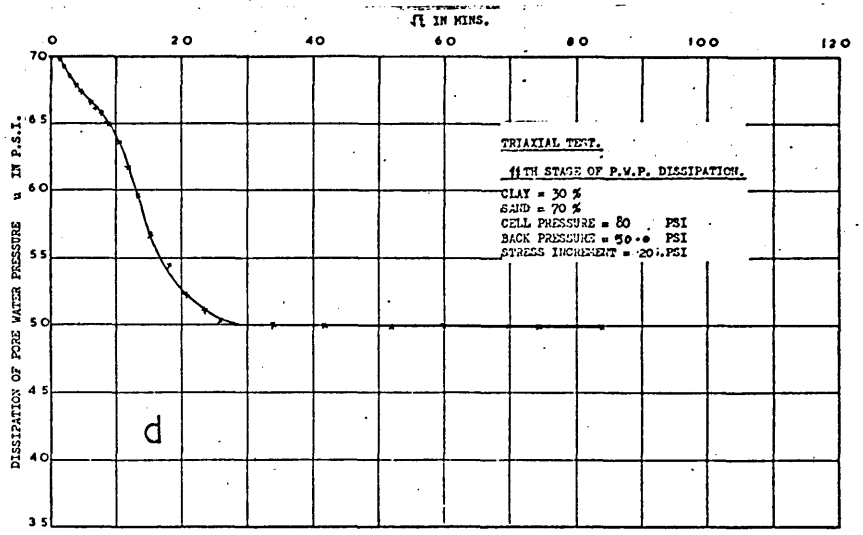

FIG.NO.4.38 (11th. Stage)

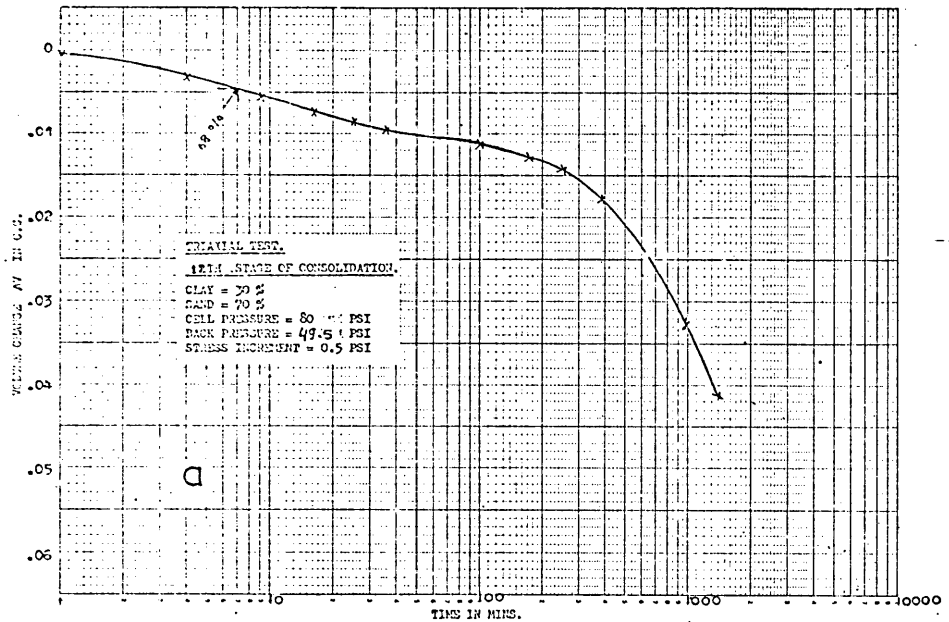

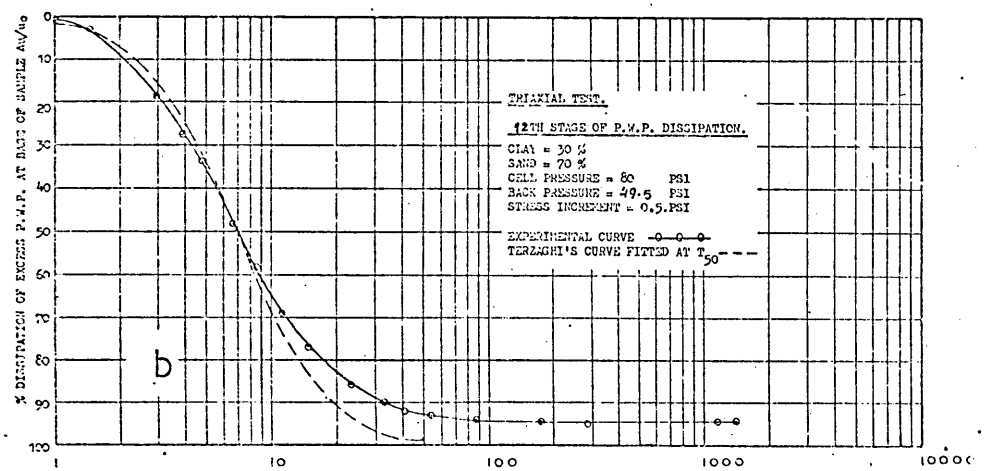

FIG.NO. 4.39 (12th. Stage)

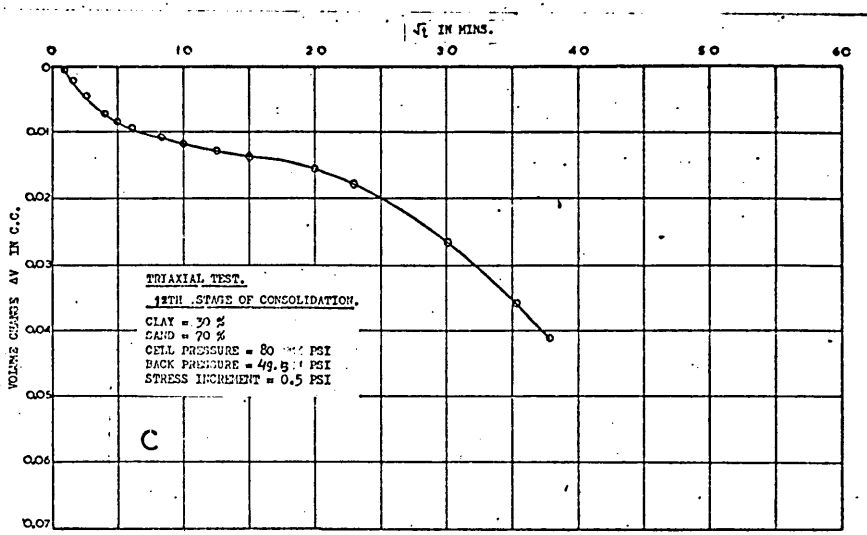

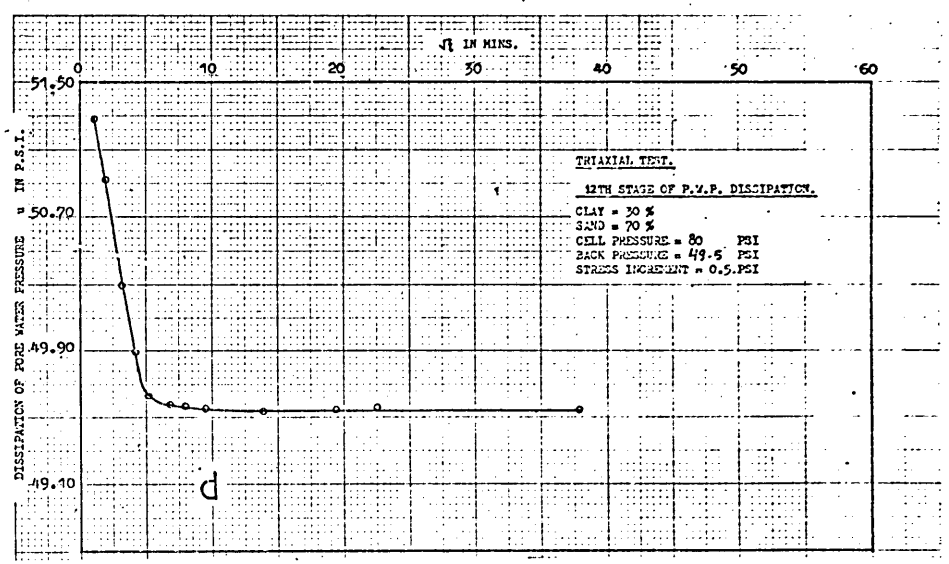

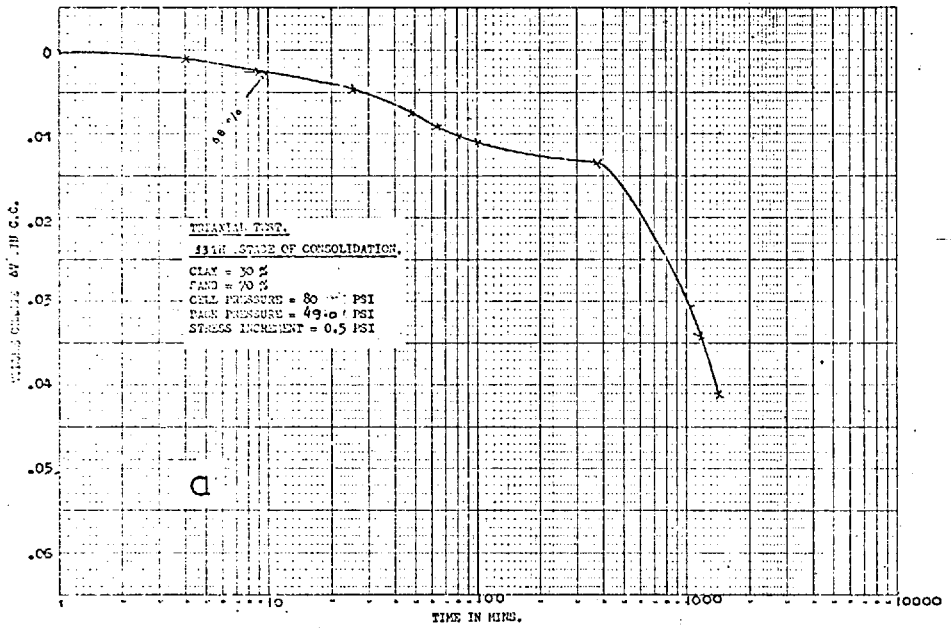

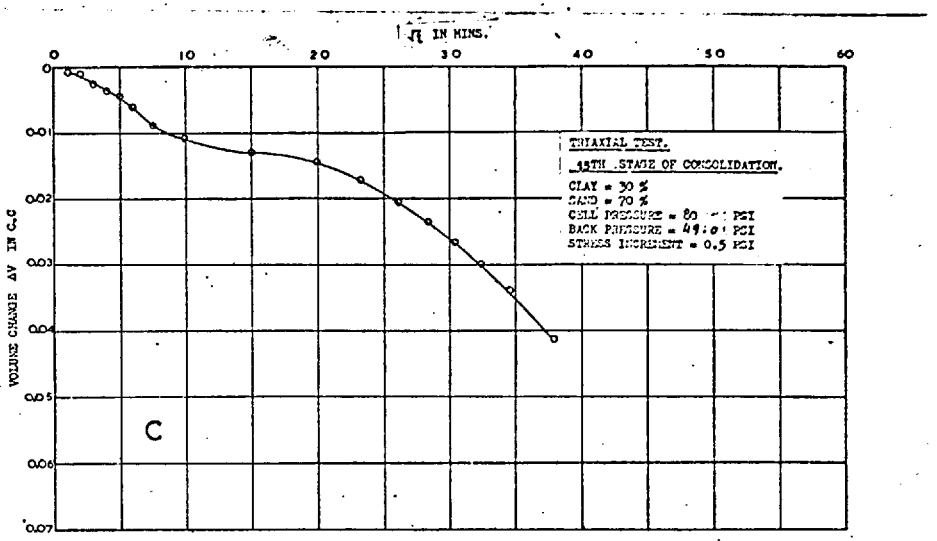

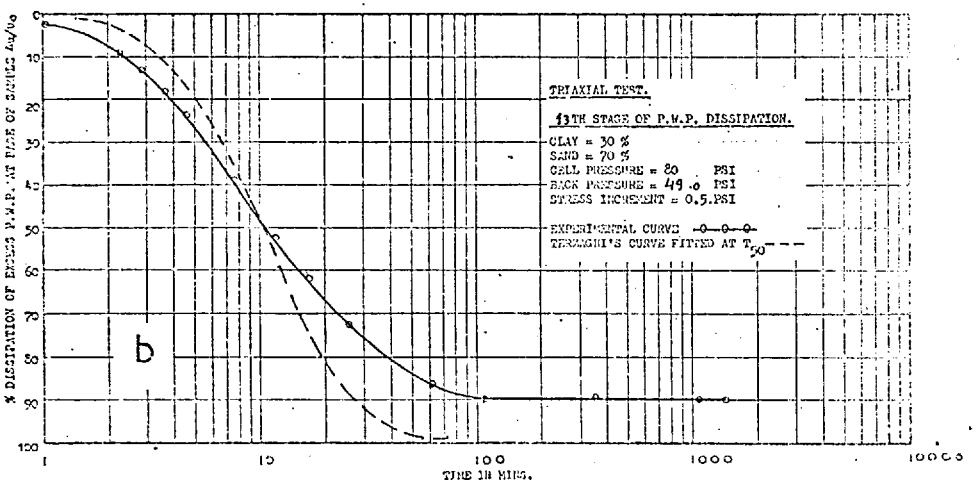

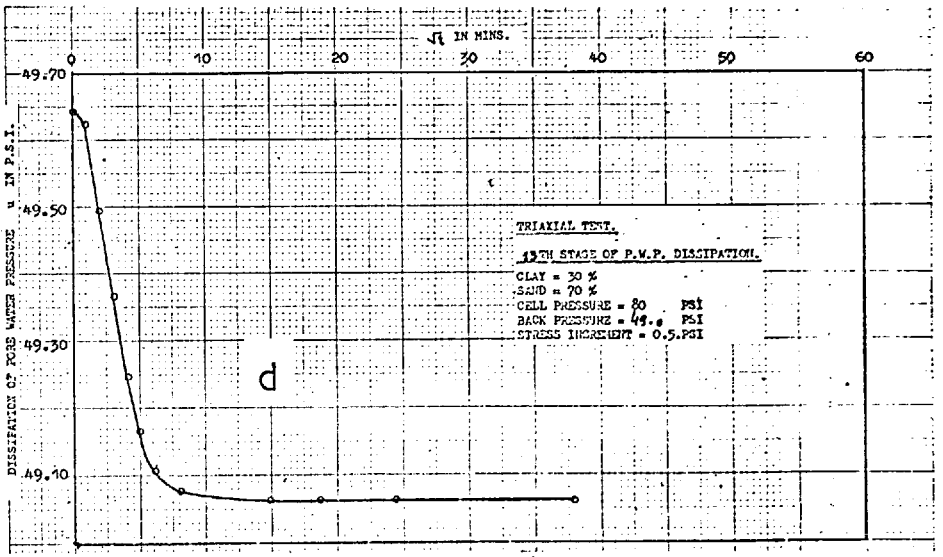

FIG. NO. 4. 40 (13th. Stage)

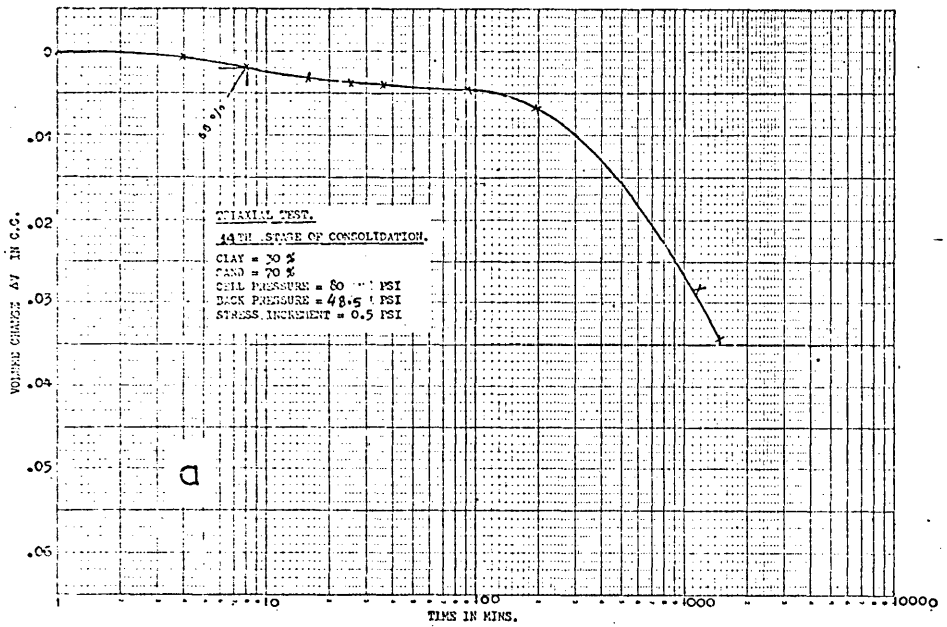

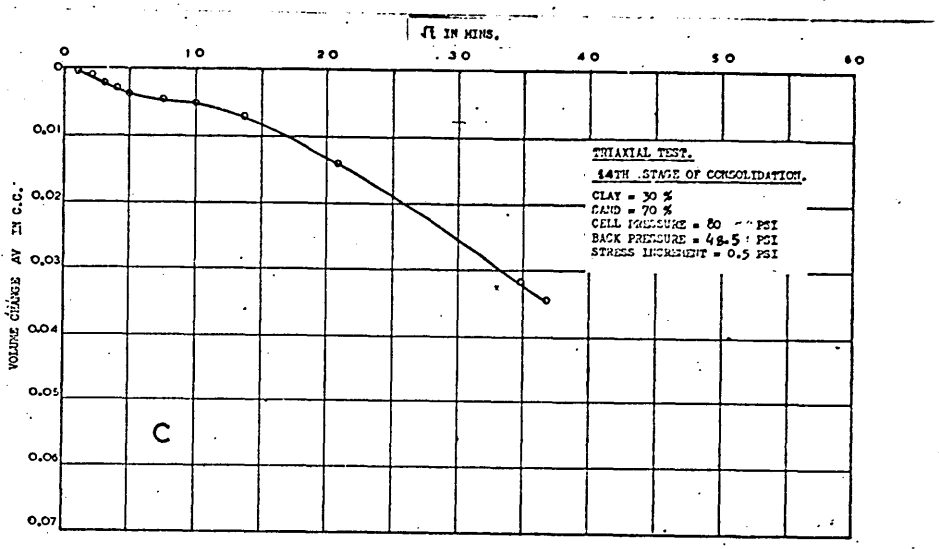

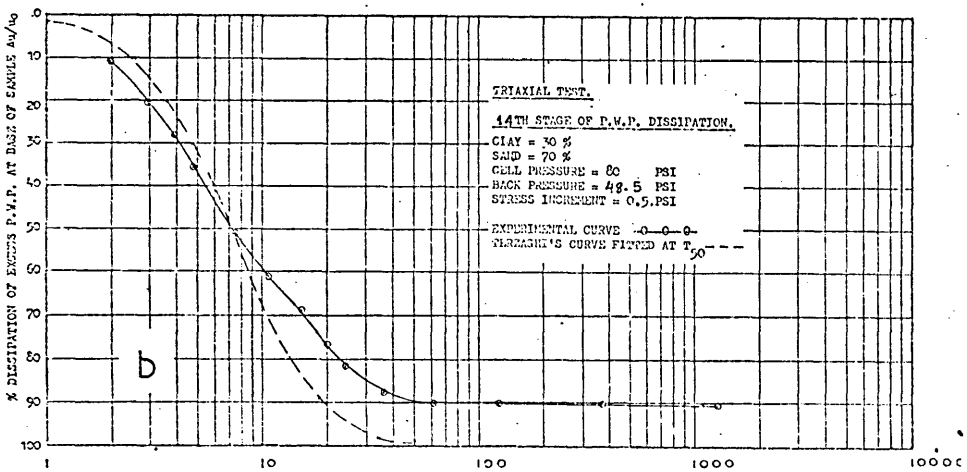

FIG.NO. 4.41 (14th. Stage)

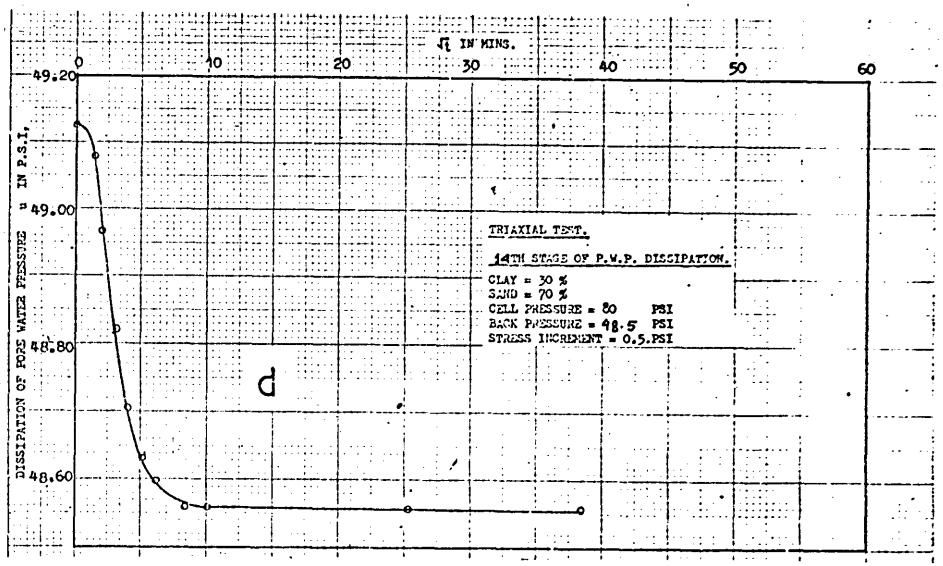

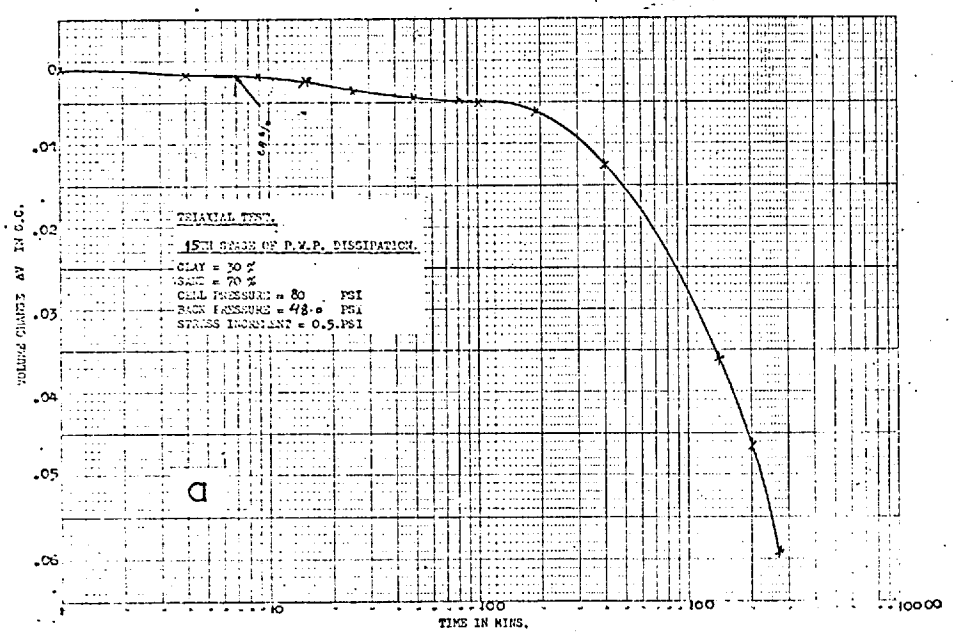

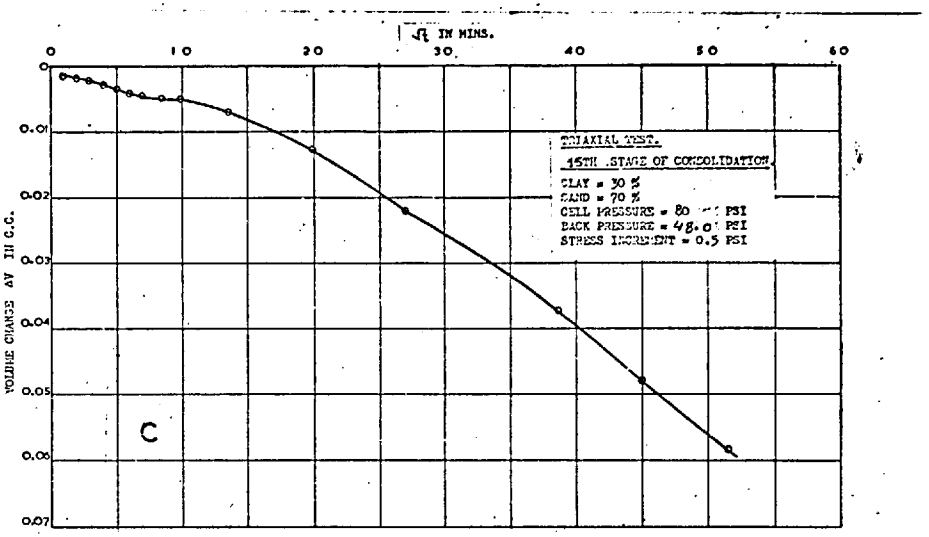

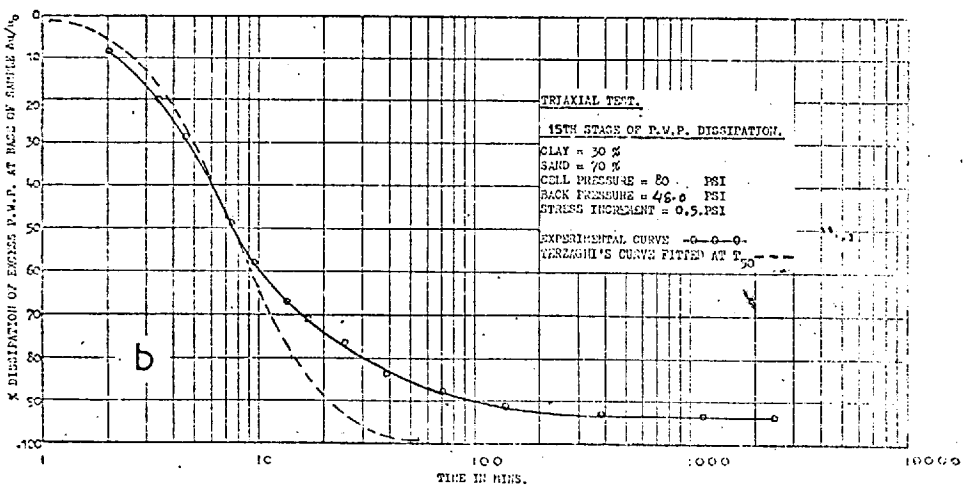

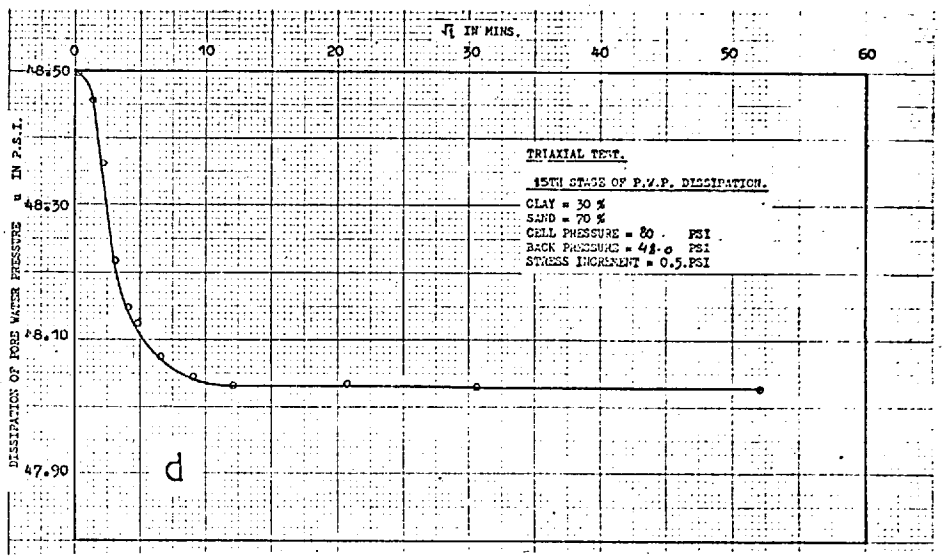

FIG. NO. 4. 42 (15th. Stage)

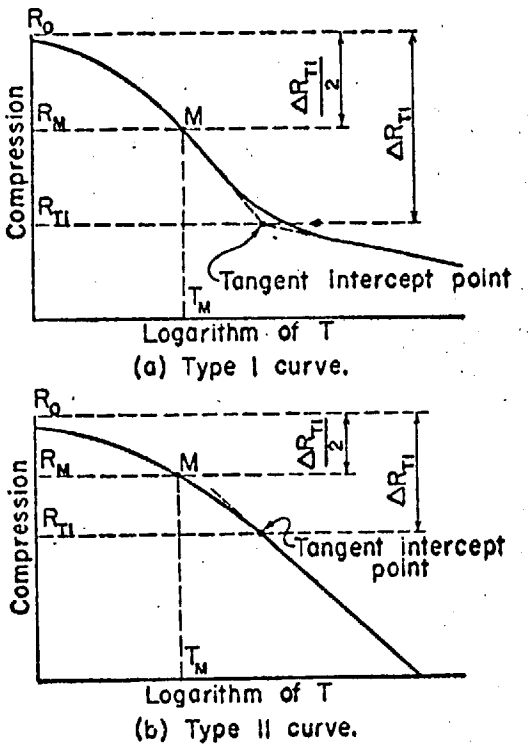

(i) –POSITION OF TANGENT INTERCEPT POINT

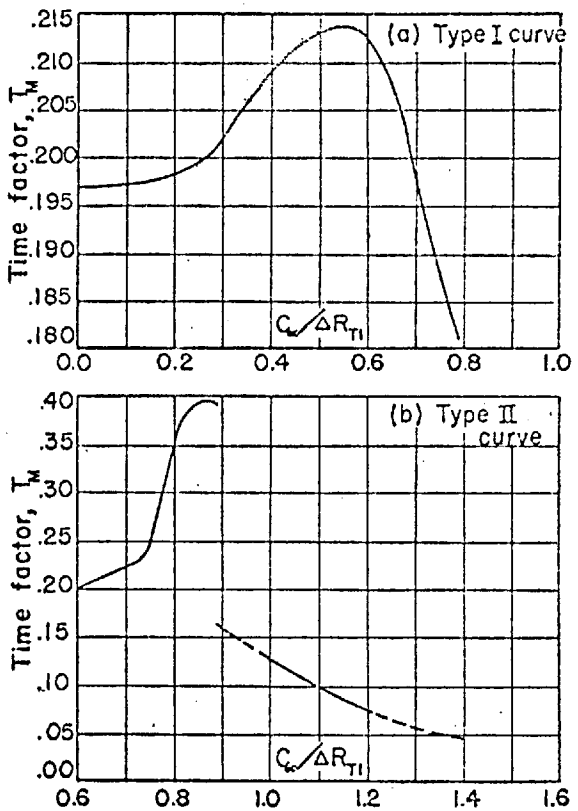

(ii) –TIME FACTOR, T_M, VERSUS $C_\alpha/\Delta R_{TI}$

FIGURE NO: 4.43. CURVE-FITTING METHOD. (AFTER WAHLS, 1962)

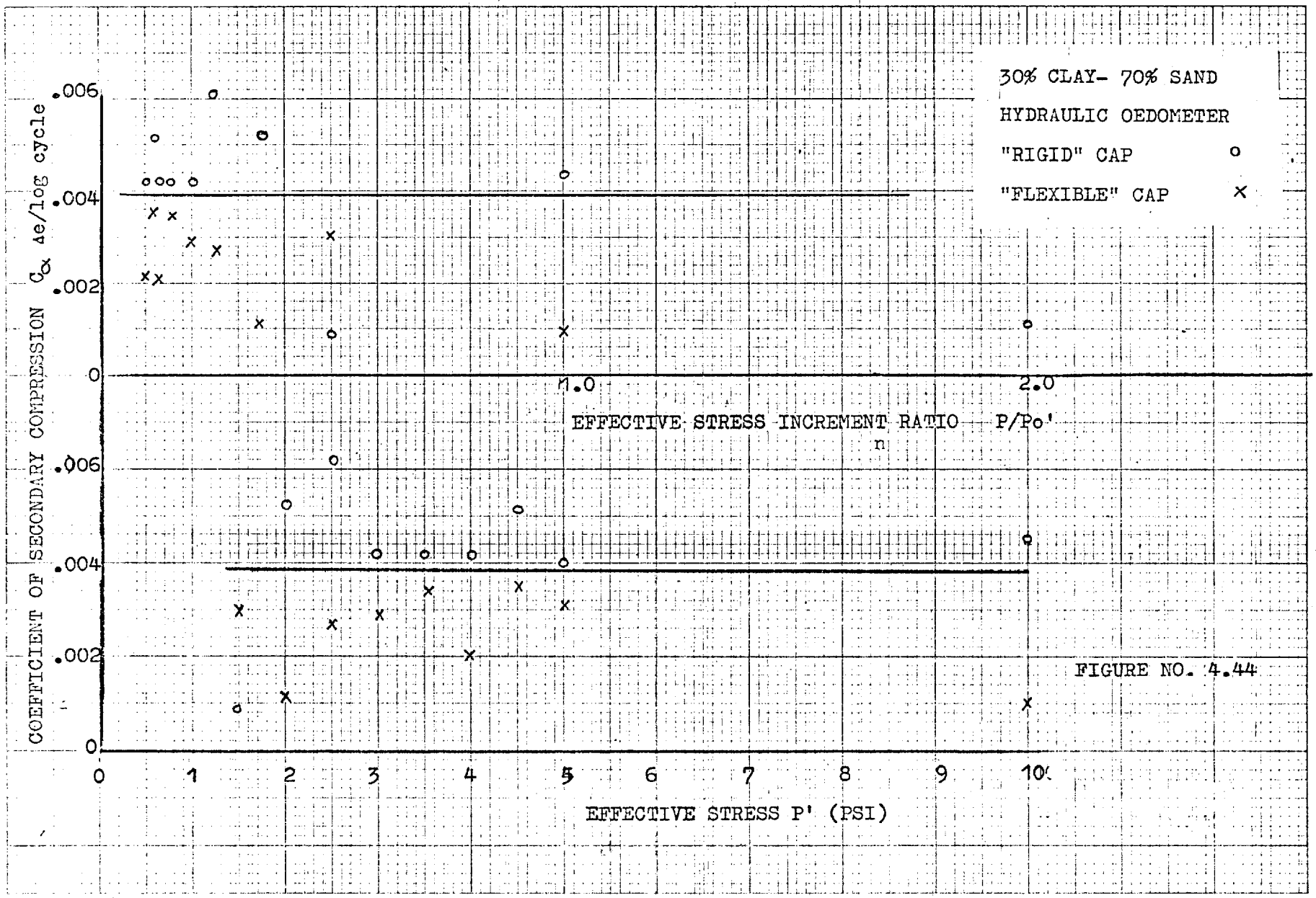

FIGURE NO. 4.44

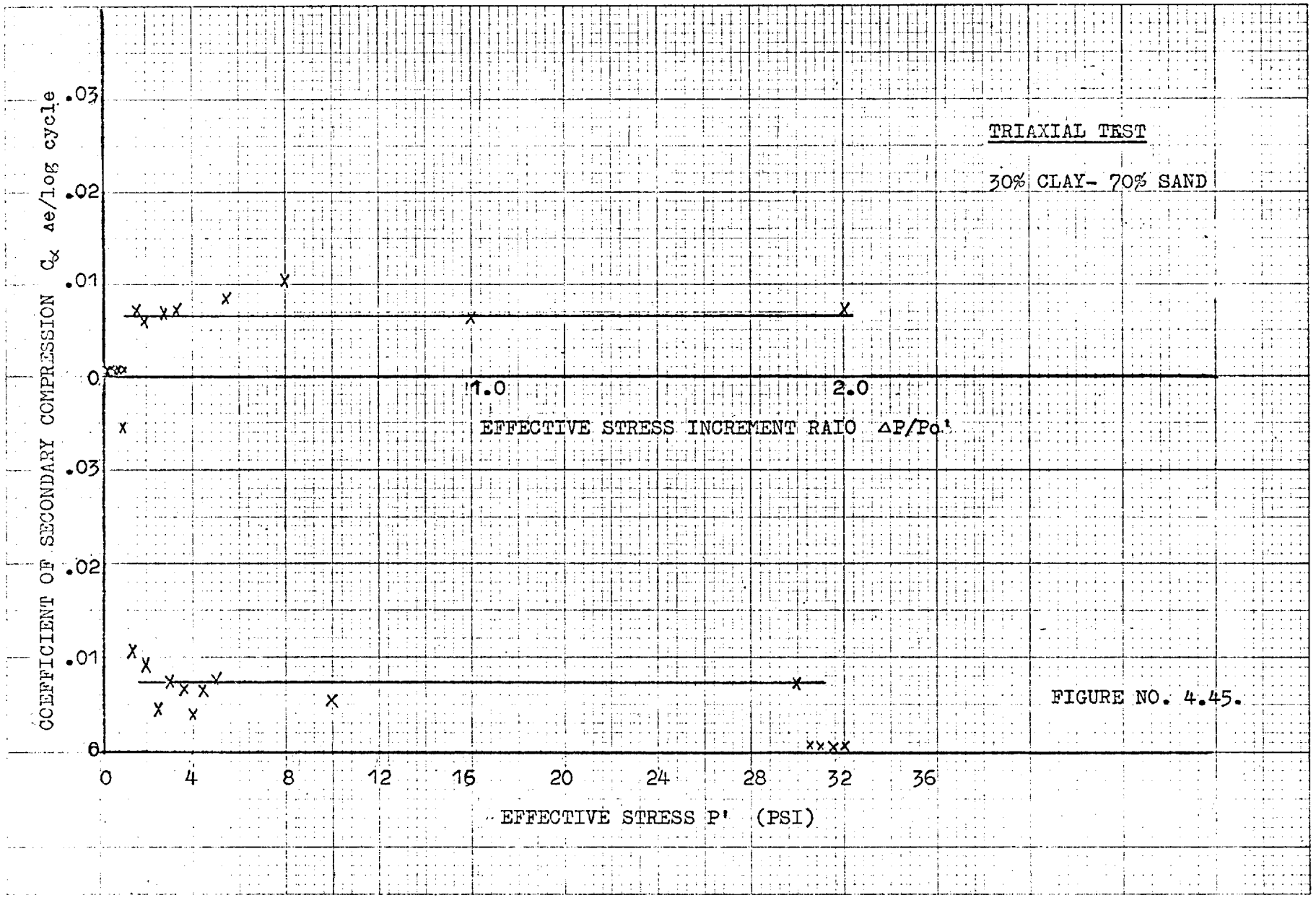

FIGURE NO. 4.45.

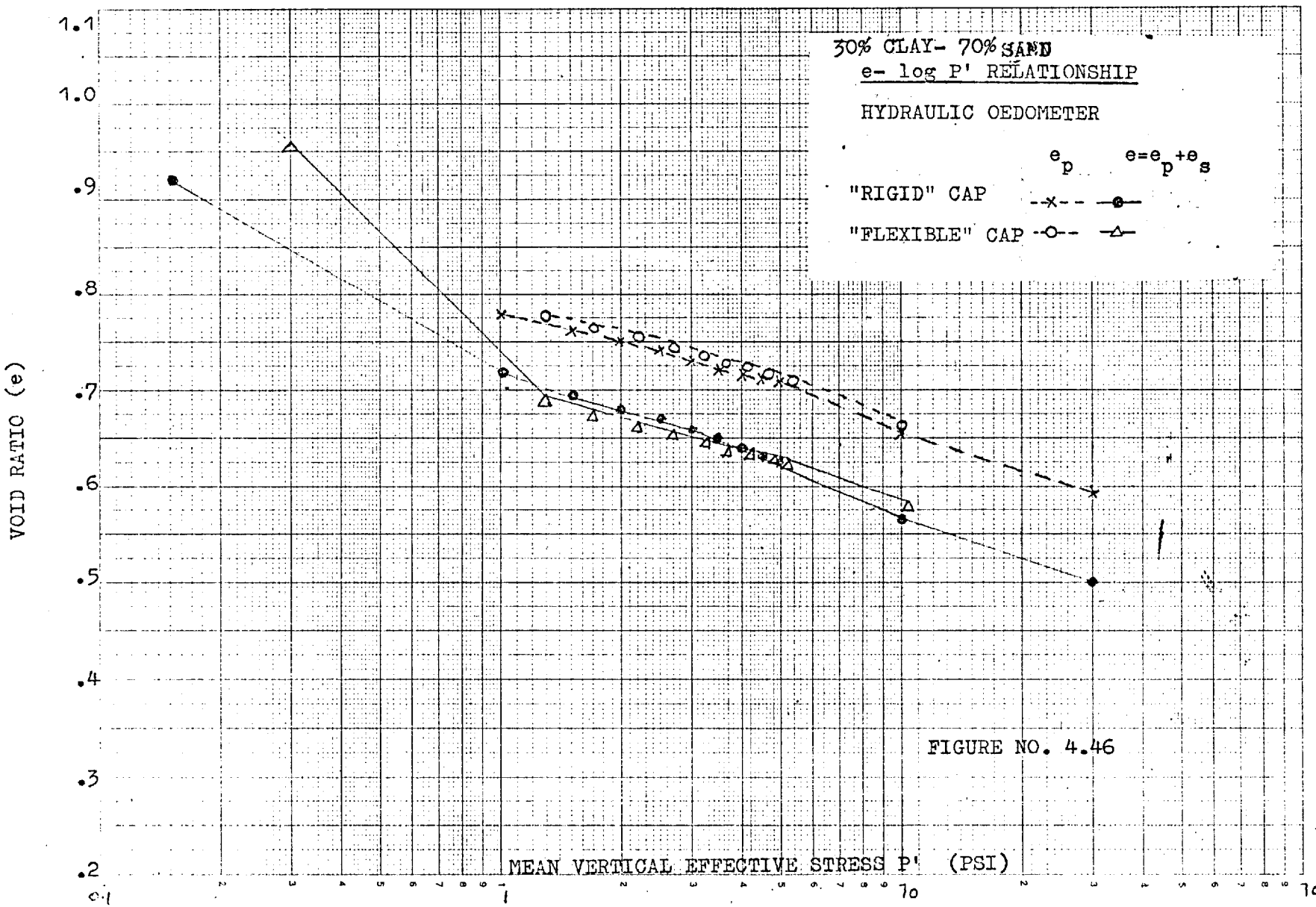

FIGURE NO. 4.46

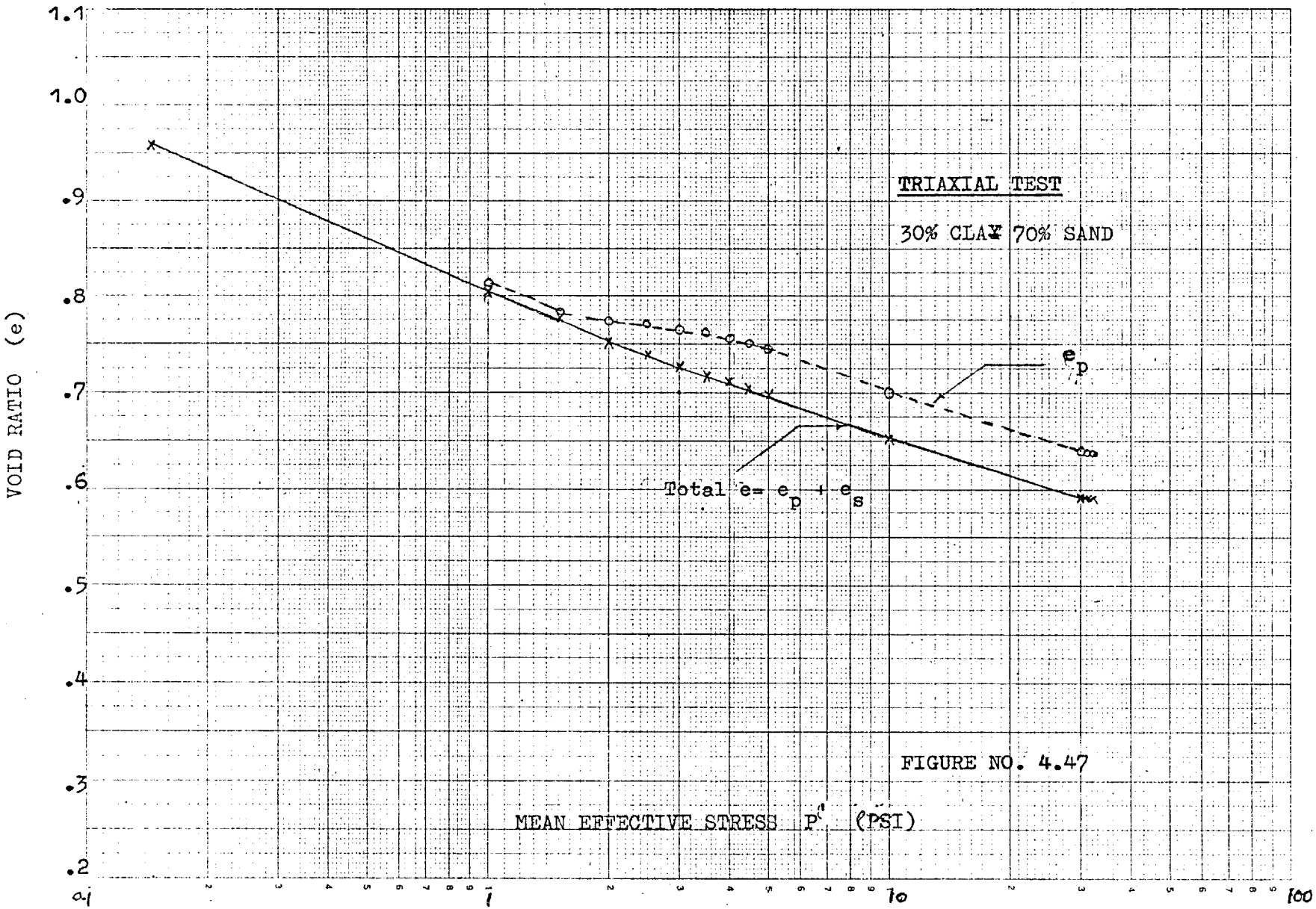

FIGURE NO. 4.47

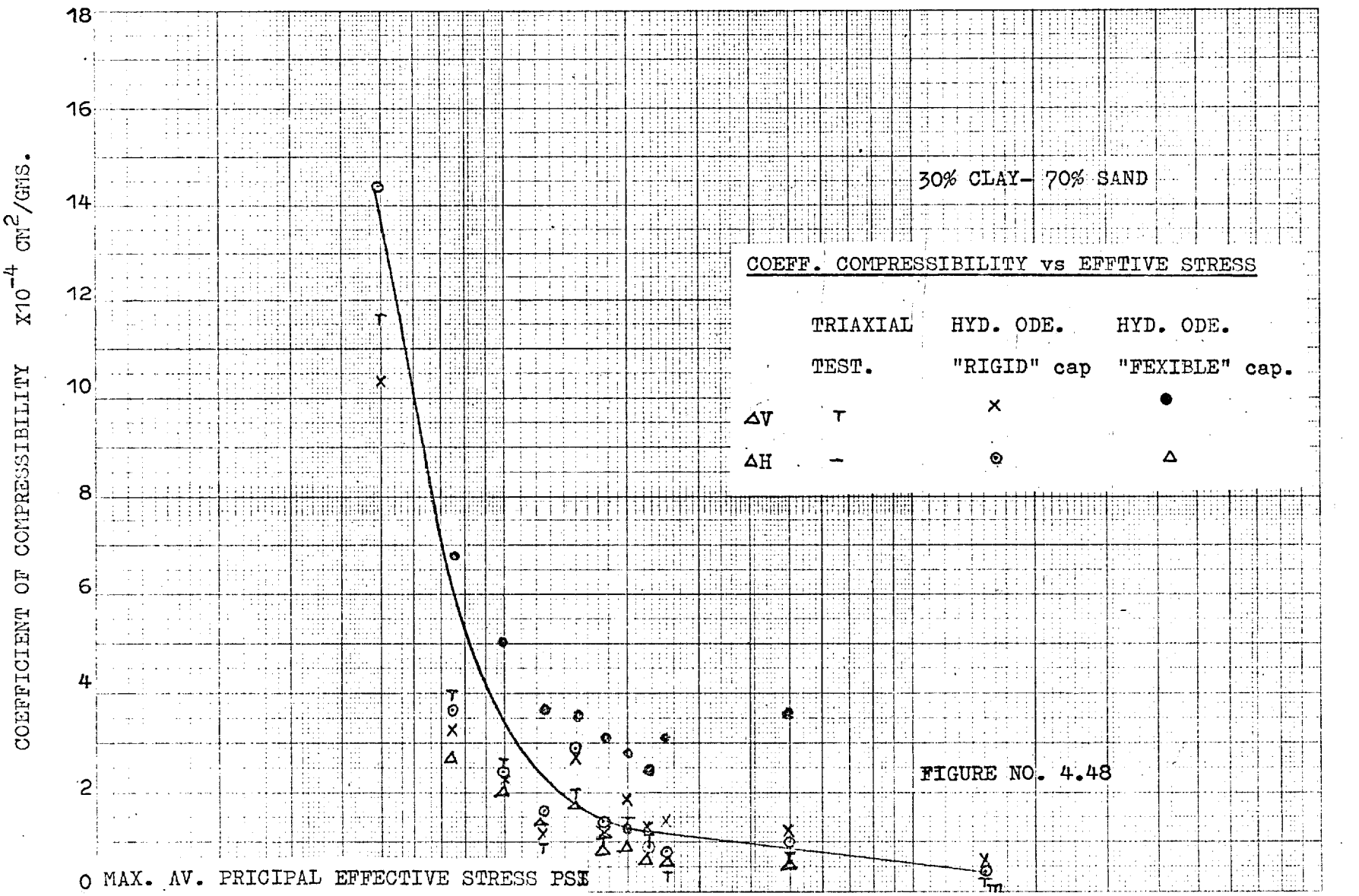

FIGURE NO. 4.48

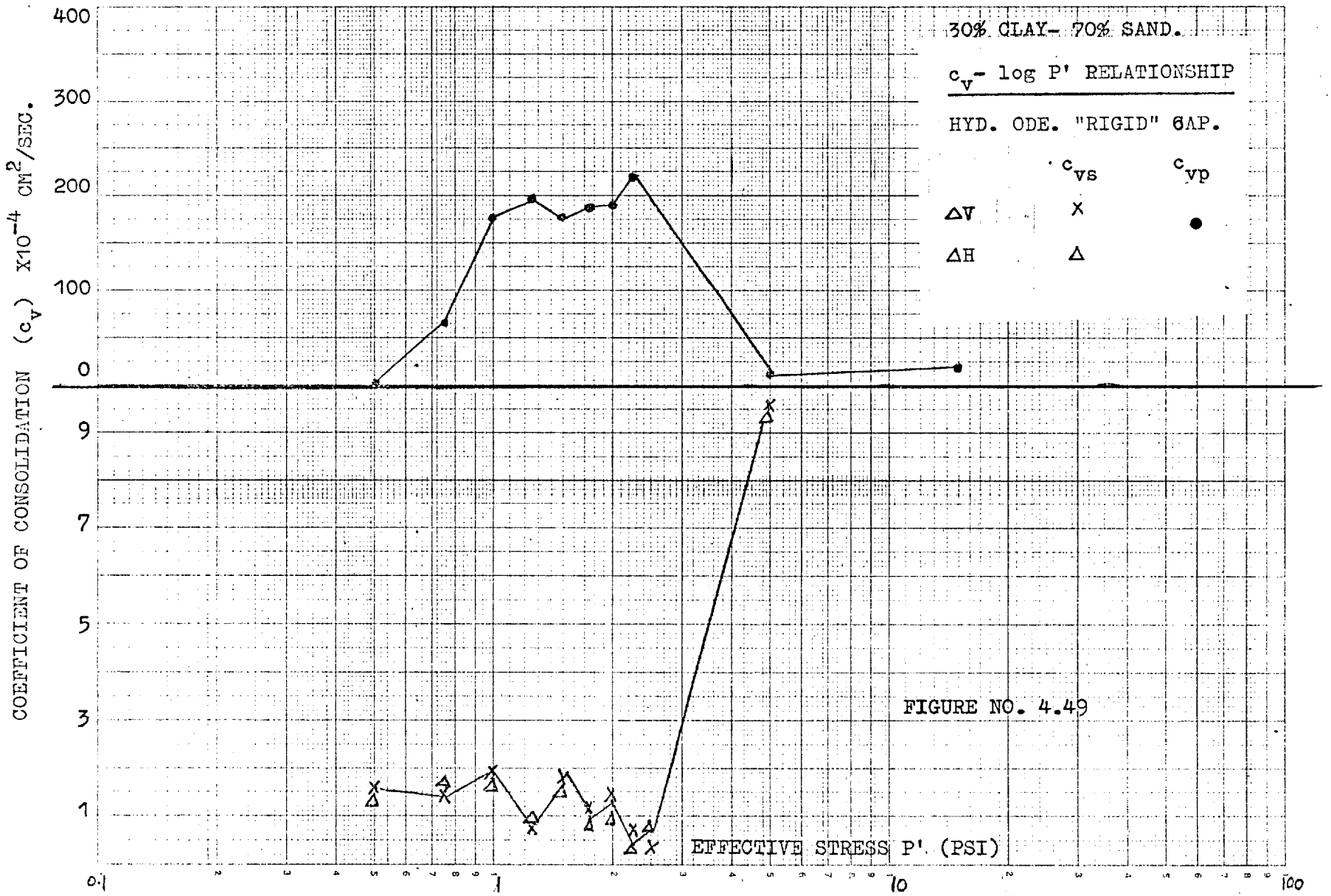

FIGURE NO. 4.49

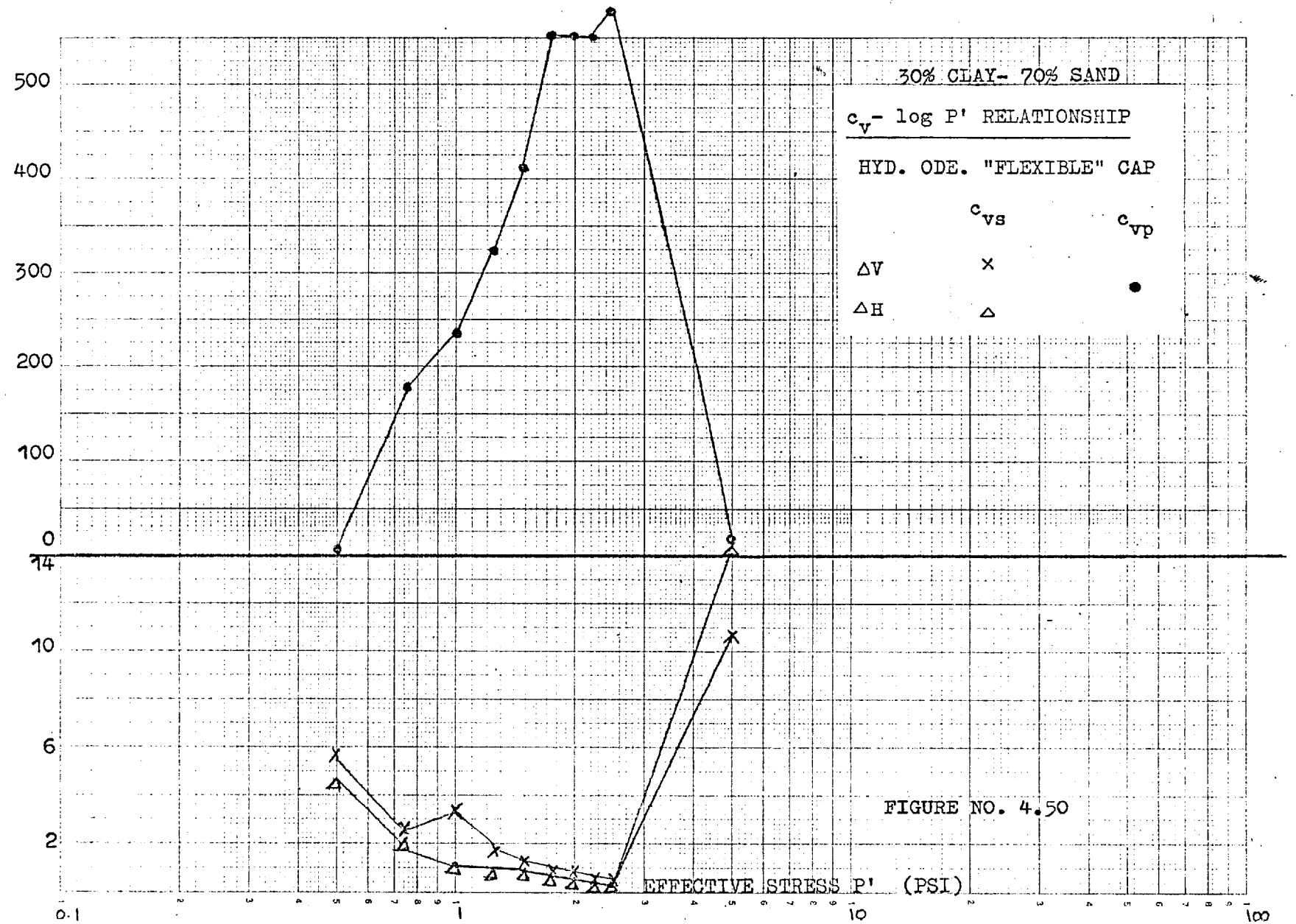

FIGURE NO. 4.50

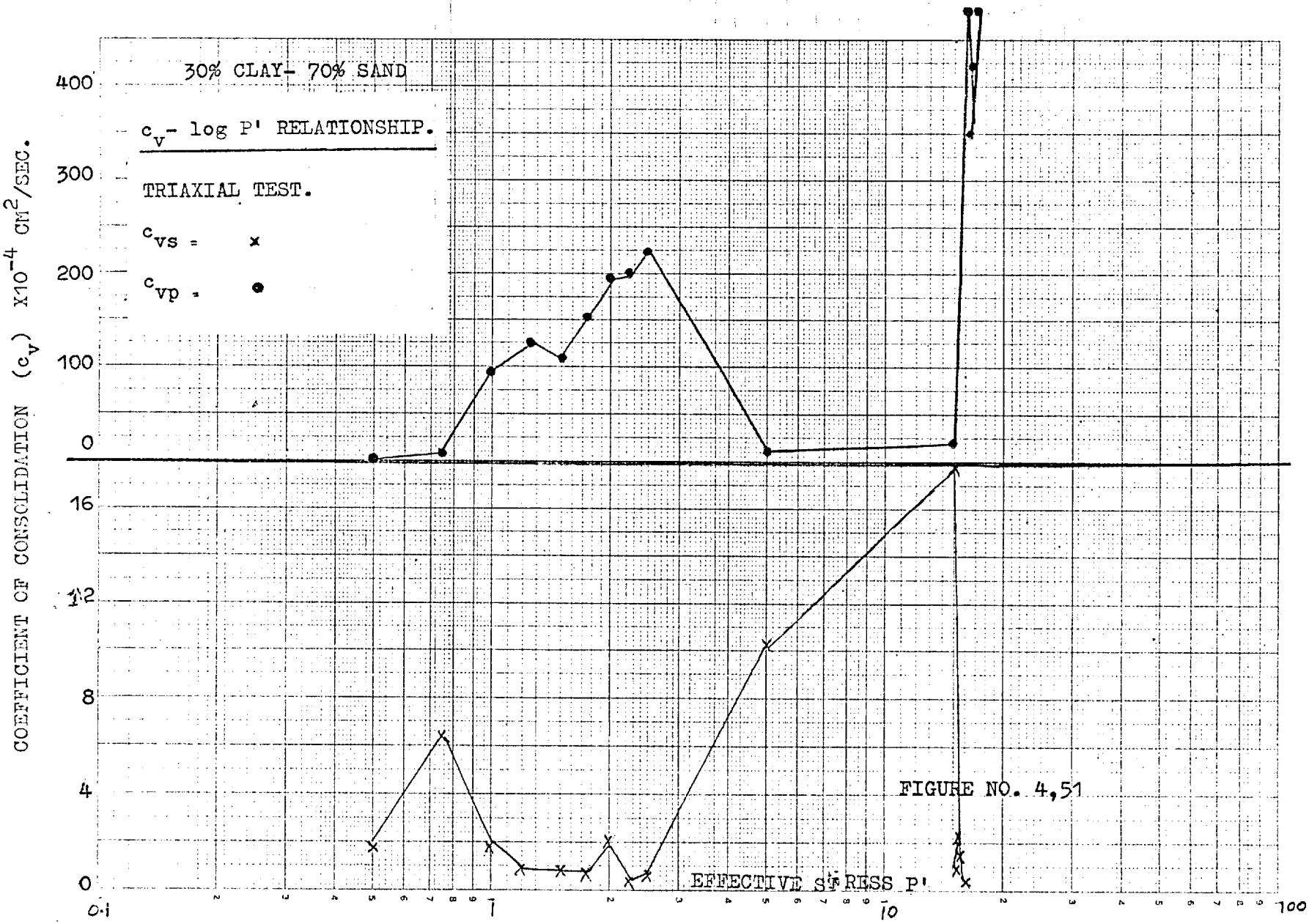

FIGURE NO. 4,51

5. THE MICROSTRUCTURE STUDY OF SAND-CLAY MIXTURES

5.1 Introduction (General Review)

The need to understand the macro-* and micro-* structure of clay soils was appreciated in the early days of Soil Mechanics so that the engineering behaviour of such materials could be more easily explained. To this end, a number of investigators have postulated different models (particle arrangements) as shown in Figure 5.1. The well-known honeycomb structure was proposed by Terzaghi (1925). He suggested that the minerals adhere to one another at the points of contact with forces sufficiently strong for the building up of the honeycomb structure. In this structure a comparatively large amount of water can be enclosed within the voids. In 1932 a somewhat similar model for sensitive clays was presented by Casagrande, the important difference being the presence of silt size particles contained in the clay honeycomb matrix (see Figure 5.1(c). Mitchell and Houston (1969) have discussed the importance of sand and silt size particles in a clay matrix and believe that the structure of sensitive clays is truely represented by Casagrande's honeycomb model.

Goldschmidt (1926), experimenting with different clay pore fluids discovered that if the pore fluid was non-polar, the clay no longer exhibited plastic behaviour. A typical non-polar fluid used in his study was Carbon Tetrachloride. On the basis of this and other work he proposed the edge-to-face or "flocculated" structure.

---

* In this chapter macro- will refer to the clay structure as seen under the optical microscope, while micro- will be used to describe the more detailed arrangement as seen under the electron microscope.

According to him the flaky minerals in the highly sensitive clays are arranged in an unstable cardhouse array (Figure 5.1(a)). This resulting structure was due to the clay particles* being deposited in a saline environment.** Subsequent isostatic movement+ and leaching of the pore fluid leads to an unstable clay. Many clays in Scandinavia exhibit such a structure as indicated in several publications of the Norwegian Geotechnical Institute (e.g. Bjerrum, 1954, 1967, Aas, 1965). Skempton and Northey (1952) point out that chemical tests indicate a drop in sensitivity++ with increasing salt concentration. in pore fluid.

Lambe (1953) agreed with the Goldschmidt cardhouse structure as a model for clays deposited under marine conditions. However, for fresh water deposits the structure was thought to be somewhat denser or "dispersed (Figure 5.1(d)) and in remoulded clays the particles were thought of as having a high degree of parallelism and a short order range between flakes. Tan (1957) presented the schematic picture of clay-minerals network dominated by contacts between a corner of one mineral and the plane of another. In recent years, the concepts proposed by Goldschmidt and Lambe have been verified by Mitchell (1956) and Rosenqvist (1959) through the use of optical and electron microscopy respectively. Trollope and Chan (1960) have taken into consideration Lambe's cardhouse concept to explain a soil structure hypothesis (step-strain theory) for a composite soil which can be represented as coarse (sand, silt) grains randomly distributed in a colloidal (clay) matrix.

---

* typically illite clays

** sea water contains about 35 gm/l Sodium Chloride ($Na^{+}cl^{-}$).

+ lowering of the sea level relative to the land

++ degree of sensitivity of clay is expressed by the ratio between the unconfined compressive strength of an undisturbed sample and the strength of the same sample at the same water content, but in a remoulded state.

Sloane and Kell (1966) in a microscopy study of compacted kaolin proposed the term "book house" structure (Figure 5.1(b)), for the packets of clay which they observed. They concluded that the packets persisted throughout the preparation of clay samples for compaction testing, and that the packets were probably present in kaolin before the addition of water.* Aylmore and Quirk (1960) proposed a "turbostratic" arrangement for a dispersed structure as shown in Figure 5.1(e). The turbostratic structure is described as consisting of domains and since these are randomly orientated, the material is isotropic on the macroscale, although locally anisotropic on the microscale. Finally the arrangement of Figure 5.1(f), described by Barden and Sides (1971) as being a "stack" represents a domain of perfectly oriented clay plates.

The above concepts of structure are presented in a simplified form. In nature however, the actual soil structure is rather more complex and difficult to analyse. The presence of sand and silt size particles complicates matters, and necessitates the introduction of further concepts. Anyhow, in the present study an attempt is made to investigate the microstructure of coarse particles (sand and silt) in the clay phase before and after consolidation.

Optical studies of thin sections of several undisturbed and remoulded clays by Mitchell (1956) have shown that coarse particles are seldom in contact, but are separated by the clay phase. Recent studies by Paduana and Mitchell (1967), on the consolidation and strength characteristics of sand-clay mixtures establish clearly, however, that the consolidation of clay is inhibited by the presence of sand, even when the amount of clay is considerably greater than required to prevent direct intereaction between the sand particles, (Mitchell and Houston, 1969). They have graphically demonstrated

---

* The flocculated structure noted in some of the compacted samples consisted of stacks rather than individual particles.

this effect showing that the water content of the soil mixture and the clay phase alone as a function of clay content in the case of an illite-sand mixture consolidated to 2.0 Kg. per sq. cm. While investigating the sensitivity of clays Mitchell and Houston have expressed a similar opinion about the sand or silt particles existing in a clay matrix, and on this basis they support the Casagrande model.

Trollope and Chan (1960) agree on the initial random distribution of coarse grains separated by the clay phase for a remoulded sand-clay mixture. However, they suggest that when these mixtures are subjected to high shear stresses, the coarser grains move or migrate to a position of intergranular contact on the potential failure plane. Trollope and Chan have formulated a hypothesis known as the "step-strain" theory which is based on the above mechanism. It is interesting to note that Mitchell and Houston (1969) do not agree with the "step-strain" hypothesis on the pretext that the coarser grains do not come into direct contact with each other at all, even after the sample is subjected to an external pressure. A discussion of this phenomenon in relation to the present investigation is deferred till later.

Other aspects of soil behaviour such as effects of remoulding treatment with solution etc., on the mechanical properties of a soil have also been the focus of research work by many investigators. For instance Jiminez Salas and Serratosa (1953) while examining the physico-chemical factors influencing the compressibility of clay, have pointed out that the difference in the coefficient of consolidation and the compressibility due to different treatments such as kneading with organic liquid and remoulding of the clay, cannot be be explained by simple mechanical theories alone. Bolt (1956) has dealt with this using the physics of colloids. He has demonstrated

that the compressibility can be partly affected by the attractive and repulsive forces interacting via the layers of absorbed water.

Tchalenko (1967) carried out an extensive optical microscope study on kaolin, while earlier similar investigations on a number of soils were made by Mitchell (1956). They took into consideration fibre orientation to explain the engineering behaviour such as strength, permeability and compressibility of a soil. Lambe (1958) and Seed and Chan (1959) on the other hand have shown that the method of remoulding induces various arrangements of the clay particles in compacted clays resulting in very different pore pressure responses.

5.2 Microscopy

Since its invention in the seventeenth century, the optical microscope has been extensively used to investigate complex mineral structure. Despite some limitations, the optical microscope has proved invaluable and still finds considerable use. A great many research workers have made use of this type of optical microscope so that a study of thin sections of different clays could be made (e.g. Mitchell, 1956; Tchalenko, 1967; Morgernstern and Tchalenko, 1967; Garga, 1970, and others). Although the sample preparation is somewhat laborious, an examination of the macrograph obtained will yield information about the deformation and degree of orientation of the clay particles.

In studying the behaviour of an electron beam, it was realized that it could be manipulated using electrostatic and magnetic lenses in a similar way to light using lenses. By the late thirties a few commercial electron microscopes had been developed and the magnification was no longer limited by the wavelength of light but by the wavelength of an electron beam. With the development of the

electron microscope, the resolving power has been greatly increased, i.e. the ability to resolve the texture of a specimen down to a fraction of an Angstrom (less than 10^{-8} cm.) depending upon which microscope is used (Hall, 1966). Some of the major types of electron microscopes commercially available are as follows:

1) Scanning electron microscope

2) Transmission electron microscope

3) Reflection and mirror electron microscope

4) Field-ion microscope

5) Field-emission microscope.

In the present study, use was made of the scanning electron microscope only. For the purpose of identifying the elements, a special instrument known as Ortec Energy Dispersive X-Ray detector coupled with a Northern Scientific Econ II multi-channel analyser was also used.

5.2.1 Scanning electron microscope

This instrument was first used in the study of soil structure by Roscoe (1967). Since then it has been widely used by many research workers to study the microstructure of clays (e.g. Tovey, 1970; Barden and Sides, 1971, and others). Basically the instrument consists of the following three sets of components (Thornton, 1968):

1) The electron column and associated electronic devices

2) Specimen chamber, stage and vacuum system.

3) Signal detection and display systems.

A schematic representation of the scanning electron microscope (S.E.M.) is shown in Figure 5.2. The electron beam supplied by an electron gun, passes through a series of magnetic or electrostatic lenses and is demagnified so that when it strikes the sample surface in the form of a spot of 250 A^{o} or less depending upon the area under investigation. Before passing into the specimen chamber the 'pencil' ray, so formed, passes through a modulator, which causes the beam to scan across the area of the sample in a way similar to the scanning of an electron beam across the surface of a Cathode Ray Tube.

Indeed this scanning motion is so timed that it is synchronised with the scanning of a cathode ray tube in the display system so that an image of the sample surface can be directly viewed. The sample is of the order of 1 cm x 1 cm x 1 cm, and the complete face of the cube can be scanned at low magnifications in the range 20 x to 100 x and then specific features selected for detailed investigation at higher magnification up to 50,000 x.

The instrument has a high depth of focus making it possible to see clearly many particles in depth providing a strong three-dimensional picture. This stereoscopic effect allows very rough unpolished surfaces including quartz and silt grains to be viewed. True stereo-pairs are very easily obtained by tilting the sample holder through a small angle of approximately 3^{o}, and the interpretation of structure is greatly facilitated by such micrographs.

Stereoscan Mark II A and the Stereoscan S600 (Cambridge Instrument Company) were used in the present investigation. For the identification of sand grains being coated with clay or not, Ortec Energy Dispersive X-Ray detector coupled with a Northern Scientific Econ II multi-channel analyser was used in conjunction with Stereoscan Mark II A. With the beam set at a particular

location on the surface of a specimen this device could identify the elements present by analysing the form of a wave containing peaks* of different heights. For example, by knowing the chemical composition of kaolin and quartz distinguishing the two minerals is fairly simple. However, where a number of clay minerals are present, as is the case for a naturally occurring clay sediment, where traces of clay minerals such as chlorite or vermiculite can be present with the main mineral, identification can become difficult, if not impossible. Other methods of mineral identification for instance Differential Thermal analysis or chemical analysis may have to be used. This problem of course, did not exist in this study.

5.3 Sample Preparation

Since the sample had to be subjected to high vacuum when placed in the steroscan, it was therefore essential that it did not contain any pore water.** For this reason, the sample had to be either dried or impregnated. Two methods of sample preparation were used for this purpose:

1) Carbowax Impregnation

2) Air-drying.

For completeness some of the main methods of sample preparation are also briefly outlined later in the section.

---

* The peaks are calibrated and assigned to the individual elements accordingly.

** A small amount of water can be removed from the sample by vacuum. Large amounts of water present in a sample can perhaps cause damage to the instrument, resulting in poor quality micrographs and large suction forces capable of collapsing a sensitive clay structure.

5.3.1 Carbowax Impregnation

Mitchell (1956) was the first to use carbowax 6000 (Polyethylene Glycol) for the preparation of thin sections of moist clays. Since then it has been successfully used by many investigators (e.g. Martin, 1966; Tchalenko, 1967; Tovey, 1970; Green-Kelly, Chapman and Pettifer, 1970; Barden and Sides, 1971; and others). The impregnation of moist soil samples usually presents no special problems and requires no elaborate equipment. Samples that are saturated and therefore contain negligible amounts of air, are impregnated by immersion on wire grids in aqueous Carbowax 6000. The initial concentration of Carbowax is chosen to avoid a large osmotic pressure difference between samples and solution. That is, some clays having fairly sensitive structure are likely to be disturbed by the pressure difference unless a step-by-step impregnation process is carried out, starting with aqueous solutions of Carbowax, before proceeding to pure Carbowax.

The specimens to be impregnated were carefully marked and numbered by lightly scratching the surface with a knife and submerged on a wire grid in aqueous Carbowax 6000. Samples with 50% and more clay content were allowed 5 minutes immersion at room temperature in 10%, followed by 2 hours in 25% and 4 hours in 50% aqueous solution, as recommended by Greene-Kelly, Chapman and Pettifer (1970). The specimens were then left overnight at 60^{o} to 70^{o} C temperature. The 50% Carbowax was replaced by molten pure Carbowax, which was changed twice during a further impregnation period of 5 to 6 days. A similar process of impregnation was adopted in the case of 70% and more sand samples, except that they were immersed directly in 50% Carbowax which was later replaced with the pure molten wax. After the advised duration for complete impregnation, the samples were removed from the Carbowax container to be allowed to cool and harden at room temperature.

5.3.2 Air-drying

This is the simplest and perhaps the quickest method of preparing a specimen for the scanning electron microscope. The sample is allowed to dry out at room temperature. A period of 24 hours air-drying is normally considered as adequate for a specimen to be thoroughly dried and ready for the study. Unfortunately, the greatest disadvantage of the method is shrinkage, which in the case of wet clays, is close to the shrinkage limit, e.g. Tovey (1970) carried out a survey on the degree of swelling or shrinkage of consolidated samples of clay, prepared by various methhods for S.E.M. (refer Table 5.1). On the basis of these results, it appears that the greatest amount of shrinkage occurs by oven or air-drying the samples, with a reduction in volume of over 30%. Therefore, this method is normally not used where the orientation of clay particles is the main subject of study. Since this was not the purpose of the present investigation, the air-drying method could be considered as reasonably satisfactory.

Next approximately 1 cm cuboids were made out of the Carbowaxed and air-dried samples for observation in S.E.M. Each cubical specimen was obtained by grinding and later fractured at one end. The smooth surface opposite the fractured face was then fixed to a stub using "Durofix" glue. While doing so, extreme care was taken not to touch the surface about to be examined. Prior to further treatment, the fractured face of the specimen was subjected to an air-jet and peeled* with "Sellotape" in the manner described by Barden and Sides (1971). This method was used to remove any loose debris present on the fractured surface.

---

* Use of peeling technique was of little use with impregnated samples because of the wax coating.

The sides of the cubical specimen not to be viewed were painted with colloidal silver right down to the edges to make an effective electrical contact with the stub. It was then mounted between two electrodes in a coating unit so that approximately 100A^{o} of gold palladium could be sprayed on to the fractured surface under a vacuum. During this process the sample was rotated to avoid shadowing. It must be pointed out that all non-metallic specimens have to be coated with silver and gold as described above before proceeding with the S.E.M. investigation. Omission of this procedure will result in partial or complete loss of a picture caused by the local charging of the clay particles.

5.3.3 Other Methods of Sample Preparation

Different methods of sample preparation have been used by various investigators. Weatherland (1940) and later Weymouth and Williamson (1953) prepared thin sections by impregnating previously dried soft rock and kaolinite surface with pyroxlin. Rosenqvist (1955) impregnated some soft Norwegian clays with sulphonated alcohol at 60^{o}C and the sample was then cut with a microtome at a temperature of -10^{o}C. This method results in an extremely small thin section and any coarse intrusion of silt or sand in clay makes the use of a microtome rather difficult. This is normally employed for examination of clays using the transmission electron microscope. Fitz-Patrick (1970) describes the preparation of ultra thin specimens of clay after displacing the pore water with Carbowax 6000 in a similar way to that described previously.

An alternative method of sample preparation for T.E.M. is the replica technique. Cromer and Turley (1955) were among the early workers to apply this technique to the study of clay. Later Rosenqvist (1959) and Sloane and Kell (1966) also used this method.

The procedure of producing a replica consists essentially of coating the surface of the specimen with carbon or metal to a thickness which is suitable for subsequent handling and which, of course, is not too great so as to prevent electron penetration.

Freeze drying for the preparation of samples has been used by Rosenqvist (1959) Leonards and Altschaeffl (1964) Gillot (1969) and others. The technique comprises of simply placing a specimen in liquid gas such as nitrogen, oxygen or air. Later sublimination of ice is carried out under a vacuum. Although the samples prepared by this method are less disturbed because the process involves low shrinkage, the method is not very popular because of the difficulties in the procedure along with the problems of prevention of melting during the sublimination stage, as pointed out by Gillot (1959).

The replacement of pore water by a number of volatile liquids including methanol, ether, isopontane, acetone and cellusolve has been attempted by Tovey (1970). After the substitution of these liquids the samples were dried. The overall swelling/shrinkage of clay samples prepared by various methods have been compared in Table 5.1 (after Tovey, 1970). It can be observed that the methods examined by Tovey are reasonable, though the shrinkage in the horizontal direction is much higher with comparison to impregnated samples. Recently Barden and Sides (1971) have studied the impregnation of samples with gelatine and water dispersable epoxy resin (W.D.E.R.). The technique of partial impregnation involved in W.D.E.R. seems to involve a considerable disturbance of the structure and therefore is unreliable. However, according to them, the gelatine impregnation, followed by etching with hydrofluoric acid, produces improved micrographs and compartively low shrinkage of 4%.

As can be seen from Table 5.1, freeze-drying produces the lowest degree of contraction or expansion, whereas the oven/air dried specimens reduce in volume by over 30%. In the present study, however, these effects are ignored as the object is not the precise clay structure as much as the arrangement of sand particles in the clay matrix.

5.4 Observations and Discussion

The fragile structure of clay is vulnerable to disturbance caused by shrinkage and cracking during the impregnation and drying up process. Additional damage to the microstructure is likely to be caused by fracturing, although this effect is minimised by peeling (Barden and Sides, 1971). The resulting pictures are occasionally not very clear as in the case of carbowaxed specimens where peeling has little effect. In general, the results are satisfactory. The problem arising from various methods of preparation examined, e.g. by Tovey (1970) and Barden and Sides (1971) show that some disturbance to the microstructure is almost inevitable. This is in-spite of taking all the precautions during the preparation of a specimen for S.E.M. A comparison between the air-dried and carbowaxed specimen can be drawn from their respective micrographs (a) and (b) presented in Plate 5.4. It will be seen that there are no obvious differences in the structures revealed by the two methods. This, however, is not a quantitive but a subjective assessment based on visual observation alone. The micrographs of sand-clay mixture specimens before and after consolidation shown in Plates 5.2 to 5.5 are representative examples chosen from a large number of micro-graphs.

In order to examine the particle arrangement of remoulded basic (unconsolidated) clay samples, the micrographs of 100% kaolin carbowaxed specimens are shown in Plate 5.1. These micrographs can also help in idenfitying the clay particles in a carbowaxed sand-clay mixture specimen, where a slight obscuring is likely to cause some confusion. At magnifications of 1000 x to 5000 x, the clay particles can be seen to be randomly orientated prior to the consoli-dation process. Since the samples were carbowaxed, the question of loose debris hanging around the surface under observation does not

arise, as discussed by Barden and Sides (1971). Thus the micrographs 5.1(a) to (d) may be considered as true representatives of the unconsolidated microstructure of 100% clay.

Plates 5.2 and 5.3 show the sand particles in the clay matrix before consolidation of the sand-clay mixtures. In table 5.2 the percentage of constituents, the method of preparation etc., of a specimen represented by the micrograph are given. The selected views of the sand-clay microstructure show that generally clay particles do not adhere to the surface of the sand particles prior to compression. These observations were verified by spectral analysis obtained using the O.E.D. X-Ray detector coupled with N.S. Econ. II. multi-channel analyser in conjunction with Stereoscan Mark II A, as described in section 5.2.1. The smooth surfaces of sand particles can be seen from the micrographs in Plates 5.2 and 5.3. The spectral analysis verified this by indicating, the absence of elements constituting the clay, while the predominance of silicon during tracing across the suspected sand grains on the fractured surface of an unconsolidated specimen.

The micrographs of sand-clay mixture samples after consolidation are illustrated in Plates 5.4 and 5.5. The percentages of the constituents in a soil mixture, the type of consolidation test and the method of preparation of a specimen etc., for the respective micrographs are given in Table 5.2. From these micrographs it will be seen that almost all the sand grains are coated with clay particles. Using the detector, a spectrum of elements was obtained which showed the peaks representing large quantities of Aluminium and Silicon, and small amount of Gold*. Since the kaolin is an aluminium-silicate having chemical composition $Al_4 Si_4 O_{10} (OH)_8$,

---

* Due to the gold-palladium coating on the surface of the specimen as described in section 5.3.2, the detector had picked up gold as one of the elements which, of course, was ignored.

therefore these elements indicated the presence of clay particles across the traced surface of a specimen. The larger quantity of silican, besides the geometrical shapes of the quartz confirmed the presence of sand particles underneath the thin film of clay coating. Micrographs of a magnification of 500 x - 2000 x and more in Plates 5.4 and 5.5 show these large geometrical shaped sand grains coated with the stacks of clay particles.

Looking again at the series of micrographs in Plates 5.4 and 5.5 a variety of sand clay particles can be viewed. The contacts between the clay particles themselves appear to be essentially face to face forming a turbostratic arrangement similar to the one proposed by Aylmore and Quirk (1960) as shown in Figure 5.1(e). These large groups of approximately oriented particles known as "domins" or "stacks" (Barden and Sides, 1971) then adhere to the surface of sand grains in an edge-face, or face-face arrangement. This effect seems to depend upon the degree of realignment of the clay particles between the adjacent sand grains during the consolidation process. The series of micrographs in Plate 5.5 illustrates a good example of this phenomenon. In the case of sand-clay mixtures containing 70% and more sand particles are likely to prevent the development of orientation in any one direction over a large area. Similar observations were reported by Mitchell (1956) on the arrangements of particles in a few one-dimensionally compressed U.S.A. clays (Cincinnati, Pump Site and Dow Field). All these clays contained more than 75% of silt and fine sand.

The examination of thin sections under the optical microscope of the above mentioned clays by Mitchell showed that the orientation of silt particles was random in almost every case. But the clay particles were orientated around the surfaces of silt particles.

After the macrostructure study of 14 undisturbed and remoulded clays, he came to the conclusion that the silt particles did not generally touch one another. This was found to be true even in clays which contained more than 75% coarse particles (silt, sand) and less than 25% finer than 2 microns (clay). Thus Mitchell thinks that the silt or sand particles "float" in a matrix of clay and that they have probably little influence on the strength properties of the material.

Trollope and Chan (1960) while presenting a "step-strain" hypothesis, postulated that a composite soil can be represented as coarse (sand, silt) grains distributed at ramdom in a colloidal (clay) matrix. When such a soil is subjected to sufficiently high shear stresses a yield condition is first developed in the colloidal matrix. This condition of matrix yield is achieved when the applied shear stresses are sufficient to force the colloid particles into such a position that they tend to be orientated parallel to one another and in the direction of a potential failure surface. Subsequently it is thought that the coarser grains migrate towards the potential failure surface and come in direct contact with each other, causing an additional resistance in the form of intergrannular friction. While studying the sensitivity of clays Mitchell and Houston (1969) have found no existence of such a phenomenon. Their study (Paduana and Mitchell, 1968) on the consolidation and strength characteristics of sand-clay mixtures show little evidence of direct interaction between granular particles. It is believed that a silt or sand grain-bond clay skeleton exists with matrix clay filler similar to Casagrande's model.

Although no direct shear strength tests were carried out in the present course of study, it is understood that sufficiently high shear stresses must have been caused due to the displacement of particles of a sample undergoing anisotropic consolidation in an oedometer. Whereas particles would tend to move closer in a more tight packing

under isotropic consolidation. It has already been described that the specimens obtained from both tests showed no sign of direct contact between the granular particles, but were separated by clay particles adhering to their surface. This characteristic behaviour of the particle arrangements in a sand-clay mixture thus confirms the findings of Mitchell (1956), Paduana and Mitchell (1968) and Mitchell and Houston (1969).

A similar picture emerges from the basic (unconsolidated) sand-clay mixture sample, but with a slight difference. That is, the sand grains neither come in contact with each other nor with the clay particles directly but float in the clay-water matrix. In other words, clay particles do not adhere to the surface of sand grains before consolidation. This is perhaps due to the "free" or "pore" water forming a thin film between the sand grains and the clay particles around it.

The whole phenomenon of inter-particle action is very complex, as it greatly depends upon physio-chemical properties of a soil, which cannot be easily explained by simple mechanical theories. However, a hypothetical explanation to the above phenomenon is presented.

The fact that electro-static charges exist on the surface of colloidal (clay) particles provides a wide understanding of micro-structural arrangements of different clays. To explain this, a number of models has been proposed by various investigators as described earlier. Anyhow, when these particles are in the presence of water, the polar structure of the water molecules results in a weak attraction of a layer of water molecules on to the surface of the particle (i.e. forming an adsorbed water layer). Yet another important feature of colloidal behaviour which has to be taken into account is the ionic distribution within these layers (i.e. the concept of an

electric double-layer described by Bolt, 1956; and Lambe, 1958). Similarly, when a sand particle is brought into contact with water, the surface attracts and strongly binds a few layers of water molecules.* The capillary force is mainly responsible for water retention in sands (Yong and Warkentin, 1966). Thus, sand and clay particles are separated by this adsorbed water. As such, when an unconsolidated air-dried or impregnated specimen is viewed under S.E.M., the uncoated sand grains are seen embedded in the clay matrix as illustrated by micrographs in Plates 5.2 and 5.3.

If the sand-clay mixture sample is now subjected to a direct compressive pressure the sand and clay particles will tend to move closer to each other. It is postulated that the highly viscous adsorbed water coating the clay and sand particle surfaces is squeezed out from between the points of contact. The resulting close approach of the particles leads to the attractive forces between clay particles and the surfaces of sand grains. Since there are no charges on the sand particle surface, therefore the clay particles will not adhere to the sand with a strong bonding such as the ionic bond. But weak Van der Waal's force may be set up as a result of the compressive pressure bringing sand and clay particles together. The process of consolidation may afford such a system whereby the electrically charged clay particles will come into contact with and build up on the surfaces of sand particles as illustrated in the micrographs in Plate 5.4 and 5.5.

Now an attempt is made to explain the effects of the observed microstructural phenomenon on the consolidation process described in the previous chapters. The relative amounts of final particle adjustment that occur during the process of consolidation are unknown quantities. However, it is possible that these adjustments are functions

---

* While explaining the phenomenon of loss of strength by remoulding, Terzaghi presented a concept of the water film where each particle may be visualized as coated with a film of water (Taylor, 1948).

of the arrangement of particles before the application of a load and of the forces which bind the particles in this arrangement and also the pressure to which the samples are subjected. The pore-pressure dissipation and the time-settlement behaviour of a soil is known to depend closely upon these factors. As shown in the micrographs, the initial structure prior to consolidation is randomly orientated. The application of a load to this type of structure will cause a decrease in inter-particle spacing accompanied by a complete reorientation of particles. The pore pressure so generated will dissipate with time. It has already been pointed out that a sample in an oedometer when subjected to a load increment will cause a considerable displacement of particles and thus impart high shear stresses within the soil, whereas under isotropic consolidation there will be comparitively less relative displacement, though the particles will tend to move closer in a very tight packing resulting in a decrease in the inter-particle spacing.

The pore pressure response and its rate of dissipation has already been shown to depend upon the load increment ratio and its duration. The phenomenon can further be interpreted as a function of the bonds between clay particles and with sand grains. It is thought that when small $\frac{\Delta P}{Po'}$ is applied, these bonds are not easily disrupted thus the maximum pore pressure generated is less than the applied increment as demonstrated in Chapter 2. On the other hand, large shear stresses caused due to large $\frac{\Delta P}{Po'}$ will tend to overcome the inter-particle resistance by breaking up the bonds, thus the subsequent collapse will give rise to a higher pore pressure build-up than in the case of small $\frac{\Delta P}{Po'}$. The dissipation of pore pressure during primary consolidation observed by Skinner and the author, as reported in Chapter 3, is postulated to be caused by inter-particle action such as concurrent breaking and mending of bonds while moving closer and closer together.

A secondary consolidation, or the void ratio decrease that occurs after the hydrostatic pressure in the pore water is dissipated, has been attributed by Lambe (1953) to the break down of aggregates and the shifting of particles under pressure. As most of the water available for movement under the applied stress drains from the soil, the remaining stresses sustained in the fluid phase are carried in water that is held between the soil particles. The adsorbed water is extruded from between particles at a very slow rate, however, this process can occur with very small volume change. Besides this the inter-particle forces of repulsion resist further decrease in inter-particle spacing during the secondary consolidation, giving rise to the characteristic time-settlement curves, as shown in Chapter 4.

After the sample is subjected to long duration of rest under a constant load increment, the bonds would have build up. Consequently when an additional load increment is applied, part of the load is carried by these structural bonds of the soil instead of being wholly transferred to the pore water. This will result in less pore pressure response than the applied increment. The stiffening of the soil structure with the long rest period has been observed by many research workers (e. g. Taylor, 1942; Skempton and Northey, 1952; Leonards and Ramiah, 1967; and Bjerrum, 1967). Leonards and Altschaeffl (1964) came to similar conclusions while studying the effects of load increment ratio and its duration on freeze-dried kaolin.

Sample	Shrinkage or Swelling on drying		
	No. of samples	Overall	
		SH%	SV%
1) Oven-dried	2	-6.7	-23.5
2) Quick air-dried	2	-7.7	-22.6
3) Slow air-dried	4	-12.5	-28.5
4) Freeze-dried	1 (3)	+0.63	+ 0.74
SUBSTITUTION DRIED			
1) Methanol	5	-3.8	- 6.8
2) Ether	4	-3.2	- 6.8
3) Isopartane	2	-2.5	- 5.9
4) Acetone	2	-2.8	- 8.5
5) Cellusolve	1	-1.2	- 6.6
IMPREGNATION			
1) Carbowax	-	variable	- 5.7
2) Araldite	4	+0.4	+ 9.5
3) Vestopal	3	+0.5	+ 9.5
4) Durcupan	1	-0.3	+11.0

Degree of swelling/shrinkage of consolidated specimens of clay prepared for the S.E.M. (after Tovey 1970).

Table 5.1

Plate No.	Micrograph	Sample		Method of Preparation	Test	Sample Plane	Magnification
		Clay %	Sand %				
5.1	a	100	-	Carbowaxed	Unconsolidated	-	1000 X
	b	100	-	"	"	-	1000 X
	c	100	-	"	"	-	2000 X
	d	100	-	"	"	-	5000 X
5.2	a	30	70	Carbowaxed	Unconsolidated	-	1000 X
	b	30	70	"	"	-	2000 X
	c	30	70	"	"	-	1000 X
	d	30	70	"	"	-	2000 X
5.3	a	30	70	Carbowaxed	Unconsolidated	-	2000 X
	b	70	30	"	"	-	1000 X
	c	50	50	"	"	-	2000 X
	d	70	30	"	"	-	2000 X
5.4	a	30	70	Air-dried	Hyd. Oed.	Horizontal	2000 X
	b	30	70	Carbowaxed	" "	"	2000 X
	c	70	30	Air-dried	Triaxial	Vertical	2000 X
	d	70	30	"	Conv. Oed.	"	5000 X
5.5	a	30	70	Carbowaxed	Hyd. Oed.	Horizontal	500 X
	b	30	70	"	" "	"	1000 X
	c	30	70	"	" "	"	2000 X
	d	30	70	"	" "	"	5000 X

TABLE 5.2

Samples for S.E.M.

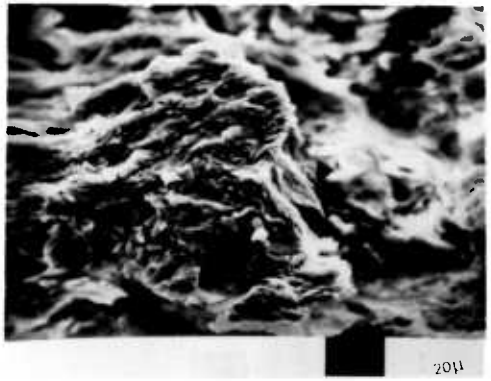

a

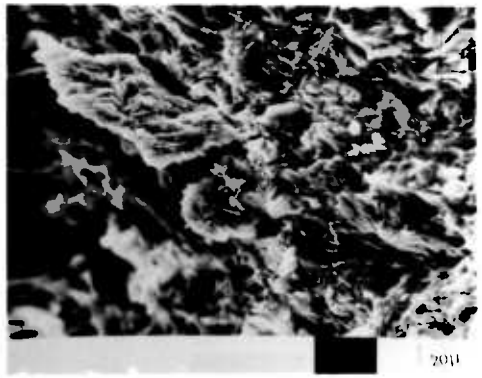

b

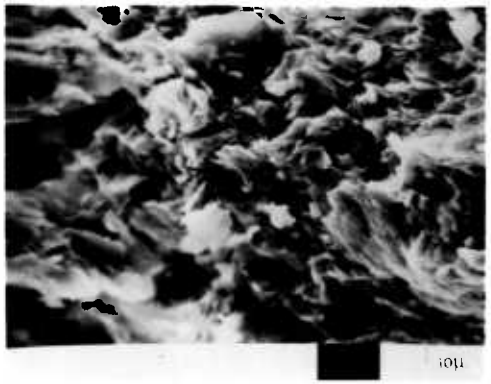

c

d

Plate No. 5·1. Micrographs of 100 % clay – Kaolin –

a

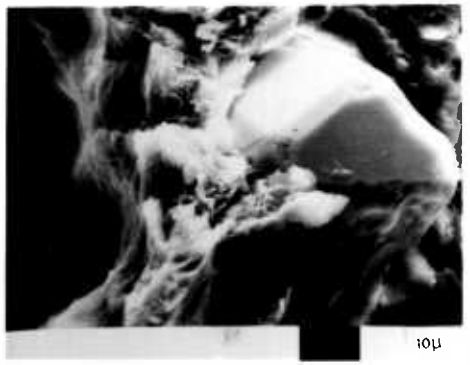

b

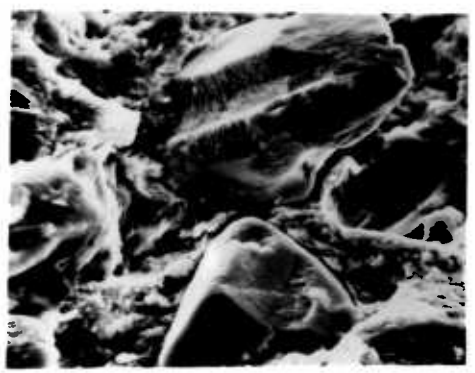

c

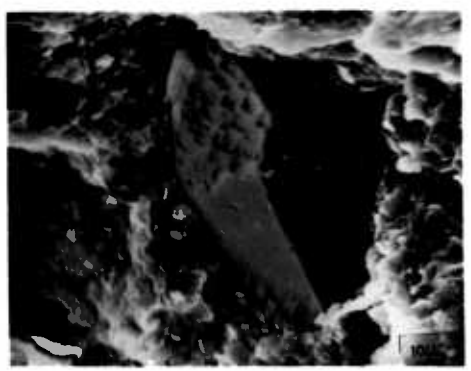

d

Plate No. 5·2. Sand grains embedded in clay matrix without being coated with clay particles before the consolidation of sand-clay mixtures.

a

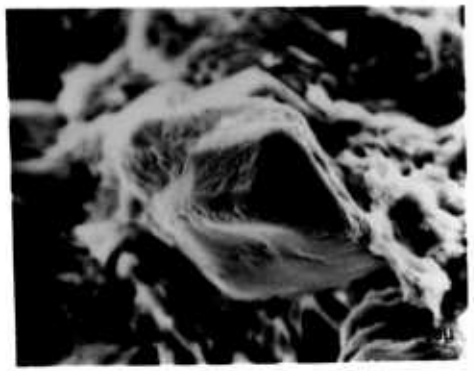

b

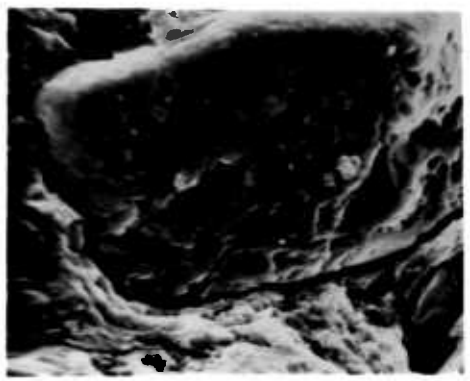

c

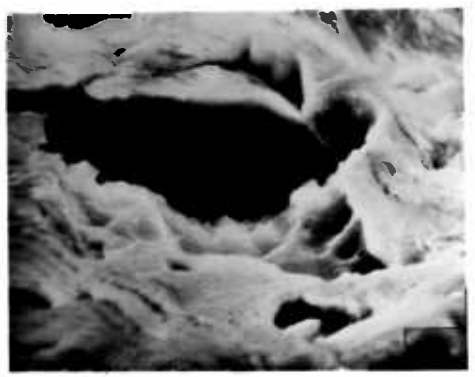

d

Plate No. 5·3. Sand grains embedded in clay matrix without being coated with clay particles before the consolidation of sand–clay mixtures.

a

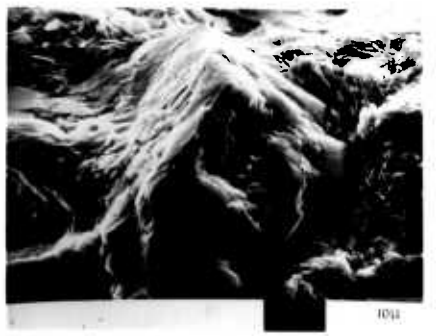

b

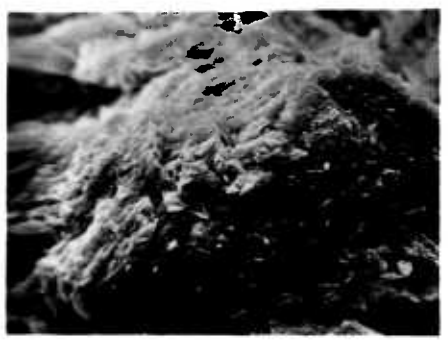

c

d

Plate No. 5·4. Sand grains in the clay matrix are coated with clay particles after the consolidation of sand–clay mixtures.

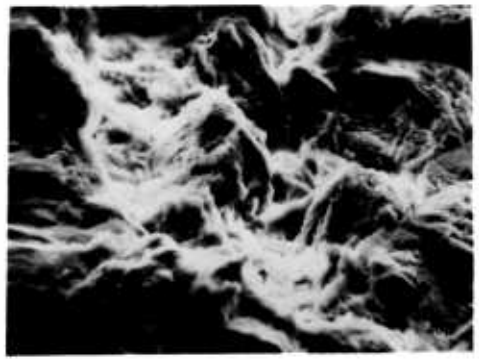

a

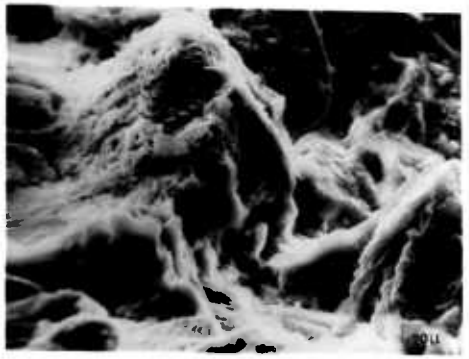

b

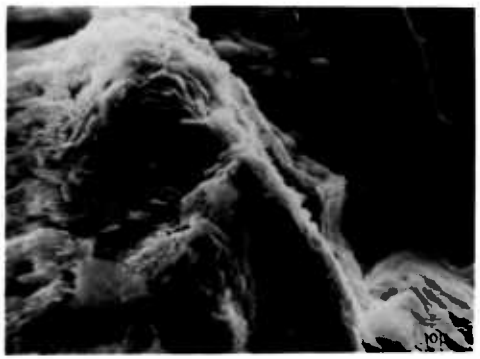

c

d

Plate No. 5·5. Sand grains in the clay matrix are coated with clay particles after the consolidation of sand–clay mixtures.

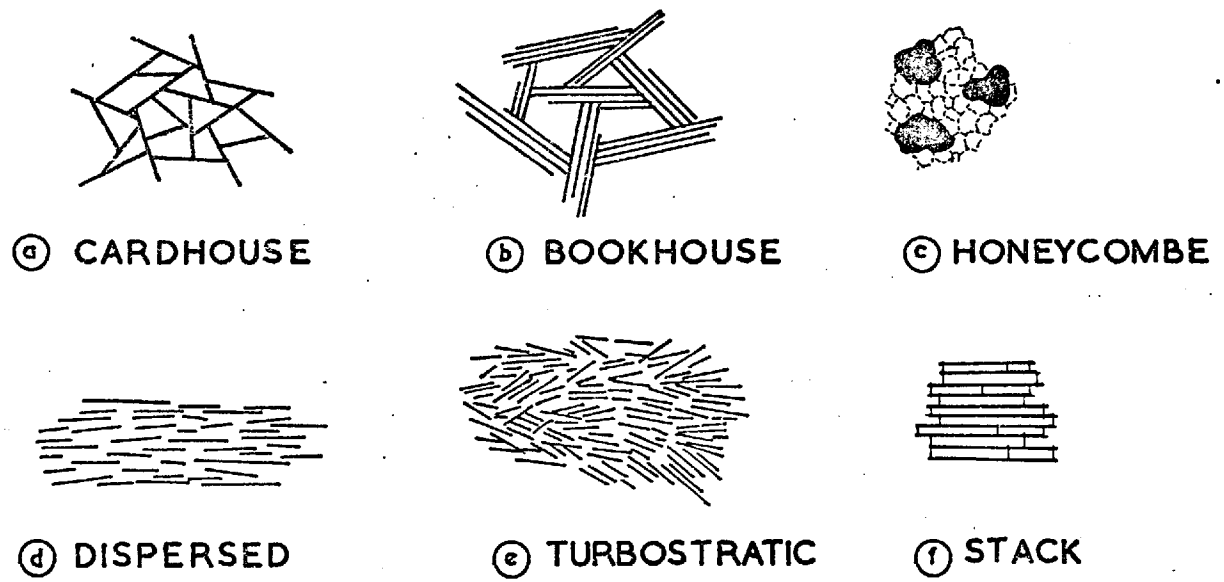

Figure No. 5.1, Idealized Clay Structures (after Barden & Sides, 1971).

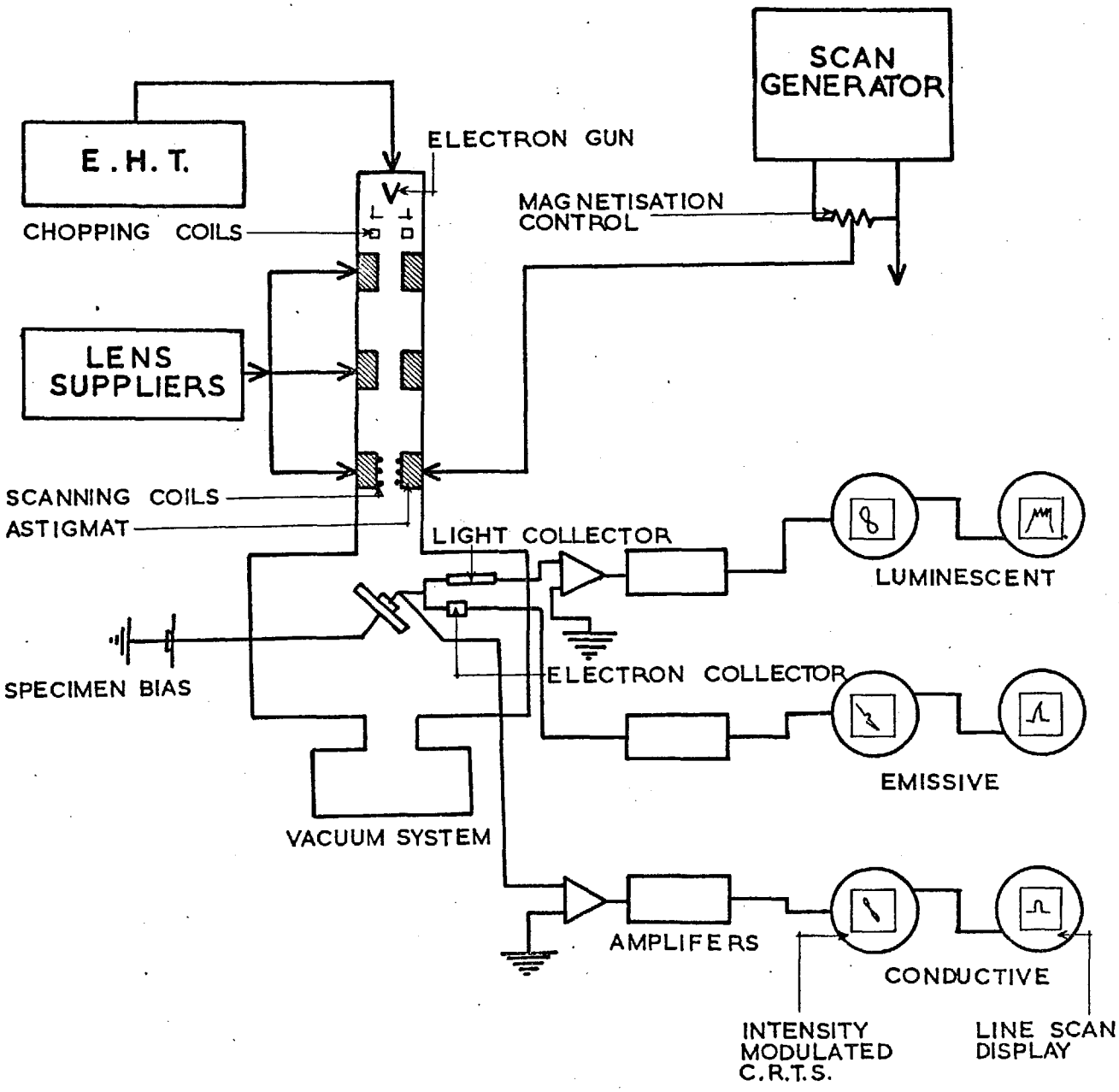

Figure No. 5.2, Schematic Diagram of Scanning Electron Microscope.

6. CONCLUSIONS

In the sand-clay mixtures considered here, 20% clay content is the minimum at which the material exhibits significant plasticity. Beyond 80% sand, the sand-clay mixture behaves like a non-plastic material.

The isotropic and anisotropic consolidation tests show that the dissipation of excess pore water pressure is highly dependent on the stress increment ratio. Terzaghi's theory is found to predict the dissipation of excess pore water pressure reliably, provided large stress increment ratio is applied; this ratio for the sand-clay mixtures is two or more. If the stress increment ratio is decreased in the subsequent stages of consolidation, the excess pore water pressure dissipates extremely rapidly and shows absolutely no agreement with the theory at all. The pore pressure response and maximum build-up is also a function of these ratios; for example, when large stress increment ratio is used, high build-up of pore pressure is obtained and vice-versa.

The coefficients of compressibility and permeability decrease with logarithm of effective stress for the range investigated. The coefficient of consolidation increases with effective stress, provided stress increment ratio is kept constant or increased. The compressibilities from isotropic consolidation are larger than those of anisotropic consolidation, which is due to different stress-strain conditions (Skempton and Bishop, 1954). The void ratio shows linear relationship with logarithm of effective stress.

The rate of settlement is not affected by the stress increment ratio to a greater extent, except when very small pressure increments are applied. In the case of small pressure increment the secondary compression is predominant; consequently it becomes difficult to distinguish

one from the other. Wahls' (1962) curve-fitting method may prove useful at these events to determine 100% primary consolidation, i.e. when pore pressure ceases to dissipate any further. The experimental work reveals that the relative amount of secondary to primary consolidation depends on the stress increment ratio.

The microstructure study seems to indicate that the consolidation process is a function of particle arrangement caused by sustained stressing of the soil and leads to a possible hypothesis for the behaviour of the material. Before consolidation the sand grains are separated from clay particles by a thin film of water. With the external pressure, the sand and clay particles move closer to each other as the pore water is drained out. Tighter packing and decrease in interparticle spacing increase stronger bond between the particles. Small stress increment ratios will cause less slippage amongst particles, or in other words, the bonds will be able to resist the small pressures fairly successfully. The compressibility will therefore be smaller than would be the case if large stress increment ratios were applied. Due to the low compressibility, the dissipation of pore water pressure will be more rapid for a small stress increment ratio than for a large one.

REFERENCES

AAS, G. (1965) "A Study of the effects of vane shape and rate of strain on the measured values of in-situ shear strength of clays". Proc. 6th Int. Conf. SMFE, 1:141-145

AYLMORE, L. and QUIRK, J.P. (1960) "Domain or turbostratic structure of clay". Nature, 187, 1046.

BARDEN, L. (1965) "Consolidation of clay with Non-linear Viscosity" Geotechnique, 15: 345-362.

BARDEN, L and BERRY, P.L. (1965) "Consolidation of normally consolidated clay" J. ASCE, SMFD, Vol. 91, SM5.

BARDEN, L. and SIDES, G. (1971) "Sample disturbance in the investigation of clay structure" Geotechnique, 21: 211-222.

BARRY, P.L. and WILKINSON, W.B. (1969) "The radial consolidation of clay soils" Geotechnique, 19: 253-284.

BERRE, T. and IVERSEN, K. (1972) "Oedometer test with different specimen heights on a clay exhibiting large secondary compression" Geotechnique, 22: 53-70.

BIOT, M.A. (1941) "General theory of three-dimensional consolidation" Journ. Appl. Phys. Vol. 12: 155-164.

BIOT, M.A. (1956) "General solutions of the equations of elasticity and consolidation for a porous material" Appl. Mech. Trans., ASME, Vol. 78.

BISHOP, A.W. and GIBSON, R.E. (1963) "The influence of provisions for boundary drainage on strength and consolidation characteristics of soil measured on the triaxial apparatus" ASTM, Spec. Tech. Publ. No. 361.

BISHOP, A.W. and HENKEL, D.J. (1962) "The measurement of soil properties in the triaxial test". Edward Arnold, London, 2nd Edition.

BJERRUM, L. (1954) "Geotechnical properties of Norwegian marine clays" Geotechnique, 4: 49-69.

BJERRUM, L. (1967) "Engineering geology of normally-consolidated marine clays as related to settlements of buildings" 7th Rankine Lecture, Geotechnique, 17: 81-118.

BOLT, G.H. (1956) "Physico-chemical analysis of the compressibility of pure clays" Geotechnique, 6: 86-93.

BUISMAN, A.S.K. (1936) "Results of long duration settlement tests" Proc. Ist. Int. Conf. SMFE, Vol. 1, p. 103.

CHRISTIE, I.F. (1964) "A re-appraisal of Merchant's contribution to the theory of consolidation" Geotechnique, 14: 4.

CHRISTIE, I.F. (1965) "Secondary compression during one-dimensional consolidation tests". Proc. 6th Int. Conf. SMFE, 1: 198-202.

CRAWFORD, C.B. (1964) "Interpretation of the consolidation tests". J. ASCE, SMFD, Vol. 90. SM5.

CRAWFORD, C.B. (1965) "The resistance of soil structures to consolidation" Canadian Geotech. Journal. Vol. 2, No.2.

CROMER, J.J. and TURLEY, J.W. (1955) "Replica studies of bulk clays" Jour. Appl. Phys., p. 346-350.

DAVIS, E.H. and RAYMOND, G.P. (1965) "A non-linear theory of consolidation" Geotechnique, 15: 161-173.

FINN, F.N. (1951) "The effects of temperature on the consolidation characteristics of remoulded clay" ASTM, Spec. Tech. Publ. No. 126.

FITZPATRICK, E.A. (1970) "A technique for the preparation of large thin sections of soils and unconsolidated materials". Agric. Res. Coun. Technical Monograph No. 2: 3-13.

GARGA, V.K. (1970) "Residual shear strength under large strains and the effects of sample size on consolidation of fissured clay". Ph.D. thesis, University of London.

GIBSON, R.E. (1963). "An analysis of system flexibility and its effect on time-lag in pore-water pressure measurements". Geotechnique, 13: 1-11.

GIBSON, R.E. (1970) "An extension to the theory of the constant head in-situ permeability test" Geotechnique, 20: 193-197.

GIBSON, R.E. ENGLAND, G.L. and HUSSEY, M.J.L. (1967) "The theory of one-dimensional consolidation of saturated clays". Geotechnique, 17: 261-273.

GIBSON, R.E. and LO, K.Y. (1961) "A theory of consolidation for soils exhibiting secondary compression" N.G.I. Publ. No. 41.

GIBSON, R.E. and McNAMEE, J (1957) "The consolidation settlement of a load uniformly distributed over a rectangular area" Proc. 4th Int. Conf. SMFE, 1: 297-299.

GIBSON, R.E. and McNAMEE, J. (1963) "A three-dimensional problem of the consolidation of a semi-infinite clay stratum" Qtly. Jour. of Mech. and Appl. Maths, Vol. 16, p. 115.

GILBOY, G. (1928) "The compressibility of sand-mica mixtures" Proc. ASCE, No. 54, p. 555-568.

GILLOT, J.E. (1969) "Study of fabric of fine-grained sediments with the Scanning electron microscope". Jour. of sedimentary petrology, 39: 90-105.

GOLDSCHMIDT, V.M. (1926) "Undersokelser over lersendimenter" Nordisk jordbrugsforskning Nos. 4-7, p. 434-445.

GRAY, H. (1936) "Progress report on research on the consolidation of fine-grained soil". Proc. Ist. Int. Conf. SMFE, 2: 138-141.

GREEN-Kelly, R. and CAPMAN, S. with PITTIFER, K (1970) "The preparation of thin sections of soils using Polyethylene Glycols". Agric. Res. Coun. Technical Monograph No. 2: 15-24.

HALL, C.E. (1966) "Introduction to electron microscopy" McGraw-Hill.

HAMILTON, J.J. and CRAWFORD, C.B. (1959) "Improved determination of preconsolidation pressure of sensitive clay" ASTM, Spec. Tech. Publ. No. 254.

HANSBO, S. (1960) "Consolidation of clays with special reference to influence of vertical sand drains" Proc. Royal Swedish Geotech. Inst. No. 18.

ISHII, Y. (1951) "General discussion" Symposium on consolidation testing of soils. ASTM, Spec. Tech. Publ. No. 126.

JIMENEZ SALAS, J.A. and SERRATOSA, J.M. (1953) "Compressibility of clays" Proc. 3rd Int. Conf. SMFE, Vol. 1.

KALLSTENIUS, T. (1963) "Studies on clay samples taken with standard sampler" Proc. Royal Swed. Geotech. Inst. No. 21.

KENNEY, T.C. (1966) "Residual strength of fine-grained minerals and mineral mixtures" N.G.I. Publication, p. 53-58.

KONDNER, R.L. and VENDRELL, J.R. (1964) "Consolidation Coefficient: cohesive soil mixtures" J. ASCE, SMFD, Vol. 90, SM5.

KOPPENJAN, A.W. (1948) "A formula combining the Terzaghi load-compression relationship and the Buisman secular effect" Proc. 2nd Int. Conf. SMFE, Vol. 3.

LAMBE, T.W. (1953) "The structure of inorganic soil". J. ASCE, SMFD, separate paper 135.

LAMBE, T.W. (1958) "The structure of compacted clay" J. ASCE, SMFD, Vol. 84, SM2.

LANGER, K. (1936) "The influence of the speed of loading on the pressure void ratio diagram of undisturbed samples" Proc. Ist. Int. Conf. SMFE, 2: 116-120.

LEONARDS, G.A. and ALTSCHAEFFL, M. (1964) "Compressibility of clay" J. ASCE, SMFD, Vol. 90, SM5.

LEONARDS, G.A. and GIRAULT, P. (1961) "A study of one-dimensional consolidation" Proc. 5th Int. Conf. SMFE, 1: 213-218.

LEONARDS, G.A. and RAMIAH, B.K. (1959) "Time effects in the consolidation of clay" ASTM, Spec. Tech. Publ. No. 254.

LEWIS, W.A. (1950) An investigation of the consolidation test for soils" DSIR, Road Research Lab., Note No. RN/1349/WAL, Hamondsworth England.

LO, K.Y. (1960) "Correspondence on measurement of coefficient of consolidation of Lacustrine clay" Geotechnique, 10: 36-39.

LOWE, J., ZACCHEO, P.F. and FELDMAN, H.S. (1964) "Consolidation testing with back pressure" J. ASCE, SMFD, Vol. 90, SM4.

MANDEL, J. (1957) "Consolidation of clay layers" Proc. 4th Int. Conf. SMFE, Vol. 1.

MARTIN, R.T. (1962) "Research on the physical properties of marine soils" Research Rept. R.62-42. Soil Eng. Div., Publ. No. 127.

MARTIN, R.T. (1966) "Quantitative fabric of wet kaolinite" Clay and Clay Minerals, 14: 271-287. Pergamon Press. London.

MARTIN, W.B. (1962) "Some factors controlling the consolidation of saturated soils" M.Sc. thesis, University of London.

MATLOCK, H. and DAWSON, R.F. (1951) "Aids in the interpretation of the consolidation test" ASTM, Spec. Tech. Publ. No. 126.

MATYAS, E. L. (1966) "Air and water permeability of compacted soils" ASTM, Spec. Tech. Publ. No. 417.

McNABB, A. (1960) "A mathematical treatment of one-dimensional soil consolidation" Qtly. Appl. Maths. Providence, R. I. 27: 4 p. 337-347.

MIKASA, M. (1965) "The consolidation of soft clay: a new consolidation theory and its application" Japanese Soc. Civil Engg. (reprint from Civil Engineering in Japan 1965).

MITCHELL, J.K. (1956) "The fabric of natural clays and its relation to engineering properties". Proc. Highway Res. Board, 35: 693-713.

MITCHELL, J.K. and HOUSTON, W. N. (1969) "Causes of clay sensitivity" J. ASCE, SMFD, Vol. 95, SM3.

MITCHELL, J.K. and YOUNGER, J.S. (1966) "Abnormalities in hydraulic flow through fine-grained soils". ASTM, Spec. Tech. Publ. No. 417.

MORGENSTERN, N.R. AND TCHALENKO, J.S. (1967) "Microstructure in kaolin subjected to direct shear" Geotechnique, 17: 309-328.

MUHS, H. and KANY, M. (1954). "Einfluss von Feblerquellen beim Kompressions versuch Mitteilung" Degebo.

MURAYAMA, S. and SHIBATA (1964) "Flow and stress relaxation of clay" (International Union of Theoretical and Applied Mechanics) Symp. Rheol. soil Mech. Grenoble, p. 99.

NAKASE, A. (1963) "Side friction in conventional tests" Report of Port and Harbour Tech. Res. Inst. No. 3., Japan Ministry of Transportation.

NEWLAND, P.L. and ALLELY, B.H. (1956) "Results of some investigation on two sensitive clays" Proc. 2nd Aust.-N.Z. Conf. SMFE.

NEWLAND, P.L. and ALLELY, B.H. (1960) "A study of the consolidation characteristics of a clay" Geotechnique 10: 62-74.

NORTHEY, R.D. (1956) "Rapid consolidation tests for routine investigations" Proc. 2nd Aust.-N.Z. Conf. SMFE.

NORTHEY, R.D. and THOMAS, R.F. (1965) "Consolidation test pore pressures" Proc. 6th Int. Conf. SMFE, Vol. 1.

OLSEN, H.W. (1965) "Deviations from Darcy's law in saturated clays" Proc. of Soil Science Soc. Am. p. 135-140.

PADUANA, J.A. and MITCHELL, J.K. (1968) "Clay-sand interaction in consolidated mixtures" Soil Mech. and Bituminous Materials Lab., University of California, Berkeley.

PERLOFF, W.H., NAIR, K. and SMITH, J.G. (1965) "Effects of measuring system on pore water pressures in the consolidation test" Proc. 6th Int. Conf. SMFE, Vol. 2.

POSKITT, T.J. (1969) "The consolidation of saturated clay with variable permeability and compressibility" Geotechnique, 19: 243-252.

POULOS, S.G. (1964) "Control of leakage in the triaxial test" Harvard Soil Mechanics Series No. 71, Cambridge, Mass.

RAYMOND, G.P. (1965) "Discussion" - The resistance of soil structure to consolidation. Canadian Geotech. Jr. 2: 100-115.

RAYMOND, G.P. (1966) "Laboratory consolidation of some normally consolidated soils" Canadian Geotech. Jr. 3: 217-234.

RICHART, F.E. (1957) "A review of the theories for sand drains" J. ASCE, SMFD, Vol. 83, SM3.

ROSCOE, K.H. (1967) "Discussion of session 2" Proc. Geotech. Conf. Oslo, 2, p. 167-170.

ROWE, P.W. and BARDEN, L. (1966) "A new consolidation cell" Geotechnique, 16:162.

ROSENQVIST, I. Th. (1955) "Investigation in the clay-electrolyte-water system" N.G.I. Publ. No. 9.

ROSENQVIST, I. Th. (1959) "Physico-chemical properties of soils: soil-water systems" J.ASCE, SMFD, Vol. 1, SM1.

SCHIFFMAN, R.L. (1958) "Consolidation of soil under time-dependent loading and varying permeability" Proc. Highway Res. Bd. 37: 584-617.

SCHIFFMAN, R.L. and GIBSON, R.E. (1964) "Consolidation of non-homogeneous clay layers" J.ASCE, SMFD, Vol. 90, SM5.

SEED, H.B. and CHAN, C.K. (1959) "Structure and strength characteristics of compacted clays" J. ASCE, SMFD, Vol. 85, SM5.

SIDES, G.R. (1971) "Soil microstructure and sample disturbance in the Stereoscan electron microscope" Soils Proc. of Roscoe Memorial Symp. G.T. Foulis.

SIMONS, N.E. (1965) "Consolidation investigation of undisturbed Fornebu clay" N.G.I. Publ. No. 62.

SKEMPTON, A.W. (1954) "The pore pressure coefficients A and B" Geotechnique, 4: 143-147.

SKEMPTON, A.W. and BISHOP, A.W. (1954) "Soils" Chapter X of building material. North-Holland Publ. Co. Amsterdam.

SKEMPTON, A.W. and NORTHEY, R.D. (1952) "The sensitivity of clays" Geotechnique 3.

SKINNER, A.E. (1970) Postgraduate Lectures, DIC course.

SLOANE, R. L. and KELL, T.R. (1966) "The fabric of mechanically compacted kaolin" Proc. 14th NCCCM, p.289-296.

SOM, N.N. (1968) "The effect of stress path on the deformation and consolidation of London clay" Ph.D. thesis, University of London.

TAN, S.B. (1968) "Consolidation of soft clays with special reference to sand drains" Ph.D. thesis, University of London.

TAN, T.K. (1953) "Contribution to discussion" Proc. 3rd. Int. Conf. SMFE, Vol. 3.

TAN, T.K. (1957) "Secondary time effects and consolidation of clays" Academia Sinica. Inst. Civil Engg. and Archit., Harbin, China.

TAYLOR, D.W. (1942) "Research on consolidation of clays" Publ. Serial 82, Dept. of Civil and Sanitary Eng., M.I.T.

TAYLOR, D.W. (1948) "Fundamentals of soil mechanics" John Wiley, New York.

TAYLOR, D.W. and MERCHANT, W. (1940) "A theory of clay consolidation accounting for secondary compression" J. Maths. Phys. 19:3:167-185

TCHALENKO, J.S. (1967) "The influence of shear and consolidation on the microscopic structure of some clays" Ph.D. thesis, University of London.

TERZAGHI, K. (1943) "Theoretical soil mechanics" John Wiley, New York.

THORTON, P.R. (1968) "Scanning electron microscopy" Chapman and Hall.

TOVEY, N.K. (1970) "Electron microscopy of clays" Ph.D. thesis, Cambridge University.

TROLLOPE, D.H. and CHAN, C.K. (1960) "Soil structure and the step-strain phenomenon" J. ASCE, SMFD, Vol. 86, SM2.

TROLLOPE, D.H. and ZAFAR, S.M. (1956) "A study of sand and sand-clay mixtures in triaxial compression" Proc. 2nd Aust.-N.Z. Conf. SMFE.

VAN ZELST, T.W. (1948) "An investigation of the factors affecting laboratory consolidation of clays" Proc. 2nd Int. Conf. SMFE, Vol. 7.

WAHLS, H.E. (1962) "Analysis of primary and secondary consolidation" J. ASCE, SMFD, Vol. 88, SM6.

WEATHERHEAD, A.V. (1940) Minerals Magazine, Vol. 25, p. 529.

WEYMOUTH, J.H. and WILLIAMSON, W.O. (1953) "The effects of extrusion and some other process on the microstructure of clay" Am. J. of Science Vol. 251, P. 89.

WHITMAN, R.V., RICHARDSON, A. and HEALY, K.A. (1961) "Time lags in pore pressure measurements" Proc. 5th Int. Conf. SMFE, Vol. 1.

WHITMAN, R.V. and MILLER (1965) " Yielding and locking of confined sand" J. ASCE, SMFD, Vol. 91, SM4.

WU, T.H., RESENDIZ, D. and NEUKIRCHNER, R.J. (1966) "Analysis of consolidation by rate process theory" J.ASCE, SMFD, Vol. 92, SM6.

YONG, R.N. and WARKENTIN, B.P. (1966) "Introduction to soil behaviour" Macmillan Co. New York.

ZEEVAERT, L. (1957) "Consolidation of Mexico City volcanic clay" ASTM, Spec. Tech. Publ. No. 232.

APPENDIX A

Relaxation Method for the Radial Flow (isotropic media), axisymmetric. The governing equation is

$$\frac{\partial^2 h}{\partial r^2} + \frac{1}{r}\frac{\partial h}{\partial r} + \frac{\partial^2 h}{\partial z^2} = 0 \qquad \ldots\ldots\ldots (1)$$

where h is the head and r and z are the coordinates as shown in the following figure (1A)

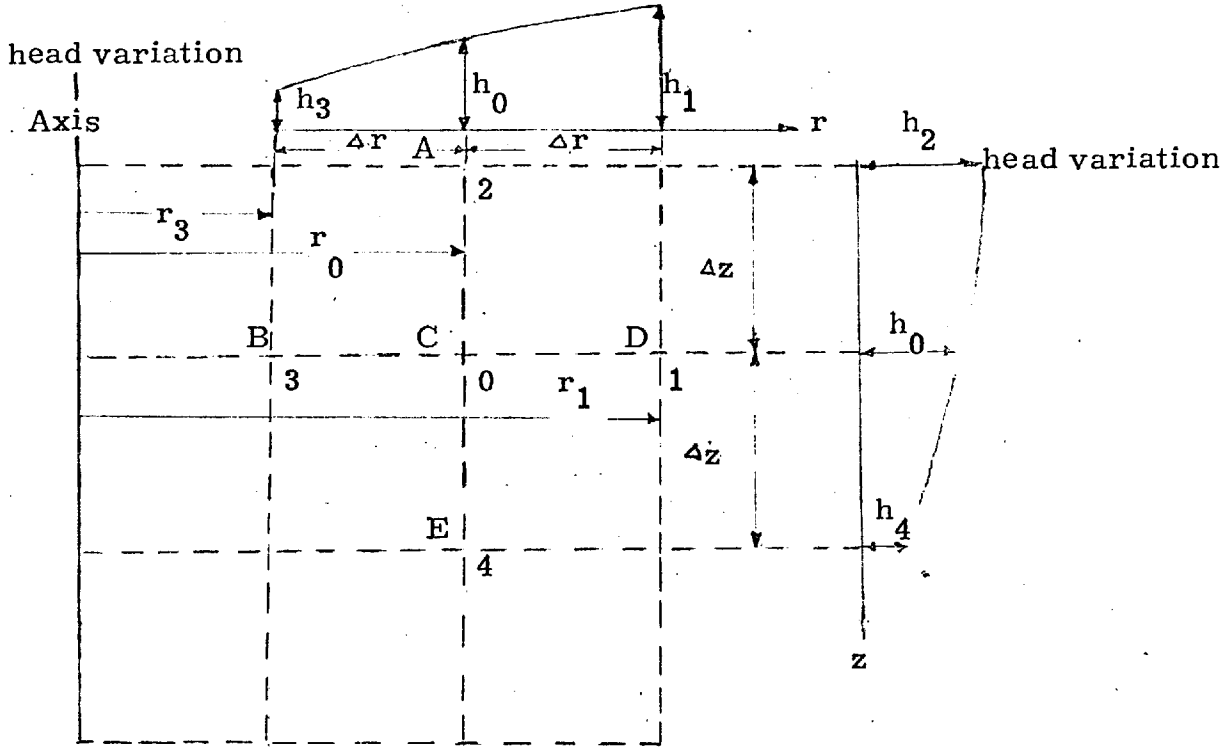

Figure (1A)

For variation in head in - direction Taylor's theorem is used.

$$h_1 = h_0 + \Delta r \left(\frac{\partial h}{\partial r}\right)_0 + \frac{\Delta r^2}{2!} \left(\frac{\partial^2 h}{\partial r^2}\right)_0 + \ldots\ldots \quad (2)$$

$$h_3 = h_0 - \Delta r \left(\frac{\partial h}{\partial r}\right)_0 + \frac{\Delta r^2}{2!} \left(\frac{\partial^2 h}{\partial r^2}\right)_0 + \ldots\ldots \quad (3)$$

where subscripts 0, 1, 3 indicate the values of function or derivative at the points 0, 1, 3.

By adding equations (1) and (2), and rearranging, the following approximate derivatives can be obtained.

i.e. $$\left(\frac{\partial^2 h}{\partial r^2}\right)_0 \simeq \frac{1}{\Delta r^2} (h_1 + h_3 - 2h_0) \quad \ldots\ldots (4)$$

and $$\left(\frac{\partial h}{\partial r}\right)_0 \simeq \frac{1}{2\Delta r} (h_1 - h_3) \quad \ldots\ldots (5)$$

Now using these finite difference approximations in equation (1), gives for a typical node "0"

$$\frac{h_1 + h_3 - 2h_0}{(\Delta r)^2} + \frac{1}{r_0} \frac{h_1 - h_3}{2(\Delta r)} + \frac{h_2 + h_4 - 2h_0}{(\Delta z)^2} = 0 \quad \ldots\ldots (6)$$

if $\Delta r = \Delta z$

the residual formula is

$$\left(1 + \frac{\Delta r}{2 r_0}\right) h_1 + h_2 + \left(1 - \frac{\Delta r}{2 r_0}\right) h_3 + h_4 - 4h_0 = R_0 . \quad \ldots\ldots (7)$$

(where R_0 made to $\rightarrow$ 0)

In order to find out a reasonably accurate difference between actual and the measured permeability, the square grid of lines having $\Delta r = \Delta z = \frac{1}{4}''$ is considered. Thus by substituting $\Delta r = \frac{1}{4}$ in equation (7) the following residual formula is obtained:

$$(1 + \frac{1}{8r_0})\ h_1 + h_2 + (1 + \frac{1}{8r_0})\ h_3 + h_4 - 4h_0 = R_0$$

$$\text{or} \quad h_1 + h_2 + h_3 + h_4 - 4h_0 + \frac{1}{8r_0}(h_1 + h_3) = R_0 \quad \ldots \ldots \ldots (8)$$

∴ Relaxation pattern for a typical point C will be:

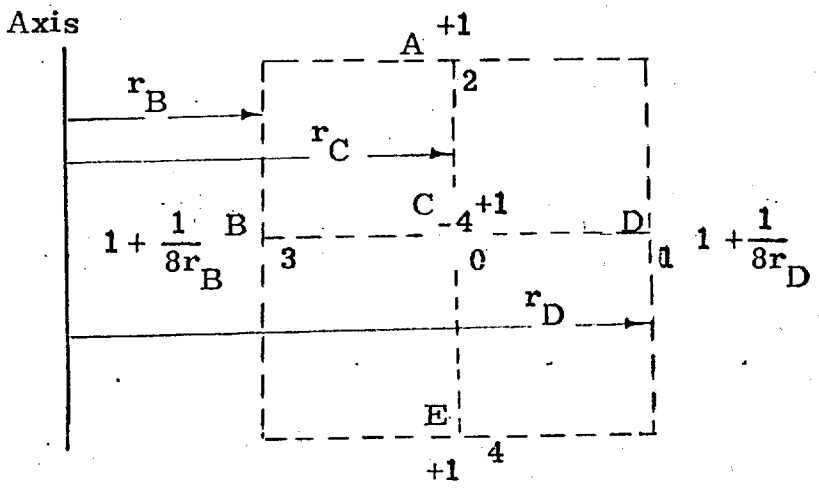

Figure (2A)

where $(1 + \frac{1}{8r_B})$ and $(1 + \frac{1}{8r_D})$ denote changes in the residuals in the residual formula for points B and D respectively, due to a unit increase in the head at point C.

The problem is solved by assigning an arbitrary value to each node point and the resulting residuals can be systematically

eliminated by adding to them equal residuals of opposite sign. However, eliminating a residual at one point produces a change in the surrounding residuals since the operation of residual at a point implies changing the head at that point. Equation (8) shows that if a positive unit change is applied to the head point 0 this produces change in the residual at C of -4 and $1 - \frac{1}{8r_D}$, $+1$, $1 + \frac{1}{8r_D}$ and $+1$ to each of the surrounding residuals R_1, R_2, R_3 and R_4 at the nodes D, A, B and E respectively, while at all nodes on the permeable boundary, the corresponding values are kept constant.